THE GRAND UNIFIED THEORY
OF CLASSICAL QUANTUM MECHANICS

Dr. Randell L. Mills

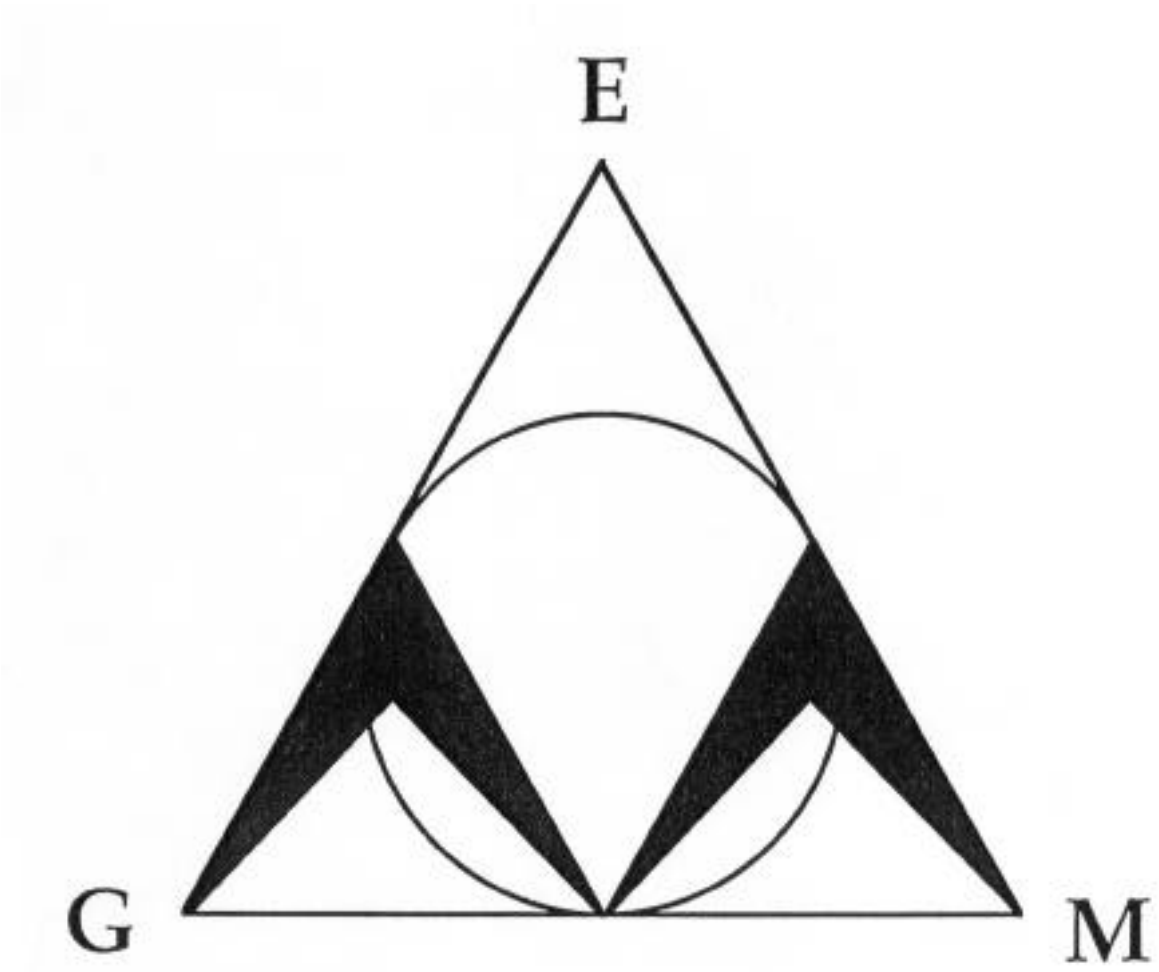

THE GRAND UNIFIED THEORY
OF CLASSICAL
QUANTUM MECHANICS

THE GRAND UNIFIED THEORY OF CLASSICAL QUANTUM MECHANICS

BY

Dr. Randell L. Mills

BLACKLIGHT SM, TM
POWER inc.

493 Old Trenton Road

Cranbury, NJ 08512

January 2000 EDITION

ISBN 0-9635171-4-7

Library of Congress Catalog Card Number 00 091384

Table Of Contents

SYMBOLS

μ_o	permeability of free-space
ε_o	permittivity or capacitivity of free-space
$\eta = \sqrt{\frac{\mu_o}{\varepsilon_o}}$	intrinsic impedance of free-space
$c = \sqrt{\frac{1}{\mu_o \varepsilon_o}}$	speed of light
$\alpha = \frac{\mu_o e^2 c}{2h}$	fine structure constant
$\hbar$	Planck constant bar
e^2	electron charge squared
$a_o = \frac{4\pi\varepsilon_0 \hbar^2}{e^2 \mu_e}$	Bohr radius
$\Phi_0 = \frac{h}{2e}$	magnetic flux quantum
$\mu_N = \frac{e\hbar}{2m_P}$	nuclear magneton
$\mu_B = \frac{e\hbar}{2m_e}$	Bohr magneton
$\lambda\!\!\!^{-}_c$	Compton wavelength bar
$\lambda\!\!\!^{-}_c = \alpha a_o = \frac{\hbar}{m_e c}$	electron Compton wavelength bar
G	gravitational constant
m_e	mass of the electron
m_μ	rest mass of the muon
m_τ	rest mass of the tau
μ_e	reduced electron mass
m_N	rest mass of the neutron
m_P	rest mass of the proton

And God said, "Let there be light"; and there was light. And God saw that the light was good; and God separated the light from the darkness.

Genesis 1:3

Apparently there is color, apparently sweetness, apparently bitterness; actually there are only atoms and the void.

Democritus 420 BC

I cannot believe that God would choose to play dice with the universe.

Albert Einstein

All truth goes through three steps. First, it is ridiculed. Second, it is violently opposed, and finally it is accepted as self-evident.

Arthur Schopenhauer
German Philosopher

FOREWORD

BLACKLIGHT POWER, inc. (BLP) of Malvern, Pennsylvania, is developing a revolutionary energy technology--catalytic hydrogen collapse. More explicitly, thermal energy is catalytically released as the electrons of atomic hydrogen atoms are induced to undergo transitions to lower energy levels corresponding to fractional quantum numbers. The Company uses a hot refractory metal (e.g.. a hot tungsten filament) to break hydrogen molecules into individual, normal hydrogen atoms. A vaporized inorganic catalyst causes the normal hydrogen atoms to collapse to smaller-than-normal hydrogen atoms. The hydrogen collapse is accompanied by a release of energy that is intermediate between chemical and nuclear energies. BLP's new technology can operate under the conditions of many existing electric power plants. It should be possible to retrofit these power plants to accommodate the new technology. The advantages are that the hydrogen fuel can be obtained by diverting a fraction of the output energy of the process to split water into its elemental constituents, and pollution which is inherent with fossil and nuclear fuels is eliminated.

BLP is not developing so-called "Cold Fusion", which refers to the failed attempt of producing substantial nuclear energy at room temperature. In contrast, BLP has obtained compelling theoretical and experimental support for fractional quantum energy states of hydrogen, which is the basis of a new hydrogen energy source. Some revisions to standard quantum theory are implied. Quantum mechanics becomes a real physical description as opposed to a purely mathematical model where the old and the revised versions are interchangeable by a Fourier Transform operation [1]. These revisions transform Schrödinger's and Heisenberg's quantum theory into what may be termed a ***classical quantum theory***. Physical descriptions flow readily from the theory. For example, in the old quantum theory the spin angular momentum of the electron is called the "intrinsic angular momentum". This term arises because it is difficult to provide a physical interpretation for the electron's spin angular momentum. Quantum Electrodynamics provides somewhat of a physical interpretation by proposing that the "vacuum" contains fluctuating electric and magnetic fields. In contrast, in Mills' theory proposed herein, spin angular momentum results from the motion of negatively charged mass moving systematically, and the equation for angular momentum, $\mathbf{r} \times \mathbf{p}$, can be applied directly to the wave function (a current density function) that describes the electron.

The quantum number $n = 1$ is routinely used to describe the "ground" electronic state of the hydrogen atom. I will show that the $n = 1$

state is the "ground" state for "pure" photon transitions (the $n=1$ state can absorb a photon and go to an excited electronic state, but it cannot release a photon and go to a lower-energy electronic state). However, an electron transition from the ground state to a lower-energy state is possible by a "resonant collision" mechanism. These lower-energy states have fractional quantum numbers, $n=\frac{1}{\text{integer}}$. Processes that occur without photons and that require collisions are common. For example, the exothermic chemical reaction of $H+H$ to form H_2 does not occur with the emission of a photon. Rather, the reaction requires a collision with a third body, M, to remove the bond energy- $H+H+M \rightarrow H_2+M^*$. The third body distributes the energy from the exothermic reaction, and the end result is the H_2 molecule and an increase in the temperature of the system. Similarly, the $n=1$ state of hydrogen and the $n=\frac{1}{\text{integer}}$ states of hydrogen are nonradiative, but a transition between two nonradiative states is possible via a resonant collision, say $n=1$ to $n=1/2$. In these cases, during the collision the electron couples to another electron transition or electron transfer reaction which can absorb the exact amount of energy that must be removed from the hydrogen atom, a resonant energy sink. The end result is a lower-energy state for the hydrogen and an increase in the temperature of the system.

NEW QUANTUM THEORY

J. J. Balmer showed in 1885 that the frequencies for some of the lines observed in the emission spectrum of atomic hydrogen could be expressed with a completely empirical relationship. This approach was later extended by J. R. Rydberg, who showed that all of the spectral lines of atomic hydrogen were given by the equation:

$$\bar{\nu}=R\left(\frac{1}{n_f^2}-\frac{1}{n_i^2}\right) \tag{1}$$

where $R=109{,}677\ cm^{-1}$, $n_f=1,2,3,...$, $n_i=2,3,4,...$, *and* $n_i>n_f$.

Niels Bohr, in 1913, developed a theory for atomic hydrogen that gave energy levels in agreement with Rydberg's equation. An identical equation, based on a totally different theory for the hydrogen atom, was developed by E. Schrödinger, and independently by W. Heisenberg, in 1926.

$$E_n=-\frac{e^2}{n^2 8\pi\varepsilon_o a_H}=-\frac{13.598\ eV}{n^2} \tag{2a}$$

$$n=1,2,3,... \tag{2b}$$

where a_H is the Bohr radius for the hydrogen atom ($52.947\ pm$), e is the magnitude of the charge of the electron, and ε_o is the vacuum permittivity.

Recently, I have built on this work by deriving a new atomic theory based on first principles. The novel theory hereafter referred to as Mills' theory unifies Maxwell's Equations, Newton's Laws, and General and Special Relativity. The central feature of this theory is that all particles (atomic-size and macroscopic particles) obey the same physical laws. Whereas Schrödinger postulated a boundary condition: $\Psi \to 0$ as $r \to \infty$, the boundary condition in Mills' theory was derived from Maxwell's equations [2]:

> *For non-radiative states, the current-density function must not possess space-time Fourier components that are synchronous with waves traveling at the speed of light.*

Application of this boundary condition leads to a physical model of particles, atoms, molecules, and, in the final analysis, cosmology. The closed-form mathematical solutions contain fundamental constants only, and the calculated values for physical quantities agree with experimental observations. In addition, the theory predicts that Eq. (2b), should be replaced by Eq. (2c).

$$n = 1,2,3,..., \text{ and, } n = \frac{1}{2},\frac{1}{3},\frac{1}{4},... \tag{2c}$$

FRACTIONAL QUANTUM ENERGY LEVELS OF HYDROGEN

A number of experimental observations lead to the conclusion that atomic hydrogen can exist in fractional quantum states that are at lower energies than the traditional "ground" ($n = 1$) state. For example, the existence of fractional quantum states of hydrogen atoms explains the spectral observations of the extreme ultraviolet background emission from interstellar space [3], which may characterize dark matter as demonstrated in Table 1. (In these cases, a hydrogen atom in a fractional quantum state, $H\left(n_i\right)$, collides, for example, with a $n = \frac{1}{2}$ hydrogen atom, $H\left(\frac{1}{2}\right)$, and the result is an even lower-energy hydrogen atom, $H\left(n_f\right)$, and $H\left(\frac{1}{2}\right)$ is ionized.

$$H\left(n_i\right) + H\left(\frac{1}{2}\right) \to H\left(n_f\right) + H^+ + e^- + photon \tag{3}$$

The energy released, as a photon, is the difference between the energies of the initial and final states given by Eqs. (2a-2c) minus the ionization energy of $H\left(\frac{1}{2}\right)$, 54.4 *eV*.)

Table 1. Observed emission data. (Raw extreme ultraviolet background spectral data taken from raw data and Figure 4 of Labov and Bowyer).

Peak #	Observed Wavelength (Å)	Observed Energy (eV)	Peak Assignment	Predicted Energy[a] (eV)	Predicted Wavelength (Å)
1	84.8	146.2	1/7 → 1/8 H transtiton	149.6	82.9
2	101.5	122.2	1/6 → 1/7 H transition	122.4	101.3
3	116.8	106.2	1/2 → 1/4 H transition	108.8	114.0
4	129.6	95.6	1/5 → 1/6 H transition	95.2	130.2
5	139.6	88.8	He scattered peak #3	87.6	141.5
6	163.2	75.9	Second order of peak #1	74.8	165.7
7	181.7	68.3	1/4 → 1/5 H transition	68.0	182.3
8	200.6	61.8	Second order of peak #2	61.2	202.6
9*	233.8	53.0	1 → 1/3 H transition	54.4	227.9
10	261.2	47.5	He scattered peak #7	46.8	265.0
11	302.5	41.0	1/3 → 1/4 H transition	40.8	303.9
12	459.1	27.0	Second order of peak #9	27.2	455.8
13	584	21.2	He resonance scattered emission	21.2	584
14	607.5	20.4	Second order of peak #11	20.4	607.8
15	633.0	19.7	He scattered peak #11	19.6	633.0
16			1/2 → 1/3 H transition	13.6	912.3

For excited state hydrogen transitions, $n_i \rightarrow n_f \quad n = 1,2,3,\ldots,$

$$E = \left(\frac{1}{n_f^2} - \frac{1}{n_i^2}\right) X 13.6\ eV$$

[a]For lower-energy transitions, $n = 1, \frac{1}{2}, \frac{1}{3}, \frac{1}{4}, \ldots,$ and $n_i > n_f$ induced by a disproportionation reaction with $H\left[\frac{a_H}{2}\right]$

$$E = \left(\frac{1}{n_f^2} - \frac{1}{n_i^2}\right) X 13.6\ eV - 54.4\ eV$$

[a]For helium inelastic scattered peaks of hydrogen transitions, $n_i \rightarrow n_f$

$$E = \left(\frac{1}{n_f^2} - \frac{1}{n_i^2}\right) X 13.6\ eV - 54.4\ eV - 21.21\ eV$$

* Bowyer and Labov used three monochrometers for maximal sensitivity in each energy range: 80-230Å, 230-430Å, and 430-650Å. The monochrometer change at 230Å resulted in the 6 Å discrepancy between the calculated and observed lines.

Table 2. Representative analytical tests performed on BlackLight's novel hydride compounds with the corresponding laboratory.

Laboratory	Analytical Test
Lehigh University	X-ray Photoelectron Spectroscopy (XPS)
Virginia Tech	Raman Spectroscopy
Charles Evans & Associates East	TOFSIMS, XPS, EDS, Scanning Electron Spectroscopy
University of Massachusetts	Proton NMR
Charles Evans & Associates West	ToF-SIMS
Xerox	ToF-SIMS, XPS
Physical Electronics, Inc.	ToF-SIMS
Spectral Data Services	Proton & K NMR
Surface Science Associates	FTIR
IC Laboratories	XRD
Ricerca, Inc.	LC/MS
PerSeptive Biosystems	ESIToFMS
INP	EUV Spectroscopy
Galbraith Laboratories	Elemental Analysis
Franklin & Marshall College	XRD
Pennsylvania State University	Calvet calorimetry, XRD
TA Instruments	TGA/DTA
Northeastern University	Mossbauer Spectroscopy
M-Scan Inc.	FABMSMS, ESIMS, Solids Probe Magnetic Sector Mass Spectroscopy
Micromass	ESITOFMS
Southwest Research Institute	Solids Probe, Direct Exposure Probe Magnetic Sector Mass Spectroscopy
BlackLight Power, Inc.	Calvet and Heat Loss Calorimetry, Cryogenic Gas Chromatography, ToF-SIMS, XPS, LC/MS, UV and EUV Spectroscopy, Thermal Decomposition/Gas Chromatography, MS of Gasses Solids Probe Quadrapole Mass Spectroscopy, ESIToFMS

Other aspects of Mills' theory include the relationship of the mechanism that determines the masses of the fundamental particles to cosmology:

- Fundamental particle production occurs when the energy of the particle given by the Planck equation, Maxwell's Equations, and Special Relativity is equal to mc^2, and the proper time is equal to the coordinate time according to General Relativity. The gravitational equations with the equivalence of the particle production energies permit the equivalence of mass/energy and the spacetime metric from which the gravitational constant and the masses of the leptons, the quarks, and nucleons are derived.

- The gravitational equations with the equivalence of the particle production energies permit the equivalence of mass/energy ($E = mc^2$) and spacetime ($\frac{c^3}{4\pi G} = 3.22\ X\ 10^{34}\ \frac{kg}{\sec}$). Spacetime expands as mass is released as energy which provides the basis of the atomic, thermodynamic, and cosmological arrows of time. Entropy and the expansion of the universe are large scale consequences.

- The universe is closed independently of the total mass of the universe, and different regions of space are isothermal even though they are separated by greater distances than that over which light could travel during the time of the expansion of the universe. The calculated microwave background temperature is 2.7 °K.

- The universe is oscillatory in matter/energy and spacetime with a finite minimum radius, the gravitational radius ($3.12\ X\ 10^{11}\ light\ years$); thus, the gravitational force causes celestial structures to evolve on a time scale that is greater than the period of oscillation ($9.83\ X\ 10^{11}\ light\ years$).

- The value of the Hubble constant (Mills) is $H_0 = 78.6\ \frac{km}{\sec\ Mpc}$.

  Presently, stars exist which are older than the elapsed time of the present expansion as stellar evolution occurred during the contraction phase. The maximum energy release of the universe which occurs at the beginning of the expansion phase is $2.89\ X\ 10^{51}\ W$.

References

1. The theories of Bohr, Schrödinger, and presently Mills all give the identical equation for the principal energy levels of the hydrogen atom.

$$E_{ele} = -\frac{Z^2 e^2}{8\pi\varepsilon_o n^2 a_H} = -\frac{Z^2}{n^2}\ X\ 2.1786\ X\ 10^{-18}\ J = -Z^2\ X\ \frac{13.598}{n^2}\ eV \qquad (4)$$

The present theory solves the two dimensional wave equation for the charge density function of the electron. And, the Fourier transform of the charge density function is a solution of the three dimensional wave equation in frequency (k,ω) space. Whereas, the Schrödinger equation solutions are three dimensional in spacetime. The energy is given by

$$\int_{-\infty}^{\infty} \psi H \psi \, dv = E \int_{-\infty}^{\infty} \psi^2 dv; \qquad (5)$$

$$\int_{-\infty}^{\infty} \psi^2 dv = 1 \qquad (6)$$

Thus,

$$\int_{-\infty}^{\infty} \psi H \psi \, dv = E \qquad (7)$$

In the case that the potential energy of the Hamiltonian, H, is a constant times the wavenumber, the Schrödinger equation is the well known Bessel equation. Then with one of the solutions for ψ, Eq. (7) is equivalent to an inverse Fourier transform. According to the duality and scale change properties of Fourier transforms, the energy equation of the present theory and that of quantum mechanics are identical, the energy of a radial Dirac delta function of radius equal to an integer multiple of the radius of the hydrogen atom (Eq. (4)). And, Bohr obtained the same energy formula by postulating nonradiative states with angular momentum

$$L_z = m\hbar \qquad (8)$$

and solving the energy equation classically.

The mathematics for all three theories converge to Eq. (4). However, the physics is quite different. Only the Mills theory is derived from first principles and holds over a scale of spacetime of 45 orders of magnitude: it correctly predicts the nature of the universe from the scale of the quarks to that of the cosmos.

2. Haus, H. A., "On the radiation from point charges", American Journal of Physics, 54, (1986), pp. 1126-1129.
3. Labov, S., Bowyer, S., "Spectral observations of the extreme ultraviolet background", The Astrophysical Journal, 371, (1991), pp. 810-819.

INTRODUCTION

GENERAL CONSIDERATIONS

Toward the end of the 19th century, many physicists believed that all of the principles of physics had been discovered. The accepted principles, now called ***classical physics***, included laws relating to Newton's mechanics, Gibbs' thermodynamics, LaGrange's and Hamilton's elasticity and hydrodynamics, Maxwell-Boltzmann molecular statistics, and Maxwell's Equations. However, the discovery that the intensity of blackbody radiation goes to zero, rather than infinity as predicted by the prevailing laws, provided an opportunity for new principles to be discovered. In 1900, Planck made the revolutionary assumption that energy levels were quantized, and that atoms of the blackbody could emit light energy only in amounts given by $h\nu$, where ν is the radiation's frequency and h is a proportionality constant (now called Planck's constant). This assumption also led to our understanding of the photoelectric effect and ultimately to the concept of light as a particle called a photon. A similar course arose in the development of the model of the electron. In 1923, de Broglie suggested that the motion of an electron has a wave aspect where the wavelength, λ, is inversely proportional to the electron's momentum, p, as — $\lambda = \frac{h}{p}$. This concept seemed unlikely according to the familiar properties of electrons such as charge, mass and adherence to the laws of particle mechanics. But, the wave nature of the electron was confirmed by Davisson and Germer in 1927 by observing diffraction effects when electrons were reflected from metals.

Experiments by the early part of the 20th century had revealed that both light and electrons behave as waves in certain instances and as particles in others. This was unanticipated from preconceptions about the nature of light and the electron. Early 20th century theoreticians proclaimed that light and atomic particles have a "wave-particle duality" that was unlike anything in our common-day experience. The wave-particle duality is the central mystery of the presently accepted atomic model, ***quantum mechanics***, the one to which all other mysteries could ultimately be reduced.

Three atomic theories have been developed to explain the seemingly mysterious physics of the atomic scale. The earlier theories of Bohr and Schrödinger assume that the laws of physics that are valid in the macroworld do not hold true in the microworld of the atom. In contrast, the Mills theory is based on the foundation that laws of physics

valid in the macroworld do hold true in the microworld of the atom. In the present case, the predictions which arise from the equations of light and atomic particles are completely consistent with observation, including the wave-particle duality of light and atomic particles.

Three Atomic Theories

The theories of Bohr, Schrödinger, and presently Mills all give the identical equation, Eq. (I.1), for the principal energy levels of the hydrogen atom.

$$E = -\frac{Z^2 e^2}{8\pi\varepsilon_o n^2 a_H} = -\frac{Z^2}{n^2}\ X\ 2.1786\ X\ 10^{-18}\ J = -\frac{Z^2}{n^2}\ X\ 13.598\ eV \qquad (I.1)$$

However, only Mills theory is derived from first principles. The theories of Bohr and Schrödinger depend on specific postulates to yield Eq. (I.1). A relationship exists between the theories of Bohr and Schrödinger with respect to that of Mills which involves these postulates.

Mills Theory-*a classical quantum theory*

One-electron atoms include the hydrogen atom, He II, Li III, Be IV, and so on. The mass-energy and angular momentum of the electron are constant; this requires that the equation of motion of the electron be temporally and spatially harmonic. Thus, the classical wave equation applies and

$$\left[\nabla^2 - \frac{1}{v^2}\frac{\delta^2}{\delta t^2}\right]\rho(r,\theta,\phi,t) = 0 \qquad (I.2)$$

where $\rho(r,\theta,\phi,t)$ is the charge density function of the electron in time and space. In general, the wave equation has an infinite number of solutions. To arrive at the solution which represents the electron, a suitable boundary condition must be imposed. It is well known from experiments that each single atomic electron of a given isotope radiates to the same stable state. Thus, Mills chose the physical boundary condition of nonradiation of the bound electron to be imposed on the solution of the wave equation for the charge density function of the electron. The condition for radiation by a moving charge is derived from Maxwell's equations. To radiate, the spacetime Fourier transform of the current-density function must possess components synchronous with waves traveling at the speed of light [1]. Alternatively,

> *For non-radiative states, the current-density function must not possess spacetime Fourier components that are synchronous with waves traveling at the speed of light.*

Proof that the condition for nonradiation by a moving point charge

is that its spacetime Fourier transform does not possess components that are synchronous with waves traveling at the speed of light is given by Haus [1]. The Haus derivation applies to a moving charge-density function as well because charge obeys superposition. The Haus derivation is summarized below.

The Fourier components of the current produced by the moving charge are derived. The electric field is found from the vector equation in Fourier space (**k**, ω-space). The inverse Fourier transform is carried over the magnitude of **k**. The resulting expression demonstrates that the radiation field is proportional to $\mathbf{J}\left(\frac{\omega}{c}\mathbf{n},\omega\right)$, where $\mathbf{J}(\mathbf{k},\omega)$ is the spacetime Fourier transform of the current perpendicular to **k** and $\mathbf{n} \equiv \frac{\mathbf{k}}{|k|}$. Specifically,

$$\mathbf{E}(\mathbf{r},\omega)\frac{d\omega}{2\pi} = \frac{c}{2\pi}\int \rho(\omega,\Omega)d\omega d\Omega \sqrt{\frac{\mu_0}{\varepsilon_0}}\mathbf{n}\,X\left(\mathbf{n}\,X\,\mathbf{J}\left(\frac{\omega}{c}\mathbf{n},\omega\right)e^{i\left(\frac{\omega}{c}\right)\mathbf{n}\cdot\mathbf{r}}\right) \tag{I.3}$$

The field $\mathbf{E}(\mathbf{r},\omega)\frac{d\omega}{2\pi}$ is proportional to $\mathbf{J}\left(\frac{\omega}{c}\mathbf{n},\omega\right)$, namely, the Fourier component for which $\mathbf{k} = \frac{\omega}{c}$. Factors of ω that multiply the Fourier component of the current are due to the density of modes per unit volume and unit solid angle. An unaccelerated charge does not radiate in free space, not because it experiences no acceleration, but because it has no Fourier component $\mathbf{J}\left(\frac{\omega}{c}\mathbf{n},\omega\right)$.

The time, radial, and angular solutions of the wave equation are separable. The motion is time harmonic with frequency ω_n. To be a harmonic solution of the wave equation in spherical coordinates, the angular functions must be spherical harmonic functions. A zero of the spacetime Fourier transform of the product function of two spherical harmonic angular functions, a time harmonic function, and an unknown radial function is sought. The solution for the radial function which satisfies the boundary condition is a delta function

$$f(r) = \frac{1}{r^2}\delta(r - r_n) \tag{I.4}$$

where r_n is an allowed radius. Thus, bound electrons are described by a charge-density (mass-density) function which is the product of a radial delta function ($f(r) = \frac{1}{r^2}\delta(r - r_n)$), two angular functions (spherical harmonic functions), and a time harmonic function. Thus, an electron is a spinning, two-dimensional spherical surface, called an ***electron***

orbitsphere, that can exist in a bound state at only specified distances from the nucleus. More explicitly, the orbitsphere comprises a two-dimensional spherical shell of moving charge. The corresponding current pattern of the orbitsphere comprises an infinite series of correlated orthogonal great circle current loops. The current pattern (shown in Figure 1.4) is generated over the surface by two orthogonal sets of an infinite series of nested rotations of two orthogonal great circle current loops where the coordinate axes rotate with the two orthogonal great circles. Each infinitesimal rotation of the infinite series is about the new x-axis and new y-axis which results from the preceding such rotation. For each of the two sets of nested rotations, the angular sum of the rotations about each rotating x-axis and y-axis totals $\sqrt{2}\pi$ radians. The current pattern gives rise to the phenomenon corresponding to the spin quantum number.

Mills has built on this result by deriving a complete atomic theory based on first principles. The novel theory unifies Maxwell's Equations, Newton's Laws, and General and Special Relativity. The central feature of this theory is that all particles (atomic-size particles and macroscopic particles) obey the same physical laws.

The Mills theory solves the wave equation for the charge density function of the electron. The radial function for the electron indicates that the electron is two-dimensional. Therefore, the angular mass-density function of the electron, $A(\theta,\phi,t)$, must be a solution of the wave equation in two dimensions (plus time),

$$\left[\nabla^2 - \frac{1}{v^2}\frac{\delta^2}{\delta t^2}\right]A(\theta,\phi,t) = 0 \tag{I.5}$$

where $\rho(r,\theta,\phi,t) = f(r)A(\theta,\phi,t) = \frac{1}{r^2}\delta(r-r_n)A(\theta,\phi,t)$ and $A(\theta,\phi,t) = Y(\theta,\phi)k(t)$

$$\left[\frac{1}{r^2\sin\theta}\frac{\delta}{\delta\theta}\left(\sin\theta\frac{\delta}{\delta\theta}\right)_{r,\phi} + \frac{1}{r^2\sin^2\theta}\left(\frac{\delta^2}{\delta\phi^2}\right)_{r,\theta} - \frac{1}{v^2}\frac{\delta^2}{\delta t^2}\right]A(\theta,\phi,t) = 0 \tag{I.6}$$

where v is the linear velocity of the electron. The charge-density functions including the time-function factor are

$\ell = 0$

$$\rho(r,\theta,\phi,t) = \frac{e}{8\pi r^2}[\delta(r-r_n)]\left[Y_\ell^m(\theta,\phi) + Y_0^0(\theta,\phi)\right] \tag{I.7}$$

$\ell \neq 0$

$$\rho(r,\theta,\phi,t) = \frac{e}{4\pi r^2}[\delta(r-r_n)]\left[Y_0^0(\theta,\phi) + \mathrm{Re}\left\{Y_\ell^m(\theta,\phi)\left[1+e^{i\omega_n t}\right]\right\}\right] \tag{I.8}$$

where

$$\mathrm{Re}\left\{Y_\ell^m(\theta,\phi)\left[1+e^{i\omega_n t}\right]\right\} = \mathrm{Re}\left[Y_\ell^m(\theta,\phi)+Y_\ell^m(\theta,\phi)e^{i\omega_n t}\right] = P_\ell^m(\cos\theta)\cos m\phi + P_\ell^m(\cos\theta)\cos(m\phi+\omega_n t)$$

and $\omega_n = 0$ for $m = 0$. And, the Fourier transform of the charge density function which is derived in the Spacetime Fourier Transform of the Electron Function Section is a solution of the four-dimensional wave equation in frequency space (**k**, ω-space).

$$M(s,\Theta,\Phi,\omega) = 4\pi\frac{\sin(2s_n r_n)}{2s_n r_n}\quad 2\pi\sum_{\upsilon=1}^{\infty}\frac{(-1)^{\upsilon-1}(\pi\sin\Theta)^{2(\upsilon-1)}}{(\upsilon-1)!(\upsilon-1)!}\frac{\Gamma\left(\frac{1}{2}+\upsilon\right)}{\Gamma\left(\frac{1}{2}\right)}\frac{2\upsilon!}{(\pi\cos\Theta)^{2\upsilon+1}2^{\upsilon+1}}\frac{s^{-2\upsilon}}{(\upsilon-1)!} \tag{I.9}$$

$$2\pi\sum_{\upsilon=1}^{\infty}\frac{(-1)^{\upsilon-1}(\pi\sin\Phi)^{2(\upsilon-1)}}{(\upsilon-1)!(\upsilon-1)!}\frac{\Gamma\left(\frac{1}{2}+\upsilon\right)}{\Gamma\left(\frac{1}{2}\right)}\frac{2\upsilon!}{(\pi\cos\Phi)^{2\upsilon+1}2^{\upsilon+1}}\frac{s^{-2\upsilon}}{(\upsilon-1)!}\frac{1}{4\pi}[\delta(\omega-\omega_n)+\delta(\omega+\omega_n)]$$

The motion on the orbitsphere is angular; however, a radial component exists due to Special Relativistic effects. Consider the radial wave vector of the sinc function. When the radial projection of the velocity is c

$$\mathbf{s}_n\cdot\mathbf{v}_n = \mathbf{s}_n\cdot\mathbf{c} = \omega_n \tag{I.10}$$

the relativistically corrected wavelength is

$$r_n = \lambda_n \tag{I.11}$$

(i.e. the lab frame motion in the angular direction goes to zero as the velocity approaches the speed of light). Substitution of Eq. (I.11) into the sinc function results in the vanishing of the entire Fourier transform of the current-density function. Thus, spacetime harmonics of $\frac{\omega_n}{c} = k$ or $\frac{\omega_n}{c}\sqrt{\frac{\varepsilon}{\varepsilon_o}} = k$ for which the Fourier transform of the current-density function is nonzero do not exist. Radiation due to charge motion does not occur in any medium when this boundary condition is met.

Relationship Between the Theories of Bohr and Schrödinger with Respect to that of Mills

J. J. Balmer showed, in 1885, that the frequencies for some of the lines observed in the emission spectrum of atomic hydrogen could be expressed with a completely empirical relationship. This approach was later extended by J. R. Rydberg, who showed that all of the spectral lines of atomic hydrogen were given by the equation:

$$\bar{\nu} = R\left(\frac{1}{n_f^2}-\frac{1}{n_i^2}\right) \tag{I.12}$$

where $R = 109{,}677\ cm^{-1}$, $n_f = 1,2,3,\ldots$, $n_i = 2,3,4,\ldots$, and $n_i > n_f$. In 1911, Rutherford proposed a planetary model for the atom where the electrons revolved about the nucleus (which contained the protons) in various orbits. There was, however, a fundamental conflict with this

model and the prevailing classical physics. According to classical electromagnetic theory, an accelerated particle radiates energy (as electromagnetic waves). Thus, an electron in a Rutherford orbit, circulating at constant speed but with a continually changing direction of its velocity vector is being accelerated; thus, the electron should constantly lose energy by radiating and spiral into the nucleus.

An explanation was provided by Bohr in 1913, when he assumed that the energy levels were quantized and the electron was constrained to move in only one of a number of allowed states. Niels Bohr's theory for atomic hydrogen was based on an unprecedented postulate of stable circular orbits that do not radiate. Although no explanation was offered for the existence of stability for these orbits, the results gave energy levels in agreement with Rydberg's equation. Bohr's theory was a straightforward application of Newton's laws of motion and Coulomb's law of electric force. According to Bohr's model, the point particle electron was held to a circular orbit about the relatively massive point particle nucleus by the balance between the coulombic force of attraction between the proton and the electron and centrifugal force of the electron.

$$\frac{e^2}{4\pi\varepsilon_0 r^2} = \frac{m_e v^2}{r} \tag{I.13}$$

Bohr postulated the existence of stable orbits in defiance of classical physics (Maxwell's Equations), but he applied classical physics according to Eq. (I.13). Then Bohr realized that the energy formula Eq. (I.1) was given by postulating nonradiative states with angular momentum

$$L_z = m_e v r = n\hbar \qquad n = 1,2,3... \tag{I.14}$$

and by solving the energy equation classically. The Bohr radius is given by substituting the solution of Eq. (I.14) for v into Eq. (I.13).

$$r = \frac{4\pi\varepsilon_0 \hbar^2 n^2}{m_e e^2} = n^2 a_0 \qquad n = 1,2,3... \tag{I.15}$$

The total energy is the sum of the potential energy and the kinetic energy. In the present case of an inverse squared central field, the total energy (which is the negative of the binding energy) is one half the potential energy [2]. The potential energy, $\phi(\mathbf{r})$, is given by Poisson's Equation

$$\phi(\mathbf{r}) = -\int_{V'} \frac{\rho(\mathbf{r}')dv'}{4\pi\varepsilon_0|\mathbf{r}-\mathbf{r}'|} \tag{I.16}$$

For a point charge at a distance r from the nucleus the potential is

$$\phi(r) = -\frac{e^2}{4\pi\varepsilon_0 r} \tag{I.17}$$

Thus, the total energy is given by

$$E = -\frac{Z^2 e^2}{8\pi\varepsilon_o r} \tag{I.18}$$

Substitution of Eq. (I.15) into Eq.(I.18) with the replacement of the electron mass by the reduced electron mass gives Eq. (I.1).

Bohr's model was in agreement with the observed hydrogen spectrum, but it failed with the helium spectrum, and it could not account for chemical bonds in molecules. The prevailing wisdom was that the Bohr model failed because it was based on the application of Newtonian mechanics for discrete particles. And, its limited applicability was attributed to the unwarranted assumption that the energy levels are quantized.

In 1923, de Broglie suggested that the motion of an electron has a wave aspect— $\lambda = \frac{h}{p}$. This was confirmed by Davisson and Germer in 1927 by observing diffraction effects when electrons were reflected from metals. Schrödinger reasoned that if electrons have wave properties, there must be a wave equation that governs their motion. And, in 1926, he proposed the Schrödinger equation

$$H\Psi = E\Psi \tag{I.19}$$

where Ψ is the wave function, H is the wave operator, and E is the energy of the wave. The Schrödinger equation solutions are three dimensional in space and four dimensional in spacetime

$$\left[\nabla^2 - \frac{1}{v^2}\frac{\delta^2}{\delta t^2}\right]\Psi(r,\theta,\phi,t) = 0 \tag{I.20}$$

where $\Psi(r,\theta,\phi,t)$ according to quantum theory is the probability density function of the electron as described below. When the time harmonic function is eliminated [3],

$$-\frac{\hbar^2}{2\mu}\left[\frac{1}{r^2}\frac{\delta}{\delta r}\left(r^2\frac{\delta\Psi}{\delta r}\right) + \frac{1}{r^2\sin\theta}\frac{\delta}{\delta\theta}\left(\sin\theta\frac{\delta\Psi}{\delta\theta}\right)_{r,\phi} + \frac{1}{r^2\sin^2\theta}\left(\frac{\delta^2\Psi}{\delta\phi^2}\right)_{r,\theta}\right] + U(r)\Psi(r,\theta,\phi) = E\Psi(r,\theta,\phi) \tag{I.21}$$

In general, the Schrödinger equation has an infinite number of solutions. To arrive at the solution which represents the electron, a suitable boundary condition must be imposed. Schrödinger postulated a boundary condition: $\Psi \to 0$ as $r \to \infty$, which leads to a purely mathematical model of the electron. The general form of the solutions for $\psi(r,\theta,\phi)$ are

$$\psi(r,\theta,\phi) = \sum_{l,m} f_{lm}(r) Y_{lm}(\theta,\phi) \tag{I.22}$$

where the solutions for the angular part of Eq. (I.21), $Y_{lm}(\theta,\phi)$, are the spherical harmonics

$$Y_{lm}(\theta,\phi)=\sqrt{\frac{(2l+1)(l-m)!}{4\pi(l+m)!}}P_l^m(\cos\theta)e^{im\phi} \tag{I.23}$$

The angular part of Eq. (I.21) is the generalized Legendre equation which is derived from the Laplace equation by Jackson (Eq. (3.9) of Jackson [4]). For the case that the potential energy is a constant times the wavenumber of the electron, k (a constant times the inverse of the de Broglie wavelength of the electron--$k=\frac{2\pi}{\lambda}$; $\lambda=\frac{h}{p}$), the radial part of Eq. (I.21) is just the Bessel equation, Eq. (3.75) of Jackson [4] with $\upsilon=l+\frac{1}{2}$. (In the present case of an inverse squared central field, the magnitude of each of the binding energy and the kinetic energy is one half the potential energy [2], and the de Broglie wavelength requires that the kinetic energy, $\frac{p^2}{2m_e}$, is a constant times the wavenumber squared.)

Thus, the solutions for $f_{lm}(r)$ are

$$f_{lm}(r)=\frac{A_{lm}}{r^{1/2}}J_{l+1/2}(kr)+\frac{B_{lm}}{r^{1/2}}N_{l+1/2}(kr) \tag{I.24}$$

It is customary to define the spherical Bessel and Hankel functions, denoted by $j_l(x)$, $n_l(x)$, $h_l^{(1,2)}(x)$, as follows:

$$\begin{aligned} j_l(x)&=\left(\frac{\pi}{2x}\right)^{1/2}J_{l+1/2}(x)\\ n_l(x)&=\left(\frac{\pi}{2x}\right)^{1/2}N_{l+1/2}(x)\\ h_l^{(1,2)}(x)&=\left(\frac{\pi}{2x}\right)^{1/2}\left[J_{l+1/2}(x)\pm iN_{l+1/2}(x)\right] \end{aligned} \tag{I.25}$$

For $l=0$, the explicit forms are:

$$\begin{aligned} j_0(x)&=\frac{\sin x}{x}\\ n_0(x)&=-\frac{\cos x}{x}\\ h_0^{(1)}(x)&=\frac{e^{ix}}{ix} \end{aligned} \tag{I.26}$$

Eq. (I.21) has the general form

$$H\psi=E\psi \tag{I.27}$$

The energy is given by

$$\int_{-\infty}^{\infty}\psi H\psi\,dv=E\int_{-\infty}^{\infty}\psi^2 dv; \tag{I.28}$$

Typically, the solutions are normalized.

$$\int_{-\infty}^{\infty} \psi^2 dv = 1 \tag{I.29}$$

Thus,

$$\int_{-\infty}^{\infty} \psi H \psi dv = E \tag{I.30}$$

A physical interpretation of Eq. (I.30) is sought. Schrödinger interpreted $e\Psi^*(x)\Psi(x)$ as the charge-density or the amount of charge between x and $x+dx$ (Ψ^* is the complex conjugate of Ψ). Presumably, then, he pictured the electron to be spread over large regions of space. Three years after Schrödinger's interpretation, Max Born, who was working with scattering theory, found that this interpretation led to logical difficulties, and he replaced the Schrödinger interpretation with the probability of finding the electron between x and $x+dx$ as

$$\int \Psi(x)\Psi^*(x)dx \tag{I.31}$$

Born's interpretation is generally accepted. Nonetheless, interpretation of the wave function is a never-ending source of confusion and conflict. Many scientists have solved this problem by conveniently adopting the Schrödinger interpretation for some problems and the Born interpretation for others. This duality allows the electron to be everywhere at one time—yet have no volume. Alternatively, the electron can be viewed as a discrete particle that moves here and there (from $r=0$ to $r=\infty$), and $\Psi\Psi^*$ gives the time average of this motion. According to the Copenhagen interpretation, every observable exists in a state of superposition of possible states and observation or the potential for knowledge causes the wavefunction corresponding to the possibilities to collapse into a definite state. The postulate of quantum measurement asserts that the process of measuring an observable forces the state vector of the system into an eigenvector of that observable, and the value measured will be the eigenvalue of that eigenvector. Thus, Eq.(I.30) corresponds to collapsing the wave function, and E is the eigenvalue of the eigenvector.

However, an alternative interpretation of Eq. (I.30) and the corresponding solutions for ψ exist. In the case that ψ is a function given by Eqs. (I.24-I.26), Eq. (I.30) is equivalent to an inverse Fourier transform. The spacetime inverse Fourier transform in three dimensions in spherical coordinates is given [5,6] as follows:

$$M(s,\Theta,\Phi) = \int_0^{\infty}\int_0^{\pi}\int_0^{2\pi} \rho(r,\theta,\phi)\exp(-i2\pi sr[\cos\Theta\cos\theta + \sin\Theta\sin\theta\cos(\phi-\Phi)])r^2\sin\theta\, dr d\theta d\phi \tag{I.32}$$

With circular symmetry [5]

$$M(s,\Theta) = 2\pi \int_0^{\infty} \int_0^{\pi} \rho(r,\theta) J_o\left(2\pi sr \sin\Theta \sin\theta\right) \exp\left(-i2\pi sr \cos\Theta \cos\theta\right) r^2 \sin\theta \, dr d\theta \qquad (I.33)$$

With spherical symmetry [5],

$$M(s) = 4\pi \int_0^{\infty} \rho(r) \mathrm{sinc}(2sr) r^2 dr = 4\pi \int_0^{\infty} \rho(r) \frac{\sin sr}{sr} r^2 dr \qquad (I.34)$$

The Schrödinger equation (Eq. (I.21)) can be transformed into a sum comprising a part that depends only on the radius and a part that is a function of angle only. By separation of variables, and substitution of the eigenvalues corresponding to the angular part [7], the Schrödinger equation becomes the radial equation, $R(r)$, given by

$$-\frac{\hbar^2}{2\mu r^2} \frac{d}{dr}\left(r^2 \frac{dR}{dr}\right) + \left[\frac{\hbar^2 l(l+1)}{2\mu r^2} + U(r)\right] R(r) = ER(r) \qquad (I.35)$$

Consider the case that $l = 0$, that the potential energy is a constant times the wavenumber, and that the radial function is a spherical Bessel function as given by Eqs. (I.24-I.26). In this case, Eq. (I.35) is given by

$$4\pi \int_0^{\infty} \frac{\sin sr}{sr} \left[-\frac{\hbar^2}{2\mu r^2} \frac{d}{dr}\left(r^2 \frac{d}{dr}\right) + U(r)\right] \frac{\sin sr}{sr} r^2 dr = E 4\pi \int_0^{\infty} \frac{\sin sr}{sr} \frac{\sin sr}{sr} r^2 dr \qquad (I.36)$$

Eq. (I.34) is the Fourier transform integral in spherical coordinates with spherical symmetry. The left hand side (LHS) of Eq. (I.36) is equivalent to the LHS of Eq. (I.30) wherein ψ is given by Eq. (I.26). Then the LHS of Eq. (I.36) is the Fourier transform integral of $H\psi$ wherein the kernel is $r^2 \frac{\sin sr}{sr}$. The integral of Eq. (I.30) gives E which is a constant. The energy E of Eq. (I.27) is a constant such as b. Thus, $H\psi$ according to Eq. (I.27) is a constant times ψ.

$$H\psi = b\psi \qquad (I.37)$$

where b is a constant. Since is b is an <u>arbitrary</u> constant, consider the following case wherein b is the Rydberg formula:

$$b = -\frac{Z^2 e^2}{8\pi\varepsilon_0 n^2 a_H} \qquad (I.38)$$

Then the energy of Eq. (I.30) is that given by Eq. (I.1). But, the Schrödinger equation can be solved to give the energy corresponding to the radial function given by Eq. (I.4) of the Mills theory. The radial function used to calculate the energy is a delta function which corresponds to an inverse Fourier transform of the solution for ψ.

$$\Psi(s) = \delta(s - s_n) \qquad (I.39)$$

With a change of variable, Eq. (I.39) becomes Eq.(I.4).

Eq. (I.36) can be expressed as follows

$$4\pi \int_0^{\infty} \frac{\sin sr}{sr} \left[-\frac{\hbar^2}{2\mu r^2} \frac{d}{dr}\left(r^2 \frac{d}{dr}\right) + U(r)\right] \frac{\sin s_n r}{s_n r} r^2 dr = E 4\pi \int_0^{\infty} \frac{\sin sr}{sr} \frac{\sin s_n r}{s_n r} r^2 dr \qquad (I.40)$$

It follows from Eq. (I.34) that the right side integral is the Fourier transform of a radial Dirac delta function.

$$4\pi E\int_0^\infty \frac{\sin s_n r}{s_n r}\frac{\sin sr}{sr}r^2 dr = E\frac{\delta(s-s_n)}{4\pi s_n^2} \tag{I.41}$$

Substitution of Eq. (I.37) into Eq. (I.40) gives

$$4\pi b\int_0^\infty \frac{\sin s_n r}{s_n r}\frac{\sin sr}{sr}r^2 dr = b\frac{\delta(s-s_n)}{4\pi s_n^2} \tag{I.42}$$

Substitution of Eq. (I.41) and Eq. (I.42) into Eq. (I.40) gives

$$b\delta(s-s_n) = E\delta(s-s_n) \tag{I.43}$$

Consider the case where b is given by

$$b = -\frac{\hbar^2}{2m_e n\frac{a_0}{Z^2}s} = -\frac{\frac{1}{n}Z^2e^2}{8\pi\varepsilon_0 s} \tag{I.44}$$

and s_n is given by

$$s_n = na_H \tag{I.45}$$

where $r_n = na_H$. According to the duality and change of scale properties of Fourier transforms [8], ***the energy equation of the Mills theory and that of quantum mechanics are identical***, the energy of a radial Dirac delta function of radius equal to an integer multiple of the radius of the hydrogen atom. The total energy of the electron is given by Poisson's Equation (Eq. (I.17)) and the relationship that the total energy is one half the potential energy in the case of an inverse squared central force [2].

$$E = \int_{-\infty}^{\infty} E\delta(r-r_n)dr = -\int_{-\infty}^{\infty}\delta(r-r_n)\frac{\frac{1}{n}Z^2e^2}{8\pi\varepsilon_0 r}dr = -\frac{\frac{1}{n}Z^2e^2}{8\pi\varepsilon_0 r_n} = -\frac{Z^2e^2}{8\pi\varepsilon_o n^2 a_H} \tag{I.46}$$

As was the case with the Bohr theory, quantum mechanics which is based on the Schrödinger equation and modifications of the Schrödinger equation has encountered several obstacles that have proved insurmountable. For examples:

1.) The Schrödinger equation failed to predict the electron spin, and it provides no rational basis for the phenomenon of spin, the Pauli exclusion principle, or Hund's rules. Instantaneous exchange of information between particles is required, which violates Special Relativity. According to this model, the electron must spin in one dimension and give rise to a Bohr magneton; yet, classically the energy of a magnetic moment is $\frac{\mu^2}{r^3}$ which in the present case is infinity (by substitution of $r = 0$ for the model that the electron is a point particle), not the required mc^2. This interpretation is in violation of Special Relativity [9]. A modification of the Schrödinger

equation was developed by Dirac to explain spin which relies on the unfounded notions of negative energy states of the vacuum, virtual particles, and gamma factors.

2.) Quantum mechanics assumes that atomic-size particles obey different physical laws than macroscopic objects. For example, according to Maxwell's equations the electron described by a Schrödinger one-electron wave function would radiate. Quantum Electrodynamics (QED) based on vacuum energy fluctuations (zero point fluctuation (ZPF) energy) was invented to address some of these issues, but rigorous solutions of QED result in no solutions other than infinities. (Radiated photons make an infinite contribution to the perturbation series).

The failure of quantum mechanics is attributed to the unwarranted assumption that first principles such as Maxwell's Equations do not apply to the electron and the incorrect notion that the electron is described by a probability distribution function of a point particle. The success of the Schrödinger equation can be understood in terms of the nature of the solutions to the wave equation. In general, the solutions are separable, provide three quantum numbers, and yield eigenvalues. By adjusting the arbitrary constants of the separable solutions, the desired eigenvalues can be obtained.

The fourth quantum number arises naturally in the Mills theory as derived in The Electron g Factor Section. The Stern-Gerlach experiment implies a magnetic moment of one Bohr magneton and an associated angular momentum quantum number of 1/2. Historically, this quantum number is called the spin quantum number, s ($s = \frac{1}{2}; m_s = \pm\frac{1}{2}$). Conservation of angular momentum of the orbitsphere permits a discrete change of its "kinetic angular momentum" ($\mathbf{r} \times m\mathbf{v}$) by the field of $\frac{\hbar}{2}$, and concomitantly the "potential angular momentum" ($\mathbf{r} \times e\mathbf{A}$) must change by $-\frac{\hbar}{2}$. The flux change, ϕ, of the orbitsphere for $r < r_n$ is determined as follows:

$$\Delta\mathbf{L} = \frac{\hbar}{2} - \mathbf{r} \times e\mathbf{A} \tag{I.47}$$

$$= \frac{\hbar}{2} - \frac{e2\pi rA}{2\pi} \tag{I.48}$$

$$= \frac{\hbar}{2} - \frac{e\phi}{2\pi} \tag{I.49}$$

In order that the change of angular momentum, $\Delta\mathbf{L}$, equals zero, ϕ must be $\Phi_0 = \frac{h}{2e}$, the magnetic flux quantum. Thus, to conserve angular

momentum in the presence of an applied magnetic field, the orbitsphere magnetic moment can be parallel or antiparallel to an applied field as observed with the Stern-Gerlach experiment, and the flip between orientations (a rotation of $\frac{\pi}{2}$) is accompanied by the "capture" of the magnetic flux quantum by the orbitsphere. And, the total energy of the flip transition is the sum of Eq. (1.148), the energy of a fluxon treading the orbitsphere and Eq. (1.136), the energy of reorientation of the magnetic moment.

$$\Delta E_{mag}^{spin} = 2\left(\mu_B \mathbf{B} + \frac{\alpha}{2\pi}\mu_B \mathbf{B}\right) \quad \text{(I.50)}$$

$$\Delta E_{mag}^{spin} = 2\left(1 + \frac{\alpha}{2\pi}\right)\mu_B \mathbf{B} \quad \text{(I.51)}$$

$$\Delta E_{mag}^{spin} = 2g\mu_B \mathbf{B} \quad \text{(I.52)}$$

The spin-flip transition can be considered as involving a magnetic moment of g times that of a Bohr magneton. The factor g is redesignated the fluxon g factor as opposed to the anomalous g factor and its value is 1.00116. The experimental value is 1.00116.

The orbitsphere is a resonator cavity which traps photons of discrete frequencies. The radius of an orbitsphere increases with the absorption of electromagnetic energy. The solutions to Maxwell's equations for modes that can be excited in the orbitsphere resonator cavity give rise to four quantum numbers, and the energies of the modes are the experimentally known hydrogen spectrum.

The subscript n is used in Eq. (I.46); the quantization condition appears in the Excited States of the One Electron Atom (Quantization) Section. Quantization arises as "allowed" solutions of the wave equation corresponding to a resonance between the electron and a photon.

More explicitly, it is well known that resonator cavities can trap electromagnetic radiation of discrete resonant frequencies. The orbitsphere is a resonator cavity which traps photons of discrete frequencies. Thus, photon absorption occurs as an excitation of a resonator mode. The "trapped photon" is a "standing electromagnetic wave" which actually is a circulating wave that propagates along each great circle current loop of the orbitsphere. The time-function factor, $k(t)$, for the "standing wave" is identical to the time-function factor of the orbitsphere in order to satisfy the boundary (phase) condition at the orbitsphere surface. Thus, the angular frequency of the "trapped photon" has to be identical to the angular frequency of the electron

orbitsphere, ω_n. Furthermore, the phase condition requires that the angular functions of the "trapped photon" have to be identical to the spherical harmonic angular functions of the electron orbitsphere. Combining $k(t)$ with the ϕ-function factor of the spherical harmonic gives $e^{i(m\phi-\omega_n t)}$ for both the electron and the "trapped photon" function. The photon is "glued" to the inner orbitsphere surface and the outer nuclear surface as photon source charge-density with a radial electric field.

From the application of the nonradiative boundary condition, the instability of excited states as well as the stability of the "ground" state arise naturally in the Mills theory as derived in Stability of Atoms and Hydrinos Section. In addition to the above known states of hydrogen (Eq. (I.1), the theory predicts the existence of a previously unknown form of matter: hydrogen atoms and molecules having electrons of lower energy than the conventional "ground" state, called ***hydrinos*** and ***dihydrinos***, respectively, where each energy level corresponds to a fractional quantum number.

The central field of the proton corresponds to integer one charge. Excited states comprise an electron with a trapped photon. In all energy states of hydrogen, the photon has an electric field which superposes with the field of the proton. In the $n=1$ state, the sum is one, and the sum is zero in the ionized state. In an excited state, the sum is a fraction of one (i.e. between zero and one). Derivations from first principles given by Mills demonstrate that each "allowed" fraction corresponding to an excited state is $\frac{1}{\text{integer}}$. The relationship between the electric field equation and the "trapped photon" source charge-density function is given by Maxwell's equation in two dimensions.

$$\mathbf{n}\cdot\left(\mathbf{E}_1-\mathbf{E}_2\right)=\frac{\sigma}{\varepsilon_0} \tag{I.53}$$

where $\mathbf{n}$ is the radial normal unit vector, $\mathbf{E}_1=0$ ($\mathbf{E}_1$ is the electric field outside of the orbitsphere), $\mathbf{E}_2$ is given by the total electric field at $r_n=na_H$, and σ is the surface charge-density. The electric field of an excited state is fractional; therefore, the source charge function is fractional. It is well known that fractional charge is not "allowed". The reason is that fractional charge typically corresponds to a radiative current density function. The excited states of the hydrogen atom are examples. They are radiative; consequently, they are not stable. Thus, an excited electron decays to the first nonradiative state corresponding to an integer field, $n=1$. Equally valid from first principles are electronic states where the sum of the photon field and the central field are an integer. These states are nonradiative. A catalyst can effect a transition

between these states.

Instability of Excited States

For the excited (integer quantum) energy states of the hydrogen atom, σ_{photon}, the two dimensional surface charge due to the "trapped photons" at the orbitsphere, is given by Eqs. (2.6) and (2.11).

$$\sigma_{photon} = \frac{e}{4\pi(r_n)^2}\left[Y_0^0(\theta,\phi) - \frac{1}{n}\left[Y_0^0(\theta,\phi) + \mathrm{Re}\left\{Y_\ell^m(\theta,\phi)\left[1+e^{i\omega_n t}\right]\right\}\right]\right]\delta(r-r_n) \quad n = 2,3,4,..., \text{(I.54)}$$

Whereas, $\sigma_{electron}$, the two dimensional surface charge of the electron orbitsphere is

$$\sigma_{electron} = \frac{-e}{4\pi(r_n)^2}\left[Y_0^0(\theta,\phi) + \mathrm{Re}\left\{Y_\ell^m(\theta,\phi)\left[1+e^{i\omega_n t}\right]\right\}\right]\delta(r-r_n) \quad \text{(I.55)}$$

The superposition of σ_{photon} (Eq. (I.54)) and $\sigma_{electron}$ (Eq. (I.55)), where the spherical harmonic functions satisfy the conditions given in the Angular Function Section, is equivalent to the sum of a radial electric dipole represented by a doublet function and a radial electric monopole represented by a delta function.

$$\sigma_{photon} + \sigma_{electron} = \frac{e}{4\pi(r_n)^2}\left[Y_0^0(\theta,\phi)\dot{\delta}(r-r_n) - \frac{1}{n}Y_0^0(\theta,\phi)\delta(r-r_n) - \left(1+\frac{1}{n}\right)\left[\mathrm{Re}\left\{Y_\ell^m(\theta,\phi)\left[1+e^{i\omega_n t}\right]\right\}\right]\delta(r-r_n)\right]$$
$$n = 2,3,4,..., \quad \text{(I.56)}$$

where

$$\left[+\delta(r-r_n) - \delta(r-r_n)\right] = \dot{\delta}(r-r_n) \quad \text{(I.57)}$$

The spacetime Fourier transform of Eq. (I.56), the superposition of σ_{photon} (Eq. (I.54)) and $\sigma_{electron}$ (Eq. (I.55)) is

$$M(s,\Theta,\Phi,\omega) = 4\pi s_n \frac{\cos(2s_n r_n)}{2s_n r_n} \quad 2\pi\sum_{\upsilon=1}^{\infty}\frac{(-1)^{\upsilon-1}(\pi\sin\Theta)^{2(\upsilon-1)}}{(\upsilon-1)!(\upsilon-1)!}\frac{\Gamma\left(\frac{1}{2}\right)\Gamma\left(\upsilon+\frac{1}{2}\right)}{(\pi\cos\Theta)^{2\upsilon+1}2^{\upsilon+1}}\frac{2\upsilon!}{(\upsilon-1)!}s^{-2\upsilon}$$

$$2\pi\sum_{\upsilon=1}^{\infty}\frac{(-1)^{\upsilon-1}(\pi\sin\Phi)^{2(\upsilon-1)}}{(\upsilon-1)!(\upsilon-1)!}\frac{\Gamma\left(\frac{1}{2}\right)\Gamma\left(\upsilon+\frac{1}{2}\right)}{(\pi\cos\Phi)^{2\upsilon+1}2^{\upsilon+1}}\frac{2\upsilon!}{(\upsilon-1)!}s^{-2\upsilon}\frac{1}{4\pi}\left[\delta(\omega-\omega_n)+\delta(\omega+\omega_n)\right] \quad \text{(I.58)}$$

Consider the radial wave vector of the cosine function of Eq. (I.58). When the radial projection of the velocity is c

$$\mathbf{s}_n \cdot \mathbf{v}_n = \mathbf{s}_n \cdot \mathbf{c} = \omega_n \quad \text{(I.59)}$$

the relativistically corrected wavelength is

$$r_n = \lambda_n \quad \text{(I.60)}$$

Substitution of Eq. (I.60) into the cosine function does not result in the vanishing of the Fourier Transform of the current-density function. Thus, spacetime harmonics of $\frac{\omega_n}{c} = k$ or $\frac{\omega_n}{c}\sqrt{\frac{\varepsilon}{\varepsilon_o}} = k$ do exist for which the

Fourier Transform of the current-density function is nonzero. An excited state is metastable because it is the sum of nonradiative (stable) and radiative (unstable) components and de-excites with a transition probability given by the ratio of the power to the energy of the transition [10].

Stability of "Ground" and Hydrino States

For the below "ground" (fractional quantum) energy states of the hydrogen atom, σ_{photon}, the two dimensional surface charge due to the "trapped photon" at the electron orbitsphere, is given by Eqs. (5.13) and (2.11).

$$\sigma_{photon} = \frac{e}{4\pi(r_n)^2}\left[Y_0^0(\theta,\phi) - \frac{1}{n}\left[Y_0^0(\theta,\phi) + \mathrm{Re}\left\{Y_\ell^m(\theta,\phi)\left[1+e^{i\omega_n t}\right]\right\}\right]\right]\delta(r-r_n) \quad n = 1,\frac{1}{2},\frac{1}{3},\frac{1}{4},..., \tag{I.61}$$

And, $\sigma_{electron}$, the two dimensional surface charge of the electron orbitsphere is

$$\sigma_{electron} = \frac{-e}{4\pi(r_n)^2}\left[Y_0^0(\theta,\phi) + \mathrm{Re}\left\{Y_\ell^m(\theta,\phi)\left[1+e^{i\omega_n t}\right]\right\}\right]\delta(r-r_n) \tag{I.62}$$

The superposition of σ_{photon} (Eq. (I.61)) and $\sigma_{electron}$, (Eq. (I.62)) where the spherical harmonic functions satisfy the conditions given in the Angular Function Section is a radial electric monopole represented by a delta function.

$$\sigma_{photon} + \sigma_{electron} = \frac{-e}{4\pi(r_n)^2}\left[\left(1-\frac{1}{n}\right)Y_0^0(\theta,\phi) + \left(1+\frac{1}{n}\right)\mathrm{Re}\,Y_\ell^m(\theta,\phi)\left[1+e^{i\omega_n t}\right]\right]\delta(r-r_n) \quad n = 1,\frac{1}{2},\frac{1}{3},\frac{1}{4},..., \tag{I.63}$$

As given in the Spacetime Fourier Transform of the Electron Function Section, the radial delta function does not possess spacetime Fourier components synchronous with waves traveling at the speed of light (Eqs. (I.9-I.11)). Thus, the below "ground" (fractional quantum) energy states of the hydrogen atom are stable. The "ground" ($n = 1$ quantum) energy state is just the first of the nonradiative states of the hydrogen atom; thus, it is the state to which excited states decay.

Catalytic Lower-Energy Hydrogen Electronic Transitions

Comparing transitions between below "ground" (fractional quantum) energy states as opposed to transitions between excited (integer quantum) energy states, it can be appreciated that the former are not effected by photons; whereas, the latter are. Transitions are symmetric with respect to time. Current density functions which give rise to photons according to the boundary condition are created by photons in the reverse process. Excited (integer quantum) energy states correspond to this case. And, current density functions which do not give rise to photons according to the nonradiative boundary condition

are not created by photons in the reverse process. Below "ground" (fractional quantum) energy states correspond to this case. But, atomic collisions and nonradiative energy transfer can cause a stable state to undergo a transition to the next stable state. The transition between two stable nonradiative states effected by a collision with an resonant energy sink is analogous to the reaction of two atoms to form a diatomic molecule which requires a third-body collision to remove the bond energy [11].

Energy Hole Concept

The nonradiative boundary condition and the relationship between the electron and the photon give the "allowed" hydrogen energy states which are quantized as a function of the parameter n. Each value of n corresponds to an allowed transition effected by a resonant photon which excites the electronic transition. In addition to the traditional integer values (1, 2, 3,...,) of n, values of fractions are allowed which correspond to transitions with an increase in the central field (charge) and decrease in the size of the hydrogen atom. This occurs, for example, when the electron couples to another electronic transition or electron transfer reaction which can absorb energy, an energy sink. This transition reaction of the electron of hydrogen to a lower energy state occurs by the ***absorption of an energy hole by the hydrogen atom.*** The absorption of an energy hole destroys the balance between the centrifugal force and the resulting increased central electric force. Consequently, the electron undergoes a transition to a lower energy nonradiative state. Thus, the corresponding reaction from an initial energy state to a lower energy state effected by an energy hole is called a ***transition reaction***.

From energy conservation, the energy hole of a hydrogen atom which excites resonator modes of radial dimensions $\frac{a_H}{m+1}$ is

$$m \times 27.2\ eV \qquad \text{(I.64)}$$

where $m = 1,2,3,4,...$

After resonant absorption of the energy hole, the radius of the orbitsphere, a_H, decreases to $\frac{a_H}{m+1}$ and after p cycles of transition reaction, the radius is $\frac{a_H}{mp+1}$. In other words, the radial ground state field can be considered as the superposition of Fourier components. The removal of negative Fourier components of energy $m \times 27.2\ eV$, where m is an integer increases the positive electric field inside the spherical shell by m times the charge of a proton. The resultant electric field is a time-harmonic solution of Laplace's Equations in spherical coordinates. In

this case, the radius at which force balance and nonradiation are achieved is $\frac{a_H}{m+1}$ where m is an integer. In decaying to this radius from the "ground" state, a total energy of $[(m+1)^2-1^2]X13.6\ eV$ is released. The transition reaction is hereafter referred to as the **BlackLight Process.** The source of energy holes may not be consumed in the transition reaction; therefore it is a hydrogen catalyst.

An efficient catalytic system that hinges on the coupling of three resonator cavities involves potassium. For example, the second ionization energy of potassium is $31.63\ eV$. This energy hole is obviously too high for resonant absorption. However, K^+ releases $4.34\ eV$ when it is reduced to K. The combination of K^+ to K^{2+} and K^+ to K, then, has a net energy change of $27.28\ eV$.

$$27.28\ eV + K^+ + K^+ + H\left[\frac{a_H}{p}\right] \rightarrow K + K^{2+} + H\left[\frac{a_H}{(p+1)}\right] + [(p+1)^2 - p^2]X13.6\ eV \qquad (I.65)$$

$$K + K^{2+} \rightarrow K^+ + K^+ + 27.28\ eV \qquad (I.66)$$

And, the overall reaction is

$$H\left[\frac{a_H}{p}\right] \rightarrow H\left[\frac{a_H}{(p+1)}\right] + [(p+1)^2 - p^2]X13.6\ eV \qquad (I.67)$$

Note that the energy given off as the atom undergoes a transition to a lower energy level is much greater than the energy lost to the energy hole. Also, the energy released is large compared to conventional chemical reactions.

Disproportionation of Energy States

Lower-energy hydrogen atoms, ***hydrinos***, can act as a source of energy holes that can cause transition reactions because the excitation and/or ionization energies are $m\,X\,27.2\ eV$ (Eq. (I.64)). The general equation for the absorption of an energy hole of $27.21\ eV$, $m=1$ in Eq. (I.64), during the transition cascade for the pth cycle of the hydrogen-type atom, $H\left[\frac{a_H}{p}\right]$, with the hydrogen-type atom, $H\left[\frac{a_H}{m'}\right]$, that is ionized as the source of energy holes that causes the transition reaction is represented by

$$27.21\ eV + H\left[\frac{a_H}{m'}\right] + H\left[\frac{a_H}{p}\right] \rightarrow H^+ + e^- + H\left[\frac{a_H}{(p+1)}\right] + [(p+1)^2 - p^2]X13.6\ eV - \left(m'^2 - 2\right)X13.6\ eV$$

(I.68)

$$H^+ + e^- \rightarrow H\left(\frac{a_H}{1}\right) + 13.6\ eV \tag{I.69}$$

And, the overall reaction is

$$H\left(\frac{a_H}{m'}\right) + H\left(\frac{a_H}{p}\right) \rightarrow H\left(\frac{a_H}{1}\right) + H\left(\frac{a_H}{(p+1)}\right) + [2p + 1 - m'^2]X13.6\ eV + 13.6\ eV \tag{I.70}$$

For example, the equation for the absorption of an energy hole of $27.21\ eV$, $m = 1$ in Eq. (I.64), during the transition cascade for the third cycle of the hydrogen-type atom, $H\left(\frac{a_H}{3}\right)$, with the hydrogen-type atom, $H\left(\frac{a_H}{2}\right)$, that is ionized as the source of energy holes that causes the transition reaction is represented by

$$27.21\ eV + H\left(\frac{a_H}{2}\right) + H\left(\frac{a_H}{3}\right) \rightarrow H^+ + e^- + H\left(\frac{a_H}{4}\right) + [4^2 - 3^2]X13.6\ eV - 27.21\ eV \tag{I.71}$$

$$H^+ + e^- \rightarrow H\left(\frac{a_H}{1}\right) + 13.6\ eV \tag{I.72}$$

And, the overall reaction is

$$H\left(\frac{a_H}{2}\right) + H\left(\frac{a_H}{3}\right) \rightarrow H\left(\frac{a_H}{1}\right) + H\left(\frac{a_H}{4}\right) + [4^2 - 3^2 - 4]X13.6\ eV + 13.6eV \tag{I.73}$$

Disproportionation may be the predominant mechanism of hydrogen electronic transitions to lower energy levels of interstellar and solar hydrogen and hydrinos. Hydrogen transitions to electronic energy levels below the "ground" state corresponding to fractional quantum numbers match the spectral lines of the extreme ultraviolet background of interstellar space and from the sun. This assignment given in the Spectral Data of Hydrinos from the Dark Interstellar Medium and Spectral Data of Hydrinos, Dihydrinos, and Hydrino Hydride Ions from the Sun Section resolves the paradox of the identity of dark matter, accounts for many celestial observations such as: diffuse Hα emission is ubiquitous throughout the Galaxy whereby widespread sources of flux shortward of $912\ Å$ are required [12], and resolves many solar problems. The energy of the emission line for the transition given by Eqs. (I.71-

I.73) whereby $H\left(\frac{a_H}{2}\right)$ is ionized as the source of the energy hole of 27.2 eV, $m=1$ in Eq. (I.64), that causes transition reaction is 40.8 eV (See Table 1 of the Foreword Section).

$$H\left(\frac{a_H}{3}\right) + H\left(\frac{a_H}{2}\right) \rightarrow H\left(\frac{a_H}{4}\right) \tag{I.74}$$

In summary, the mathematics of the theories of Bohr, Schrödinger, and presently Mills converge to Eq. (I.1) as the principal energy levels of the hydrogen atom.

$$E_n = -\frac{e^2}{n^2 8\pi\varepsilon_o a_H} = -\frac{13.598\ eV}{n^2} \tag{I.75a}$$

$$n = 1,2,3,... \tag{I.75b}$$

where a_H is the Bohr radius for the hydrogen atom (52.947 pm), e is the magnitude of the charge of the electron, and ε_o is the vacuum permittivity. However, the physics is quite different. Only the Mills theory is derived from first principles and holds over a scale of spacetime of 45 orders of magnitude-it correctly predicts the nature of the universe from the scale of the quarks to that of the cosmos. And, only the Mills theory predicts fractions as "allowed" states. Explicitly, Mills theory gives Eq. (I.75a) as the energy-level equation for atomic hydrogen, but the restriction on "n", Eq. (I.75b), should be replaced by Eq. (I.75c).

$$n = 1,2,3,...,\ and,\ n = \frac{1}{2},\frac{1}{3},\frac{1}{4},... \tag{I.75c}$$

A number of experimental observations lead to the conclusion that atomic hydrogen can exist in fractional quantum states that are at lower energies than the traditional "ground" ($n=1$) state. The corresponding process, the catalytic release of thermal energy as electrons are induced undergo transitions to lower energy levels corresponding to fractional quantum numbers, represents a virtually limitless source of clean, inexpensive energy.

References

1. Haus, H. A., "On the radiation from point charges", American Journal of Physics, 54, (1986), pp. 1126-1129.
2. Fowles, G. R., Analytical Mechanics, Third Edition, Holt, Rinehart, and Winston, New York, (1977), pp. 154-156.
3. McQuarrie, D. A., Quantum Chemistry, University Science Books, Mill Valley, CA, (1983), pp. 78-79.
4. Jackson, J. D., Classical Electrodynamics, Second Edition, John Wiley &

Sons, New York, (1962), pp. 84-108.
5. Bracewell, R. N., The Fourier Transform and Its Applications, McGraw-Hill Book Company, New York, (1978), pp. 252-253.
6. Siebert, W. McC., Circuits, Signals, and Systems, The MIT Press, Cambridge, Massachusetts, (1986), p. 415.
7. McQuarrie, D. A., Quantum Chemistry, University Science Books, Mill Valley, CA, (1983), pp. 221-224.
8. Siebert, W. McC., Circuits, Signals, and Systems, The MIT Press, Cambridge, Massachusetts, (1986), p. 416.
9. Pais, A., "George Uhlenbeck and the discovery of electron spin", Physics Today, 42, Dec., (1989), pp. 34-40.
10. Jackson, J. D., Classical Electrodynamics, Second Edition, John Wiley & Sons, New York, (1962), pp. 758-763.
11. N. V. Sidgwick, The Chemical Elements and Their Compounds, Volume I, Oxford, Clarendon Press, (1950), p.17.
12. Labov, S., Bowyer, S., "Spectral observations of the extreme ultraviolet background", The Astrophysical Journal, 371, (1991), pp. 810-819.

A NEW ATOMIC THEORY DERIVED FROM FIRST PRINCIPLES

To overcome the limitations of quantum mechanics, physical laws which are exact on all scales are sought. Rather than engendering the electron with a wave nature as suggested by the Davisson-Germer experiment and fabricating a set of associated postulates and mathematical rules for wave operators, a new theory is derived from first principles.

The novel theory unifies Maxwell's Equations, Newton's Laws, and General and Special Relativity. Theoretical predictions conform with experimental observations. The closed form calculations of a broad spectrum of fundamental phenomena contain fundamental constants only. Equations of the one electron atom are derived which give four quantum numbers, the spin/nuclear hyperfine structure, the Rydberg constant, the stability of atoms, the ionization energies, the equation of the photon, the equation of the electron in free space, the results of the Stern-Gerlach experiment, the electron g factor, the spin angular momentum energies, the excited states, the results of the Davisson-Germer experiment, the parameters of pair production, and the hyperfine structure interval of positronium. Ionization energies of two and three electron atoms are given as well as the bond energies, vibrational energies, rotational energies, and bond distances of hydrogen-type molecules and molecular ions.

From the closed form solution of the helium atom, the predicted electron scattering intensity is derived. The closed form scattering equation matches the experimental data; whereas, calculations based on the Born model of the atom utterly fail at small scattering angles. The implications for the invalidity of the Schrödinger and Born model of the atom and the dependent Heisenberg Uncertainty Principle are discussed. The theory of collective phenomena including statistical mechanics, superconductivity, Quantum Hall effects, and the Aharonov-Bohm effect is given. Atomic equations of gravitation are derived which provide the basis of the atomic, thermodynamic, and cosmological arrows of time, and the equation of the expansion of the universe. The gravitational equations with the equivalence of the particle production energies permit the equivalence of mass/energy and the spacetime metric from which the gravitational constant and the masses of the leptons, the quarks, and nucleons are derived. The basis of the antigravitational force is presented with supporting experimental evidence. The magnetic moments of the nucleons are derived. The beta decay energy of the neutron, and the binding energy of deuterium are calculated. The theory of alpha decay is derived.

In addition to the above known phenomena and characteristics of

fundamental particles and forces, the theory predicts the existence of a previously unknown form of matter: hydrogen atoms and molecules having electrons of lower energy than the conventional "ground" state called ***hydrinos*** and ***dihydrinos***, respectively, where each energy level corresponds to a fractional quantum number. The existence of hydrinos explains the spectral observations of the extreme ultraviolet background emission from interstellar space, which characterizes dark matter, and it provides an explanation of the solar neutrino paradox. The experimental confirmation of the existence of fractional quantum energy levels of hydrogen atoms and molecules is presented. The data shows the process of hydrino production to be an exothermic reaction that represents a limitless clean energy source.
The principles are as follows:

Foundations:

- Conservation of mass-energy;
- Conservation of linear and angular momentum;
- Maxwell's Equations;
- Newton's Laws;
- Special Relativity.

Next, the condition that a bound electron cannot radiate energy is imposed. The mathematical formulation for zero radiation is that the function that describes the motion of the electron must not possess spacetime Fourier components that are synchronous with waves traveling at the speed of light. The permissible solutions of the electron function are derived as a boundary value problem with the application of the nonradiative boundary condition.

Solution to the Electron Functions

From these laws and the non-radiative condition the following are a summary of some of the salient features of the theory derived in subsequent sections:

- Bound electrons are described by a charge-density (mass-density) function which is the product of a radial delta function ($f(r) = \delta(r - r_n)$), two angular functions (spherical harmonic functions), and a time harmonic function. Thus, an electron is a spinning, two-dimensional spherical surface, called an electron

orbitsphere, that can exist in a bound state at only specified distances from the nucleus. More explicitly, the orbitsphere comprises a two dimensional spherical shell of moving charge. The corresponding current pattern of the orbitsphere comprises an infinite series of correlated orthogonal great circle current loops. The current pattern (shown in Figure 1.4) is generated over the surface by two orthogonal sets of an infinite series of nested rotations of two orthogonal great circle current loops where the coordinate axes rotate with the two orthogonal great circles. Each infinitesimal rotation of the infinite series is about the new x-axis and new y-axis which results from the preceding such rotation. For each of the two sets of nested rotations, the angular sum of the rotations about each rotating x-axis and y-axis totals $\sqrt{2}\pi$ radians. The current pattern gives rise to the phenomenon corresponding to the spin quantum number.

- The total function that describes the spinning motion of each electron orbitsphere is composed of two functions. One function, the spin function, is spatially uniform over the orbitsphere, spins with a quantized angular velocity, and gives rise to spin angular momentum. The other function, the modulation function, can be spatially uniform—in which case there is no orbital angular momentum and the magnetic moment of the electron orbitsphere is one Bohr magneton—or not spatially uniform—in which case there is orbital angular momentum. The modulation function also rotates with a quantized angular velocity. Numerical values for the angular velocity, radii of allowed orbitspheres, energies, and associated quantities are calculated.

- Orbitsphere radii are calculated by setting the centripetal force equal to the electric and magnetic forces.

- The orbitsphere is a resonator cavity which traps photons of discrete frequencies. The radius of an orbitsphere increases with the absorption of electromagnetic energy. The solutions to Maxwell's equations for modes that can be excited in the orbitsphere resonator cavity give rise to four quantum numbers, and the energies of the modes are the experimentally known hydrogen spectrum. The spectrum of helium is the solution of Maxwell's equations for the energies of modes of this resonator cavity with a contribution from electron-electron spin and orbital interactions.

- Excited states are unstable because the charge-density function of the electron plus photon have a radial doublet function component which corresponds to an electric dipole. The doublet possesses spacetime Fourier components synchronous with waves traveling at the speed of light; thus it is radiative. The charge-density function of the electron plus photon for the $n = 1$ principal quantum state of the hydrogen atom as well as for each of the $n = \frac{1}{\text{integer}}$ states mathematically is purely a radial delta function. The delta function does not possess spacetime Fourier components synchronous with waves traveling at the speed of light; thus, each is nonradiative.

- The spectroscopic linewidth arises from the classical rise-time band-width relationship, and the Lamb Shift is due to conservation of energy and linear momentum and arises from the radiation reaction force between the electron and the photon.

- The photon is an orbitsphere with electric and magnetic field lines along orthogonal great circles.

- Upon ionization, the orbitsphere radius goes to infinity and the electron becomes a plane wave (consistent with double-slit experiments) with the de Broglie wave length, $\lambda = h / p$.

- The energy of atoms is stored in their electric and magnetic fields. Chemical bonding occurs when the total energy of the participant atoms can be lowered with the formation of two dimensional equipotential energy surfaces (molecular orbitals) where the motion is along geodesics, and a general form of the nonradiative boundary condition is met. Zero order vibration occurs because it gives rise to a nonradiative lower energy state.

- Certain atoms and ions serve as catalysts to release energy from hydrogen to produce an increased binding energy hydrogen atom having a binding energy of $\frac{13.6\ eV}{\left(1 - \frac{1}{p}\right)^2}$ where p is an integer greater than 1, designated as $H\left[\frac{a_H}{p}\right]$ where a_H is the radius of the hydrogen atom. Increased binding energy hydrogen atoms called

hydrinos are predicted to form by reacting an ordinary hydrogen atom with a catalyst having a net enthalpy of reaction of about the potential energy of hydrogen in its first nonradiative state, $m\ 27.2\ eV$, where m is an integer. This catalysis releases energy from the hydrogen atom with a commensurate decrease in size of the hydrogen atom, $r_n = n a_H$. For example, the catalysis of $H(n=1)$ to $H(n=1/2)$ releases $40.8\ eV$, and the hydrogen radius decreases from a_H to $\frac{1}{2} a_H$. For example, potassium ions can provide a net enthalpy of a multiple of that of the potential energy of the hydrogen atom. The second ionization energy of potassium is $31.63\ eV$; and K^+ releases $4.34\ eV$ when it is reduced to K. The combination of reactions K^+ to K^{2+} and K^+ to K, then, has a net enthalpy of reaction of $27.28\ eV$. The process is hereafter referred to as the Atomic BlackLight Process.

- The existence of fractional quantum energy levels of hydrogen atoms, molecules, and hydride ions as the product of the BlackLight Process-a new energy source has been confirmed experimentally.

- The Schwarzschild metric gives the relationship whereby matter causes relativistic corrections to spacetime that determines the curvature of spacetime and is the origin of gravity. The correction is based on the boundary conditions that no signal can travel faster that the speed of light including the gravitational field that propagates following particle production from a photon wherein the particle has a finite gravitational velocity given by Newton's Law of Gravitation.

- It is possible to give the electron a spatial velocity function having negative curvature and, therefore, cause antigravity. An engineered spacecraft may be feasible.

- Fundamental particle production occurs when the energy of the particle given by the Planck equation, Maxwell's Equations, and Special Relativity is equal to mc^2, and the proper time is equal to the coordinate time according to General Relativity. The gravitational equations with the equivalence of the particle production energies permit the equivalence of mass/energy and the spacetime metric from which the gravitational constant and the masses of the leptons, the quarks, and nucleons are derived.

- The gravitational equations with the equivalence of the particle production energies permit the equivalence of mass/energy ($E = mc^2$) and spacetime ($\frac{c^3}{4\pi G} = 3.22\ X\ 10^{34}\ \frac{kg}{\sec}$). Spacetime expands as mass is released as energy which provides the basis of the atomic, thermodynamic, and cosmological arrows of time. Entropy and the expansion of the universe are large scale consequences. The universe is closed independently of the total mass of the universe, and different regions of space are isothermal even though they are separated by greater distances than that over which light could travel during the time of the expansion of the universe. The universe is oscillatory in matter/energy and spacetime with a finite minimum radius, the gravitational radius; thus, the gravitational force causes celestial structures to evolve on a time scale that is greater than the period of oscillation. The equation of the radius of the universe, R, is $R = \left(\frac{2Gm_U}{c^2} + \frac{\frac{cm_U}{c^3}}{\frac{c^3}{4\pi G}}\right) - \frac{cm_U}{\frac{c^3}{4\pi G}} \cos\left(\frac{2\pi t}{\frac{2\pi G m_U}{c^3}} \sec\right) m$. The calculated Hubble constant is $H_0 = 78.6\ \frac{km}{\sec\ Mpc}$. Presently, stars exist which are older than the elapsed time of the present expansion as stellar evolution occurred during the contraction phase. The maximum energy release of the universe which occurs at the beginning of the expansion phase is

$$P_U = \frac{\frac{m_e c^2}{\sqrt{\frac{2GM}{c^2 \lambda_c}}}}{\tau\sqrt{\frac{2GM}{c^2 \lambda_c}}} = \frac{c^5}{4\pi G} = 2.89\ X\ 10^{51}\ W.$$

- Superconductivity arises when the lattice is a band-pass for the magnetic field of an array of magnetic dipoles; so, no energy is dissipated with current flow.

- The Quantum Hall Effect arises when the forces of crossed electric and magnetic fields balance and the lattice is a band-pass for the magnetic field of an array of magnetic dipoles.

- The vector potential component of the electron's angular momentum gives rise to the Aharonov-Bohm Effect.

- Alpha decay occurs as a transmission of a plane wave through a potential barrier.

- The proton and neutron functions each comprise a linear combination of a constant function and three orthogonal spherical harmonic functions resulting in three quark/gluon functions per nucleon. The nucleons are locally two dimensional.

SECTION I

Atoms and Molecules

THE ONE ELECTRON ATOM

One-electron atoms include the hydrogen atom, He(II), Li(III), Be(IV), and so on. The mass-energy and angular momentum of the electron are constant; this requires that the equation of motion of the electron be temporally and spatially harmonic. Thus, the classical wave equation (4-dimensional Laplace equation) applies and

$$\left[\nabla^2 - \frac{1}{v^2}\frac{\delta^2}{\delta t^2}\right]\rho(r,\theta,\phi,t) = 0 \qquad (1.1)$$

where $\rho(r,\theta,\phi,t)$ is the function of the electron in time and space. In each case, the nucleus contains Z protons and the atom has a net positive charge of $(Z-1)e$. All forces are central and Special Relativity applies. Thus, the coordinates must be three dimensional spherically harmonic coordinates plus time. The time, radial, and angular solutions of Laplace's Equation are separable. The motion is time harmonic with frequency ω_n. To be a harmonic solution of Laplace's equation in spherical coordinates, the angular functions must be spherical harmonic functions.

THE BOUNDARY CONDITION OF NONRADIATION AND THE RADIAL FUNCTION - THE CONCEPT OF THE "ORBITSPHERE"

A zero of the spacetime Fourier transform of the product function of two spherical harmonic angular functions, a time harmonic function, and an unknown radial function is sought.

The Boundary Condition

The condition for radiation by a moving charge is derived from Maxwell's equations. To radiate, the spacetime Fourier transform of the current-density function must possess components synchronous with waves traveling at the speed of light [1]. Alternatively,

> *For non-radiative states, the current-density function must not possess spacetime Fourier components that are synchronous with waves traveling at the speed of light.*

Derivation of the Condition for Nonradiation

Proof that the condition for nonradiation by a moving point charge is that its spacetime Fourier transform does not possess components that are synchronous with waves traveling at the speed of light is given by Haus [1]. The Haus derivation applies to a moving charge-density function as well because charge obeys superposition. The Haus

derivation is summarized below.

The Fourier components of the current produced by the moving charge are derived. The electric field is found from the vector equation in Fourier space ($\mathbf{k}$, ω-space). The inverse Fourier transform is carried over the magnitude of $\mathbf{k}$. The resulting expression demonstrates that the radiation field is proportional to $\mathbf{J}\left(\frac{\omega}{c}\mathbf{n},\omega\right)$, where $\mathbf{J}(\mathbf{k},\omega)$ is the spacetime Fourier transform of the current perpendicular to $\mathbf{k}$ and $\mathbf{n} \equiv \frac{\mathbf{k}}{|k|}$. Specifically,

$$\mathbf{E}(\mathbf{r},\omega)\frac{d\omega}{2\pi} = \frac{c}{2\pi}\int \rho(\omega,\Omega)d\omega d\Omega\sqrt{\frac{\mu_0}{\varepsilon_0}}\mathbf{n}\,X\left(\mathbf{n}\,X\,\mathbf{J}\left(\frac{\omega}{c}\mathbf{n},\omega\right)e^{i\left(\frac{\omega}{c}\mathbf{n}\cdot\mathbf{r}\right)}\right) \quad (1.2)$$

The field $\mathbf{E}(\mathbf{r},\omega)\frac{d\omega}{2\pi}$ is proportional to $\mathbf{J}\left(\frac{\omega}{c}\mathbf{n},\omega\right)$, namely, the Fourier component for which $\mathbf{k} = \frac{\omega}{c}$. Factors of ω that multiply the Fourier component of the current are due to the density of modes per unit volume and unit solid angle. An unaccelerated charge does not radiate in free space, not because it experiences no acceleration, but because it has no Fourier component $\mathbf{J}\left(\frac{\omega}{c}\mathbf{n},\omega\right)$.

Derivation of the Boundary Condition

In general, radial solutions of the Helmholtz wave equation are spherical Bessel functions, Neumann functions, Hankel functions, associated Laguerre functions, and the radial Dirac delta function. The Dirac delta function eliminates the radial dependence and reduces the number of dimensions of the Helmholtz wave equation from four to three. The solution for the radial function which satisfies the boundary condition is three dimensional delta function in spherical coordinates--a spherical shell [2]

$$f(r) = \frac{1}{r^2}\delta(r - r_n) \quad (1.3)$$

where r_n is an allowed radius. The Fourier Transform of the radial Dirac delta function is a sinc function. For time harmonic motion, with angular velocity, ω, the relationship between the radius and the wavelength is

$$2\pi r = \lambda \quad (1.4)$$

Consider the radial wave vector of the sinc function, when the radial projection of the velocity is c, the relativistically corrected wavelength is

$$r = \lambda \quad (1.5)$$

Substitution of Eq. (1.5) into the sinc function results in the vanishing of the entire Fourier Transform of the current-density function.

SPACETIME FOURIER TRANSFORM OF THE ELECTRON FUNCTION

The electron charge-density (mass-density) function is the product of a radial delta function ($f(r) = \frac{1}{r^2}\delta(r - r_n)$), two angular functions (spherical harmonic functions), and a time harmonic function. The spacetime Fourier transform in three dimensions in spherical coordinates plus time is given [3,4] as follows:

$$M(s,\Theta,\Phi,\omega) = \int_0^{\infty}\int_0^{\infty}\int_0^{\pi}\int_0^{2\pi}\rho(r,\theta,\phi,t)\exp(-i2\pi sr[\cos\Theta\cos\theta + \sin\Theta\sin\theta\cos(\phi - \Phi)]) \exp(-i\omega t)r^2\sin\theta\, dr d\theta d\phi dt \quad (1.6)$$

With circular symmetry [3]

$$M(s,\Theta,\omega) = 2\pi\int_0^{\infty}\int_0^{\infty}\int_0^{\pi}\rho(r,\theta,t)J_o(2\pi sr\sin\Theta\sin\theta)\exp(-i2\pi sr\cos\Theta\cos\theta)r^2\sin\theta\exp(-i\omega t)dr d\theta dt \quad (1.7)$$

With spherical symmetry [3],

$$M(s,\omega) = 4\pi\int_0^{\infty}\int_0^{\infty}\rho(r,t)\mathrm{sinc}(2sr)r^2\exp(-i\omega t)dr dt \quad (1.8)$$

The solutions of the classical wave equation are separable.

$$\rho(r,\theta,\phi,t) = f(r)g(\theta)h(\phi)k(t) \quad (1.9)$$

The orbitsphere function is separable into a product of functions of independent variables, r,θ,ϕ, and t. The radial function which satisfies the boundary condition is a delta function. The time functions are of the form $e^{i\omega t}$, the angular functions are spherical harmonics, sin or cosine trigonometric functions or sums of these functions, each raised to various powers. The spacetime Fourier transform is derived of the separable variables for the angular space function of $\sin\phi$ and $\sin\theta$. It follows from the spacetime Fourier transform given below that other possible spherical harmonics angular functions give the same form of result as the transform of $\sin\theta$ and $\sin\phi$. Using Eq. (1.8), $F(s)$, the space Fourier transform of ($f(r) = \delta(r - r_n)$) is given as follows:

$$F(s) = 4\pi\int_0^{\infty}\frac{1}{r^2}\delta(r - r_n)\mathrm{sinc}(2sr)r^2 dr \quad (1.10)$$

$$F(s) = 4\pi\mathrm{sinc}(2sr_n) \quad (1.11)$$

The subscript n is used hereafter; however, the quantization condition appears in the Excited States of the One Electron Atom (Quantization) Section. Quantization arises as

"allowed" solutions of the wave equation corresponding to a resonance between the electron and a photon.

Using Eq. (1.7), $G(s,\Theta)$,, the space Fourier transform of $g(\theta) = \sin\theta$ is given
as follows where there is no dependence on ϕ:

$$G(s,\Theta) = 2\pi \int_0^\infty \int_0^\pi \sin\theta J_o\left(2\pi sr \sin\Theta \sin\theta\right) \exp\left(-i2\pi sr \cos\Theta\cos\theta\right) \sin\theta r^2 d\theta dr \tag{1.12}$$

$$G(s,\Theta) = 2\pi \int_0^\infty \int_0^\pi r^2 \sin^2\theta J_o\left(2\pi sr \sin\Theta \sin\theta\right) \cos\left(2\pi sr \cos\Theta\cos\theta\right) d\theta dr \tag{1.13}$$

From Luke [5] and [6]:

$$J_\upsilon(z) = \left(\frac{1}{2} z\right)^\nu \sum_{n=0}^\infty \frac{(-1)^n \left(\frac{z}{2}\right)^{2n}}{n!\Gamma(\nu+n+1)} = \left(\frac{1}{2} z\right)^\nu \sum_{n=0}^\infty \frac{(-1)^n \left(\frac{z}{2}\right)^{2n}}{n!(\nu+n)!} \tag{1.14}$$

Let

$$Z = 2\pi sr \sin\Theta \sin\theta \tag{1.15}$$

With substitution of Eqs. (1.15) and (1.14) into Eq. (1.13),

$$G(s,\Theta) = 2\pi \int_0^\infty \int_0^\pi r^2 \sin^2\theta \left[\sum_{n=0}^\infty \frac{(-1)^n \left(\pi sr \sin\Theta \sin\theta\right)^{2n}}{n!\,n!}\right] \cos(2\pi sr \cos\Theta\cos\theta) d\theta dr \tag{1.16}$$

$$G(s,\Theta) = 2\pi \int_0^\infty r^2 \int_0^\pi \sum_{n=0}^\infty \frac{(-1)^n \left(\pi sr \sin\Theta\right)^{2n}}{n!\,n!} \sin^{2(n+1)}\theta \cos\left(2\pi sr \cos\Theta\cos\theta\right) d\theta dr \tag{1.17}$$

$$G(s,\Theta) = 2\pi \int_0^\infty r^2 \int_0^\pi \sum_{n=1}^\infty \frac{(-1)^{n-1} \left(\pi sr \sin\Theta\right)^{2(n-1)}}{(n-1)!(n-1)!} \sin^{2n}\theta \cos(2\pi sr \cos\Theta\cos\theta) d\theta dr \tag{1.18}$$

From Luke [7], with $\mathrm{Re}(\upsilon) > -\frac{1}{2}$:

$$J_\upsilon(z) = \frac{\left(\frac{1}{2} z\right)^\upsilon}{\Gamma\left(\frac{1}{2}\right)\Gamma\left(\upsilon + \frac{1}{2}\right)} \int_0^\pi \cos\left(z\cos\theta\right) \sin^{2\upsilon}\theta d\theta \tag{1.19}$$

Let

$$z = 2\pi sr\cos\theta, \text{ and } n = \upsilon \tag{1.20}$$

Applying the relationship, the integral of a sum is equal to the sum of the integral to Eq. (1.18), and transforming Eq. (1.18) into the form of Eq. (1.19) by multiplication by

$$1 = \frac{\Gamma\left(\frac{1}{2}\right)\Gamma\left(\upsilon + \frac{1}{2}\right)(\pi sr\cos\Theta)^{\upsilon}}{(\pi sr\cos\Theta)^{\upsilon}\Gamma\left(\frac{1}{2}\right)\Gamma\left(\upsilon + \frac{1}{2}\right)} \tag{1.21}$$

and by moving the constant outside of the integral gives:

$$G(s,\Theta) = 2\pi\int_0^{\infty} r^2 \sum_{\upsilon=1}^{\infty}\int_0^{\pi} \frac{(-1)^{\upsilon-1}(\pi r\sin\Theta)^{2(\upsilon-1)}}{(\upsilon-1)!(\upsilon-1)!} \frac{\Gamma\left(\frac{1}{2}\right)\Gamma\left(\upsilon+\frac{1}{2}\right)(\pi sr\cos\Theta)^{\upsilon}}{(\pi sr\cos\Theta)^{\upsilon}\Gamma\left(\frac{1}{2}\right)\Gamma\left(\upsilon+\frac{1}{2}\right)} \sin^{2\upsilon}\theta\cos(2\pi sr\cos\Theta\cos\theta)\,d\theta\,dr \tag{1.22}$$

$$G(s,\Theta) = 2\pi\int_0^{\infty} r^2 \sum_{\upsilon=1}^{\infty} \frac{(-1)^{\upsilon-1}(\pi r\sin\Theta)^{2(\upsilon-1)}}{(\upsilon-1)!(\upsilon-1)!} \frac{\Gamma\left(\frac{1}{2}\right)\Gamma\left(\upsilon+\frac{1}{2}\right)(\pi sr\cos\Theta)^{\upsilon}}{(\pi sr\cos\Theta)^{\upsilon}\Gamma\left(\frac{1}{2}\right)\Gamma\left(\upsilon+\frac{1}{2}\right)} \int_0^{\pi} \sin^{2\upsilon}\theta\cos(2\pi sr\cos\Theta\cos\theta)\,d\theta\,dr \tag{1.23}$$

Applying Eq. (1.19),

$$G(s,\Theta) = 2\pi\int_0^{\infty} r^2 \sum_{\upsilon=1}^{\infty} \frac{(-1)^{\upsilon-1}(\pi r\sin\Theta)^{2(\upsilon-1)}}{(\upsilon-1)!(\upsilon-1)!} \frac{\Gamma\left(\frac{1}{2}\right)\Gamma\left(\upsilon+\frac{1}{2}\right)}{(\pi sr\cos\Theta)^{\upsilon}} J_{\upsilon}(2\pi sr\cos\Theta)\,dr \tag{1.24}$$

Using the Hankel transform formula from Bateman [8]:

$$\int_0^{\infty} r^{-\left(\frac{1}{2}\right)}(rs)^{\left(\frac{1}{2}\right)} J_{\upsilon}(rs)\,dr = s^{\left(\frac{1}{2}\right)} \tag{1.25}$$

and the Hankel transform relationship from Bateman [9], the general Eq. (1.31) is derived as follows:

$$f(x) <=======> g(y;\upsilon) = \int_0^{\infty} f(x)(xy)^{\left(\frac{1}{2}\right)} J_{\upsilon}(xy)\,dx \tag{1.26}$$

$$x^m f(x), m = 0,1,2... <=======> y^{\left(\frac{1}{2}\right)-\upsilon}\left(\frac{d}{ydy}\right)^m \left[y^{m+\upsilon-\frac{1}{2}} g(y;m+\upsilon)\right] \tag{1.27}$$

$$\int_0^{\infty} r^{\upsilon} r^{-\left(\frac{1}{2}\right)}(rs)^{\left(\frac{1}{2}\right)} J_{\upsilon}(rs)\,dr = s^{\left(\frac{1}{2}\right)-\upsilon}\left(\frac{d}{sds}\right)^{\upsilon}\left[s^{\upsilon-\frac{1}{2}} s^{\left(\frac{1}{2}\right)}\right] \tag{1.28}$$

$$\int_0^\infty r^\upsilon s^{\left(\frac{1}{2}-\upsilon\right)} J_\upsilon(rs)\,dr = \frac{s^{\left(\frac{1}{2}-\upsilon\right)}}{s^\upsilon}\left(\frac{d}{ds}\right)^\upsilon \left[s^{(2\upsilon)}\right] \tag{1.29}$$

$$\int_0^\infty r^\upsilon s^{\left(\frac{1}{2}\right)} J_\upsilon(rs)\,dr = s^{\left(\frac{1}{2}-2\upsilon\right)} \frac{2\upsilon!}{(\upsilon-1)!}\, s^\upsilon = \frac{2\upsilon!}{(\upsilon-1)!}\, s^{\left(\frac{1}{2}-\upsilon\right)} \tag{1.30}$$

$$\int_0^\infty r^\upsilon s^{-\left(\frac{1}{2}\right)} s^{\left(\frac{1}{2}\right)} J_\upsilon(rs)\,dr = \frac{2\upsilon!}{(\upsilon-1)!}\, s^{-\upsilon} \tag{1.31}$$

Collecting the r raised to a power terms, Eq. (1.24) becomes,

$$G(s,\Theta) = 2\pi \sum_{\upsilon=1}^{\infty} \int_0^\infty \frac{(-1)^{\upsilon-1}(\pi \sin\Theta)^{2(\upsilon-1)}}{(\upsilon-1)!(\upsilon-1)!} \frac{\Gamma\left(\frac{1}{2}\right)\Gamma\left(\upsilon+\frac{1}{2}\right)}{(\pi s\cos\Theta)^\upsilon} r^\upsilon J_\upsilon(2\pi sr\cos\Theta)\,dr \tag{1.32}$$

Let $r = \dfrac{r'}{2\pi\cos\Theta}$; $dr = \dfrac{dr'}{2\pi\cos\Theta}$,

$$G(s,\Theta) = 2\pi \sum_{\upsilon=1}^{\infty} \int_0^\infty \frac{(-1)^{\upsilon-1}(\pi \sin\Theta)^{2(\upsilon-1)}}{(\upsilon-1)!(\upsilon-1)!} \frac{\Gamma\left(\frac{1}{2}\right)\Gamma\left(\upsilon+\frac{1}{2}\right)}{(\pi s\cos\Theta)^\upsilon} \frac{r^\upsilon}{(2\pi\cos\Theta)^{\upsilon+1}} J_\upsilon(sr')\,dr' \tag{1.33}$$

By applying Eq. (1.31), Eq. (1.33) becomes,

$$G(s,\Theta) = 2\pi \sum_{\upsilon=1}^{\infty} \frac{(-1)^{\upsilon-1}(\pi \sin\Theta)^{2(\upsilon-1)}}{(\upsilon-1)!(\upsilon-1)!} \frac{\Gamma\left(\frac{1}{2}\right)\Gamma\left(\upsilon+\frac{1}{2}\right)}{(\pi s\cos\Theta)^\upsilon (2\pi\cos\Theta)^{\upsilon+1}} \frac{2\upsilon!}{(\upsilon-1)!}\, s^{-\upsilon} \tag{1.34}$$

By collecting power terms of s, Eq. (1.34) becomes,

$$G(s,\Theta) = 2\pi \sum_{\upsilon=1}^{\infty} \frac{(-1)^{\upsilon-1}(\pi \sin\Theta)^{2(\upsilon-1)}}{(\upsilon-1)!(\upsilon-1)!} \frac{\Gamma\left(\frac{1}{2}\right)\Gamma\left(\upsilon+\frac{1}{2}\right)}{(\pi\cos\Theta)^{2\upsilon+1} 2^{\upsilon+1}} \frac{2\upsilon!}{(\upsilon-1)!}\, s^{-2\upsilon} \tag{1.35}$$

$H(s,\Phi)$, the space Fourier transform of $h(\phi) = \sin\phi$ is given as follows where there is no dependence on θ:

The spectrum of $\sin\phi$ and $\sin\theta$ are equivalent. Applying a change of variable to the Fourier transform of $g(\theta) = \sin\theta$.

θ ======>ϕ implies Θ =======>Φ

Therefore, Φ replaces Θ in Eq. (1.35),

$$H(s,\Phi) = 2\pi \sum_{\upsilon=1}^{\infty} \frac{(-1)^{\upsilon-1}(\pi \sin\Phi)^{2(\upsilon-1)}}{(\upsilon-1)!(\upsilon-1)!} \frac{\Gamma\left(\frac{1}{2}\right)\Gamma\left(\upsilon+\frac{1}{2}\right)}{(\pi\cos\Phi)^{2\upsilon+1} 2^{\upsilon+1}} \frac{2\upsilon!}{(\upsilon-1)!}\, s^{-2\upsilon} \tag{1.36}$$

The time Fourier transform of $K(t) = \mathrm{Re}\{\exp(i\omega_n t)\}$ where ω_n is the

angular frequency is given [4] as follows:

$$\int_0^\infty \cos\omega_n t \exp(-i\omega t)dt = \frac{1}{2\pi}\frac{1}{2}[\delta(\omega-\omega_n)+\delta(\omega+\omega_n)] \quad (1.37)$$

A very important theorem of Fourier analysis states that the Fourier transform of a product is the convolution of the individual Fourier transforms [10]. By applying this theorem, the spacetime Fourier transform of an orbitsphere, $M(s,\Theta,\Phi,\omega)$ is of the following form:

$$M(s,\Theta,\Phi,\omega) = F(s) \quad G(s,\Theta) \quad H(s,\Phi)K(\omega) \quad (1.38)$$

Therefore, the spacetime Fourier transform, $M(s,\Theta,\Phi,\omega)$, is the convolution of Eqs. (1.11), (1.35), (1.36), and (1.37).

$$M(s,\Theta,\Phi,\omega) = 4\pi\,\mathrm{sinc}(2sr_n) \quad 2\pi\sum_{\upsilon=1}^{\infty}\frac{(-1)^{\upsilon-1}(\pi\sin\Theta)^{2(\upsilon-1)}}{(\upsilon-1)!(\upsilon-1)!}\frac{\Gamma\left(\frac{1}{2}\right)\Gamma\left(\upsilon+\frac{1}{2}\right)}{(\pi\cos\Theta)^{2\upsilon+1}2^{\upsilon+1}}\frac{2\upsilon!}{(\upsilon-1)!}s^{-2\upsilon}$$

$$2\pi\sum_{\upsilon=1}^{\infty}\frac{(-1)^{\upsilon-1}(\pi\sin\Phi)^{2(\upsilon-1)}}{(\upsilon-1)!(\upsilon-1)!}\frac{\Gamma\left(\frac{1}{2}\right)\Gamma\left(\upsilon+\frac{1}{2}\right)}{(\pi\cos\Phi)^{2\upsilon+1}2^{\upsilon+1}}\frac{2\upsilon!}{(\upsilon-1)!}s^{-2\upsilon}\frac{1}{4\pi}[\delta(\omega-\omega_n)+\delta(\omega+\omega_n)] \quad (1.39)$$

The condition for nonradiation of a moving charge-density function is that the spacetime Fourier transform of the current-density function must not have waves synchronous with waves traveling at the speed of light, that is synchronous with $\frac{\omega_n}{c}$ or synchronous with $\frac{\omega_n}{c}\sqrt{\frac{\varepsilon}{\varepsilon_o}}$ where ε is the dielectric constant of the medium. The Fourier transform of the charge-density function of the orbitsphere (bubble of radius r) is given by Eq. (1.39). In the case of time harmonic motion, the current-density function is given by the time derivative of the charge-density function. Thus, the current-density function is given by the product of the constant angular velocity and the charge-density function. The Fourier transform of current-density function of the orbitsphere is given by the product of the constant angular velocity and Eq. (1.39). Consider the radial and time parts of, J , the Fourier transform of the current-density function where the angular transforms are not zero:

$$J \quad \omega_n\,\mathrm{sinc}2sr_n\frac{1}{4\pi}[\delta(\omega-\omega_n)+\delta(\omega+\omega_n)] = \omega_n\frac{\sin 2\pi sr_n}{2\pi sr_n}\frac{1}{4\pi}[\delta(\omega-\omega_n)+\delta(\omega+\omega_n)] \quad (1.40)$$

For the case that the current-density function is constant, the delta function of Eq. (1.40) is replaced by a constant. For time harmonic motion, with angular velocity, ω_n, Eq. (1.40) is nonzero only for $\omega=\omega_n$; thus, $-\infty < s < \infty$ becomes finite only for the corresponding wavenumber,

s_n. The relationship between the radius and the wavelength is

$$v_n = \lambda_n f_n \tag{1.41}$$

$$v_n = 2\pi r_n f_n = \lambda_n f_n \tag{1.42}$$

$$2\pi r_n = \lambda_n \tag{1.43}$$

The motion on the orbitsphere is angular; however, a radial component exists due to Special Relativistic effects. Consider the radial wave vector of the sinc function. When the radial projection of the velocity is c

$$\mathbf{s}_n \cdot \mathbf{v}_n = \mathbf{s}_n \cdot \mathbf{c} = \omega_n \tag{1.44}$$

the relativistically corrected wavelength is[1]

$$r_n = \lambda_n \tag{1.45}$$

(i.e. the lab frame motion in the angular direction goes to zero as the velocity approaches the speed of light as given by Eq. (24.15)). Substitution of Eq. (1.45) into the sinc function results in the vanishing of the entire Fourier Transform of the current-density function. Thus, spacetime harmonics of $\frac{\omega_n}{c} = k$ or $\frac{\omega_n}{c}\sqrt{\frac{\varepsilon}{\varepsilon_o}} = k$ do not exist for which the Fourier Transform of the current-density function is nonzero. Radiation due to charge motion does not occur in any medium when this boundary condition is met. [Note that the boundary condition for the solution of the radial function of the hydrogen atom with the Schrödinger equation is that $\Psi \to 0$ as $r \to \infty$. Here, however, the boundary condition is derived from Maxwell's equations: For non-radiative states, the current-density function must not possess spacetime Fourier components that are synchronous with waves traveling at the speed of light. An alternative derivation which provides acceleration without radiation is given by Abbott [11]] Bound electrons are described by a charge-density (mass-density) function which is the product of a radial delta function, Eq. (1.3), two angular functions (spherical harmonic functions), and a time harmonic function. This is a solution of Laplace's Equation. Thus,

---

[1] The special relativistic length contraction relationship observed for a laboratory frame relative to an inertial frame moving at constant velocity v in the direction of velocity v is

$$l = l_o\sqrt{1 - \frac{v^2}{c^2}}$$

Consider the distance on a great circle given by

$$\int_0^{2\pi} r d\theta = r\theta\Big|_0^{2\pi} = 2\pi r$$

The distance undergoes length contraction only in the θ direction as $v \to c$. Thus, as $v \to c$ the distance on a great circle approaches its radius which is the relativistically contracted electron wavelength.

this radial function implies that allowed states are two-dimensional spherical shells (zero thickness) of charge-density (and mass density) at specific radii r_n. These shells are referred to as electron orbitspheres. See Figure 1.1 for a pictorial representation of an orbitsphere.

Figure 1.1. The orbitsphere is a two dimensional spherical shell with the Bohr radius of the hydrogen atom.

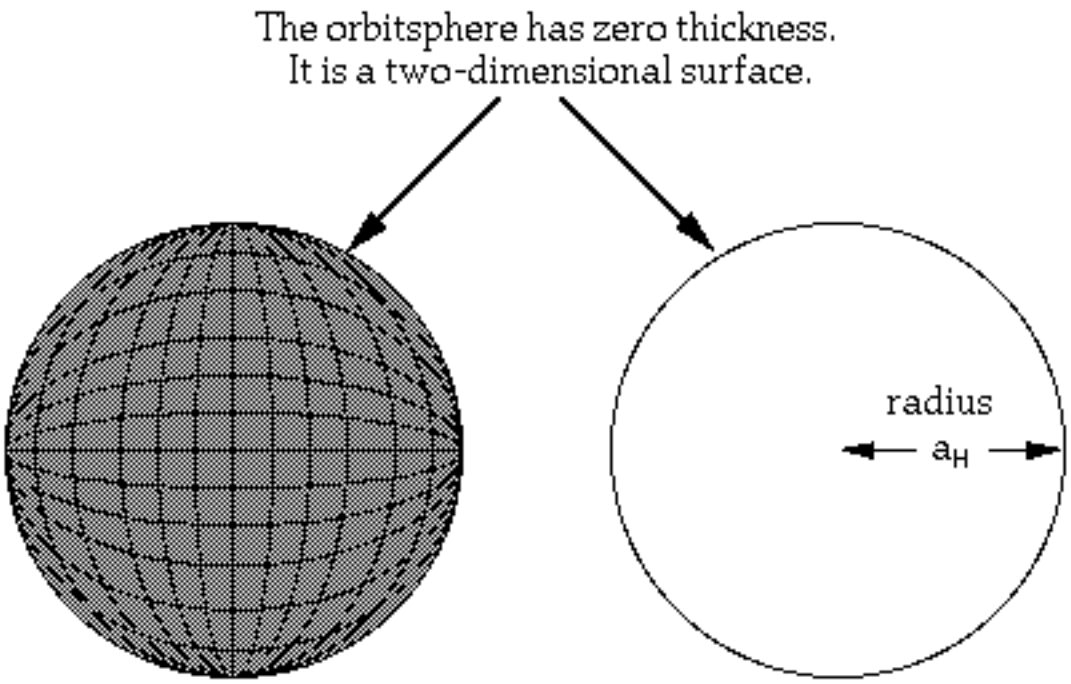

Given time harmonic motion and a radial delta function, the relationship between an allowed radius and the electron wavelength is given by Eq. (1.43). Using the de Broglie relationship for the electron mass where the coordinates are spherical,

$$\lambda_n = \frac{h}{p_n} = \frac{h}{m_e v_n} \tag{1.46}$$

and the magnitude of the velocity for every point on the orbitsphere is

$$v_n = \frac{\hbar}{m_e r_n} \tag{1.47}$$

THE ANGULAR FUNCTION

The radial function for the electron indicates that the electron is two-dimensional. Therefore, the angular mass-density function of the electron , $A(\theta,\phi,t)$, must be a solution of the Laplace equation in two dimensions (plus time),

$$\left[\nabla^2 - \frac{1}{v^2}\frac{\delta^2}{\delta t^2}\right]A(\theta,\phi,t) = 0 \tag{1.48}$$

where $\rho(r,\theta,\phi,t) = f(r)A(\theta,\phi,t) = \frac{1}{r^2}\delta(r-r_n)A(\theta,\phi,t)$ *and* $A(\theta,\phi,t) = Y(\theta,\phi)k(t)$

$$\left[\frac{1}{r^2\sin\theta}\frac{\delta}{\delta\theta}\left(\sin\theta\frac{\delta}{\delta\theta}\right)_{r,\phi} + \frac{1}{r^2\sin^2\theta}\left(\frac{\delta^2}{\delta\phi^2}\right)_{r,\theta} - \frac{1}{v^2}\frac{\delta^2}{\delta t^2}\right]A(\theta,\phi,t) = 0 \tag{1.49}$$

where v is the linear velocity of the electron. Conservation of momentum and energy allows the angular functions and time functions to be separated.

$$A(\theta,\phi,t) = Y(\theta,\phi)k(t) \tag{1.50}$$

Charge is conserved as well, and the charge of an electron is superimposable with its mass. That is, the angular mass-density function, $A(\theta,\phi,t)$, is also the angular charge-density function.

The electron orbitsphere experiences a constant potential energy because it is fixed at $r = r_n$. In general, the kinetic energy for an inverse squared electric force is half the potential energy. It is the rotation of the orbitsphere that causes spin angular momentum. The rotational energy of a rotating body, E_{rot}, is

$$E_{rot} = \frac{1}{2}I\omega^2 \tag{1.51}$$

where I is the moment of inertia and ω is the angular velocity. The angular velocity must be constant (at a given n) because r is constant and the energy and angular momentum are constant. The allowed angular velocities are related to the allowed frequencies by

$$\omega_n = 2\pi\nu_n \tag{1.52}$$

The allowed frequencies are related to allowed velocities by

$$v_n = \nu_n\lambda_n \tag{1.53}$$

The allowed velocities and angular frequencies are related to r_n by

$$v_n = r_n\omega_n \tag{1.54}$$

$$\omega_n = \frac{\hbar}{m_e r_n^2} \tag{1.55}$$

$$v_n = \frac{\hbar}{m_e r_n} \tag{1.56}$$

The sum of the $\mathbf{L}_i$, the magnitude of the angular momentum of each infinitesimal point of the orbitsphere of mass m_i, must be constant. The constant is $\hbar$.

$$\sum|\mathbf{L}_i| = \sum|\mathbf{r}\times m_i\mathbf{v}| = m_e r_n\frac{\hbar}{m_e r_n} = \hbar \tag{1.57}$$

where the velocity is given by Eq. (1.47). The vector projections of the

orbitsphere spin angular momentum relative to the Cartesian coordinates are given in the Spin Angular Momentum of the Orbitsphere with $\ell = 0$ Section.

In the case of an excited state, the charge density function of the electron orbitsphere can be modulated by the corresponding "trapped" photon to give rise to orbital angular momentum about the z-axis. The "trapped photon" is a "standing electromagnetic wave" which actually is a circulating wave that propagates around the z-axis. Its source current superimposes with each great circle current loop of the orbitsphere. In order to satisfy the boundary (phase) condition at the orbitsphere surface, the angular and time functions of the photon must match those of its source current which modulates the orbitsphere charge density function as given in the Equation of the Electric Field Inside the Orbitsphere Section. The time-function factor, $k(t)$, for the photon "standing wave" is identical to the time-function factor of the orbitsphere. Thus, the angular frequency of the "trapped photon" has to be identical to the angular frequency of the electron orbitsphere, ω_n given by Eq. (1.55). However, the linear velocity of the modulation component is not given by Eq. (1.54)--the orbital angular frequency is with respect to the z-axis; thus, the distance from the z-axis must be substituted for the orbitsphere radius of Eq. (1.54). The vector projections of the orbital angular momentum and the spin angular momentum of the orbitsphere are given in the Rotational Parameters of the Electron (Angular Momentum, Rotational Energy, and Moment of Inertia) Section. Eq. (1.49) becomes

$$-\frac{\hbar^2}{2I}\left[\frac{1}{\sin\theta}\frac{\delta}{\delta\theta}\left(\sin\theta\frac{\delta}{\delta\theta}\right)_{r,\phi}+\frac{1}{\sin^2\theta}\left(\frac{\delta^2}{\delta\phi^2}\right)_{r,\theta}\right]A(\theta,\phi,t)=E_{rot}A(\theta,\phi,t) \qquad (1.58)$$

The spacetime angular function, $A(\theta,\phi,t)$, is separated into an angular and a time function, $Y(\theta,\phi)k(t)$. The solution of the time harmonic function is $k(t)=e^{i\omega_n t}$. When the time harmonic function is eliminated,

$$-\frac{\hbar^2}{2I}\left[\frac{1}{\sin\theta}\frac{\delta}{\delta\theta}\left(\sin\theta\frac{\delta}{\delta\theta}\right)_{r,\phi}+\frac{1}{\sin^2\theta}\left(\frac{\delta^2}{\delta\phi^2}\right)_{r,\theta}\right]Y(\theta,\phi)=E_{rot}Y(\theta,\phi) \qquad (1.59)$$

Eq. (1.59) is the equation for the rigid rotor. The angular function can be separated into a function of θ and a function of ϕ and the solutions are well known [11]. The energies are given by

$$E_{rot}=\frac{\hbar^2\ell(\ell+1)}{2I} \quad \ell = 0,1,2,3,..., \qquad (1.60)$$

where the moment of inertia, I, is derived in the Rotational Parameters of the Electron (Angular Momentum, Rotational Energy, and Moment of Inertia) Section. The angular functions are the spherical harmonics,

$Y_\ell^m(\phi,\theta) = P_\ell^m(\cos\theta)e^{im\phi}$. The spherical harmonic $Y_0^0(\phi,\theta) = 1$ is also a solution. The real part of the spherical harmonics vary between −1 and 1. But the mass of the electron cannot be negative; and the charge cannot be positive. Thus, to insure that the function is positive definite, the form of the angular solution must be a superposition:

$$Y_0^{\,0}(\theta,\phi) + Y_\ell^{\,m}(\theta,\phi) \tag{1.61}$$

(Note that $Y_\ell^m(\phi,\theta) = P_\ell^m(\cos\theta)e^{im\phi}$ are not normalized here as given by Eq. (3.53) of Jackson [12]; however, it is implicit that magnitude is made to satisfy the boundary condition that the function is positive definite and Eq. (1.63) is satisfied.) $Y_0^{\,0}(\theta,\phi)$ is called the angular spin function corresponding to the quantum numbers $s = \frac{1}{2}; m_s = \pm\frac{1}{2}$ as given in the Spin Angular Momentum of the Orbitsphere with ℓ = 0 Section and the Stern-Gerlach Experiment Section. $Y_\ell^{\,m}(\theta,\phi)$ is called the angular orbital function corresponding to the quantum numbers $\ell = 0, 1, 2, 3, 4,...; m_\ell = -\ell, -\ell+1, ..., 0, ..., +\ell$. $Y_\ell^{\,m}(\theta,\phi)$ can be thought of as a modulation function. The charge-density of the entire orbitsphere is the total charge divided by the total area, $\frac{-e}{4\pi r_n^2}$. The fraction of the charge of an electron in any area element is given by

$$N\left[Y_0^{\,0}(\theta,\phi) + Y_\ell^{\,m}(\theta,\phi)\right] r_n^2 \sin\theta d\theta d\phi, \tag{1.62}$$

where N is the normalization constant. Therefore, the normalization constant is given by

$$-e = N r_n^2 \int_0^{\pi}\int_0^{2\pi}\left[Y_0^{\,0}(\theta,\phi) + Y_\ell^{\,m}(\theta,\phi)\right]\sin\theta d\theta d\phi \tag{1.63}$$

For ℓ = 0, $N = \frac{-e}{8\pi r_n^2}$. For $\ell \neq 0$, $N = \frac{-e}{4\pi r_n^2}$. The charge-density functions including the time-function factor are

ℓ = 0

$$\rho(r,\theta,\phi,t) = \frac{e}{8\pi r^2}[\delta(r - r_n)]\left[Y_\ell^m(\theta,\phi) + Y_0^0(\theta,\phi)\right] \tag{1.64}$$

$\ell \neq 0$

$$\rho(r,\theta,\phi,t) = \frac{e}{4\pi r^2}[\delta(r - r_n)]\left[Y_0^0(\theta,\phi) + \mathrm{Re}\left\{Y_\ell^m(\theta,\phi)\left[1 + e^{i\omega_n t}\right]\right\}\right] \tag{1.65}$$

where

$$\mathrm{Re}\left\{Y_\ell^m(\theta,\phi)\left[1 + e^{i\omega_n t}\right]\right\} = \mathrm{Re}\left[Y_\ell^m(\theta,\phi) + Y_\ell^m(\theta,\phi)e^{i\omega_n t}\right] = P_\ell^m(\cos\theta)\cos m\phi + P_\ell^m(\cos\theta)\cos(m\phi + \omega_n t)$$

and $\omega_n = 0$ for $m = 0$. The photon equations which correspond to the orbitsphere states, Eqs. (1.64) and (1.65) are given in the Excited States

of the One Electron Atom (Quantization) Section. For $n = 1$, and $\ell = 0$, $m = 0$, and $s = 1/2$, the charge (and mass) distribution is spherically symmetric and $M_{1,0,0,1/2} = -14.41\ Cm^{-2}$ everywhere on the orbitsphere. Similarly, for $n = 2$, $\ell = 0$, $m = 0$, and $s = 1/2$, the charge distribution everywhere on the sphere is $M_{2,0,0,1/2} = -3.602\ Cm^{-2}$. For $n = 2$, $\ell = 1$, $m = 0$, and $s = 1/2$, the charge distribution varies with θ. $Y_1^0(\phi,\theta)$ is a maximum at $\theta = 0°$ and the charge-density is also a maximum at this point, $M_{2,1,0,1/2}(\theta = 0°) = -7.203\ Cm^{-2}$. The charge-density decreases as θ increases; a minimum in the charge-density is reached at $\theta = 180°$, $M_{2,1,0,1/2}(\theta = 180°) = 0\ Cm^{-2}$.

For $\ell = 1$ and $m = \pm 1$, the spherical harmonics are complex, and the angular functions comprise linear combinations of

$$Y_{1,x} = \sin\theta\cos\phi \tag{1.66}$$

$$Y_{1,y} = \sin\theta\sin\phi \tag{1.67}$$

Each of $Y_{1,x}$ and $Y_{1,y}$ is the component factor part of a phasor. They are not components of a vector; however, the x and y designation corresponds, respectively, to the historical p_x and p_y probability density functions of quantum mechanics. $Y_{1,x}$ is a maximum at $\theta = 90°$ and $\phi = 0°$; $M_{2,1,x,1/2}(90°,0°) = -3.602\ Cm^{-2}$. Figure 1.2 gives pictorial representation of how the modulation function changes the electron density on the orbitsphere for several ℓ values. (When the electron charge appears throughout this text in a function involving a linear combination of the spin and orbital functions, it is implicit that the charge is normalized.)

Figure 1.2 The orbital function modulates the constant (spin) function. (shown for t = 0; cross-sectional view)

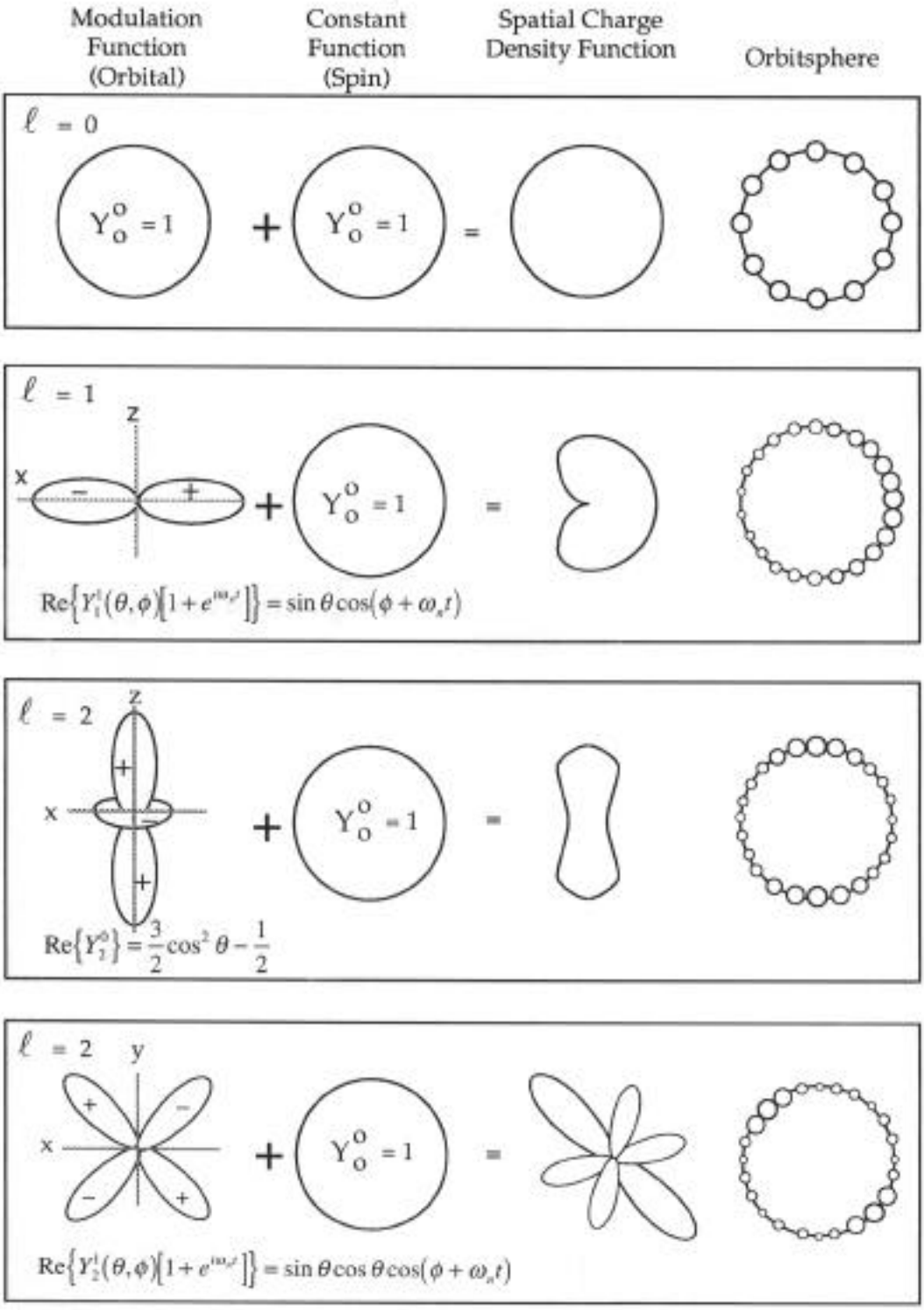

THE ORBITSPHERE EQUATION OF MOTION FOR $\ell = 0$

The orbitsphere equation of motion for $\ell = 0$ is solved as a boundary value problem. The boundary conditions are: 1.) each infinitesimal point of the orbitsphere must move along a great circle; 2.) every such infinitesimal point must have the same angular and linear velocity given by Eqs. (1.55) and (1.56), respectively; 3.) the current of the orbitsphere must give rise a magnetic moment of a Bohr magneton and the corresponding magnetic field; 4.) the magnetic moment must align completely parallel or antiparallel with an applied magnetic field in agreement with the Stern-Gerlach experiment; 5.) the energy of the transition of the alignment of the magnetic moment with an applied magnetic field must be given by Eq. (1.151); 6.) the projection of the angular momentum of the orbitsphere onto the z-axis must be $\pm\frac{\hbar}{2}$, and 7.) the projection of the angular momentum of the orbitsphere onto an axis which precesses about the z-axis must be $\pm\sqrt{\frac{3}{4}}\hbar$.

In the derivation of Eqs. (1.58) and (1.59), the moment of inertia, typically caused by a point particle or a reduced mass, is mr^2. Here, however, the mass is in the form of a two-dimensional, spherical shell. Assume that $\ell = 0$ and that the electron mass and charge is uniformly distributed over the orbitsphere. Each point on the sphere with mass m_i has the same angular velocity (ω_n), the same magnitude of linear velocity (v_n), and the same moment of inertia ($m_i r_n^2$). The motion of each point of the orbitsphere is along a great circle, and the motion of each great circle is correlated with the motion on all other great circles. The orbitsphere is *not* analogous to a globe, where $I = \frac{2}{3}mr^2$, spinning about some axis. The velocity of a point mass on a spinning globe is a function of θ. On the orbitsphere, however, each point mass has the same velocity (magnitude); the velocity is not a function of θ. Each point must travel on a great circle such that all points have the same velocity (magnitude) and angular frequency. The uniform charge-density function of the orbitsphere is constant in time due to the motion of the current along great circles. The current flowing into any given point of the orbitsphere equals the current flowing out, but the current pattern of the orbitsphere is not uniform. The equation of motion for each point mass which gives the current pattern of the orbitsphere is generated as follows:

(Here a procedure is used to generate the current pattern of the orbitsphere from which the physical properties are derived in the Spin

Angular Momentum of the Orbitsphere with $\ell = 0$ Section and are shown to match the boundary conditions.)

Consider the electron to be evenly distributed within two orthogonal great circle current loops. Then consider two infinitesimal point masses (charges), one and two, of two orthogonal great circle current loops. The Cartesian coordinate system wherein the first current loop lies in the
yz-plane, and the second current loop lies in the xz-plane is designated the orbitsphere reference frame.

Figure 1.3 Two infinitesimal point masses (charges) of two orthogonal great circle current loops in the orbitsphere frame.

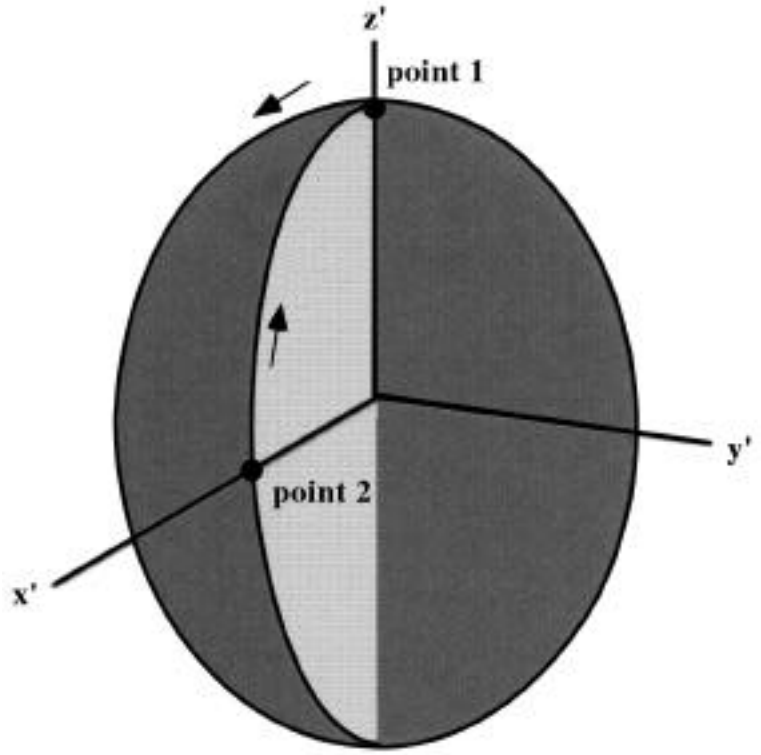

The current pattern of the orbitsphere comprises an infinite series of correlated orthogonal great circle current loops. It is generated by an infinite series of nested rotations of two orthogonal great circle current loops each about the new x-axis and new y-axis which results from the preceding such rotation. Each such two orthogonal great circle current loops wherein the first current loop lies in the yz-plane, and the second current loop lies in the xz-plane of the orbitsphere reference frame is an element of the infinite series. The first such orthogonal great circle

current loops is shown in Figure 1.3. The second element of the series is generated by rotation of the first element by an infinitesimal angle $\Delta\alpha$ about the first x-axis followed by a rotation by the same infinitesimal angle $\Delta\alpha$ about the new (second) y-axis to form a second x-axis. The third element of the series is generated by the rotation of the second element by the infinitesimal angle $\Delta\alpha$ about the second x-axis followed by the rotation by the same infinitesimal angle $\Delta\alpha$ about the new (third) y-axis. In general, the $(n+1)$th element of the series is generated by the rotation of the nth orbitsphere coordinate system by the infinitesimal angle $\Delta\alpha$ about the nth x-axis followed by the rotation of the nth orbitsphere coordinate system by the infinitesimal angle $\Delta\alpha$ about the $(n+1)$th new y-axis. The orbitsphere is given by reiterations of the successive rotations where the summation of the rotation about each of the x-axis and the y-axis is $\sum_{n=1}^{\frac{\sqrt{2}\pi}{\Delta\alpha}} \Delta\alpha = \sqrt{2}\pi$ which rotates the final z-axis to the first negative z-axis, the final x-axis to the first -y-axis, and the final y-axis to the first -x-axis. (The total angle, $\sqrt{2}\pi$, is the hypotenuse of the triangle having the sides of π radians corresponding to x-axis rotations and π radians corresponding to y-axis rotations.) Then the reiterations of the successive rotations is continued about the nth x-axis followed by the rotation of the nth orbitsphere coordinate system by the infinitesimal angle $\Delta\alpha' = -\Delta\alpha$ about the $(n+1)$th new y-axis where the magnitude of the summation of the rotation about each of the x-axis and the y-axis is $\sum_{n=1}^{\frac{\sqrt{2}\pi}{|\Delta\alpha'|}} |\Delta\alpha'| = \sqrt{2}\pi$. The final step rotates the final z-axis to the first z-axis, the final x-axis to the first x-axis, and the final y-axis to the first y-axis. Thus, the orbitsphere is generated from two orthogonal great circle current loops which are rotated about the nth x-axis then about the $(n+1)$th y-axis in two steps. The first step comprises all rotations by $\Delta\alpha$, and the second step comprises all rotations by $\Delta\alpha'$. In the case of the nth element of the first step, the intersection of the two orthogonal great circle current loops occurs at the nth z-axis which is along a great circle in a plane rotated $\frac{\pi}{4}$ with respect to the 1st xz-plane and 1st yz-plane of Figure 1.3. In the case of the nth element of the second step, the intersection of the two orthogonal great circle current loops occurs at the nth z-axis which is along a great circle in a plane rotated $\frac{\pi}{4}$ with respect to the 1st yz-plane and the 1st negative xz-plane (the plane containing the negative x-axis and the positive z-axis) of Figure 1.3.

Consider two point masses, one and two, in the reference frame of the orbitsphere at time zero. Point one is at $x'=0$, $y'=0$, and $z'=r_n$ and point two is at $x'=r_n$, $y'=0$, and $z'=0$. Let point one move on a great circle toward the negative y'-axis, as shown in Figure 1.3, and let point two move on a great circle toward the positive z'-axis, as shown in Figure 1.3. The equations of motion, in the reference frame of the orbitsphere are given by

point one:

$$x_1' = 0 \qquad y_1' = -r_n \sin(\omega_n t) \qquad z_1' = r_n \cos(\omega_n t) \tag{1.68}$$

point two:

$$x_2' = r_n \cos(\omega_n t) \qquad y_2' = 0 \qquad z_2' = r_n \sin(\omega_n t) \tag{1.69}$$

The great circles are rotated by an infinitesimal angle $\Delta\alpha$ (a rotation around the x-axis) and then by $\Delta\alpha$ (a rotation around the new y-axis). The coordinates of each point on the rotated great circle is expressed in terms of the first (x,y,z) coordinates by the following transforms:

point one:

$$\begin{bmatrix} x_1 \\ y_1 \\ z_1 \end{bmatrix} = \begin{bmatrix} \cos(\Delta\alpha) & -\sin^2(\Delta\alpha) & -\sin(\Delta\alpha)\cos(\Delta\alpha) \\ 0 & \cos(\Delta\alpha) & -\sin(\Delta\alpha) \\ \sin(\Delta\alpha) & \cos(\Delta\alpha)\sin(\Delta\alpha) & \cos^2(\Delta\alpha) \end{bmatrix} \begin{bmatrix} x_1' \\ y_1' \\ z_1' \end{bmatrix} \tag{1.70}$$

and $\Delta\alpha' = -\Delta\alpha$ replaces $\Delta\alpha$ for $\sum_{n=1}^{\frac{\sqrt{2}\pi}{\Delta\alpha}} \Delta\alpha = \sqrt{2}\pi$; $\sum_{n=1}^{\frac{\sqrt{2}\pi}{|\Delta\alpha'|}} |\Delta\alpha'| = \sqrt{2}\pi$

point two:

$$\begin{bmatrix} x_2 \\ y_2 \\ z_2 \end{bmatrix} = \begin{bmatrix} \cos(\Delta\alpha) & -\sin^2(\Delta\alpha) & -\sin(\Delta\alpha)\cos(\Delta\alpha) \\ 0 & \cos(\Delta\alpha) & -\sin(\Delta\alpha) \\ \sin(\Delta\alpha) & \cos(\Delta\alpha)\sin(\Delta\alpha) & \cos^2(\Delta\alpha) \end{bmatrix} \begin{bmatrix} x_2' \\ y_2 \\ z_2' \end{bmatrix} \quad (1.71)$$

and $\Delta\alpha' = -\Delta\alpha$ replaces $\Delta\alpha$ for $\sum_{n=1}^{\frac{\sqrt{2}\pi}{\Delta\alpha}} \Delta\alpha = \sqrt{2}\pi$; $\sum_{n=1}^{\frac{\sqrt{2}\pi}{|\Delta\alpha'|}} |\Delta\alpha'| = \sqrt{2}\pi$

The total orbitsphere is given by reiterations of Eqs. (1.70) and (1.71). The output given by the non primed coordinates is the input of the next iteration corresponding to each successive nested rotation by the infinitesimal angle where the summation of the rotation about each of the x-axis and the y-axis is $\sum_{n=1}^{\frac{\sqrt{2}\pi}{\Delta\alpha}} \Delta\alpha = \sqrt{2}\pi$ and $\sum_{n=1}^{\frac{\sqrt{2}\pi}{|\Delta\alpha'|}} |\Delta\alpha'| = \sqrt{2}\pi$.

The current pattern corresponding to point one and point two shown with 8.49 degree increments of the infinitesimal angular variable $\Delta\alpha(\Delta\alpha')$ of Eqs. (1.70) and (1.71) is shown from three perspectives in Figures 1.4 A, 1.4 B, and 1.4 C. The complete orbitsphere current pattern corresponds to all such correlated points, point one and point two, of the orthogonal great circles shown in Figure 1.3 which are rotated according to Eqs. (1.70) and (1.71) where $\Delta\alpha(\Delta\alpha')$ approaches zero and the summation of the infinitesimal angular rotations of $\Delta\alpha(\Delta\alpha')$ about the successive x-axes and y-axes is $\sqrt{2}\pi$.

Figure 1.4 A. The current pattern of the orbitsphere shown with 8.49 degree increments of the infinitesimal angular variable $\Delta\alpha(\Delta\alpha')$ from the perspective of looking along the z-axis.

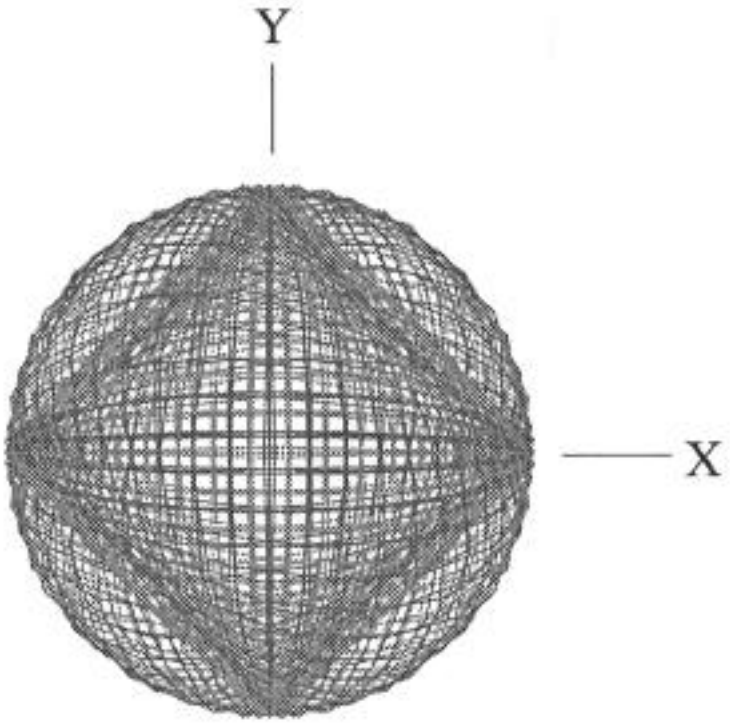

VIEW ALONG THE Z AXIS

Figure 1.4 B. The current pattern of the orbitsphere shown with 8.49 degree increments of the infinitesimal angular variable $\Delta\alpha(\Delta\alpha')$ from the perspective of looking along the x-axis.

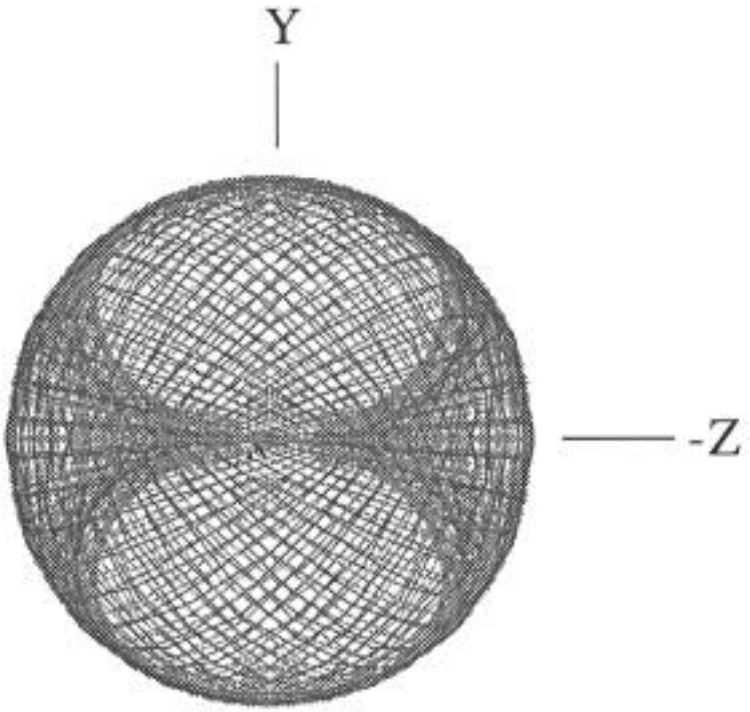

VIEW ALONG THE +X AXIS

Figure 1.4 C. The current pattern of the orbitsphere shown with 8.49 degree increments of the infinitesimal angular variable $\Delta\alpha(\Delta\alpha')$ from the perspective of looking along the y-axis.

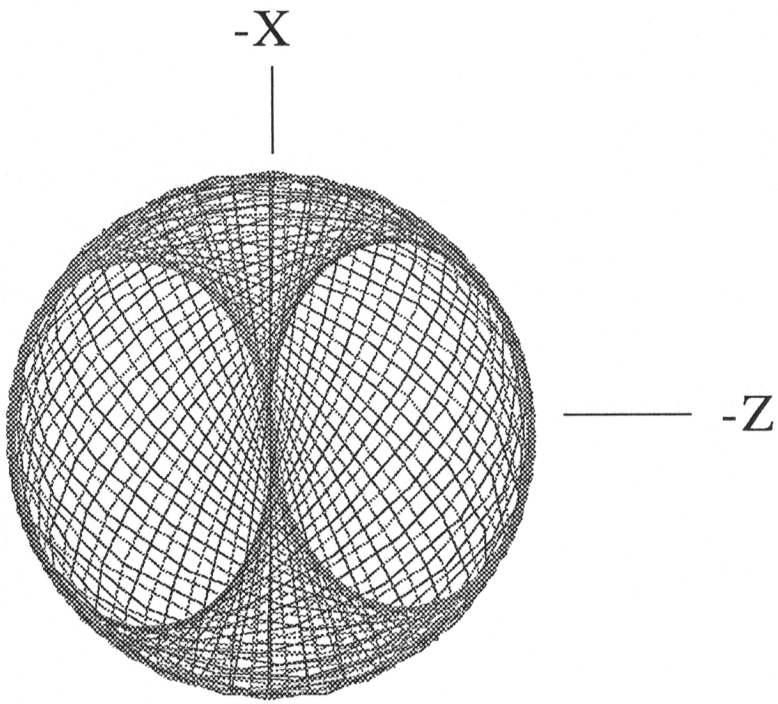

SPIN ANGULAR MOMENTUM OF THE ORBITSPHERE WITH $\ell = 0$

As demonstrated in Figures 1.3 and 1.4, the orbitsphere is generated from two orthogonal great circle current loops which are rotated about the nth x-axis then about the $(n+1)$th y-axis in two steps. The first step comprises all rotations by $\Delta\alpha$, and the second step comprises all rotations by $\Delta\alpha'$. In the case of the nth element of the first step, the intersection of the two orthogonal great circle current loops occurs at the nth z-axis which is along a great circle in a plane rotated $\frac{\pi}{4}$ with respect to the 1st xz-plane and the 1st yz-plane of Figure 1.3. In the case of the nth element of the second step, the intersection of the two orthogonal great circle current loops occurs at the nth z-axis which is along a great circle in a plane rotated $\frac{\pi}{4}$ with respect to the 1st yz-plane and the 1st negative xz-plane (the plane containing the negative x-

axis and the positive z-axis) of Figure 1.3. The mass density, $\frac{m_e}{4\pi r_1^2}$, of the orbitsphere of radius r_1 is uniform. However, the projections of the angular momentum of the great circle current loops of the orbitsphere onto the z-axis and onto the xy-plane can be derived by considering two orthogonal great circle current loops of Figure 1.5 each of mass $\frac{m_e}{2}$ which generate the current pattern of the orbitsphere in two steps. (Here the physical properties of the orbitsphere are derived following the procedure used to generate the current pattern of the orbitsphere given in the Orbitsphere Equation of Motion for $\ell = 0$ Section and are shown to match the boundary conditions.)

Figure 1.5 A. The angular momentum of the orthogonal great circle current loops in the xy-plane is $\frac{\hbar}{\sqrt{2}}$.

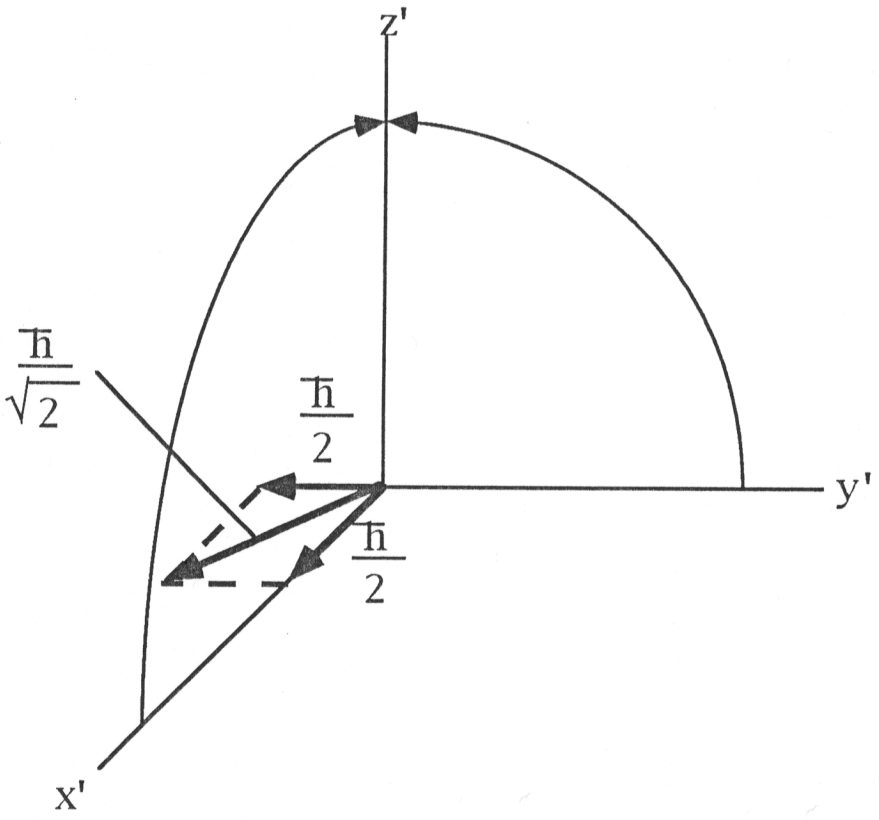

For step one, the resultant angular momentum vector of the orthogonal great circle current loops of magnitude $\frac{\hbar}{\sqrt{2}}$ moves along a

great circle oriented at an angle of $\frac{\pi}{4}$ to the 1st xz-plane and the 1st yz-plane. For the vector current directions shown in Figure 1.5 A, as the $Y_0^0(\phi,\theta)$ orbitsphere function is partially generated in step one, the resultant angular momentum vector moves along the great circle from the 1st xy-plane to the 1st negative z-axis and back to the xy-plane. The trajectory of the resultant angular momentum vector is shown in Figure 1.5 B.

Figure 1.5 B. The trajectory of the resultant angular momentum vector of the orthogonal great circle current loops of magnitude $\frac{\hbar}{\sqrt{2}}$ during step one.

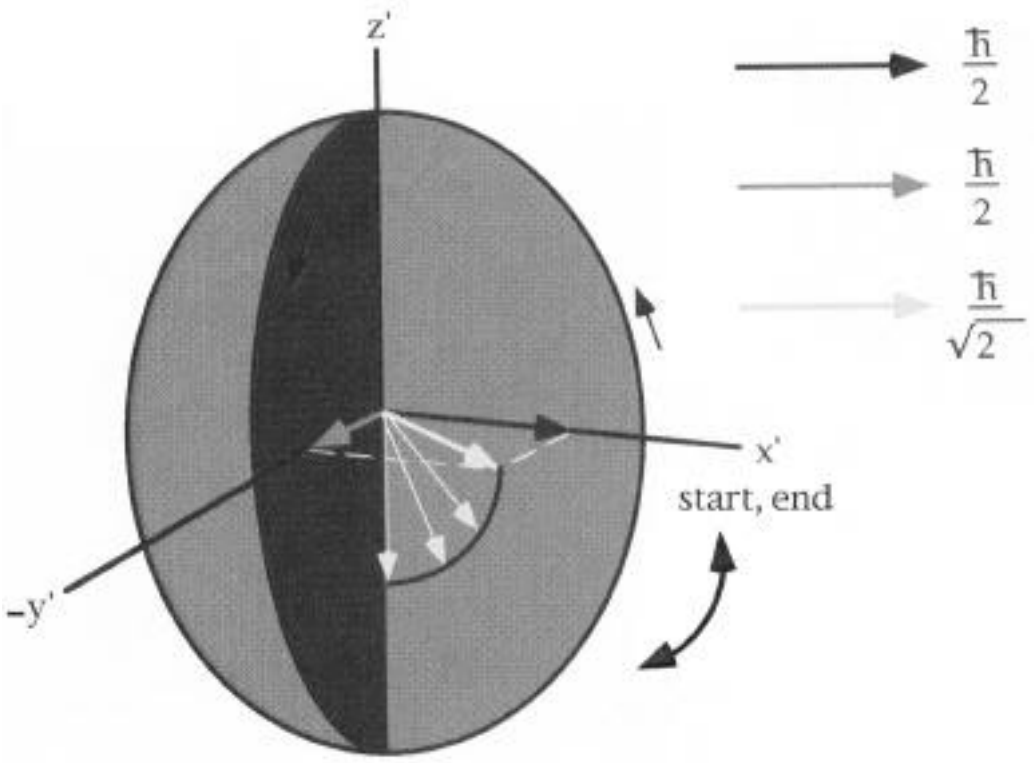

The total sum of the magnitude of the angular momentum of each infinetesimal point of the orbitsphere is $\hbar$ (Eq. (1.57)). Thus, the angular momentum of each great circle is $\frac{\hbar}{2}$. The planes of the great circles are oriented at an angle of $\frac{\pi}{2}$ with respect to each other, and the resultant angular momentum is $\frac{\hbar}{\sqrt{2}}$ in the xy-plane. Now, allow the

summation of the rotations by $\Delta\alpha$ to go from zero to $\sqrt{2}\pi$. For step one, the vector projection of the angular momentum onto the xy-plane goes as the magnitude of $\frac{\hbar}{\sqrt{2}}\cos\theta$ ($\left|\frac{\hbar}{\sqrt{2}}\cos\theta\right|$) for $0 \le \theta \le \frac{\pi}{2}$ where θ is defined as the angle of the resultant angular momentum vector of the orthogonal great circle current loops that moves along a great circle oriented at an angle of $\frac{\pi}{4}$ to the 1st xz-plane and the 1st yz-plane as shown in Figure 1.5 B. The trajectory of the resultant angular momentum vector is from $\theta = 0$ to $\theta = \frac{\pi}{2}$, and then from $\theta = \frac{\pi}{2}$ to $\theta = 0$. The vector projection of the angular momentum onto the negative z-axis goes as $\left|\frac{\hbar}{\sqrt{2}}\sin\theta\right|$ as shown in Figure 1.5 B. In each case, the projection of the angular momentum is periodic over the range of θ corresponding to $\Sigma\Delta\alpha$ which generates the angular momentum distribution. The projection in the xy-plane varies in magnitude from a maximum of $\frac{\hbar}{\sqrt{2}}$ to zero to $\frac{\hbar}{\sqrt{2}}$ again. The projection onto the negative z-axis varies in magnitude from zero to a maximum of $\frac{\hbar}{\sqrt{2}}$ to zero again. The total of each projection, $\langle \mathbf{L}_{xy} \rangle_{\Sigma\Delta\alpha}$ and $\langle \mathbf{L}_z \rangle_{\Sigma\Delta\alpha}$, is the integral of the magnitude of the vector as a function of θ. The result is the root mean square value (rms) of the maximum magnitude which is multiplied by one half corresponding to two steps (i.e. the electron angular momentum is distributed over 1/2 of the surface of a sphere in the first step, and the mirror image of the angular momentum distribution is generated in the second step given *infra*).

$$\langle \mathbf{L}_{xy} \rangle_{\Sigma\Delta\alpha} = \frac{1}{2}\frac{\hbar}{\sqrt{2}}\ \frac{1}{\sqrt{2}} = \frac{\hbar}{4} \tag{1.72}$$

$$\langle \mathbf{L}_z \rangle_{\Sigma\Delta\alpha} = \frac{1}{2}\frac{\hbar}{\sqrt{2}}\ \frac{1}{\sqrt{2}} = \frac{\hbar}{4} \tag{1.73}$$

For step two, the resultant angular momentum vector of the orthogonal great circle current loops of magnitude $\frac{\hbar}{\sqrt{2}}$ moves along a great circle oriented at an angle of $\frac{\pi}{4}$ to the 1st yz-plane and the 1st negative xz-plane (the plane containing the negative x-axis and the positive z-axis). For the vector current directions shown in Figure 1.5 A, as the $Y_0^0(\phi,\theta)$ orbitsphere equation of motion is completely generated in step two, the resultant angular momentum vector moves along the great circle from the xy-plane to the negative z-axis and back to the xy-plane such that the vector projections on to the z-axis all add positively and

the vector projections into the xy-plane sum to zero. The trajectory of the resultant angular momentum vector is shown in Figure 1.5 C.

Figure 1.5 C. The trajectory of the resultant angular momentum vector of the orthogonal great circle current loops of magnitude $\frac{\hbar}{\sqrt{2}}$ during step two.

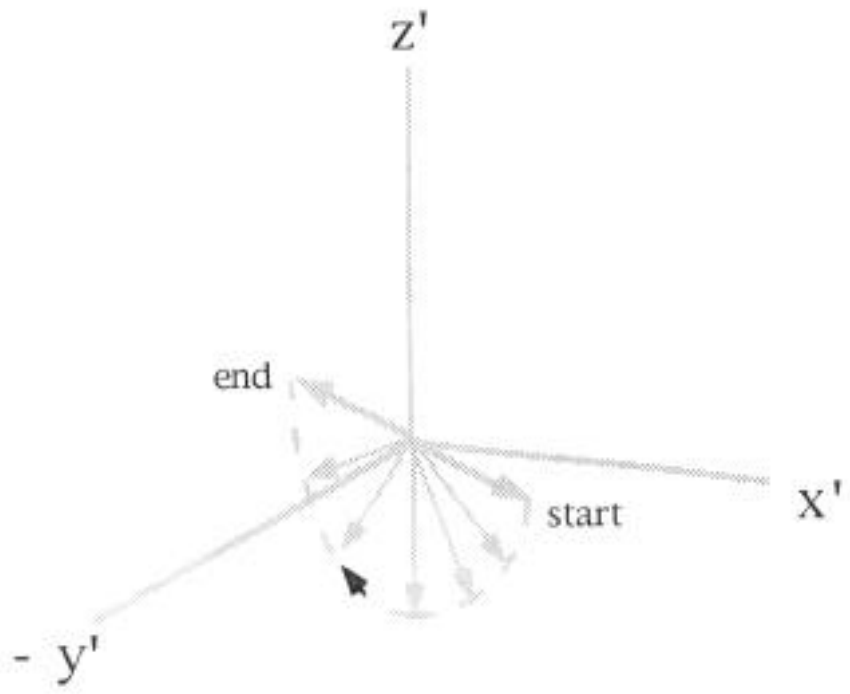

For step two, the trajectory of the resultant angular momentum vector is from $\theta = 0$ to $\theta = \pi$. The vector projection of the angular momentum onto the xy-plane goes as $\left|\frac{\hbar}{\sqrt{2}}\cos\theta\right|$ for $0 \le \theta \le \frac{\pi}{2}$ and $-\left|\frac{\hbar}{\sqrt{2}}\cos\theta\right|$ for $\frac{\pi}{2} \le \theta \le \pi$ as shown in Figure 1.5 C. The projection of the angular momentum is a periodic function of θ corresponding to $\Sigma\Delta\alpha'$ which generates the angular momentum distribution. The projection in the xy-plane varies in magnitude from a maximum of $\frac{\hbar}{\sqrt{2}}$ to zero to $-\frac{\hbar}{\sqrt{2}}$. For step two, the vector projection into the xy-plane, $\left\langle \mathbf{L}_{xy} \right\rangle_{\sum\Delta\alpha'}$ is zero, but the scalar sum of the angular momentum in the xy-plane is the absolute value of the integral of the magnitude of the vector as a function of θ. The result is the root mean square value (rms) of the maximum magnitude which is multiplied by one half corresponding to two steps

(i.e. the electron angular momentum is distributed over 1/2 of the surface of a sphere in the first step, and the mirror image of the angular momentum distribution is generated in the second step). The scalar sum is given by the magnitude of Eq. (1.72).

The vector projection of the angular momentum onto the negative z-axis goes as $\left|\frac{\hbar}{\sqrt{2}}\sin\theta\right|$ for $0 \le \theta \le \pi$ as shown in Figure 1.5 C. The vector projection onto the z-axis is periodic over the range of θ corresponding to $\Sigma\Delta\alpha$ which generates the angular momentum distribution and varies in magnitude from zero to a maximum of $\frac{\hbar}{\sqrt{2}}$ to zero again. The total of each projection, $\langle \mathbf{L}_z \rangle_{\sum \Delta\alpha'}$, is the integral of the magnitude of the vector as a function of θ. The result is the root mean square value (rms) of the maximum magnitude which is multiplied by one half corresponding to two steps (i.e. the electron angular momentum is distributed over 1/2 of the surface of a sphere in the first step, and the mirror image of the angular momentum distribution is generated in the second step). The vector sum is given by Eq. (1.73).

The total angular momentum of the orbitsphere is $\hbar$ (Eq. (1.57)). The vector projection of the angular momentum into the xy-plane is given by Eq. (1.72), and the scalar sum of the projection of the angular momentum into the xy-plane is $\frac{\hbar}{2}$. Consider steps one and two. As demonstrated by Figures 1.3, 1.4, and 1.5, each contribution to vector sum of the z component of the orbitsphere angular momentum is positive. Thus, the z-projection of the angular momentum is $\frac{\hbar}{2}$. Consider the case of a magnetic field applied to the orbitsphere. The magnetic moment corresponding to the angular momentum along the z-axis results in the alignment of the z-axis of the orbitsphere with the magnetic field. The angular momentum in the xy-plane precesses about the applied field; thus, the time average angular momentum in the xy-plane is zero. The angular momentum of the precessing orbitsphere can be given as an equivalent vector which precesses about the z-axis which possesses a scalar projection of the angular momentum into the xy-plane of $\frac{\hbar}{2}$ and a vector projection of the angular momentum onto the z-axis of $\frac{\hbar}{2}$. **S** the projection of the orbitsphere angular momentum that precesses about the z-axis called the spin axis at an angle of $\theta = \frac{\pi}{3}$ and an angle of $\phi = \pi$ with respect to $\langle \mathbf{L}_{xy} \rangle_{\sum \Delta\alpha}$ given by Eq. (1.72) is

$$\mathbf{S} = \pm\sqrt{\frac{3}{4}}\hbar \tag{1.74}$$

S rotates about the z-axis at the Larmor frequency; thus, $\langle \mathbf{S}_z \rangle$, the time averaged projection of the orbitsphere angular momentum onto the axis of the applied magnetic field is $\pm\frac{\hbar}{2}$. To verify the validity of Eq. (1.74), consider the components of the angular momentum along the z-axis and in the xy-plane from the perspective of a frame that rotates with **S** and from the presepective of the stationary or laboratory frame. In the rotating frame $\phi = 0$ is defined in the direction of the resultant angular momentum vector shown in Figure 1.5A. From Eq. (1.72), the angular momentum in this direction is $\frac{\hbar}{4}$. The angular momentum in the direction $\phi = \pi$ with respect to this direction is $\sqrt{\frac{3}{4}}\hbar\sin\frac{\pi}{3} = \frac{3}{4}\hbar$. Thus, in the rotating frame, the resultant scalar angular momentum in the xy plane is $\frac{\hbar}{2}$. **S** forms a cone in the nonrotating laboratory frame with a total angular momentum of $\hbar$. The projection of this angular momentum onto the z-axis is $\pm\hbar\cos\frac{\pi}{3} = \pm\frac{\hbar}{2}$. (The same result is obtained from the approach given by Eq. (3.35).) The plus or minus sign corresponds to the two possible vector orientations which are observed with the Stern-Gerlach experiment described below.

ROTATIONAL PARAMETERS OF THE ELECTRON (ANGULAR MOMENTUM, ROTATIONAL ENERGY, AND MOMENT OF INERTIA)

One result of the correlated motion along great circles is that some of the kinetic energy is not counted in the rotational energy. That is, for any spin axis there will be an infinite number of great circles with planes passing through that axis with θ angles other than 90°. All points on any one of these great circles will be moving, but not all of that motion will be part of the rotational energy; only that motion perpendicular to the spin axis will be part of the rotational energy. Thus, the rotational kinetic energy will always be less than the total kinetic energy. Furthermore, the following relationships must hold.

$$E_{rotational} = \frac{1}{2} I\omega^2 \le \frac{1}{2} m_e v^2 \tag{1.75}$$

$$I\omega \le \hbar \tag{1.76}$$

$$I \le m_e r^2 \tag{1.77}$$

Furthermore, it is known from the Stern-Gerlach experiment that a beam of silver atom splits into two components when passed through an

inhomogeneous magnetic field. This experiment implies a magnetic moment of one Bohr magneton and an associated angular momentum quantum number of 1/2. Historically, this quantum number is called the spin quantum number, and that designation will be retained. The angular momentum can be thought of arising from a spin component or equivalently an orbital component of the spin. The z-axis projection of the spin angular momentum was derived in the Spin Angular Momentum of the Orbitsphere with $\ell = 0$ Section.

$$L_z = I\omega \mathbf{i}_z = \pm\frac{\hbar}{2} \tag{1.78}$$

where ω is given by Eq. (1.55); so,

$\ell = \mathbf{0}$

$$|L_z| = I\frac{\hbar}{m_e r^2} = \frac{\hbar}{2} \tag{1.79}$$

Thus,

$$I_z = I_{spin} = \frac{m_e r_n^{\ 2}}{2} \tag{1.80}$$

From Eq. (1.51),

$$E_{rotational\ spin} = \frac{1}{2}\left[I_{spin}\omega^2\right] \tag{1.81}$$

From Eqs. (1.55) and (1.80),

$$E_{rotational} = E_{rotational\ spin} = \frac{1}{2}\left[I_{spin}\left(\frac{\hbar}{m_e r_n^{\ 2}}\right)^2\right] = \frac{1}{2}\left[\frac{m_e r_n^{\ 2}}{2}\left(\frac{\hbar}{m_e r_n^{\ 2}}\right)^2\right] = \frac{1}{4}\left[\frac{\hbar^2}{2I_{spin}}\right] \tag{1.82}$$

When $\ell \neq 0$, the spherical harmonic is not a constant and the charge-density function is not uniform over the orbitsphere. Thus, the angular momentum can be thought of arising from a spin component and an orbital component.

Derivation of the Rotational Parameters of the Electron

In the derivation of Eq. (1.59) and its solution for $E_{rotational}$ (Eq. (1.60)), the moment of inertia, I, was assumed by McQuarrie [11] to be the moment of inertia of a point particle, mr_n^2. However, the correct equation of the electron is a two dimensional shell with constant or a constant plus a spherical harmonic angular dependence. In that case, the relationships given by Eqs. (1.75) to (1.77) must hold.

The substitution of NI for I in the rigid rotor problem [11] where N is a constant does not change the form of the previous solution given by Eq. (1.60). However, the result that

$$N = \left[\frac{\ell(\ell+1)}{\ell^2 + 2\ell + 1}\right]^{\frac{1}{2}} < 1 \tag{1.83}$$

derived below gives

$$E_{rotational} = \frac{\hbar^2 \ell(\ell+1)}{2I(\ell^2+2\ell+1)} \tag{1.84}$$

and gives the moment of inertia of the orbitsphere, $I_{orbital}$, where $\ell \neq 0$ as

$$NI = I_{orbital} = m_e r_n^2 \left[\frac{\ell(\ell+1)}{(\ell^2+2\ell+1)}\right]^{\frac{1}{2}} \tag{1.85}$$

The solution of Eq. (1.59) for $|L|$, the magnitude of the orbital angular momentum is [11]

$$|L| = \hbar\sqrt{\ell(\ell+1)} \tag{1.86}$$

where I of Eq. (1.59) is the moment of inertia of a point charge. It is demonstrated by Eq. (1.57) that the total sum of the magnitudes of the angular momenta of the infinitesimal points of the electron orbitsphere is $\hbar$; therefore, the magnitude of the angular momentum of an electron orbitsphere must be less than $\hbar$, and the moment of inertia must be less than that given by $m_e r_n^2$. For example, the moment of inertia of the uniform spherical shell, I_{RS}, is [13]

$$I_{RS} = \frac{2}{3} m r_n^2 \tag{1.87}$$

Thus, Eq. (1.86) must be multiplied by a fraction, $\frac{1}{K}$, to give the correct angular momentum. Given that generally **L** is

$$\mathbf{L} = I\omega\mathbf{i}_z \tag{1.88}$$

then

$$I_{orbital}\omega\mathbf{i}_z = \hbar\frac{1}{K}\sqrt{\ell(\ell+1)}, \tag{1.89}$$

where ω is given by Eq. (1.55). The orbital moment of inertia, $I_{orbital}$, is

$$I_{orbital} = m_e r_n^2 \frac{1}{K}\sqrt{\ell(\ell+1)} \tag{1.90}$$

The total kinetic energy, T, of the orbitsphere is

$$T = \frac{1}{2} m_e v_n^2 \tag{1.91}$$

Substitution of Eq. (1.56) gives

$$T = \frac{\hbar^2}{2 m_e r_n^2} \tag{1.92}$$

$E_{rotational}$ of the rigid shell is given by Eq. (1.51) with I given by Eq. (1.87). $E_{rotational\,\mathrm{orbital}}$ of the orbitsphere is given by Eq. (1.60) multiplied by the fraction $\frac{1}{K^2}$ so that Eqs. (1.75) to (1.77) hold with $I = m_e r_n^2$.

$$E_{rotational\,\mathrm{orbital}} = \frac{\hbar^2}{2I}\left[\frac{\ell(\ell+1)}{K^2}\right] \tag{1.93}$$

Eq. (1.59) can be expressed in terms of the variable x which is

substituted for $\cos\theta$. The resulting function $P(x)$ is called Legendre's equation and is a well-known equation in classical physics. It occurs in a variety of problems that are formulated in spherical coordinates. When the power series method of solution is applied to $P(x)$, the series must be truncated in order that the solutions be finite at $x = \pm 1$. The solution to Legendre's equation given by Eq. (1.60) is the maximum term of a series of solutions corresponding to the m and ℓ values [11,14]. The rotational energy must be normalized by the total number of states-each corresponding to a set of quantum numbers of the power series solution. As demonstrated in the Excited States of the One Electron Atom (Quantization) Section, the quantum numbers of the excited states are

$$n = 2,3,4,...$$
$$\ell = 1,2,..., n-1$$
$$m = -\ell, -\ell+1,...,0,...,+\ell$$

In the case of an orbitsphere excited state, each rotational state solution of Eq. (1.59) (Legendre's equation) corresponds to a multipole moment of the charge-density function (Eq. (1.65)). $E_{rotational\,\mathrm{orbital}}$ is normalized by N, the total number of multipole moments. N, the total number of multipole moments where each corresponds to an ℓ and m_ℓ quantum number of an energy level corresponding to a principal quantum number of n is

$$N = \sum_{\ell=0}^{n-1} \sum_{m_\ell=-\ell}^{+\ell} = \sum_{\ell=0}^{n-1} 2\ell+1 = n^2 = \ell^2 + 2\ell + 1 \tag{1.94}$$

Thus, K^2 is equal to N given by Eq. (1.94). Substitution of Eq. (1.94) into Eq. (1.93) gives

$$E_{rotational\,\mathrm{orbital}} = \frac{\hbar^2}{2I}\left[\frac{\ell(\ell+1)}{\ell^2+2\ell+1}\right] \tag{1.95}$$

Substitution of Eq. (1.94) into Eq. (1.90) gives the orbital moment of inertia.

$$I_{orbital} = m_e r_n^{\,2}\left[\frac{\ell(\ell+1)}{\ell^2+2\ell+1}\right]^{\frac{1}{2}} \tag{1.96}$$

In the case of the excited states, the orbitsphere charge-density function for $\ell \neq 0$, Eq. (1.65), is the sum of two functions of equal magnitude. $\mathbf{L}_z$, total is given by the sum of the spin and orbital angular momenta. The principal energy levels of the excited states are split when a magnetic field is applied. The energy shift due to spin and orbital angular momenta are given in the Spin and Orbital Splitting Section.

$\ell \neq 0$

$$L_{z\,total} = L_{z\,spin} + L_{z\,orbital} \tag{1.97}$$

Similarly, the orbital rotational energy arises from a spin function (spin angular momentum) modulated by a spherical harmonic angular function (orbital angular momentum). The time-averaged orbital rotational energy is zero; the magnitude is given by Eq. (1.95); the rotational energy due to spin is given by Eq. (1.82); the total kinetic energy is given by Eq. (1.92).

$$\langle E_{rotational\,\mathrm{orbital}} \rangle = 0 \tag{1.98}$$

The demonstration that the modulated orbitsphere solutions are solutions of the wave equation appears in Box 1.1.

BOX 1.1. DERIVATION OF THE ROTATIONAL PARAMETERS OF THE ELECTRON FROM A SPECIAL CASE OF THE WAVE EQUATION--THE RIGID ROTOR EQUATION

For a time harmonic charge density function, Eq. (1.49) becomes

$$\left[\frac{1}{r^2\sin\theta}\frac{\delta}{\delta\theta}\left(\sin\theta\frac{\delta}{\delta\theta}\right)_{r,\phi} + \frac{1}{r^2\sin^2\theta}\left(\frac{\delta^2}{\delta\phi^2}\right)_{r,\theta} + \frac{\omega^2}{v^2}\right]A(\theta,\phi) = 0 \tag{1}$$

Substitution of the velocity about a Cartesian coordinate axis, $v = \rho\omega$, into Eq. (1) gives

$$\left[\frac{1}{r^2\sin\theta}\frac{\delta}{\delta\theta}\left(\sin\theta\frac{\delta}{\delta\theta}\right)_{r,\phi} + \frac{1}{r^2\sin^2\theta}\left(\frac{\delta^2}{\delta\phi^2}\right)_{r,\theta} + \frac{\omega^2}{(\rho\omega)^2}\right]A(\theta,\phi) = 0 \tag{2}$$

Substitution of Eq. (1.55) into Eq. (1.2) gives

$$\left[\frac{1}{r^2\sin\theta}\frac{\delta}{\delta\theta}\left(\sin\theta\frac{\delta}{\delta\theta}\right)_{r,\phi} + \frac{1}{r^2\sin^2\theta}\left(\frac{\delta^2}{\delta\phi^2}\right)_{r,\theta} + \frac{\omega_n^2}{\left(\rho\frac{\hbar}{m_e r_n^2}\dot{\phi}\right)^2}\right]A(\theta,\phi) = 0 \tag{4}$$

Multiplication by the denominator of the second term in Eq. (3) gives

$$\left(\rho\frac{\hbar}{m_e r_n^2}\dot{\phi}\right)^2\left[\frac{1}{r^2\sin\theta}\frac{\delta}{\delta\theta}\left(\sin\theta\frac{\delta}{\delta\theta}\right)_{r,\phi} + \frac{1}{r^2\sin^2\theta}\left(\frac{\delta^2}{\delta\phi^2}\right)_{r,\theta} + \omega_n^2\right]A(\theta,\phi) = 0 \tag{4}$$

Substitution of Eq. (1.51) gives

$$\left(\rho\frac{\hbar}{m_e r_n^2}\dot{\phi}\right)^2\left[\frac{1}{r^2\sin\theta}\frac{\delta}{\delta\theta}\left(\sin\theta\frac{\delta}{\delta\theta}\right)_{r,\phi} + \frac{1}{r^2\sin^2\theta}\left(\frac{\delta^2}{\delta\phi^2}\right)_{r,\theta} + \frac{2E_{rot}}{I}\right]A(\theta,\phi) = 0 \tag{5}$$

The total rotational energy is given by the superposition of ℓ quantum states corresponding to a multipole expansion of total rotational energy of the orbitsphere. The total number, N, of multipole moments where

each corresponds to an ℓ and m_ℓ quantum number of an energy level corresponding to a principal quantum number of n is

$$N = \sum_{\ell=0}^{n-1} \sum_{m_\ell=-\ell}^{+\ell} = \sum_{\ell=0}^{n-1} 2\ell + 1 = \ell^2 + 2\ell + 1 = n^2 \tag{6}$$

Summing over all quantum states gives

$$\left[\sum_{\ell=0}^{n-1} \sum_{m_\ell=-\ell}^{+\ell} \left(\rho \frac{\hbar}{m_e r_n^2}\right)^2 \left[\frac{1}{r^2 \sin\theta} \frac{\delta}{\delta\theta}\left(\sin\theta \frac{\delta}{\delta\theta}\right)_{r,\phi} + \frac{1}{r^2 \sin^2\theta}\left(\frac{\delta^2}{\delta\phi^2}\right)_{r,\theta}\right] + \sum_{\ell=0}^{n-1} \sum_{m_\ell=-\ell}^{+\ell} \frac{2E_{rot}}{I}\right] A(\theta,\phi) = 0 \tag{7}$$

Each of the orbital energy, orbital moment of inertia, and orbital angular momentum is a modulation of the orbitsphere function. Thus, the sum of ρ^2 over all ℓ quantum numbers is r_n. Substitution of $\rho_z = r_n \cos\theta$; $\rho_x = r_n \sin\theta \cos\phi$; $\rho_y = r_n \sin\theta \sin\phi$ into Eq. (7) gives

$$\left[r_n \frac{\hbar}{m_e r_n^2}\right]^2 \left[\frac{1}{r_n^2 \sin\theta} \frac{\delta}{\delta\theta}\left(\sin\theta \frac{\delta}{\delta\theta}\right)_{r,\phi} + \frac{1}{r_n^2 \sin^2\theta}\left(\frac{\delta^2}{\delta\phi^2}\right)_{r,\theta}\right] + \left(\ell^2 + 2\ell + 1\right)\frac{2E_{rot}}{I}\right] A(\theta,\phi) = 0 \tag{8}$$

where $\frac{2E_{rot}}{I}$ is the constant, ω_n given by Eq. (1.55), and $r = r_n$. Eq. (8) can be expressed in terms of the rotational energy of any given mode by dividing the denominator of the first term by, K^2, the factor corresponding to the vector projection of the rotational energy onto the z-axis.

$$\left[\frac{I\hbar^2}{2m_e^2 r_n^4\left(\ell^2 + 2\ell + 1\right)}\left[\frac{1}{\sin\theta} \frac{\delta}{\delta\theta}\left(\sin\theta \frac{\delta}{\delta\theta}\right)_{r,\phi} + \frac{1}{\sin^2\theta}\left(\frac{\delta^2}{\delta\phi^2}\right)_{r,\theta}\right] + E_{rot}\right] A(\theta,\phi) = 0 \tag{9}$$

In the case that E_{rot} is the total rotational energy which is equal to the kinetic energy of the orbitsphere given by Eq. (1.92) and that the moment of inertia is given by

$$I = m_e r_n^2 \tag{10}$$

Eq. (9) becomes equivalent to Eq. (1.59).

$$\left[\frac{1}{N}\frac{\hbar^2}{2I}\left[\frac{1}{\sin\theta} \frac{\delta}{\delta\theta}\left(\sin\theta \frac{\delta}{\delta\theta}\right)_{r,\phi} + \frac{1}{\sin^2\theta}\left(\frac{\delta^2}{\delta\phi^2}\right)_{r,\theta}\right] + E_{rot\ total}\right] A(\theta,\phi) = 0 \tag{11}$$

where N is one. Eq. (11) applies to all of the multipole modes of the rotational energy with the appropriate moment of inertia, I, and factor N; thus, the rotational energy of each mode is given by Eq. (1.58) with these conditions. Eq. (9) can be expressed in terms of the rotational energy of any given mode by dividing the first term by, K^2, the factor corresponding to the vector projection of the rotational energy and the

moment of inertia onto the z-axis.

$$\frac{I\hbar^2}{2m_e^2 r_n^4 K^2\left(\ell^2+2\ell+1\right)}\left[\frac{1}{\sin\theta}\frac{\delta}{\delta\theta}\left(\sin\theta\frac{\delta}{\delta\theta}\right)_{r,\phi}+\frac{1}{\sin^2\theta}\left(\frac{\delta^2}{\delta\phi^2}\right)_{r,\theta}\right]+E_{rot}\right]A(\theta,\phi)=0 \tag{12}$$

where in the case of the spherical harmonics, $N=\ell^2+2\ell+1$. From Eq. (1.51) and Eq. (1.88), Eq. (12) can be expressed as

$$\left[\frac{\hbar^2}{m_e^2 r_n^4 K^2\left(\ell^2+2\ell+1\right)}\left[\frac{1}{\sin\theta}\frac{\delta}{\delta\theta}\left(\sin\theta\frac{\delta}{\delta\theta}\right)_{r,\phi}+\frac{1}{\sin^2\theta}\left(\frac{\delta^2}{\delta\phi^2}\right)_{r,\theta}\right]+\frac{L^2}{I^2}\right]A(\theta,\phi)=0 \tag{13}$$

In the case of the spherical harmonic functions with Eq. (1.88) and Eq. (1.55), Eq. (12) gives

$$\sqrt{\frac{\hbar^2\left(\ell(\ell+1)\right)}{m_e^2 r_n^4 K^2\left(\ell^2+2\ell+1\right)}}=\frac{L}{I}=\frac{\hbar}{m_e r_n^2} \tag{14}$$

Thus,

$$\sqrt{\frac{\left(\ell(\ell+1)\right)}{\left(\ell^2+2\ell+1\right)}}=K \tag{15}$$

Eq. (12) becomes Eq. (11) where the rotational energy is given by Eq. (1.95).

$$E_{rotational\,\text{orbital}}=\frac{\hbar^2}{2I}\left[\frac{\ell(\ell+1)}{\ell^2+2\ell+1}\right] \tag{16}$$

and the orbital moment of inertia is given by Eq. (1.96).

$$I_{orbital}=m_e r_n^{\,2}\left[\frac{\ell(\ell+1)}{\ell^2+2\ell+1}\right]^{\frac{1}{2}} \tag{17}$$

The Substitution of Eqs. (1.65), (6), and (16) into Eq. (11) gives

$$-\frac{\hbar^2}{2I}\left[\frac{\ell(\ell+1)}{\ell^2+2\ell+1}\right]+\frac{\hbar^2}{2m_e r_n^2}\sqrt{\frac{\ell(\ell+1)}{\ell^2+2\ell+1}}=0 \tag{18}$$

Substitution of Eq. (17) into Eq. (18) gives

$$-\frac{\hbar^2}{2m_e r_n^2\sqrt{\frac{\ell(\ell+1)}{\ell^2+2\ell+1}}}\left[\frac{\ell(\ell+1)}{\ell^2+2\ell+1}\right]+\frac{\hbar^2}{2m_e r_n^2}\sqrt{\frac{\ell(\ell+1)}{\ell^2+2\ell+1}}=0 \tag{19}$$

$$0=0 \tag{20}$$

Thus, the modulated orbitsphere solutions are shown to be solutions of the wave equation by their substitution into the wave equation (Eqs. (18-20). The present derivation of the rigid rotor equation given by the substitution of

$$\begin{aligned} E_{rot}&=\frac{1}{2}I\omega_n^2 \\ \omega_n&=\frac{\hbar}{m_e r_n^2} \\ v&=\rho\omega_n \end{aligned} \tag{21}$$

is consistent with the wave equation relationship:

$$v = \lambda \frac{\omega}{2\pi} \tag{22}$$

Whereas, Schrodinger's derivation from the Helmholtz equation [1] with the substitution of

$$\lambda = \frac{h}{m_e v} \tag{23}$$

gives the rigid rotor equation with the paradox that

$$v^2 = \frac{h}{m_e} \frac{\omega}{2\pi} \tag{24}$$

which is not the wave relationship,

$$v = \lambda \frac{\omega}{2\pi} \tag{25}$$

References

1. McQuarrie, D. A., Quantum Chemistry, University Science Books, Mill Valley, CA, (1983), pp. 78-79.

MAGNETIC PARAMETERS OF THE ELECTRON (BOHR MAGNETON)

The Magnetic Field of an Orbitsphere from Spin

The orbitsphere is a shell of negative charge current comprising correlated charge motion along great circles. For $\ell = 0$, the orbitsphere gives rise to a magnetic moment of 1 Bohr magneton [16] as shown in the Derivation of the Magnetic Field Section,

$$\mu_B = \frac{e\hbar}{2m_e} = 9.274\ X\ 10^{-24}\ JT^{-1}, \tag{1.99}$$

and a magnetic field derived below.

$$\mathbf{H} = \frac{e\hbar}{m_e r_n^3}(\mathbf{i}_r \cos\theta - \mathbf{i}_\theta \sin\theta) \qquad \text{for } r < r_n \tag{1.100}$$

$$\mathbf{H} = \frac{e\hbar}{2m_e r^3}(\mathbf{i}_r 2\cos\theta - \mathbf{i}_\theta \sin\theta) \qquad \text{for } r > r_n \tag{1.101}$$

It follows from Eq. (1.99), the relationship for the Bohr magneton, and relationship between the magnetic dipole field and the magnetic moment **m** [17] that Eqs. (1.100) and (1.101) are the equations for the magnetic field due to a magnetic moment of a Bohr magneton, $\mathbf{m} = \mu_B \mathbf{i_z}$ where $\mathbf{i_z} = \mathbf{i_r}\cos\theta - \mathbf{i}_\theta \sin\theta$. Note that the magnetic field is a constant for $r < r_n$. See Figure 1.6. It is shown in the Magnetic Parameters of the Electron

(Bohr Magneton) Section that the energy stored in the magnetic field of the electron orbitsphere is

$$E_{mag,total} = \frac{\pi \mu_o e^2 \hbar^2}{m_e^2 r_1^3} \tag{1.102}$$

Figure 1.6. The magnetic field of an electron orbitsphere.

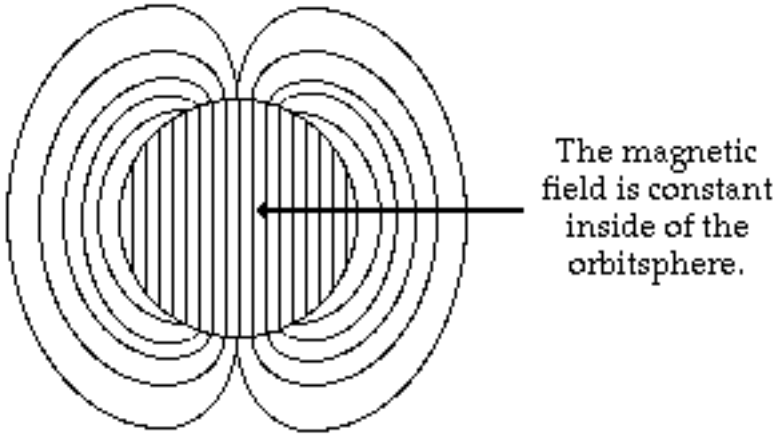

Derivation of the Magnetic Field

Consider Figure 1.6. The magnetic field must satisfy the following relationships:

$$\mathrm{H} = 0 \textit{ in free space} \tag{1.103}$$

$$\mathbf{n} X (\mathbf{H}_a - \mathbf{H}_b) = \mathbf{K} \tag{1.104}$$

$$\mathbf{n} \cdot (\mathbf{H}_a - \mathbf{H}_b) = 0 \tag{1.105}$$

$$\mathbf{H} = -\nabla \psi \tag{1.106}$$

The z component of the current, $|i|$, for a current loop of total charge, e, oriented at an angle θ with respect to the z-axis is given as the product of the charge, the angular velocity (The orbitsphere angular velocity is given by Eq. (1.55).), and $\sin\theta$.

$$|i| = \frac{e\hbar}{m_e r_n^2} \sin\theta \tag{1.107}$$

Consider the orbitsphere depicted in Figures 1.3, 1.4, and 1.5. The surface current-density function, $\mathbf{K}i_\phi$, is perpendicular to the angular momentum. As shown in the Spin Angular Momentum Section, the

vector projection of the orbitsphere angular momentum onto the xy-plane goes as $|\cos\Delta\alpha|$ as shown in Figure 1.5 B. It is periodic over the range of $\Sigma\Delta\alpha$ and $\Sigma\Delta\alpha'$ and varies in magnitude from a maximum of $\frac{\hbar}{\sqrt{2}}$ to zero to $\frac{\hbar}{\sqrt{2}}$ again. The projection of the charge-density of the orbitsphere onto the xy-plane (perpendicular to the z-axis) which carries the incremental current, $\mathbf{i}i_\phi$, is a function of $\sin\theta$. The angular function of the current-density of the orbitsphere is normalized to that of one electron.

$$N = \frac{1}{\int_0^\pi \sin^2\theta \sin\theta d\theta} = \frac{3}{4} \tag{1.108}$$

Due to the precession of the **S**-axis about the z axis, the time averaged projection of the angular momentum of the electron orbitsphere onto the xy-plane is zero. Therefore, the current corresponding to the total charge of the electron is about the z-axis, and the angular velocity of the spinning orbitsphere is twice that of a stationary orbitsphere. As shown in Figure 1.5 B, the projection of the angular momentum is only onto the negative z-axis of length r_n. Thus, the incremental current-density $d\mathbf{K}i_\phi$ along the z-axis is given by dividing $\mathbf{i}i_\phi$ by the length, r_n. The current-density of the orbitsphere in the incremental length dz is

$$\mathbf{K}(\rho,\phi,z) = \mathbf{i}_\phi 2N\frac{e\hbar}{m_e r_n^3} = \mathbf{i}_\phi \frac{3}{2}\frac{e\hbar}{m_e r_n^3} \tag{1.109}$$

Because

$$z = r\cos\theta \tag{1.110}$$

a differential length

$$dz = -\sin\theta r_n d\theta \tag{1.111}$$

and so the current-density in the differential length $r_n d\theta$ as measured along the periphery of the orbitsphere is a function of $\sin\theta$. Thus, the surface current-density function is given by

$$\mathbf{K}(r,\theta,\varphi) = \mathbf{i}_\phi \frac{3}{2}\frac{e\hbar}{m_e r_n^3}\sin\theta \tag{1.112}$$

Substitution of Eq. (1.112) into Eq. (1.104) gives

$$H_\theta^a - H_\theta^b = \frac{3}{2}\frac{e\hbar}{m_e r_n^3}\sin\theta \tag{1.113}$$

To obtain H_θ, the derivative of Ψ with respect to θ must be taken, and this suggests that the θ dependence of Ψ be taken as $\cos\theta$. The field is finite at the origin and is zero at infinity; so, solutions of Laplace's equation in spherical coordinates are selected because they are consistent with these conditions [18].

$$\Psi = C\left(\frac{r}{r_n}\right)\cos\theta \; ; \qquad r < r_n \tag{1.114}$$

$$\Psi = A\left(\frac{r_n}{r}\right)^2\cos\theta \; ; \qquad r > r_n \tag{1.115}$$

The negative gradient of these potentials is

$$\mathbf{H} = \frac{-C}{r_n}(\mathbf{i}_r\cos\theta - \mathbf{i}_\theta\sin\theta) \quad \text{for } r < r_n \tag{1.116}$$

$$\mathbf{H} = \frac{A}{r_n}\left(\frac{r_n}{r}\right)^3(\mathbf{i}_r 2\cos\theta + \mathbf{i}_\theta\sin\theta) \quad \text{for } r > r_n \tag{1.117}$$

The continuity conditions of Eqs. (1.104), (1.105), (1.112), and (1.113) and are applied to obtain the following relationships among the variables

$$\frac{-C}{r_n} = \frac{2A}{r_n} \tag{1.118}$$

$$\frac{A}{r_n} - \frac{C}{r_n} = \frac{3}{2}\frac{e\hbar}{m_e r_n^3} \tag{1.119}$$

Solving the variables algebraically gives the magnetic fields of an electron:

$$\mathbf{H} = \frac{e\hbar}{m_e r_n^3}(\mathbf{i}_r\cos\theta - \mathbf{i}_\theta\sin\theta) \qquad \text{for } r < r_n \tag{1.120}$$

$$\mathbf{H} = \frac{e\hbar}{2m_e r^3}(\mathbf{i}_r 2\cos\theta - \mathbf{i}_\theta\sin\theta) \quad \text{for } r > r_n \tag{1.121}$$

Derivation of the Energy

The energy stored in the magnetic field of the electron is

$$E_{mag} = \frac{1}{2}\mu_o\int_0^{2\pi}\int_0^{\pi}\int_0^{\infty} H^2 r^2\sin\theta\, dr d\theta d\Phi \tag{1.122}$$

$$E_{mag\,\text{total}} = E_{mag\,\text{external}} + E_{mag\,\text{internal}} \tag{1.123}$$

$$E_{mag\,\text{internal}} = \frac{1}{2}\mu_o\int_0^{2\pi}\int_0^{\pi}\int_0^{r_1}\left(\frac{e\hbar}{m_e r_1^3}\right)^2\left(\cos^2\theta + \sin^2\theta\right)r^2\sin\theta\, dr d\theta d\Phi \tag{1.124}$$

$$= \frac{2\pi\mu_o e^2\hbar^2}{3m_e^2 r_1^3} \tag{1.125}$$

$$E_{mag\ \text{external}} = \frac{1}{2}\mu_o \int_0^{2\pi}\int_0^{\pi}\int_{r_1}^{\infty} \left(\frac{e\hbar}{2m_e r_1^3}\right)^2 \left(4\cos^2\theta + \sin^2\theta\right) r^2 \sin\theta\, dr\, d\theta\, d\Phi \tag{1.126}$$

$$= \frac{\pi\mu_o e^2\hbar^2}{3m_e^2 r_1^3} \tag{1.127}$$

$$E_{mag\ \text{total}} = \frac{2\pi\mu_o e^2\hbar^2}{3m_e^2 r_1^3} + \frac{\pi\mu_o e^2\hbar^2}{3m_e^2 r_1^3} \tag{1.128}$$

$$E_{mag\ \text{total}} = \frac{\pi\mu_o e^2\hbar^2}{m_e^2 r_1^3} \tag{1.129}$$

STERN-GERLACH EXPERIMENT

The sum of the $\mathbf{L}_i$, the magnitude of the angular momentum of each infinitesimal point of the orbitsphere of mass m_i, must be constant. The constant is $\hbar$.

$$\sum |\mathbf{L}_i| = \sum |\mathbf{r} \times m_i \mathbf{v}| = m_e r_n \frac{\hbar}{m_e r_n} = \hbar \tag{1.130}$$

where the velocity is given by Eq. (1.47). Furthermore, it is known from the Stern-Gerlach experiment that a beam of silver atoms is split into two components when passed through an inhomogeneous magnetic field. The measured angular momentum in the direction of the applied field (spin axis) is $\pm\frac{\hbar}{2}$, and the magnitude of the angular momentum vector which precesses about the spin axis is $\sqrt{\frac{3}{4}}\hbar$ As demonstrated in the Orbitsphere Equation of Motion Section, the projection of the total orbitsphere angular momentum onto the spin axis is $\pm\frac{\hbar}{2}$, and the projection onto **S**, the axis which precesses about the spin axis, is $\sqrt{\frac{3}{4}}\hbar$. The Stern-Gerlach experiment implies a magnetic moment of one Bohr magneton and an associated angular momentum quantum number of 1/2. Historically, this quantum number is called the spin quantum number, s ($s = \frac{1}{2}; m_s = \pm\frac{1}{2}$), and that designation is maintained.

ELECTRON g FACTOR

As demonstrated by Purcell [19], when a magnetic field is applied to an electron in a central field which comprises a current loop, the

orbital radius does not change, but the velocity changes as follows:

$$\Delta \mathbf{v} = \frac{er\mathbf{B}}{2m_e} \tag{1.131}$$

The angular momentum of the electron orbitsphere is $\hbar$ as given by Eq. (1.57), and as demonstrated in Figure 1.5, $\frac{\hbar}{2}$ of the orbitsphere angular momentum is in the plane perpendicular to any applied magnetic field. The angular momentum in the presence of an applied magnetic field is

$$\mathbf{L} = \mathbf{r} \times (m_e \mathbf{v} + e\mathbf{A}) \tag{1.132}$$

where $\mathbf{A}$ is the vector potential of the external field evaluated at the location of the orbitsphere. Conservation of angular momentum of the orbitsphere permits a discrete change of its "kinetic angular momentum" ($\mathbf{r} \times m\mathbf{v}$) by the field of $\frac{\hbar}{2}$, and concomitantly the "potential angular momentum" ($\mathbf{r} \times e\mathbf{A}$) must change by - $\frac{\hbar}{2}$. The flux change, ϕ, of the orbitsphere for $r < r_n$ is determined as follows:

$$\Delta \mathbf{L} = \frac{\hbar}{2} - \mathbf{r} \times e\mathbf{A} \tag{1.133}$$

$$= \frac{\hbar}{2} - \frac{e 2\pi r A}{2\pi} \tag{1.134}$$

$$= \frac{\hbar}{2} - \frac{e\phi}{2\pi} \tag{1.135}$$

In order that the change of angular momentum, $\Delta \mathbf{L}$, equals zero, ϕ must be $\Phi_0 = \frac{h}{2e}$, the magnetic flux quantum. Thus, to conserve angular momentum in the presence of an applied magnetic field, the orbitsphere magnetic moment can be parallel or antiparallel to an applied field as observed with the Stern-Gerlach experiment, and the flip between orientations (a rotation of $\frac{\pi}{2}$) is accompanied by the "capture" of the magnetic flux quantum by the orbitsphere "coils" comprising infinitesimal loops of charge moving along geodesics (great circles).

The energy to flip the orientation of the orbitsphere due to its magnetic moment of a Bohr magneton, μ_B, is

$$\Delta E_{mag}^{spin} = 2\mu_B \mathbf{B} \tag{1.136}$$

where

$$\mu_B = \frac{e\hbar}{2m_e} \tag{1.137}$$

The energy change corresponding to the "capture" of the magnetic flux quantum is derived below. From Eq. (1.129) for one electron,

$$E_{mag} = \frac{\pi\mu_0 e^2\hbar^2}{(m_e)^2 r_n^3} \tag{1.138}$$

is the energy stored in the magnetic field of the electron. The orbitsphere is equivalent to a Josephson junction which can trap integer numbers of fluxons where the quantum of magnetic flux is $\Phi_0 = \frac{h}{2e}$.

Consider Eq. (1.138). During the flip transition a fluxon treads the orbitsphere at the speed of light; therefore, the radius of the orbitsphere in the lab frame is 2π times the relativistic radius in the fluxon frame. Thus, the energy of the transition corresponding to the "capture" of a fluxon by the orbitsphere, ΔE_{mag}^{fluxon}, is

$$\Delta E_{mag}^{fluxon} = \frac{\pi\mu_o e^2\hbar^2}{(m_e)^2(2\pi r_n)^3} \tag{1.139}$$

$$= \frac{\mu_o e^2}{4\pi^2 m_e r_n}\left(\frac{e\hbar}{2m_e}\right)\left(\frac{h}{2e\pi r_n^2}\right) \tag{1.140}$$

$$= \frac{\mu_o e^2}{4\pi^2 m_e r_n}\mu_B\left(\frac{\Phi_0}{A}\right) \tag{1.141}$$

where **A** is the area and Φ_0 is the magnetic flux quantum.

$$\Delta E_{mag}^{fluxon} = 2\left[\frac{e^2\mu_o}{2m_e r_n}\right]\frac{1}{4\pi^2}\mu_B B \tag{1.142}$$

where the nth fluxon treading through the area of the orbitsphere is equivalent to the applied magnetic flux. Furthermore, the term in brackets can be expressed in terms of the fine structure constant, α ,as follows:

$$\frac{e^2\mu_o}{2m_e r_n} = \frac{e^2\mu_o cv}{2m_e v r_n c} \tag{1.143}$$

Substitution of Eq. (1.47) gives

$$\frac{e^2\mu_o cv}{2\hbar c} \tag{1.144}$$

Substitution of

$$c = \sqrt{\frac{1}{\varepsilon_o\mu_o}} \tag{1.145}$$

and

$$\alpha = \frac{\mu_o e^2 c}{2h} \tag{1.146}$$

gives

$$\frac{e^2\mu_o cv}{2\hbar c} = 2\pi\alpha\frac{v}{c} \tag{1.147}$$

The fluxon treads the orbitsphere at $v = c$. Thus,

$$\Delta E_{mag}^{fluxon} = 2\frac{\alpha}{2\pi}\mu_B B \tag{1.148}$$

The principal energy of the transition of reorientation of the orbitsphere is given by Eq. (1.136). And, the total energy of the flip transition is the sum of Eq. (1.148), the energy of a fluxon treading the orbitsphere and Eq. (1.136), the energy of reorientation of the magnetic moment.

$$\Delta E_{mag}^{spin} = 2\left(\mu_B \mathbf{B} + \frac{\alpha}{2\pi}\mu_B \mathbf{B}\right) \tag{1.149}$$

$$\Delta E_{mag}^{spin} = 2\left(1+\frac{\alpha}{2\pi}\right)\mu_B \mathbf{B} \tag{1.150}$$

$$\Delta E_{mag}^{spin} = 2g\mu_B \mathbf{B} \tag{1.151}$$

The magnetic moment of Eq. (1.136) is twice that from the gyromagnetic ratio as given by Eq. (2.36) of the Orbital and Spin Splitting Section. The magnetic moment of the electron is the sum of the component corresponding to the kinetic angular momentum, $\frac{\hbar}{2}$, and the component corresponding to the vector potential angular momentum, $\frac{\hbar}{2}$, (Eq. (1.132). The spin-flip transition can be considered as involving a magnetic moment of g times that of a Bohr magneton. The factor g is redesignated the fluxon g factor as opposed to the anomalous g factor and its value is 1.00116. The experimental value is 1.00116. Additional small corrective terms to the g factor arise as a result of the radiative reaction force [20].

DETERMINATION OF ORBITSPHERE RADII, r_n

The one-electron orbitsphere is a spherical shell of negative charge (total charge = $-e$) of zero thickness at a distance r_n from the nucleus (charge = $+Ze$). It is well known that the field of a spherical shell of charge is zero inside the shell and that of a point charge at the origin outside the shell [21]. See Figure 1.7.

Figure 1.7 The electric fields of a proton, an electron, and a hydrogen atom.

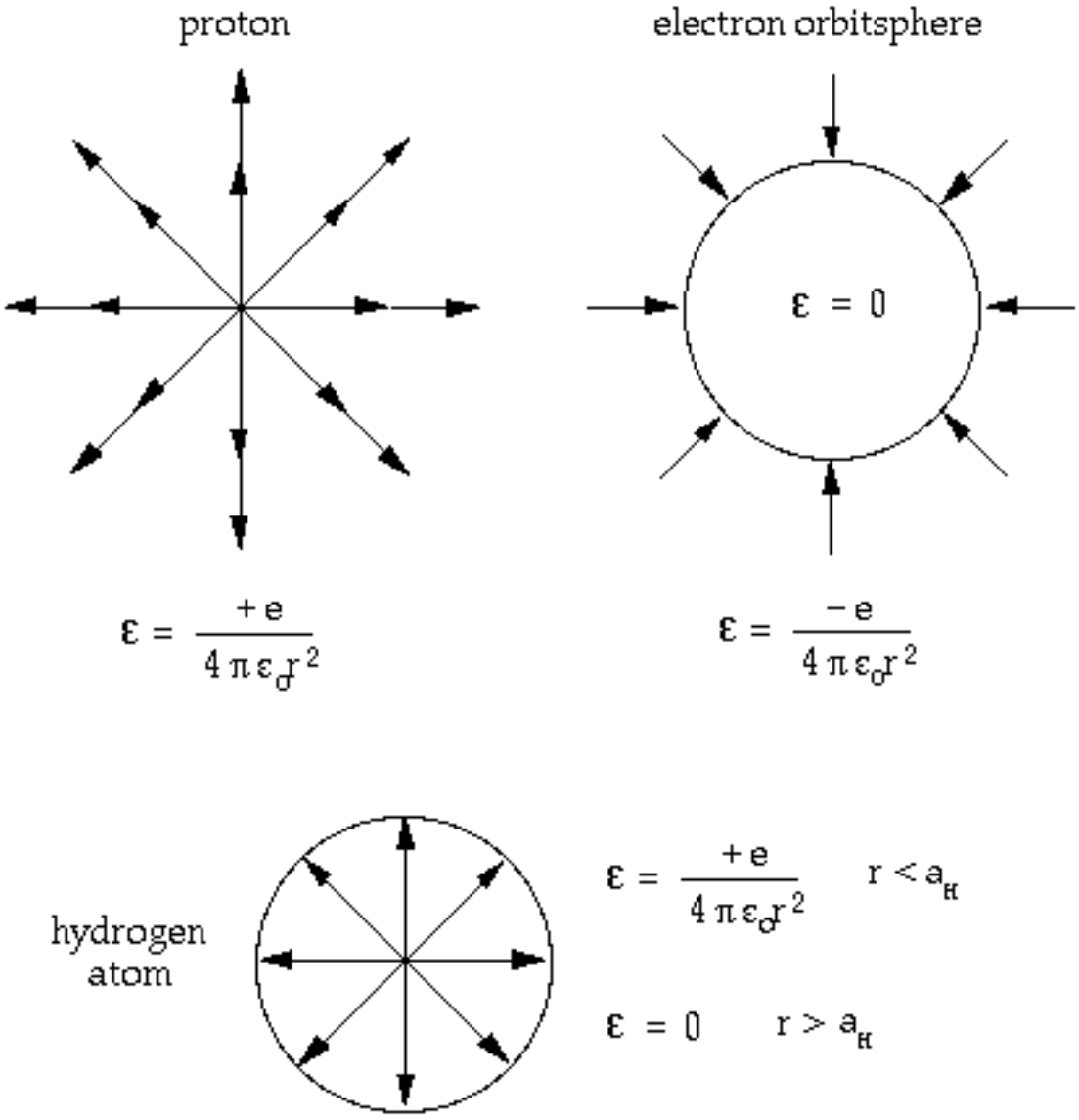

Thus, for a nucleus of charge Z, the force balance equation for the electron orbitsphere is obtained by equating the forces on the mass and charge densities. For the ground state, $n=1$, the centrifugal force of the electron is given by

$$\mathbf{F}_{centrifugal} = \frac{m_e}{4\pi r_1^2}\frac{\mathbf{v}_1^2}{r_1} \tag{1.152}$$

where $\frac{m_e}{4\pi r_1^2}$ is the mass density of the orbitsphere. The centripetal force

is the electric force, $\mathbf{F}_{ele}$, between the electron and the nucleus.

$$\mathbf{F}_{ele} = \frac{e}{4\pi r_1^2}\frac{Ze}{4\pi\varepsilon_o r_1^2} \tag{1.153}$$

where ε_o is the permittivity of free-space.

The second centripetal force is an electrodynamic force, a force dependent on the second derivative of charge position which respect to time, which arises between the electron and the nucleus. The motion of each point in the magnetic field of the nucleus will cause a relativistic central force, $\mathbf{F}_{mag}$, which acts on each point mass. The magnetic central force is derived as follows from the Lorentzian force which is relativistically corrected. Each infinitesimal point of the orbitsphere moves on a great circle, and each point charge has the charge-density $\frac{e}{4\pi r_n^2}$. As given in the Proton and Neutron Section, the proton is comprised of a linear combination of three constant functions and three orthogonal spherical harmonic quark/gluon functions. From the photon inertial reference frame at the radius of each infinitesimal point of the electron orbitsphere, the proton charge distribution is given as the product of the quark and gluon functions which gives rise to a uniform distribution. The magnetic flux of the proton in the $v = c$ inertial frame at the electron radius follows from McQuarrie [16]:

$$\mathbf{B} = \frac{\mu_o e\hbar}{2m_p r_n^3} \tag{1.154}$$

And, the magnetic flux due to a nucleus of charge Z and mass m is

$$\mathbf{B} = \frac{\mu_o Z_1 e\hbar}{2mr_n^3} \tag{1.155}$$

The motion of each point will cause a relativistic central force, $\mathbf{F}_{i\,mag}$, which acts on each point mass. The magnetic central force is derived as follows from the Lorentzian force which is relativistically corrected. The Lorentzian force density on each point moving at velocity v given by Eq. (1.47) is

$$\mathbf{F}_{mag} = \frac{e}{4\pi r_n^2}\mathbf{v}\times\mathbf{B} \tag{1.156}$$

Substitution of Eq. (1.47) for $\mathbf{v}$ and Eq. (1.155) for $\mathbf{B}$ gives

$$\mathbf{F}_{mag} = \frac{1}{4\pi r_1^2}\left[\frac{Z_1 e^2\mu_o}{2m_e r_n}\right]\frac{\hbar^2}{mr_n^3} \tag{1.157}$$

The term in brackets can be expressed in terms α. From Eqs. (1.143-1.147)

$$\frac{Z_1 e^2\mu_o}{2m_e r_n} = 2\pi\alpha Z_1\frac{v}{c} \tag{1.158}$$

It can be shown that the relativistic correction to Eq. (1.157) is the

reciprocal of Eq. (1.158). Consider an inertial frame following a great circle of radius r_n with $v = c$. The motion is tangential to the radius; thus, r_n is Lorentzian invariant. But, the tangential distance along a great circle is $2\pi r_n$ in the laboratory frame and r_n in the $v = c$ frame. The charge is relativistically invariant, whereas, the mass is not. The relativistic correction to the laboratory frame mass relative to the $v = c$ frame is 2π. The correction follows from the Lorentz transformation of the electron's invariant angular momentum of $\hbar$. It is shown by Purcell [22] that the force on a moving charge due to a moving line of charge is a relativistic electric force due to Lorentzian contraction of the line charge density. The force is proportional to $\frac{v}{c}$ where v is the electron's velocity. Thus, it follows that the electron mass in the laboratory frame relative to the $v = c$ inertial frame is which is also proportional to $\frac{v}{c}$. Following the derivation of Purcell with the substitution of the relativistic mass density for the charge density gives the electron mass correction to the electrodynamic force as

$$m_e = 2\pi \frac{v}{c} m_{e\text{Rest}} \tag{1.159}$$

Furthermore, due to invariance of charge under Gauss's Integral Law, the radius term in the brackets of Eq. (1.157) is relativistically corrected. The radius of the electron relative to the $v = c$ frame, r_α^*, is relativistically corrected as follows. From Eq. (1.43) the relationship between the radius and the electron wavelength is

$$2\pi r = \lambda \tag{1.160}$$

Using the de Broglie Eq. (1.46) with $v = c$

$$\lambda = \frac{h}{mv} = \frac{h}{mc} \tag{1.161}$$

With substitution of Eq. (1.160) into Eq. (1.161)

$$r_\alpha^* = \frac{\hbar}{mc} = \lambda\!\!\!^{-}_c = \alpha a_o \tag{1.162}$$

where $\lambda\!\!\!^{-}_C$ is the Compton wavelength bar, and where a_o is the Bohr radius. The radius of the electron orbitsphere in the $v = c$ frame is $\lambda\!\!\!^{-}_C$, and the relativistic correction due to length contraction can be determined as a boundary value problem. Eq. (1.162) can be expressed in terms of a relativistic correction, n, which multiplies, r_1, the radius of the electron orbitsphere in the lab frame. The lab frame electron radius is taken as $\frac{a_o}{Z_2}$ which is consistent with Eq. (1.169); thus, it is the solution of our boundary value problem as shown as follows.

$$r_\alpha^* = \frac{\hbar}{mc} = \lambda\!\!\!^{-}_c = \alpha a_o = \frac{n a_o}{Z_2} = n r_1 \tag{1.163}$$

It follows from Eq. (1.163) that the radius, r_n, of Eq. (1.157) must be corrected by the factor αZ_2. By correcting the radius and the mass, the relativistic correction is $\frac{1}{2\pi\alpha Z_2 \frac{v}{c}}$. In this case, $Z_1 = Z_2$; thus, 1 is substituted for the term in brackets in Eq. (1.157); therefore,

$$\mathbf{F}_{mag} = -\frac{1}{4\pi r_1^{\,2}} \frac{\hbar^2}{m r_n^{\,3}} \tag{1.164}$$

The force balance equation is given by equating the centrifugal and centripetal force densities:

$$\frac{m_e}{4\pi r_1^{\,2}} \frac{v_1^{\,2}}{r_1} = \frac{e}{4\pi r_1^{\,2}} \frac{Ze}{4\pi\varepsilon_o r_1^{\,2}} - \frac{1}{4\pi r_1^{\,2}} \frac{\hbar^2}{m r_n^{\,3}} \tag{1.165}$$

Using Eq. (1.47),

$$r_1 = \frac{4\pi\varepsilon_o \hbar^2}{Ze^2 \mu_e} \tag{1.166}$$

where the reduced electron mass, μ_e, is

$$\mu_e = \frac{m_e m}{m_e + m} \tag{1.167}$$

The Bohr radius is

$$a_o = \frac{4\pi\varepsilon_o \hbar^2}{e^2 m_e} \tag{1.168}$$

And, the radius given by force balance between the centifugal force and central electrostatic force alone is

$$r_1 = \frac{4\pi\varepsilon_o \hbar^2}{Ze^2 m_e} = \frac{a_0}{Z} \tag{1.169}$$

And, for hydrogen, m of Eq. (1.167) is

$$m = m_p \tag{1.170}$$

Substitution of the reduced electron mass for the electron mass gives, a_H, the Bohr radius of the hydrogen atom.

$$a_H = \frac{4\pi\varepsilon_o \hbar^2}{e^2 \mu_e} \tag{1.171}$$

Thus, Eq. (1.166) becomes

$$r_1 = \frac{a_H}{Z} \tag{1.172}$$

ENERGY CALCULATIONS

The potential energy V between the electron and the nucleus separated by the radial distance radius r_1 is,

$$V = \frac{-Ze^2}{4\pi\varepsilon_o r_1} = \frac{-Z^2e^2}{4\pi\varepsilon_o a_H} = -Z^2\ X\ 4.3675\ X\ 10^{-18}\ J = -Z^2\ X\ 27.2\ eV \qquad (1.173)$$

Because this is a central force problem, the kinetic energy, T, is $-\frac{1}{2}V$.

$$T = \frac{Z^2e^2}{8\pi\varepsilon_o a_H} = Z^2\ X\ 13.59\ eV \qquad (1.174)$$

The same result can be obtained from $T = \frac{1}{2}m_e v_1^2$ and Eq. (1.47).

Alternatively, the kinetic energy, which is equal to the stored electric energy, E_{ele}, can be calculated from

$$T = E_{ele} = -\frac{1}{2}\varepsilon_o \int_{\infty}^{r_1} \mathbf{E}^2 dv \qquad (1.175)$$

where $\mathbf{E} = -\frac{Ze}{4\pi\varepsilon_o r^2}$. Thus, as the orbitsphere shrinks from ∞ *to* r_1,

$$E_{ele} = -\frac{Z^2e^2}{8\pi\varepsilon_o a_H} = -Z^2\ X\ 2.1786\ X\ 10^{-18}\ J = -Z^2\ X\ 13.598\ eV \qquad (1.176)$$

The calculated Rydberg constant is 109,677.58 cm^{-1}; the experimental Rydberg constant is 109,677.58 cm^{-1}. Furthermore, a host of parameters can be calculated for the hydrogen atom, as shown in Table 1.1.

Table 1.1. Some calculated parameters for the hydrogen atom ($n=1$).

radius	$r_1 = a_H$	$5.2918\ X\ 10^{-11}\ m$
potential energy	$V = \frac{-e^2}{4\pi\varepsilon_o a_H}$	$-27.196\ eV$
kinetic energy	$T = \frac{e^2}{8\pi\varepsilon_o a_H}$	$13.598\ eV$
angular velocity (spin)	$\omega_1 = \frac{\hbar}{m_e r_1^2}$	$4.13\ X\ 10^{16}\ rads^{-1}$
linear velocity	$v_1 = r_1\omega_1$	$2.19\ X\ 10^{6}\ ms^{-1}$
wavelength	$\lambda_1 = 2\pi r_1$	$3.325\ X\ 10^{-10}\ m$
spin quantum number	$s = \frac{1}{2}$	$\frac{1}{2}$
moment of Inertia	$I = m_e r_1^2\sqrt{s(s+1)}$	$2.209\ X\ 10^{-51}\ kgm^2$
angular kinetic energy	$E_{angular} = \frac{1}{2} I\omega_1^2$	$11.78\ eV$
magnitude of the angular momentum	$\hbar$	$1.0545\ X\ 10^{-34}\ Js$
projection of the angular momentum onto the S-axis	$S = \hbar\sqrt{s(s+1)}$	$9.133\ X\ 10^{-35}\ Js$
projection of the angular momentum onto the z-axis	$S_z = \frac{\hbar}{2}$	$5.273\ X\ 10^{-35}\ Js$
mass density	$\frac{m_e}{4\pi r_1^2}$	$2.589\ X\ 10^{-11}\ kgm^{-2}$
charge-density	$\frac{e}{4\pi r_1^2}$	$14.41\ Cm^{-2}$

Table 1.2 gives the radii and energies for some one-electron atoms.

In addition to the energies, the wavelength, angular frequency, and the linear velocity can be calculated for any one-electron atom from Eqs. (1.46), (1.55), and (1.56). Values are given in Table 1.3.

Table 1.2. Calculated energies (non-relativistic) and calculated ionization energies for some one-electron atoms.

Atom	Calculated r_1[a] (a_0)	Calculated Kinetic Energy[b] (eV)	Calculated Potential Energy[c] (eV)	Calculated Ionization Energy[d] (eV)	Experimental Ionization Energy[e] (eV)
H	1.000	13.59	–27.18	13.59	13.59
He^+	0.500	54.35	–108.70	54.35	54.58
Li^{2+}	0.333	122.28	–244.56	122.28	122.45
Be^{3+}	0.250	217.40	–438.80	217.40	217.71
B^{4+}	0.200	339.68	–679.36	339.68	340.22
C^{5+}	0.167	489.14	–978.28	489.14	489.98
N^{6+}	0.143	665.77	–1331.54	665.77	667.03
O^{7+}	0.125	869.58	–1739.16	869.58	871.39

[a] from Equation (1.169)
[b] from Equation (1.174)
[c] from Equation (1.173)
[d] from Equation (1.176)
[e] experimental

It is noteworthy that the potential energy is a constant (at a given n) because the electron is at a fixed distance, r_n, from the nucleus. And, the kinetic energy and velocity squared are constant because the atom does not radiate at r_n and the potential energy is constant.

Table 1.2. Calculated radii, angular frequencies, linear velocities, and wavelengths for the $n=1$ state of some one-electron atoms (non-relativistic).

Atom	r_1 [a] (a_0)	angular[b] velocity ($10^{17} rad\ s^{-1}$)	linear[c] velocity ($10^6\ ms^{-1}$)	wavelength[d] ($10^{-10}\ m$)
H	1.000	0.413	2.19	3.325
He^+	0.500	1.65	4.38	1.663
Li^{2+}	0.333	3.72	6.56	1.108
Be^{3+}	0.250	6.61	8.75	0.831
B^{4+}	0.200	10.3	10.9	0.665
C^{5+}	0.167	14.9	13.1	0.554
N^{6+}	0.143	20.3	15.3	0.475
O^{7+}	0.125	26.5	17.5	0.416

[a] from Equation (1.169)
[b] from Equation (1.55)
[c] from Equation (1.56)
[d] from Equation (1.46)

It should be noted that the linear velocity is an appreciable percent of the velocity of light for some of the atoms in Table 1.2—5.9% for O^{7+} for example. Relativistic corrections must be applied before a comparison between the total energy and ionization energy (Table 1.2) is made.

References

1. Haus, H. A., "On the radiation from point charges", American Journal of Physics, 54, (1986), pp. 1126-1129.
2. Jackson, J. D., Classical Electrodynamics, Second Edition, John Wiley & Sons, New York, (1962), p. 111.
3. Bracewell, R. N., The Fourier Transform and Its Applications, McGraw-Hill Book Company, New York, (1978), pp. 252-253.
4. Siebert, W. McC., Circuits, Signals, and Systems, The MIT Press, Cambridge, Massachusetts, (1986), p. 415.

5. Luke, Y. L., Integrals of Bessel Functions, McGrall-Hill, New York, p.22.
6. Abramovitz and Stegagun (3rd Printing 1965), p. 366, eq. 9.1.10, and p. 255, eq. 6.1.6.
7. Luke, Y. L., Integrals of Bessel Functions, McGrall-Hill, New York, p.30.
8. Bateman, H., Tables of Integral Transforms, Vol. III, McGraw-Hill, New York, (1954), p. 33.
9. Bateman, H., Tables of Integral Transforms, Vol. III, McGraw-Hill, New York, (1954), p. 5.
10. Reynolds, G. O., DeVelis, J. B., Parrent, G. B., Thompson, B. J., The New Physical Optics Notebook, SPIE Optical Engineering Press, (1990).
11. Abbott, T. A., Griffiths, D. J., Am. J. Phys., Vol. 153, No. 12, (1985), pp. 1203-1211.
12. McQuarrie, D. A., Quantum Chemistry, University Science Books, Mill Valley, CA, (1983), pp. 206-221.
13. Jackson, J. D., Classical Electrodynamics, Second Edition, John Wiley & Sons, New York, (1962), p. 99.
14. Fowles, G. R., Analytical Mechanics, Third Edition, Holt, Rinehart, and Winston, New York, (1977), p. 196.
15. Pauling, Linus, Wilson, E., Bright, Introduction to Quantum Mechanics with Applications to Chemistry, McGraw-Hill Book Company, New York, (1935), pp. 118-121.
16. McQuarrie, D. A., Quantum Chemistry, University Science Books, Mill Valley, CA, (1983), pp. 238-241.
17. Jackson, J. D., Classical Electrodynamics, Second Edition, John Wiley & Sons, New York, (1962), p. 178.
18. Jackson, J. D., Classical Electrodynamics, Second Edition, John Wiley & Sons, New York, (1962), pp. 194-197.
19. Purcell, E. M., Electricity and Magnetism, McGraw-Hill, New York, (1965), pp. 370-375.
20. Jackson, J. D., Classical Electrodynamics, Second Edition, John Wiley & Sons, New York, (1962), Chapter 17.
21. Bueche, F., Introduction to Physics for Scientists and Engineers, McGraw-Hill, (1975), pp. 352-353.
22. Purcell, E. M., Electricity and Magnetism, McGraw-Hill, New York, (1965), pp. 170-199.

EXCITED STATES OF THE ONE ELECTRON ATOM (QUANTIZATION)

EQUATION OF THE ELECTRIC FIELD INSIDE THE ORBITSPHERE

It is well known that resonator cavities can trap electromagnetic radiation of discrete resonant frequencies. The orbitsphere is a resonator cavity which traps photons of discrete frequencies. Thus, photon absorption occurs as an excitation of a resonator mode. The "trapped photon" is a "standing electromagnetic wave" which actually is a circulating wave that propagates around the z-axis, and its source current superimposes with each great circle current loop of the orbitsphere. The time-function factor, $k(t)$, for the "standing wave" is identical to the time-function factor of the orbitsphere in order to satisfy the boundary (phase) condition at the orbitsphere surface. Thus, the angular frequency of the "trapped photon" has to be identical to the angular frequency of the electron orbitsphere, ω_n given by Eq. (1,55). Furthermore, the phase condition requires that the angular functions of the "trapped photon" have to be identical to the spherical harmonic angular functions of the electron orbitsphere. Combining $k(t)$ with the ϕ-function factor of the spherical harmonic gives $e^{i(m\phi-\omega_n t)}$ for both the electron and the "trapped photon" function. The photon is "glued" to the inner orbitsphere surface and the outer nuclear surface as photon source charge-density with a radial electric field. Thus, the "trapped photon" is analogous to a gluon described in the Proton and Neutron Section and is different from a photon in free space as described in the Equation of the Photon Section.

For a spherical resonator cavity, the relationship between an allowed radius and the "photon standing wave" wavelength is

$$2\pi r = n\lambda \tag{2.1}$$

where n is an integer. Now, the question arises: given that this is a resonator cavity, which nonradiative states are possible where the transition is effected by a "trapped photon"? For the electron orbitsphere, a spherical resonator cavity, the relationship between an allowed radius and the electron wavelength is

$$2\pi(nr_1) = 2\pi r_n = n\lambda_1 = \lambda_n \tag{2.2}$$

where

$n = 1,2,3,4,...$

$n = \frac{1}{2},\frac{1}{3},\frac{1}{4},...$

λ_1 is the allowed wavelength for $n = 1$

r_1 is the allowed radius for $n = 1$

An electron in the ground state, $n = 1$, is in force balance including the electrodynamic force which is included by using the reduced electron

mass as given by Eqs. (1.166), (1.171), and (1.172).

$$\frac{m_e v_1^2}{r_1} = \frac{Ze^2}{4\pi\varepsilon_o r_1^2} \tag{2.3}$$

When an electron in the ground state absorbs a photon of sufficient energy to take it to a new non-radiative state, $n = 2,3,4,...,$ force balance must be maintained. This is possible only if the central field is equivalent to that of a central charge of $\frac{Ze}{n}$, and the excited state force balance equation is

$$\frac{m_e v_n^2}{r_n} = \frac{1}{n}\frac{Ze^2}{4\pi\varepsilon_o r_n^2} \tag{2.4}$$

where r_1 is the "ground" state radius of the electron, and r_n is the nth excited state radius of the electron. The radius of the nth excited state follows from Eq. (1.172) and Eq. (2.4).

$$r_n = na_H \tag{2.5}$$

The reduction of the charge from Ze to $\frac{Ze}{n}$ is caused by trapping a photon in the orbitsphere, a spherical resonator cavity. The photon's electric field creates a "standing wave" in the cavity with an effective charge of $\left(-1+\frac{1}{n}\right)Ze\,(at\ r_n)$. The total charge experienced by the electron is the sum of the proton and "trapped photon" charge components. The equation for these "trapped photons" can be solved as a boundary value problem of Laplace's equation. For the hydrogen atom, the boundary conditions are that the electric field is in phase with the orbitsphere and that the radial function for the electric field of the "trapped photon" at r_n is

$$\mathbf{E}_{rphoton} = \left(-1+\frac{1}{n}\right)\frac{e}{4\pi\varepsilon_o (r_n)^2} \qquad n = 2,3,4,..., \tag{2.6}$$

The general form of the solution to Laplace's equation in spherical coordinates is

$$\Phi(r,\theta,\phi) = \sum_{\ell=0}^{\infty}\sum_{m=-\ell}^{\ell}\left[A_{\ell,m}r^{\ell} + B_{\ell,m}r^{-(\ell+1)}\right]\left[Y_0^0(\theta,\phi) + Y_\ell^m(\theta,\phi)\right] \tag{2.7}$$

All $A_{\ell,m}$ are zero because the electric field given by the potential must be inversely proportional to the radius to obtain force balance. The electric field is the gradient of the potential

$$\mathbf{E} = -\ \Phi \tag{2.8}$$

$$\mathbf{E}_r = -\frac{\delta\Phi}{\delta r}\hat{i}_r$$
$$\mathbf{E}_\theta = -\frac{1}{r}\frac{\delta\Phi}{\delta\theta}\hat{i}_\theta \qquad (2.9)$$
$$\mathbf{E}_\phi = -\frac{1}{r\sin\theta}\frac{\delta\Phi}{\delta\phi}\hat{i}_\phi$$

Thus,

$$\mathbf{E}_r = \sum_{\ell=0}^{\infty}\sum_{m=-\ell}^{\ell} B_{\ell,m}(\ell+1)r^{-(\ell+2)}\left[Y_0^0(\theta,\phi) + Y_\ell^m(\theta,\phi)\right] \qquad (2.10)$$

Given that $\mathbf{E}(proton) = \frac{+e}{4\pi\varepsilon_o r_n^2}$, and that the electric fields of the proton and "trapped photon" must superimpose to yield a field equivalent to a central point charge of $\frac{+Ze}{n}$, the "trapped photon" electric field for each mode is determined as follows. The time-function factor and the angular-function factor of the charge-density function of the orbitsphere (Eqs. (1.64) and (1.65)) at force balance must be in phase with the electric field of the "trapped photon". The relationship between the electric field equation and the "trapped photon" source charge-density function is given by Maxwell's equation in two dimensions.

$$\mathbf{n}\cdot\left(\mathbf{E}_1 - \mathbf{E}_2\right) = \frac{\sigma}{\varepsilon_0} \qquad (2.11)$$

where $\mathbf{n}$ is the radial normal unit vector, $\mathbf{E}_1 = 0$ ($\mathbf{E}_1$ is the electric field outside of the orbitsphere), $\mathbf{E}_2$ is given by the total electric field at $r_n = na_H$, and σ is the surface charge-density. Thus,

$$\mathbf{E}_{r_{photon\,n,l,m}|_{r_n=na_H}} = \frac{e}{4\pi\varepsilon_o(na_H)^2}\left\{-1 + \frac{1}{n}\left[Y_0^0(\theta,\phi) + \mathrm{Re}\left\{Y_\ell^m(\theta,\phi)\left[1+e^{i\omega_n t}\right]\right\}\right]\right\}$$
$$\omega_n = 0 \text{ for } m = 0 \qquad (2.12)$$
$$= \sum_{\ell=0}^{\infty}\sum_{m=-\ell}^{\ell} -B_{\ell,m}(\ell+1)(na_H)^{-(\ell+2)}\left[Y_0^0(\theta,\phi) + \mathrm{Re}\left\{Y_\ell^m(\theta,\phi)\left[1+e^{i\omega_n t}\right]\right\}\right]$$
$$\omega_n = 0 \text{ for } m = 0 \qquad (2.13)$$

Therefore,

$$\sum_{\ell=0}^{\infty}\sum_{m=-\ell}^{\ell} -B_{\ell,m} = \frac{e(na_H)^\ell}{4\pi\varepsilon_o(\ell+1)}\left\{-1 + \frac{1}{n}\right\}, \text{ and} \qquad (2.14)$$

$$\mathbf{E}_{r_{photon\,n,l,m}} = \frac{e(na_H)^\ell}{4\pi\varepsilon_o}\frac{1}{r^{(\ell+2)}}\left\{-Y_0^0(\theta,\phi) + \frac{1}{n}\left[Y_0^0(\theta,\phi) + \mathrm{Re}\left\{Y_\ell^m(\theta,\phi)\left[1+e^{i\omega_n t}\right]\right\}\right]\right\}$$
$$\omega_n = 0 \text{ for } m = 0 \qquad (2.15)$$
$$n = 1,2,3,4,\ldots$$
$$\ell = 1,2,\ldots, n-1$$

$$m = -\ell, -\ell+1,...,0,...,+\ell$$

$\mathbf{E}_{r_{total}}$ is the sum of the "trapped photon" and proton electric fields,

$$\mathbf{E}_{r_{total}} = \frac{e}{4\pi\varepsilon_o r^2} + \frac{e(na_H)^\ell}{4\pi\varepsilon_o}\frac{1}{r^{(\ell+2)}}\left[-Y_0^0(\theta,\phi) + \frac{1}{n}\left[Y_0^0(\theta,\phi) + \mathrm{Re}\left\{Y_\ell^m(\theta,\phi)\left[1+e^{i\omega_n t}\right]\right\}\right]\right]$$

$$\omega_n = 0 \text{ for } m = 0 \tag{2.16}$$

For $r = na_H$ and $m = 0$, the total radial electric field is

$$\mathbf{E}_{rtotal} = \frac{1}{n}\frac{e}{4\pi\varepsilon_o(na_H)^2} \tag{2.17}$$

All boundary conditions are met for the electric fields and the wavelengths of the "trapped photon" and the electron. Thus, Eq. (2.16) is the solution for the excited modes of the orbitsphere, a spherical resonator cavity. And, the quantum numbers of the electron are n, ℓ, m (m_ℓ), and m_s (Described in the Stern-Gerlach Experiment Section).

PHOTON ABSORPTION

The energy of the photon which excites a mode in a stationary spherical resonator cavity from radius a_H to radius na_H is

$$E_{photon} = \frac{e^2}{4\pi\varepsilon_o a_H}\left[1 - \frac{1}{n^2}\right] = h\nu = \hbar\omega \tag{2.18}$$

After multiplying Eq. (2.18) by $\frac{a_H}{a_H} = \frac{4\pi\varepsilon_0\hbar^2}{e^2\mu_e a_H}$, where a_H is given by Eq. (1.171), ω_{photon} is

$$\omega_{photon} = \frac{\hbar}{m_e a_H^2}\left[1 - \frac{1}{n^2}\right] \tag{2.19}$$

In the case of an electron orbitsphere, the resonator possesses kinetic energy before and after the excitation. The kinetic energy is always one-half of the potential energy because the centripetal force is an inverse squared central force. As a result, the energy and angular frequency to excite an electron orbitsphere is only one-half of the values above, Eqs. (2.18) and (2.19). From Eq. (1.55), the angular velocity of an electron orbitsphere of radius na_H is

$$\omega_n = \frac{\hbar}{m_e(na_H)^2} \tag{2.20}$$

The change in angular velocity of the orbitsphere for an excitation from $n = 1$ to $n = n$ is

$$\Delta\omega = \frac{\hbar}{m_e(a_H)^2} - \frac{\hbar}{m_e(na_H)^2} = \frac{\hbar}{m_e(a_H)^2}\left[1 - \frac{1}{n^2}\right] \tag{2.21}$$

The kinetic energy change of the transition is

$$\frac{1}{2} m_e (\Delta v)^2 = \frac{1}{2} \frac{e^2}{4\pi\varepsilon_0 a_H} \left[1 - \frac{1}{n^2}\right] = \frac{1}{2} \hbar\omega \qquad (2.22)$$

The change in angular velocity of the electron orbitsphere, Eq. (2.21), is identical to the angular velocity of the photon necessary for the excitation, ω_{photon} (Eq. (2.21)). The energy of the photon necessary to excite the equivalent transition in an electron orbitsphere is one-half of the excitation energy of the stationary cavity because the change in kinetic energy of the electron orbitsphere supplies one-half of the necessary energy. The change in the angular frequency of the orbitsphere during a transition and the angular frequency of the photon corresponding to the superposition of the free space photon and the photon corresponding to the kinetic energy change of the orbitsphere during a transition are equivalent. The correspondence principle holds. It can be demonstrated that the resonance condition between these frequencies is to be satisfied in order to have a net change of the energy field [1].

The excited states of hydrogen are given in Table 2.1.

Table 2.1. Calculated energies (non-relativistic; no spin-orbit interaction; no electronic spin/nuclear spin interaction) and ionization energies for the hydrogen atom in the ground state and some excited states.

n	Z	Calculated r_n[a] (a_H)	Calculated Kinetic Energy[b] (eV)	Calculated Potential Energy[c] (eV)	Calculated Ionization Energy[d] (eV)	Experimental Ionization Energy[e] (eV)
1	1	1.000	13.589	–27.21	13.598	13.595
2	$\frac{1}{2}$	2.000	3.397	–6.803	3.400	3.393
3	$\frac{1}{3}$	3.000	1.510	–3.023	1.511	1.511
5	$\frac{1}{5}$	5.000	0.544	–1.088	0.544	0.544
10	$\frac{1}{10}$	10.000	0.136	–0.272	0.136	0.136

[a] from Equation (2.5)
[b] from $T = -\frac{1}{2}V$
[c] from Equation (1.173)
[d] from Equation (2.22)
[e] experimental

SELECTION RULES

The multipole fields of a radiating source can be used to calculate the energy and angular momentum carried off by the radiation [2]. For definiteness we consider a linear superposition of electric (l, m) multipoles with different m values, but all having the same l, and following Eq. (16.46) of Jackson [2], write the fields as

$$\mathbf{B}_l = \sum_m a_E(l,m)\mathbf{X}_{lm}h_l^{(1)}(kr)e^{i\omega t}$$
$$\mathbf{E}_l = \frac{i}{k} \times \mathbf{B}_l \qquad (2.23)$$

For harmonically varying fields, the time-averaged energy density is

$$u = \frac{1}{16\pi}\left(\mathbf{E}\cdot\mathbf{E}^{*} + \mathbf{B}\cdot\mathbf{B}^{*}\right) \tag{2.24}$$

In the radiation zone, the two terms are equal. Consequently, the energy in a spherical shell between r and $(r+dr)$ ($for\ kr >> 1$) is

$$dU = \frac{dr}{8\pi k^2}\sum_{m,m'} a_E^{*}(l,m')a_E(l,m)\int \mathbf{X}_{lm'}^{*}\cdot\mathbf{X}_{lm}\,d\Omega \tag{2.25}$$

where the asymptotic form (Eq. (16.13) of Jackson [2]) of the spherical Hankel function has been used. With the orthogonality integral (Eq. (16.44) of Jackson [2]) this becomes

$$\frac{dU}{dr} = \frac{1}{8\pi k^2}\sum_{m}\left|a_E(l,m)\right|^2 \tag{2.26}$$

independent of the radius. For a general superposition of electric and magnetic multipoles, the sum over m becomes a sum over l and m and $|a_E|^2$ becomes $|a_E|^2 + |a_M|^2$. The total energy is a spherical shell in the radiation zone is thus an *incoherent sum* over all multipoles.

The time-averaged angular-momentum density is

$$\mathbf{m} = \frac{1}{8\pi c}\,\mathrm{Re}\left[\mathbf{r}\times\left(\mathbf{E}\times\mathbf{B}^{*}\right)\right] \tag{2.27}$$

The triple cross product can be expanded, and the electric field substituted to yield, for a superposition of electric multipoles,

$$\mathbf{m} = \frac{1}{8\pi\omega}\,\mathrm{Re}\left[\mathbf{B}^{*}\left(\mathbf{L}\cdot\mathbf{B}\right)\right] \tag{2.28}$$

Then the angular momentum in a spherical shell between r and $(r+dr)$ in the radiation zone is

$$d\mathbf{M} = \frac{dr}{8\pi\omega k^2}\,\mathrm{Re}\sum_{m,m'} a_E^{*}(l,m')a_E(l,m)\int\left(\mathbf{L}\cdot\mathbf{X}_{lm'}\right)^{*}\mathbf{X}_{lm}\,d\Omega \tag{2.29}$$

With the explicit form (Eq. (16.43) of Jackson [2]) for X_{lm}, Eq. (2.29) can be written

$$\frac{d\mathbf{M}}{dr} = \frac{1}{8\pi\omega k^2}\,\mathrm{Re}\sum_{m,m'} a_E^{*}(l,m')a_E(l,m)\int Y_{lm'}^{*}\mathbf{L}Y_{lm}\,d\Omega \tag{2.30}$$

From the properties of LY_{lm} listed in Eq. (16.28) of Jackson [2] and the orthogonality of the spherical harmonics, we obtain the following expressions for the Cartesian components of $\frac{dM}{dr}$

$$\frac{dM_x}{dr} = \frac{1}{16\pi\omega k^2}\,\mathrm{Re}\sum_{m}\left[\sqrt{(l-m)(l+m+1)}\,a_E^{*}(l,m+1) + \sqrt{(l+m)(l-m+1)}\,a_E^{*}(l,m-1)\right]a_E(l,m) \tag{2.31}$$

$$\frac{dM_y}{dr} = \frac{1}{16\pi\omega k^2}\,\mathrm{Im}\sum_{m}\left[\sqrt{(l-m)(l+m+1)}\,a_E^{*}(l,m+1) - \sqrt{(l+m)(l-m+1)}\,a_E^{*}(l,m-1)\right]a_E(l,m) \tag{2.32}$$

$$\frac{dM_z}{dr} = \frac{1}{8\pi\omega k^2}\sum_{m} m\left|a_E(l,m)\right|^2 \tag{2.33}$$

These equations show that for a general lth order electric multipole that

consists of a superposition of different m values, only the z component of the angular momentum is relatively simple.

For a multipole with a single m value, M_x and M_y vanish, while a comparison of Eq. (2.33) and Eq. (2.25) shows that

$$\frac{dM_z}{dr} = \frac{m}{\omega}\frac{dU}{dr} \tag{2.34}$$

independent of r. Experimentally, the photon can carry $\pm \hbar$. units of angular momentum. Thus, during excitation the spin, orbital, or total angular momentum of the orbitsphere can change by zero or $\pm \hbar$ The electron transition rules arise from conservation of angular momentum. The selection rules for multipole transitions between quantum states arise from conservation of total angular momentum and component angular momentum where the photon carries $\hbar$ of angular momentum. The radiation of a multipole of order (l, m) carries $m\hbar$ units of the z component of angular momentum per photon of energy $\hbar\omega$.

ORBITAL AND SPIN SPLITTING

The ratio of the square of the angular momentum, M^2, to the square of the energy, U^2, for a pure (l,m) multipole follows from Eq. (2.25) and Eqs. (2.31-2.33)

$$\frac{M^2}{U^2} = \frac{m^2}{\omega^2} \tag{2.35}$$

The magnetic moment is defined [3] as

$$\mu = \frac{\text{charge x angular momentum}}{\text{2 x mass}} \tag{2.36}$$

The radiation of a multipole of order (l, m) carries $m\hbar$ units of the z component of angular momentum per photon of energy $\hbar\omega$. Thus, the z component of the angular momentum of the corresponding excited state electron orbitsphere is

$$L_z = m\hbar \tag{2.37}$$

Therefore,

$$\mu_z = \frac{em\hbar}{2m_e} = m\mu_B \tag{2.38}$$

where μ_B is the Bohr magneton. The presence of a magnetic field causes the principal excited state energy levels of the hydrogen atom (Eq. (2.22)) to split by the energy E_{mag}^{orb} corresponding to the interaction of the magnetic flux with the magnetic moment given by Eq. (2.38). This energy is called orbital splitting.

$$E_{mag}^{orb} = m\mu_B \mathbf{B} \tag{2.39}$$

As is the case with spin splitting given by one half the energy of Eq. (1.151) which corresponds to the transition between spin states, the energy of the electron is increased in the case that the magnetic flux is

antiparallel to the magnetic moment, or the energy of the electron is decreased in the case that the magnetic flux is parallel to the magnetic moment. The spin and orbital splitting energies superimpose; thus, the principal excited state energy levels of the hydrogen atom (Eq. (2.22)) are split by the energy $E_{mag}^{spin/orb}$

$$E_{mag}^{spin/orb} = m\frac{e\hbar}{2m_e}\mathbf{B} + m_s g\frac{e\hbar}{m_e}\mathbf{B} \tag{2.40}$$

where it follows from Eq.(2.15) that

$n = 2,3,4,...$

$\ell = 1,2,..., n-1$

$m = -\ell, -\ell+1,...,0,..., +\ell$

$m_s = \pm\frac{1}{2}$

For the electric dipole transition, the selection rules are

$$\Delta m = 0, \pm 1$$
$$\Delta m_s = 0 \tag{2.41}$$

Splitting of the energy levels in addition to that given by Eq. (2.40) occurs due to a relativistic effect described in the Spin-Orbital Coupling Section. Also, a very small shift which is observable by radio-frequency spectroscopy is due to conservation of energy and linear momentum and arises from the radiation reaction force between the electron and the photon. This so-called Lamb Shift is described in the Resonant Line Shape and Lamb Shift Section.

Decaying spherical harmonic currents on the surface of the orbitsphere give rise to spherical harmonic radiation fields during emission; conversely, absorbed spherical harmonic radiation fields produce spherical harmonic currents on the surface of the orbitsphere to effect a transition. Transition intensities, I, are given by the integral of the product of the multipole of the photon, ${}^{p}X_{l,m}(\theta,\phi)$, and the initial, ${}^{i}X_{l,m}(\theta,\phi)$, and final, ${}^{f}X_{l,m}(\theta,\phi)$, states as is the case with classical electrodynamics calculations involving antennas.

$$I \quad I_0\left|\int_0^{\pi}\int_0^{2\pi} {}^{i}X_{l,m}(\theta,\phi)\,{}^{p}X_{l,m}(\theta,\phi)\,{}^{f}X_{l,m}(\theta,\phi)\sin\theta\, d\phi\, d\theta\right|^2 \tag{2.42}$$

The distribution of multipole radiation and the multipole moments of the orbitsphere for absorption and emission are derived in Jackson [4]. Some of the simpler angular distributions are listed in Table 2.2.

Table 2.2. Some of the simpler angular distributions of multipole radiation

and the multipole moments of the orbitsphere for absorption and emission.

---

	m		
l	0	±1	±2
1 Dipole	$\frac{3}{8\pi}\sin^2\theta$	$\frac{3}{16\pi}\left(1+\cos^2\theta\right)$	
2 Quadrapole	$\frac{15}{8\pi}\sin^2\theta\cos^2\theta$	$\frac{5}{16\pi}\left(1-3\cos^2\theta+4\cos^4\theta\right)$	$\frac{5}{16\pi}\left(1-\cos^4\theta\right)$

RESONANT LINE SHAPE AND LAMB SHIFT

The spectroscopic linewidth arises from the classical rise-time band-width relationship, and the Lamb Shift is due to conservation of energy and linear momentum and arises from the radiation reaction force between the electron and the photon. It follows from the Poynting Power Theorem (Eq. (7.27)) with spherical radiation that the transition probabilities are given by the ratio of power and the energy of the transition [5]. The transition probability in the case of the electric multipole moment given by Jackson [5] as

$$Q_{lm} = \frac{3}{l+3}e\left(na_0\right)^l \tag{2.43}$$

is [5]

$$\frac{1}{\tau} = \frac{power}{energy}$$

$$\frac{1}{\tau} = \frac{\left[\frac{2\pi c}{\left[(2l+1)!!\right]^2}\left(\frac{l+1}{l}\right)k^{2l+1}\left|Q_{lm}+Q_{lm}^{'}\right|^2\right]}{\left[\hbar\omega\right]} = 2\pi\left(\frac{e^2}{h}\right)\sqrt{\frac{\varepsilon_0}{\mu_0}}\frac{2\pi}{\left[(2l+1)!!\right]^2}\left(\frac{l+1}{l}\right)\left(\frac{3}{l+3}\right)^2\left(kna_0\right)^{2l}\omega \tag{2.44}$$

This rise-time gives rise to, Γ, the spectroscopic line-width. The relationship between the rise-time and the band-width is given by Siebert [6].

$$\tau^2 = 4\left[\frac{\int_{-\infty}^{\infty} t^2 h^2(t)dt}{\int_{-\infty}^{\infty} h^2(t)dt} - \left(\frac{\int_{-\infty}^{\infty} t h^2(t)dt}{\int_{-\infty}^{\infty} h^2(t)dt}\right)^2\right] \tag{2.45}$$

$$\Gamma^2 = 4\frac{\int_{-\infty}^{\infty} f^2 |H(f)|^2 df}{\int_{-\infty}^{\infty} |H(f)|^2 df} \tag{2.46}$$

By application of the Schwartz inequality, the relationship between the rise-time and the band-width is

$$\tau\Gamma \geq \frac{1}{\pi} \tag{2.47}$$

From Eq. (2.44), the line-width is proportional to the ratio of the Quantum Hall resistance, $\frac{h}{e^2}$, and, η, the radiation resistance of free space.

$$\eta = \sqrt{\frac{\mu_0}{\varepsilon_0}} \tag{2.48}$$

And, the Quantum Hall resistance given in the Quantum Hall Effect Section was derived using the Poynting Power Theorem. Also, from Eq. (2.44), the line-width is proportional to the fine structure constant, α,

$$\alpha = \frac{1}{4\pi}\sqrt{\frac{\mu_o}{\varepsilon_o}}\frac{e^2}{\hbar} \tag{2.49}$$

During a transition, the total energy of the system decays exponentially. Applying Eqs. (2.45) and (2.46) to the case of exponential decay,

$$h(t) = e^{-\frac{1}{T}t}u(t) \tag{2.50}$$

$$|H(f)| = \frac{1}{\sqrt{\left(\frac{1}{T}\right)^2 + (2\pi f)^2}} \tag{2.51}$$

where the rise-time, τ, is the time required for $h(t)$ of Eq. (2.50) to decay to $1/e$ of its initial value and where the band-width, Γ, is the half-power bandwidth, the distance between points at which

$$|H(f)| = \frac{|H(0)|}{\sqrt{2}} \tag{2.52}$$

From Eq. (2.45),

$$\tau = T \tag{2.53}$$

From Eq. (2.46),

$$\Gamma = \frac{1}{\pi T} \tag{2.54}$$

From Eq. (2.53) and Eq. (2.54), the relationship between the rise-time and the band-width for exponential decay is

$$\tau\Gamma = \frac{1}{\pi} \tag{2.55}$$

Photons obey Maxwell-Boltzmann statistics as given in the Statistical Mechanics Section. The emitted radiation, the summation of an assemble of emitted photons each of an exact frequency and energy given by Eq. (4.8), appears as a wave train with effective length c/Γ. Such a finite pulse of radiation is not exactly monochromatic but has a frequency spectrum covering an interval of the order Γ. The exact shape of the frequency spectrum is given by the square of the Fourier Transform of the electric field. Thus, the amplitude spectrum is proportional to

$$\mathbf{E}(\omega) \quad \int_0^\infty e^{-\alpha t} e^{-i\omega t} dt = \frac{1}{\alpha - i\omega} \tag{2.56}$$

The coefficient α corresponds to the spectroscopic linewidth and also to a shift in frequency that arises from the radiation reaction force between the electron and the photon. The energy radiated per unit frequency interval is therefore

$$\frac{dI(\omega)}{d\omega} = I_0 \frac{\Gamma}{2\pi} \frac{1}{\left(\omega - \omega_0 - \Delta\omega\right)^2 + \left(\Gamma/2\right)^2} \tag{2.57}$$

where I_0 is the total energy radiated. The spectral distribution is called a resonant line shape. The width of the distribution at half-maximum intensity is called the half-width or line-breadth and is equal to Γ. Shown in Figure 2.1 is such a spectral line. Because of the reactive effects of radiation the line is shifted in frequency. The small radiative shift of the energy levels of atoms was first observed by Lamb in 1947 [7] and is called the Lamb Shift in his honor.

Figure 2.1. Broadening of the spectral line due to the rise-time and shifting of the spectral line due to the radiative reaction. The resonant line shape has width Γ. The level shift is $\Delta\omega$.

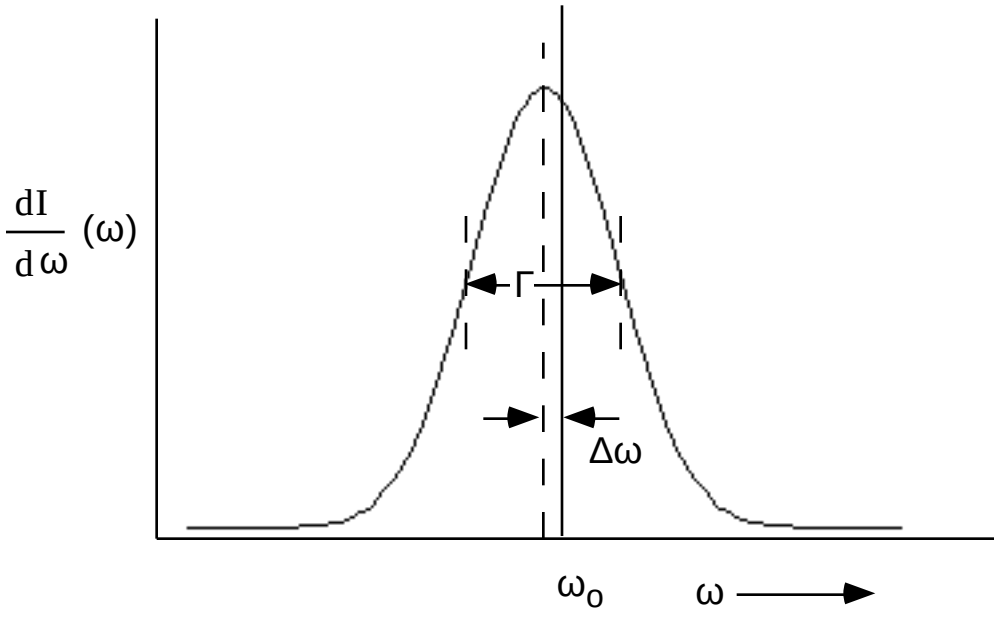

The Lamb Shift of the $^2P_{1/2}$ state of the hydrogen atom having the quantum number $\ell = 1$ is calculated by applying conservation of energy and linear momentum to the emitted photon, electron, and atom. The photon emitted by an excited state atom carries away energy, linear momentum, and angular momentum. The initial and final values of the energies and momenta must be conserved between the atom, the electron, and the photon. (Conservation of angular momentum is used to derive the photon's equation in the Equation of the Photon Section). Consider an isolated atom of mass M having an electron of mass m_e in an excited state level at an energy E and moving with velocity $\mathbf{V}$ along the direction in which the photon is to be emitted (the components of motion perpendicular to this direction remain unaffected by the emission and may be ignored). The energy above the "ground" state at rest is

$$\left(E + \frac{1}{2} M\mathbf{V}^2\right) \tag{2.58}$$

When a photon of energy $E_{h\upsilon}$ is emitted, the atom and/or electron recoils and has a new velocity

$$\mathbf{V} + \mathbf{v} \tag{2.59}$$

(which is a vector sum in that $\mathbf{V}$ and $\mathbf{v}$ may be opposed), and a total energy of

$$\frac{1}{2}M(\mathbf{V}+\mathbf{v})^2 \tag{2.60}$$

By conservation of energy,

$$E+\frac{1}{2}M\mathbf{V}^2 = E_{h\upsilon} + \frac{1}{2}M(\mathbf{V}+\mathbf{v})^2 \tag{2.61}$$

so, that the actual energy of the photon emitted is given by

$$\begin{aligned} E_{h\upsilon} &= E - \frac{1}{2}M\mathbf{v}^2 - M\mathbf{v}\mathbf{V} \\ E_{h\upsilon} &= E - E_R - E_D \end{aligned} \tag{2.62}$$

The photon is thus deficient in energy by a recoil kinetic energy

$$E_R = \frac{1}{2}M\mathbf{v}^2 \tag{2.63}$$

which is independent of the initial velocity $\mathbf{V}$, and by a thermal or Doppler energy

$$E_D = M\mathbf{v}\mathbf{V} \tag{2.64}$$

which depends on $\mathbf{V}$; therefore, it can be positive or negative.

Momentum must also be conserved in the emission process. The energy, E, of the photon is given by Eq. (4.8)

$$E = \hbar\omega = h\frac{\omega}{2\pi} = h\nu = hf = h\frac{c}{\lambda} \tag{2.65}$$

From Special Relativity,

$$E = \hbar\omega = mc^2 \tag{2.66}$$

Thus, $\mathbf{p}$, the momentum of the photon is

$$\mathbf{p} = mc = \frac{E_{h\nu}}{c} \tag{2.67}$$

where c is the velocity of light, so that

$$M\mathbf{V} = M(\mathbf{V}+\mathbf{v}) + \frac{E_{h\nu}}{c} \tag{2.68}$$

And, the recoil momentum is

$$M\mathbf{v} = -\frac{E_{h\nu}}{c} \tag{2.69}$$

Thus, the recoil energy is given by

$$E_R = \frac{E_{h\nu}^2}{2Mc^2} \tag{2.70}$$

and depends on the mass of the electron and/or atom and the energy of the photon. The Doppler energy, E_D, is dependent on the thermal motion of the atom, and will have a distribution of values which is temperature dependent. A mean value, E_D, can be defined which is related to the mean kinetic energy per translational degree of freedom

$$\bar{E}_D \quad \frac{1}{2}kT \tag{2.71}$$

by

$$\bar{E}_D \quad 2\sqrt{E_k E_R} = E_{h\nu}\sqrt{\frac{2\bar{E}_k}{Mc^2}} \tag{2.72}$$

where k is Boltzmann's constant and T is the absolute temperature. As a result, the statistical distribution in energy of the emitted photons is displaced from the true excited-state energy by $-E_R$ and broadened by E_D into a Gaussian distribution of width $2\bar{E}_D$. The distribution for absorption has the same shape but is displaced by $+E_R$.

For the transition of the hydrogen atom with $n=2$ and $\ell=0$ in the initial and final states, the emitted angular radiation power pattern is uniform. The linear momentum of the photon is balanced by the recoil momentum of the entire atom of mass m_H. The recoil frequency of the hydrogen atom, Δf, is given by the combining Eqs. (2.65) and (2.70).

$$\Delta f = \frac{\Delta\omega}{2\pi} = \frac{E_{h\upsilon}}{h} = \frac{\left(E_{h\upsilon}\right)^2}{2m_H c^2} = 13\ MHz \tag{2.73}$$

where $E_{h\upsilon}$ is

$$E_{h\upsilon} = 13.6\left(1-\frac{1}{n^2}\right) - h\Delta f \quad ; h\Delta f <<< 1 \quad E_{h\upsilon} = 13.6\left(1-\frac{1}{n^2}\right) \tag{2.74}$$

However, during the emission of a photon by an excited state atom, with $\ell \neq 0$, the angular radiation power pattern is not uniform, and the electron receives the recoil momentum as the charge-density of the electron changes from uniform to uniform plus a spherical harmonic function (angular modulation) as given in the One Electron Atom Section. In the case of $\ell=1$; $m_\ell = 0$, the angular charge-density function is

$$\rho(r,\theta,\phi,t) = \frac{e}{4\pi r_n^2}[\delta(r-r_n)]\left[Y_0^0(\theta,\phi) + Y_\ell^m(\theta,\phi)\,\mathrm{Re}\left[1+e^{i\omega_n t}\right]\right] \tag{2.75}$$

where

$$Y_\ell^m(\theta,\phi)\,\mathrm{Re}\left[1+e^{i\omega_n t}\right] = \mathrm{Re}\left[Y_\ell^m(\theta,\phi) + Y_\ell^m(\theta,\phi)e^{i\omega_n t}\right] = P_\ell^m(\cos\theta)\cos m\phi + P_\ell^m(\cos\theta)\cos(m\phi+\omega_n t)$$

and $\omega_n = 0$ for $m=0$.

$$Y_{1,z} = \cos\theta \tag{2.76}$$

Figure 1.2 gives pictorial representation of how the modulation function changes the electron density on the orbitsphere for several ℓ values.

The angular function , $|X_{lm}|^2$, of the radiation power pattern of the electron in the $^2P_{1/2}$ ($\ell=1$; $m_\ell = 0$) state is equivalent to that of a Hertzian dipole.

$$|X_{lm}|^2 = \sin^2\theta \tag{2.77}$$

The integral of Eq. (2.77) over the surface of a spherical shell is

$$|X_{lm}|^2_{\ell=1} = \frac{8\pi}{3} \tag{2.78}$$

Thus, the inverse of Eq. (2.78) is the weighting factor of momentum

transfer due to the radiation power pattern. Photons obey Maxwell-Boltzmann statistics as given in the Statistical Mechanics Section. The distribution of the linear momentum transferred from the emitted photons to the electrons is given by the projection of the photon momentum distribution onto the x, y, or z-axis which corresponds to 3 degrees of freedom. The Lamb Shift of the ${}^2P_{1/2}$ state of the hydrogen atom is given by the combining Eqs. (2.65), (2.78), and (2.70)

$$\Delta f = \frac{\Delta\omega}{2\pi} = \frac{E_{h\upsilon}}{h} = 3\frac{\left(E_{h\upsilon}\right)^2}{h2m_e c^2} = 1052\ MHz \tag{2.79}$$

where $E_{h\upsilon}$ is

$$E_{h\upsilon} = 13.6\left(1 - \frac{1}{n^2}\right)\frac{1}{\left|X_{lm}\right|^2_{\ell=1}} - h\Delta f$$

$$E_{h\upsilon} = 13.6\left(1 - \frac{1}{n^2}\right)\frac{3}{8\pi} - h\Delta f; \tag{2.80}$$

$$h\Delta f <<< 1$$

$$E_{h\upsilon} = 13.6\left(1 - \frac{1}{n^2}\right)\frac{3}{8\pi}$$

Furthermore, it follows from Eq. (2.75), that the recoil energy of the photon corresponding to momentum transfer to the atom for the case of $\ell = 1$ is one half that of the case where $\ell = 0$ (Eq. (2.73)).

$$\Delta f = \frac{\Delta\omega}{2\pi} = \frac{E_{h\upsilon}}{h} = \frac{1}{2}\frac{\left(E_{h\upsilon}\right)^2}{2m_H c^2} = 6.5\ MHz \tag{2.81}$$

The recoiling electron transfers momentum to the nucleus which binds the electron, and some linear momentum is transferred to the atom as angular momentum. Linear momentum of the electron, atom, and photon are conserved where the propagation vector of the photon does not go through the nucleus; thus, it possesses an equal and opposite component of angular momentum with respect to the atom. The total recoil energy is the sum of the electron component (Eq. (2.79)) and the atom component (Eq. (2.81)). Thus, the calculated Lamb Shift due to both components of linear momentum transfer is

$$\Delta f = 1052\ MHz + 6.5\ MHz = 1058.5\ MHz$$

$$\Delta f = 1052\ MHz + 6.5 MHz = 1058.5 MHz \tag{2.82}$$

The experimental Lamb Shift is $1058\ MHz$.

The present calculations used the electron rest mass; however, the relativistic mass is required in order to be exact. It is given by Eq. (7.31). In addition to the Lamb Shift, the spectral lines of hydrogen are Zeeman split by spin-orbital coupling and electron-nuclear magnetic interactions.

(As a further example, conservation of linear momentum of the

photon is central to the Mössbauer phenomenon. See Mills patent [8]).

SPIN-ORBITAL COUPLING

The spin-orbital coupling split is given by the Dirac equation [9] which applies Special Relativity to a spherically symmetric charge distribution in a central field as is the case with the orbitsphere. And, Dirac's spin-orbital interaction operator follows from Eq. (1.164) and Eq. (1.173).

$$E = m_e c^2 \left[1 + \frac{\alpha}{n - \left(j + \frac{1}{2}\right) + \sqrt{\left(j + \frac{1}{2}\right)^2 - \alpha^2}}\right]^{-\frac{1}{2}} \quad ; \quad n = 1,2,3,\ldots\infty \qquad j + \frac{1}{2} \le n \tag{2.83}$$

The predicted energy difference between the $^2P_{1/2}$ and $^2P_{3/2}$, $^2S_{1/2}$ levels of the hydrogen atom, $E_{s/o}$, given by Eq. (2.83) is

$$E_{s/o} \quad \frac{\alpha^4 m_e c^2}{32} \tag{2.84}$$

which corresponds to a frequency of about 11,000 *MHz* or a wavelength of about 2.7 *cm*. The experimental value is 10,950 *MHz*.

KNIGHT SHIFT

The unpaired electron of the hydrogen atom gives rise to a uniform magnetic field at the nucleus which is given by Eq. (1.120).

$$\mathbf{H} = \frac{e\hbar}{m_e r_n^3}(\mathbf{i}_r \cos\theta - \mathbf{i}_\theta \sin\theta) \qquad r < r_n \tag{2.85}$$

Multiplication of Eq. (2.85) by the permeability of free space, μ_0, and substitution of the Bohr radius of the hydrogen atom, a_H, given by Eq. (1.171) for r_n of Eq. (2.85) gives the magnetic flux, $\mathbf{B_s}$, at the nucleus due to electron spin.

$$\mathbf{B_s} = \frac{\mu_0 e\hbar}{m_e a_H^3}\mathbf{i}_z = 157.29\ T \tag{2.86}$$

The proton possesses a magnetic moment which is derived in the Proton and Neutron Section and is given by

$$\mu_P = \frac{\left(\frac{2}{3}\right)^2 e\hbar}{2\frac{m_p}{2\pi}} \tag{2.87}$$

$\Delta E_{mag}^{\text{proton spir}}$, the energy to flip the orientation of the proton's magnetic moment, μ_P, from parallel to antiparallel to the direction of the magnetic flux $\mathbf{B_s}$ is

$$\Delta E_{mag}^{\text{proton spin}} = -2\mu_P \mathbf{B}_s \tag{2.88}$$

As given in the Spin Angular Momentum of the Orbitsphere with $\ell = 0$ Section, the z directed magnetic field of the nucleus corresponding to the proton magnetic moment given by Eq. (2.87) gives rise to a projection of the angular momentum of the electron onto an axis which precesses about the z-axis of $\sqrt{\frac{3}{4}}\hbar$. The projection of the magnetic energy between the electron orbitsphere and the proton is equivalent to that of the angular momentum onto the axis which precesses about the z-axis, $\sqrt{\frac{3}{4}}$ times that of a Bohr magneton. In the case of the hydrogen atom, the energy to flip the orientation of the proton's magnetic moment, μ_P, from parallel to antiparallel to the direction of the magnetic flux $\mathbf{B}_s$ of the electron is given by the substitution of the magnetic flux $\mathbf{B}_s$ of Eq. (2.86) multiplied by $\sqrt{\frac{3}{4}}$ into Eq. (2.88).

$$\Delta E_{mag}^{\text{proton spin}} = -2\mu_P \frac{\mu_0 e\hbar}{m_e a_H^3}\sqrt{\frac{3}{4}} = -3.837\ X\ 10^{-24}\ J = -2.395\ X\ 10^{-5}\ eV \tag{2.89}$$

The frequency, f, can be determined from the energy using the Planck relationship, Eq. (2.18).

$$f = \frac{3.837\ X\ 10^{-24}\ J}{h} = 5.790\ GHz \tag{2.90}$$

The shift of the NMR frequency of a nucleus by an unpaired electron is called the Knight Shift. The Knight Shift of the hydrogen atom is given by Eq. (2.90) which corresponds to the magnetic flux given by Eq. (2.86). The experimental value is unknown; however, magnetic hyperfine structure shifts of Mossbauer spectra corresponding to magnetic fluxes of 100 T or more due unpaired electrons are common.

SPIN-NUCLEAR COUPLING

The radius of the hydrogen atom is increased or decreased very slightly due to the force between the magnetic moment of the electron and the magnetic field of the nucleus. The magnetic moment of the electron is a Bohr magneton, μ_B, given by Eq. (1.99). The magnetic moment $\mathbf{m}$ of the proton is given by Eq. (2.87), and the magnetic field of the proton follows from the relationship between the magnetic dipole field and the magnetic moment $\mathbf{m}$ as given by Jackson [10] where $\mathbf{m} = \mu_P \mathbf{i}_z$.

$$\mathbf{H} = \frac{\mu_P}{r^3}(\mathbf{i}_r 2\cos\theta - \mathbf{i}_\theta \sin\theta) \tag{2.91}$$

Multiplication of Eq. (2.91) by the permeability of free space, μ_0, gives

the magnetic flux, $\mathbf{B_P}$, due to the nucleus.

$$\mathbf{B_P} = \frac{\mu_0 \mu_P}{r^3}(\mathbf{i}_r 2\cos\theta - \mathbf{i}_\theta \sin\theta) \tag{2.92}$$

The force between the magnetic moment of the electron and the magnetic flux of the proton, $\mathbf{F_{S/N}}$, is

$$\mathbf{F_{S/N}} = \frac{1}{4\pi r_1^2}\mu_B \mathbf{i}_z \cdot \quad \mathbf{B_P} \tag{2.93}$$

Substitution of Eq. (2.92) into Eq. (2.93) gives

$$\mathbf{F_{S/N}} = \pm \frac{1}{4\pi r_1^2}\mu_B 3\frac{\mu_0}{r^4}\ \mu_P \int_0^\pi (\mathbf{i}_r \cos\theta - \mathbf{i}_\theta \sin\theta)\cdot(\mathbf{i}_r 2\cos\theta - \mathbf{i}_\theta \cos\theta)d\theta \tag{2.94}$$

$$\mathbf{F_{S/N}} = \pm \frac{1}{4\pi r_1^2}\mu_B 3\frac{\mu_0}{r^4}\ \mu_P \mathbf{i}_r \tag{2.95}$$

where the plus corresponds to parallel alignment of the magnetic moments of the electron and proton, and the minus corresponds to antiparallel alignment of the magnetic moments of the electron and proton. The force must be corrected for the vector projection of the angular momentum onto the z-axis. As given in the Spin Angular Momentum of the Orbitsphere with $\ell = 0$ Section, the z directed magnetic field of the nucleus corresponding to the proton magnetic moment given by Eq. (1.120) gives rise to a projection of the angular momentum of the electron onto an axis which precesses about the z-axis of $\sqrt{\frac{3}{4}}\hbar$. The projection of the magnetic force between the electron orbitsphere and the proton is equivalent to that of the angular momentum onto the axis which precesses about the z-axis, $\sqrt{\frac{3}{4}}$ times that of a Bohr magneton. The force balance equation of the hydrogen atom including the spin/nuclear force is given by substituting Eq. (2.95) multiplied by $\sqrt{\frac{3}{4}}$ into Eq. (1.165).

$$\frac{m_e}{4\pi r_1^2}\frac{v_1^2}{r_1} = \frac{e}{4\pi r_1^2}\frac{e}{4\pi\varepsilon_o r_1^2} - \frac{1}{4\pi r_1^2}\frac{\hbar^2}{m r_n^3} \pm \frac{1}{4\pi r_1^2}\mu_B 3\frac{\mu_0}{r^4}\ \mu_P\sqrt{\frac{3}{4}} \tag{2.96}$$

Using Eq. (1.47),

$$r_{1\pm} = \frac{a_H + \sqrt{a_H^2 \pm \frac{6\mu_o e \mu_P a_o \sqrt{\frac{3}{4}}}{\hbar}}}{2} \tag{2.97}$$

where r_{1+} corresponds to parallel alignment of the magnetic moments of the electron and proton, r_{1-} corresponds to antiparallel alignment of the magnetic moments of the electron and proton, a_H is the Bohr radius of

the hydrogen atom given by Eq. (1.171), and a_o is the Bohr radius given by Eq. (1.168).

Energy Calculations

The change in the electric energy of the electron due to the slight shift of the radius of the electron is given by the difference between the electric energies associated with the two possible orientations of the magnetic moment of the electron with respect to the magnetic moment of the proton, parallel versus antiparallel. Each electric energy is given by the substitution of the corresponding radius given by Eq. (2.97) into Eq. (1.176). The change in electric energy for the flip from parallel to antiparallel alignment, $\Delta E_{ele}^{S/N}$, is

$$\Delta E_{ele}^{S/N} = \frac{e^2}{8\pi\varepsilon_o}\left[\frac{1}{r_{1-}} - \frac{1}{r_{1+}}\right] = 2.878\ X\ 10^{-24}\ J \tag{2.98}$$

The magnetic energy to flip the orientation of the proton's magnetic moment, μ_P, from parallel to antiparallel to the direction of the magnetic flux $\mathbf{B}_s$ of the electron is given by Eq. (2.89).

$$\Delta E_{mag}^{\text{proton spin}} = -2\mu_P \frac{\mu_0 e\hbar}{m_e a_H^3}\sqrt{\frac{3}{4}} = -3.837\ X\ 10^{-24}\ J \tag{2.99}$$

The total energy of the transition from parallel to antiparallel alignment, $\Delta E_{total}^{S/N}$, is given as the sum of Eqs. (2.98) and (2.99).

$$\Delta E_{total}^{S/N} = \frac{e^2}{8\pi\varepsilon_o}\left[\frac{1}{r_{1-}} - \frac{1}{r_{1+}}\right] - 2\mu_P \frac{\mu_0 e\hbar}{m_e a_H^3}\sqrt{\frac{3}{4}} \tag{2.100}$$

$$\Delta E_{total}^{S/N} = 2.878\ X\ 10^{-24}\ J - 3.837\ X\ 10^{-24}\ J = -9.592\ X\ 10^{-25}\ J \tag{2.101}$$

The energy is expressed in terms of wavelength using the Planck relationship, Eq. (2.65).

$$\lambda = \frac{hc}{\Delta E_{total}^{S/N}} = 21\ cm \tag{2.102}$$

The experimental value from astrophysical studies and from electron spin resonance measurements is $21\ cm$.

SPIN-NUCLEAR AND ORBITAL-NUCLEAR COUPLING OF HYDRINOS

The theory of a previously unknown form of matter: hydrogen atoms having electrons of lower energy than the conventional "ground" state called ***hydrinos***, where each energy level corresponds to a fractional quantum number is given in the Atomic Coulomb Field Collapse--Hydrino Theory--BlackLight Process Section. The radius of the hydrino atom corresponding to the fractional quantum number $\frac{1}{n}$ where n is an integer is the Bohr radius of the hydrogen atom divided by n, $\frac{a_H}{n}$,

and the central field is n times that of the proton. The quantum numbers of the electron for below "ground" states are n, ℓ, m (m_ℓ), and m_s as described in the Atomic Coulomb Field Collapse--Hydrino Theory--BlackLight Process Section. The relationship between the quantum numbers is given by Eq. (5.13).

$$\begin{aligned} n &= 2,3,4,... \\ \ell &= 1,2,...,n-1 \\ m &= -\ell,-\ell+1,...,0,...,+\ell \end{aligned} \tag{2.103}$$

Photons obey Maxwell's Equations. At the two dimensional surface of the orbitsphere containing a "trapped photon", the relationship between the photon's electric field and its two dimensional charge-density at the orbitsphere is

$$\mathbf{n}\cdot\left(\mathbf{E}_1-\mathbf{E}_2\right)=\frac{\sigma}{\varepsilon_0} \tag{2.104}$$

Thus, the photon's electric field acts as surface charge. According to Eq. (2.104), the "photon standing wave" in the electron orbitsphere resonator cavity gives rise to a two dimensional surface charge at the orbitsphere two dimensional surface. The surface charge is given by Eq. (2.104) for a central field strength equal in magnitude to ne. This surface charge possesses the same angular velocity as the orbitsphere; thus, it is a current with a corresponding magnetic field. As demonstrated in the Orbital and Spin Splitting Section, the z component of the angular momentum of an excited state electron orbitsphere corresponding to a "trapped photon" multipole of order (ℓ, m) is

$$L_z = m\hbar \tag{2.105}$$

Eq. (2.105) also applies in the case of ***hydrinos***, hydrogen atoms with below "ground" state electronic energy levels.

The "trapped photon" is a "standing electromagnetic wave" which actually is a circulating wave that propagates along each great circle current loop of the orbitsphere. The time-function factor, $k(t)$, for the "standing wave" is identical to the time-function factor of the orbitsphere in order to satisfy the boundary (phase) condition at the orbitsphere surface. Thus, the angular frequency of the "trapped photon" has to be identical to the angular frequency of the electron orbitsphere, ω_n. Furthermore, the phase condition requires that the angular functions of the "trapped photon" have to be identical to the spherical harmonic angular functions of the electron orbitsphere. The rotational parameters of the surface current of the "photon standing wave" are given in the Derivation of the Rotational Parameters of the Electron Section. The solution to Legendre's equation given by Eq. (1.60) is the maximum term of a series of solutions corresponding to the m and

ℓ values [11,12]. From Eq. (1.86), $\left|\mathbf{L}_o^{photon}\right|$, the magnitude of the orbital angular momentum along the axis which precesses about the z-axis is

$$\left|\mathbf{L}_o^{photon}\right| = \hbar\sqrt{\ell(\ell+1)} \tag{2.106}$$

Therefore, from Eq. (2.36),

$$\mu = \frac{e\hbar}{2m_e}\sqrt{\ell(\ell+1)} = \mu_B\sqrt{\ell(\ell+1)} \tag{2.107}$$

where μ_B is the Bohr magneton. The magnetic moment gives rise to a magnetic field at the nucleus. The magnetic field follows from the relationship between the magnetic dipole field and the magnetic moment **m** as given by Jackson [10] where $\mathbf{m} = \mu_B\sqrt{\ell(\ell+1)}$ where the z-axis is redesignated as the precessing axis.

$$\mathbf{H} = \frac{2\mu_B}{r_n^3}\sqrt{\ell(\ell+1)}(\mathbf{i}_r\cos\theta - \mathbf{i}_\theta\sin\theta) \qquad r < r_n \tag{2.108}$$

Multiplication of Eq. (2.108) by the permeability of free space, μ_0, and substitution of the Bohr radius of the hydrogen atom, a_H, given by Eq. (1.171) for r_n of Eq. (2.108) gives the magnetic flux, $\mathbf{B}_o$, at the nucleus due to the orbital angular momentum of the electron.

$$\mathbf{B}_o = \frac{\mu_0 e\hbar}{m_e a_H^3}\sqrt{\ell(\ell+1)}\mathbf{i}_z \tag{2.109}$$

The orbital-nuclear coupling energy, $\Delta E_{\text{mag}}^{\text{proton orb}}$, the energy to flip the orientation of the proton's magnetic moment, μ_P, from parallel to antiparallel to the direction of the magnetic flux $\mathbf{B}_o$ due to the orbital angular momentum of the electron given by Eq. (2.109), is

$$\Delta E_{\text{mag}}^{\text{proton orb}} = -2\mu_P\mathbf{B}_o \tag{2.110}$$

The spin-nuclear and orbital-nuclear coupling energies superimpose. Thus, $E_{\text{mag}}^{\text{proton spin orb}}$, the energy to flip the orientation of the proton's magnetic moment, μ_P, from parallel to antiparallel to the direction of the magnetic flux $\mathbf{B}_s$ due to electron spin and the magnetic flux $\mathbf{B}_o$ due to the orbital angular momentum of the electron is the sum of Eqs. (2.89) and (2.110).

$$E_{\text{mag}}^{\text{proton spin orb}} = -2\mu_P\mathbf{B}_o - 2\mu_P\mathbf{B}_s\sqrt{\frac{3}{4}} \tag{2.111}$$

The spin and orbital moments of inertia, spin and orbital angular momenta, and spin and orbital kinetic energies of an excited state electron orbitsphere are given in the Derivation of the Rotational Parameters of the Electron Section. Substitution of Eq. (1.55) and Eq. (1.96) into Eq. (1.88) gives the magnitude of the orbital component of the angular momentum of an excited state electron orbitsphere corresponding to a multipole of order (ℓ, m). $\left|\mathbf{L}_o^{electron}\right|$, the magnitude of the orbital angular momentum along the axis which precesses about the

z-axis is

$$\left|\mathbf{L}_o^{electron}\right| = \hbar\left(\frac{\ell(\ell+1)}{\ell^2+\ell+1}\right)^{\frac{1}{2}} \tag{2.112}$$

Eq. (2.112) also applies in the case of ***hydrinos***, hydrogen atoms with below "ground" state electronic energy levels. Therefore, from Eq. (2.36),

$$\mu = \frac{e\hbar}{2m_e}\left(\frac{\ell(\ell+1)}{\ell^2+2\ell+1}\right)^{\frac{1}{2}} = \mu_B\left(\frac{\ell(\ell+1)}{\ell^2+2\ell+1}\right)^{\frac{1}{2}} \tag{2.113}$$

where μ_B is the Bohr magneton. The force between the magnetic moment of the electron due to orbital angular momentum and the magnetic flux of the proton, $\mathbf{F}_{O/N}$, is

$$\mathbf{F}_{O/N} = \frac{1}{4\pi r_1^2}\mu_B\left(\frac{\ell(\ell+1)}{\ell^2+2\ell+1}\right)^{\frac{1}{2}}\mathbf{i}_z \cdot \quad \mathbf{B}_P \tag{2.114}$$

where the z-axis is redesignated as the precessing axis. Substitution of Eq. (2.92) into Eq. (2.114) gives

$$\mathbf{F}_{O/N} = \pm\frac{1}{4\pi r_1^2}\mu_B\left(\frac{\ell(\ell+1)}{\ell^2+2\ell+1}\right)^{\frac{1}{2}}3\frac{\mu_0}{r^4}\ \mu_P\int_0^{\pi}(\mathbf{i}_r\cos\theta - \mathbf{i}_\theta\sin\theta)\cdot(\mathbf{i}_r 2\cos\theta - \mathbf{i}_\theta\cos\theta)d\theta \tag{2.115}$$

$$\mathbf{F}_{O/N} = \pm\frac{1}{4\pi r_1^2}\mu_B\left(\frac{\ell(\ell+1)}{\ell^2+2\ell+1}\right)^{\frac{1}{2}}3\frac{\mu_0}{r^4}\ \mu_P\mathbf{i}_r \tag{2.116}$$

where the plus corresponds to parallel alignment of the magnetic moments of the electron and proton, and the minus corresponds to antiparallel alignment of the magnetic moments of the electron and proton. The force balance equation of the hydrino atom including the spin-nuclear force and the orbital-nuclear force is given by Eq. (5.14), Eq. (2.116), Eq. (1.94), and Eq. (2.96) where the magnitude of the central field is an integer, n.

$$\frac{m_e}{4\pi r_1^2}\frac{v_1^2}{r_1} = \frac{e}{4\pi r_1^2}\frac{ne}{4\pi\varepsilon_o r_1^2} - \frac{1}{4\pi r_1^2}\frac{\hbar^2}{m_e r_n^3} \pm \frac{1}{4\pi r_1^2}\frac{1}{n}\left(\sqrt{\ell(\ell+1)} + \sqrt{\frac{3}{4}}\right)\mu_B 3\frac{\mu_0}{r^4}\ \mu_P \tag{2.117}$$

Using Eq. (1.47),

$$r_{1\pm} = \frac{a_H + \sqrt{a_H^2 \pm \frac{6\mu_o e\left(\sqrt{\ell(\ell+1)} + \sqrt{\frac{3}{4}}\right)\mu_P a_o}{\hbar}}}{2n} \tag{2.118}$$

where r_{1+} corresponds to parallel alignment of the magnetic moments of the electron and proton, r_{1-} corresponds to antiparallel alignment of the magnetic moments of the electron and proton, a_H is the Bohr radius of the hydrogen atom given by Eq. (1.171), and a_o is the Bohr radius given by Eq. (1.168).

Energy Calculations

The change in the electric energy of the electron due to the slight shift of the radius of the electron is given by the difference between the electric energies associated with the two possible orientations of the magnetic moment of the electron with respect to the magnetic moment of the proton, parallel versus antiparallel. Each electric energy is given by the substitution of the corresponding radius given by Eq. (2.118) into Eq. (1.176) where the magnitude of the central field of the hydrino atom is n times that of a proton. The change in electric energy for the flip from parallel to antiparallel alignment, $\Delta E_{ele}^{S/N\ O/N}$, is

$$\Delta E_{ele}^{S/N\ O/N} = \frac{ne^2}{8\pi\varepsilon_o}\left(\frac{1}{r_{1-}} - \frac{1}{r_{1+}}\right) \tag{2.119}$$

The magnetic energy to flip the orientation of the proton's magnetic moment, μ_P, from parallel to antiparallel to the direction of the magnetic flux $\mathbf{B}_s$ due to electron spin and the magnetic flux $\mathbf{B}_o$ due to the orbital angular momentum of the electron follows from Eqs. (2.109) and (2.111) where the radius of the hydrino atom is $\frac{a_H}{n}$.

$$E_{\text{mag}}^{\text{proton spin orb}} = -2\mu_P \frac{n^3\mu_0 e\hbar}{m_e a_H^3}\sqrt{\ell(\ell+1)} - 2\mu_P \frac{n^3\mu_0 e\hbar}{m_e a_H^3}\sqrt{\frac{3}{4}} = -\left(\sqrt{\ell(\ell+1)} + \sqrt{\frac{3}{4}}\right)2\mu_P \frac{n^3\mu_0 e\hbar}{m_e a_H^3} \tag{2.120}$$

The total energy of the transition from parallel to antiparallel alignment, $\Delta E_{total}^{S/N\ O/N}$, is given as the sum of Eqs. (2.119) and (2.120).

$$\Delta E_{total}^{S/N\ O/N} = \frac{ne^2}{8\pi\varepsilon_o}\left(\frac{1}{r_{1-}} - \frac{1}{r_{1+}}\right) - \left(\sqrt{\ell(\ell+1)} + \sqrt{\frac{3}{4}}\right)2\mu_P \frac{n^3\mu_0 e\hbar}{m_e a_H^3} \tag{2.121}$$

For the case that $\ell = 0$,

$$\Delta E_{total}^{S/N\ O/N} = n^2\, 2.878\ X\ 10^{-24}\ J - n^3\, 3.837\ X\ 10^{-24}\ J \tag{2.122}$$

The frequency, f, can be determined from the energy using the Planck relationship, Eq. (2.65).

$$f = \frac{\Delta E_{total}^{S/N\ O/N}}{h} \tag{2.123}$$

From Eq. (2.122), Eq. (2.102), and the Planck relationship, Eq. (2.123), the energy, the wavelength, and the frequency corresponding to the spin-nuclear coupling energy of the hydrino atom with the lower energy state quantum numbers n and ℓ and with the radius $\frac{a_H}{n}$ are given in Table 2.3.

Table 2.3. The spin-nuclear coupling energy of the hydrino atom with the lower energy state quantum numbers n and ℓ and with the radius $\frac{a_H}{n}$.

n	ℓ	Energy ($JX10^{23}$)	Lambda (cm)	Wave Number (cm^{-1})	Frequency (GHz)
1	0	0.09592	20.71	0.04829	1.447
2	0	1.918	1.0355	0.9657	28.95
2	1	5.051	0.3933	2.543	76.23
3	0	7.769	0.2557	3.911	117.2
3	1	20.46	0.09710	10.30	308.7
3	2	29.74	0.06678	14.97	448.9
4	0	19.95	0.09957	10.04	301.1
4	1	52.53	0.03781	26.44	792.8
4	2	76.38	0.02601	38.45	1153
4	3	99.76	0.01991	50.22	1505
5	0	40.77	0.04873	20.52	615.2
5	1	107.3	0.01851	54.03	1620
5	2	156.1	0.01273	78.57	2355
5	3	203.8	0.009746	102.6	3076
5	4	251.3	0.007905	126.5	3792

EINSTEIN A COEFFICIENT

An estimate of the transition probability for magnetic multipoles is given by Eq. (16.105) of Jackson [13]. For a magnetic dipole $\ell=1$, and Eq. (16.105) of Jackson is

$$\frac{1}{\tau_M} \left(\frac{g}{mc}\right)^2 \left(\frac{\hbar e^2}{c}\right) \frac{\pi}{16} k^2 \omega \tag{2.124}$$

Substitution of

$$k = \frac{\omega}{c} \tag{2.125}$$

into Eq. (2.124) gives

$$\frac{1}{\tau_M} \left(\frac{g}{mc}\right)^2 \left(\frac{\hbar e^2}{c}\right) \frac{\pi}{16} \frac{\omega^3}{c^2} \tag{2.126}$$

From Eq. (2.126), the transition probability is proportional to the frequency cubed. The experimental Einstein A coefficient for hydrogen $H(n=1)$ [14] is

$$A = 2.87\ X\ 10^{-15}\ \sec^{-1} \tag{2.127}$$

The frequencies for the spin/nuclear hyperfine transition of hydrogen $H(n=1)$ and hydrino $H(n=1/2)$ are given in Table 2.3. The Einstein A coefficient for hydrino $H(n=1/2)$ is given by Eq. (2.126) and Eq. (2.127) and the frequencies of Table 2.3.

$$A_{H(n=1/2)} = A_{H(n=1)}\left(\frac{\omega_{H(n=1/2)}}{\omega_{H(n=1)}}\right)^3 = 2.87\ X\ 10^{-15}\left(\frac{28.95}{1.447}\right)^3 \sec^{-1} = 2.30\ X\ 10^{-11}\ \sec^{-1} \tag{2.128}$$

INTENSITY OF SPIN-NUCLEAR AND ORBITAL-NUCLEAR COUPLING TRANSITIONS OF HYDRINOS

The intensity, I, of spin-nuclear and orbital-nuclear coupling transitions of hydrinos can be calculated from the column density of hydrogen or hydrino atoms, $N(H)$, and the Einstein A coefficient, A_{ul}. The column density is given by the product of the number of hydrogen or hydrino atoms per unit volume, n_H, and the path length, ℓ, which is calculated in steradians from its integral.

$$I = \frac{1}{4\pi} A_{ul} N(H) = \frac{1}{4\pi} A_{ul} n_H \ell \tag{2.129}$$

The number of hydrogen or hydrino atoms per unit volume, n_H, can be determined from the experimental results of Labov and Bowyer [15]. The number of electronic transitions per atom per second, k_1 (Eq. (5.69) of the Interstellar Disproportionation Rate Section), is equivalent to the number of photons per atom per second, A_{ul} (Eq. (2.129). Equating intensities of photon flux (Eq. (2.129) and the rate of the disproportionation reaction, $r_{m,m',p}$ Eq. (5.70), gives

$$I = \frac{1}{4\pi} A_{ul} N(H) = \frac{1}{\sqrt{2}} n_H \left(\frac{a_H}{p}\right)^2 \sqrt{\frac{3kT}{m_H}} N(H) \tag{2.130}$$

where $N(H) = n_H \ell$ is the column density. The intensity reported by Labov and Bowyer for the 304 $\AA$ line which is herein assigned as the $1/3 \rightarrow 1/4$ H transition is $I = 2080^{+740}_{-720}\ photons\ cm^{-2} s^{-1} sr^{-1}$ [15]. In the case that $m=1$, $m'=2$, and $p=3$ in Eqs. (5.50-5.52); $T=50\ K$, and $g_{m,p}=1$ (the result of Förster's theory for the efficiencies of dipole-dipole resonant energy transfers), the column density of hydrino atoms, $H\left(\frac{a_H}{3}\right)$, is calculated along the sight-line at b=48 deg to be

$$N(H) = 2\ X\ 10^{18}\ cm^{-2} \tag{2.131}$$

The calculated density of hydrino atoms, $H\left(\frac{a_H}{3}\right)$, is

$$n_H = 4\,X\,10^3\ atom/m^3 \tag{2.132}$$

Substitution of Eq. (2.132) and Eq. (2.128) into Eq. (2.129) gives the intensity as a function of the path length, ℓ, which is calculated in steradians from its integral.

$$I = \frac{1}{4\pi} A_{ul} N(H) = \frac{1}{4\pi}\left(2.30\,X\,10^{-11}\ \sec^{-1}\right)\left(4\,X\,10^3\ \frac{atom}{m^3}\right)\left(\frac{1\ photon}{atom}\right)\ell \tag{2.133}$$

References

1. Mizushima, M., Quantum Mechanics of Atomic Spectra and Atomic Structure, W.A. Benjamin, Inc., New York, (1970), p.17.
2. Jackson, J. D., Classical Electrodynamics, Second Edition, John Wiley & Sons, New York, (1962), pp. 739-752.
3. McQuarrie,D. A., Quantum Chemistry, University Science Books, Mill Valley, CA, (1983), pp. 238-241.
4. Jackson, J. D., Classical Electrodynamics, Second Edition, John Wiley & Sons, New York, (1962), pp. 752-763.
5. Jackson, J. D., Classical Electrodynamics, Second Edition, John Wiley & Sons, New York, (1962), pp. 758-763.
6. Siebert, W. McC., Circuits, Signals, and Systems, The MIT Press, Cambridge, Massachusetts, (1986), pp. 488-502.
7. Lamb, W. E., Retherford, R. C., Phys. Rev., Vol. 72, (1947), pp. 241-243.
8. R. L. Mills, EPO Patent Number 86103694.5/0 198 257, Method and Apparatus for Selective Irradiation of Biological Materials, (1986).
9. Berestetskii, V. B., Lifshitz, E. M., Pitaevskii, Quantum Electrodynamics, Pergamon Press, Oxford, (1982), pp. 118-128.
10. Jackson, J. D., Classical Electrodynamics, Second Edition, John Wiley & Sons, New York, (1962), p. 178.
11. McQuarrie, D. A., Quantum Chemistry, University Science Books, Mill Valley, CA, (1983), pp. 206-221.
12. Pauling, Linus, Wilson, E., Bright, Introduction to Quantum Mechanics with Applications to Chemistry, McGraw-Hill Book Company, New York, (1935), pp. 118-121.
13. Jackson, J. D., Classical Electrodynamics, Second Edition, John Wiley & Sons, New York, (1962), pp. 758-760.
14. Allen, C. W., Astrophysical Quantities, 3 rd Edition, (1973), University of London, The Athlone Press, p. 79.
15. Labov, S., Bowyer, S., "Spectral observations of the extreme ultraviolet background", The Astrophysical Journal, 371, (1991), pp. 810-819.

ELECTRON IN FREE SPACE

CHARGE DENSITY FUNCTION

The radius of an electron orbitsphere increases with the absorption of electromagnetic energy [1]. With the absorption of a photon of energy exactly equal to the ionization energy, the electron is at rest; the de Broglie wavelength, $\lambda = h/p$, is infinite, and the electron is infinitely large. Upon ionization, the radius of the spherical shell, orbitsphere, goes to infinity as is the case with a spherical wavefront of light emitted from a symmetrical source; the free electron propagates with linear velocity, and the de Broglie wavelength is finite. The ionized electron is a plane wave that propagates as a wavefront with the de Broglie wavelength where the size of the electron is the de Broglie wavelength as shown below. Analogously, as the radius of a spherical wavefront of light goes to infinity its propagation is given by the plane wave equation:

$$\mathbf{E} = E_o e^{-ik_z z} \tag{3.1}$$

Light and electrons display identical propagation and diffraction behavior. (This is expected because an electron is created from a photon as derived in the Pair Production Section). Electrons behave as two dimensional wavefronts with the de Broglie wave length, $\lambda = h/p$, in double-slit experiments (Davisson-Germer experiment) [2]. The plane wave nature of free electrons is demonstrated in the Electron Scattering by Helium Section. (The proton and neutron also demonstrate interference patterns during diffraction because they are locally two dimensional having the de Broglie wavelength.)

As r goes to infinity the electron becomes ionized and is a plane wave with the de Broglie wavelength. The ionized electron traveling at constant velocity is nonradiative and is a two dimensional surface having a total charge of e and a total mass of m_e. The solution of the spacetime charge-density function of the ionized electron is solved as a boundary value problem as described previously for the bound electron in the One Electron Atom Section. The de Broglie wavelength relationship given by Eq. (1.46) must hold independent of the radius of the electron. The relationship between the electron orbitsphere radius and its wavelength, is given by Eq. (1.43). The scalar sum of the magnitude of the angular momentum is $\hbar$ (Eq. (1.57)) independent of the electron radius; thus, for both the bound electron and the free electron, the scalar sum of the magnitude of the angular momentum is $\hbar$. The spacetime charge-density function of the free electron is a solution of the Classical Wave Equation (Eq. (1.1)) The current-density function possesses no spacetime Fourier components synchronous with waves traveling at the speed of light; thus

it is nonradiative. As shown below, the solution of the boundary value problem of the free electron is given by the projection of the orbitsphere into a plane that linearly propagates along an axis perpendicular to the plane where the velocity of the plane and the orbitsphere is given by Eq. (1.47) where the radius of the orbitsphere in spherical coordinates is equal to the radius of the free electron in cylindrical coordinates.

Consider an electron orbitsphere of radius r_0. The boundary condition that the de Broglie wavelength holds for any electron radius requires that the ionized electron is the projection of the orbitsphere into $\pi(z)$, the Cartesian xy-plane that propagates linearly along the z-axis with the same linear velocity as the electron orbitsphere. The mass density function, $\rho_m(\rho,\phi,z)$, of the electron with linear velocity along the z-axis of v_z ***in the inertial frame of the proton*** given by Eq. (1.47)

$$\mathbf{v}_z = \frac{\hbar}{m_e r_n} = \frac{\hbar}{m_e r_0} = \frac{\hbar}{m_e \rho_o} \tag{3.2}$$

is given by the projection into the xy-plane of the convolution, , of the xy-plane, $\pi(z)$, with an orbitsphere of radius r_o. The convolution is

$$\pi(z) \quad \delta(r - r_o) = \sqrt{r_o^2 - z^2}\,\delta(r - \sqrt{r_o^2 - z^2}) \tag{3.3}$$

where the orbitsphere function is given in spherical coordinates. The equation of the free electron is given as the projection of Eq. (3.3) into the xy-plane which is

$$\rho_m(\rho,\phi,z) = N\pi\left(\frac{\rho}{2\rho_o}\right)\sqrt{\rho_0^2 - \rho^2}\,\delta(z) \tag{3.4}$$

where $\rho_m(\rho,\phi,z)$ is given in cylindrical coordinates, N is the normalization factor, and the function, $\pi\left(\frac{\rho}{2\rho_o}\right)$ represents a two dimensional disk of radius ρ_o. The total mass is m_e. Thus, Eq. (3.4) must be normalized.

$$m_e = N\int_0^{2\pi}\int_{-\infty}^{\infty}\sqrt{\rho_0^2 - \rho^2}\,\rho\, d\rho\, d\phi \tag{3.5}$$

$$N = \frac{m_e}{\frac{2}{3}\pi\rho_0^3} \tag{3.6}$$

The mass density function of a free electron is a two dimensional disk having the mass density distribution in the xy(ρ)-plane

$$\rho_m(\rho,\phi,z) = \frac{m_e}{\frac{2}{3}\pi\rho_0^3}\pi\left(\frac{\rho}{2\rho_o}\right)\sqrt{\rho_0^2 - \rho^2}\,\delta(z) \tag{3.7}$$

and charge-density distribution, $\rho_e(\rho,\phi,z)$, in the xy-plane

$$\rho_e(\rho,\phi,z) = \frac{e}{\frac{2}{3}\pi\rho_0^{\,3}}\pi\left(\frac{\rho}{2\rho_o}\right)\sqrt{\rho_0^{\,2}-\rho^2}\,\delta(z) \qquad (3.8)$$

where $\rho_e(\rho,\phi,z)$ is given in cylindrical coordinates. The magnitude of each distribution is shown in Figure 3.1. ***The charge density distribution of the free electron given by Eq. (3.8) and shown in Figure 3.1 has recently been confirmed experimentally*** [3-4]. Researchers working at the Japanese National Laboratory for High Energy Physics (KEK) demonstrated that the charge of the free electron increases toward the particle's core and is symmetrical as a function of ϕ.

Figure. 3.1. The front view of the magnitude of the mass (charge) density function in the xy-plane of a free electron; side view of a free electron along the axis of propagation--z-axis.

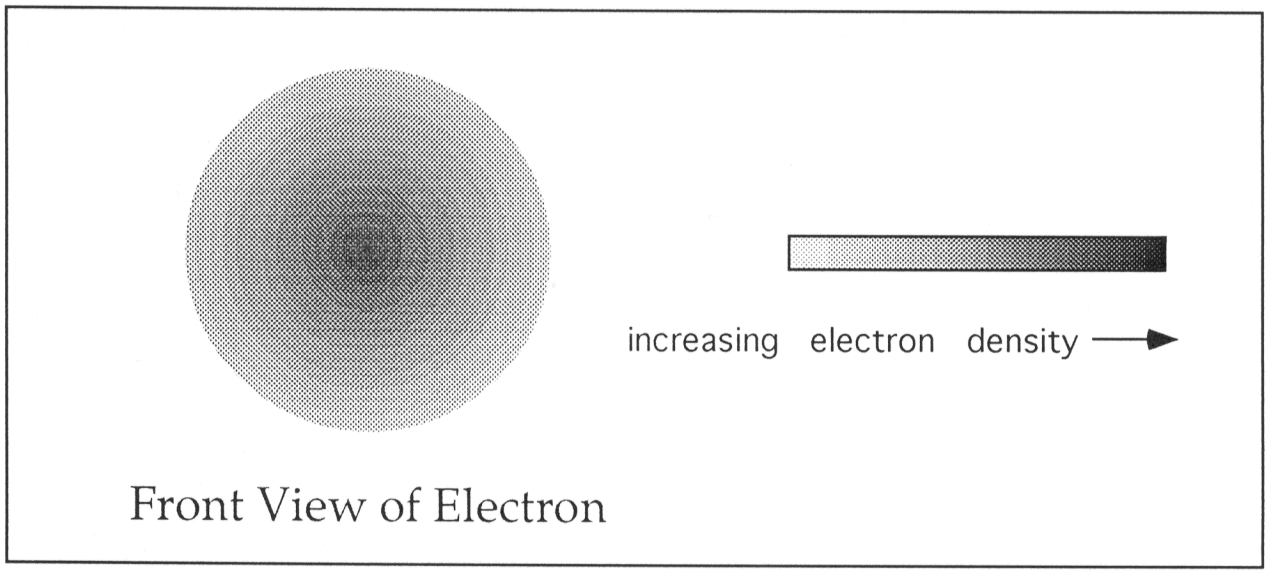

$$\rho_0 = \frac{\hbar}{mv_z}$$

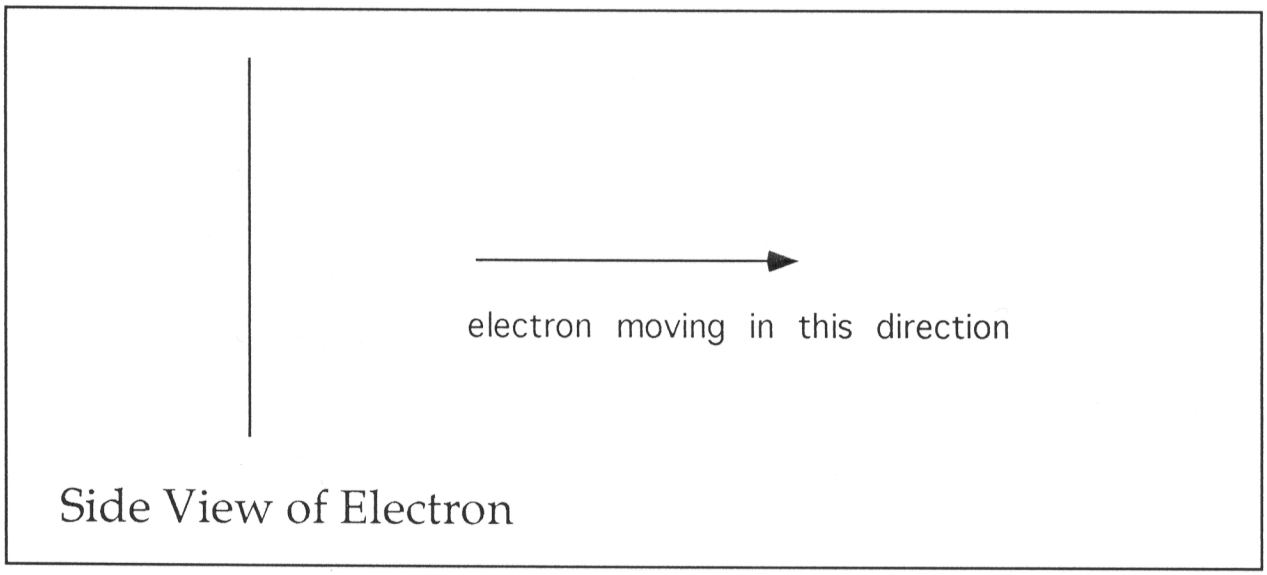

CURRENT DENSITY FUNCTION

This surface has an electric field equivalent to a point charge at the origin along the z-axis as shown in the Electric Field of the Electron in Free Space Section. The free electron possesses time harmonic charge motion in the xy-plane. In general, the current-density function is the product of the charge-density function times the angular velocity function. During ionization of the electron, the scalar sum of the magnitude of the angular momentum, $\hbar$, must be conserved. The current-density function of a free electron propagating with ***velocity*** v_z ***along the z-axis in the inertial frame of the proton*** is given by the vector projections of the current into xy-plane for $r = r_o$ to $r = \infty$ which corresponds to the ionization of the electron initially bound as an orbitsphere of radius $r = r_n = r_o$. The magnitude of the angular velocity of the orbitsphere is given by Eq. (1.55) is

$$\omega = \frac{\hbar}{m_e r^2} \tag{3.9}$$

The current-density function of the free electron, $\mathbf{K}(\rho,\phi,z,t)$, is the projection into the xy-plane of the integral of the product of the projections of the charge of the orbitsphere (Eq. (3.3)) times the angular velocity as a function of the radius r of the ionizing orbitsphere (Eq. (3.9)) for $r = r_o$ to $r = \infty$. The integral is

$$\int_{r_o}^{\infty} \omega \Pi(z) \quad \delta(r - r_o)dr = \frac{e}{\frac{2}{3}\pi r_0^{\,3}} \int_{r_o}^{\infty} \frac{\hbar}{m_e r^2} \sqrt{r_0^2 - z^2}\, \delta(r - \sqrt{r_0^2 - z^2})dr \tag{3.10}$$

The projection of Eq. (3.10) into the xy-plane is

$$\mathbf{J}(\rho,\phi,z,t) = \begin{bmatrix} \\ \Pi\left(\frac{\rho}{2\rho_o}\right) \frac{e}{\frac{4}{3}\pi\rho_0^{\,3}} \frac{\hbar}{m_e\sqrt{\rho_0^{\,2} - \rho^2}} \end{bmatrix} \mathbf{i}_\phi \tag{3.11}$$

where $\rho_o = r_o$. The factor of $\frac{1}{2}$ in Eq. (3.11) arises from the vector projection of the angular momentum of the orbitsphere into the xy-plane as follows from Eqs. (1.68 - 1.71) and Figures 1.3, 1.4, and 1.5. The angular momentum, **L**, is given by

$$\mathbf{L}\mathbf{i}_z = m_e r^2 \omega \tag{3.12}$$

Substitution of m_e for e in Eq. (3.11) followed by substitution into Eq. (3.12) gives the angular momentum density function, **L**

$$\mathbf{L}\mathbf{i}_z = \Pi\left(\frac{\rho}{2\rho_o}\right) \frac{m_e}{\frac{4}{3}\pi\rho_0^{\,3}} \frac{\hbar}{m_e\sqrt{\rho_0^{\,2} - \rho^2}} \rho^2 \tag{3.13}$$

The total angular momentum of the free electron is given by integration over the two dimensional disk having the angular momentum density

given by Eq. (3.13).

$$\mathbf{L}\mathbf{i}_z = \int_0^{2\pi}\int_0^{\rho_0} \pi\left(\frac{\rho}{2\rho_o}\right)\frac{m_e}{\frac{4}{3}\pi\rho_0^{\,3}}\frac{\hbar}{m_e\sqrt{\rho_0^{\,2}-\rho^2}}\rho^2 d\rho d\rho d\phi \tag{3.14}$$

$$\mathbf{L}\mathbf{i}_z = \hbar \tag{3.15}$$

Eq. (3.15) is in agreement with Eq. (1.130); thus, the scalar sum of the magnitude of the angular momentum is conserved. The four dimensional spacetime current-density function of the free electron that propagates along the z-axis with velocity given by Eq. (3.2) corresponding to $r = r_o$ is given by substitution of Eq. (3.2) into Eq. (3.11) and is shown in Figure 3.2.

$$\mathbf{J}(\rho,\phi,z,t) = \left[\pi\left(\frac{\rho}{2\rho_o}\right)\frac{e}{\frac{4}{3}\pi\rho_0^{\,3}}\frac{\hbar}{m_e\sqrt{\rho_0^{\,2}-\rho^2}}\,\mathbf{i}_\phi + \frac{e\hbar}{m_e\rho_0}\delta\left(z-\frac{\hbar}{m_e\rho_0}t\right)\mathbf{i}_z\right] \tag{3.16}$$

Figure 3.2. The magnitude of the current-density function, $|\mathbf{J}|$, of the free electron in the xy-plane cutaway through the top and side.

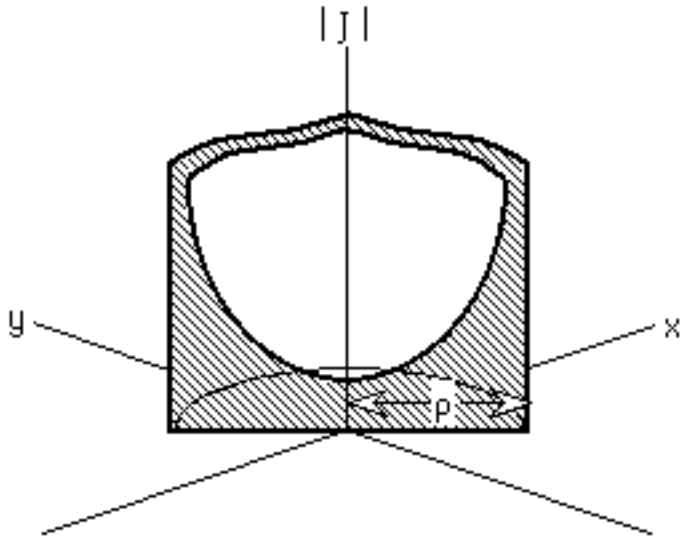

The spacetime Fourier Transform of Eq. (3.16) is [5-6]

$$\frac{e}{\frac{4}{3}\pi\rho_0^{\,3}}\frac{\hbar}{m_e}\mathrm{sinc}(2\pi s\rho_o) + 2\pi e\frac{\hbar}{m_e\rho_0}\delta(\omega - \mathbf{k}_z\cdot\mathbf{v}_z) \tag{3.17}$$

The condition for nonradiation of a moving charge-density function is that the spacetime Fourier transform of the current-density function must not possess waves synchronous with waves traveling at the speed

of light, that is synchronous with $\frac{\omega_n}{c}$ or synchronous with $\frac{\omega_n}{c}\sqrt{\frac{\varepsilon}{\varepsilon_o}}$ where ε is the dielectric constant of the medium. The Fourier transform of the current-density function of the free electron is given by Eq. (3.17). Consider the radial part of, J , the Fourier transform of the current-density function where the z spatial dimensional transform is not zero:

$$J \quad \text{sinc}(s\rho_o) = \frac{\sin 2\pi s\rho_o}{2\pi s\rho_o} \tag{3.18}$$

For time harmonic motion corresponding to the electron parameters ω_0 and s_o, Eq. (1.43),

$$2\pi\rho_o = \lambda_o \tag{3.19}$$

The charge motion of the free electron is angular; however, a radial component exists due to Special Relativistic effects. Consider the radial wave vector of the sinc function, when the radial projection of the velocity is c

$$\mathbf{s}\cdot\mathbf{v} = \mathbf{s}\cdot\mathbf{c} = \omega_0 \tag{3.20}$$

The relativistically corrected wavelength is

$$\rho_o = \lambda_o \tag{3.21}$$

(i.e. the lab frame motion in the angular direction goes to zero as the velocity approaches the speed of light). Substitution of Eq. (3.21) into the sinc function results in the vanishing of the entire Fourier Transform of the current-density function. Thus, spacetime harmonics of $\frac{\omega_n}{c} = k$ or $\frac{\omega_n}{c}\sqrt{\frac{\varepsilon}{\varepsilon_o}} = k$ do not exist. Radiation due to charge motion does not occur in any medium when this boundary condition is met.

Furthermore, consider the z spatial dimensional transform of, J , the Fourier transform of the current-density function:

$$J \quad 2\pi e\frac{\hbar}{m_e\rho_0}\delta(\omega - \mathbf{k}_z\cdot\mathbf{v}_z) \tag{3.22}$$

The only nonzero Fourier components are for

$$k_z = \frac{\omega}{v_z\cos\theta} > \frac{\omega}{c} \tag{3.23}$$

where θ is the angle between $\mathbf{k}_z$ and $\mathbf{v}_z$. Thus, no Fourier components that are synchronous with light velocity with the propagation constant $|\mathbf{k}_z| = \frac{\omega}{c}$ exist. Radiation due to charge motion does not occur when this boundary condition is met. It follows from Eq. (3.2) and Eq. (3.19) that the wavelength of the free electron is

$$\lambda_o = \frac{h}{m_e v_z} = 2\pi\rho_o \tag{3.24}$$

which is the de Broglie wavelength.

The free electron is a two dimensional disk with a charge distribution given by Eq. (3.8) having a radius ρ_o given by Eq. (3.24). This distribution is a minimal energy surface. An attractive magnetic force exists between current circles in the xy-plane. The force balance equation is given by equating the centrifugal and centripetal magnetic electrodynamic force as given in the Two Electron Atom Section. The magnetic field, **B**, of each current loop of current, **i**, is

$$\mathbf{B} = \frac{\mu_o \mathbf{i}}{2\pi r} \tag{3.25}$$

The force balance between the Lorentzian Force and the centrifugal force is

$$m\mathbf{vw} = \frac{1}{2} e\mathbf{v} \times \mathbf{B} = \frac{1}{2} evB \tag{3.26}$$

Substitution of Eq. (3.25) and

$$\mathbf{i} = e\frac{\omega}{2\pi} \tag{3.27}$$

into Eq. (3.26) gives

$$\omega = \left[\frac{e^2\mu_o}{2m_e r}\right]\frac{\omega}{(2\pi)^2} \tag{3.28}$$

According to invariance of charge under Gauss's Integral Law, the relativistic correction for current, i, and the charge, e, is 2π, and it follows from that Eq. (7.6) and Eq. (7.15) of the Two Electron Atom Section that the term in brackets is factored out as the relativistic correction for the electrodynamic force between current loops. Thus, from Eq. (3.28),

$$\omega = \omega \tag{3.29}$$

And, the electron is in force balance.

Furthermore, the free electron possesses a total charge e, a total mass m_e, and a scalar sum of the magnitude of the angular momentum of $\hbar$. The magnetic moment is given by Eq. (2.36); thus,

$$\mu_B = \frac{e\hbar}{2m_e} = 9.274\ X\ 10^{-24}\ JT^{-1} \tag{3.30}$$

which is the Bohr magneton. Conservation of angular momentum with the linking of the magnetic flux quantum gives rise to the spin quantum number, m_S, and the fluxon g factor which is the same as given previously in the Electron g Factor Section.

The free electron possesses current in the xy-plane given by Eq. (3.16), the current along the z-axis follows from Eqs. (1.54), (3.2), and (3.27)

$$\mathbf{i} = e\frac{\omega}{2\pi} = \frac{e\hbar}{2\pi m_e \rho_o^2} \tag{3.31}$$

STERN-GERLACH EXPERIMENT

The free electron arises during pair production and ionization. In both cases the production photon or the ionizing photon carries $\hbar$ of angular momentum. The derivations of the parameters of the free electron were made with the conservation of the photon angular momentum implicit. The vector and scalar parameters of the bound electron in a magnetic field are conserved in the case of a free electron in a magnetic field. Consider the case where a magnetic field is applied to the free electron. The energy of interaction of the magnetic moment of a Bohr magneton of the free electron with the applied magnetic field is minimized. The z'-axis (the former z-axis before the application of the magnetic field) of the free electron precesses about the direction of the applied field, the z-axis called the spin axis. The precessing free electron comprising a two dimensional disk rotates time harmonically about the x'-axis and by the same angle, θ, at any time point, about the y'-axis (the primed axis refers to the coordinate system of the free electron where the two dimensional disk lies in each new x'y'(ρ)-plane corresponding to each new set of axes established by rotations about the x' and y' axes) over the continuous angular range, $-\frac{\pi}{2} \le \theta \le \frac{\pi}{2}$. The scalar sum of the magnitude of the angular momentum of the free electron is $\hbar$ (Eq. (3.15)). Now, allow the rotations about the x'-axis and y'-axis by θ to go from $-\frac{\pi}{2}$ to $\frac{\pi}{2}$. (During the precession of the free electron function, this motion results in a sphere being swept out in space relative to the coordinate system that travels at v_z with the free electron). The vector projection of the angular momentum onto the xy-plane, $\mathbf{L}_{xy}$, due to the rotation about each axis goes as $|\sin\theta|$. The vector projection of the angular momentum onto the z-axis, $\mathbf{L}_z$, due to the rotation about each axis goes as $|\cos\theta|$. Because rotation occurs about two orthogonal axes, each of the total angular projections, $\mathbf{L}_{xy}$ and $\mathbf{L}_z$, is the root mean square value (rms) squared of the total angular momentum, $\hbar$.

$$\mathbf{L}_{xy} = \mathbf{L}_z = \hbar \frac{1}{\sqrt{2}} \ \frac{1}{\sqrt{2}} = \frac{\hbar}{2} \tag{3.32}$$

The z'-axis precesses about the spin axis; thus, the time average projection of the angular momentum onto the xy-plane, $\langle \mathbf{L}_{xy} \rangle$ is zero, and $\langle \mathbf{L}_z \rangle$, the time average projection of the angular momentum onto the z-axis, is

$$\langle \mathbf{L}_z \rangle = \frac{\hbar}{2} \tag{3.33}$$

Given that the time average angular momentum in the xy-plane is zero,

S, the projection of the free electron angular momentum that precesses about the z-axis called the spin axis follows from Eq. (3.15), and the relationship between the components:

$$\left\langle \mathbf{L}_{xy} \right\rangle_{\sum \Delta\alpha}^{2} + \mathbf{S}^2 = \hbar^2 \tag{3.34}$$

It follows from Eq. (3.32) and Eq. (3.34) that **S** is

$$\mathbf{S} = \sqrt{\left(1 - \frac{1}{4}\right)\hbar^2} = \pm\sqrt{\frac{3}{4}}\hbar \tag{3.35}$$

S rotates about the z-axis; thus, $\langle \mathbf{S}_z \rangle$, the time averaged projection of the orbitsphere angular momentum onto the axis of the applied magnetic field is $\pm\frac{\hbar}{2}$. The plus or minus sign corresponds to the two possible vector orientations which are observed with the Stern-Gerlach described below.

The precessing free electron sweeps out a sphere in space relative to the free electron's inertial frame, and the spatial distribution of angular momentum is equivalent to that given is Figure 1.5 and in the Orbitsphere Equation of Motion for $\ell = 0$ Section. The total angular momentum of the free electron of magnitude $\hbar$ is conserved. The projection of the total angular momentum onto the **S** axis is $\pm\sqrt{\frac{3}{4}}\hbar$, and the angular momentum in the direction of the applied field is $\pm\frac{\hbar}{2}$. Magnetic flux is linked by the electron in units of the magnetic flux quantum with conservation of angular momentum as in the case of the orbitsphere as the projection of the angular momentum along the magnetic field axis of $\frac{\hbar}{2}$ reverses direction. The energy, ΔE_{mag}^{spin}, of the spin flip transition corresponding to the $m_S = \frac{1}{2}$ quantum number is given by Eq. (1.151).

$$\Delta E_{mag}^{spin} = 2g\mu_B B \tag{3.36}$$

The Stern-Gerlach experiment implies a magnetic moment of one Bohr magneton and an associated angular momentum quantum number of 1/2. Historically, this quantum number is called the spin quantum number, m_S, and that designation is maintained.

ELECTRIC FIELD OF A FREE ELECTRON

The electric potential of a free electron is given by Poisson's Equation for a charge-density function, $\rho(x', y', z')$

$$\Phi(x,y,z) = \iiint \frac{\rho(x', y', z')dv'}{4\pi\varepsilon_o\sqrt{(x-x')^2+(y-y')^2+(z-z')^2}} \quad (3.37)$$

and the charge-density function of the electron, Eq. (3.8)

$$\Phi(x,y,z) = -\frac{e}{\frac{2}{3}\pi\rho_0{}^3}\frac{1}{4\pi\varepsilon_o}\int_{-\infty}^{\infty}\int_{-\rho_o}^{\rho_o}\int_{-\sqrt{\rho_0{}^2-y^2}}^{+\sqrt{\rho_0{}^2-y^2}}\frac{\sqrt{\rho_o{}^2-x'^2-y'^2}\,\delta(z')dx'\,dy'\,dz'}{\sqrt{(x-x')^2+(y-y')^2+z^2}} \quad (3.38)$$

For $x = y = 0$; $r = z$,

$$\Phi(r) = -\frac{e}{4\pi\varepsilon_o r} \quad (3.39)$$

For $r = \sqrt{x^2+y^2+z^2} >> \rho_o$

$$\Phi(r) = -\frac{e}{4\pi\varepsilon_o r} \quad (3.40)$$

Eqs. (3.39) and (3.40) are equivalent to the potential of a point charge at the origin. The electric field, **E**, is the gradient of the electric potential given by Eqs. (3.38-3.40)

$$\mathbf{E} = -\ \Phi \quad (3.41)$$

References

1. Clark, D., "Very large hydrogen atoms in interstellar space", Journal of Chemical Education, 68, No. 6, (1991), pp. 454-455.
2. Matteucci, G., "Electron wavelike behavior: a historical and experimental introduction", Am. J. Phys., 58, No. 12, (1990), pp. 1143-1147.
3. Gribbin, J., New Scientist, January, 25, (1997), p. 15.
4. Levine, I., et al., Physical Review Letters, Vol. 78., No. 3, (1997), pp. 424-427.
5. Bracewell, R. N., The Fourier Transform and Its Applications, McGraw-Hill Book Company, New York, (1978), pp. 248-249.
6. Haus, H. A., "On the radiation from point charges", American Journal of Physics, 54, (1986), pp. 1126-1129.

EQUATION OF THE PHOTON

RIGHT AND LEFT HAND CIRCULAR AND ELLIPTICALLY POLARIZED PHOTONS

The equation of the photon in free space is derived as a boundary value problem involving the transition from the ground state to an excited state of the hydrogen atom. The "ground" state function of the hydrogen atom is an orbitsphere given in the Orbitsphere Equation of Motion Section, and the excited state function comprising the orbitsphere and a resonant trapped photon is given in the Excited States of the One Electron Atom (Quantization) Section. During the transition from an excited state having a "trapped photon" given by Eq. (2.15) and with the orbitsphere equation given by Eq. (2.11) to the ground state orbitsphere having the equation given by Eqs. (1.68 - 1.71) and Figures 1.3, 1.4, and 1.5, the orbitsphere angular momentum, $\hbar$ (Eq. (1.57), and photon angular momentum, $\hbar$, are conserved. The time-averaged angular-momentum density, $\mathbf{m}$, of the emitted photon is given by Eq. (16.61) of Jackson [1]

$$\mathbf{m} = \frac{1}{8\pi} \mathrm{Re}[\mathbf{r} \times (\mathbf{E} \times \mathbf{B}^*)] \tag{4.1}$$

Thus, the photon equation is given by the superposition of two orbitspheres at the same radius- one with electric field lines which follow great circles and one with magnetic field lines which follow great circles. The magnetic orbitsphere is rotated $\frac{\pi}{2}$ relative to the electric orbitsphere; thus, the magnetic field lines are orthogonal to the electric field lines.

$$X\mathbf{E} = \frac{\delta \mu_o \mathbf{H}}{\delta t} \tag{4.2}$$

$$X\mathbf{H} = \frac{\delta \varepsilon_o \mathbf{E}}{\delta t} \tag{4.3}$$

A right-handed circularly polarized photon orbitsphere is generated as follows: Consider two orthogonal great circle field lines. The Cartesian coordinate system wherein the first great circle magnetic field line lies in the yz-plane, and the second great circle electric field line lies in the xz-plane is designated the photon orbitsphere reference frame.

The electric and magnetic field lines of the right-handed circularly polarized photon are given in Figure 4.1.

Figure 4.1. The Cartesian coordinate system wherein the first great circle magnetic field line lies in the yz-plane, and the second great circle electric field line lies in the xz-plane is designated the photon

orbitsphere reference frame of a right-handed circularly polarized photon orbitsphere.

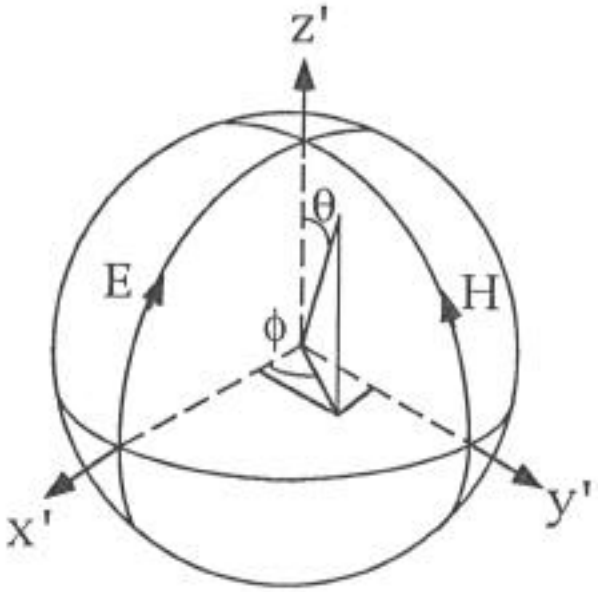

The photon orbitsphere comprises an infinite series of correlated orthogonal great circle field lines. It is generated by an infinite series of nested rotations of two orthogonal great circle field lines each about the new x-axis and new y-axis which results from the preceding such rotation. Each such two orthogonal great circle field lines wherein the first great circle magnetic field line lies in the yz-plane, and the second great circle magnetic field line lies in the xz-plane of the photon orbitsphere reference frame is an element of the infinite series. The first such orthogonal great circle field lines is shown in Figure 4.1. The second element of the series is generated by rotation of the first element by an infinitesimal angle $\Delta\alpha$ about the first x-axis followed by a rotation by the same infinitesimal angle $\Delta\alpha$ about the new (second) y-axis to form a second x-axis. The third element of the series is generated by the rotation of the second element by the infinitesimal angle $\Delta\alpha$ about the second x-axis followed by the rotation by the same infinitesimal angle $\Delta\alpha$ about the new (third) y-axis. In general, the $(n+1)$th element of the series is generated by the rotation of the nth photon orbitsphere coordinate system by the infinitesimal angle $\Delta\alpha$ about the nth x-axis followed by the rotation of the nth photon orbitsphere coordinate system by the infinitesimal angle $\Delta\alpha$ about the $(n+1)$th new y-axis. The total photon orbitsphere is given by reiterations of the successive rotations where the summation of the rotation about each of the x-axis

and the y-axis is $\sum_{n=1}^{\frac{\sqrt{2}\pi}{\Delta\alpha}} \Delta\alpha = \sqrt{2}\pi$.

Consider a point of each of the two orthogonal great circle field lines, one and two, in the reference frame of the orbitsphere at time zero. Point one is at $x' = 0$, $y' = 0$, and $z' = r_n$ and point two is at $x' = r_n$, $y' = 0$, and $z' = 0$. Let point one move on a great circle toward the negative y'-axis, as shown in Figure 4.1, and let point two move on a great circle toward the positive z'-axis, as shown in Figure 4.1. The equations of motion, in the reference frame of the photon orbitsphere are given by

point one:

$$x_1' = 0 \qquad y_1' = -r_n \sin(\omega_n t) \qquad z_1' = r_n \cos(\omega_n t) \tag{4.4}$$

point two:

$$x_2' = r_n \cos(\omega_n t) \qquad y_2' = 0 \qquad z_2' = r_n \sin(\omega_n t) \tag{4.5}$$

The great circles are rotated by an infinitesimal angle $\Delta\alpha$ (a rotation around the x-axis) and then by $\Delta\alpha$ (a rotation around the new y-axis). The coordinates of each point on the rotated great circle is expressed in terms of the first (x,y,z) coordinates by the following transforms:

point one:

$$\begin{bmatrix} x_1 \\ y_1 \\ z_1 \end{bmatrix} = \begin{bmatrix} \cos(\Delta\alpha) & -\sin^2(\Delta\alpha) & -\sin(\Delta\alpha)\cos(\Delta\alpha) \\ 0 & \cos(\Delta\alpha) & -\sin(\Delta\alpha) \\ \sin(\Delta\alpha) & \cos(\Delta\alpha)\sin(\Delta\alpha) & \cos^2(\Delta\alpha) \end{bmatrix} \begin{bmatrix} x_1' \\ y_1' \\ z_1' \end{bmatrix} \tag{4.6}$$

point two:

$$\begin{bmatrix} x_2 \\ y_2 \\ z_2 \end{bmatrix} = \begin{bmatrix} \cos(\Delta\alpha) & -\sin^2(\Delta\alpha) & -\sin(\Delta\alpha)\cos(\Delta\alpha) \\ 0 & \cos(\Delta\alpha) & -\sin(\Delta\alpha) \\ \sin(\Delta\alpha) & \cos(\Delta\alpha)\sin(\Delta\alpha) & \cos^2(\Delta\alpha) \end{bmatrix} \begin{bmatrix} x_2' \\ y_2' \\ z_2' \end{bmatrix} \tag{4.7}$$

The total photon orbitsphere is given by reiterations of Eqs. (4.6) and

(4.7). The output given by the non primed coordinates is the input of the next iteration corresponding to each successive nested rotation by the infinitesimal angle where the summation of the rotation about each of the x-axis and the y-axis is $\sum_{n=1}^{\frac{\sqrt{2}\pi}{\Delta\alpha}} \Delta\alpha = \sqrt{2}\pi$.

The field line pattern corresponding to the first great circle magnetic field line and the second great circle electric field line shown with 8.49 degree increments of the infinitesimal angular variable $\Delta\alpha$ of Eqs. (4.6) and (4.7) is shown from two perspectives in Figures 4.2 A and 4.2 B. The complete photon orbitsphere distribution of field lines corresponds to all such correlated orthogonal great circles shown in Figure 4.1 which are rotated according to Eqs. (4.6) and (4.7) where $\Delta\alpha$ approaches zero and the summation of the infinitesimal angular rotations about the successive x-axes and y-axes is $\sqrt{2}\pi$.

Figure 4.2 A. The field line pattern from the perspective of looking along the z-axis of a right-handed circularly polarized photon orbitsphere corresponding to the first great circle magnetic field line, and the second great circle electric field line shown with 8.49 degree increments of the infinitesimal angular variable $\Delta\alpha$. (Electric field lines-solid; Magnetic field lines-dashed).

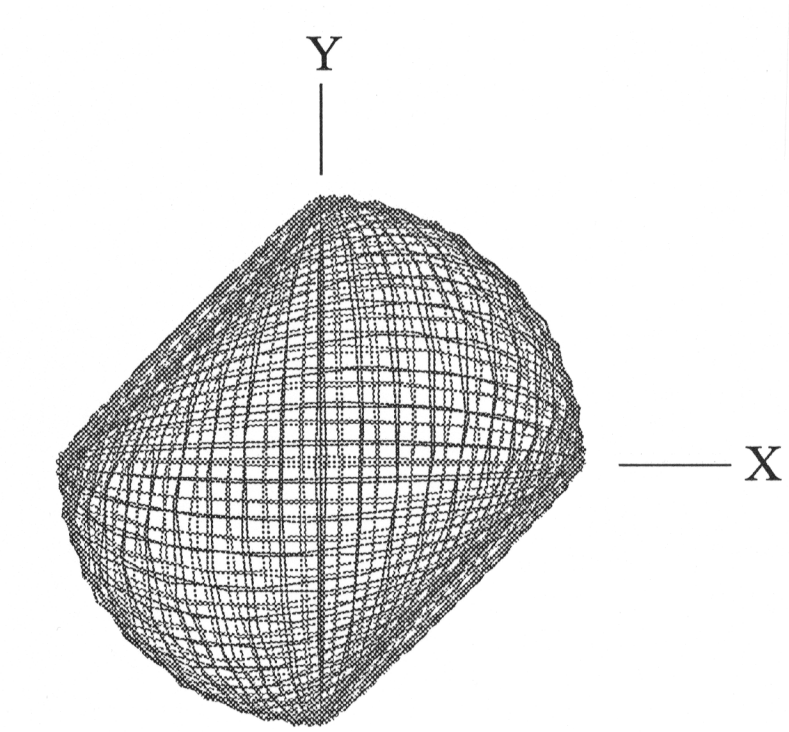

Figure 4.2 B. The field line pattern from the perspective of looking along the x-axis of a right-handed circularly polarized photon orbitsphere corresponding to the first great circle magnetic field line, and the second great circle electric field line shown with 8.49 degree increments of the infinitesimal angular variable $\Delta\alpha$. (Electric field lines-solid; Magnetic field lines-dashed).

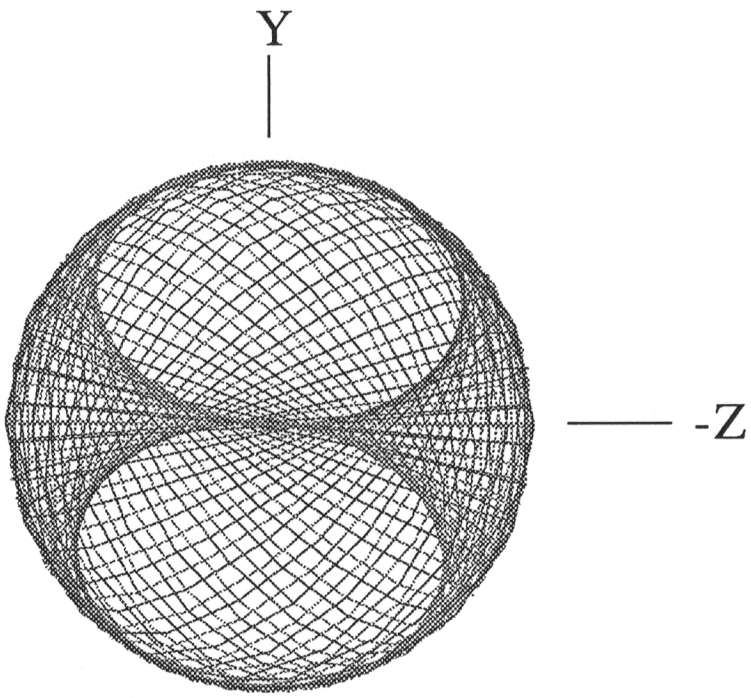

VIEW ALONG THE X AXIS

The angular velocity of the photon orbitsphere is equal to the change in angular velocity of the electron orbitsphere for a de-excitation from the energy level with principal quantum number $n = n_i$ to $n = n_f$, where $n_i > n_f$, given by Eq. (2.21) for $n_f = 1$. From Eq. (2.22), the photon is an electromagnetic wave that carries energy, E, given by

$$E = \hbar\omega \tag{4.8}$$

Given the relationships, Eqs. (4.2) and (4.3) for the electric and magnetic fields, the solution of the classical wave Eq. (1.1) requires that the linear velocity of each point along a great circle of the photon orbitsphere is c,

$$c = \sqrt{\frac{1}{\varepsilon_o \mu_o}} \tag{4.9}$$

and, that the velocity of the orbitsphere in the lab frame is c. Therefore,

the velocity in all frames of reference is c; thus, it follows from Eq. (24.14) that the photon has zero rest mass. The field lines in the lab frame follow from the relativistic invariance of charge as given by Purcell [2]. The relationship between the relativitic velocity and the electric field of a moving charge are shown schematically in Figure 4.3 A and 4.3 B.

Figure 4.3 A. The electric field of a moving point charge ($v = \frac{1}{3}c$).

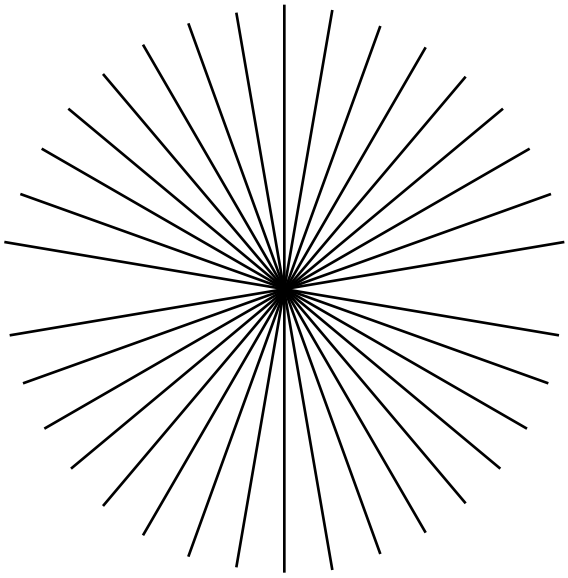

Figure 4.3 B. The electric field of a moving point charge ($v = \frac{4}{5}c$).

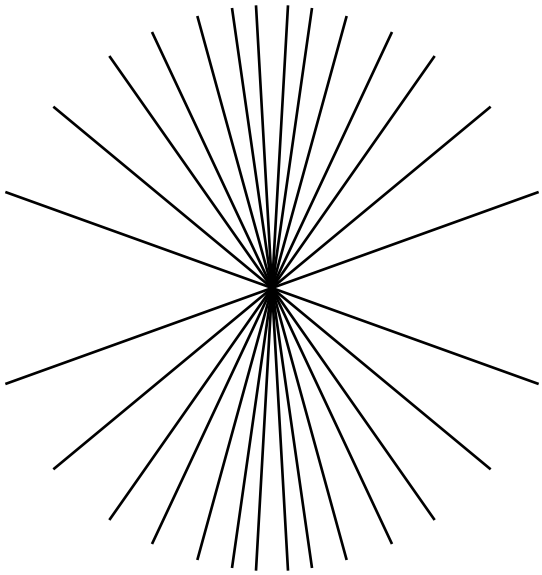

The photon equation in the lab frame (shown in Figures 4.4 and 4.5) of a right-handed circularly polarized photon orbitsphere is

$$\mathbf{E} = \mathbf{E}_0[\mathbf{x} + i\mathbf{y}]e^{-jk_z z}e^{-j\omega t}$$

$$\mathbf{H} = \left(\frac{\mathbf{E}_0}{\eta}\right)[\mathbf{y} - i\mathbf{x}]e^{-jk_z z}e^{-j\omega t} = \mathbf{E}_0\sqrt{\frac{\varepsilon}{\mu}}[\mathbf{y} - i\mathbf{x}]e^{-jk_z z}e^{-j\omega t} \quad (4.10)$$

with a wavelength of

$$\lambda = 2\pi\frac{c}{\omega} \quad (4.11)$$

The relationship between the photon orbitsphere radius and wavelength is

$$2\pi r_0 = \lambda_0 \quad (4.12)$$

Figure 4.4. The electric field lines of a right-handed circularly polarized photon orbitsphere as seen along the axis of propagation in the lab inertial reference frame.

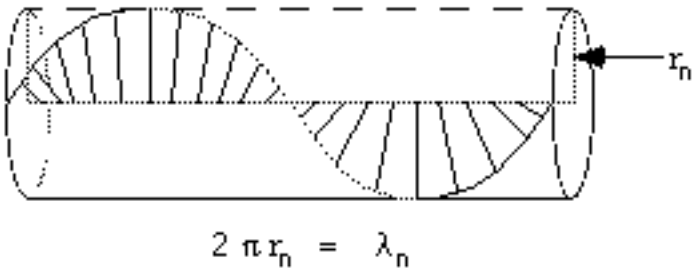

Figure 4.5. The electric field rotation of a right-handed circularly polarized photon orbitsphere as seen transverse to the axis of propagation in the lab inertial reference frame.

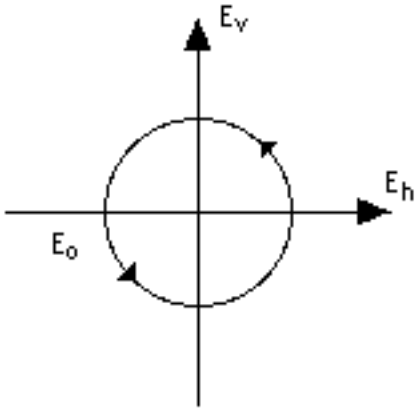

The cross section, σ, transverse to the the propagation direction of the photon is

$$\sigma = \pi \left(\frac{\lambda}{2\pi} \right)^2 \tag{4.13}$$

The photon orbitsphere may comprise magnetic and electric field lines that are constant in magnitude as a function of angle over the surface, or the magnitude may vary as a function of angular position (ϕ,θ) on the orbitsphere. The general photon equation for the electric field is

$$\mathbf{E}_{\phi,\theta} = \frac{e}{4\pi\varepsilon_o r_n^2} \left(-1 + \frac{1}{n} \left[Y_0^0(\theta,\phi) + \mathrm{Re}\left\{ Y_\ell^m(\theta,\phi) \left[1 + e^{i\omega_n t} \right] \right\} \right] \right) \delta\left(r - \frac{\lambda}{2\pi} \right); \ \omega_n = 0 \text{ for } m = 0 \tag{4.14}$$

where r_n is the radius of the photon orbitsphere which is equal to $\Delta n a_H$, the change in electron orbitsphere radius given by Eq. (2.21), λ is the photon wavelength which is equal to $\Delta\lambda$, the change in orbitsphere de Broglie wavelength given by Eqs. (2.21), (1.54), and (1.46), and $\omega = \frac{2\pi c}{\lambda}$ is the photon angular velocity which is equal to $\Delta\omega$, the change in orbitsphere angular velocity given by Eqs. (2.21). The magnetic field photon orbitsphere is given by Eqs. (4.14) and (4.2). In the case of $Y_\ell^m(\phi,\theta) = 0$ in Eq. (4.14), a right-handed and a left-handed circularly polarized photon orbitsphere are superimposed to comprise a linearly polarized photon orbitsphere. A right-handed or left-handed circularly polarized photon is obtained by attenuating the oppositely polarized component. For Eq. (4.14), the power density per unit area, **S**, is

$$\mathbf{S} = \mathbf{E} \times \mathbf{B}^* \tag{4.15}$$

LINEAR POLARIZED PHOTONS

As in the case of the circularly polarized photon orbitsphere, the linearly polarized photon orbitsphere is given by reiterations of the successive rotations where the summation of the rotation about each of the x-axis and the y-axis is $\sum_{n=1}^{\frac{\sqrt{2}\pi}{\Delta\alpha}} \Delta\alpha = \sqrt{2}\pi$ which rotates the final z-axis to the first negative z-axis, the final x axis to the first -y axis, and the final y-axis to the first -x-axis. Then the reiterations of the successive rotations is continued about the nth x-axis followed by the rotation of the nth orbitsphere coordinate system by the infinitesimal angle $\Delta\alpha' = -\Delta\alpha$ about the $(n+1)$th new y-axis where the magnitude of the summation of the rotation about each of the x-axis and the y-axis is $\sum_{n=1}^{\frac{\sqrt{2}\pi}{|\Delta\alpha'|}} |\Delta\alpha'| = \sqrt{2}\pi$. In Eqs. (4.6) and (4.7), $\Delta\alpha' = -\Delta\alpha$ replaces $\Delta\alpha$ for $\sum_{n=1}^{\frac{\sqrt{2}\pi}{\Delta\alpha}} \Delta\alpha = \sqrt{2}\pi$; $\sum_{n=1}^{\frac{\sqrt{2}\pi}{|\Delta\alpha'|}} |\Delta\alpha'| = \sqrt{2}\pi$. The final step rotates the final z-axis to the first z-axis, the final x-axis to the first x-axis, and the final y-axis to the first y-axis. Thus, the orbitsphere is generated from two orthogonal great circle field lines which are rotated about the nth x-axis then about the $(n+1)$th y-axis in two steps. The first step comprises all rotations by $\Delta\alpha$, and the second step comprises all rotations by $\Delta\alpha'$. In the case of the nth element of the first step, the intersection of the two orthogonal great circle field lines occurs at the nth z-axis which is along a great circle in a plane rotated $\frac{\pi}{4}$ with respect to the 1st xz-plane and 1st yz-plane of Figure 4.1. In the case of the nth element of the second step, the intersection of the two orthogonal great circle field lines occurs at the nth z-axis which is along a great circle in a plane rotated $\frac{\pi}{4}$ with respect to the 1st yz-plane and the 1st negative xz-plane of Figure 4.1. The first step generates the right-handed circularly polarized photon orbitsphere shown with the view along the z-axis in Figure 4.2 A. The second step generates the left-handed circularly polarized photon orbitsphere shown with the view along the z-axis in Figure 4.6.

Figure 4.6. The field line pattern from the perspective of looking along the z-axis of a left-handed circularly polarized photon orbitsphere corresponding to the first great circle magnetic field line, and the second great circle electric field line shown with 8.49 degree increments

of the infinitesimal angular variable $\Delta\alpha'$. (Electric field lines-solid; Magnetic field lines-dashed).

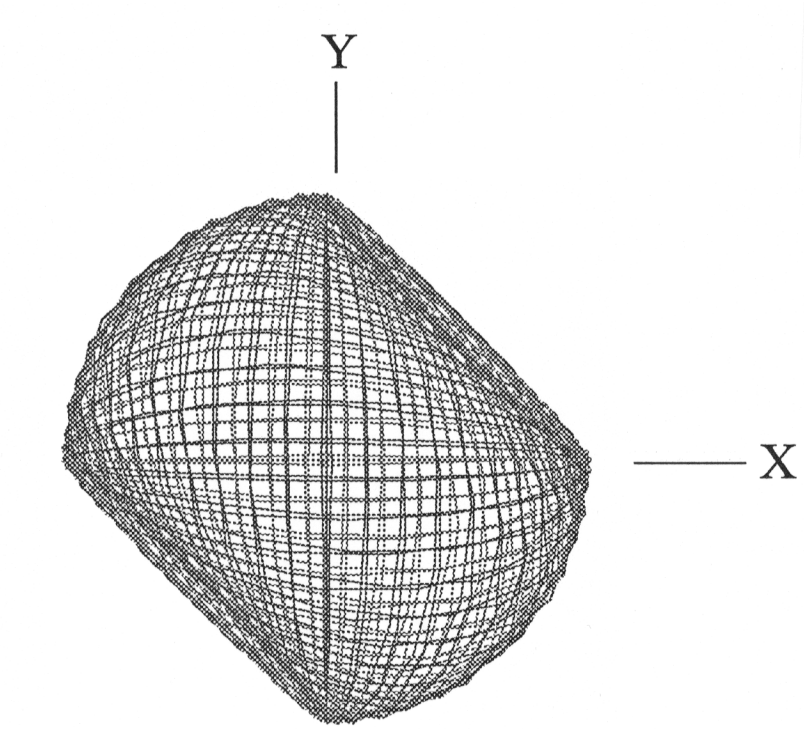

VIEW ALONG THE Z AXIS

The left-handed circularly polarized photon orbitsphere is the mirror image of the right-handed circularly polarized photon orbitsphere, and the superposition of the two is the linearly polarized photon orbitsphere. The electric and magnetic field lines of a linearly polarized photon orbitsphere are shown from three different perspectives in Figures 4.7 A, 4.7 B, and 4.7 C. The field lines pattern of a linearly polarized photon orbitsphere shown in Figures 4.7 A, 4.7 B, and 4.7 C is equivalent to the current density pattern of the electron orbitsphere shown in Figures 1.4 A, 1.4 B, and 1.4 C. The conditions whereby a photon becomes an electron and a positron are given in the Pair Production and the Leptons Sections.

Figure 4.7 A. The field lines pattern of a linearly polarized photon orbitsphere shown with 8.49 degree increments of the infinitesimal angular variable $\Delta\alpha(\Delta\alpha')$ from the perspective of looking along the z-axis. (Electric field lines-solid; Magnetic field lines-dashed).

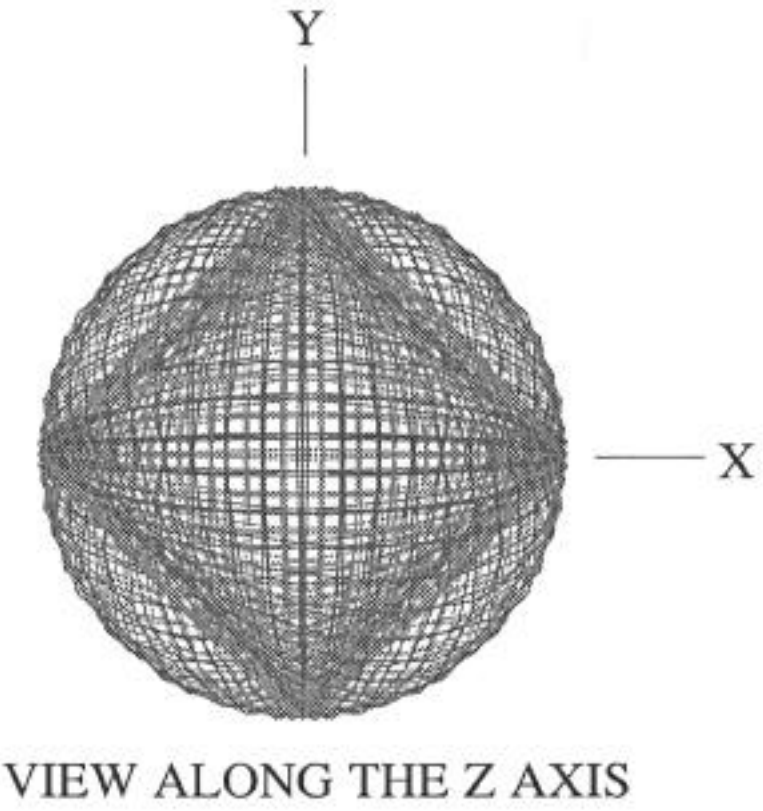

Figure 4.7 B. The field lines pattern of a linearly polarized photon orbitsphere shown with 8.49 degree increments of the infinitesimal angular variable $\Delta\alpha(\Delta\alpha')$ from the perspective of looking along the x-axis. (Electric field lines-solid; Magnetic field lines-dashed).

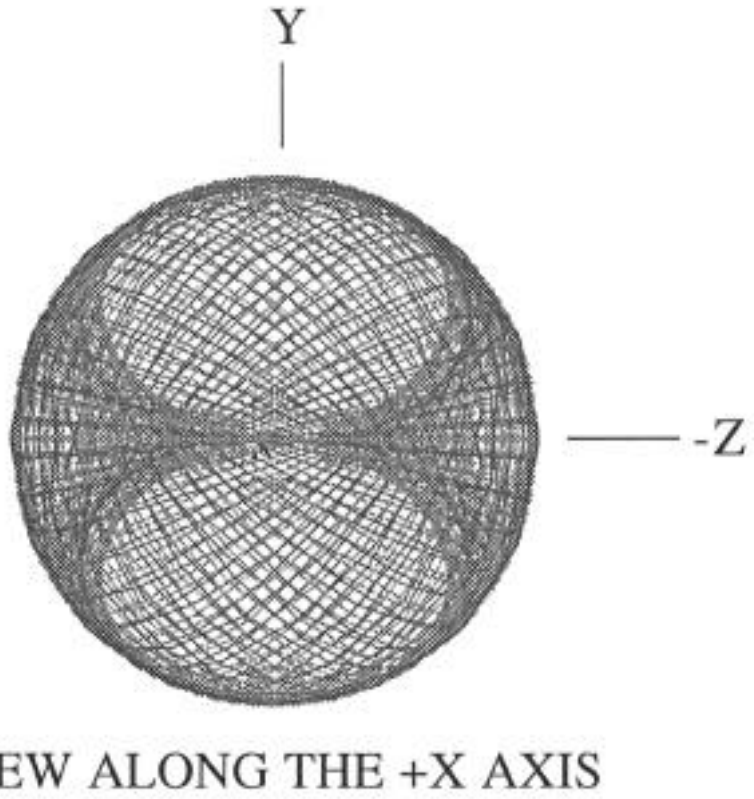

Figure 4.7 C. The field lines pattern of a linearly polarized photon orbitsphere shown with 8.49 degree increments of the infinitesimal angular variable $\Delta\alpha(\Delta\alpha')$ from the perspective of looking along the y-axis. (Electric field lines-solid; Magnetic field lines-dashed).

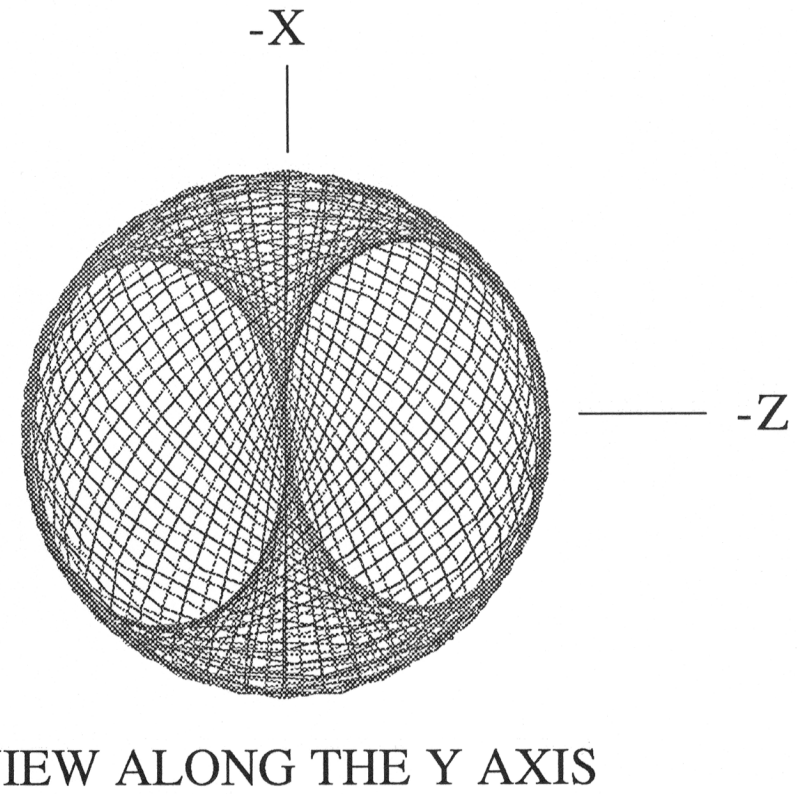

The linearly polarized photon orbitsphere equation in the lab frame is

$$\mathbf{E} = E_0 e^{-jk_z z} e^{-j\omega t} \tag{4.16}$$

In the case of $Y_\ell^m(\phi,\theta) \neq 0$ in Eq. (4.14), a right-handed and a left-handed elliptically polarized photon orbitsphere are superimposed to comprise a linearly polarized photon orbitsphere with the plane of polarization rotated relative to the case of $Y_\ell^m(\phi,\theta) = 0$. A right-handed or left-handed elliptically polarized photon is obtained by attenuating the oppositely polarized component.

SPHERICAL WAVE

Photons superimpose and the amplitude due to N photons is

$$\mathbf{E}_{total} = \sum_{n=1}^{N} \frac{e^{-ik_r|\mathbf{r}-\mathbf{r}'|}}{4\pi|\mathbf{r}-\mathbf{r}'|} f(\phi,\theta) \tag{4.17}$$

When the observation point is very far from the source as shown in

Figure 4.8, the distance in Eq. (4.17) becomes

$$|\mathbf{r}-\mathbf{r}'| \approx r - \hat{\mathbf{r}}\cdot\mathbf{r}' \tag{4.18}$$

where $\hat{\mathbf{r}}$ is the radial unit vector. Substitution of Eq. (4.18) into Eq. (4.17) gives

$$\mathbf{E}_{total} = \frac{e^{-ikr}}{r}\sum_{n=1}^{N} e^{-i\mathbf{k}\cdot\mathbf{r}'} f(\phi,\theta) \tag{4.19}$$

where we neglect $\hat{\mathbf{r}}\cdot\mathbf{r}'$ in the denominator, and

$$\mathbf{k} = \hat{\mathbf{r}}k \tag{4.20}$$

For an assembly of incoherent emitters

$$\sum_{n=1}^{N} e^{i\mathbf{k}\cdot\mathbf{r}'} f(\phi,\theta) = 1 \tag{4.21}$$

Thus, in the far field, the emitted wave is a spherical wave

$$\mathbf{E}_{total} = E_o \frac{e^{-ikr}}{r} \tag{4.22}$$

The Green Function, (Eq. (6.62) of Jackson [1]) is given as the solution of the wave equation (Eq. (6.58) of Jackson [1]). Thus, the superposition of photons gives the classical result.

Figure 4.8. Far field approximation.

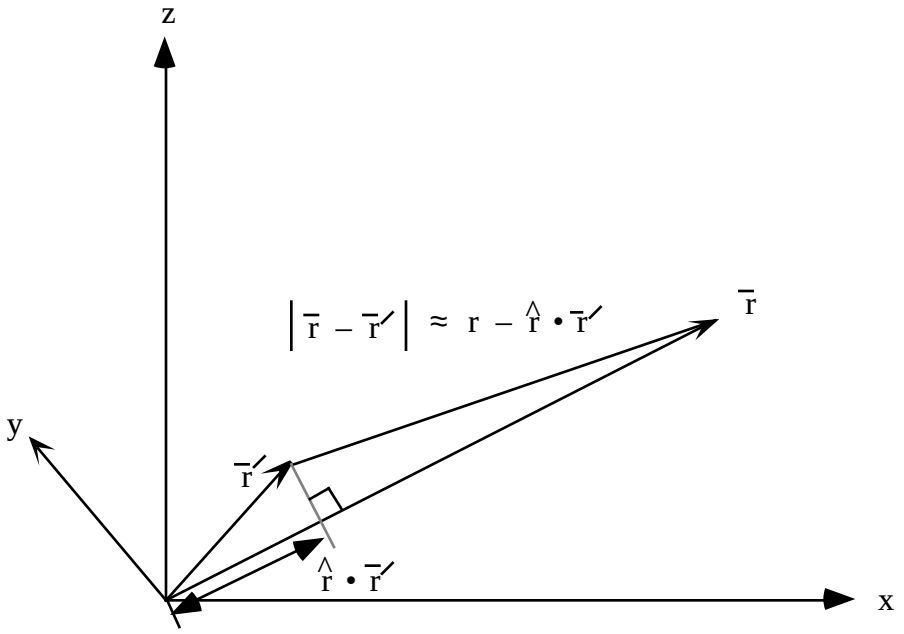

The photon spin angular momentum corresponding to the first term of Eq. (4.14) and the orbital angular momentum corresponding to the second term of Eq. (4.14) are conserved during electronic excitation as described in the Excited States of the One Electron Atom (Quantization) Section. And, the spin and orbital angular momentum of photons superimpose to give the classical result. For example, second harmonic generation has been obtained by Dholakia et al. [3] by use of

Laguerre-Gaussian beams in a variety of mode orders. Each mode becomes doubled in frequency and transformed to a higher order which is shown to be a consequence of the phase-matching conditions. The experiment is consistent with the interpretation that the orbital angular momentum of the Laguerre-Gaussian mode is directly proportional to the azimuthal mode index ℓ where each photon posses orbital angular momentum of $\ell\hbar$ in addition to any spin angular momentum due to its state of polarization.

PHOTON TORPEDOES

Recent evidence suggests that energy packets like photon torpedoes are creeping toward reality [4]. The possibility of solutions of the scalar wave equation and Maxwell's equations that describe localized, slowly decaying transmission of energy in space-time has been suggested by several groups in recent years. These include exact pulse solutions (focus wave modes [5,6], electromagnetic directed energy pulse trains [7], splash modes [8], transient beams [9],), continuous-wave modes (Bessel beams [10]), and asymptotic fields (electromagnetic missiles [11], electromagnetic bullets [12], Gaussian wave packets[13]).

A macroscopic surface current having a distribution given as an orbitsphere transition comprises a means to emit electromagnetic energy having electric and magnetic field lines which comprise a photon orbitsphere. In this case, energy is not diminished in intensity as the electromagnetic wave propagates through space. Thus, "photon torpedoes" can be realized. High power densities can be achieved by increasing the magnitude of the electric and magnetic fields of the photon where the energy is given by Eq. (1.175) and Eq. (1.122). Also, neutrino-type photons described in the Weak Nuclear Force: Beta Decay of the Neutron Section represent a means to transfer energy without scattering or attenuation between matched emitters and receivers. Applications in both cases include power transfer, communications, weapons, and artificial intelligence.

References

1. Jackson, J. D., Classical Electrodynamics, Second Edition, John Wiley & Sons, New York, (1962), pp. 739-779.
2. Purcell, E., Electricity and Magnetism, McGraw-Hill, New York, (1965), pp.156-167.
3. Dholakia, K., Simpson, N. B., Padgett, M. J., Allen, L., Physical Review A, Volume 54, Number 5, (1996), pp. R3742-R3745.
4. Ziolkowski, R. W., Lewis, K. D., Phys. Rev. Letts., Vol. 62, No. 2, (1989), pp. 147-150.
5. Brittingham, J. B., J. Appl. Phys., Vol. 54, (1983), p. 1179.

6. Ziolkowski, R. W., J. Math. Phys., Vol. 26, (1985), p. 861.
7. Ziolkowski, R. W., Microwave and Particle Beam Sources and Propagation, edited by N. Rostoker, SPIE Conference Proceedings, No. 873, (SPIE, Bellingham, WA, 1988).
8. Hillion, P., J. Appl. Phys., Vol. 60, (1986), p. 2981; Hillion, P., J. Math. Phys., Vol. 28, (1987), p. 1743.
9. Heyman, E., Felsen, L. B., IEEE Trans. Antennas Propag., Vol. 34, (1986), p. 1062; Heyman, E., Steinberg, B. Z., J. Opt. Soc. Am. A, Vol. 4, (1987), p. 473; Heyman, E., Steinberg, B. Z., Felsen, L. P., J. Opt. Soc. Am. A, Vol. 4, (1987), p. 2081.
10. Durnin, J. J., Opt. Soc. Am. A, Vol. 4, (1987), p. 651; Durnin, J., Miceli, J., Eberly, J. H., Phys. Rev. Lett., Vol. 58, (1987), p. 1499.
11. Wu, T. T., J. Appl. Phys., Vol. 57, (1985), p. 2370; Wu, T., T., King, R. W. P., Shen, H., J. Appl. Phys., Vol. 62, (1987), p. 4036; Shen, H., Microwave and Particle Beam Sources and Propagation, edited by N. Rostoker, SPIE Conference Proceedings, No. 873, (SPIE, Bellingham, WA, 1988).
12. Moses, H. E., J. Math. Phys., Vol. 25, (1984), p. 1905; Moses, H. E., Prosser, R. T., IEEE Trans. Antennas Propag., Vol. 34, (1986), p. 188.
13. Norris, A. N., White, B., Schrieffer, S, Proc. Roy. Soc. London A, Vol. 412, (1987), p. 93.

BLACKLIGHT PROCESS

Certain atoms or ions serve as catalysts to release energy from hydrogen to produce an increased binding energy hydrogen atom called a *hydrino atom* having a binding energy of

$$Binding\ Energy = \frac{13.6\ eV}{n^2} \tag{5.1}$$

where

$$n = \frac{1}{2}, \frac{1}{3}, \frac{1}{4}, ..., \frac{1}{p} \tag{5.2}$$

and p is an integer greater than 1, designated as $H\left(\frac{a_H}{p}\right)$ where a_H is the radius of the hydrogen atom. Hydrinos are predicted to form by reacting an ordinary hydrogen atom with a catalyst having a net enthalpy of reaction of about

$$m\ \ 27.2\ eV \tag{5.3}$$

where m is an integer. This catalysis releases energy from the hydrogen atom with a commensurate decrease in size of the hydrogen atom, $r_n = na_H$. For example, the catalysis of $H(n=1)$ to $H(n=1/2)$ releases $40.8\ eV$, and the hydrogen radius decreases from a_H to $\frac{1}{2}a_H$.

The excited energy states of atomic hydrogen are also given by Eq. (5.1) except that

$$n = 1,2,3,... \tag{5.4}$$

The $n=1$ state is the "ground" state for "pure" photon transitions (the $n=1$ state can absorb a photon and go to an excited electronic state, but it cannot release a photon and go to a lower-energy electronic state). However, an electron transition from the ground state to a lower-energy state is possible by a nonradiative energy transfer such as multipole coupling or a resonant collision mechanism. These lower-energy states have fractional quantum numbers, $n = \frac{1}{\text{integer}}$. Processes that occur without photons and that require collisions are common. For example, the exothermic chemical reaction of $H+H$ to form H_2 does not occur with the emission of a photon. Rather, the reaction requires a collision with a third body, M, to remove the bond energy-$H+H+M \rightarrow H_2+M^*$ [1]. The third body distributes the energy from the exothermic reaction, and the end result is the H_2 molecule and an increase in the temperature of

the system. Some commercial phosphors are based on nonradiative energy transfer involving multipole coupling. For example, the strong absorption strength of Sb^{3+} ions along with the efficient nonradiative transfer of excitation from Sb^{3+} to Mn^{2+}, are responsible for the strong manganese luminescence from phosphors containing these ions. Similarly, the $n=1$ state of hydrogen and the $n=\frac{1}{\text{integer}}$ states of hydrogen are nonradiative, but a transition between two nonradiative states is possible via a nonradiative energy transfer, say $n=1$ to $n=1/2$. In these cases, during the transition the electron couples to another electron transition, electron transfer reaction, or inelastic scattering reaction which can absorb the exact amount of energy that must be removed from the hydrogen atom, a resonant energy sink called an ***energy hole***. Thus, a **catalyst** is a source of an energy hole *infra.* because it provides a net positive enthalpy of reaction of $m\ 27.2\ eV$ (i.e. it absorbs or provides an energy sink of $m\ 27.2\ eV$). The reaction of hydrogen-type atoms to lower-energy states is referred to as a ***transition reaction***. Certain atoms or ions serve as transition catalysts which resonantly accept energy from hydrogen atoms and release the energy to the surroundings to effect electronic transitions to fractional quantum energy levels.

An example of *nonradiative energy transfer* is the basis of commercial fluorescent lamps. Consider Mn^{2+} which when excited sometimes emits yellow luminescence. The absorption transitions of Mn^{2+} are spin-forbidden. Thus, the absorption bands are weak, and the Mn^{2+} ions cannot be efficiently raised to excited states by direct optical pumping. Nevertheless, Mn^{2+} is one of the most important luminescence centers in commercial phosphors. For example, the double-doped phosphor $Ca_5(PO_4)_3F:Sb^{3+},Mn^{2+}$ is used in commercial fluorescent lamps where it converts mainly ultraviolet light from a mercury discharge into visible radiation. When 2536 Å mercury radiation falls on this material, the radiation is absorbed by the Sb^{3+} ions rather than the Mn^{2+} ions. Some excited Sb^{3+} ions emit their characteristic blue luminescence, while other excited Sb^{3+} ions transfer their energy to Mn^{2+} ions. These excited Mn^{2+} ions emit their characteristic yellow luminescence. The efficiency of transfer of ultraviolet photons through the Sb^{3+} ions to the Mn^{2+} ions can be as high as 80%. The strong absorption strength of Sb^{3+} ions along with the efficient transfer of excitation from Sb^{3+} to Mn^{2+}, are responsible for the strong manganese luminescence from this material.

This type of *nonradiative energy transfer* is common. The ion which emits the light and which is the active element in the material is

called the *activator*; and the ion which helps to excite the activator and makes the material more sensitive to pumping light is called the *sensitizer*. Thus, the sensitizer ion absorbs the radiation and becomes excited. Because of a coupling between sensitizer and activator ions, the sensitizer transmits its excitation to the activator, which becomes excited, and the activator may release the energy as its own characteristic radiation. The sensitizer to activator transfer is *not* a radiative emission and absorption process, rather a *nonradiative transfer*. The nonradiative transfer may be by electric or magnetic multipole interactions. In the transfer of energy between dissimilar ions, the levels will, in general, not be in resonance, and some of the energy is released as a phonon or phonons. In the case of similar ions the levels should be in resonance, and phonons are not needed to conserve energy.

Sometimes the host material itself may absorb (usually in the ultraviolet) and the energy can be transferred nonradiatively to dopant ions. For example, in $YVO_4:Eu^{3+}$, the vanadate group of the host material absorbs ultraviolet light, then transfers its energy to the Eu^{3+} ions which emit characteristic Eu^{3+} luminescence.

The catalysis of hydrogen involves the nonradiative transfer of energy from atomic hydrogen to a catalyst which may then release the transferred energy by radiative and nonradiative mechanisms. As a consequence of the nonradiative energy transfer, the hydrogen atom becomes unstable and emits further energy until it achieves a lower-energy nonradiative state having a principal energy level given by Eq. (5.1).

ENERGY HOLE CONCEPT

For a spherical resonator cavity, the nonradiative boundary condition and the relationship between the electron and the photon give the "allowed" hydrogen energy states which are quantized as a function of the parameter n. That is the nonradiative boundary condition and the relationship between an allowed radius and the photon standing wave wavelength Eq. (2.1) gives rise to Eq. (2.2), the boundary condition for allowed radii and allowed electron wavelengths as a function of the parameter n. Each value of n corresponds to an allowed transition effected by a resonant photon which excites the transition in the orbitsphere resonator cavity. In addition to the traditional integer values (1, 2, 3,...,) of n, values of fractions are allowed by Eq. (2.2) which correspond to transitions with an increase in the central field (charge) and decrease in the radius of the orbitsphere. This occurs, for example, when the orbitsphere couples to another resonator cavity which can absorb energy. This is the ***absorption of an energy hole by***

the hydrogen-type atom. The absorption of an energy hole destroys the balance between the centrifugal force and the increased central electric force. Consequently, the electron undergoes a transition to a lower energy nonradiative state. Thus, the corresponding reaction from an initial energy state to a lower energy state requiring an energy hole is called a ***transition reaction***.

From energy conservation, the energy hole of a hydrogen atom which excites resonator modes of radial dimensions $\frac{a_H}{m+1}$ is

$$m\,X\,27.2\,eV, \quad \text{where } m = 1,2,3,4,.... \tag{5.5}$$

After resonant absorption of the energy hole, the radius of the orbitsphere, a_H, shrinks to $\frac{a_H}{m+1}$ and after t cycles of transition, the radius is $\frac{a_H}{mt+1}$. In other words, the radial ground state field can be considered as the superposition of Fourier components. The removal of negative Fourier components of energy $m\,X\,27.2\,eV$, where m is an integer increases the positive electric field inside the spherical shell by m times the charge of a proton. The resultant electric field is a time harmonic solution of Laplace's Equations in spherical coordinates. In this case, the radius at which force balance and nonradiation are achieved is $\frac{a_H}{m+1}$ where m is an integer. In decaying to this radius from the "ground" state, a total energy of $[(m+1)^2 - 1^2]X13.6\,eV$ is released. The process is hereafter referred to as the Atomic BlackLight Process. (See Mills International Patent Application [2]). An appropriate technical term is "Coulomb Field Collapse".

For the hydrogen atom, the radius of the ground state orbitsphere is a_H. This orbitsphere contains no photonic waves and the centripetal force and the electric force balance including the electrodynamic force which is included by using the reduced electron mass as given by Eqs. (1.166), (1.171), and (1.172) is

$$\frac{m_e v_1^2}{a_H} = \frac{e^2}{4\pi\varepsilon_o a_H^2} \tag{5.6}$$

where v_1 is the velocity in the "ground" state. It was shown in the Excited States of the One Electron Atom (Quantization) Section that the electron orbitsphere is a resonator cavity which can trap electromagnetic radiation of discrete frequencies. The photon electric field functions are solutions of Laplace's equation. The "trapped photons" decrease the nuclear charge to $1/n$ and increase the radius of the orbitsphere to na_H. The new configuration is also in force balance.

$$\frac{\hbar^2}{m_e r_n^3} = \frac{Z_{eff} e^2}{4\pi\varepsilon_o r_n^2} \tag{5.12}$$

A transition occurs because the effective nuclear charge increases by an integer, m, when Eqs. (5.10-5.12) are satisfied by the introduction of an energy hole. The source of energy holes may not be consumed in the transition reaction; therefore it is a transition catalyst. The catalyst provides energy holes and affects the transition from the initial radius $\frac{a_H}{p}$ and an effective nuclear charge of p to the second radius $\left[\frac{a_H}{p+m}\right]$ and an effective nuclear charge of $p+m$. Energy conservation and the boundary condition that "trapped photons" must be a solution to Laplace's equation determine that the energy hole to cause a transition is given by Eq. (5.5). As a result of coupling, the hydrogen atom nonradiatively transfers $m\,X\,27.21\,eV$ to the catalyst. Stated another way, the hydrogen atom absorbs an energy hole of $m\,X\,27.21\,eV$. The energy hole absorption causes a standing electromagnetic wave ("photon") to be trapped in the hydrogen atom electron orbitsphere. Recall from the Excited States of the One Electron Atom (Quantization) Section that electromagnetic radiation of discrete energy can be trapped in a resonator cavity. As shown previously, the photonic equation must be a solution of Laplace's equation in spherical coordinates. The "trapped photon" field comprises an electric field which provides force balance and a nonradiative orbitsphere. The solution to this boundary value problem of the radial photon electric field is given by

$$\mathbf{E}_{r\,photonn,l,m} = \frac{e}{4\pi\varepsilon_o}\left(\frac{a_H}{n}\right)^{\ell}\frac{1}{r^{(\ell+2)}}\left[-Y_0^0(\theta,\phi) + n\left[Y_0^0(\theta,\phi) + \mathrm{Re}\left\{Y_\ell^m(\theta,\phi)\left[1+e^{i\omega_n t}\right]\right\}\right]\right]$$

$$\omega_n = 0 \quad for\ m = 0 \tag{5.13}$$

$$n = 2,3,4,\ldots$$

$$\ell = 1,2,\ldots, n-1$$

$$m = -\ell, -\ell+1,\ldots,0,\ldots,+\ell$$

And, the quantum numbers of the electron are n, ℓ, m (m_ℓ), and m_s as described previously. It is apparent from this equation that given an initial radius of $\frac{a_H}{p}$ and a final radius of $\left[\frac{a_H}{p+m}\right]$ that the central field is increased by m with the absorption of an energy hole of $m\,X\,27.2\,eV$. The potential energy decreases by this energy; thus, energy is conserved. However, the force balance equation is not initially satisfied as the effective nuclear charge increases by m. Further energy is emitted as force balance is achieved at the final radius. By replacing the initial radius with the final radius, and by increasing the charge by m in Eq.

(5.12).

$$[p+m]^3 \frac{\hbar^2}{m_e a_H^3} = [p+m]^2 \frac{((p+m)e)e}{4\pi\varepsilon_o a_H^2} \tag{5.14}$$

force balance is achieved and the orbitsphere is non-radiative. The energy balance for $m=1$ is as follows. An initial energy of $27.21\ eV$ is transferred as the energy hole absorption event. This increases the effective nuclear charge by one and decreases the potential by $27.21\ eV$. More energy is emitted until the total energy released is $[(p+1)^2 - p^2]X13.6\ eV$. The potential energy diagram of the electron is given in Figure 5.1.

Figure 5.1. Potential Energy well of a Hydrogen Atom.

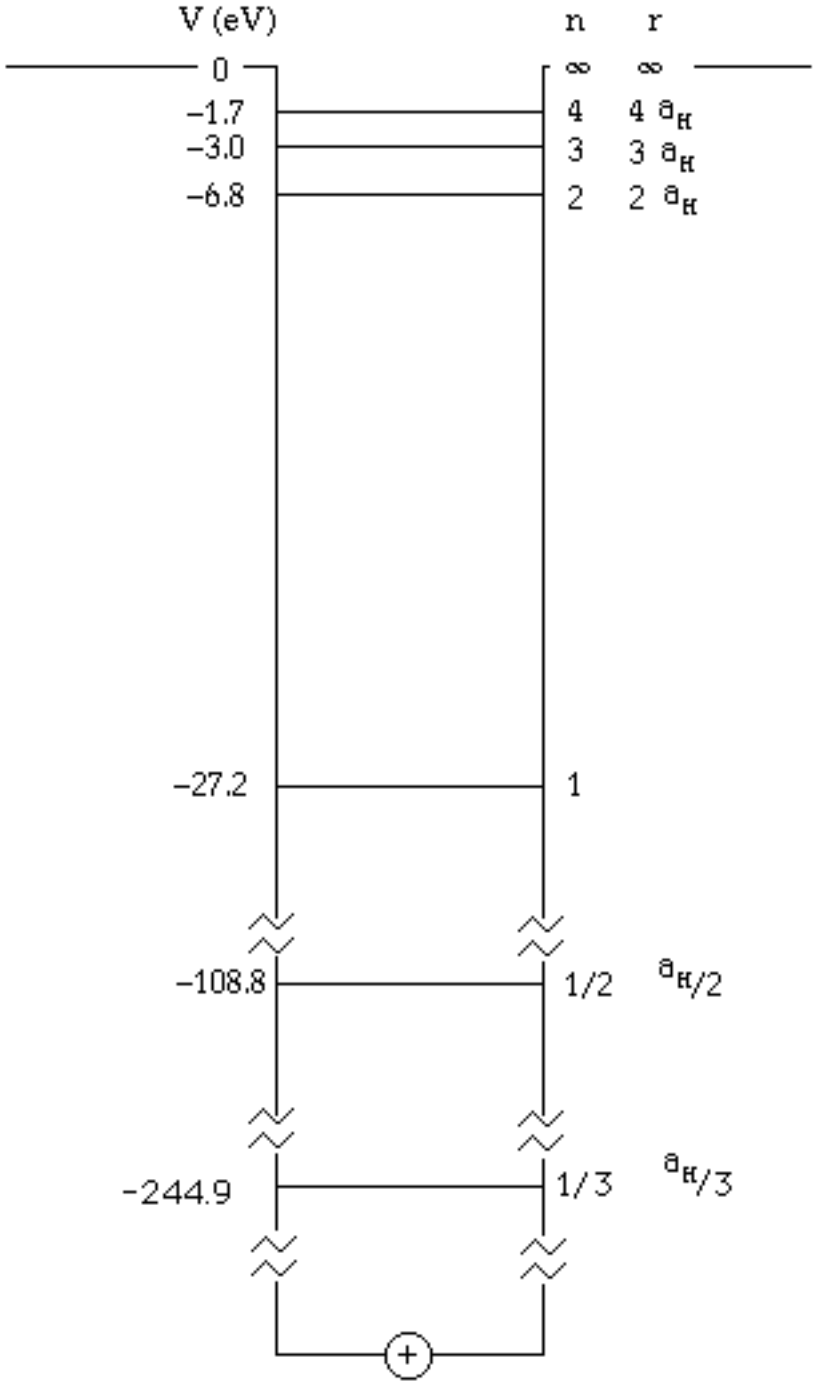

The energy hole ($m\,X\,27.21\,eV$) required to cause a hydrogen atom to undergo a transition reaction to form a given hydrino atom ($H\left(\frac{a_H}{m+1}\right)$) as well as the corresponding radius ($\frac{a_H}{(m+1)}$), effective nuclear charge ($m+1$) and energy parameters of several states of atomic hydrogen are given in

Table 5.1.

Table 5.1. Principal quantum number, radius, potential energy, kinetic energy, effective nuclear charge, energy hole required to form the hydrino from atomic hydrogen (n=1), and hydrino binding energy, respectively, for several states of hydrogen.

$H(n)$	R	V (eV)	T (eV)	Z_{eff}	Energy Hole (eV)	Binding Energy (eV)
1	a_H	-27.2	13.6	1	0	13.6
$\frac{1}{2}$	$\frac{a_H}{2}$	-108.8	54.4	2	27.2	54.4
$\frac{1}{3}$	$\frac{a_H}{3}$	-244.9	122.4	3	54.4	122.4
$\frac{1}{4}$	$\frac{a_H}{4}$	-435.4	217.7	4	81.6	217.7
$\frac{1}{5}$	$\frac{a_H}{5}$	-680.2	340.1	5	108.8	340.1
$\frac{1}{6}$	$\frac{a_H}{6}$	-979.6	489.6	6	136.1	489.6
$\frac{1}{7}$	$\frac{a_H}{7}$	-1333.3	666.4	7	163.3	666.4
$\frac{1}{8}$	$\frac{a_H}{8}$	-1741.4	870.4	8	190.5	870.4
$\frac{1}{9}$	$\frac{a_H}{9}$	-2204.0	1101.6	9	217.7	1101.6
$\frac{1}{10}$	$\frac{a_H}{10}$	-2721.0	1360.5	10	244.9	1360.5

The size of the electron orbitsphere as a function of potential energy is given in Figure 5.2.

Figure 5.2. Quantized sizes of hydrogen atoms.

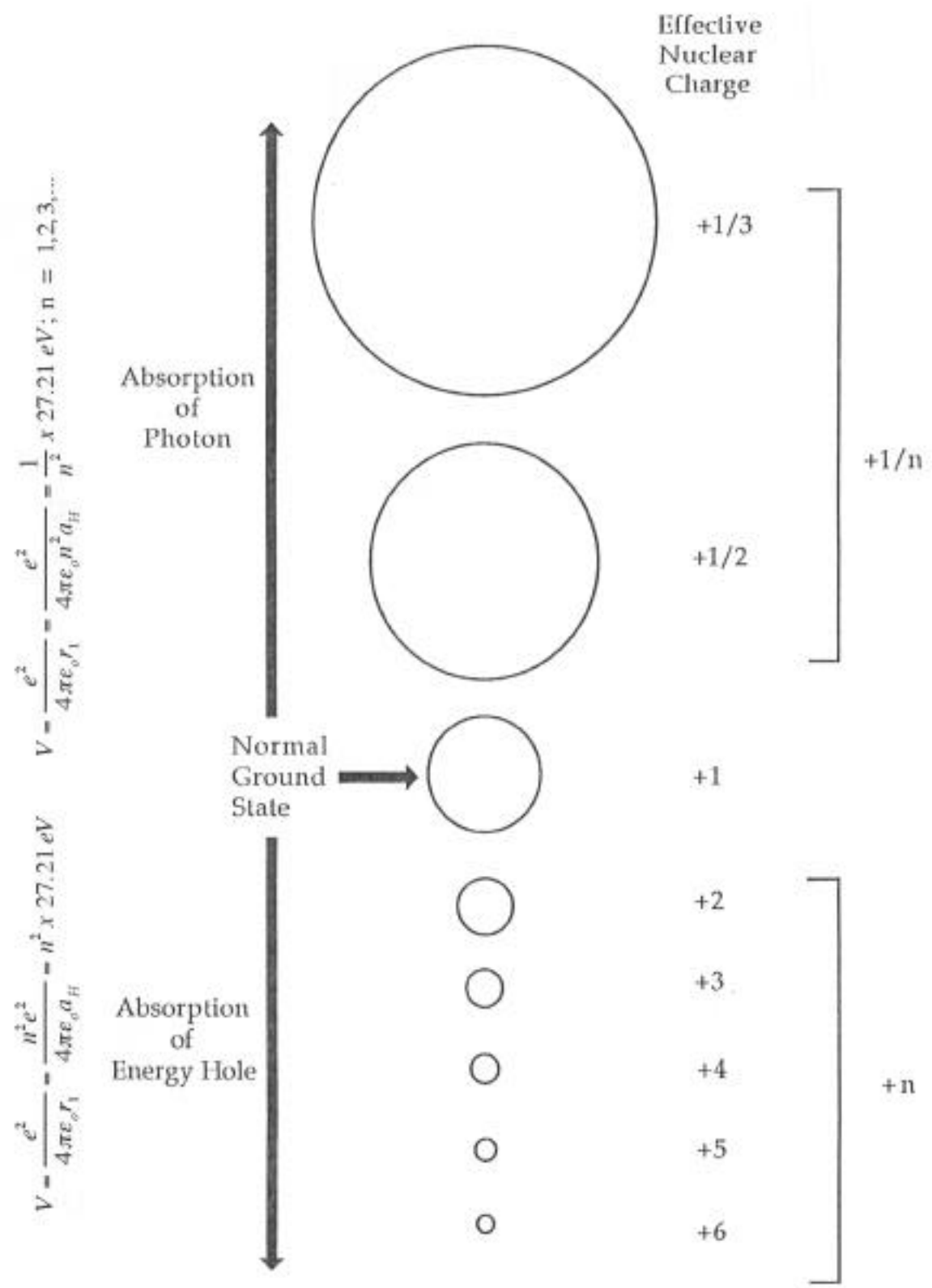

CATALYSTS

A catalytic system is provided by the ionization of t electrons from an atom each to a continuum energy level such that the sum of the ionization energies of the t electrons is approximately $m\,X\,27.2\ eV$ where m is an integer. One such catalytic system involves cesium. The first and second ionization energies of cesium are $3.89390\ eV$ and $23.15745\ eV$, respectively [3]. The double ionization ($t=2$) reaction of Cs to Cs^{2+}, then, has a net enthalpy of reaction of $27.05135\ eV$, which is equivalent to $m=1$ in Eq. (5.5).

$$27.05135\ eV + Cs(m) + H\left[\frac{a_H}{p}\right] \rightarrow Cs^{2+} + 2e^- + H\left[\frac{a_H}{(p+1)}\right] + [(p+1)^2 - p^2]X13.6\ eV \tag{5.15}$$

$$Cs^{2+} + 2e^- \rightarrow Cs(m) + 27.05135\ eV \tag{5.16}$$

And, the overall reaction is

$$H\left[\frac{a_H}{p}\right] \rightarrow H\left[\frac{a_H}{(p+1)}\right] + [(p+m)^2 - p^2]X13.6\ eV \tag{5.17}$$

where $m=1$ in Eq. (5.17). The energy given off during catalysis is much greater than the energy lost to the catalyst. The energy released is large as compared to conventional chemical reactions. For example, when hydrogen and oxygen gases undergo combustion to form water

$$H_2(g) + \frac{1}{2}O_2(g) \rightarrow H_2O(l) \tag{5.18}$$

the known enthalpy of formation of water is $\Delta H_f = -286\ kJ/mole$ or 1.48 eV per hydrogen atom. By contrast, each ($n=1$) ordinary hydrogen atom undergoing catalysis releases a net of $40.8\ eV$. Moreover, further catalytic transitions may occur: $n=\frac{1}{2} \rightarrow \frac{1}{3}$, $\frac{1}{3} \rightarrow \frac{1}{4}$, $\frac{1}{4} \rightarrow \frac{1}{5}$, and so on. Once catalysis begins, hydrinos autocatalyze further in a process called disproportionation discussed in the Disproportionation of Energy States Section. This mechanism is similar to that of an inorganic ion catalysis. But, hydrino catalysis should have a higher reaction rate than that of the inorganic ion catalyst due to the better match of the enthalpy to $m\ 27.2\ eV$.

Hydrogen catalysts capable of providing a net enthalpy of reaction of approximately $m \times 27.2\ eV$ where m is an integer to produce hydrino whereby t electrons are ionized from an atom or ion are given in Table 5.2. The atoms or ions given in the first column are ionized to provide the net enthalpy of reaction of $m \times 27.2\ eV$ given in the tenth column where m is given in the eleventh column. The electrons which are ionized are given with the ionization potential (also called ionization energy or binding energy). The ionization potential of the nth electron of the atom or ion is designated by IP_n and is given by the CRC [3]. That is for example, $Cs + 3.89390\ eV \rightarrow Cs^+ + e^-$ and $Cs^+ + 23.15745\ eV \rightarrow Cs^{2+} + e^-$. The first ionization potential, $IP_1 = 3.89390\ eV$, and the second ionization potential, $IP_2 = 23.15745\ eV$, are given in the second and third columns, respectively. The net enthalpy of reaction for the double ionization of Cs is $27.05135\ eV$ as given in the tenth column, and $m = 1$ in Eq. (5.5) as given in the eleventh column.

Table 5.2. Hydrogen Catalysts.

Catalyst	IP1	IP2	IP3	IP4	IP5	IP6	IP7	IP8	Enthalpy	m
Li	5.39172	75.6402							81.032	3
Be	9.32263	18.2112							27.534	1
K	4.34066	31.63	45.806						81.777	3
Ca	6.11316	11.8717	50.9131	67.27					136.17	5
Ti	6.8282	13.5755	27.4917	43.267	99.3				190.46	7
V	6.7463	14.66	29.311	46.709	65.2817				162.71	6
Cr	6.76664	16.4857	30.96						54.212	2
Mn	7.43402	15.64	33.668	51.2					107.94	4
Fe	7.9024	16.1878	30.652						54.742	2
Fe	7.9024	16.1878	30.652	54.8					109.54	4
Co	7.881	17.083	33.5	51.3					109.76	4
Co	7.881	17.083	33.5	51.3	79.5				189.26	7
Ni	7.6398	18.1688	35.19	54.9	76.06				191.96	7
Ni	7.6398	18.1688	35.19	54.9	76.06	108			299.96	11
Cu	7.72638	20.2924							28.019	1
Zn	9.39405	17.9644							27.358	1
Zn	9.39405	17.9644	39.723	59.4	82.6	108	134	174	625.08	23
As	9.8152	18.633	28.351	50.13	62.63	127.6			297.16	11
Se	9.75238	21.19	30.8204	42.945	68.3	81.7	155.4		410.11	15
Kr	13.9996	24.3599	36.95	52.5	64.7	78.5			271.01	10
Kr	13.9996	24.3599	36.95	52.5	64.7	78.5	111		382.01	14
Rb	4.17713	27.285	40	52.6	71	84.4	99.2		378.66	14
Rb	4.17713	27.285	40	52.6	71	84.4	99.2	136	514.66	19
Sr	5.69484	11.0301	42.89	57	71.6				188.21	7
Nb	6.75885	14.32	25.04	38.3	50.55				134.97	5
Mo	7.09243	16.16	27.13	46.4	54.49	68.8276			151.27	8
Mo	7.09243	16.16	27.13	46.4	54.49	68.8276	125.664	143.6	489.36	18
Pd	8.3369	19.43							27.767	1
Sn	7.34381	14.6323	30.5026	40.735	72.28				165.49	6
Te	9.0096	18.6							27.61	1
Te	9.0096	18.6	27.96						55.57	2
Cs	3.8939	23.1575							27.051	1
Ce	5.5387	10.85	20.198	36.758	65.55				138.89	5
Ce	5.5387	10.85	20.198	36.758	65.55	77.6			216.49	8
Pr	5.464	10.55	21.624	38.98	57.53				134.15	5
Sm	5.6437	11.07	23.4	41.4					81.514	3
Gd	6.15	12.09	20.63	44					82.87	3
Dy	5.9389	11.67	22.8	41.47					81.879	3
Pb	7.41666	15.0322	31.9373						54.386	2
Pt	8.9587	18.563							27.522	1
He+		54.4178							54.418	2
Na+		47.2864	71.6200	98.91					217.816	8
Rb+		27.285							27.285	1
Fe3+				54.8					54.8	2
Mo2+			27.13						27.13	1
Mo4+					54.49				54.49	2
In3+				54					54	2

An additional catalytic system involving potassium metal is provided by the ionization of t electrons from a potassium atom each to a continuum energy level such that the sum of the ionization energies of the t electrons is approximately $m\,X\,27.2\,eV$ where m is an integer. The first, second, and third ionization energies of potassium are $4.34066\,eV$, $31.63\,eV$, $45.806\,eV$, respectively [3]. The triple ionization ($t=3$) reaction of K to K^{3+}, then, has a net enthalpy of reaction of $81.7426\,eV$, which is equivalent to $m=3$ in Eq. (5.5).

$$81.7426\,eV + K(m) + H\left[\frac{a_H}{p}\right] \rightarrow K^{3+} + 3e^- + H\left[\frac{a_H}{(p+3)}\right] + [(p+3)^2 - p^2]X13.6\,eV \qquad (5.19)$$

$$K^{3+} + 3e^- \rightarrow K(m) + 81.7426\,eV \qquad (5.20)$$

And, the overall reaction is

$$H\left[\frac{a_H}{p}\right] \rightarrow H\left[\frac{a_H}{(p+3)}\right] + [(p+3)^2 - p^2]X13.6\,eV \qquad (5.21)$$

Potassium ions can also provide a net enthalpy of a multiple of that of the potential energy of the hydrogen atom. The second ionization energy of potassium is $31.63\,eV$; and K^+ releases $4.34\,eV$ when it is reduced to K. The combination of reactions K^+ to K^{2+} and K^+ to K, then, has a net enthalpy of reaction of $27.28\,eV$, which is equivalent to $m=1$ in Eq. (5.5).

$$27.28\,eV + K^+ + K^+ + H\left[\frac{a_H}{p}\right] \rightarrow K + K^{2+} + H\left[\frac{a_H}{(p+1)}\right] + [(p+1)^2 - p^2]\,X\,13.6\,eV \qquad (5.22)$$

$$K + K^{2+} \rightarrow K^+ + K^+ + 27.28\,eV \qquad (5.23)$$

The overall reaction is

$$H\left[\frac{a_H}{p}\right] \rightarrow H\left[\frac{a_H}{(p+1)}\right] + [(p+1)^2 - p^2]\,X\,13.6\,eV \qquad (5.24)$$

Rubidium ions can also provide a net enthalpy of a multiple of that of the potential energy of the hydrogen atom. The second ionization energy of rubidium is $27.28\,eV$. The reaction Rb^+ to Rb^{2+} has a net enthalpy of reaction of $27.28\,eV$, which is equivalent to $m=1$ in Eq. (5.5).

$$27.28\ eV + Rb^{+} + H\left[\frac{a_H}{p}\right] \rightarrow Rb^{2+} + e^{-} + H\left[\frac{a_H}{(p+1)}\right] + [(p+1)^2 - p^2]X13.6\ eV \quad (5.25)$$

$$Rb^{2+} + e^{-} \rightarrow Rb^{+} + 27.28\ eV \quad (5.26)$$

The overall reaction is

$$H\left[\frac{a_H}{p}\right] \rightarrow H\left[\frac{a_H}{(p+1)}\right] + [(p+1)^2 - p^2]\ X\ 13.6\ eV \quad (5.27)$$

In another example, a catalytic system transfers two electrons from one ion to another such that the sum of the total ionization energy of the electron donating species minus the total ionization energy of the electron accepting species equals approximately $m\ X\ 27.2\ eV$ where m is an integer. One such catalytic system involves lanthanum. The only stable oxidation state of lanthanum is La^{3+}. The fourth and fifth ionization energies of lanthanum are $49.95\ eV$ and $61.6\ eV$, respectively. The third and second ionization energies of lanthanum are $19.1773\ eV$ and $11.060\ eV$, respectively [3]. The combination of reactions La^{3+} to La^{5+} and La^{3+} to La^{+}, then, has a net enthalpy of reaction of $81.3127\ eV$, which is equivalent to $m = 3$ in Eq. (5.5).

$$81.3127\ eV + La^{3+} + La^{3+} + H\left[\frac{a_H}{p}\right] \rightarrow La^{5+} + La^{+} + H\left[\frac{a_H}{(p+3)}\right] + [(p+3)^2 - p^2]\ X\ 13.6\ eV \quad (5.28)$$

$$La^{5+} + La^{+} \rightarrow La^{3+} + La^{3+} + 81.3127\ eV \quad (5.29)$$

The overall reaction is

$$H\left[\frac{a_H}{p}\right] \rightarrow H\left[\frac{a_H}{(p+3)}\right] + [(p+3)^2 - p^2]\ X\ 13.6\ eV \quad (5.30)$$

For sodium, no electrocatalytic reaction of approximately $27.21\ eV$ is possible by the transfer of an electron between two Na^{+} ions as is the case with K^{+}. For example, $42.15\ eV$ of energy is absorbed by the reverse of the reaction given in Eq. (5.23) where Na^{+} replaces K^{+}:

$$Na^{+} + Na^{+} + 42.15\ eV \rightarrow Na + Na^{2+} \quad (5.31)$$

However a catalytic system is provided by the ionization of 3 electrons from Na^+ to a continuum energy level such that the sum of the ionization energies of the 3 electrons is approximately $m\,X\,27.2\,eV$ where m is an integer. The second, third, and fourth ionization energies of sodium are $47.2864\,eV$, $71.6200\,eV$, and $98.91\,eV$, respectively [3]. The triple ionization reaction of Na^+ to Na^{4+}, then, has a net enthalpy of reaction of $217.8164\,eV$, which is equivalent to $m=8$ in Eq. (5.5).

$$217.8164\,eV + Na^+ + H\left(\frac{a_H}{p}\right) \rightarrow Na^{4+} + 3e^- + H\left(\frac{a_H}{(p+8)}\right) + [(p+8)^2 - p^2]X13.6\,eV \tag{5.32}$$

$$Na^{4+} + 3e^- \rightarrow Na^+ + 217.8164\,eV \tag{5.33}$$

And, the overall reaction is

$$H\left(\frac{a_H}{p}\right) \rightarrow H\left(\frac{a_H}{(p+8)}\right) + [(p+8)^2 - p^2]X13.6\,eV \tag{5.34}$$

For lithium, no electrocatalytic reaction of approximately $27.21\,eV$ is possible by the transfer of an electron between two Li^+ ions as is the case with K^+.. For example, $70.246\,eV$ of energy is absorbed by the reverse of the reaction given in Eq. (5.23) where Li^+ replaces K^+:

$$Li^+ + Li^+ + 70.246\,eV \rightarrow Li + Li^{2+} \tag{5.35}$$

However, lithium metal is a catalyst as shown in Table 5.2.

DISPROPORTIONATION OF ENERGY STATES

Lower-energy hydrogen atoms, ***hydrinos***, can act as catalysts because each of the metastable excitation, resonance excitation, and ionization energy of a hydrino atom is $m\,X\,27.2\,eV$ (Eq. (5.5)). The transition reaction mechanism of a first hydrino atom affected by a second hydrino atom involves the resonant coupling between the atoms of m degenerate multipoles each having $27.21\,eV$ of potential energy. (See the Energy Hole as a Multipole Expansion Section). The energy transfer of $m\,X\,27.2\,eV$ from the first hydrino atom to the second hydrino atom causes the central field of the first to increase by m and the electron of the first to drop m levels lower from a radius of $\frac{a_H}{p}$ to a

radius of $\frac{a_H}{p+m}$. The second lower-energy hydrogen is excited to a metastable state, excited to a resonance state, or ionized by the resonant energy transfer. The resonant transfer may occur in multiple stages. For example, a nonradiative transfer by multipole coupling may occur wherein the central field of the first increases by m, then the electron of the first drops m levels lower from a radius of $\frac{a_H}{p}$ to a radius of $\frac{a_H}{p+m}$ with further resonant energy transfer. The energy transferred by multipole coupling may occur by a mechanism that is analogous to photon absorption involving an excitation to a virtual level. Or, the energy transferred by multipole coupling and during the electron transition of the first hydrino atom may occur by a mechanism that is analogous to two photon absorption involving a first excitation to a virtual level and a second excitation to a resonant or continuum level [4-6]. The transition energy greater than the energy transferred to the second hydrino atom may appear as a photon in a vacuum medium.

For example, $H\left[\frac{a_H}{4}\right]$ may serve as a catalyst to form $H\left[\frac{a_H}{5}\right]$. The transition of $H\left[\frac{a_H}{4}\right]$ to $H\left[\frac{a_H}{5}\right]$ induced by a resonance transfer of $27.21\,eV$, $m=1$ in Eq. (5.5) with a metastable state excited in $H\left[\frac{a_H}{4}\right]$ is represented by

$$27.2\,eV + H\left[\frac{a_H}{4}\right] + H\left[\frac{a_H}{4}\right] \rightarrow H^*\left[\frac{a_H}{4}\right] + H\left[\frac{a_H}{5}\right] + 27.2\,eV + 95.2\,eV \tag{5.36}$$

$$H^*\left[\frac{a_H}{4}\right] \rightarrow H\left[\frac{a_H}{4}\right] + 27.2\,eV \tag{5.37}$$

$$H\left[\frac{a_H}{4}\right] \rightarrow H\left[\frac{a_H}{5}\right] + 95.2\,eV + 27.2eV \tag{5.38}$$

$H\left[\frac{a_H}{4}\right]$ may serve as both a catalyst and a reactant to form $H\left[\frac{a_H}{3}\right]$ and $H\left[\frac{a_H}{6}\right]$. The transition of $H\left[\frac{a_H}{4}\right]$ to $H\left[\frac{a_H}{6}\right]$ induced by a multipole resonance transfer of $54.4\,eV$, $m=2$ in Eq. (5.5) and a transfer of $40.8\,eV$ with a resonance state of $H\left[\frac{a_H}{3}\right]$ excited in $H\left[\frac{a_H}{4}\right]$ is represented by

$$H\left[\frac{a_H}{4}\right]+H\left[\frac{a_H}{4}\right]\rightarrow H\left[\frac{a_H}{6}\right]+H\left[\frac{a_H}{3}\right]+176.8\,eV \tag{5.39}$$

In general, the transition of $H\left[\frac{a_H}{p}\right]$ to $H\left[\frac{a_H}{p+m}\right]$ induced by a resonance transfer of $m\ 27.21\,eV$ (Eq. (5.5)) with a metastable state excited in $H\left[\frac{a_H}{p'}\right]$ is represented by

$$m\ 27.2\,eV+H\left[\frac{a_H}{p'}\right]+H\left[\frac{a_H}{p}\right]\rightarrow H^*\left[\frac{a_H}{p'}\right]+H\left[\frac{a_H}{p+m}\right]+[(p+m)^2-p^2]\,X\,13.6\,eV \tag{5.40}$$

$$H^*\left[\frac{a_H}{p'}\right]\rightarrow H\left[\frac{a_H}{p'}\right]+m\ 27.2\,eV \tag{5.41}$$

And, the overall reaction is

$$H\left[\frac{a_H}{p}\right]\rightarrow H\left[\frac{a_H}{p+m}\right]+[(p+m)^2-p^2]\,X\,13.6\,eV \tag{5.42}$$

where p, p', and m are integers and the asterisk represents an excited metastable state.

The transition of $H\left[\frac{a_H}{p}\right]$ to $H\left[\frac{a_H}{p+m}\right]$ induced by a multipole resonance transfer of $m\ 27.21\,eV$ (Eq. (5.5)) and a transfer of $[(p')^2-(p'-m')^2]\,X\,13.6\,eV-m\ 27.2\,eV$ with a resonance state of $H\left[\frac{a_H}{p'-m'}\right]$ excited in $H\left[\frac{a_H}{p'}\right]$ is represented by

$$H\left[\frac{a_H}{p'}\right]+H\left[\frac{a_H}{p}\right]\rightarrow H\left[\frac{a_H}{p'-m'}\right]+H\left[\frac{a_H}{p+m}\right]+[\left((p+m)^2-p^2\right)-\left(p'^2-(p'-m')^2\right)]\,X\,13.6\,eV \tag{5.43}$$

where p, p', m, and m' are integers.

The second lower-energy hydrogen may be ionized by the resonant energy transfer. For an example, the equation for the absorption of an energy hole of $27.21\,eV$, $m=1$ in Eq. (5.5), during the transition cascade for the third cycle of the hydrogen-type atom, $H\left[\frac{a_H}{3}\right]$, with the hydrogen-type atom, $H\left[\frac{a_H}{2}\right]$, that is ionized as the source of energy holes that causes the transition is represented by

$$27.21\ eV + H\left[\frac{a_H}{2}\right] + H\left[\frac{a_H}{3}\right] \rightarrow H^+ + e^- + H\left[\frac{a_H}{4}\right] + [4^2 - 3^2]X13.6\ eV - 27.21\ eV \qquad (5.44)$$

$$H^+ + e^- \rightarrow H\left[\frac{a_H}{1}\right] + 13.6\ eV \qquad (5.45)$$

And, the overall reaction is

$$H\left[\frac{a_H}{2}\right] + H\left[\frac{a_H}{3}\right] \rightarrow H\left[\frac{a_H}{1}\right] + H\left[\frac{a_H}{4}\right] + [4^2 - 3^2 - 4]X13.6\ eV + 13.6\ eV \qquad (5.46)$$

The general equation for the absorption of an energy hole of $27.21\ eV$, $m = 1$ in Eq. (5.5), during the transition cascade for the pth cycle of the hydrogen-type atom, $H\left[\frac{a_H}{p}\right]$, with the hydrogen-type atom, $H\left[\frac{a_H}{m'}\right]$, that is ionized as the source of energy holes that causes the transition is represented by

$$27.21\ eV + H\left[\frac{a_H}{m'}\right] + H\left[\frac{a_H}{p}\right] \rightarrow H^+ + e^- + H\left[\frac{a_H}{(p+1)}\right] + [(p+1)^2 - p^2]X13.6\ eV - \left(m'^2 - 2\right)X13.6\ eV \qquad (5.47)$$

$$H^+ + e^- \rightarrow H\left[\frac{a_H}{1}\right] + 13.6\ eV \qquad (5.48)$$

And, the overall reaction is

$$H\left[\frac{a_H}{m'}\right] + H\left[\frac{a_H}{p}\right] \rightarrow H\left[\frac{a_H}{1}\right] + H\left[\frac{a_H}{(p+1)}\right] + [2p + 1 - m'^2]X13.6\ eV + 13.6\ eV \qquad (5.49)$$

Transitions to nonconsecutive energy levels involving the absorption of an energy hole of an integer multiple of $27.21\ eV$ are possible. Lower-energy hydrogen atoms, ***hydrinos***, can act as a source of energy holes that can cause transition reactions with the absorption of energy holes each of $m\,X\,27.2\ eV$ (Eq. (5.5)). Thus, the transition cascade for the pth cycle of the hydrogen-type atom, $H\left[\frac{a_H}{p}\right]$, with the hydrogen-type atom, $H\left[\frac{a_H}{m'}\right]$, that is ionized as the source of energy holes that causes the transition is represented by

$$m\,X\,27.21\ eV + H\left(\frac{a_H}{m'}\right) + H\left(\frac{a_H}{p}\right) \rightarrow H^+ + e^- + H\left(\frac{a_H}{(p+m)}\right) + [(p+m)^2 - p^2 - (m'^2 - 2m)]X13.6\ eV \quad (5.50)$$

$$H^+ + e^- \rightarrow H\left(\frac{a_H}{1}\right) + 13.6\ eV \quad (5.51)$$

And, the overall reaction is

$$H\left(\frac{a_H}{m'}\right) + H\left(\frac{a_H}{p}\right) \rightarrow H\left(\frac{a_H}{1}\right) + H\left(\frac{a_H}{(p+m)}\right) + \left[2pm + m^2 - m'^2\right]X13.6\ eV + 13.6\ eV \quad (5.52)$$

Disproportionation may be the predominant mechanism of hydrogen electronic transitions to lower energy levels of interstellar hydrogen and hydrinos. Hydrogen transitions to electronic energy levels below the "ground" state corresponding to fractional quantum numbers exactly match the spectral lines of the extreme ultraviolet background of interstellar space. This assignment given in the Spectral Data of Hydrinos from the Dark Interstellar Medium and Spectral Data of Hydrinos, Dihydrinos, and Hydrino Hydride Ions from the Sun Section resolves the paradox of the identity of dark matter and accounts for many celestial observations such as: diffuse Hα emission is ubiquitous throughout the Galaxy, and widespread sources of flux shortward of 912 *Å* are required [7]. The energy of the emission line for the transition given by Eqs. (5.44-5.46) involving the absorption of an energy hole of $27.21\,eV$, $m = 1$ in Eq. (5.5), is $40.8\,eV$.

$$H\left(\frac{a_H}{3}\right) \xrightarrow{H\left(\frac{a_H}{2}\right)} H\left(\frac{a_H}{4}\right) \quad (5.53)$$

The energy of the emission line for the transition given by Eqs. (5.50-5.52) where $m = 2$, $m' = 2$, and $p = 1$ involving the absorption of an energy hole of $2\,X\,27.21\,eV$, $m = 2$ in Eq. (5.5), is $54.4\,eV$.

$$H\left(\frac{a_H}{1}\right) \xrightarrow{H\left(\frac{a_H}{2}\right)} H\left(\frac{a_H}{3}\right) \quad (5.54)$$

Stars are sources of lower-energy hydrogen for reactants for interstellar disproportionation reactions given by Eqs. (5.47-5.49). The source of energy holes in stellar production are hydrogen and singly ionized helium, He^+. The ionization energy of hydrogen is $13.6\,eV$. Disproportionation can occur between three hydrogen atoms whereby two atoms provide an energy hole of $27.21\,eV$ for the third hydrogen atom. Thus, the transition cascade for the pth cycle of the hydrogen-

type atom, $H\left[\frac{a_H}{p}\right]$, with two hydrogen atoms, $H\left[\frac{a_H}{1}\right]$, as the source of energy holes that causes the transition is represented by

$$27.21\ eV + 2H\left[\frac{a_H}{1}\right] + H\left[\frac{a_H}{p}\right] \rightarrow 2H^+ + 2e^- + H\left[\frac{a_H}{(p+1)}\right] + [(p+1)^2 - p^2]X13.6\ eV \quad (5.55)$$

$$2H^+ + 2e^- \rightarrow 2H\left[\frac{a_H}{1}\right] + 27.21\ eV \quad (5.56)$$

And, the overall reaction is

$$H\left[\frac{a_H}{p}\right] \rightarrow H\left[\frac{a_H}{(p+1)}\right] + [(p+1)^2 - p]X13.6\ eV \quad (5.57)$$

Helium II is one of the catalysts that can cause a transition reaction because the second ionization energy is $54.4\ eV$, $m = 2$ in Eq. (5.5). Thus, the transition cascade for the pth cycle is represented by

$$54.4\ eV + He^+ + H\left[\frac{a_H}{p}\right] \rightarrow He^{2+} + e^- + H\left[\frac{a_H}{(p+2)}\right] + [(p+2)^2 - p^2]X13.6\ eV \quad (5.58)$$

$$He^{2+} + e^- \rightarrow He^+ + 54.4\ eV \quad (5.59)$$

And, the overall reaction is

$$H\left[\frac{a_H}{p}\right] \rightarrow H\left[\frac{a_H}{(p+2)}\right] + [(p+2)^2 - p]X13.6\ eV \quad (5.60)$$

Also, Helium II is a catalyst that can cause a transition reaction with the absorption of an energy hole of $27.21\ eV$, $m = 1$ in Eq. (5.5). Thus, the transition cascade for the pth cycle is represented by

$$27.21\ eV + He^+ + H\left[\frac{a_H}{p}\right] \rightarrow He^{2+} + e^- + H\left[\frac{a_H}{(p+1)}\right] + [(p+1)^2 - p^2]X13.6\ eV - 27.21\ eV \quad (5.61)$$

$$He^{2+} + e^- \rightarrow He^+ + 54.4\ eV \quad (5.62)$$

And, the overall reaction is

$$H\left[\frac{a_H}{p}\right] \rightarrow H\left[\frac{a_H}{(p+1)}\right] + [(p+1)^2 - p]X13.6\ eV \tag{5.63}$$

The majority of the solar power can be attributed to disproportionation reactions as given in the Spectral Data of Hydrinos from the Dark Interstellar Medium and Spectral Data of Hydrinos, Dihydrinos, and Hydrino Hydride Ions from the Sun Section. This assignment resolves the solar neutrino problem and the mystery of the cause of sunspots and other solar activity and why the Sun emits X-rays. It also provides the reason for the abrupt change in the speed of sound and transition from "radiation zone" to "convection zone" at a radius of 0.7 the solar radius, $0.7R_S$.

INTERSTELLAR DISPROPORTIONATION RATE

Disproportionation may be the predominant mechanism of hydrogen electronic transitions to lower energy levels of interstellar hydrogen and hydrinos. The reaction rate is dependent on the collision rate between the reactants and the coupling factor for resonant energy transfer. The collision rate can be calculated by determining the collision frequency. The collision frequency, f, and the mean free path, ℓ, for a gas containing n_u spherical particles per unit volume, each with radius r and velocity v is given by Bueche [8].

$$f = 4\pi\sqrt{2}n_u r^2 v \tag{5.64}$$

$$\ell = \frac{1}{4\pi\sqrt{2}n_u r^2} \tag{5.65}$$

The average velocity, v_{avg}, can be calculated from the temperature, T, [8].

$$\frac{1}{2}m_H v_{avg}^2 = \frac{3}{2}kT \tag{5.66}$$

where k is Boltzmann's constant. Substitution of Eq. (5.66) into Eq. (5.64) gives the collision rate, $f_{H\left[\frac{a_H}{p}\right]}$, in terms of the temperature, T, the number of hydrogen or hydrino atoms per unit volume, n_H, and the radius of each hydrogen atom or hydrino, $\frac{a_H}{p}$.

$$f_{H\left[\frac{a_H}{p}\right]} = 4\pi\sqrt{2}n_H\left(\frac{a_H}{p}\right)^2\sqrt{\frac{3kT}{m_H}} \tag{5.67}$$

The rate constant of the disproportionation reaction, $k_{m,m',p}$, to the transition reaction, Eqs. (5.44-5.52), is given by the product of the collision rate per atom, Eq. (5.67), and the coupling factor for resonant

energy transfer, $g_{m,m',p}$.

$$k_{m,m',p} = g_{m,p} 4\pi\sqrt{2} n_H \left(\frac{a_H}{p}\right)^2 \sqrt{\frac{3kT}{m_H}} \tag{5.68}$$

The coupling factor for resonant energy transfer, $g_{m,m',p}$, can be determined from the experimental results of Labov and Bowyer [7]. Consider the case that $m=1$, $m'=2$, and $p=3$ in Eqs. (5.50-5.52); $T=50\ K$, and the column density of hydrogen and hydrino atoms is estimated from typical values of the column density of H in diffuse hydrogen regions along the sight-line at b=48 deg. The intensity is calculated as the rate constant times the column density and equated to the experimental intensity of the 304 $\AA$ line which is assigned in the Spectral Data of Hydrinos from the Dark Interstellar Medium and Spectral Data of Hydrinos, Dihydrinos, and Hydrino Hydride Ions from the Sun Section as the $1/3 \rightarrow 1/4$ H transition. This yields a value of $g_{m,m',p}$ in the range of 1 which is consistent with the efficiencies of dipole-dipole resonant energy transfers [9-12]. Thus, an estimate of the rate constant of the disproportionation reaction, $k_{m,m',p}$, to cause the transition reaction, Eqs. (5.44-5.52), is given by substitution of $g_{m,m',p}=1$ into Eq. (5.68).

$$k_{m,m',p} = 4\pi\sqrt{2} n_H \left(\frac{a_H}{p}\right)^2 \sqrt{\frac{3kT}{m_H}} \ \sec^{-1} \tag{5.69}$$

The rate of the disproportionation reaction, $r_{m,m',p}$, to cause the transition reaction, Eqs. (5.44-5.52), is given by the product of the rate constant, $k_{m,m',p}$ given by Eq. (5.69), and the total number of hydrogen or hydrino atoms, N_H.

$$r_{m,m',p} = N_H 4\pi \frac{1}{2}\sqrt{2} n_H \left(\frac{a_H}{p}\right)^2 \sqrt{\frac{3kT}{m_H}} \ \frac{transitions}{\sec} \tag{5.70}$$

The factor of one half in Eq. (5.70) corrects for double counting of collisions [13]. The power, $P_{m,m',p}$, is given by the product of the rate of the transition, Eq. (5.70), and the energy of the transition, Eq. (5.49)

$$P_{m,m',p} = \frac{N_H^2}{V}\frac{4\pi}{\sqrt{2}}\left(\frac{a_H}{p}\right)^2 \sqrt{\frac{3kT}{m_H}}\left[2mp + m^2 - m'^2 + 1\right] X 2.2 X 10^{-18}\ W \tag{5.71}$$

where V is the volume.

COULOMBIC ANNIHILATION FUSION (CAF)

The electric field of a hydrogen atom is zero for $r > r_n$, where r_n is the radius of the orbitsphere of the electron (See Figure 1.7). Thus, as the orbitsphere shrinks with transitions to lower-energy states, approaching nuclei experience a smaller electric barrier and the internuclear distance (between two deuterium or tritium atoms, for

example) shrinks as well. As the internuclear separation decreases, fusion is more probable. In muon catalyzed fusion, for example, the internuclear separation is reduced by about 200 (the muon to electron mass ratio) and the fusion rate increases by about 80 orders of magnitude. In a catalytic system that produces energy holes of $27.21\,eV$, deuterium atoms can be repeatedly shrunk and the internuclear separation can be much smaller than the muon reduction. These smaller internuclear distances yield much higher fusion rates. The cold fusion process is hereafter referred to as Coulombic Annihilation Fusion (CAF).

It is important to note that the products of CAF are tritium, ${}^3H$, and protons, ${}^1H$. In hot fusion, deuterium nuclei collide randomly and produce about 50% ${}^3H$ plus ${}^1H$ and about 50% ${}^3He$ plus a neutron. In CAF, however, the nuclei are moving slowly and will collide in the most favored Coulombic arrangement—with the two protons as far from each other as possible. Thus, for CAF significantly more ${}^3H$ will be produced than ${}^3He$.

NEW "GROUND" STATE

Hydrogen atoms can undergo transitions to energy states below the ground state until the total potential energy of the proton is converted to relativistically corrected kinetic energy and total energy (the negative of the binding energy). The potential energy V of the electron and the proton separated by the radial distance radius r_1 is,

$$V = \frac{-e^2}{4\pi\varepsilon_o r_1} \tag{5.72}$$

where the radius r_1 is the proton radius given by Eq. (28.1)

$$r_p = 1.3\,X\,10^{-15}\,m \tag{5.73}$$

Substitution of Eq.(5.73) into Eq.(5.72) gives the total potential energy V of the electron and the proton

$$V = \frac{-e^2}{4\pi\varepsilon_o r_p} = 1.1\,\mathrm{X}\,10^6\ \mathrm{eV} \tag{5.74}$$

With electron capture, the electron orbitsphere superimposes that of the proton, and a neutral particle is formed that is energy deficient with respect to the neutron. To conserve spin, electron capture requires the concurrent capture of an electron antineutrino with decay to a photon and an electron neutrino as given in the Gravity Section.
Disproportionation reactions to the lowest-energy states of hydrogen followed by electron capture with gamma ray emission may be a source of nonthermal γ-ray bursts from interstellar regions [14]. Hydrino present in neutron stars may effect Coulombic Annihilation Fusion. This may be the mechanism of principally gamma emission by neutron stars.

With sufficient energy/mass release, a chain reaction of neutron decay to release electron antineutrinos which react with hydrinos according to Eq. (23.173) may be the cause of γ-ray bursts.

References

1. N. V. Sidgwick, The Chemical Elements and Their Compounds, Volume I, Oxford, Clarendon Press, (1950), p.17.
2. R. L. Mills, International Application Number: PCT/US96/07949, Lower-Energy Hydrogen Methods and Structures, January, 26, 1996; R. L. Mills, International Application Number: PCT/US98/14029, Inorganic Hydrogen Compounds, Separation Methods, and Fuel Applications, July 7, 1998.
3. David R. Linde, CRC Handbook of Chemistry and Physics, 79 th Edition, CRC Press, Boca Raton, Florida, (1998-9), p. 10-175.
4. Thompson, B. J., Handbook of Nonlinear Optics, Marcel Dekker, Inc., New York, (1996), pp. 497-548.
5. Shen, Y. R., The Principles of Nonlinear Optics, John Wiley & Sons, New York, (1984), pp. 203-210.
6. B. de Beauvoir, F. Nez, L. Julien, B. Cagnac, F. Biraben, D. Touahri, L. Hilico, O. Acef, A. Clairon, and J. J. Zondy, Physical Review Letters, Vol. 78, No. 3, (1997), pp. 440-443.
7. Labov, S., Bowyer, S., "Spectral observations of the extreme ultraviolet background", The Astrophysical Journal, 371, (1991), pp. 810-819.
8. Bueche, F. J., Introduction to Physics for Scientists and Engineers, McGraw-Hill Book Company, New York, (1986), pp. 261-265.
9. Morawetz, H., Science, 240, (1988), pp. 172-176.
10. Schnepp, O., Levy, M., J. Am. Chem. Soc., 84, (1962), pp. 172-177.
11. Wilkinson, F., Luminescence in Chemistry, Edited by E. J. Bowen, D. Van Nostrand Co. Ltd., London, (1968), pp. 155-182.
12. Förster, Th., Comparative Effects of Radiation, Report of a Conference held at the University of Puerto Rico, San Juan, February 15-19, (1960), sponsored by the National Academy of Sciences; National Research Council, Edited by Milton Burton, J. S. Kirby-Smith, and John L. Magee, John Wiley & Sons, Inc., New York pp. 300-325.
13. Levine, I., Physical Chemistry, McGraw-Hill Book Company, New York, (1978), pp. 420-421.
14. Hurley, K., et. al., Nature, 372, (1994), pp. 652-654.

STABILITY OF ATOMS AND HYDRINOS

The central field of the proton corresponds to integer one charge. Excited states comprise an electron with a trapped photon. In all energy states of hydrogen, the photon has an electric field which superposes with the field of the proton. In the $n=1$ state, the sum is one, and the sum is zero in the ionized state. In an excited state, the sum is a fraction of one (i.e. between zero and one). Derivations from first principles given in the Excited States of the One Electron Atom Section demonstrate that each "allowed" fraction corresponding to an excited state is $\frac{1}{\text{integer}}$. The relationship between the electric field equation and the "trapped photon" source charge-density function is given by Maxwell's equation in two dimensions.

$$\mathbf{n}\cdot\left(\mathbf{E}_1-\mathbf{E}_2\right)=\frac{\sigma}{\varepsilon_0} \tag{6.1}$$

where $\mathbf{n}$ is the radial normal unit vector, $\mathbf{E}_1=0$ ($\mathbf{E}_1$ is the electric field outside of the orbitsphere), $\mathbf{E}_2$ is given by the total electric field at $r_n=na_H$, and σ is the surface charge-density. The electric field of an excited state is fractional; therefore, the source charge function is fractional. It is well known that fractional charge is not "allowed". The reason given below in the Instability of Excited States Section is that fractional charge typically corresponds to a radiative current density function. The excited states of the hydrogen atom are examples. They are radiative; consequently, they are not stable. Thus, an excited electron decays to the first nonradiative state corresponding to an integer field, $n=1$. Equally valid from first principles are electronic states where the sum of the photon field and the central field are an integer. These states are nonradiative. A catalyst can effect a transition between these states as described in the Atomic Coulomb Field collapse--Hydrino Theory--BlackLight Process Section.

The condition for radiation by a moving charge is derived from Maxwell's equations. To radiate, the spacetime Fourier transform of the current-density function must possess components synchronous with waves traveling at the speed of light [1]. Alternatively,

> *For non-radiative states, the current-density function must not possess spacetime Fourier components that are synchronous with waves traveling at the speed of light.*

As given in the One Electron Atom Section, the relationship between the radius and the wavelength of the electron is

$$v_n=\lambda_n f_n \tag{6.2}$$

$$v_n=2\pi r_n f_n=\lambda_n f_n \tag{6.3}$$

$$2\pi r_n = \lambda_n \tag{6.4}$$

Consider the radial wave vector of the sinc function of Eq. (1.39), the Fourier transform of the electron current density function. When the radial projection of the velocity is c

$$\mathbf{s}_n \cdot \mathbf{v}_n = \mathbf{s}_n \cdot \mathbf{c} = \omega_n \tag{6.5}$$

the relativistically corrected wavelength is

$$\mathbf{r}_n = \lambda_n \tag{6.6}$$

Substitution of Eq. (6.6) into the sinc function results in the vanishing of the entire Fourier Transform of the current-density function. Thus, spacetime harmonics of $\frac{\omega_n}{c} = k$ or $\frac{\omega_n}{c}\sqrt{\frac{\varepsilon}{\varepsilon_o}} = k$ do not exist for which the Fourier Transform of the current-density function is nonzero.

In the case of below "ground" (fractional quantum) energy states, the sum of the source current corresponding to the photon and the electron current results in a radial Dirac delta function as shown in the Stability of Atoms and Hydrinos Section. Whereas, in the case of above "ground" or excited (integer quantum) energy states, the sum of the source current corresponding to the photon and the electron current results in a radial doublet function which has Fourier components of $\frac{\omega_n}{c} = k$. Thus, excited states are radiative as shown below.

INSTABILITY OF EXCITED STATES

For the excited (integer quantum) energy states of the hydrogen atom, σ_{photon}, the two dimensional surface charge due to the "trapped photons" at the orbitsphere, is given by Eqs. (2.6) and (2.11).

$$\sigma_{photon} = \frac{e}{4\pi(r_n)^2}\left[Y_0^0(\theta,\phi) - \frac{1}{n}\left[Y_0^0(\theta,\phi) + \mathrm{Re}\left\{Y_\ell^m(\theta,\phi)\left[1+e^{i\omega_n t}\right]\right\}\right]\right]\delta(r-r_n) \quad n = 2,3,4,..., \tag{6.7}$$

Whereas, $\sigma_{electron}$, the two dimensional surface charge of the electron orbitsphere is

$$\sigma_{electron} = \frac{-e}{4\pi(r_n)^2}\left[Y_0^0(\theta,\phi) + \mathrm{Re}\left\{Y_\ell^m(\theta,\phi)\left[1+e^{i\omega_n t}\right]\right\}\right]\delta(r-r_n) \tag{6.8}$$

The superposition of σ_{photon} (Eq. (6.7)) and $\sigma_{electron}$ (Eq. (6.8)) where the spherical harmonic functions satisfy the conditions given in the Angular Function Section is equivalent to the sum of a radial electric dipole represented by a doublet function and an radial electric monopole represented by a delta function.

$$\sigma_{photon} + \sigma_{electron} = \frac{e}{4\pi(r_n)^2}\left[Y_0^0(\theta,\phi)\delta(r-r_n) - \frac{1}{n}Y_0^0(\theta,\phi)\delta(r-r_n) - \left(1+\frac{1}{n}\right)\left[\mathrm{Re}\left\{Y_\ell^m(\theta,\phi)\left[1+e^{i\omega_n t}\right]\right\}\right]\delta(r-r_n)\right]$$
$$n = 2,3,4,..., \tag{6.9}$$

where

$$\left[+\delta(r-r_n)-\delta(r-r_n)\right]=\dot{\delta}(r-r_n) \tag{6.10}$$

is the Dirac doublet function [2] which is defined by the property

$$\begin{aligned} x(t)\quad \dot{\delta}(t) &= \dot{x}(t) \\ \int_{-\infty}^{\infty} x(\tau)\dot{\delta}(t-\tau)d\tau &= \dot{x}(t) \end{aligned} \tag{6.11}$$

or equivalently by the property

$$\int_{-\infty}^{\infty} x(t)\dot{\delta}(t)dt = -\dot{x}(0) \tag{6.12}$$

The Dirac doublet is the impulse response of an ideal differentiator and corresponds to the radial electrostatic dipole. The symbol $\dot{\delta}(t)$ is appropriate since operationally the doublet is the derivative of the impulse.

The doublet does possess spacetime Fourier components synchronous with waves traveling at the speed of light. Whereas, the radial delta function does not as demonstrated in the Spacetime Fourier Transform of the Electron Function Section. The Spacetime Fourier Transform of the orbitsphere comprising a radial Dirac delta function is given by Eq. (1.39).

$$\begin{aligned} M(s,\Theta,\Phi,\omega) = 4\pi\,\mathrm{sinc}(2s_n r_n)\quad & 2\pi\sum_{\upsilon=1}^{\infty}\frac{(-1)^{\upsilon-1}(\pi\sin\Theta)^{2(\upsilon-1)}}{(\upsilon-1)!(\upsilon-1)!}\frac{\Gamma\left(\frac{1}{2}\right)\Gamma\left(\upsilon+\frac{1}{2}\right)}{(\pi\cos\Theta)^{2\upsilon+1}2^{\upsilon+1}}\frac{2\upsilon!}{(\upsilon-1)!}s^{-2\upsilon} \\ & 2\pi\sum_{\upsilon=1}^{\infty}\frac{(-1)^{\upsilon-1}(\pi\sin\Phi)^{2(\upsilon-1)}}{(\upsilon-1)!(\upsilon-1)!}\frac{\Gamma\left(\frac{1}{2}\right)\Gamma\left(\upsilon+\frac{1}{2}\right)}{(\pi\cos\Phi)^{2\upsilon+1}2^{\upsilon+1}}\frac{2\upsilon!}{(\upsilon-1)!}s^{-2\upsilon}\frac{1}{4\pi}\left[\delta(\omega-\omega_n)+\delta(\omega+\omega_n)\right] \end{aligned} \tag{6.13}$$

The radial doublet function is the derivative of the radial Dirac delta function; thus, the Fourier transform of the doublet function can be obtained from the Fourier transform of the Dirac delta function, Eq. (6.13) and the differentiation property of Fourier transforms [3].

$$x(t)=\int_{-\infty}^{\infty}X(f)e^{j2\pi ft}df \qquad X(t)=\int_{-\infty}^{\infty}x(t)e^{-j2\pi ft}dt \tag{6.14}$$

$$\textit{Differentiation}\qquad \frac{dx(t)}{dt} \quad\Leftrightarrow\quad j2\pi fX(f)$$

From Eq. (6.13) and Eq. (6.14), the spacetime Fourier transform of Eq. (6.9), the superposition of σ_{photon} (Eq. (6.7)) and $\sigma_{electron}$ (Eq. (6.8)) is

$$M(s,\Theta,\Phi,\omega) = 4\pi s_n e^{j\frac{\pi}{2}} \frac{\sin(2s_n r_n)}{2s_n r_n} \quad 2\pi \sum_{\upsilon=1}^{\infty} \frac{(-1)^{\upsilon-1}(\pi \sin\Theta)^{2(\upsilon-1)}}{(\upsilon-1)!(\upsilon-1)!} \frac{\Gamma\left(\frac{1}{2}\right)\Gamma\left(\upsilon+\frac{1}{2}\right)}{(\pi\cos\Theta)^{2\upsilon+1}2^{\upsilon+1}} \frac{2\upsilon!}{(\upsilon-1)!} s^{-2\upsilon}$$

$$2\pi \sum_{\upsilon=1}^{\infty} \frac{(-1)^{\upsilon-1}(\pi \sin\Phi)^{2(\upsilon-1)}}{(\upsilon-1)!(\upsilon-1)!} \frac{\Gamma\left(\frac{1}{2}\right)\Gamma\left(\upsilon+\frac{1}{2}\right)}{(\pi\cos\Phi)^{2\upsilon+1}2^{\upsilon+1}} \frac{2\upsilon!}{(\upsilon-1)!} s^{-2\upsilon} \frac{1}{4\pi} [\delta(\omega-\omega_n)+\delta(\omega+\omega_n)] \tag{6.15}$$

$$M(s,\Theta,\Phi,\omega) = 4\pi s_n \frac{\cos(2s_n r_n)}{2s_n r_n} \quad 2\pi \sum_{\upsilon=1}^{\infty} \frac{(-1)^{\upsilon-1}(\pi \sin\Theta)^{2(\upsilon-1)}}{(\upsilon-1)!(\upsilon-1)!} \frac{\Gamma\left(\frac{1}{2}\right)\Gamma\left(\upsilon+\frac{1}{2}\right)}{(\pi\cos\Theta)^{2\upsilon+1}2^{\upsilon+1}} \frac{2\upsilon!}{(\upsilon-1)!} s^{-2\upsilon}$$

$$2\pi \sum_{\upsilon=1}^{\infty} \frac{(-1)^{\upsilon-1}(\pi \sin\Phi)^{2(\upsilon-1)}}{(\upsilon-1)!(\upsilon-1)!} \frac{\Gamma\left(\frac{1}{2}\right)\Gamma\left(\upsilon+\frac{1}{2}\right)}{(\pi\cos\Phi)^{2\upsilon+1}2^{\upsilon+1}} \frac{2\upsilon!}{(\upsilon-1)!} s^{-2\upsilon} \frac{1}{4\pi} [\delta(\omega-\omega_n)+\delta(\omega+\omega_n)] \tag{6.16}$$

Consider the radial wave vector of the cosine function of Eq. (6.16). When the radial projection of the velocity is c

$$\mathbf{s}_n \cdot \mathbf{v}_n = \mathbf{s}_n \cdot \mathbf{c} = \omega_n \tag{6.17}$$

the relativistically corrected wavelength is

$$\mathbf{r}_n = \lambda_n \tag{6.18}$$

Substitution of Eq. (6.18) into the cosine function does not result in the vanishing of the Fourier Transform of the current-density function. Thus, spacetime harmonics of $\frac{\omega_n}{c} = k$ or $\frac{\omega_n}{c}\sqrt{\frac{\varepsilon}{\varepsilon_o}} = k$ do exist for which the Fourier Transform of the current-density function is nonzero. An excited state is metastable because it is the sum of nonradiative (stable) and radiative (unstable) components and de-excites with a transition probability given by the ratio of the power to the energy of the transition [4].

STABILITY OF "GROUND" AND HYDRINO STATES

For the below "ground" (fractional quantum) energy states of the hydrogen atom, σ_{photon}, the two dimensional surface charge due to the "trapped photon" at the electron orbitsphere, is given by Eqs. (5.13) and (2.11).

$$\sigma_{photon} = \frac{e}{4\pi(r_n)^2}\left[Y_0^0(\theta,\phi) - \frac{1}{n}\left[Y_0^0(\theta,\phi) + \mathrm{Re}\left\{Y_\ell^m(\theta,\phi)\left[1+e^{i\omega_n t}\right]\right\}\right]\right]\delta(r-r_n) \quad n = 1,\frac{1}{2},\frac{1}{3},\frac{1}{4},\ldots, \tag{6.19}$$

And, $\sigma_{electron}$, the two dimensional surface charge of the electron

orbitsphere is

$$\sigma_{electron} = \frac{-e}{4\pi(r_n)^2}\left[Y_0^0(\theta,\phi) + \mathrm{Re}\left\{Y_\ell^m(\theta,\phi)\left[1+e^{i\omega_n t}\right]\right\}\right]\delta(r-r_n) \qquad (6.20)$$

The superposition of σ_{photon} (Eq. (6.19)) and $\sigma_{electron}$, (Eq. (6.20)) where the spherical harmonic functions satisfy the conditions given in the Angular Function Section is a radial electric monopole represented by a delta function.

$$\sigma_{photon} + \sigma_{electron} = \frac{-e}{4\pi(r_n)^2}\left[\frac{1}{n}Y_0^0(\theta,\phi) + \left(1+\frac{1}{n}\right)\mathrm{Re}\left\{Y_\ell^m(\theta,\phi)\left[1+e^{i\omega_n t}\right]\right\}\right]\delta(r-r_n) \quad n = 1,\frac{1}{2},\frac{1}{3},\frac{1}{4},..., \qquad (6.21)$$

In the case of lower-energy states, the superposition given by Eq. (6.21) involves integer charge only. Whereas, in the case of excited states, the superposition given by Eq. (6.9) involves the sum of a delta function with a fractional charge (radial monopole term) and of two delta functions of charge plus one and minus one which is a doublet function (radial dipole term). As given in the Spacetime Fourier Transform of the Electron Function Section, the radial delta function does not possess spacetime Fourier components synchronous with waves traveling at the speed of light. Thus, the below "ground" (fractional quantum) energy states of the hydrogen atom are stable. The "ground" ($n=1$ quantum) energy state is just the first of the nonradiative states of the hydrogen atom; thus, it is the state to which excited states decay.

DISPROPORTIONATION MECHANISM

Comparing transitions between below "ground" (fractional quantum) energy states as opposed to transitions between excited (integer quantum) energy states, it can be appreciated that the former are not effected by photons; whereas, the latter are. Transitions are symmetric with respect to time (ignoring the minuscule effects of spacetime expansion given in the Gravity Section). Current density functions which give rise to photons according to the boundary condition are created by photons by the reverse process. Excited (integer quantum) energy states correspond to this case. And, current density functions which do not give rise to photons according to the boundary condition are not created by photons by the reverse process. Below "ground" (fractional quantum) energy states correspond to this case. But, atomic collisions can cause a stable state to undergo a transition to the next stable state. The transition between two stable nonradiative states effected by a collision with an energy hole is analogous to the energy-releasing reaction of two atoms to form a diatomic molecule which requires a third-body collision to remove the bond energy [5]. The process referred to as the Atomic BlackLight Process is described in the Atomic Coulomb Field collapse--Hydrino

Theory--BlackLight Process Section. (Also see Mills International Patent Application [6]).

Exemplary of an inelastic collision with resonant energy transfer to form an excited state atom is the Franck-Hertz experiment [7]. And, the $n \leq 1$ ("ground" ($n=1$) and below "ground" (fractional quantum)) energy states are stable until an inelastic collision occurs with resonant energy transfer. Then the force balance is altered, and the electron radiates energy in the form of a photon until the next nonradiative level is achieved. Chemical reactions are analogous. The former type which give rise to high energy photons are chemiluminescent.

In a system containing two fluorescent species such that the emission spectrum of one (the "donor") overlaps the absorption spectrum of the other (the "acceptor"), the excitation energy of the donor atoms may be transferred by a resonance Coulombic electromagnetic interaction mechanism over relatively large distances to the acceptor species (energy hole) rather than the donors radiating into free space. The total Coulombic interaction may be taken as the sum of terms including dipole-dipole, dipole-quadrapole, and terms involving higher order multipoles. The Förster theory [8-12] is general to dipole-dipole energy transfer which is often predominant. It applies to the case of lower-energy hydrogen following a collision with a concomitant electron current alteration. The hydrogen-type electron orbitsphere is a spherical shell of negative charge (total charge = $-e$) of zero thickness at a distance r_n from the nucleus (charge = $+Ze$). It is well known that the field of a spherical shell of charge is zero inside the shell and that of a point charge at the origin outside the shell [13]. The electric field of the proton is that of a point charge at the origin. And, the superposition, **E**, of the electric fields of the electron and the proton is that of a point charge inside the shell and zero outside.

$$\mathbf{E} = \frac{e}{4\pi\varepsilon_0 r^2} \qquad \text{for } r < r_n \tag{6.22}$$

$$\mathbf{E} = 0 \qquad \text{for } r > r_n \tag{6.23}$$

The magnetic field of the electron, **H**, is derived in the Derivation of the Magnetic Field Section:

$$\mathbf{H} = \frac{e\hbar}{m_e r_n^3}(\mathbf{i}_r \cos\theta - \mathbf{i}_\theta \sin\theta) \qquad \text{for } r < r_n \tag{6.24}$$

$$\mathbf{H} = \frac{e\hbar}{2m_e r^3}(\mathbf{i}_r 2\cos\theta - \mathbf{i}_\theta \sin\theta) \qquad \text{for } r > r_n \tag{6.25}$$

Power flow is governed by the Poynting power theorem,

$$\cdot(\mathbf{E}\times\mathbf{H}) = -\frac{\delta}{\delta t}\left(\frac{1}{2}\right)\mu_o\mathbf{H}\cdot\mathbf{H} - \frac{\delta}{\delta t}\left(\frac{1}{2}\right)\varepsilon_o\mathbf{E}\cdot\mathbf{E} - \mathbf{J}\cdot\mathbf{E} \tag{6.26}$$

It follows from Eqs. (6.22-6.26) that $\cdot(\mathbf{E}\times\mathbf{H})$ is zero until a collision occurs between two hydrogen-type atoms. As given in Jackson [14], each current distribution can be written as a multipole expansion. A catalytic collision gives rise to radiative terms including a dipole term. (There is at least current in the radial direction until force balance is achieved again at the next nonradiative level). Förster's theory [8], leads to the following equation for $n(R)$, the transfer rate constant

$$n(R) = \frac{9000(\ln 10)\kappa^2\Phi_D}{128\pi^5 n^4 N_A \tau_D R^6}\int_0^\infty f_D(\bar{\nu})\varepsilon_A(\bar{\nu})\frac{d\bar{\nu}}{\bar{\nu}^4} \tag{6.27}$$

where $\varepsilon_A(\bar{\nu})$ is the molar decadic extinction coefficient of the acceptor (at wave-number $\bar{\nu}$), $f_D(\bar{\nu})$ is the spectral distribution of the fluorescence of the donor (measured in quanta and normalized to unity on a wave-number scale), N_A is Avogadro's number, τ_D is the mean lifetime of the excited state, Φ_D is the quantum yield of the fluorescence of the donor, n is the refractive index , R is the distance between the donor and acceptor, and κ is an orientative factor which for a random distribution equals $\left(\frac{2}{3}\right)^{\frac{1}{2}}$. The collision of two lower-energy hydrogen atoms will result in an elastic collision, an inelastic collision with a hydrogen-type molecular reaction, or an inelastic collision with a disproportionation reaction as described in the Disproportionation of Energy States Section. An estimate of the transition probability for electric multipoles is given by Eq. (16.104) of Jackson [15]. For an electric dipole $\ell = 1$, and Eq. (16.104) of Jackson is

$$\frac{1}{\tau_E} \quad \left(\frac{e^2}{\hbar c}\right)\frac{\pi}{16}(ka)^2\omega \tag{6.28}$$

where a is the radius of the hydrogen-type atom, and k is the wave-number of the transition. Substitution of

$$k = \frac{\omega}{c} \tag{6.29}$$

into Eq. (6.28) gives

$$\frac{1}{\tau_E} \quad \left(\frac{e^2}{\hbar c}\right)\frac{\pi}{16}\left(\frac{a}{c}\right)^2\omega^3 \tag{6.30}$$

From Eq. (6.30), the transition probability is proportional to the frequency cubed. Thus, the disproportionation reaction of lower-energy hydrogen is favored over the molecular reaction because it is the most energetic transition for the donor lower-energy hydrogen atom. In the

case that nonradiative energy transfer occurs between two lower-energy hydrogen atoms, the mean lifetime of the excited state of Eq. (6.27), τ_D, corresponds to the vibrational period of the corresponding lower-energy hydrogen molecule which follows from Eq. (12.107) and Planck's Equation (Eq. (2.65)), the distance between the donor and acceptor, R, is given by the internuclear distance which is twice c' of Eq. (12.95), and the orientative factor, κ, equals one because of the spherical symmetry of the lower-energy hydrogen atoms. Electronic transitions of lower-energy hydrogen atoms occur only by nonradiative energy transfer; thus, the quantum yield of the fluorescence of the donor, Φ_D, is equal to one. In free space, the overlap integral between the emission spectrum of the donor lower-energy hydrogen atom and the absorption spectrum of the acceptor lower-energy hydrogen atom is one. Consider the following disproportionation reaction where the energy of the emission line for the transition given by $m=1$, $m'=2$ and $p=2$ in Eqs. (5.50-5.52) involving the absorption of an energy hole of $27.21\,eV$, $m=1$ in Eq. (5.5), is $13.6\,eV$.

$$H\left(\frac{a_H}{2}\right) + H\left(\frac{a_H}{2}\right) \rightarrow H\left(\frac{a_H}{3}\right) \tag{6.31}$$

The transfer rate constant, $n(R)$, for Eq. (6.31) using Eq. (6.27) is

$$n(R) = \frac{9000(\ln 10)(1)^2 1}{128\pi^5(1)^4\left(6.02\ X\ 10^{23}\right)\left(1.77\ X\ 10^{-15}\right)\left(3.73\ X\ 10^{-11}\right)^6\left(6.91\ X\ 10^7\right)} = 8\ X\ 10^{21}\ \text{sec}^{-1} \tag{6.32}$$

According to Förster's theory [9], the efficiency E of such nonradiative energy transfer given by the product of the transfer rate constant and the mean lifetime of the excited state may be expressed by

$$E = \frac{1}{1+\left(\frac{r}{R_0}\right)^6} \tag{6.33}$$

$$R_0^6 = \left(8.8\ X\ 10^{-25}\right) J \eta^{-4} \phi_D^0 \kappa^2$$

where r is the distance between the donor and the acceptor, J is the overlap integral between the emission spectrum of the donor and the absorption spectrum of the acceptor, η is the dielectric constant, ϕ_D^0 is the fluorescence quantum yield of the donor in the absence of acceptors, and κ^2 is a function of the mutual orientation of the donor and acceptor transition moments. In the case that the radius of Eq. (6.32) is a fraction of the Bohr radius, the efficiency of energy transfer is approximately one as given in the Interstellar Disproportionation Rate Section.

(As an additional reference to the application of Förster theory see Mills patent [16]).

ENERGY HOLE AS A MULTIPOLE EXPANSION

The potential energy (Eq. (1.173)) of the below "ground" state hydrogen atom of radius $\frac{a_H}{n}$ having a central field of magnitude n is

$$n^2 X 27.2\ eV, \tag{6.34}$$

where n is an integer. The potential energy is given as the superposition of ℓ energy-degenerate quantum states corresponding to a multipole expansion of the central electromagnetic field. One multipole moment of all those possible, need be excited to stimulate the below "ground" state transition. The total number, N, of multipole moments where each corresponds to an ℓ and m_ℓ quantum number of an energy level corresponding to a principal quantum number of n is

$$N = \sum_{\ell=0}^{n-1} \sum_{m_\ell=-\ell}^{+\ell} = \sum_{\ell=0}^{n-1} 2\ell + 1 = n^2 \tag{6.35}$$

Thus, the energy hole to stimulate a transition of a hydrogen atom from radius $\frac{a_H}{n}$ to radius $\frac{a_H}{n+1}$ with an increase in the central field from n to $n+1$ where n is an integer is

$$(n+1)^2 27.2 \frac{1}{(n+1)^2} = 27.2\ eV \tag{6.36}$$

Energy conservation occurs during the absorption of an energy hole. For a hydrogen atom with a principal quantum number of n having a radius of $\frac{a_H}{n}$, the absorption of an energy hole of $n X 27.2\ eV$ instantaneously decreases the potential energy by $n X 27.2\ eV$. The calculation of instantaneous potential energy change due to the absorption of the energy hole of equal but opposite energy is given by the summation over all possible multipoles of the integral of the product of the photon standing wave corresponding to the absorbed energy hole and the multipoles of the electron charge-density function. The multipole of the photon standing wave and each multipole of the electron charge-density function corresponds to an ℓ and m_ℓ quantum number.

POWER DENSITY OF GAS ENERGY CELL

A pressurized hydrogen gas energy reactor for the release of energy by a catalytic or disproportionation reaction, wherein the electrons of hydrogen atoms undergo transitions to lower energy states, comprises a vessel containing a source of hydrogen, a means to control the pressure and flow of hydrogen into the vessel, a material to dissociate the molecular hydrogen into atomic hydrogen, and a material

which is a source of energy holes. The reaction that produces lower-energy hydrogen referred to as a ***transition reaction*** is a catalytic reaction as given in the BlackLight Process Section. The ***disproportionation reaction*** given in the Disproportionation of Energy States Section is also a transition reaction. Each energy sink or means to remove energy resonant with the hydrogen electronic energy released to effect each transition is hereafter referred to as an ***energy hole***.

The rate of the disproportionation reaction, $r_{m,m',p}$, to cause the transition reaction, Eqs. (5.44-5.52), is dependent on the collision rate between the reactants and the efficiency of resonant energy transfer. It is given by the product of the rate constant, $k_{m,m',p}$,(Eq. (5.69)), the total number of hydrogen or hydrino atoms, N_H, and the efficiency, E (Eq. (6.33)), of the transfer of the energy from the donor hydrino atom to the energy hole provided by the acceptor hydrino atom,

$$E = \frac{1}{1 + \left(\frac{r}{R_0}\right)^6} \qquad (6.37)$$

$$R_0^6 = \left(8.8\ X\ 10^{-25}\right) J \eta^{-4} \phi_D^0 \kappa^2$$

where r is the distance between the donor and the acceptor, J is the overlap integral between the energy distribution of the donor hydrino atom and the distribution of the energy hole provided by the acceptor hydrino atom, η is the dielectric constant, and κ^2 is a function of the mutual orientation of the donor and acceptor transition moments. Electronic transitions of lower-energy hydrogen atoms occur only by nonradiative energy transfer; thus, the quantum yield of the fluorescence of the donor, Φ_D, of Eq. (6.37) is equal to one. The rate of the disproportionation reaction, $r_{m,m',p}$, to cause a transition reaction is

$$r_{m,m',p} = E\, N_H 4\pi \frac{1}{2} \sqrt{2} n_H \left(\frac{a_H}{p}\right)^2 \sqrt{\frac{3kT}{m_H}} \qquad (6.38)$$

The factor of one half in Eq. (6.38) corrects for double counting of collisions [17]. The power, $P_{m,m',p}$, is given by the product of the rate of the transition, Eq. (6.38), and the energy of the disproportionation reaction (Eq. (5.49)).

$$P_{m,m',p} = E\, \frac{N_H^2}{V} 4\pi \frac{1}{\sqrt{2}} \left(\frac{a_H}{p}\right)^2 \sqrt{\frac{3kT}{m_H}} \left[2pm + m^2 - m'^2 + 1\right] X\, 2.2\, X 10^{-18}\ W \qquad (6.39)$$

where V is the volume. For a disproportionation reaction in the gas phase, the energy transfer efficiency is one. The power given by substitution of

$$E = 1, p = 2, m = 1, m' = 2, V = 1\, m^3, N = 3\ X\ 10^{21}, T = 675\ K \qquad (6.40)$$

into Eq. (6.39) is

$$P_{m,m',p} = 1\,GW(1\,kW/cm^3) \tag{6.41}$$

In the case that the reaction of hydrogen to lower-energy states occurs by the reaction of a catalytic source of energy holes with hydrogen or hydrino atoms, the reaction rate is dependent on the collision rate between the reactants and the efficiency of resonant energy transfer. The hydrogen-or-hydrino-atom/catalyst-atom collision rate per unit volume, $Z_{H\left(\frac{a_H}{p}\right)\text{Catalyst}}$, for a gas containing n_H hydrogen or hydrino atoms per unit volume, each with radius $\frac{a_H}{p}$ and velocity v_H and n_C catalyst atoms per unit volume, each with radius r_{Catalyst} and velocity v_C is given by the general equation of Levine [17] for the collision rate per unit volume between atoms of two dissimilar gases.

$$Z_{H\left(\frac{a_H}{p}\right)\text{Catalyst}} = \pi\left(\frac{a_H}{p} + r_{\text{Catalyst}}\right)^2\left[\langle v_H\rangle^2 + \langle v_C\rangle^2\right]^{1/2} n_H n_C \tag{6.42}$$

The average velocity, v_{avg}, can be calculated from the temperature, T, [18].

$$\frac{1}{2}m_H v_{avg}^2 = \frac{3}{2}kT \tag{6.43}$$

where k is Boltzmann's constant. Substitution of Eq. (5.66) into Eq. (5.64) gives the collision rate per unit volume, $Z_{H\left(\frac{a_H}{p}\right)\text{Catalyst}}$, in terms of the temperature, T.

$$Z_{H\left(\frac{a_H}{p}\right)\text{Catalyst}} = \pi\left(\frac{a_H}{p} + r_{\text{Catalyst}}\right)^2\left[3kT\left(\frac{1}{m_H} + \frac{1}{m_C}\right)\right]^{1/2} n_H n_C \tag{6.44}$$

The rate of the catalytic reaction, $r_{m,p}$, to cause a transition reaction is given by the product of the collision rate per unit volume, $Z_{H\left(\frac{a_H}{p}\right)\text{Catalyst}}$, the volume, V, and the efficiency, E, of resonant energy transfer given by Eq. (6.37).

$$r_{m,p} = E\,\pi\left(\frac{a_H}{p} + r_{\text{Catalyst}}\right)^2\left[3kT\left(\frac{1}{m_H} + \frac{1}{m_C}\right)\right]^{1/2}\frac{N_H N_C}{V} \tag{6.45}$$

The power, $P_{m,p}$, is given by the product of the rate of the transition, Eq. (6.45), and the energy of the transition, Eq. (5.17).

$$P_{m,p} = E\,\pi\left(\frac{a_H}{p} + r_{\text{Catalyst}}\right)^2\left[3kT\left(\frac{1}{m_H} + \frac{1}{m_C}\right)\right]^{1/2}\frac{N_H N_C}{V}\left[2mp + m^2\right]X2.2\,X10^{-18}\,W \tag{6.46}$$

In the case of a gas phase catalytic transition reaction of a single cationic catalyst having an ionization energy of $27.21\,eV$ with hydrogen or hydrino

atoms, the energy transfer efficiency is one. Rubidium II is a catalyst with a second ionization energy of 27.28 eV. The power for the reaction given by Eqs. (5.25-5.27) with the substitution of

$$E = 1, p = 1, m = 1, V = 1\ m^3, N_H = 3\ X\ 10^{21}, N_C = 3\ X\ 10^{21}, \quad m_C = 1.4\ X\ 10^{-25}\ \text{kg}, r_C = 2.16\ X\ 10^{-10}\ \text{m}, T = 675\ K \tag{6.47}$$

into Eq. (6.46) is

$$P_{m,p} = 55\ GW\ (55\ \text{kW}/cm^3) \tag{6.48}$$

In the case that the catalytic reaction of hydrogen to lower-energy states occurs on a surface, the energy transfer efficiency is less than one due to differential surface interactions of the absorbed hydrogen or hydrino atoms and the catalyst. The power given by Eqs. (6.46) and (6.47) with

$$E = 0.001 \tag{6.49}$$

is

$$P_{m,p} = 55\ MW\ (55\ W/cm^3) \tag{6.50}$$

Less efficient catalytic systems hinge on the coupling of three resonator cavities. For example, an electron transfer occurs between two cations which comprises an energy hole for a hydrogen or hydrino atom. The reaction rate is dependent on the collision rate between catalytic cations and hydrogen or hydrino atoms and the efficiency of resonant energy transfer with a concomitant electron transfer with each transition reaction. The rate of the catalytic reaction, $r_{m,p}$, to cause a transition reaction is given by the product of the collision rate per unit volume, $Z_{H\left(\frac{a_H}{p}\right)\text{Catalyst}}$, the volume, V, and the efficiency, E_e, of resonant energy transfer given by Eq. (6.37) where r is given by the average distance between cations in the reaction vessel.

$$r_{m,p} = E_c\ \pi\left(\frac{a_H}{p} + r_{\text{Catalyst}}\right)^2\left(3kT\left(\frac{1}{m_H} + \frac{1}{m_C}\right)\right)^{1/2}\frac{N_H N_C}{V} \tag{6.51}$$

The power, $P_{m,p}$, is given by the product of the rate of the transition, Eq. (6.51), and the energy of the transition, Eq. (5.17).

$$P_{m,p} = E_c\ \pi\left(\frac{a_H}{p} + r_{\text{Catalyst}}\right)^2\left(3kT\left(\frac{1}{m_H} + \frac{1}{m_C}\right)\right)^{1/2}\frac{N_H N_C}{V}\left[2mp + m^2\right]X\,2.2\,X10^{-18}\ W \tag{6.52}$$

A catalytic system that hinges on the coupling of three resonator cavities involves potassium. For example, the second ionization energy of potassium is 31.63 eV. This energy hole is obviously too high for resonant absorption. However, K^+ releases 4.34 eV when it is reduced to K. The combination of K^+ to K^{2+} and K^+ to K, then, has a net energy change of 27.28 eV. Consider the case of a gas phase catalytic transition reaction of hydrogen or hydrino atoms by potassium ions as the catalyst having an energy hole of 27.28 eV. The energy transfer efficiency is given by Eq.

(6.37) where r is given by the average distance between cations in the reaction vessel. When the K^+ concentration is $3 X 10^{22} \frac{K^+}{m^3}$, r is approximately $5 X 10^{-9}\ m$. For $J = 1$, $\Phi_D = 1$, $\kappa^2 = 1$, $\tau_D = 10^{-13}$ sec (based on the vibrational frequency of KH^+), and $m = 1$ in Eq (5.8), the energy transfer efficiency, E_c, is approximately 0.001. The power for the reaction given by Eqs. (5.22-5.24) with the substitution of

$$E = 0.001,\ p = 1,\ m = 1,\ V = 1\,m^3,\ N_H = 3 X 10^{21},\ N_C = 3 X 10^{22},$$
$$m_C = 6.5 X 10^{-26}\ \text{kg},\ r_C = 1.38 X 10^{-10}\ \text{m},\ T = 675\ K \qquad (6.53)$$

into Eq. (6.52) is

$$P_{m,p} = 300\ MW\ (300\ W / cm^3) \qquad (6.54)$$

References

1. Haus, H. A., "On the radiation from point charges", American Journal of Physics, 54, (1986), pp. 1126-1129.
2. Siebert, W. McC., Circuits, Signals, and Systems, The MIT Press, Cambridge, Massachusetts, (1986), pp. 338-339.
3. Siebert, W. McC., Circuits, Signals, and Systems, The MIT Press, Cambridge, Massachusetts, (1986), p. 416.
4. Jackson, J. D., Classical Electrodynamics, Second Edition, John Wiley & Sons, New York, (1962), pp. 758-763.
5. N. V. Sidgwick, The Chemical Elements and Their Compounds, Volume I, Oxford, Clarendon Press, (1950), p.17.
6. R. L. Mills, International Application Number: PCT/US96/07949, Lower-Energy Hydrogen Methods and Structures, (1996).
7. Beiser, A., Concepts of Modern Physics, Fourth Edition, McGraw-Hill Book Company, New York, (1978), pp. 153-155.
8. F. Wilkinson, "Intramolecular Electronic Energy Transfer Between Organic Molecules", Luminescence in Chemistry, Edited by E. J. Bowen, D. Van Nostrand Co. Ltd., London, (1968), Chapter 8, pp. 154-182.
9. Morawetz, H., Science, 240, (1988), pp. 172-176.
10. Schnepp, O., Levy, M., J. Am. Chem. Soc., 84, (1962), pp. 172-177.
11. Wilkinson, F., Luminescence in Chemistry, Edited by E. J. Bowen, D. Van Nostrand Co. Ltd., London, (1968), pp. 155-182.
12. Förster, Th., Comparative Effects of Radiation, Report of a Conference held at the University of Puerto Rico, San Juan, February 15-19, (1960), sponsored by the National Academy of Sciences; National Research Council, Edited by Milton Burton, J. S. Kirby-Smith, and John L. Magee, John Wiley & Sons, Inc., New York pp. 300-325.
13. Bueche, F., Introduction to Physics for Scientists and Engineers, McGraw-Hill, (1975), pp. 352-353.

14. Jackson, J. D., Classical Electrodynamics, Second Edition, John Wiley & Sons, New York, (1962), pp. 739-747.
15. Jackson, J. D., Classical Electrodynamics, Second Edition, John Wiley & Sons, New York, (1962), pp. 758-760.
16. R. L. Mills, US Patent Number: 5,428,163, Prodrugs for Selective Drug Delivery, (1995); R. L. Mills, US Patent Number: 5,773,592 Prodrugs for Selective Drug Delivery, (1998).
17. Levine, I., Physical Chemistry, McGraw-Hill Book Company, New York, (1978), pp. 420-421.
18. Bueche, F. J., Introduction to Physics for Scientists and Engineers, McGraw-Hill Book Company, New York, (1986), pp. 261-265.

TWO ELECTRON ATOMS

Two electron atoms comprise two indistinguishable electrons bound to a nucleus of $+Z$. Each electron experiences a centrifugal force, and the balancing centripetal force (on each electron) is produced by the electric force between the electron and the nucleus and the magnetic force between the two electrons causing the electrons to pair.

DETERMINATION OF ORBITSPHERE RADII, r_n

According to the Mills theory of the electron derived from first principles bound electrons are described by a charge-density (mass-density) function which is the product of a radial delta function ($f(r) = \delta(r - r_n)$), two angular functions (spherical harmonic functions), and a time harmonic function. Thus, an electron is a spinning, two-dimensional spherical surface, called an electron orbitsphere, that can exist in a bound state at only specified distances from the nucleus. More explicitly, the orbitsphere comprises a two dimensional spherical shell of moving charge. The corresponding current pattern of the orbitsphere comprises an infinite series of correlated orthogonal great circle current loops. The current pattern (shown in Figure 1.4) is generated over the surface by two orthogonal sets of an infinite series of nested rotations of two orthogonal great circle current loops where the coordinate axes rotate with the two orthogonal great circles. Each infinitesimal rotation of the infinite series is about the new x-axis and new y-axis which results from the preceding such rotation. For each of the two sets of nested rotations, the angular sum of the rotations about each rotating x-axis and y-axis totals $\sqrt{2}\pi$ radians. The current pattern gives rise to the phenomenon corresponding to the spin quantum number. Each one-electron orbitsphere is a spherical shell of negative charge ($\text{total charge} = -e$) of zero thickness at a distance r_n from the nucleus ($\text{charge} = +Ze$). It is well known that the field of a spherical shell of charge is zero inside the shell and that of a point charge at the origin outside the shell [1] (See Figure 1.7). Thus, for a nucleus of charge Z, the force balance equation for the electron orbitsphere is obtained by equating the forces on the mass and charge densities. The centrifugal force of each electron is given by

$$\mathbf{F}_{centrifugal} = \frac{m_e}{4\pi r_n^2}\frac{\mathbf{v}_n^2}{r_n} \tag{7.1}$$

where r_n is the radius of electron n which has velocity $\mathbf{v}_n$. In order to be nonradiative, the velocity for every point on the orbitsphere is given by Eq. (1.47).

$$\mathbf{v}_n = \frac{\hbar}{m_e r_n} \tag{7.2}$$

Now, consider electron 1 initially at $r = r_1 = \frac{a_0}{Z}$ (the radius of the one electron atom of charge Z given in the One Electron Atom Section where $a_0 = \frac{4\pi\varepsilon_0\hbar^2}{e^2 m_e}$ and electron 2 initially at $r_n = \infty$. Each electron can be treated as $-e$ charge at the nucleus with $\mathbf{E} = \frac{-e}{4\pi\varepsilon_o r_n^2}$ for $r > r_n$ and $\mathbf{E} = 0$ for $r < r_n$ where r_n is the radius of the electron orbitsphere. The centripetal force is the electric force, $\mathbf{F}_{ele}$, between the electron and the nucleus. Thus, the electric force between electron 2 and the nucleus is

$$\mathbf{F}_{ele(electron2)} = \frac{(Z-1)e^2}{4\pi\varepsilon_o r_n^2} \tag{7.3}$$

where ε_o is the permittivity of free-space. The magnetic force, the second centripetal force, on the electron 2 (at infinity) from electron 1 (at r_1) is the relativistic corrected magnetic force, $\mathbf{F}_{mag}$, between each point of the electron two and electron one. Each infinitesimal point of each orbitsphere moves on a great circle, and each point charge has the charge-density $\frac{e}{4\pi r_n^2}$. From the photon inertial reference frame at the radius of each infinitesimal point of electron 2, the magnetic field of electron 1 in the point's inertial frame follows from McQuarrie [2]:

$$\mathbf{B} = \frac{\mu_o e\hbar}{2m_e r_n^3} \tag{7.4}$$

where μ_o is the permeability of free-space ($4\pi X 10^{-7} N/A^2$). An electrodynamic force, a force dependent on the second derivative of the charge's position which respect to time, arises between the two electrons. The motion of each point will cause a relativistic central force, $\mathbf{F}_{i\,mag}$, which acts on each point mass comprising the orbitsphere. The magnetic central force is derived as follows from the Lorentzian force which is relativistically corrected. The Lorentzian force density on each point moving at velocity $\mathbf{v}$ given by Eq. (1.47) is

$$\mathbf{F}_{mag} = \frac{e}{4\pi r_n^2}\mathbf{v}\times\mathbf{B} \tag{7.5}$$

Substitution of Eq. (1.47) for $\mathbf{v}$ and Eq. (7.4) for $\mathbf{B}$ gives

$$\mathbf{F}_{mag} = \frac{1}{4\pi r_1^2}\left[\frac{e^2\mu_o}{2m_e r_n}\right]\left[\frac{\hbar^2}{m_e r_n^3}\right] \tag{7.6}$$

Furthermore, the term in brackets can be expressed in terms of the fine structure constant, α. From Eqs. (1.143-1.147) where $Z_1 = 1$

$$\frac{e^2\mu_o}{2m_e r_n} = 2\pi\alpha\frac{v}{c} \tag{7.7}$$

It can be shown that the relativistic correction to Eq. (7.6) is $\frac{1}{Z_2}$ times the reciprocal of Eq. (7.7). Consider an inertial frame following a great circle of radius r_n with $v = c$. The motion is tangential to the radius; thus, r_n is Lorentzian invariant. But, the tangential distance along a great circle is $2\pi r_n$ in the electron frame and r_n in the $v = c$ frame. The charge is relativistically invariant, whereas, the mass is not. The relativistic correction to the laboratory frame mass relative to the $v = c$ frame is 2π. The correction follows from the Lorentz transformation of the electron's invariant angular momentum of $\hbar$. It is shown by Purcell [3] that the force on a moving charge due to a moving line of charge is a relativistic electric force due to Lorentzian contraction of the line charge density. The force is proportional to $\frac{v}{c}$ where v is the electron's velocity. Thus, it follows that the electron mass in the laboratory frame relative to the $v = c$ inertial frame is also proportional to $\frac{v}{c}$. Following the derivation of Purcell with the substitution of the relativistic mass density for the charge density gives the electron mass correction to the electrodynamic force as

$$m_e = 2\pi\frac{v}{c}m_{e\,Rest} \tag{7.8}$$

Furthermore, due to invariance of charge under Gauss's Integral Law, the radius term in the brackets of Eq. (7.6) is relativistically corrected. The radius of the electron relative to the $v = c$ frame, r_α^*, is relativistically corrected as follows. The wave equation relationship is

$$v = \lambda\frac{\omega}{2\pi} \tag{7.9}$$

It can be demonstrated that the velocity of the electron orbitsphere satisfies the relationship for the velocity of a wave by substitution of Eqs. (1.43) and (1.55) into Eq. (7.9), which gives Eq. (1.47). The result of the substitution into Eq. (7.9) of c for v_n, of λ_n given by Eq. (2.2)

$$2\pi(kr_1) = 2\pi r_n = n\lambda_1 = \lambda_n \tag{7.10}$$

with r_1 given by Eq. (1.169)

$$r_1 = \frac{a_o}{Z_2} \tag{7.11}$$

for λ, and of ω_n given by Eq. (1.55)

$$\omega_n = \frac{\hbar}{m_e r_n^2} \tag{7.12}$$

for ω is

$$c = 2\pi \frac{na_o}{Z_2} \frac{\hbar}{m_e \left[\frac{na_o}{Z_2}\right]^2 2\pi} \tag{7.13}$$

$$n = \frac{Z_2 m_e c a_o}{\hbar} = \frac{Z_2 m_e}{\hbar\sqrt{\varepsilon_o \mu_o}} \frac{4\pi\varepsilon_0 \hbar^2}{e^2 m_e} = 4\pi Z_2 \sqrt{\frac{\varepsilon_o}{\mu_o}} \frac{\hbar}{e^2} = Z_2 \alpha \tag{7.14}$$

It follows from Eq. (7.14) that the radius, r_n, of Eq. (7.6) must be corrected by the factor αZ_2. By correcting the radius and the mass, the relativistic correction is $\frac{1}{2\pi\alpha Z_2 \frac{v}{c}}$. In this case, $Z_1 = 1$ and Z_2 is the nuclear charge, Z; thus, $\frac{1}{Z}$ is substituted for the term in brackets in Eq. (7.6).

The force must be corrected for the vector projection of the velocity onto the z-axis. As given in the Spin Angular Momentum of the Orbitsphere with $\ell = 0$ Section, the application of a z directed magnetic field of electron two given by Eq. (1.120) to the inner orbitsphere gives rise to a projection of the angular momentum of electron one onto an axis which precesses about the z-axis of $\sqrt{\frac{3}{4}}\hbar$. The projection of the force between electron two and electron one is equivalent to that of the angular momentum onto the axis which precesses about the z-axis, and is $\sqrt{s(s+1)} = \sqrt{\frac{3}{4}}$ times that of a point mass. Thus, Eq. (7.6) becomes

$$\mathbf{F}_{mag} = \frac{1}{4\pi r_1^2} \frac{1}{Z} \frac{\hbar^2}{m_e r^3} \sqrt{s(s+1)} \tag{7.15}$$

The outward centrifugal force on electron 2 is balanced by the electric force and the magnetic force (on electron 2),

$$\frac{m_e}{4\pi r_2^2} \frac{v_2^2}{r_2} = \frac{e}{4\pi r_2^2} \frac{(Z-1)e}{4\pi\varepsilon_o r_2^2} + \frac{1}{4\pi r_2^2} \frac{\hbar^2}{Z m_e r_2^3} \sqrt{s(s+1)} \tag{7.16}$$

From Eq. (1.47)

$$v_2^2 = \frac{\hbar^2}{m_e^2 r_2^2} \tag{7.17}$$

Then,

$$\frac{m_e v_2^2}{r_2} = \frac{\hbar^2}{m_e r_2^3} = \frac{(Z-1)e^2}{4\pi\varepsilon_o r_2^2} + \frac{1}{Z} \frac{\hbar^2}{m_e r_2^3} \sqrt{s(s+1)} \tag{7.18}$$

Solving for r_2,

$$r_2 = r_1 = a_0 \left[\frac{1}{Z-1} - \frac{\sqrt{s(s+1)}}{Z(Z-1)}\right]; \; s = \frac{1}{2} \tag{7.19}$$

That is, the final radius of electron 2, r_2, is given by Eq. (7.19); this is

also the final radius of electron 1. The energies and radii of several two-electron atoms are given in Table 7.1.

ENERGY CALCULATIONS

The electric work to bring electron 2 to $r_2 = r_1$ is given by the integral of the electric force from infinity to r_1,

$$work(electric, electron 2) = \frac{(Z-1)e^2}{8\pi\varepsilon_o r_1} \tag{7.20}$$

And the electric energy is the negative of the electric work,

$$E(electric) = \frac{-(Z-1)e^2}{8\pi\varepsilon_o r_1} \tag{7.21}$$

The potential energy of each electron at $r = r_1$, is given as

$$V = \frac{-(Z-1)^2 e^2}{4\pi\varepsilon_o r_1} \tag{7.22}$$

The kinetic energy is $\frac{1}{2} m_e v^2$, where v is given by Eq. (1.47).

$$T = \frac{1}{2}\frac{\hbar^2}{m_e r_1^2} \tag{7.23}$$

The magnetic work is the integral of the magnetic force from infinity to r_1,

$$work(magnetic, electron 2) = -\frac{1}{2}\frac{1}{Z}\frac{\hbar^2}{m_e r_1^2}\sqrt{s(s+1)} \tag{7.24}$$

Conservation of Energy

Energy is conserved. Thus, the potential energy (electron 2 at r_1) with the nucleus plus the magnetic work (electron 2 going from infinity to r_1) must equal the sum of the negative of the electric work (electron 2 going from infinity to r_1) and the kinetic energy (electron 2 at r_1). This is shown below with Eq. (7.25) and Eq. (7.26).

$$-V(electron\ 2\ at\ r_1) = \frac{(Z-1)e^2}{8\pi\varepsilon_o r_1} + \frac{1}{2}\frac{1}{Z}\frac{\hbar^2}{m_e r_1^2}\sqrt{s(s+1)} - \frac{1}{2}\frac{\hbar^2}{m_e r_1^2} \tag{7.25}$$

and using r_1 for Eq. (7.19),

$$V(electron\ 2\ at\ r_1) = -\frac{(Z-1)e^2}{4\pi\varepsilon_o r_1} \tag{7.26}$$

This is also the potential energy of electron 1 where their potential energies are indistinguishable when $r_1 = r_2$.

Ionization Energies

During ionization, power must be conserved. Power flow is governed by the Poynting power theorem,

$$\cdot(\mathbf{E}\times\mathbf{H}) = -\frac{\delta}{\delta t}\left(\frac{1}{2}\right)\mu_o\mathbf{H}\cdot\mathbf{H} - \frac{\delta}{\delta t}\left(\frac{1}{2}\right)\varepsilon_o\mathbf{E}\cdot\mathbf{E} - \mathbf{J}\cdot\mathbf{E} \tag{7.27}$$

Energy is superposable; thus, the calculation of the ionization energy is determined as a sum of contributions. Energy must be supplied to overcome the electric force of the nucleus, and this energy contribution is the negative of the electric work given by Eq. (7.21). By the selection rules for absorption of electromagnetic radiation dictated by conservation of angular momentum, absorption of a photon causes the spin axes of the antiparallel spin-paired electrons to become parallel. Thus, a repulsive magnetic force exists on the electron to be ionized due to the parallel alignment of the spin axes; consequently, no magnetic work is necessary for ionization. However, initially the electrons were paired producing no magnetic fields; whereas, following ionization, the electrons possess magnetic fields. For helium, the contribution to the ionization energy is given as the energy stored in the magnetic fields of the two electrons. For helium, which has no electric field beyond r_1 the ionization energy is given by the general formula:

$$Ionization\ Energy(He) = -E(electric) + E(magnetic) \tag{7.28}$$

where,

$$E(electric) = -\frac{(Z-1)e^2}{8\pi\varepsilon_o r_1} \tag{7.29}$$

$$E(magnetic) = \frac{2\pi\mu_0 e^2\hbar^2}{m_e^2 r_1^3} \tag{7.30}$$

Eq. (7.30) is derived for each of the two electrons as Eq. (1.129) of the Magnetic Parameters of the Electron (Bohr Magneton) Section,

$$m_e = \gamma m_0 \ with\ \gamma = \frac{1}{\sqrt{1-\left(\frac{v}{c}\right)^2}} \tag{7.31}$$

and v is given by Eq. (1.47) with the mass of the electron given by Eq. (7.31) and the radius given by Eq. (7.19)[1].

---

[1]Relativistic Corrections:

$$r_1 = a_o\left(\frac{1}{Z-1} - \frac{\sqrt{\frac{3}{4}}}{Z(Z-1)}\right) \tag{1}$$

$$v = \frac{\hbar c}{\sqrt{\left(\frac{4\pi\varepsilon_0\hbar^2}{e^2}c\left(\frac{1}{Z-1} - \frac{\sqrt{\frac{3}{4}}}{Z(Z-1)}\right)\right)^2 + \hbar^2}} \tag{2}$$

For a nuclear charge Z greater than two, an electric field exists outside of the orbitsphere of the unionized atom. During ionization, the energy contribution of the expansion of the orbitsphere of the ionized electron (electron two) from r_1 to infinity in the presence of the electric fields present inside and outside of the orbitsphere is calculated as the $\mathbf{J} \cdot \mathbf{E}$ term of the Poynting theorem. This energy contribution can be determined by designing an energy cycle and considering the individual contributions of each electron (electron one and electron two) in going from the initial unionized to the final ionized state. Consider two paired orbitspheres. Expansion of an orbitsphere in the presence of an electric field which is positive in the outward radial direction requires energy, and contraction of an orbitsphere in this field releases energy. Thus, the contribution of the $\mathbf{J} \cdot \mathbf{E}$ term to ionization is the difference in the energy required to expand one orbitsphere (electron two) from r_1 to infinity and to contract one orbitsphere (electron one) from infinity to r_1. The energy contribution is calculated for the expanding orbitsphere by considering the reverse of the process used to derive Eq. (7.15) of the Determination of Orbitsphere Radii, r_n Section as follows:

The magnetic force on electron two due to electron one is

$$\mathbf{F}_{mag} = -\frac{1}{Z}\frac{\hbar^2}{m_e r_2^3}\sqrt{s(s+1)} \tag{7.32}$$

The expansion of the orbitsphere of electron two produces a current. The current over time $\Delta t\mathbf{J}$ is

---

$$m_e = \gamma m_0 \; with \; \gamma = \frac{1}{\sqrt{1 - \left(\frac{v}{c}\right)^2}} \tag{3}$$

where v is given by Eq. (2) and Eq. (3) is transformed into spherical coordinates. For helium, which has no electric field beyond r_1 the ionization energy is given by the general formula:

$$Ionization\,Energy(He) = -E(electric) + E(magnetic) \tag{4}$$

where,

$$E(electric) = -\frac{(Z-1)e^2}{8\pi\varepsilon_o r_1} \tag{5}$$

and

$$E(magnetic) = \frac{2\pi\mu_0 e^2\hbar^2}{m_e^2 r_1^3} \tag{6}$$

The ionization energies of positively charged two electron atoms are given by

$$Ionization\,Energy = -Electric\;\;Energy - \frac{1}{Z}\,Magnetic\;\;Energy \tag{7}$$

$$\Delta t\mathbf{J} = \Delta t\sigma \mathbf{E}_f \tag{7.33}$$

where $\mathbf{J}$ is the current-density, Δt is the time interval, σ is the conductivity, and $\mathbf{E}_f$ is the effective electric field defined as follows:

$$\mathbf{F} = q\mathbf{E}_f \tag{7.34}$$

where $\mathbf{F}$ is the magnetic force given by Eq. (7.32), and q is the charge-density given as follows:

$$q = \frac{e}{4\pi} \tag{7.35}$$

The orbit expands in free space; thus, the relation for the conductivity is

$$\Delta t\sigma = \varepsilon_o \tag{7.36}$$

The electric field provided by the nucleus for the expanding orbitsphere is

$$\mathbf{E} = \frac{(Z-2)e}{4\pi\varepsilon_o r_2^2} \tag{7.37}$$

where ε_o is the permittivity of free space ($8.854\ X\ 10^{-12}\ C^2\ /\ N\ m^2$). Using Eqs. (7.6), (7.7) and (7.15) and Eqs. (7.32-7.37), the $\mathbf{J}\cdot\mathbf{E}$ energy density over time for the expansion of electron two with the contraction of electron one is

$$\Delta t(\mathbf{J}\cdot\mathbf{E}) = \frac{(Z-2)e}{4\pi\varepsilon_o r_2^2}\frac{\hbar^2}{Zm_e r_2^3}2\sqrt{s(s+1)}\frac{4\pi\varepsilon_o}{e} \tag{7.38}$$

$$\Delta t(\mathbf{J}\cdot\mathbf{E}) = \frac{(Z-2)e}{4\pi\varepsilon_o r_2^2}\frac{\hbar^2}{Zm_e r_2^3}\frac{\mu_0 e^2}{m_e r_2}\frac{4\pi\varepsilon_o}{e} \tag{7.39}$$

$$\Delta t(\mathbf{J}\cdot\mathbf{E}) = \frac{(Z-2)}{Z}\frac{\mu_0 e^2\hbar^2}{m_e^2 r_2^6} \tag{7.40}$$

The $\mathbf{J}\cdot\mathbf{E}$ energy over time is the volume integral of the energy density over time

$$[\Delta t(\mathbf{J}\cdot\mathbf{E})]_{energy\ \text{external}} = \int_0^{2\pi}\int_0^{\pi}\int_{\infty}^{r_1}\frac{(Z-2)}{Z}\frac{\mu_0 e^2\hbar^2}{m_e^2 r_2^6} r^2\sin\theta\, dr d\theta d\Phi \tag{7.41}$$

$$[\Delta t(\mathbf{J}\cdot\mathbf{E})]_{energy\ \text{external}} = \frac{(Z-2)}{Z}\frac{2\pi\mu_0 e^2\hbar^2}{3m_e^2 r_1^3} \tag{7.42}$$

The $\mathbf{J}\cdot\mathbf{E}$ energy over time involving the electric field external to the orbitsphere of electron two is $\frac{(Z-2)}{Z}$ times the magnetic energy stored in the space external to the orbitsphere as given by Eq. (1.127). The left and right sides of the Poynting theorem must balance. Given the form of the $\mathbf{J}\cdot\mathbf{E}$ energy over time involving the electric field external to the orbitsphere of electron two and given that the electric field inside of the orbitsphere is $Z-1$ times the electric field of a point charge, the $\mathbf{J}\cdot\mathbf{E}$ energy over time involving the electric field internal to the orbitsphere

of electron two is $\frac{(Z-1)}{Z}$ times the magnetic energy stored inside of the orbitsphere as given by Eq. (1.125). This energy is

$$[\Delta t(\mathbf{J}\cdot\mathbf{E})]_{energy\ \text{internal}} = \frac{(Z-1)}{Z}\frac{4\pi\mu_0 e^2\hbar^2}{3m_e^2 r_1^3} \tag{7.43}$$

Thus, the total $\mathbf{J}\cdot\mathbf{E}$ energy over time of electron two is the sum of Eqs. (7.42) and (7.43). The $\mathbf{J}\cdot\mathbf{E}$ energy over time of electron one during contraction from infinity to r_1 is negative, and the equations for the external and internal contributions are of the same form as Eqs. (7.42) and (7.43) where the appropriate effective charge is substituted. The $\mathbf{J}\cdot\mathbf{E}$ energy over time involving the electric field external to the orbitsphere of electron one is

$$[\Delta t(\mathbf{J}\cdot\mathbf{E})]_{energy\ \text{external}} = \frac{(Z-1)}{Z}\frac{2\pi\mu_0 e^2\hbar^2}{3m_e^2 r_1^3} \tag{7.44}$$

And, the $\mathbf{J}\cdot\mathbf{E}$ energy over time involving the electric field internal to the orbitsphere of electron one is

$$[\Delta t(\mathbf{J}\cdot\mathbf{E})]_{\text{energy internal}} = \frac{Z}{Z}\frac{4\pi\mu_0 e^2\hbar^2}{3m_e^3 r_1^3} \tag{7.45}$$

The difference, Δ, between the $\mathbf{J}\cdot\mathbf{E}$ energy over time for expanding electron two from r_1 to infinity and contracting electron one from infinity to r_1 is $-\frac{1}{Z}$ times the stored magnetic energy given by Eq. (7.30).

$$\Delta = -\frac{1}{Z}\frac{2\pi\mu_0 e^2\hbar^2}{m_e^2 r_1^3} \tag{7.46}$$

Thus, the ionization energies are given by

$$Ionization\ Energy = -Electric\ \ Energy - \frac{1}{Z}\,Magnetic\ \ Energy \tag{7.47}$$

The energies of several two-electron atoms are given in Table 7.1.

Table 7.1. The calculated electric (per electron), magnetic (per electron), and ionization energies for some two-electron atoms.

Atom	r_1 (a_o) [a]	Electric Energy [b] (eV)	Magnetic Energy [c] (eV)	Calculated Ionization Energy [d] (eV)	Experimental [e] Ionization [4-5] Energy (eV)
He	0.567	-23.96	0.63	24.59	24.59
Li^+	0.356	-76.41	2.54	75.56	75.64
Be^{2+}	0.261	-156.08	6.42	154.48	153.89
B^{3+}	0.207	-262.94	12.96	260.35	259.37
C^{4+}	0.171	-396.98	22.83	393.18	392.08
N^{5+}	0.146	-558.20	36.74	552.95	552.06
O^{6+}	0.127	-746.59	55.35	739.67	739.32
F^{7+}	0.113	-962.17	79.37	953.35	953.89
Ne^{8+}	0.101	-1204.9	109.5	1194	1195.90
Na^{9+}	0.0921	-1474.8	146.4	1462	1465.14
Mg^{10+}	0.8043	-1771.9	190.7	1756	1761.86
Al^{11+}	0.0778	-2096.2	243.2	2077	2086.05
Si^{12+}	0.0722	-2447.6	304.5	2426	2437.76
P^{13+}	0.0673	-2826.3	375.3	2801	2817.04
S^{14+}	0.0631	-3232.1	456.4	3204	3223.95
Cl^{15+}	0.0593	-3665.0	548.3	3633	3658.55
Ar^{16+}	0.0560	-4125.2	651.9	4089	4120.92
K^{17+}	0.0530	-4612.5	767.7	4572	4611.11

[a] from Equation (7.19)
[b] from Equation (7.29)
[c] from Equation (7.30)
[d] from Equations (7.28) and (7.47)
[e] from theoretical calculations for ions Ne^{8+} to K^{17+}

HYDRIDE ION

The hydride ion comprises two indistinguishable electrons bound to a proton of $Z = +1$. Each electron experiences a centrifugal force, and the balancing centripetal force (on each electron) is produced by the electric force between the electron and the nucleus. In addition, a magnetic force exists between the two electrons causing the electrons to pair.

Determination of the Orbitsphere Radius, r_n

Consider the binding of a second electron to a hydrogen atom to form a hydride ion. The second electron experiences no central electric force because the electric field is zero outside of the radius of the first electron. However, the second electron experiences a magnetic force due to electron 1 causing it to pair with electron 1. Thus, electron 1 experiences the reaction force of electron 2 which acts as a centrifugal force. The force balance equation can be determined by equating the total forces acting on the two bound electrons taken together. The force balance equation for the paired electron orbitsphere is obtained by equating the forces on the mass and charge densities. The centrifugal force of both electrons is given by Eq. (7.1) and Eq. (7.2) where the mass is $2m_e$. Electric field lines end on charge. Since both electrons are paired at the same radius, the number of field lines ending on the charge density of electron 1 equals the number that end on the charge density of electron 2. The electric force is proportional to the number of field lines; thus, the centripetal electric force, $\mathbf{F}_{ele}$, between the electrons and the nucleus is

$$\mathbf{F}_{ele(electron1,2)} = \frac{\frac{1}{2}e^2}{4\pi\varepsilon_o r_n^2} \tag{7.48}$$

where ε_o is the permittivity of free-space. The outward magnetic force on the two paired electrons is given by the negative of Eq. (7.15) where the mass is $2m_e$. The outward centrifugal force and magnetic forces on electrons 1 and 2 are balanced by the electric force

$$\frac{\hbar^2}{2m_e r_2^3} = \frac{\frac{1}{2}e^2}{4\pi\varepsilon_o r_2^2} - \frac{1}{Z}\frac{\hbar^2}{2m_e r_2^3}\sqrt{s(s+1)} \tag{7.49}$$

where $Z = 1$. Solving for r_2,

$$r_2 = r_1 = a_0\left(1 + \sqrt{s(s+1)}\right);\ s = \frac{1}{2} \tag{7.50}$$

That is, the final radius of electron 2, r_2, is given by Eq. (7.50); this is also the final radius of electron 1.

Ionization Energy

During ionization, electron 2 is moved to infinity. By the selection rules for absorption of electromagnetic radiation dictated by conservation of angular momentum, absorption of a photon causes the spin axes of the antiparallel spin-paired electrons to become parallel. The unpairing energy, $E_{unpairing}(magnetic)$, is given by Eq. (7.30) and Eq. (7.50) multiplied by two because the magnetic energy is proportional to the square of the magnetic field as derived in Eqs. (1.122-1.129). A repulsive magnetic force exists on the electron to be ionized due to the parallel alignment of the spin axes. The energy to move electron 2 to a radius which is infinitesimally greater than that of electron 1 is zero. In this case, the only force acting on electron 2 is the magnetic force. Due to conservation of energy, the potential energy change to move electron 2 to infinity to ionize the hydride ion can be calculated from the magnetic force of Eq. (7.49). The magnetic work, $E_{magwork}$, is the negative integral of the magnetic force (the second term on the right side of Eq. (7.49)) from r_2 to infinity,

$$E_{magwork} = \int_{r_2}^{\infty} \frac{\hbar^2}{2m_e r^3}\sqrt{s(s+1)}dr \tag{7.51}$$

where r_2 is given by Eq. (7.50). The result of the integration is

$$E_{magwork} = -\frac{\hbar^2\sqrt{s(s+1)}}{4m_e a_0^2\left[1+\sqrt{s(s+1)}\right]^2} \tag{7.52}$$

where $s = \frac{1}{2}$. By moving electron 2 to infinity, electron 1 moves to the radius $r_1 = a_H$, and the corresponding magnetic energy, $E_{electron\,1\,final}(magnetic)$, is given by Eq. (7.30). In the present case of an inverse squared central field, the binding energy is one half the negative of the potential energy [5]. Thus, the ionization energy is given by subtracting the two magnetic energy terms from one half the negative of the magnetic work wherein m_e is the electron reduced mass μ_e given by Eq. (1.167) due to the electrodynamic magnetic force between electron 2 and the nucleus given by one half that of Eq. (1.164). The factor of one half follows from Eq. (7.49).

$$\begin{aligned} Ionization\,Energy &= -\frac{1}{2}E_{magwork} - E_{electron1\ final}(magnetic) - E_{unpairing}(magnetic) \\ &= \frac{\hbar^2\sqrt{s(s+1)}}{8\mu_e a_0^2\left[1+\sqrt{s(s+1)}\right]^2} - \frac{\pi\mu_0 e^2\hbar^2}{m_e^2 a_0^3}\left(1+\frac{2^2}{\left[1+\sqrt{s(s+1)}\right]^3}\right) \end{aligned} \tag{7.53}$$

From Eq. (7.53), the calculated ionization energy of the hydride ion is $0.75402\,eV$. The experimental value given by Dean [6] is $0.754209\,eV$ which

corresponds to a wavelength of $\lambda = 1644\ nm$.

HYDRINO HYDRIDE ION

The hydrino atom $H(1/2)$ can form a stable hydride ion. The central field is twice that of the hydrogen atom, and it follows from Eq. (7.49) that the radius of the hydrino hydride ion $H^-(n=1/2)$ is one half that of atomic hydrogen hydride, $H^-(n=1)$, given by Eq. (7.50).

$$r_2 = r_1 = \frac{a_0}{2}\left(1+\sqrt{s(s+1)}\right);\ s=\frac{1}{2} \tag{7.54}$$

The energy follows from Eq. (7.53) and Eq. (7.54).

$$Ionization\ Energy = -\frac{1}{2}E_{magwork} - E_{electron1\ final}(magnetic) - E_{unpairing}(magnetic)$$

$$= \frac{\hbar^2\sqrt{s(s+1)}}{8\mu_e a_0^2\left[\frac{1+\sqrt{s(s+1)}}{2}\right]^2} - \frac{\pi\mu_0 e^2\hbar^2}{m_e^2 a_0^3}\left(1+\frac{2^2}{\left[\frac{1+\sqrt{s(s+1)}}{2}\right]^3}\right) \tag{7.55}$$

From Eq. (7.55), the calculated ionization energy of the hydrino hydride ion $H^-(n=1/2)$ is $3.047\ eV$ which corresponds to a wavelength of $\lambda = 407\ nm$. In general, the central field of hydrino atom $H(n=1/p);\ p=\text{integer}$ is p times that of the hydrogen atom. Thus, the force balance equation is

$$\frac{\hbar^2}{2m_e r_2^3} = \frac{\frac{p}{2}e^2}{4\pi\varepsilon_o r_2^2} - \frac{1}{Z}\frac{\hbar^2}{2m_e r_2^3}\sqrt{s(s+1)} \tag{7.56}$$

where $Z=1$ because the field is zero for $r > r_1$. Solving for r_2,

$$r_2 = r_1 = \frac{a_0}{p}\left(1+\sqrt{s(s+1)}\right);\ s=\frac{1}{2} \tag{7.57}$$

From Eq. (7.57), the radius of the hydrino hydride ion $H^-(n=1/p);\ p=\text{integer}$ is $\frac{1}{p}$ that of atomic hydrogen hydride, $H^-(n=1)$, given by Eq. (7.50). The energy follows from Eq. (7.53) and Eq. (7.57).

$$Ionization\ Energy = -\frac{1}{2}E_{magwork} - E_{electron1\ final}(magnetic) - E_{unpairing}(magnetic)$$

$$= \frac{\hbar^2\sqrt{s(s+1)}}{8\mu_e a_0^2\left[\frac{1+\sqrt{s(s+1)}}{p}\right]^2} - \frac{\pi\mu_0 e^2\hbar^2}{m_e^2 a_0^3}\left(1+\frac{2^2}{\left[\frac{1+\sqrt{s(s+1)}}{p}\right]^3}\right) \tag{7.58}$$

From Eq. (7.58), the calculated ionization energy of the hydrino hydride ion $H^-(n=1/p)$ as a function of p is given in Table 7.2.

Table 7.2. The ionization energy of the hydrino hydride ion $H^-(n=1/p)$ as a function of p.

Hydride Ion	r_1 (a_o) [a]	Calculated Ionization Energy [b] (eV)	Calculated Wavelength (nm)
$H^-(n=1)$	1.8660	0.754	1645
$H^-(n=1/2)$	0.9330	3.047	407
$H^-(n=1/3)$	0.6220	6.610	188
$H^-(n=1/4)$	0.4665	11.23	110
$H^-(n=1/5)$	0.3732	16.70	74.2
$H^-(n=1/6)$	0.3110	22.81	54.4
$H^-(n=1/7)$	0.2666	29.34	42.3
$H^-(n=1/8)$	0.2333	36.08	34.4
$H^-(n=1/9)$	0.2073	42.83	28.9
$H^-(n=1/10)$	0.1866	49.37	25.1
$H^-(n=1/11)$	0.1696	55.49	22.34
$H^-(n=1/12)$	0.1555	60.98	20.33
$H^-(n=1/13)$	0.1435	65.62	18.89
$H^-(n=1/14)$	0.1333	69.21	17.91
$H^-(n=1/15)$	0.1244	71.53	17.33
$H^-(n=1/16)$	0.1166	72.38	17.13
$H^-(n=1/17)$	0.1098	71.54	17.33
$H^-(n=1/18)$	0.1037	68.80	18.02
$H^-(n=1/19)$	0.0982	63.95	19.39
$H^-(n=1/20)$	0.0933	56.78	21.83
$H^-(n=1/21)$	0.0889	47.08	26.33
$H^-(n=1/22)$	0.0848	34.63	35.80
$H^-(n=1/23)$	0.0811	19.22	64.49
$H^-(n=1/24)$	0.0778	0.6535	1897
$H^-(n=1/25)$		not stable	

[a] from Equation (7.57)
[b] from Equation (7.58)

HYDRINO HYDRIDE ION NUCLEAR MAGNETIC RESONANCE SHIFT

The proton gyromagnetic ratio $\gamma_p / 2\pi$ is

$$\gamma_p / 2\pi = 42.57602\ MHz\ T^{-1} \tag{7.59}$$

The NMR frequency f is the product of the proton gyromagnetic ratio given by Eq. (7.59) and the magnetic flux **B**.

$$f = \gamma_p / 2\pi \mathbf{B} = 42.57602\ MHz\ T^{-1}\mathbf{B} \tag{7.60}$$

A typical flux for a superconducting NMR magnet is $1.5\ T$. According to Eq. (7.60) this corresponds to a radio frequency (RF) of $63.86403\ MHz$. With a constant magnetic field, the frequency is scanned to yield the spectrum. Or, in a common type of NMR spectrometer, the radiofrequency is held constant at $60\ MHz$, the applied magnetic field H_0 ($H_0 = \frac{B}{\mu_0}$) is varied over a small range, and the frequency of energy absorption is recorded at the various valves for H_0. The spectrum is typically scanned and displayed as a function of increasing H_0. The protons that absorb energy at a lower H_0 give rise to a downfield absorption peak; whereas, the protons that absorb energy at a higher H_0 give rise to an upfield absorption peak. The electrons of the compound of a sample influence the field at the nucleus such that it deviates slightly from the applied value. For the case that the chemical environment has no NMR effect, the value of H_0 at resonance with the radiofrequency held constant at $60\ MHz$ is

$$\frac{2\pi f}{\mu_0 \gamma_p} = \frac{(2\pi)(60\ MHz)}{\mu_0 42.57602\ MHz\ T^{-1}} = H_0 \tag{7.61}$$

In the case that the chemical environment has a NMR effect, a different value of H_0 is required for resonance. This chemical shift is proportional to the electronic magnetic flux change at the nucleus due to the applied field which in the case of each hydrino hydride ion is a function of its radius. The change in the magnetic moment, $\Delta\mathbf{m}$, of each electron of the hydride ion due to an applied magnetic flux **B** is [8]

$$\Delta\mathbf{m} = -\frac{e^2 r_1^2 \mathbf{B}}{4m_e} \tag{7.62}$$

The change in magnetic flux $\Delta\mathbf{B}$ at the nucleus due to the change in magnetic moment, $\Delta\mathbf{m}$, of each electron follows from Eq. (1.100).

$$\Delta\mathbf{B} = \mu_0 \frac{\Delta m}{r_n^3}(\mathbf{i}_r \cos\theta - \mathbf{i}_\theta \sin\theta) \qquad \text{for } r < r_n \tag{7.63}$$

where μ_0 is the permeability of vacuum. It follows from Eqs. (7.62-7.63) that the diamagnetic flux (flux opposite to the applied field) at the nucleus is inversely proportional to the radius. For resonance to occur, ΔH_0, the change in applied field from that given by Eq. (7.61), must

compensate by an equal and opposite amount as the field due to the electrons of the hydrino hydride ion. According to Eq. (7.57), the ratio of the radius of the hydrino hydride ion $H^-(1/p)$ to that of the hydride ion $H^-(1/1)$ is the reciprocal of an integer. It follows from Eqs. (7.59-7.63) that compared to a proton with a no chemical shift, the ratio of ΔH_0 for resonance of the proton of the hydrino hydride ion $H^-(1/p)$ to that of the hydride ion $H^-(1/1)$ is a positive integer (i.e. the absorption peak of the hydrino hydride ion occurs at a valve of ΔH_0 that is a multiple of p times the value of ΔH_0 that is resonant for the hydride ion compared to that of a proton with no shift where p is an integer).

References

1. Bueche, F., Introduction to Physics for Scientists and Engineers, McGraw-Hill, (1975), pp. 352-353.
2. McQuarrie,D. A., Quantum Chemistry, University Science Books, Mill Valley, CA, (1983), pp. 238-241.
3. Purcell, E. M., Electricity and Magnetism, McGraw-Hill, New York, (1965), pp. 170-199.
4. C. E. Moore, "Ionization Potentials and Ionization Limits Derived from the Analyses of Optical Spectra, Nat. Stand. Ref. Data Ser.-Nat. Bur. Stand. (U.S.), No. 34, 1970.
5. Robert C. Weast, CRC Handbook of Chemistry and Physics, 58 Edition, CRC Press, West Palm Beach, Florida, (1977), p. E-68.
6. Fowles, G. R., Analytical Mechanics, Third Edition, Holt, Rinehart, and Winston, New York, (1977), pp. 154-156.
7. John A. Dean, Editor, Lange's Handbook of Chemistry, Thirteenth Edition, McGraw-Hill Book Company, New York, (1985), p. 3-10.
8. Purcell, E., Electricity and Magnetism, McGraw-Hill, New York, (1965), pp. 370-389.

DERIVATION OF ELECTRON SCATTERING BY HELIUM

CLASSICAL SCATTERING OF ELECTROMAGNETIC RADIATION

Light is an electromagnetic disturbance which is propagated by vector wave equations which are readily derived from Maxwell's equations. The Helmholtz wave equation results from Maxwell's equations. The Helmholtz equation is linear; thus, superposition of solutions is allowed. Huygens' principle is that a point source of light will give rise to a spherical wave emanating equally in all directions. Superposition of this particular solution of the Helmholtz equation permits the construction of a general solution. An arbitrary wave shape may be considered as a collection of point sources whose strength is given by the amplitude of the wave at that point. The field, at any point in space, is simply a sum of spherical waves. Applying Huygens' principle to a disturbance across a plane aperture gives the amplitude of the far field as the Fourier Transform of the aperture distribution, i.e., apart from constant factors,

$$\psi(x,y) = \iint A(\xi,\eta)\exp\left[\frac{-ik}{f}(\xi x + \eta y)\right]d\xi\, d\eta \tag{8.1}$$

Here $A(\xi,\eta)$ describes the amplitude and phase distribution across the aperture and $\psi(x,y)$ describes the far field [1] where f is the focal length.

Delta Function

In many diffraction and interference problems, it proves convenient to make use of the Dirac delta function. This function is defined by the following property: let $f(\xi)$ be any function (satisfying some very weak convergence conditions which need not concern us here) and let $\delta(\xi - \xi')$ be a delta function centered at the point ξ'; then

$$\int_a^b f(\xi)\delta(\xi - \xi')d\xi = f(\xi') \qquad (a < \xi' < b);\ 0\ \textit{otherwise} \tag{8.2}$$

We note, therefore, that

$$\int_{-\infty}^{\infty}\delta(\xi - \xi')d\xi = 1 \tag{8.3}$$

the Fourier transform of the delta function is given by

$$\psi(x) = \int\delta(\xi - \xi')\exp\left[\frac{-ikx\xi}{f}\right]d\xi \tag{8.4}$$

which by definition of the delta function becomes

$$\psi(x) = \exp\left[\frac{-ikx\xi'}{f}\right] \tag{8.5}$$

The amplitude is constant and the phase function $\exp\left(\frac{-ikx\xi'}{f}\right)$ depends on the origin.

The Array Theorem

A large number of interference problems involve the mixing of similar diffraction patterns. That is, they arise in the study of the combined diffraction patterns of an array of similar diffracting apertures. This entire class of interference effects can be described by a single equation, the array theorem. This unifying theorem is easily developed as follows: Let $\psi(\xi)$ represent the amplitude and phase distribution across one aperture centered in the diffraction plane, and let the total diffracting aperture consist of a collection of these elemental apertures at different locations ξ_n. We require first a method of representing such an array. The appropriate representation is obtained readily by means of the delta function. Thus, if an elemental aperture is positioned such that its center is at the point ξ_n, the appropriate distribution function is $\psi(\xi - \xi_n)$. The combining property of the delta function allows us to represent this distribution as follows:

$$\psi(\xi - \xi_n) = \int \psi(\xi - \alpha)\delta(\alpha - \xi_n)d\alpha \tag{8.6}$$

The integral in Eq. (8.6) is termed a "convolution" integral and plays an important role in Fourier analysis. Thus, if we wish to represent a large number N of such apertures with different locations, we could write the total aperture distribution $\Psi(\xi)$ as a sum, i.e.,

$$\Psi(\xi) = \sum_{n=1}^{N} \psi(\xi - \xi_n) \tag{8.7}$$

Or in terms of the delta function we could write, combining the features of Eqs. (8.6) and (8.7),

$$\Psi(\xi) = \sum_{n=1}^{N} \int \psi(\xi - \alpha)\delta(\alpha - \xi_n)d\alpha \tag{8.8}$$

Eq. (8.8) may be put in a more compact form by introducing the notation

$$A(\alpha) = \sum_{n=1}^{N} \delta(\alpha - \xi_n) \tag{8.9}$$

thus, Eq. (8.8) becomes

$$\Psi(\xi) = \int \psi(\xi - \alpha)A(\alpha)d\alpha \tag{8.10}$$

which is physically pleasing in the sense that $A(\alpha)$ characterizes the array itself. That is, $A(\alpha)$ describes the location of the apertures and $\psi(\xi)$ describes the distribution across a single aperture. We are in a position to calculate the far field or Fraunhofer diffraction pattern associated with the array. We have the theorem that the Fraunhofer

pattern is the Fourier transform of the aperture distribution. Thus, the Fraunhofer pattern $\tilde{\Psi}(x)$ of the distribution $\Psi(\xi)$ is given by

$$\tilde{\Psi}(x) = \int \psi(\xi) \exp\left(\frac{-2\pi i \xi \, x}{\lambda f}\right) d\xi \tag{8.11}$$

substituting from Eq. (8.10) gives

$$\tilde{\Psi}(x) = \left[\iint (\xi - \alpha) A(\alpha) d\alpha\right] \exp\left(\frac{-2\pi i \xi \, x}{\lambda f}\right) d\xi \tag{8.12}$$

A very important theorem of Fourier analysis states that the Fourier transform of a convolution is the product of the individual Fourier transforms [1]. Thus, Eq. (8.12) may be written as

$$\tilde{\Psi}(x) = \tilde{\psi}(x)\tilde{A}(x) \tag{8.13}$$

where $\tilde{\psi}(x)$ and $\tilde{A}(x)$ are the Fourier transforms of $\psi(\xi)$ and $A(\alpha)$. Eq. (8.13) is the array theorem and states that the diffraction pattern of an array of similar apertures is given by the product of the elemental pattern $\tilde{\psi}(x)$ and the pattern that would be obtained by a similar array of point sources, $\tilde{A}(x)$. Thus, the separation that first arose in Eq. (8.10) is retained. To analyze the complicated patterns that arise in interference problems of this sort, one may analyze separately the effects of the array and the effects of the individual apertures.

Applications of the Array Theorem

Two-Beam Interference

We use Eq. (8.13) to describe the simplest of interference experiments, Young's double-slit experiment in one dimension. The individual aperture will be described by

$$\Psi(\xi) = (C \quad |\xi| < a; \qquad 0 \quad |\xi| > a) = rec(\xi | a) \tag{8.14}$$

Here C is a constant representing the amplitude transmission of the apertures. This is essentially a one-dimensional problem and the diffraction integral may be written as

$$\tilde{\Psi}(x) = \int \psi(\xi) \exp\left(\frac{-ik\xi \, x}{f}\right) d\xi = C \int_{-a}^{a} \exp\left(\frac{-ik\xi \, x}{f}\right) d\xi \tag{8.15}$$

The integral in Eq. (8.15) is readily evaluated to give

$$\tilde{\Psi}(x) = \frac{-Cf}{ikx}\left[\exp\left(\frac{-ikax}{f}\right) - \exp\left(\frac{+ikax}{f}\right)\right] = 2aC \frac{\sin\left(\frac{kax}{f}\right)}{\left(\frac{kax}{f}\right)} \tag{8.16}$$

The notation $\mathrm{sinc}\theta = \dfrac{\sin\theta}{\theta}$ is frequently used and in terms of this function $\tilde{\Psi}(x)$ may be written as

$$\tilde{\Psi}(x) = 2aC\,\mathrm{sinc}\left(\frac{kax}{f}\right) \tag{8.17}$$

Thus the result that the elemental distribution in the Fraunhofer plane is Eq. (8.17). The array in this case is simply two delta functions; thus,

$$A(\xi) = \delta(\xi - b) + \delta(\xi + b) \tag{8.18}$$

The array pattern is, therefore,

$$\tilde{A}(x) = \int \left[\delta(\xi - b) + \delta(\xi + b)\right] \exp\left(\frac{-2\pi i \xi \mathbf{x}}{\lambda f}\right) d\xi \tag{8.19}$$

Eq. (8.19) is readily evaluated by using the combining property of the delta function, thus,

$$\tilde{A}(x) = \exp\left(\frac{2\pi i b x}{\lambda f}\right) + \exp\left(\frac{-2\pi i b x}{\lambda f}\right) = 2\cos\left(\frac{2\pi b x}{\lambda f}\right) \tag{8.20}$$

Finally, the diffraction pattern of the array of two slits is

$$\tilde{\Psi}(x) = 4aC\,\mathrm{sinc}\left(\frac{2\pi a x}{\lambda f}\right)\cos\left(\frac{2\pi b x}{\lambda f}\right) \tag{8.21}$$

The intensity is

$$I(x) = 16a^2C^2\,\mathrm{sinc}^2\left(\frac{2\pi a x}{\lambda f}\right)\cos^2\left(\frac{2\pi b x}{\lambda f}\right) \tag{8.22}$$

From Eq. (8.22), it is clear that the resulting pattern has the appearance of cosine^2 fringes of period $\lambda f / b$ with an envelope $\mathrm{sinc}^2(2\pi a x / \lambda f)$. The distribution pattern observed with diffracting electrons is equivalent to that for diffracting light. Note that Eq. (8.15) represents a plane wave. In the case of the Davison-Germer experiment, the intensity is given by Eq. (8.13) as the product of the elemental pattern corresponding to a plane wave of wavelength $\lambda = h / p$ and the array pattern of the nickel crystal.

CLASSICAL WAVE THEORY OF ELECTRON SCATTERING

The following mathematical development of scattering is adapted from Bonham [2] with the exception that the Mills model is a Fourier optics derivation for an exact elemental pattern, a plane wave, and an exact array pattern, an orbitsphere. In contrast, Bonham derives similar scattering equations for an incident plane wave via an averaged probability density function description of the electron, the Born model.

In scattering experiments in which Fraunhofer diffraction is the most important mode for scattering, measurements are made in momentum or reciprocal space. The data is then transformed in terms of real space, where the structure of the scatterer is expressed in terms of distances from its center of mass. There are, fortunately, well known mathematical techniques for making this transformation. If we are given a model of the scattering system, we can, in general, uniquely calculate the results to be expected in reciprocal space for scattering from the

model. Unfortunately, the converse--deducing the nature of the scatterer uniquely by transforming the experimental results obtained in reciprocal space--is not always possible. But, as we will see, certain possibilities can be eliminated because they violate fundamental physical laws such as Special Relativity.

In classical optics, a diffraction pattern results whenever light is scattered by a slit system whose dimensions are small compared to the wavelength of light. In order to develop a mathematical model for diffraction scattering, let us represent the amplitude of an incident plane wave traveling from left to right as $e^{i(\mathbf{k}\,\mathbf{r}-\omega t)}$, where the absolute magnitude of the wave vector $\mathbf{k}$ is $|\mathbf{k}| = \frac{2\pi}{\lambda}$. The quantity λ is the wavelength of the incident radiation and $\hbar\mathbf{k}$ is the momentum $\mathbf{p}$. The vector $\mathbf{r}$ represents the position in real space at which the amplitude is evaluated, and ω and t are the frequency and time, respectively. A plane wave traveling in the opposite direction is $e^{-i(\mathbf{k}\,\mathbf{r}+\omega t)}$ where the sign of $\mathbf{k}\,\mathbf{r}$ changes, but not the sign of t. That is, we may reflect a wave from a mirror and reverse its direction, but we cannot change the sign of the time since that would indicate a return to the past. The intensity of a classical wave is the square magnitude of the amplitude, and thus the intensity of a plane wave is constant in space and time. If a plane wave is reflected back on itself by a perfectly reflecting mirror, then the resultant amplitude is $e^{i(\mathbf{k}\,\mathbf{r}-\omega t)} + e^{-i(\mathbf{k}\,\mathbf{r}+\omega t)} = e^{-i\omega t} 2\cos \mathbf{k}\,\mathbf{r}$, and the intensity is $I = 4\cos^2 \mathbf{k}\,\mathbf{r} e^{i\omega t} e^{-i\omega t}$ which is independent of time and given as $4\cos^2 \mathbf{k}\,\mathbf{r}$ which clearly exhibits maxima and minima dictated by the wavelength of the radiation and the position in space at which intensity is measured.

In an experiment, we measure the intensity of scattered particles, which is related to plane waves in a simple fashion. To see this, consider a collimated plane-wave source, whose width is small compared to the scattering angle region where the scattering is to be investigated, incident upon a diffraction grating. If we integrate the incident intensity over a time interval Δt, we obtain a number proportional to the energy content of the incident wave. We may safely assume in most cases that the scattering power of the diffraction image does not change with time, so that a constant fraction of the incident radiation and hence constant energy will be transferred into the scattered wave. We further assume that the effect of the diffraction grating on the incident radiation occurs only in a region very close to the grating in comparison to its distance from the detection point. For elastic scattering (no energy transfer to the grating), once the scattered portion of the wave has left the field of influence of the scatterer, all parts of the scattered amplitude at the same radial distance from the scatterer must travel at the velocity of the incident wave. For simplicity, we neglect resonance effects, which can

introduce significant time delays in the scattering process even if the waves are scattered elastically. The effects of resonance states on the scattering at high energies is usually negligible and hence will not be discussed here. In the case of inelastic scattering, in which waves are scattered with various velocities, we can focus our attention successively on parts of the outgoing scattered radiation which have velocities falling within a certain narrow band, and the following argument will hold for each such velocity segment. The result of the integration of a constant-velocity segment of the scattered intensity over the volume element,

$$\int_{R}^{R+\Delta R} r^2 dr \int_{0}^{\pi} \sin\theta d\theta \int_{0}^{2\pi} d\Phi, \tag{8.23}$$

is proportional to the energy content in that portion of the scattered wave, and the result must be independent of R. This restriction, which is a direct consequence of conservation of energy, then demands that the outgoing scattered waves have in polar coordinates the form

$$\Psi_{sc}(R,\theta,\phi) = \frac{e^{ikR}}{R} f(\theta,\phi) \tag{8.24}$$

where the term 1/R is a dilution effect to guarantee energy on an ever-spreading wave.

Ψ_{sc} only describes the scattered amplitude after the scattered wave has left the field of influence of the scatterer and is thus an asymptotic form. The function $f(\theta,\varphi)$ is called the scattered amplitude and depends on the nature of the scatterer. The classical theory tells us that the scattered intensity is proportional to the square magnitude of the scattered amplitude; so, the intensity will be directly proportional to $\frac{|f(\theta,\varphi)|^2}{R^2}$.

Let us next consider the expression for the scattering of a plane wave by a number of disturbances in some fixed arrangement in space. Consider the scatterers comprising a nucleus and electrons; this would correspond to a plane wave scattered by an atom.

We shall choose the center of mass of the scatterer as our origin and shall for the most part consider dilute-gas electron scattering in the keV energy range, where the electron wavelength λ lies in the range $0.03\,\text{Å} < \lambda < 0.1\,\text{Å}$. The scattering experimental conditions are such that to a high degree of approximation, at least 0.1% or better, we can consider the scattering as a single electron scattered by a single atom. Note also that no laboratory to center-of-mass coordinate system transformation is required because the ratio of the electron mass to the mass of the target will be on the order of 10^{-3} or smaller.

Let us consider an ensemble of scattering centers as shown in

Figure 8.1.

Figure 8.1. An ensemble of scattering centers.

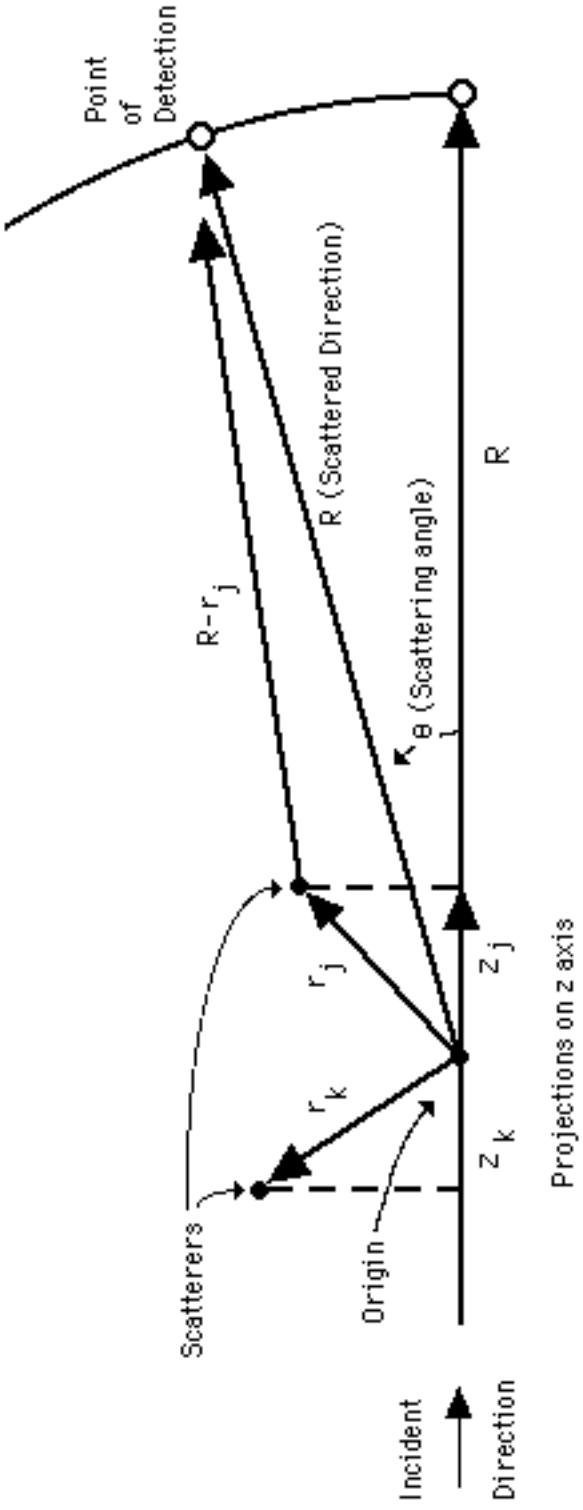

We may write the total scattered amplitude in the first approximation as

a sum of amplitudes, each of which is produced by scattering from one of the single scattering centers. In this view, we generally neglect multiple scattering, the rescattering of portions of the primary scattered amplitudes whenever they come in contact with other centers, except in the case of elastic scattering in the heavier atoms. Clearly a whole hierarchy of multiple-scattering processes may result. The incident wave may experience a primary scattering from one center, a portion of the scattered amplitude may rescatter from a second center, and part of this amplitude may in turn be scattered by a third center (which can even be the first center), and so on.

An incident plane wave will obviously travel a distance along the incident direction before scattering from a particular center, depending on the instantaneous location of that center. To keep proper account of the exact amplitude or phase of the incident wave at the instant it scatters from a particular center, we select our origin, as mentioned previously, to lie at the center of mass. The phase of the scattered wave depends on the total distance traveled from the center of mass to the detector. We can now write the scattered amplitude as

$$\Psi_{total} = \sum_{l=1}^{N} \left(\frac{\exp\left[ik\left(z_l + |\mathbf{R} - \mathbf{r}_l| \right) \right]}{|\mathbf{R} - \mathbf{r}_l|} \right) f_l(\theta,\phi) \tag{8.25}$$

where $z_l + |\mathbf{R} - \mathbf{r}_l|$ is the distance traveled from a plane perpendicular to the incident direction and passing through the center of mass and $f_l(\theta,\phi)$ is the scattered amplitude characteristic of the $l-th$ scattering center. It should be clear at this point that the term $\left(\frac{\exp\left[ik|\mathbf{R} - \mathbf{r}_l| \right]}{|\mathbf{R} - \mathbf{r}_l|} \right) f_l(\theta,\phi)$ is made up of a plane wave in the scattered direction with the dilution factor $\frac{1}{|\mathbf{R} - \mathbf{r}_l|}$ to account for energy conservation and with allowances made through $f_l(\theta,\phi)$ for any special influence that the scatterer may have on the scattering because of the detailed structure of the scatterer. The additional term e^{ikz_1} enters whenever two or more scattering centers are encountered and accounts for the fact that the instantaneous location of our scattering centers may not coincide with planes of equal amplitude of the incident plane wave. That is, in a two-center case, the first particle may scatter a plane wave of amplitude +1 while at the same time a second scatterer may encounter an amplitude of -1. The amplitudes of the incident plane wave which the various particles encounter depend on their separation from each other along the z-axis and on the wavelength of the incident radiation. By adding to the phase, the projections of the various $\mathbf{r}_l$ vectors onto the incident direction, referred to the same

origin, this problem is automatically corrected. As long as our composite scatterer is on the order of atomic dimensions, the magnitude of R will be enormously larger than either $\mathbf{z}_l$ or $\mathbf{r}_l$. This allows us to expand $|\mathbf{R}-\mathbf{r}_l|$ in a binomial expansion through first-order terms as $R-\left(\frac{\mathbf{R}}{|\mathbf{R}|}\right)\mathbf{r}_l$. In the denominator, the first-order correction term R can be neglected but not in the phase.

To see this, suppose that R is $\pi X 10^6$ and $\frac{\mathbf{R}}{|\mathbf{R}|}\mathbf{r}_l$ is $\pi/2$. Clearly $\pi/2$ would seem negligible compared to $\pi X 10^6$, but look what a difference the value of a sin or cos function has if $\pi/2$ is retained or omitted from the sum of the two terms. The product kz_l may be rewritten as $\mathbf{k_i}\ \mathbf{r}_l$, where the subscript i on $\mathbf{k}$ denotes the fact that $\mathbf{k}_l$ is a vector parallel to the incident direction with magnitude $k=\frac{2\pi}{\lambda}$. Similarly, since $\frac{\mathbf{R}}{|\mathbf{R}|}$ is a unit vector whose sense is essentially in the direction of the scattered electron, we may write $k\frac{\mathbf{R}}{|\mathbf{R}|}\mathbf{r}_l$ as $\mathbf{k}_s\ \mathbf{r}_l$ where $\mathbf{k}_s$ is a wave vector in the scattering direction. The phase of Eq. (8.25) now contains the term $(\mathbf{k}_i-\mathbf{k}_s)\ \mathbf{r}_l$, where $\mathbf{k}_i-\mathbf{k}_s$ must be proportional to the momentum change of the incident particle on scattering, since $\hbar\mathbf{k}_i$ is the initial momentum and $\hbar\mathbf{k}_s$ is the final momentum of the scattered electron. This vector difference is labeled by the symbol **s**. The asymptotic total amplitude is now expressible as

$$\Psi_{total}=\frac{e^{ikR}}{R}\sum_{l=1}^{N}e^{i\mathbf{s}\,\mathbf{r}_l}f_l(\theta,\phi) \tag{8.26}$$

Classical Wave Theory Applied to Scattering from Atoms and Molecules.

Let us first apply Eq. (8.26) to scattering from atoms. We will consider the theoretical side of high-energy electron scattering and x-ray scattering from gaseous targets as well. In the x-ray case, the intensity for an x-ray scattered by an electron is found experimentally to be a constant, usually denoted by I_{cl}, which varies inversely as the square of the mass of the scatterer where I_{cl} is the Thompson x-ray scattering constant. This means that x-rays are virtually unscattered by the nucleus, since the ratio of electron to nuclear scattering will be greater than $\left(\frac{m_p}{m_e}\right)^2\approx\left(\frac{1\ X\ 10^{-24}}{9X10^{-28}}\right)^2\sim 10^6$, where m_p is the proton rest mass and m_e is the electron rest mass. The total amplitude for x-ray scattering by an

atom can then be written as

$$\Psi^{xr}_{total} = \sqrt{I_{cl}}\, e^{i\eta_{cl}} e^{ikR} \sum_{l=1}^{N} e^{i\mathbf{s}\cdot\mathbf{r}_l} \tag{8.27}$$

where η_{cl} is a phase factor introduced because of a possibility that the x-ray scattered amplitude may be complex. The intensity can be written as

$$I^{xr}_{total} = I_{cl}\left(N + \sum_{l\neq k}^{N}\sum_{l\neq k}^{N} e^{i\mathbf{s}\cdot\mathbf{r}_{lk}}\right) \tag{8.28}$$

where $\mathbf{r}_{lk} = \mathbf{r}_l - \mathbf{r}_k$ is an interelectron distance. Both expressions, Eqs. (8.27) and (8.28), correspond to a fixed arrangement of electrons in space. For electrons, the intensity of scattering by another charged particle proceeds according to the Rutherford experimental law $I = \frac{I_e Z^2}{s^4}$, where Z is the charge of the scatterer and I_e is a characteristic constant. Note that both I_{cl} and I_e include the $\frac{1}{R^2}$ dilution factor and depend on the incident x-ray or electron beam flux I_o and on the number N_o of target particles per cubic centimeter in the path of the incident beam as the product $I_o N_o$. We may take $f_l(\theta,\phi) = \sqrt{I_e}\left(\frac{Z}{s^2}\right)\exp[i\eta(Z)]$, where $\eta(Z)$ is again an unknown phase shift introduced because of the possibility that the amplitude may be complex. In the x-ray case for scattering by an atom, the intensity is independent of the phase η_{cl}, and we need not investigate it further. In electron scattering, this term is different for electrons and nuclei since they contain charges of opposite sign and usually different magnitude. The amplitude for this case is

$$\Psi^{ed}_{total} = \sqrt{I_e}\left(\frac{e^{ikR}}{s^2}\right)\left[Ze^{\left(i\eta(Z)+i\mathbf{s}\cdot\mathbf{r}_n\right)} + \sum_{i=1}^{N} e^{\left(i\eta(-1)+i\mathbf{s}\cdot\mathbf{r}_i\right)}\right] \tag{8.29}$$

which for an atom simplifies further, since the nuclear position vector $\mathbf{r}_n$ is zero because the nucleus lies at the center of mass. The term $\eta(Z)$ is the nuclear phase and $\eta(-1)$ is the phase for scattering by an individual electron. The notation -1 signifies a unit negative charge on each electron as opposed to $+Z$ on the nucleus, where Z is the atomic number. The intensity with $\mathbf{r}_n = 0$ becomes

$$I^{ed}_{total} = \left(\frac{I_e}{s^4}\right)\left\{Z^2 + 2Z\sum_{i=1}^{N}\cos[\eta(Z) - \eta(-1) - \mathbf{s}\cdot\mathbf{r}_i] + N + \sum_{i\neq j}^{N}\sum_{i\neq j}^{N} e^{i\mathbf{s}\cdot\mathbf{r}_{ij}}\right\} \tag{8.30}$$

Note that the last two terms on the right in Eq. (8.30) are identical to those in Eq. (8.28).

According to Huygens' principle, the function $\sum_{i=1}^{N} e^{i\mathbf{s}\cdot\mathbf{r}_i}$ of Eq. (8.29) represents the sum over each spherical wave source arising from the

scattering of an incident plane wave from each point of the electron function where the wavelength of the incident plane wave is given by the de Broglie equation $\lambda = h/p$. The sum is replaced by the integral over ρ and ϕ of the single point element aperture distribution function. The single point element aperture distribution function, $a(\rho,\phi,z)$, for the scattering of an incident plane wave by the an atom is given by the convolution of a plane wave function with the electron orbitsphere function. The convolution is $a(\rho,\phi,z) = \pi(z) \quad [\delta(r - r_o)]Y_\ell^m(\theta,\phi)$ where $a(\rho,\phi,z)$ is given in cylindrical coordinates, $\pi(z)$, the xy-plane wave is given in Cartesian coordinates with the propagation direction along the z-axis, and the orbitsphere function, $[\delta(r - r_o)]Y_\ell^m(\theta,\phi)$, is given in spherical coordinates. Using cylindrical coordinates,

$$\sum_{i=1}^{N} e^{i\mathbf{s}\cdot\mathbf{r}_i} = \int_0^{\infty}\int_0^{2\pi}\int_{-\infty}^{\infty} a(\rho,\phi,z)e^{-i[s\rho\cos(\phi-\Phi)+wz]}\rho^2 d\rho d\phi dz \tag{8.31}$$

The general Fourier transform integral is given in reference [3].

For an aperture distribution with circular symmetry, the Fourier transform of the aperture array distribution function, $A(z)$, is [3]:

$$\sum_{i=1}^{N} e^{i\mathbf{s}\cdot\mathbf{r}_i} = 2\pi\int_0^{\infty}\int_{-\infty}^{\infty} a(\rho,z)J_o(s\rho)e^{-iwz}\rho d\rho dz \tag{8.32}$$

$$= \int_0^{\infty} A(z)e^{-iwz}dz \tag{8.33}$$

$$= F(s) \tag{8.34}$$

The same derivation applies for the two-point term $\sum_{}^{N} e^{i\mathbf{s}\cdot\mathbf{r}_{ij}}$ of Eq. (8.30).

The sum is replaced by the integral over ρ and ϕ of the single point element autocorrelation function, $\mathrm{r}(\rho,\phi,z)$, of the single point element aperture distribution function. For circular symmetry [3],

$$\mathrm{r}(\rho,\phi,z) = a(\rho,\phi,z) \quad a(\rho,\phi,z) \tag{8.35}$$

and

$$\sum_{i\neq j}^{N}\sum_{i\neq j}^{N} e^{i\mathbf{s}\cdot\mathbf{r}_{ij}} = 2\pi\int_0^{\infty}\int_{-\infty}^{\infty} a(\rho,z)J_o(s\rho)e^{-iwz}\rho d\rho dz \tag{8.36}$$

$$= \int_0^{\infty} R(z)e^{-iwz}dz \tag{8.37}$$

And

$$R(z) = A(z) \quad A(z) \tag{8.38}$$

For closed shell atoms in single states such as rare gases, $Y(\theta,\phi)$, the spherical harmonic angular function of the electron function is a constant, and only two expressions are possible from all orders of averaging over all possible orientations in space. For the x-ray case the

scattered intensities are

$$I_1^{xr} = I_{cl}[\int_0^\infty A(z)e^{-iwz}dz]^2 = I_{cl}F(s)^2 \tag{8.39}$$

and

$$I_2^{xr} = I_{cl}[N + \int_0^\infty R(z)e^{-iwz}dz] \tag{8.40}$$

while for electrons, the scattered intensities are

$$I_1^{ed} = \left(\frac{I_e}{s^4}\right)\{Z^{2+} 2Z\cos[\eta(Z) - \eta(-1)]F(s) + F(s)^2\} \tag{8.41}$$

and

$$I_2^{ed} = \left(\frac{I_e}{s^4}\right)\{Z^2 + 2Z\cos[\eta(Z) - \eta(-1)]F(s) + N + \int_0^\infty R(z)e^{-iwz}dz\} \tag{8.42}$$

where the subscript 1 denotes an amplitude derivation and 2 an intensity derivation. The aperture function of the nucleus is a delta function of magnitude Z, the nuclear charge. The Fourier Transform is a constant of magnitude Z as appears in Eqs. (8.41) and (8.42). Note that the Fourier convolution theorem proves the equivalence of Eq. (8.39) and Eq. (8.40) and the equivalence of Eq. (8.41) and Eq. (8.42).

The aperture array distribution function, A(z), Eq. (8.33), corresponds to the electron radial distribution function of Bonham, and the aperture array autocorrelation function R(z), Eq. (8.37), corresponds to the electron pair correlation function of Bonham [2].

ELECTRON SCATTERING EQUATION FOR THE HELIUM ATOM BASED ON THE ORBITSPHERE MODEL

The closed form solution of all two electron atoms is given in the Two Electron Atom Section. In the helium ground state, both electrons orbitspheres are at a radius

$$r_1 = 0.567a_o$$

The helium atom comprises a central nucleus of charge two which is at the center of an infinitely thin spherical shell comprising two bound electrons of charge minus two. Thus, the helium atom is neutrally charged, and the electric field of the atom is zero for $r > 0.567a_o$. The Rutherford scattering equation for isolated charged particles does <u>not</u> apply. The appropriate scattering equation for helium in the ground state can be derived as a Fourier optics problem as given in the Classical Scattering of Electromagnetic Radiation Section.

The aperture distribution function, $a(\rho,\phi,z)$, for the scattering of an incident plane wave by the He atom is given by the convolution of the plane wave function with the two electron orbitsphere Dirac delta

function of *radius* $= 0.567a_o$ and charge/mass density of $\frac{2}{4\pi(0.567a_o)^2}$. For radial units in terms of a_o

$$a(\rho,\phi,z) = \pi(z) \quad \frac{2}{4\pi(0.567a_o)^2}[\delta(r-0.567a_o)] \tag{8.43}$$

where $a(\rho,\phi,z)$ is given in cylindrical coordinates, $\pi(z)$, the xy-plane wave is given in Cartesian coordinates with the propagation direction along the z-axis, and the He atom orbitsphere function, $\frac{2}{4\pi(0.567a_o)^2}[\delta(r-0.567a_o)]$, is given in spherical coordinates.

$$a(\rho,\phi,z) = \frac{2}{4\pi(0.567a_o)^2}\sqrt{(0.567a_o)^2 - z^2}\,\delta\left(r - \sqrt{(0.567a_o)^2 - z^2}\right) \tag{8.44}$$

For circular symmetry [3],

$$F(s) = \frac{2}{4\pi(0.567a_o)^2} 2\pi \int_0^{\infty}\int_{-\infty}^{\infty} \sqrt{(0.567a_o)^2 - z^2}\,\delta\left(\rho - \sqrt{(0.567a_o)^2 - z^2}\right) J_o(s\rho) e^{-iwz} \rho\, d\rho\, dz \tag{8.45}$$

$$F(s) = \frac{4\pi}{4\pi(0.567a_o)^2} \int_{-z_o}^{z_o} (z_0^2 - z^2) J_o\left(s\sqrt{z_o^2 - z^2}\right) e^{-iwz} dz \;;\; z_0 = 0.567a_0 \tag{8.46}$$

Substitute $\frac{z}{z_o} = -\cos\theta$

$$F(s) = \frac{4\pi z_o^2}{4\pi z_o^2} \int_0^{\pi} \sin^3\theta J_o(sz_o \sin\theta) e^{iz_0 w\cos\theta} d\theta \tag{8.47}$$

Substitution of the recurrence relationship,

$$J_o(x) = \frac{2J_1(x)}{x} - J_2(x) \;;\; x = sz_0\sin\theta \tag{8.48}$$

into Eq. (8.47), and, using the general integral of Apelblat [4]

$$\int_0^{\pi} (\sin\theta)^{\upsilon+1} J_\upsilon(b\sin\theta) e^{ia\cos\theta} d\theta = \left[\frac{2\pi}{a^2+b^2}\right]^{\frac{1}{2}} \left[\frac{b}{\sqrt{a^2+b^2}}\right]^{\upsilon} J_{\upsilon+1/2}\left[(a^2+b^2)^{\frac{1}{2}}\right] \tag{8.49}$$

with $a = z_o w$ and $b = z_o s$ gives:

$$F(s) = \left[\frac{2\pi}{(z_o w)^2 + (z_o s)^2}\right]^{\frac{1}{2}} \left\{ 2\left[\frac{z_o s}{(z_o w)^2 + (z_o s)^2}\right] J_{3/2}\left[((z_o w)^2 + (z_o s)^2)^{1/2}\right] - \left[\frac{z_o s}{(z_o w)^2 + (z_o s)^2}\right]^2 J_{5/2}\left[((z_o w)^2 + (z_o s)^2)^{1/2}\right] \right\} \tag{8.50}$$

The magnitude of the single point element autocorrelation function, $|r(\rho,\phi,z)|$, is given by the convolution of the magnitude of the single point element aperture distribution function, $a(\rho,\phi,z)$, with its self.

$$|r(\rho,\phi,z)| = |a(\rho,\phi,z)| \quad |a(\rho,\phi,z)| \tag{8.51}$$

The Fourier convolution theorem permits Eq. (8.51) to be determined by Fourier transformation.

$$|r(\rho,\phi,z)| = \int_0^{\infty} e^{i\mathbf{w}\cdot\mathbf{z}} \left[\int_0^{\infty} \sqrt{(0.567a_o)^2 - z^2}\, e^{-i\mathbf{w}\cdot\mathbf{z}} dz \right]^2 dw \tag{8.52}$$

$$|r(\rho,\phi,z)| = -e^{i\pi} \left\{ \int_0^{\infty} \sin(\mathbf{w}\cdot\mathbf{z}) \left[\frac{J_1(0.567a_o w)}{w} \right]^2 dw \right\} + C \tag{8.53}$$

where C is an integration constant for which $R(\rho)$ equals zero at $r = 1.134a_o$

$$|r(\rho,\phi,z)| = \left[\frac{1}{2} - \left(\frac{4z_o}{3\pi} \right) \left(\left[1 + \frac{z^2}{4z_o^2} \right] E\left(\frac{z}{2z_0} \right) + \left[1 - \frac{z^2}{4z_o^2} \right] K\left(\frac{z}{2z_o} \right) \right) \right] + C$$

$$0 < z \le 2z_o;\ z_o = 0.567a_o \tag{8.54}$$

Eq. (8.54) was derived from a similar transform by Bateman [5]. The electron elastic scattering intensity is given by a constant times the square of the amplitude given by Eq. (8.50).

$$I_1^{ed} = I_e \left\{ \left[\frac{2\pi}{((z_o w)^2 + (z_o s)^2)^{1/2}} \right]^{\frac{1}{2}} \left\{ 2 \left[\frac{z_o s}{((z_o w)^2 + (z_o s)^2)^{1/2}} \right] J_{3/2}\left[((z_o w)^2 + (z_o s)^2)^{1/2} \right] - \left[\frac{z_o s}{((z_o w)^2 + (z_o s)^2)^{1/2}} \right]^2 J_{5/2}\left[((z_o w)^2 + (z_o s)^2)^{1/2} \right] \right\}^2 \right\} \tag{8.55}$$

$$s = \frac{4\pi}{\lambda} \sin\frac{\theta}{2};\ w = 0\ (\textit{units of } \text{Å}^{-1}) \tag{8.56}$$

Results

The magnitude of the single point element aperture distribution function, $a(\rho,\phi,z)$, convolved with the function $\delta(z - 0.567a_o)$ is shown graphically in Figure 8.2 in units of a_o. The function was normalized to 2.

Figure. 8.2. The magnitude of the single point element aperture distribution function, $a(\rho,\phi,z)$, convolved with the function $\delta(z-0.567a_o)$ in units of a_o.

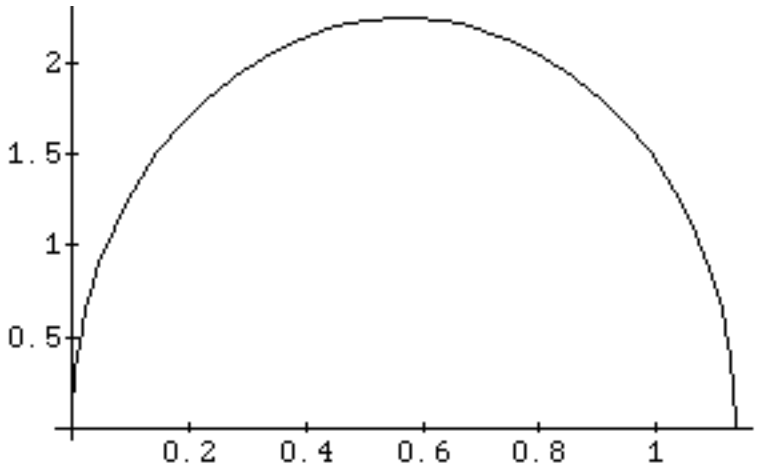

The magnitude of the single point element autocorrelation function, $r(\rho,\phi,z)$, convolved with the function $\delta(z-1.134a_o)$ is shown graphically in Figure 8.3 in units of a_o. The function was normalized to 2 and the constant of 0.352183 was added to meet the boundary condition for the convolution integral.

Figure. 8.3. The magnitude of the single point element autocorrelation function, $r(\rho,\phi,z)$, convolved with the function $\delta(z-1.134a_o)$ is shown graphically in units of a_o.

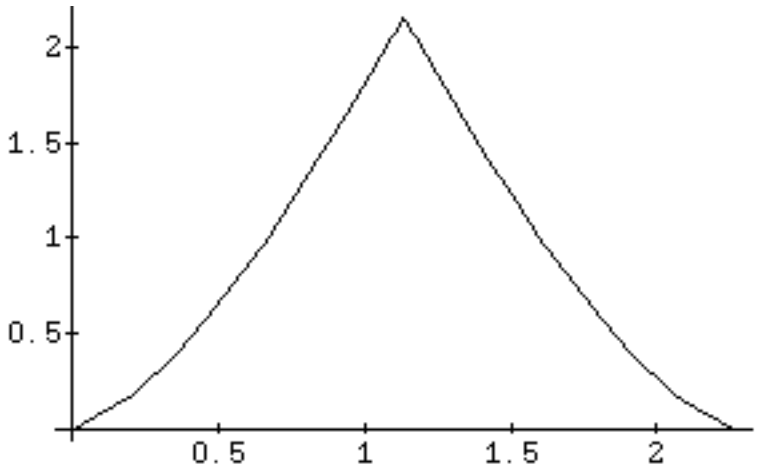

The experimental results of Bromberg [6], the extrapolated experimental data of Hughes [6], the small angle data of Geiger [7] and the semiexperimental results of Lassettre [6] for the elastic differential cross

section for the elastic scattering of electrons by helium atoms is shown graphically in Figure 8.4. The elastic differential cross section as a function of angle numerically calculated by Khare [6] using the first Born approximation and first-order exchange approximation also appear in Figure 8.4.

Figure. 8.4. The experimental results of Bromberg [6], the extrapolated experimental data of Hughes [6], the small angle data of Geiger [7] and the semiexperimental results of Lassettre [6] for the elastic differential cross section for the elastic scattering of electrons by helium atoms and the elastic differential cross section as a function of angle numerically calculated by Khare [6] using the first Born approximation and first-order exchange approximation.

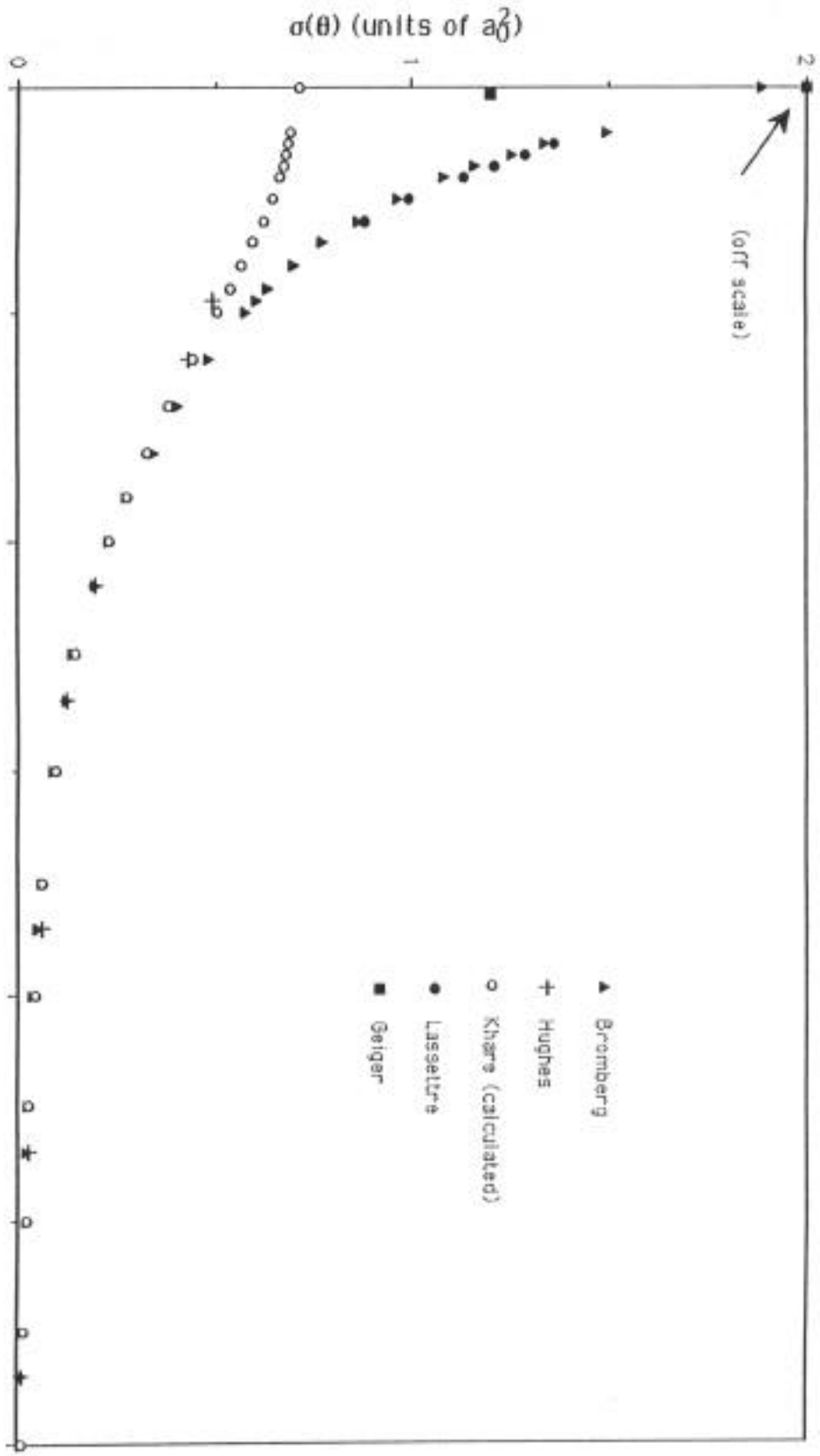

These results which are based on a quantum mechanical model are compared with experimentation [6,7]. The closed form function (Eqs. (8.55) and (8.56)) for the elastic differential cross section for the elastic scattering of electrons by helium atoms is shown graphically in Figure 8.5. The scattering amplitude function, $F(s)$ (Eq. (8.50), is shown as an insert.

Figure. 8.5. The closed form function (Eqs. (8.55) and (8.56)) for the elastic differential cross section for the elastic scattering of electrons by helium atoms. The scattering amplitude function, $F(s)$ (Eq. (8.50), is shown as an insert.

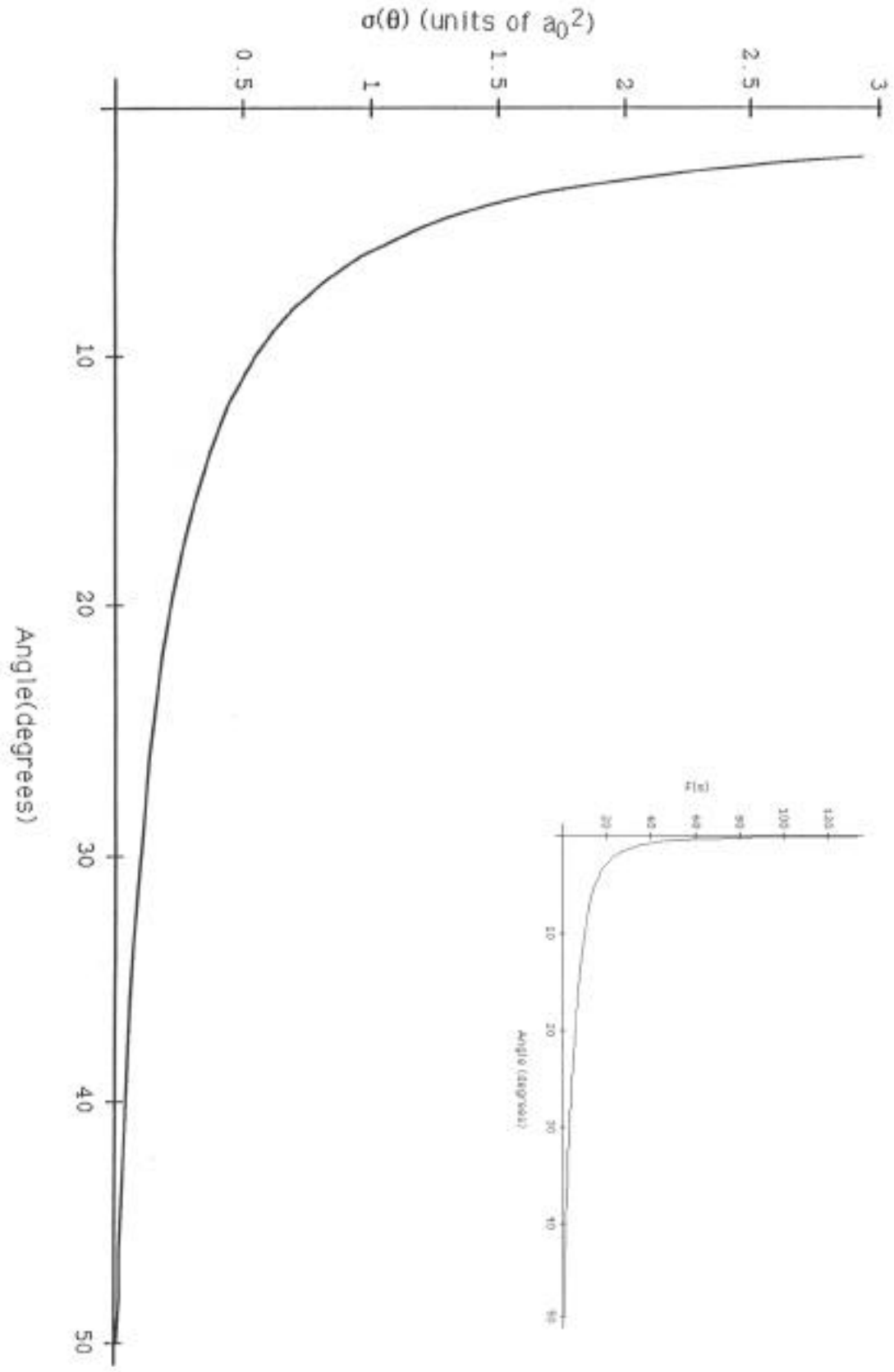

DISCUSSION

The magnitude of the single point element autocorrelation function, $r(\rho,\phi,z)$, convolved with the function $\delta(z-0.567a_o)$ (Figure 8.3) and the electron pair correlation function, $P(r)$, of Bonham [8] are similar. According to Bonham [8], the electron radial distribution function, $D(r)$, calculated from properly correlated CI wave functions for He is similar in shape to the $P(r)$ function but its maximum occurs at a value of r almost exactly half of that for $P(r)$. Thus, the function $D(r)$ is similar to the magnitude of the single point element aperture distribution function, $a(r,\theta,z)$, (Figure 8.2). $D(r)$ and $P(r)$ lead to a most probable structure for the He atom in which the electrons and the nucleus are collinear with the nucleus lying between the two electrons [2]. This is an average picture compared to the Mills model. However, it is apparent from Figure 8.4 that the quantum mechanical calculations fail completely at predicting the experimental results at small scattering angles; whereas, Eq. (8.55) predicts the correct scattering intensity as a function of angle.

In the far field, the solution of the Schrödinger equation for the amplitude of the scattered plane wave incident on a three dimensional static potential field $U(r)$ is identical to Eq. (8.25) only if one assumes a continuous distribution of scattering points and replaces the sum over l in Eq. (8.25) with an integral over the scattering power f_l of point l replaced by the instantaneous value of the potential at the same point. This result is the basis of the failure of Schrödinger's interpretation that $\Psi(x)$ is the amplitude of the electron in some sense which was superseded by the Born interpretation that $\Psi(x)$ represents a probability function of a point electron. The Born interpretation can only be valid if the speed of the electron is equal to infinity. (The electron must be in all positions weighted by the probability density function during the time of the scattering event). The correct aperture function for the Born interpretation is a Dirac delta function, $\delta(r)$, having a Fourier transform of a constant divided by $\mathbf{s}^2$ which is equivalent to the case of the point nucleus (Rutherford Equation). The Born interpretation must be rejected because the electron velocity can not exceed c without violating Special Relativity.

Solutions to the Schrödinger equation involve the set of Laguerre functions, spherical Bessel functions, and Newmann functions. From the infinite set of solutions to real problems, a linear combination of functions and the amplitude and phases of these functions are sought which gives results that are consistent with scattering experiments. The Schrödinger equation is a statistical model representing an approximation to the actual nature of the bound electron. Statistical

models are good at predicting averages as exemplified by the reasonable agreement between the calculated and experimental scattering results at large angles. However, in the limit of zero scattering angle, the results calculated via the Schrödinger equation are not in agreement with experimentation. In the limit, the "blurred" representation can not be averaged, and only the exact description of the electron will yield scattering predictions which are consistent with the experimental results.

Also, a contradiction arises in the quantum mechanical scattering calculation. For hydrogen electron orbitals, the $n = \infty$ orbital is equivalent to an ionized electron. According to the quantum mechanical scattering model, the incident ionized electron is a plane wave. However, substitution of $n = \infty$ into the solution of the Schrödinger equation yields a radial function that has an infinite number of nodes and exists over all space. The hydrogen-like radial functions have $n - \ell - 1$ nodes between $r = 0$ and $r = \infty$. The results of the Davison-Germer experiment confirm that the ionized electron is a plane wave. In contrast, for the present orbitsphere model, as n goes to infinity the electron is a plane wave with wavelength $\lambda = h / p$ as shown in the Electron in Free Space Section.

Although there are parallels in the mathematical derivations wherein the Schwartz inequality is invoked, the physics of the Heisenberg Uncertainty Principle is quite distinct from the physics of the rise-time/band-width relationship of classical mechanics [10] as given in the Resonant Line Shape and Lamb Shift Section. The Heisenberg Uncertainty Principle is derived from the probability model of the electron by applying the Schwartz inequality [9]; whereas, the rise-time/band-width relationship of classical mechanics is an energy conservation statement according to Parseval's Theorem. The Born model of the electron violates Special Relativity. The failure of the Born and Schrödinger model of the electron to provide a consistent representation of the states of the electron from a bound state to an ionized state to a scattered state also represents a failure of the dependent Heisenberg Uncertainty Principle.

In contrast, the present exact orbitsphere model provides a continuous representation of all states of the electron and is consistent with the scattering experiments of helium.

References

1. Reynolds, G. O., DeVelis, J. B., Parrent, G. B., Thompson, B.J., The New Physical Optics Notebook, SPIE Optical Engineering Press, (1990).
2. Bonham, R. A., Fink, M., High Energy Electron Scattering, ACS Monograph, Van Nostrand Reinhold Company, New York, (1974).

3. Bracewell, R. N., The Fourier Transform and Its Applications, McGraw-Hill Book Company, New York, (1978), pp. 252-253.
4. Apelblat, A., Table of Definite and Infinite Integrals, Elsevier Scientific Publishing Company, Amsterdam, (1983).
5. Bateman, H., Tables of Integral Transforms, Vol. I, McGraw-Hill Book Company, New York, (1954).
6. Bromberg, P. J., "Absolute differential cross sections of elastically scattered electrons. I. He, N_2, and CO at 500 eV", The Journal of Chemical Physics, Vol. 50, No. 9, (1969), pp. 3906-3921.
7. Geiger, J., "Elastische und unelastische streuung von elektronen an gasen", Zeitschrift fur Physik, Vol. 175, (1963), pp. 530-542.
8. Peixoto,E. M., Bunge, C. F., Bonham, R. A., "Elastic and inelastic scattering by He and Ne atoms in their ground states", Physical Review, Vol. 181, (1969), pp. 322-328.
9. McQuarrie, D. A., Quantum Chemistry, University Science Books, Mill Valley, CA, (1983), p.139.
10. Siebert, W. McC., Circuits, Signals, and Systems, The MIT Press, Cambridge, Massachusetts, (1986), pp. 488-502.

EXCITED STATES OF HELIUM

In the ground state of the helium atom, both electrons are at $r_1 = 0.567a_o$ as given in the Two Electron Atom Section. When a photon is absorbed by the ground state helium atom, one electron can move to a radius at $r > r_1$, the radius of electron one. The photon will generate an effective charge, Z_{P-eff}, within the first orbitsphere to keep electron 1 at the allowed radius $0.567a_o$. We can determine Z_{P-eff} of the "trapped photon" electric field by requiring that the force balance equation is satisfied with the superposition of the electric fields of the nucleus and the "trapped photon". From Eqs. (1.56) and (1.153), the force balance equation for electron one, at $r_1 = 0.567a_o$ is

$$\frac{m_e v^2}{r_1} = \frac{\hbar^2}{m_e \left(0.567 a_o\right)^3} = \frac{Z_{T-eff} e^2}{4\pi\varepsilon_0 \left(0.567 a_o\right)^2} \tag{9.1}$$

$$Z_{T-eff} = 1.7636 \tag{9.2}$$

where Z_{T-eff} is the effective charge of the central field of the "trapped photon" plus the nucleus. The electric field of the nucleus for $r < 0.567a_o$ is

$$\mathbf{E}_{nucleus} = \frac{+2e}{4\pi\varepsilon_o r^2} \tag{9.3}$$

From Eq. (2.15), the equation of the electric field of the "trapped photon" for $r < 0.567a_o$, is

$$\mathbf{E}_{r\,photonn,l,m} = Z_{P-eff} \frac{e\left(0.567 a_0\right)^{\ell}}{4\pi\varepsilon_o} \frac{1}{r_1^{(\ell+2)}} \left[Y_0^0(\theta,\phi) + Y_\ell^m(\theta,\phi) \mathrm{Re}\left[1 + e^{i\omega_n t}\right] \right]$$

$$\omega_n = 0 \text{ for } m = 0 \tag{9.4}$$

The total central field for $r < 0.567a_o$ is given by the sum of the electric field of the nucleus and the electric field of the "trapped photon".

$$\mathbf{E}_{total} = \mathbf{E}_{nucleus} + \mathbf{E}_{photon} \tag{9.5}$$

From Eqs. (9.2-9.5) and the force balance boundary condition at $r_1 = 0.567a_o$, the electric field of the "trapped photon" for $r < 0.567a_o$, is

$$\mathbf{E}_{r\,photonn,l,m} = [-2 + 1.7636] \frac{e\left(0.567 a_0\right)^{\ell}}{4\pi\varepsilon_o} \frac{1}{r_1^{(\ell+2)}} \left[Y_0^0(\theta,\phi) + Y_\ell^m(\theta,\phi) \mathrm{Re}\left[1 + e^{i\omega_n t}\right] \right]$$

$$\omega_n = 0 \text{ for } m = 0 \tag{9.6}$$

Substitution of Eqs. (9.3) and (9.6) into Eq. (9.5) gives for $r < 0.567a_o$,

$$\mathbf{E}_{r\,total} = \frac{2e}{4\pi\varepsilon_o r_1^2} - 0.2364 \frac{e\left(0.567 a_0\right)^{\ell}}{4\pi\varepsilon_o} \frac{1}{r^{(\ell+2)}} \left[Y_0^0(\theta,\phi) + Y_\ell^m(\theta,\phi) \mathrm{Re}\left[1 + e^{i\omega_n t}\right] \right]$$

$$\omega_n = 0 \text{ for } m = 0 \tag{9.7}$$

Recall from Eq. (2.17) of the Excited States of the One Electron Atom

(Quantization) Section that the solution of Z_{T-eff} of the boundary value problem of "trapped photons" which excite modes in the orbitsphere resonator cavity is $\frac{Z'}{n}$. In this case, $Z' = Z - 1 = 1$ where Z is the nuclear charge. Thus, for $0.567a_o < r < r_2$ where r_2 is the radius of electron 2,

$$\mathbf{E}_{r_{total}} = \frac{e}{4\pi\varepsilon_o r_2^2}\frac{1}{n}\left[Y_0^0(\theta,\phi) + Y_\ell^m(\theta,\phi)\,\mathrm{Re}\left[1 + e^{i\omega_n t}\right]\right]$$
$$\omega_n = 0 \text{ for } m = 0 \tag{9.8}$$

The force balance equation for electron 2 is the same as the equation derived to determine the ionization energies of two electron atoms as given in the Two Electron Atom Section (Eq. (7.18)):

$$\frac{m_e v^2}{r_2} = \frac{\hbar^2}{m_e r_2^3} = \frac{1}{n}\frac{e^2}{4\pi\varepsilon_o r_2^2} + \frac{1}{2}\frac{1}{n}\frac{\hbar^2}{2m_e r_2^3}\sqrt{s(s+1)} \tag{9.9}$$

with the exception that the magnetic force is multiplied by one-half because electron 1 is held at a fixed radius. With $s = \frac{1}{2}$,

$$r_2 = \left[n - \frac{\sqrt{s(s+1)}}{4}\right]a_o \qquad n = 2,3,4,... \tag{9.10}$$

The energy stored in the electric field, E_{ele}, is given by Eqs. (1.175) and (1.176)

$$E_{ele} = -\frac{1}{n}\frac{e^2}{8\pi\varepsilon_o r_2} \tag{9.11}$$

where r_2 is given by Eq. (9.10).

The energy stored in the magnetic fields of two unpaired electrons initially paired at radius r_2, E_{mag}, is given by Eq. (7.30)

$$E_{mag} = \frac{2\pi\mu_o e^2\hbar^2}{m_e^2 r_2^3} \tag{9.12}$$

where r_2 is given by Eq. (9.10).

$E_{magwork}$ is the integral of the magnetic force (the second term on the right side of Eq. (9.9) multiplied by two because with ionization, the second term of Eq.(9.9) corresponds to the center of mass force balance of electron two and electron one wherein the electron mass replaced by the reduced mass $\frac{1}{2}m_e$):

$$E_{magwork} = \int_{\infty}^{r_2}\frac{\hbar^2}{2nm_e r^3}\sqrt{s(s+1)}\,dr \tag{9.13}$$

where r_2 is given by Eq. (9.10).

$$E_{magwork} = \frac{\hbar^2 \sqrt{s(s+1)}}{4nm_e a_0^2 \left(n - \frac{\sqrt{s(s+1)}}{4}\right)^2}; \quad s = \frac{1}{2} \tag{9.14}$$

The magnetic transition energy, E_{HF}, can be calculated from the spin/spin coupling energy and the magnetic energy stored in the surface currents produced by the "trapped resonant photon". The spin/spin coupling energy arises from the interaction of the magnetic moment associated with the spin of one electron with the magnetic field generated by the current produced by the spin motion of the other electron. The spin/spin coupling energy in the excited state between the inner orbitsphere and the outer orbitsphere is given by Eq. (1.136) where μ_B, the magnetic moment of the outer orbitsphere is given by Eq. (1.137). The magnetic flux, **B**, of the inner orbitsphere at the position of the outer is

$$\mathbf{B} = \frac{\mu_o e \hbar}{2 m_e r_2^3} \tag{9.15}$$

Substitution of Eq. (9.15) and (1.137) into Eq. (1.136) gives

$$E = 2g \frac{\mu_o e^2 \hbar^2}{4 m_e^2 r_2^3} \tag{9.16}$$

Photons obey Maxwell's Equations. At the two dimensional surface of the orbitsphere containing a "trapped photon", the relationship between the photon's electric field and its two dimensional charge-density at the orbitsphere is

$$\mathbf{n} \cdot (\mathbf{E}_1 - \mathbf{E}_2) = \frac{\sigma}{\varepsilon_0} \tag{9.17}$$

Thus, the photon's electric field acts as surface charge. According to Eq. (9.17), the "photon standing wave" in the helium orbitsphere resonator cavity gives rise to a two dimensional surface charge at the orbitsphere two dimensional surface at r_1^+, infinitesimally greater than the radius of the inner orbitsphere, and r_2^-, infinitesimally less than the radius of the outer orbitsphere. For an electron in a central field, the magnitude of the field strength of each excited state corresponding to a transition from the state with $n = 1$ and radius $r_1 = 0.567 a_o$ to the state with $n = n$ and radius r_2 is $\frac{1}{n} e$ (Eq. (2.17)) as given in the Excited States of the One Electron Atom (Quantization) Section. The energy corresponding to the surface charge which arises from the "trapped photon standing wave" is given by the energy stored in the magnetic fields of the corresponding currents. The surface charge is given by Eq. (9.17) for a central field strength equal in magnitude to $\frac{1}{n} e$. This surface charge possesses the

same angular velocity as each orbitsphere; thus, it is a current with a corresponding stored magnetic energy. The energy corresponding to the surface currents, E_{sc}, is the sum of $E_{mag,\,\text{internal}}$ and $E_{mag,\,\text{external}}$ for a charge of $\frac{1}{n}e$ substituted into Eqs. (1.125) and (1.127) for both electrons initially at r_1.

$$E_{sc} = \left(\frac{2}{3}\frac{\pi\mu_o e^2\hbar^2}{n^2 m_e^2 r_1^3} + \frac{1}{3}\frac{\pi\mu_o e^2\hbar^2}{n^2 m_e^2 r_1^3}\right) \tag{9.18}$$

E_{sc}, the magnetic surface current energy corresponding to absorbing a photon such the second electron with principal quantum number n is ionized is given by multiplying Eq. (9.18) by the projection of the electric fields-the ratio of the magnitude of the electric field for $0.567a_o < r < r_2$, $\frac{1}{n}$, given by Eq. (9.8) to the magnitude of the electric field change, $1-\frac{1}{n}$.

$$E_{SC} = \frac{\frac{1}{n}}{\left(1-\frac{1}{n}\right)}\frac{\pi\mu_o e^2\hbar^2}{n^2 m_e^2 r_1^3} = \frac{1}{(n-1)}\frac{\pi\mu_o e^2\hbar^2}{n^2 m_e^2 r_1^3} \tag{9.19}$$

The energy corresponding to the a singlet to triplet transition-the hyperfine structure energy, E_{HF}, is given by the sum of Eq. (9.16) and Eq. (9.19)

$$E_{HF} = 2g\left(\frac{\mu_o e^2\hbar^2}{4m_e^2 r_2^3} + \frac{1}{(n-1)}\frac{\pi\mu_o e^2\hbar^2}{n^2 m_e^2 r_1^3}\right) \tag{9.20}$$

where $r_1 = 0.567a_o$ and r_2 is given by Eq. (9.10).

The ionization energy of helium is given by Eq. (7.28). The ionization energy of triplet states with $\ell = 0$ is given as the sum of $E_{magwork}$, (Eq. (9.14)), the energy to remove the second electron following the absorption of an ionizing photon which flips the electrons such that they are antiparallel, and the energies terms of Eq. (7.28) where E_{ele} is given by Eq. (9.11) and E_{mag} is given by Eq. (9.12). The ionization energy of singlet states with $\ell = 0$ is given by the sum of E_{ele} (Eq. (9.11)) and E_{HF} (Eq. (9.20)), the energy of the transition of the electrons from antiparallel to parallel such that they repel each other; so, the second electron is ionized. The ionization energy of triplet states with $\ell \neq 0$ is given by E_{ele} (Eq. (9.11)) minus the magnetic energy corresponding to the spin and orbital angular energies which follow from Eq. (1.95): E_{HF} (Eq. (9.20)) is multiplied by the magnitude of the maximum spin projection which follows from Eqs. (1.74) and (1.95) and the magnitude

of the maximum orbital projection given by Eq. (1.95). The ionization energy of singlet states with $\ell \neq 0$ is given by E_{ele} (Eq. (9.11)) minus the magnetic work energy corresponding to the orbital angular energy which follows from Eq. (1.95): $E_{magwork}$ (Eq. (9.14)) is multiplied by the magnitude of the maximum orbital projection given by Eq. (1.95). The energy of the excited states of helium are given by the sum of the component electric and magnetic energies and their interactions as follows:

Excited States with ℓ = Zero

$$1s^2 = 1s^1(ns)^1 \tag{9.21}$$

Triplet States

$$E = -E_{ele} + E_{magwork} + E_{mag} \tag{9.22}$$

Singlet States

$$E = -E_{ele} + E_{HF} \tag{9.23}$$

Excited States with $\ell \neq$ Zero

Triplet States

$$E = -E_{ele} - \left[s(s+1) + \frac{\ell(\ell+1)}{\ell^2 + 2\ell + 1}\right] E_{HF};\ s = \frac{1}{2} \tag{9.24}$$

Singlet States

$$E = -E_{ele} - \frac{\ell(\ell+1)}{\ell^2 + 2\ell + 1} E_{magwork} \tag{9.25}$$

Table 9.1 gives the orbital factor as a function of ℓ.

Table 9.1. Orbital factor $\frac{\ell(\ell+1)}{\ell^2+2\ell+1}$ as a function of ℓ.

ℓ	orbitsphere designation	$\frac{\ell(\ell+1)}{\ell^2+2\ell+1}$
0	s	0
1	p	$\frac{1}{2}$
2	d	$\frac{2}{3}$
3	f	$\frac{3}{4}$

Table 9.2 gives the radius of electron 2 and the energy terms as a function of n.

Table 9.2. The radius of electron 2 and the energy terms as a function of n.

	$n=1$	$n=2$	$n=3$	$n=4$
r_n (a_o)	0.567	1.7835	2.7835	3.7835
E_{ele}	–23.98	–3.813	–1.6286	–0.8986
$E_{mag\ work}$	0	0.9257	0.2533	0.1028
E_{mag}	0.63	0.02024	0.005	0.002
E_{HF}	0	0.159	0.0354	0.0133

The magnetic splitting energies due to spin angular momentum and orbital angular momentum are given by Eq. (2.40). In the case that $m>1$ ($\ell>1$), the magnetic splitting is nonzero, and a spin/orbital coupling energy arises from the surface currents corresponding to the "trapped resonant photon" which gives rise to the net orbital angular momentum.

The spin/orbital coupling energy arises from the interaction of the magnetic moment associated with the orbital angular momentum of one electron with the magnetic field generated by the current produced by the orbital motion of the other electron. From Eq. (2.40) and Eq. (9.18), $E_{s/o}$, the spin/orbital coupling energy is

$$E_{s/o} = \frac{(\ell - 1)}{(n-1)} \frac{2\pi\mu_o e^2 \hbar^2}{n^2 m_e^2 r_1^3} \tag{9.26}$$

Spin/orbital coupling increases the ionization energy of singlet states ($mm_s < 0$) and decreases the energy of triplet states ($mm_s > 0$) [1]. Table 9.3 gives the spin/orbital coupling energy terms as a function of n and ℓ (Eq. (9.26)).

Table 9.3. The spin/orbital coupling energy terms as a function of n and ℓ.

Term Designation	n	ℓ	$r_n(a_o)$	$E_{s/o}$
3D	3	2	2.7835	0.0354
4D	4	2	3.7835	0.0133
4F	4	3	3.7835	0.0266

An electrodynamic spin/orbital coupling energy arises from the interaction of the magnetic moment associated with the spin of each electron with the magnetic field generated by the current produced by the electron's own orbital motion (Eq. (2.84)).

The energies of the various states of helium with spin-orbital coupling corrections appear in Table 9.4.

Table 9.4. Calculated and experimental energies of excited states of helium with spin-orbital coupling corrections.

Configuration	Term Designation	Energy (Calculated)	Energy (Experimental)
$1s^2$	^1S	24.59	24.59
$1s^12s^1$	^3S	4.76	4.76
$1s^12s^1$	^1S	3.97	3.97
$1s^12p^1$	^3P	3.62	3.62
$1s^12p^1$	^1P	3.35	3.36
$1s^13s^1$	^3S	1.88	1.87
$1s^13s^1$	^1S	1.66	1.66
$1s^13p^1$	^3P	1.58	1.58
$1s^13p^1$	^1P	1.51	1.51
$1s^13d^1$	^3D	1.53	1.51
$1s^13d^1$	^1D	1.50	1.51
$1s^14s^1$	^3S	1.00	0.99
$1s^14s^1$	^1S	0.91	0.91
$1s^14p^1$	^3P	0.88	0.88
$1s^14p^1$	^1P	0.85	0.85
$1s^14d^1$	^3D	0.86	0.85
$1s^14d^1$	^1D	0.85	0.85
$1s^14f^1$	^3F	0.85	0.85
$1s^14f^1$	^1F	0.85	0.85

References

1. Karplus, M., Porter, R. N., Atoms & Molecules: An Introduction for Students of Physical Chemistry, Benjamin/Cummings Publishing Company, Menlo Park, CA, (1970), p.155.

THE THREE ELECTRON ATOM

THE LITHIUM ATOM

For Li^+, there are two spin-paired electrons in an orbitsphere with

$$r_1 = r_2 = a_o \left[\frac{1}{2} - \frac{\sqrt{3}}{6} \right] \tag{10.1}$$

as given by Eq. (7.19) where r_n is the radius of electron n which has velocity v_n. The next electron is added to a new orbitsphere because of the repulsive diamagnetic force between the two spin-paired electrons and the spin-unpaired electron. This repulsive magnetic force arises from the phenomenon of diamagnetism involving the magnetic field of the outer spin-unpaired electron and the two spin-paired electrons of the inner shell. The diamagnetic force on the outer electron is determined below. The central force on each electron of the inner shell due to the magnetic flux **B** of the outer electron follows from Purcell [1]

$$\mathbf{F} = \frac{2m_e \mathbf{v}_n \Delta \mathbf{v}}{r} \tag{10.2}$$

where

$$\frac{\Delta \mathbf{v}}{r} = \frac{e\mathbf{B}}{2m_e} \tag{10.3}$$

The velocity $\mathbf{v}_n$ is given by the boundary condition for no radiation as follows:

$$\mathbf{v}_1 = \frac{\hbar}{m_e r_1} \tag{10.4}$$

where r_1 is the radius of the first orbitsphere; therefore, the force on each of the inner electrons is given as follows:

$$\mathbf{F} = \frac{\hbar e \mathbf{B}}{m_e r_1} \tag{10.5}$$

The change in magnetic moment, $\Delta\mathbf{m}$, of each electron of the inner shell due to the magnetic flux **B** of the outer electron is [1]

$$\Delta \mathbf{m} = -\frac{e^2 r_1^2 \mathbf{B}}{4m_e} \tag{10.6}$$

The diamagnetic force on the outer electron due to the two inner shell electrons is in the opposite direction of the force given by Eq. (10.5), and this diamagnetic force on the outer electron is proportional to the sum of the changes in magnetic moments of the two inner electrons due to the magnetic flux **B** of the outer electron. Because changes in the magnetic moments are involved, the determination of the diamagnetic force on the outer electron is simplified by considering the two inner

electrons as a single entity of twice the mass. The total change in magnetic moments of the inner shell electrons due to the field of the outer electron is then given by Eq. (10.6) where m_e is replaced by $2m_e$. It is then apparent that the force given by Eq. (10.5) is proportional to the flux **B** of the outer electron; whereas, the total of the change in magnetic moments of the inner shell electrons given by Eq. (10.6) applied to the combination of the inner electrons is proportional to one eighth of the flux, **B**. Thus, the force on the outer electron due to the reaction of the inner shell to the flux of the outer electron is given as follows:

$$\mathbf{F}_{diamagnetic} = -\frac{\hbar}{8r_1}\frac{e\mathbf{B}}{m_e} \tag{10.7}$$

where r_1 is the radial distance of the first orbitsphere from the nucleus. The magnetic flux, **B**, is supplied by the constant field inside the orbitsphere of the outer electron at radius r_3 and is given by the product of μ_o times Eq. (1.120).

$$\mathbf{B} = \frac{\mu_o e\hbar}{m_e r_3^3} \tag{10.8}$$

The result of substitution of Eq. (10.8) into Eq. (10.7) is

$$\mathbf{F}_{diamagnetic} = -\left[\frac{e^2\mu_o}{2m_e r_3}\right]\frac{\hbar^2}{4m_e r_1 r_3^2} \tag{10.9}$$

The term in brackets can be expressed in terms of the fine structure constant, α. From Eqs. (1.143-1.147)

$$\frac{e^2\mu_o}{2m_e r_3} = 2\pi\alpha\frac{v}{c} \tag{10.10}$$

It is demonstrated in the Two Electron Atom Section that the relativistic correction to Eq. (10.9) is $\frac{1}{Z_2}$ times the reciprocal of Eq. (10.10). Z_2 for electron three is one; thus, one is substituted for the term in brackets in Eq. (10.9).

The force must be corrected for the vector projection of the velocity onto the z-axis. As given in the Spin Angular Momentum of the Orbitsphere with $\ell = 0$ Section, the application of a z directed magnetic field of electron three given by Eq. (1.120) to the two inner orbitspheres gives rise to a diamagnetic field and a projection of the angular momentum of electron three onto an axis which precesses about the z-axis of $\sqrt{\frac{3}{4}}\hbar$. The projection of the force between electron three and electron one and two is equivalent to that of the angular momentum onto the axis which precesses about the z-axis, and is $\sqrt{s(s+1)} = \sqrt{\frac{3}{4}}$ times that of a point mass. Thus, Eq. (10.9) becomes

$$\mathbf{F}_{diamagnetic} = -\frac{\hbar^2}{4m_e r_3^2 r_1}\sqrt{s(s+1)} \tag{10.11}$$

THE RADIUS OF THE OUTER ELECTRON OF THE LITHIUM ATOM

The radius for the outer electron is calculated by equating the outward centrifugal force to the sum of the electric and diamagnetic forces as follows:

$$\frac{m_e v_3^2}{r_3} = \frac{e^2}{4\pi\varepsilon_o r_3^2} - \frac{\hbar^2}{4m_e r_3^2 r_1}\sqrt{s(s+1)} \tag{10.12}$$

With $v_3 = \frac{\hbar}{m_e r_3}$ (Eq. (1.56), $r_1 = a_o\left[\frac{1}{2} - \frac{\sqrt{\frac{3}{4}}}{6}\right]$ (Eq. (7.19)), and $s = \frac{1}{2}$, we solve for r_3.

$$r_3 = \frac{a_o}{\left[1 - \frac{\sqrt{3/4}}{4\left(\frac{1}{2} - \frac{\sqrt{3/4}}{6}\right)}\right]} \tag{10.13}$$

$$r_3 = 2.5559\ a_o$$

THE IONIZATION ENERGY OF LITHIUM

From Eq. (1.176), the energy stored in the electric field is

$$\frac{e^2}{8\pi\varepsilon_o r_3} = 5.318\ eV \tag{10.14}$$

The magnetic field of the outer electron changes the angular velocities of the inner electrons. However, the magnetic field of the outer electron provides a central Lorentzian force which exactly balances the change in centripetal force because of the change in angular velocity [1]. Thus, the electric energy of the inner orbitsphere is unchanged upon ionization. The magnetic field of the outer electron, however, also changes the magnetic moment, m, of each of the inner orbitsphere electrons. From Eq. (10.6), the change in magnetic moment, Δm, (per electron) is

$$\Delta\mathbf{m} = -\frac{e^2 r_1^2}{4m_e}\mathbf{B} \tag{10.15}$$

where **B** is the magnetic flux of the outer electron given by the product of μ_o times Eq. (1.120).

$$\mathbf{B} = \frac{\mu_o e\hbar}{m_e r_3^3} \tag{10.16}$$

Substitution of Eq. (10.16) and $2m_e$ for m_e (because there are two electrons) into Eq. (10.15) gives

$$\Delta\mathbf{m} = -\left[\frac{e^2\mu_o}{2m_e r_3}\right]\left[\frac{e\hbar r_1^2}{4m_e r_3^2}\right] \tag{10.17}$$

Furthermore, we know from Eqs. (10.9) and (10.11) that the term in brackets is replaced by $\sqrt{s(s+1)}$.

$$\Delta\mathbf{m} = -\frac{e\hbar r_1^2}{4m_e r_3^2}\sqrt{s(s+1)} \tag{10.18}$$

Substitution of Eq. (10.1) for r_1, Eq. (10.13) for r_3, and given that the magnetic moment of an electron is one Bohr magneton according to Eq. (1.99),

$$\mu_B = \frac{e\hbar}{2m_e}, \tag{10.19}$$

the fractional change in magnetic moment of an inner shell electron, $\Delta\mathbf{m}_f$, is given as follows:

$$\Delta\mathbf{m}_f = \frac{\dfrac{e\hbar r_1^2\sqrt{s(s+1)}}{4m_e r_3^2}}{\dfrac{e\hbar}{2m_e}} \tag{10.20}$$

$$= \frac{1}{2}\frac{r_1^2}{r_3^2}\sqrt{s(s+1)} \tag{10.21}$$

With r_1 given by Eq. (10.1), r_3 given by Eq. (10.13), and $s = \frac{1}{2}$,

$$\Delta \mathbf{m}_f = \frac{\left[\left(\frac{1}{2}\right)\left[a_o\left[\left(\frac{1}{2}\right) - \frac{\sqrt{\frac{3}{4}}}{6}\right]\right]\sqrt{\frac{3}{4}}\right]^2}{\left[\frac{a_o}{1 - \frac{\sqrt{\frac{3}{4}}}{4\left(\left(\frac{1}{2}\right) - \frac{\sqrt{\frac{3}{4}}}{6}\right)}}\right]^2} \tag{10.22}$$

$$\Delta \mathbf{m}_f = 0.01677$$

We add one (corresponding to $\mathbf{m}_f$) to $\Delta \mathbf{m}_f$ which is the fractional change in the magnetic moment. The energy stored in the magnetic field is proportional to the magnetic field strength squared as given by Eq. (1.122); thus, the sum is squared

$$(1.0168)^2 = 1.03382 \tag{10.23}$$

Thus, the change in magnetic energy of the inner orbitsphere is 3.382 %, or

$$0.3382\ X\ 2.543\ eV = 0.0860\ eV \tag{10.24}$$

where the magnetic energy for Helium from Eq. (7.30) which is given in Table 7.1 is 2.543 eV. And, the ionization energy is

$$E(ionization;\ Li) = 0.0860\ eV + 5.3178\ eV = 5.4038\ eV \tag{10.25}$$

The experimental ionization energy of lithium is 5.392 eV.

THREE ELECTRON ATOMS WITH THE NUCLEAR CHARGE Z>3

Three electron atoms having $Z > 3$ possess an electric field of

$$\mathbf{E} = \frac{(Z-3)e}{4\pi\varepsilon_o r_3^2} \tag{10.26}$$

for $r > r_3$. For three electron atoms having $Z > 3$, the diamagnetic force given by Eq. (10.11) is unchanged. However, for three electron atoms having $Z > 3$, an electric field exists for $r > r_3$. This electric field gives rise to an additional diamagnetic force term which adds to Eq. (10.11). The additional diamagnetic force is derived as follows. The diamagnetic

force repels the third (outer) electron, and the electric force attracts the third electron. Consider the reverse of ionization where the third electron is at infinity and the two spin paired electrons are at $r_1 = r_2$ given by Eq. (7.19).

Power must be conserved as the net force of the diamagnetic and electric forces cause the third electron to move from infinity to its final radius. Power flow is given by the Poynting Power Theorem:

$$\cdot(\mathbf{E}\times\mathbf{H}) = -\frac{\delta}{\delta t}\left(\frac{1}{2}\right)\mu_o\mathbf{H}\cdot\mathbf{H} - \frac{\delta}{\delta t}\left(\frac{1}{2}\right)\varepsilon_o\mathbf{E}\cdot\mathbf{E} - \mathbf{J}\cdot\mathbf{E} \tag{10.27}$$

During binding, the radius of electron three decreases. The electric force

$$\mathbf{F}_{ele} = \frac{(Z-2)e^2}{4\pi\varepsilon_o r_3^2} \tag{10.28}$$

increases the stored electric energy which corresponds to the power term, $-\frac{\delta}{\delta t}\left(\frac{1}{2}\right)\varepsilon_o\mathbf{E}\cdot\mathbf{E}$, of Eq. (10.27). The diamagnetic force given by Eq. (10.7) changes the stored magnetic energy which corresponds to the power term, $-\frac{\delta}{\delta t}\left(\frac{1}{2}\right)\mu_o\mathbf{H}\cdot\mathbf{H}$, of Eq. (10.27). An additional diamagnetic force arises when $Z-3>0$. This diamagnetic force corresponds to that given by Purcell [1] for a charge moving in a central field having an imposed magnetic field perpendicular to the plane of motion. The second diamagnetic force $\mathbf{F}_{diamagnetic2}$ is given by

$$\mathbf{F}_{diamagnetic2} = -2\frac{m_e\Delta\mathbf{v}^2}{r_1} \tag{10.29}$$

where $\Delta\mathbf{v}$ is derived from Eq. (10.3). The result of substitution of $\Delta\mathbf{v}$ into Eq. (10.29) is

$$\mathbf{F}_{diamagnetic2} = -\frac{2m_e}{r_1}\left(\frac{er_1\mathbf{B}}{2m_e}\right)^2 \tag{10.30}$$

The magnetic flux, $\mathbf{B}$, at electron three for $r < r_3$ is given by the product of μ_o times Eq. (1.120). The result of the substitution of the flux into Eq. (10.30) is

$$\mathbf{F}_{diamagnetic2} = -2\left(\frac{e^2\mu_o}{2m_e r_3}\right)^2\frac{r_1\hbar^2}{m_e r_3^4} \tag{10.31}$$

The term in brackets can be expressed in terms of the fine structure constant, α. From Eqs. (1.143-1.147)

$$\frac{Z_1 e^2\mu_o}{2m_e r_3} = 2\pi\alpha Z_1\frac{v}{c} \tag{10.32}$$

It is demonstrated in the One Electron Atom Section that the relativistic

correction to Eq. (10.31) is $\frac{1}{Z_2}$ times the reciprocal of Eq. (10.32). The relativistic correction to Eq. (10.31) can be considered the product of two corrections-a correction of electron three relative to electron one and two and electron one and two relative to electron three. In the former case, Z_1 and $Z_2 = 1$ which corresponds to electron three. In the latter case, $Z_1 = Z - 3$, and $Z_2 = Z - 2$ which corresponds to r_3^+, infinitesimally greater than the radius of the outer orbitsphere and r_3^-, infinitesimally less than the radius of the outer orbitsphere, respectively, where Z is the nuclear charge. Thus, $\frac{Z-3}{Z-2}$ is substituted for the term in brackets in Eq. (10.31). The force must be corrected for the vector projection of the velocity onto the z-axis. As given in the Spin Angular Momentum of the Orbitsphere with $\ell = 0$ Section, the application of a z directed magnetic field of electron three given by Eq. (1.120) to the two inner orbitspheres gives rise to a diamagnetic field and a projection of the angular momentum of electron three onto an axis which precesses about the z-axis of $\sqrt{\frac{3}{4}}\hbar$. The projection of the force between electron three and electron one and two is equivalent to that of the angular momentum onto the axis which precesses about the z-axis, and is $\sqrt{s(s+1)} = \sqrt{\frac{3}{4}}$ times that of a point mass. Thus, Eq. (10.31) becomes

$$\mathbf{F}_{diamagnetic2} = -2\frac{(Z-3)r_1\hbar^2}{(Z-2)m_e r_3^4}\sqrt{s(s+1)} \tag{10.33}$$

As given previously in the Two Electron Section, this force corresponds to the dissipation term of Eq. (10.27), $\mathbf{J}\cdot\mathbf{E}$. The current $\mathbf{J}$ is proportional to the sum of one for the outer electron and two times two-the number of spin paired electrons. For the inner electrons, the factor of two arises because they possess mutual inductance which doubles their contribution to $\mathbf{J}$. (Recall the general relationship that the current is equal to the flux divided by the inductance.) Thus, the second diamagnetic force is

$$\mathbf{F}_{diamagnetic2} = -2\left(\frac{Z-3}{Z-2}\right)\frac{(1+4)r_1\hbar^2}{m_e r_3^4}\sqrt{s(s+1)}; \quad s = \frac{1}{2} \tag{10.34}$$

$$\mathbf{F}_{diamagnetic2} = -\left(\frac{Z-3}{Z-2}\right)\frac{r_1\hbar^2}{m_e r_3^4}10\sqrt{3/4} \tag{10.35}$$

THE RADIUS OF THE OUTER ELECTRON OF THREE ELECTRON ATOMS WITH THE NUCLEAR CHARGE Z>3

The radius of the outer electron is calculated by equating the outward centrifugal force to the sum of the electric and diamagnetic forces as follows:

$$\frac{m_e v_3^2}{r_3} = \frac{(Z-2)e^2}{4\pi\varepsilon_o r_3^2} - \frac{\hbar^2}{4m_e r_3^2 r_1}\sqrt{s(s+1)} - \left[\frac{Z-3}{Z-2}\right]\frac{r_1\hbar^2}{r_3^4 m_e}10\sqrt{s(s+1)} \tag{10.36}$$

With $v_3 = \frac{\hbar}{m_e r_3}$ (Eq. (1.56), $r_1 = a_0\left(\frac{1}{Z-1} - \frac{\sqrt{s(s+1)}}{Z(Z-1)}\right)$ (Eq. (7.19), and $s = \frac{1}{2}$, we solve for r_3 using the quadratic formulae or reiteratively.

$$r_3 = \frac{a_o\left[1 + \left[\frac{Z-3}{Z-2}\right]\frac{r_1}{r_3}10\sqrt{\frac{3}{4}}\right]}{(Z-2) - \frac{\sqrt{\frac{3}{4}}}{4r_1}}, \; r_1 \textit{ in units of } a_o \tag{10.37}$$

THE IONIZATION ENERGIES OF THREE ELECTRON ATOMS WITH THE NUCLEAR CHARGE Z>3

The energy stored in the electric field, **E** (electric), is

$$\mathbf{E}(electric) = \frac{(Z-2)e^2}{8\pi\varepsilon_o r_3} \tag{10.38}$$

where r_3 is given by Eq. (10.37). The magnetic field of the outer electron charges the angular velocities of the inner electrons. However, the magnetic field of the outer electron provides a central Lorentzian field which balances the change in centripetal force because of the change in angular velocity. Thus, the electric energy of the inner orbitsphere is unchanged upon ionization. The change in the angular velocities of the inner electrons upon ionization gives rise to a change in kinetic energies of the inner electrons. The change in velocity, $\Delta\mathbf{v}$, is given by Eq. (10.3)

$$\Delta\mathbf{v} = \frac{er_1\mathbf{B}}{2m_e} \tag{10.39}$$

Substitution of the flux, **B**, given by the product of μ_o and Eq. (1.120), into Eq. (10.39) is

$$\Delta v = \left[\frac{e^2\mu_o}{2m_e r_1}\right]\frac{r_1^2\hbar^2}{m_e r_3^3} \tag{10.40}$$

It is demonstrated in the One Electron Section and the Two Electron Atom Section that the relativistic correction to Eq. (10.40) is $\frac{1}{Z_2}$ times the reciprocal of the term in brackets. In this case, Z_2 corresponding to

electron three is one; thus, one is substituted for the term in brackets in Eq. (10.40). Thus, Eq. (10.40) becomes,

$$\Delta v = \frac{r_1^2 \hbar^2}{r_3^3 m_e} \tag{10.41}$$

where is r_1 given by Eq. (7.19), and r_3 is given by Eq. (10.37). The change in kinetic energy, ΔE_T, of the two inner shell electrons is given by

$$\Delta E_T = 2\frac{1}{2} m \Delta v^2 \tag{10.42}$$

The ionization energy is the sum of the electric energy, Eq. (10.38), and the change in the kinetic energy, Eq. (10.42), of the inner electrons.

$$E(Ionization) = E(Electric) + E_T \tag{10.43}$$

The ionization energies for several three electron atoms are given in Table 10.1.

Table 10.1. The calculated radii of the inner paired electrons and the outer unpaired electron, electric energy of the outer electron, change in kinetic energy of the two inner electrons, and ionization energies for some three-electron atoms.

Atom	Z	r_1[a] (a_o)	r_3[b] (a_o)	Electric Energy[c] (eV)	Δv[d] 10^4 (m/sec)	ΔE_T[e] (eV)	Calculated Ionization Energy[f] (eV)	Experimental Ionization Energy [2] (eV)
Li	3	0.567	2.556	5.318	-	-	5.40	5.392
Be^+	4	0.261	1.498	18.16	4.44	0.0112	18.17	18.211
B^{2+}	5	0.207	1.078	37.86	7.51	0.032	37.9	37.93
C^{3+}	6	0.171	0.8459	64.33	10.58	0.064	64.4	64.492
N^{4+}	7	0.146	0.697	97.6	13.80	0.108	97.71	97.888
O^{5+}	8	0.127	0.593	137.6	16.95	0.163	137.76	138.116
F^{6+}	9	0.113	.516	184.56	20.37	0.236	184.8	185.182
Ne^{7+}	10	0.101	0.456	238.68	23.48	0.313	239.0	239.09

a from Equation (7.19)
b from Equation (10.37)
c from Equation (10.38)
d from Equation (10.41)
e from Equation (10.42)
f from Equation (10.43)

References

1. Purcell, E., Electricity and Magnetism, McGraw-Hill, New York, (1965), pp. 370-389.
2. DeKock, R. L., Gray, H. B., Chemical Structure and Bonding, Benjamin/Cummings Publishing Company, Menlo Park, California, (1980), pp. 76-77.

THE ELECTRON CONFIGURATION OF ATOMS

The electrons of multielectron atoms all exist as orbitspheres of discrete radii which are given by r_n of the radical Dirac delta function, $\delta(r - r_n)$. These electron orbitspheres may be paired or unpaired depending on the force balance which applies to each electron. Ultimately, the electron configuration must be a minimum of energy. Minimum energy configurations are given by solutions to Laplace's Equation. The general form of the solution is

$$\Phi(r,\theta,\phi) = \sum_{\ell=0}^{\infty} \sum_{m=-\ell}^{\ell} B_{\ell,m} r^{-(\ell+1)} Y_\ell^m(\theta,\phi) \tag{11.1}$$

As demonstrated previously, this general solution gives the functions of the resonant photons. This general solution is also the minimum energy configuration for any atom. The configuration is given by the product of this general solution and the sum of the Dirac delta functions comprising the discrete radii of the electron orbitspheres. In general, the electron configuration of an atom approximately parallels that of the excited modes of the helium atom: 1s < 2s < 2p < 3s < 3p < 3d < 4s < 4p < 4d < 4f. (See Excited States of Helium Section.)

In general, electrons of an atom with the same principal and ℓ quantum numbers align parallel until each of the m_ℓ levels are occupied, and then pairing occurs until each of the m_ℓ levels contain paired electrons. Exceptions occur due to the relative importance of spin and orbital interactions and paramagnetic, diamagnetic, and electric forces for a given atom or ion.

THE NATURE OF THE CHEMICAL BOND OF HYDROGEN-TYPE MOLECULES AND MOLECULAR IONS

Two hydrogen atoms react to form a diatomic molecule, the hydrogen molecule.

$$2H\left[a_H\right] \rightarrow H_2\left[2c' = \sqrt{2}a_o\right] \tag{12.1}$$

where 2c' is the internuclear distance. Also, two hydrino atoms react to form a diatomic molecule, a dihydrino molecule.

$$2H\left[\frac{a_H}{p}\right] \rightarrow H_2^*\left[2c' = \frac{\sqrt{2}a_o}{p}\right] \tag{12.2}$$

where p is an integer.

Hydrogen molecules form hydrogen molecular ions when they are singly ionized.

$$H_2\left[2c' = \sqrt{2}a_o\right] \rightarrow H_2\left[2c' = 2a_o\right]^+ + e^- \tag{12.3}$$

Also, dihydrino molecules form dihydrino molecular ions when they are singly ionized.

$$H_2^*\left[2c' = \frac{\sqrt{2}a_o}{p}\right] \rightarrow H_2^*\left[2c' = \frac{2a_o}{p}\right]^+ + e^- \tag{12.4}$$

HYDROGEN-TYPE MOLECULAR IONS

Each hydrogen-type molecular ion comprises two protons and an electron where the equation of motion of the electron is determined by the central field which is p times that of a proton at each focus (p is one for the hydrogen molecular ion, and p is an integer greater than one for each dihydrino molecular ion). The differential equations of motion in the case of a central field are

$$m(\ddot{r} - r\dot{\theta}^2) = f(r) \tag{12.5}$$

$$m(2\dot{r}\dot{\theta} + r\ddot{\theta}) = 0 \tag{12.6}$$

The second or transverse equation, Eq. (12.6), gives the result that the angular momentum is constant.

$$r^2\dot{\theta} = \text{constant} = L/m \tag{12.7}$$

where L is the angular momentum ($\hbar$ in the case of the electron). The central force equations can be transformed into an orbital equation by the substitution, $u = \frac{1}{r}$. The differential equation of the orbit of a particle moving under a central force is

$$\frac{\delta^2 u}{\delta\theta^2} + u = \frac{-1}{\frac{mL^2u^2}{m^2}} f(u^{-1}) \tag{12.8}$$

Because the angular momentum is constant, motion in only one plane

need be considered; thus, the orbital equation is given in polar coordinates. The solution of Eq. (12.8) for an inverse square force

$$f(r) = -\frac{k}{r^2} \tag{12.9}$$

is

$$r = r_0 \frac{1+e}{1+e\cos\theta} \tag{12.10}$$

$$e = A\frac{m\frac{L^2}{m^2}}{k} \tag{12.11}$$

$$r_0 = \frac{m\frac{L^2}{m^2}}{k(1+e)} \tag{12.12}$$

where e is the eccentricity of the ellipse and A is a constant. The equation of motion due to a central force can also be expressed in terms of the energies of the orbit. The square of the speed in polar coordinates is

$$v^2 = (\dot{r}^2 + r^2\dot{\theta}^2) \tag{12.13}$$

Since a central force is conservative, the total energy, E, is equal to the sum of the kinetic, T, and the potential, V, and is constant. The total energy is

$$\frac{1}{2}m(\dot{r}^2 + r^2\dot{\theta}^2) + V(r) = E = \text{ constant} \tag{12.14}$$

Substitution of the variable $u = \frac{1}{r}$ and Eq. (12.7) into Eq. (12.14) gives the orbital energy equation.

$$\frac{1}{2}m\frac{L^2}{m^2}[(\frac{\delta^2 u}{\delta\theta^2}) + u^2] + V(u^{-1}) = E \tag{12.15}$$

Because the potential energy function $V(r)$ for an inverse square force field is

$$V(r) = -\frac{k}{r} = -ku \tag{12.16}$$

the energy equation of the orbit, Eq. (12.15),

$$\frac{1}{2}m\frac{L^2}{m^2}[(\frac{\delta^2 u}{\delta\theta^2}) + u^2] - ku = E \tag{12.17}$$

which has the solution

$$r = \frac{m\frac{L^2}{m^2}k^{-1}}{1+[1+2Em\frac{L^2}{m^2}k^{-2}]^{1/2}\cos\theta} \tag{12.18}$$

where the eccentricity, e, is

$$e = [1+2Em\frac{L^2}{m^2}k^{-2}]^{1/2} \tag{12.19}$$

Eq. (12.19) permits the classification of the orbits according to the total energy, E, as follows:

$E < 0, \quad e < 1$ closed orbits (ellipse or circle)

$E = 0, \quad e = 1$ parabolic orbit

$E > 0, \quad e > 1$ hyperbolic orbit

Since $E = T + V$ and is constant, the closed orbits are those for which $T \leq |V|$, and the open orbits are those for which $T \geq |V|$. It can be shown that the time average of the kinetic energy, $< T >$, for elliptic motion in an inverse square field is $1/2$ that of the time average of the potential energy, $< V >$. $< T > = 1/2 < V >$.

As demonstrated in the One Electron Atom Section, the electric inverse square force is conservative; thus, the angular momentum of the electron, $\hbar$, and the energy of atomic orbitspheres is constant. In addition, the orbitspheres are nonradiative when the boundary condition is met.

The central force equation, Eq. (12.14), has orbital solutions which are circular, elliptic, parabolic, or hyperbolic. The former two types of solutions are associated with atomic and molecular orbitals. These solutions are nonradiative. The boundary condition for nonradiation given in the One Electron Atom Section, is the absence of components of the space-time Fourier transform of the charge-density function synchronous with waves traveling at the speed of light. The boundary condition is met when the velocity for ***every*** point on the orbitsphere is

$$v_n = \frac{\hbar}{m_e r_n} \tag{12.20}$$

The allowed velocities and angular frequencies are related to r_n by

$$v_n = r_n \omega_n \tag{12.21}$$

$$\omega_n = \frac{\hbar}{m_e r_n^2} \tag{12.22}$$

As demonstrated in the One Electron Atom Section and by Eq. (12.22), this condition is met for the product function of a radial Dirac delta function and a time harmonic function where the angular frequency, ω, is constant and given by Eq. (12.22).

$$\omega_n = \frac{\hbar}{m_e r_n^2} = \frac{\frac{\pi L}{m_e}}{A} \tag{12.23}$$

where L is the angular momentum and A is the area of the closed geodesic orbit. Consider the solution of the central force equation

comprising the product of a two dimensional ellipsoid and a time harmonic function. The spatial part of the product function is the convolution of a radial Dirac delta function with the equation of an ellipsoid. The Fourier transform of the convolution of two functions is the product of the individual Fourier transforms of the functions; thus, the boundary condition is met for an ellipsoidal-time harmonic function when

$$\omega_n = \frac{\pi\hbar}{m_e A} = \frac{\hbar}{m_e ab} \tag{12.24}$$

where the area of an ellipse is

$$A = \pi ab \tag{12.25}$$

where $2b$ is the length of the semiminor axis and $2a$ is the length of the semimajor axis. The geometry of molecular hydrogen is elliptic with the internuclear axis as the principal axis; thus, the electron orbital is a two dimensional ellipsoidal-time harmonic function. The mass follows geodesics time harmonically as determined by the central field of the protons at the foci. Rotational symmetry about the internuclear axis further determines that the orbital is a prolate spheroid. In general, ellipsoidal orbits of molecular bonding, hereafter referred to as ellipsoidal molecular orbitals (M. O. ‘s), have the general equation

$$\frac{x^2}{a^2} + \frac{y^2}{b^2} + \frac{z^2}{c^2} = 1 \tag{12.26}$$

The semiprincipal axes of the ellipsoid are a, b, c.

In ellipsoidal coordinates the Laplacian is

$$(\eta - \zeta)R_\xi \frac{\delta}{\delta\xi}\left(R_\xi \frac{\delta\phi}{\delta\xi}\right) + (\zeta - \xi)R_\eta \frac{\delta}{\delta\eta}\left(R_\eta \frac{\delta\phi}{\delta\eta}\right) + (\xi - \eta)R_\zeta \frac{\delta}{\delta\zeta}\left(R_\zeta \frac{\delta\phi}{\delta\zeta}\right) = 0 \tag{12.27}$$

An ellipsoidal M. O. is equivalent to a charged conductor whose surface is given by Eq. (12.26). It carries a total charge q, and it's potential is a solution of the Laplacian in ellipsoidal coordinates, Eq. (12.27).

Excited states of orbitspheres are discussed in the Excited States of the One Electron Atom (Quantization) Section. In the case of ellipsoidal M. O. ‘s, excited electronic states are created when photons of discrete frequencies are trapped in the ellipsoidal resonator cavity of the M. O. The photon changes the effective charge at the M. O. surface where the central field is ellipsoidal and arises from the protons and the effective charge of the "trapped photon" at the foci of the M. O. Force balance is achieved at a series of ellipsoidal equipotential two dimensional surfaces confocal with the ground state ellipsoid. The "trapped photons" are solutions of the Laplacian in ellipsoidal coordinates, Eq. (12.27).

As is the case with the orbitsphere, higher and lower energy states are equally valid. The photon standing wave in both cases is a solution of the Laplacian in ellipsoidal coordinates. For an ellipsoidal resonator

cavity, the relationship between an allowed circumference, $4aE$, and the photon standing wavelength, λ, is

$$4aE = n\lambda \tag{12.28}$$

where n is an integer and where

$$k = \frac{\sqrt{a^2 - b^2}}{a} \tag{12.29}$$

is used in the elliptic integral E of Eq. (12.28). Applying Eqs. (12.28) and (12.29), the relationship between an allowed angular frequency given by Eq. (12.24) and the photon standing wave angular frequency, ω, is:

$$\frac{\pi\hbar}{m_e A} = \frac{\hbar}{m_e n a_1 n b_1} = \frac{\hbar}{m_e a_n b_n} = \frac{1}{n^2}\omega_1 = \omega_n \tag{12.30}$$

where $n = 1,2,3,4,...$

$$n = \frac{1}{2}, \frac{1}{3}, \frac{1}{4}, ...$$

ω_1 is the allowed angular frequency for $n = 1$

a_1 and b_1 are the allowed semimajor and semiminor axes for $n = 1$

Let us compute the potential of an ellipsoidal M. O. which is equivalent to a charged conductor whose surface is given by Eq. (12.26). It carries a total charge q, and we assume initially that there is no external field. We wish to know the potential, ϕ, and the distribution of charge, σ, over the conducting surface. To solve this problem a potential function must be found which satisfies Eq. (12.27), which is regular at infinity, and which is constant over the given ellipsoid. Now ξ is the parameter of a family of ellipsoids all confocal with the standard surface $\xi = 0$ whose axes have the specified values a, b, c. The variables ζ and η are the parameters of confocal hyperboloids and as such serve to measure position on any ellipsoid $\xi = \text{constant}$. On the surface $\xi = 0$; therefore, ϕ must be independent of ζ and η. If we can find a function depending only on ξ which satisfies Eq. (12.27) and behaves properly at infinity, it can be adjusted to represent the potential correctly at any point outside the ellipsoid $\xi = 0$.

Let us assume, then, that $\phi = \phi(\xi)$. The Laplacian reduces to

$$\frac{\delta}{\delta\xi}\left(R_\xi \frac{\delta\phi}{\delta\xi}\right) = 0 \qquad R_\xi = \sqrt{(\xi + a^2)(\xi + b^2)(\xi + c^2)} \tag{12.31}$$

which on integration leads to

$$\phi(\xi) = C_1 \int_\xi^\infty \frac{\delta\xi}{R_\xi} \tag{12.32}$$

where C_1 is an arbitrary constant. The choice of the upper limit is such as to ensure the proper behavior at infinity. When ξ becomes very

large, R_ξ approaches $\xi^{3/2}$ and

$$\phi \sim \frac{2C_1}{\sqrt{\xi}} \qquad (\xi \to \infty) \tag{12.33}$$

On the other hand, the equation of an ellipsoid can be written in the form

$$\frac{x^2}{1+\frac{a^2}{\xi}} + \frac{y^2}{1+\frac{b^2}{\xi}} + \frac{z^2}{1+\frac{c^2}{\xi}} = \xi \tag{12.34}$$

If $r^2 = x^2 + y^2 + z^2$ is the distance from the origin to any point on the ellipsoid ξ, it is apparent that as ξ becomes very large $\xi \to r^2$ and hence at great distances from the origin

$$\phi \sim \frac{2C_1}{r} \tag{12.35}$$

The solution Eq. (12.32) is, therefore, regular at infinity. Moreover Eq. (12.35) enables us to determine at once the value of C_1; for it has been shown that whatever the distribution, the dominant term of the expansion at remote points is the potential of a point charge at the origin equal to the total charge of the distribution - in this case q.

Hence $C_1 = \frac{q}{8\pi\varepsilon_o}$, and the potential at any point is

$$\phi(\xi) = \frac{q}{8\pi\varepsilon_o}\int_\xi^\infty \frac{\delta\xi}{R_\xi} \tag{12.36}$$

The equipotential surfaces are the ellipsoids $\xi = \text{constant}$. Eq. (12.36) is a elliptic integral and its values have been tabulated [1].

To obtain the normal derivative we must remember that distance along a curvilinear coordinate u^1 is measured not by du^1 but by $h_1 du^1$. In ellipsoidal coordinates

$$h_1 = \frac{1}{2}\frac{\sqrt{(\xi-\eta)(\xi-\zeta)}}{R_\xi} \tag{12.37}$$

$$\frac{\delta\phi}{\delta n} = \frac{1}{h_1}\frac{\delta\phi}{\delta\xi} = \frac{-q}{4\pi\varepsilon_o}\frac{1}{\sqrt{(\xi-\eta)(\xi-\zeta)}} \tag{12.38}$$

The density of charge, σ, over the surface $\xi = 0$ is

$$\sigma = \varepsilon_o\left(\frac{\delta\phi}{\delta n}\right)_{\xi=0} = \frac{q}{4\pi\sqrt{\eta\zeta}} \tag{12.39}$$

Defining x, y, z in terms of ξ, η, ζ we put $\xi = 0$, it may be easily verified that

$$\frac{x^2}{a^4} + \frac{y^2}{b^4} + \frac{z^2}{c^4} = \frac{\zeta\eta}{a^2b^2c^2} \qquad (\xi = 0) \tag{12.40}$$

Consequently, the charge-density in rectangular coordinates is

$$\sigma = \frac{q}{4\pi abc}\frac{1}{\sqrt{(\frac{x^2}{a^4}+\frac{y^2}{b^4}+\frac{z^2}{c^4})}} \tag{12.41}$$

(The mass density function of an M. O. is equivalent to its charge-density function where m replaces q of Eq. (12.41)). The equation of the plane tangent to the ellipsoid at the point x_0, y_0, z_0 is

$$X\frac{x_0}{a^2}+Y\frac{y_0}{b^2}+Z\frac{z_0}{c^2}=1 \tag{12.42}$$

where X, Y, Z are running co-ordinates in the plane. After dividing through by the square root of the sum of the squares of the coefficients of $X, Y,$ and Z, the right member is the distance D from the origin to the tangent plane. That is,

$$D = \frac{1}{\sqrt{(\frac{x^2}{a^4}+\frac{y^2}{b^4}+\frac{z^2}{c^4})}} \tag{12.43}$$

so that

$$\sigma = \frac{q}{4\pi abc}D \tag{12.44}$$

In other words, the surface density at any point on a charged ellipsoidal conductor is proportional to the perpendicular distance from the center of the ellipsoid to the plane tangent to the ellipsoid at the point. The charge is thus greater on the more sharply rounded ends farther away from the origin.

In the case of hydrogen-type molecules and molecular ions, rotational symmetry about the internuclear axis requires that two of the axes be equal. Thus, the M. O. is a spheroid, and Eq. (12.36) can be integrated in terms of elementary functions. If $a > b = c$, the spheroid is prolate, and the potential is given by

$$\phi = \frac{1}{8\pi\varepsilon_o}\frac{q}{\sqrt{a^2-b^2}}\ln\frac{\sqrt{\xi+a^2}+\sqrt{a^2-b^2}}{\sqrt{\xi+a^2}-\sqrt{a^2-b^2}} \tag{12.45}$$

Spheroidal Force Equations

Electric Force

The spheroidal M. O. is a two dimensional surface of constant potential given by Eq. (12.45) for $\xi = 0$. For an isolated electron M. O. the electric field inside is zero as given by Gauss' Law

$$\int_S \mathbf{E}dA = \int_V \frac{\rho}{\varepsilon_o}dV \tag{12.46}$$

where the charge-density, ρ, inside the M. O. is zero. Gauss' Law at a two dimensional surface is

$$\mathbf{n}\cdot\left(\mathbf{E}_1-\mathbf{E}_2\right)=\frac{\sigma}{\varepsilon_0} \tag{12.47}$$

$\mathbf{E}_2$ is the electric field inside which is zero. The electric field of an ellipsoidal M. O. is given by substituting σ given by Eq. (12.38) and Eq. (12.39) into Eq. (12.47).

$$\mathbf{E}=\frac{\sigma}{\varepsilon_o}=\frac{q}{4\pi\varepsilon_o}\frac{1}{\sqrt{(\xi-\eta)(\xi-\zeta)}} \tag{12.48}$$

The electric field in spheroid coordinates is

$$\mathbf{E}=\frac{q}{8\pi\varepsilon_o}\frac{1}{\sqrt{\xi+a^2}}\frac{1}{\xi+b^2}\frac{1}{c}\sqrt{\frac{\xi^2-1}{\xi^2-\eta}} \tag{12.49}$$

From Eq. (12.30), the magnitude of the elliptic field corresponding to a below "ground state" hydrogen-type molecular ion is an integer. The integer is one in the case of the hydrogen molecular ion and an integer greater than one in the case of each dihydrino molecular ion. The central electric force from the two protons, $\mathbf{F}_e$, is

$$\mathbf{F}_e = Ze\mathbf{E}=\frac{p2e^2}{8\pi\varepsilon_o}\frac{1}{\sqrt{\xi+a^2}}\frac{1}{\xi+b^2}\frac{1}{c}\sqrt{\frac{\xi^2-1}{\xi^2-\eta}} \tag{12.50}$$

where p is one for the hydrogen molecular ion, and p is an integer greater than one for each dihydrino molecule and molecular ion.

Centripetal Force

Each infinitesimal point mass of the electron M. O. moves along a geodesic orbit of a spheroidal M. O. in such a way that its eccentric angle, θ, changes at a constant rate. That is $\theta=\omega t$ at time t where ω is a constant, and

$$r(t)=\mathbf{i}a\cos\omega t+\mathbf{j}b\sin\omega t \tag{12.51}$$

is the parametric equation of the ellipse of the geodesic. If $\mathbf{a}(t)$ denotes the acceleration vector, then

$$\mathbf{a}(t)=-\omega^2 r(t) \tag{12.52}$$

In other words, the acceleration is centripetal as in the case of circular motion with constant angular speed ω. The centripetal force, $\mathbf{F}_c$, is

$$\mathbf{F}_c=ma=-m\omega^2 r(t) \tag{12.53}$$

Recall that nonradiation results when $\omega=\text{constant}$ given by Eq. (12.30). Substitution of ω given by Eq. (12.30) into Eq. (12.53) gives

$$\mathbf{F}_c=\frac{-\hbar^2}{m_e a^2 b^2}r(t)=\frac{-\hbar^2}{m_e a^2 b^2}D \tag{12.54}$$

where D is the distance from the origin to the tangent plane as given by Eq. (12.43). If X is defined as follows

$$X=\frac{1}{\sqrt{\xi+a^2}}\frac{1}{\xi+b^2}\frac{1}{c}\sqrt{\frac{\xi^2-1}{\xi^2-\eta}} \tag{12.55}$$

Then, it follows from Eqs. (12.38), (12.44), (12.48), and (12.50) that

$$D = 2ab^2X \tag{12.56}$$

FORCE BALANCE OF HYDROGEN-TYPE MOLECULAR IONS

Force balance between the electric and centripetal forces is

$$\frac{\hbar^2}{m_e a^2 b^2} 2ab^2X = \frac{pe^2}{4\pi\varepsilon_o} X \tag{12.57}$$

which has the parametric solution given by Eq. (12.51) when

$$a = \frac{2a_0}{p}. \tag{12.58}$$

ENERGIES OF HYDROGEN-TYPE MOLECULAR IONS

From Eq. (12.30), the magnitude of the elliptic field corresponding to a below "ground state" hydrogen-type molecule is an integer, p. The potential energy, V_e, of the electron M. O. in the field of magnitude p times that of the protons at the foci ($\xi = 0$) is

$$V_e = \frac{-4pe^2}{8\pi\varepsilon_o\sqrt{a^2-b^2}} \ln\frac{a+\sqrt{a^2-b^2}}{a-\sqrt{a^2-b^2}} \tag{12.59}$$

where

$$\sqrt{a^2-b^2} = c' \tag{12.60}$$

$2c'$ is the distance between the foci which is the internuclear distance. The kinetic energy, T, of the electron M. O. is given by the integral of the left side of Eq. (12.57)

$$T = \frac{2\hbar^2}{m_e a\sqrt{a^2-b^2}} \ln\frac{a+\sqrt{a^2-b^2}}{a-\sqrt{a^2-b^2}} \tag{12.61}$$

From the orbital equations in polar coordinates, Eqs. (12.10-12.12), the following relationship can be derived:

$$a = \frac{m\frac{L^2}{m^2}}{k(1-e^2)} \tag{12.62}$$

For any ellipse,

$$b = a\sqrt{1-e^2} \tag{12.63}$$

Thus,

$$b = a\sqrt{\frac{\frac{L^2}{m^2}m}{ka}} \quad \text{(polar coordinates)} \tag{12.64}$$

Using Eqs. (12.54) and (12.61), and (12.16) and (12.61), respectively, it can be appreciated that b of polar coordinates corresponds to $c' = \sqrt{a^2-b^2}$ of elliptic coordinates, and k of polar coordinates with one

attracting focus is replaced by $2k$ of elliptic coordinates with two attracting foci. In elliptic coordinates, k is given by Eq. (12.48) and (12.50)

$$k = \frac{2pe^2}{4\pi\varepsilon_o} \tag{12.65}$$

and L for the electron equals $\hbar$; thus, in elliptic coordinates

$$c' = a\sqrt{\frac{\hbar^2 4\pi\varepsilon_o}{me^2 2pa}} = \sqrt{\frac{aa_0}{2p}} \tag{12.66}$$

Substitution of a given by Eq. (12.58) into Eq. (12.66) is

$$c' = \frac{a_0}{p} \tag{12.67}$$

The internuclear distance from Eq. (12.67) is $2c' = \frac{2a_o}{p}$. One half the length of the semiminor axis of the prolate spheroidal M. O., $b = c$, is

$$b = \sqrt{a^2 - c'^2} \tag{12.68}$$

Substitution of $a = \frac{2a_o}{p}$ and $c' = \frac{a_o}{p}$ into Eq. (12.68) is

$$b = \frac{\sqrt{3}}{p} a_o \tag{12.69}$$

The eccentricity, e, is

$$e = \frac{c'}{a} \tag{12.70}$$

Substitution of $a = \frac{2a_o}{p}$ and $c' = \frac{a_o}{p}$ into Eq. (12.70) is

$$e = \frac{1}{2} \tag{12.71}$$

The potential energy, V_p, due to proton-proton repulsion in the field of magnitude p times that of the protons at the foci ($\xi = 0$) is

$$V_p = \frac{pe^2}{8\pi\varepsilon_o\sqrt{a^2 - b^2}} \tag{12.72}$$

Substitution of a and b given by Eqs. (12.58) and (12.69), respectively, into Eqs. (12.59), (12.61), and (12.72) is

$$V_e = \frac{-4p^2e^2}{8\pi\varepsilon_o a_o} \ln 3 \tag{12.73}$$

$$V_p = \frac{p^2e^2}{8\pi\varepsilon_o a_o} \tag{12.74}$$

$$T = \frac{2p^2e^2}{8\pi\varepsilon_o a_o} \ln 3 \tag{12.75}$$

$$E_T = V_e + V_p + T \tag{12.76}$$

$$E_T = 13.6\ eV(-4p^2 \ln 3 + p^2 + 2p^2 \ln 3) \tag{12.77}$$

The bond dissociation energy, E_D, is the difference between the total energy of the corresponding hydrogen atom or hydrino atom and E_T.

$$E_D = E(H\left(\frac{a_H}{p}\right)) - E_T \tag{12.78}$$

VIBRATION OF HYDROGEN-TYPE MOLECULAR IONS

It can be shown that a perturbation of the orbit determined by an inverse square force results in simple harmonic oscillatory motion of the orbit. For the case of a circular orbit of radius a, an approximation of the angular frequency of this oscillation is

$$\omega = \sqrt{\frac{\left(\frac{-3}{a}\right) f(a) + f'(a)}{m}} = \sqrt{\frac{k}{m}} \tag{12.79}$$

Oscillating charges radiate. However, molecules and molecular ions including the hydrogen molecule, the hydrogen molecular ion, dihydrino molecules, and dihydrino molecular ions demonstrate nonradiative zero order vibration which is time harmonic oscillation of the position of the protons along the principal axis. The protons are located at the foci, and nonradiation is due to the geometry of the ellipse where the electron M. O. is ellipsoidal. A fundamental property of an ellipse is that a light ray emitted from a focus in any direction is reflected off of the ellipse to the other focus, and the sum of the lengths of the ray paths is constant, $2a$. An oscillating charge $\mathbf{r}_0(t) = \mathbf{d}\sin\omega_0 t$ has a Fourier spectrum

$$\mathbf{J}(\mathbf{k},\omega) = \frac{q\omega_0 d}{2} J_m(k\cos\theta d)\{\delta[\omega - (m+1)\omega_0] + \delta[\omega - (m-1)\omega_0]\} \tag{12.80}$$

where J_m's are Bessel functions of order m. These Fourier components can, and do, acquire phase velocities that are equal to the velocity of light. Consider two oscillating charges at the foci of an ellipsoidal resonator cavity, an ellipsoidal M. O. A nonradiative standing electromagnetic wave can be excited which has higher order harmonics in addition to the fundamental frequency as given in Eq. (12.80). This nonradiative standing wave gives rise to zero order vibration of the molecule. The zero order mode is a standing wave with destructive interference of all harmonics of the fundamental frequency, ω_0. A ray undergoes a 180° phase shift upon reflection, and the protons oscillate in opposite relative directions. Thus, mutual destructive interference occurs when x, the distance from one focus to the other for a reflected ray is equal to a wavelength, λ, where λ is

$$\lambda = \frac{h}{mv} \tag{12.81}$$

It follows that

$$v = \frac{h}{m\lambda} = \frac{h}{mx} \tag{12.82}$$

For time harmonic motion,

$$v = v_{average} = \frac{v_{maximum}}{\sqrt{2}} \tag{12.83}$$

The kinetic energy, T, is given by

$$T = \frac{1}{2} mv^2 \tag{12.84}$$

The vibrational energy of the protons, E_{Pvib}, is equal to the maximum vibrational kinetic energy of the protons. Substitution of Eqs. (12.82) and (12.83) into Eq. (12.84) and multiplication by two corresponding to the two protons is

$$T = T_{\max} = 2\frac{1}{2} m \frac{h^2}{m^2 x^2} (\sqrt{2})^2 = 2\frac{h^2}{mx^2} \tag{12.85}$$

The vibrational energy is the sum of the vibrational energy of the electron M. O. and that of the protons which are equal.

$$E_{vib} = \frac{4h^2}{mx^2} \tag{12.86}$$

where m is the sum of the masses of the protons, each of mass m_p.

$$m = m_p \tag{12.87}$$

And, X is $2a$. Thus, the vibrational energy is

$$E_{vib} = \frac{h^2}{m_p a^2} \tag{12.88}$$

For a in units of a_o,

$$E_{vib} = \frac{0.59}{a^2} \ eV \tag{12.89}$$

The time average internuclear distance is increased by the zero order vibration because the total energy versus internuclear distance function is asymmetrical with a lower slope for internuclear distances greater than the internuclear distance at which the total energy is a minimum. Elongation occurs along the principal axis, and shifts the total energy versus internuclear distance function to a new function which includes the contribution due to vibration. The perturbation of E_T, the total energy of the M. O. given by Eq. (12.76) with a fractional increase in the semimajor axis, a, and the reciprocal decrease in the semiminor axis, b is calculated by reiteration. The angular frequency of the M.O. given by Eq. (12.24) is unchanged when a and b are changed by reciprocal fractions. The corrected a and b are obtained when the change in E_T is equal to the vibrational energy. The vibrational energy is the sum of two equal components, the vibrational energy of the protons and the vibrational energy of the electron M. O. Vibration causes a redistribution of energy within the molecule. The M.O. potential and

kinetic energy terms given by Eqs. (12.59), (12.61), and (12.72) add π radians out of phase with the potential and kinetic energies of vibration; thus, the energy of the molecule will decrease by this amount which is equal to one half the vibrational energy. An x% increase in the semimajor axis and the reciprocal decrease in the semiminor axis decreases E_T by the vibrational energy and releases energy equal to one half vibrational energy.

Substitution of $a = (1+\frac{x}{100})\frac{2a_o}{p}$ and $b = \frac{1}{(1+\frac{x}{100})}\frac{\sqrt{3}}{p}a_o$ into Eqs. (12.73), (12.74), (12.75), and (12.76) and (12.78) with the reduction of the total energy by one half the vibrational energy is

$$E_D = E(H\left(\frac{a_H}{p}\right)) - E_{T_{zeroorder}} - \frac{E_{vib}}{2} \tag{12.90}$$

Eq. (12.90) is the bond dissociation energy where E_{vib} is given by Eq. (12.91). Substitution of $a = (1+\frac{x}{100})\frac{2a_o}{p}$ into Eq. (12.89) is

$$E_{vib} = \frac{0.59}{\left((1+\frac{x}{100})\frac{2a_o}{p}\right)^2}\ eV \tag{12.91}$$

HYDROGEN-TYPE MOLECULES

FORCE BALANCE OF HYDROGEN-TYPE MOLECULES

Hydrogen-type molecules comprise two indistinguishable electrons bound by an elliptic field. Each electron experiences a centrifugal force, and the balancing centripetal force (on each electron) is produced by the electric force between the electron and the elliptic electric field and the magnetic force between the two electrons causing the electrons to pair. In the present case of hydrogen-type molecules, if the eccentricity equals $\frac{1}{\sqrt{2}}$, then the vectorial projection of the magnetic force between the electrons, $\sqrt{\frac{3}{4}}$ of Eq. (7.15) of the Two Electron Atom Section, is one. The molecules will be solved by self consistency. Assume $e = \frac{1}{\sqrt{2}}$, then the force balance equation given by Eq. (7.18) of the Two Electron Atom Section and Eq. (12.57) is

$$\frac{\hbar^2}{m_e a^2 b^2} 2ab^2 X = \frac{pe^2}{4\pi\varepsilon_o} X + \frac{\hbar^2}{2m_e a^2 b^2} 2ab^2 X \tag{12.92}$$

$$\frac{2a_o}{pa} - \frac{a_o}{pa} = 1 \tag{12.93}$$

$$a = \frac{a_o}{p} \tag{12.94}$$

Substitution of Eq. (12.94) into (12.66) is

$$c' = \frac{1}{p\sqrt{2}} a_o \tag{12.95}$$

Substitution of Eqs. (12.94) and (12.95) into Eq. (12.68) is

$$b = c' = \frac{1}{p\sqrt{2}} a_o \tag{12.96}$$

Substitution of Eqs. (12.94) and (12.95) into Eq. (12.70) is

$$e = \frac{1}{\sqrt{2}} \tag{12.97}$$

The eccentricity is $\frac{1}{\sqrt{2}}$; thus, the present self consistent solution which was obtained as a boundary value problem is correct. The internuclear distance given by multiplying Eq. (12.95) by two is $\frac{a_o\sqrt{2}}{p}$.

ENERGIES OF HYDROGEN-TYPE MOLECULES

The energy components defined previously for the molecular ion, Eqs. (12.73-12.77), apply in the case of the corresponding molecule. And, each molecular energy component is given by the integral of corresponding force in Eq. (12.92) where each energy component is the total for the two equivalent electrons. The parameters a and b are given by Eqs. (12.94) and (12.96), respectively.

$$V_e = \frac{-2pe^2}{8\pi\varepsilon_o\sqrt{a^2-b^2}} \ln\frac{a+\sqrt{a^2-b^2}}{a-\sqrt{a^2-b^2}} \tag{12.98}$$

$$V_p = \frac{p}{8\pi\varepsilon_o} \frac{e^2}{\sqrt{a^2-b^2}} \tag{12.99}$$

$$T = \frac{\hbar^2}{2m_e a\sqrt{a^2-b^2}} \ln\frac{a+\sqrt{a^2-b^2}}{a-\sqrt{a^2-b^2}} \tag{12.100}$$

The energy, V_m, corresponding to the magnetic force of Eq. (12.92) is

$$V_m = \frac{-\hbar^2}{4m_e a\sqrt{a^2-b^2}} \ln\frac{a+\sqrt{a^2-b^2}}{a-\sqrt{a^2-b^2}} \tag{12.101}$$

$$E_T = V_e + T + V_m + V_p \tag{12.102}$$

$$E_T = -13.6\,eV\left\{2p^2\sqrt{2} - p^2\sqrt{2} + \frac{p^2\sqrt{2}}{2}\ln\frac{\sqrt{2}+1}{\sqrt{2}-1} - p^2\sqrt{2}\right\} \tag{12.103}$$

$$E(2H\left(\frac{a_H}{p}\right)) = -2p^2 13.6\ eV \tag{12.104}$$

The bond dissociation energy, E_D, is the difference between the total energy of the corresponding hydrogen atoms or hydrino atoms and E_T.

$$E_D = E(2H\left(\frac{a_H}{p}\right)) - E_T \tag{12.105}$$

VIBRATION OF HYDROGEN-TYPE MOLECULES

As in the case of the hydrogen-type molecular ion, the time averaged internuclear distance is increased by the zero order molecular vibration. A y% increase in the semimajor axis and the reciprocal decrease in the semiminor axis releases energy which is equal to one half the vibrational energy. Substitution of $a = (1+\frac{y}{100})\frac{a_o}{p}$ and $b = \frac{1}{(1+\frac{y}{100})}\frac{1}{p\sqrt{2}}a_o$ into Eqs. (12.98-12.105) with the reduction of the total energy by one half the vibrational energy is

$$E_D = E(2H\left(\frac{a_H}{p}\right)) - E_{T_{zeroorder}} - \frac{E_{vib}}{2} \tag{12.106}$$

Eq. (12.106) is the bond dissociation energy where E_{vib} is given by Eq. (12.107). Substitution of $a = (1+\frac{y}{100})\frac{a_o}{p}$ into Eq. (12.89) is

$$E_{vib} = \frac{0.59}{\left((1+\frac{y}{100})\frac{a_o}{p}\right)^2}\ eV \tag{12.107}$$

THE HYDROGEN MOLECULAR ION $H_2[2c' = 2a_o]^+$

FORCE BALANCE OF THE HYDROGEN MOLECULAR ION

Force balance between the electric and centripetal forces is given by Eq. (12.57) where $p = 1$

$$\frac{\hbar^2}{m_e a^2 b^2} 2ab^2 X = \frac{e^2}{4\pi\varepsilon_o} X \tag{12.108}$$

which has the parametric solution given by Eq. (12.51) when

$$a = 2a_o \tag{12.109}$$

The semimajor axis, a, is also given by Eq. (12.58) where $p = 1$. The internuclear distance, $2c'$, which is the distance between the foci is given by Eq. (12.67) where $p = 1$.

$$2c' = 2a_o \tag{12.110}$$

The experimental internuclear distance is $2a_o$. The semiminor axis is

given by Eq. (12.69) where $p=1$.

$$b=\sqrt{3}a_o \tag{12.111}$$

The eccentricity, e, is given by Eq. (12.71).

$$e=\frac{1}{2} \tag{12.112}$$

ENERGIES OF THE HYDROGEN MOLECULAR ION

The potential energy, V_e, of the electron M. O. in the field of the protons at the foci ($\xi=0$) is given by Eq. (12.59) where $p=1$

$$V_e=\frac{-4e^2}{8\pi\varepsilon_o\sqrt{a^2-b^2}}\ln\frac{a+\sqrt{a^2-b^2}}{a-\sqrt{a^2-b^2}} \tag{12.113}$$

The potential energy, V_p, due to proton-proton repulsion is given by Eq. (12.72) where $p=1$

$$V_p=\frac{e^2}{8\pi\varepsilon_o\sqrt{a^2-b^2}} \tag{12.114}$$

The kinetic energy, T, of the electron M. O. is given by Eq. (12.61) where $p=1$

$$T=\frac{2\hbar^2}{m_e a\sqrt{a^2-b^2}}\ln\frac{a+\sqrt{a^2-b^2}}{a-\sqrt{a^2-b^2}} \tag{12.115}$$

Substitution of a and b given by Eqs. (12.109) and (12.111), respectively, into Eqs. (12.113), (12.114), and (12.115) is

$$V_e=\frac{-4e^2}{8\pi\varepsilon_o a_o}\ln 3=-59.763\ eV \tag{12.116}$$

$$V_p=\frac{e^2}{8\pi\varepsilon_o a_o}=13.6\ eV \tag{12.117}$$

$$T=\frac{2e^2}{8\pi\varepsilon_o a_o}\ln 3=29.88\ eV \tag{12.118}$$

$$E_T=V_e+V_p+T \tag{12.119}$$

$$E_T=-16.282\ eV \tag{12.120}$$

$$E(H[a_H])=-13.6\ eV$$

$$E_T=V_e+V_p+T \tag{12.121}$$

$$E_T=13.6\ eV(-4\ln 3+1+2\ln 3) \tag{12.122}$$

The bond dissociation energy, E_D, is the difference between the total energy of the corresponding hydrogen atom and E_T.

$$E_D=E(H[a_H])-E_T=2.68eV \tag{12.123}$$

Eqs. (12.116-12.123) are equivalent to Eqs. (12.73-12.78) where $p=1$.

VIBRATION OF THE HYDROGEN MOLECULAR ION

It can be shown that a perturbation of the orbit determined by an

inverse square force results in simple harmonic oscillatory motion of the orbit. Zero order vibration arises because the state is nonradiative and is an energy minimum. The time average internuclear distance is increased by the zero order vibration. A 0.1% increase in the semimajor axis and the reciprocal decrease in the semiminor axis decreases E_T by the vibration energy and releases energy equal to one half the vibrational energy. Substitution of $a = 2.002\ a_o$ and $b = 1.7303\ a_o$ into Eqs. (12.113), (12.114), (12.115), and (12.121) and (12.123) with the reduction of the total energy by one half the vibrational energy is

$$E_D = E(H[a_H]) - E_{T_{zeroorder}} - \frac{E_{vib}}{2} = 2.76\ eV \tag{12.124}$$

Eq. (12.124) is the bond dissociation energy where E_{vib} is given by Eq. (12.125). The experimental value is $2.78\ eV$. Substitution of $a = 2.002\ a_o$ into Eq. (12.89) is

$$E_{vib} = 0.147\ eV \tag{12.125}$$

THE HYDROGEN MOLECULE $H_2[2c' = \sqrt{2}a_o]$

FORCE BALANCE OF THE HYDROGEN MOLECULE

The force balance equation for the hydrogen molecule is given by Eq. (12.92) where $p = 1$

$$\frac{\hbar^2}{m_e a^2 b^2} 2ab^2 X = \frac{e^2}{4\pi\varepsilon_o} X + \frac{\hbar^2}{2m_e a^2 b^2} 2ab^2 X \tag{12.126}$$

which has the parametric solution given by Eq. (12.51) when

$$a = a_o \tag{12.127}$$

The semimajor axis, a, is also given by Eq. (12.94) where $p = 1$. The internuclear distance, $2c'$, which is the distance between the foci is given by Eq. (12.95) where $p = 1$.

$$2c' = \sqrt{2}a_o \tag{12.128}$$

The experimental internuclear distance is $\sqrt{2}a_o$. The semiminor axis is given by Eq. (12.96) where $p = 1$.

$$b = \frac{1}{\sqrt{2}} a_o \tag{12.129}$$

The eccentricity, e, is given by Eq. (12.97).

$$e = \frac{1}{\sqrt{2}} \tag{12.130}$$

The finite dimensions of the hydrogen molecule are evident in the plateau of the resistivity versus pressure curve of metallic hydrogen [2].

ENERGIES OF THE HYDROGEN MOLECULE

The energies of the hydrogen molecule are given by Eqs. (12.98-

12.104) where $p=1$

$$V_e = \frac{-2e^2}{8\pi\varepsilon_o\sqrt{a^2-b^2}}\ln\frac{a+\sqrt{a^2-b^2}}{a-\sqrt{a^2-b^2}} = -67.813\ eV \quad (12.131)$$

$$V_p = \frac{e^2}{8\pi\varepsilon_o\sqrt{a^2-b^2}} = 19.23\ eV \quad (12.132)$$

$$T = \frac{\hbar^2}{2m_e a\sqrt{a^2-b^2}}\ln\frac{a+\sqrt{a^2-b^2}}{a-\sqrt{a^2-b^2}} = 33.906\ eV \quad (12.133)$$

The energy, V_m, of the magnetic force is

$$V_m = \frac{-\hbar^2}{4m_e a\sqrt{a^2-b^2}}\ln\frac{a+\sqrt{a^2-b^2}}{a-\sqrt{a^2-b^2}} = -16.9533\ eV \quad (12.134)$$

$$E_T = V_e + T + V_m + V_p \quad (12.135)$$

$$E_T = -13.6\ eV\left(2\sqrt{2} - \sqrt{2} + \frac{\sqrt{2}}{2}\ln\frac{\sqrt{2}+1}{\sqrt{2}-1} - \sqrt{2}\right) = -31.63\ eV \quad (12.136)$$

$$E(2H[a_H]) = -27.21\ eV \quad (12.137)$$

The bond dissociation energy, E_D, is the difference between the total energy of the corresponding hydrogen atoms and E_T.

$$E_D = E(2H[a_H]) - E_T = 4.43\ eV \quad (12.138)$$

VIBRATION OF THE HYDROGEN MOLECULE

As in the case of the hydrogen molecular ion, the time averaged internuclear distance is increased by the zero order molecular vibration. A 0.7% increase in the semimajor axis and the reciprocal decrease in the semiminor axis releases energy which is equal to one half the vibrational energy. Substitution of $a = 1.007\,a_o$ and $b = 0.702\,a_o$ into Eqs. (12.131-12.138) with the reduction of the total energy by one half the vibrational energy is

$$E_D = E(2H[a_H]) - E_{T_{zeroorder}} - \frac{E_{vib}}{2} = -27.21 + 31.94 = 4.73\ eV \quad (12.139)$$

Eq. (12.139) is the bond dissociation energy where E_{vib} is given by Eq. (12.140). The experimental value is $4.75\ eV$. Substitution of $a = 1.007\,a_o$ into Eq. (12.89) is

$$E_{vib} = 0.582\ eV \quad (12.140)$$

The experimental value is $0.55\ eV$ which is calculated using the quantum harmonic oscillator approximation with the experimental value of the first vibrational transition.

THE DIHYDRINO MOLECULAR ION $H_2^*[2c' = a_o]^+$

FORCE BALANCE OF THE DIHYDRINO MOLECULAR ION

Force balance between the electric and centripetal forces is given by Eq. (12.57) where $p = 2$

$$\frac{\hbar^2}{m_e a^2 b^2} 2ab^2 X = \frac{2e^2}{4\pi\varepsilon_o} X \tag{12.141}$$

which has the parametric solution given by Eq. (12.51) when

$$a = a_o \tag{12.142}$$

The semimajor axis, a, is also given by Eq. (12.58) where $p = 2$. The internuclear distance, $2c'$, which is the distance between the foci is given by Eq. (12.67) where $p = 2$.

$$2c' = a_o \tag{12.143}$$

The semiminor axis is given by Eq. (12.69) where $p = 2$.

$$b = \frac{\sqrt{3}}{2} a_o \tag{12.144}$$

The eccentricity, e, is given by Eq. (12.71).

$$e = \frac{1}{2} \tag{12.145}$$

ENERGIES OF THE DIHYDRINO MOLECULAR ION

The potential energy, V_e, of the electron M. O. in the field of magnitude twice that of the protons at the foci ($\xi = 0$) is given by Eq. (12.59) where $p = 2$

$$V_e = \frac{-8e^2}{8\pi\varepsilon_o \sqrt{a^2 - b^2}} \ln \frac{a + \sqrt{a^2 - b^2}}{a - \sqrt{a^2 - b^2}} \tag{12.146}$$

The potential energy, V_p, due to proton-proton repulsion in the field of magnitude twice that of the protons at the foci ($\xi = 0$) is given by Eq. (12.72) where $p = 2$

$$V_p = \frac{2e^2}{8\pi\varepsilon_o \sqrt{a^2 - b^2}} \tag{12.147}$$

The kinetic energy, T, of the electron M. O. is given by Eq. (12.61) where $p = 2$

$$T = \frac{2\hbar^2}{m_e a \sqrt{a^2 - b^2}} \ln \frac{a + \sqrt{a^2 - b^2}}{a - \sqrt{a^2 - b^2}} \tag{12.148}$$

Substitution of a and b given by Eqs. (12.142) and (12.144), respectively, into Eqs. (12.146), (12.147), and (12.148) is

$$V_e = \frac{-16e^2}{8\pi\varepsilon_o a_o} \ln 3 = -239.058\ eV \tag{12.149}$$

$$V_p = \frac{4e^2}{8\pi\varepsilon_o a_o} = 54.42\ eV \tag{12.150}$$

$$T = \frac{8e^2}{8\pi\varepsilon_o a_o} \ln 3 = 119.53\ eV \tag{12.151}$$

$$E\left(H\left(\frac{a_H}{2}\right)\right) = -54.4\ eV \tag{12.152}$$

$$E_T = V_e + V_p + T \tag{12.153}$$

$$E_T = 13.6\ eV(-16\ln 3 + 4 + 8\ln 3) = -65.09\ eV \tag{12.154}$$

The bond dissociation energy, E_D, is the difference between the total energy of the corresponding hydrino atom and E_T.

$$E_D = E\left(H\left(\frac{a_H}{2}\right)\right) - E_T = 10.69\ eV \tag{12.155}$$

Eqs. (12.149-12.155) are equivalent to Eqs. (12.73-12.78) where $p = 2$.

VIBRATION OF THE DIHYDRINO MOLECULAR ION

It can be shown that a perturbation of the orbit determined by an inverse square force results in simple harmonic oscillatory motion of the orbit. Zero order vibration arises because the state is nonradiative and is an energy minimum. The time average internuclear distance is increased by the zero order vibration. A 0.15% increase in the semimajor axis and the reciprocal decrease in the semiminor axis decreases E_T by the vibrational energy and releases energy equal to one half the vibrational energy. Substitution of $a = 1.0015\,a_o$ and $b = 0.8647\,a_o$ into Eqs. (12.146), (12.147), (12.148), and (12.153) and (12.155) with the reduction of the total energy by one half the vibrational energy is

$$E_D = E\left(H\left(\frac{a_H}{2}\right)\right) - E_{T_{zeroorder}} - \frac{E_{vib}}{2} = -54.4 + 65.39 = 10.99\ eV \tag{12.156}$$

Eq. (12.156) is the bond dissociation energy where E_{vib} is given by Eq. (12.157). Substitution of $a = 1.0015\,a_o$ into Eq. (12.89) is

$$E_{vib} = 0.588\ eV \tag{12.157}$$

THE DIHYDRINO MOLECULE $H_2^*\left(2c' = \frac{\mathbf{a_o}}{\sqrt{\mathbf{2}}}\right)$

FORCE BALANCE OF THE DIHYDRINO MOLECULE

The force balance equation for the dihydrino molecule $H_2^*\left(2c' = \frac{a_o}{\sqrt{2}}\right)$ is given by Eq. (12.92) where $p = 2$

$$\frac{\hbar^2}{m_e a^2 b^2} 2ab^2 X = \frac{2e^2}{4\pi\varepsilon_o} X + \frac{\hbar^2}{2m_e a^2 b^2} 2ab^2 X \tag{12.158}$$

which has the parametric solution given by Eq. (12.51) when

$$a = \frac{a_o}{2} \tag{12.159}$$

The semimajor axis, a, is also given by Eq. (12.94) where $p = 2$. The internuclear distance, $2c'$, which is the distance between the foci is given by Eq. (12.95) where $p = 2$.

$$2c' = \frac{1}{\sqrt{2}} a_o \tag{12.160}$$

The semiminor axis is given by Eq. (12.96) where $p = 2$.

$$b = c = \frac{1}{2\sqrt{2}} a_o \tag{12.161}$$

The eccentricity, e, is given by Eq. (12.97).

$$e = \frac{1}{\sqrt{2}} \tag{12.162}$$

ENERGIES OF THE DIHYDRINO MOLECULE

The energies of the dihydrino molecule $H_2^*\left[2c' = \frac{a_o}{\sqrt{2}}\right]$ are given by Eqs. (12.98-12.104) where $p = 2$

$$V_e = \frac{-4e^2}{8\pi\varepsilon_o\sqrt{a^2 - b^2}} \ln\frac{a + \sqrt{a^2 - b^2}}{a - \sqrt{a^2 - b^2}} = -271.23\,eV \tag{12.163}$$

$$V_p = \frac{2}{8\pi\varepsilon_o}\frac{e^2}{\sqrt{a^2 - b^2}} = 76.93\,eV \tag{12.164}$$

$$T = \frac{\hbar^2}{2m_e a\sqrt{a^2 - b^2}} \ln\frac{a + \sqrt{a^2 - b^2}}{a - \sqrt{a^2 - b^2}} = 135.614\ eV \tag{12.165}$$

The energy, V_m, of the magnetic force is

$$V_m = \frac{-\hbar^2}{4m_e a\sqrt{a^2 - b^2}} \ln\frac{a + \sqrt{a^2 - b^2}}{a - \sqrt{a^2 - b^2}} = -67.8069\ eV \tag{12.166}$$

$$E_T = V_e + T + V_m + V_p \tag{12.167}$$

$$E_T = -13.6\ eV\left[8\sqrt{2} - 4\sqrt{2} + \frac{4\sqrt{2}}{2}\ln\frac{\sqrt{2}+1}{\sqrt{2}-1} - 4\sqrt{2}\right] = -126.5\ eV \tag{12.168}$$

$$E\left(2H\left[\frac{a_H}{2}\right]\right) = -2(54.4)\ eV \tag{12.169}$$

The bond dissociation energy, E_D, is the difference between the total energy of the corresponding hydrino atoms and E_T.

$$E_D = E\left(2H\left[\frac{a_H}{2}\right]\right) - E_T = 17.688\ eV \tag{12.170}$$

VIBRATION OF THE DIHYDRINO MOLECULE

As in the case of the dihydrino molecular ion, the time averaged internuclear distance is increased by the zero order molecular vibration.

A 0.7% increase in the semimajor axis and the reciprocal decrease in the semiminor axis releases energy which is equal to one half the vibrational energy. Substitution of $a = 0.5035a_o$ and $b = 0.351a_o$ into Eqs. (12.163-12.170) with the reduction of the total energy by one half the vibrational energy is

$$E_D = E(2H\frac{a_H}{2}) - E_{T_{zeroorder}} - \frac{E_{vib}}{2} = -108.8 + 127.66 = 18.86\ eV \tag{12.171}$$

Eq. (12.171) is the bond dissociation energy where E_{vib} is given by Eq. (12.172). Substitution of $a = 0.5035a_o$ into Eq. (12.89) is

$$E_{vib} = 2.33\ eV \tag{12.172}$$

GEOMETRY

The internuclear distance can also be determined geometrically. The spheroidal M. O. of the hydrogen molecule is an equipotential energy surface which is an energy minimum surface. For the hydrogen molecule, the electric field is zero for $\xi > 0$. Consider two hydrogen atoms A and B approaching each other. Consider that the two electrons form a spheroidal M. O. as the two atoms overlap, and the charge is distributed such that an equipotential two dimensional surface is formed. The electric fields of atoms A and B add vectorially as the atoms overlap. The energy at the point of intersection of the overlapping orbitspheres decreases to a minimum as they superimpose and then rises with further overlap. When this energy is a minimum the internuclear distance is determined. It can be demonstrated [3] that when two hydrogen orbitspheres superimpose such that the radial electric field vector from nucleus A and B makes a 45° angle with the point of intersection of the two original orbitspheres, the electric energy of interaction between orbitspheres given by

$$E_{\text{interaction}} = 2X\frac{1}{2}\varepsilon_o\int \Delta\mathbf{E}^2 dv \tag{12.173}$$

is a minimum (Figure 7.1 of [3]). The M. O. is a minimum potential energy surface; therefore, a minimum of energy of one point on the surface is a minimum for the entire surface- M. O. Thus,

$$R_{H_2} = \sqrt{2}a_o = 0.748\,\text{Å} \tag{12.174}$$

The experimental internuclear bond distance is 0.746 Å.

IONIZATION ENERGIES

The first ionization energy, IP_1, of the dihydrino molecule

$$H_2^*\left[2c' = \frac{\sqrt{2}a_o}{2}\right] \rightarrow H_2^*\left[2c' = a_o\right]^+ + e^- \tag{12.175}$$

is given by Eqs. (12.153) and (12.167) with zero order vibration, Eqs.

(12.156) and (12.171), respectively.

$$IP_1 = E_T\left(H_2^*\left[2c' = a_o\right]\right) - E_T\left(H_2^*\left(2c' = \frac{\sqrt{2}a_0}{2}\right)\right) \quad (12.176)$$

$$IP_1 = -65.39\ eV + 127.66\ eV = 62.27\ eV \quad (12.177)$$

The second ionization energy, IP_2, is given by Eq. (12.153) with zero order vibration, Eq. (12.156).

$$IP_2 = 65.39\ eV \quad (12.178)$$

A hydrino atom can react with a hydrogen, deuterium, or tritium nucleus to form a dihydrino molecular ion that further reacts with an electron to form a dihydrino molecule.

$$H\left(\frac{a_H}{p}\right) + H^+ + e^- \rightarrow H_2^*\left(2c' = \frac{\sqrt{2}a_o}{p}\right) \quad (12.179)$$

The energy released is

$$E = E\left(H\left(\frac{a_H}{p}\right)\right) - E_T \quad (12.180)$$

where E_T is given by Eq. (12.102) with zero order vibration, Eqs. (12.106-12.107).

A hydrino atom can react with a hydrogen, deuterium, or tritium atom to form a dihydrino molecule.

$$H\left(\frac{a_H}{p}\right) + H\left[a_H\right] \rightarrow H_2^*\left(2c' = \frac{\sqrt{2}a_o}{p}\right) \quad (12.181)$$

The energy released is

$$E = E\left(H\left(\frac{a_H}{p}\right)\right) + E\left(H\left[a_H\right]\right) - E_T \quad (12.182)$$

where E_T is given by Eq. (12.102) with zero order vibration, Eqs. (12.106-12.107).

SIZES OF REPRESENTATIVE ATOMS AND MOLECULES

Atoms

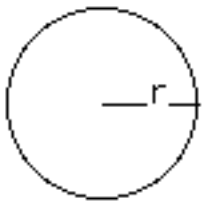

Helium Atom (He)

Helium comprises the nucleus at the origin and two electrons as a

spherical shell at
$r = 0.567 a_0$

Hydrogen Atom ($H\left[a_H\right]$)

Hydrogen comprises the nucleus at the origin and the electron as a spherical shell at
$r = a_H$

Hydrino Atom ($H\left[\frac{a_H}{2}\right]$)

Hydrino atom (1/2) comprises the nucleus at the origin and the electron as a spherical shell at
$r = \frac{a_H}{2}$

Molecules

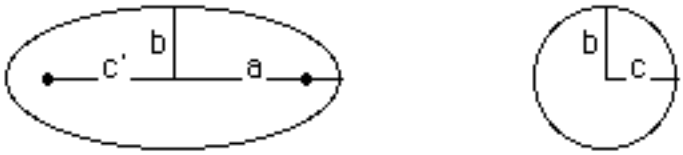

All the following molecules and molecular ions comprise prolate spheroids where

- a is the semiminor axis
- $2a$ is the total length of the molecule or molecular ion along the principal axis
- $b = c$ is the semiminor axis
- $2b = 2c$ is the total width of the molecule or molecular ion along the minor axis
- c' is the distance from the origin to a focus (nucleus)
- $2c'$ is the internuclear distance

Hydrogen Molecular Ion ($H_2\left[2c' = 2a_o\right]^+$)

$a = 2a_0$
$b = c = \sqrt{3}a_0$
$c' = a_0$
$2c' = 2a_0$

Hydrogen Molecule ($H_2\left[2c' = \sqrt{2}a_o\right]$)

$a = a_0$

$b = c = \frac{1}{\sqrt{2}} a_0$

$c' = \frac{1}{\sqrt{2}} a_0$

$2c' = \sqrt{2} a_0$

Dihydrino Molecular Ion ($H_2^*[2c' = a_o]^+$)

$a = a_0$

$b = c = \frac{\sqrt{3}}{2} a_0$

$b = c = \frac{1}{2} a_0$

$2c' = a_0$

Dihydrino Molecule ($H_2^*\left[2c' = \frac{1}{\sqrt{2}} a_o\right]$)

$a = \frac{1}{2} a_0$

$b = c = \frac{1}{2\sqrt{2}} a_0$

$c' = \frac{1}{2\sqrt{2}} a_0$

$2c' = \frac{1}{\sqrt{2}} a_0$

ORTHO-PARA TRANSITION OF HYDROGEN-TYPE MOLECULES

Each proton of hydrogen-type molecules possesses a magnetic moment which is derived in the Proton and Neutron Section and is given by

$$\mu_P = \frac{\left(\frac{2}{3}\right)^2 e\hbar}{2\frac{m_p}{2\pi}} \tag{12.183}$$

The magnetic moment **m** of the proton is given by Eq. (12.183), and the magnetic field of the proton follows from the relationship between the magnetic dipole field and the magnetic moment **m** as given by Jackson [4] where $\mathbf{m} = \mu_P \mathbf{i}_z$.

$$\mathbf{H} = \frac{\mu_P}{r^3}(\mathbf{i}_r 2\cos\theta - \mathbf{i}_\theta \sin\theta) \tag{12.184}$$

Multiplication of Eq. (12.184) by the permeability of free space, μ_0, gives the magnetic flux, **B**, due to proton one at proton two.

$$\mathbf{B} = \frac{\mu_0 \mu_P}{r^3}(\mathbf{i}_r 2\cos\theta - \mathbf{i}_\theta \sin\theta) \tag{12.185}$$

$\Delta E_{mag}^{\text{ortho/para}}$, the energy to flip the orientation of proton two's magnetic moments, μ_P, from ortho (parallel magnetic moments) to para (antiparallel magnetic moments) with respect to the direction of the magnetic moment of proton one with corresponding magnetic flux **B** is

$$\Delta E_{mag}^{\text{ortho/para}} = -2\mu_P \mathbf{B} = \frac{-2\mu_0 \mu_P^2}{r^3} \tag{12.186}$$

where r is the internuclear distance 2c' where c' is given by Eq. (12.95). Substitution of the internuclear distance into Eq. (12.186) for r gives

$$\Delta E_{mag}^{\text{ortho/para}} = -2\mu_P \mathbf{B} = \frac{-2\mu_0 \mu_P^2 n^3}{\left(\sqrt{2} a_o\right)^3} \tag{12.187}$$

The frequency, f, can be determined from the energy using the Planck relationship, Eq. (2.18).

$$f = \frac{\Delta E_{mag}^{\text{ortho/para}}}{h} = \frac{\dfrac{-2\mu_0 \mu_P^2 n^3}{\left(\sqrt{2} a_o\right)^3}}{h} \tag{12.188}$$

From Eq. (12.188) with $n = 2$, the ortho-para transition energy of the dihydrino molecule is 14.4 *MHz*.

References

1. Jahnke-Emde, Tables of Functions, 2nd ed., Teubner, (1933).
2. W. J. Nellis, "Making Metallic Hydrogen", Scientific American, May, (2000), pp. 84-90.
3. Mills, R. L., Farrell, J. J., The Grand Unified Theory, Science Press, (1989), pp. 46-47; 117-119.
4. Jackson, J. D., Classical Electrodynamics, Second Edition, John Wiley & Sons, New York, (1962), p. 178.

MOLECULAR COULOMB FIELD COLLAPSE--BLACKLIGHT PROCESS

BELOW "GROUND" STATE TRANSITIONS OF HYDROGEN-TYPE MOLECULES AND MOLECULAR IONS

Excited states of orbitspheres are discussed in the Excited States of the One Electron Atom (Quantization) Section. In the case of ellipsoidal M. O. 's, excited electronic states are created when photons of discrete frequencies are trapped in the ellipsoidal resonator cavity of the M. O. The photon changes the effective charge at the M. O. surface where the central field is ellipsoidal and arises from the protons and the effective charge of the "trapped photon" at the foci of the M. O. Force balance is achieved at a series of ellipsoidal equipotential two dimensional surfaces confocal with the ground state ellipsoid. The "trapped photons" are solutions of the Laplacian in ellipsoidal coordinates, Eq. (12.27).

As is the case with the orbitsphere, higher and lower energy states are equally valid. The photon standing wave in both cases is a solution of the Laplacian in ellipsoidal coordinates. For an ellipsoidal resonator cavity, the relationship between an allowed circumference, $4aE$, and the photon standing wavelength, λ, is

$$4aE = n\lambda \tag{13.1}$$

where n is an integer and where

$$k = \frac{\sqrt{a^2 - b^2}}{a} \tag{13.2}$$

is used in the elliptic integral E of Eq. (13.1). Applying Eqs. (13.1) and (13.2), the relationship between an allowed angular frequency given by Eq. (12.24) and the photon standing wave angular frequency, ω, is:

$$\frac{\pi\hbar}{m_e A} = \frac{\hbar}{m_e n a_1 n b_1} = \frac{\hbar}{m_e a_n b_n} = \frac{1}{n^2}\omega_1 = \omega_n \tag{13.3}$$

where $n = 1,2,3,4,...$

$$n = \frac{1}{2}, \frac{1}{3}, \frac{1}{4}, ...$$

ω_1 is the allowed angular frequency for $n = 1$

a_1 and b_1 are the allowed semimajor and semiminor axes for $n = 1$

ENERGY HOLES

From Eq. (13.3), the magnitude of the elliptic field corresponding to a below "ground state" transition of the hydrogen molecule is an integer. The potential energy equations of hydrogen-type molecules are

$$V_e = \frac{-p2e^2}{8\pi\varepsilon_o\sqrt{a^2 - b^2}} \ln\frac{a + \sqrt{a^2 - b^2}}{a - \sqrt{a^2 - b^2}} \tag{13.4}$$

$$V_p = \frac{pe^2}{8\pi\varepsilon_o\sqrt{a^2 - b^2}} \tag{13.5}$$

where

$$a = \frac{a_o}{p} \tag{13.6}$$

$$b = \frac{1}{p\sqrt{2}}\, a_o \tag{13.7}$$

$$c' = \sqrt{a^2 - b^2} = \frac{\sqrt{2}a_o}{2p} \tag{13.8}$$

and where p is an integer. (These energies are approximate in that they do not include the energy component corresponding to zero order vibration. The exact energies are given by Eqs. (13.4-13.5) where the parameters a and b are those given by Eqs. (13.6-13.7) with the correction for zero order vibration as given in the Vibration Section). From energy conservation, the resonance energy hole of a hydrogen-type molecule which causes the transition

$$H_2^*\left(2c' = \frac{\sqrt{2}a_o}{p}\right) \rightarrow H_2^*\left(2c' = \frac{\sqrt{2}a_o}{p+m}\right) \tag{13.9}$$

is

$$mp^2\, X\, 48.6\ eV \tag{13.10}$$

where m and p are integers. During the transition, the elliptic field is increased from magnitude p to magnitude $p+m$. The corresponding potential energy change equals the energy absorbed by the energy hole.

$$Energy\ hole = -V_e - V_p = mp^2\, X\, 48.6\ eV \tag{13.11}$$

Further energy is released by the hydrogen-type molecule as the internuclear distance "shrinks". The total energy, E_T, released during the transition is

$$E_T = -13.6\ eV\left[2(m+p)^2\sqrt{2} - (m+p)^2\sqrt{2} + \frac{(m+p)^2\sqrt{2}}{2}\ln\frac{\sqrt{2}+1}{\sqrt{2}-1} - (m+p)^2\sqrt{2}\right] + 13.6\ eV\left[2p^2\sqrt{2} - p^2\sqrt{2} + \frac{p^2\sqrt{2}}{2}\ln\frac{\sqrt{2}+1}{\sqrt{2}-1} - p^2\sqrt{2}\right] \tag{13.12}$$

(This energy is approximate in that it does not include the energy component corresponding to zero order vibration. The exact energy is given by Eq. (13.12) with the correction for zero order vibration as given in the Vibration Section).

A schematic drawing of the total energy well of hydrogen-type molecules and molecular ions is given in Figure 13.1. The exothermic reaction involving transitions from one potential energy level to a lower level is also hereafter referred to as the Molecular BlackLight Process.

Figure 13.1. The total energy well of hydrogen-type molecules and molecular ions.

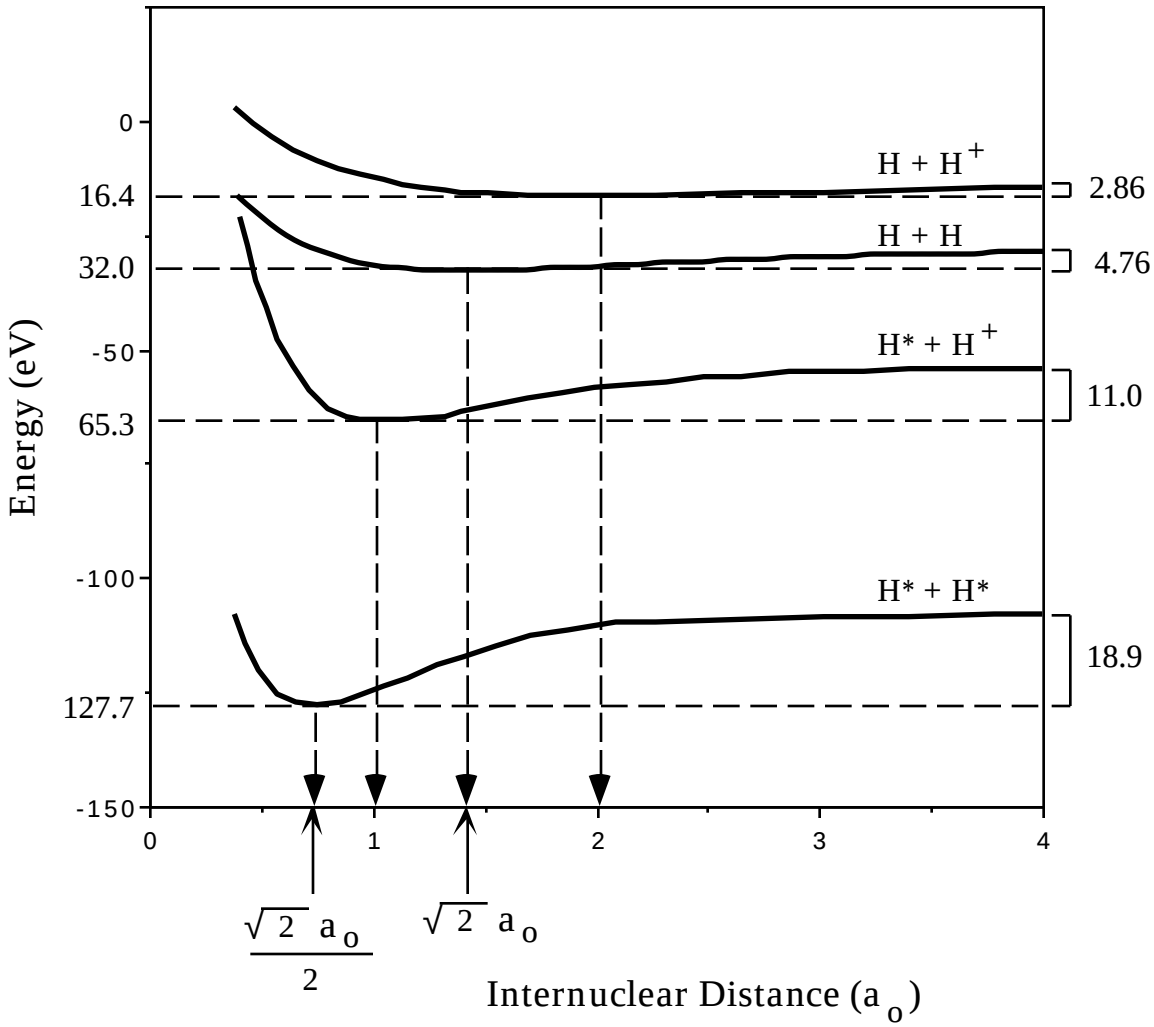

A hydrogen-type molecule with its electrons in a lower than "ground state" energy level corresponding to a fractional quantum number is hereafter referred to as a dihydrino molecule. The designation for a dihydrino molecule of internuclear distance, $2c' = \frac{\sqrt{2}a_o}{p}$ where p is an integer, is $H_2^*\left[2c' = \frac{\sqrt{2}a_o}{p}\right]$. A schematic drawing of the size of hydrogen-type molecules as a function of total energy is given in Figure 13.2.

Figure 13.2. The size of hydrogen-type molecules as a function of total energy.

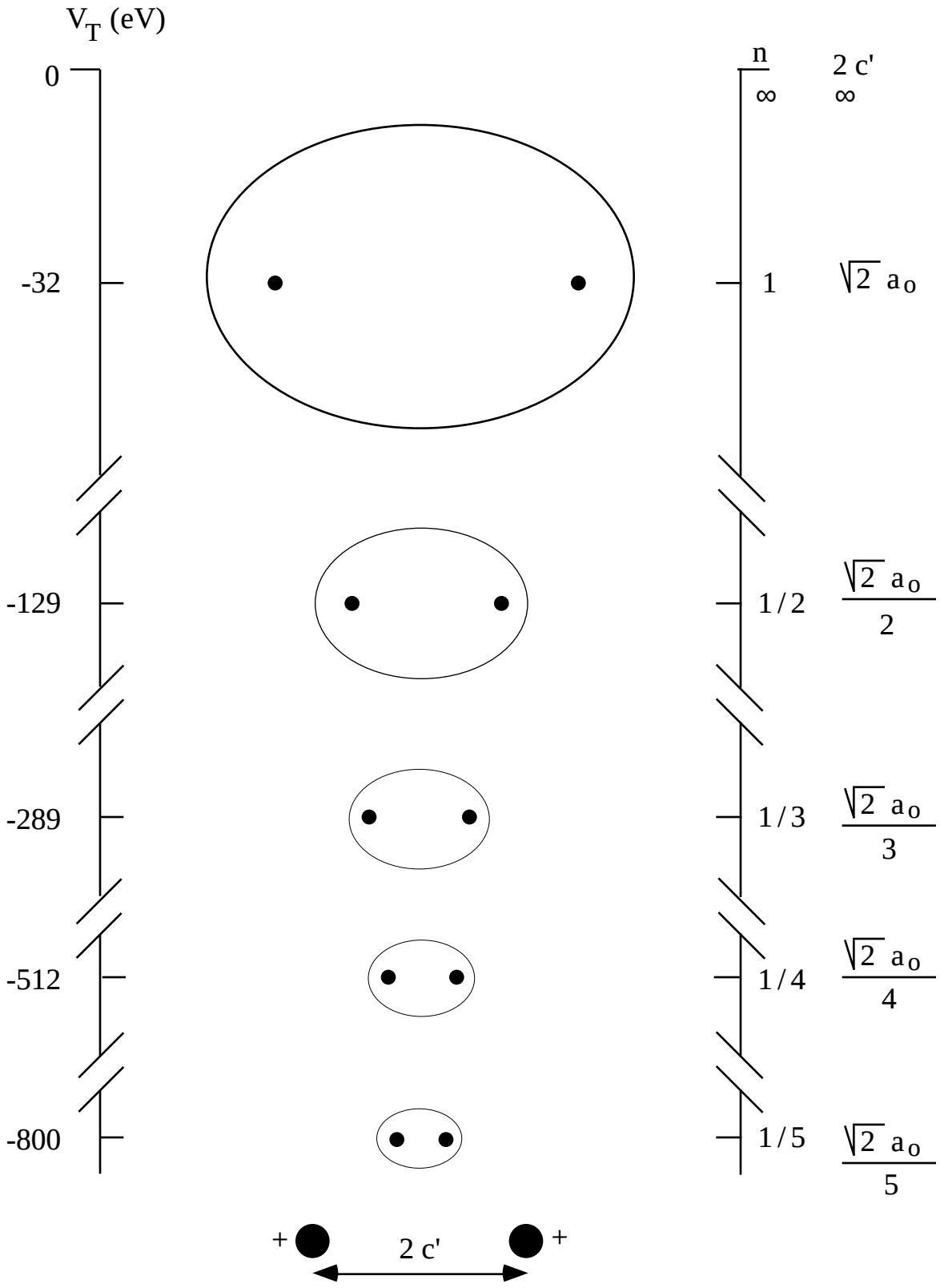

The magnitude of the elliptic field corresponding to the first below "ground state" transition of the hydrogen molecule is 2. From energy conservation, the resonance energy hole of a hydrogen molecule which excites the transition of the hydrogen molecule with internuclear distance $2c' = \sqrt{2}a_o$ to the first below "ground state" with internuclear distance $2c' = \frac{1}{\sqrt{2}}a_o$ is given by Eqs. (13.4-13.8) where the elliptic field is increased from magnitude one to magnitude two:

$$V_e = \frac{-2e^2}{8\pi\varepsilon_o\sqrt{a^2-b^2}}\ln\frac{a+\sqrt{a^2-b^2}}{a-\sqrt{a^2-b^2}} = -67.813\ eV \tag{13.13}$$

$$V_p = \frac{e^2}{8\pi\varepsilon_o\sqrt{a^2-b^2}} = 19.23\ eV \tag{13.14}$$

$$Energy\ hole = -V_e - V_p = 48.6\ eV \tag{13.15}$$

In other words, the elliptic "ground state" field of the hydrogen molecule can be considered as the superposition of Fourier components. The removal of negative Fourier components of energy

$$m\ X\ 48.6\ eV \tag{13.16}$$

where m is an integer, increases the positive electric field inside the ellipsoidal shell by m times the charge of a proton at each focus. The resultant electric field is a time harmonic solution of the Laplacian in ellipsoidal coordinates. The corresponding potential energy change equals the energy absorbed by the energy hole.

$$Energy\ hole = -V_e - V_p = m\ X\ 48.6\ eV \tag{13.17}$$

Further energy is released by the hydrogen molecule as the internuclear distance "shrinks". The hydrogen molecule with internuclear distance $2c' = \sqrt{2}a_o$ is caused to undergo a transition to the below "ground state" level, and the internuclear distance for which force balance and nonradiation are achieved is $2c' = \frac{\sqrt{2}a_o}{1+m}$. In decaying to this internuclear distance from the "ground state", a total energy of

$$-13.6\ eV\left\{2(1+m)^2\sqrt{2} - (1+m)^2\sqrt{2} + \frac{(1+m)^2\sqrt{2}}{2}\ln\frac{\sqrt{2}+1}{\sqrt{2}-1} - (1+m)^2\sqrt{2}\right\}$$
$$+13.6\ eV\left\{2\sqrt{2} - \sqrt{2} + \frac{\sqrt{2}}{2}\ln\frac{\sqrt{2}+1}{\sqrt{2}-1} - \sqrt{2}\right\} \tag{13.18}$$

is released.

CATALYTIC ENERGY HOLES FOR HYDROGEN-TYPE MOLECULES

An efficient catalytic system that hinges on the coupling of three resonator cavities involves iron and lithium. For example, the fourth

ionization energy of iron is 54.8 eV. This energy hole is obviously too high for resonant absorption. However, Li^+ releases 5.392 eV when it is reduced to Li. The combination of Fe^{3+} to Fe^{4+} and Li^+ to Li, then, has a net energy change of 49.4 eV.

$$49.4\ eV + Fe^{3+} + Li^+ + H_2\left[2c' = \sqrt{2}a_o\right] \rightarrow Fe^{4+} + Li + H_2^*\left[2c' = \frac{\sqrt{2}a_o}{2}\right] + 95.7\ eV \quad (13.19)$$

$$Li + Fe^{4+} \rightarrow Li^+ + Fe^{3+} + 49.4\ eV \quad (13.20)$$

And, the overall reaction is

$$H_2\left[2c' = \sqrt{2}a_o\right] \rightarrow H_2^*\left[2c' = \frac{\sqrt{2}a_o}{2}\right] + 95.7\ eV \quad (13.21)$$

Note that the energy given off as the molecule shrinks is much greater than the energy lost to the energy hole. And, the energy released is large compared to conventional chemical reactions.

An efficient catalytic system that hinges on the coupling of three resonator cavities involves scandium. For example, the fourth ionization energy of scandium is 73.47 eV. This energy hole is obviously too high for resonant absorption. However, Sc^{3+} releases 24.76 eV when it is reduced to Sc^{2+}. The combination of Sc^{3+} to Sc^{4+} and Sc^{3+} to Sc^{2+}, then, has a net energy change of 48.7 eV.

$$48.7\ eV + Sc^{3+} + Sc^{3+} + H_2\left[2c' = \sqrt{2}a_o\right] \rightarrow Sc^{4+} + Sc^{2+} + H_2^*\left[2c' = \frac{\sqrt{2}a_o}{2}\right] + 95.7\ eV \quad (13.22)$$

$$Sc^{2+} + Sc^{4+} \rightarrow Sc^{3+} + Sc^{3+} + 48.7\ eV \quad (13.23)$$

And, the overall reaction is

$$H_2\left[2c' = \sqrt{2}a_o\right] \rightarrow H_2^*\left[2c' = \frac{\sqrt{2}a_o}{2}\right] + 95.7\ eV \quad (13.24)$$

An efficient catalytic system that hinges on the coupling of three resonator cavities involves yttrium. For example, the fourth ionization energy of gallium is 64.00 eV. This energy hole is obviously too high for resonant absorption. However, Pb^{2+} releases 15.03 eV when it is reduced to Pb^+. The combination of Ga^{3+} to Ga^{4+} and Pb^{2+} to Pb^+, then, has a net energy change of 48.97 eV.

$$48.97\ eV + Ga^{3+} + Pb^{2+} + H_2\left[2c' = \sqrt{2}a_o\right] \rightarrow Ga^{4+} + Pb^+ + H_2^*\left[2c' = \frac{\sqrt{2}a_o}{2}\right] + 95.7\ eV \quad (13.25)$$

$$Ga^{4+} + Pb^+ \rightarrow Ga^{3+} + Pb^{2+} + 48.97\ eV \quad (13.26)$$

And, the overall reaction is

$$H_2\left[2c' = \sqrt{2}a_o\right] \rightarrow H_2^*\left[2c' = \frac{\sqrt{2}a_o}{2}\right] + 95.7\ eV \quad (13.27)$$

The rates of electronic transitions of molecules is a function of the change in internuclear distance during the transition. Transitions between electronic states that have equivalent internuclear distances at

some point during their vibrational cycles have much greater rates than transitions that require the energy level of the electrons to change as well as the internuclear distance to change simultaneously. As shown in Figure 13.1, the transition from the $n=1$ state to the $n=1/2$ state of molecular hydrogen is not favored for this reason. A more likely transition pathway is a vibrational excitation of molecular hydrogen ($n=1$) that breaks the bond, followed by a transition reaction of each of the hydrogen atoms via a 27.2 eV energy hole catalyst as given in the Atomic Coulomb Field Collapse-Hydrino Theory-BlackLight Process Section, followed by reaction of the two hydrino atoms ($n=1/2$) to form dihydrino molecule ($n=1/2$).

DIATOMIC MOLECULAR ENERGY STATES

EXCITED ELECTRONIC STATES OF ELLIPSOIDAL M.O.'S

Excited states of orbitspheres are discussed in the Excited States of the One Electron Atom (Quantization) Section. In the case of ellipsoidal M. O. 's, excited electronic states are created when photons of discrete frequencies are trapped in the ellipsoidal resonator cavity of the M. O. The photon changes the effective charge at the M. O. surface where the central field is ellipsoidal and arises from the protons at the foci of the M. O. Force balance is achieved at a series of ellipsoidal equipotential two dimensional surfaces confocal with the ground state ellipsoid. The "trapped photons" are solutions of the Laplacian in ellipsoidal coordinates and are given by Eq. (12.27).

MAGNETIC MOMENT OF AN ELLIPSOIDAL M.O.

The magnetic dipole moment, μ, of a current loop is

$$\mu = iA \tag{14.1}$$

The area of an ellipse is given by Eq. (12.25). For any elliptic orbital due to a central field, the frequency, f, is

$$f = \frac{\frac{L}{m}}{2\pi ab} \tag{14.2}$$

where L is the angular momentum. The current, i, is

$$i = ef = \frac{\frac{eL}{m_e}}{2\pi ab} \tag{14.3}$$

where e is the charge. Substitution of Eqs. (14.3) and (12.25) into Eq. (14.1) where L is the angular momentum of the electron, $\hbar$, gives

$$\mu = \frac{e\hbar}{2m_e} \tag{14.4}$$

which is the Bohr magneton.

MAGNETIC FIELD OF AN ELLIPSOIDAL M.O.

The magnetic field can be solved as a magnetostatic boundary value problem which is equivalent to that of a uniformly magnetized ellipsoid.[1] The magnetic scalar potential inside the ellipsoidal M. O., ϕ^-, is

$$\phi^- = \frac{e\hbar}{2m_e} x \int_0^\infty \frac{ds}{(s+a^2)R_s} \tag{14.5}$$

The magnetic scalar potential outside of the M. O., ϕ^+, is

$$\phi^{+} = \frac{e\hbar}{2m_e} x \int_{\xi}^{\infty} \frac{ds}{(s+a^2)R_s} \tag{14.6}$$

The magnetic field inside the ellipsoidal M. O., $\mathbf{H}_x^-$, is

$$\mathbf{H}_x^- = -\frac{\delta\phi^-}{\delta x} = \frac{-e\hbar}{2m_e} \int_0^{\infty} \frac{ds}{(s+a^2)R_s} \tag{14.7}$$

The magnetic field inside the ellipsoidal M. O. is uniform and parallel to the minor axis.

DIATOMIC MOLECULAR VIBRATION

It can be shown that a perturbation of the orbit determined by an inverse square force results in simple harmonic oscillatory motion of the orbit. For the case of a circular orbit of radius a, an approximation of the angular frequency of this oscillation is

$$\omega = \sqrt{\frac{\left[\frac{-3}{a} f(a) + f'(a)\right]}{m}} = \sqrt{\frac{k}{m}} \tag{14.8}$$

Oscillating charges radiate. However, molecules and molecular ions including the hydrogen molecule, the hydrogen molecular ion, dihydrino molecules, and dihydrino molecular ions demonstrate nonradiative zero order vibration which is time harmonic oscillation of the position of the protons along the principal axis. The protons are located at the foci, and nonradiation is due to the geometry of the ellipse where the electron M. O. is ellipsoidal. A fundamental property of an ellipse is that a light ray emitted from a focus in any direction is reflected off of the ellipse to the other focus, and the sum of the lengths of the ray paths is constant, $2a$.

An oscillating charge $r_o(t) = \mathbf{d}\sin\omega_o t$ has a Fourier spectrum

$$\mathbf{J}(\mathbf{k},\omega) = \frac{q\omega_o d}{2} J_m(k\cos\theta d)\{\delta[\omega - (m+1)\omega_o] + \delta[\omega - (m-1)\omega_o]\} \tag{14.9}$$

where J_m's are Bessel functions of order m. These Fourier components can, and do, acquire phase velocities that are equal to the velocity of light. Consider two oscillating charges at the foci of an ellipsoidal resonator cavity, an ellipsoidal M. O. A nonradiative standing electromagnetic wave can be excited which has higher order harmonics in addition to the fundamental frequency as given in Eq. (14.9). This nonradiative standing wave gives rise to zero order vibration of the molecule. The zero order mode is a standing wave with destructive interference of all harmonics of the fundamental frequency, ω_0. A ray undergoes a 180° phase shift upon reflection, and the protons oscillate in opposite relative directions. Thus, mutual destructive interference occurs when x, the distance from one focus to the other for a reflected

ray is equal to a wavelength, λ, where λ is

$$\lambda = \frac{h}{mv} \tag{14.10}$$

It follows that

$$v = \frac{h}{m\lambda} = \frac{h}{mx} \tag{14.11}$$

For time harmonic motion,

$$v = v_{average} = \frac{v_{\max imum}}{\sqrt{2}} \tag{14.12}$$

The kinetic energy, T, is given by

$$T = \frac{1}{2} mv^2 \tag{14.13}$$

The vibrational energy of the protons, E_{Pvib}, is equal to the maximum vibrational kinetic energy of the protons. Substitution of Eqs. (14.11) and (14.12) into Eq. (14.13) and multiplication by two corresponding to the two protons is

$$T = T_{\max} = 2\frac{1}{2} m \frac{h^2}{m^2 x^2} (\sqrt{2})^2 = 2\frac{h^2}{mx^2} \tag{14.14}$$

The vibrational energy is the sum of the vibrational energy of the electron M. O. and that of the protons which are equal.

$$E_{vib} = \frac{4h^2}{mx^2} \tag{14.15}$$

where m is the sum of the masses of the protons, each of mass m_p.

$$m = m_p \tag{14.16}$$

And, X is $2a$. Thus, the vibrational energy is

$$E_{vib} = \frac{h^2}{m_p a^2} \tag{14.17}$$

For a in units of a_o,

$$E_{vib} = \frac{0.59}{a^2}\ eV \tag{14.18}$$

The time average internuclear distance is increased by the zero order vibration because the total energy versus internuclear distance function is asymmetrical with a lower slope for internuclear distances greater than the internuclear distance at which the total energy is a minimum. Elongation occurs along the principal axis, and shifts the total energy versus internuclear distance function to a new function which includes the contribution due to vibration. The perturbation of E_T, the total energy of the M. O. given by Eq. (12.72) with a fractional increase in the semimajor axis, a, and the reciprocal decrease in the semiminor axis, b is calculated by reiteration. The angular frequency of the M.O. given by Eq. (12.24) is unchanged when a and b are changed by reciprocal fractions. The corrected a and b are obtained when the change in E_T is

equal to the vibrational energy. The vibrational energy is the sum of two equal components, the vibrational energy of the protons and the vibrational energy of the electron M. O. Vibration causes a redistribution of energy within the molecule. The M.O. potential and kinetic energy terms given by Eqs. (12.59), (12.61), and (12.72) add π radians out of phase with the potential and kinetic energies of vibration; thus, the energy of the molecule will decrease by this amount which is equal to one half the vibrational energy. An x% increase in the semimajor axis and the reciprocal decrease in the semiminor axis decreases E_T by the vibrational energy and releases energy equal to one half vibrational energy. The vibrational energies and bond distances for hydrogen-type molecules and molecular ions are given in the Nature of the Chemical Bond Section.

Zero order vibration arises because the state is nonradiative and is an energy minimum. Furthermore, electromagnetic radiation of discrete energies given by Eq. (14.18) can be trapped in the resonator cavity where constructive interference occurs at the foci. These standing waves change the electric field at the ellipse surface as described in the Excited Electronic States of Ellipsoidal M. O.'s Section; thus, the major and minor axes increase and the total energy of the molecule given by Eqs. (12.73), (12.74), (12.75), and (12.76) increases. The photons of these standing waves drive the vibration of the molecule at a higher frequency than the zero order frequency, but are reradiated. The energy of a vibrational transition is given by the difference of the sum of the energies of the modes excited before and after the transition. The modes are quantized, and from Eq. (14.18), the energy spacing of the modes is closer together as the total vibrational energy increases.

DIATOMIC MOLECULAR ROTATION

A molecule with a permanent dipole moment can resonantly absorb a photon which excites a rotational mode about the center of mass of the molecule. Nonradiative rotational states require that the space-time Fourier Transform of the rotational current-density function not possess Fourier components synchronous with waves traveling at the speed of light. As demonstrated previously in the Spacetime Fourier Transform of the Electron Function Section, the product of a radial Dirac delta function, two spherically harmonic angular functions, and a time harmonic function is nonradiative and is a solution of the wave equation (Eq. (1.11)). Furthermore, momentum must be conserved with excitation of a rotational mode. The photon carries $\hbar$ of angular momentum; thus, the rotational angular momentum of the molecule changes by $\hbar$. And, the rotational charge-density function is equivalent to the rigid rotor problem considered in the Rotational Parameters of the

Electron (Angular Momentum, Rotational Energy, Moment of Inertia) Section with the exception that for a diatomic molecule having atoms of masses m_1 and m_2, the moment of inertia is

$$I = \mu r^2 \tag{14.19}$$

where μ is the reduced mass

$$\mu = \frac{m_1 m_2}{m_1 + m_2} \tag{14.20}$$

and where r is the distance between the centers of the atoms, the internuclear distance. The rotational energy levels follow from Eq. (1.95)

$$E_{rotational\,orbital} = \frac{\hbar^2}{2I} J(J+1) \tag{14.21}$$

where J is an integer. For Eq. (14.21), $J = 0$ corresponds to rotation about the z-axis where the internuclear axis is along the y-axis, and $J \neq 0$ corresponds to a linear combination of rotations about the z and x-axis.

As given in the Selection Rules Section, the radiation of a multipole of order (l, m) carries $m\hbar$ units of the z component of angular momentum per photon of energy $\hbar\omega$. Thus, the z component of the angular momentum of the corresponding excited rotational state is

$$L_z = m\hbar \tag{14.22}$$

Thus, the selection rule for rotational transitions is

$$\Delta J = \pm 1 \tag{14.23}$$

In addition, the molecule must posses a permanent dipole moment. In the case of absorption of electromagnetic radiation, the molecule goes from a state with a quantum number J to one with a quantum number of $J+1$. Using Eq. (14.21), the energy difference is

$$\Delta E = E_{J+1} - E_J = \frac{\hbar^2}{I}[J+1] \tag{14.24}$$

DIATOMIC MOLECULAR ROTATION OF HYDROGEN-TYPE MOLECULES

The reduced mass of hydrogen-type molecules, μ_{H_2}, having two protons is given by Eq. (14.20) where $m_1 = m_2 = m_p$, and m_p is the mass of the proton.

$$\mu_{H_2} = \frac{m_p m_p}{m_p + m_p} = \frac{1}{2} m_p \tag{14.25}$$

The moment of inertia of hydrogen-type molecules is given by substitution of the reduced mass, Eq. (14.25), for μ of Eq. (14.19) and substitution of the internuclear distance, two times Eq. (12.95), for r of Eq. (14.19).

$$I = m_p \frac{a_o^2}{n^2} \tag{14.26}$$

where n is an integer which corresponds to , $\frac{1}{n}$, the fractional quantum number of the hydrogen-type molecule. Using Eqs. (14.24) and (14.26), the rotational energy absorbed by a hydrogen-type molecule with the transition from the state with the rotational quantum number J to one with the rotational quantum number $J+1$ is

$$\Delta E = E_{J+1} - E_J = \frac{n^2\hbar^2}{m_p a_o^2}[J+1] = n^2[J+1]\,2.37\ X\ 10^{-21}\ J \tag{14.27}$$

The energy can be expressed in terms of wavelength in angstroms (Å) using the Planck relationship, Eq. (2.65).

$$\lambda = 10^{10}\frac{hc}{\Delta E}\ \text{Å} = \frac{8.38\ X\ 10^5}{n^2[J+1]}\ \text{Å} \tag{14.28}$$

Vibration increases the internuclear distance, r of Eq. (14.19), which decreases the rotational energy. The rotational wavelength including vibration given in the Vibration of Hydrogen -Type Molecules Section is

$$\lambda = \frac{8.43\ X\ 10^5}{n^2[J+1]}\ \text{Å} \tag{14.29}$$

The calculated wavelength for the $J=0$ to $J=1$ transition of the hydrogen molecule $H_2(n=1)$ including vibration is $8.43\ X\ 10^5\ Å$. The experimental value is $8.43X10^5\ Å$. The wavelength calculated from Eq. (14.29) for the $J=0$ to $J=1$ transition of the hydrogen-type molecule $H_2^*\left(2c' = \frac{\sqrt{2}a_o}{p}\right)$ including vibration is given in Table 14.1.

The rotational wavelength for $p=8$ is given in Table 14.1 as $13{,}175\ Å$. Recently, an interstellar band has been discovered for which no satisfactory assignment exists [2]. The experimentally measured wavelength which matches the predicted wavelength is $13{,}175\ Å$.

Table 14.1. The wavelength calculated from Eq. (14.29) for the $J = 0$ to $J = 1$ transition of the hydrogen-type molecule $H_2^*\left(2c' = \frac{\sqrt{2}a_o}{p}\right)$ including vibration.

p of $H_2\left(\frac{1}{p}\right)$	Lambda (Å)
1	$8.431\ X\ 10^5$
2	$2.108\ X\ 10^5$
3	$9.368\ X\ 10^4$
4	$5.269\ X\ 10^4$
5	$3.372\ X\ 10^4$
6	$2.342\ X\ 10^4$
7	$1.721\ X\ 10^4$
8	$1.317\ X\ 10^4$
9	$1.041\ X\ 10^4$
10	$8.431\ X\ 10^3$
11	$6.968\ X\ 10^3$
12	$5.855\ X\ 10^3$
13	$4.989\ X\ 10^3$
14	$4.302\ X\ 10^3$
15	$3.747\ X\ 10^3$
16	$3.293\ X\ 10^3$
17	$2.917\ X\ 10^3$
18	$2.602\ X\ 10^3$

DIATOMIC MOLECULAR ROTATION OF HYDROGEN-TYPE MOLECULAR IONS

The moment of inertia of hydrogen-type molecular ions is given by substitution of the reduced mass, Eq. (14.25), for μ of Eq. (14.19) and substitution of the internuclear distance, two times Eq. (12.67), for r of Eq. (14.19).

$$I = m_p \frac{2a_o^2}{n^2} \tag{14.30}$$

where n is an integer which corresponds to , $\frac{1}{n}$, the fractional quantum number of the hydrogen-type molecular ion. Using Eqs. (14.24) and (14.26), the rotational energy absorbed by a hydrogen-type molecular ion with the transition from the state with the rotational quantum number J to one with the rotational quantum number $J+1$ is

$$\Delta E = E_{J+1} - E_J = \frac{n^2\hbar^2}{m_p 2a_o^2}[J+1] = n^2[J+1]\ 1.89\,X\,10^{-21}\ J \tag{14.31}$$

The energy can be expressed in terms of wavelength in microns (μm) using the Planck relationship, Eq. (2.65).

$$\lambda = 10^6 \frac{hc}{\Delta E}\ \mu m = \frac{168}{n^2[J+1]}\ \mu m \tag{14.32}$$

Vibration increases the internuclear distance, r of Eq. (14.19), which decreases the rotational energy. The rotational wavelength including vibration given in the Vibration of Hydrogen -Type Molecular Ions Section is

$$\lambda = \frac{169}{n^2[J+1]}\ \mu m \tag{14.33}$$

The calculated wavelength for the $J=0$ to $J=1$ transition of the hydrogen molecular ion $H_2[2c' = 2a_o]^+$ including vibration is 169 μm. The experimental value is 169 μm. The wavelength calculated from Eq. (14.33) for the $J=0$ to $J=1$ transition of the hydrogen-type molecular ion $H_2^*\left[2c' = \frac{2a_o}{p}\right]^+$ including vibration is given in Table 14.2.

The rotational wavelength for $p=6$ given in Table 14.2 is 4.7 μm. A broad 4.7 μm solar chromospheric absorption line is observed which was previously assigned to cool carbon monoxide clouds; however, the temperature of the chromosphere, $>6000\,K$, is higher than that at which carbon monoxide completely decomposes into carbon and oxygen, $<4000\,K$ [3]. The assignment of the 4.7 μm absorption line to the $J=0$ to $J=1$ transition rotational transition of $H_2^*\left[2c' = \frac{a_o}{3}\right]^+$ provides a resolution of the problem of cool carbon monoxide clouds.

Table 14.2. The wavelength calculated from Eq. (14.33) for the $J = 0$ to $J = 1$ transition of the hydrogen-type molecular ion $H_2^*\left(2c' = \frac{2a_o}{p}\right)^+$ including vibration.

p of $H_2^+\left(\frac{1}{p}\right)$	Lambda (μm)
1	$1.69\ X\ 10^2$
2	42.2
3	18.7
4	10.5
5	6.74
6	4.68
7	3.44
8	2.63
9	2.08
10	1.69
11	1.39
12	1.17
13	0.998
14	0.860
15	0.749
16	0.659
17	0.583
18	0.520

References

1. See Stratton, J. A., Electromagnetic Theory, McGraw-Hill Book Company, (1941), p. 257.
2. C. Joblin, J. P. Maillard, L. d'Hendecourt, and A. Leger, Nature, 346, (1990), pp. 729-732.
3. Phillips, J. H., Guide to the Sun, Cambridge University Press, Cambridge, Great Britain, (1992), pp. 126-127; 360.

SECTION II

Collective Phenomena

STATISTICAL MECHANICS

The distribution functions of statistical mechanics according to the Mills theory are as usual [1]. However, the nature of each distribution is related to the present classical quantum mechanical model. The underlying physics is deterministic which can be modeled with chaos theory.

Bose-Einstein- indistinguishable photons having $\hbar$ of angular momentum excite quantized energy levels of electron resonator cavities where superposition and conservation of angular momentum are obeyed.

Fermi-Dirac- identical, indistinguishable electrons occupy the lowest energy configuration as given in the Two Electron Atom Section. The Pauli Exclusion Principle arises as a minimum of energy for interacting electrons each having a Bohr magneton of magnetic moment.

Maxwell-Boltzmann- identical, discrete particles such as molecules which are separated such that the predominant interaction is scattering possess a continuum of momenta.

References

1. Beiser, A., Concepts of Modern Physics, Fourth Edition, McGraw-Hill Book Company, New York, (1978), pp. 312-354.

In the case of a superconductor, an applied voltage gives rise to a transient constant electric field in the z direction

$$\mathbf{E}_z = r\cos\theta\mathbf{i}_z \tag{16.1}$$

$$\mathbf{E}_z = E_0\mathbf{i}_z \tag{16.2}$$

where $\mathbf{i}_z$ is the unit vector along the z-axis.

The applied field polarizes the material into a superconducting current comprised of current dipoles-magnetic dipoles. In Cartesian coordinates, the magnetic field, **H**, at the point (x,y,z) due to a magnetic dipole having a magnetic dipole moment of a Bohr magneton, μ_B, at the position (x_0,y_0,z_0) is

$$\mathbf{H} = \frac{\mu_B\left(2(z-z_0)^2-(x-x_0)^2-(y-y_0)^2\right)}{[(x-x_0)^2+(y-y_0)^2+(z-z_0)^2]^{5/2}}\mathbf{i}_z \tag{16.3}$$

$$\mathbf{H} = \frac{\left(2z^2-x^2-y^2\right)}{[x^2+y^2+z^2]^{5/2}} \quad \mu_B\delta(x-x_0,y-y_0,z-z_0)\mathbf{i}_z \tag{16.4}$$

The field is the convolution of the system function, $h(x,y,z)$ *or* $h(\rho,\phi,z)$, (the left-handed part of Eq. (16.4)) with the delta function (the right-hand part of Eq. (16.4)) at the position (x_0,y_0,z_0). A very important theorem of Fourier analysis states that the Fourier Transform of a convolution is the product of the individual Fourier Transforms [1]. The Fourier Transform of the system function, $h(x,y,z)$ *or* $h(\rho,\phi,z)$, is given in Box 16.1.

BOX 16.1. FOURIER TRANSFORM OF THE SYSTEM FUNCTION

The system function, $h(\rho,\phi,z)$, in cylindrical coordinates is

$$h(\rho,\phi,z) = \frac{2z^2-x^2-y^2}{[x^2+y^2+z^2]^{5/2}} = \frac{2z^2-\rho^2}{[\rho^2+z^2]^{5/2}} \tag{1}$$

The spacetime Fourier transform in three dimensions in cylindrical coordinates, $H(k_\rho,\Phi,k_z)$, is given [1] as follows:

$$H(k_\rho,\Phi,k_z) = \int_{-\infty}^{\infty}\int_0^{2\pi}\int_0^{\infty} h(\rho,\phi,z)\exp\left(-i2\pi\left[k_\rho\rho\cos(\Phi-\phi)+k_z z\right]\right)\rho d\rho d\phi dz \tag{2}$$

With circular symmetry [1]

$$H(k_\rho,k_z) = 2\pi\int_0^{\infty}\int_{-\infty}^{\infty} h(\rho,z)J_o(k_\rho\rho)e^{-iwz}\rho d\rho dz \tag{3}$$

The Fourier transform of the system function is given by the substitution of Eq. (1) into Eq. (3).

$$H = \int_{-\infty}^{\infty} 2\pi \int_0^{\infty} \frac{2z^2 - \rho^2}{[\rho^2 + z^2]^{5/2}} J_0[k_\rho \rho] \rho d\rho e^{-jk_z z} dz \tag{4}$$

Consider the integral of Eq. (4) with respect to $d\rho$ only. Factorization of $h(\rho, \phi, z)$ gives

$$2\pi \int_0^{\infty} \left[\frac{2z^2 \rho}{[\rho^2 + z^2]^{5/2}} - \frac{\rho^3}{[\rho^2 + z^2]^{5/2}} \right] J_0[k_\rho \rho] d\rho \tag{5}$$

Consider the definite integral

$$\int_0^{\infty} \frac{t^{v+1} J_v[at] dt}{[t^2 + z^2]^{u+1}} = \frac{a^u z^{v-u} K_{v-u}[az]}{2^u \Gamma[u+1]} \tag{6}$$

and the modified Bessel function of the third kind relationship,

$$K_{-\upsilon}[x] = K_{\upsilon}[x] \tag{7}$$

The first factor of Eq. (5) is the same form as Eq. (6) with $v = 0; u = \frac{3}{2}$, thus,

$$2z^2 (2\pi) \int_0^{\infty} \frac{\rho}{[\rho^2 + z^2]^{5/2}} J_o[k_\rho \rho] d\rho = \frac{2z^2 (2\pi) k_\rho^{3/2} z^{-3/2}}{2^{3/2} \Gamma[5/2]} K_{-3/2}[k_\rho z] = \frac{[2^{1/2}] \pi z^{1/2} k_\rho^{3/2}}{\Gamma[5/2]} K_{3/2}[k_\rho z] \tag{8}$$

where $K_{-3/2}[k_\rho z] = K_{3/2}[k_\rho z]$ (Eq. (7)). The second factor of Eq. (5) can be made into the same form as Eq. (6) using the Bessel function of the first kind recurrence relationship

$$J_{v-1}[x] + J_{v+1}[x] = \frac{2v}{x} J_v[x] \tag{9}$$

Consider the second factor of the integral of Eq. (5).

$$-2\pi \int_0^{\infty} \frac{\rho^3}{[\rho^2 + z^2]} J_o[k_p \rho] d\rho \tag{10}$$

Eq. (9) with $\upsilon = 1$ is

$$J_o[x] + J_2[x] = \frac{2}{x} J_1[x] \tag{11}$$

$$J_0[x] = \frac{2}{x} J_1[x] - J_2[x] \tag{12}$$

Let

$$x = k_\rho \rho \tag{13}$$

Substitution of Eq. (13) into Eq. (12) is

$$J_o[k_\rho \rho] = \frac{2}{k_\rho \rho} J_1[k_\rho \rho] - J_2[k_\rho \rho] \tag{14}$$

Substitution of Eq. (10) into Eq. (14) is

$$\begin{aligned} -2\pi \int_0^{\infty} \frac{\rho^3}{[\rho^2 + z^2]} J_o[k_\rho \rho] d\rho &= -2\pi \int_0^{\infty} \frac{\rho^3}{[\rho^2 + z^2]^{5/2}} \left[\frac{2}{k_\rho \rho} J_1[k_\rho \rho] - J_2[k_\rho \rho] \right] d\rho \\ &= -2\pi \int_0^{\infty} \frac{2\rho^2}{k_\rho [\rho^2 + z^2]^{5/2}} J_1[k_\rho \rho] d\rho + 2\pi \int_0^{\infty} \frac{\rho^3}{[\rho^2 + z^2]^{5/2}} J_2[k_\rho \rho] d\rho \end{aligned} \tag{15}$$

The first factor of the right hand side of Eq. (15) is the same form as Eq.

(6) with $\nu = 1; u = \frac{3}{2}$, thus,

$$-2\pi\int_0^\infty \frac{2\rho^2}{k_\rho[\rho^2+z^2]^{5/2}} J_1[k_\rho\rho]d\rho = \frac{-(4\pi)k_\rho^{3/2}z^{-1/2}}{k_\rho 2^{3/2}\Gamma[5/2]} K_{-1/2}[k_\rho z] = -\frac{\left[2^{1/2}\right]\pi z^{-1/2}k_\rho^{1/2}}{\Gamma[5/2]} K_{1/2}[k_\rho z] \quad (16)$$

where $K_{-1/2}[k_\rho z] = K_{1/2}[k_\rho z]$ (Eq.(7)). The second factor of the right hand side of Eq. (15) is the same form as Eq. (6) with $\nu = 2; u = \frac{3}{2}$, thus,

$$2\pi\int_0^\infty \frac{\rho^3}{[\rho^2+z^2]^{5/2}} J_2[k_\rho\rho]d\rho = \frac{(2\pi)k_\rho^{3/2}z^{1/2}}{2^{3/2}\Gamma[5/2]} K_{1/2}[k_\rho z] = \frac{\pi z^{1/2}k_\rho^{3/2}}{\left[2^{1/2}\right]\Gamma[5/2]} K_{1/2}\left[k_\rho z\right] \quad (17)$$

Combining the parts of the integration with respect to $d\rho$ of Eq. (4) by adding Eq. (8), Eq. (16), and Eq. (17) gives

$$\int_{-\infty}^{\infty} \left\{\frac{\left[2^{1/2}\right]\pi z^{1/2}k_\rho^{1/2}}{\Gamma[5/2]} K_{3/2}[k_\rho z] - \frac{\left[2^{1/2}\right]\pi z^{1/2}k_\rho^{1/2}}{\Gamma[5/2]} K_{1/2}[k_\rho z] + \frac{\pi z^{1/2}k_\rho^{3/2}}{\left[2^{1/2}\right]\Gamma[5/2]} K_{1/2}[k_\rho z]\right\} e^{-jk_z z}dz \quad (18)$$

The modified Bessel function of the third kind formulae is

$$K_{n+1/2}[x] = \left[\frac{\pi}{2x}\right]^{1/2} e^{-x}\sum_{m=0}^{n}[2x]^{-m}\frac{\Gamma[n+m+1]}{m!\Gamma[n+1-m]} \quad (19)$$

Substitution of Eq. (13) into Eq. (19) with $\upsilon = 1$ is

$$K_{3/2}[k_\rho z] = \left[\frac{\pi}{2k_\rho z}\right]^{1/2} e^{-k_\rho z}\left[1+\frac{1}{2k_\rho z}\Gamma[3]\right] \quad (20)$$

Substitution of Eq. (13) into Eq. (19) with $\upsilon = 0$ is

$$K_{1/2}[k_\rho z] = \left[\frac{\pi}{2k_\rho z}\right]^{1/2} e^{-k_\rho z} \quad (21)$$

Substitution of Eq. (20) and Eq. (21) into Eq. (18) is

$$\int_{-\infty}^{\infty}\left\{\frac{(2^{1/2})\pi z^{1/2}k_\rho^{3/2}}{\Gamma[5/2]}\left[1+\frac{1}{2k_\rho z}\Gamma[3]\right] - \frac{(2^{1/2})\pi z^{1/2}k_\rho^{1/2}}{\Gamma[5/2]} + \frac{\pi z^{1/2}k_\rho^{3/2}}{(2^{1/2})\Gamma[5/2]}\left[\frac{\pi}{2k_\rho z}\right]^{1/2}\right\} e^{-k_\rho z}e^{-jk_z z}dz \quad (22)$$

$$\int_{-\infty}^{\infty}\left\{\frac{\pi^{3/2}}{\Gamma[5/2]}k_\rho e^{-[jk_z+k_\rho]z} + \frac{z^{-1}\pi^{3/2}\Gamma[3]}{\Gamma[5/2]2}e^{-[jk_z+k_\rho]z} - \frac{z^{-1}\pi^{3/2}}{\Gamma[5/2]}e^{-[jk_z+k_\rho]z} + \frac{\pi^{3/2}}{\Gamma[5/2]2}k_\rho e^{-[jk_z+k_\rho]z}\right\}dz \quad (23)$$

Collecting terms gives

$$\int_{-\infty}^{\infty}\frac{\pi^{3/2}}{\Gamma[5/2]}\left\{k_\rho[1+1/2]+\left[\frac{\Gamma[3]}{2}-1\right]z^{-1}\right\}e^{-[jk_z+k_\rho]z}dz \quad (24)$$

With $\Gamma[3] = 2$ and $\Gamma[5/2] = 3/4\pi^{1/2}$, Eq. (24) is

$$\int_{-\infty}^{\infty}\frac{\pi^{3/2}}{\Gamma[5/2]}\left\{k_\rho[3/2]+[1-1]z^{-1}\right\}e^{-k_\rho z}e^{-jk_z z}dz \quad (25)$$

$$\int_{-\infty}^{\infty}\frac{\pi^{3/2}}{3/4\pi^{1/2}}3/2k_\rho e^{-k_\rho z}e^{-jk_z z}dz \quad (26)$$

$$2\pi k_\rho \int_{-\infty}^{\infty} e^{-k_\rho z} e^{-jk_z z} dz \tag{27}$$

$$4\pi k_\rho \int_{0}^{\infty} e^{-k_\rho z} e^{-jk_z z} dz \tag{28}$$

$$4\pi k_\rho \int_{0}^{\infty} e^{-[jk_z + k_\rho]z} dz \tag{29}$$

Integration of Eq. (29) with respect to *dz* gives

$$4\pi k_\rho \left\{ \frac{-1}{jk_z + k_\rho} e^{-[jk_z + k_\rho]z} \Big|_0^{\infty} \right\} \tag{30}$$

$$4\pi k_\rho \left[\frac{1}{jk_z + k_\rho} \right] \tag{31}$$

Multiplication of Eq. (31) by

$$1 = \left[\frac{-jk_z + k_\rho}{-jk_z + k_\rho} \right] \tag{32}$$

gives

$$4\pi k_\rho \left[\frac{-jk_z + k_\rho}{k_z^{\,2} + k_\rho^{\,2}} \right] \tag{33}$$

The system function (Eq. (1)) is an even function; thus, the spacetime Fourier transform in three dimensions in cylindrical coordinates, $H(k_\rho, k_z)$, is given by taking the real part of Eq. (33) [2].

$$H[k_\rho, k_z] = \frac{4\pi k_\rho^{\,2}}{k_z^{\,2} + k_\rho^{\,2}} \tag{34}$$

The spacetime Fourier transform in three dimensions in Cartesian coordinates, $H(k_\rho, k_z)$, is

$$H[k_x, k_y, k_z] = \frac{4\pi[k_x^{\,2} + k_y^{\,2}]}{[k_x^{\,2} + k_y^{\,2} + k_z^{\,2}]} \tag{35}$$

where the relationship between the wavenumbers and the spatial Cartesian coordinates is as follows:

$$k_x = \frac{2\pi}{\lambda_x} = \frac{1}{x} \tag{36}$$

$$k_y = \frac{2\pi}{\lambda_y} = \frac{1}{y} \tag{37}$$

$$k_z = \frac{2\pi}{\lambda_z} = \frac{1}{z} \tag{38}$$

References

1. Bracewell, R. N., The Fourier Transform and Its Applications, McGraw-Hill Book Company, New York, (1978), pp. 252-253.
2. Siebert, W. McC., Circuits, Signals, and Systems, The MIT Press, Cambridge, Massachusetts, (1986), p. 399.

BAND-PASS FILTER

The z component of a magnetic dipole oriented in the z direction has the system function, $h(x,y,z)$, which has the Fourier Transform, $H[k_x,k_y,k_z]$, which is shown in Figure 16.1.

$$H[k_x,k_y,k_z] = \frac{4\pi[k_x^2 + k_y^2]}{[k_x^2 + k_y^2 + k_z^2]} \tag{16.5}$$

$$= H[k_\rho,k_z] = \frac{4\pi k_\rho^2}{k_z^2 + k_\rho^2} = \frac{4\pi}{1 + \frac{k_z^2}{k_\rho^2}} \tag{16.6}$$

Figure 16.1. The Fourier Transform $H[k_x,k_y,k_z]$ of the system function $h(x,y,z)$ corresponding to the z component of a magnetic dipole oriented in the z direction.

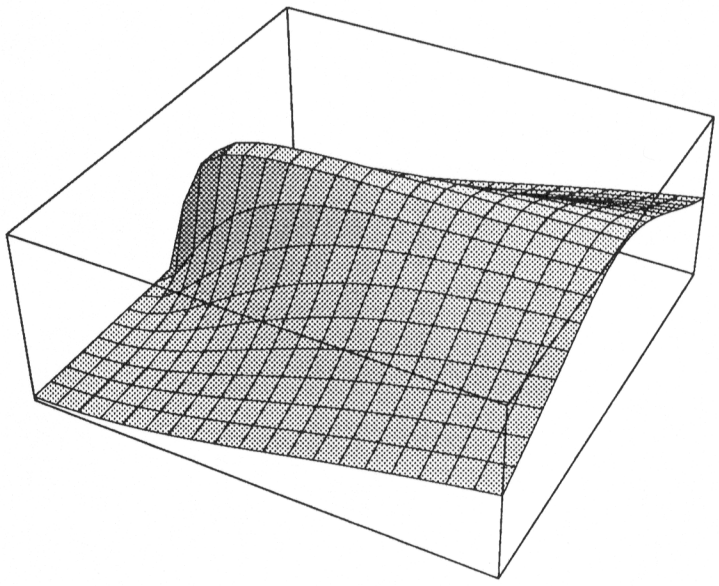

As shown in the Electron Scattering by Helium Section, in the far field, the amplitude of the scattered electromagnetic radiation or scattered electron flux density is the Fourier Transform of the aperture function. In the case of a superconductor, the electric field is zero-no voltage drop occurs; however, a magnetic field is present. The relationship between the amplitude of the scattered energy and the Fourier Transform of the aperture function can be applied to the present case of the scattering of magnetic energy by the lattice of the potential superconductor. The spatial aperture function is the convolution of the

array pattern with the elemental pattern. The elemental pattern is the system function, $h(x,y,z)$,-the geometric transfer function for the z component of a z oriented magnetic dipole. And, the array pattern is a periodic array of delta functions each at the position of a magnetic dipole corresponding to a current carrying electron.

$$\frac{\left(2z^2 - x^2 - y^2\right)}{[x^2 + y^2 + z^2]^{5/2}} \quad \sum_{n=-\infty}^{\infty} \mu_B \delta\left(x - nx_0, y - ny_0, z - nz_0\right) \tag{16.7}$$

The Fourier Transform of a periodic array of delta functions (the right-hand side of Eq. (16.7)) is also a periodic array of delta functions in k-space

$$\frac{1}{x_0 y_0 z_0} \sum_{n=-\infty}^{\infty} \mu_B \delta\left(k_x - \frac{n}{x_0}, k_y - \frac{n}{y_0}, k_z - \frac{n}{z_0}\right) \tag{16.8}$$

By the Fourier Theorem, the Fourier Transform of the spatial aperture function, Eq. (16.7), is the product of the Fourier Transform of the elemental function, system function given by Eq. (16.6), and the Fourier Transform of the array function given by Eq. (16.8).

$$\frac{4\pi}{1 + \frac{k_z^2}{k_\rho^2}} \frac{1}{x_0 y_0 z_0} \sum_{n=-\infty}^{\infty} \mu_B \delta\left(k_x - \frac{n}{x_0}, k_y - \frac{n}{y_0}, k_z - \frac{n}{z_0}\right) \tag{16.9}$$

The space-time aperture function corresponding to the current-density function is given by multiplying the spatial aperture function (Eq. (16.7)) by a time harmonic function

$$\exp(-i\omega t) \tag{16.10}$$

Thus, the space-time aperture function is

$$\frac{\left(2z^2 - x^2 - y^2\right)}{[x^2 + y^2 + z^2]^{5/2}} \quad \sum_{n=-\infty}^{\infty} \mu_B \delta\left(x - nx_0, y - ny_0, z - nz_0\right) \exp(-i\omega t) \tag{16.11}$$

The Fourier Transform of the time harmonic function (Eq. (16.10)) is

$$\frac{[\delta(\omega - \omega_z) + \delta(\omega + \omega_z)]}{2} \tag{16.12}$$

A very important theorem of Fourier analysis states that the Fourier Transform of a product is the convolution of the individual Fourier Transforms. Thus, the Fourier Transform of Eq. (16.11) is the convolution of Eqs. (16.9) and (16.12)

$$\frac{4\pi}{1 + \frac{k_z^2}{k_\rho^2}} \frac{1}{x_0 y_0 z_0} \sum_{n=-\infty}^{\infty} \mu_B \delta\left(k_x - \frac{n}{x_0}, k_y - \frac{n}{y_0}, k_z - \frac{n}{z_0}\right) \frac{[\delta(\omega - \omega_z) + \delta(\omega + \omega_z)]}{2} \tag{16.13}$$

In the special case that

$$k_\rho = k_z \tag{16.14}$$

the Fourier Transform of the system function (the left-hand side of Eq. (16.13)) is given by

$$H = 4\pi \tag{16.15}$$

Thus, the Fourier Transform of the system function band-passes the Fourier Transform of the time dependent array function. Both the space-time aperture function, Eq. (16.11) and its Fourier Transform, Eq. (16.13), are a periodic array of delta functions. No frequencies of the Fourier Transform of the space-time aperture function are attenuated; thus, no energy is lost in this special case where Eq. (16.14) holds. (This result is also central to a powerful new medical imaging technology-Resonant Magnetic Susceptibility Imaging (ReMSI) [2-3]). No energy loss corresponds to a superconducting state. And the relationship between k-space and real space is

$$\begin{aligned} k_x &= \frac{2\pi}{\lambda_x} = \frac{1}{x} \\ k_y &= \frac{2\pi}{\lambda_y} = \frac{1}{y} \\ k_z &= \frac{2\pi}{\lambda_z} = \frac{1}{z} \end{aligned} \tag{16.16}$$

From Eqs. (16.14) and (16.16), it follows that a cubic array ($x_0 = y_0 = z_0$) of magnetic dipoles centered on the nuclei of the lattice is a superconductor when the temperature is less than the critical temperature such that the superconducting electrons can propagate. Propagating electrons which carry the superconducting current and comprise magnetic dipoles form standing waves centered on the nuclear centers of the cubic lattice. Fermi-Dirac statistic apply to electrons as given in the Statistical Mechanics Section. It follows from Eqs. (16.14) and (16.16) that the Fermi energy is calculated for a cubical cavity L on a side. The number standing waves in a cubical cavity L on a side is given by Eq. (9.33) of Beiser [4]

$$g(j)dj = \pi j^2 dj \tag{16.17}$$

where

$$j = \frac{2L}{\lambda} \tag{16.18}$$

The de Broglie wavelength of an electron is

$$\lambda = \frac{h}{p} \tag{16.19}$$

Electrons in superconductors have non relativistic velocities; so,

$$p = \sqrt{2m_e\varepsilon} \tag{16.20}$$

and

$$j = \frac{2L}{\lambda} = \frac{2Lp}{h} = \frac{2L\sqrt{2m_e\varepsilon}}{h} \tag{16.21}$$

$$dj = \frac{L}{h}\sqrt{\frac{2m_e}{\varepsilon}}d\varepsilon \tag{16.22}$$

Using these expressions for j and dj in Eq. (16.17) gives

$$g(\varepsilon)d\varepsilon = \frac{8\sqrt{2}\pi L^3 m_e^{3/2}}{h^3}\sqrt{\varepsilon}\,d\varepsilon \tag{16.23}$$

Substitution of V for L^3 gives the number of electron states, $g(\varepsilon)$

$$g(\varepsilon)d\varepsilon = \frac{8\sqrt{2}\pi V m_e^{3/2}}{h^3}\sqrt{\varepsilon}\,d\varepsilon \tag{16.24}$$

The Fermi energy, E_F, is calculated by equating the number of free electrons, N, to the integral over the electron states of energy ε from zero to the highest energy, the Fermi energy, $E = E_F$.

$$N = \int_0^{E_F} g(\varepsilon)d\varepsilon = \frac{8\sqrt{2}\pi V m_e^{3/2}}{h^3}\int_0^{E_F}\sqrt{\varepsilon}\,d\varepsilon \tag{16.25}$$

$$= \frac{16\sqrt{2}\pi V m_e^{3/2}}{3h^3}E_F^{3/2} \tag{16.26}$$

and the Fermi energy is

$$E_F = \frac{h^2}{2m_e}\left(\frac{3N}{8\pi V}\right)^{2/3} = \frac{h^2}{2m_e}\left(\frac{3}{8\pi}\right)^{2/3} n^{2/3} \tag{16.27}$$

The quantity $N/V = n$ is the density of free electrons.

In the case of superconducting electrons, comprising an array of magnetic dipoles (each dipole in the xy-plane and oriented along the z-axis), the dimensions of Eq. (9.33) of Beiser [4] is reduced to 2 from 3.

$$2\frac{1}{4}2\pi j = g(j) \tag{16.28}$$

For $g(j) = 1$ with the substitution of Eq. (16.18),

$$2\pi L = \lambda \tag{16.29}$$

As the temperature of a superconducting material rises from a temperature below the critical temperature, T_c, the number density, n_s, of superconducting electrons decreases. At the transition temperature, the superconducting electrons condense into a nondissipative electron current ensemble which obeys the statistics of a Bose gas (each electron is identical and indistinguishable as indicated in Eq. (16.8) with the constraint of Eq. (16.14)), and Eqs. (16.28) and (16.29) apply

$$\left(\frac{2\pi}{\lambda}\right)^3 = \left(\frac{1}{L}\right)^3 = n_s \tag{16.30}$$

where

$$n_s E_F = n k_B T_c \tag{16.31}$$

n_s is the number density of superconducting electrons within $k_B T_c$ of the Fermi energy and n is the number density of free electrons. The current carried by each superconducting electron corresponds to a translational

or kinetic energy. The relationship between the electron de Broglie wavelength (Eqs. (16.19) and (16.20)) and the average electron energy, $\bar{\varepsilon}$, per degree of freedom, f, given by Beiser [5]

$$\bar{\varepsilon} = \frac{f}{2} k_B T_c = \Delta \qquad f = 3, 2, or\ 1 \tag{16.32}$$

is

$$\lambda = \frac{h}{\left(2 m_e \left(\frac{1}{2} f k_B T_c\right)\right)^{1/2}} = \frac{h}{\left(m_e f k_B T_c\right)^{1/2}} \tag{16.33}$$

where in the present case of an inverse squared central field, the binding energy or energy gap, Δ, of the superconducting state is one half the negative of the potential energy and equal to the kinetic energy [6]. Consider the case wherein the Fermi energy is that of a three dimensional system, but the motion of superconducting electrons is restricted to 3, 2, *or* 1 directions corresponding to $f = 3, 2, or\ 1$, respectively. Combining Eqs. (16.30-16.33) gives the transition temperature

$$T_c = \frac{8}{(2\pi)^6} \left(\frac{8\pi}{3}\right)^2 \frac{E_F}{k_B f^3} \tag{16.34}$$

where the Fermi energy, E_F, is given by Eq. (16.27). An isotope effect can be manifest indirectly by changing the rms. position of atoms which effects the condition of Eq. (16.14) or the Fermi energy by changing the bond and vibrational energies.

CRITICAL TEMPERATURE, T_c

T_c for Conventional Three Dimensional Metallic Superconductors

In the case of conventional three dimensional metallic superconductors, the number density of conduction electrons is comparable to the number density of atoms-approximately $10^{29} / m^3$. Thus, the calculated transition temperature (Eq. (16.34)) is

$$T_c = 30.8\ K$$

As a comparison, the material of this class with the highest known transition of 23.2 K is Nb_3Ge [7].

T_c for One, Two, or Three Dimensional Ceramic Oxide Superconductors

In the case of ceramic oxide superconductors, one, two, and three dimensional conduction mechanisms are possible. The number density of conduction electrons is less than that of metallic superconductors-

approximately $10^{28} / m^3$.

For the three dimensional case, the calculated transition temperature (Eq. (16.34)) is

$$T_c = 7\ K$$

As a comparison, a possible material of this class, Li_2TiO_3 has a transition temperature of 13.7 K [8].

For the two dimensional case,

$$T_c = 22\ K$$

As a comparison, a possible material of this class, the original Bednorz and Muller $Ba-La-Cu-O$ material has a transition temperature of 35 K [7].

For the one dimensional case,

$$T_c = 180\ K$$

As a comparison, a possible material of this class, $Tl-Ca-Ba-Cu-O$ has a transition temperature of $120-125\ K$ [9]. The existence of superconductivity confined to stripes has been observed experimentally by neutron scattering [10].

Transition temperatures which are intermediate of each of these limiting cases are possible where combinations of conduction mechanism are present.

JOSEPHSON JUNCTION, WEAK LINK

As shown in the Electron g Factor Section, the electron links flux in units of the magnetic flux quantum. Thus, the magnetic flux that links a superconducting loop with a weak link is the magnetic flux quantum, Φ_0.

$$\Phi_0 = \frac{h}{2e} \tag{16.35}$$

The factor of $2e$ in the denominator has been erroneously interpreted [11] as evidence that Cooper pairs are the superconducting current carriers which is central to the BCS theory of superconductors. This theory fails to explain so called High Temperature Superconductors. These materials have a transition temperature which corresponds to an internal electron energy that is well above the energy limits at which the BCS theory permits conduction electron pairing. According to the present theory, Cooper pairs do not exist, and the present theory is consistent with the existence of High Temperature Superconductors as well as the experimental result that the magnetic flux that links a superconducting loop with a weak link is the magnetic flux quantum, Φ_0.

References

1. Reynolds, G. O., DeVelis, J. B., Parrent, G. B., Thompson, B.J., The New Physical Optics Notebook, SPIE Optical Engineering Press, (1990).

2. Mills, R., Magnetic Susceptibility Imaging (MSI), U.S. Patent No. 5,073,858 (1991).
3. Mills, R., Resonant Magnetic Susceptibility Imaging (ReMSI), Provisional US Patent Application No. 60/065,318, filed November 13, 1997.
4. Beiser, A, Concepts of Modern Physics, Fourth Edition, McGraw-Hill, New York, (1987),. p. 333.
5. Beiser, A, Concepts of Modern Physics, Fourth Edition, McGraw-Hill, New York, (1987),. p. 344.
6. Fowles, G. R., Analytical Mechanics, Third Edition, Holt, Rinehart, and Winston, New York, (1977), pp. 154-156.
7. Bednorz, J. G., Muller, K.A. Science, Vol. 237, (1987), pp. 1133-1139.
8. Johnston, D. C., Prakash, H., Zachariasen, W.H., and Viswanathan, V., Materials Research Bulletin, Vol. 8, (1973), pp. 777.
9. Sheng, Z. Z., Hermann, A.M., Nature, Vol. 322, (1988), pp. 55.
10. Service, R. F., Science, Vol. 283, (1999), pp. 1106-1108.
11. Gough, C. E., Colclough, M. S., Forgan, E. M., Jordan, R. G., Keene, M., Muirhead, C. M., Rae, A. I. M., Thomas, N., Abell, J. S., Sutton, S., Nature, Vol. 326, (1987), P. 855.

QUANTUM HALL EFFECT

GENERAL CONSIDERATIONS

When confined to two dimensions and subjected to a magnetic field, electrons exhibit a range of extraordinary behavior, most notably the Quantum Hall Effect (QHE). Two distinct versions of this phenomenon are observed, the Integral Quantum Hall Effect (IQHE) and the Fractional Quantum Hall Effect (FQHE). The former involves the condition for re-establishment of a superconducting state of one well in the presence of a magnetic field; whereas, the latter involves the condition for re-establishment of a superconducting state of two magnetically linked wells in the presence of a magnetic field.

Consider a conductor in a uniform magnetic field and assume that it carries a current driven by an electric field perpendicular to the magnetic field. The current in this case is not parallel to the electric field, but is deflected at an angle to it by the magnetic field. This is the Hall Effect, and it occurs in most conductors.

In the Quantum Hall Effect, the applied magnetic field quantizes the Hall conductance. The current is then precisely perpendicular to the magnetic field, so that no dissipation (that is no ohmic loss) occurs. This is seen in two-dimensional systems, at cryogenic temperatures, in quite high magnetic fields. Furthermore, the ratio of the total electric potential drop to the total current, the Hall resistance, R_H, is precisely equal to

$$R_H = \frac{h}{ne^2} \tag{17.1}$$

The factor n is an integer in the case of the Integral Quantum Hall Effect, and n is a small rational fraction in the case of the Fractional Quantum Hall Effect. In an experimental plot [1] as the function of the magnetic field, the Hall resistance exhibits flat steps precisely at these quantized resistance values; whereas, the regular resistance vanishes (or is very small) at these Hall steps. Thus, the quantized Hall resistance steps occur for a transverse superconducting state.

As shown in the Superconductivity Section, superconductivity arises for an array of current carrying magnetic dipoles when

$$k_p = k_z \tag{17.2}$$

Thus, the Fourier Transform of the system function band-passes the Fourier Transform of the time dependent array function. Both the space-time aperture function and its Fourier Transform are a periodic array of delta functions. No frequencies of the Fourier Transform of the space-time aperture function are attenuated; thus, no energy is lost in this special case where Eq. (17.2) holds. Consider the case that an external magnetic field is applied along the x-axis to a two dimensional

superconductor in the yz-plane which exhibits the Integral Quantum Hall Effect. (See Figure 17.1.) The magnetic field is expelled from the bulk of the superconductor by the supercurrent (Meissner Effect). The supercurrent-density function is a minimum energy surface; thus, the magnetic flux decays exponentially at the surface as given by the London Equation [2]. The Meissner current increases as a function of the applied flux. The energy of the superconducting electrons increases with flux. This energy increase is equivalent to lowering the critical temperature in Eq. (16.31) of the Superconductivity Section which is given by

$$n_s E_F = nkT_c \tag{17.3}$$

where n_s is the number density of superconducting electrons within kT_c of the Fermi energy and n is the number density of free electrons. At the critical current, the material loses superconductivity and becomes normal at a temperature below that of the critical temperature in the absence of an applied field. Conduction electrons align with the applied field in the x direction as the field permeates the material. The normal current carrying electrons experience a Lorentzian force, $\mathbf{F}_L$, due to the magnetic flux. The y directed Lorentzian force on an electron having a velocity $\mathbf{v}$ in the z direction by an x directed applied flux, $\mathbf{B}$, is

$$\mathbf{F}_L = e\mathbf{v} \times \mathbf{B} \tag{17.4}$$

The electron motion is a cycloid where the center of mass experiences an $\mathbf{E} \times \mathbf{B}$ drift [3]. Consequently, the normal Hall Effect occurs. Conduction electron energy states are altered by the applied field and by the electric field corresponding to the Hall Effect. The electric force, $\mathbf{F}_H$, due to the Hall electric field, $\mathbf{E}_y$, is

$$\mathbf{F}_L = e\mathbf{E}_y \tag{17.5}$$

When these two forces are equal and opposite, conduction electrons propagate in the z direction alone. For this special case, it is demonstrated in Jackson [3] that the ratio of the corresponding Hall electric field and the applied magnetic flux is

$$E/B = v \tag{17.6}$$

where $\mathbf{v}$ is the electron velocity. At a temperature below T_c, given by Eq. (17.3) where E_F is the Fermi energy, Eq. (17.6) is satisfied. The further conditions for superconductivity are

$$n\omega_\rho = \omega_z \tag{17.7}$$

$$nk_p = k_z \tag{17.8}$$

And, it is demonstrated in the Integral Quantum Hall Effect Section that the Hall resistance, R_H, in the superconducting state is given by

$$R_H = \frac{h}{ne^2} \tag{17.9}$$

where n of Eqs. (17.7), (17.8), and (17.9) is the same integer for the case of a single superconducting well. It is demonstrated in the Fractional Quantum Hall Effect Section that electrons in different superconducting wells can interact when the two wells are separated by a distance comparable to the magnetic length, ℓ_0.

$$\ell_0 = \left(\frac{\hbar c}{eB}\right)^{1/2} \tag{17.10}$$

In this case, it is further demonstrated that the Hall resistance, R_H, in the superconductivity state is given by Eq. (17.9) where n is a fraction.

INTEGRAL QUANTUM HALL EFFECT

A superconducting current-density function is nonradiative and does not dissipate energy as was the case for single electron current-density functions described previously in the One Electron Atom Section, the Two Electron Atom Section, the Three Electron Atom Section, the Electron in Free Space Section, and the Nature of the Chemical Bond Section. Furthermore, a superconducting current-density function is the superposition of single electron current-density functions-which are spatially two dimensional in nature. Thus, a superconducting current-density function is an electric and magnetic equipotential energy surface.

From Eq. (1.55), the angular frequency in spherical coordinates which satisfies the boundary condition for nonradiation is

$$\omega = \frac{\hbar}{m_e r^2} = \frac{(2\pi)^2 \hbar}{m_e (2\pi r)^2} \tag{17.11}$$

The relationship between the electron wavelength and the radius which satisfies the nonradiative boundary condition in spherical coordinates is given by Eq. (1.43)

$$2\pi r = \lambda \tag{17.12}$$

Substitution of Eq. (17.12) into Eq. (17.11) gives

$$\omega = \frac{\hbar}{m_e} k^2 \tag{17.13}$$

where

$$k = \frac{2\pi}{\lambda} \tag{17.14}$$

It follows from Eq. (1.47) that

$$v = \frac{\hbar}{m_e r} = \frac{\hbar}{m_e} k \tag{17.15}$$

In a solid lattice, the coordinates are Cartesian rather than spherical. The relationship between the wavelength of a standing wave of a superconducting electron and the length, x, of a cubical unit cell follows from Eqs. (16.28) and (16.29) of the Superconductivity Section

$$\lambda = 2\pi x \tag{17.16}$$

The de Broglie wavelength, λ, is given by

$$\lambda = \frac{h}{m_e v} \tag{17.17}$$

It follows from Eqs. (17.14), (17.16), and (17.17) that the angular velocity, ω, and linear velocity, v, for an electron held in force balance by a periodic array of nuclei comprising a cubical unit cell with internuclear spacing x are given by Eqs. (17.13) and (17.15) where

$$k = \frac{2\pi}{\lambda} = \frac{1}{x} \tag{17.18}$$

In general, the Cartesian coordinate wavenumber, k, given by Eq. (17.18) replaces $\frac{1}{r}$ of spherical coordinates.

In the case of an exact balance between the Lorentzian force (Eq. (17.4)) and the electric force corresponding to the Hall voltage (Eq. (17.5)), each superconducting electron propagates along the z-axis where

$$E/B = v \tag{17.19}$$

where v is given by Eq. (17.15). Substitution of Eqs. (17.15) and (17.18) into Eq. (17.19) gives

$$E/B = \frac{\hbar}{m_e} k = \frac{\hbar}{m_e x} \tag{17.20}$$

Eq. (17.20) is the condition for superconductivity in the presence of crossed electric and magnetic fields. The Hall resistance for this superconducting state is derived as follows using the coordinate system shown in Figure 17.1.

Figure 17.1. Coordinate system of crossed electric field, $\mathbf{E}_y$, corresponding to the Hall voltage, magnetic flux, $\mathbf{B}_x$, due to applied field, and superconducting current $\mathbf{i}_z$.

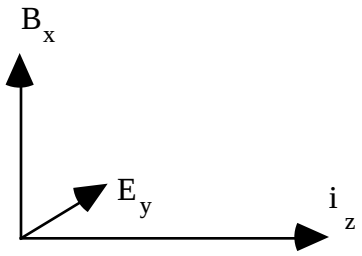

The current is perpendicular to $\mathbf{E}_y$, thus there is no dissipation. This occurs when

$$e\mathbf{E} = e\mathbf{v} \times \mathbf{B} \tag{17.21}$$

or

$$E/B = v \tag{17.22}$$

The magnetic flux, **B**, is quantized in terms of the Bohr magneton because an electron, and therefore a superconductor, links flux in units of the magnetic flux quantum,

$$\Phi_0 = \frac{h}{2e} \tag{17.23}$$

The electric field, $\mathbf{E}_y$, corresponding to the Hall voltage, V_H, is quantized in units of e because this electric field arises from conduction electrons-each of charge e. The energy, E_H, corresponding to the Hall voltage is calculated using the Poynting Power Theorem. The Hall energy of an integer number of electrons, Z, each in the presence of a magnetic dipole and an electric field of magnitude Ze due to the Z electrons follows for Eqs. (7.30) and (7.47) of the Two Electron Atom Section

$$E_H = ZE_{mag} = \frac{Z\pi\mu_0 e^2\hbar^2 k^3}{Zm_e^2} \tag{17.24}$$

where k is given by Eq. (17.13) and where the electric energy of Eq. (7.47) is zero because each electron is a conduction electron. In the limit to a superconducting state, the trajectory of each electron is a cycloid where ω_p is the frequency in the xy-plane and ω_z is the frequency along the z-axis. In this case, the dipole array function given in the Superconductivity Section is multiplied by a time harmonic function with argument ω_p

$$\frac{\left(2z^2 - x^2 - y^2\right)}{[x^2 + y^2 + z^2]^{5/2}} \quad \sum_{n=-\infty}^{\infty} \mu_B \delta\left(x - nx_0, y - ny_0, z - nz_0\right) \exp(-i\omega t) \tag{17.25}$$

where

$$\omega = \omega_\rho + \omega_z \tag{17.26}$$

The Fourier Transform of the convolved functions of Eq. (17.25) is given in the Superconductivity Section as

$$\frac{4\pi}{1 + \frac{k_z^2}{k_\rho^2}} \frac{1}{x_0 y_0 z_0} \sum_{n=-\infty}^{\infty} \mu_B \delta\left(k_x - \frac{n}{x_0}, k_y - \frac{n}{y_0}, k_z - \frac{n}{z_0}\right) \tag{17.27}$$

The Fourier Transforn of the time harmonic function is

$$\frac{[\delta(\omega - (\omega_p + \omega_z)) + \delta(\omega + (\omega_p + \omega_z))]}{2} \tag{17.28}$$

A very important theorem of Fourier analysis states that the Fourier Transform of a product is the convolution of the individual Fourier Transforms. Thus, the Fourier Transform of Eq. (17.25) is the convolution of Eqs. (17.27) and (17.28)

$$\frac{4\pi}{1 + \frac{k_z^2}{k_\rho^2}} \frac{1}{x_0 y_0 z_0} \sum_{n=-\infty}^{\infty} \mu_B \delta\left(k_x - \frac{n}{x_0}, k_y - \frac{n}{y_0}, k_z - \frac{n}{z_0}\right) \frac{[\delta(\omega - (\omega_p + \omega_z)) + \delta(\omega + (\omega_p + \omega_z))]}{2} \tag{17.29}$$

Eq. (17.29) is a band-pass when

$$nk_p = k_z \tag{17.30}$$

and when

$$\frac{\omega_z}{\omega_\rho} = n \tag{17.31}$$

where n is an integer. The cyclotron frequency, ω_p, is derived as follows:

The force balance between the Lorentzian force and the centrifugal force is

$$\frac{m_e \mathbf{v}^2}{r} = e\mathbf{v} \times \mathbf{B} \tag{17.32}$$

The magnetic flux, **B**, from a magnetic moment of a Bohr magneton is

$$B = \frac{\mu_0 e\hbar}{2m_e} k^3 \tag{17.33}$$

Cancelation of **v** on both sides of Eq. (17.32) gives

$$m_e \omega = e \times \mathbf{B} \tag{17.34}$$

$$\omega_\rho = \frac{eB}{m_e} \tag{17.35}$$

Substitution of Eq. (17.33) into Eq. (17.35) gives

$$\omega_\rho = \frac{\mu_0 e^2 \hbar}{2m_e^2} k^3 \tag{17.36}$$

Substitution of Eq. (17.31) into Eq. (17.36) gives

$$\omega_z = \frac{n\mu_0 e^2 \hbar}{2m_e^2} k^3 \tag{17.37}$$

The current, $\mathbf{i}_z$, along the z-axis is given as the product of the charge, e, and ω_z, the frequency along the z-axis

$$\mathbf{i}_z = e\omega_z = \frac{n\mu_0 e^3 \hbar}{2m_e^2} k^3 \tag{17.38}$$

The Hall voltage is given as the energy per coulomb:

$$V_H = \frac{E_{mag}}{e} = \frac{\pi\mu_0 e\hbar^2 k^3}{m_e^2} \tag{17.39}$$

Thus, the Hall resistance, R_H, is given as the ratio of the Hall voltage (Eq. (17.39)) and the current, $\mathbf{i}_z$, (Eq. (17.38))

$$R_H = \frac{V_H}{i_z} = \frac{\frac{\pi\mu_0 e\hbar^2 k^3}{2m_e^2}}{\frac{n\mu_0 e^3 \hbar k^3}{2m_e^2}} = \frac{h}{ne^2} \tag{17.40}$$

The velocity of each superconducting electron according to Eq. (17.22) is

$$E/B = v \tag{17.41}$$

which is derived as follows:

The Hall electric field, $\mathbf{E}_y$, is given by the ratio of the Hall voltage and the distance of the cyclotron orbit, $2\pi x$, where the unit cell distance, x, wavenumber, k, by Eq. (17.16)

$$\mathbf{E}_y = V_H \frac{k}{2\pi}$$

where V_H is given by Eq. (17.39)

$$\mathbf{E}_y = \frac{\pi\mu_0 e\hbar^2 k^4}{2\pi m_e^2} \tag{17.42}$$

The magnetic field, $\mathbf{B}$, is given by Eq. (17.33); thus the velocity $\mathbf{v}$ is given as

$$\mathbf{v} = \frac{\frac{\pi\mu_0 e\hbar^2 k^4}{2\pi m_e^2}}{\frac{\mu_0 e\hbar k^3}{2m_e}} \tag{17.43}$$

$$= \frac{\hbar}{m_e} k \tag{17.44}$$

Eq. (17.44) is equivalent to the velocity for nonradiation given by Eq. (1.47), where

$$\frac{2\pi}{2\pi r} = \frac{2\pi}{\lambda} = k \tag{17.45}$$

This superconducting phenomenon whereby the Hall resistance occurs as inverse integer multiples of

$$\frac{h}{e^2} \tag{17.46}$$

is the Integral Quantum Hall Effect (IQHE)

FRACTIONAL QUANTUM HALL EFFECT

For two superconducting wells separated by the magnetic length, ℓ_o,

$$\ell_0 = \left(\frac{\hbar c}{eB}\right)^{1/2} = \left(\frac{\Phi_0}{\pi B}\right)^{1/2} \tag{17.47}$$

where Φ_0 given by Eq. (17.23) is the magnetic flux quantum, the wells are linked. Electrons can propagate from one well to the other with activation energy

$$\left|\frac{\Delta E_{mag}}{E_{mag}}\right| \quad \frac{e^2}{\ell_0} \tag{17.48}$$

In the case that a magnetic field is applied to both well one and well two, and that an exact balance between the Lorentzian force (Eq. (17.4)) and the electric force corresponding to the Hall voltage (Eq. (17.5)) exists, each superconducting electron propagates along the z-axis where

$$\frac{E_1}{B_1} = v_1 \tag{17.49}$$

$$\frac{E_2}{B_2} = v_2 \tag{17.50}$$

Because the two wells are linked

$$v_1 = jv_2 \tag{17.51}$$

where j is an integer. Eq. (17.51) provides that the electrons are in phase with

$$\frac{2\pi}{\lambda_1} = k_1 = j \quad k_2 = j\frac{2\pi}{\lambda_2} \tag{17.52}$$

where the de Broglie wavelength is given by Eq. (17.19). Otherwise, $E_z \neq 0$, and the state is not superconducting. It follows from the derivation of Eq. (17.40) of the Integral Quantum Hall Effect Section that

$$\frac{E_1}{n_1 B_{01}} = v_1 \tag{17.53}$$

And,

$$\frac{E_2}{n_2 B_{01}} = v_2 \tag{17.54}$$

where n_1 and n_2 are integers. From Eqs. (17.52), (17.53), and (17.54)

$$E_1 = j\frac{n_1}{n_2}\frac{E_2}{B_{01}}B_{01} \tag{17.55}$$

The resistance of each well is proportional to the transverse velocity as shown previously, and the resistance across both linked wells which are in series is the sum of the individual resistances. Thus, the total resistance is proportional to the sum of the individual velocities.

$$R \quad \left(\frac{E_1}{n_1 B_{01}} + \frac{E_2}{n_2 B_{01}}\right) \tag{17.56}$$

Substitution of Eq. (17.55) into Eq. (17.56) gives

$$R \quad \frac{E_2}{B_{01}}\frac{1}{n_2}(j+1) \tag{17.57}$$

It follows from the derivation of Eq. (17.40) of the Integral Quantum Hall Effect Section that Hall resistance, R_H, is

$$R_{H=}\frac{V_H}{i_z} = \frac{(j+1)\frac{\pi\mu_0 e\hbar^2 k^3}{m_e^2}}{\frac{n_2\mu_0 e^3\hbar k^3}{2m_e^2}} = \frac{h}{ne^2} \tag{17.58}$$

where n is a fraction. This superconducting phenomenon whereby the Hall resistance occurs as inverse fractional multiples of

$$\frac{h}{e^2} \tag{17.59}$$

is the Fractional Quantum Hall Effect (FQHE)

References

1. Das Sarma, S., Prange, R. E., Science, Vol. 256, (1992), pp. 1284-1285.
2. Matsen, F. A., Journal of Chemical Education, Vol. 64, No. 10, (1987), pp. 842-845.
3. Jackson, J. D., Classical Electrodynamics, Second Edition, John Wiley & Sons, New York, (1962), pp. 582-584.

AHARONOV-BOHM EFFECT

The resistance of a circuit corresponds to the decrease in the energy of the current carrying electrons as they propagate through the circuit. Scattering of the electrons is a principal mechanism. In the case where a magnetic field is applied such that the field lines are perpendicular to the plane of a current carrying ring, the current carrying electrons lose energy through the effect of the field on the current.

The application of the magnetic field to the current carrying ring initially gives rise to a changing flux through the ring. The changing flux gives rise to an electric field which reduces the current in the ring; thus, the magnetic field contributes a term called magnetoresistance to the resistance of the ring. This term can be derived from the change in velocity (assuming no scattering) of a current carrying electron of charge e and mass m_e by the application of a magnetic field of strength $\mathbf{B}$ which is given as Eq. (29) of Purcell [1]

$$\frac{\Delta \mathbf{v}}{r} = \frac{e\mathbf{B}}{2m_e} \tag{18.1}$$

where r is the radius of the ring. The changes in the force on the electron due to the electric field is

$$\Delta \mathbf{F} = e\Delta \mathbf{E} \tag{18.2}$$

The change in kinetic energy of the electron over length s is

$$\frac{1}{2} m_e \Delta \mathbf{v}^2 = \Delta \mathbf{F} s = e\Delta \mathbf{E} s = e\Delta V \tag{18.3}$$

where ΔV is the change in voltage over the distance s. From Eq. (18.3), the voltage change is

$$\Delta V = \frac{m_e \Delta v^2}{2e} \tag{18.4}$$

The change in current, $\Delta \mathbf{i}$, per electron due to the change in velocity, $\Delta \mathbf{v}$, is given by Eq. (20) of Purcell [1].

$$\Delta \mathbf{i} = \frac{e\Delta \mathbf{v}}{2\pi r} \tag{18.5}$$

And, the total change in current, $\Delta \mathbf{i}$, is

$$\Delta \mathbf{i} = NWt\frac{e\Delta \mathbf{v}}{2\pi r} \tag{18.6}$$

where N is the density of current carrying electrons in the current ring cross section, W is the width of the current ring, and t is the thickness of the ring.

The resistance change, ΔR, follows from Eqs. (18.4) and (18.6)

$$\Delta R = \frac{\Delta V}{\Delta i} = \frac{2\pi r m_e \Delta v^2}{NWt2ee\Delta v} = \frac{\pi r m_e \Delta v}{NWte^2} \tag{18.7}$$

Substitution of Δv given by Eq. (18.1) into Eq. (18.7) gives the change in

resistance corresponding to the magnetoresistance.

$$\Delta R = \frac{\pi r^2 B}{NWt2e} \tag{18.8}$$

An additional critically damped, over damped, or underdamped oscillatory resistive term may arise due to both the magnetoresistance and the vector potential of the electron. The electron possesses an angular momentum of $\hbar$. As shown in the Electron g Factor Section, the electron angular momentum comprises kinetic and vector potential components. Angular momentum is conserved in the presence of an applied magnetic field when the electron links flux in units of the magnetic flux quantum, Φ_0.

$$\Phi_0 = \frac{h}{2e} \tag{18.9}$$

This occurs when the electron rotates by $\frac{\pi}{2}$ radians about an axis perpendicular to the axis parallel to the magnetic flux lines. This electron rotation corresponds to an $\frac{\hbar}{2}$ magnitude, $180°$, rotation of the electron's angular momentum vector. In the case that the electrons carry current, this change in momentum of a given current carrying electron increases or decreases the current depending on the vector projection of the momentum change onto the direction of the current. Recently, it has been demonstrated that 50-nm-diameter rings of *InAs* on a *GaAs* surface have can host a single circulating electron in a pure quantum state, that is easily controlled by magnetic fields and voltages on nearby plates. The electrons were observed to link flux in the unit of the magnetic flux quantum with a gain in a unit of angular momentum in a specific direction with the linkage [2].

At low temperature, the de Broglie wavelength of an electron

$$\lambda = \frac{h}{m_e v} \tag{18.10}$$

has macroscopic dimensions, and the electron scattering length for a given electron in a current carrying ring may be comparable to the dimensions of the ring. A current carrying ring having a magnetic field applied perpendicularly to the plane of the ring may be constructed and operated at a temperature, current, and applied magnetic field strength such that resonance occurs between the vector potential of a current carrying electron and the flux of the applied magnetic field. This coupling can give rise to a contribution to the resistance which behaves as an underdamped harmonic oscillator in response to the applied magnetic flux. The general form of the equation for this component of the resistance is the product of an exponential dampening function and a harmonic function as given by Fowles [3]. Each electron links flux only

in units of the magnetic flux quantum, Φ_0, given by Eq. (18.9). Thus, the natural frequency in terms of the applied flux, Φ, is the magnetic flux quantum, Φ_0. According to Eq. (18.8), the magnetoresistance is proportional to the applied flux Φ where

$$\Phi = \pi r^2 B \tag{18.11}$$

Thus, the argument of the dampening function is proportional to $\frac{\Phi}{\Phi_0}$.

Furthermore, the magnetoresistance gives rise to a distribution of electron velocity changes centered about the average velocity change given by Eq. (18.1) where each electron's current contributing drift velocity along the ring contributes a component to the kinetic term of the electron's angular momentum. The distribution of velocity changes, dampens the coupling between each electron vector potential and the applied magnetic flux at the natural frequency corresponding to the average electron velocity. And, each electron de Broglie wavelength change corresponding to its velocity change alters the electron-lattice scattering cross section which also contributes to the dampening of the oscillatory resistance behavior. The argument of the dampening function is the product of $\frac{\Phi}{\Phi_0}$ and the corresponding dimensionless damping factor, α_D, which incorporates both dampening effects. The underdamped oscillatory resistance change due to the applied magnetic field is

$$\Delta R = \frac{\pi r^2 B}{NWt2e} e^{-\alpha_D \left(\frac{\Phi}{\Phi_0}\right)} \cos 2\pi \frac{\Phi}{\Phi_0} \tag{18.12}$$

The total resistance change due to the applied field is the sum of the magnetoresistance and the underdamped oscillatory resistance

$$\Delta R = \frac{\pi r^2 B}{NWt2e} \left[1 + e^{-\alpha_D \left(\frac{\Phi}{\Phi_0}\right)} \cos 2\pi \frac{\Phi}{\Phi_0}\right] \tag{18.13}$$

This type of contribution to the resistance that is an oscillatory function of the applied flux with a period of $\Phi_0 = \frac{h}{2e}$ is known as the Aharonov-Bohm Effect. The resistance contribution given by Eq. (18.13) is consistent with the observed behavior [4] as shown in Figure 18.1.

Figure 18.1. The change in the resistance divided by the resistance as a function of the applied flux which demonstrates the Aharonov-Bohm effect.

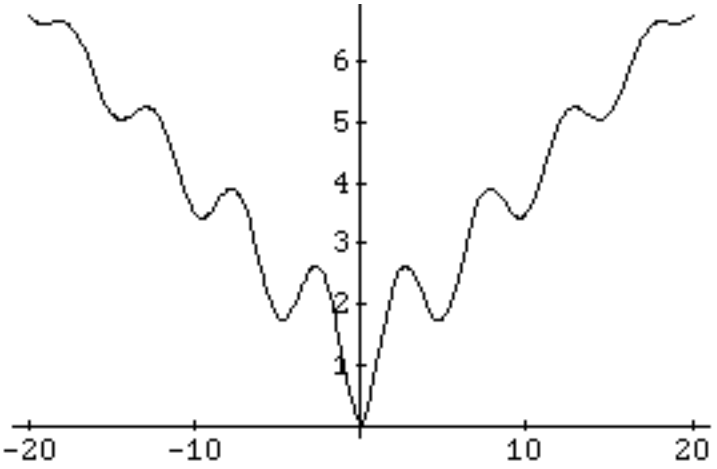

References

1. Purcell, E., Electricity and Magnetism, McGraw-Hill, New York, (1965), pp. 373.
2. A. Lorke, R. J. Luyken, A. O. Govorov, J. P. Kotthaus, J. M. Garcia, and P. M. Petroff, Phys. Rev. Lett., Vol. 84, March 6, (2000), p. 2223.
3. Fowles, G. R., Analytical Mechanics, Third Edition, Holt, Rinehart, and Winston, New York, (1977), pp. 62-66.
4. Chandrasekhar, V., Rooks, M. J., Wind, S., and Prober, D. E., Physical Review Letters, Vol. 55, No. 15, (1985), pp. 1610-1613.

SECTION III

Gravity, Cosmology, Elementary Particles, and Nuclear Physics

CREATION OF MATTER FROM ENERGY

[The general result of equations and relationships derived in the Pair Production and Gravity Sections are given herein.]

Matter and energy are interconvertible and are in essence different *states* of the same entity. The state, matter or energy, is determined by the laws of nature and the properties of spacetime. A photon propagates according to Maxwell's Equations at the speed of light in spacetime having intrinsic impedance η. Matter as a fundamental particle is created in spacetime from a photon. Matter obeys the laws of Special Relativity, the relationship of motion to spacetime, and spacetime is curved by matter according to the laws of General Relativity. Relationships must exist between these laws and the implicit fundamental constants. The fundamental elements which determine the evolution of the universe are the fundamental constants of spacetime, ε_o and μ_o with the property of charge; the capacity of spacetime to be curved by mass/energy; and the photon's angular momentum of $\hbar$. The conversion of energy into matter requires a transition state for which the identification of the entity as matter or energy is impossible. From the properties of the entity, as matter or energy, and from the physical laws and the properties of spacetime, the transition state hereafter called a transition state orbitsphere are derived. Concomitantly, the equations for the interconversion of matter and energy are determined, and the fundamental constant relationships are determined exactly. The results are: matter and energy possess mass; matter possesses charge, and energy is stored in the electric and magnetic fields of matter as a consequence of its charge and the motion of its charge. Matter can trap photons as an absorption event. The mass of the matter possessing a "trapped photon" increases by the mass/energy of the photon, and the photon acts as if it possesses charge. (The electric fields of "trapped photons" is given in the Excited States of the One Electron Atom (Quantization) Section). Photons obey Maxwell's Equations. At the two dimensional surface of the orbitsphere containing a "trapped photon", the relationship between the photon's electric field and its charge at the orbitsphere (See Eq. 2.10) is

$$\mathbf{n} \cdot \left(\mathbf{E}_1 - \mathbf{E}_2\right) = \frac{\sigma}{\varepsilon_0} \tag{19.1}$$

Thus, the photon's electric field acts as surface charge. This property of a photon is essential because *charge arises from electromagnetic radiation in the creation of matter*. Furthermore, energy is proportional to the mass of matter as given by

$$E = mc^2 \tag{19.2}$$

And, energy is proportional to frequency as given by Planck's equation,

$$E = \hbar\omega \tag{19.3}$$

It is shown in the Gravity Section (Eq. (23.29)) that the de Broglie relationship can be derived from Planck's equation.

$$\lambda = \frac{h}{mv} \tag{19.4}$$

Matter and light obey the wave equation relationship

$$v = \lambda \frac{\omega}{2\pi} \tag{19.5}$$

and Eqs. (19.2) through (19.4). Light and matter exist as orbitspheres, as given in the Photon Equation Section and the One Electron Atom Section, respectively.

The boundary condition for nonradiation by *a transition state orbitsphere* is

$$2\pi(r_n^*) = 2\pi(nr_1^*) = n\lambda_1^* = \lambda_n^* \tag{19.6}$$

where r^* and λ^* are allowed radii and allowed wavelengths for the transition state matter in question, and n is a positive real number. A general relationship derived for the electron in the Pair Production Section is that when $r = \alpha a_o$, v of Eq. (19.5) of a transition state orbitsphere equals the velocity of light in the inertial reference frame of the photon of angular frequency ω^* and energy $\hbar\omega^* = m_e c^2$ which forms the transition state orbitsphere of rest mass m_e. Substitution of Eq. (19.4) into Eq. (19.6) with $v = c$ and $r^* = \alpha a_o$ gives the result that the radius of the transition state orbitsphere is the Compton wavelength bar, $\lambda\!\!\!^{-}_c$, which gives the general condition for particle production.

$$r^*_\alpha = \alpha a_o = \lambda\!\!\!^{-}_c = \frac{\hbar}{m_0 c} \tag{19.7}$$

With the substitution of Eq. (19.7) and the appropriate special relativistic corrections into the orbitsphere energy equations , the following energies, written in general form, are equal

$$E = \hbar\omega^* = m_0 c^2 = V \tag{19.8}$$

where V is the potential energy. In the case of an electron orbitsphere, the rest mass $m_0 = m_e$, the radius $r_\alpha^* = \alpha a_o$, and the electron and positron each experience an effective charge of $\alpha^{-1}e$.

$$V = \frac{\alpha^{-1}e^2}{4\pi\varepsilon_o \alpha a_o} \tag{19.9}$$

This energy and mass are that of the transition state orbitsphere which can be considered to be created from the photon of frequency ω^*. Furthermore, the relativistic factor, γ ,

$$\gamma = \frac{1}{\sqrt{1 - \left(\frac{v}{c}\right)^2}} \tag{19.10}$$

for the lab frame relative to the photon frame of the transition state orbitsphere of radius αa_o is 2π where Eq. (19.10) is transformed from Cartesian coordinates to spherical coordinates[1]. (For example, the relativistic mass of the electron transition state orbitsphere of radius αa_o is $2\pi m_e$.) Using the relativistic mass, the Lorentzian invariance of charge, and the radius of the transition state orbitsphere as αa_o, it is demonstrated in the Pair Production Section that the electrical potential energy is equal to the energy stored in the magnetic field which gives the following equalities of energies written in general form

$$E = V = E_{mag} = \hbar\omega^* = m_0 c^2 \tag{19.11}$$

The energy stored in the electric and magnetic fields of any photon are equal, and equivalence of these energies occurs for an LC circuit excited at its resonance frequency

$$\omega^* = \frac{1}{\sqrt{LC}} \tag{19.12}$$

where L is the inductance and C is the capacitance of the circuit. Spacetime is an LC circuit with resonance frequency

$$\omega^* = \frac{1}{\sqrt{LC}} = \frac{1}{\sqrt{\varepsilon_o \mu_o d^2}} = \frac{1}{\sqrt{\varepsilon_o \mu_o \lambda_C^2}} \tag{19.13}$$

where d is the circuit dimensions. (This equation is derived in the Pair Production Section.) For $d = \alpha a_o$, this frequency is equivalent to that of a photon of energy $m_e c^2$. When the resonance frequency of an LC circuit is excited, the impedance becomes infinite. Thus, spacetime is excited at its resonance frequency when a photon of angular frequency ω^* forms a transition state orbitsphere of mass/energy $m_e c^2$. At this event, the

---

[1] For time harmonic motion, with angular velocity, ω, the relationship between the radius and the wavelength given Eq. (1.43) by is

$$2\pi r_n = \lambda_n$$

The de Broglie wave length is given by Eq. (1.46)

$$\lambda_n = \frac{h}{p_n} = \frac{h}{m_e v_n}$$

In the relativistically corrected case given by Eq. (1.45),

$$r_n = \lambda_n$$

Then from Eq. (1.46),

$$r_n = \lambda_n = \frac{h}{p_n} = \frac{h}{(2\pi m_e) v_n}$$

Thus, the relativistically corrected electron mass is $2\pi m_e$.

equivalence of all energies given previously provides that matter and energy are indistinguishable. (For the transition state orbitsphere, the potential energy corresponds to the stored electrical energy of an LC circuit which, in turn, corresponds to the energy stored in the electric field of a photon.) The impedance for the propagation of electromagnetic radiation becomes infinite and a photon of energy $m_e c^2$ becomes a fundamental particle as the transition state orbitsphere becomes real. The energy of the photon is equal to the rest mass of the particle at zero potential energy. Therefore, in the case of charged particle production, a particle and an antiparticle each of mass $\frac{\hbar\omega^*}{c^2}$ is produced at infinity relative to the mutual central field of

$$\mathbf{E} = \frac{+e}{4\pi\varepsilon_o r^2} \tag{19.14}$$

And, momentum is conserved by a third body such as an atomic nucleus.

The boundary condition, Eq. (1.43) and Eq. (19.6), precludes the existence of the Fourier components of the current-density function of the orbitsphere that are synchronous with waves traveling at the speed of light. The nonradiative condition is Lorentzian invariant because the velocity is perpendicular to the radius. However, the constancy of the speed of light must also hold which requires relativistic corrections to spacetime. The Schwarzschild metric gives the relationship whereby matter causes relativistic corrections to spacetime that determines the curvature of spacetime and is the origin of gravity. Thus, the creation of matter causes local spacetime to become curved. The geometry of spacetime is transformed from flat (Euclidean) to curved (Riemannian). Time and distances are distorted. At particle production, the proper time of the particle must equal the coordinate time given by Special Relativity for Riemannian geometry affected by the creation of matter of mass m_0 where the metric of spacetime is given by the Schwarzschild metric. This boundary condition determines the masses of the fundamental particles. The gravitational radius, α_G or r_G, which arises from the solution of the Schwarzschild metric is defined as

$$\alpha_G = \frac{Gm_0}{c^2} = r_G \tag{19.15}$$

where G is the gravitational constant. The radius of the transition state orbitsphere is

$$r_\alpha^* = \lambda\!\!\!^{-}_c = \frac{\hbar}{m_0 c} \tag{19.16}$$

These radii are equal when the gravitational potential, E_{grav}, is

$$E_{grav} = \frac{Gm_0^2}{r_\alpha^*} = \frac{Gm_0^2}{\lambda\!\!\!^{-}_c} = \hbar\omega \quad = V = E_{mag} \tag{19.17}$$

These relationships represent the unification of the fundamental laws of the universe, Maxwell's Equations, Newtonian Mechanics, Special and General Relativity, and the Planck equation and the de Broglie relationship where the latter two can be derived from Maxwell's Equations as demonstrated in the Gravity Section.

PAIR PRODUCTION

Matter and energy are interconvertible and are in essence different states of the same entity. The state, matter or energy, is determined by the laws of nature and the properties of spacetime. A photon propagates according to Maxwell's Equations at the speed of light in spacetime having intrinsic impedance η. Matter as a fundamental particle is created in spacetime from a photon. Matter obeys the laws of Special Relativity, the relationship of motion to spacetime, and spacetime is curved by matter according to the laws of General Relativity. Relationships must exist between these laws and the implicit fundamental constants. The conversion of energy into matter requires a transition state for which the identification of the entity as matter or energy is impossible. From the properties of the entity, as matter or energy, and from the physical laws and the properties of spacetime, the transition state hereafter called a transition state orbitsphere is derived. For example, a photon of energy 1.02 *MeV* in the presence of a third particle becomes a positron and an electron. This phenomenon, called pair production, involves the conservation of mass/energy, charge, and angular and linear momentum. Pair production occurs as an event in spacetime where all boundary conditions are met according to the physical laws: Maxwell's Equations, Newton's Laws, and Special and General Relativity, where matter and energy are indistinguishable by any physical property. Matter and photons exist as orbitspheres; thus, the conversion of energy to matter must involve the orbitsphere equations derived in the previous sections. It must also depend on the equations of electromagnetic radiation and the properties of spacetime because matter is created from electromagnetic radiation as an event in spacetime.

Matter and light obey the wave equation relationship

$$v = \lambda \frac{\omega}{2\pi} \tag{20.1}$$

The boundary condition for nonradiation by a transition state orbitsphere is

$$2\pi(r_n^*) = 2\pi(nr_1^*) = n\lambda_1^* = \lambda_n^* \tag{20.2}$$

where r^* and λ^* are allowed radii and allowed wavelengths for the transition state matter in question, and n is a positive real number.

Consider the production of an electron and a positron providing a mutual central field. The relationship between the potential energy of an electron orbitsphere and the angular velocity of the orbitsphere is

$$V = \hbar\omega \quad = \frac{1}{n}\frac{e^2}{4\pi\varepsilon_o n a_o} \tag{20.3}$$

It can be demonstrated that the velocity of the electron orbitsphere satisfies the relationship for the velocity of a wave by substitution of Eqs. (1.43) and (1.55) into Eq. (20.1), which gives Eq. (1.56). Similarly, the relationship between c, the velocity of light in free space, and frequency ω and wavelength λ is

$$c = \lambda \frac{\omega}{2\pi} \tag{20.4}$$

And, the energy of a photon of frequency ω is

$$E = \hbar\omega \tag{20.5}$$

Recall from the Excited States of the One Electron (Quantization) Section that a photon of discrete frequency, ω, can be trapped in the orbitsphere of an electron which serves as a resonator cavity of radius r_n where the resonance excitation energy of the cavity is given by Eq. (20.3).

As demonstrated in the Excited States of the One Electron Atom (Quantization) Section, with the inclusion of the contribution of the electron kinetic energy change, the change in the orbitsphere angular velocity is equal to the angular velocity of the resonant photon of the corresponding electron transition. The ratio of their linear velocities is given by Eq. (20.4).

$$\frac{\Delta v_n}{c_{photon}} = \frac{\Delta\lambda_n \frac{\Delta\omega_n}{2\pi}}{\lambda_{photon}\frac{\omega_{photon}}{2\pi}} = \frac{\Delta\lambda_n}{\lambda_{photon}} \tag{20.6}$$

where the n subscripts refer to orbitsphere quantities.

Consider a transition state electron orbitsphere which is defined as the transition state between light and matter where light and matter are indistinguishable, and where $\Delta v_n = v_n$ and $\Delta\lambda_n = \lambda_n$. For this case, the velocity of the electron transition state orbitsphere is the speed of light in the inertial reference frame of the photon which formed the transition state orbitsphere. The result of the substitution into Eq. (20.1) of c for v, of λ_n given by Eq. (2.2) where r_1 is given by Eq. (1.169) for λ, and of ω_n given by Eq. (1.55) for ω is

$$c = 2\pi n a_o \frac{\hbar}{m_e (n a_0)^2 2\pi} \tag{20.7}$$

Maxwell's Equations provide that

$$c = \sqrt{\frac{1}{\varepsilon_o \mu_o}} \tag{20.8}$$

The result of substitution of Eqs. (1.168) and (20.8) into Eq. (20.7) is

$$n^{-1} = \frac{m_e c a_o}{\hbar} = \frac{m_e}{\hbar\sqrt{\varepsilon_o\mu_o}} \frac{4\pi\varepsilon_0\hbar^2}{e^2 m_e} = 4\pi\sqrt{\frac{\varepsilon_o}{\mu_o}}\frac{\hbar}{e^2} = \alpha^{-1} \tag{20.9}$$

In fact, α is the fine structure constant (a dimensionless constant for pair production) [1]. The experimental value is 0.0072973506 . Recently, alterations to the most up-to-date, self consistent set of the recommended values of the MKS basic constants and conversion factors of physics and chemistry resulting from the 1986 least-squares adjustment have been proposed [2]. Eq. (20.9), the equations of pair production given below, and the equations in the Unification of Spacetime, the Forces, Matter, and Energy Section and Gravity Section permit the derivation of a more accurate self consistent set.

Continuing with the present MKS units, the radius of the transition state electron orbitsphere is αa_o, and the potential energy, V, is given by Eq. (20.3) where n is α where α arises from Gauss's law surface integral and the relativistic invariance of charge.

$$V = \frac{-\alpha^{-2} e^2}{4\pi\varepsilon_o a_o} \tag{20.10}$$

$$V = m_e c^2 \tag{20.11}$$

Furthermore, the result of the multiplication of both sides of Eq. (1.55) by $\hbar$, $r_n = n a_0$, and the substitution of $n = \alpha$ yields

$$\hbar\omega_\alpha^* = m_e c^2 \tag{20.12}$$

The relativistic factor,

$$\gamma = \frac{1}{\sqrt{1 - \left(\frac{v}{c}\right)^2}} \tag{20.13}$$

for an orbitsphere at radius r_α^* (αa_o in the case of the electron) is 2π where Eq. (20.13) is transformed from Cartesian coordinates to spherical coordinates. The energy stored in the magnetic field of the electron orbitsphere is

$$E_{mag} = \frac{\pi\mu_o e^2 \hbar^2}{(m_e)^2 r_n^3} \tag{20.14}$$

Eq. (20.15) is the result of the substitution of αa_o for r_n , the relativistic mass, $2\pi m_e$, for m_e, and multiplication by the relativistic correction, α^{-1}, which arises from Gauss's law surface integral and the relativistic invariance of charge.

$$E_{mag} = m_e c^2 \tag{20.15}$$

Thus, the energy stored in the magnetic field of the transition state electron orbitsphere equals the electrical potential energy of the transition state orbitsphere. The magnetic field is a relativistic effect of the electrical field; thus, equivalence of the potential and magnetic energies when $v = c$ is given by Special Relativity where these energies are calculated using Maxwell's Equations. The energy stored in the electric and magnetic fields of a photon are equivalent. The corresponding

equivalent energies of the transition state orbitsphere are the electrical potential energy and the energy stored in the magnetic field of the orbitsphere.

Spacetime is an electrical LC circuit with an intrinsic impedance of exactly

$$\eta = \sqrt{\frac{\mu_o}{\varepsilon_o}} \tag{20.16}$$

The lab frame circumference of the transition state electron orbitsphere is $2\pi\alpha a_o$; whereas, the circumference for the $v = c$ inertial frame is αa_o. The relativistic factor for the radius of αa_o is 2π; thus, due to relativistic length contraction, the total capacitance of free space of the transition state orbitsphere of radius αa_o is

$$C = \frac{2\pi\alpha a_o \varepsilon_o}{2\pi} = \varepsilon_o \alpha a_o \tag{20.17}$$

where ε_o is the capacitance of spacetime per unit length (F/m). Similarly, the inductance is

$$L = \frac{2\pi\alpha a_o \mu_o}{2\pi} = \mu_o \alpha a_o \tag{20.18}$$

where μ_o is the inductance per unit length (H/m).

Thus, the resonance frequency of a transition state electron orbitsphere is

$$\omega = \frac{1}{\sqrt{LC}} = \frac{1}{\sqrt{\varepsilon_o \alpha a_o \mu_o \alpha a_o}} \tag{20.19}$$

Thus,

$$\omega = \frac{m_e c^2}{\hbar} \tag{20.20}$$

Thus, the LC resonance frequency of free space for a transition state electron orbitsphere equals the angular frequency of the photon which forms the transition state orbitsphere.

The impedance of any LC circuit goes to infinity when it is excited at the resonance frequency. Thus, the electron transition state orbitsphere is an LC circuit excited at the corresponding resonance frequency of free space. The impedance of free space becomes infinite, and electromagnetic radiation cannot propagate. At this event, the frequency, wavelength, velocity, and energy of the transition state orbitsphere equals that of the photon. The energy of the photon is equal to the rest mass of the particle at zero potential energy, and charge is conserved. Therefore, a free electron and a free positron each of mass $\frac{\hbar\omega^*}{c^2}$ is produced at infinity relative to the mutual central field of

$$\mathbf{E} = \frac{+e}{4\pi\varepsilon_o r^2} \tag{20.21}$$

where all of the electron transition state orbitsphere equations developed herein apply to this central field. The equation of the free electron is given in the Electron in Free Space Section. The transition state is equivalent to the equation of the photon given in the Photon Equation Section. Photons superimpose; thus, pair production occurs with a single photon of energy equal to twice the rest mass of an electron. Linear momentum is conserved by a third body such as a nucleus which recoils in the opposite direction as the particle pair; thus, permitting pair production to occur.

For pair production, angular momentum is conserved. All photons carry $\pm\hbar$ of angular momentum, and the angular momentum of all matter as orbitspheres is $\pm\hbar$; see Eq. (1.57). The radius of particle creation is αr_1^*. This radius is equal to $\lambda\!\!\!^{-}_c$, the Compton wavelength bar, where $\lambda\!\!\!^{-}_c = \frac{\hbar}{m_e c}$. It arises naturally from the boundary condition of no radiation, Eq. (1.43) and Eq. (20.2) where $n = \alpha$, the de Broglie relationship, Eq. (1.46), and that the velocity of the transition state orbitsphere equals c.

$$r_\alpha^* = \frac{\hbar}{m_e c} = \lambda\!\!\!^{-}_c \tag{20.22}$$

The equations derived for the electron in the present section are generally applicable to all fundamental particles, and it is shown in the Gravity Section that the masses of the fundamental particles are determined by these equations and the curvature of spacetime by matter. During the creation of matter, the constancy of the speed of light must hold which requires relativistic corrections to spacetime. The Schwarzschild metric gives the relationship whereby matter causes relativistic corrections to spacetime that determines the curvature of spacetime and is the origin of gravity. Thus, the creation of matter causes local spacetime to become curved. The geometry of spacetime is transformed from flat (Euclidean) to curved (Riemannian). Time and distances are distorted. At particle production, the proper time of the particle must equal the coordinate time given by Special Relativity for Riemannian geometry affected by the creation of matter of mass m_0 (in the case of pair production, $m_0 = m_e$) where the metric of spacetime is given by the Schwarzschild metric. This boundary condition determines the masses of the fundamental particles.

References

1. Hughes, I. S., Elementary Particles, Cambridge University Press, (1972),

pp. 100-102.
2. Cohen, B., Taylor, B., "The fundamental physical constants", Physics Today, August, (1991), BG 9-BG13.

POSITRONIUM

Pair production, the creation of a positron/electron pair occurs such that the radius of one orbitsphere has a radius infinitesimally greater than the radius of the antiparticle orbitsphere. The inner orbitsphere is held in force balance by a photon such as the case of the proton and neutron (See Proton and Neutron Section). The forces are central, and the radius of the outer orbitsphere (electron or positron) is calculated as follows. The centrifugal force is given by Eq. (1.152). The centripetal electric force of the inner orbitsphere on the outer orbitsphere is given by Eq. (1.153). A second centripetal force is the relativistic corrected magnetic force, $\mathbf{F}_{mag}$, between each point of the particle and the inner antiparticle given by Eq. (1.164) with m_e substituted for m. The force balance equation is given by Eq. (1.165) with m_e substituted for m. Thus,

$$r_1 = \frac{4\pi\varepsilon_0\hbar^2}{e^2\mu} \tag{21.1}$$

where $r_1 = r_2$ is the radius of the positron and the electron and where the reduced mass, μ, is

$$\mu = \frac{m_e}{2} \tag{21.2}$$

The Bohr radius given by Eq. (21.3) and Eq. (21.2) is substituted into Eq. (21.1),

$$a_o = \frac{4\pi\varepsilon_0\hbar^2}{e^2 m_e} \quad \text{, and} \tag{21.3}$$

$$r_1 = 2a_o \tag{21.4}$$

Energy Calculations

The potential energy V between the particle and the antiparticle having the radius r_1 is,

$$V = \frac{-e^2}{4\pi\varepsilon_o r_1} = \frac{-Z^2e^2}{8\pi\varepsilon_o a_o} = -2.18375\ X\ 10^{-18}\ J = 13.59\ eV. \tag{21.5}$$

The calculated ionization energy is $\frac{1}{2}V$ which is

$$E_{ele} = 6.795\ eV. \tag{21.6}$$

The experimental ionization energy is $6.795\ eV$.

Parapositronium, a singlet state hydrogen-like atom comprising an electron and a positron, can absorb a photon which excites the atom to the first triplet state, orthopositronium. In parapositronium, the electron and positron angular momentum vectors are parallel; whereas, the magnetic moment vectors are antiparallel. The opposite relationships exist for orthopositronium. The principal energy levels for

the singlet excited states are given by Eq. (2.22) with the electron reduced mass substituted for the mass of the electron.

$$E_n = \frac{e^2\mu}{8\pi\varepsilon_o a_o n^2} = \frac{6.8}{n^2}\ eV;\quad n \text{ is an integer} \tag{21.7}$$

which are the experimental energy levels. The energy of the transition from parapositronium to orthopositronium is the hyperfine structure interval. Parapositronium possesses orbital angular momentum states corresponding to the quantum number $m_\ell = 0$; whereas, orthopositronium possesses orbital angular momentum states corresponding to $m_\ell = 0,\pm 1$. The orbital angular momentum states of orthopositronium are degenerate in the absence of an applied magnetic field. The magnitude of the central field of the first excited triplet state of positronium is $\frac{1}{2}e$ as given in the Excited States of the One Electron Atom (Quantization) Section and $\mathbf{F}_{mag}$ of Eq. (1.164) with m_e substituted for m is zero for the parallel spins having antiparallel angular momentum vectors. Thus, the radii of the two orbitspheres of the first triplet excited state are given by the force balance equating the centrifugal and centripetal forces:

$$\frac{m_e}{4\pi r_1^2}\frac{v_1^2}{r_1} = \frac{e}{4\pi r_1^2}\frac{1}{2}\frac{Ze}{4\pi\varepsilon_o r_1^2} \tag{21.8}$$

$$r_1 = r_2 = 2a_o \tag{21.9}$$

Thus, E_{ele}, Eq. (21.6) is unchanged from the "ground" state energy. The hyperfine structure interval of positronium can be calculated from the spin/spin coupling energy and the magnetic energy stored in the surface currents produced by the "trapped resonant photon". The spin/spin coupling energy between the inner orbitsphere and the outer orbitsphere is given by Eq. (1.136) where μ_B, the magnetic moment of the outer orbitsphere is given by Eq. (1.137). The magnetic flux, **B**, of the inner orbitsphere at the position of the outer is

$$\mathbf{B} = \frac{\mu_o e\hbar}{2m_e r_2^3} \tag{21.10}$$

Substitution of Eq. (21.10) and (1.137) into Eq. (1.136) gives

$$E = \frac{2\mu_o e^2\hbar^2}{4m_e^2 r_2^3} \tag{21.11}$$

Photons obey Maxwell's Equations. At the two dimensional surface of the orbitsphere containing a "trapped photon", the relationship between the photon's electric field and its charge at the orbitsphere is

$$\mathbf{n}\cdot\left(\mathbf{E}_1 - \mathbf{E}_2\right) = \frac{\sigma}{\varepsilon_0} \tag{21.12}$$

Thus, the photon's electric field acts as surface charge. According to Eq.

(21.12), the photon standing wave in the positronium orbitsphere resonator cavity gives rise to a two dimensional surface charge at the orbitsphere two dimensional surface at r_1^+, infinitesimally greater than the radius of the inner orbitsphere, and r_2^-, infinitesimally less than the radius of the outer orbitsphere. For an electron in a central field, the magnitude of the field strength of the first excited state corresponding to a transition from the state with $n=1$ and radius $2a_o$ to the state with $n=2$ is $\frac{1}{4}e$ as given in the Excited States of the One Electron Atom (Quantization) Section. The energy corresponding to the surface charge which arises from the "trapped photon standing wave" is given by the energy stored in the magnetic fields of the corresponding currents. The surface charge is given by Eq. (21.12) for a central field strength equal in magnitude to $\frac{1}{4}e$. This surface charge possesses the same angular velocity as each orbitsphere; thus, it is a current with a corresponding stored magnetic energy. The energy corresponding to the surface currents, E_{sc}, is the difference of $E_{mag\ \text{internal}}$ and $E_{mag\ \text{external}}$ for a single charge of $\frac{1}{4}e$ substituted into Eqs. (1.125) and (1.127).

$$E_{sc} = \frac{2}{3}\frac{\pi\mu_o e^2\hbar^2}{4^2 m_e^2 r_1^3} - \frac{1}{3}\frac{\pi\mu_o e^2\hbar^2}{4^2 m_e^2 r_1^3} \tag{21.13}$$

The hyperfine structure interval of positronium, E_{HF}, is given by the sum of Eq. (21.11) and Eq. (21.13) where $r_1 = 2a_o$.

$$E_{HF} = \frac{\mu_o e^2\hbar^2}{4m_e^2 8a_0^3} - \frac{\pi\mu_o e^2\hbar^2}{(4^2)(3)m_e^2 8a_0^3} \tag{21.14}$$

Eq. (21.14) is the hyperfine structure interval calculated for an electron or a positron magnetic moment of one Bohr magneton; however, the exact magnetic moment in the case of an orbitsphere includes the electron (fluxon) g factor which is given by Eq. (1.151). Thus, Eq. (21.14) becomes

$$E_{HF} = 2g\frac{\mu_o e^2\hbar^2}{32 m_e^2 a_0^3}\left(1 - \frac{\pi}{12}\right) \tag{21.15}$$

$$E_{HF,calculated} = 8.4111\ X\ 10^{-4}\ eV$$

$$E_{HF,\text{experimental}} = 8.4111\ X\ 10^{-4}\ eV$$

RELATIVITY

Basis of a Theory of Relativity[1]

To describe any phenomenon such as the motion of a body or the propagation of light, a definite frame of reference is required. A frame restricts the maximun sdonsisting of a defined origin and three axes equipped with graduated rules and clocks. Bodies in motion then have definite positions and definite motions with respect to the base. The motion of planets is commonly described in the heliocentric system. The origin is defined as the mass center, and the three axes are chosen to point to three fixed stars to establish the fixed orientation of the axes. In general, the mathematical form of the laws of nature will be different in different frames. For example, the motion of bodies relative to the Earth may be described either in a frame with axes pointing to three fixed stars or in one rigidly fixed to the Earth. In the latter case, Coriolis forces arise in the equations of motion. There exist frames of reference in which the equations of motion have a particular simple form; in a certain sense these are the most "natural" frames of reference. They are the *inertial* frames in which the motion of a body is uniform and rectilinear, provided no forces act on it. In pre-relativistic physics the notion of an inertial systems was related only to the laws of mechanics. Newton's first law of motion is, in fact, nothing but a definition of an inertial frame.

But it is impossible to define absolute velocity, and the speed of light is the conversion factor from time to length. The laws of light propagation play a fundamental part in the definition of the basic concepts relating to space and time. Therefore it proves more correct to relate the notion of an inertial frame not only to the laws of mechanics but also to those of light propagation.

The usual form of Maxwell's equations refers to some inertial frame. It is obvious and has always been assumed, even before relativity, that at least one reference frame exists that is inertial with respect to mechanics and in which at the same time Maxwell's equations are true. The law of propagation of an electromagnetic wave front in the form

$$\frac{1}{c^2}\left(\frac{\partial \omega}{\partial t}\right)^2 - \left[\left(\frac{\partial \omega}{\partial x}\right)^2 + \left(\frac{\partial \omega}{\partial y}\right)^2 + \left(\frac{\partial \omega}{\partial z}\right)^2\right] = 0 \qquad (22.1)$$

also refers to this inertial frame. A frame for which Eq. (22.1) is valid may be called inertial in the electromagnetic sense. A frame that is

---

1 A good reference for the historical concepts of the theory of special relativity which are partially included herein is Fock [1].

inertial both in the mechanical and in the electromagnetic senses will be simply called inertial.

Thus, by the definition we have adopted, an inertial frame which is characterized by the following two properties:

1. In an inertial frame, a body moves uniformly and in a straight line, provided no forces act on it. (The inertial property in the usual mechanical sense.)
2. In an inertial frame, the equation of propagation of an electromagnetic wave front has the form Eq. (22.1). (The inertial property for the field.)

Eq. (22.1) applies not only to the propagation of an electromagnetic wave. The electromagnetic field has no preference over other fields. The maximum speed of propagation of all fields must be the same such that Eq. (22.1) is of universal validity.

The fundamental postulate of the theory of relativity, also called the principle of relativity, asserts that phenomena occurring in a closed system are independent of any non-accelerated motion of the system as a whole. The principle of relativity asserts that the two sequences of events will be exactly the same (at least insofar as they are determined at all). If a process in the original systems can be described in terms of certain functions of the space and time coordinates of the first frame, the same functions of the space and time coordinates of the second frame will describe a process occurring in the copy. *The uniform rectilinear motion of a material system as a whole has no influence on the course of any process occurring within it.*

The theory of relativity is based on two postulates, namely, the principle of relativity and another principle that states that the velocity of light is independent of the velocity of its source. The latter principle is a consequence of the first. The latter principle is implicit in the law of the propagation of an electromagnetic wave front given by Eq. (22.1). The basis for defining inertial reference frames is Eq. (22.1) together with the fact of the uniform rectilinear motion of a body not subject to forces. The principle of relativity holds in the case that the reference frames are inertial.

It is appropriate to give here a generalized interpretation of the law of wave front propagation and to formulate the following general postulate:

There exists a maximum speed for the propagation of any kind of action -- the speed of light in free space.

This principle is very significant because the transmission of signals with greatest possible speed plays a fundamental part in the definition of concepts concerning space and time. The very notion of a definite frame of reference for describing events in space and time depends on the existence of such signals. The principle formulated above, by asserting the existence of a general upper limit for all kinds of action and signal, endows the speed of light with a universal significance, independent of the particular properties of the agency of transmission and reflecting a certain objective property of space-time. This principle has a logical connection with the principle of relativity. For if there was no single limiting velocity but instead different agents, e.g. light and gravitation, propagated in vacuum with different speeds, then the principle of relativity would necessarily be violated as regards at least one of the agents. The principle of the universal limiting velocity can be made mathematically precise as follows:

For any kind of wave advancing with limiting velocity and capable of transmitting signals, the equation of front propagation is the same as the equation for the front of a light wave.

Thus, the equation

$$\frac{1}{c^2}\left(\frac{\delta\omega}{\delta t}\right)^2 - (grad\omega)^2 = 0 \qquad (22.2)$$

acquires a general character; it is more general than Maxwell's equations from which Maxwell originally derived it. As a consequence of the principle of the existence of a universal limiting velocity one can assert the following: the differential equations describing any field that is capable of transmitting signals must be of such a kind that the equation of their characteristics is the same as the equation for the characteristics of light waves. In addition to the governing the propagation of any form of energy, the wave equation governs fundamental particles created from energy and vice versa, the associated effects of mass on spacetime, and the evolution the universe itself. The equation that describes the electron given by Eq. (1.48) is the wave equation, the relativistic correction of spacetime due to particle production travels according to the wave equation as given in the Gravity Section, and the evolution of the universe is according to the wave equation as given in the Gravity Section and the Unification of Spacetime, the Forces, Matter, and Energy Section (Eq. (24.46)).

The presence of a gravitational field somewhat alters the appearance of the equation of the characteristics from the form of Eq. (22.2), but in this case one and the same equation still governs the propagation of all kinds of wave fronts traveling with limiting velocity,

including electromagnetic and gravitational ones. The basis for defining inertial reference frames is Eq. (22.2) asserting the universality of the equation together with the fact of the uniform rectilinear motion of a body not subject to forces.

Let one and the same phenomenon be described in two inertial frames of reference. The question arises of relating measurements in one frame to this in another. For example, consider transforming radar data obtained by a satellite circling the Earth to that recorded on the ground. For such a transformation, the relationship between the space and time coordinates x, y, z and t in the first frame and the corresponding x', y', z' and t' in the second. Before relativity one accepted as self-evident the existence of a universal time t that was the same for all frames. In this case $t' = t$ or $t' = t - t_0$, if a change of time origin was used. Considering two events occurring at t' and τ, the old point of view required the time elapsed between them to be the same in all reference frames so that

$$t - \tau = t' - \tau' \tag{22.3}$$

Furthermore, it was considered to be evident that the length of a rigid rod, measured in the two frames, would have the same value. (This applies equally to the distance between the "simultaneous" positions of two points which need not necessarily be rigidly connected.) Denoting the spatial coordinates of the two ends of the rod (or the two points) by (x, y, z) and (ξ, η, ζ) in the one frame and by (x', y', z') and (ξ', η', ζ') in the other, the old theory required

$$(x-\xi)^2 + (y-\eta)^2 + (z-\zeta)^2 = (x'-\xi')^2 + (y'-\eta')^2 + (z'-\zeta')^2 \tag{22.4}$$

Eqs. (22.3) and (22.4) determine uniquely the general form of the transformation connecting x, y, z and t with x', y', z' and t'. It consists of a change in origin of spatial coordinates and of time, of a rotation of the spherical axes, and of a transformation such as

$$\begin{aligned} x' &= x - V_x t \\ y' &= y - V_y t \\ z' &= z - V_z t \\ t' &= t \end{aligned} \tag{22.5}$$

where V_x, V_x, and V_x are the constants of velocity with which the primed frame moves relative to the unprimed one; more exactly they are the components of this velocity in the unprimed frame. The transformation (Eq. (22.5)) is known as a Galileo transformation. Thus, pre-relativistic physics asserted that, given an inertial frame (x, y, z), space and time coordinates in any other frame moving uniformly and rectilinearly relative to the former are connected by a Galileo transformation, apart from a displacement of the origin.

Galileo transformations satisfy the principle of relativity as far as the laws of (Newtonian) mechanics are concerned, but not in relation to the propagation of light. Indeed the wave front equation changes its appearance when subjected to a Galileo transformation. If Galileo transformations were valid and the Principle of Relativity in its generalized form was not, then there would exist only one inertial system as defined above. The changed form of the wave front equation in any other frame would allow one to detect even uniform rectilinear motion relative to the single inertial system - the "immobile ether" - and to determine the velocity of this motion. Experiments devised to discover such motion relative to the "ether" have unquestionably eliminated the "ether" as a possibility and confirm that the form of the law of wave front propagation is the same in all non-accelerated frames[2]. Therefore the principle of relativity is certainly also applicable to electromagnetic phenomena. It also follows that the Galileo transformation is in general wrong and should be replaced by another. The problem can be stated as follows. Let a reference frame be given which is inertial according to the definition given above (i.e. both mechanically and electromagnetically). The space time coordinates in this frame are given by x, y, z and t. Let the space time coordinates in another inertial frame be given by (x', y', z', t'). The connection between (x,y,z,t) and (x', y', z', t') is to be found. The problem of finding a transformation between two inertial frames is purely mathematical; it can be solved without any further physical assumptions other than the definition of an inertial frame given above. The transformations are given by Lorentz.

---

2 The most famous of such experiments is the Michelson-Morley experiment. In 1887 in collaboration with Edward Morley, Albert Michelson performed an experiment to measure the motion of the Earth through the "ether", a hypothetical medium pervading the universe in which light waves propagated. The notion of the ether was carried over from the days before light waves were recognized as electromagnetic. At that time, the physics community was unwilling to discard the idea that light propagates relative to some universal frame of reference. The extremely sensitive Michelson-Morley experiment could find no motion through an ether, which meant that there could be no ether and no principle of "absolute motion" relative to it. All motion is relative to a specific frame of reference, not a universal one. The experiment which in essence compared the speeds of light parallel to and perpendicular to the Earth's motion around the Sun, also showed that the speed of light is the same for all observers. This is not true in the case of waves that need a material medium in which to occur such as sound and water waves. The experimental results of the Michelson-Morley experiment comprised the basis of a theory by Einstein that stated the impossibility of an absolute reference frame and that the speed of light is a constant maximum for all observers. Thus, the Michelson-Morley experiment set the stage for Einstein's 1905 special theory of relativity as Michelson was reluctant to accept this result.

Lorentz Transformations

A Lorentz transformation is a set of equations for transforming the space and time coordinates in one inertial frame into those of another that moves uniformly and in a straight line relative to the first. The transformation can be characterized by the fact that the quantity

$$ds^2 = dx_0^2 - \left(dx_1^2 + dx_2^2 + dx_3^2\right) \tag{22.6}$$

or

$$ds^2 = c^2dt^2 - \left(dx^2 + dy^2 + dz^2\right) \tag{22.7}$$

remains invariant in the strict sense (not only the numerical value, but also the mathematical form of the expression remain unchanged.) Newtonian mechanics is corrected by Lorentz transformations of the time, length, mass, momentum, and energy of an object. Newtonian mechanics with Galileo transforms give mechanical forces for $v << c$:

$$\mathbf{F} = \frac{d\mathbf{p}}{dt} = \frac{d(m\mathbf{v})}{dt} = m\frac{d\mathbf{v}}{dt} = m\mathbf{a} \tag{22.8}$$

$$T = \frac{1}{2}mv^2 \tag{22.9}$$

In the case that v approaches c, Lorentz transforms apply.

Time Dilation

The relativity of time

The postulates of relativity may be used to derive the Lorentz transformation that described how relative motion affects measurements of time intervals.

A clock that moves with respect to an observer appears to tick less rapidly than it does when at rest with respect to him. That is, if someone is a spacecraft finds that the time interval between two events in the spacecraft is t_0, we on the ground would find that the same interval has the longer duration t. The quantity t_0, which is determined by events that occur *at the same place* in a observer's frame of reference, is called the *proper time* of the interval between the events. When witnessed from the ground, the events that mark the beginning and end of the time interval occur at different places, and as a consequence the duration of the interval appears longer than the proper time. This effect is called time dilation (to dilate is to become larger).

To see how time dilation comes about, let us consider two clocks of the particularly simple kind shown in Figure 22.1.

Figure 22.1. A simple clock. Each "tick" corresponds to a round trip of the light pulse from the lower mirror to the upper one and back.

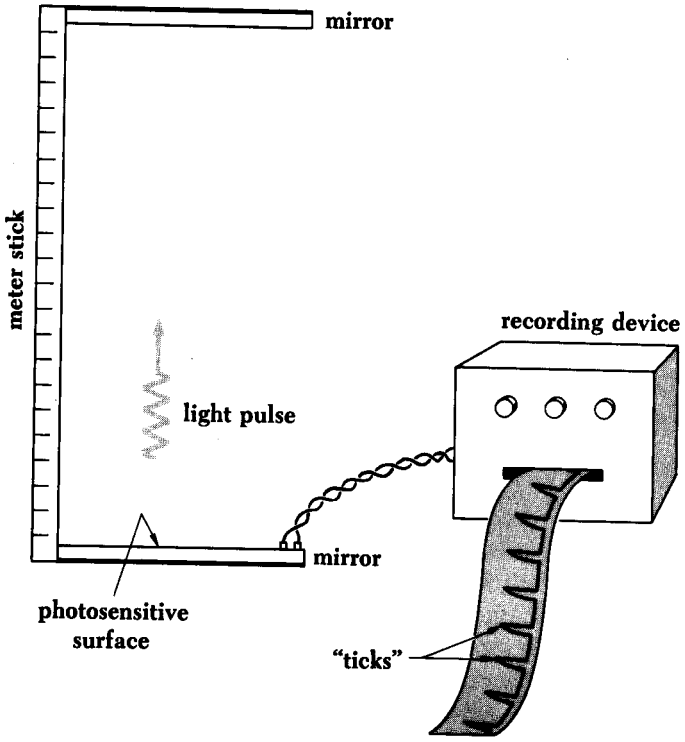

Such a clock consists of a stick L_0 long with a mirror at each end. A pulse of light is reflected up and down between the mirrors, and a device attached to one of them produces a "tick" of some kind each time the light pulse strikes it. Such a device might be a photosensitive coating on the mirror that gives an electric signal when the pulse arrives.

One clock is at rest in a laboratory on the ground and the other is in a spacecraft that moves at the v relative to the ground. An observer in the laboratory watches both clocks and finds that they tick at different rates.

Figure 22.2 shows the laboratory clock in operation. The time interval between ticks is the proper time t_0. The time needed for the light pulse to travel between the mirrors at the speed of light c is $\frac{t_0}{2}$; hence $\frac{t_0}{2} = \frac{L_0}{c}$ and

$$t_0 = \frac{2L_0}{c} \qquad (22.10)$$

Figure 22.3 shows the moving clock with its mirrors perpendicular to the direction of motion relative to the ground.

Figure 22.2. A light-pulse clock at rest on the ground as seen by an observer on the ground. The dial represents a conventional clock on the ground.

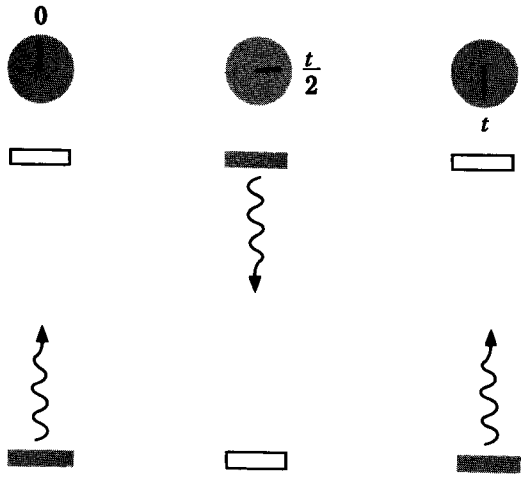

Figure 22.3. A light-pulse clock in a spacecraft as seen by an observer on the ground. The mirrors are parallel to the direction of motion of the spacecraft. The dial represents a conventional clock on the ground.

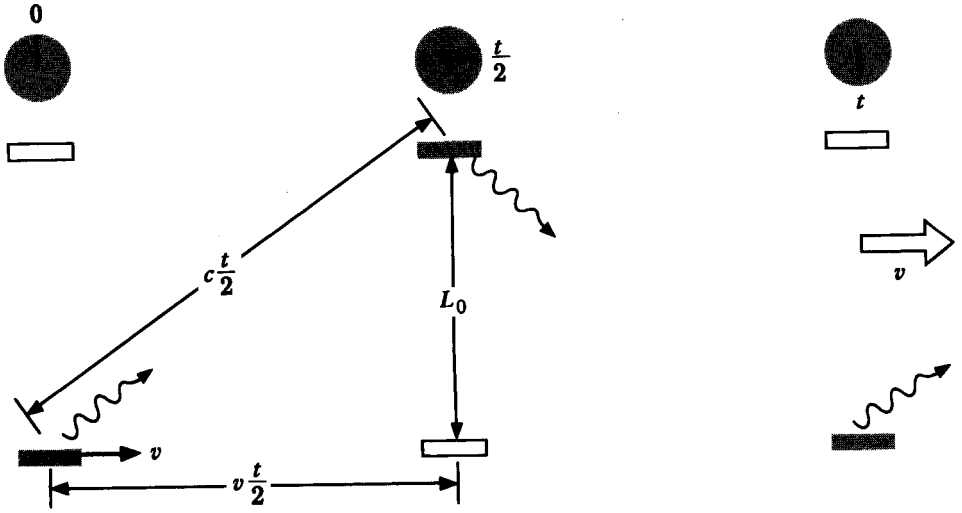

The time interval between ticks is t. Because the clock is moving, the light pulse, as seen from the ground, follows a zigzag path. On its way from the lower mirror to the upper one in the time $\frac{t}{2}$, the pulse travels a horizontal distance of $v\frac{t}{2}$ and a total distance of $c\frac{t}{2}$. Since L_0 is the vertical distance between the mirrors,

$$\left(c\frac{t}{2}\right)^2 = L_0^2 + \left(v\frac{t}{2}\right)^2 \tag{22.11}$$

$$\frac{t^2}{4}\left(c^2 - v^2\right) = L_0^2 \tag{22.12}$$

$$t^2 = \frac{4L_0^2}{c^2 - v^2} = \frac{\left(2L_0\right)^2}{c^2\left(1 - \frac{v^2}{c^2}\right)} \tag{22.13}$$

$$t = \frac{\frac{2L_0}{c}}{\sqrt{1 - \frac{v^2}{c^2}}} \tag{22.14}$$

But $\frac{2L_0}{c}$ is the time interval t_0 between ticks on the clock on the ground, as in Eq. (22.10), and so the **time dilation relationship** is

$$t = \frac{t_0}{\sqrt{1 - \frac{v^2}{c^2}}} \tag{22.15}$$

wherein the parameters are:

t_0 = time interval on clock at rest relative to an observer
t = time interval on clock in motion relative to an observer
v = speed of relative motion
c = speed of light

Because the quantity $\sqrt{1 - \frac{v^2}{c^2}}$ is always smaller than 1 for a moving object, t is always greater than t_0. The moving clock in the spacecraft appears to tick at a slower rate than the stationary one on the ground, as seen by an observer on the ground.

Exactly the same analysis holds for measurements of the clock on the ground by the pilot of the spacecraft. To him, the light pulse of the ground clock follows a zigzag path that requires a total time t per round trip. His own clock, at rest in the spacecraft, ticks at intervals of t_0. He too finds that

$$t = \frac{t_0}{\sqrt{1 - \frac{v^2}{c^2}}} \tag{22.16}$$

so the effect is reciprocal: (every observer finds that clocks in motion relative to him tick more slowly than clocks at rest relative to him.

The Lorentz transformation of time, length, mass, momentum, and energy which are significant when v approaches c can be derived by a similar procedure [2]. The Lorentz transformations are:

$$t = \frac{t_0}{\sqrt{1-\frac{v^2}{c^2}}} \tag{22.17}$$

$$l = l_o\sqrt{1-\frac{v^2}{c^2}} \tag{22.18}$$

$$m = \frac{m_0}{\sqrt{1-\frac{v^2}{c^2}}} \tag{22.19}$$

$$p = \frac{m_0 v}{\sqrt{1-\frac{v^2}{c^2}}} \tag{22.20}$$

$$E = mc^2 = \frac{m_0 c^2}{\sqrt{1-\frac{v^2}{c^2}}} \tag{22.21}$$

$$E^2 = m_0^2 c^4 + p^2 c^2 \tag{22.22}$$

When speaking of the relativity of a frame of reference or simply of relativity, one usually means that there exist identical physical processes in different frames of reference. According to the generalized Galilean principle of relativity identical processes are possible in all inertial frames of reference related by Lorentz transformations. On the other hand, Lorentz transformations characterize the uniformity of Galilean space-time.

The Relativity Principle and the Covariance of Equations in Galilean or Euclidean Spacetime and Riemann Spacetime

From the geometrical point of view the theory of space and time naturally divides into the theory of uniform, Galilean, space and the theory of non-uniform, Riemannian, space.

Galilean space is of maximal uniformity. This means that in it:

(a) All points in space and instants in time are equivalent.

(b) All directions are equivalent, and

(c) All inertial systems, moving uniformly and in a straight line relative to one another, are equivalent (Galilean principle of relativity).

The uniformity of space and time manifests itself in the existence of a group of transformations which leave invariant the four-

dimensional distance or interval between two points. The expression for this interval plays an important part in the theory of space and time because its form is directly related to the form taken by the basic laws of physics, viz. the law of motion of a free mass-point and the law of propagation in free space of the front of a light wave.

The indications (a), (b) and (c) of the uniformity of Galilean space are related to the following transformations:

(a) To the equivalence of all points and instants corresponds the transformation of displacing the origins of the spatial coordinates and of time; the transformation involves four parameters, namely, the three space coordinates and the time coordinate of the origin.

(b) To the equivalence of all directions corresponds the transformation of rotating the spatial coordinate axes, this involves three parameters, the three angles of rotation.

(c) To the equivalence of inertial frames corresponds a change from one frame of reference to another moving uniformly in a straight line with respect to the first: this transformation involves three parameters, the three components of relative velocity.

The most general transformation involves ten parameters. This is the Lorentz transformation. It is well known that in a space of n dimensions the group of transformations which leave invariant the expression for the squared distance between infinitely near points, can contain at most $\frac{1}{2}n(n+1)$ parameters. If there is a group involving all $\frac{1}{2}n(n+1)$ parameters then the space is of maximal uniformity; it may be a space of constant curvature, or, if the curvature vanishes, a Euclidean or pseudo-Euclidean space.

In the case of space-time the number of dimensions is four and therefore the greatest possible number of parameters is ten. This is also the number of parameters in the Lorentz transformation, so that Galilean space, to which the transformation relates, is indeed of maximal uniformity. It is customary to call the theory based on the Lorentz transformations the special theory of relativity. More precisely, the subject of that theory is the formulation of physical laws in accordance with the properties of Galilean space.

A formulation of the principle of relativity given *supra*. which

together with the postulate that the velocity of light has a limiting character, may be made the basis of relativity theory. We shall now investigate in more detail the question of the connection of the physical principle of relativity with the requirement that the equations be covariant.

In the first place, we shall attempt to give a generally covariant formulation of the principle of relativity, without as yet making this concept more precise. In its most general form, the principle of relativity states the equivalence of the coordinate systems (or frames of reference) that belong to a certain class and are related by transformations of the form

$$x'_\alpha = f_\alpha(x_0, x_1, x_2, x_3) \tag{22.23}$$

which may be stated more briefly as

$$x = f(x) \tag{22.24}$$

It is essential to remember that, in addition to the group of permissible transformations, the class of coordinate systems must be characterized by certain supplementary conditions. Thus, for instance, if we consider Lorentz transformations, it is self-evident that these linear transformations must connect not any arbitrary coordinates, but only the Galilean coordinates in two inertial reference frames. To consider linear transformations between any other (non-Galilean) coordinates has no sense, because the Galilean principle of relativity has no validity in relation to such artificial linear transformations. On the other hand, if one introduces any other variables in place of the Galilean coordinates, a Lorentz transformation can evidently be expressed in terms of these variables, but then the transformation formulae will have a more complicated form.

Let us now state more precisely what is meant in the formulation of the principle of relativity by equivalence of reference frames. Two reference frames (x) and (x') may be called physically equivalent if phenomena proceed in the same way in them. This means that if a possible process is described in the coordinates (x) by the functions

$$\phi_1(x),\ \phi_2(x),\ ...,\ \phi_n(x) \tag{22.25}$$

then there is another possible process which is describable by the same functions

$$\phi_1(x'),\ \phi_2(x'),\ ...,\ \phi_n(x') \tag{22.26}$$

in the coordinates (x'). Conversely any process of the form Eq. (22.26) in the second system corresponds to a possible process of the form Eq. (22.25) in the first system. Thus a relativity principle is a statement concerning the existence of corresponding processes in a set of reference frames of a certain class; the systems of this class are then accepted as equivalent. It is clear from this definition that both the

principle of relativity itself and the equivalence of two reference frames are physical concepts, and the statement that the one or the other is valid involves a definite physical hypothesis and is not just conventional. In addition, it follows that the very notion of a "principle of relativity" becomes well defined only when a definite class of frames of reference has been singled out. In the usual theory of relativity this class is that of inertial systems.

The functions Eq. (22.25) or Eq. (22.26) describing a physical process will be called field functions or functions of state. In a generally covariant formulation of the equations describing physical processes the components $g_{\mu\nu}$ of the metric tensor must be included among the functions of state such as the collection of field functions:

$$F_{\mu\nu}(x), \qquad j_{\nu}(x), \qquad g_{\mu\nu}(x) \tag{22.27}$$

i.e. the electromagnetic field, the current vector, and the metric tensor, respectively. The requirement entering the formulation of a principle of relativity that in two equivalent reference frames corresponding phenomena should proceed in the same way applies equally to the metric tensor. Thus, if we compare two corresponding phenomena in to physically equivalent reference frames, then for the first phenomenon, described in the old coordinates, not only the components of electromagnetic field and of current density, but also the components of the metric tensor must have the same mathematical form as for the second phenomenon described in the new coordinates.

What can be concluded further will depend on whether we assume that the metric is fixed or whether we take into consideration phenomena which themselves influence the metric. In the usual theory of relativity it is assumed that the metric is given once and for all and does not depend on any physical processes. The generally covariant formulation of the theory of relativity does not change anything in this. As long as the assumption remains in force that the character of space-time is Galilean and the $g_{\mu\nu}$ are introduced only to achieve general covariance, these quantities will depend only on the choice of coordinate system, not on the nature of the physical process discussed. They are functions of state only in a formula sense. In the theory of gravitation on the other hand, a different assumption is made concerning the nature of spacetime. There the $g_{\mu\nu}$ are functions of state, not only in a formal sense, but in fact: they describe a certain physical field, namely the field of gravitation.

To give a definite meaning to the principle of relativity in such circumstances, it is essential to specify more closely not only the class of coordinate systems, but also the nature of the physical processes for which the principle is being formulated. We shall first start from the

assumption that the metric is fixed ("rigid"), or else that it may be considered as fixed for a certain class of physical processes. We return to the above definition of corresponding phenomena in two physically equivalent coordinate systems, according to which all field functions, including the components of the metric tensor, must have the same mathematical form for the first process described in the old coordinates as for the second process described in the new coordinates. If the $g_{\mu\nu}$ are independent of the nature of the physical phenomenon, then in relation to those quantities we need not make a distinction between the first and second process, and need consider only transformations of the coordinates. But then the quantities

$$g_{\mu\nu}(x) \quad \text{and} \quad g'_{\mu\nu}(x') \tag{22.28}$$

will be connected by the tensor transformation rule; the requirement of the relativity principle that they should have one and the same mathematical form reduces (for infinitesimal coordinate transformations) to the equations $\delta g_{\mu\nu} = 0$.

We know that the most general class of transformations that satisfies these equations contains 10 parameters and is possible only in uniform space-time, where the relation

$$R_{\mu\nu,\alpha\beta} = K\ (g_{\nu\alpha}g_{\mu\beta} - g_{\mu\alpha}g_{\nu\beta}) \tag{22.29}$$

is valid. (A space in which the curvature tensor $R_{\mu\nu,\alpha\beta}$ has the form of Eq. (22.29) is called a space of constant curvature; it is a four-dimensional generalization of Friedmann-Lobachevsky space. The constant K is called the constant of curvature.) If in these relations K is zero, the space-time is Galilean and the transformations in questions are Lorentz transformations, except when other (non-Galilean) coordinates are used.

Thus with the rigidity assumption for the metric, the principle of relativity implies the uniformity of space-time, and if the additional condition $K = 0$ holds, we obtain a Galilean metric in appropriate coordinates. The relativity principle in general form then reduces to the Galilean relativity principle. As for the condition $K = 0$, it results in an additional uniformity of space-time; if the scale of the Galilean coordinates is changed, then the scale of the elementary interval changes in the same proportion. This property implies in turn that there is no absolute scale for space-time, unlike the absolute scale that exists for velocities in terms of the velocity of light; the absence of an absolute scale for space-time leads conversely to the equation $K = 0$.

If we now go over to discuss phenomena which may influence the metric, we must reckon with the possibility that under certain conditions the principle of relativity will be valid in non-uniform space also. For this to be so, it is necessary that the motion of the masses

producing the non-uniformity be included in the description of the phenomena.

It can be shown that under the assumption that space-time is uniform at infinity (where it must be Galilean) one can single out a class of coordinate systems that are analogous to inertial systems and defined up to a Lorentz transformation. In relation to this class of coordinate systems a principle of relativity will hold in the same form as in the usual theory of relativity, in spite of the fact that a finite distance from the masses the space is non-uniform. Here however one must bear in mind the essential role played by the boundary conditions that require uniformity at infinity. Thus in the last analysis the relativity principle is here also a result of uniformity.

Since the greatest possible uniformity is expressed by Lorentz transformations there cannot be a more general principle of relativity than that discussed in ordinary relativity theory. Moreover, there cannot be a general principle of relativity, as a physical principle, which would hold with respect to arbitrary frames of reference. In order to make this fact clear, it is essential to distinguish sharply between a physical principle that postulates the existence of corresponding phenomena in different frames of reference and the simple requirement that equations should be covariant in the passage from one frame of reference to another. It is clear that a principle of relativity implies a covariance of equations, but the converse is not true: covariance of differential equations is possible also when no principle of relativity is satisfied. Covariance of equations in itself is in no way the expression of any kind of physical law. For instance, in the mechanics of systems of mass-points, Lagrange's equations of the second kind are covariant with respect to arbitrary transformations of the coordinates, although they do not express any new physical law compared to, for instance, Lagrange's equations of the first kind, which are stated in Cartesian coordinates and are not covariant. In the case of Lagrange's equations, covariance is achieved by introducing as new auxiliary functions the coefficients of the Lagrangian considered as an expression quadratic, but not necessarily homogeneous in the velocities. Quite apart from the fact that not all laws of nature reduce to differential equations, even fields described by differential equations require for their definitions not only these equations, but also all kinds of initial, boundary and other conditions. These conditions are not covariant. Therefore, the preservation of their physical content requires a change in their mathematical form and, conversely, preservation of their mathematical form implies a change of their physical content. But, the realization of a process with a new physical content is an independent question which cannot be solved *a priori*. If within a given class of reference systems

"corresponding" physical processes are possible, then a principle of relativity holds. In the opposite case it does not. It is clear, however, that such a model representation of physical processes, and in particular such a model representation of the metric, is possible at most for a narrow class of reference systems, and certainly cannot be unlimited. This argument shows once again (without invoking the concept of uniformity) that a general principle of relativity, as a physical principle, holding in relation to arbitrary frames of reference, is impossible.

But as a motivation of the requirement of covariance of the equations a general principle of relativity is also unnecessary. The covariance requirement can be justified independently. It is a self-evident, purely logical requirement that in all cases in which the coordinate system is not fixed in advance, equations written down in different coordinate systems should be mathematically equivalent. The class of transformations with respect to which the equations must be covariant must correspond to the class of coordinate systems considered. Thus if one deals with inertial systems related by Lorentz transformations and if Galilean coordinates are used, it is sufficient to require covariance with respect to Lorentz transformations. If , however, arbitrary coordinates are employed, it is necessary to demand general covariance.

It should be noted that covariance of coordinate systems acquires definite physical meaning if, and only if, a principle of relativity exists for the class of reference frames used. Such is the covariance with respect to Lorentz transformations. This concept was so useful in the formulation of physical laws because it contains concrete temporal and geometric elements (rectilinearity and uniformity of motion) and also dynamic elements (the concept of inertia in the mechanical and the electromagnetic sense). Because of this, it is related to the physical principle of relativity and itself becomes concrete and physical.

If, however, in place of the Lorentz transformations one discusses arbitrary transformations, one ceases to single out that class of coordinate systems relative to which the principle of relativity exists, and by doing this one destroys the connection between physics and the concept of covariance. There remains a purely logical side to the concept of covariance as a consistency requirement on equations written in different coordinate systems. Naturally this requirement is necessary, and it can always be satisfied.

In dealing with classes of reference frames that are more general than that relative to which a principle of relativity holds, the necessity arises of replacing the explicit formulation of the principle by some other statement. The explicit formulation consists in indicating a class of physically equivalent frames of reference; the new formulation must

express those properties of space and time by virtue of which the principle of relativity is possible. With the assumption of a rigid metric this is achieved by introducing an additional Eq. (22.29). With the additional assumption of the absence of a universal scale ($K=0$) these equations lead to a generally covariant formulation of the theory of relativity, without any alteration of its physical content. The Galileo-Lorentz principle of relativity is then maintained to its full extent.

The very possibility of formulating the ordinary theory of relativity in a general covariant form shows particularly clearly the difference between the principle of relativity as a physical principle and the covariance of the equations as a logical requirement. In addition, such a formulation opens the way to generalizations based on a relaxation of the assumption of a rigid metric. This relaxation provides the possibility of replacing the supplementary conditions Eq. (22.29) by others which reflect better the properties of space and time. This leads us to the theory of gravitation.

Universal gravitation does not fit into the framework of uniform Galilean space because not only the inertial mass, but also the gravitational mass of a body depends on its energy. In the latter case, it is possible to ameliorate the effects of gravity by transforming to an accelerating frame of reference. A theory of universal gravitation is derived below wherein Euclidean, or rather pseudo-Euclidean, geometry is abandoned in favor of the geometry of Riemann.

In Riemannian geometry the new functions at our disposal are the coefficients $g_{\mu\nu}$ of the quadratic form for the squared infinitesimal distance. The law according to which these functions transform in passing to a new coordinate system follows from their definition as coefficients of a quadratic form, together with the condition that this form is an invariant; in the following we shall always assume that a transformation of the coordinates is accompanied by a transformation of the metric $g_{\mu\nu}$ according to this law. The set of quantities metric $g_{\mu\nu}$ is called the metric tensor.

Having introduced the metric tensor, one can form expressions that are covariant with respect to any coordinate transformation. If we consider only those metric tensors which are obtainable from a particular one (e.g. from the Galilean tensor) by coordinate transformation, this will give us nothing new except the fact that our equations are covariant. But, if we extend the discussion to metric tensors of a more general form, tensors which cannot be transformed into one another by coordinate transformations, the generalization so obtained is an essential one. In this case, the metric tensor will express not only properties of the coordinate system but also properties of

space, and the latter can be related to the phenomenon of gravitation. It is shown below that the origin of gravity is the relativistic correction of spacetime itself as opposed to the relativistic correction of mass, length, and time of objects of inertial frames in constant relative motion. The production of a massive particle from a photon with zero rest mass traveling at the speed of light requires time dilation and length contraction of spacetime. The present theory of gravity also maintains the constant maximum speed of light for the propagation of any form of energy.

Having clarified the concept of covariance as applied to Riemannian geometry, let us now consider it together with the previously discussed concept of the uniformity of space. As was shown above, the property of uniformity in Galilean space manifests itself in the existence of transformations that leave unchanged the expression for the four-dimensional distance between two points. More precisely, these transformations leave unchanged the coefficients of this expression, i.e. the quantities $g_{\mu\nu}$. If the $g_{\mu\nu}$ are functions of the coordinates we mean by this that the mathematical form of these functions is unchanged: the dependence of the new $g_{\mu\nu}$ on the new coordinates has the same mathematical form as that of the old $g_{\mu\nu}$ on the old coordinates. In the general case of Riemannian geometry, there are no transformations that leave the $g_{\mu\nu}$ unchanged because Riemannian space is not uniform. One deals with transformations of coordinates accompanied by transformations of the $g_{\mu\nu}$, and neither such a combined transformation nor covariance with respect to it, has any relation to the uniformity or non-uniformity of space.

The geometrical properties of real physical space and time correspond not to Euclidean but to Riemannian geometry. Any deviation of geometrical properties from their Euclidean, or to be precise, pseudo-Euclidean form appears in Nature as a gravitational field. The geometrical properties are inseparably linked with the distribution and motion of ponderable matter. This relationship is mutual. On the one hand the deviations of geometrical properties from the Euclidean are determined by the presence of gravitating masses, on the other, the motion of masses in the gravitational field is determined by these deviations. In short, masses determine the geometrical properties of space and time, and these properties determine the movement of the masses. The description of the gravitational field demands the introduction of no functions other than the metric tensor itself which is uniquely determined by the presence and motion of matter. Differing from other kinds of forces, gravity which influences the motion of the matter by determining the properties of space-time, is itself described

by the metric of space-time. For this principle of relativity, the class of coordinate systems relative to which the principle of relativity exists is the spherical coordinate systems. Spherical harmonic coordinates arise naturally due to the spherical symmetry of the particle production (energy/matter conversion) event and its effect on spacetime and provide the connection between physics and the concept of covariance as shown in the Gravity Section.

References

1. Fock, V., The Theory of Space, Time, and Gravitation, The MacMillan Company, (1964).
2. Beiser, A., Concepts of Modern Physics, Fourth Edition, McGraw-Hill Book Company, New York, (1978), pp. 2-40.

GRAVITY

QUANTUM GRAVITY OF FUNDAMENTAL PARTICLES

The attractive gravitational force has been the subject of investigation for centuries. Traditionally, gravitational attraction has been investigated in the field of astrophysics applying a large scale perspective of cosmological spacetime, as distinguished from currently held theories of atomic and subatomic structure. However, gravity originates on the atomic scale. In Newtonian gravitation, the mutual attraction between two particles of masses m_1 and m_2 separated by a distance r is

$$\mathbf{F} = G\frac{m_1 m_2}{r^2} \tag{23.1}$$

where G is the gravitational constant, its value being $6.67\ X\ 10^{-11}\ Nm^2kg^{-2}$. Although Newton's theory gives a correct quantitative description of the gravitational force, the most elementary feature of gravitation is still not well defined. What is the most important feature of gravitation in terms of fundamental principles? By comparing Newton's second law,

$$\mathbf{F} = m\mathbf{a} \tag{23.2}$$

with his law of gravitation, we can describe the motion of a freely falling object by using the following equation:

$$m_i\mathbf{a} = m_g\frac{GM}{r^3}\mathbf{r} \tag{23.3}$$

where m_i and m_g represent respectively the object's inertial mass (inversely proportional to acceleration) and the gravitational mass (directly proportional to gravitational force), M is the gravitational mass of the Earth, and r is the position vector of the object taken from the center of the Earth. The above equation can be rewritten as

$$\mathrm{a} = \frac{m_g}{m_i}\left(\frac{GM}{r^2}\right) \tag{23.4}$$

Extensive experimentation dating from Galileo's Pisa experiment to the present has shown that irrespective of the object chosen, the acceleration of an object produced by the gravitational force is the same, which from Eq. (23.4) implies that the value of m_g / m_i should be the same for all objects. In other words, we have

$$\frac{m_g}{m_i} = \text{universal constant} \tag{23.5}$$

the equivalence of the gravitational mass and the inertial mass- the fractional deviation of Eq. (23.5) from a constant is experimentally confirmed to less $1\ X\ 10^{-11}$ [1]. In physics, the discovery of a universal constant often leads to the development of an entirely new theory. From the universal constancy of the velocity of light c, the special theory of

relativity was derived; and from Planck's constant h, the quantum theory was deduced. Therefore, the universal constant m_g / m_i should be the key to the gravitational problem. The theoretical difficulty with Newtonian gravitation is to explain just why relation, Eq. (23.5), exists implicitly in Newton's theory as a separate law of nature besides Eqs. (23.1) and (23.2). Furthermore, discrepancies between certain astronomical observations and predictions based on Newtonian celestial mechanics exist, and they apparently could not be reconciled until the development of Einstein's theory of general relativity which can be transformed to Newtonian gravitation on the scale in which Newton's theory holds.

Einstein's general relativity is the geometric theory of gravitation developed by Albert Einstein, whereby he intended to incorporate and extend the special theory of relativity to accelerated frames of reference. Einstein's theory of general relativity is based on a flawed dynamic formulation of Galileo's law. Einstein took as the basis to postulate his gravitational field equations a certain kinematical consequence of a law which he called the "Principle of Equivalence" which states that it is impossible to distinguish a uniform gravitational field from an accelerated frame. However, the two are not equivalent since they obviously depend on the direction of acceleration relative to the gravitation body and the distance from the gravitating body since the gravitational force is a central force. (In the latter case, only a line of a massive body may be exactly radial, not the entire mass.) And, this assumption leads to conflicts with special relativity. The success of Einstein's gravity equation can be traced to a successful solution which arises from assumptions and approximations whereby the form of the solution ultimately conflicts with the properties of the original equation, no solution is consistent with the experimental data in the case of the possible cosmological solutions of Einstein's general relativity. Furthermore, Einstein's general relativity is a partial theory in that it deals with matter on a cosmological scale, but not an atomic scale. All gravitating bodies are composed of matter and are collections of atoms which are composed of fundamental particles such as electrons, which are leptons, and quarks which make up protons and neutrons. Gravity originates from the fundamental particles.

The popular theory of Einstein has as its foundation that gravity is a force unique from electromagnetism. The magnetic force was unified with the Coulomb force by Maxwell. Lorentz derived the transformations named after him which formalize the origin of the magnetic force as a relativistic a relativistic correction of the Coulomb force. The unification of electricity and magnetism by Maxwell permitted him to derive a wave equation which predicted the propagation of electromagnetic waves at the speed of light. Maxwell's

wave equation defines a four dimensional spacetime and the speed of light as a maximum permitted according to the permeability and permittivity of spacetime. Minkowski originated the concept of a four dimensional spacetime formally expressed as the Minkowski tensor [2]. The Minkowski tensor corresponds to the electromagnetic wave equation derived by Maxwell and can be derived from it [3]. Special relativity is implicit in the wave equation of electromagnetic waves that travel at the speed of light. The generalization of this metric to mass as well as charge requiring application of Lorentz transformations comprises the theory of special relativity which is credited to Einstein[3]. The Lorentz transformations quantify the increase in mass, length contraction, and time dilation in the direction of constant relative motion of separate inertial frames. Einstein's goal was to generalize relativity to accelerated frames of reference as well as inertial frames moving at constant relative velocity. But, gravity is not a force separable from electromagnetism. The true origin of gravity is the relativistic correction of spacetime itself as opposed to the relativistic correction of mass, length, and time of objects of inertial frames in constant relative motion. The production of a massive particle from a photon with zero rest mass traveling at the speed of light requires time dilation and length contraction of spacetime. The present theory of gravity also maintains the constant maximum speed of light for the propagation of any form of energy. And, the origin of the gravitational force is also a relativistic correction. In the metric which arises due to the presence of mass, spacetime itself must be relativistically corrected as a consequence of the presence of mass in order to that 1.) the speed of light is constant and a maximum, 2.) the angular momentum of a photon, $\hbar$, is conserved, and 3.) the energy of the photon is conserved as mass. Spacetime must undergo time dilation and length contraction due to the production event. The event must be spacelike even though the photon of the particle production event travels at the speed of light and the particle must travel at a velocity less that the speed of light. The relativistically altered spacetime gives rise to a gravitational force between separated masses. Thus, the production of matter and its motion alters spacetime and the altered spacetime effects the motion of matter which must follow geodesics.

When speaking of the relativity of a frame of reference or simply

---

3 In 1900 Lorentz conjectured that gravitation could be attributed to actions which propagate with the velocity of light. Poincare', in a paper in July 1905 (submitted days before Einstein's special relativity paper), suggested that all forces should transform according to Lorentz transformations. In this case, he notes that Newton's Law of Gravitation is not valid and proposed gravitational waves which propagated with the velocity of light.

of relativity, one usually means that there exist identical physical processes in different frames of reference. According to the generalized Galilean principle of relativity identical processes are possible in all inertial frames of reference related by Lorentz transformations. On the other hand, Lorentz transformations characterize the uniformity of Galilean space-time. Using the four-dimensional coordinates x^{μ} for describing the events and the world-line in spacetime the separation of proper time between two events x^{μ} and $x^{\mu} + dx^{\mu}$ is

$$d\tau^2 = -g_{\mu\nu} dx^{\mu} dx^{\nu} \tag{23.6}$$

where $g_{\mu\nu}$ is the metric tensor which determines the geometric character of spacetime. For different coordinate systems, the dx^{μ} may not be the same, but the separation $d\tau^2$ remains unchanged.
The metric $g_{\mu\nu}$ for Euclidean space called the Minkowski tensor $\eta_{\mu\nu}$ is

$$\eta_{\mu\nu} = \begin{pmatrix} -1 & 0 & 0 & 0 \\ 0 & \frac{1}{c^2} & 0 & 0 \\ 0 & 0 & \frac{1}{c^2} & 0 \\ 0 & 0 & 0 & \frac{1}{c^2} \end{pmatrix} \tag{23.7}$$

In this case, the separation of proper time between two events x^{μ} and $x^{\mu} + dx^{\mu}$ is

$$d\tau^2 = -\eta_{\mu\nu} dx^{\mu} dx^{\nu} \tag{23.8}$$

A spherically symmetrical system of mass m_0 applies to the production of a particle which implies spherical coordinates with the origin at 0. Thus, a family of curved surfaces, each with constant r, is a series of concentric spheres on which it is natural to adopt the coordinate r so that a sphere with constant r has area $4\pi r^2$, and the metric on the surface of the sphere would then be

$$ds^2 = r^2 d\theta^2 + r^2 \sin^2\theta d\phi^2 \tag{23.9}$$

Such a definition of r is no longer the distance from the origin to the surface, because of the spacetime contraction caused by the mass m_0.
The form of the out going gravitational field front traveling at the speed of light is

$$f\left(t - \frac{r}{c}\right) \tag{23.10}$$

Therefore the spatial metric should be expressed as

$$ds^2 = f(r)^{-1} dr^2 + r^2 d\theta^2 + r^2 \sin^2\theta d\phi^2 \tag{23.11}$$

In addition, the existence of mass m_0 also causes time dilation of spacetime such that the clock on each r-sphere is no longer observed from each r-sphere to run at the same rate. Therefore, the general form

of the metric due to the relativistic effect on spacetime due to mass m_0 is

$$d\tau^2 = f(r)dt^2 - \frac{1}{c^2}\left[f(r)^{-1}dr^2 + r^2 d\theta^2 + r^2 \sin^2\theta d\phi^2\right] \tag{23.12}$$

In the case where $m_0 = 0$, space would be flat which corresponds to

$$f(r) = f(r)^{-1} = 1 \tag{23.13}$$

Then the spacetime metric is the Minkowski tensor. In the case that the mass m_0 is finite, the Minkowski tensor is corrected by the time dilation and length contraction of spacetime.

The creation of a particle from light requires that the event to be spacelike; yet, particle production arises from a photon traveling at the speed of light. At production, the particle must have a finite velocity called the Newtonian gravitational velocity according to Newton's Law of Gravitation that may not exceed the speed of light. The Newtonian gravitational velocity must have an associated gravitational energy. The photon initially traveling at the speed of light undergoes particle production and must produce a gravitational field that travels at the speed of light. The gravitational energy associated with the field must have an inverse radius dependence according to the spreading wave. Since the gradient of the gravitational energy gives rise gravitational field, the gravitational field must have an inverse radius squared dependence. In order that the velocity of light does not exceed c in any frame including that of the particle having a finite Newtonian gravitational velocity, the laboratory frame of an incident photon, and that of a gravitational field propagating outward at the speed of light spacetime must undergo time dilation and length contraction due to the production event. During particle production the speed of light as a constant maximum as well as phase matching and continuity conditions require the following form of the squared displacements due to constant motion along two orthogonal axes in polar coordinates:

$$(c\tau)^2 + (v_g t)^2 = (ct)^2 \tag{23.14}$$

$$(c\tau)^2 = (ct)^2 - (v_g t)^2 \tag{23.15}$$

$$\tau^2 = t^2\left(1 - \frac{v_g}{c}\right)^2 \tag{23.16}$$

Thus,

$$f(r) = \left(1 - \frac{v_g}{c}\right)^2 \tag{23.17}$$

(The derivation and result of spacetime time dilation is analogous to the derivation and result of special relativistic time dilation given by Eqs. (22.11-22.15).) Therefore, the general form of the metric due to the relativistic effect on spacetime due to mass m_0 is

$$d\tau^2 = \left(1 - \left(\frac{v_g}{c}\right)^2\right) dt^2 - \frac{1}{c^2}\left(1 - \left(\frac{v_g}{c}\right)^2\right)^{-1} dr^2 + r^2 d\theta^2 + r^2 \sin^2\theta d\phi^2 \qquad (23.18)$$

The gravitational energy of a particle during production given by Newton's Law of Gravitation may be unified with the inertial and electromagnetic energies given by Planck's equation and Maxwell's equations, respectively. The physical basis is the law of Galileo that in the absence of a resistive medium all bodies fall equally fast, or, more accurately, with equal acceleration. The law of Galileo can be stated in generalized form as the law of the equality of inertial and gravitational mass. The equivalence of the Planck equation, electric potential, and the stored magnetic energies occurs for a transition state orbitsphere during pair production as shown in the Pair Production Section. During particle production the transition state orbitsphere has a charge density function σ given by

$$\sigma = \frac{e}{4\pi r^2}\delta(r - r_n) \qquad (23.19)$$

where e is the fundamental charge. The corresponding mass density function is

$$\mu = \frac{m_0}{4\pi r^2}\delta(r - r_n) \qquad (23.20)$$

where mass m_0 is the rest mass of the particle produced. In both cases, the radius, r_n, is the Compton wavelength bar, $\lambda\!\!\!^{-}_C$, given by

$$\lambda\!\!\!^{-}_C = \frac{\hbar}{m_0 c} = r_\alpha^* \qquad (23.21)$$

Consider the definition of the gravitational radius, α_G or r_G, of an orbitsphere of mass m_0 defined as

$$\alpha_G = r_G = \frac{Gm_0}{c^2} \qquad (23.22)$$

where G is the Newtonian gravitational constant. Notice that as m_0 increases the gravitational radius r_G increases (i.e. the curvature of spacetime increases), and the radius of the transition state orbitsphere, r_α^*, decreases. Remarkably, when the $r_G = r_\alpha^* = \lambda\!\!\!^{-}_C$, the gravitational potential energy equals $m_0 c^2$ where m_0 is the rest mass of the fundamental particle created as the transition state orbitsphere becomes real.

$$\frac{Gm_0}{c^2} = \lambda\!\!\!^{-}_c = \frac{\hbar}{m_0 c} \qquad (23.23)$$

$$\frac{Gm_0^2}{\lambda^*} = \frac{\hbar c}{\lambda^*} \qquad (23.24)$$

$$\frac{Gm_0^2}{\frac{\lambda^*}{2\pi}} = \frac{hc}{\lambda^*} \tag{23.25}$$

$$\frac{Gm_0^2}{\lambda\!\!\!^{-}_C} = \frac{Gm_0^2}{r_\alpha^*} = \hbar\omega^* \tag{23.26}$$

Thus, from Eq. (19.11) and Eq. (23.26), the following energies are equivalent

$$E = m_0c^2 = V = \hbar\omega^* = E_{mag} = \frac{Gm_0^2}{\lambda\!\!\!^{-*}_C} \tag{23.27}$$

where ω^* is the frequency of the photon which forms the transition state orbitsphere, and ω^* is also the spacetime resonance frequency for this particle. Furthermore, given

$$E = m_0c^2 = \hbar\omega^* = \frac{hc}{\lambda^*} \tag{23.28}$$

It follows that

$$\lambda = \frac{h}{mc} = \frac{h}{mv} = \frac{h}{p} \tag{23.29}$$

This equation is the de Broglie relationship; it must hold for matter and energy. The mass/energy which causes the gravitational radius r_G to equal $\lambda\!\!\!^{-}_C$ is hereafter called the Grand Unification Mass/Energy which is equal to $\hbar$ times the angular frequency of the photon which becomes the transition state orbitsphere. This angular frequency is also the spacetime resonance frequency of the Grand Unification Mass/Energy as given by Eq. (19.13). The Grand Unification Mass/Energy is further equal to the corresponding electric potential, stored magnetic, and gravitational potential energy. The equality of radii unifies de Broglie's equation, Planck's equation, Maxwell's equations, Newton's equations, and Special and General Relativity which comprise the fundamental laws of the universe.

The Grand Unification Mass/Energy, m_u, can be expressed in terms of Planck's constant.

$$m_0c^2 = \frac{Gm_0^2}{\lambda\!\!\!^{-*}_C} \tag{23.30}$$

$$m_u = m_0 = \sqrt{\frac{\hbar c}{G}} \tag{23.31}$$

The Grand Unification Mass/Energy, m_u, given by Eq. (23.31) is the ***Planck mass***. From Eq. (19.11), the relationship of the equivalent particle production energies (mass energy = Planck equation energy = electric potential energy = magnetic energy = gravitational potential energy) is

$$m_0c^2 = \hbar\omega^* = V = E_{mag} = E_{grav} \tag{23.32a}$$

where m_0 is the rest mass of a fundamental particle of the Planck mass m_u when the gravitational energy is the gravitational potential energy given by Eq. (23.30). A corresponding general relationship of the equivalent particle production energies (mass energy = Planck equation energy = electric potential energy = magnetic energy = gravitational energy) is

$$m_0c^2 = \left(\hbar\omega^* = \frac{\hbar^2}{m_0\lambda\!\!\!^{-2}_C}\right) = \alpha^{-1}\frac{e^2}{4\pi\varepsilon_0\lambda\!\!\!^{-}_C} = \alpha^{-1}\frac{\pi\mu_0e^2\hbar^2}{\left(2\pi m_0\right)^2\lambda\!\!\!^{-3}_C} = \alpha^{-1}\frac{\mu_0e^2c^2}{2h}\sqrt{\frac{Gm_0}{\lambda\!\!\!^{-}_C}}\sqrt{\frac{\hbar c}{G}} \tag{23.32b}$$

where m_0 is the rest mass of a fundamental particle. For particle production, the gravitational velocity, v_G, is defined as

$$v_G = \sqrt{\frac{Gm_0}{r}} = \sqrt{\frac{Gm_0}{\lambda\!\!\!^{-}_C}} \tag{23.33}$$

Substitution of the gravitational velocity, v_G, given by Eq. (23.33) and the Grand Unification Mass/Energy, m_U, given by Eq. (23.31) into Eq. (23.32) followed by division by the speed of light squared gives the mass of a fundamental particle in terms of the Grand Unification Mass/Energy.

$$m_0 = \alpha^{-1}\frac{\mu_0e^2c}{2h}\frac{\sqrt{\frac{Gm_0}{\lambda\!\!\!^{-}_C}}}{c}m_u = \alpha^{-1}\frac{\mu_0e^2c}{2h}\sqrt{\frac{Gm_0}{c^2\lambda\!\!\!^{-}_C}}m_u = \alpha^{-1}\frac{\mu_0e^2c}{2h}\frac{v_G}{c}m_u = \frac{v_G}{c}m_u \tag{23.34}$$

The equivalence of the gravitational and inertial masses according to experiments and Eq. (23.32) prove that Newton's Gravitational Law is exact on a local scale. The production of a particle requires that the velocity of each of the point masses of the particle is equivalent to the Newtonian gravitational escape velocity v_g of the superposition of the point masses of the antiparticle. According to Newton's Law of Gravitation the eccentricity is one and the particle production trajectory is a parabola relative to the center of mass of the antiparticle. The correction to Newton's Gravitational Law due to the relativistic effect of the presence of mass on spacetime may be determined by substitution of the gravitational escape velocity, v_g, given by [4]

$$v_g = \sqrt{\frac{2Gm}{r}} = \sqrt{\frac{2Gm_0}{\lambda\!\!\!^{-}_C}} \tag{23.35}$$

into Eq.(23.18) for v_g. The corresponding Newtonian gravitational radius is given by

$$r_g = \frac{2Gm_0}{c^2} \tag{23.36}$$

In the case of the boundary conditions of Eq. (23.32), Eq. (23.35) and Eq

(23.36), three families of leptons and quarks are predicted wherein each particle corresponds to a unique orbitsphere radius equal to its Compton wavelength bar. At particle production, a photon having a radius and a wavelength equal to the Compton wavelength bar of the particle forms a transition state orbitsphere of the particle of the same wavelength. However, a pair of particles each of the Planck mass corresponding to the conditions of Eq. (23.22), Eq. (23.32), and Eq. (23.33) is not observed since the velocity of each of the point masses of the transition state orbitsphere is the gravitational velocity v_G that in this case is the speed of light; whereas, the Newtonian gravitational escape velocity v_g of the superposition of the point masses of the antiparticle is twice the speed of light (Eq. (23.35)). In this case, an electromagnetic wave of mass energy equivalent to the Planck mass travels in a circular orbit about the center of mass of another electromagnetic wave of mass energy equivalent to the Planck mass wherein the eccentricity is equal to zero (Eq. (26.20)), and the escape velocity can never be reached. The Planck mass is a "measuring stick". The extraordinarily high Planck mass ($\sqrt{\frac{\hbar c}{G}} = 2.18\ X\ 10^{-8}\ kg$) is the unobtainable mass bound imposed by the angular momentum and speed of the photon relative to the gravitational constant. It is analogous to the unattainable bound of the speed of light for a particle possessing finite rest mass imposed by the Minkowski tensor. It has a physical significance for the fate of blackholes as given in the Composition of the Universe Section.

Eq. (23.34) gives the relationship between the mass of each fundamental particle and the ratio of the gravitational velocity v_G to the speed of light times the Planck mass, the mass at which the gravitational radius r_G is the Compton wavelength bar and the production energy is equal to the gravitational potential energy given by Eq. (23.30). The square of the ratio of the gravitational escape velocity v_g of each particle relative to the speed of light gives the corresponding spacetime contraction according to Eqs. (23.17-23.18). During particle production, a particle having the gravitational escape velocity v_g is formed from a photon traveling at the speed of light. The spacetime contraction during particle production is analogous to Lorentzian length contraction and time dilation of an object in one inertial frame relative to another moving at constant relative velocity. In the latter case, the correction is the square of the ratio of the relative velocity of two inertial frames to the speed of light according to Eqs. (22.17-22.18). The theory of the masses of fundamental particles is given in the Particle Production Section, the Leptons Section, and The Quarks Section.

The resulting metric is valid for the external region of particles and

spherically symmetric bodies comprised of fundamental particles such as the celestial bodies. The metric $g_{\mu\nu}$ for non-Euclidean space due to the relativistic effect on spacetime due to mass m_0 is

$$g_{\mu\nu} = \begin{pmatrix} -\left(1 - \frac{2Gm_0}{c^2 r}\right) & 0 & 0 & 0 \\ 0 & \frac{1}{c^2}\left(1 - \frac{2Gm_0}{c^2 r}\right)^{-1} & 0 & 0 \\ 0 & 0 & \frac{1}{c^2} r^2 & 0 \\ 0 & 0 & 0 & \frac{1}{c^2} r^2 \sin^2\theta \end{pmatrix} \tag{23.37}$$

In this case, the separation of proper time between two events x^μ and $x^\mu + dx^\mu$ is

$$d\tau^2 = \left(1 - \frac{2Gm_0}{c^2 r}\right) dt^2 - \frac{1}{c^2}\left[\left(1 - \frac{2Gm_0}{c^2 r}\right)^{-1} dr^2 + r^2 d\theta^2 + r^2 \sin^2\theta d\phi^2\right] \tag{23.38}$$

The origin of gravity is fundamental particles, and the masses and fields from particles superimpose. So, m_0, the mass of a fundamental particle, may be replaced by M, the sum of the masses of the particles which make up a massive body. In this case, Eq. (23.38) is equivalent to the a modified version of the Schwarzschild metric [5 and footnote 7].

One interpretation of the relativistic correction of spacetime due to conversion of energy into matter and matter into energy is that spacetime contracts and expands, respectively, in the radial and time dimensions. Thus, matter-energy conversion can be considered to conserve spacetime. Also, since matter causes spacetime to deviate from flat or Euclidean, matter-energy conversion can be considered to curve spacetime. The result is that spacetime is positively curved to match the boundary condition of the positive curvature of particles during production. The two dimensional nature of fundamental particles requires that the radial and time dimensions are distinct from the angular dimensions. The curvature of spacetime results from a discontinuity of matter having curvature confined to two spatial dimensions. This is the property of all matter as an orbitsphere. A space in which the curvature tensor has the following form:

$$R_{\mu\nu,\alpha\beta} = K\ (g_{\nu\alpha} g_{\mu\beta} - g_{\mu\alpha} g_{\nu\beta}) \tag{23.39}$$

is called a space of constant curvature; it is a four-dimensional generalization of Friedmann-Lobachevsky space. The constant K is called the constant of curvature. Consider an isolated orbitsphere and radial distances, r, from its center. For r less than r_n there is no mass; thus, spacetime is flat or Euclidean. The curvature tensor applies to all space of the inertial frame considered; thus, for r less than r_n, $K = 0$. At

$r = r_n$ there exists a discontinuity of mass of the orbitsphere. This results in a discontinuity of the metric tensor for radial distances greater than or equal to r_n which defines the curvature tensor given by Eq. (23.39).

Gauss and Riemann [5-6] developed the theory of curved spacetime and proposed that our universe may be curved rather than flat. A generation later, Einstein formalized the ideas of Gauss, Riemann, and Clifford [5-6, 7] that matter curved spacetime to give rise to a gravitational field[4]. Einstein proposed the principle of equivalence as the basis that gravity could be explained in terms of a spacetime metric that is different from Euclidean [5-6]. According to Einstein's Theory of general relativity, his field equations give the relationship whereby matter determines the curvature of spacetime[5], which is the origin of gravity. The definitive form of the equations are as follows[6]:

---

4 It is easy to discuss two-dimensional surfaces since we live in three dimensional space. Gauss considered the problem of whether a being that lives in and measures only in a two dimensional surface and can not travel in a three dimensional space can determine whether the surface in which it exists is curved or flat. The solution is not obvious. "One cannot be sure of the true sights of Lu mountain, since one is on it." Gauss found the solution that the two dimensional being could determine whether the surface on which it exists is curved by measuring the angle sum of a "geodesic triangle" on the surface. Euclidean plane geometry asserts that in a plane, the sum of the angles of a triangle add up to 180 °. On the surface of a sphere, however, the sum of the angles of a "geodesic triangle" exceed 180°. Gauss reasoned that the question of whether the three dimensional space in which we live is curved or flat could be resolved analogously. Gauss himself measured the angle sum of a triangle formed by three mountains as vertices, but failed to detect any departure from 180° within the limits of accuracy of his experiments. A generation later Einstein paraphrased this concept, "When a blind beetle crawls over the surface of the globe, he doesn't realize that the track he has covered is curved. I was lucky enough to have spotted it."

5 It is important to realize the distinction between the rationalization that the origin of gravity is by virtue of matter causing spacetime to be curved, and a physical basis consistent with Maxwell's equations and special relativity that the origin of gravity is time dilation and length contraction of spacetime based on the speed of light which is a constant maximum for the propagation of any form of energy at particle production. The relativistic correction of spacetime may be viewed as matter causing spacetime to be curved, but this is a consequence rather than the cause of the origin of gravity.

6 Although historically Einstein is credited with Eq. (23.40), David Hilbert discovered the same form of the field equations days before Einstein. Einstein had reached his final version of general relativity after a slow road with progress but many errors along the way. In December 1915, he said of himself, "That fellow Einstein suits his convenience. Each year he retracts what he wrote the year before." A reference describing the tremendous broad-based effort to develop the theory of general relativity in the early 20 th century is the web site :www-history.mcs.st-and.ac.uk/history//HistTopics/General_relativity.html#49. Also see D. Overbye, "Einstein, Confused in Love, and Sometimes, Physics", New York Times, August 31, 1999, F4.

$$R_{\mu\nu} - \frac{1}{2} g_{\mu\nu} R = \frac{-8\pi G}{c^4} T_{\mu\nu} \qquad (23.40)$$

where $R_{\mu\nu} = g^{\alpha\beta} R_{\mu\alpha\nu\beta}$, $R = g^{\mu\nu} R_{\mu\nu}$, the left-half of Eq. (23.40) is Einstein's Tensor $G_{\mu\nu}$, and $T_{\mu\nu}$ is the stress-energy-momentum tensor. Einstein proposed Eq. (23.40) starting with the assumption of the local equivalence of accelerated and gravitational inertial reference frames called the Principal of Equivalence. Einstein's infamous equation postulates that a conservative Riemannian tensor is proportional to a conservative stress energy momentum tensor wherein the proportionality constant contains Newton's gravitational constant. The uniqueness of the radial and time dimension for particle production (Eq. (23.32) and Eqs. (23.37-23.38)) and the corresponding effect on spacetime reveals a fatal flaw in Einstein's gravity equations. The tensors can not be conservative. All cosmological solutions of general relativity predict a decelerating universe from a postulated initial condition of a "Big Bang" expansion [8]. The astrophysical data reveals an accelerating cosmos [9] which invalidates Einstein's equation as discussed in the Cosmology Section. It has been shown that the correct basis of gravitation is not according to Einstein's equation (Eq. (23.40)); instead the origin of gravity is the relativistic correction of spacetime itself which is analogous to the special relativistic corrections of inertial parameters-- increase in mass, dilation in time, and contraction in length in the direction of constant relative motion of separate inertial frames. On this basis, the observed acceleration of the cosmos is predict as given in the Cosmology Section.

The popular terms for these effects, general relativity and special relativity, respectively, are confusing at best. The special relativistic corrections of an object corresponding to Newton's law of mechanics applied to inertial frames with constant relative motion are more appropriately named Newtonian Inertial Corrections or Newtonian Corrections of the First Kind. The gravitational relativistic corrections of spacetime which correspond to Newton's Laws of Gravitation applied to massive bodies are more appropriately named Newtonian Gravitational Corrections or Newtonian Corrections of the Second Kind. The nomenclature used herein will adhere to tradition, but it is implicit that Special Relativity refers to spacetime defined by the Minkowski tensor, and General Relativity refers not to Einstein's equations but to the spacetime defined by the Schwarzschild metric wherein the physical basis for the latter is the time dilation and length contraction of spacetime due to particle production[7].

---

7 The Schwarzschild metric was originally derived from Einstein's field equations and is widely used in astrophysical calculations. This metric is widely regarded as a

triumph of Einstein's theory of gravitation. Implicit in the Schwarzschild solution is a privileged system of coordinates. Yet, Einstein denied the existence of a privileged system of coordinates in all cases based on his view of the local method of discussing properties of space. The equivalence principle used by Einstein as the basis for Riemannian geometry of space is only valid locally. Einstein underestimated the importance of considering space as a whole. Having obtained his equation based on the Principal of Equivalence, Einstein realized that the mass of the universe would cause it to collapse. He would accept only a static universe. Thus, he added a cosmological constant to his equation. This type of antigravity of spacetime was intended to exactly balance the tendency of matter to cause spacetime to collapse. But, according to his basic postulates, the absence of a gravitational field signifies the absence of deviations of the geometry of spacetime from Euclidean, and therefore, also vanishing of the curvature tensor $R^{\mu\nu}$ and of its invariant R. Also, the gravitational field will be absent if the mass tensor $T^{\mu\nu}$ is zero everywhere. Therefore, the equations $T^{\mu\nu} = 0$ and $R^{\mu\nu} = 0$ must certainly be compatible, and this is only possible if the equations relating $G^{\mu\nu} = R^{\mu\nu} - \frac{1}{2} g^{\mu\nu} R$ to $T^{\mu\nu}$ do not contain the term $\lambda g^{\mu\nu}$. The cosmological constant must be zero. This is also the case in order to obtain consistency with Newton's Law of Gravitation in the same limit. After Hubble's redshift observations in 1929 demonstrated the expansion of the universe, the original motivation for the introduction of Λ was lost. Nevertheless, Λ has been reintroduced on numerous occasions when discrepancies have arisen between theory and observations, only to be abandoned again when these discrepancies have been resolved. Einstein abandoned the constant calling it the greatest mistake of his life. Einstein failed to notice two other tremendously important features of the universe which further undermines his view of a static universe. A positively curved spacetime has a finite radius based on the mass and energy. And, the universe is converting about 10^{33} kilograms of matter into energy per second. He also failed to develop an atomic theory of gravity which is the means to determine the impact of matter to energy conversion on the expansion of the universe.

In Einstein's equation in its original form, a conservative tensor (the divergence of the tensor is zero) which expresses the curvature of spacetime is equated with a conservative stress-energy-momentum tensor of matter. This approach conserves momentum, matter, and energy. The Schwarzschild metric given as Eq. (57.54) of Fock [10]

$$ds^2 = c^2\left(1 - \frac{GM}{c^2 r}\right)\left(1 + \frac{GM}{c^2 r}\right)^{-1} dt^2 - \left(1 + \frac{GM}{c^2 r}\right)^2 \left(dr^2 + r^2\left(d\theta^2 + \sin^2\theta d\phi^2\right)\right) \tag{23.41}$$

is an exact solution of the Einstein's equation based on a preferred system of coordinates. According to a theorem by Birkoff [11] the Schwarzschild metric is the only solution of Einstein's gravity equations for the corresponding boundary conditions of a spherically symmetric time-independent or dynamic solution with zero cosmological constant for the metric of a space which is empty apart from a central spherical body.

The Schwarzschild metric is consistent with observations wherein the radius applies to distances between gravitating bodies. For example, it solves the precession of the perihelion of Mercury and the deflection of light in a

gravitational field. However, Einstein's equation with general coordinates has an infinite number of solutions, and none of the possible solutions are consistent with cosmological observations as shown in the Cosmology Section. These solutions are all conservative (the divergence of each metric tensor is zero). The Schwarzschild metric given by Eq. (23.41) is also conservative; whereas, the Schwarzschild metric in the form given by Eq. (23.38) is not conservative.

The Schwarzschild metric (Eq. 23.38)) gives the relationship whereby matter (energy) causes relativistic corrections to spacetime that determines the curvature of spacetime and is the origin of gravity. The Minkowski space is obtained in the limit of no mass or at infinity. Eq. (23.41) may be transformed into Eq. (23.38) by the substitution of the radial coordinate r with the reduced radial coordinate, $r - \frac{GM}{c^2}$.

The origin of gravity is fundamental particles, and the masses and fields from particles superimpose. The derivation of the correct form of the Schwarzschild metric (Eq. (23.38)) is based on contraction of spacetime during particle production that requires a privileged system of coordinates. Einstein's approach to his equation conserves momentum, matter, and energy. Derivation of the Schwarzschild metric is based on the wave equation which conserves momentum, matter, and energy and additionally requires a maximum constant velocity for the propagation of any signal including a graviational field at particle production. As a consequence of particle production the radius of the universe contracts by 2π times the gravitational radius of each particle with the gravitational radius given by Eq. (23.36) which applies to the observed leptons and quarks formed at the gravitational velocity v_g which is the escape velocity given by Eq. (23.35)). Thus, Q the mass/energy to expansion/contraction quotient of spacetime (Eq. (23.140)) is given by the ratio of the mass of a particle at production divided by T the period of production given by Eq. (23.149) wherein the gravitational radius is the Newtonian gravitational radius is given by Eq. (23.36). By superposition, obtaining the correct solution of the Schwarzschild metric (Eq. (23.38)) requires that the radius of the metric (Eq. (23.41)) be replaced by the radius decreased by the gravitational radius of the central mass (Eq. (23.22) which applies to a particle of the Planck mass). The gravitational radius may be considered the "effective thickness" of fundamental particles which are two dimensional.

It is shown in the Cosmology Section that a 3-sphere spatial geometry describes the universe which is finite but has no boundary. The radius of the universe oscillates harmonically between two finite radii. It expands as matter is transformed into energy, and it contracts as the radiation filled universe reverts back to a matter filled universe. Matter causes spacetime to become curved like a dimple on a ball, but in three spatial dimensions plus time. Consider such a dimple caused by the Sun which is converting $5\ billion\ kg$ of matter into energy per second. If the conversion persisted indefinitely, the Sun would vanish. The local spacetime dimple would vanish also. Thus, spacetime must expand as matter is converted into energy. The same applies to the universe as a whole. Due to matter converting to energy the radius of the universe expands by 2π times the gravitational radius of the converted matter (Eq. (23.140) with the gravitational radius given by Eq. (23.36) wherein m_0, the mass of a fundamental particle, is replaced by M, the sum of the masses of the particles which make up the massive body). The Hubble constant is consistent with the experimental mass to energy conversion rate of the universe

PARTICLE PRODUCTION

The equations which *unify de Broglie's Equation, Planck's Equation, Maxwell's Equations, Newton's Equations, and Special and General Relativity define the mass of fundamental particles in terms of the spacetime metric.* Eq. (23.32) (Eq. (23.48) *infra.*) gives the equivalence of particle production energies corresponding to mass, charge, current, and gravity according to the proportionality constants which are given in terms of a self consistent set of units. This equivalence is a consequence of equivalence of the gravitational mass and the inertial mass together with special relativity. Charge is relativistically invariant; whereas, mass and spacetime are not. The fine structure constant is dimensionless and is the proportionality constant corresponding to the relativistic invariance of charge. Thus, it is absolute. All the other constants are not, and any property of mass/energy or spacetime is measurable only in terms of the remaining properties where the metrics and definitions of the properties are in terms of experiments which define a self consistent circular system of units. In addition to the equivalence of particle production energies corresponding to mass, charge, current, and gravity according to the proportionality constants which are given in terms of a self consistent set of units, general relativity further provides for the further proportional equivalence with the metric of spacetime of the same self consistent system of units. The metric of spacetime is used to calculate the mass of the fundamental particles in terms of the same consistent system of units.

Satisfaction of the nonradiative boundary condition precludes emission of electromagnetic radiation. Continuity of boundary conditions requires that particle production gives rise to a gravitational

---

calculated from the number of galaxies ($400\ billion$) times the number of stars per galaxy ($400\ billion$) times the average mass to energy conversion rate per star ($5\ billion\ kg/\sec\ star$). The Schwarzschild metric (Eq. 23.38)) is shown to explain all current cosmological observations as well as permit the derivation of an equation which correctly predicts the masses of fundamental particles. It is proposed that the Schwarzschild metric (Eq. 23.38)) is an exact description of reality which has as its basis the gravitational velocity v_g of a massive object according to Newton's Law of Gravitation and the constant maximum speed of light. It provides that any discontinuities in the gravitational field caused by matter to energy conversion or vice versa must propagate as a front like a light wave in empty space, this equation does not conserve matter, energy, and momentum separately from spacetime. In this case, matter, energy, momentum, and spacetime are conserved as a totality. The wave equation conserves matter, energy, and momentum. It further provides for the conservation of these physical entities with spacetime and provides a unifying physical principal that gives an oscillating universe as given in the Wave Equation Section.

field front which satisfies the same wave equation as electromagnetic radiation and travels at the speed of light. The charge and mass density functions of an orbitsphere are interchangeable by interchanging the fundamental charge and the particle mass; thus, satisfaction of the boundary condition of no Fourier components of the current-density function which are synchronous with waves traveling at the speed of light also holds for the mass density function. The transverse electric field of the photon of zero rest mass is replaced by a central electric and gravitational field and a particle and anti particle. For Euclidean spacetime, the radius of the boundary condition is invariant because the velocity is perpendicular to the radius of the orbitsphere. (The radius of the boundary condition is not length contracted by special relativistic effects.) However, the nonradiative boundary condition and the constancy of the speed of light must hold which requires relativistic corrections to spacetime.

Mass and charge are concomitantly created with the transition of a photon to a particle or antiparticle. Thus, the energies which are equal to the mass energies apply for the proper time of the particle (antiparticle) given by the general relativity, Eq. (23.38). The transition state from two photons to a particle and antiparticle pair comprises two concentric orbitspheres called transition state orbitspheres. The gravitational effect of a spherical shell on an object outside of the radius of the shell is equivalent to that of a point of equal mass at the origin. Thus, the proper time of the concentric orbitsphere with radius $^{+}r_n^*$ (the radius is infinitesimally greater than that of the inner transition state orbitsphere with radius r_n) is given by the Schwarzschild metric, Eq. (23.38). The proper time applies to each point on the orbitsphere. Therefore, consider a general point in the xy-plane having $r = \lambda\!\!\!^{-}_C$; $dr = 0$; $d\theta = 0$; $\sin^2\theta = 1$. Substitution of these parameters into Eq. (23.38) gives

$$d\tau = dt\left(1 - \frac{2Gm_0}{c^2 r_\alpha^*} - \frac{v^2}{c^2}\right)^{\frac{1}{2}} \tag{23.42}$$

with $v^2 = c^2$, Eq. (23.42) becomes

$$\tau = ti\sqrt{\frac{2GM}{c^2 r_\alpha^*}} = ti\sqrt{\frac{2GM}{c^2 \lambda\!\!\!^{-}_c}} = ti\frac{v_g}{c} \tag{23.43}$$

The production of a real particle from a transition state orbitsphere is a spacelike event in terms of special relativity wherein spacetime is contracted by the gravitational radius of the particle during its production. Thus, the coordinate time is imaginary as given by Eq. (23.43). On a cosmological scale, imaginary time corresponds to spacetime expansion and contraction as a consequence of the harmonic interconversion of matter and energy as given by Eq. (24.40). The left-

hand side of Eq. (23.43) represents the proper time of the particle/antiparticle as the photon orbitsphere becomes matter. The right-hand side of Eq. (23.43) represents the correction to the laboratory coordinate metric for time corresponding to the relativistic correction of spacetime by the particle production event. Riemannian space is conservative, and only changes in the metric of spacetime during particle production must be considered. The changes must be conservative. For example, pair production occurs in the presence of a heavy body. A nucleus which existed before the production event only serves to conserve momentum but is not a factor in determining the change in the properties of spacetime as a consequence of the pair production event. The effect of this and other external gravitating bodies are equal on the photon and resulting particle and antiparticle and do not effect the boundary conditions for particle production. For particle production to occur, the particle must possess the escape velocity relative to the antiparticle where Eqs. (23.34), (23.48), and (23.140) apply.

Eq. (23.43) is valid in the case that $v_g < c$. The velocity of each of the point masses of the particle is equivalent to the gravitational escape velocity v_g of the superposition of the point masses of the antiparticle (Eq. (23.43)). According to Newton's Law of Gravitation the eccentricity is one and the particle production trajectory is a parabola relative to the center of mass of the antiparticle. The mass of each member of a lepton pair corresponds to an energy of Eq. (23.32). The electron and antielectron correspond to the Planck equation energy. The muon and antimuon correspond to the electric energy. And, the tau and antitau correspond to the magnetic energy. However, a pair of particles each of the Planck mass corresponding to the conditions of Eq. (23.22), Eq. (23.32), and Eq. (23.33) is not observed since the velocity of each of the point masses of the transition state orbitsphere is the gravitational velocity v_G that in this case is the speed of light; whereas, the Newtonian gravitational escape velocity v_g of the superposition of the point masses of the antiparticle is twice the speed of light (Eq. (23.35)). In this case, an electromagnetic wave of mass energy equivalent to the Planck mass travels in a circular orbit about the center of mass of another electromagnetic wave of mass energy equivalent to the Planck mass wherein the eccentricity is equal to zero (Eq. (26.20)), and the escape velocity can never be reached. The relative velocity of Eq. (23.18) given by the velocity addition formula of special relativity for two photons corresponding to a particle and an antiparticle each of the Planck mass is c. In this case, the Compton wavelength bar is the gravitational radius given by Eq. (23.22) where the mass m is the Planck mass, and no matter can escape. Thus, for example, only three pairs of leptons are observed.

And, a lepton having the Planck mass is not observed. From Eq. (23.43), the masses of fundamental particles are calculated in the Leptons and Quarks Sections.

As stated in the Relativity Section, to describe any phenomenon such as the motion of a body or the propagation of light, a definite frame of reference is required. A frame of reference is a certain base consisting of a defined origin and three axes equipped with graduated rules and clocks. Given the unified relationships between the mass energy, the Planck equation energy, electric potential, magnetic energy, the gravitational potential energy, and the mass/spacetime metric energy given by Eqs. (23.32-23.34) and Eq. (23.48) *infra.*, it is possible to reduce the graduated rules and clocks to a clock alone. The units of measure are interdependent. Eqs. (23.32-23.34) and Eq. (23.48) *infra.* which unify the energies also unify the relationships of the units of measurement. *A measure of spacetime does exist a priori. Thus, one must be defined.* Based on the unification, only the metric of time need be set in the equations such that the other calculable parameters of matter and energy may be expressed relative to the time metric in terms of an internally consistent system of units such as the MKS units. The permeability of free space μ_0 is defined in terms of the MKS unit NA^{-2} as

$$\mu_0 = 4\pi X 10^{-7}\ NA^{-2} \tag{23.44}$$

The permeability of free space μ_0 and the permittivity of free space ε_0 are derived by converting the Coulombic force law and the magnetic force law from CGS units to MKS units. In CGS units, the unit of charge is defined such that the Coulomb force equation is

$$F(dynes) = k\frac{e^2(esu^2)}{r^2(cm^2)} \text{ where } k = 1 \tag{23.45}$$

From the magnetic force per unit length law, μ_0, is given by the conversion of

$$F(dynes/cm) = \frac{2I^2(esu/\sec)^2}{rc^2(cm^3/\sec^2)} \text{ where } k = 1 \tag{23.46}$$

to

$$F(dynes/cm) = \frac{\mu_0}{4\pi}\frac{2I^2}{r}\left(\frac{A^2}{m}\right) \tag{23.47}$$

defined exactly as $\mu_0 = 4\pi X 10^{-7}\ NA^{-2}$. The experimental definition of charge in MKS units is based on the speed of light. The Coulomb force law gives ε_0 in terms of the MKS charge; thus, ε_0 in terms of MKS units is based on the experimentally measured speed of light. The speed of light is the conversion factor from time to length. Time can also be converted to inertial and gravitational mass and charge according to Eqs.

(23.32-23.34) and Eq. (23.48) *infra*.. MKS units are selected. In the case of MKS units, the time metric is the second which is substituted for the variable t of Eq. (23.43). [Eq. (23.43) gives the equivalence of time in the proper and coordinate frames according to a dimensionless correction factor. But, Eq. (23.43) gives the mass in terms of a self consistent system of units independent of the particular system because of the circularity of the properties of mass, charge, momentum, and spacetime and their measurement. In the case of MKS units, it represents a time normalization which reduces the number of units from meters, kilograms and seconds (three unit system) to seconds (one unit system). Eq. (23.43) also applies to the cosmos wherefore time and distance are interchangeable by the speed of light as given in the Cosmology Section].

Conversely, the unification equation provides a superior means to define a self consistent set of units based only on time.

$$m_0c^2 = \hbar\omega^* = V = E_{mag} = E_{grav} = E_{spacetime} \tag{23.48a}$$

$$m_0c^2 = \hbar\omega^* = \frac{\hbar^2}{m_0\lambda\!\!\!^{-2}_C} = \alpha^{-1}\frac{e^2}{4\pi\varepsilon_0\lambda\!\!\!^{-}_C} = \alpha^{-1}\frac{\pi\mu_0e^2\hbar^2}{\left(2\pi m_0\right)^2\lambda\!\!\!^{-3}_C} = \alpha^{-1}\frac{\mu_0e^2c^2}{2h}\sqrt{\frac{Gm_0}{\lambda\!\!\!^{-}_C}}\sqrt{\frac{\hbar c}{G}} = \frac{\alpha h}{1\ \mathrm{sec}}\sqrt{\frac{\lambda\!\!\!^{-}_Cc^2}{2Gm}} \tag{23.48b}$$

A superior measure of time is an atomic standard. Using Eq. (23.48b) all other standards are determined according to the metric of time, and the speed of light is the conversion factor for time and distance.

ORBITAL MECHANICS

Newton's differential equations of motion in the case of the central field are

$$m(\ddot{r} - r\dot{\theta}^2) = f(r) \tag{23.49}$$

$$m(2\dot{r}\dot{\theta} + r\ddot{\theta}) = 0 \tag{23.50}$$

where $f(r)$ is the central force. The second or transverse equation, Eq. (23.50), gives the result that the angular momentum is constant.

$$r^2\dot{\theta} = \text{constant} = L/m \tag{23.51}$$

where L is the angular momentum. The central force equations can be transformed into an orbital equation by the substitution, $u = \frac{1}{r}$. The differential equation of the orbit of a particle moving under a central force is

$$\frac{\delta^2u}{\delta\theta^2} + u = \frac{-1}{\frac{mL^2u^2}{m^2}}\ f(u^{-1}) \tag{23.52}$$

Because the angular momentum is constant, motion in only one plane need be considered; thus, the orbital equation is given in polar coordinates. The solution of Eq. (23.52) for an inverse square force

$$f(r) = -\frac{k}{r^2} \tag{23.53}$$

is

$$r = r_0 \frac{1+e}{1+e\cos\theta} \tag{23.54}$$

$$e = A\frac{m\frac{L^2}{m^2}}{k} \tag{23.55}$$

$$r_0 = \frac{m\frac{L^2}{m^2}}{k(1+e)} \tag{23.56}$$

where e is the eccentricity and A is a constant. The equation of motion due to a central force can also be expressed in terms of the energies of the orbit. The square of the speed in polar coordinates is

$$v^2 = (\dot{r}^2 + r^2\dot{\theta}^2) \tag{23.57}$$

Since a central force is conservative, the total energy, E, is equal to the sum of the kinetic, T, and the potential, V, and is constant. The total energy is

$$\frac{1}{2}m(\dot{r}^2 + r^2\dot{\theta}^2) + V(r) = E = \text{ constant} \tag{23.58}$$

Substitution of the variable $u = \frac{1}{r}$ and Eq. (23.51) into Eq. (23.58) gives the orbital energy equation.

$$\frac{1}{2}m\frac{L^2}{m^2}[(\frac{\delta^2 u}{\delta\theta^2}) + u^2] + V(u^{-1}) = E \tag{23.59}$$

Because the potential energy function $V(r)$ for an inverse square force field is

$$V(r) = -\frac{k}{r} = -ku \tag{23.60}$$

the energy equation of the orbit, Eq. (23.59),

$$\frac{1}{2}m\frac{L^2}{m^2}[(\frac{\delta^2 u}{\delta\theta^2}) + u^2] - ku = E \tag{23.61}$$

which has the solution

$$r = \frac{m\frac{L^2}{m^2}k^{-1}}{1+[1+2Em\frac{L^2}{m^2}k^{-2}]^{1/2}\cos\theta} \tag{23.62}$$

where the eccentricity, e, is

$$e = [1+2Em\frac{L^2}{m^2}k^{-2}]^{1/2} \tag{23.63}$$

Eq. (23.63) permits the classification of the orbits according to the total energy, E, as follows:

$$\begin{aligned} E<0, \quad e<1 &\qquad \text{ellipse} \\ E<0, \quad e=0 &\qquad \text{circle (special case of ellipse)} \\ E=0, \quad e=1 &\qquad \text{parabolic orbit} \\ E>0, \quad e>1 &\qquad \text{hyperbolic orbit} \end{aligned} \tag{23.64}$$

Since $E=T+V$ and is constant, the closed orbits are those for which $T \lhd |V|$, and the open orbits are those for which $T \geq |V|$. It can be shown that the time average of the kinetic energy, $<T>$, for elliptic motion in an inverse square field is $1/2$ that of the time average of the potential energy, $<V>$. $<T>=1/2<V>$.

In Newtonian gravitation, the central force between two particles of masses m_1 and m_2 separated by a distance r is

$$F=G\frac{m_1 m_2}{r^2} \tag{23.65}$$

where G is the gravitational constant, its value being $6.67\ X\ 10^{-11}\ Nm^2kg^{-2}$. The theoretical difficulty with Newtonian gravitation is to explain just why Eq. (23.5) exists implicitly in Newton's theory as a separate law of nature besides Eq. (23.1) and Eq. (23.2). Even so, Newtonian gravitation and mechanics was the first truly successful dynamics, and its most well-known application was in celestial mechanics. The verification of the prediction of the existence of Neptune marked the peak of the success of celestial mechanics, but the first real difficulty was also met here. It was first pointed out in 1850, based on astronomical observations, that there was a discrepancy between certain observations of the orbit of Mercury and the predictions made by Newtonian mechanics. According to Newton's theory of gravitation, the Sun's gravitational force acting on Mercury causes its orbit to be a closed ellipse. In fact it is not a precise ellipse: with every revolution, its major axis rotates slightly. The observed rate of Mercury's precession (rotation) of the perihelion (major axis) is 1° 33'20" per century. This value ought to be due to the gravitational perturbations of all other planets and the effect of rotation of our Earth-based coordinate system. However, the value calculated from Newtonian mechanics is 1° 32'37" per century. The discrepancy between them of

$$1°\ 33'20" - 1°\ 32'\ 37 = 43" \tag{23.66}$$

is extremely small, but it has been observed with a negligible amount of

observational error, and it represents a tremendous outstanding problem for Newtonian mechanics.

Relativistic Corrections of Newtonian Mechanics and Newtonian Gravity

Newtonian mechanics (Eqs. (23.2)) is corrected by Lorentz transformations of the time, length, mass, momentum, and energy of an object (Eqs. (22.17-22.22)). Similarly Newtonian gravitation is corrected by relativistic corrections of the metric. The Schwarzschild metric is relativistically correct and may be solved to provide the orbital equation. The force is central; therefore, the angular momentum per unit mass is constant. The transverse differential equation of motion in the case of the central field,

$$m(2\dot{r}\dot{\phi} + r\ddot{\phi}) = 0 \tag{23.67}$$

gives the result that the angular momentum is constant

$$r^2\dot{\phi} = \text{constant} = L_\phi / m \tag{23.68}$$

where L_ϕ is the ϕ component of the angular momentum of an orbiting body of mass m. Eq. (23.38) may be expressed as

$$1 = \left(1 - \frac{2Gm_0}{c^2 r}\right)\left(\frac{dt}{d\tau}\right)^2 - \frac{1}{c^2}\left[\left(1 - \frac{2Gm_0}{c^2 r}\right)^{-1}\left(\frac{dr}{d\tau}\right)^2 + r^2\left(\frac{d\phi}{d\tau}\right)^2\right] \tag{23.69}$$

The relativistic correction for time is

$$\tau^2 = t^2\left(1 - \left(\frac{v_g}{c}\right)^2\right) \tag{23.70}$$

It has the same form as the special relativistic correction for time with v_g in place of v. This correction may be determined by considering an object of mass m orbiting an object of mass M. The gravitational force is central; thus the angular momentum is constant. Consider that a radial force is applied to increase the radius r of the object's orbit with a change of its energy E. The angular momentum is conserved; thus,

$$mr_i^2\left(\frac{d\phi}{dt}\right)_i = mr_f^2\left(\frac{d\phi}{dt}\right)_f \tag{23.71}$$

where $\left(\frac{d\phi}{dt}\right)_i$ is the initial angular velocity, $\left(\frac{d\phi}{dt}\right)_f$ is the final angular velocity, r_i is the initial radius and r_f is the final radius. At fixed radius, dr^2 is zero, but dt^2 is finite. Applying the time relativistic correction given by Eq. (23.38) and Eqs. (23.14-23.17) gives the mass m_f at r_f with respect to the mass m_i of the inertial frame of r_i as

$$m_i\sqrt{1 - \frac{2GM}{rc^2}} = m_f \tag{23.72}$$

where r is the increase in the radius. The proper energy E_p of the object is given by

$$m_i c^2 \sqrt{\left(1 - \frac{2GM}{rc^2}\right)} = E_p \tag{23.73}$$

The relativistic correction for energy is of the same form as the special relativistic correction for mass (Eq. (22.19)) with v_g in place of v.

$$\frac{E}{\sqrt{1 - \left(\frac{v_g}{c}\right)^2}} = mc^2 \tag{23.74}$$

where m in the coordinate mass of the orbiting body and E is the energy of the orbiting object. In the case that the gravitational velocity is much less that the speed of light ($v_g << c$), the gravitational energy E_g converges to that given by Newton.

$$E \approx mc^2 \left(1 - \frac{1}{2}\left(\frac{2GM}{rc^2}\right)\right) \tag{23.75}$$

$$E \approx mc^2 - \frac{GMm}{r} \tag{23.76}$$

$$E_g = -\frac{GMm}{r} \tag{23.77}$$

Precession of the Perihelion

Combining Eq. (23.73) and Eq. (23.38) in terms of the time differentials gives

$$\left(1 - \frac{2GM}{rc^2}\right)\frac{dt}{d\tau} = \frac{E}{mc^2} \tag{23.78}$$

Eq. (23.78) is herein derived from first principals. It is *postulated* in pervious solutions [5, 6]. Having arrived at the basis for the orbital equation using the correct physics, the derivation follows from Fang and Ruffini [5]. Eqs. (23.69), (23.78) and (23.68) are the equations of motion of the geodesic, which give

$$\left(\frac{dr}{d\phi}\right)^2 = \frac{r^4}{L_\phi^2}\left[\left(\frac{E}{c}\right)^2 - \left(1 - \frac{2GM}{c^2 r}\right)\left(\frac{L_\phi^2}{r^2} + m^2 c^2\right)\right] \tag{23.79}$$

The central force equations can be transformed into an orbital equation by the substitution, $u = \frac{1}{r}$. The relativistically corrected differential equation of the orbit of a particle moving under a central force is

$$\left(\frac{du}{d\phi}\right)^2 + u^2 = \frac{\left(\frac{E}{c}\right)^2 - m^2 c^2}{L_\phi^2} + \frac{m^2 c^2}{L_\phi^2}\left(\frac{2GM}{c^2}\right)u + \left(\frac{2GM}{c^2}\right)u^3 \tag{23.80}$$

By differentiating with respect to ϕ, noting that $u = u(\phi)$ gives

$$\frac{d^2u}{d\phi^2} + u = \frac{GM}{a^2} + \frac{3}{2}\left(\frac{2GM}{c^2}\right)u^2 \tag{23.81}$$

where

$$a = \frac{L_\phi}{m} \tag{23.82}$$

In the case of a weak field,

$$\left(\frac{2GM}{c^2}\right)u << 1 \tag{23.83}$$

and the second term on the right-hand of Eq. (23.81) can then be neglected in the zero-order. In such a case the solution is

$$u_0 - \frac{GM}{a^2} = A\cos(\phi + \phi_0) \tag{23.84}$$

where A and ϕ_0 denote the constants of integration. The orbits of Eq. (23.84) are conic sections and are specified in terms of eccentricity

$$e = \frac{Aa^2}{GM} \tag{23.85}$$

and perihelion distance

$$r_{\min} = \frac{a^2}{GM(1+e)} \tag{23.86}$$

If $e < 1$, the orbits are bound and elliptical in shape. In the case for which the minor axis is parallel to $\phi = 0$ (i.e. $\phi_0 = 0$), the ellipse can be written as

$$u_0 = \frac{1}{r} = \frac{GM}{a^2}(1 + e\cos\phi) \tag{23.87}$$

We shall calculate the correction to the elliptical orbits caused by the relativistic term $\frac{3}{2}\left(\frac{2GM}{c^2}\right)u^2$ in Eq. (23.81). The value of this term is only about 10^{-7} for Mercury and far less for other planets, so that it is only necessary to calculate the lowest order corrections, called the ***post-Newtonian corrections***. Substituting Eq. (23.87) into the second term on the right-hand side of Eq. (23.81), we get

$$\frac{d^2u}{d\phi^2} + u = \frac{GM}{a^2} + \varepsilon\frac{3GM}{a^2}\left[2e\cos\phi + \left(1 + e^2\cos^2\phi\right)\right] \tag{23.88}$$

where $\varepsilon = \left(\frac{GM}{ca}\right)^2 << 1$. Let $u = u_0 + u_1$. Then the equation for the first-order correction function u_1 is

$$\frac{d^2u_1}{d\phi^2} + u_1 = \varepsilon\frac{3GM}{a^2}\left[2e\cos\phi + \left(1 + e^2\cos^2\phi\right)\right] \tag{23.89}$$

This is an equation for forced oscillations. In Eq. (23.89) , the only important term on the right-hand side is the first one, which is resonant, while the second non-resonant term will only cause a slight periodic variation in the position of the perihelion. Thus, after neglecting the

non-resonant term, Eq. (23.87) becomes

$$\frac{d^2u_1}{d\phi^2} + u_1 = \varepsilon \frac{6GM}{a^2} e\cos\phi \tag{23.90}$$

A solution can be obtained as

$$u_1 = \varepsilon \frac{3GMe}{a^2} \phi\sin\phi \tag{23.91}$$

It is obvious that the presence of a multiplicative factor ϕ in the solution causes a cumulative effect which can be observed clearly after a sufficiently large number of revolutions.

Using the above solution, by considering the relativistic correction up to the first order, the orbit is

$$u = u_0 + u_1 = \frac{GM}{a^2}\left[1 + e\left(\cos\phi + 3\varepsilon\phi\sin\phi\right)\right] \tag{23.92}$$

or

$$r \approx \frac{\frac{a^2}{GM}}{\left\{1 + e\cos\left[\phi\left(1 - 3\varepsilon\right)\right]\right\}} \tag{23.93}$$

as ε is small.

We know that perihelia occur when the cosine is unity, and are therefore determined by the following equation:

$$\phi\left(1 - 3\varepsilon\right) = 2\pi n \tag{23.94}$$

where n is any integer. This can be approximated as

$$\phi = 2\pi n + 6\pi n\varepsilon \tag{23.95}$$

Therefore, the azimuth angle ϕ increases with increasing n, that is, the major axis of the ellipse has a precession. The angular precession $\Delta\phi_1$ per revolution is

$$\Delta\phi_1 = \frac{6\pi GM}{c^2 r_{\min}\left(1 + e\right)} \tag{23.96}$$

and the centennial precession $\Delta\phi$ is

$$\Delta\phi = \frac{6\pi GMN}{c^2 r_{\min}\left(1 + e\right)} \tag{23.97}$$

where N is the number of revolutions per century.

Only for the planets Mercury, Venus, and the Earth, and the asteroid Icarus, is $r_{\min}$ small enough and M large enough for $\Delta\phi$ to be measured. The results are as shown in Table 23.1. The large uncertainty in the measured precession of Venus arises from the near-circularity of the orbit (e is only 0.0068), which makes it difficult to locate the precession. These results support the verification of general relativity (Schwarzschild metric).

Table 23.1. Observed and theoretical angle of procession of the perihelion of Mercury, Venus, Earth, and Icarus.

Planet	Observed $\Delta\phi^{100}$ (seconds of arc)	Theoretical $\Delta\phi^{100}$ (seconds of arc)
Mercury	43.11 ± 0.45	43.03
Venus	8.4 ± 4.8	8.6
Earth	5.0 ± 1.2	3.8
Icarus	9.8 ± 0.8	10.3

To confirm that all of the remaining precession of a star arises from general relativity, it is of course necessary to be able to rule out other possibilities which may also cause some precession, the most important of which is the non-spherical symmetry of the Sun. If the Sun is slightly oblate, its gravitational potential would be

$$V = \frac{GM}{r}\left(1 - J_2 \frac{R_{Sun}^2}{r^2}\left(\frac{3\cos^2\theta - 1}{2}\right)\right) \tag{23.98}$$

where J_2 is the oblateness of the Sun. In this field, there is already a certain rotation of the perihelion, the value of which per revolution of the star would be

$$\Delta\phi = \frac{6\pi GM}{r_{\min}(1+e)} J_2 \frac{\frac{R_{Sun}^2}{MG}}{2r_{\min}(1+e)} \tag{23.99}$$

The lack of data of J_2 is the outstanding serious problem that prevents us from isolating the relativistic contribution to the precession. Inference of J_2 from measurements of the visual oblateness of the Sun is difficult; this method has been tried, but the results are in dispute. Dicke and Goldenberg have claimed that this oblateness is as large as $J_2 = 5\,X\,10^{-5}$ [5], which should account for about 20% of the remaining precession. However, recent observations indicate that the oblateness of the Sun is far less than the above value with only $J_2 = (1.84 \pm 1.25)\,X\,10^{-6}$. Inference of J_2 by comparing results for Mercury and Mars is also difficult. The effect for Mars is very small, and the influences of the asteroid belt on the orbit of Mars make the interpretation of a measured precession difficult.

The best approach for measuring J_2 would be to track a spacecraft that passes close to the Sun. In one possible version of such a method,

the spacecraft would be sent from the Earth to pass by Jupiter to obtain a "gravity assist". Due to the Jupiter encounter, the spacecraft would be made to travel perpendicular to the ecliptic. After several years of flight, the spacecraft would pass by the Sun in less than a day and J_2 would be estimated from that brief encounter.

Deflection of Light

The principle of equivalence implies that light is deflected in a gravitational field. For instance, imagine a laboratory falling freely in the gravitational field near the Earth's surface, and suppose a light ray is emitted from the left end propagates horizontally towards the right. According to the principle of equivalence, the laboratory is an inertial frame in which gravity is eliminated. Ignoring special relativistic considerations, this is true to extent that the acceleration is exactly radial. In the frame accelerated by gravity, the light ray is observed to travel along a straight line according to the demands of special relativity. However, for an observer on the ground, the laboratory is accelerated downwards, and the light ray which propagates horizontally to the right for an observer in the laboratory, would in the ground frame be accelerated downwards in a curved path. Due to the weakness of the gravitational field near the Earth's surface, deflection of the light is very small (a light ray propagating horizontally has a deflection of only about 1 Å, due to a curved trajectory, for every kilometer traveled) and difficult to observe. Nevertheless, the deflection of light in the Sun's gravitational field has a magnitude that can be observed. To obtain a correct calculation of the total deflection caused by the Sun's gravitational field, it is necessary to consider many different local inertial frames and their connections. It is not sufficient to employ just the single laboratory falling freely as mentioned above.

Newtonian mechanics predicts the bending of the trajectory of light in a gravitational field. The deflection predicted by Newtonian gravitation is less than the experimental value, but closely matches the experimental value when relativistically corrected. As early as in 1801, Soldner calculated the deflection of light in gravitational fields using Newtonian mechanics. Eq. (23.87) corresponds to unbound hyperbolic orbits if the eccentricity e exceeds unit. The asymptotes, where $r \to \infty$, correspond to angles to the angles shown in Figure 23.1 having the following relationship

$$\phi_{\pm} = \pm\left(\frac{\pi}{2} + \frac{1}{2}\delta\right) \tag{23.100}$$

where δ is the total Newtonian deflection of the ray, given by

$$\cos\phi_{\pm} = -\frac{1}{e} \tag{23.101}$$

which is equivalent to

$$\sin\frac{1}{2}\delta = \frac{1}{e} \tag{23.102}$$

Figure 23.1. The coordinate parameters of the deflection of light in the gravitational field of the Sun.

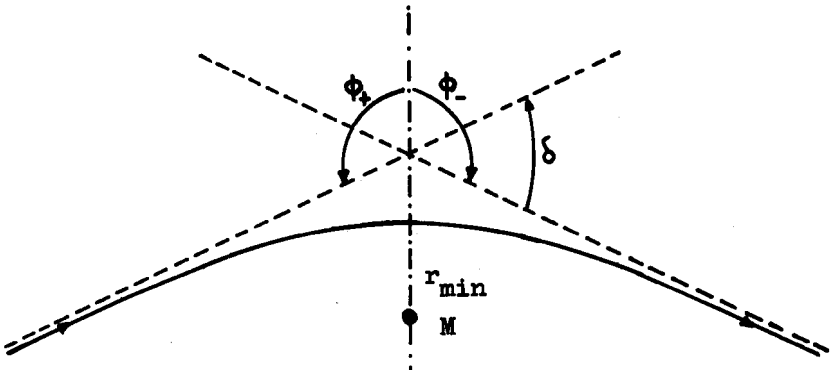

Using the speed of light c, Eq.(23.51) and $a = \frac{L_\phi}{m}$, the angular momentum per unit mass of the photon, a, is approximately

$$a \approx r_{\min} c \tag{23.103}$$

The eccentricity follows from Eq. (23.85) and Eq. (23.86)

$$e = \frac{a^2}{GMr_{\min}} - 1 \approx \frac{c^2 r_{\min}}{GM} - 1 \approx \frac{c^2 r_{\min}}{GM} \tag{23.104}$$

Since $\frac{c^2 r_{\min}}{GM} >> 1$, e is very large and δ is very small, so that we have approximately,

$$\sin\left(\frac{1}{2}\delta\right) \approx \frac{1}{2}\delta = \frac{1}{e} \tag{23.105}$$

that is

$$\delta = \frac{2GM}{c^2 r_{\min}} \tag{23.106}$$

For light grazing the surface of the Sun, $r_{\min} = R_{Sun}$ and $M = M_{Sun}$, giving

$$\delta = 0".875 \tag{23.107}$$

The Newtonian deflection must be corrected relativistically to calculate the true deflection δ. The results obtained in the Precession of the Perihelion Section can be applied to light propagation in gravitational fields wherein the rest mass of light is zero. Substitution of $m = 0$ in Eq. (23.81) gives

$$\frac{d^2u}{d\phi^2} + u = \frac{3GM}{c^2}u^2 \tag{23.108}$$

If $M = 0$, the path of the light would be a straight line with the orbit

equation,

$$u_0 = \frac{1}{r_{\min}} \cos(\phi + \phi_0) \tag{23.109}$$

where $r_{\min}$ and ϕ_0 are constants of integration. By making $\phi_0 = 0$, up to the first order correction, Eq. (23.108) gives

$$\frac{d^2u}{d\phi^2} + u = \frac{3GM}{c^2 r_{\min}^2} \cos^2\phi \tag{23.110}$$

which has a solution:

$$u = \frac{1}{r_{\min}} \cos\phi + \frac{GM}{c^2 r_{\min}^2}\left(1 + \sin^2\phi\right) \tag{23.111}$$

The asymptote is determined by taking $r \to \infty$, namely,

$$0 = -\frac{1}{r_{\min}} \sin\frac{\delta}{2} + \frac{GM}{c^2 r_{\min}^2}\left(1 + \cos^2\frac{\delta}{2}\right) \tag{23.112}$$

Since $\delta \approx 0$ and $\frac{GM}{c^2 r_{\min}} << 1$, the deflection δ is

$$\delta \approx \frac{4GM}{c^2 r_{\min}} \tag{23.113}$$

This is twice the unrelativistically corrected Newtonian value. For light grazing the Sun,

$$\delta = 1".75 \tag{23.114}$$

It is only possible to measure the deflection of light from a star during a total eclipse of the Sun. Measuring the relative positions of the stars around the Sun during an eclipse and repeating the measurements for the same celestial region six months later (i.e. in the absence of the Sun's gravitational field in the region), a comparison between the two results would give the required deflection. In this way $\Delta\phi$ has been measured for about 400 stars since 1919. The experimental results all lie within the limits 1".57-2".37, the mean value being 1".89. These results disagree with the prediction of unrelativistically corrected Newtonian theory. But, ***the predicted and experimentally observed values agree quite well after general relativistic correction of Newton's Law of Gravitation.***

There are many problems that are difficult to overcome in the observation of deflections. First of all, the effect of the solar corona limits us to measurements of the star with $r_{\min} > 2R_{Sun}$. Secondly, total eclipses of the Sun are not usually observable at locations where large telescopes are available. The size of the diffraction disc of a telescope of 10 cm in diameter is about $5X10^{-6}$ arc, which restricts the accuracy of the measurement. Moreover, exposures and developing which are made at different times also bring in systematic errors.

Radiosources have been employed for detecting the deflection of

light in the last few years. The results of direction measurements using very long baseline interferometry are better than those using the optical method, since the precision of the former can be very high. For example, QSO 3C279 is occulted annually by the Sun. By measuring the angle between 3C279 and 3C273, before and after an occultation, the required results on the deflection are obtained. Some of these results are listed in Table 23.2.

Table 23.2. The angle of deflection of the propagation of a light ray $\Delta\phi$ by a gravitating body.

Name of Observatory	Frequency (MHz)	Length of Baseline (km)	$\Delta\phi$
OWENSVALLEY	9602	1	1".7 ± 0".20
GOLDSTONE	2388	21.566	1".82 ± 0".24 0".17
GOLDSTONE HAYSTACK	7840	3899.22	1"80 ± 0".2
NRAO	2695 8085	2.7	1".57 ± 0".08
NRAO	2697 4993.8	1.41	1".87 ± 0".3

In addition, radiosources 0119+11, 0116+08, and 0111+02 are collinear so that when the ecliptic of the Sun crosses 0116+08, 0119+11 and 0111+02 are each on one side of the ecliptic, making angles of 4° and 6° with the ecliptic, respectively. The Sun passes through the celestial region near 0116+08 in the first ten days of the month every April. Using two frequencies, 2695 and 8085 MHz, eliminates the effects of the corona. Fomaleont and Sramek have measured the change in the relative positions of the three radiosources by using 35 km baseline interferometry at NRAO when the Sun passed 0116+08. Their result is $\Delta\phi = 1".761 \pm 0".010$.

COSMOLOGY

A space in which the curvature tensor $R_{\mu\nu,\alpha\beta}$ having the form

$$R_{\mu\nu,\alpha\beta} = K\ (g_{\nu\alpha}g_{\mu\beta} - g_{\mu\alpha}g_{\nu\beta}) \tag{23.115}$$

is satisfied (with $K = \text{constant}$) is called a space of constant curvature; it is a four-dimensional generalization of Friedmann-Lobachevsky space. The constant K is called the constant of curvature. If in these relations K is zero, the space-time is Galilean and the transformations in questions are

Lorentz transformations, except when other (non-Galilean) coordinates are used. It can be shown [12] that any two spaces of constant curvature of the same dimension and metric signature which have equal values of K must be (locally) isometric. Thus, our task of determining the possible spatial geometries of a hypersurface Σ_t will be completed if we enumerate spaces of constant curvature encompassing all values of K. This is easily done. All positive values of K are attained by the 3-spheres, defined as the surfaces in four-dimensional flat Euclidean space R^4 whose Cartesian coordinates satisfy

$$x^2 + y^2 + z^2 + w^2 = R^2 \tag{23.116}$$

In spherical coordinates, the metric of the unit 3-sphere is

$$ds^2 = d\psi^2 + \sin^2\psi\left(d\theta^2 + \sin^2\theta d\phi^2\right) \tag{23.117}$$

The value $K = 0$ is attained by ordinary three-dimensional flat space. In Cartesian coordinates, this metric is

$$ds^2 = dx^2 + dy^2 + dz^2 \tag{23.118}$$

Finally, all negative values of K are attained by the three-dimensional hyperboloids, defined as the surfaces in a four-dimensional flat Lorentz signature spaces (i.e., Minkowski space-time) whose global inertial coordinates satisfy

$$t^2 - x^2 - y^2 - z^2 = R^2 \tag{23.119}$$

In hyperbolic coordinates, the metric of the unit hyperboloid is

$$ds^2 = d\psi^2 + \sinh^2\psi\left(d\theta^2 + \sin^2\theta d\phi^2\right) \tag{23.120}$$

The new possibilities for the global spatial structure of our universe should be stressed. In prerelativity physics, as well as in special relativity, it was assumed that space had the flat structure given by the possibility $K = 0$ above. But even under the very restrictive assumptions of homogeneity and isotropy, the framework of general relativity admits two other distinct possibilities. The possibility of a 3-sphere spatial geometry is particularly interesting, as it is a compact manifold and thus describes a universe which is finite but has no boundary. Such a universe is called "closed", while the universes with noncompact spatial sections such as those given by flat and hyperboloid geometries are called "open". (One could construct closed universes with flat or hyperboloid geometries by making topological identifications, but it does not appear to be natural to do so.) Thus, an intriguing question raised by general relativity is whether our universe is closed or open.

Consider isotropic observers orthogonal to the homogeneous hypersurfaces Σ_t. In this case, we may express the four-dimensional space-time metric g_{ab} as

$$g_{ab} = -u_a u_b + h_{ab}(t) \tag{23.121}$$

where for each t, $h_{ab}(t)$ is the metric of either (a) a sphere, (b) flat

Euclidean space, or (c) a hyperboloid, on Σ_t. We can choose, respectively, either (a) spherical coordinates, (b) Cartesian coordinates, or (c) hyperbolic coordinates on one of the homogeneous hypersurfaces. We then "carry" these coordinates to each of the other homogeneous hypersurfaces by means of our isotropic observers; i.e., we assign a fixed spatial coordinate label to each observer. Finally, we label each hypersurface by the proper time, τ, of a clock carried by any of the isotropic observers. (By homogeneity, all the isotropic observes must agree on the time difference between any two hypersurfaces.) Thus, τ and our spatial coordinates label each event in the universe.

Expressed in these coordinates, the space-time metric takes the form

$$ds^2 = -d\tau^2 + a^2(\tau)\begin{cases} d\psi^2 + \sin^2\psi\left(d\theta^2 + \sin^2\theta d\phi^2\right) \\ dx^2 + dy^2 + dz^2 \\ d\psi^2 + \sinh^2\psi\left(d\theta^2 + \sin^2\theta d\phi^2\right) \end{cases} \tag{23.122}$$

where the three possibilities in the bracket correspond to the three possible spatial geometries. The metric for the spatially flat case could be made to look more similar to the other cases by writing it in spherical coordinates as

$$d\psi^2 + \psi^2\left(d\theta^2 + \sin^2\theta d\phi^2\right) \tag{23.123}$$

The general form of the metric, Eq. (23.122) is called a Robertson-Walker cosmological model. The assumptions of homogeneity and isotropy alone determine the spacetime metric up to three discrete possibilities of spatial geometry and arbitrary positive function $a(\tau)$. Einstein's equation can be solved for the spatial geometry and $a(\tau)$. The result is that all possible solutions of Einstein's equation are inconsistent with the observation of the acceleration of the expansion of the cosmos shown *infra*.

Einstein Cosmological Predictions

Dynamical predictions for the evolution of the universe according to Einstein's equation may be found by substituting the metric into Eq. (23.40). In the cases of spherical, flat, and hyperbolic geometries, the general evolution equations for homogeneous, isotropic cosmology are

$$3\frac{\dot{a}^2}{a^2} = 8\pi\rho - 3\frac{k}{a^2} \tag{23.124}$$

$$3\frac{\ddot{a}}{a} = -4\pi(\rho + 3P) \tag{23.125}$$

where $k = +1$ for the 3-sphere, $k = 0$ for flat space, and $k = -1$ for the hyperboloid and ρ is the (average) mass density of matter, $\dot{a} = \frac{da}{d\tau}$, and P

is the pressure. The exact solutions of these equations for the cases of dust ($P=0$) and radiation ($P=\frac{\rho}{3}$) are given below in Table 23.3.

Table 23.3. Dust and Radiation Filled Robertson-Walker Cosmologies.

	TYPE OF MATTER	
	"Dust"	Radiation
SPATIAL GEOMETRY	$P=0$	$P=\frac{\rho}{3}$
3-sphere, $k=+1$	$a=\frac{1}{2}C(1-\cos\eta)$ $\tau=\frac{1}{2}C(\eta-\sin\eta)$	$a=\sqrt{C'}\left[1-\left(1-\frac{\tau}{\sqrt{C'}}\right)^2\right]^{\frac{1}{2}}$
Flat, $k=0$	$a=\left(\frac{9C}{4}\right)^{\frac{1}{3}}\tau^{\frac{2}{3}}$	$a=(4C')^{\frac{1}{4}}\tau^{\frac{1}{2}}$
Hyperboloid, $k=-1$	$a=\frac{1}{2}C(\cosh\eta-1)$ $\tau=\frac{1}{2}C(\sinh\eta-\eta)$	$a=\sqrt{C'}\left[\left(1+\frac{\tau}{\sqrt{C'}}\right)^2-1\right]^{\frac{1}{2}}$

Consider some of the important qualitative properties of the solutions. The first striking result is that the universe cannot be static, provided only that $\rho>0$ and $P\geq 0$. This conclusion follows immediately from ***Eq. (23.125) which tells us that*** $\ddot{a}<0$. Thus, the universe must always either be expanding ($\dot{a}>0$) or contracting ($\dot{a}<0$) (with the possible exception of an instant of time when expansion changes over to contraction). Note the nature of this expansion or contraction: The distance scale between all isotropic observers (in particular, between galaxies) changes with time, but there is no preferred center of expansion or contraction. Indeed, if the distance (measured in the homogeneous surface) between two isotropic observers at time τ is R, the rate of change of R is

$$v\equiv\frac{dR}{d\tau}=\frac{R}{a}\frac{da}{d\tau}=HR \qquad (23.126)$$

where $H(\tau)=\frac{\dot{a}}{a}$ is called Hubble's constant. (Note, however, that the value of H changes with time.) Eq. (23.126) is known as Hubble's law.

Note that v can be greater than the speed of light if $H(\tau)=\frac{\dot{a}}{a}$ is large enough. This represents a contradiction of special relativity that no signal may travel faster than c the speed of light for any observer. (The maximum expansion rate for a 3-sphere is $4\pi c$ which is given in Eq. (23.186).

The expansion of the universe in accordance with Eq. (23.126) has been confirmed by the observation of the redshifts of distant galaxies. The confirmation of this striking prediction of Einstein's general relativity is regarded as a dramatic success of the theory. Unfortunately, the historical development of events clouded this success and recent data reveals a fatal flaw in the nature of the expansion. Einstein was sufficiently unhappy with the prediction of a dynamic universe that he proposed a modification of his equation, the addition of a new term, as follows:

$$G_{ab}+\Lambda g_{ab}=8\pi T_{ab} \tag{23.127}$$

where Λ is a new fundamental constant of nature, called the cosmological constant. (It can be shown [13] that a linear combination of G_{ab} and g_{ab} is the most general two-index symmetric tensor which is divergence free and can be constructed locally from the metric and its derivatives up to second order; so Eq. (23.127) gives the most general modification which does not grossly alter the basic properties of Einstein's equation. If $\Lambda \neq 0$, *one does* ***not*** *obtain Newtonian theory* in the slow motion, weak field limit; but if Λ is small enough, the deviations from Newtonian theory would not be noticed.) With this additional one-parameter degree of freedom, static solutions exist, though they require exact adjustment of the parameters and are unstable, much like a pencil standing on its point. Thus, Einstein was able to modify the theory to yield static solutions. After Hubble's redshift observations in 1929 demonstrated the expansion of the universe, the original motivation for the introduction of Λ was lost. Nevertheless, Λ has been reintroduced on numerous occasions when discrepancies have arisen between theory and observations, only to be abandoned again when these discrepancies have been resolved. In the following, we shall assume that $\Lambda = 0$.

Given that the universe is expanding, $\dot{a} > 0$, we know from Eq. (23.125) that $\ddot{a} < 0$, so the universe must have been expanding at a faster and faster rate as one goes backward in time. Einstein's equation predict that the universe must be decelerating for all time.

In fact, the opposite is observed experimentally [9].

If the universe had always expanded at its present rate, then at the time $T = \frac{a}{\dot{a}} = H^{-1}$ ago, we would have had $a = 0$. Since its expansion actually was faster, the time at which a was zero was even closer to the present. Thus, under the assumption of homogeneity and isotropy, Einstein's general relativity makes the prediction that at a time less than H^{-1} ago, the universe was in a singular state: The distance between all "points of space" was zero; the density of matter and the curvature of space-time was infinite. This singular state of the universe is referred to as the *big bang.*

> *Such a spacetime structure makes no physical sense. Furthermore, big bang theory requires the existence of a center of the universe from which the universe originated. No such point of origin is observed.*

For many years it was generally believed that the prediction of a singular origin of the universe was due merely to the assumptions of exact homogeneity and isotropy, that if these assumptions were relaxed one would get a non-singular "bounce" at small a rather than a singularity. However, the singularity theorems of general relativity [14] show that singularities are generic features of cosmological solutions; they have ruled out the possibility of "bounce" models close to the homogeneous, isotropic modes.

In order to determine the qualitative predictions of Einstein's general relativity for the future evolution of the universe, it is useful to first obtain an equation for the evolution of the mass density. Multiplying Eq. (23.124) by a^2, differentiating it with respect to τ, and then eliminating $\ddot{a}$ via Eq. (23.125) gives an equation for the evolution of the mass density.

$$\dot{\rho} + 3(\rho + P)\frac{\dot{a}}{a} = 0 \tag{23.128}$$

In the case of a dust filled universe ($P = 0$), the equation for the predicted evolution of the mass density of the universe is

$$\rho a^3 = \text{constant} \tag{23.129}$$

which expresses conservation of rest mass, while in the case of a radiation filled universe ($P = \frac{\rho}{3}$)

$$\rho a^4 = \text{constant} \tag{23.130}$$

In this case, the explanation is that the energy density decreases more rapidly as a increases than by the volume factor a^3, since the radiation in each volume element does work on its surroundings as the universe

expands. (Alternatively, in terms of photons, the photon number density decreases as a^{-3}, but each photon loses energy as a^{-1} because of redshift. Comparison of Eq. (23.129) and Eq. (23.130) shows that although the radiation content of the present universe may be negligible, its contribution to the total mass density far enough into the past ($a \to 0$) should dominate over that of ordinary matter.

The qualitative features of the future evolution of the universe predicted by Einstein's general relativity may now be determined. If $k = 0$ or -1, Eq. (23.124) shows that $\dot{a}$ never can become zero. Thus, if the universe is presently expanding, it must continue to expand forever. Indeed, for any matter with $P \geq 0$, ρ must decrease as a increases at least as rapidly as a^{-3}, the value for dust. Thus, $\rho a^2 \to 0$ as $a \to \infty$. Hence, if $k = 0$, the "expansion velocity" $\dot{a}$ asymptotically approaches zero as $\tau \to \infty$, while if $k = -1$ we have $\dot{a} \to 1$ as $\tau \to \infty$.

However, if $k = +1$, the universe cannot expand forever. The first term on the right hand of Eq. (23.124) decreases with a more rapidly than the second term, and thus, since the left-hand side must be positive, there is a critical value, a_c such that $a \leq a_c$. Furthermore, a cannot asymptotically approach a_c as $\tau \to \infty$ because the magnitude of $\ddot{a}$ is bounded from below on account of Eq. (23.125). Thus, if $k = +1$, then at a finite time after the big bang origin of the universe, the universe will achieve a maximum size a_c and then will begin to recontract. The same argument as given above for the occurrence of a big bang of the universe now shows that a finite time after recontraction begins, a "big crunch" end of the universe will occur. Thus, the dynamical equations of Einstein's general relativity show that the spatially closed 3-sphere universe will exist for only a finite span of time.

Let us now turn our attention to solving Eq. (23.124) and Eq. (23.125) exactly for the cases of dust and radiation. The most efficient procedure for doing this is to eliminate ρ using Eq. (23.129) or, respectively, Eq. (23.130), and substitute into Eq. (23.124). The result for dust is

$$\dot{a}^2 - \frac{C}{a} + k = 0 \tag{23.131}$$

where $C = \frac{8\pi\rho a^3}{3}$ is constant; and for radiation,

$$\dot{a}^2 - \frac{C'}{a^2} + k = 0 \tag{23.132}$$

where $C' = \frac{8\pi\rho a^4}{3}$. Given Eq. (23.129) (or Eq. (23.130)), Eq. (23.125) is redundant; so, the only first order ordinary differential Eq. (23.131) (or, respectively, Eq. (23.132)) need be solved. The solutions for $a(\tau)$ are

readily obtained by elementary methods. These solutions for the six cases of interest are given in Table 23.3. Graphs of $a(\tau)$ versus τ for dust-filled Robertson-Walker universes are shown in Figure 23.2. Similar graphs are obtained for radiation-filled Robertson-Walker universes. The solution for the dust-filled universe with 3-sphere geometry was first given by Friedmann (1922) and is called the Friedmann cosmology, although in some references all the solutions in Table 23.3 are referred to as Friedmann solutions.

Figure. 23.2. The dynamics of dust-filled Robertson-Walker universes.

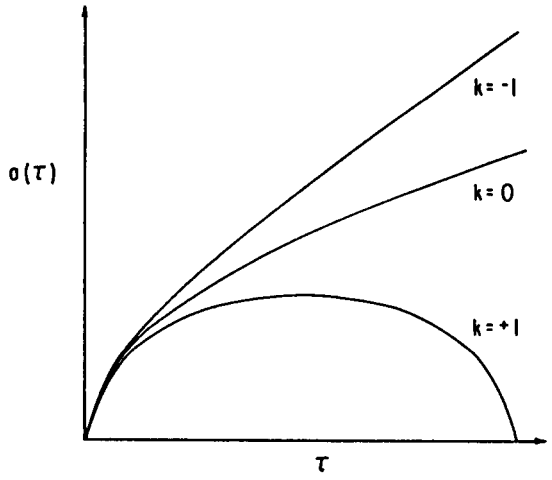

Solutions to Einstein's general relativity yield multiple possible outcomes of $a(\tau)$ with regard to future evolution such as whether our universe is "open" or "closed," i.e., whether it corresponds to the cases $k=0$, $k=-1$, or the case $k=+1$. If the universe is open, it will expand forever, while if it is closed it will eventually recontract. The basic equations (Eq. (23.124) and Eq. (23.125)) governing the dynamics of the universe may be expressed in terms of Hubble's constant, $H=\frac{\dot{a}}{a}$, and the deceleration parameter, q, defined by

$$q=-\ddot{a}\frac{a}{(\dot{a})^2} \tag{23.133}$$

Assuming $P\approx 0$ in the present universe, gives

$$H^2=\frac{8\pi G\rho}{3}-\frac{kc^2}{a^2} \tag{23.134}$$

$$q=\frac{4\pi G\rho}{3H^2} \tag{23.135}$$

Defining Ω as

$$\Omega=\frac{8\pi G\rho}{3H^2} \tag{23.136}$$

gives the result

$$q = \frac{\Omega}{2} \tag{23.137}$$

and the universe is closed ($k = +1$) if and only if $\Omega > 1$, i.e., $\rho > \rho_c \equiv \frac{3H^2}{8\pi G}$.

Dynamical predictions for the evolution of the universe according to Einstein's equation are consistent with the expansion of the cosmos; but are fatally flawed since they predict the possibility of an expansion velocity that exceeds the speed of light, and all cosmological solutions of Einstein's general relativity predict a decelerating universe from a postulated initial condition of a "big bang" expansion [8][8]. The astrophysical data reveals an accelerating cosmos [9] which invalidates Einstein's equation. Furthermore, multiple solutions with dramatically different consequences are equally valid. The solutions to Einstein's equation can not account for the power spectrum of the cosmos or the nature or uniformity of the cosmic microwave background radiation. Einstein's universe is static with expanding dust, expanding radiation, or a static expanding mixture. In actuality, the universe comprises predominantly matter which is under going conversion into radiation with a concomitant expansion of spacetime. The Einstein solutions predict the opposite of the actual evolution of the cosmos wherein radiation dominates in the early universe with matter dominant latter. The equations are derived *infra.* that reconcile the short comings of Einstein's general relativity. The correct basis of gravitation is not according to Einstein's equation (Eq. (23.40)); instead the origin of gravity is the relativistic correction of spacetime itself which is analogous to the special relativistic corrections of inertial parameters--increase in mass, dilation in time, and contraction in length in the direction of constant relative motion of separate inertial frames. As matter converts into energy spacetime undergoes expansion. On this basis, the observed acceleration of the expansion of the cosmos is predicted.

COSMOLOGY BASED ON THE RELATIVISTIC EFFECTS OF MATTER/ENERGY CONVERSION ON SPACETIME

The Arrow of Time and Entropy

The first principle laws are time symmetrical. They are equally valid for reverse time as they are for forward time. The principle of

---

8 Some of the failings of the "Big Bang" model as well as an even more far fetched model is given by Linde [15].

entropy was invented to provide an explanation for the direction of time as it pertains to macroscopic processes. And, it is not based on first principles. It does not provide an atomic arrow of time or provide insight into its existence. It is not clear whether entropy applies to the entire universe, and the relationship of entropy to the observed large scale expansion of the universe is not obvious.

The following retrospect of entropy is adapted from Levine [16]. Consider the spontaneous mixing of two different gases. In the mixing process, the molecules move according to Newton's second law, Eq. (23.2). This law is symmetric with respect to time, meaning that if t is replaced by $-t$ and $\mathbf{v}$ by $-\mathbf{v}$, the law is unchanged. Thus, a reversal of all particle motions gives a set of motions that is also a valid solution of Newton's equation. Hence it is possible for the molecules to become spontaneously unmixed, and this unmixing does not violate the laws of motion. However, motions that correspond to a detectable degree of unmixing are extremely improbable (even though not absolutely impossible). Although Newton's laws of motion (which govern the motion of individual molecules) do not single out a direction of time, when the behavior of a very large number of molecules is considered, the second law of thermodynamics (which is a statistical law) tells us that states of an isolated system with lower entropy must precede in time states with higher entropy. The second law is not time-symmetric but singles out the direction of increasing time; we have $\frac{dS}{dt} > 0$ for an isolated system, so that the signs of dS and dt are the same. If someone showed us a film of two gases mixing spontaneously and then ran the film backward, we would not see any violation of $\mathbf{F} = m\mathbf{a}$ in the unmixing process, but the second law would tell us which showing of the film corresponded to how things actually happened. Likewise, if we saw a film of someone being spontaneously propelled out of a swimming pool of water, with the concurrent subsidence of waves in the pool, we would know that we were watching a film run backward; although tiny pressure fluctuations in a fluid can propel colloidal particles about, the Brownian motion of an object the size of a person is too improbable to occur.

The second law of thermodynamics singles out the direction of increasing time. The astrophysicist Eddington put things nicely with his statement that "entropy is time's arrow." The fact that $\frac{dS}{dt} > 0$ for an isolated system gives us the *thermodynamic arrow* of time. Besides the thermodynamic arrow, there is a *cosmological arrow* of time. Spectral lines in light reaching us from other galaxies show wavelengths that are longer than the corresponding wavelengths of light from objects at rest (the famous red shift). This red shift indicates that all galaxies are moving away from us. Thus the universe is expanding with increasing time, and this expansion gives the cosmological arrow. Many physicists believe that the thermodynamic and the cosmological arrows are directly related, but this question is still undecided [17].

Particle physicists feel that there is strong (but not conclusive) evidence that the decay of one of the elementary particles (the neutral K meson) follows a law that is not symmetric with respect to time reversal. Thus, they speculate that there may also be a *microscopic arrow of time*, in addition to the thermodynamic and cosmological arrows [18-20].

The second law of thermodynamics shows that S increases with time for an isolated system. Can this statement be applied to the entire physical universe? Scientists use universe to mean the system plus those parts of the world which

interact with the system. In the present contexts, universe shall mean everything that exists - the entire cosmos of galaxies, intergalactic matter, electromagnetic radiation, etc. Physicists in the late nineteenth century generally believed that the second law is valid for the entire universe, but presently they are not so sure. Scientists make the point that experimental thermodynamic observations are on systems that are not of astronomic size, and hence they are cautious about extrapolating thermodynamic results to encompass the entire universe. They feel that there is no guarantee that laws that hold on a terrestrial scale must also hold on a cosmic scale. Although there is no evidence for a cosmic violation of the second law, their experience is insufficient to rule out such a violation.

The Arrow of Time

The present theory provides an alternative explanation for the expanding universe which unifies the ***microscopic, thermodynamic, and cosmological arrows of time***.

Physical phenomena involve exchange of energy between matter and spacetime. The relationship between mass/energy and spacetime provides the arrow of time. The particle production equations which unify de Broglie's Equation, Planck's Equation, Maxwell's Equations, Newton's Equations, and Special and General Relativity, Eq. (23.48a) and Eq. (23.48b), give the equivalence of particle production energies corresponding to mass, charge, current, gravity, and spacetime according to the proportionality constants which are given in terms of a self consistent set of units. As shown by Eq. (23.38), particle production requires radial length contraction and time dilation that results in the curvature of spacetime. Thus, the creation of mass from energy causes an infinitesimal contraction or collapse of spacetime much like a dimple in a plastic ball but in three dimensions plus time; whereas, the release of energy causes an expansion of spacetime. Time goes forward in the direction of lower energy states and greater entropy because these states correspond to an expansion of spacetime relative to the higher energy states of matter. Expanded space corresponds to a smaller cross section for reverse time as opposed to forward time. Thus, the arrow of time arising on the subatomic and atomic level gives rise to the Second Law of thermodynamics;

> *In an isolated system, spontaneous processes occur in the direction of increasing entropy.*

Stated mathematically:

> *The entropy change, dS, which is equal to the change in heat, dq, divided by the temperature, T, is greater than zero.*

$$dS = \frac{dq}{T} > 0 \qquad (23.138)$$

The Expanding Universe and the Microwave Background

The atomic arrow of time also applies to cosmology and provides for the expansion of spacetime on a cosmological scale. As fundamental particles, atoms, molecules, and macroscopic configurations of fundamental particles, atoms, and molecules release energy, spacetime increases. The superposition of expanding spacetime arising at the atomic level over all scales of dimensions from the atomic to the cosmological gives rise to the observed expanding universe which continues to increase in entropy. However, due to conservation of mass/energy and spacetime as given by Eqs. (23.43), (23.48a), and (23.48b), the change in entropy of the universe over all spacetime is zero.

$$\langle dS \rangle_{spacetime} = 0 \qquad (23.139)$$

Thus, regions of the world line of the universe exist wherein entropy decreases. The implications that are developed *supra.* are that:

- ***The universe is closed*** (it is ***finite but with no boundary***)
- The total matter in the universe is sufficient to eventually stop the expansion and is less than that which would result in permanent collapse (a 3-sphere universe-Riemannian three dimensional hyperspace plus time of constant positive curvature), and
- ***The universe is oscillatory in matter/energy and spacetime***.

The amount of mass which is released as energy to cause spacetime to expand by one second can be calculated using Eqs. (27.1) and (27.3) of the Lepton Section. Eq. (23.43) gives the relationship between ***the equivalence of mass/energy conversion and the contraction/expansion of spacetime***. The proper time of the electron is given by Eq. (27.1), and the electron mass corresponding to this amount of time is given by Eq. (27.3). Thus, Q, the mass/energy to expansion/contraction quotient of spacetime is given by the ratio of Eq. (27.3) and Eq. (27.1) wherein Eq. (23.43) gives the general relativistic factor which divides the electron mass and multiplies the electron proper time to give the corresponding spacetime expansion.

$$Q = \frac{m_e}{\tau\sqrt{\frac{2GM}{c^2\lambda_c}}} = \frac{\left(\frac{h\alpha}{\sqrt{1-\sec}\,c^2}\right)^{\frac{1}{2}}\left(\frac{c\hbar}{2G}\right)^{\frac{1}{4}}}{2\pi\frac{\hbar}{m_e c^2}\frac{2Gm_e}{c^2\lambda_c}} = \frac{c^3}{4\pi G} = 3.22\ X\ 10^{34}\ \frac{kg}{\sec} \qquad (23.140a)$$

As a consequence of particle production the radius of the universe

contracts by 2π times the gravitational radius of each particle with the gravitational radius given by Eq. (23.36) which applies to the observed leptons and quarks formed at the gravitational velocity v_g which is the escape velocity given by Eq. (23.35)). Thus, Q the mass/energy to expansion/contraction quotient of spacetime is also given by the ratio of the mass of a particle at production divided by T the period of production given by Eq. (23.149) wherein the gravitational radius is the Newtonian gravitational radius is given by Eq. (23.36).

$$Q = \frac{m_0}{T} = \frac{m_0}{\frac{2\pi r_g}{c}} = \frac{m_0}{2\pi \frac{2Gm_0}{\frac{c^2}{c}}} = \frac{c^3}{4\pi G} = 3.22\,X\,10^{34}\ \frac{kg}{\sec} \qquad (23.140b)$$

As shown infra. the universe oscillates between the extremes of all matter and all energy. At the beginning of its expansion, the universe is all matter with no electromagnetic radiation; thus, ***the universe is not observable for earlier times***. The observer's light sphere determines the limits of observation thereafter; thus, the observable conversion rate is a percentage of the total. The observable mass to energy conversion rate of the universe calculated from the number of galaxies ($400\ billion$) times the number of stars per galaxy ($400\ billion$) times the average mass to energy conversion rate per star ($5\ billion\ kg/\sec\ star$) is $8\,X\,10^{32}\ \frac{kg}{\sec}$ which is 2.5% of Q given by Eq. (23.140). The time of the present expansion calculated from the observed Hubble constant and the maximum redshift is approximately 10 billion years [21]. Assuming the presently observed mass to energy conversion rate was approximately constant over this time, the amount of mass to energy released during this time is

$$3.2\,X\,10^{34}\ \frac{kg}{\sec}\ X\,3.2\,X\,10^{17}\ \sec\ =\ 1X\,10^{52}\ kg \qquad (23.141)$$

The mass of the universe is approximately $2\,X\,10^{54}\ kg$ [Eq. (23.147) with ref. 22-24]; thus, 0.5 % of the maximum mass of the universe has been converted to energy. Thus, the present universe is predominantly comprised of matter, and according to Eq. (23.141) the mass of the matter of the universe is essentially a maximum. Given time harmonic behavior, the observable universe is approximately at its minimum size. The wavefront of energy and spacetime from matter to energy conversion travel at the speed of light. Consider Eq. (23.43). At the present time in the cycle of the universe, the world line of the expanding spacetime and the released energy are approximately coincident. In terms of Eq. (23.38), the proper time and the coordinate time are approximately equal. The ratio of the gravitational radius, r_g given by

Eq. (23.36), and the radius of the universe equal to one and the gravitational escape velocity given by Eq. (23.35) is the speed of light. And, Q, (Eq. (23.140)) is equal to the matter to energy conversion rate of the time harmonic expansion/contraction cycle of the entire universe (versus the observable universe) which permits light energy (photons) to propagate (escape the gravitational hole of the universe).

When the gravitational radius r_g is the radius of the universe, the proper time is equal to the coordinate time (Eq. (23.43)), and the gravitational escape velocity v_g of the universe is the speed of light.

The cosmic microwave background radiation dominates the total radiation density of the universe. The microwave background spectrum obtained by COBE is well fitted by a blackbody with a temperature of $2.735 \pm 0.06\ K$, and the deviation from a blackbody is less than 1% of the peak intensity over the range $1 - 20\ cm^{-1}$ [25]. From the isothermal temperature of the ubiquitous microwave background radiation and the Stefan-Boltzmann law, the minimum size of the universe is calculated. Presently, the mass to energy conversion rate of the universe is approximately equal to, Q, the mass/energy to expansion/contraction quotient of spacetime given by Eq. (23.140). At the present time in the cycle of the universe, the world line of the expanding spacetime and the released energy are approximately coincident. In terms of Eq. (23.38), the proper time and the coordinate time are approximately equal. Therefore, the mass to energy conversion rate of the entire universe is equated with Q. Thus, P_U, ***the maximum power radiated by the universe*** is given by Eqs. (23.27) and (23.140).

$$P_U = \frac{\frac{m_e c^2}{\sqrt{\frac{2GM}{c^2 \lambda\!\!\!^{-}_c}}}}{\tau\sqrt{\frac{2GM}{c^2 \lambda\!\!\!^{-}_c}}} = \frac{c^5}{4\pi G} = 2.89\ X\ 10^{51}\ W \qquad (23.142)$$

The observable mass to energy conversion rate of the universe calculated from the number of galaxies (400 *billion*) times the number of stars per galaxy (400 *billion*) times the average mass to energy conversion rate per star ($5\ billion\ kg/\sec\ star$) is $7.2\ X\ 10^{49}\ W$ which is 2.5% of P_U given by Eq. (23.142).

The Stefan-Boltzmann law [26] equates the power radiated by an object per unit area, R, to the emissivity, e, times the Stefan-Boltzmann constant, σ, times the fourth power of the temperature, T^4.

$$R = e\sigma T^4 \qquad (23.143)$$

The area, A, of the universe of radius À is

$$A = 4\pi À^2 \tag{23.144}$$

The power radiated by the universe per unit area, R_U, is given by the ratio of Eq. (23.142) and Eq. (23.144).

$$R_U = \frac{\frac{c^5}{4\pi G}}{4\pi À^2} = \frac{2.89\ X\ 10^{51}\ W}{4\pi À^2} \tag{23.145}$$

The minimum radius of the universe, $À_{\min}$, is calculated in terms of the temperature of the cosmic microwave background radiation by the substitution of Eq. (23.145) into Eq. (23.143).

$$À_{\min} = \sqrt{\frac{c^5}{(4\pi)^2 Ge\sigma T^4}} = 8.52\ X\ 10^{27}\ m$$
$$À_{\min} = \frac{8.52\ X\ 10^{27}\ m}{c} = 9.01\ X\ 10^{11}\ light\ years \tag{23.146}$$

where $T = 2.735\ °K$, $e = 1$ for a blackbody, and $\sigma = 5.67\ X\ 10^{-8}\ Wm^{-2}K^{-4}$. Given that the present expansion age is 10 billion years [21] and that the power used to calculate Eq. (23.146) is an upper bound, the ***minimum radius of the universe***, $À_{\min}$, given by Eq. (23.146) ***is equal to the gravitational radius of the universe***, r_g, given by Eq. (23.36) and Eq. (23.38) where the experimental mass of the universe is $2\ X\ 10^{54}\ kg$ [Eq. (23.147) with ref. 22-24].

$$r_g = \frac{2Gm_U}{c^2} = 2.96\ X\ 10^{27}\ m = 3.12\ X\ 10^{11}\ light\ years \tag{23.147}$$

Eq. (23.147) is consistent with the mass of the universe being that which gives the ratio of the gravitational radius, r_g, and the radius of the universe equal to one and the gravitational escape velocity given by Eq. (23.35) equal to the speed of light.

The gravitational equation (Eq. (23.38)) with the equivalence of the particle production energies (Eqs. (23.48a) and (23.48b)) permit the equivalence of mass/energy ($E = mc^2$) and spacetime ($\frac{c^3}{4\pi G} = 3.22\ X\ 10^{34}\ \frac{kg}{\sec}$). Spacetime expands as mass is released as energy which provides the basis of the atomic, thermodynamic, and cosmological arrows of time. Entropy and the expansion of the universe are large scale consequences. ***The universe is closed independently of the total mass of the universe***. Because Eq. (23.140) gives a constant as the ratio of energy to spacetime expansion, the energy density is constant throughout the inhomogeneous universe for a given r-sphere; thus, ***different regions of space are isothermal even though they are separated by greater distances than that over which light could travel during the time of the expansion of the universe***. The

spacetime expansion and the energy released travel spherically outward at the speed of light. The sum of the spacetime expansion over all points in the universe and the sum of the energy release over all points in the universe are each equivalent to that of a point source at the observer's position of magnitude equal to the corresponding sum. Recent evidence reveals a fatal flaw in inflation theory and supports structure at a much larger scale. The cosmic microwave background radiation was an average temperature of 2.7 ° kelvins, with deviations of 30 or so microkelvins in different parts of the sky representing slight variations in the density of matter. The temperature fluctuations of the cosmic microwave background radiation are not Gaussian [27] which is an absolute requirement for inflation theory.

Mass/energy must be conserved during the harmonic cycle of expansion and contraction. The gravitational potential energy E_{grav} of the universe follows that given by Eq. (23.26)

$$E_{grav} = \frac{Gm_U^2}{r} \tag{23.148}$$

In the case that the radius of the universe r is the gravitational radius r_G given by Eq. (23.22), the gravitational potential energy is equal to $m_U c^2$ which follows that given by Eq. (23.27). The gravitational velocity v_G is given by Eq. (23.33) wherein an electromagnetic wave of mass/energy equivalent to the mass of the universe travels in a circular orbit wherein the eccentricity is equal to zero (Eq. (26.20)), and the escape velocity from the universe can never be reached. The wavelength of the oscillation of the universe and the wavelength corresponding to the gravitational radius r_G must be equal. Both spacetime expansion and contraction travel at the speed of light and obey the wave relationship given by Eq. (20.4). The wavelength is given in terms of the radius by Eq. (2.2). Thus, ***the harmonic oscillation period***, T, is

$$T = \frac{2\pi r_G}{c} = \frac{2\pi G m_U}{c^3} = \frac{2\pi G\left(2\ X\ 10^{54}\ kg\right)}{c^3} = 3.10\ X\ 10^{19}\ \text{sec} = 9.83\ X\ 10^{11}\ \text{years} \tag{23.149}$$

where the mass of the universe, m_U, is approximately $2\ X\ 10^{54}\ kg$ [Eq. (23.147) with ref. 22-24]. Thus, the observed universe will expand as mass is released as photons for $4.92\ X\ 10^{11}\ years$. At this point in its world line, the universe will obtain its maximum size and begin to contract.

The universe is oscillatory in matter/energy and spacetime with a finite minimum radius, the gravitational radius r_g. The minimum radius of the universe, 300 billion light years [24], is larger than that provided by the current expansion, approximately 10 billion light years [21]; even

though, presently the spacetime expansion and the released energy world lines are coincident as a consequence of the equality of Eq. (23.140) and the rate of matter to energy conversion. In terms of Eq. (23.38), the proper time and the coordinate time are approximately equal. Consequently, the radius of the universe does not go negative during the contraction phase of the oscillatory cycle.

The ***maximum radius of the universe***, the amplitude, r_o, of the time harmonic variation in the radius of the universe, is given by the quotient of the total mass of the universe and Q, the mass/energy to expansion/contraction quotient, given by Eq. (23.140).

$$r_0 = \frac{2\ X\ 10^{54}\ kg}{\frac{c^3}{4\pi G}} = 6.20\ X\ 10^{19}\ \text{sec} = 1.97\ X\ 10^{12}\ \textit{light years}$$
$$r_0 = \frac{2\ X\ 10^{54}\ kg}{\frac{c^3}{4\pi G}}\, c = 1.86\ X\ 10^{28}\ m \qquad (23.150)$$

where the conversion factor of space to time is the speed of light according to Minkowski's tensor [5]. The equation for À, the radius of the universe is

$$\text{À} = r_U - 1.97\ X\ 10^{12} \cos\left(\frac{2\pi t}{3.10\ X\ 10^{19}\ \text{sec}}\right) \textit{light years}$$
$$\text{À} = r_U - 1.86\ X\ 10^{28} \cos\left(\frac{2\pi t}{3.10\ X\ 10^{19}\ \text{sec}}\right) m \qquad (23.151)$$

where r_U is the average size of the universe.

The universe has a finite minimum size equal to its gravitational radius r_g (Eq. (23.36)), and a maximum radius given by Eq. (23.150). Therefore, the universe has an average size which represents an offset of an oscillatory cycle of expansion and contraction. The average size of the universe, r_U, is determined by substitution of Eq. (23.147) into Eq. (23.151).

$$3.12\ X\ 10^{11}\ \textit{light years} = r_U - 1.97\ X\ 10^{12}\ \cos\left(\frac{2\pi t}{3.10\ X\ 10^{19}\ \text{sec}}\right) \textit{light years}$$
$$r_U = 2.28\ X\ 10^{12}\ \textit{light years}$$
$$2.96\ X\ 10^{27}\ m = r_U - 1.86\ X\ 10^{28}\ \cos\left(\frac{2\pi t}{3.10\ X\ 10^{19}\ \text{sec}}\right) m \qquad (23.152)$$
$$r_U = 2.16\ X\ 10^{28}\ m$$

Substitution of Eq. (23.152) into Eq. (23.151) gives ***the radius of the universe as a function of time***.

$$\grave{A} = 2.28\ X\ 10^{12} - 1.97\ X\ 10^{12}\ \cos\left(\frac{2\pi t}{3.10\ X\ 10^{19}\ \text{sec}}\right) \textit{light years}$$

$$\grave{A} = 2.28\ X\ 10^{12} - 1.97\ X\ 10^{12}\ \cos\left(\frac{2\pi t}{9.83\ X\ 10^{11}\ yrs}\right) \textit{light years} \qquad (23.153)$$

$$\grave{A} = 2.16\ X\ 10^{25} - 1.86\ X\ 10^{25}\ \cos\left(\frac{2\pi t}{3.01\ X\ 10^{5}\ M\text{pc}}\right) \text{k}m$$

The expansion/contraction rate, $\dot{\grave{A}}$, is given by taking the derivative with respect to time of Eq. (23.153).

$$\dot{\grave{A}} = 3.99\ X\ 10^{-7}\ \sin\left(\frac{2\pi t}{3.10\ X\ 10^{19}\ \text{sec}}\right) \frac{\textit{light years}}{\text{sec}}$$

$$\dot{\grave{A}} = 3.77\ X\ 10^{6}\ \sin\left(\frac{2\pi t}{9.83\ X\ 10^{11}\ yrs}\right) \frac{km}{\text{sec}} \qquad (23.154)$$

$$\dot{\grave{A}} = 3.77\ X\ 10^{6}\ \sin\left(\frac{2\pi t}{3.01\ X\ 10^{5}\ M\text{pc}}\right) \frac{km}{\text{sec}}$$

The expansion/contraction acceleration, $\ddot{\grave{A}}$, is given by taking the derivative with respect to time of Eq. (23.154).

$$\ddot{\grave{A}} = H_o = 78.7\ \cos\left(\frac{2\pi t}{3.01\ X\ 10^{5}\ M\text{pc}}\right) \frac{km}{\text{sec}\ Mpc} \qquad (23.155)$$

Eq. (23.155) and Figure 23.4 are consistent with the experimental observation that the rate of the expansion of the universe is increasing [28-30].

The ***time harmonic radius of the universe*** is shown graphically in Figure 23.3. The ***time harmonic expansion/contraction rate of the radius of the universe*** is shown graphically in Figure 22.4.

Figure 23.3. The radius of the universe as a function of time.

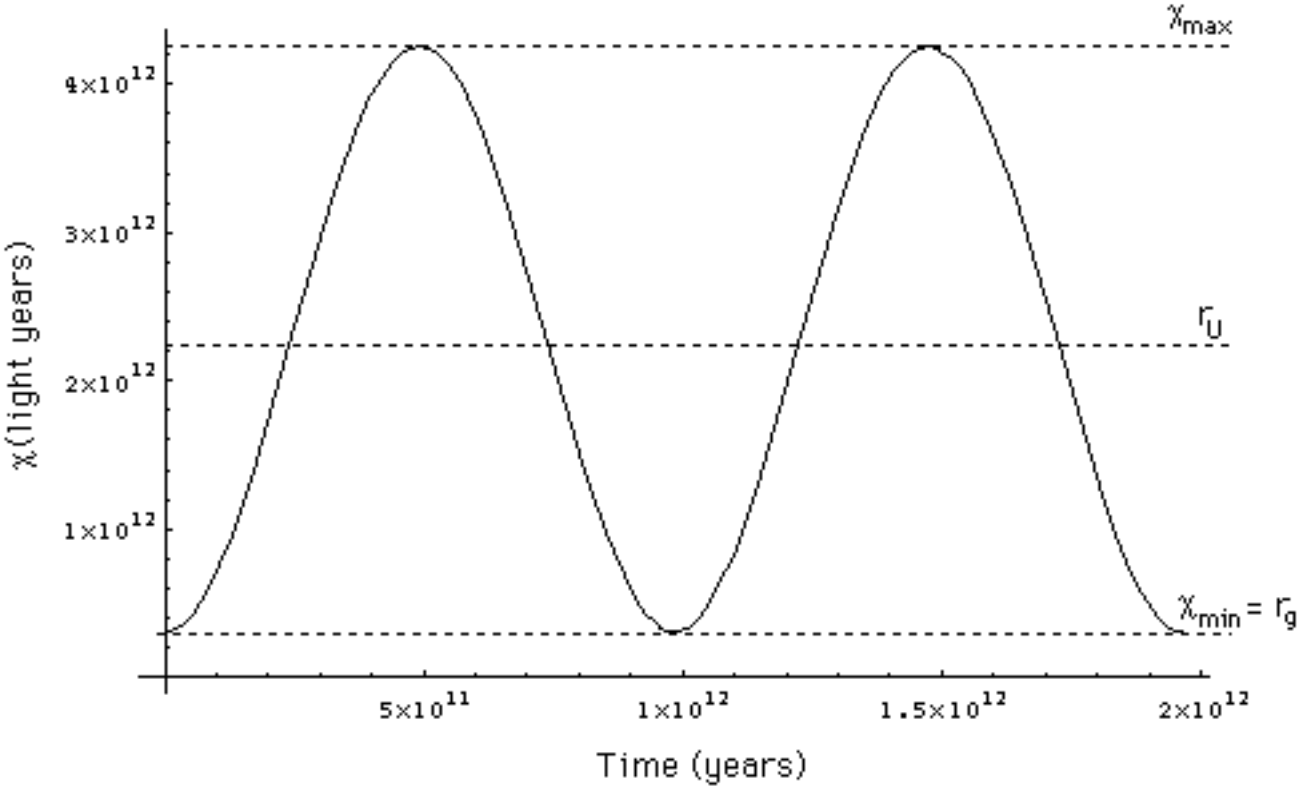

Figure 23.4. The expansion/contraction rate of the universe as a function of time.

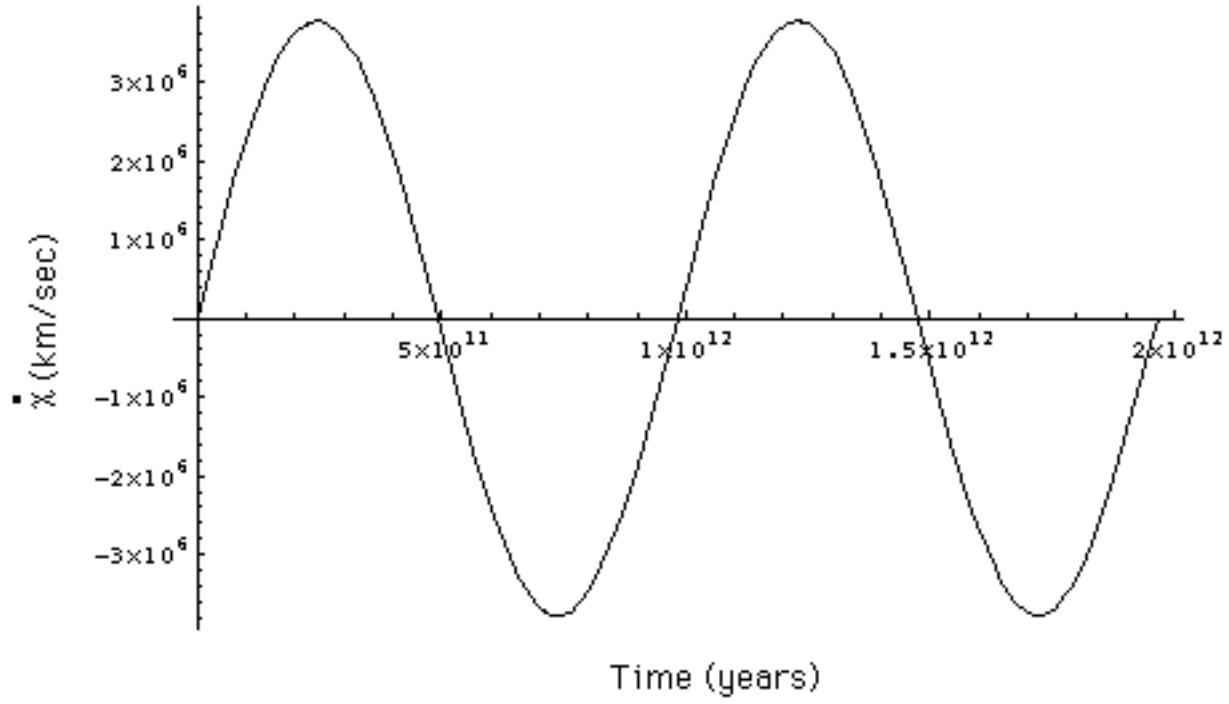

The ***Hubble constant*** defined by Eq. (23.126) is given by the ratio of the expansion rate given in units of $\frac{km}{\sec}$ divided by the radius of the expansion in Mpc (1 Megaparsec (Mpc) is $3.258\,X\,10^6$) light years). The radius of expansion is equivalent to the radius of the light sphere with an origin at the time point when the universe stopped contracting and started to expand. Thus, the radius of Eq. (23.126) is the time of expansion $t\,M\text{pc}$. From Eq. (23.154), the ***Hubble constant*** is

$$H = \frac{\dot{A}}{t} = \frac{3.77\,X\,10^6 \sin\left(\frac{2\pi t}{3.01\,X\,10^5\,M\text{pc}}\right)\frac{km}{\sec}}{t\,M\text{pc}} \tag{23.156}$$

For $t = 10^{10}$ *light years* $= 3.069\,X\,10^3 Mpc$,

$$H = \frac{3.77\,X\,10^6 \sin\left(\frac{2\pi\left(3.069\,X\,10^3\,M\text{pc}\right)}{3.01\,X\,10^5\,M\text{pc}}\right)\div\frac{km}{\sec}}{3.069\,X\,10^3\,M\text{pc}} = 78.6\frac{km}{\sec\,M\text{pc}} \tag{23.157}$$

Thus, from Eqs. (23.156-23.157), the Hubble, H_0, constant is $H_0 = 78.6\,\frac{km}{\sec\,Mpc}$. The experimental value is $H_0 = 80 \pm 17\,\frac{km}{\sec\,Mpc}$ [21]. The ***Hubble constant as a function of time*** is shown graphically in Figure 23.5.

Figure 23.5. The Hubble constant of the universe as a function of time.

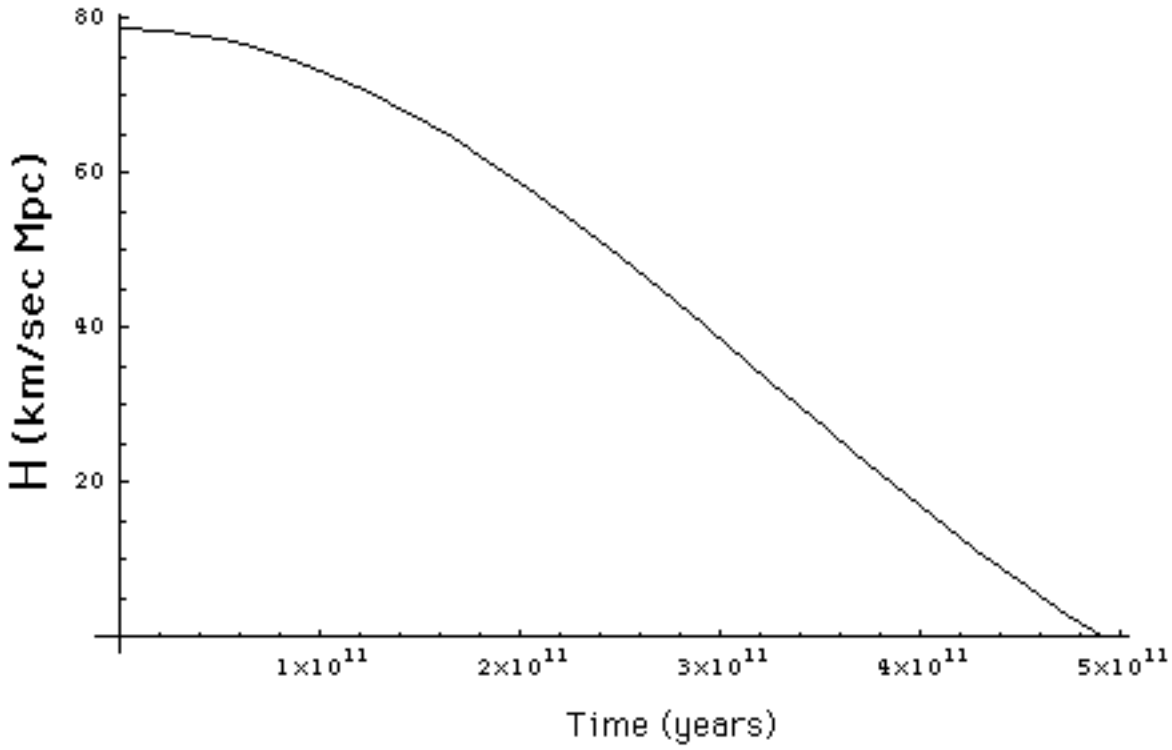

The mass of the universe as a function of time, $m_U(t)$, follows from the initial mass of $2\ X\ 10^{54}\ kg$ (based on internal consistency with the size, age, Hubble constant, temperature, density of matter, and power spectrum of the universe given herein) and Eq. (23.153)

$$m_U(t) = 2\ X\ 10^{54} \cos\left(\frac{2\pi t}{9.83\ X\ 10^{11}\ yrs}\right) kg \tag{23.158}$$

The volume of the universe as a function of time $V(t)$ follows from Eq. (23.153)

$$V(t) = \frac{4}{3}\pi R(t)^3 = \frac{4}{3}\pi\left(2.16\ X\ 10^{28} - 1.86\ X\ 10^{28} \cos\left(\frac{2\pi t}{9.83\ X\ 10^{11}\ yrs}\right) m\right)^3 \tag{23.159}$$

The density of the universe as a function of time $\rho_U(t)$ is given by the ratio of the mass as a function of time given by Eq. (23.158) and the volume as a function of time given by Eq. (23.159)

$$\rho_U(t) = \frac{m_U(t)}{V(t)} = \frac{m_U(t)}{\frac{4}{3}\pi R(t)^3} = \frac{2\ X\ 10^{54} \cos\left(\frac{2\pi t}{9.83\ X\ 10^{11}\ yrs}\right) kg}{\frac{4}{3}\pi\left(2.16\ X\ 10^{28} - 1.86\ X\ 10^{28} \cos\left(\frac{2\pi t}{9.83\ X\ 10^{11}\ yrs}\right) m\right)^3} \tag{23.160}$$

For $t = 10^{10}\ light\ years = 3.069\ X\ 10^{3} Mpc$, $\rho_U = 1.7\ X\ 10^{-35}\ g/cm^3$. The density of luminous matter of stars and gas of galaxies is about $\rho_U = 2\ X\ 10^{-31}\ g/cm^3$ [31-32]. The ***time harmonic density of the universe***, $\rho_U(t)$, is shown graphically in Figure 23.6.

Figure 23.6. The density of the universe as a function of time.

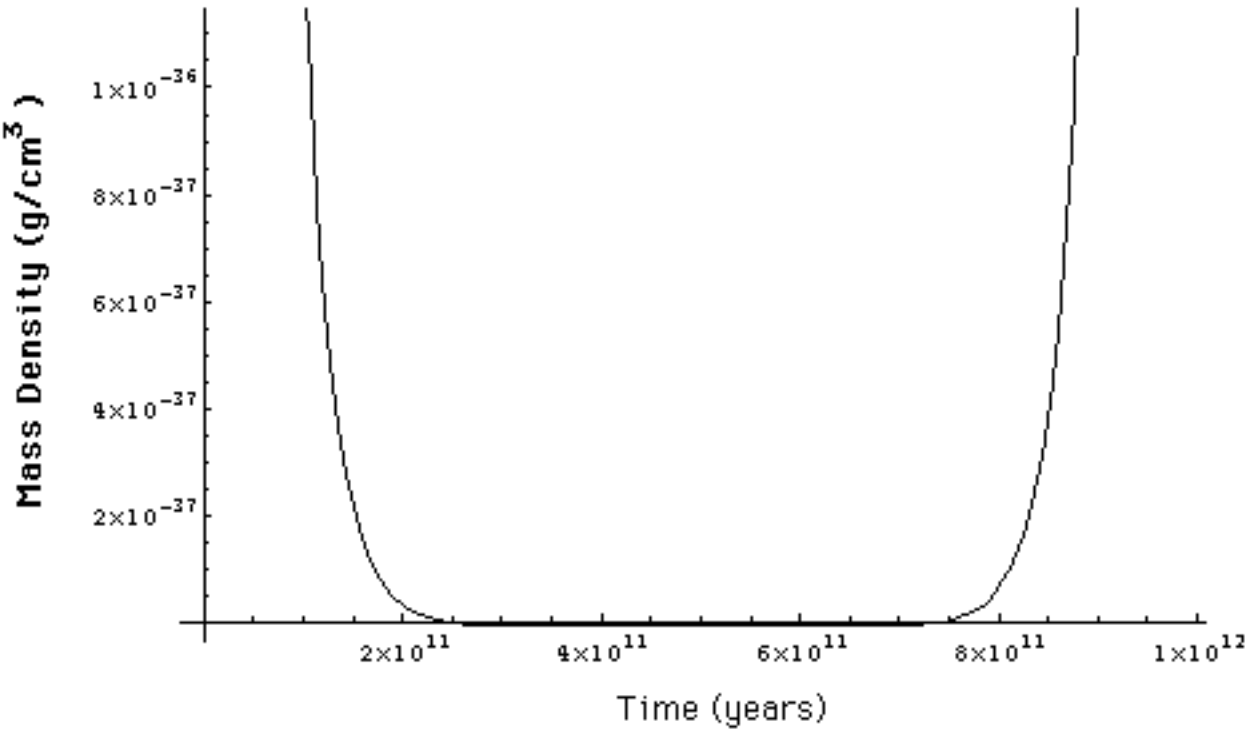

The power of the universe as a function of time, $P_U(t)$, follows from Eq. (23.142) and Eq. (23.151).

$$P_U(t) = \frac{c^5}{4\pi G}\cos\left(\frac{2\pi t}{9.83\ X\ 10^{11}\ yrs}\right) W$$

$$P_U(t) = 2.89\ X\ 10^{51}\cos\left(\frac{2\pi t}{9.83\ X\ 10^{11}\ yrs}\right) W \qquad (23.161)$$

The ***time harmonic power of the universe***, $P_U(t)$, is shown graphically in Figure 23.7.

Figure 23.7. The power of the universe as a function of time.

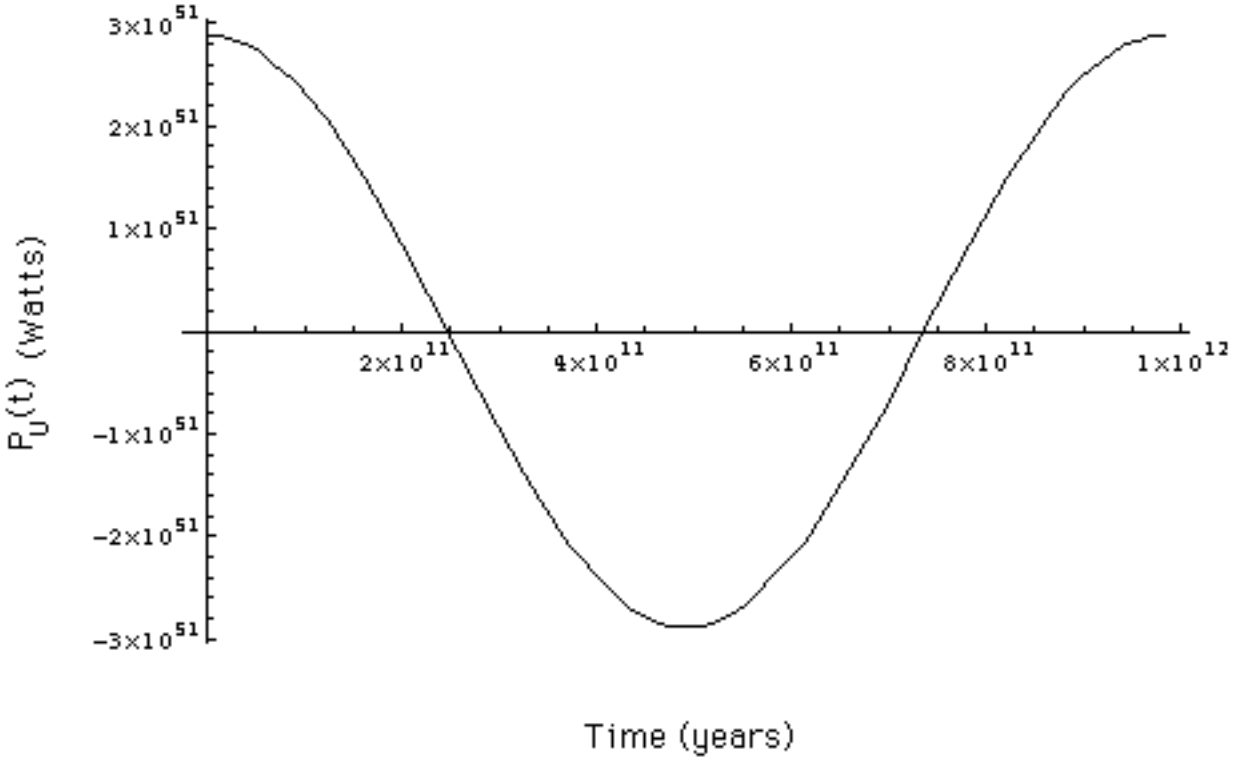

The temperature of the universe as a function of time can be derived from the Stefan-Boltzmann law. The Stefan-Boltzmann law (Eq.(23.143)) equates the power radiated by an object per unit area, R, to the emissivity, e, times the Stefan-Boltzmann constant, σ, times the fourth power of the temperature, T^4. The area of the universe as a function of time, $A(t)$, is approximately given by substitution of Eq. (23.153) into Eq. (23.144). (The universe is a four dimensional hyperspace of constant positive curvature. In the case that the radius of the universe is equal to the gravitational radius r_g, the area is given by Eq. (23.144); otherwise, the area of the sphere corresponding to the radius of the universe is less than that given by Eq. (23.144). The proper area is given by solving Eq. (23.38) for the coordinate radius as a function of the proper radius followed by the substitution of the coordinate radius into Eq. (23.144).)

$$A(t) = 4\pi\left[2.16\ X\ 10^{28} - 1.86\ X\ 10^{28}\ \cos\left(\frac{2\pi t}{3.10\ X\ 10^{19}\ \sec}\right) m\right]^2 \qquad (23.162)$$

The power radiated by the universe per unit area as a function of time, $R_U(t)$, is given by the ratio of Eq. (23.161) and Eq. (23.162).

$$R_U(t) = \frac{P_U(t)}{4\pi r(t)^2}$$

$$R_U(t) = \frac{2.89\ X\ 10^{51} \cos\left(\frac{2\pi t}{3.10\ X\ 10^{19}\ \sec}\right) W}{4\pi\left[2.16\ X\ 10^{28} - 1.86\ X\ 10^{28}\ \cos\left(\frac{2\pi t}{3.10\ X\ 10^{19}\ \sec}\right) m\right]^2} \tag{23.163}$$

The ***temperature of the universe as a function of time***, $T_U(t)$, follows from the Stefan-Boltzmann law (Eq.(23.143)) and Eq. (23.163)

$$T_U(t) = \left[\frac{R_U(t)}{e\sigma}\right]^{\frac{1}{4}}$$

$$T_U(t) = \left[\frac{2.89\ X\ 10^{51} \cos\left(\frac{2\pi t}{3.10\ X\ 10^{19}\ \sec}\right) W}{4\pi\left[2.16\ X\ 10^{28} - 1.86\ X\ 10^{28}\ \cos\left(\frac{2\pi t}{3.10\ X\ 10^{19}\ \sec}\right) m\right]^2}\right]^{\frac{1}{4}} \tag{23.164}$$

where the emissivity, e, for a blackbody is one, and $\sigma = 5.67\ X\ 10^{-8}\ Wm^{-2}K^{-4}$.

The universe is a four dimensional hyperspace of constant positive curvature. The coordinates are spherical, and the space can be described as a series of spheres each of constant radius r whose centers coincide at the origin. The existence of the mass m_U causes the area of the spheres to be less than $4\pi r^2$ and causes the clock of each r-sphere to run so that it is no longer observed from other r-spheres to be at the same rate. The Schwarzschild metric given by Eq. (23.38) is the general form of the metric which allows for these effects. Fang and Ruffini [5] show that the time effect is equivalent to a gravitational redshift of a photon. The shifted wavelength due to the gravitational field of a mass m_U is

$$\lambda(\infty) = \lambda(r)\left(1 + \frac{Gm_U}{c^2 r}\right) \tag{23.165}$$

Wien's displacement law gives the relationship between temperature and wavelength [26].

$$\lambda_{\max} T = 2.898\ X\ 10^{-3}\ m\ K \tag{23.166}$$

Thus, the temperature of the universe as a function of time, $T_U(t)$, is

$$T_U(t) = \left(\frac{1}{1+\frac{Gm_U}{c^2 R_U(t)}}\left[\frac{R_U(t)}{e\sigma}\right]\right)^{\frac{1}{4}}$$

$$T_U(t) = \left(\frac{1}{1+\frac{1.48\ X\ 10^{27}\ m}{\left[2.16\ X\ 10^{28} - 1.86\ X\ 10^{28}\cos\left(\frac{2\pi t}{3.10\ X\ 10^{19}\ \sec}\right) m\right]}}\right) X$$

$$\left[\frac{2.89\ X\ 10^{51}\cos\left(\frac{2\pi t}{3.10\ X\ 10^{19}\ \sec}\right) W}{4\pi\left[2.16\ X\ 10^{28} - 1.86\ X\ 10^{28}\cos\left(\frac{2\pi t}{3.10\ X\ 10^{19}\ \sec}\right) m\right]^2 \frac{}{5.67 X 10^{-8}\ W m^{-2} K^{-4}}}\right]^{\frac{1}{4}} \quad (23.167)$$

$$T_U(t) = \left(\frac{1}{1+\frac{1.48\ X\ 10^{27}\ m}{\left[2.16\ X\ 10^{28} - 1.86\ X\ 10^{28}\cos\left(\frac{2\pi t}{9.83\ X\ 10^{11}\ yrs}\right) m\right]}}\right) X$$

$$\left[\frac{2.89\ X\ 10^{51}\cos\left(\frac{2\pi t}{9.83\ X\ 10^{11}\ yrs}\right) W}{4\pi\left[2.16\ X\ 10^{28} - 1.86\ X\ 10^{28}\cos\left(\frac{2\pi t}{9.83\ X\ 10^{11}\ yrs}\right) m\right]^2 \frac{}{5.67 X 10^{-8}\ W m^{-2} K^{-4}}}\right]^{\frac{1}{4}} \quad (23.168)$$

The temperature of the universe as a function of time, $T_U(t)$, during the expansion phase is shown graphically in Figure 23.8.

Figure 23.8. The temperature of the universe as a function of time during the expansion phase.

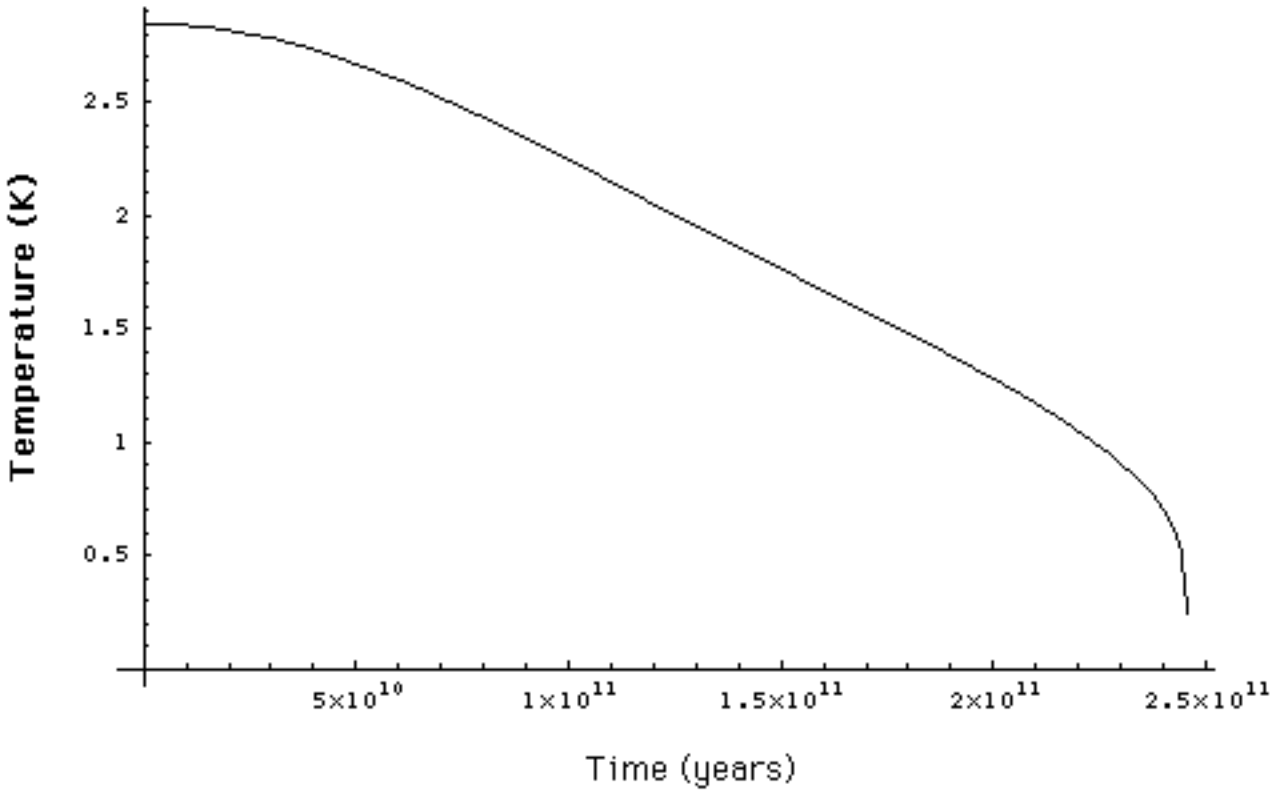

Furthermore, hydrogen transitions to electronic energy levels below the "ground" state corresponding to fractional quantum numbers exactly match the spectral lines of the extreme ultraviolet background of interstellar space. This assignment, given in the Spectral Data of Hydrinos from the Dark Interstellar Medium and Spectral Data of Hydrinos, Dihydrinos, and Hydrino Hydride Ions from the Sun Section, resolves the paradox of the identity of dark matter and accounts for many celestial observations such as: the observation that diffuse Hα emission is ubiquitous throughout the Galaxy, and that widespread sources of flux short of 912 $\AA$ are required [33]. Also, the spin/nuclear hyperfine structure transition energies of lower-energy hydrogen match closely certain spectral lines obtained by COBE [34-35] for which no other satisfactory assignment exists. The far-infrared absolute spectrometer (FIRAS) on the Cosmic Background Explorer has carried out an all-sky survey in the far infrared region ($1 \; to \; 90 \; cm^{-1}$). Averaged over many positions in the Galaxy, spectral features are observed which correspond closely with the predicted hydrino hyperfine transition

energies. The lines obtained by COBE that match the hyperfine structure transitions of lower-energy hydrogen as calculated in the Spin-Nuclear and Orbital-Nuclear Coupling of Hydrinos Section are given in the Spectral Data of Hydrinos from the Dark Interstellar Medium and Spectral Data of Hydrinos, Dihydrinos, and Hydrino Hydride Ions from the Sun Section.

Composition of the Universe

In the case that ***lower-energy hydrogen comprises the dark matter***, all matter is ordinary (baryonic) matter, and the mass of the universe is sufficient for it to be closed [22-23]. Whereas, the standard theory of big bang nucleosynthesis explains the observed abundance of light elements (H, He, and Li) only if the present density of ordinary (baryonic) matter is less than 10 % of the critical value [36-37]. According to Mills' theory, ***the abundance of the lighter elements, H, He, and Li is consistent with neutron, proton, and electron production during the collapsing phase and solar nucleosynthesis during the expansion phase of the expansion/contraction cycle***. The abundance of light elements for any r-sphere may be calculated using the power of the universe as a function of time (Eq. (23.161)) and the solar nucleosynthesis rates. During the collapsing phase of the oscillatory cycle, the electron neutrino causes neutron production from a photon. Planck's equation and Special and General Relativity define the mass of the neutron in terms of the spacetime metric as given in the Quarks Section. The Planck equation energy, which is equal to the mass energy, applies for the proper time of the neutron given by general relativity (Eq. (23.38)) that is created with the transition of a photon to a neutron. As discussed previously in the Quantum Gravity of Fundamental Particles Section, a photon gives rise to a particle and an antiparticle. The event must be spacelike or annihilation would occur. The event must also conserve energy, momentum, charge, and satisfy the condition that the speed of light is a constant maximum. Eqs. (23.14-23.17) give the relationship whereby matter causes relativistic corrections to spacetime that determines the curvature of spacetime and is the origin of gravity. To satisfy the boundary conditions, particle production from a single photon requires the production of an antimatter particle as well as a particle. The transition state from a photon to a particle and antiparticle comprises two concentric orbitspheres called transition state orbitspheres. The gravitational effect of a spherical shell on an object outside of the radius of the shell is equivalent to that of a point of equal mass at the origin. Thus, the proper time of the concentric orbitsphere with radius ${}^{+}r_n^*$ (the radius is infinitesimally greater than that

of the inner transition state orbitsphere with radius r_n) is given by the Schwarzschild metric, Eq. (23.38). The proper time applies to each point on the orbitsphere. Therefore, consider a general point in the xy-plane having $r = \lambda\!\!\!^{-}_C$; $dr = 0$; $d\theta = 0$; $\sin^2\theta = 1$. Substitution of these parameters into Eq. (23.38) gives

$$d\tau = dt\left(1 - \frac{2Gm_0}{c^2 r_\alpha^*} - \frac{v^2}{c^2}\right)^{\frac{1}{2}} \tag{23.169}$$

with $v^2 = c^2$, Eq. (23.169) becomes

$$\tau = ti\sqrt{\frac{2GM}{c^2 r_\alpha^*}} = ti\sqrt{\frac{2GM}{c^2 \lambda\!\!\!^{-}_c}} \tag{23.170}$$

The coordinate time is imaginary because particle/antiparticle production is spacelike. The left-hand side of Eq. (23.170) represents the proper time of the particle/antiparticle as the photon orbitsphere becomes matter. The right-hand side of Eq. (23.170) represents the correction to the laboratory coordinate metric for time corresponding to the curvature of spacetime by the particle production event.

During the contraction phase, the electron neutrino causes neutron production from a photon. The event must be spacelike or annihilation would occur. The event must also conserve energy, momentum, charge, and satisfy the condition that the speed of light is a constant maximum. Eqs. (23.14-23.17) give the relationship whereby matter causes relativistic corrections to spacetime that determines the curvature of spacetime and is the origin of gravity. The electron neutrino is a special type of photon as given in the Neutrino Section. The photon and the neutrino have zero rest mass and travel at the speed of light. To satisfy the boundary conditions, particle production from an electron neutrino and a photon requires the production of a single neutral particle. In this case, the transition state only comprises a single transition state orbitsphere. The left-hand side of Eq. (23.170) represents the proper time of the neutron as the photon orbitsphere becomes matter. The right-hand side of Eq. (23.170) represents the correction to the laboratory coordinate metric for time corresponding to the relativistic correction of spacetime by the particle production. Thus, ***during the collapsing phase of the oscillatory cycle, the electron neutrino causes neutron production from a photon, and the production of protons and electrons occurs by neutron beta decay.*** Typically, antimatter and matter are created in the laboratory in equal amounts; yet, ***celestial antimatter is not observed***. The reason is that no electron antineutrinos exist at the initiation of spacetime collapse, thus, antineutron production does not occur as a separate symmetrical reaction, and particle production from a neutrino and a photon

prohibits production of the antimatter twin. From Eq. (30.6), the neutron mass is

$$m_{ddu\ calculated} = (3)(2\pi)\left(\frac{1}{1-\alpha}\right)\left(\frac{2\pi h}{\sec c^2}\right)^{\frac{1}{2}}\left(\frac{2\pi(3)ch}{2G}\right)^{\frac{1}{4}} = 1.674\ X\ 10^{-27}\ kg \qquad (23.171)$$

The neutron production reaction and the nuclear reaction for the Beta decay of a neutron are

$$\begin{aligned} \gamma + \upsilon_e &\rightarrow {}^1n \\ {}^1n &\rightarrow {}^1H + \beta + \bar{\nu}_e + 0.7835\ MeV \end{aligned} \qquad (23.172)$$

where υ_e is the electron neutrino and $\bar{\nu}_e$ is the electron antineutrino. Eq. (23.172) predicts an electron neutrino background which could account for the atmospheric neutrino anomaly [38]. From Eq. (23.172), ***the number of electrons exactly balances the number of protons***. Thus, ***the universe is electrically neutral***.

During the expansion phase, protons and electrons of lower-energy hydrogen which comprises the dark matter annihilate to photons and electron neutrinos as given in the New "Ground" State Section. To conserve spin (angular momentum) the reaction is

$$\bar{\nu}_e + {}^1H\left[\frac{a_H}{n}\right] \rightarrow \gamma + \nu_e \qquad (23.173)$$

where ν_e is the electron neutrino. (A similar reaction to that of Eq. (23.173) is the reaction of a muon neutrino rather than an electron antineutrino with a hydrino to give a gamma photon and a muon antineutrino.) Disproportionation reactions to the lowest-energy states of hydrogen followed by electron capture with gamma ray emission may be *a source of nonthermal* γ*-ray bursts from interstellar regions* [39].

Alternately, the source may be due to conversion of matter to photons of the Planck mass/energy which may also give rise to cosmic rays. When the gravitational potential energy density of a massive body such as a blackhole equals that of a particle having the Planck mass as given by Eqs. (23.22-23.32), the matter may transition to photons of the Planck mass given by Eq. (23.31). In the case of the Plank mass, the gravitational potential energy (Eq, (23.30)) is equal to the Planck equation, electric, and magnetic energies which equal mc^2 (Eq. (23.32)), and the coordinate time is equal to the proper time (Eqs. (23.33-23.34 and Eq. (23.43)). However, the particle corresponding to the Planck mass may not form since its gravitational velocity (Eq. (23.33)) is the speed of light. *(The limiting speed of light eliminates the singularity problem of Einstein's equation that arises as the radius of a blackhole equals the Schwarzschild radius. General relativity with the singularity eliminated resolves the paradox of the infinite propagation velocity required for the gravitational force in order to explain why the angular*

momentum of objects orbiting a gravitating body does not increase due to the finite propagation delay of the gravitational force according to special relativity [40]). Thus, it remains a photon. Even light from a blackhole will escape when the decay rate of the trapped matter with the concomitant spacetime expansion is greater than the effects of gravity which oppose this expansion. The annihilation of a blackhole may be the source of *γ-ray bursts.* Gamma-ray bursts are the most energetic phenomenon known that can release an explosion of gamma rays packing 100 times more energy than a supernova explosion [41]. Cosmic rays are the most energetic particles known, and their origin is also a mystery [42]. In 1966, Cornell University's Kenneth Greisen predicted that interaction with the ubiquitous photons of the cosmic microwave background would result in a smooth power-law cosmic-ray energy spectrum being sharply cutoff close to $5 X 10^{19}$ *eV*. However, in 1998, Schwarzschild reported [43] that the *Akeno Giant Air Shower Array (AGASA) in Japan has collected data that show the cosmic-ray energy spectrum is extending beyond the Greisen-Zatsepin-Kuzmin (GZK) cutoff.* According to the GZK cutoff, the cosmic spectrum cannot extend beyond $5 X 10^{19}$ *eV*, but AGASA, the world's largest air shower array, has shown that the spectrum is extending beyond 10^{20} *eV* without any clear sign of cutoff. *Photons each of the Planck mass may be the source of these inexplicably energetic cosmic rays.*

Thus, the universe is oscillatory in matter, energy, and spacetime without the existence of antimatter due to conservation of spin of the electron neutrino and the relationship of particle production to spacetime contraction. During the expansion phase, ***the arrow of time runs forward*** to lower mass and higher entropy states; whereas, during collapse, ***the arrow of time runs backwards*** relative to the case of the universe in a state of expansion. Recent particle physics experiments demonstrate that the decay of kaons and antikaons follows a law that is not symmetric with respect to time reversal [30]. The data reveals that there is a microscopic arrow of time, in addition to the thermodynamic and cosmological arrows.

The universe evolves to higher mass and lower entropy states. Thus, biological organisms such as humans which rely on the spontaneity of chemical reactions with respect to the forward arrow of time cannot exist in the contracting phase of the universe. And, compared to the period of the universe, the ***origins of life*** occurred at a time very close to the beginning of the expansion of the universe when the direction of the spontaneity of reactions changed to the direction of increasing entropy and the rate of the increase in entropy of the universe was a maximum.

Expansion of the universe depends on the rate of energy release which varies throughout the universe; thus, clusters of galaxies, huge voids, and other ***large features which are observed*** [44-47] are caused by the interaction between the rate of energy release with concomitant spacetime expansion and gravitational attraction. Hydrogen-type atoms and molecules comprises most of the matter of the universe. The distinction between hydrogen and lower-energy hydrogen with respect to the interaction with electromagnetic radiation and release of energy via disproportionation reactions (Eqs. (5.36-5.63)) also has an influence on the formation of large voids and walls of matter. Lower-energy atomic hydrogen atoms, hydrinos, each have the same mass and a similar interaction as the neutron. According to Paul Steinhardt and David Spergel of Princeton University [48], these are the properties of dark matter that are necessary in order for the theory of the structure of galaxies to work out on all scales. The observation that Galaxy clusters arrange themselves as predicted for cold dark matter except that the cores are less dense than expected is explained. Hydrinos further account for the observation that small halos of dark matter are evaporated when they approach larger ones and that dark matter is easily influenced by black holes, explaining how they grew so large.

Furthermore, the universe is oscillatory with a finite minimum radius; thus, the gravitational force causes celestial structures to evolve on a time scale that is greater than the period of oscillation. Presently, ***stars exist which are older than the elapsed time of the present expansion*** as stellar evolution occurred during the contraction phase [49-50]. The maximum energy release of the universe given by Eq. (23.142) occurred at the beginning of the expansion phase, and the power spectrum is a function of the r-sphere of the observer.

Power Spectrum of the Cosmos

The power spectrum of the cosmos, as measured by the Las Campanas survey, generally follows the prediction of cold dark matter on the scales of 200 million to 600 million light-years. However, the power increases dramatically on scales of 600 million to 900 million light-years [51]. This discrepancy means that the universe is much more structured on those scales than current theories can explain. Furthermore, recent evidence reveals a fatal flaw in inflation theory and supports structure at a much larger scale. The cosmic microwave background radiation was an average temperature of 2.7 ° kelvins, with deviations of 30 or so microkelvins in different parts of the sky representing slight variations in the density of matter. The temperature fluctuations of the cosmic microwave background radiation are not Gaussian [27] which is an absolute requirement for inflation theory. The

universe is oscillatory in matter/energy and spacetime with a finite minimum radius. The minimum radius of the universe, 300 billion light years [24], is larger than that provided by the current expansion, approximately 10 billion light years [21]. The universe is a four dimensional hyperspace of constant positive curvature. The coordinates are spherical, and the space can be described as a series of spheres each of constant radius r whose centers coincide at the origin. The existence of the mass m_U causes the area of the spheres to be less than $4\pi r^2$ and causes the clock of each r-sphere to run so that it is no longer observed from other r-spheres to be at the same rate. The Schwarzschild metric given by Eq. (23.38) is the general form of the metric which allows for these effects. Consider the present observable universe that has undergone expansion for 10 billion years. The radius of the universe as a function of time from the coordinate r-sphere is of the same form as Eq. (23.153). The average size of the universe, r_U, is given as the sum of the gravitational radius, r_g, and the observed radius, 10 billion light years.

$$\begin{aligned} r_U &= r_g + 10^{10}\ \textit{light years} \\ r_U &= 3.12\ X\ 10^{11}\ \textit{light years} + 10^{10}\ \textit{light years} \\ r_U &= 3.22\ X\ 10^{11}\ \textit{light years} \end{aligned} \tag{23.174}$$

The frequency of Eq. (23.153) is one half the amplitude of spacetime expansion from the conversion of the mass of universe into energy according to Eq. (23.140). Thus, keeping the same relationships, the frequency of the current expansion function is the reciprocal of one half the current age. Substitution of the average size of the universe, the frequency of expansion, and the amplitude of expansion, 10 billion light years, into Eq. (23.153) gives ***the radius of the universe as a function of time for the coordinate r-sphere***.

$$\grave{A} = 3.22\ X\ 10^{11} - 1\ X\ 10^{10}\ \cos\left(\frac{2\pi t}{5\ X\ 10^{9}\ \textit{light years}}\right)\textit{light years} \tag{23.175}$$

The Schwarzschild metric gives the relationship between the proper time and the coordinate time (Eq. 23.38)). The infinitesimal temporal displacement, $d\tau^2$, is

$$d\tau^2 = \left(1 - \frac{2Gm_U}{c^2 r}\right)dt^2 - \frac{1}{c^2}\left[\frac{dr^2}{1 - \frac{2Gm_U}{c^2 r}} + r^2 d\theta^2 + r^2 \sin^2\theta d\phi^2\right] \tag{23.176}$$

In the case that $dr^2 = d\theta^2 = d\phi^2 = 0$, the relationship between the proper time and the coordinate time is

$$d\tau^2 = \left(1 - \frac{2Gm_U}{c^2 r}\right)dt^2 \tag{23.177}$$

$$\tau = t\sqrt{1-\frac{2Gm_U}{c^2 r}} \tag{23.178}$$

$$\tau = t\sqrt{1-\frac{r_g}{r}} \tag{23.179}$$

The maximum power radiated by the universe is given by Eqs. (23.142) which occurs when the proper radius, the coordinate radius, and the gravitational radius r_g are equal. For the present universe, the coordinate radius is given by Eq. (23.174). The gravitational radius is given by Eq. (23.147). The maximum of the power spectrum of a trigonometric function occurs at its frequency [52]. Thus, the coordinate maximum power according to Eq. (23.175) occurs at $5\,X\,10^9$ *light years*. The maximum power corresponding to the proper time is given by the substitution of the coordinate radius, the gravitational radius r_g, and the coordinate power maximum into Eq. (23.179). The power maximum in the proper frame occurs at

$$\tau = 5\,X\,10^9 \text{ light years}\sqrt{1-\frac{3.12\,X\,10^{11} \text{ light years}}{3.22\,X\,10^{11} \text{ light years}}} \tag{23.180}$$

$$\tau = 880\,X\,10^6 \text{ light years}$$

The power maximum of the current observable universe is predicted to occur on the scale of $880\,X\,10^6$ *light years*. There is excellent agreement between the predicted value and the experimental value of between 600 million to 900 million light years [51].

The Differential Equation of the Radius of the Universe

The differential equation of the radius of the universe, À, can be derived as a conservative simple harmonic oscillator having a restoring force, **F**, which is proportional to the radius. The proportionality constant, k, is given in terms of the potential energy, E, gained as the radius decreases from the maximum expansion to the minimum contraction.

$$\frac{E}{\text{À}^2} = k \tag{23.181}$$

The universe oscillates between a minimum and maximum radius as matter is created into energy and then energy is converted to matter. At the minimum radius, the gravitational velocity, v_G, is given by Eq. (23.33) and the gravitational radius r_G, is given by Eq. (23.22) wherein an electromagnetic wave of mass energy equivalent to the mass of the universe travels in a circular orbit wherein the eccentricity is equal to zero (Eq. (26.20)), and the escape velocity from the universe can never be reached. At this point in time, all of the energy of the universe is in the form of matter, and the gravitational energy (Eq. (23.148)) is equal

to $m_U c^2$. Thus, the proportionality constant of the restoring force with respect to the radius is

$$F = -k\grave{A} = -\frac{m_U c^2}{r_G^2}\grave{A} = -\frac{m_U c^2}{\left(\frac{Gm_U}{c^2}\right)^2}\grave{A} \tag{23.182}$$

The differential equation of the radius of the universe, $\grave{A}$, follows from Eq. (23.182) as given by Fowles [53].

$$\begin{aligned} m_U\ddot{\grave{A}} + \frac{m_U c^2}{r_G^2}\grave{A} &= 0 \\ m_U\ddot{\grave{A}} + \frac{m_U c^2}{\left(\frac{Gm_U}{c^2}\right)^2}\grave{A} &= 0 \end{aligned} \tag{23.183}$$

The solution of Eq. (23.183) which gives the radius of the universe as a function of time follows from Fowles [53].

$$\begin{aligned} \grave{A} &= \left(r_g + \frac{cm_U}{Q}\right) - \frac{cm_U}{Q}\cos\left(\frac{2\pi t}{\frac{2\pi r_G}{c}\sec}\right)m \\ \grave{A} &= \left(\frac{2Gm_U}{c^2} + \frac{\frac{cm_U}{c^3}}{4\pi G}\right) - \frac{\frac{cm_U}{c^3}}{4\pi G}\cos\left(\frac{2\pi t}{\frac{2\pi Gm_U}{c^3}\sec}\right)m \end{aligned} \tag{23.184}$$

The gravitation force causes the radius of Eq. (23.184) to be offset [53]. The force equations of general relativity which follow from Eq. (23.38) give the offset radius, r_U. The minimum radius corresponds to the gravitational radius r_g whereby the proper time is equal to the coordinate time. The offset radius, r_U, is

$$r_U = r_g + \frac{\frac{cm_U}{c^3}}{4\pi G} \tag{23.185}$$

The expansion/contraction rate, $\dot{\grave{A}}$, is given by taking the derivative with respect to time of Eq. (23.184).

$$\dot{\grave{A}} = 4\pi c\, X\, 10^{-3}\sin\left(\frac{2\pi t}{\frac{2\pi Gm_U}{c^3}\sec}\right)\frac{km}{\sec} \tag{23.186}$$

According to special relativity no signal may travel faster than c, the speed of light for any observer. The maximum expansion rate for a 3-sphere is $4\pi c$ which is given in Eq. (23.186). The expansion/contraction acceleration, $\ddot{\grave{A}}$, is given by taking the derivative with respect to time of

Eq. (23.186).

$$\ddot{A} = 2\pi \frac{c^4}{Gm_U} X\ 10^{-3} \cos\left(\frac{2\pi t}{\frac{2\pi Gm_U}{c^3}\ \sec}\right) \frac{km}{\sec^2} \tag{23.187}$$

The universe oscillates between the extremes of all matter and all energy. At the beginning of its expansion, the universe is all matter with no electromagnetic radiation; thus, ***the universe is not observable for earlier times***. The observer's light sphere determines the limits of observation thereafter. Furthermore, ancient stars and the large scale structure of the cosmos comprising galactic superclusters and voids that could not have formed within the elapsed time of expansion are visible [44-47; 49-51]. Recently, a uniform cosmic infrared background has been discovered which is consistent with the heating of dust with reradiation over a much longer period then the elapsed time of expansion [54]. The size of the universe may be detected by observing the early curvature, the power spectrum, and the microwave background temperature. In the latter case, the power released as a function of time over the entire universe is given by Eq. (23.161). The size of the universe as a function of time is given by Eq. (23.153). The microwave background temperature corresponds to the power density over the entire universe which is uniform on the scale of the entire universe. Thus, the microwave background temperature as a function of time for each observer within his light sphere is give by Eq. (23.168).

The Hubble constant given by the ratio of the expansion rate (Eq. (23.186)) given in units of $\frac{km}{\sec}$ and the lapsed time of expansion in units of Mpc (1 Megaparsec (Mpc) is $3.258\ X\ 10^6$) light years) is

$$H = \frac{\dot{A}}{t\ Mpc} = \frac{4\pi c\ X\ 10^{-3} \sin\left(\frac{2\pi t}{\frac{2\pi Gm_U}{c^3}\ \sec}\right) \frac{km}{\sec}}{t\ Mpc} \tag{23.188}$$

The differential in the radius of the universe ΔA due to its acceleration is given by

$$\Delta A = 1/2 \ddot{A} t^2 \tag{23.189}$$

The ***expansion of the light sphere due to the acceleration of the expansion of the cosmos*** given by Eq. (23.155) and Eq. (23.187) is shown graphically in Figure 23.9. The observed brightness of supernovae as standard candles is inversely proportional to their distance squared. As shown in Figure 23.9, ΔA increases by a factor of about three as the time of expansion increases from the midpoint to a time comparable to the elapsed time of expansion,

$t = 10^{10}$ *light years* = $3.069\ X\ 10^{3} Mpc$. As an approximation, this differential in expanded radius corresponds to a decease in brightness of a supernovae standard candle of about an order of magnitude of that expected where the distance is taken as ΔÀ. This result is consistent with the experimental observation [28-30]. Recently, the BOOMERANG telescope [55] imaged the microwave background radiation covering about 2.5% of the sky with an angular resolution of 35 times that of COBE [25]. The image revealed hundreds of complex structures that were visible as tiny fluctuations--typically only 100 millionths of a degree (0.0001 ºC)--in temperature of the Cosmic Microwave Background. Structures of about 1° in size were observed that are consistent with a universe of nearly flat geometry since the commencement of its expansion. The data is consistent with a large offset radius of the universe as given by Eq. (23.147) with a fractional increase in size (Eq. (23.153)) since the commencement of expansion about 10 billion years ago.

Figure 23.9. The differential expansion of the light sphere due to the acceleration of the expansion of the cosmos as a function of time.

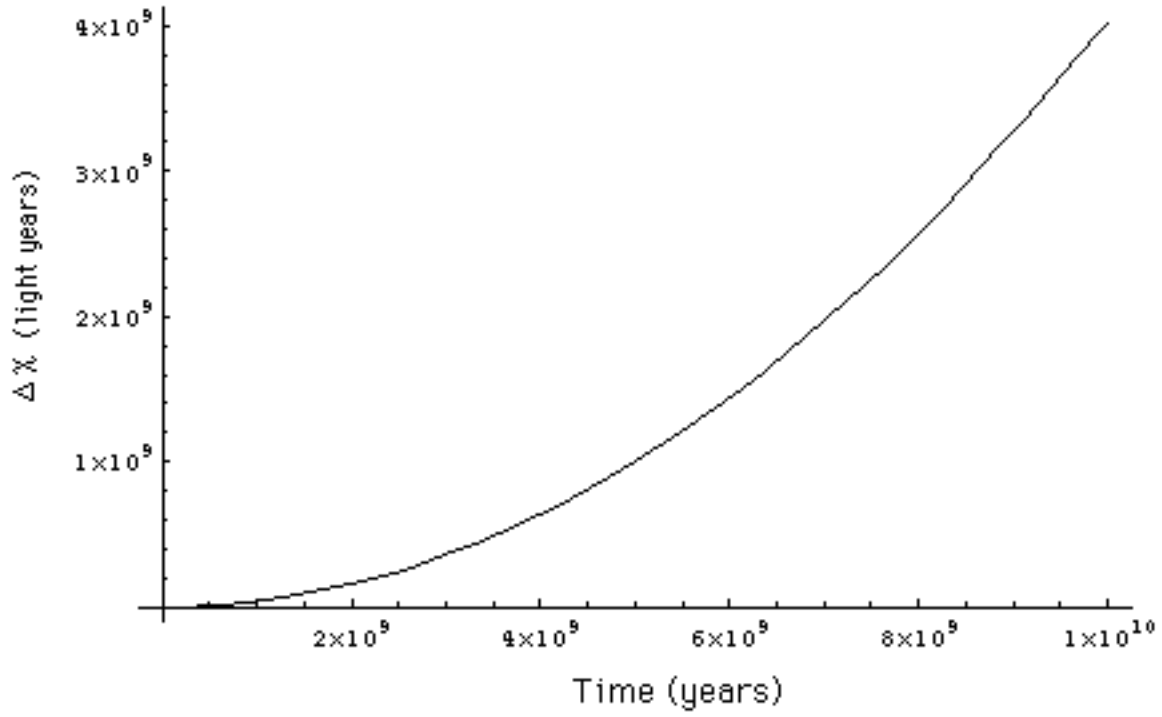

The definitive form of the field equations of general relativity follow from the Schwarzschild metric (Eq.(23.38)) and can be expressed in terms of ***the contraction of spacetime by the special relativistic***

mass of a fundamental particle (Eq. (23.140)). The masses and charges of the fundamental particles are determined by the equations of the transition state orbitsphere herein derived where the nonradiative boundary condition and the constancy of the speed of light must hold which requires relativistic corrections to spacetime. Fundamental particles can decay or interact to form an energy minimum. Thus, each stable particle arises from a photon directly or from a decaying particle which arose from a photon. The photon, and the corresponding fundamental particle, possess $\hbar$ of angular momentum. Nuclei form as binding energy is released as the orbitspheres of participating nucleons overlap. Atoms form as the potential energy of the fields of electrons and nuclei is released as the fields are partially annihilated. Molecules form as the energy stored in the fields of atoms is minimized. Planets and celestial bodies form as the gravitational potential energy is minimized. All of these energies correspond to forces, and the equations of the forces are given in the Unification of Spacetime, the Forces, Matter, and Energy Section.

References

1. Adelberger, E. G., Stubbs, C.W., Heckel, B.R., Su, Y., Swanson, H.E., Smith, G., Gundlach, J. H., Phys. Rev. D, Vol. 42, No. 10, (1990), pp. 3267-3292.
2. H. Minkowski's interpretation of special relativity in terms of a four dimensional space time was presented in the form of a lecture in Cologne, Germany in September 1908. An English translation , entitled "Space and Time," can be found in the collection *The Principle of Relativity*, Dover, New York, 1952.
3. Fock, V., The Theory of Space, Time, and Gravitation, The MacMillan Company, (1964), pp. 14-15.
4. Fowles, G. R., Analytical Mechanics, Third Edition, Holt, Rinehart, and Winston, New York, (1977), pp. 154-155.
5. Fang , L. Z., and Ruffini, R., Basic Concepts in Relativistic Astrophysics, World Scientific, (1983).
6. Fock, V., The Theory of Space, Time, and Gravitation, The MacMillan Company, (1964).
7. W. K. Clifford, The Common Sense of the Exact Sciences; Mathematical Papers, p. 21, presented to the Cambridge Philosophical Society in 1870.
8. R. M. Wald, General Relativity, University of Chicago Press, Chicago, (1984), pp. 91-101.
9. N. A. Bahcall, J. P. Ostriker, S. Perlmutter, P. J. Steinhardt, Science, May 28, 1999, Vol. 284, pp. 1481-1488.
10. Fock, V., The Theory of Space, Time, and Gravitation, The MacMillan

Company, (1964), pp. 209-215.
11. Steven Weinberg, Gravitation and Cosmology: Principles and Applications of the General Theory of Relativity, John Wiley & Sons, New York, (1972), Sect. 11/7, pp. 335 ff.
12. L. P. Eisenhart, Riemannian Geometry, Princeton: Princeton University Press, (1949).
13. D. Lovelock, "The Four Dimensionality of Space and the Einstein Tensor", J. Math. Phys., Vol. 13, (1972), pp. 874-876.
14. R. M. Wald, General Relativity, University of Chicago Press, Chicago, (1984), Chp. 9 and Chp. 14.
15. A. Linde, "The Self Reproducing Inflationary Universe", Scientific American Presents, Spring (1998), Vol. 9 pp. 98-104.
16. I. Levine, Physical Chemistry, McGraw-Hill Book Company, (1978).
17. T. Gold, Am. J. Phys., 30, 403 (1962).
18. R. S. Casella, Phys. Rev. Lett., 21, 1128 (1968).
19. R. S. Casella, Phys. Rev. Lett., 22, 554 (1969).
20. Y.. Ne'eman, Int. J. Theoret. Phys., 3, 1 (1970).
21. W. L. Freeman, et. al., Nature, 371, pp. 757-762, (1994).
22. R. F. Mushotzky, Meeting of the American Astronomical Society, Phoenix, AZ, (January 4, 1994).
23. D. N. Schramm, Physics Today, April, (1983), pp. 27-33.
24. S. W. Hawking, A Brief History of Time, Bantam Books, Toronto, (1988), p. 11.
25. J. C. Mather, et. al., The Astrophysical Journal, 354, L37-L40, (1990).
26. Beiser, A., Concepts of Modern Physics, Fourth Edition, McGraw-Hill Book Company, New York, (1978), pp. 329-339.
27. G. Musser, Scientific American, Vol. 281, No. 3, September, (1999), pp. 26-29.
28. Science, Vol. 279, Feb., (1998), pp. 1298-1299.
29. Science News, Vol. 153, May, (1998), p. 344.
30. Science News, Vol. 154, October 31, (1998), p. 277.
31. R. M. Wald, General Relativity, University of Chicago Press, Chicago, (1984), pp. 114-1116.
32. P. J. E. Peebles, J. Silk, Nature, Vol. 346, July, 19, (1990), p. 233-239.
33. Labov, S., Bowyer, S., "Spectral observations of the extreme ultraviolet background", The Astrophysical Journal, 371, (1991), pp. 810-819.
34. E. L. Wright, et. al., The Astrophysical Journal, 381, (1991), pp. 200-209.
35. J. C. Mather, et. al., The Astrophysical Journal, 420, (1994), pp. 439-444.
36. M. Davis, et. al., Nature, 356, (1992), pp. 489-493.
37. K. A. Olive, D. N. Schramm, G. Steigman, and T. P. Walker, Phys. Lett., B236, (1990), pp. 454-460.

38. CERN Courier, June, (1996), p. 1.
39. Hurley, K., et. al., Nature, 372, (1994), pp. 652-654.
40. T. Van Flandern, "The Speed of Gravity--What the Experiments Say", Physics Letters A, 250 (1998), pp. 1-11.
41. R. Cowen, Science News, May 9, (1998), p. 292.
42. M. Chown, New Scientist, May 10, (1997), p. 21.
43. B. Schwarzschild, Physics Today, Vol. 51, No. 10, October, (1998), pp. 19-21.
44. W. Sanders, et. al. Nature, 349, (1991), pp. 32-38.
45. Kirshner, R. P., Oemler, A., J., Schecter, P., L., and Schectman, A., S., A. S., (1983), AJ, 88,1285.
46. de Lapparent, V., Geller, M. J., and Huchra, J. P., ApJ, (1988), 332, 44.
47. Dressler, A., et. al., (1987), Ap. J., 313, L37.
48. G. Musser, Scientific American, May, (2000), p. 24.
49. S. Flamsteed, Discover, Vol. 16, Number 3, March, (1995), pp. 66-77.
50. Glanz, J., Science, Vol. 273, (1996), p. 581.
51. S. D. Landy, Scientific American, June, (1999), pp. 38-45.
52. Siebert, W. McC., Circuits, Signals, and Systems, The MIT Press, Cambridge, Massachusetts, (1986), pp. 597-603.
53. Fowles, G. R., Analytical Mechanics, Third Edition, Holt, Rinehart, and Winston, New York, (1977), pp. 57-60.
54. G. Musser, Scientific American, Vol. 278, No. 3, March, (1998), p. 18.
55. P. de Bernardis et al., A flat universe from high-resolution maps of the cosmic microwave background radiation, Nature, Vol. 404, (2000), p. 955; http://www.physics.ucsb.edu/~boomerang.

UNIFICATION OF SPACETIME, THE FORCES, MATTER, AND ENERGY

RELATIONSHIP OF SPACETIME AND THE FORCES

Spacetime has an intrinsic impedance of η. It provides a limiting speed of c for the propagation of any wave, including gravitational and electromagnetic waves. It further provides fields which match boundary conditions. Matter/energy acts on spacetime and spacetime acts on matter/energy. Thus, a spatial two-dimensional manifold of matter results in a gravitational field in spacetime; a three-dimensional spacetime manifold of current gives rise to a magnetic field in spacetime; a spatial two-dimensional manifold of charge gives rise to an electric field in spacetime. Thus, General Relativity and Maxwell's Equations are valid on any scale. Furthermore, the existence of matter with a determined mass as a three-dimensional spacetime manifold that is charged maximizes the volume of spacetime to the surface area of matter. This gives an energy minimum of the resulting gravitational, electric, and magnetic fields.

Matter/energy are interchangeable and are, in essence, the same entity with different boundary values imposed by spacetime where the matter/energy has a reaction effect on spacetime. The intricacy of the action/reaction is evident in that all matter/energy obeys the four-dimensional wave equation, and the magnetic, electric, photonic, and gravitational fields can be derived as a boundary value problem of the wave equation of spacetime where space provides the respective force fields for the matter/energy. That spacetime is four-dimensional is evident because the fundamental forces of gravity and electric attraction which are time dependent have a one-over-distance-squared relationship. This relationship is equivalent to the distance dependence of the area of a spherically symmetric wavefront which carries the forces. The force at the wavefront is nonradial and has an inverse r-dependence, traveling at the limiting speed of light provided by spacetime in accordance with Special Relativity.

The action/reaction relationships of the third fundamental force, the mechanical force, is given by Newton's Laws. They provide the motion of matter including charged matter, which can give rise to gravitational, magnetic, and photonic fields. The action/reaction provided by forces in one inertial frame is given in a different inertial frame by the Lorentz Transformations of Special Relativity, which are valid for Euclidean spacetime and are a consequence of the limiting speed of light. For example, the magnetic field in one inertial frame is given as electric field in another inertial frame as consequence of their relative motion. The presence of matter causes the geometry of spacetime to deviate from Euclidean which is manifest as a gravitational

field. The gravitational equation is derived for all scales from the present orbitsphere model where spacetime is Riemannian.

The provision of the equivalence of inertial and gravitational mass by the Mills theory of fundamental particles permits the correct derivation of the General Theory. And, the former provision of the two-dimensional nature of matter permits the unification of atomic, subatomic, and cosmological gravitation. The unified theory of gravitation is derived by first establishing a metric.

A space in which the curvature tensor has the following form:

$$R_{\mu\nu,\alpha\beta} = K\ (g_{\nu\alpha}g_{\mu\beta} - g_{\mu\alpha}g_{\nu\beta}) \tag{24.1}$$

is called a space of constant curvature; it is a four-dimensional generalization of Friedmann-Lobachevsky space. The constant K is called the constant of curvature. *The curvature of spacetime will be shown to result from a discontinuity of matter having curvature confined to two spatial dimensions. This is the property of all matter as an orbitsphere.* Consider an isolated orbitsphere and radial distances, r, from its center. *For r less than r_n there is no mass; thus, spacetime is flat or Euclidean.* The curvature tensor applies to all space of the inertial frame considered; thus, for r less than r_n, $K = 0$. At $r = r_n$ there exists a discontinuity of mass of the orbitsphere. This results in a discontinuity of the curvature tensor for radial distances greater than or equal to r_n. The discontinuity requires relativistic corrections to spacetime itself. It requires radial length contraction and time dilation that results in the curvature of spacetime. The gravitational radius r_g of the orbitsphere and infinitesimal temporal displacement in spacetime which is curved by the presence of the orbitsphere are derived in the Gravity Section.

The Schwarzschild metric gives the relationship whereby matter causes relativistic corrections to spacetime that determines the curvature of spacetime and is the origin of gravity. The separation of proper time between two events x^μ and $x^\mu + dx^\mu$ given by the Schwarzschild metric is

$$d\tau^2 = \left(1 - \frac{2Gm_0}{c^2 r}\right)dt^2 - \frac{1}{c^2}\left[\left(1 - \frac{2Gm_0}{c^2 r}\right)^{-1} dr^2 + r^2 d\theta^2 + r^2 \sin^2\theta\, d\phi^2\right] \tag{24.2}$$

Eq. (24.2) can be reduced to Newton's Law of Gravitation for $\frac{r_g}{r_\alpha^*} << 1$,

where $r_\alpha^* = \lambda\!\!\!^{-}_c$

$$\mathbf{F} = \frac{Gm_1m_2}{r^2} \tag{24.3}$$

where G is the Newtonian gravitational constant. Eq. (24.2) relativistically corrects Newton's gravitational theory. In an analogous

manner, Lorentz transformations correct Newton's Laws of Mechanics.

Maxwell's Equations give the electromagnetic forces:

$$\nabla \times \mathbf{E} = \frac{\delta \mu_o \mathbf{H}}{\delta t} \tag{24.4}$$

$$\nabla \times \mathbf{H} = \mathbf{J} + \frac{\delta \varepsilon_o \mathbf{E}}{\delta t} \tag{24.5}$$

$$\nabla \cdot \varepsilon_o \mathbf{E} = \rho \tag{24.6}$$

$$\nabla \cdot \mu_o \mathbf{H} = 0 \tag{24.7}$$

Maxwell's Integral Laws in Free Space are:

Ampere's Law

$$\oint_C \mathbf{H} \cdot d\mathbf{s} = \int_S \mathbf{J} \cdot d\mathbf{a} + \frac{d}{dt}\int_S \varepsilon_0 \mathbf{E} \cdot d\mathbf{a} \tag{24.8}$$

Faraday's Law

$$\oint_C \mathbf{E} \cdot d\mathbf{s} = -\frac{d}{dt}\int_S \mu_0 \mathbf{H} \cdot d\mathbf{a} \tag{24.9}$$

Power flow is governed by the Poynting power theorem:

$$\nabla \cdot (\mathbf{E} \times \mathbf{H}) = -\frac{\delta}{\delta t}\left(\frac{1}{2}\mu_o \mathbf{H} \cdot \mathbf{H}\right) - \frac{\delta}{\delta t}\left(\frac{1}{2}\varepsilon_o \mathbf{E} \cdot \mathbf{E}\right) - \mathbf{J} \cdot \mathbf{E} \tag{24.10}$$

Newtonian mechanics gives mechanical forces for $v << c$:

$$\mathbf{F} = \frac{d\mathbf{p}}{dt} = \frac{d(m\mathbf{v})}{dt} = m\frac{d\mathbf{v}}{dt} = m\mathbf{a} \tag{24.11}$$

$$T = \frac{1}{2}mv^2 \tag{24.12}$$

Special Relativity applies when v approaches c:

$$E = mc^2 \tag{24.13}$$

$$m = \frac{m_0}{\sqrt{1 - \frac{v^2}{c^2}}} \tag{24.14}$$

$$l = l_o\sqrt{1 - \frac{v^2}{c^2}} \tag{24.15}$$

$$t = \frac{t_0}{\sqrt{1 - \frac{v^2}{c^2}}} \tag{24.16}$$

where the subscript denotes the value in the moving frame.

The following equations are boundary conditions:

$$2\pi(nr_1) = 2\pi r_n = n\lambda_1 = \lambda_n \tag{24.17}$$

where

λ_1 is the allowed wavelength for $n = 1$

r_1 is the allowed radius for $n = 1$

For pair production:

$n = \alpha$

For hydrogen:

$n = 1,2,3,4,...$

$n = \frac{1}{2}, \frac{1}{3}, \frac{1}{4}, ...$

$$v_n = \frac{\hbar}{m_e r_n} \tag{24.18}$$

The weak and strong nuclear forces are discussed in the Weak Nuclear Force: Beta Decay of the Neutron Section and the Strong Nuclear Force Section. These forces are electromagnetic in nature. They arise as a minimization of the stored field energies. This also applies for the case of the force of the chemical bond as described in the Nature of the Chemical Bond Section.

RELATIONSHIP OF SPACETIME, MATTER, AND CHARGE

In addition to the force laws, the nature of the universe is determined by the following experimentally observed parameters:

- Four dimensional spacetime;
- The fundamental constants which comprise the fine structure constant;
- The Newtonian gravitational constant, G;
- The mass of the universe, and
- The spin of the electron neutrino.

General Relativity gives the relationship between the proper time and the coordinate time of particle production.

$$\tau = ti\sqrt{\frac{2GM}{c^2 r_\alpha^*}} = ti\sqrt{\frac{2GM}{c^2 \lambda_c}} \tag{24.19}$$

The following boundary condition applies at the creation of matter from energy:

$$2\pi r_n = \lambda_n \qquad n = \alpha \tag{24.20}$$

The particle production energies given in the Gravity Section are the mass energy, the Planck equation energy, electric potential energy, magnetic energy, the gravitational potential energy, and the

mass/spacetime metric energy[9].

$$m_o c^2 = \hbar\omega^* = V = E_{mag} = E_{grav} = E_{spacetime}$$

$$m_0 c^2 = \hbar\omega^* = \frac{\hbar^2}{m_0 \lambda\!\!\!^{-2}_C} = \alpha^{-1}\frac{e^2}{4\pi\varepsilon_0 \lambda\!\!\!^{-}_C} = \alpha^{-1}\frac{\pi\mu_0 e^2\hbar^2}{(2\pi m_0)^2 \lambda\!\!\!^{-3}_C} = \alpha^{-1}\frac{\mu_0 e^2 c^2}{2h}\sqrt{\frac{Gm_0}{\lambda\!\!\!^{-}_C}}\sqrt{\frac{\hbar c}{G}} = \frac{\alpha h}{1\,\mathrm{sec}}\sqrt{\frac{\lambda\!\!\!^{-}_C c^2}{2Gm}} \tag{24.21}$$

When m_o is the Grand Unification Mass, m_U,

$$m_U c^2 = \hbar\omega^* = V = E_{mag} = \frac{Gm_U^2}{\lambda\!\!\!^{-*}_C} \tag{24.22}$$

$$m_U = m_0 = \sqrt{\frac{\hbar c}{G}}$$

The gravitational velocity, v_G, is defined as

$$v_G = \sqrt{\frac{Gm_0}{\lambda\!\!\!^{-}_C}} \tag{24.23}$$

Substitution of the gravitational velocity, v_G, given by Eq. (24.23) and the Grand Unification Mass/Energy, m_U, given by Eq. (24.22) into Eq. (24.21) followed by division by the speed of light squared gives the particle mass in terms of the Grand Unification Mass/Energy.

$$m_0 = \alpha^{-1}\frac{\mu_0 e^2 c}{2h}\frac{\sqrt{\frac{Gm_0}{\lambda\!\!\!^{-}_C}}}{c} m_u = \alpha^{-1}\frac{\mu_0 e^2 c}{2h}\sqrt{\frac{Gm_0}{c^2\lambda\!\!\!^{-}_C}} m_u = \alpha^{-1}\frac{\mu_0 e^2 c}{2h}\frac{v_G}{c} m_u = \frac{v_G}{c} m_u \tag{24.24}$$

The relationships between the fundamental constants are given by the equivalence of the particle production energies. The magnitude of the quantized angular momentum of the photon and fundamental particles is Planck's constant bar, $\hbar$. The wave equation gives the relationship between the velocity, wavelength, and frequency of the wave.

$$v = \lambda\frac{\omega}{2\pi} \tag{24.25}$$

When $v = c$ the radius at particle production is given by Eq. (20.22).

$$r_\alpha = \frac{\hbar}{m_o c} = \lambda\!\!\!^{-}_C \tag{24.26}$$

Substitution of Eq. (24.25) and (24.26) into Eq. (24.21) with $v = c$ gives the relationship between $\hbar$ and the fundamental charge squared.

---

9 Eq. (24.21) is the relationship between matter and energy with an implicit physical basis for particle production. The relationship derived by Einstein [2] related the kinetic energy of an object to the increase in its mass times the speed of light squared. Thus, Eq. (24.21) is the complete form of the popular equation, $E = m_0 c^2$.

$$\hbar\omega^* = h\frac{c}{\lambda} = \alpha^{-1}\frac{e^2}{4\pi\varepsilon_0\lambda\!\!\!^{-}_C}$$

$$\hbar\frac{c}{\lambda\!\!\!^{-}_C} = \alpha^{-1}\frac{e^2}{4\pi\varepsilon_0\lambda\!\!\!^{-}_C} \tag{24.27}$$

$$\hbar c = \alpha^{-1}\frac{e^2}{4\pi\varepsilon_0}$$

Thus, charge is quantized as a consequence of the quantization of the angular momentum of the photon. The relationship between the speed of light, c, and the permittivity of free space, ε_0, and the permeability of free space, μ_0, is

$$c = \frac{1}{\sqrt{\mu_0\varepsilon_0}} \tag{24.28}$$

The fine structure constant given by Eqs. (1.146) and (20.9) is the dimensionless factor that corresponds to the relativistic invariance of charge.

$$\alpha = \frac{1}{4\pi}\sqrt{\frac{\mu_0}{\varepsilon_0}}\frac{e^2}{\hbar} = \frac{1}{2}\frac{\sqrt{\frac{\mu_0}{\varepsilon_0}}}{\frac{h}{e^2}} = \frac{\mu_0 e^2 c}{2h} \tag{24.29}$$

It is equivalent to one half the ratio of the radiation resistance of free space, $\sqrt{\frac{\mu_0}{\varepsilon_0}}$, and the hall resistance, $\frac{h}{e^2}$. The radiation resistance of free space is equal to the ratio of the electric field and the magnetic field of the photon (Eq. (4.10)). The Hall resistance is given by Eq. (17.46). Substitution of Eq. (24.28) into Eq. (24.27) gives the relationship for the radiation resistance of free space, η.

$$\eta = \sqrt{\frac{\mu_0}{\varepsilon_0}} = 4\pi\alpha\frac{\hbar}{e^2} \tag{24.30}$$

It provides a limiting speed of c for the propagation of any wave, including gravitational and electromagnetic waves and expanding spacetime.

PERIOD EQUIVALENCE

The universe undergoes time harmonic expansion and contraction corresponding to matter/energy conversion. The equation of the radius of the universe, À, which is derived in the Gravity Section is

$$\text{À} = \left(\frac{2Gm_U}{c^2} + \frac{\frac{cm_U}{c^3}}{\frac{c^3}{4\pi G}} - \frac{cm_U}{\frac{c^3}{4\pi G}}\cos\left(\frac{2\pi t}{\frac{2\pi G m_U}{c^3}}\sec\right)\right) m \tag{24.31}$$

The gravitational equation (Eq. (23.38)) with the equivalence of the particle production energies (Eqs. (23.48a-23.48b)) permit the equivalence of mass/energy ($E = mc^2$) and spacetime ($\frac{c^3}{4\pi G} = 3.22\ X\ 10^{34}\ \frac{kg}{\sec}$). Spacetime expands as mass is released as energy which provides the basis of the atomic, thermodynamic, and cosmological arrows of time. Q, the mass/energy to expansion/contraction quotient of spacetime is given by the ratio of Eq. (27.3) and Eq. (27.1) wherein Eq. (23.43) gives the General Relativistic factor which divides the electron mass and multiplies the electron proper time to give the corresponding spacetime expansion.

$$Q = \frac{\frac{m_e}{\sqrt{\frac{2GM}{c^2\lambda\!\!\!^{-}_c}}}}{\tau\sqrt{\frac{2GM}{c^2\lambda\!\!\!^{-}_c}}} = \frac{\left(\frac{h\alpha}{1\ \sec\ c^2}\right)^{\frac{1}{2}}\left(\frac{c\hbar}{2G}\right)^{\frac{1}{4}}}{2\pi\frac{\hbar}{m_e c^2}\frac{2Gm_e}{c^2\lambda\!\!\!^{-}_c}} = \frac{c^3}{4\pi G} = 3.22\ X\ 10^{34}\ \frac{kg}{\sec} \tag{24.32}$$

From Eq. (24.31), the period of the expansion/contraction cycle of the radius of the universe, T, is

$$T = \frac{2\pi G m_U}{c^3}\ \sec \tag{24.33}$$

It is herein derived that ***the periods of spacetime expansion/contraction and particle decay/production for the universe are equal***. It follows from the Poynting Power Theorem (Eq. (7.27)) with spherical radiation that the transition lifetimes are given by the ratio of energy and the power of the transition [1]. Magnetic energy is a Special Relativistic consequence of electric energy and kinetic energy. Thus, only transitions involving electric energy need be considered. The transition lifetime, τ, in the case of the electric multipole moment given by Jackson [1] as

$$Q_{lm} = \frac{3}{\ell + 3} e\left(r_n\right)^{\ell} \tag{24.34}$$

is [1]

$$\tau = \frac{energy}{power}$$

$$\tau = \frac{[\hbar\omega]}{\left[\frac{2\pi c}{[(2l+1)!!]^2}\left(\frac{l+1}{l}\right)k^{2l+1}\left|Q_{lm} + Q'_{lm}\right|^2\right]} = \frac{1}{2\pi}\left(\frac{h}{e^2}\right)\sqrt{\frac{\mu_0}{\varepsilon_0}}\frac{[(2l+1)!!]^2}{2\pi}\left(\frac{l}{l+1}\right)\left(\frac{l+3}{3}\right)^2\frac{1}{(kr_n)^{2l}\omega} \tag{24.35}$$

where in the exemplary case of an excited state of atomic hydrogen r_n is the radius of the electron orbitsphere which is na_0 (Eq. (27.17)). From

Eq. (24.35), the transition lifetime is proportional to the ratio of η, the radiation resistance of free space.

$$\eta = \sqrt{\frac{\mu_0}{\varepsilon_0}} \tag{24.36}$$

and, the Quantum Hall resistance, $\frac{h}{e^2}$. The Quantum Hall resistance given in the Quantum Hall Effect Section was derived using the Poynting Power Theorem. Also, from Eq. (24.35), the transition lifetime is proportional to the fine structure constant, α,

$$\alpha = \frac{1}{4\pi}\sqrt{\frac{\mu_o}{\varepsilon_o}}\frac{e^2}{\hbar} \tag{24.37}$$

From Eq. (24.17) and Eq. (24.35), the lifetime an excited state of a hydrogen atom is inversely proportional to the frequency of the transition. This is also the case for the universe which is a 3-sphere universe. (More explicitly, the universe is a Riemannian three dimensional hyperspace plus time with a constant positive curvature). During an electromagnetic transition, the total energy of the system decays exponentially. Applying Eqs. (2.45) and (2.46) to the case of exponential decay,

$$h(t) = e^{-\frac{1}{T}t}u(t) \tag{24.38}$$

However, Eq. (24.19) determines that ***the coordinate time is imaginary*** because energy transitions are spacelike due to General Relativistic effects. For example, Eq. (27.2) gives the mass of the electron (a fundamental particle) in accordance with Eq. (24.19).

$$\frac{2\pi\lambda\!\!\!^{-}_C}{\sqrt{\frac{2Gm_e}{\lambda\!\!\!^{-}_C}}} = \frac{2\pi\lambda\!\!\!^{-}_C}{v_g} = i\alpha^{-1}\sec \tag{24.39}$$

where Newtonian gravitational velocity v_g is given by Eq. (23.35). Replacement of the coordinate time, t, of Eq. (24.38) by the spacelike time, it, gives.

$$h(t) = e^{-i\frac{1}{T}t} = \cos\frac{2\pi}{T}t \tag{24.40}$$

where the period is T. The periods of spacetime expansion/contraction and particle decay/production for the universe are equal due to the Eq. (24.19) which determines the masses of fundamental particles, the equivalence of inertial and gravitational mass, the phase matching condition of mass to the speed of light and charge to the speed of light, and that the coordinate time is imaginary because energy transitions are spacelike due to general relativistic effects. From Eq. (24.19)

$$\frac{\text{proper time}}{\text{coordinate time}} = \frac{\text{gravitational wave condition}}{\text{electromagnetic wave condition}} = \frac{\text{gravitational mass phase matching}}{\text{charge/inertial mass phase matching}}$$

$$\frac{\text{proper time}}{\text{coordinate time}} = i\frac{\sqrt{\frac{2Gm}{c^2\lambda\!\!\!^{-}_C}}}{\alpha} = i\frac{v_g}{\alpha c} \tag{24.41}$$

where Newtonian gravitational velocity v_g is given by Eq. (23.35). Eq. (24.24) gives the ratio of Eq. (24.41) in terms of the coordinate particle mass and the Grand Unification Mass/Energy.

$$\frac{\text{proper time}}{\text{coordinate time}} = \frac{m_0}{m_u} = \alpha^{-1}\frac{\mu_0 e^2 c}{2h}\frac{\sqrt{\frac{Gm_0}{\lambda\!\!\!^{-}_C}}}{c} = \alpha^{-1}\frac{\mu_0 e^2 c}{2h}\sqrt{\frac{Gm_0}{c^2\lambda\!\!\!^{-}_C}} = \alpha^{-1}\frac{\mu_0 e^2 c}{2h}\frac{v_G}{c} = \frac{v_G}{c} \tag{24.42}$$

As fundamental particles, atoms, molecules, and macroscopic configurations of fundamental particles, atoms, and molecules release energy, spacetime increases. The superposition of expanding spacetime arising at the atomic level over all scales of dimensions from the atomic to the cosmological gives rise to the observed expanding universe. The wavefront of energy and spacetime from matter to energy conversion travel at the speed of light. Consider Eq. (23.43). As given in the Gravity Section, at the present time in the cycle of the universe, the world line of the expanding spacetime and the released energy are approximately coincident. In terms of Eq. (23.38), the proper time and the coordinate time are approximately equal. The ratio of the gravitational radius, r_g given by Eq. (23.36), and the radius of the universe equal to one and the gravitational escape velocity given by Eq. (23.35) is the speed of light. And, Q, (Eq. (23.140)) is equal to the matter to energy conversion rate of the time harmonic expansion/contraction cycle of the universe which permits light energy (photons) to propagate (escape the gravitational hole of the universe).

When the gravitational radius r_g is the radius of the universe, the proper time is equal to the coordinate time (Eq. (23.43)), and the gravitational escape velocity v_g of the universe is the speed of light.

Mass/energy must be conserved during the harmonic cycle of

expansion and contraction. The gravitational potential energy E_{grav} of the universe follows that given by Eq. (23.26)

$$E_{grav} = \frac{Gm_U^2}{r} \tag{24.43}$$

In the case that the radius of the universe r is the gravitational radius r_G given by Eq. (23.22), the gravitational potential energy is equal to $m_U c^2$ which follows that given by Eq. (23.27). The gravitational velocity v_G is given by Eq. (23.33) wherein an electromagnetic wave of mass/energy equivalent to the mass of the universe travels in a circular orbit wherein the eccentricity is equal to zero (Eq. (26.20)), and the escape velocity from the universe can never be reached. The wavelength of the oscillation of the universe and the wavelength corresponding to the gravitational radius r_G must be equal. Electromagnetic energy and gravitational mass obey superposition, and both spacetime expansion/contraction and electromagnetic energy corresponding to particle decay/production travel at the speed of light and obey the wave relationship given by Eq. (20.4). The wavelength is given in terms of the radius by Eq. (2.2). Thus, ***the harmonic oscillation period***, T, is

$$T = \frac{2\pi r_G}{c} = \frac{2\pi G m_U}{c^3} = \frac{2\pi G\left(2\ X\ 10^{54}\ kg\right)}{c^3} = 3.10\ X\ 10^{19}\ \text{sec} = 9.83\ X\ 10^{11}\ \text{years} \tag{24.44}$$

where the mass of the universe, m_U.

WAVE EQUATION

The equation

$$\frac{1}{c^2}\left(\frac{\delta\omega}{\delta t}\right)^2 - (grad\,\omega)^2 = 0 \tag{24.45}$$

acquires a general character; it is more general than Maxwell's equations from which Maxwell originally derived it. As a consequence of the principle of the existence of a universal limiting velocity one can assert the following: the differential equations describing any field that is capable of transmitting signals must be of such a kind that the equation of their characteristics is the same as the equation for the characteristics of light waves. In addition to the governing the propagation of any form of energy, the wave equation governs fundamental particles created from energy and vice versa, the associated effects of mass on spacetime, and the evolution the universe itself. The equation that describes the electron given by Eq. (1.48) is the wave equation, the relativistic correction of spacetime due to particle production travels according to the wave equation as given in the

Gravity Section, and the evolution of the universe is according to the wave equation. The speed of light is the conversion factor from time to distance. Thus, the equation of the radius of the universe, À, (Eq. (24.31)) may be written as

$$\text{À} = \left(\frac{2Gm_U}{c^2} + \frac{\frac{cm_U}{c^3}}{\frac{4\pi G}{}}\right) - \frac{\frac{cm_U}{c^3}}{\frac{4\pi G}{}} \cos\left(\frac{2\pi}{\frac{2\pi G m_U}{c^3}} \sec\left(t - \frac{\text{À}'}{c}\right)\right) m \qquad (24.46)$$

which is a solution to the wave equation.

References

1. Jackson, J. D., Classical Electrodynamics, Second Edition, John Wiley & Sons, New York, (1962), pp. 758-763.
2. Beiser, A., Concepts of Modern Physics, Fourth Edition, McGraw-Hill Book Company, New York, (1978), pp. 27-30.

INERTIA

Charge, Mass, and Momentum

The photon possesses electric and magnetic fields, energy, and momentum. Charge arises from the fields, mass arises from the energy, and momentum is conserved as the particle is created from a photon as given in the Unification of Spacetime, the Forces, Matter, and Energy Section.

Inertia

Inertia arises from the nature of matter being comprised of fundamental particles which exist in *nonradiative states* having a balance between the electromagnetic forces and centrifugal forces and *the nature of space-time* which provides for the relativistic invariance of charge and a limiting velocity for the propagation of any field according to special relativity.

All matter is comprised of charged fundamental particles such as quarks and leptons. Charge is relativistically invariant. Consider a particle which acquires a finite constant velocity. As the magnitude of the velocity increases, the electric field lines of the particle increase in density relative to the stationary observer in a direction perpendicular to the direction of motion of the particle. The field lines of a stationary proton, electron, and hydrogen atom are shown in Figure 1.7. The field lines of a moving point charge are shown in Figures 4.3A and 4.3B A. The particle resists a change in motion (i.e. energy has to be transferred to the particle in order for it to change its velocity). The energy in an electric field E_{ele} is given by the integral of the electric field **E** squared over all space (Eq. (1.175)).

$$E_{ele} = -\frac{1}{2}\varepsilon_o \int_{\infty}^{r_1} \mathbf{E}^2 dv \tag{25.1}$$

where the space is relativistically contracted (Eq. (24.15)) in the direction of constant velocity relative to the stationary observer. Newton's first law can be understood in terms of the relative invariance of charge which is manifest as the inertia of a particle. The mass density and charge density functions of fundamental particles are interchangeable by interchanging the fundamental charge and the relativistic mass of the particle. The mass/charge density functions are in force balance with the central field which binds particles in atoms and molecules. Since field lines end on charge, charge and mass redistribute in the moving frame relative to the stationary frame; thus, an inertial force is required to cause a velocity with a concomitant redistribution of the field lines and mass/charge density functions of the particles

comprising matter which is made to acquire a finite velocity. The force is given by the time derivative of the momentum. Consider the case of an electron. The velocity for every point on the orbitsphere is given by Eq. (1.47).

$$v_n = \frac{\hbar}{m_e r_n} \tag{25.2}$$

The momentum is the mass times Eq. (25.2). Newton's second law gives the force as the time derivative of the momentum. The time derivative of the momentum is

$$\frac{d}{dt} m v_n = \frac{dp}{dt} = \frac{d}{dt} m_e \frac{\hbar}{m_e r_n} = \frac{\hbar}{r_n^2} \frac{dr}{dt} = \frac{k}{r_n^2} \tag{25.3}$$

where p is the momentum and k is a constant since the final velocity is a constant. The inertial force on a fundamental particle to give it a constant velocity is of the same form as the inverse squared central force of a charge. Thus, Newton's second law can be understood in terms of the relative invariance of charge which requires an inertial force to move of a particle. The nature of spacetime which is described by special relativity provides a limiting velocity for the propagation of any field including light. Consequently, spacetime provides that the limiting velocity for the propagation of any matter is the speed of light since its is comprised of charged matter wherein charge is relativistically invariant. The corresponding relationship of relative mass to the velocity of a particle is given by Eq. (24.14). The inertial mass is increased as a function of relative velocity according to special relativity. As demonstrated in the Gravity Section the gravitational mass and the inertial mass of fundamental particles are equivalent. Thus, Newton's second law and Newton's Law of Gravitation may be understood in terms of the nature of spacetime in relationship to charge and the limiting speed for the propagation of fields where the increase of mass energy of a moving particle is equivalent to that given by Eq. (25.1).

POSSIBILITY OF A NEGATIVE ELECTRON GRAVITATIONAL MASS

GENERAL CONSIDERATIONS

The provision of the equivalence of inertial and gravitational mass by the Mills theory of fundamental particles wherein spacetime is Riemannian due to its relativistic correction with particle production permits the correct derivation of the General Theory. In the case of ordinary matter (an example of an extraordinary state of matter called a hyperbolic electron is given *infra*), the nature of chemical bonding is electric and magnetic, and the angular momentum of each bound electron is always $\hbar$ independent of material such as wood or metal. The angular momentum with a central field is given by Eq. (1.57). In this case, each infinitesimal point of the orbitsphere of mass m_i is the inertial mass according to the inertial angular momentum. It also is the gravitational mass according to the gravitational angular momentum. The inertial and gravitational mass of electrons and nucleons in ordinary matter are equivalent.

The provision of the two-dimensional nature of matter permits the unification of atomic, subatomic, and cosmological gravitation. The unified theory of gravitation is derived by first establishing a metric. A space in which the curvature tensor has the following form:

$$R_{\mu\nu,\alpha\beta} = K\ (g_{\nu\alpha}g_{\mu\beta} - g_{\mu\alpha}g_{\nu\beta}) \tag{26.1}$$

is called a space of constant curvature; it is a four-dimensional generalization of Friedmann-Lobachevsky space. The constant K is called the constant of curvature. *The curvature of spacetime results from a discontinuity of matter having curvature confined to two spatial dimensions. This is the property of all matter as an orbitsphere.* Consider an isolated orbitsphere and radial distances, r, from its center. *For r less than r_n there is no mass; thus, spacetime is flat or Euclidean.* The curvature tensor applies to all space of the inertial frame considered; thus, for r less than r_n, $K = 0$. At $r = r_n$ there exists a discontinuity of mass of the orbitsphere. This results in a discontinuity of the curvature tensor for radial distances greater than or equal to r_n. The discontinuity requires relativistic corrections to spacetime itself. It requires radial length contraction and time dilation that results in the curvature of spacetime. The gravitational radius of the orbitsphere and infinitesimal temporal displacement in spacetime which is curved by the presence of the orbitsphere are derived in the Gravity Section.

The Schwarzschild metric gives the relationship whereby matter causes relativistic corrections to spacetime that determines the curvature of spacetime and is the origin of gravity. The correction is

based on the boundary conditions that no signal can travel faster that the speed of light including the gravitational field that propagates following particle production from a photon wherein the particle has a finite gravitational velocity given by Newton's Law of Gravitation. The separation of proper time between two events x^μ and $x^\mu + dx^\mu$ given by Eq. (23.38), the Schwarzschild metric [1-2], is

$$d\tau^2 = \left(1 - \frac{2Gm_0}{c^2 r}\right) dt^2 - \frac{1}{c^2}\left[\left(1 - \frac{2Gm_0}{c^2 r}\right)^{-1} dr^2 + r^2 d\theta^2 + r^2 \sin^2\theta d\phi^2\right] \tag{26.2}$$

Eq. (26.2) can be reduced to Newton's Law of Gravitation for r_g, the gravitational radius of the particle, much less than r_α^*, the radius of the particle at production ($\frac{r_g}{r_\alpha^*} << 1$), where the radius of the particle is its Compton wavelength bar ($r_\alpha^* = \lambda\!\!\!^{-}_c$).

$$F = \frac{Gm_1 m_2}{r^2} \tag{26.3}$$

where G is the Newtonian gravitational constant. Eq. (26.2) relativistically corrects Newton's gravitational theory. In an analogous manner, Lorentz transformations correct Newton's laws of mechanics.

The effects of gravity preclude the existence of inertial frames in a large region, and only local inertial frames, between which relationships are determined by gravity are possible. In short, the effects of gravity are only in the determination of the local inertial frames. The frames depend on gravity, and the frames describe the spacetime background of the motion of matter. Therefore, differing from other kinds of forces, gravity which influences the motion of matter by determining the properties of spacetime is itself described by the metric of spacetime. It was demonstrated in the Gravity Section that gravity arises from the two spatial dimensional mass density functions of the fundamental particles.

It is demonstrated in the One Electron Atom Section that a bound electron is a two-dimensional spherical shell— an orbitsphere. On the atomic scale, the curvature, K, is given by $\frac{1}{r_n^2}$, where r_n is the radius of the radial delta function of the orbitsphere. The velocity of the electron is a constant on this two dimensional sphere. It is this local, positive curvature of the electron that causes gravity. It is worth noting that all ordinary matter, comprised of leptons and quarks, has positive curvature. Euclidean plane geometry asserts that (in a plane) the sum of the angles of a triangle equals 180°. In fact, this is the definition of a flat surface. For a triangle on an orbitsphere the sum of the angles is greater than 180°, and the orbitsphere has *positive curvature*. For some surfaces the sum of the angles of a triangle is less than 180°; these are

said to have *negative curvature.*

sum of angles of a triangle	type of surface
> 180°	positive curvature
= 180°	flat
< 180°	negative curvature

The measure of Gaussian curvature, K, at a point on a two dimensional surface is

$$K = \frac{1}{r_1 r_2} \tag{26.4}$$

the inverse product of the radius of the maximum and minimum circles, r_1 and r_2, which fit the surface at the point, and the radii are normal to the surface at the point. By a theorem of Euler, these two circles lie in orthogonal planes. For a sphere, the radii of the two circles of curvature are the same at every point and equivalent to the radius of a great circle of the sphere. Thus, the sphere is a surface of constant curvature;

$$K = \frac{1}{r^2} \tag{26.5}$$

at every point. In case of positive curvature of which the sphere is an example, the circles fall on the same side of the surface, but when the circles are on opposite sides, the curve has negative curvature. A saddle, a cantenoid, and a pseudosphere are negatively curved. The general equation of a saddle is

$$z = \frac{x^2}{a^2} - \frac{y^2}{b^2} \tag{26.6}$$

where a and b are constants. The curvature of the surface of Eq. (26.6) is

$$K = \frac{-1}{4a^2b^2}\left(\frac{x^2}{a^4} + \frac{y^2}{b^4} + \frac{1}{4}\right)^{-2} \tag{26.7}$$

A saddle is shown schematically in Figure 26.1.

Figure 26.1. A saddle.

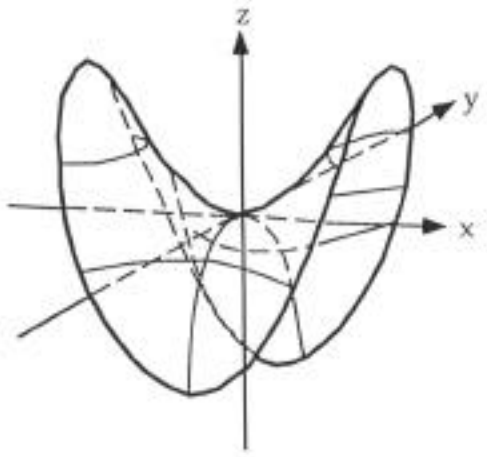

A pseudosphere is constructed by revolving the tractrix about its asymptote. For the tractrix, the length of any tangent measured from the point of tangency to the x-axis is equal to the height R of the curve from its asymptote-in this case the x-axis. The pseudosphere is a surface of constant negative curvature. The curvature, K

$$K = \frac{-1}{r_1 r_2} = \frac{-1}{R^2} \tag{26.8}$$

given by the product of the two principal curvatures on opposite sides of the surface is equal to the inverse of R squared at every point where R is the equitangent. R is also known as the radius of the pseudosphere. A pseudosphere is shown schematically in Figure 26.2.

Figure 26.2. A pseudosphere.

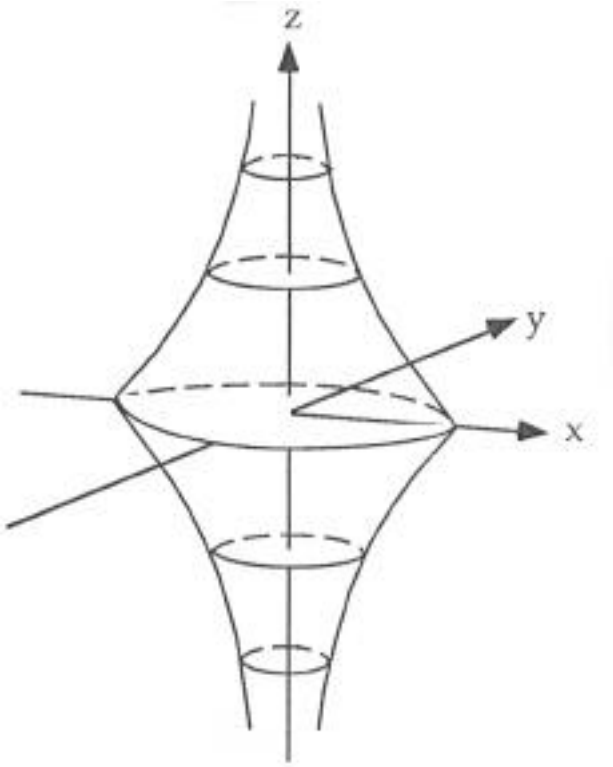

In the case of a sphere, surfaces of constant potential are concentric spherical shells. The general law of potential for surfaces of constant curvature is

$$V = \frac{1}{4\pi\varepsilon_o}\sqrt{\frac{1}{r_1 r_2}} = \frac{1}{4\pi\varepsilon_o R} \tag{26.9}$$

In the case of a pseudosphere the radii r_1 and r_2, the two principal curvatures, represent the distances measured along the normal from the negative potential surface to the two sheets of its evolute, envelop of normals (cantenoid and x-axis). The force is given as the gradient of the potential which is proportional to $\frac{1}{r^2}$ in the case of a sphere.

All matter is comprised of fundamental particles, and all fundamental particles exists as mass confined to two spatial dimensions. The particle's velocity surface is positively curved in the case of an orbitsphere, or the velocity surface is negatively curved in the case of an electron as a hyperboloid (hereafter called a hyperbolic electron given in the Hyperbolic Electrons Section). The effect of this "local" curvature on the non-local spacetime is to cause it to be Riemannian, in the case of an orbitsphere, or hyperbolic, in the case of a hyperbolic electron, as opposed to Euclidean which is manifest as a gravitational field or an antigravitational field, respectively. Thus, the spacetime is curved with

constant spherical curvature in the case of an orbitsphere, or spacetime is curved with hyperbolic curvature in the case of a hyperbolic electron.

The relativistic correction for spacetime dilation and contraction due to the production of a particle with positive curvature is given by Eq. (23.17)

$$f(r) = \sqrt{1 - \left(\frac{v_g}{c}\right)^2} \tag{26.10}$$

The derivation of the relativistic correction factor of spacetime was based on the constant maximum velocity of light and a finite positive Newtonian gravitational velocity v_g of the particle given by

$$v_g = \sqrt{\frac{2Gm_0}{r}} = \sqrt{\frac{2Gm_0}{\lambda\!\!\!^{-}_C}} \tag{26.11}$$

Consider a Newtonian gravitational radius, r_g, of each orbitsphere of the particle production event, each of mass m

$$r_g = \frac{2Gm}{c^2} \tag{26.12}$$

where G is the Newtonian gravitational constant. Substitution of Eq. (26.11) or Eq. (26.12) into the Schwarzschild metric Eq. (26.2), gives

$$d\tau^2 = \left(1 - \left(\frac{v_g}{c}\right)^2\right) dt^2 - \frac{1}{c^2}\left[\left(1 - \left(\frac{v_g}{c}\right)^2\right)^{-1} dr^2 + r^2 d\theta^2 + r^2 \sin^2\theta d\phi^2\right] \tag{26.13}$$

and

$$d\tau^2 = \left(1 - \frac{r_g}{r}\right) dt^2 - \frac{1}{c^2}\left[\left(1 - \frac{r_g}{r}\right)^{-1} dr^2 + r^2 d\theta^2 + r^2 \sin^2\theta d\phi^2\right] \tag{26.14}$$

respectively. The solutions for the Schwarzschild metric exist wherein the relativistic correction to the gravitational velocity v_g and the gravitational radius r_g are of the opposite sign (i.e. negative). In these cases the Schwarzschild metric Eq. (26.2), is

$$d\tau^2 = \left(1 + \left(\frac{v_g}{c}\right)^2\right) dt^2 - \frac{1}{c^2}\left[\left(1 + \left(\frac{v_g}{c}\right)^2\right)^{-1} dr^2 + r^2 d\theta^2 + r^2 \sin^2\theta d\phi^2\right] \tag{26.15}$$

and

$$d\tau^2 = \left(1 + \frac{r_g}{r}\right) dt^2 - \frac{1}{c^2}\left[\left(1 + \frac{r_g}{r}\right)^{-1} dr^2 + r^2 d\theta^2 + r^2 \sin^2\theta d\phi^2\right] \tag{26.16}$$

The metric given by Eqs. (26.13-26.14) corresponds to positive curvature. The metric given by Eqs. (26.15-26.16) corresponds to negative curvature. The negative solution arises naturally as a match to the boundary condition of matter with a velocity function having negative curvature. Consider the case of pair production given in the Gravity Section. The photon equation given in the Equation of the

Photon Section is equivalent to the electron and positron functions given by in the One Electron Atom Section. The velocity of any point on the positively curved electron orbitsphere is constant which correspond to the trigonometric function given in Eqs. (1.68-1.69). At particle production, the relativistic corrections to spacetime due to the constant gravitational velocity v_g are given by Eqs. (26.13-26.14). In the case of negative curvature, the electron velocity as a function of position is not constant. It may be described by a harmonic variation which corresponds to an imaginary velocity. The trigonometric function of the positively curved electron orbitsphere given in Eqs. (1.68-1.69) becomes a hyperbolic function (e.g. cosh) in the case of a negatively curved electron. Substitution of an imaginary velocity with respect to a gravitating body into Eq. (26.13) givens Eq. (26.15). Substitution a negative radius of curvature with respect to a gravitating body into Eq. (26.14) gives Eq. (26.16). Thus, antigravity can be created by forcing matter into negative curvature of the velocity surface. A fundamental particle with negative curvature of the velocity surface would experience a central but repulsive force with a gravitating body comprised of matter of positive curvature of the velocity surface.

POSITIVE, ZERO, AND NEGATIVE GRAVITATIONAL MASS

In the case of Einstein's gravity equation (Eq. (23.40)), the Einstein's Tensor $G_{\mu\nu}$, is equal to the stress-energy-momentum tensor $T_{\mu\nu}$. The only possibility is for the gravitational mass to be equivalent to the inertial mass. A particle of zero or negative gravitational mass is not possible. However, it is shown in the Gravity Section that the correct basis of gravitation is not according to Einstein's equation (Eq. (23.40)); instead the origin of gravity is the relativistic correction of spacetime itself which is analogous to the special relativistic corrections of inertial parameters-- increase in mass, dilation in time, and contraction in length in the direction of constant relative motion of separate inertial frames. On this basis, the observed acceleration of the cosmos is predict as given in the Cosmology Section.

The Schwarzschild metric gives the relationship whereby matter causes relativistic corrections to spacetime that determines the curvature of spacetime and is the origin of gravity. Matter arises during particle production from a photon. According to Newton's Law of Gravitation, the production of a particle of finite mass gives rise to a gravitational velocity of the particle. The gravitational velocity determines the energy and the corresponding eccentricity and trajectory of the gravitational orbit of the particle. The eccentricity e given by Newton's differential equations of motion in the case of the central field

(Eq. (23.49-23.50)) permits the classification of the orbits according to the total energy E as follows [3]:

$E<0, \quad e<1$ ellipse

$E<0, \quad e=0$ circle (special case of ellipse)

$E=0, \quad e=1$ parabolic orbit

$E>0, \quad e>1$ hyperbolic orbit (26.17)

Since $E=T+V$ and is constant, the closed orbits are those for which $T \leq |V|$, and the open orbits are those for which $T \geq |V|$. It can be shown that the time average of the kinetic energy, $<T>$, for elliptic motion in an inverse square field is $1/2$ that of the time average of the potential energy, $<V>$. $<T>=1/2<V>$.

In the case that a particle of inertial mass m is observed to have a speed v_0, a distance from a massive object r_0, and a direction of motion makes that an angle ϕ with the radius vector from the object (including a particle) of mass M, the total energy is given by

$$E=\frac{1}{2}mv^2-\frac{GMm}{r}=\frac{1}{2}mv_0^2-\frac{GMm}{r_0}=\text{constant} \tag{26.18}$$

The orbit will be elliptic, parabolic, or hyperbolic, according to whether E is negative, zero, or positive. Accordingly, if v_0^2 is less than, equal to, or greater than $\frac{2GM}{r_0}$, the orbit will be an ellipse, a parabola, or a hyperbola, respectively. Since h, the angular momentum per unit mass, is

$$h=L/m=|\mathbf{r}\times\mathbf{v}|=r_0v_0\sin\phi \tag{26.19}$$

The eccentricity e, from Eq. (23.63) may be written as

$$e=[1+\left(v_0^2-\frac{2GM}{r_0}\right)\frac{r_0^2v_0^2\sin^2\phi}{G^2M^2}]^{1/2} \tag{26.20}$$

As shown in the Gravity Section (Eq. (23.35)), the production of a particle requires that the velocity of each of the point masses of the particle is equivalent to the Newtonian gravitational escape velocity v_g of the superposition of the point masses of the antiparticle.

$$v_g=\sqrt{\frac{2Gm}{r}}=\sqrt{\frac{2Gm_0}{\lambda_C}} \tag{26.21}$$

From Eq. (26.20) and Eq. (26.17), the eccentricity is one and the particle

production trajectory is a parabola relative to the center of mass of the antiparticle. The right-hand side of Eq. (23.43) represents the correction to the laboratory coordinate metric for time corresponding to the relativistic correction of spacetime by the particle production event. Riemannian space is conservative. Only changes in the metric of spacetime during particle production must be considered. The changes must be conservative. For example, pair production occurs in the presence of a heavy body. A nucleus which existed before the production event only serves to conserve momentum but is not a factor in determining the change in the properties of spacetime as a consequence of the pair production event. The effect of this and other external gravitating bodies are equal on the photon and resulting particle and antiparticle and do not effect the boundary conditions for particle production. For particle production to occur, the particle must possess the escape velocity relative to the antiparticle where Eqs. (23.34), (23.48), and (23.140) apply. In other cases not involving particle production such as a special electron scattering event wherein hyperbolic electron production occurs as given *infra*, the presence of an external gravitating body must be considered. The curvature of spacetime due to the presence of a gravitating body and the constant maximum velocity of the speed of light comprise boundary conditions for hyperbolic electron production from a free electron.

With particle production, the form of the outgoing gravitational field front traveling at the speed of light (Eq. (23.10)) is

$$f\left(t-\frac{r}{c}\right) \tag{26.22}$$

At production, the particle must have a finite velocity called the gravitational velocity according to Newton's Law of Gravitation. In order that the velocity does not exceed c in any frame including that of the particle having a finite gravitational velocity, the laboratory frame of an incident photon that gives rise to the particle, and that of a gravitational field propagating outward at the speed of light, spacetime must undergo time dilation and length contraction due to the production event. During particle production the speed of light as a constant maximum as well as phase matching and continuity conditions require the following form of the squared displacements due to constant motion along two orthogonal axes in polar coordinates:

$$(c\tau)^2+\left(v_g t\right)^2=(ct)^2 \tag{26.23}$$

$$(c\tau)^2=(ct)^2-\left(v_g t\right)^2 \tag{26.24}$$

$$\tau^2=t^2\left(1-\left(\frac{v_g}{c}\right)^2\right) \tag{26.25}$$

Thus,

$$f(r) = \left(1 - \left(\frac{v_g}{c}\right)^2\right) \tag{26.26}$$

(The derivation and result of spacetime time dilation is analogous to the derivation and result of special relativistic time dilation given by Eqs. (22.11-22.15).) Consider a gravitational radius, r_g, of each orbitsphere of the particle production event, each of mass m

$$r_g = \frac{2Gm}{c^2} \tag{26.27}$$

where G is the Newtonian gravitational constant. Substitution of Eq. (26.11) or Eq. (26.12) into the Schwarzschild metric Eq. (26.2), gives the general form of the metric due to the relativistic effect on spacetime due to mass m_0.

$$d\tau^2 = \left(1 - \left(\frac{v_g}{c}\right)^2\right) dt^2 - \frac{1}{c^2}\left[\left(1 - \left(\frac{v_g}{c}\right)^2\right)^{-1} dr^2 + r^2 d\theta^2 + r^2 \sin^2\theta d\phi^2\right] \tag{26.28}$$

and

$$d\tau^2 = \left(1 - \frac{r_g}{r}\right) dt^2 - \frac{1}{c^2}\left[\left(1 - \frac{r_g}{r}\right)^{-1} dr^2 + r^2 d\theta^2 + r^2 \sin^2\theta d\phi^2\right] \tag{26.29}$$

respectively. Masses and their effects on spacetime superimpose; thus, the metric corresponding to the Earth is given by substitution of the mass of the Earth M for m in Eqs. (26.13-26.14). The corresponding Schwarzschild metric Eq. (26.2) is

$$d\tau^2 = \left(1 - \frac{2GM}{c^2 r}\right) dt^2 - \frac{1}{c^2}\left[\left(1 - \frac{2GM}{c^2 r}\right)^{-1} dr^2 + r^2 d\theta^2 + r^2 \sin^2\theta d\phi^2\right] \tag{26.30}$$

Gravitational and electromagnetic forces are both inverse squared central forces. The inertial mass corresponds to the inertial angular momentum and the gravitational mass corresponds to the gravitational angular momentum. In the case that an electron is bound in by electromagnetic forces in a nonradiative orbit, the following condition from the particle production relationships given by Eq. (24.41) hold

$$\frac{\text{proper time}}{\text{coordinate time}} = \frac{\text{gravitational wave condition}}{\text{electromagnetic wave condition}} = \frac{\text{gravitational mass phase matching}}{\text{charge/inertial mass phase matching}}$$

$$\frac{\text{proper time}}{\text{coordinate time}} = i\frac{\sqrt{\frac{2Gm}{c^2 \lambda_C}}}{\alpha} = i\frac{v_g}{\alpha c} \tag{26.31}$$

The gravitational and inertial angular momentum correspond to the

same mass; thus, the inertial and gravitational masses are identically equal for all matter in a stable bound state.

Consider the case that the radius in Eq. (26.30) goes to infinity. From Eq. (26.20) and Eq. (26.17) in the case that r_0 goes to infinity, the eccentricity is always greater than or equal to one and approaches infinity, and the trajectory is a parabola or a hyperbola. The gravitational velocity (Eq. (26.21)) where $m = M$ goes to zero. This condition must hold from all r_0; thus, the free electron is not effected by the gravitational field of a massive object, but has inertial mass determined by the conservation of the angular momentum of $\hbar$ as shown by Eqs. (3.14-3.15). From the Electron in Free Space Section, the free electron has a velocity distribution given by

$$\mathbf{v}(\rho,\phi,z,t) = \left[\pi\left(\frac{\rho}{2\rho_o}\right)\frac{\hbar}{m_e\sqrt{\rho_0^{\,2}-\rho^2}}\right]\mathbf{i}_\phi$$

$$\mathbf{v}(\rho,\phi,z,t) = \left[\pi\left(\frac{\rho}{2\rho_o}\right)\frac{\hbar}{m_e\rho_o\sqrt{1-\left(\frac{\rho}{\rho_o}\right)^2}}\right]\mathbf{i}_\phi \qquad (26.32)$$

The velocity function is a paraboloid in a two dimensional plane. The corresponding gravity field front corresponds to a radius at infinity in Eq. (26.22). As a consequence, an ionized or free electron has a gravitational mass that is zero; whereas, the inertial mass is constant (e.g. equivalent to its mass energy given by Eq. (24.13)). Minkowski space applies to the free electron.

In the Electron in Free Space Section, a free electron is shown to be a two-dimensional plane wave—a flat surface. Because the gravitational mass depends on the positive curvature of a particle, a free electron has inertial mass but not gravitational mass. The experimental mass of the free electron measured by Witteborn [4] using a free fall technique is less than $0.09\,m_e$, where m_e is the inertial mass of the free electron $\left(9.109534\,X\,10^{-31}\,kg\right)$. Thus, ***a free electron is not gravitationally attracted to ordinary matter, and the gravitational and inertial masses are not equivalent***. Furthermore, it is possible to give the electron velocity function negative curvature and, therefore, cause antigravity.

As is the case of special relativity, the velocity of a particle in the presence of a gravitating body is relative. In the case that the relative gravitational velocity is imaginary, the eccentricity is always greater than one, and the trajectory is a hyperbola. This case corresponds to a

hyperbolic electron wherein gravitational mass is effectively negative and the inertial mass is constant (e.g. equivalent to its mass energy given by Eq. (24.13)). The formation of a hyperbolic electron occurs over the time that the plane wave free electron scatters from the neutral atom. Huygens' principle, Newton's law of Gravitation, and the constant speed of light in all inertial frames provide the boundary conditions to determine the metric corresponding to the hyperbolic electron. From Eq. (26.71), the velocity $\mathbf{v}(\rho,\phi,z,t)$ on a two dimensional sphere in spherical coordinates is

$$\mathbf{v}(r,\theta,\phi,t) = \left(\frac{\hbar}{m_e r_0 \sin\theta}\delta\left(r - r_0\right)\mathbf{i}_\phi\right) \tag{26.33}$$

With hyperbolic electron production, the form of the outgoing gravitational field front traveling at the speed of light (Eq. (23.10)) is

$$f\left(t - \frac{r}{c}\right) \tag{26.34}$$

During hyperbolic electron production the speed of light as a constant maximum as well as phase matching and continuity conditions require the following form of the squared displacements due to constant motion along two orthogonal axes in polar coordinates:

$$(c\tau)^2 + \left(v_g t\right)^2 = (ct)^2 \tag{26.35}$$

According to Eq. (3.11), the velocity of the electron on the two dimension sphere approaches the speed of light at the angular extremes ($\theta = 0$ and $\theta = \pi$), and the velocity is harmonic as a function of theta. The speed of any signal can not exceed the speed of light. Therefore, the outgoing two dimensional spherical gravitational field front traveling at the speed of light and the velocity of the electron at the angular extremes require that the relative gravitational velocity must be radially outward. The relative gravitational velocity squared of the term $\left(v_g t\right)^2$ of Eq. (26.35) must be negative. In this case, the relative gravitational velocity may be considered imaginary which is consistent with the velocity as a harmonic function of theta. The energy of the orbit of the hyperbolic electron must always be greater than zero which corresponds to a hyperbolic trajectory and an eccentricity greater than one (Eq. (26.17) and Eq. (26.20)). From Eq. (26.20) and Eq. (26.21) with the requirements that the relative gravitational velocity must be imaginary and the energy of the orbit must always be positive, the relative gravitational velocity for a hyperbolic electron produced in the presence of the gravitational field of the Earth is

$$v_g = i\sqrt{\frac{2GM}{r}} \tag{26.36}$$

where M is the mass of the Earth. Substitution of Eq. (26.36) into Eq.

(26.35) gives

$$(c\tau)^2 = (ct)^2 + (v_g t)^2 \tag{26.37}$$

$$\tau^2 = t^2\left(1 + \left(\frac{v_g}{c}\right)^2\right) \tag{26.38}$$

Thus,

$$f(r) = \left(1 + \left(\frac{v_g}{c}\right)^2\right) \tag{26.39}$$

Consider a gravitational radius, r_g, of a massive object of mass M relative to a hyperbolic electron at the production event that is negative to match the boundary condition of a negatively curved velocity surface

$$r_g = -\frac{2GM}{c^2} \tag{26.40}$$

where G is the Newtonian gravitational constant. Substitution of Eq. (26.36) or Eq. (26.40) into the Schwarzschild metric Eq. (26.2), gives the general form of the metric due to the relativistic effect on spacetime due to a massive object of mass M relative to the hyperbolic electron.

$$d\tau^2 = \left(1 + \left(\frac{v_g}{c}\right)^2\right)dt^2 - \frac{1}{c^2}\left[\left(1 + \left(\frac{v_g}{c}\right)^2\right)^{-1} dr^2 + r^2 d\theta^2 + r^2 \sin^2\theta d\phi^2\right] \tag{26.41}$$

and

$$d\tau^2 = \left(1 + \frac{r_g}{r}\right)dt^2 - \frac{1}{c^2}\left[\left(1 + \frac{r_g}{r}\right)^{-1} dr^2 + r^2 d\theta^2 + r^2 \sin^2\theta d\phi^2\right] \tag{26.42}$$

respectively.

ANTIGRAVITY DEVICE

It is possible to give the velocity function of electrons negative curvature by elastically scattering electrons of an electron beam from atoms such that electrons with negatively curved velocity surfaces (hyperbolic electrons) emerge. The emerging beam of electrons with negatively curved velocity surfaces experience an antigravitational force (on the Earth), and the beam will tend to move upward (away from the Earth). To use this invention for propulsion or levitation, the antigravitational force of the electron beam must be transferred to a negatively charged plate. The Coulombic repulsion between the beam of electrons and the negatively charged plate will cause the plate (and anything connected to the plate) to lift. Figure 26.3 gives a schematic of an antigravity levitation device.

Figure 26.3. An antigravity device.

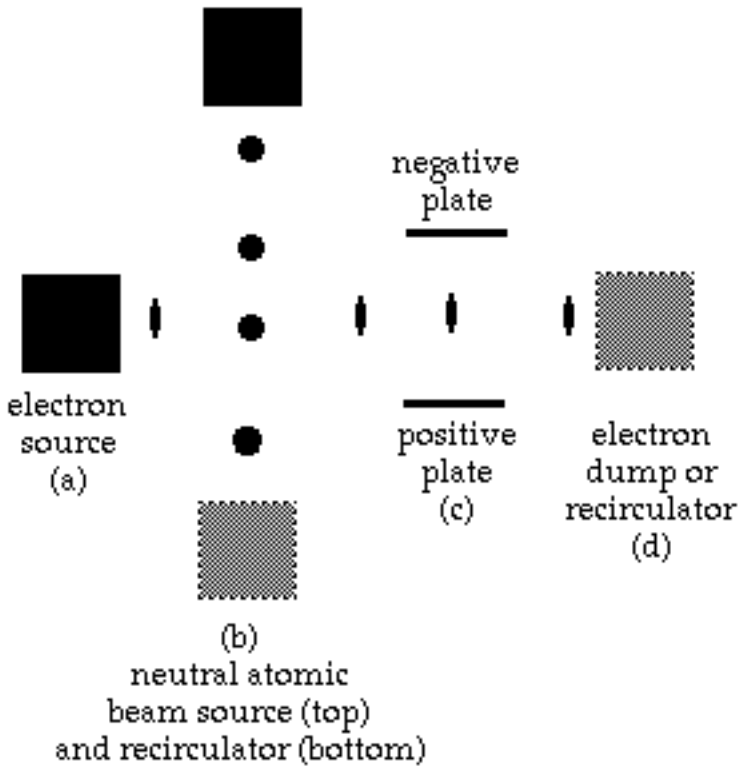

(a) a beam of electrons is generated and directed to the neutral atomic beam

(b) scattering of the electrons of the electron beam by the neutral atom beam gives the electrons negative curvature of their velocity surfaces, and the electrons experience an antigravitational force upward (away from the earth)

(c) the electrons, which would normally bend down toward the positive plate but do not because of the antigravitational force, repel the negative plate and attract the positive plate, and transfer the antigravity force to the object to be lifted or propelled

(d) the electrons are collected or recirculated back to the electron beam

HYPERBOLIC ELECTRONS

A method and means to produce an antigravitational force for propulsion and/or levitation comprises a source of fundamental particles including electrons and a source of neutral atoms. The source of electrons produces a free electron beam, and the source of neutral atoms produces a free atom beam. The two beams intersect such that the neutral atoms cause elastic incompressible scattering of the

electrons of the electron beam to form hyperbolic electrons. In a preferred embodiment, the de Broglie wavelength of each electron is given by

$$\lambda_o = \frac{h}{m_e v_z} = 2\pi\rho_o \tag{26.43}$$

where ρ_o is the radius of the free electron in the xy-plane, the plane perpendicular to its direction of propagation. The velocity of each electron follows from Eq. (26.43)

$$v_z = \frac{h}{m_e \lambda_o} = \frac{h}{m_e 2\pi\rho_o} = \frac{\hbar}{m_e \rho_o} \tag{26.44}$$

The elastic electron scattering in the far field is given by the Fourier Transform of the aperture function as described in Electron Scattering by Helium Section. The convolution of a uniform plane wave with on orbitsphere of radius z_o is given by Eq. (8.43) and Eq. (8.44).

The aperture distribution function, $a(\rho,\phi,z)$, for the scattering of an incident plane wave by the He atom is given by the convolution of the plane wave function with the two electron orbitsphere Dirac delta function of $radius = 0.567a_o$ and charge/mass density of $\frac{2}{4\pi(0.567a_o)^2}$. For radial units in terms of a_o

$$a(\rho,\phi,z) = \pi(z) \quad \frac{2}{4\pi(0.567a_o)^2}[\delta(r - 0.567a_o)] \tag{26.45}$$

where $a(\rho,\phi,z)$ is given in cylindrical coordinates, $\pi(z)$, the xy-plane wave is given in Cartesian coordinates with the propagation direction along the z-axis, and the He atom orbitsphere function, $\frac{2}{4\pi(0.567a_o)^2}[\delta(r - 0.567a_o)]$, is given in spherical coordinates.

$$a(\rho,\phi,z) = \frac{2}{4\pi(0.567a_o)^2}\sqrt{(0.567a_o)^2 - z^2}\,\delta\left(r - \sqrt{(0.567a_o)^2 - z^2}\right) \tag{26.46}$$

The convolution of the charge-density equation of a free electron given by Eq. (3.7) with an orbitsphere of radius z_o follows from Eq. (3.7) and Eq. (26.46)

$$\rho_m(\rho,\phi,z) = \sqrt{\rho_0^2 - \rho^2}\sqrt{z_0^2 - z^2}\,\delta\left(\rho - \sqrt{z_0^2 - z^2}\right) \tag{26.47}$$

Substitution of Eq. (26.47) into Eq. (8.45) gives

$$F(s) = \frac{1}{z_o^2}\int_{-z_o}^{z_o}\sqrt{\rho_o^2 - (z_o^2 - z^2)}(z_o^2 - z^2)J_o\left(s\sqrt{z_o^2 - z^2}\right)e^{iwz}dz \tag{26.48}$$

Substitution $\frac{z}{z_o} = -\cos\theta$ into Eq. (26.48) gives

$$F(s) = \int_0^{\pi} \sqrt{\rho_o{}^2 - z_o{}^2 \sin^2\theta}\, \sin^3\theta J_o\left(sz_o \sin\theta\right) e^{iz_0 w\cos\theta} d\theta \tag{26.49}$$

when $\rho_o = z_o$, Eq. (26.49) becomes

$$F(s) = z_o \int_0^{\pi} \cos\theta \sin^3\theta J_o(sz_o \sin\theta) e^{iz_0 w\cos\theta} d\theta \tag{26.50}$$

The function of the scattered electron in the far field is given by the Fourier Transform integral, Eq. (26.50). Eq. (26.50) is equivalent to the Fourier Transform integral of $\cos\theta$ times the Fourier Transform integral given by of Eq. (8.47) with the latter result given by Eq. (8.50).

$$F(s) = \left[\frac{2\pi}{(z_o w)^2 + (z_o s)^2}\right]^{\frac{1}{2}} \left\{ 2\left[\frac{z_o s}{(z_o w)^2 + (z_o s)^2}\right] J_{3/2}\left[((z_o w)^2 + (z_o s)^2)^{1/2}\right] - \left[\frac{z_o s}{(z_o w)^2 + (z_o s)^2}\right]^2 J_{5/2}\left[((z_o w)^2 + (z_o s)^2)^{1/2}\right] \right\} \tag{26.51}$$

where

$$s = \frac{4\pi}{\lambda} \sin\frac{\theta}{2};\ w = 0\ (units\ of\ \AA^{-1}) \tag{26.52}$$

A very important theorem of Fourier analysis states that the Fourier Transform of a product is the convolution of the individual Fourier Transforms. The Fourier Transform of $\cos\theta$ is

$$\frac{[\delta(\Theta - \Theta_o) + \delta(\Theta + \Theta_o)]}{2} \tag{26.53}$$

The Fourier Transform integral, Eq. (26.50), is the convolution of Eqs. (26.51-26.52) and Eq. (26.53). The convolution gives the result that Eq. (26.52) is given by

$$s = \frac{4\pi}{\lambda} \sin\left(\frac{\theta - \Theta_o}{2}\right);\ w = 0\ (units\ of\ \AA^{-1}) \tag{26.54}$$

Given that $z = z_o \cos\theta$, the mass density function of each electron having a de Broglie wavelength λ_o given by Eq. (26.43) corresponding to λ in Eq. (26.54) which is elastically scattered by an atom having a radius of $z_o = \rho_o$ is given by Eqs. (26.51) and (26.54). The replacement of $\Pi(z)$, the xy-plane wave corresponding to the superposition of many electrons scattered from an atomic beam with the function of a single electron propagating in the z-direction (Eq. (3.7)) gives rise to the ***electron density function on a two dimensional sphere*** of

$$\rho_m(\rho, \phi, z) = Nm_e \sqrt{\rho_0{}^2 - z^2}\, \delta\left(\rho - \sqrt{\rho_0{}^2 - z^2}\right) \tag{26.55}$$

centered at a scattering angle of Θ_o. With the condition $z_o = \rho_o$, the

elastic electron scattering angle in the far field Θ_o is determined by the boundary conditions of the curvature of spacetime due to the presence of a gravitating body and the constant maximum velocity of the speed of light. The far field condition must be satisfied with respect to electron scattering and the gravitational orbital equation. The former condition is met by Eq. (26.51) and Eq. (26.54). The latter is derived in the Preferred Embodiment of an Antigravity Device Section and is met by Eq. (26.103) where the far field angle of the hyperbolic gravitational trajectory ϕ is equivalent to Θ_o.

The electron mass/charge density function, $\rho_m(\rho,\phi,z)$, is given in cylindrical coordinates, and N is the normalization factor. The charge density, mass density, velocity, current density, and angular momentum functions are derived in the same manner as for the free electron given in the Electron in Free Space Section except that the scattered electron is symmetric about the z-axis. The total mass is m_e. Thus, Eq. (26.55) must be normalized.

$$m_e = N \int_{-\rho_0}^{\rho_0} \int_{0}^{2\pi} \int_{-\infty}^{\infty} \sqrt{\rho_0^{\,2} - z^2}\,\delta\left(\rho - \sqrt{\rho_0^{\,2} - z^2}\right)\rho\, d\rho\, d\phi\, dz \tag{26.56}$$

$$N = \frac{m_e}{\frac{8}{3}\pi\rho_0^{\,3}} \tag{26.57}$$

The mass density function, $\rho_m(\rho,\phi,z)$, of the scattered electron is

$$\rho_m(\rho,\phi,z) = \frac{m_e}{\frac{8}{3}\pi\rho_0^{\,3}} \sqrt{\rho_0^{\,2} - z^2}\,\delta\left(\rho - \sqrt{\rho_0^{\,2} - z^2}\right)$$

$$\rho_m(\rho,\phi,z) = \frac{m_e}{\frac{8}{3}\pi\rho_0^{\,3}} \rho_0 \sqrt{1 - \left(\frac{z}{\rho_0}\right)^2}\,\delta\left(\rho - \rho_0\sqrt{1 - \left(\frac{z}{\rho_0}\right)^2}\right) \tag{26.58}$$

and charge-density distribution, $\rho_e(\rho,\phi,z)$, is

$$\rho_e(\rho,\phi,z) = \frac{e}{\frac{8}{3}\pi\rho_0^{\,3}} \sqrt{\rho_0^{\,2} - z^2}\,\delta\left(\rho - \sqrt{\rho_0^{\,2} - z^2}\right)$$

$$\rho_e(\rho,\phi,z) = \frac{e}{\frac{8}{3}\pi\rho_0^{\,3}} \rho_0 \sqrt{1 - \left(\frac{z}{\rho_0}\right)^2}\,\delta\left(\rho - \rho_0\sqrt{1 - \left(\frac{z}{\rho_0}\right)^2}\right) \tag{26.59}$$

The magnitude of the angular velocity of the helium orbitsphere is given by Eq. (1.55) is

$$\omega = \frac{\hbar}{m_e r^2} \tag{26.60}$$

where $r = r_0 = \rho_0 = z_0 = 0.567 a_0$ and a_0 is the Bohr radius. The current-

density function of the scattered electron, $\mathbf{K}(\rho,\phi,z,t)$, is the projection along the z-axis of the integral of the product of the projections of the charge of the orbitsphere (Eq. (3.3)) times the angular velocity as a function of the radius r of an ionizing orbitsphere (Eq. (3.9)) for $r = r_o$ to $r = \infty$. The integral is

$$\int_{r_o}^{\infty} \omega\pi(z) \quad \delta(r - r_o)dr = \frac{e}{\frac{8}{3}\pi r_0^3}\int_{r_o}^{\infty} \frac{\hbar}{m_e r^2}\sqrt{r_0^2 - z^2}\,\delta(r - \sqrt{r_0^2 - z^2})dr \tag{26.61}$$

The projection of Eq. (26.61) along the z-axis is

$$\mathbf{J}(\rho,\phi,z,t) = \left[\frac{e}{\frac{8}{3}\pi\rho_0^3}\frac{\hbar}{m_e\sqrt{\rho_0^2 - z^2}}\delta\left(\rho - \sqrt{\rho_0^2 - z^2}\right)\mathbf{i}_\phi\right] \tag{26.62}$$

The velocity $\mathbf{v}(\rho,\phi,z,t)$ along the z-axis is

$$\mathbf{v}(\rho,\phi,z,t) = \left[\frac{\hbar}{m_e\sqrt{\rho_0^2 - z^2}}\delta\left(\rho - \sqrt{\rho_0^2 - z^2}\right)\mathbf{i}_\phi\right]$$

$$\mathbf{v}(\rho,\phi,z,t) = \left[\frac{\hbar}{m_e\rho_0\sqrt{1 - \left(\frac{z}{\rho_0}\right)^2}}\delta\left(\rho - \rho_0\sqrt{1 - \left(\frac{z}{\rho_0}\right)^2}\right)\mathbf{i}_\phi\right] \tag{26.63}$$

where $\rho_o = r_o$. The angular momentum, $\mathbf{L}$, is given by

$$\mathbf{L}\mathbf{i}_z = m_e r^2\omega = \mathbf{L} = mr^2\mathbf{w} = m\mathbf{r}\times\mathbf{v} \tag{26.64}$$

Substitution of m_e for e in Eq. (26.62) followed by substitution into Eq. (26.64) gives the angular momentum density function, $\mathbf{L}$

$$\mathbf{L}\mathbf{i}_z = \frac{m_e}{\frac{8}{3}\pi\rho_0^3}\frac{\hbar}{m_e\sqrt{\rho_0^2 - z^2}}\rho^2\delta\left(\rho - \sqrt{\rho_0^2 - z^2}\right) \tag{26.65}$$

The total angular momentum of the scattered electron is given by integration over the two dimensional negatively curved surface having the angular momentum density given by Eq. (26.65).

$$\mathbf{L}\mathbf{i}_z = \int_{-\rho_0}^{\rho_0}\int_0^{2\pi}\int_{-\infty}^{\infty}\frac{m_e}{\frac{8}{3}\pi\rho_0^3}\frac{\hbar}{m_e\sqrt{\rho_0^2 - z^2}}\delta\left(\rho - \sqrt{\rho_0^2 - z^2}\right)\rho^2\,\rho d\rho\, d\phi dz \tag{26.66}$$

$$\mathbf{L}\mathbf{i}_z = \hbar \tag{26.67}$$

Eq. (26.67) is in agreement with Eq. (1.130); thus, the scalar sum of the magnitude of the angular momentum is conserved.

The mass, charge, and current of the scattered electron exist on a two dimension sphere which may be given in spherical coordinates where theta is with respect to the z-axis of the original cylindrical

coordinate system. The mass density function, $\rho_m(r,\theta,\phi)$, of the scattered electron in spherical coordinates is

$$\rho_m(r,\theta,\phi) = \frac{m_e}{\frac{8}{3}\pi r_0^3} r_0 \sin^2\theta\,\delta(r - r_0) \tag{26.68}$$

The charge-density distribution, $\rho_e(r,\theta,\phi)$, in spherical coordinates is

$$\rho_e(r,\theta,\phi) = \frac{e}{\frac{8}{3}\pi r_0^3} r_0 \sin^2\theta\,\delta(r - r_0) \tag{26.69}$$

The current density function $\mathbf{J}(r,\theta,\phi,t)$, in spherical coordinates is

$$\mathbf{J}(r,\theta,\phi,t) = \left[\frac{e}{\frac{8}{3}\pi r_0^2}\frac{\hbar}{m_e r_0^2}\sin\theta\,\delta(r - r_0)\,\mathbf{i}_\phi\right] \tag{26.70}$$

The velocity $\mathbf{v}(\rho,\phi,z,t)$ in spherical coordinates is

$$\mathbf{v}(r,\theta,\phi,t) = \left[\frac{\hbar}{m_e r_0 \sin\theta}\delta(r - r_0)\,\mathbf{i}_\phi\right] \tag{26.71}$$

The total angular momentum of the scattered electron is given by integration over the two dimensional negatively curved surface having the angular momentum density in spherical coordinates given by

$$\mathbf{L}\mathbf{i}_z = \int_0^{2\pi}\int_0^{\pi}\int_0^{\infty}\frac{m_e}{\frac{8}{3}\pi r_0^3}\frac{\hbar}{m_e r_0} r^2\sin^2\theta\,\delta(r - r_0) r^2\sin\theta\,dr\,d\theta\,d\phi \tag{26.72}$$

$$\mathbf{L}\mathbf{i}_z = \hbar \tag{26.73}$$

where $\rho_o = r_o$.

The electron orbitsphere of an atom has a constant velocity as a function of angle. ***Whereas, the electron orbitsphere formed when the radius of the incoming electron is equal to the radius of the scattering atom (i.e.*** $z_o = \rho_o$***) has a velocity function whose magnitude is harmonic in theta (Eq. (26.71)). The velocity function (Eq. (26.63) or Eq. (26.71)) is a hyperboloid. It exists on a two dimension sphere; thus, it is spatially bounded. The mass and charge functions given by Eq. (26.68) and Eq. (26.69), respectively, are finite on a two dimensional sphere; thus, they are bounded. The scattered electron having a negatively curved two dimensional velocity surface is called a hyperbolic electron.*** The magnetic field of the current-density function of the hyperbolic electron provides the force balance of the centrifugal force of the mass density function as was the case for the free electron given in the Electron in Free Space Section. The current density function is also nonradiative as given in that section. Hyperbolic electrons can be focused into a beam by electric and/or magnetic fields to form a hyperbolic electron beam. The velocity distribution along the

z-axis of a hyperbolic electron is shown schematically in Figure 26.4A. A cutaway of the velocity distribution of a hyperbolic electron is shown schematically in Figure 26.4B.

Figure 26.4A. The magnitude of the velocity distribution ($|\mathbf{v}_\phi|$) on a two dimension sphere along the z-axis (vertical axis) of a hyperbolic electron.

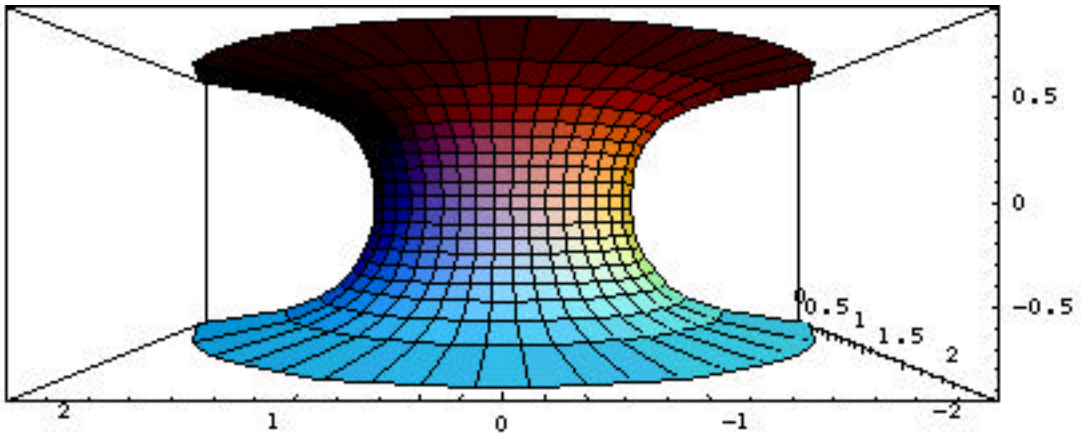

Figure 26.4B. A cutaway of the magnitude of the velocity distribution ($|\mathbf{v}_\phi|$) on a two dimension sphere along the z-axis (vertical axis) of a hyperbolic electron.

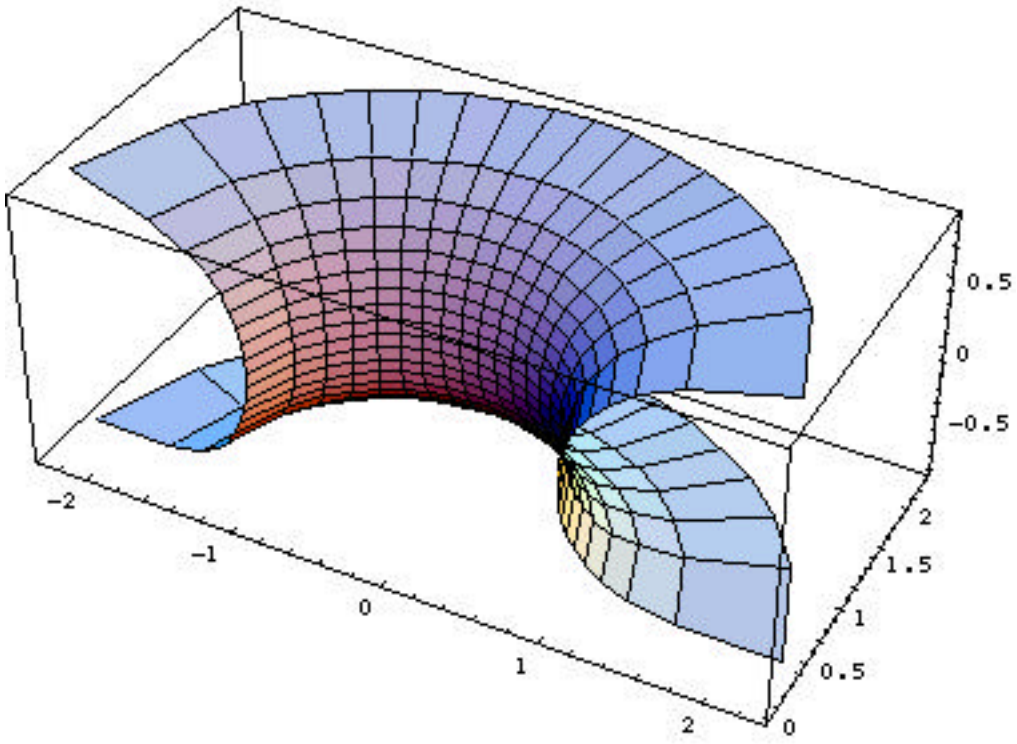

The velocity is harmonic or imaginary as a function of theta. Therefore, the gravitational velocity of the Earth relative to that of the hyperbolic electron is imaginary. This case corresponds to an eccentricity greater than one and a hyperbolic orbit of Newton's Law of Gravitation. The metric for the imaginary gravitational velocity is derived based on the center of mass of the scattering event. The Earth, helium, and the hyperbolic electron are spherically symmetrical; thus, the Schwarzschild metric (Eqs. (26-41-26.42)) applies. The velocity distribution defines a surface of negative curvature relative to the positive curvature of the Earth. This case corresponds to a negative radius of Eq. (26.40) or an imaginary gravitational velocity of Eq. (26.36). The lift due to the resulting antigravitational force is given in the Preferred Embodiment of an Antigravitational Device Section. According to Eq. (23.48) and Eq. (23.140), matter, energy, and spacetime are conserved with respect to creation of a particle which is repelled from a gravitating body. The gravitationally ejected particle gains energy as it is repelled. The ejection of a particle having a negatively curved velocity surface such as a hyperbolic electron from a gravitating body such as the Earth must result in an infinitesimal decrease in its radius of the gravitating body (e.g. r of the Schwarzschild metric given by Eq. (26.2) where $m_0 = M$ is the mass of the Earth). The amount that the gravitational potential energy of the gravitating body is lowered is equivalent to the energy gained by the repelled particle. The physics is time reversible. The process may be run backwards to achieve the original state before the repelled particle such as a hyperbolic electron was created.

In a preferred embodiment, the neutral atoms of the neutral atom beam comprise helium, and the velocity of the free electrons of the electron beam is

$$v_z = \frac{\hbar}{m_e \rho_o} = 3.858361\ X\ 10^6\ m/s \tag{26.74}$$

where $\rho_o = 0.567 a_o = 3.000434\ X\ 10^{-11}\ m$.

In another preferred embodiment, each atom of the neutral atomic beam comprises hydrino atom $H(1/p)$, $\rho_o = \frac{a_H}{p}$; p is an integer). The velocity of each electron of the free electron beam is

$$v_z = \frac{\hbar}{m_e \rho_o} = 2.187691\ X\ 10^6\ m/s \tag{26.75}$$

where $\rho_o = \frac{a_H}{n} = \frac{5.29177\ X\ 10^{-11}}{n}\ m$

For a nonrelativistic electron of velocity v_z, the kinetic energy, T, is

$$T = \frac{1}{2} m_e v_z^2 \quad (26.76)$$

In the case of helium with the substitution of Eq. (26.74) into Eq. (26.76),

$$T = 42.3\ eV \quad (26.77)$$

In the case of hydrogen with the substitution of Eq. (26.75) into Eq. (26.76),

$$T = p^2 13.6\ eV \quad (26.78)$$

PREFERRED EMBODIMENT OF AN ANTIGRAVITY DEVICE

As shown schematically in Figure 26.5, the device 10 of Mills [5] to provide an antigravitational force for levitation or propulsion comprises a source 1 of a gas jet of atoms 101 such as helium atoms such as described by Bonham [6] and an energy tunable electron beam source 2 which supplies an electron beam 102 having electrons of a precise energy such that the radius of each electron is equal to the radius of each atom of the gas jet 101. Such a source is described by Bonham [6]. The gas jet 101 and electron beam 102 intersect such that the velocity function of each electron is elastically scattered and warped into a hyperboloid of negative curvature (hyperbolic electron). The hyperbolic electron beam 103 passes into an electric field provided by a capacitor means 3. In a preferred embodiment, the capacitor means 3 is along to the electron beam 102, and the intersection of the gas jet 101 and the electron beam 102 occurs inside of the capacitor means 3. The hyperbolic electrons experience an antigravitational force due to their velocity surfaces of negative curvature and are accelerated away from the center of the gravitating body such as the Earth. This upward force is transferred to the capacitor means 3 via a repulsive electric force between the hyperbolic electrons and the electric field of the capacitor means 3. The capacitor means 3 is rigidly attached to the body to be levitated or propelled by structural attachment 4. The present antigravity means further includes a means to trap unscattered and hyperbolic electrons and recirculate them through the beam 102. Such a trap means 5 includes a Faraday cage as described by Bonham [6]. The present antigravity means 10 further includes a means 6 to trap and recirculate the atoms of the gas jet 101. Such a gas trap means 6 includes a pump such as a diffusion pump as described by Bonham [6].

Figure 26.5. Antigravity device driven by hyperbolic electrons.

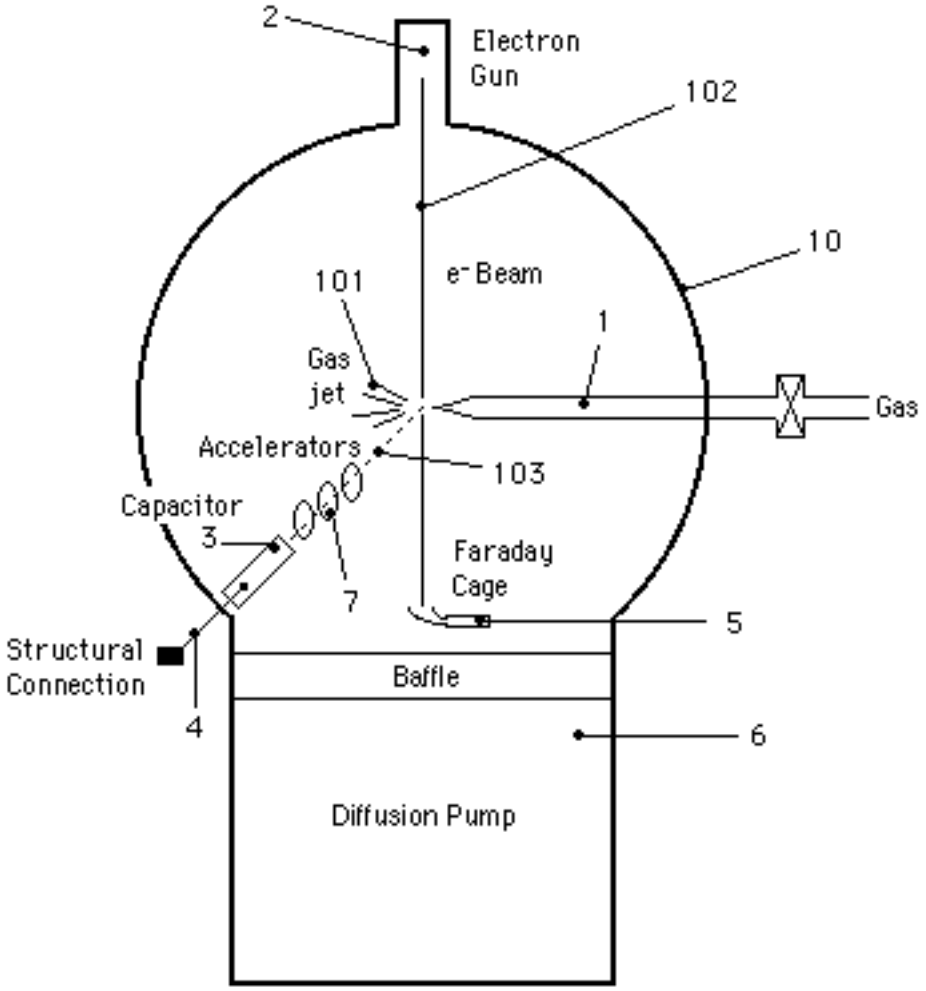

In the case of a hyperbolic electron which is much smaller then the size of a capacitor, the electric force of the hyperbolic electron on the capacitor is equivalent to that of a point charge. This force provides lift to the capacitor due to the gravitational repulsion of the hyperbolic electron from the Earth as it undergoes a trajectory through the capacitor. A close approximation of the trajectory of hyperbolic electrons generated by the antigravity levitation and propulsion means can be found by solving the Newtonian inverse-square gravitational force equations for the case of a repulsive force. The trajectory follows from the Newtonian gravitational force and the solution of motion in an inverse-square repulsive field given by Fowles [7]. The trajectory can be calculated rigorously by solving the orbital equation from the Schwarzschild metric (Eqs. (26.15-26.16)) for a two-dimensional spatial velocity density function of negative curvature which is produced by the apparatus and repelled by the Earth. The rigorous solution is equivalent

to that given for the case of a positive gravitational velocity given in the Orbital Mechanics Section except that the gravitational velocity is imaginary, or the gravitational radius is negative.

In the case of a velocity function having negative curvature, Eq. (23.78) becomes

$$\left(1+\frac{2GM}{rc^2}\right)\frac{dt}{d\tau}=\frac{E}{mc^2} \tag{26.79}$$

where M is the mass of the Earth and m is the mass of the hyperbolic electron. Eq. (23.79) is based on the equations of motion of the geodesic, which in the case of an imaginary gravitation velocity or a negative gravitational radius becomes

$$\left(\frac{dr}{d\theta}\right)^2=\frac{r^4}{L_\theta^2}\left[\left(\frac{E}{c}\right)^2-\left(1+\frac{2GM}{c^2r}\right)\left(\frac{L_\theta^2}{r^2}+m^2c^2\right)\right] \tag{26.80}$$

The repulsive central force equations can be transformed into an orbital equation by the substitution, $u=\frac{1}{r}$. The relativistically corrected differential equation of the orbit of a particle moving under a repulsive central force is

$$\left(\frac{du}{d\theta}\right)^2+u^2=\frac{\left(\frac{E}{c}\right)^2-m^2c^2}{L_\theta^2}-\frac{m^2c^2}{L_\theta^2}\left(\frac{2GM}{c^2}\right)u-\left(\frac{2GM}{c^2}\right)u^3 \tag{26.81}$$

By differentiating with respect to θ, noting that $u=u(\theta)$ gives

$$\frac{d^2u}{d\theta^2}+u=-\frac{GM}{a^2}-\frac{3}{2}\left(\frac{2GM}{c^2}\right)u^2 \tag{26.82}$$

where

$$a=\frac{L_\theta}{m} \tag{26.83}$$

In the case of a weak field,

$$\left(\frac{2GM}{c^2}\right)u<<1 \tag{26.84}$$

and the second term on the right-hand of (26.37) can then be neglected in the zero-order. The equation of the orbit is

$$u_0=\frac{1}{r}=A\cos(\theta+\theta_0)-\frac{GM}{a^2} \tag{26.85}$$

$$r=\frac{1}{A\cos(\theta+\theta_0)-\frac{GM}{a^2}} \tag{26.86}$$

where A and θ_0 denote the constants of integration. Consider E_t, the sum of the kinetic and gravitational potential energy:

$$E_t=\frac{1}{2}mv^2+\frac{GMm}{r} \tag{26.87}$$

where m is the mass of the hyperbolic electron. The orbit equation may

also be expressed in terms of E_t as given by Fowles [8]

$$r = \frac{\frac{a^2}{GM}}{-1 + \left(1 + \frac{2Ema^2}{(GMm)^2}\right)^{\frac{1}{2}} \cos(\theta - \theta_0)} \tag{26.88}$$

In a repulsive field, the energy is always greater than zero. Thus, the eccentricity e, the coefficient of $\cos(\theta - \theta_0)$, must be greater than unity ($e > 1$) which requires that the orbit must be hyperbolic. Consider the trajectory of a hyperbolic electron shown in Figure 26.6.

Figure 26.6. Hyperbolic path of a hyperbolic electron of mass m in an inverse-square repulsive field of a gravitating body comprised of positively curved matter of total mass M.

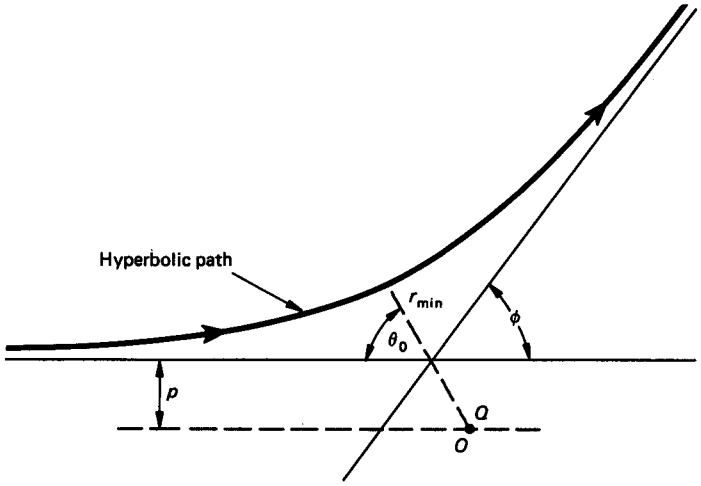

It approaches along one asymptote and recedes along the other. The direction of the polar axis is selected such that the initial position of the hyperbolic electron is $\theta = 0$, $r = \infty$. According to either of the equations of the orbit (Eq. (26.86) or Eq. (26.88)) r assumes its minimum value when $\cos(\theta - \theta_0) = 1$, that is, when $\theta = \theta_0$. Since $r = \infty$ when $\theta = 0$, then r is also infinite when $\theta = 2\theta_0$. Therefore, the angle between the two asymptotes of the hyperbolic path is $2\theta_0$, and the angle ϕ through which the incident hyperbolic electron is deflected is given by

$$\phi = \pi - 2\theta_0 \tag{26.89}$$

Furthermore, the denominator of Eq. (26.88) vanishes when $\theta = 0$ and $\theta = 2\theta_0$. Thus,

$$-1+\left(1+\frac{2Ema^2}{(GMm)^2}\right)^{\frac{1}{2}}\cos(\theta_0)=0 \tag{26.90}$$

Using Eq. (26.89) and Eq. (26.90), the scattering angle ϕ is given in terms of θ as

$$\tan\theta_0=\frac{(2Em)^{\frac{1}{2}}a}{GMm}=\cot\frac{\phi}{2} \tag{26.91}$$

For convenience, the constant $a=\frac{L_\theta}{m}$ may be expressed in terms of another parameter p called the impact parameter. The impact parameter is the perpendicular distance from the origin (deflection or scattering center) to the initial line of motion of the hyperbolic electron as shown in Figure 26.6. The relationship between a the angular momentum per unit mass and v_0 the initial velocity of the hyperbolic electron is

$$a=|\mathbf{r}\times\mathbf{v}|=pv_0 \tag{26.92}$$

A massive gravitational body such as the Earth will not be moved by the encounter with a hyperbolic electron. Thus, the energy E_t of the deflected hyperbolic electron is constant and is equal to T the initial kinetic energy because the initial potential energy is zero ($r=\infty$).

$$T=\frac{1}{2}mv_0^2 \tag{26.93}$$

Using the impact parameter, the deflection or scattering equation is given by

$$\cot\frac{\phi}{2}=\frac{pv_0^2}{GM}=\frac{2pE}{GMm} \tag{26.94}$$

$$\phi=2\arctan\left(\frac{pv_0^2}{GM}\right)^{-1}=2\arctan\left(\frac{2pE}{GMm}\right)^{-1} \tag{26.95}$$

The gravitational velocity of the Earth v_{g_E} is approximately

$$v_{g_E}\approx\sqrt{\frac{2GM}{p}} \tag{26.96}$$

Thus, Eq. (26.95) is given by

$$\phi=2\arctan\left(\frac{1}{2}\left(\frac{v_{g_E}}{v_0}\right)^2\right) \tag{26.97}$$

Consider the postulate that the hyperbolic electron must follow the trajectory for an inverse squared force in the far field. In the limit, the far field trajectory is the asymptote. As a method to obtain a first approximation of the asymptote, consider the case that the hyperbolic electron is generated at the surface of the Earth with an initial trajectory as shown in Figure 26.6. The initial radial position is $r_{\min}$ which is the

radius of the Earth. Also, the impact parameter p is essentially equal to the radius of the Earth. Substitution of Eq. (26.87) and Eq. (26.92) into Eq. (26.91) gives

$$\frac{\left(v_0^2 + \frac{2GM}{p}\right)^{\frac{1}{2}} p v_0}{GM} = \cot\frac{\phi}{2} \tag{26.98}$$

Substitution of Eq. (26.96) into Eq. (26.98) gives

$$2\left(v_0^2 + v_{g_E}^2\right)^{\frac{1}{2}} \frac{v_0}{v_{g_E}^2} = \cot\frac{\phi}{2} \tag{26.99}$$

$$\phi = 2\arctan\left(\frac{1}{2}\frac{v_{g_E}^2}{\left(v_0^2 + v_{g_E}^2\right)^{\frac{1}{2}} v_0}\right) \tag{26.100}$$

The gravitational velocity of the Earth v_{g_E} is

$$v_{g_E} = \sqrt{\frac{2GM}{R}} = 1.1\,X\,10^8\ m/\sec \tag{26.101}$$

where R is the radius of the Earth. Consider the case of the generation of hyperbolic electrons via elastic scattering from helium atoms. Substitution of the hyperbolic electron velocity of $2.187691\,X\,10^6\,m/s$ given by Eq. (26.75) and the gravitational velocity of the Earth given by Eq. (26.101) into Eq. (26.100) gives

$$\phi = 2\arctan\left(\frac{1}{2}\frac{\left(1.1\,X\,10^8\ m/\sec\right)^2}{\left(\left(1.1\,X\,10^8\ m/\sec\right)^2 + \left(2.2\,X\,10^6\ m/\sec\right)^2\right)^{\frac{1}{2}}\left(2.2\,X\,10^6\ m/\sec\right)}\right) \tag{26.102}$$

The angle of the asymptote is

$$\phi = 175° \approx \pi \tag{26.103}$$

Thus, the asymptote of the trajectory of a hyperbolic electron is essentially radial from the Earth. Since the trajectory in a conservative inverse field is reversible going from $+\infty$ to $-\infty$ or vice versa, the entire trajectory of a hyperbolic electron with $v_0 = 2.187691\,X\,10^6\,m/s$ at $r_{\min}$ equal to the radius of the Earth is essentially radial with respect to the Earth. From this result, it can be concluded that the far field trajectory of a hyperbolic electron formed from a free electron with an initial kinetic energy of $42.3\,eV$ and an initial electron velocity of $2.187691\,X\,10^6\,m/s$ in an arbitrary initial direction relative to the Earth is essentially radial from the Earth since 1.) v_0 is much less than v_{g_E}, 2.) the impact parameter is essentially $r_{\min}$ which is the radius of the Earth since the radius of the

Earth is so large, and 3.) the free electron has zero gravitational mass. The trajectory forms the gravitational boundary condition to be matched with the additional scattering boundary condition.

The scattering distribution of hyperbolic electrons given by Eq. (26.51) is centered at a scattering angle of Θ_o given by Eq. (26.54). With the condition $z_o = \rho_o$, the elastic electron scattering angle in the far field Θ_o is determined by the boundary conditions of the curvature of spacetime due to the presence of a gravitating body and the constant maximum velocity of the speed of light. The far field condition must be satisfied with respect to electron scattering and the gravitational orbital equation. The former condition is met by Eq. (26.51) and Eq. (26.54). The latter is met by Eq. (26.103) where the far field angle of the hyperbolic gravitational trajectory ϕ is equivalent to Θ_o.

The elastic scattering condition is possible due to the large mass of the helium atom and the Earth relative to the electron wherein the recoil energy transferred during a collision is inversely proportional to the mass as given by Eq. (2.70). Satisfaction of the far field conditions of the elastic electron scattering to produce hyperbolic electrons and the hyperbolic gravitational trajectory requires that the hyperbolic electrons elastically scatter in a direction radially from the Earth with a kinetic energy in the radial direction that is essentially equal to the initial kinetic energy corresponding to the condition $z_o = \rho_o$.

According to Eq. (23.48) and Eq. (23.140), matter, energy, and spacetime are conserved with respect to creation of the hyperbolic electron which is repelled from a gravitating body, the Earth. The gravitationally ejected hyperbolic electron gains energy as it is repelled ($> 10^4\ eV$). The ejection of a hyperbolic electron having a negatively curved velocity surface from the Earth must result in an infinitesimal decrease in its radius of the Earth (e.g. r of the Schwarzschild metric given by Eq. (26.2) where $m_0 = M$ is the mass of the Earth). The amount that the gravitational potential energy of the Earth is lowered is equivalent to the energy gained by the repelled hyperbolic electron.

Momentum is also conserved for the electron, Earth, and helium atom wherein the gravitating body that repels the hyperbolic electron, the Earth, receives an equal and opposite change of momentum with respect to that of the electron.

Causing a satellite to follow a hyperbolic trajectory about a gravitating body is a common technique to achieve a gravity assist to further propel the satellite. In this case, the energy and momentum gained by the satellite is also equal and opposite that lost by the gravitating body.

The kinetic energy of the hyperbolic electron corresponding to a

velocity of $2.187691\,X\,10^6\,m/s$ is $T = 42.3\,eV$. Thus, $42.3\,eV$ may be imparted to the antigravity device per hyperbolic electron. With a beam current of 10^5 amperes achieved in one embodiment by multiple beams such as 100 beams each providing 10^3 amperes, the power transferred to the device P_{AG} is

$$P_{AG} = \frac{10^5 \text{ coulomb}}{\text{sec}} \text{ X } \frac{1 \text{ electron}}{1.6 \text{ X } 10^{-19} \text{ coulombs}} \text{ X } \frac{42.3 \text{ eV}}{\text{electron}} \text{ X } \frac{1.6 \text{ X } 10^{-19} \text{J}}{\text{eV}} = 4.2 \text{ MW} \tag{26.104}$$

The power dissipated against gravity P_G is given by

$$P_G = m_c g v_c \tag{26.105}$$

where m_c is the mass of the craft, g is the acceleration of gravity, v_c is the velocity of the craft. In the case of a $10^4\,kg$ craft, the 4.2 MW of power provided by Eq. (26.104) sustains a steady lifting velocity of 43 m/sec. Thus, significant lift is possible using hyperbolic electrons.

In the case of a $10^4\,kg$ craft, F_g, the gravitational force is

$$F_g = m_c g = \left(10^4\ kg\right)\left(9.8\ \frac{m}{\sec^2}\right) = 9.8\ X\,10^4\ N \tag{26.106}$$

where m_c is the mass of the craft and g is the standard gravitational acceleration. The lifting force may be determined from the gradient of the energy which is approximately the energy dissipated divided by the vertical (relative to the Earth) distance over which it is dissipated. The antigravitational force provided by the hyperbolic electrons may be controlled by adjusting the electric field of the capacitor. For example, the electric field of the capacitor may be increased such that the levitating force overcomes the gravitational force. In an embodiment of the capacitor, the electric field, E_{cap}, is constant and is given by the capacitor voltage, V_{cap}, divided by the distance between the capacitor plates, d, of a parallel plate capacitor.

$$E_{cap} = \frac{V_{cap}}{d} \tag{26.107}$$

In the case that V_{cap} is $10^6\,V$ and d is $1\,m$, the electric field is

$$E_{cap} = \frac{10^6\ V}{m} \tag{26.108}$$

The force of the electric field of the capacitor on a hyperbolic electron, F_{ele}, is the electric field, E_{cap}, times the fundamental charge

$$F_{ele} = eE_{cap} = \left(1.6\ X\,10^{-19}\ C\right)\left(10^6\ \frac{V}{m}\right) = 1.6\ X\,10^{-13}\ N \tag{26.109}$$

The distance traveled away from the Earth, Δr_z, by a hyperbolic electron having an energy of $E = 42.3\,eV = 6.77\,X\,10^{-18}\,J$ is given by the energy divided by the electric field F_{ele}

$$\Delta r_z = \frac{E}{F_{ele}} = \frac{6.77\ X\ 10^{-18}\ J}{1.6\ X\ 10^{-13}\ N} = 4.23\ X\ 10^{-5}\ m = 0.0423\ mm \qquad (26.110)$$

The number of electrons N_e is given by

$$N_e = \frac{I}{e v_e r_i} \qquad (26.111)$$

where I is the current, e is the fundamental electron charge, v_e is the hyperbolic electron velocity, r_i is the length of the current. Substitution of $I = 10^5\ A$, $v_e = v_0 = 2.187691\ X\ 10^6\ m/s$, and $r_i = 0.2\ m$, the number of electrons is

$$N_e = 1.5\ X\ 10^{18}\ \text{electrons} \qquad (26.112)$$

The antigravitational force, F_{AG}, is given by multiplying the number of electrons (Eq. (26.112)) by the force per electron (Eq. (26.109)).

$$F_{AG} = N_e F_e = \left(1.5\ X\ 10^{18}\ \text{electrons}\right)\left(1.6\ X\ 10^{-13}\ N\right) = 2.4\ X\ 10^5\ N \qquad (26.113)$$

Thus, the present example of an antigravity device may provide a levitating force that is capable of overcoming the gravitational force on the craft to achieve a maximum vertical velocity of 43 m/sec as given by Eq. (26.105). In an embodiment of the antigravity device, the hyperbolic electron current and the electric field of the capacitor are adjusted to control the vertical acceleration and velocity.

Levitation by an antigravitational force is orders of magnitude more energy efficient than conventional rocketry. In the former case, the energy dissipation is converted directly to gravitational potential energy as the craft is lifted out of the gravitation field. Whereas, in the case of rocketry, matter is expelled at a higher velocity than the craft to provide thrust or lift. The basis of rocketry's tremendous inefficiency of energy dissipation to gravitational potential energy conversion may be determined from the thrust equation. In a case wherein external forces including gravity are taken as zero for simplicity, the thrust equation is [9]

$$v = v_0 + V \ln \frac{m_0}{m} \qquad (26.114)$$

where v is the velocity of the rocket at any time, v_0 is the initial velocity of the rocket, m_0 is the initial mass of the rocket plus unburned fuel, m is the mass at any time, and V is the speed of the ejected fuel relative to the rocket. Owing to the nature of the logarithmic function, it is necessary to have a large fuel to payload ratio in order to attain the large speeds needed for satellite launching, for example.

The antigravitational force of hyperbolic electrons can be increased by using atoms of the neutral atom beam of relativistic kinetic energy. The electrons of the electron beam and the relativistic atoms of the neutral atomic beam intersect at an angle such that the

relativistically contracted radius of each atom, z_o, is equal to ρ_o, the radius of each free electron of the electron beam. Elastic scattering produces hyperbolic electrons at relativistic energies. The relativistic radius of helium is calculated by substitution of the relativistic mass (Eq. (24.14)) of helium

$$m = \frac{m_0}{\sqrt{1 - \frac{v^2}{c^2}}} \tag{26.115}$$

into Eq. (7.19) with a_o given by Eq. (1.168) where Eq. (26.115) is transformed from Cartesian coordinates to spherical coordinates. In a preferred embodiment, the relativistic atomic beam which intersects the electron beam directed along the negative x-axis is oriented at an angle of $\frac{\pi}{4}$ to both the xz and yz-planes with the relativistic radius of each neutral atom equal to the radius of each free electron.

In another embodiment, high energy hyperbolic electrons are created by scattering according to Eq. (26.75) and Eq. (26.78) from hydrino atoms of small radii. Since hydrino atoms form hydrino hydride ions for $p \leq 24$, hydrino atoms of $p > 24$ are preferably used.

In another embodiment shown in Figure 26.5, hyperbolic electrons are accelerated to relativistic energies by an acceleration means 7 before entering or within the capacitor means 3 to provide relativistic hyperbolic electrons with increased energy to be converted to gravitational potential energy as the body to be levitated is levitated.

In the case of relativistic hyperbolic electrons, the distance traveled in order to transfer a substantial amount of the kinetic energy of the hyperbolic electron to an axis parallel to that of the radius of the Earth is much greater than the case of low hyperbolic electron velocities. With a relativistic hyperbolic electron initially propagating in the direction perpendicular to the radius of the Earth, a path length of many meters may be required for the hyperbolic electron to act on the capacitor. In one embodiment of the antigravity device, a capacitor may further comprise a synchrotron for forcing the hyperbolic electron in a orbit with a component of the velocity in the xy-plane such as that shown in Figure 26.7 which is perpendicular to the radius of the Earth. The hyperbolic electron held in a synchrotron orbit in the xy-plane is repelled by the Earth and transfers a force to the capacitor in the z direction as shown in Figure 26.7.

Figure 26.7. Helical motion of a hyperbolic electron in a synchrotron orbit in the xy-plane with an antigravitational acceleration along the +z axis which is transferred to the capacitor.

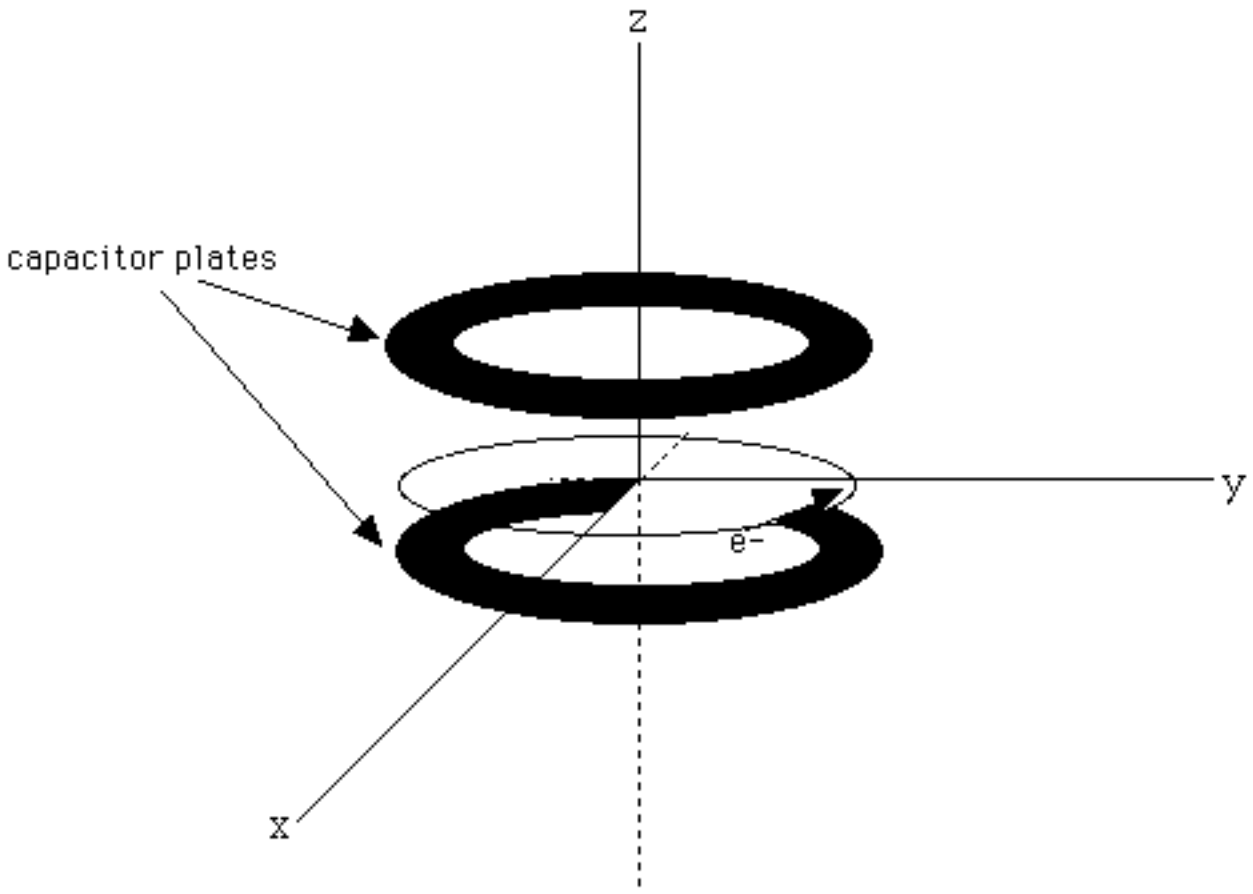

MECHANICS

In addition to levitation, acceleration in a direction tangential to the gravitating body's surface can be effected via conservation of angular momentum. Thus, a radially accelerated structure such as an aerospace vehicle to be tangentially accelerated possesses a cylindrically or spherically symmetrically movable mass having a moment of inertia, such as a flywheel device. The flywheel is rotated by a driving device which provides angular momentum to the flywheel. Such a device is the electron beams which are the source of hyperbolic electrons. The electrons move rectilinearly until being elastically scattered from an atomic beam to form hyperbolic electrons which are deflected in a radial direction from the center of the gravitating body. A component

to the initial momentum of the electron beam is transferred to the gravitating body as the hyperbolic electrons are deflected upward by the gravitating body. The opposite momentum is transferred to the source of the electron beam. This momentum may be used to translate the craft in a direction tangential to the gravitating body's surface or to cause it to spin. Thus, the electron beam serves the additional function of a source of transverse or angular acceleration. Thus, it may be considered an ion rocket.

The vehicle is levitated using antigravity means to overcome the gravitational force of the gravitating body where the levitation is such that the angular momentum vector of the flywheel is parallel to the radial or central vector of the gravitational force of the gravitating body. The angular momentum vector of the flywheel is forced to make a finite angle with the radial vector of gravitational force by tuning the symmetry of the levitating (antigravitational) forces provided by an antigravity apparatus comprising multiple elements at different spatial locations of the vehicle. A torque is produced on the flywheel as the angular momentum vector is reoriented with respect to the radial vector due to the interaction of the central force of gravity of the gravitating body, the force of antigravity of the antigravity means, and the angular momentum of the flywheel device. The resulting acceleration which conserves angular momentum is perpendicular to the plane formed by the radial vector and the angular momentum vector. Thus, the resulting acceleration is tangential to the surface of the gravitating body.

Large translational velocities are achievable by executing a trajectory which is vertical followed by a precession with a large radius that gives a translation to the craft. The latter motion is effected by tilting the spinning craft to cause it to precess with a radius that increases due to the force provided by the craft acting as an airfoil. The tilt is provided by the activation and deactivation of multiple antigravitational devices spaced so that the desired torque perpendicular to the spin axis is maintained. The craft also undergoes a controlled fall and gains a velocity that provides the centrifugal force to the precession as the craft acts as an airfoil. During the translational acceleration, energy stored in the flywheel is converted to kinetic energy of the vehicle. As the radius of the precession goes to infinity the rotational energy is entirely converted into transitional kinetic energy. The equation for rotational kinetic energy E_R and translational kinetic energy E_T are given as follows:

$$E_R = \frac{1}{2} I\omega^2 \tag{26.116}$$

where I is the moment of inertia and ω is the angular rotational frequency;

$$E_T = \frac{1}{2} m v^2 \tag{26.117}$$

where m is the total mass and v is the translational velocity of the craft. The equation for the moment of inertia I of the flywheel is given as:

$$I = \sum m_i r^2 \tag{26.118}$$

where m_i is the infinitesimal mass at a distance r from the center of mass. Eqs. (26.116) and (26.118) demonstrate that the rotational kinetic energy stored for a given mass is maximized by maximizing the distance of the mass from the center of mass. Thus, ideal design parameters are cylindrical symmetry with the rotating mass, flywheel, at the perimeter of the vehicle.

The equation that describes the motion of the vehicle with a moment of inertia I, a spin moment of inertial I_s, a total mass m, and a spin frequency of its flywheel of S is given as follows [10]:

$$mgl\sin\theta = I\ddot{\theta} + I_s S\dot{\phi}\sin\theta - I\dot{\phi}^2\cos\theta\sin\theta \tag{26.119}$$

$$0 = I\frac{d}{dt}\left(\dot{\phi}\sin\theta\right) - I_s S\dot{\theta} + I\dot{\theta}\dot{\phi}\cos\theta \tag{26.120}$$

$$0 = I_s\dot{S} \tag{26.121}$$

where θ is the tilt angle between the radial vector and the angular momentum vector, $\ddot{\theta}$ is the acceleration of the tilt angle θ, g is the acceleration due to gravity, l is the height to which the vehicle levitates, and $\dot{\phi}$ is the angular precession frequency resulting from the torque which is a consequence of tilting the craft. Eq. (26.121) shows that S, the spin of the craft about the symmetry axis, remains constant. Also, the component of the angular momentum along that axis is constant.

$$L_z = I_s S = \text{constant} \tag{26.122}$$

Eq. (26.120) is then equivalent to

$$0 = \frac{d}{dt}\left(I\dot{\phi}\sin^2\theta + I_s S\cos\theta\right) \tag{26.123}$$

so that

$$I\dot{\phi}\sin^2\theta + I_s S\cos\theta = B = \text{constant} \tag{26.124}$$

The craft is an airfoil which provides the centrifugal force to move the center of mass of the craft away from the Z axis of the stationary frame. The schematic appears in Figure 26.8.

Figure 26.8. Schematic of the forces on a spinning craft which is caused to tilt.

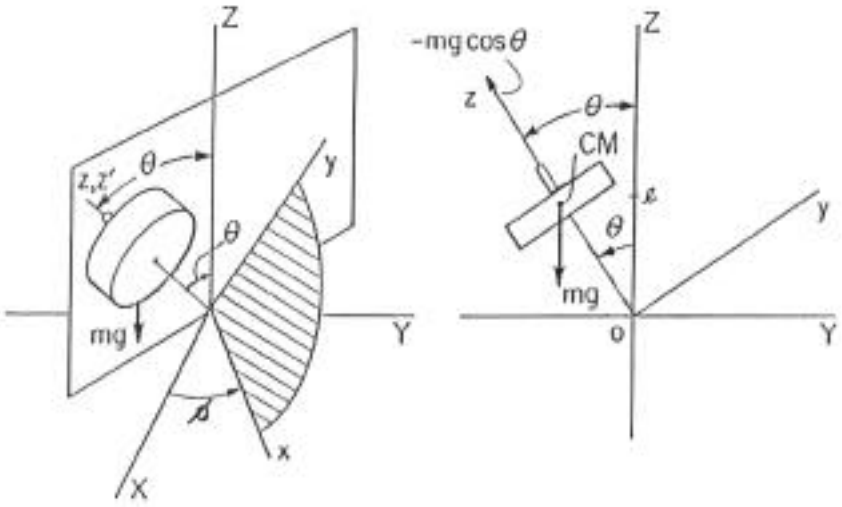

If there is no drag acting on the spinning craft to dissipate its energy E, then the total energy E equal to the kinetic T and potential V remains constant:

$$\frac{1}{2}\left(I\omega_x^2 + I\omega_y^2 + I_s S^2\right) + mgl\cos\theta = E \tag{26.125}$$

or equivalently in terms of Eulerian angles,

$$\frac{1}{2}\left(I\dot{\theta}^2 + I\dot{\phi}^2\sin^2\theta + I_s S^2\right) + mgl\cos\theta = E \tag{26.126}$$

From Eq. (26.124), $\dot{\phi}$ may be solved and substituted into Eq. (26.126). The result is

$$\frac{1}{2}I\dot{\theta}^2 + \frac{\left(B - I_s S\cos\theta\right)^2}{2I\sin^2\theta} + \frac{1}{2}I_s S^2 + mgl\cos\theta = E \tag{26.127}$$

which is entirely in terms of θ. Eq. (26.126) permits θ to be obtained as a function of time t by integration. The following substitution may be made:

$$u = \cos\theta \tag{26.128}$$

Then

$$\dot{u} = -(\sin\theta)\dot{\theta} = -\left(1-u^2\right)^{1/2}\dot{\theta} \tag{26.129}$$

Eq. (26.127) is then

$$\dot{u}^2 = \left(1-u^2\right)\left(2E - I_s S^2 - 2mglu\right)I^{-1} - \left(B - I_s Su\right)^2 I^{-2} \tag{26.130}$$

or

$$\dot{u}^2 = f(u) \tag{26.131}$$

from which u (hence θ) may be solved as a function of t by integration:

$$t = \int \frac{du}{\sqrt{f(u)}} \tag{26.132}$$

In Eq. (26.132), $f(u)$ is a cubic polynomial, thus, the integration may be carried out in terms of elliptic functions. Then the precession velocity $\dot{\phi}$ may be solved may be solved by substitution of θ into Eq. (26.124) wherein the constant B is the initial angular momentum of the craft along the spin axis, $I_s S$ given by Eq. (26.122). The radius of the precession is given by

$$R = l\sin\theta \tag{26.133}$$

And the linear velocity v of the precession is given by

$$v = R\dot{\phi} \tag{26.134}$$

The maximum rotational speed for steel is approximately 1100 m/sec [11]. For a craft with a radius of 10 m, the corresponding angular velocity is $\frac{110\ cycles}{\text{sec}}$. In the case that most of the mass of a $10^4\ kg$ was at this radius, the initial rotation energy (Eq. (26.116)) is $6\ X\ 10^9\ J$. As the craft tilts and changes altitude (increases or decreases), the airfoil pushes the craft away from the axis that is radial with respect to the Earth. For example, as the craft tilts and falls, the airfoil pushes the craft into a trajectory which is analogous to that of a gyroscope as shown in Figure 26.8. From Figure 26.8, the centrifugal force provided by the airfoil ($mg\cos\theta$) is always less than the force of gravity on the craft. From Eq. (26.124), the rotational energy is transferred from the initial spin to the precession as the angle θ increases. From Eq. (26.125), the precessional energy may become essentially equal to the initial rotational energy plus the initial gravitational potential energy. Thus, the linear velocity of the craft may reach approximately 1100 m/sec (2500 mph). During the transfer, the craft falls approximately one half the distance of the radius of the precession of the center of mass about the Z axis. Thus, the initial vertical height l must be greater.

In the cases of solar system and interstellar travel, velocities approaching the speed of light may be obtained by using gravity assists from massive gravitating bodies wherein the antigravitational capability of the craft establishes the desired trajectory to maximize the assist.

EXPERIMENTAL

The electron-impact energy-loss spectrum of helium taken in the forward direction with 100 eV incident electrons with a resolution of 0.15 eV by Simpson, Mielczarek, and Cooper [12] showed large energy-loss peaks at 57.7 eV, 60.0 eV, and 63.6 eV. Resonances in the photoionization continuum of helium at 60 eV and in the 63.6 eV region have been observed spectroscopically by Madden and Codling [13] using

synchrotron radiation. Absent was a resonance at 57.7 *eV*. Both Simpson and Madden assign the peaks of their data to two-electron excitation states in helium. Each of these states decays with the emission of an ionization electron of energy equal to the excitation energy minus the ionization energy of helium, 24.59 *eV*. The data of Goruganthu and Bonham [14] shows ejected-energy peaks at 35.5 *eV* and at 39.1 *eV* corresponding to the energy loss peaks of Simpson of 60.0 *eV* and 63.6 *eV*, respectively. The absence of an ejected-energy peak corresponding to the energy-loss peak at 57.7 *eV* precludes the assignment of this peak to a two-electron resonance. The energy of each inelastically scattered electron of incident energy of 100 *eV* corresponding to the energy-loss of 57.7 *eV* is 42.3 *eV*. This is the resonance energy of hyperbolic electron production by electron scattering from helium given by Eq. (26.77). Thus, the 57.7 *eV* energy-loss peak of Simpson arises from inelastic scattering of electrons of 42.3 *eV* from helium with resonant hyperbolic electron production. The production of electrons with velocity functions having negative curvature is experimentally supported.

The electron-impact energy-loss spectrum of helium taken in the forward direction with 400 *eV* incident electrons by Priestley and Whiddington [15] showed large energy-loss peaks at 42.4 *eV*, and 60.8 *eV*. A resonance in the photoionization continuum of helium at 60 *eV* has been observed spectroscopically by Madden and Codling [13] using synchrotron radiation. Absent was a resonance at 42.4 *eV*. Both Priestley and Madden assign the peaks of their data to two-electron excitation states in helium. Each of these states decay with the emission of an ionization electron of energy equal to the excitation energy minus the ionization energy of helium, 24.59 *eV*. The data of Goruganthu and Bonham [14] shows an ejected-energy peak at 35.5 *eV* corresponding to the energy loss peak of Priestley of 60.8 *eV*. The absence of an ejected-energy peak at 17.8 *eV* corresponding to the energy-loss peak at 42.4 *eV* precludes the assignment of this peak to a two-electron resonance. This is the resonance energy of hyperbolic electron production by electron scattering from helium given by Eq. (26.77). Thus, the 42.4 *eV* energy-loss peak of Priestley arises from inelastic scattering of electrons of 42.3 *eV* from helium with resonant hyperbolic electron production. The production of electrons with velocity functions having negative curvature is experimentally further supported.

References

1. Fock, V., The Theory of Space, Time, and Gravitation, The MacMillan Company, (1964).
2. Fang , L. Z., and Ruffini, R., Basic Concepts in Relativistic Astrophysics,

World Scientific, (1983).
3. Fowles, G. R., Analytical Mechanics, Third Edition, Holt, Rinehart, and Winston, New York, (1977), pp. 154-155.
4. Witteborn, F. C., and Fairbank, W. M., Physical Review Letters, Vol. 19, No. 18, (1967), pp. 1049-1052.
5. R. L. Mills, Apparatus and Method for Providing an Antigravitational Force, PCT Patent Appln. No.: PCT/US95/006140 (1994).
6. Bonham, R. F., Fink, M., High Energy Electron Scattering, ACS Monograph, Van Nostrand Reinhold Company, New York, (1974).
7. Fowles, G. R., Analytical Mechanics, Third Edition, Holt, Rinehart, and Winston, New York, (1977), pp. 140-164.
8. Fowles, G. R., Analytical Mechanics, Third Edition, Holt, Rinehart, and Winston, New York, (1977), pp. 154-160.
9. Fowles, G. R., Analytical Mechanics, Third Edition, Holt, Rinehart, and Winston, New York, (1977), pp. 182-184.
10. Fowles, G. R., Analytical Mechanics, Third Edition, Holt, Rinehart, and Winston, New York, (1977), pp. 243-247.
11. J. W. Beams, "Ultrahigh-Speed Rotation", pp. 135-147.
12. Simpson, J. A., Mielczarek, S. R., Cooper, J., Journal of the Optical Society of America, Vol. 54, (1964), pp. 269-270.
13. Madden, R. B., Codling, K., Astrophysical Journal, Vol. 141, (1965), pp. 364-375.
14. Goruganthu, R. R., Bonham, R. A., Physical Review A, Vol. 34, No. 1, (1986), pp. 103-125.
15. Priestley, H., Whiddington, R., Proc. Leeds Phil. Soc., Vol. 3, (1935), p. 81.

LEPTONS

Only three lepton particles can be formed from photons corresponding to the Planck equation energy, the potential energy, and the magnetic energy, where each is equal to the mass energy (Eq. (23.27). As opposed to a continuum of energies, leptons arise from photons of only three energies. Each "resonant" photon can be considered to be the superposition of two photons- each possessing the energy given by Planck's equation, Eq. (23.28) which is equal to the mass energy of the lepton or antilepton, each possessing $\hbar$ of angular momentum, and each traveling at the speed of light in the lab inertial frame.

At particle production, a photon having a radius and a wavelength equal to the Compton wavelength bar of the particle forms a transition state orbitsphere of the particle of the same wavelength. Eq. (23.43) equates the proper and coordinate times at particle production wherein the velocity of the transition state orbitsphere in the coordinate frame is the speed of light and the relationships between the masses energies given by Eq. (23.32) hold. To describe any phenomenon such as the motion of a body or the propagation of light, a definite frame of reference is required. A frame of reference is a certain base consisting of a defined origin and three axes equipped with graduated rules and clocks as described in the Relativity Section. In the case of particle production wherein the velocity is the speed of light, only the time ruler need be defined. By defining a standard ruler for time in the coordinate frame, the mass of the particle is then given in terms of the self consistent system of units based on the definition of the time ruler. The mass of the particle must be experimental measured with the same time ruler as part of a consistent system of units. In the case that MKS units are used, the coordinate time is defined as the second, the permeability of free space is defined as $\mu_0 = 4\pi X 10^{-7}\ Hm^{-1}$, and the mass of the particle is given in kilograms as given in the Particle Production Section. The production of a real particles from a transition state orbitsphere is a spacelike event in terms of special relativity wherein spacetime is contracted by the gravitational radius of the particle during its production as given in the Gravity Section. Thus, the coordinate time is imaginary as given by Eq. (23.43). On a cosmological scale, imaginary time corresponds to spacetime expansion and contraction as a consequence of the harmonic interconversion of matter and energy as given by Eq. (24.40).

THE ELECTRON-ANTIELECTRON LEPTON PAIR

Consider the Planck energy equation, Eq. (23.28). The proper time

is given by

$$\frac{2\pi}{\omega} = 2\pi \frac{\hbar}{mc^2} \tag{27.1}$$

In the lab frame, the relativistic correction of the radius in the derivation of the Planck's equation for the transition state orbitsphere (Eq. (20.12)) is α^{-2}. Substitution of $\alpha^{-2}r$, the relativistically corrected radius; the second which is the definition for the coordinate time in MKS units, and the Compton wavelength bar for the radius r, (Eq. (23.21), into Eq. (23.43) gives

$$2\pi \frac{\hbar}{mc^2} = \sec\sqrt{\frac{2Gm^2}{c\alpha^2\hbar}} \tag{27.2}$$

The Special relativistic factor, α^{-1}, also follows from Eq. (23.34), from Eqs. (2.44) and (2.49), and from Eq. (5.45) of Fowles [1]. The mass of the electron/antielectron in MKS units based on the definition of the coordinate time in terms of the second is

$$m_e = \left(\frac{h\alpha}{\sec c^2}\right)^{\frac{1}{2}} \left(\frac{c\hbar}{2G}\right)^{\frac{1}{4}} = 9.1097\ X\ 10^{-31}\ kg \tag{27.3}$$

A neutrino/antineutrino pair are formed in each of three cases of lepton/antilepton production to conserve linear and angular momentum during the separation of the world lines of each particle and its antiparticle. The neutrino and antineutrino are photons which travel at velocity c and have energy, but no rest mass. The electron/antielectron mass is corrected for the experimental mass/energy deficit of the $18\ eV$ neutrino.

$$m_e = 9.1097\ X\ 10^{-31}\ kg - 18\ eV(\nu_e) = 9.1094\ X\ 10^{-31}\ kg \tag{27.4}$$

$$m_{e\ \text{experimental}} = 9.1095\ X\ 10^{-31}\ kg$$

Conversely, the Newtonian Gravitational Constant, G, can be calculated from Eq. (27.2) by substitution of the experimentally determined mass of the electron.

$$G_{calculated} = 6.644\ X\ 10^{-11}\ \frac{Nm^2}{kg^2}$$

$$G_{\text{experimental}} = 6.666\ X\ 10^{-11}\ \frac{Nm^2}{kg^2}$$

THE MUON-ANTIMUON LEPTON PAIR

Given that the electron is "allowed" by the Planck energy equation (Eq. (23.28)) and that the proper time is given by General Relativity (Eq. (23.38)), the muon (antimuon) mass can be calculated from the potential energy, V, (Eq. (23.27)) and the proper time relative to the electron inertial frame. The muon (antimuon) decays to the electron (antielectron) and may be considered a transient resonance which

decays to the stable lepton, the electron (antielectron). For the lab inertial frame, the relativistic correction of the radius of the transition state orbitsphere given by the potential energy equations (Eq. (20.10) and (20.11)) is α^{-2}. For the electron inertial frame, the relativistic correction relative to the proper frame is the inverse, α^2. Furthermore, the potential energy equation gives an electrostatic energy; thus, the electron inertial time must be corrected by the relativistic factor of 2π relative to the proper time. Multiplication of the right side of Eq. (23.43) by 2π; substitution of m_e, the mass of the electron, for M; substitution of the second which is the definition for the coordinate time in MKS units; substitution of $\alpha^2 r$, the relativistically corrected radius for r, and substitution of the Compton wavelength bar for the radius r, (Eq. (23.21)), into Eq. (23.43) gives the relationship between the proper time and the electron coordinate time.

$$2\pi \frac{\hbar}{mc^2} = 2\pi \sec \sqrt{\frac{2Gm_e\alpha^2 m}{c\hbar}} \tag{27.5}$$

The mass of the muon/antimuon is

$$m_\mu = \frac{\hbar}{c}\left(\frac{1}{2Gm_e(\alpha \sec)^2}\right)^{\frac{1}{3}} = 1.8902\ X\ 10^{-28}\ kg \tag{27.6}$$

The muon/antimuon mass is corrected for the experimental mass/energy deficit of the 0.25 MeV neutrino.

$$m_\mu = 1.890563\ X\ 10^{-28}\ kg - 0.25\ MeV(\nu_\mu) = 1.8857\ X\ 10^{-28}\ kg$$

$$m_{\mu experimental} = 1.8836\ X\ 10^{-28}\ kg$$

THE TAU-ANTITAU LEPTON PAIR

Given that the electron is "allowed" by the Planck energy equation (Eq. (23.28)) and that the proper time is given by General Relativity (Eq. (23.38)), the tau (antitau) mass can be calculated from the magnetic energy (Eq. (23.27)) and the proper time relative to the electron inertial frame. For the lab inertial frame, the relativistic correction of the radius of the transition state orbitsphere given by the magnetic energy equations (Eq. (20.14) and (20.15)) is $\frac{1}{(2\pi)^2\alpha^4}$. For the electron inertial frame, the relativistic correction relative to the proper frame is the inverse, $(2\pi)^2\alpha^4$. Furthermore, the transition state comprises two magnetic moments. For $v = c$, the magnetic energy equals, the potential energy equals the Planck equation energy equals mc^2. The magnetic energy is given by the square of the magnetic field as given by Eqs. (1.122-1.129). The magnetic energy corresponding to particle production is given by Eq. (23.32). Because two magnetic moments are produced the magnetic energy (and corresponding photon frequency) in

the proper frame is two times that of the electron frame. Thus, the electron time is corrected by a factor of two relative to the proper time. Another way Multiplication of the right side of Eq. (23.43) by 2; substitution of m_e, the mass of the electron, for M; substitution of the second which is the definition for the coordinate time in MKS units; substitution of $(2\pi)^2\alpha^4 r$, the relativistically corrected radius for r, and substitution of the Compton wavelength bar for the radius r, (Eq. (23.21)), into Eq. (23.43) gives the relationship between the proper time and the electron coordinate time.

$$2\pi\frac{\hbar}{mc^2} = 2\sec\sqrt{\frac{2Gm_e(2\pi)^2\alpha^4 m}{c\hbar}} \tag{27.7}$$

The mass of the tau/antitau is

$$m_\tau = \frac{\hbar}{c}\left(\frac{1}{2Gm_e}\right)^{\frac{1}{3}}\left(\frac{1}{2\sec\alpha^2}\right)^{\frac{2}{3}} = 3.17\ X\ 10^{-27}\ kg \tag{27.8}$$

The tau/antitau mass is corrected for the experimental mass/energy deficit of the 17 keV neutrino.

$$m_\tau = 3.17\ X\ 10^{-27}\ kg - 17\ keV(\nu_\tau) = 3.17\ X\ 10^{-27}\ kg$$

$$m_{\tau\ \text{experimental}} = 3.17\ X\ 10^{-27}\ kg$$

In each case a nucleus is present during particle/antiparticle production to conserve momentum.

A fourth particle/antiparticle pair can arise by the gravitational potential energy of Eq. (23.27). However, the pair is not observable because the mass gives rise to a singularity for Eq. (23.38).

References

1. Fowles, G. R., Analytical Mechanics, Third Edition, Holt, Rinehart, and Winston, New York, (1977), p. 157.

PROTON AND NEUTRON

Experimental evidence [1] indicates that the proton and neutron each comprise three charged fundamental particles called quarks and three massive photons called gluons. Each quark is found in combination with a gluon. It is demonstrated in the Excited States of the One Electron Atom (Quantization) Section and by Eq. (2.11) that photons trapped inside of an orbitsphere resonator cavity can provide an effective charge at the two dimensional orbitsphere. A model of the nucleons which is consistent with experimentation and the present theory is an orbitsphere of mass and charge held in positive curvature by photons trapped inside of the orbitsphere. This model explains the experimental result that half of the angular momentum of each nucleon is associated with the quarks and half is associated with the gluons. Fundamental particles and photons each carry $\hbar$ of angular momentum. The experimental radius of a proton is $1.3\,X\,10^{-15}\,m$.

$$r_p = 1.3\,X\,10^{-15}\,m \tag{28.1}$$

The Compton wavelength of the proton, $\lambda_{C,p}$, is

$$\lambda_{C,p} = \frac{h}{m_p c} = 1.3214\,X\,10^{-15}\,m \tag{28.2}$$

Substitution of Eq. (1.162) and using Eq. (1.168) yields

$$\lambda_{C,p} = \frac{2\pi a_o m_e}{\alpha^{-1} m_P} = 1.3214\,X\,10^{-15}\,m \tag{28.3}$$

It appears that $\lambda_{C,p} = r_p$. To test this assumption we proceed as follows. We know that a proton is comprised of three quarks and three gluons ("trappe 29.2 The Neutrinopose to form an orbitsphere of radius r_q s

$$r_p = r_q, \text{ and that} \tag{28.4}$$

$$m_P = m_q + m_g'' = m_q'', \tag{28.5}$$

where r_q is the radius of the quarks, m_q is the rest mass of the quarks, m_g'' is the relativistic mass of the gluons, and m_q'' is the relativistic mass of the quarks. The proton is in the ground state and

$$2\pi r_{1,p} = \lambda_{1,p} = 2\pi\lambda_{C,p} \tag{28.6}$$

The boundary condition for the quarks is

$$2\pi r_{n,q} = \lambda_{n,q} = \frac{h}{m_q v_{nq}} = 2\pi r_{1,p} = 2\pi\frac{h}{m_p c} = 2\pi\lambda_{C,p} \tag{28.7}$$

A solution to Eq. (28.7) is $v_{nq} = c$ and $m_q = \frac{m_P}{2\pi}$. When the quark velocity is the speed of light in the photon frame (gluon frame in this case), the relativistic factor, γ, for the lab frame is 2π. Thus, the mass of the quarks in the lab frame (the relativistic mass) is

$$2\pi m_q = 2\pi\, X\, \frac{m_P}{2\pi} = m_P = m_q'' \tag{28.8}$$

Furthermore, the (relativistic) mass of the gluons can be determined.

$$m_g'' = m_P - m_q = m_P\left[1 - \frac{1}{2\pi}\right] \tag{28.9}$$

This is consistent with the experimental result that the gluons [1] comprise the majority of the mass of the proton. The radius of the orbitsphere for $v_{nq} = c$ is then

$$r_{n,q} = r_{1,p} = \lambda_{C,p} = \frac{h}{m_P c} = \frac{\hbar}{m_q c} = 2\pi \text{ x } \frac{a_o m_e}{\alpha^{-1} m_P} = \lambda\!\!\!^{-}_{C,q} \tag{28.10}$$

where $\lambda\!\!\!^{-}_{c,q}$ is the Compton wavelength bar for the quarks. This result is internally consistent and represents the solution of the boundary value problem of the rest mass of the proton.

The quark mass/charge functions and the gluon mass/charge functions must have the same angular dependence. Thus, the force balance equation is

$$\frac{m_q v_n^2}{r_n} = \frac{Z_{eff} e^2}{4\pi\varepsilon_o r_n^2} = \frac{m_q v_n^2}{r_{1p}} = \frac{Z_{eff} e^2}{4\pi\varepsilon_o r_{1p}^2}, \text{ where} \tag{28.11}$$

$$v_n = \frac{\hbar}{m_q r_{1p}} \tag{28.12}$$

The result of the substitution of Eq. (28.12) in Eq. (28.11), $r_{1,p} = \lambda_{C,p}$, and $m_q = \frac{m_P}{2\pi}$ is that $Z_{eff} = \alpha^{-1}$, and $n = \alpha$. Thus, Z_{eff}, the magnitude of the gluon field is α^{-1}. The potential energy of the quarks is then

$$V_q = \frac{\alpha^{-1} e^2}{4\pi\varepsilon_o r_{1p}} = \frac{m_p}{2\pi} c^2 \tag{28.13}$$

Thus, the total energy of the proton is

$$E = m_q c^2 + m_g c^2 = \frac{m_p}{2\pi} c^2 + m_P\left[1 - \frac{1}{2\pi}\right] c^2 = m_P c^2 \tag{28.14}$$

The neutron rest mass, m_N, the rest mass for the neutron quarks, the Compton wavelength of the neutron, and the Compton wavelength bar of the neutron quarks are obtained in a similar fashion.

$$\lambda_{C,n} = \lambda\!\!\!^{-}_{c,q} = \frac{2\pi a_o m_e}{\alpha^{-1} m_N} = 1.3196\, X\, 10^{-15}\ m = r_{1,n} \tag{28.15}$$

$$m_q = \frac{m_N}{2\pi} \tag{28.16}$$

$$m_g'' = m_N - m_q = m_N\left[1 - \frac{1}{2\pi}\right] \tag{28.17}$$

QUARK AND GLUON FUNCTIONS

Spherical harmonics are solutions to Laplace's Equations in spherical coordinates, and the constant orbitsphere is also a solution. All matter and energy is a linear combination of these functions. Thus, matter is created as an orbitsphere with mass/charge being linear combinations of spherical harmonics and constant functions. And, photons whose electric fields are linear combinations of solutions to Laplace's Equation, spherical harmonics and constant angular functions, can be trapped in the orbitsphere at the creation of matter from energy. (See the Excited States of the One Electron Atom (Quantization) Section and Atomic Coulomb Field Collapse--Hydrino Theory--BlackLight Process Section for the equations of these photons.) The proton and the neutron are such hybrids of matter and energy. The proton and neutron can each be viewed as being comprised of a linear combination of three quarks possessing mass and charge and three gluons (photons) which hold the orbitsphere comprised of three quarks per nucleon in positive curvature. The proton orbitsphere is comprised of an up, up, and a down quark, and the neutron is comprised of a down, down, and an up quark where the charge of an up quark is $+\frac{2}{3}e$ and the charge of a down quark is $-\frac{1}{3}e$. Each quark is associated with its gluon where the quark mass/charge function has the same angular dependence as the gluon mass/charge function.

To be consistent with experimentation, we choose a solution that is a linear combination of the three spherical harmonic functions, corresponding to $\ell = 1$, and three constant orbitspheres. This resultant function can be viewed as being comprised of three separate particles. The three functions are orthogonal, and the corresponding gluon potentials have the same angular dependence as each other and each quark where there exists a one to one correspondence between each quark and each gluon.

The Proton

The proton functions can be viewed as a linear combination of three fundamental particles, three quarks, of $+\frac{2}{3}e$, $+\frac{2}{3}e$, $-\frac{1}{3}e$. The magnitude of Z_{eff} of the radial gluon electric field for a proton is given by the solution of Eq. (28.11) as α^{-1}, and $r_1 = \frac{2\pi a_o m_e}{\alpha^{-1} m_p}$. The unnormalized quark mass function of a proton is

$$\frac{m_P}{2\pi}\left\{\frac{1}{3}(1+\sin\theta\sin\phi)+\frac{1}{3}(1+\sin\theta\cos\phi)+\frac{1}{3}(1+\cos\theta)\right\} \quad (28.18)$$

The unnormalized charge function of the quarks of a proton is

$$e\left\{\frac{2}{3}(1+\sin\theta\sin\phi)+\frac{2}{3}(1+\sin\theta\cos\phi)-\frac{1}{3}(1+\cos\theta)\right\} \quad (28.19)$$

The gluons comprise three orthogonal elliptical polarized photon orbitsphere as given in the Equation of the Photon Section. The gluons travel with the quarks at $v = c$ (Eq. (28.7); thus, the gluons provide a central field. The potential function of the gluons of a proton is

$$\Phi(r,\theta,\phi)=\frac{\alpha^{-1}e}{8\pi\varepsilon_o r^2}\left\{\frac{3}{2}(1+\sin\theta\sin\phi)+\frac{3}{2}(1+\sin\theta\cos\phi)-3(1+\cos\theta)\right\} \quad (28.20)$$

The radial electric field of the gluons of a proton is

$$E_r=\frac{-\alpha^{-1}e}{4\pi\varepsilon_o r^3}\frac{2\pi a_o}{\frac{m_N}{m_e}\alpha^{-1}}\left\{\frac{3}{2}(1+\sin\theta\sin\phi)+\frac{3}{2}(1+\sin\theta\cos\phi)-3(1+\cos\theta)\right\} \quad (28.21)$$

The Neutron

The neutron functions can be viewed as a linear combination of three fundamental particles, three quarks, of charge $+\frac{2}{3}e$, $-\frac{1}{3}e$, and $-\frac{1}{3}e$. The magnitude of Z_{eff} of the radial gluon electric field for a neutron is given by the solution of Eq. (28.11) as α^{-1}, and $r_1=\frac{2\pi a_o m_e}{\alpha^{-1}m_N}$ where m_N is the rest mass of the neutron. The unnormalized quark mass function of a neutron is

$$\frac{m_N}{2\pi}\left\{\frac{1}{3}(1+\sin\theta\sin\phi)+\frac{1}{3}(1+\sin\theta\cos\phi)+\frac{1}{3}(1+\cos\theta)\right\} \quad (28.22)$$

The unnormalized charge function of the quarks of a neutron is

$$e\left\{\frac{2}{3}(1+\sin\theta\sin\phi)-\frac{1}{3}(1+\sin\theta\cos\phi)-\frac{1}{3}(1+\cos\theta)\right\} \quad (28.23)$$

The gluons comprise three orthogonal elliptical polarized photon orbitsphere as given in the Equation of the Photon Section. The gluons travel with the quarks at $v = c$ (Eq. (28.15); thus, the gluons provide a central field The potential function of the gluons of a neutron is

$$\Phi(r,\theta,\phi)=\frac{\alpha^{-1}e}{8\pi\varepsilon_o r^2}\frac{2\pi a_o}{\frac{m_N}{m_e}\alpha^{-1}}\left\{\frac{3}{2}(1+\sin\theta\sin\phi)-3(1+\sin\theta\cos\phi)-3(1+\cos\theta)\right\} \quad (28.24)$$

The radial electric field of the gluons of a neutron is

$$E_r=\frac{-\alpha^{-1}e}{4\pi\varepsilon_o r^3}\frac{2\pi a_o}{\frac{m_N}{m_e}\alpha^{-1}}\left\{\frac{3}{2}(1+\sin\theta\sin\phi)-3(1+\sin\theta\cos\phi)-3(1+\cos\theta)\right\} \quad (28.25)$$

MAGNETIC MOMENTS

The time dependent charge distributions of the proton and the neutron give rise to quadrapole moments and magnetic moments. It is demonstrated in the derivations of the magnetic moments that follow, that the magnetic moment of the proton is purely orbital, the magnetic moment of the neutron is spin and orbital, and only about 30 percent ($\frac{2}{2\pi}$) of the proton's and neutron's spin is found among the quarks based on their contribution to the angular momentum and their contribution to the nucleon mass. The remainder is due to the gluons wherein their angular momentum is given by Eq. (28.31). The predicted parameters are consistent with the experimental evidence [1,2].

Proton Magnetic Moment

The proton is comprised of three orthogonal mass functions-spherical harmonics with ℓ = 1; these are the quarks. In addition, the proton is comprised of three "trapped orthogonal photons", called gluons, of the same angular dependence as the quarks. Each gluon is in phase with a quark.

The combination of a quark and its associated gluon is hereafter referred to as a quark/gluon. The projection of the quark/gluon angular momentum onto the z-axis is given by the sum of the independent projections. The angular momentum of the photon is $\hbar$, and the proton is generated from a photon as demonstrated in the Neutron and Proton Production Section. Thus, the sum of the magnitude of the angular momenta of the three quark/gluons is $\hbar$, and the magnitude of the angular momentum of each quark/gluons is $\frac{\hbar}{3}$. As demonstrated in the Orbital and Spin Splitting Section, the z component of the angular momentum of an excited state electron orbitsphere corresponding to a multipole of order (ℓ, m) is

$$L_z = m\hbar \tag{28.26}$$

Thus, the z projection of the angular momentum of a quark/gluon corresponding to $m_\ell = \pm 1$ is $\pm\frac{\hbar}{3}$. In the case that the two orthogonal up quark/gluons each of charge $+\frac{2}{3}$ are in the xy-plane with $m_\ell = 1$ and the down quark/gluon of charge $-\frac{1}{3}$ is along the z-axis, the magnetic moment is aligned along the z-axis. The magnetic moment is defined [3] as

$$\mu = \frac{\text{charge X angular momentum}}{2 \text{ X mass}} \tag{28.27}$$

The down quark/gluon corresponding to quantum number $m_\ell = 0$ has no magnetic projection on the z-axis. From Eq. (28.7), the mass of the quark function which describes the three quarks is $\frac{m_P}{2\pi}$ and the charge of each up quark/gluon is $+\frac{2}{3}e$. The angular momentum of Eq. (28.27) for the proton is the sum of the z projections of the two up quark/gluons.

$$L_z = \frac{1}{3}\hbar + \frac{1}{3}\hbar = \frac{2}{3}\hbar \tag{28.28}$$

Therefore,

$$\mu_{proton} = \frac{\frac{2}{3}e\frac{2}{3}\hbar}{2\frac{m_P}{2\pi}} = \frac{4}{9}2\pi\frac{e\hbar}{2m_P} = 2.79253\mu_N \tag{28.29}$$

where μ_N is the nuclear magneton $\frac{e\hbar}{2m_p}$. The experimental magnetic moment of the proton is $2.79268\mu_N$.

Neutron Magnetic Moment

The neutron is unstable and undergoes beta decay with a half-life of 12 minutes. Thus, the neutron can be viewed as the sum of an electron, a proton, and the beta decay energy. (The calculation of the energy of beta decay of a neutron is given below.) The magnetic moment of a neutron can be calculated as the sum of the following: $-\mu_N$, the magnetic moment of a constant orbitsphere of charge $-e$ and mass m_N, which corresponds to the beta particle, $\frac{4}{9}2\pi\mu_N$, the magnetic moment of a proton, and the magnetic moment associated with changing an up quark/gluon to a down quark/gluon [See Quark and Gluon Functions of the Proton and Neutron Section]. The contribution due to the transformation of an up quark/gluon to a down quark/gluon is determined as follows:

The fractional change in the quark functions equals the fractional change in the gluon function.

$$\frac{3/2}{3+3+3/2} = \frac{1}{5} \tag{28.30}$$

Substitution of the equation for the time-averaged angular-momentum density, **m**, of a photon (Eq. (4.1)

$$\mathbf{m} = \frac{1}{8\pi}\text{Re}[\mathbf{r} \times (\mathbf{E} \times \mathbf{B}^*)] \tag{28.31}$$

into the vector identity

$$\mathbf{A}\times(\mathbf{B}\times\mathbf{C})=\mathbf{B}(\mathbf{A}\ \mathbf{C})-\mathbf{C}(\mathbf{A}\ \mathbf{B}) \tag{28.32}$$

gives

$$\mathbf{m}=\frac{1}{8\pi}\mathrm{Re}\left[\mathbf{E}(\mathbf{r}\ \mathbf{B}^*)-\mathbf{E}(\mathbf{r}\ \mathbf{E})\right] \tag{28.33}$$

The first term of Eq. (28.33) is zero, and the electric field is radial. Thus,

$$\mathbf{m}=\frac{1}{8\pi}\mathrm{Re}\left[-\mathbf{E}(\mathbf{r}\ \mathbf{E})\right]=-\frac{1}{8\pi}\mathrm{Re}\left[-\mathbf{r}(\mathbf{E}\ \mathbf{E})\right] \tag{28.34}$$

The gluon is a photon that is phase-matched to a quark. The quark/gluon is analogous to the case of an absorbed photon and the corresponding electron in an excited state as described in the Excited States of the One Electron Atom (Quantization) Section. From Eq. (28.27), Eq. (28.30), and Eq. (28.34), the contribution to the change in the magnetic moment of the nucleon from the quark/gluon function is proportional to the dot product of the change in the electric field of the quark/gluon,

$$\frac{1}{5}\ \frac{1}{5}=\frac{1}{25} \tag{28.35}$$

The contribution to the change in the nucleon magnetic moment from a quark/gluon with ℓ = 1 is a factor of three times greater than that of a constant angular distribution of mass (ℓ = 0). The integral of the dot product of the modulation functions (spherical harmonic functions) of each quark/gluon function with itself over all space for all three orthogonal quark/gluons is one, and the integral of the modulation function of the mass of each quark/gluon over the nucleon is zero. The change of an up quark/gluon to a down quark/gluon involves one of the three where ℓ = 1. With the mass of parameter of Eq. (28.27) equal to one third the mass of the nucleon, the contribution to the change in the magnetic moment due to the transformation of an up quark/gluon to a down quark/gluon is

$$3\,X\,\frac{1}{25}\,X\,\mu_N \tag{28.36}$$

The sum of the three components, the magnetic moment of the neutron, μ_n, is

$$\mu_n=\left[1-\frac{4}{9}2\pi-\frac{3}{25}\right]\mu_N=-1.91253\mu_N \tag{28.37}$$

The direction of the positive z-axis is taken as the spin part of the magnetic moment. The experimental magnetic moment of the neutron is $-1.91315\mu_N$.

NEUTRON and PROTON PRODUCTION

Eq. (23.43) equates the proper and coordinate times in the special

case that the velocity of the transition state orbitsphere in the coordinate frame is the speed of light. In this case, the mass of the particle is given by defining a standard ruler for time in the coordinate frame whereby the mass of the particle must be experimental measured with the same time ruler as part of a consistent system of units. In the case that MKS units are used, the coordinate time is defined as the second, the permeability of free space is defined as $\mu_0 = 4\pi X 10^{-7}\ Hm^{-1}$, and the mass of the particle is given in kilograms. The production of a real particles from a transition state orbitsphere is a space-like event in terms of special relativity wherein spacetime is contracted by the gravitational radius of the particle during its production as given in the Gravity Section. Thus, the coordinate time is imaginary as given by Eq. (23.43).

The considerations for the production of leptons and baryons are the same as those for leptons as described in the Leptons Section. Consider the relativistic corrections of the variables of the relationship between the proper and coordinate times, Eq. (23.43), for the production of a neutral particle/antiparticle pair, each comprised of three quarks and three gluons of equivalent mass. The charges of each set of three quarks must sum to zero and the lowest energy nonuniform spherical harmonics are those corresponding to $\ell = 1$; thus, the charges are $-\frac{1}{3}$, $-\frac{1}{3}$, and $+\frac{2}{3}$ for the neutron quarks and $+\frac{1}{3}$, $+\frac{1}{3}$, $-\frac{2}{3}$ for the antineutron quarks. The neutron possesses three quarks of total mass $\frac{m_N}{2\pi}$ (Eq. (28.16)); thus, the mass of each quark is

$$m_{1q} = \frac{m_N}{(3)2\pi} \tag{28.38}$$

The quarks/gluons possess magnetic stored energy. Concomitant with the "capture" of the gluons by the quark resonator cavity, the magnetic flux of the gluons is "captured." To conserve the total quark angular momentum, $\hbar$, the flux is trapped in quanta of the magnetic quantum of flux. The quark/gluon velocity is $v = c$; thus, the magnetic stored energy is $m_N c^2$ (Eq. (20.14 and 20.15)) with m_e replaced by m_N). The mass (energy) released due to magnetic flux "capture" (gluon "capture") follows from Eq. (1.148).

$$mass\ deficit = m_N \frac{\alpha}{2\pi} \tag{28.39}$$

The force corresponding to this mass deficit is the strong nuclear force (which is calculated for the deuterium nucleus in the Strong Nuclear Force Section). Combining Eqs. (28.38) and (28.39) gives the bound individual quark mass

$$m_{1q} = \frac{m_N}{3}\left[\frac{1}{2\pi} - \frac{\alpha}{2\pi}\right] \tag{28.40}$$

The radius of the quark orbitsphere at neutron production and thereafter is given by Eq. (28.15). No particles or fields propagate out from the event radius at the speed of light; thus, the lab frame radius relativistically corrected relative to the $v = c$ inertial frame is given by Eq. (20.13) and Eq. (28.15) as $(2\pi)^2 r$. The velocity of the quarks in the proper frame is $v = c$ (Proton and Neutron Section); thus, the proper time is relativistically dilated by a factor of 2π. Multiplication of the left side of Eq. (23.43) by 2π; substitution of the second which is the definition for the coordinate time in MKS units; substitution of $(2\pi)^2 r$ for r; substitution of the Compton wavelength bar for the radius r (Eq. (23.21)), and substitution of Eq. (28.40) for M into Eq. (23.43) gives the relationship between the neutron proper time and the coordinate time.

$$2\pi \frac{2\pi\hbar}{\frac{m_N}{3}\left[\frac{1}{2\pi} - \frac{\alpha}{2\pi}\right]c^2} = \sec\sqrt{\frac{2G\left[\frac{m_N}{3}\left[\frac{1}{2\pi} - \frac{\alpha}{2\pi}\right]\right]^2}{3c(2\pi)^2\hbar}} \tag{28.41}$$

The neutron mass in MKS units based on the definition of the coordinate time in terms of the second is

$$\begin{aligned} m_{N\ calculated} &= (3)(2\pi)\left(\frac{1}{1-\alpha}\right)\left(\frac{2\pi\hbar}{\sec c^2}\right)^{\frac{1}{2}}\left(\frac{2\pi(3)c\hbar}{2G}\right)^{\frac{1}{4}} \\ &= 1.6744X10^{-27}\ kg \\ m_{N\text{experimental}} &= 1.6749X10^{-27}\ kg \end{aligned} \tag{28.42}$$

The energy of the neutron can be lowered by neutron decay to a proton and a beta. The proton mass calculated from the neutron decay reaction given in the Weak Nuclear Force: Beta Decay of the Neutron Section is $1.672648\,X\,10^{-27}\,kg$. The experimental proton mass is $1.672648\,X\,10^{-27}\,kg$.

Three families of quarks arise from Eq. (23.27) as given in the case of the leptons in the Leptons Section.

Proton production is given in the Weak Nuclear Force: Beta Decay of the Neutron Section via Beta decay of the neutron.

References

1. Science News, Vol. 135, (1989), p. 215.
2. Science News, Vol. 152, (1997), pp. 158-159.
3. McQuarrie,D. A., Quantum Chemistry, University Science Books, Mill Valley, CA, (1983), pp. 238-241.

THE WEAK NUCLEAR FORCE: BETA DECAY OF THE NEUTRON

BETA DECAY ENERGY

The nuclear reaction for the beta decay of a neutron is

$$^1n \rightarrow ^1H + \beta + \bar{\nu}_e + 0.7835\ MeV \tag{29.1}$$

where $\bar{\nu}_e$ is the electron antineutrino. The beta decay energy, E_β, can be calculated from conservation of mass/energy

$$E_\beta = E_n - E_p - E_e \tag{29.2}$$

where E_n, E_p, and E_e are the mass/energy of the neutron, proton, and electron. Thus,

$$E_{beta\ decay} = (m_n - m_P - m_e)c^2 \tag{29.3}$$
$$= 0.7835 MeV$$

The experimental value is 0.7835 MeV.

Neutron decay results in the change of the nuclear moment from that of a neutron $\left(1 - \frac{4}{9}2\pi - \frac{3}{25}\right)\mu_N$ to that of a proton $(\frac{4}{9}2\pi\mu_N)$ where these terms were determined in the Magnetic Moment Section. The beta decay energy can be calculated from the magnetic, electric, and kinetic energy transformations which occur during the decay. The energy components are the sum of the following:

- the release of E_{mag}, the magnetic energy stored in one μ_N corresponding to the emitted Beta particle-following Beta decay, the Beta particle no longer contains the magnetic fields of the gluons at a radius of $\frac{2\pi a_0}{\frac{m_p}{m_e}\alpha^{-1}} = r_1$, the radius of the proton;
- minus E_{mag} (gluon), the energy to change the gluon field corresponding to a down quark to that corresponding to an up quark;
- minus E_{ele}, the electric energy stored in the electric field of the proton;
- plus T, the initial kinetic energy of the electron at $r_1 = \frac{2\pi a_0}{\frac{m_p}{m_e}\alpha^{-1}}$.

The magnitude of the beta decay contributions are

$$E_{mag} = m_P c^2 \frac{\alpha}{2\pi} = 1.09\ X\ 10^6\ eV\ (Eq.(30.27)) \tag{29.4}$$

$$T = \frac{1}{2}mv^2 = \frac{1}{2}\frac{m_e\hbar^2}{\left(\frac{m_p}{2\pi}\right)^2 r_1^2} = 2.553\ X\ 10^5\ eV \text{ with (Eq. (1.47))} \tag{29.5}$$

$$E_{ele} = \frac{e^2}{8\pi\varepsilon_o r_1} = 5.46\ X\ 10^5\ eV\ (Eq.(1.176)) \quad (29.6)$$

$$E_{mag}(gluon) = \left(\frac{3}{25}\right)^2 E_{mag} = 15.7\ X\ 10^3\ eV \quad (29.7)$$

where the change in the magnetic moment contribution of quark/gluon function is $\frac{3}{25}$ (Eq. (28.36)) and the change in the energy stored in the magnetic field is proportional to the change magnetic moment squared (Eq. (1.122)). Thus, the sum is

$$E_\beta = E_{mag} - E_{mag}(gluon) - E_{ele} + T \quad (29.8)$$

$$E_\beta = 1.09\ X\ 10^6 - 15.7\ X\ 10^3 - 5.46\ X\ 10^5 + 2.553\ X\ 10^5$$

$$E_\beta = 0.7836\ MeV$$

The weak force is the negative gradient of the weak energy.

NEUTRINOS

Furthermore, to conserve energy and linear and angular momentum an electron antineutrino, $\bar{\nu}_e$, is emitted with the beta particle. The antineutrino is a ***unique elliptically polarized photon*** that has handedness (the neutrino and antineutrino have opposite handedness), zero rest mass, and travels at the speed c. Consider the photon orbitsphere given in the Equation of the Photon Section. It may comprise magnetic and electric field lines that are constant in magnitude as a function of angle over the surface. Or, the magnitude may vary as a function of angular position (ϕ,θ) on the orbitsphere which corresponds to an elliptically polarized photon. The general photon equation for the electric field is

$$\mathbf{E}_{\phi,\theta} = \frac{e}{4\pi\varepsilon_o r_n^2}\left(-1 + \frac{1}{n}\left[Y_0^0(\theta,\phi) + \mathrm{Re}\left\{Y_\ell^m(\theta,\phi)\left[1 + e^{i\omega_n t}\right]\right\}\right]\right)\delta\left(r - \frac{\lambda}{2\pi}\right);\ \omega_n = 0 \text{ for } m = 0 \quad (29.9)$$

where r_n is the radius of the photon orbitsphere which is equal to $\Delta n a_H$, the change in electron orbitsphere radius given by Eq. (2.21), λ is the photon wavelength which is equal to $\Delta\lambda$, the change in orbitsphere de Broglie wavelength given by Eqs. (2.21), (1.54), and (1.46), and $\omega = \frac{2\pi c}{\lambda}$ is the photon angular velocity which is equal to $\Delta\omega$, the change in orbitsphere angular velocity given by Eqs. (2.21). The magnetic field photon orbitsphere is given by Eqs. (4.14) and (4.2). The nature of the unique elliptically polarized photon orbitsphere which is the antineutrino (neutrino) is determined by the nature of quark/gluon functions and the change in the quark/gluon angular harmonic functions during the transition from a neutron to a proton (proton to a neutron) with the emission of a beta particle (positron). A free quark or a free

gluon is not a stable state of matter, and both are precluded from existence in isolation. Quarks and gluons can only exist in pairs, each comprising a quark and a gluon. In the case of beta decay, a down quark/gluon is converted to an up quark/gluon. Energy and linear momentum are conserved by the emission of an electron antineutrino, $\bar{\nu}_e$, with the beta particle where the maximum energy of the antineutrino is that of the mass deficit. To conserve angular momentum, the electric field, $\mathbf{E}_\theta$, of the electron antineutrino has an angular dependence given by a harmonic function squared corresponding to the change between the initial and final quark/gluon functions where the electric field of each gluon and its corresponding quark are radial and Eq. (28.34) applies.

$$\mathbf{E}_\theta \quad \mathrm{Re}\left\{\left(Y_\ell^m(\theta,\phi)\right)^2\left(1+e^{i\omega_n t}\right)\right\}\delta\left(r-\frac{\lambda}{2\pi}\right)$$
$$\cos^2\theta\,\mathrm{Re}\left(1+e^{i\omega_n t}\right)\delta\left(r-\frac{\lambda}{2\pi}\right)=\left(\frac{1}{2}+\frac{\cos 2\theta}{2}\right)\mathrm{Re}\left(1+e^{i\omega_n t}\right)\delta\left(r-\frac{\lambda}{2\pi}\right) \tag{29.10}$$

where $\ell=1$ and the power is given by Eq. (4.15). In contrast, the electric field of a photon corresponding to electronic transitions (Eq. (29.9) is given by the sum of a constant function plus a spherical harmonic modulation function which averages to zero over a period. The angular momentum of an antineutrino (neutrino) is $-\frac{\hbar}{2}$ ($\frac{\hbar}{2}$); whereas, that of a photon corresponding to an electronic transition is $\pm\hbar$. Due to its unusual angular momentum, the antineutrino and neutrino interact extremely weakly with matter. Essentially, it only has a finite cross-section for processes which involve transitions of two fundamental particles simultaneously. Such cases include beta decay, inverse beta decay, and the hydrino decay reaction (Eq. (23.173))

$$\bar{\nu}_e + {}^1H\left(\frac{a_H}{n}\right) \rightarrow \gamma + \nu_e \tag{29.11}$$

where ν_e is the electron neutrino and $\bar{\nu}_e$ is the electron antineutrino. There are three classes of neutrinos (antineutrinos) corresponding to the electron (antielectron), muon (antimuon), and tau (antitau) as described in the Leptons Section. In the case of the electron neutrino and antineutrino, the energy of the electric and magnetic fields given by Eq. (1.122) and Eq. (1.175), respectively, equals the energy given by the Planck equation (Eq. (4.8)). This equivalence does not hold for the other two types of neutrinos due to Special Relativistic effects that determine the production conditions with General relativistic effects as given in the Leptons Section. Thus, each type of neutrino (antineutrino) is unique, and they cannot be interconverted or interchanged.

QUARKS

Only three quark families can be formed from photons corresponding to the Planck equation energy, the potential energy, and the magnetic energy, where each is equal to the mass energy (Eq. (23.27). As opposed to a continuum of energies, fundamental quark families arise from photons of only three energies. The considerations for the production of baryons are described in the Neutron and Proton Production Section. Consider the relativistic corrections of the variables of the relationship between the proper and coordinate times, Eq. (23.43), for the production of three types of neutral baryon/antibaryon pairs, each comprised of three quarks and three gluons. The charges of each set of three quarks must sum to zero and the lowest energy nonuniform spherical harmonics are those corresponding to $\ell = 1$; thus, the charges are $-\frac{1}{3}$, $-\frac{1}{3}$, and $+\frac{2}{3}$ for the baryon quarks and $+\frac{1}{3}$, $+\frac{1}{3}$, $-\frac{2}{3}$ for the antibaryon quarks. The radius of the quark orbitsphere at baryon production and thereafter follows from by Eq. (28.15). The baryon possesses three quarks of total mass $\frac{m_B}{2\pi}$ (Eq. (28.16)); thus, the mass of each quark is

$$m_{1q} = \frac{m_B}{(3)2\pi} \tag{30.1}$$

The quarks/gluons possess magnetic stored energy. Concomitant with the "capture" of the gluons by the quark resonator cavity, the magnetic flux of the gluons is "captured." To conserve the total quark angular momentum, $\hbar$, the flux is trapped in quanta of the magnetic quantum of flux. The quark/gluon velocity is $v = c$; thus, the magnetic stored energy is $m_B c^2$ (Eq. (20.14) and (20.15)) with m_e replaced by m_B). The mass (energy) released due to magnetic flux "capture" (gluon "capture") follows from Eq. (1.148).

$$mass\ deficit = m_B \frac{\alpha}{2\pi} \tag{30.2}$$

The force corresponding to this mass deficit is the strong nuclear force (which is calculated for the deuterium nucleus in the Strong Nuclear Force Section). Combining Eqs. (30.1) and (30.2) gives the bound individual quark mass

$$m_{1q} = \frac{m_B}{3}\left(\frac{1}{2\pi} - \frac{\alpha}{2\pi}\right) \tag{30.3}$$

No particles or fields propagate out from the event radius at the speed of light; thus, the lab frame radius relativistically corrected relative to the $v = c$ inertial frame is given by Eq. (20.13) and Eq. (28.15) as $(2\pi)^2 r$.

The velocity of the quarks in the proper frame is $v = c$ (Proton and Neutron Section); thus, the proper time is relativistically dilated by a factor of 2π.

Multiplication of the left side of Eq. (23.43) by 2π; substitution of the second which is the definition for the coordinate time in MKS units; substitution of $(2\pi)^2 r$ for r; substitution of the Compton wavelength bar for the radius r (Eq. (23.21)) gives the general equation for principal baryon production as the relationship between the particular neutron proper time and the coordinate time.

$$2\pi \frac{2\pi\hbar}{\frac{m_B}{3}\left(\frac{1}{2\pi} - \frac{\alpha}{2\pi}\right)c^2} = \sec\sqrt{\frac{2GM\left(\frac{m_B}{3}\left(\frac{1}{2\pi} - \frac{\alpha}{2\pi}\right)\right)}{3c(2\pi)^2\hbar}} \tag{30.4}$$

DOWN-DOWN-UP NEUTRON (ddu)

The down-down-up neutron is comprised of a down, down, and an up quark where the charge of a down quark is $-\frac{1}{3}e$, and the charge of an up quark is $+\frac{2}{3}e$. The mass of the down-down-up neutron corresponds to the Planck equation energy given by Eq. (23.28). Substitution of Eq. (30.3) for M into Eq. (30.4) gives the relationship between the down-down-up neutron proper time and the coordinate time.

$$2\pi \frac{2\pi\hbar}{\frac{m_{ddu}}{3}\left(\frac{1}{2\pi} - \frac{\alpha}{2\pi}\right)c^2} = \sec\sqrt{\frac{2G\left(\frac{m_{ddu}}{3}\left(\frac{1}{2\pi} - \frac{\alpha}{2\pi}\right)\right)^2}{3c(2\pi)^2\hbar}} \tag{30.5}$$

The neutron mass in MKS units is

$$m_{ddu\ calculated} = (3)(2\pi)\left(\frac{1}{1-\alpha}\right)\left(\frac{2\pi h}{\sec c^2}\right)^{\frac{1}{2}}\left(\frac{2\pi(3)ch}{2G}\right)^{\frac{1}{4}} \tag{30.6}$$

$$m_{ddu\ calculated} = 1.6744\ X\ 10^{-27}\ kg \tag{30.7}$$

$$m_{ddu\ experimental} = 1.6749\ X\ 10^{-27}\ kg \tag{30.8}$$

STRANGE-STRANGE-CHARMED NEUTRON (ssc)

The strange-strange-charmed neutron is comprised of a strange, strange, and a charmed quark where the charge of a strange quark is $-\frac{1}{3}e$, and the charge of an charmed quark is $+\frac{2}{3}e$. Given that the down-down-up neutron is a solution to Eq. (30.4), other solutions follow from this solution and the other energy solutions.

Consider the case of the potential energy. Given that the down-

down-up neutron is "allowed" by the Planck energy equation (Eq. (23.28)) and that the proper time is given by General Relativity (Eq. (23.38)), the strange-strange-charmed neutron mass can be calculated from the potential energy, V, (Eq. (23.27)) and the proper time relative to the down-down-up neutron inertial frame. Baryons comprised of charmed and strange quarks (antiquarks) decay to baryons of up and down quarks (antiquarks) and may be considered a transient resonance which decays to the stable baryons, the neutron or proton (antineutron or antiproton). For the lab inertial frame, the relativistic correction of the radius of the transition state orbitsphere given by the potential energy equations (Eq. (20.10) and (20.11)) is α^{-2}. For the down-down-up neutron inertial frame, the relativistic correction relative to the proper frame is the inverse, α^2. Furthermore, the potential energy equation gives an electrostatic energy; thus, the down-down-up neutron inertial time must be corrected by the relativistic factor of 2π relative to the proper time. Multiplication of the right side of Eq. (30.4) by 2π and substitution of m_{ddu}, the mass of the down-down-up neutron, for M into Eq. (30.4) gives the relationship between the proper time and the down-down-up neutron coordinate time.

$$2\pi \frac{2\pi\hbar}{\frac{m_{ssc}}{3}\left(\frac{1}{2\pi}-\frac{\alpha}{2\pi}\right)c^2} = 2\pi \sec\sqrt{\frac{2G\alpha^2 m_{ddu}\left(\frac{m_{ssc}}{3}\left(\frac{1}{2\pi}-\frac{\alpha}{2\pi}\right)\right)}{3c(2\pi)^2\hbar}} \tag{30.9}$$

The strange-strange-charmed neutron mass in MKS units is

$$m_{ssc\,calculated} = (3)(2\pi)\left(\frac{1}{1-\alpha}\left(\frac{h}{\sec c^2}\right)^{\frac{2}{3}}\left(\frac{2\pi(3)ch}{2m_{ddu}G\alpha^2}\right)^{\frac{1}{3}}\right) \tag{30.10}$$

$$m_{ssc\,calculated} = 4.90\,X10^{-27}\ kg = 2.75\ GeV/c^2 \tag{30.11}$$

The observed mass of the Ω^- hyperon that contains three strange quarks (sss) is [1].

$$m_{\Omega^-} = 1673\ MeV/c^2 \tag{30.12}$$

Thus, an estimate for the dynamical mass of the strange quark, m_s, is

$$m_s = \frac{m_{\Omega^-}}{3} = \frac{1673\ MeV/c^2}{3} = 558\ MeV/c^2 \tag{30.13}$$

The dynamical mass of the charmed quark, m_c, has been determined by fitting quarkonia spectra; and from the observed masses of the charmed pseudoscalar mesons $D^0(1865)$ and $D^+(1869)$ [2].

$$m_c = 1.580\ GeV/c^2 \tag{30.14}$$

Thus,

$$m_{ssc\,experimental} = 2m_s + m_c = 2(558\ MeV/c^2) + 1673\ MeV/c^2 \tag{30.15}$$

$$m_{ssc\,experimental} = 2.79\ GeV/c^2 \tag{30.16}$$

Eqs. (30.11) and (30.16) are in agreement.

BOTTOM-BOTTOM-TOP NEUTRON (bbt)

The bottom-bottom-top neutron is comprised of a bottom, bottom, and a top quark where the charge of a bottom quark is $-\frac{1}{3}e$, and the charge of a top quark is $+\frac{2}{3}e$. Given that the down-down-up neutron is a solution to Eq. (30.4), other solutions follow from this solution and the other energy solutions.

Consider the case of the magnetic energy. Given that the down-down-up neutron is "allowed" by the Planck energy equation (Eq. (23.28)) and that the proper time is given by General Relativity (Eq. (23.38)), the bottom-bottom-top neutron mass can be calculated from the magnetic energy (Eq. (23.27)) and the proper time relative to the down-down-up neutron inertial frame. As given in the Proton and Neutron Section for the neutron and proton, the bottom-bottom-top neutron and the antibottom-bottom-top neutron radius, r, is given by the Compton wavelength.

$$r = \lambda_{C,bbt} = \frac{h}{m_{bbt}c} \tag{30.17}$$

Furthermore, the transition state comprises two magnetic moments. For $v = c$, the magnetic energy equals the potential energy equals the Planck equation energy equals mc^2. The magnetic energy is given by the square of the magnetic field as given by Eqs. (1.122-1.129). The magnetic energy corresponding to particle production is given by Eq. (23.32). Because two magnetic moments are produced, the magnetic energy (and corresponding photon frequency) in the proper frame is two times that of the down-down-up neutron frame. Thus, the down-down-up neutron time is corrected by a factor of two relative to the proper time. Both the bottom-bottom-top neutron and the antibottom-bottom-top neutron exit the production event in opposite directions with the radius given by Eq. (30.17). Whereas, in the case of tau-antitau production given in the Leptons Section, the radius of the lepton and antilepton increased symmetrically to produce lepton plane waves at infinity relative to each other. Thus, in the lab frame, the mass of the bottom-bottom-top neutron is not corrected by $(2\pi)^2$, and the bottom-bottom-top neutron mass is given by the center of mass for the two baryonic magnetic dipoles.

$$m_{bbt}(center\ of\ mass) = \frac{m_{bbt}}{2} \tag{30.18}$$

Furthermore, for the lab inertial frame, the relativistic correction of the radius of the transition state orbitsphere given by the magnetic energy

equations (Eq. (20.14) and (20.15)) is $\frac{1}{\alpha^4}$. For the down-down-up neutron inertial frame, the relativistic correction relative to the proper frame is the inverse, α^4. Multiplication of the right side of Eq. (23.43) by 2; substitution of m_{ddu}, the mass of the down-down-up neutron, for M and substitution of $\alpha^4 r$, the relativistically corrected radius for r which is multiplied by a factor of two as the correction of the radius corresponding to the reduced bottom-bottom-top neutron mass into Eq. (30.4) gives the relationship between the proper time and the down-down-up neutron coordinate time.

$$2\pi \frac{2\pi\hbar}{\frac{m_{bbt}}{3}\left(\frac{1}{2\pi} - \frac{\alpha}{2\pi}\right)c^2} = 2\sec\sqrt{\frac{2G\alpha^4 m_{ddu}\left(\frac{m_{bbt}}{3}\left(\frac{1}{2\pi} - \frac{\alpha}{2\pi}\right)\right)}{3c2(2\pi)^2\hbar}} \tag{30.19}$$

The bottom-bottom-top neutron mass in MKS units is

$$m_{bbt\ calculated} = (3)(2\pi)\left(\frac{1}{1-\alpha}\right)\left(\frac{2\pi h}{2\sec c^2}\right)^{\frac{2}{3}}\left(\frac{2\pi(3)ch}{m_{ddu}G\alpha^4}\right)^{\frac{1}{3}} \tag{30.20}$$

$$m_{bbt\ calculated} = 3.48\ X\ 10^{-25}\ kg = 195\ GeV/c^2$$

The dynamical mass of the bottom quark, m_b, has been determined by fitting quarkonia spectra; and from the observed masses of the bottom pseudoscalar mesons $B^0(5275)$ and $B^+(5271)$ [2].

$$m_b = 4.580\ GeV/c^2 \tag{30.21}$$

Thus, the predicted dynamical mass of the top quark based on the dynamical mass of the bottom quark is

$$m_{t\ calculated} = m_{bbt\ calculated} - 2m_b = 195\ GeV/c^2 - 2(4.580\ GeV/c^2) \tag{30.22}$$

$$m_{t\ calculated} = 186\ GeV/c^2$$

Recently, two independent groups have reported the experimental mass of the top quark [3]. From about 21 top quark events, the CDF collaboration calculates the mass of the top quark as $176 \pm 13\ GeV/c^2$. From about 17 top quark events, the D0 collaboration calculates the mass of the top quark as $199 \pm 30\ GeV/c^2$.

All other hadrons are given as linear combinations of the fundamental quarks.

References

1. Hughes, I. S., Elementary Particles, Cambridge University Press, (1972), pp. 124-125.
2. Kenyon, I. R., Elementary Particle Physics, Routledge & Kegan Paul, London, (1987), p.196.
3. M. W., Browne, The New York Times, March 3, (1995), A1.

4. I. Peterson, Science News, July 1, (1995), Vol. 148, p. 10.

THE STRONG NUCLEAR FORCE

The Deuterium Nucleus.

The deuterium nucleus is a minimum energy superposition of a neutron and a proton. Thus, the deuterium quark/gluon function is a spherical coordinate orbitsphere solution of Laplace's equation (Eq. (1.1)). The neutron is electrically neutral; thus, no electric term arises in the energy calculation. The neutron and proton quarks of the same kind or flavor are indistinguishable and superimpose to form the deuterium orbitsphere. The gluon electric and magnetic fields of each nucleon superimpose with conservation of stored electric energy density (Eq. (1.175)) and stored magnetic energy density (Eq. (1.122)); however, gluon mass/energy is released as the proton and neutron gluon fields superimpose to provide the central field of the deuterium orbitsphere comprising the linear combination of quarks from both nucleons. The quark/gluons possess magnetic stored energy. Concomitant with the superposition of the neutron with the proton, the quark resonator cavity of the proton traps the magnetic flux of the neutron gluons, and the neutron quark resonator cavity captures the flux of the proton gluons. To conserve the total quark angular momentum of each nucleon, $\hbar$, the flux is trapped in quanta of the quantum of magnetic flux. As shown in the Quark and Gluon Functions of the Proton and Neutron Section, the quark/gluon proper velocity is c. Therefore, the quark/gluon stored magnetic energy is $m_P c^2$ and $m_N c^2$ for the proton and the neutron, respectively (Eqs. (20.14) and (20.15) with m_e replaced by the nucleon mass). The energy released due to the magnetic flux capture, the deuterium binding energy ($E_{Binding}$), follows from Eq. (1.148).

$$E_{Binding} = \left(\frac{\alpha}{2\pi} m_P + \frac{\alpha}{2\pi} m_N\right) c^2 \tag{31.1}$$

$$E_{Binding} = \left(m_P + m_N\right)\frac{\alpha}{2\pi} c^2 \tag{31.2}$$

The calculated mass of deuterium is

$$Mass = \left(m_P + m_N\right)\left(1 - \frac{\alpha}{2\pi}\right) = 2.0141\ AMU \tag{31.3}$$

The experimental mass of deuterium is 2.0140 *AMU*.

K-CAPTURE

Nuclear transition probabilities are derived by Jackson [1]. Formula 16.104 of Jackson applies for K capture where $|Q_{lm} + Q_{lm}^{'}|^2$ and $|M_{lm} + M_{lm}^{'}|^2$ are, respectively, the magnitudes of the electric and magnetic multipole moments between the electron and the nucleus which correspond to equivalent multipole components of the two dimensional charge-density functions of the electron and the nucleus.

References

1. Jackson, J. D., Classical Electrodynamics, Second Edition, John Wiley & Sons, New York, (1962), pp. 758-763.

ALPHA DECAY

ELECTRON TRANSMISSION AND REFLECTION AT A POTENTIAL ENERGY STEP [1]

The electron in free space has its charge-density in a two dimensional plane as given in the Electron in Free Space Section. Electron transition and reflection can be modeled as a plane wave at a potential energy barrier. An electron of total energy E is incident at an angle θ_i upon a potential energy barrier of height V_B as shown in Figure 33.1. The incident and transmitted electron wave vectors are shown in Figure 33.2a.

Figure 33.1. An electron plane wave of wave vector k_i incident at an angle θ_i upon a potential barrier of height V_B.

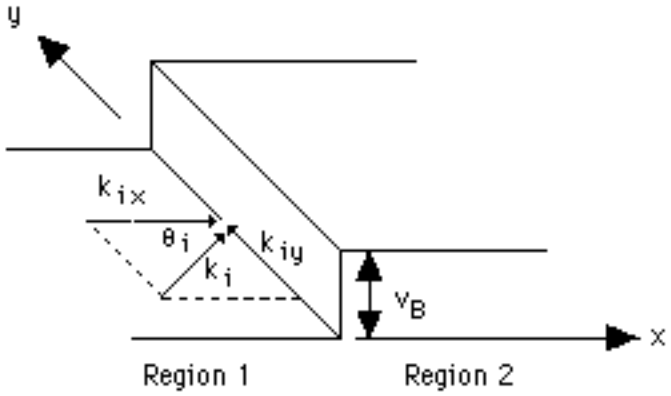

Figure 33.2. Electron wave-vector components parallel (y) and perpendicular (x) to the potential barrier for (a) incident and transmitted electron plane waves and (b) incident and reflected electron plane waves.

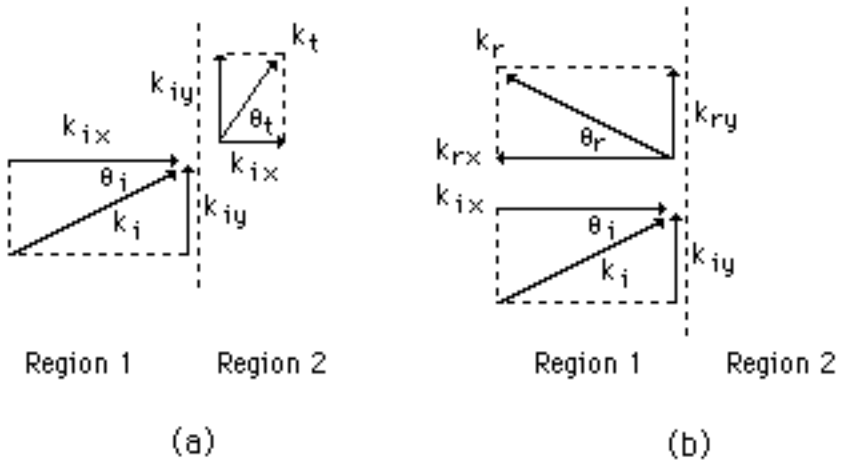

The kinetic energy of an incident electron (region 1) is

$$E = \left(\hbar^2 / 2m_1^*\right)\left(k_{ix}^2 + k_{iy}^2\right) = \left(\hbar^2 / 2m_1^*\right)k_i^2, \tag{33.1}$$

where, m^* is the electron effective mass, k_{ix} and k_{iy} are the components of the incident electron wave vector normal and parallel to the boundary, respectively, and k_i, is the magnitude of the incident electron wave vector which is given by

$$k_i = \left(2m_1^* E\right)^{1/2} / \hbar \tag{33.2}$$

The incident and reflected electron wave vectors are shown in Figure 33.2b. The kinetic energy of a transmitted electron (region 2) is

$$E - V_B = \left(\hbar^2 / 2m_2^*\right)\left(k_{tx}^2 + k_{ty}^2\right) = \left(\hbar^2 / 2m_2^*\right)k_t^2, \tag{33.3}$$

where k_{tx} and k_{ty} are the components of the transmitted electron wave vector normal and parallel to the boundary, respectively, and k_t is the magnitude of the transmitted wave vector which is given by

$$k_t = \left[2m_2^*\left(E - V_B\right)\right]^{1/2} / \hbar \tag{33.4}$$

The phase of the transmitted electron along the boundary must be identical to that of the incident electron wave. This requirement of the continuity of the instantaneous phase at a boundary is commonly referred to as "phase matching." For the transmitted electron wave, the component of the wave parallel to the boundary is

$$k_{ty} = k_{iy} \tag{33.5}$$

The transmitted wave vector normal to the boundary can be obtained by combining Eqs. (33.2), (33.4), and (33.5). The result is

$$k_{tx} = \left[\left(m_2^* / m_1^*\right)\left(k_{ix}^2 + k_{iy}^2\right) - k_{iv}^2 - \left(2m_2^* / \hbar^2\right)V_B\right]^{1/2} \quad (33.6)$$

The kinetic energy of the reflected electron wave (region 1) is

$$E = \left(\hbar^2 / 2m_1^*\right)\left(k_{rx}^2 + k_{ry}^2\right) = \left(\hbar^2 / 2m_1^*\right)k_r^2, \quad (33.7)$$

where k_{rx} and k_{ry} are the components of the reflected electron wave vector normal and parallel to the boundary, respectively, and k_r, is the magnitude of the reflected wave vector which is given by

$$k_r = \left(2m_1^* E\right)^{1/2} / \hbar \quad (33.8)$$

The requirement that the reflected wave also be phase matched to the incident wave means that

$$k_{ry} = k_{iy} \quad (33.9)$$

Since the kinetic energy of a reflected electron is the same as that of an incident electron, then

$$k_{rx} = -k_{ix}, \quad (33.10)$$

and thus implies the angle of reflection, θ_r, is equal to the angle of incidence, θ_i. That is

$$\theta_r = \theta_i \quad (33.11)$$

Equation (33.5) represents the equivalent of Snell's law for electrons. It can be rewritten as

$$k_t \sin\theta_t = k_i \sin\theta_i \quad (33.12)$$

In terms of the electron energies, Eq. (33.5) becomes

$$\frac{\sin\theta_t}{\sin\theta_i} = \frac{k_i}{k_t} = \left(\frac{m_1^* E}{m_2^*\left(E - V_B\right)}\right)^{1/2} \quad (33.13)$$

For isotropic materials, the electron allowed wave-vector surfaces are spheres. For an electron wave obliquely incident upon an infinitely thick potential barrier as shown in Figure 33.1, the allowed wave-vector surfaces may be depicted as shown in Figure 33.3.

Figure 33.3. Allowed wave-vector surfaces for the incident and reflected electron plane wave vectors and for the transmitted plane wave vector.

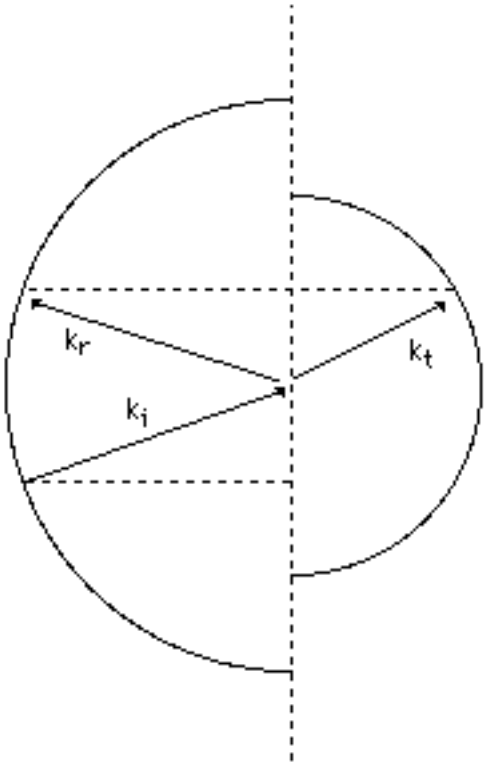

In general the radius of the allowed wave vector surface is

$$k = \left[2m^*(E-V)\right]^{1/2} / \hbar, \tag{33.14}$$

where $E-V$ is the kinetic energy of the electron. The onset of total internal reflection occurs when $\theta_t = 90°$. This happens when the angle of incidence is equal to the critical angle, θ_{ic}. Thus from Eq. (33.13), the critical angle is

$$\theta_{ic} = \begin{cases} \sin^{-1}\left[m_2^* E - V_B / m_1^* E\right]^{1/2} & for \quad E - V_B > 0 \\ 0 & for \quad E - V_B \le 0 \end{cases} \tag{33.15}$$

For an electron wave incident at an angle greater than θ_{ic}, the wave is totally internally reflected for an infinitely thick barrier. At steady state, all of the electron current is reflected back into region 1. The electron wave function decays exponentially into region 2. If the kinetic energy $E - V_B \le 0$, then total internal reflection occurs for any angle of incidence including normal incidence. This is in contrast to the electromagnetic case where total internal reflection can never occur at normal incidence due to the nonzero value of the minimum (free-space) wave-vector magnitude.

TRANSMISSION OUT OF A NUCLEUS - ALPHA DECAY [2]

The equation for the propagation of the electron in free space, a two dimensional plane, is given by the plane wave equation Eq. (3.1):

$$E = E_0 e^{-ik_z z} \tag{33.16}$$

In the case where electrons of kinetic energy K are incident on a rectangular potential barrier whose height V_B is greater than K. V is substituted for V_B and K is substituted for E and the wave vector given by Eq. (33.4) becomes imaginary. An approximate value of T, the transmission probability - the ratio between the number of electrons that pass through the barrier and the number that arrive is given by

$$T = \left[\frac{E}{E_0}\right]^2 \tag{33.17}$$

From Eqs. (33.4), (33.16), and (33.17) the transmission probability is

$$T = e^{-2k_2 L} \tag{33.18}$$

where

$$k_2 = \frac{\sqrt{2m(V-K)}}{\hbar} \tag{33.19}$$

and L is the width of the barrier. Eqs. (33.18) and (33.19) were derived for electrons. However, protons and neutrons are also two dimensional in nature, and alpha particles are comprised of protons and neutrons. Thus, the model applies to alpha particles. Furthermore, Eqs. (33.18) and (33.19) were derived for electrons incident on a rectangular potential barrier; whereas, an alpha particle inside a nucleus is faced with a barrier of varying height, as shown in Figure 33.4.

Figure 33.4. The potential energy of an alpha particle as a function of its distance from the center of the nucleus.

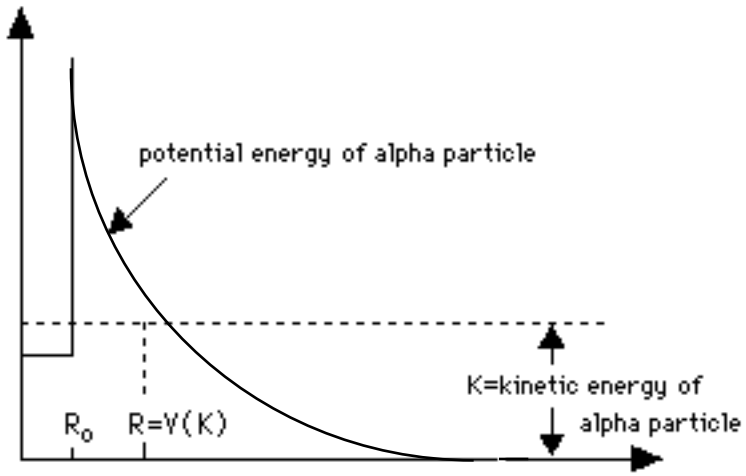

Eqs. (33.18) and (33.19) can be adapted to the case of a nuclear alpha particle. The first step is to rewrite Eqs. (33.18) and (33.19) in the form

$$\ln T = -2k_2 L \tag{33.20}$$

and then express them as the integral

$$\ln T = -2\int_0^L k_2(x)dx = -2\int_{R_0}^R k_2(x)dx \tag{33.21}$$

where R_0 is the radius of the nucleus and R is the distance from its center at which $V = K$. The kinetic energy K is greater than the potential energy V for $x > R$; so, if it can get past R, the alpha particle will have permanently escaped from the nucleus.

The electrical potential energy of an alpha particle at the distance x from the center of a nucleus of charge Ze is given by

$$V(x) = \frac{2Ze^2}{4\pi\varepsilon_0 x} \tag{33.22}$$

Here Ze is the nuclear charge minus the alpha-particle charge of $2e$; thus, Z is the atomic number of the daughter nucleus.

We therefore have

$$k_2 = \frac{\sqrt{2m(V-K)}}{\hbar} = \left(\frac{2m}{\hbar^2}\right)^{1/2}\left(\frac{2Ze^2}{4\pi\varepsilon_0 x} - K\right)^{1/2} \tag{33.23}$$

Since $V = K$ when $x = R$,

$$K = \frac{2Ze^2}{4\pi\varepsilon_0 R} \tag{33.24}$$

and we can express k_2 in the form

$$k_2 = \left(\frac{2mK}{\hbar^2}\right)^{1/2}\left(\frac{R}{x} - 1\right)^{1/2} \tag{33.25}$$

Hence

$$\ln T = -2\int_{R_0}^R k_2(x)dx \tag{33.26}$$

$$= -2\left(\frac{2mK}{\hbar^2}\right)^{1/2}\int_{R_0}^R \left(\frac{R}{x} - 1\right)^{1/2} dx \tag{33.27}$$

$$= -2\left(\frac{2mK}{\hbar^2}\right)^{1/2} R\left[\cos^{-1}\left(\frac{R_0}{R}\right)^{1/2} - \left(\frac{R_0}{R}\right)^{1/2}\left(1 - \frac{R_0}{R}\right)^{1/2}\right]$$

Because the potential barrier is relatively wide, $R >> R_o$, and

$$\cos^{-1}\left(\frac{R_0}{R}\right)^{1/2} \approx \frac{\pi}{2} - \left(\frac{R_0}{R}\right)^{1/2} \tag{33.28}$$

$$\left(1 - \frac{R_0}{R}\right)^{1/2} \approx 1$$

with the result that

$$\ln T = -2\left(\frac{2mK}{\hbar^2}\right)^{1/2} R\left(\frac{\pi}{2} - 2\left(\frac{R_o}{R}\right)^{1/2}\right) \tag{33.29}$$

From the Eq. (33.24)

$$R = \frac{2Ze^2}{4\pi\varepsilon_0 K} \tag{33.30}$$

and so

$$\ln T = \frac{4e}{\hbar}\left(\frac{m}{\pi\varepsilon_0}\right)^{1/2} Z^{1/2}R_0^{1/2} - \frac{e^2}{\hbar\varepsilon_0}\left(\frac{m}{2}\right)^{1/2} ZK^{-1/2} \tag{33.31}$$

The result of evaluating the various constants in Eq. (33.31) is

$$\ln T = 2.97\,Z^{1/2}R_0^{1/2} - 3.95ZK - 1/2 \tag{33.32}$$

where K (alpha-particle kinetic energy) is expressed in MeV, R_o (the nuclear radius) is expressed in fermis ($1\,fm = 10^{-15}\,m$), and Z is the atomic number of the nucleus minus the alpha particle. The decay probability per unit time, λ, can be expressed as the product of the number of times per second, υ, that an alpha particle within the nucleus strikes the potential barrier and the probability, T, that a particle will be transmitted through the barrier. And, υ can be expressed as the alpha particle velocity divided by the nuclear distance. Thus, the decay constant, λ, is given by

$$\lambda = \upsilon T = \frac{v}{2R_0}T \tag{33.33}$$

Taking the natural logarithm of both sides and substituting for the transmission probability ,T, gives

$$\ln\lambda = \ln\left(\frac{v}{2R_0}\right) + 2.97\,Z^{1/2}R_0^{1/2} - 3.95ZK^{-1/2} \tag{33.34}$$

To express Eq. (33.34) in terms of common logarithms, we note that

$$\ln A = \frac{\log_{10} A}{\log_{10} e} = \frac{\log_{10} A}{0.4343} \tag{33.35}$$

and so

$$\log_{10}\lambda = \log_{10}\left(\frac{v}{2R_0}\right) + 0.4343(2.97Z^{1/2}R_0^{1/2} - 3.95ZK^{-1/2}) \tag{33.36}$$

$$\text{Alpha decay constant} = \log_{10}\left(\frac{v}{2R_0}\right) + 1.29Z^{1/2}R_0^{1/2} - 1.72ZK^{-1/2} \tag{33.37}$$

Figure 33.5 is a plot of $\log_{10}\lambda$ *versus* $ZK^{-1/2}$ for a number of alpha-radioactive nuclides.

Figure 33.5. Plot of $\log_{10}\lambda$ *versus* $ZK^{-1/2}$ for a number of alpha-radioactive nuclides.

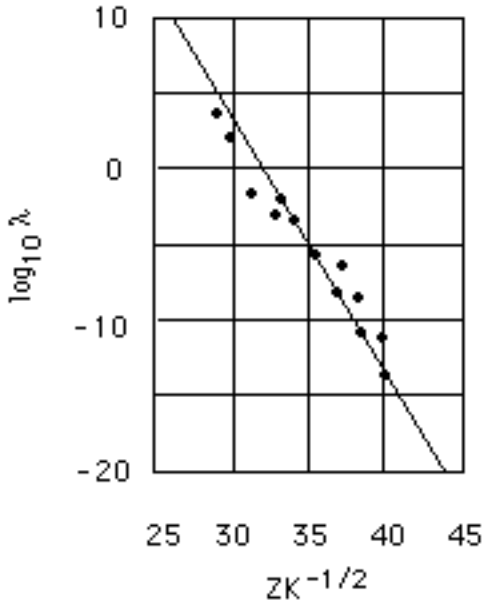

The straight line fitted to the experimental data has the -1.72 slope predicted throughout the entire range of decay constants which is in excellent agreement with the experimental data. We can use the position of the line to determine R_o, the nuclear radius. The result agrees with the results obtained from nuclear scattering experiments. This approach thus constitutes an independent means of determining nuclear sizes.

References

1. Gaylord, T. K., Brennan, K.F., J. Appl. Phys., Vol. 65 (2), (1989), pp. 814-820.
2. Beiser, A, Concepts of Modern Physics, Fourth Edition, McGraw-Hill, New York, (1987),. pp. 462-467.

MÖSSBAUER PHENOMENON

The gluon field of proton or a neutron can transform to another solution of Laplace's Equation by the absorption of a gamma ray which becomes trapped inside the resonator cavity of the orbitsphere comprising the nucleon. This is the Mössbauer Effect. The nuclear size may increase or decrease depending on the effect of the excitation on the strong nuclear force via the absorbed photon field superposing with the gluon field affecting a change in the energy.

SECTION IV

Retrospect

THE SCHRÖDINGER WAVEFUNCTION IN VIOLATION OF MAXWELL'S EQUATIONS

The Schrödinger equation implicitly postulates time harmonic motion of the spatial charge function of the electron. A wave equation was assumed, and the time harmonic motion was eliminated by Schrödinger [1] by substituting de Broglie waves, kinetic and potential energy relationships, and the equation,

$$v = \lambda f \tag{35.1}$$

The solution to the Schrödinger equation is a wave function $\psi(x)$. An interpretation of $\psi(x)$ is required. Schrödinger postulated that $\psi(x)$ represents the amplitude of the particle in some sense, and because the intensity of a wave is the square of the amplitude the "intensity of the particle" is proportional to $\psi^*(x)\psi(x)$ [$\psi^*(x)$ is the complex conjugate of $\psi(x)$]. A controversy arose over the meaning of intensity. Schrödinger considered $e\psi^*(x)\psi(x)$ to be the charge-density or $e\psi^*(x)\psi(x)$ to be the amount of charge between x and $x+dx$. Thus, he presumed the electron to be spread all over the region. The electron has kinetic energy and angular momentum and energy must be conserved; thus, the motion of an electron must be time harmonic. It is demonstrated in the One Electron Atom Section that emission of electromagnetic radiation occurs if the spacetime Fourier transform possesses waves that are synchronous with waves traveling at the speed of light. It is demonstrated below that the Schrödinger wave equations have such components; thus, they must radiate. That no radiation is observed demonstrates the invalidity of these equations as an accurate description of an electron.

The angular functions of Schrödinger wave equations are spherical harmonics and their spacetime Fourier transform is given in the One Electron Atom Section (Spacetime Fourier Transform of the Electron Function) as the transforms of $g(\theta)$, $h(\phi)$, and $k(t)$. The radial solutions (solutions which are a function of the radial variable r) are of the form of r raised to a power times a negative exponential of r. Thus, it is appropriate to take the spacetime Fourier transform of the general solution for psi squared times a time harmonic function (which is proportional to qdr/dt) and apply Haus' nonradiative condition [2]. The most fundamental solution is chosen for analysis. Additional powers of the radial functions would give rise to convolution integrals in Fourier space and additional terms that do not go to zero. The same applies to additional linear terms. It is only necessary to demonstrate that one component does not vanish for $k = \frac{\omega}{c}$.

The spacetime Fourier transform of the radial function $f(r) = re^{-r/a_o}$ follows:

With spherical symmetry [3],

$$G(s) = 4\pi \int_0^\infty g(r)\,\mathrm{sinc}(2sr) r^2 dr\,, \tag{35.2}$$

$$G(s) = 4\pi \int_0^\infty re^{-r/a_o}\,\mathrm{sinc}(2sr) r^2 dr \tag{35.3}$$

Using the definition of the function

$$Sinc\ x = \frac{\sin \pi x}{\pi x} \tag{35.4}$$

Eq. (35.3) becomes,

$$= 4\pi \int_0^\infty r^3 e^{-r/a_o} \frac{\sin 2\pi sr dr}{\pi sr} \tag{35.5}$$

$$= \frac{4}{s} \int_0^\infty r^2 e^{-r/a_o} \sin 2\pi sr dr \tag{35.6}$$

Let

$$r = \frac{r'}{2\pi} \quad and \quad dr = \frac{dr'}{2\pi} \tag{35.7}$$

$$G(s) = \frac{1}{2s\pi^3} \int_0^\infty r'^2 \exp\left(\frac{-r'}{2\pi a_o}\right) \sin sr'\, dr' \tag{35.8}$$

From Bateman [4]:

$$\int_0^\infty x^n e^{-\alpha x} \sin(xy) dx =$$

$$n! \left(\frac{\alpha}{\alpha^2 + y^2}\right)^{n+1} \sum_{m=0}^{\frac{n}{2}} (-1)^m \binom{n+1}{2m+1} \left(\frac{y}{\alpha}\right)^{2m+1} \tag{35.9}$$

Let

$$x = r,\ s = y,\ \alpha = \frac{1}{2\pi a_o},\ n = 2 \tag{35.10}$$

and apply Eq. (35.9) to Eq. (35.8).

$$G(s) = \frac{1}{2s\pi^3} \int_0^\infty r'^2 \exp\left(\frac{-r'}{2\pi a_o}\right) \sin sr'\, dr' = \frac{1}{2s\pi^3} 2! \left(\frac{\frac{1}{2\pi a_o}}{\left(\frac{1}{2\pi a_o}\right)^2 + s^2}\right)^3 \sum_{m=0}^{1} (-1)^m \binom{3}{2m+1} \left(\frac{s}{\frac{1}{2\pi a_o}}\right)^{2m+1} \tag{35.11}$$

The Fourier Transforms of the angular functions are given by Eqs. (1.35) and (1.36), and the Fourier transform of the time harmonic function is given by Eq. (1.37). By Eq. (1.38), the complete spacetime Fourier transform of a Schrödinger wave equation, $W(s,\Theta,\Phi,\omega)$, is the convolution of Eqs. (35.11), (1.35), (1.36), and (1.37).

$$W(s,\Theta,\Phi,\omega) = \frac{1}{2s\pi^3}\, 2!\left(\frac{\frac{1}{2\pi a_o}}{\left(\frac{1}{2\pi a_o}\right)^2 + s^2}\right)^3 \sum_{m=0}^{1}(-1)^m \left(\frac{3}{2m+1}\right)\left(\frac{\frac{s}{1}}{2\pi a_o}\right)^{2m+1}$$

$$2\pi \sum_{\upsilon=1}^{\infty} \frac{(-1)^{\upsilon-1}(\pi\sin\Theta)^{2(\upsilon-1)}}{\upsilon(\upsilon-1)!} \frac{\Gamma\left(\frac{1}{2}\right)\Gamma\left(\upsilon+\frac{1}{2}\right)}{(\pi\cos\Theta)^{2\upsilon+1}2^{\upsilon+1}} \frac{2\upsilon!}{\upsilon!} s^{-2\upsilon}$$

$$2\pi \sum_{\upsilon=1}^{\infty} \frac{(-1)^{\upsilon-1}(\pi\sin\Phi)^{2(\upsilon-1)}}{\upsilon(\upsilon-1)!} \frac{\Gamma\left(\frac{1}{2}\right)\Gamma\left(\upsilon+\frac{1}{2}\right)}{(\pi\cos\Phi)^{2\upsilon+1}2^{\upsilon+1}} \frac{2\upsilon!}{\upsilon!} s^{-2\upsilon}$$

$$\frac{1}{4\pi}\left[\delta(\omega-\omega_n)+\delta(\omega+\omega_n)\right] \tag{35.12}$$

This transform has components $\frac{\omega_n}{c} = k$ which are not zero and are synchronous with waves traveling at the speed of light. Thus, a charge-density function given by the Schrödinger wave equation must radiate in accordance with Maxwell's Equations.

References

1. McQuarrie,D. A., Quantum Chemistry, University Science Books, Mill Valley, CA, (1983), pp. 78-79.
2. Haus, H. A., "On the radiation from point charges", American Journal of Physics, 54, (1986), pp. 1126-1129.
3. Bracewell, R. N., The Fourier Transform and Its Applications, McGraw-Hill Book Company, New York, (1978), pp. 252-253.
4. Bateman, H., Tables of Integral Transforms, Vol. III, McGraw-Hill, New York, (1954), p. 72.

CLASSICAL ELECTRON RADIUS

Electron scattering from neutral atoms and the classical electron radius are tests of the nature of bound electrons as orbitspheres of the Mills model as opposed to point particles of the Schrödinger-Born model.

Electron scattering experiments support the nature of bound electrons as orbitspheres of the Mills model, and the data is inconsistent with the probability point particle model of Schrödinger and Born. Consider the case given in the Derivation of Electron Scattering by Helium Section wherein experimental results by Bromberg [1] were presented. Quoting from Bromberg [1], "At smaller angles; however, the Born approximation calculation fails utterly, the experimental curve rising much more steeply than the theoretical". This point is explicitly demonstrated in Figure 8.4. In contrast, the closed form function (Eqs. (8.55) and (8.56)) for the elastic differential cross section for the elastic scattering of electrons by helium atoms is in agreement with the data of Bromberg as demonstrated in Figure 8.5. In principle, Quantum mechanics cannot adequately describe the results of electron scattering from neutral atoms or the results of the Davidson-Germer experiment. An assembly of point particles cannot give rise to neutral scattering in the absence of the violation of Special Relativity. Otherwise, an internal inconsistency arises - namely violation of the Uncertainty Principle. Rutherford scattering would be predicted from a point particle model.

Furthermore, the radius of the electron according to quantum mechanics is zero and not the classical electron radius as required according to Einstein. The electron must spin in one dimension and give rise to a Bohr magneton, μ_B,

$$\mu_B = \frac{e\hbar}{2m_e} = 9.274\ X\ 10^{-24}\ JT^{-1}, \tag{36.1}$$

The magnetic energy corresponding to the magnetic moment of Eq. (36.1) is

$$E_{mag} = \frac{1}{2}\mu_o \int_0^{2\pi}\int_0^{\pi}\int_0^{\infty} H^2 r^2 \sin\theta\, dr d\theta d\Phi \tag{36.2}$$

$$\mathbf{H} = \frac{e\hbar}{2m_e r^3}(\mathbf{i}_r 2\cos\theta - \mathbf{i}_\theta \sin\theta) \quad for\ r > r_n \tag{36.3}$$

which in the present case is infinity (by substitution of $r = 0$ for the model that the electron is a point particle) not the required mc^2. This interpretation is in violation of Special Relativity [2].

Eq. (20.14) of the Pair Production Section gives the magnetic energy correctly as mc^2. The "effective" orbitsphere radius to be used to calculate the cross section for pair production using the electric energy

of Eq. (20.10) and Eq. (20.11) is the classical electron radius,

$$\alpha^2 a_o = \alpha\lambda\!\!\!^{-}_c = 2.82\,X10^{-13}\ cm\ (CGSunits) \qquad (36.4)$$
$$= 2.82\,X10^{-15}\ m\ (MKS\ units)$$

$$V = -\frac{\alpha^{-2}e^2}{4\pi\varepsilon_o a_o} \qquad (36.5)$$

$$V = m_e c^2 \qquad (36.6)$$

Based on Eqs. (36.5) and (36.6), σ, the geometric cross section of the electron can be derived using the classical electron radius.

$$\sigma = \pi\left(\frac{e^2}{m_e c^2}\right)^2 \qquad (36.7)$$

$$\sigma = \pi\left[\alpha\lambda\!\!\!^{-}_C\right]^2 \qquad (36.8)$$

From the geometric cross section of the electron, the equation for radiation scattering follows from the equation for radiation by a Hertzian dipole

$$I = I_o\frac{8\pi}{3}\frac{\sigma}{\pi} = I_o\frac{8\pi}{3}\left(\frac{e^2}{m_e c^2}\right)^2\ (cgs\ units) \qquad (36.9)$$

which is the formula proposed by Einstein.

Electron-proton force balance exits and the orbitsphere is nonradiative. Mechanics and electrodynamics can both be satisfied simultaneously to achieve these conditions of force balance with cancellation of all radiation fields. Directional antennae arrays are designed using identical principles of achieving cancellation of desired radiation fields. For the electron orbitsphere,

$$\left(\nabla^2 - \frac{1}{v^2}\frac{\delta^2}{\delta t^2}\right)\rho(r,\theta,\phi,t) = 0 \qquad (36.10)$$

And, the Fourier transform of the orbitsphere is zero when,

$$\left(k^2 - \left(\frac{\omega}{c}\right)^2\right) = 0 \qquad (36.11)$$

In contrast, the electron described by a Schrödinger one-electron wave function would radiate. (See The Schrödinger Wavefunction in Violation of Maxwell's Equation Section).

Furthermore, the correct prediction of the elastic scattering of electrons by helium atoms wherein the electron radius is a crucial parameter (Eq. (8.55)), the results of the Stern-Gerlach experiment, the results of the Davidson-Germer experiment, as well as the correct derivation of the electron (fluxon) g factor, the resonant line shape, the Lamb, Shift, spin-orbital coupling energies, and the excited state spectrum of hydrogen wherein ***the correspondence principle holds*** are direct verifications that the electron is an orbitsphere with the calculated radius. Quantum mechanics has failings in each of these

cases.

Two dimensional distributions are common in classical physics. A two dimensional discontinuity in surface current gives rise to a magnetic field; a discontinuity in surface charge gives rise to an electric field. Ampere's and Gauss's Laws also apply in the present theory with respect to the electron. Furthermore, a two dimensional discontinuity in mass according to the Mills model gives rise to a gravitational field which is consistent with General Relativity which leads to the correct prediction of the masses of leptons (Leptons Section), the quarks (Quarks Section), and the classical electron radius as given in Eq. (20.14) of the Pair Production Section wherein the magnetic energy is correctly given as $m_e c^2$ as shown previously.

Furthermore, Born postulated that the electron is a one dimensional delta function -- zero volume and infinite mass. The Schrödinger solutions for the hydrogen atom exclude the existence of energy levels below the "ground" state corresponding to $n = \frac{1}{\text{integer}}$ in the Rydberg formula [3]

$$\bar{\nu} = R\left(\frac{1}{n_f^2} - \frac{1}{n_i^2}\right) \tag{36.12}$$

where $R = 109{,}677\ cm^{-1}$, $n = \frac{1}{2}, \frac{1}{3}, \frac{1}{4}, \ldots$, and $n_i > n_f$. The data given in the Experimental Section proves that the Schrödinger-Born model is incorrect because it is clearly inconsistent with the experimental findings. The two dimensional function given for a bound electron in the One Electron Atom Section and for a free electron in the Electron in Free Space Section is the correct description of the electron. Also, the two dimensional function given in the Photon Equation Section is the correct description for electromagnetic radiation which can give rise to the electron. The models of the Mills theory are supported by the close agreement between experimental observation and theoretical predictions.

References

1. Bromberg, P. J., "Absolute differential cross sections of elastically scattered electrons. I. He, N_2, and CO at 500 eV", The Journal of Chemical Physics, Vol. 50, No. 9, (1969), pp. 3906-3921.
2. Pais, A., "George Uhlenbeck and the discovery of electron spin", Physics Today, 40, (1989), pp. 34-40
3. Maly, J. A., Vavra, J., Fusion Tech., Vol. 24, Nov. (1993), pp. 307-318.

WAVE-PARTICLE DUALITY

> [My father] said, "I understand that they say that light is emitted from an atom when it goes from one state to another, from an excited state to a state of lower energy."
>
> I said, "That's right."
>
> "And light is kind of a particle, a photon, I think they call it."
>
> "Yes."
>
> "So if the photon comes out of the atom when it goes from the excited to the lower state, the photon must have been in the atom in the excited state."
>
> I said, "Well no."
>
> He said, "Well, how do you look at it so you can think of a particle photon coming out without it having been there in the excited state?"
>
> I thought a few minutes, and I said, "I'm sorry; I don't know. I can't explain it to you."
>
> -Richard P. Feynman, *The Physics Teacher* (September 1969).

Many great physicists rejected Quantum Mechanics. Feynman also attempted to use first principles including Maxwell's Equations to discover new physics to replace quantum mechanics [1]. Other great physicists of the 20th century searched. "Einstein [...] insisted [...] that a more detailed, wholly deterministic theory must underlie the vagaries of quantum mechanics" [2]. He felt that scientists were misinterpreting the data. In fact, this is the case. Experiments by the early part of the 20th century had revealed that both light and electrons behave as waves in certain instances and as particles in others. This was unanticipated from preconceptions about the nature of light and the electron. Early 20th century theoreticians proclaimed that light and atomic particles have a wave-particle duality that was unlike anything in our common day experience. The wave-particle duality is the central mystery of quantum mechanics - the one to which all others could ultimately be reduced. Consider the two-slit experiment. A gun (obeying classical physics) sprays bullets towards a target. Before they reach the target, they must pass through a screen with two slits. The pattern they make shows how their probability of arrival varies from place to place. They are more likely to strike directly behind the one slit that they went through as shown in Figure 37.1. The pattern happens to be simply the sum of the patterns for each slit considered separately: if half the bullets were fired with only the left slit open and then half were fired with just the right slit open, the result would be the same.

Figure 37.1. Two-slit experiment with macroscopic particles.

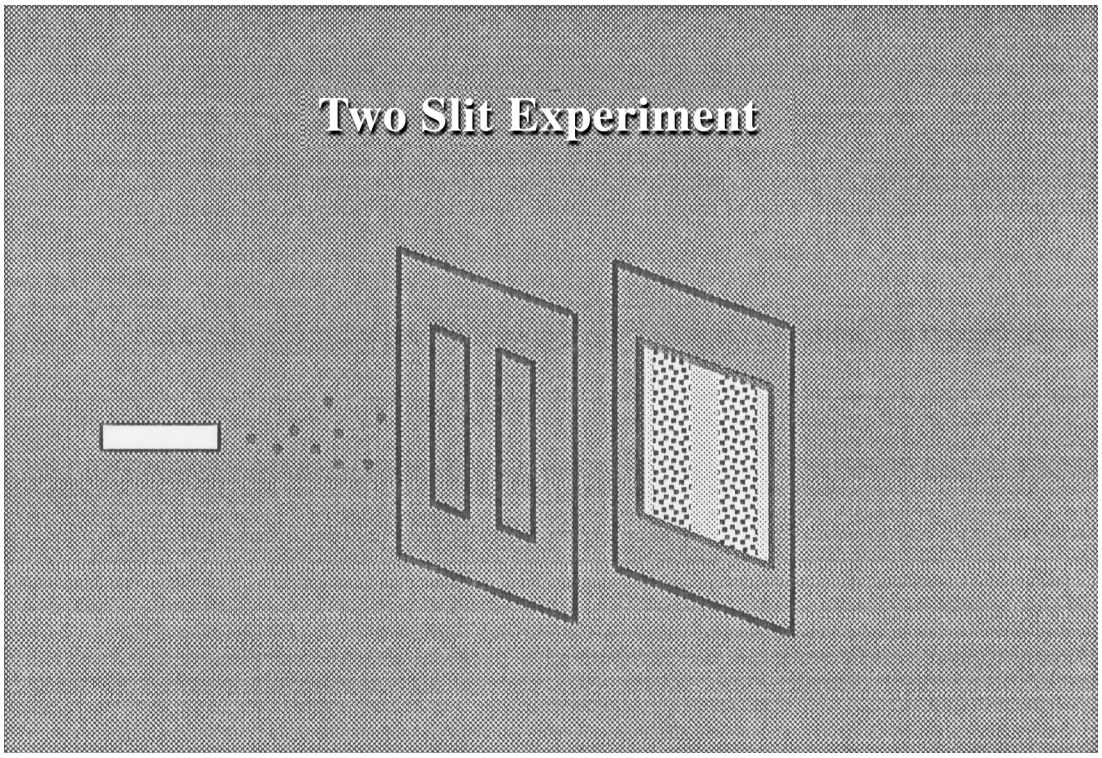

With waves, however, the result is very different, because of interference. If the slits were opened one at a time, the pattern would resemble the pattern for bullets: two distinct peaks. But, when the slits are open at the same time, the waves pass through both slits at once and interfere with each other: where they are in phase they reinforce each other; where they are out of phase they cancel each other out as shown in Figure 37.2.

Figure 37.2. Two-slit experiment with waves.

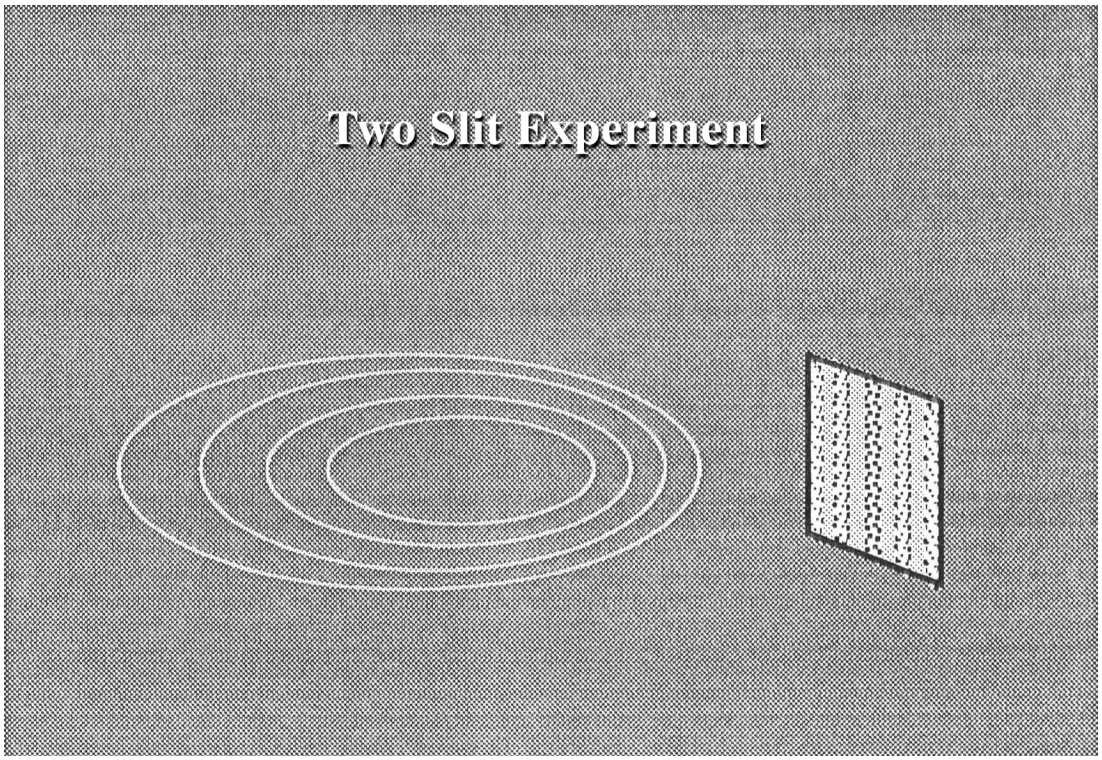

Now the quantum paradox: Electrons, like bullets, strike the target one at a time. Yet, like waves, they create an interference pattern as shown in Figure 37.3.

Figure 37.3. Two-slit experiment with electrons.

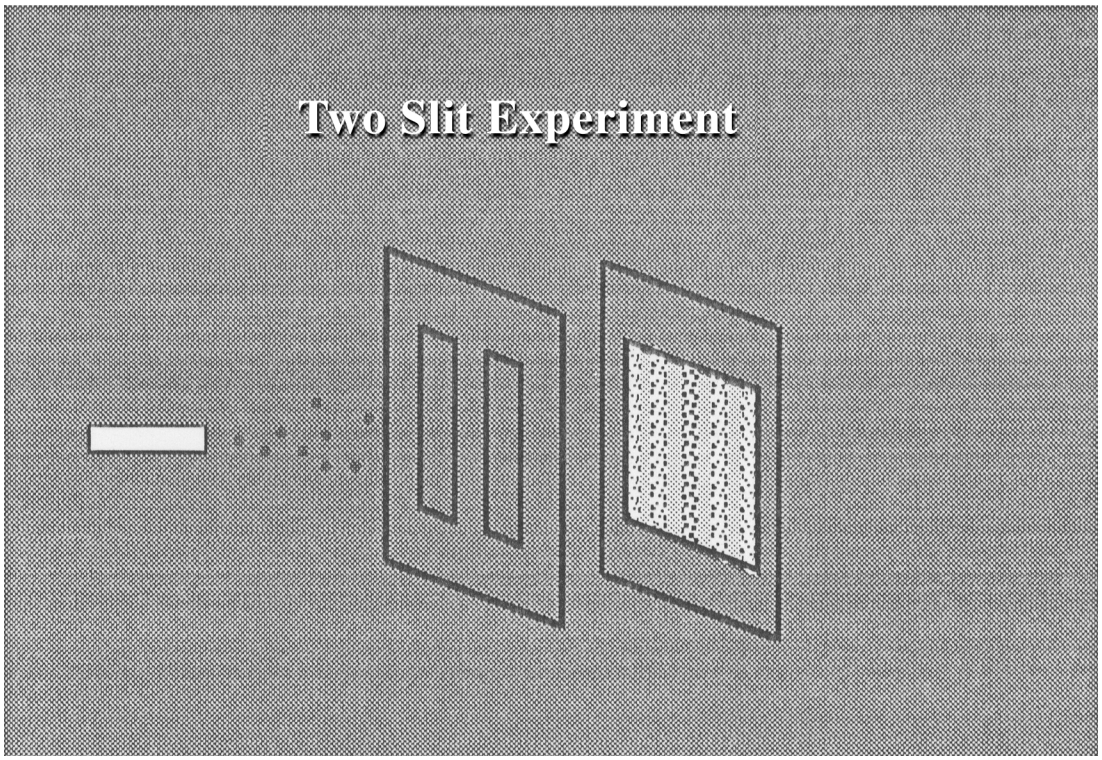

If each electron passes individually through one slit, with what does it "interfere"? Although each electron arrives at the target at a single place and a single time, it seems that each has passed through - or somehow felt the presence of both slits at once. Thus, the electron is understood in terms of a wave-particle duality as represented in Figure 37.4.

Figure 37.4. Interpretation of the two-slit experiment with electrons in terms of a wave-particle duality to the nature of the electron.

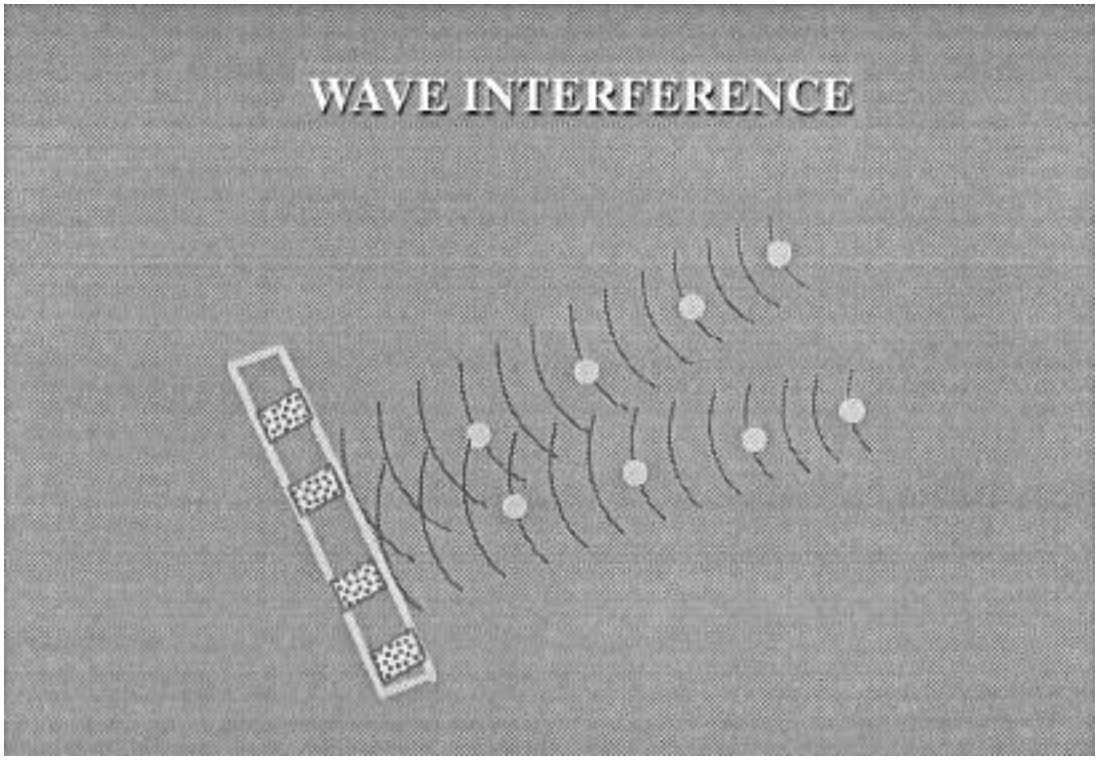

The mistake in the direction of the development of the theory of light and the atom occurred when theoreticians concluded: The laws of physics that are valid in the macroworld do not hold true in the microworld of the atom. In contrast, Mills' theory is based on the foundation that the laws of physics that are valid in the macroworld do hold true in the microworld of the atom. In the present case, the predictions which arise from the equations of light and atomic particles are completely consistent with observation including the wave-particle duality of light and atomic particles.

Maxwell unified electricity and magnetism by proposing the existence of electromagnetic waves which travel at the velocity c. In 1888, Hertz showed that electromagnetic waves exist and behave exactly as Maxwell had predicted - they had electric and magnetic components, and they could be reflected, refracted, and diffracted. Toward the end of the 19th century, many physicists believed that all of the principles of physics had been discovered. The accepted principles, now called ***classical physics***, included laws relating to Newton's mechanics, Gibbs' thermodynamics, LaGrange's and Hamilton's elasticity and hydrodynamics, Maxwell-Boltzmann molecular statistics, and Maxwell's Equations. However, the discovery that the intensity of blackbody

radiation goes to zero, rather than infinity as predicted by the prevailing laws of electromagnetism, led theoreticians to question the validity of Maxwell's Equations on the atomic scale. In 1900, Planck made the revolutionary assumption that energy levels were quantized, and that atoms of the blackbody could emit light energy only in amounts given by $h\nu$, where ν is the radiation's frequency and h is a proportionality constant (now called Planck's constant). This assumption does not conflict with the notion that light is a wave. However, Hertz's experiments with light further revealed that photoelectrons were emitted from illuminated metals, and the photoelectron energy increases with the frequency of incident light and not its intensity. Einstein explained this photoelectron effect by proposing that light of a given frequency is composed of individual photons whose energy is proportional to that frequency according to Planck's relationship[1]. Einstein's proposal that light has a particle nature in that it travels through space as distinct photons[2] is opposed to the wave view whereby light waves spread out from a source, and the energy is spread continuously throughout the wave pattern. Thus, light has since been regarded as both a wave and a particle which exhibits one feature or the other during observation but never both simultaneously. Early 20th century theoreticians proclaimed that light has a wave-particle duality that was unlike anything in our common day experience [3].

A similar course arose in the development of the model of the atom. J. J. Balmer showed, in 1885, that the frequencies for some of the lines observed in the emission spectrum of atomic hydrogen could be expressed with a completely empirical relationship. This approach was later extended by J. R. Rydberg, who showed that all of the spectral lines of atomic hydrogen were given by the equation:

$$\bar{\nu} = R\left(\frac{1}{n_f^2} - \frac{1}{n_i^2}\right) \tag{37.1}$$

where $R = 109{,}677\ cm^{-1}$, $n_f = 1,2,3,\ldots$, $n_i = 2,3,4,\ldots$, and $n_i > n_f$. Niels Bohr, in 1913, developed a theory for atomic hydrogen based on an unprecedented postulate of stable circular orbits that do not radiate. Although no explanation was offered for the existence of stability for these orbits, the results gave energy levels in agreement with Rydberg's

---

[1] In 1900, Planck made the revolutionary assumption that energy levels were quantized, and that atoms of the blackbody could emit light energy only in amounts given by $h\nu$, where ν is the radiation's frequency and h is a proportionality constant (now called Planck's constant). This assumption also led to our understanding of the photoelectric effect and ultimately to the concept of light as a particle called a photon.

[2] This view was first proposed by Newton.

equation. Bohr's theory was a straightforward application of Newton's laws of motion and Coulomb's law of electric force - both pillars of classical physics and is in accord with the experimental observation that atoms are stable. However, it is not in accord with electromagnetic theory - another pillar of classical physics which predicts that accelerated charges radiate energy in the form of electromagnetic waves. An electron pursuing a curved path is accelerated and therefore should continuously lose energy, spiraling into the nucleus in a fraction of a second. The predictions of electromagnetic theory have always agreed with experiment, yet atoms do not collapse. To the early 20th century theoreticians, this contradiction could mean only one thing: The laws of physics that are valid in the macroworld do not hold true in the microworld of the atom. In 1923, de Broglie suggested that the motion of an electron has a wave aspect— $\lambda = \frac{h}{p}$. This concept seemed unlikely according to the familiar properties of electrons such as charge, mass and adherence to the laws of particle mechanics. But, the wave nature of the electron was confirmed by Davisson and Germer in 1927 by observing diffraction effects when electrons were reflected from metals. Schrödinger reasoned that if electrons have wave properties, there must be a wave equation that governs their motion. And in 1926, he proposed the Schrödinger equation, $H\Psi = E\Psi$, where Ψ is the wave function, H is the wave operator, and E is the energy of the wave. This equation, and its associated postulates, is now the basis of ***quantum mechanics***, and it is the basis for the world view that the atomic realm including the electron and photon cannot be described in terms of "pure" wave and "pure" particle but in terms of a wave-particle duality. The wave-particle duality based on the fundamental principle that physics on an atomic scale is very different from physics on a macroscopic scale is central to present day atomic theory [4].

The hydrogen atom is the only real problem for which the Schrödinger equation can be solved without approximations; however, it only provides three quantum numbers - not four. Nevertheless, the application of the Schrödinger equation to real problems has provided useful approximations for physicists and chemists. Schrödinger interpreted $e\Psi^*(x)\Psi(x)$ as the charge-density or the amount of charge between x and $x+dx$ (Ψ^* is the complex conjugate of Ψ). Presumably, then, he pictured the electron to be spread over large regions of space. Three years after Schrödinger's interpretation, Max Born, who was working with scattering theory, found that this interpretation led to inconsistencies and he replaced the Schrödinger interpretation with the probability of finding the electron between x and $x+dx$ as

$$\int \Psi(x)\Psi^*(x)dx \tag{37.2}$$

Born's interpretation is generally accepted. Nonetheless, interpretation of the wave function is a never-ending source of confusion and conflict. Many scientists have solved this problem by conveniently adopting the Schrödinger interpretation for some problems and the Born interpretation for others. This duality allows the electron to be everywhere at one time—yet have no volume. Alternatively, the electron can be viewed as a discrete particle that moves here and there (from $r = 0$ to $r = \infty$), and $\Psi\Psi^*$ gives the time average of this motion.

According to the quantum mechanical view, a moving particle is regarded as a wave group. To regard a moving particle as a wave group implies that there are fundamental limits to the accuracy with which such "particle" properties as position and momentum can be measured. Quantum predicts that the particle may be located anywhere within its wave group with a probability $|\Psi|^2$. An isolated wave group is the result of superposing an infinite number of waves with different wavelengths. The narrower the wave group, the greater range of wavelengths involved. A narrow de Broglie wave group thus means a well-defined position (Δx smaller) but a poorly defined wavelength and a large uncertainty $\Delta \mathbf{p}$ in the momentum of the particle the group represents. A wide wave group means a more precise momentum but a less precise position. The infamous Heisenberg Uncertainty Principle is a formal statement of the standard deviations of properties implicit in the probability model of fundamental particles.

$$\Delta x \Delta \mathbf{p} \geq \frac{\hbar}{2} \tag{37.3}$$

According to the standard interpretation of quantum mechanics, the act of measuring the position or momentum of a quantum mechanical entity collapses the wave-particle duality because the principle forbids both quantities to be simultaneously known with precision.

THE WAVE-PARTICLE DUALITY IS NOT DUE TO THE UNCERTAINTY PRINCIPLE

Quantum entities can behave like particles or waves, depending on how they are observed. They can be diffracted and produce interference patterns (wave behavior) when they are allowed to take different paths from some source to a detector--in the usual example, electrons or photons go through two slits and form an interference pattern on the screen behind. On the other hand, with an appropriate detector put along one of the paths (at a slit, say), the quantum entities can be detected at a particular place and time, as if they are point-like particles.

But any attempt to determine which path is taken by a quantum object destroys the interference pattern. Richard Feynman described this as the central mystery of quantum physics.

Bohr called this vague principle 'complementarity, and explained it in terms of the uncertainty principle, put forward by Werner Heisenberg, his postdoc at the time. In an attempt to persuade Einstein that wave-particle duality is an essential part of quantum mechanics, Bohr constructed models of quantum measurements that showed the futility of trying to determine which path was taken by a quantum object in an interference experiment. As soon as enough information is acquired for this determination, the quantum interferences must vanish, said Bohr, because any act of observing will impart uncontrollable momentum kicks to the quantum object. This is quantified by Heisenberg's uncertainty principle, which relates uncertainty in positional information to uncertainty in momentum--when the position of an entity is constrained, the momentum must be randomized to a certain degree.

More than 60 years after the famous debate between Niels Bohr and Albert Einstein on the nature of quantum reality, a question central to their debate --the nature of quantum interference--has resurfaced. The usual textbook explanation of wave-particle duality in terms of unavoidable 'measurement disturbances' is experimentally proven incorrect by an experiment reported in the September 3, 1998 issue of *Nature* [5] by Durr, Nonn, and Rempe. Durr, Nonn, and Rempe report on the interference fringes produced when a beam of cold atoms is diffracted by standing waves of light. Their interferometer displayed fringes of high contrast--but when they manipulated the electronic state within the atoms with a microwave field according to which path was taken, the fringes disappeared entirely. The interferometer produced a spatial distribution of electronic populations which were observed via fluorescence. The microwave field canceled the spatial distribution of electronic populations. The key to this new experiment was that although the interferences are destroyed, the initially imposed atomic momentum distribution left an envelope pattern (in which the fringes used to reside) at the detector. A careful analysis of the pattern demonstrated that it had not been measurably distorted by a momentum kick of the type invoked by Bohr, and therefore that any locally realistic momentum kicks imparted by the manipulation of the internal atomic state according to the particular path of the atom are too small to be responsible for destroying interference.

Durr et al. conclude that the "Heisenberg Uncertainty relationship has nothing to do with wave-particle duality" and

further conclude that the phenomenon is based on entanglement and correlation. Their interpretation of the principles of the experiment is that directional information is encoded by manipulating the internal state of an atom with a microwave field, which entangles the atom's momentum with its internal electronic state. Like all such entangled states, the constituent parts lose their separate identity. But the attachment of a distinguishable electronic label to each path means that the total electronic-plus-path wavefunction along one path becomes orthogonal to that along the other, and so the paths can't interfere. By encoding information as to which path is taken within the atoms, the fringes disappear entirely. The internal labeling of paths does not even need to be read out to destroy the interferences: all you need is the option of being able to read it out.

According to Durr et al., the mere existence of information about an entity's path causes its wave nature to disappear. But, correlations are observations about relationships between quantities and do not cause physical processes to occur. **The existence of information about an entity's path is a consequence of the manipulation of the momentum states of the atoms which resulted in cancellation of the interference pattern. It was not the cause of the cancellation. The cancellation is predicted by the classical atomic theory of Mills.**

The explanation for the loss of interference in which-way experiments that endured and is present in essentially all quantum physics textbooks is that based on Heisenberg's position-momentum uncertainty relation. This has been illustrated in famous gedanken experiments like Einstein's recoiling slit [6] or Feynman's light microscope [7]. In the light microscope, electrons are illuminated with light immediately after they have passed through a double slit with slit separation d. A scattered photon localizes the electron with a position uncertainty of the order of the light wavelength, $\Delta z = \lambda_{light}$. Owing to Heisenberg's position-momentum uncertainty relation, this localization must produce a momentum uncertainty of the order of $\Delta p_z \approx h/\lambda_{light}$. This momentum uncertainty arises from the momentum kick transferred by the scattered photon. For $\lambda_{light} < d$, which-way information is obtained, but the momentum kick is so large that it completely washes out the spatial interference pattern.

The issue of whether momentum kicks are necessary to explain the two-slit experiment is revisited. Obviously, momentum is involved, because a diffraction pattern is a map of the momentum distribution in the experiment. But how is it involved? Is it everything, as Bohr would have claimed?

This is the question addressed by Durr et al. [5] who report on a which-way experiment with an atom interferometer wherein an incoming beam of atoms passes through two separated standing wave light beams. The detuning of the light frequency from the atomic resonance, $\Delta = \omega_{light} - \omega_{atom}$, is large so that spontaneous emission can be neglected. The light fields each create a conservative potential U for the atoms, the so-called light shift, with $U \quad I/\Delta$, where I is the light intensity. In a standing wave, the light intensity is a function of position

$$I(z) = I_0 \cos^2\left(k_{light} z\right) \tag{37.4}$$

where k_{light} is the wavevector of the light. Hence the light shift potential takes the form

$$U(z) = U_0 \cos^2\left(k_{light} z\right) \tag{37.5}$$

with $U_0 \quad I_0/\Delta$.

The atoms are Bragg-reflected from this periodic potential, if they enter the standing light wave at a Bragg angle. This process is similar to Bragg reflection of X-rays from the periodic structure of a solid-state crystal, but with the role of matter and light exchanged. The light creates the periodic structure, from which the matter wave is reflected.

The scheme of the interferometer is shown in Figure 37.5. The standing light wave splits the incoming atomic beam A into two beams, a transmitted beam C and a first-order Bragg-reflected beam B. The angle between the beams B and C corresponds to a momentum transfer of exactly $2\hbar k_{light}$ as determined by the spatial period of $U(z)$. By varying the light intensity, the fraction of reflected atoms can be adjusted to any arbitrary value. Durr et al. tune the reflectivity of the beam splitter to about 50%.

Figure 37.5. Scheme of the atom interferometer. The incoming atomic beam A is split into two beams: beam C is transmitted and beam B is Bragg-reflected from a standing light wave. The beams are not exactly vertical because a Bragg condition must be fulfilled. After free propagation for a time t_{sep}, the beams are displaced by a distance d. Then the beams are split again with a second standing light wave. In the far field, a spatial interference pattern is observed.

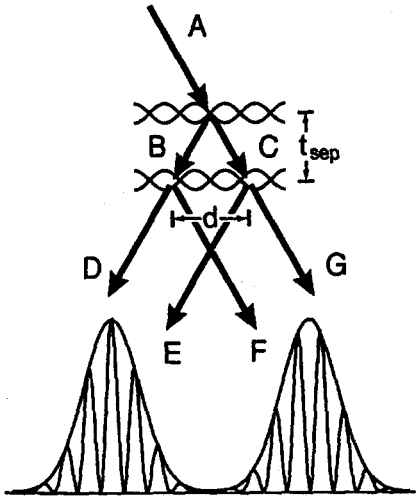

After switching off the first standing light wave, the two beams are allowed to propagate freely for a time interval t_{sep}. During this time, beam B moves a horizontal distance $d/2$ to the left, and beam C moves $d/2$ to the right. The longitudinal velocities (direction normal to the standing light wave of Figure 37. 5) of the two beams are not affected by the light field. Then a second standing light wave is switched on, which also serves as a 50% beam splitter. Now two atomic beams D and E are traveling to the left, while beams F and G are traveling to the right. In the far field, each pair of overlapping beams produces a spatial interference pattern. The fringe period is the same as in a double-slit experiment with slit separation d as given in Two-Beam Interference Section. The intensity is given by Eq. (8.22)

$$I(\mathrm{x}) = 16a^2C^2\mathrm{sinc}^2\left(\frac{2\pi a x}{\lambda f}\right)\cos^2\left(\frac{2\pi d x}{\lambda f}\right) \tag{37.6}$$

From Eq. (37.6), it is clear that the resulting pattern has the appearance of cosine^2 fringes of period $\lambda f / d$ with an envelope $\mathrm{sinc}^2(2\pi a x / \lambda f)$ where and f is the focal length and a is the slit width. In the present case, the envelope of the fringe pattern is given by the collimation properties of

the initial atomic beam A. Note that Eq. (37.6) corresponds to an amplitude transmission of a plane wave. The bound unpaired electron of each ^{85}Rb atom behaves as a plane wave of wavelength $\lambda = h/p$ as shown in the Free Electron Section. The relevant wavelength λ of Eq. (37.6) is the de Broglie wavelength associated with the momentum of the atoms (Eq. (1.46)) which is transferred to the electrons through atomic interactions.

The atomic position distribution is observed by exciting atoms with a resonant laser and detecting the fluorescence photons. The observed far-field position distribution is a picture of the atomic transverse momentum distribution after the interaction. The pattern is given by Eq. (37.6). The pattern may be altered by application of microwave pulses which transfer momentum to the electrons of the ^{85}Rb atoms which add vectorally to that transferred from the interactions with the standing light field and atomic interactions.

Microwave pulses are now added to manipulate the two internal electronic states of the atom according to whether it moved along pathway B or C. A simplified level scheme of ^{85}Rb is shown in Figure 37.6. The manipulation of internal states by two microwave fields which each apply a $\pi/2$ pulse is shown in Figure 37.7. Rabi oscillations between states $|2\rangle$ and $|3\rangle$ can be induced by applying a microwave field of about 3 GHz. To describe the manipulation of the two internal electronic states of the atom, we first investigate the properties of a single Bragg beam splitter.

Figure 37.6. Simplified level scheme of ^{85}Rb. The excited state $\left(5^2P_{3/2}\right)$ is labeled $|e\rangle$. The ground state $\left(5^2P_{1/2}\right)$ is split into two hyperfine states with total angular momentum $F = 2$ and $F = 3$, which are labeled $|2\rangle$ and $|3\rangle$, respectively. The standing light wave has angular frequency ω_{light}.

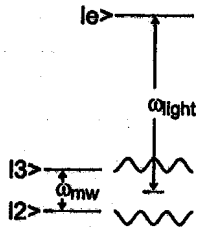

Figure 37.7. Scheme of the manipulation of internal states of ^{85}Rb by two microwave fields which each apply a $\pi/2$ pulse. The standing light wave with angular frequency ω_{light} induces a light shift for both ground states which is given as a function of position. The beam splitter produces a

phase shift that depends on the internal and external degree of freedom. A Ramsey scheme, consisting of two microwave $\pi/2$ pulses, converts this phase shift into a population difference.

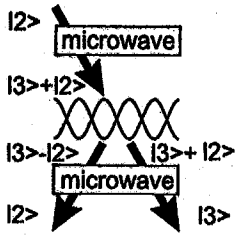

The frequency of the standing light wave, ω_{light} is tuned halfway between the $|2\rangle \rightarrow |e\rangle$ and $|3\rangle \rightarrow |e\rangle$ transitions. Hence the detunings from these transitions, Δ_{2e}, and Δ_{3e}, have the same absolute value but opposite sign. The reflectivity of the beam splitter, that is, the probability of reflecting an atom, depends on $t_{Bragg}X|U_0|$, and it is independent of the internal state.

However, the amplitude of the wavefunction experiences a phase shift which depends on the internal atomic state. A simple analogy for this phase shift can be found in light optics: a light wave reflected from an optically thicker medium experiences a phase shift of π, while reflection from an optical thinner medium or transmission into an arbitrary medium does not cause any phase shift. This argument also applies in atomic optics: in the present experiment, an atom in $|2\rangle$ sees a negative light shift potential (because $\Delta_{2e} < 0$), corresponding to an optically thicker medium, while an atom in $|3\rangle$ sees a positive potential (because $\Delta_{3e} > 0$), corresponding to an optically thinner medium. Hence an atom will experience a π phase shift only if it is reflected in $|2\rangle$.

This phase shift can be converted into a population difference between the hyperfine levels. For that purpose, two microwave $\pi/2$ pulses resonant with the hyperfine transition are applied. They form a Ramsey scheme as shown in Figure 37.7. The atom is initially prepared in state $|2\rangle$. Then a $\pi/2$ microwave pulse is applied, converting the beam into an equal mixture of internal states of $|2\rangle + |3\rangle$. After this, each atom interacts with the standing light wave. As explained above, each atom will experience a π phase shift only if it is reflected and in state $|2\rangle$. Thus the internal state of the reflected beam is changed to an equal mixture of internal states of $|3\rangle - |2\rangle$, while the internal state of the transmitted beam is not affected. As a result, the momentum of each atom is a superposition of the internal and external degree of freedom of the atom which is specific to the path. The state vector of the system

becomes:

$$|\psi\rangle \quad |\psi_B\rangle \quad (|3\rangle - |2\rangle) + |\psi_C\rangle \quad (|3\rangle + |2\rangle) \tag{37.7}$$

where $|\psi_B\rangle$ and $|\psi_C\rangle$ describe the center-of-mass motion for the reflected and transmitted beams (see Figure 37.5), respectively. The second microwave pulse action on both beams (the transmitted and the reflected), converts the internal state of the transmitted beam to state $|3\rangle$, while the reflected beam is converted to state $-|2\rangle$. Thus, the state vector after the pulse sequence shown in Figure 37.7 becomes:

$$|\psi\rangle \quad -|\psi_B\rangle \quad |2\rangle + |\psi_C\rangle \quad |3\rangle \tag{37.8}$$

Eq. (37.8) shows that the internal state is correlated with the way taken by the atom. The which-way information can be read out later by performing a measurement of the internal atomic state. The result of this measurement reveals which way the atom took: if the internal state is found to be $|2\rangle$, the atom moved along beam B, otherwise it moved along beam C.

After considering a single beam splitter, now consider the complete interferometer. Sandwiching the first Bragg beam splitter between two $\pi/2$ microwave pulses produces a reflected and transmitted beam each of a single internal atomic state, as described above. We note that the second Bragg beam splitter does not change the internal state. **No fringes are experimentally observed in this case.** The data is recorded with the same parameters with the only difference being that two microwave pulses are added to produce a single internal atomic state according to the particular path of the atom. Atoms in both hyperfine states are detected. The interference pattern is also not observed when only atoms in state $|2\rangle$ or only atoms in state $|3\rangle$ are detected. Of course, the absolute size of the signal is reduced by a factor of two in these cases. The key to this new experiment is that although the interferences are destroyed, the initially imposed atomic momentum distribution leaves an envelope pattern (in which the fringes used to reside) at the detector. **A careful analysis of the pattern finds that it has not been measurably distorted by a momentum kick of the type invoked by Bohr, and therefore that any locally realistic momentum kicks imparted by the manipulation of the internal atomic state according to the particular path of the atom are too small to be responsible for destroying interference.**

In order to investigate why the interference is lost, we consider the state vector for the interaction sequence used which causes the disappearance of the fringes. The state vector after the interaction with the first beam splitter sandwiched between the two microwave pulses is given by Eq. (37.8). The second beam splitter transforms this state

vector into a left peak and a right peak given by:

$$|\psi_{left}\rangle \quad -|\psi_D\rangle \quad |2\rangle + |\psi_E\rangle \quad |3\rangle \tag{37.9}$$

and

$$|\psi_{right}\rangle \quad |\psi_F\rangle \quad |2\rangle + |\psi_G\rangle \quad |3\rangle \tag{37.10}$$

where the sign of $|\psi_F\rangle$ is positive due to the π phase shift during the reflection from the second beam splitter. Each peak is a superposition of atoms which follow separate paths and comprise atoms of a single internal state. In each case atoms which interfere have internal states which are orthogonal; thus, in the far field, the atomic position distribution under the each peak of the envelope is given by the superposition of two single slit patterns rather than the double slit pattern in the absence of the application of the $\pi/2$ microwave pulses. In the far field, the amplitude of the atomic position distribution under each peak of the envelope $\tilde{\Psi}(x)$ is the sum of the independent Fraunhofer planes and the intensity of the atomic position distribution under each peak of the envelope $\tilde{\Psi}^2(x)$ is given by

$$\tilde{\Psi}^2(x) = (2aC)^2 \operatorname{sinc}^2\left(\frac{kax}{f}\right) \tag{37.11}$$

where f is the focal length and a is the slit width. In the present case, the envelope of the fringe pattern is given by the collimation properties of the initial atomic beam A.

A dramatic change in the spatial momentum distribution occurs when adding the microwave fields to the interferometer that manifests itself as loss of interference; even though, the microwave itself does not transfer enough momentum to the atom to wash out the fringes according to the Heisenberg Uncertainty Principle. The addition of the microwave fields modifies the probability for momentum transfer by the light fields. This modification of the momentum transfer probability is due to the manipulation of the internal atomic state according to the particular path of the atom. The disappearance of interference is explained by the classical quantum mechanics of Mills.

INCONSISTENCIES OF QUANTUM MECHANICS

Quantum mechanics failed to predict the results of the Stern-Gerlach experiment which indicated the need for an additional quantum number. Quantum electrodynamics was proposed by Dirac in 1926 to provide a generalization of quantum mechanics for high energies in conformity with the theory of Special Relativity and to provide a consistent treatment of the interaction of matter with radiation. From Weisskopf [8], "Dirac's quantum electrodynamics gave a more consistent derivation of the results of the correspondence principle, but

it also brought about a number of new and serious difficulties." Quantum electrodynamics; 1.) does not explain nonradiation of bound electrons; 2.) contains an internal inconsistency with Special Relativity regarding the classical electron radius - the electron mass corresponding to its electric energy is infinite; 3.) it admits solutions of negative rest mass and negative kinetic energy; 4.) the interaction of the electron with the predicted zero-point field fluctuations leads to infinite kinetic energy and infinite electron mass; 5.) Dirac used the unacceptable states of negative mass for the description of the vacuum; yet, infinities still arise. In 1947, Lamb discovered a 1000 *MHz* shift between the $^2S_{1/2}$ state and the $^2P_{1/2}$ state of the hydrogen atom. This so called Lamb Shift marked the beginning of modern quantum electrodynamics. In the words of Dirac [9], "No progress was made for 20 years. Then a development came initiated by Lamb's discovery and explanation of the Lamb Shift, which fundamentally changed the character of theoretical physics. It involved setting up rules for discarding ...infinities..." Renormalization is presently believed to be required of any fundamental theory of physics [10]. However, dissatisfaction with renormalization has been expressed at various times by many physicists including Dirac [11]. who felt that, "This is just not sensible mathematics. Sensible mathematics involves neglecting a quantity when it turns out to be small - not neglecting it just because it is infinitely great and you do not want it!"

Modern quantum mechanics has encountered several obstacles that have proved insurmountable as pointed out previously in the General Considerations Section and the Classical Electron Radius Section. And, quantum mechanics leads to certain philosophical interpretations [12] which are not sensible. Some conjure up multitudes of universes including "mind" universes; others require belief in a logic that allows two contradictory statements to be true. The question addressed is whether the universe is determined or influenced by the possibility of our being conscious of it. The meaning of quantum mechanics is debated, but the Copenhagen interpretation is predominant. Its asserts that "what we observe is all we can know; any speculation about what a photon, an atom or even a SQUID (Superconducting Quantum Interference Device) really is or what it is doing when we are not looking is just that speculation" [13]. According to this interpretation every observable exists in a state of superposition of possible states, and observation or the potential for knowledge causes the wavefunction corresponding to the possibilities to collapse into a definite. As shown by Platt [14] in the case of the Stern-Gerlach experiment, "the postulate of quantum measurement [which] asserts that the process of measuring

an observable forces the state vector of the system into an eigenvector of that observable, and the value measured will be the eigenvalue of that eigenvector". According to the Zeno no-go theorem which is a consequence of the postulate of quantum measurement, observation of an atom collapses its state into a definite; thus, transitions cannot occur under continuous observation. Recently, it has become possible to test this postulate via an experiment involving transitions of a single atom, and the results are inconsistent with the predictions. Quoting from the caption of Figure 10 of the article, by Dehmelt [15],

> "Shelving" the Ba^+ optical electron in the metastable D level. Illuminating the ion with a laser tuned close to its resonance line produces strong resonance fluorescence and an easily detectable photon count of 1600 photons/sec. When later an auxiliary, weak Ba^+ spectral lamp is turned on, the ion is randomly transported into the metastable $D_{5/2}$ level for 30-s lifetime and becomes invisible. After dwelling in this shelving level for 30 s on average, it drops down to the S ground state spontaneously and becomes visible again. This cycle repeats randomly. According to the Zeno no-go theorem, no quantum jumps should occur under continuous observation.

In addition to the interpretation that photons, electrons, neutrons, and even human beings [12] have no definite form until they are measured, a more disturbing interpretation of quantum mechanics is that a measurement of a quantum entity can instantaneously influence another light years away. Einstein argued that a probabilistic versus deterministic nature of atomic particles leads to disagreement with Special Relativity. In fact, the nonlocality result of the Copenhagen interpretation violates causality. As a consequence of the indefinite nature of the universe according to quantum mechanics and the implied Uncertainty Principle, Einstein, Podolsky, and Rosen (EPR) in a classic paper [16] presented a paradox which led them to infer that quantum mechanics is not a complete theory. They concluded that the quantum-mechanical description of a physical system should be supplemented by postulating the existence of "hidden variables," the specification of which would predetermine the result of measuring any observable of the system. They believed the predictions of quantum mechanics to be correct, but only as consequences of statistical distribution of the hidden variables. But, Bell [17] showed that in a Gedanken experiment of Bohm [18] (a variant of that of EPR) no local hidden-variable theory can reproduce all of the statistical predictions of quantum mechanics. Thus, a paradox arises from Einstein's conviction that quantum-mechanical predictions concerning spatially separated systems are incompatible with his condition for locality unless hidden variables exist. Bell's theorem provides a decisive test of the family of local hidden-

variable theories (LHVT). In a classic experiment involving measurement of coincident photons at spatially separated detectors, Aspect [19] showed that local hidden-variable theories are inconsistent with the experimental results. Although Aspect's results are touted as a triumph of the predictions of quantum mechanics, the correct coincidence rate of detection of photons emitted from a doubly excited state of calcium requires that the z component of the angular momentum is conserved on a photon pair basis. As a consequence, a paradox arises between the deterministic conservation of angular momentum and the Uncertainty Principle. The prediction derived from the quantum nature of the electromagnetic fields for a single photon is inconsistent with Aspect's results, and Bell's theorem also disproves quantum mechanics. However, the results of Aspect's experiment are predicted by Mills' theory wherein locality and causality hold.

THE ASPECT EXPERIMENT - SPOOKY ACTIONS AT A DISTANCE?

The Aspect experiment is often invoked as the proof of the quantum-mechanical nature of reality [19-27]. According to the quantum explanation of the Aspect experiment [19], the polarization of each photon of a pair is not determined until a measurement is made, and the act of measuring the polarization of one photon causes an action at a distance with regard to the measurement of the polarization of the other member of a given pair. These results are interpreted as proof of a spooky action at a distance. Thus, information travels faster than the speed of light in violation of Special Relativity, or nonlocality and noncausality are implicit.

Bell's theorem is a simple proof of statistical inequalities of expectation values of observables given that quantum statistics are correct and that the physical system possesses "hidden variables". Mills' theory is not a hidden-variable theory. It is a deterministic theory of classical quantum mechanics, and Bell's theorem does not apply to it. The correct interpretation of the results of the Aspect experiment follows from classical quantum-mechanical derivation of Mills' theory. The expectation value of the coincidence rate at separated randomly oriented polarization analyzers for pairs of photons emitted from a doubly excited state atom is derived from the equation of the photon which appears in the Equation of the Photon Section.

Aspect [19] reports the measurement of polarization correlation (coincidence count rate) of visible photons ($\upsilon_1 = 551.3\,nm$; $\upsilon_2 = 422.7\,nm$) emitted in a $(J=0) \rightarrow (J=1) \rightarrow (J=0)$ calcium atomic cascade $\left(4p^2\ {}^1S_0 - 4s4p\ {}^1P_1 - 4s^2\ {}^1S_0\right)$. The calcium atoms were selectively pumped to the upper level of the cascade from the ground state by the two photon

absorption via two lasers, a single-mode krypton ion laser and a cw single-mode Rhodamine 6G dye laser tuned to the resonance for the two photon process. The fluorescent light was collected by lenses and made incident on two detectors - one at position -z and the other at position +z relative to the emitting calcium atoms. The polarizers were independently rotated in the xy-plane, and the coincidence count rate was measured.

The equation for the transmission of an electromagnetic wave through a barrier as given in any text of classical electrodynamics such as that of Kong [28] is

$$\mathbf{E}_T = TE_i e^{i\mathbf{k}_z z} \tag{37.12}$$

where $\mathbf{E}_T$ is the transmitted wave, E_i is the incident wave, and T is the transmission coefficient. For a wave that propagates at an angle with respect to the z-axis, the transmitted photon is given by a sum of equations of the form of Eq. (37.12) for each vector component. Using the convention of Horne [24], the vector transmission efficiencies (coefficients) can be written in matrix form with a matrix corresponding to each linear polarizer. In a basis of linear polarizations along x_1 and y_1 in the coordinates of photon 1, the most general linear polarizer with axis along x_1 is described by an efficiency matrix

$$\varepsilon(1) = \begin{pmatrix} \varepsilon_M^1 & 0 \\ 0 & \varepsilon_m^1 \end{pmatrix} \tag{37.13}$$

where ε_M^1 is the probability of transmitting an x_1 linearly polarized photon and ε_m^1 is the probability of transmitting a y_1 linearly polarized photon (leakage). In the ideal case $\varepsilon_M^1 = 1$ and $\varepsilon_m^1 = 0$. If the polarizer is not parallel to the x_1-axis but rotated in the plane perpendicular to the interdetector axis by an angle ϕ_1 from x_1, and $\varepsilon(1)$ is expressed in the basis of right hand circular (RHC) and left hand circular (LHC) photon states formed from x_1 and y_1, then the elementary transformations give the elements of $\varepsilon(1)$ as a function of ϕ_1 in matrix form:

$$\varepsilon^1\left(\sigma_1', \sigma_1\right) \equiv \left\langle \sigma_1' | \varepsilon(1) | \sigma_1 \right\rangle = \frac{1}{2} \begin{pmatrix} \varepsilon_M^1 + \varepsilon_m^1 & -\left(\varepsilon_M^1 - \varepsilon_m^1\right) e^{-2i\phi_1} \\ -\left(\varepsilon_M^1 - \varepsilon_m^1\right) e^{2i\phi_1} & \varepsilon_M^1 - \varepsilon_m^1 \end{pmatrix} \tag{37.14}$$

where $\left\langle \sigma_1' | \varepsilon(1) | \sigma_1 \right\rangle$ is defined as the expectation value of the transmission of the photon 1 with polarization σ_1, $\sigma_1 = \pm 1$ are RHC and LHC, respectively, and the angle between polarizer 1 (P_1) and x_1 is

$$\Delta\phi_1 = \phi_1 \tag{37.15}$$

Similarly, $\varepsilon(2)$, the efficiency matrix as a function of $\phi - \phi_2$ of the second polarizer (P_2) in the circular polarization basis of photon 2, is

$$\varepsilon^2\left(\sigma_2^{'},\sigma_2\right)\equiv\left\langle\sigma_2^{'}\left|\varepsilon(1)\right|\sigma_2\right\rangle=\frac{1}{2}\begin{pmatrix}\varepsilon_M^2+\varepsilon_m^2 & -\left(\varepsilon_M^2-\varepsilon_m^2\right)e^{-2i(\phi-\phi_2)}\\ -\left(\varepsilon_M^2-\varepsilon_m^2\right)e^{2i(\phi-\phi_2)} & \varepsilon_M^2-\varepsilon_m^2\end{pmatrix} \tag{37.16}$$

where the angle between polarizer 2 and the x-polarization of photon 2 (i. e. the angle between P_2 and x_2) is

$$\Delta\phi_2=\phi-\phi_2 \tag{37.17}$$

The efficiency matrix for coincidence transmission of photon 1 and photon 2 is given by the product of their independent probabilities, $\varepsilon(1)\varepsilon(2)$. The normalized coincidence counting rate is

$$\frac{R(\phi)}{R_0}=\frac{Tr\left[\varepsilon(1)\varepsilon(2)p_f\right]}{Tr\left(Ip_f\right)} \tag{37.18}$$

The normalized coincidence counting rate with polarizer 2 removed, $\frac{R_1}{R_0}$, is

$$\frac{R_1}{R_0}=\frac{Tr\left[\varepsilon(1)p_f\right]}{Tr\left(Ip_f\right)} \tag{37.19}$$

The normalized coincidence counting rate with polarizer 1 removed, $\frac{R_2}{R_0}$, is

$$\frac{R_2}{R_0}=\frac{Tr\left[\varepsilon(2)p_f\right]}{Tr\left(Ip_f\right)} \tag{37.20}$$

where I is the identity matrix and p_f is the probability that photon 1 and photon 2 have the same polarization and is a function of solid angle of the projection of the propagation vector of each photon onto the z-axis. In terms of Eq. (37.12), p_f corresponds to the vector correlated electric field incident on the opposed detectors. It is given by the normalized electric field of photons of matched momentum projected onto the z-axis over the solid angle of the detectors. For each photon of the two photon $(J=0)\rightarrow(J=1)\rightarrow(J=0)$ cascade of calcium, the transition amplitudes, E, are given by the integral of the product of the multipole of the photon, ${}^pX_{l,m}(\theta,\phi)$, and the initial, ${}^iX_{l,m}(\theta,\phi)$, and final, ${}^fX_{l,m}(\theta,\phi)$, states as is the case with classical electrodynamics calculations involving antennas. The transition amplitudes follow from Eq. (2.42) where the intensity is proportional to the amplitude squared.

$$E\quad E_0\int_0^{\pi}\int_0^{2\pi}{}^iX_{l,m}(\theta,\phi)\,{}^pX_{l,m}(\theta,\phi)\,{}^fX_{l,m}(\theta,\phi)\sin\theta\,d\phi\,d\theta \tag{37.21}$$

The distribution of multipole radiation and the multipole moments of the electron for absorption and emission are given in the Excited State of

the Electron Section and in Jackson [29].

Horne postulates the emission as a plane wave which is replaced by a spherical multipole expansion. The spherical multipole expansion of a plane wave such as given in Jackson [30] is consistent with the Green Function as the function which corresponds to the superposition of an ensemble of photons given by Eqs. (4.17-4.22) of Mills' theory. Using Eqs. (2.34-2.35) of Mills' theory, the projection of the photon pair propagation vector onto the axis perpendicular to the plane of each detector gives a factor of one corresponding to the conservation of angular momentum for each photon pair times a solid angle correction. The result for the numerator of Eq. (37.19) is

$$Tr\left[\varepsilon(1)\varepsilon(2)p_f\right] = \sum_{\sigma_1\sigma_1'\sigma_2\sigma_2'} \sigma_1\sigma_1'\sigma_2\sigma_2'\varepsilon^1\left(\sigma_1',\sigma_1\right)\varepsilon^2\left(\sigma_2',\sigma_2\right)g\left(\sigma_1,\sigma_2\right)g^*\left(\sigma_1',\sigma_2'\right) \tag{37.22}$$

where $g\left(\sigma_1,\sigma_2\right)g^*\left(\sigma_1',\sigma_2'\right)$ is a factor corresponding to the solid angle.

Eq. (37.22) is equivalent to Eq. (5.17) of Horne. To obtain this result, Horne suppressed the integration over $d\Omega_1$ and $d\Omega_2$ as well as the explicit dependence on the photon propagation vectors, $\mathbf{k}_1$ and $\mathbf{k}_2$, respectively. (The integration was also suppressed over frequency space as well as the explicit dependence on the photon propagation vectors, $\mathbf{k}_1$ and $\mathbf{k}_2$ in the case that QED holds.) This is only valid if the z component of angular momentum is conserved on a photon by photon basis such that the polarization correlation distribution function is independent of angle. Otherwise, it **cannot** be removed from the integral. HORNE'S CALCULATION IS NOT CONSISTENT WITH THE QUANTUM-MECHANICAL NATURE OF THE ELECTROMAGNETIC FIELDS FOR A SINGLE PHOTON as described below.

Substitution of the Eq. (37.14) and (37.15) and the results of solid angle term of Eq. (37.22) into Eq. (37.18) gives the normalized coincidence count rate.

$$\frac{R(\phi)}{R_0} = \frac{1}{4}\left(\varepsilon_M^1 + \varepsilon_m^1\right)\left(\varepsilon_M^2 + \varepsilon_m^2\right) + \frac{1}{4}\left(\varepsilon_M^1 - \varepsilon_m^1\right)\left(\varepsilon_M^2 - \varepsilon_m^2\right)F_1(\theta)\cos 2\phi \tag{37.23}$$

where the solid angle factor, $F_1(\theta)$, for the $0-1-0$ electric dipole cascade is

$$F_1(\theta) = 2G_1^2(\theta)\left[G_2^2(\theta) + \frac{1}{2}G_3^2(\theta)\right]^{-1} \tag{37.24}$$

The normalized coincidence count rate with polarizer 2 removed, $\frac{R_1}{R_0}$, is

$$\frac{R_1}{R_0} = \frac{1}{2}\left(\varepsilon_M^1 + \varepsilon_m^1\right) \tag{37.25}$$

The normalized coincidence count rate with polarizer 1 removed, $\frac{R_2}{R_0}$, is

$$\frac{R_2}{R_0} = \frac{1}{2}\left(\varepsilon_M^2 + \varepsilon_m^2\right) \tag{37.26}$$

The transmittances ε_M^i and ε_m^i of the polarizers (i=1 or 2) for light polarized parallel or perpendicular to the polarization axis were measured by Aspect [19]:

$$\begin{aligned} &\varepsilon_M^1 = 0.971 \pm 0.005,\ \varepsilon_m^1 = 0.029 \pm 0.005, \\ &\varepsilon_M^2 = 0.968 \pm 0.005,\ \varepsilon_m^2 = 0.028 \pm 0.005 \end{aligned} \tag{37.27}$$

And, the solid angle factor, $F_1(\theta)$, for the $0-1-0$ electric dipole cascade which accounts for the solid angles subtended by the collecting lenses of the Aspect experiment is

$$F_1(\theta) = F_2(\theta) = 0.984 \tag{37.28}$$

Substitution of the Eqs. (37.27) and (37.28) into Eq. (37.23) gives the normalized coincidence count rate as a function of the relative angle between the polarizers.

$$\frac{R(\phi)}{R_0} = 0.2490 + 0.2178\cos 2\phi \tag{37.29}$$

The normalized coincidence count rate, $\frac{R(\phi)}{R_0}$, as a function of the relative polarizer orientation, ϕ, given by Eq. (37.29) with the results of Aspect [19] appears in Figure 37.8.

Figure 37.8. The normalized coincidence count rate as a function of the relative polarizer orientation as given by Eqs. (37.23), (37.24), and Eq. (37.29) (solid curve) with the results of Aspect [19] (•).

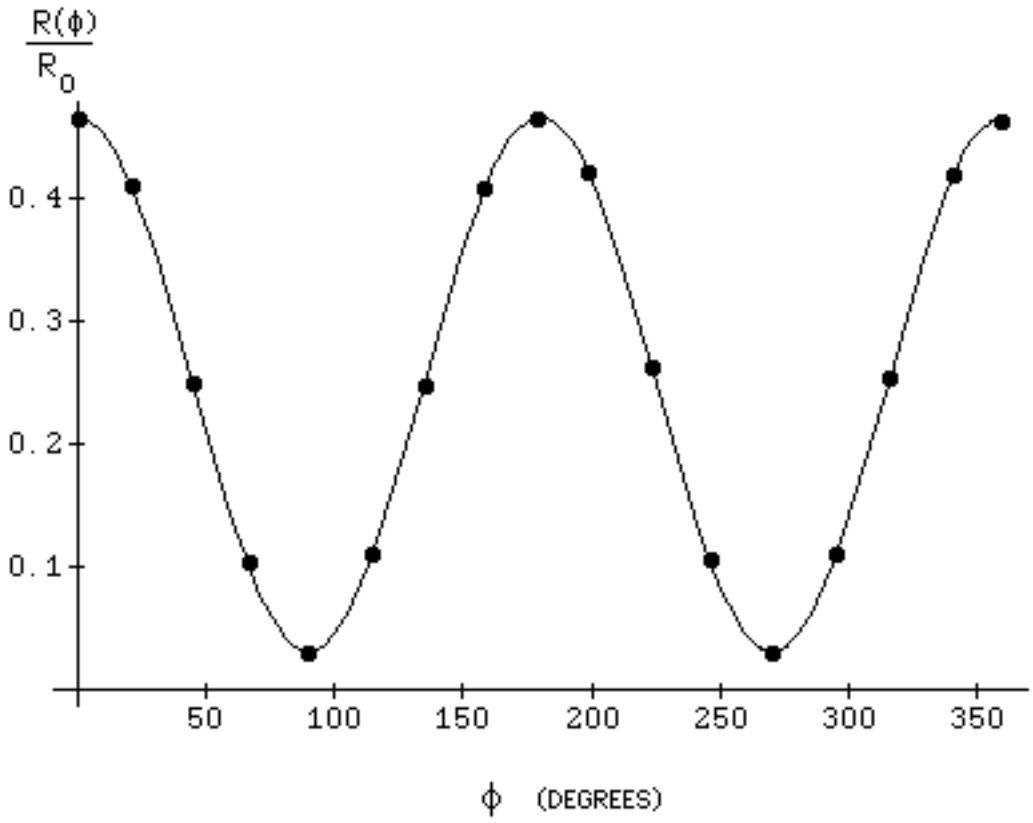

Eq. (5.17) of Horne (same as Eq. (37.22)) is the sum over the product of the transmission efficiencies of photon pairs of identical polarization at two independent detectors and a correction for the solid angle of the detectors for the photon pairs emitted from a remote isotropic source. The probability integral over momentum space was "suppressed" and set equal to one. Thus, the calculation is a deterministic equation. It does ***not correspond*** to the equation for coincident detection predicted ***by quantum mechanics***. According to Jackson [31]:

> For a multipole with a single m value, M_x and M_y vanish, while a comparison of (16.67) and (16.60) shows that
>
> $$\frac{dM_z}{dr} = \frac{m}{\omega}\frac{dU}{dr} \tag{16.68}$$
>
> independent of r. This has the obvious quantum interpretation that the

radiation from a multipole of order (l,m) carries off $m\hbar$ units of z component of angular momentum per photon of energy $\hbar\omega$. Even with a superposition of different m values, the same interpretation of (16.67) holds, with each multipole of definite m contributing incoherently its share of the z component of angular momentum. Now, however the x and y components are in general nonvanishing, with multipoles of adjacent m values contributing in a weighed coherent sum. The behavior continued in (16.64) and exhibited explicitly in (16.65)-(16.67) is familiar in the quantum mechanics of a vector operator and its representation with respect to basis states of J^2 and J_z*. The angular momentum of multipole fields affords a classical example of this behavior, with the z component being diagonal in the (l,m) multipole basis and the x and y components not.

The characteristics of the angular momentum just presented hold true generally, even though our example (16.57) was somewhat specialized. For a superposition of both electric and magnetic multipoles of various (l,m) values, the angular momentum expression (16.63) is generalized to

$$\frac{d\mathbf{M}}{dr} = \frac{1}{8\pi\omega k^2}\,\mathrm{Re}\sum_{\substack{l,m\\ l',m'}}\left\{\left[a_E^*(l',m')a_E(l,m)+a_M^*(l',m')a_M(l,m)\right]\int\left(\mathbf{L}\ \mathbf{X}_{l'm'}\right)^*\mathbf{X}_{l,m}\,d\Omega\right.$$
$$\left.+\,i^{l'-l}\left[a_E^*(l',m')a_M(l,m)-a_M^*(l',m')a_E(l,m)\right]\left(\mathbf{L}\ \mathbf{X}_{l'm'}\right)^*\mathbf{n}\times\mathbf{X}_{l,m}\,d\Omega\right\} \tag{16.69}$$

The first term in (16.69) is of the same form as (16.63) and represents the sum of the electric and magnetic multipoles separately. The second term is an interference between electric and magnetic multipoles. Examination of the structure of its angular integral shows that the interference is between electric and magnetic multipoles whose l values differ by unity. This is a necessary consequence of the parity properties of the multipole fields (see below). Apart from this complication of interference, the properties of $\frac{d\mathbf{M}}{dr}$ are as before.

The quantum-mechanical interpretation of (16.68) concerned the z component of angular momentum carried off by each photon. In further analogy with quantum mechanics, we would expect the ratio of the square of the angular momentum to the square of the energy to have the value,

$$\frac{M^{(q)^2}}{U^2} = \frac{\left(M_x^2+M_y^2+M_z^2\right)_q}{U^2} = \frac{l(l+1)}{\omega^2} \tag{16.70}$$

But from (16.60) and (16.65)-(16.67), the classical result for a pure (l,m) multipole is

$$\frac{M^{(c)^2}}{U^2} = \frac{|M_z|^2}{U^2} = \frac{m^2}{\omega^2} \tag{16.71}$$

The reason for this difference lies in the quantum nature of the electromagnetic fields for a single photon. If the z component of angular momentum of a single photon is known precisely, the uncertainty principle requires that the other components be uncertain, with mean square values such that (16.70) holds. On the other hand, for a state of the radiation field containing many photons (the classical limit) the mean square values of the transverse components of angular momentum can be made negligible compared to the square of the z component. Then the classical limit (16.71) applies. For a (l,m) multipole field containing N photons it can be shown* that

$$\frac{\left[M^{(q)}(N)\right]^2}{\left[U(N)\right]^2} = \frac{N^2m^2 + Nl(l+1) - m^2}{N^2\omega^2} \tag{16.72}$$

This contains (16.70) and (16.71) as limiting cases.

Consider the quantum nature of the electromagnetic fields for a single photon. According to Eqs. (16.70-16-72) of Jackson, photon pairs cannot have identical z components of angular momentum; therefore, each pair cannot have identical polarization. Each quantum-mechanical photon is a superposition of RHC, LHC, linear, and elliptic polarization. And, in the case of Quantum Electrodynamics (QED), each photon is also a superposition over frequency space. In the quantum-mechanical case Eq. (16.71) of Jackson applies - the z component of angular momentum is conserved on the average of many photons. Probability applies to the emission of a pair of photons of identical polarizations (the correlation of polarizations cannot be one ($P(A,B) \neq 1$) as well as to the detection of the photons of equal polarizations. Furthermore, QED requires that the probability associated with emission as well as detection applies to a distribution of photon wavelengths with expectation values of $\nu_1 = 551.3\ nm$ and $\nu_2 = 422.7\ nm$. The coincidence count rate is a function of the dot product of the electric field vector of each photon pair having correlated polarization onto the z-axis, and the probability of detection of the separate members of each pair at the separate detectors where the associated probabilities are independent. Thus, the probability of detecting a coincident event is given by the product of their independent probabilities. The quantum nature of the electromagnetic fields for a single photon requires a p_f of Eq.(37.18) that includes all distributions. Thus, the coincident rate predicted by quantum mechanics is less than the experimental rate. The extent of the error which is a function of the relative angle of the polarizers is given by Bell's theorem.

BELL'S THEOREM TEST OF LOCAL HIDDEN VARIABLE THEORIES (LHVT) AND QUANTUM MECHANICS

Using the convention of Clauser and Horne [22, 24], consider an ensemble of correlated pairs of photons emitted from the $0-1-0$ cascade of excited state calcium atoms each moving so that one enters polarizer 1 (P_1) and the other polarizer 2 (P_2), where ϕ_1 and ϕ_2 are adjustable angles of polarizer 1 and 2. In each polarizer a photon is recorded as ± 1 corresponding to RHC and LHC polarized, respectively. Let the results of these selections be represented by $A(a)$ and $B(b)$, each of which equals ± 1 according as the RHC or LHC is recorded.

Suppose now that a statistical correlation of $A(a)$ and $B(b)$ is due to information carried by and localized within each photon, and that at

some time in the past the photons constituting one pair were in contact and in communication regarding this information. The information is quantum mechanical or is part of the content of a set of hidden variables, denoted collectively by λ. The results of the two polarization outcomes are then to be functions $A(a,\lambda)$ and $B(b,\lambda)$. Locality reasonably requires $A(a,\lambda)$ to be independent of the parameter b and $B(b,\lambda)$ to be likewise independent of a, since the two outcomes may occur at an arbitrarily great distance from each other. Finally, since the pair of photons is generally emitted by a source in a manner physically independent of the adjustable parameters a and b, we assume that the normalized probability distribution $\rho(\lambda)$ characterizing the ensemble is independent of a and b. The requirement that the expectation value of a and b is equal to one ($E(a,b)=1$) (on the average, the polarization of photons incident on each polarizer are equal) implies $B(a,\lambda)=A(a,\lambda)$. Defining the correlation function $P(a,b)\equiv\int_\Gamma A(a,\lambda)B(b,\lambda)\rho(\lambda)d\lambda$ where Γ is the total λ space, generalization of Bell's theorem gives

$$\begin{aligned}|P(a,b)-P(a,c)| &\le \int_\Gamma |A(a,\lambda)B(b,\lambda)-A(a,\lambda)B(c,\lambda)|\rho(\lambda)d\lambda \\ &= \int_\Gamma |A(a,\lambda)B(b,\lambda)|\left[1-B(b,\lambda)B(c,\lambda)\right]\rho(\lambda)d\lambda \\ &= \int_\Gamma \left[1-B(b,\lambda)B(c,\lambda)\right]\rho(\lambda)d\lambda \\ &= 1-\int_\Gamma B(b,\lambda)B(c,\lambda)\rho(\lambda)d\lambda\end{aligned} \tag{37.30}$$

In the case of the $0-1-0$ cascade, the coincidence count rate, $R(\mathbf{a},\mathbf{b})$, replaces the correlation function, $P(a,b)$, of the generalization of Bell's theorem which then yields the following inequalities [19]:

$$-1\le S=\frac{\left[R(\mathbf{a},\mathbf{b})-R(\mathbf{a},\mathbf{b}')+R(\mathbf{a}',\mathbf{b})+R(\mathbf{a}',\mathbf{b}')-R_1(\mathbf{a}')-R_2(\mathbf{b}')\right]}{R_0}\le 0 \tag{37.31}$$

where $R(\mathbf{a},\mathbf{b})$ is the rate of coincidences with polarizer 1 in orientation $\mathbf{a}$ and polarizer 2 in orientation $\mathbf{b}$, $R_1(\mathbf{a}')$ is the coincidence rate with polarizer 2 removed and polarizer 1 in orientation $\mathbf{a}'$, $R_2(\mathbf{b}')$ is the coincidence rate with polarizer 1 removed and polarizer 2 in orientation $\mathbf{b}'$, and R_0 is the coincidence rate with the two polarizers removed. The maximum violation of Bell's inequalities (Eq. (37.31)) is predicted by substituting Eqs. (37.23-37.26) into Eq. (37.31) and by taking derivatives with respect to the orientation angles and setting them equal to zero [24]. Assuming the rotational invariance of $R(\mathbf{a},\mathbf{b})$, the inequalities (Eq. (37.31)) contract to [19]

$$\delta=\frac{\left|R(22.5°)-R(67.5°)\right|}{R_0}-\frac{1}{4}\le 0 \tag{37.32}$$

The calculated value, δ_{cal}, from Eqs. (37.23) and Eq. (37.32) is

$$\delta_{cal}=5.8\ X\ 10^{-2}\pm 0.2\ X\ 10^{-2} \tag{37.33}$$

The experimental value, δ_{exp}, is [19]

$$\delta_{exp} = 5.72\ X\ 10^{-2} \pm 0.43\ X\ 10^{-2} \quad (37.34)$$

The experimental value is in agreement with the calculated value and violates the inequality of Eq. (37.32) by 13 standard deviations. From Eq. (37.23) and Eq. (37.31), the inequality parameter, S_{cal}, corresponding to orientations:

$$-1 \le S = \frac{\left[R(22.5°) - R(67.5°) + R(22.5°) + R(22.5°) - R_1(44.8°) - R_2(67.5°)\right]}{R_0} \le 0 \quad (37.35)$$

is

$$S_{cal} = 0.118 \pm 0.005 \quad (37.36)$$

The experimental value, S_{exp}, is [19]

$$S_{exp} = 0.126 \pm 0.014 \quad (37.37)$$

The experimental value is in agreement with the calculated value and violates the inequality of Eq. (37.31) by 9 standard deviations. These results refute LHVT and quantum mechanics because both theories require a distribution function of correlated angular momentum. Only Mills' theory correctly predicts the coincidence count rate as a function of the relative orientation of the polarizers.

A fundamental difference exists between Mills' theory versus quantum mechanics and quantum electrodynamics (QED). In the case of Mills' theory, Eq. (16.70) of Jackson applies - the z component of angular momentum is conserved on a photon by photon basis. Whereas, in the quantum mechanical case, Eq. (16.71) of Jackson applies - the z component of angular momentum is conserved on the average of many photons. The photon is the cause of quantization in the deterministic Mills' theory; whereas, quantization arises from the expectation values of probability distribution functions in quantum mechanics and QED. Bell's theorem accepts quantum-mechanical statistics and hidden variables as correct simultaneously. The resulting inequalities predicted for the measurement of two spatially separated observables that were historically in communication with the condition that local hidden variables theories (LHVT) are correct is inconsistent with experimental results. Thus, the data refute LHVT. Furthermore, the calculation of Horne is ***not quantum mechanical***, the implicit physics is deterministic with the statistics of the measurement associated with two independent, inefficient detectors. For a true quantum-mechanical and QED calculation, the z component of angular momentum is only conserved on average over momentum space, and in the case of QED, the z component of angular momentum is only conserved on average over momentum space as well as over a continuum of frequencies centered about the expectation values of ν_1 and ν_2. (The expectation value of the

z component of angular momentum must include an integral over all momentum space and over all frequency space.) Bell's inequalities apply not only to LHVT, but also to quantum mechanics and QED. Consider the consequences of the postulate of quantum mechanics that photon momentum has a distribution function, and the change in the z component of angular momentum is zero on the average of many emission events. The associated average momentum distribution function is equivalent to a hidden variable distribution function in Eqs. (37.18) and (37.30). The observed coincidence count rate of Aspect [19] is equal to that predicted classically from the statistics of measurement at an inefficient detector only. The additional finite distribution function required in the case of quantum mechanics and QED results in incorrect predictions as demonstrated in the Bell's Theorem Test of Local Hidden Variable Theories (LHVT) and Quantum Mechanics Section. The observed results disprove LHVT, quantum mechanics, and QED and support Mills' theory.

SCHRÖDINGER "BLACK" CATS

A recent report in New York Times [32] entitled "Physicists Put Atom in 2 Places at Once" states, "a team of physicists has proved that an entire atom can simultaneously exist in two widely separated places". The article further states, "In the quantum "microscale" world, objects can tunnel magically through impenetrable barriers. A single object can exist in a multiplicity of forms and places. In principle, two quantum-mechanically "entangled" objects can respond instantly to each other's experiences, even when the two objects are at the opposite ends of the universe". (This quantum mechanical prediction of the Spooky Actions at a Distance was disproved in the previous sections--Aspect Experiment-Spooky Action at a Distance? and Bell's Theorem Test of Local Hidden Variable Theories (LHVT) and Quantum Mechanics). Experimentally, interference patterns were observed by Monroe et al. [33] for a single $^{9}Be^{+}$ ion in a trap in a continuous Stern-Gerlach experiment. The phenomenon is similar to that of the Aharonov-Bohm Effect which was erroneously interpreted as interference of electron wave-functions as given in the Aharonov-Bohm Effect Section. In this case, the erroneous interpretation of the experimental observation was that the ion wave-function interfered with itself wherein the ion was at two separate places at the same time corresponding to a wave function state called a "Schrödinger cat" state [32-34]. According to Monroe et al. [33],

> "A "Schrödinger cat"-like state of matter was generated at the single atom level. A trapped $^{9}Be^{+}$ ion was laser-cooled to the zero-point energy and then prepared in a superposition of spatially separated coherent oscillator states. This state was

created by application of a sequence of laser pulses, which entangles internal (electronic) and external (motional) states of the ion. The "Schrödinger cat" superposition was verified by detection of the quantum mechanical interference between the localized wave packets. This mesoscopic system may provide insight into the fuzzy boundary between the classical and quantum worlds by allowing controlled studies of quantum measurement and quantum decoherence."

The "Schrödinger cat" state analysis relies on the postulate that the Pauli Exclusion Principle applies to Rabi states wherein a rotation of the magnetic moment of the unpaired electron of an RF-trapped $^{9}Be^{+}$ ion is represented by a linear combination of spin 1/2 ($\left|\uparrow\right\rangle_i$) and spin -1/2 ($\left|\downarrow\right\rangle_i$) states. Three steps of rotation of the spin magnetic moment by a time harmonic field provided by pairs of copropagating off-resonant laser beams which drove two-photon-stimulated Raman magnetic resonance transitions were each separated by displacement laser pulses which excited a resonant translational harmonic oscillator level of the trapped ion by coupling only with the $\left|\uparrow\right\rangle_i$ state. According to Monroe, "this selectivity of the displacement force provides quantum entanglement of the internal state with the external motional state. Although the motional state can be thought of as nearly classical, its entanglement with the internal atomic quantum levels precludes any type of semiclassical analysis". The interference was detected by exciting a fluorescent transition which only appreciatively coupled to the $\left|\downarrow\right\rangle_i$ state. Thus, the fluorescence reading was proportional to the probability $P_{\downarrow}$ the ion was in state $\left|\downarrow\right\rangle_i$. The "Schrödinger cat" superposition was supposedly verified by detection of the quantum mechanical interference between the localized wave packets.

However, the interference arises not from the existence of the ion at two places at once. The positively charged ion was excited to a time harmonic translational energy state, and the spin quantization axis was defined by an applied 0.20 mT magnetostatic field at an angle of $\frac{\pi}{4}$ with respect to the x-axis of the RF-trap. **The frequency of the energy to "flip" the spin state was equivalent to the projection of that of the translational harmonic oscillator onto the spin axis**

$$\frac{\omega_x}{2\pi}\cos^2\frac{\pi}{4} = (11.2\ MHz)(0.5) = 5.605\ MHz = \frac{\Delta E_{mag}^{spin}}{h} \qquad (37.38)$$

given by Eqs. (37.45-37.48), *infra.* Thus, interference occurred between the Stern-Gerlach transition and the synchrotron radiation corresponding to the charged harmonic oscillator. Since the displacement beams affected only motion correlated with the

with the $|\uparrow\rangle_i$ state, a rotation of the magnetic moment such that $\delta \neq 0$ with application of the displacement beams gives rise to a phase shift of the interference pattern.

Experimental Approach

A classical approach to the description of the experiment and the results of Monroe [33] are given herein. The corresponding description according to a "Schrödinger cat" state is given by Monroe [33].

A single $^9Be^+$ ion was confined in a coaxial-resonator radio frequency (RF)-ion trap [35] that provided harmonic oscillation frequencies of $(\omega_x,\omega_y,\omega_z)/2\pi \approx (11.2, 18.2, 29.8)\ MHz$ along the principal axes of the trap. The ion was laser-cooled to the quantum ground state of motion [36], and then the electronic and motional states were coherently manipulated by applying pairs of off-resonant laser beams, which drove two-photon stimulated Raman transitions. The two internal states of interest were the stable $^2S_{1/2}(F=2,m_F=-2)$ and $^2S_{1/2}(F=1,m_F=-1)$ hyperfine ground states (denoted by $|\downarrow\rangle_i$ and $|\uparrow\rangle_i$, respectively), separated in frequency by $\omega_{HF}/2\pi \approx 1.250\ GHz$. Here, F and m_F are quantum numbers representing the total internal angular momentum of the atom and its projection along a quantization axis. The Raman beams were detuned by $\Delta \approx -12\ GHz$ from the $^2P_{1/2}(F=2,m_F=-2)$ excited state, which acted as the virtual level, providing the Raman coupling. The external motional states were characterized by the quantized vibrational harmonic oscillator states $|n\rangle_e$ in the x dimension, separated in frequency by $\omega_x/2\pi \approx 11.2\ MHz$.

When the Raman beam difference frequency was tuned near ω_{HF} and the "carrier beams" a and b were applied, the magnetic moment of the ion was rotated away from the spin axis as described by Slichter [37]. By adjusting the exposure time of the carrier beams, for example, the electronic state was "flipped"--a $|\downarrow\rangle_i$ to $|\uparrow\rangle_i$ transition by a π-pulse or rotated into the x'y'-plane (the plane perpendicular to the spin axis) of the rotating coordinate system by a $\frac{\pi}{2}$-pulse. Transitions on the carrier did not significantly affect the state of motion, because beams a and b were copropagating. When the Raman beam difference frequency was tuned near ω_x, and the "displacement" beams b and c of were applied, the displacement beams produced a "walking wave" pattern whose time-dependent dipole force resonantly excited the harmonic motion. According to Monroe [33], this force promoted an initial zero-point state of motion $|0\rangle_e$ to a coherent state

$$|\beta\rangle_e = \exp\left(\frac{-|\beta|^2}{2}\right)\sum_n \frac{\beta^n}{(n!)^{1/2}}|n\rangle_e \tag{37.39}$$

where $\beta = \alpha e^{i\theta}$ is a dimensionless complex number that represents the amplitude and phase of the motion in the harmonic potential. The probability distribution of vibrational levels in a coherent state is Poissonian with mean number of vibrational quanta

$$\langle n\rangle = \alpha^2 \tag{37.40}$$

The coherent state of motion is much like classical motion in a harmonic potential with amplitude

$$2\alpha x_0 \tag{37.41}$$

where

$$x_0 = \left(\frac{\hbar}{2M\omega_x}\right)^{1/2} = 7.1\,nm \tag{37.42}$$

was the root mean square Gaussian amplitude of the oscillating ion and M was the mass of the ion.

The polarizations of the three Raman beams, a, b, and c produced π, σ^+/σ^-, and σ^- couplings, respectively, with respect to a quantization axis defined by an applied $0.20\,mT$ magnetic field which was at an angle of $\frac{\pi}{4}$ with respect to the x-axis of the RF-trap. As a result, the displacement beams (b and c) affected only the motional state correlated with the $|\uparrow\rangle_i$ state, because the σ^- polarized beam c could not couple the $|\downarrow\rangle_i$ state to any virtual $^2P_{1/2}$ states.

The energy to flip the orientation of the orbitsphere due to its magnetic moment of a Bohr magneton, μ_B, given by Eq. (1.151) is

$$\Delta E_{mag}^{spin} = 2g\mu_B\mathbf{B} \tag{37.43}$$

where

$$\mu_B = \frac{e\hbar}{2m_e} \tag{37.44}$$

In the case that the magnetic flux density was $0.2\,mT$, the energy was

$$\Delta E_{mag}^{spin} = 2g\mu_B\mathbf{B} = 2(1.00116)\left(9.2741X10^{-24}\frac{J}{T}\right)\left(0.2\ X\ 10^{-3}\ T\right) = 3.714\ X\ 10^{-27}\ J \tag{37.45}$$

The resonance frequency is given by Planck's equation

$$\omega = \frac{\Delta E_{mag}^{spin}}{\hbar} = \frac{3.714\ X\ 10^{-27}\ J}{\hbar} = 3.522\ X\ 10^7\ \frac{rads}{s} = 5.605\,MHz \tag{37.46}$$

As demonstrated by Eq. (37.72) and Eq. (37.73), *infra.*, energy is exchanged between the harmonic oscillator state and the spin state according to the dot product of the wavenumber vector of the spin transition and the harmonic displacement vector

$$\left[\mathbf{k}\ \mathbf{u}(l,\phi)\right]^2 \quad \cos^2\frac{\pi}{4} = 0.5 \tag{37.47}$$

Because the positively charged ion was excited to a time harmonic translational energy state along the x-axis, and the spin quantization axis was defined by an applied $0.20\ mT$ magnetostatic field at an angle of $\frac{\pi}{4}$ with respect to the x-axis of the RF-trap the frequency of the energy to "flip" the spin state was equivalent to the projection of that of the translational harmonic oscillator onto the spin axis

$$\frac{\omega_x}{2\pi}\cos^2\frac{\pi}{4} = (11.2\ MHz)(0.5) = 5.605\ MHz = \frac{\Delta E_{mag}^{spin}}{h} \tag{37.48}$$

Each Raman beam contained $\approx 1\ mW$ of power at $\approx 313\ nm$. This resulted in a two-photon Rabi frequency of $\frac{\Omega}{2\pi} = 250\ kHz$ for the copropagating Raman carrier beams a and b, or a π-pulse exposure time of about $1\ \mu s$. The displacement Raman beams (b and c) were applied to the ion in directions such that their wave vector difference **dk** pointed nearly along the x-axis of the trap. Motion in the y or z dimensions was therefore highly insensitive to the displacement beams. When the displacement beams were applied to a zero-point translational state (correlated with the $\left|\uparrow\right\rangle_i$ state) for time τ on average a harmonic oscillator state of amplitude

$$\alpha = \eta\Omega_d\tau \tag{37.49}$$

was created. Here, $\eta = 0.205$ is the Lamb-Dicke parameter and $\frac{\Omega_d}{2\pi} \approx 300\ kHz$ is the coupling strength of the displacement beams. After each preparation cycle (described below), which spin state ($\left|\downarrow\right\rangle_i$ or $\left|\uparrow\right\rangle_i$) the ion occupied was detected independent of its state of motion. This was accomplished by applying a few microwatts of σ^--polarized light ("detection" beam d) resonant with the cycling $\left|\downarrow\right\rangle_i \rightarrow {}^2P_{3/2}\left(F = 3,\ m_F = -3\right)$ transition [radiative linewidth $\frac{\gamma}{2\pi} \approx 19.4\ MHz$ at wavelength $(\lambda) \approx 313\ nm$] and observing the resulting ion fluorescence. Because this radiation does not appreciably couple to the $\left|\uparrow\right\rangle_i$ state, the fluorescence reading was proportional to the probability $P_\downarrow$ the ion was in state $\left|\downarrow\right\rangle_i$. The experiment was continuously repeated--cooling, state preparation, detection--while slowly sweeping the harmonic oscillator phase ϕ.

State Preparation and Detection

The ion was first laser-cooled so that the $\left|\downarrow\right\rangle_i\left|n_x = 0\right\rangle_e$ state was

occupied about 95% of the time. Then, five sequential pulses of Raman beams were applied. In step 1, a $\frac{\pi}{2}$-pulse on the carrier rotated the magnetic moment into the plane perpendicular to the spin axis (z'-axis) in a coordinate system which rotates around the z'-axis. The moment precessed about the x'-axis of the rotating coordinate frame described by Slichter [37]. The precessing moment had a time averaged projection onto the z'-axis equivalent to an equal superposition of states $\left|\downarrow\right\rangle_i|0\rangle_e$ and $\left|\uparrow\right\rangle_i|0\rangle_e$. In step 2, the displacement beams excited the motion correlated with the $\left|\uparrow\right\rangle_i$ component to a harmonic oscillator state $\left|\alpha e^{-i\phi/2}\right\rangle_e$. In step 3, a π-pulse rotated the magnetic moment in the plane perpendicular to the spin axis such that the moment precessed about the negative x'-axis of the rotating coordinate frame described by Slichter [37]. The precessing moment was equivalent to the swap of the superposition of states $\left|\downarrow\right\rangle_i|0\rangle_e$ and $\left|\uparrow\right\rangle_i|n\rangle_e$ produced in step 1 to give component states $\left|\downarrow\right\rangle_i|n\rangle_e$ and $\left|\uparrow\right\rangle_i|0\rangle_e$. In step 4, the displacement beams excited the motion correlated with the $\left|\uparrow\right\rangle_i$ component to a second harmonic oscillator state $\left|\alpha e^{i\phi/2}\right\rangle_e$. In step 5, a final $\frac{\pi}{2}$-pulse on the carrier rotated the magnetic moment to the spin axis to give $\left|\downarrow\right\rangle_i|n\rangle_e$, the initial spin state excited to an oscillator state of quantum number n, or $\left|\uparrow\right\rangle_i|n\rangle_e$, the flipped spin state excited to an oscillator state of quantum number n. In the absence of interference between the oscillatory state and the spin state, $\left|\downarrow\right\rangle_i|n\rangle_e$ and $\left|\uparrow\right\rangle_i|n\rangle_e$ occur with equal probability. The relative phases of the above steps were determined by the phases of the RF difference frequencies of the Raman beams which were easily controlled by phase-locking RF sources. The experiment was continuously repeated--cooling, state preparation, detection--while slowly sweeping the harmonic oscillator phase ϕ. The relative populations of $\left|\downarrow\right\rangle_i$ and $\left|\uparrow\right\rangle_i$ depended on the phase difference ϕ between the two oscillator states because of the interference of these states, and each coupled (interfered) with the Stern-Gerlach transition. The state $\left|\downarrow\right\rangle_i|n\rangle_e$ underwent a transition to the higher energy spin state $\left|\uparrow\right\rangle_i$ by coupling to the energy of the oscillator state. The amplitude of the oscillation, α, given by Eq. (37.49) is modulated by the interference between the displacement beam of step 2 having a phase $\frac{\phi}{2}$ and step 4 having a phase $\frac{\phi}{2}$. The resultant amplitude,

$\langle\alpha(\phi)\rangle$, of the oscillation as a function of harmonic oscillator phase $\frac{\phi}{2}$ was given by

$$\langle\alpha(\phi)\rangle = \sqrt{\left(\alpha e^{i\frac{\phi}{2}}\right)^2} = \sqrt{\left(\alpha e^{-i\frac{\phi}{2}}\right)^2} = \alpha\sin\frac{\phi}{2} \tag{37.50}$$

where the probability (Eq. (37.81), *infra.*) of detecting the $|\downarrow\rangle_i$ was $\phi = \frac{\pi}{2}$ out of phase with the probability of the ion oscillatory state $|n\rangle_e$ because the spin flip to the higher energy state occurred--$|\downarrow\rangle_i \rightarrow |\uparrow\rangle_i$. The interference of the oscillator states with the Stern-Gerlach transition was measured by detecting the probability $P_{\downarrow}(\phi)$ that the ion was in the $|\downarrow\rangle_i$ state for a given value of ϕ. The magnitude of the harmonic oscillator state was controlled by the duration of the applied displacement beams (Eq. (37.49)) in steps 2 and 4. The phase of the harmonic oscillator state was controlled by the phase of the applied displacement beams in steps 2 and 4. Monroe et al. report [33] on average the detection of one photon per measurement cycle when the ion was in the $|\downarrow\rangle_i$ state. The data represented an average of about 4000 measurements, or 1 second of integration.

The physical behavior of a large number of continuous Stern-Gerlach experiments (an ensemble) each detecting the spin state of a harmonic oscillating RF-trapped ion is equivalent to that of the interaction of ultrasound with Mössbauer gamma rays (interference of an electronic transition and an oscillator transition). Consider the Lamb-Mössbauer formula for the absorption of a γ ray of energy E by a nucleus in a crystal given by Maradudin [38].

$$\sigma_a(E) = \frac{1}{4}\sigma_0\Gamma^2\sum_{mn} e^{-\frac{\beta E_m}{Z}} X \frac{\langle m|e^{i\frac{\mathbf{p}}{\hbar}\cdot\mathbf{R}(l)}|n\rangle\langle n|e^{-i\frac{\mathbf{p}}{\hbar}\cdot\mathbf{R}(l)}|m\rangle}{\left(E_0 - E + E_n - E_m\right)^2 + \frac{1}{4}\Gamma^2} \tag{37.51}$$

In this equation, E_0 is the energy difference between the final and initial nuclear states of the absorbing nucleus, E_m and E_n are the energies of the eigenstates $|m\rangle$ and $|n\rangle$ of the crystal, respectively, Γ is the natural width of the excited state of the nucleus, $\mathbf{p}$ is the momentum of the γ ray, $\mathbf{R}(l)$ is the instantaneous position vector of the absorbing nucleus, Z is the crystal's partition function, $T = (k\beta)^{-1}$, and σ_0 is the resonance absorption cross section for the absorbing nucleus. By expressing the denominator of Eq. (37.51) as an integral, Eq. (37.51) is equivalent to

$$\sigma_a(E) = \frac{1}{2}\sigma_0\gamma\int_{-\infty}^{\infty} dt e^{i\omega t - \gamma|t|} X\left\langle \exp\left[-i\mathbf{k}\cdot\mathbf{u}(l;t)\right]\exp\left[i\mathbf{k}\cdot\mathbf{u}(l;0)\right]\right\rangle \tag{37.52}$$

wherein the position vector $\mathbf{R}(l)$ is

$$\mathbf{R}(l) = \mathbf{x}(l) + \mathbf{u}(l) \tag{37.53}$$

For, Eq. (37.53), $\mathbf{x}(l)$ is the position vector of the mean position of the absorbing nucleus, and $\mathbf{u}(l)$ is its displacement from the mean position. Eq. (37.52) follows from Eq. (37.51) with the following substitutions:

$$\left(\frac{1}{\hbar}\right)\mathbf{p} = \mathbf{k} \tag{37.54}$$

$$\hbar\omega = E - E_0 \tag{37.55}$$

$$\gamma = \frac{\Gamma}{2\hbar} \tag{37.56}$$

and $\mathbf{u}(l;t)$ denotes the Heisenberg operator,

$$\mathbf{u}(l;t) = e^{i\left(\frac{t}{\hbar}\right)H}\,\mathbf{u}(l;0)\,e^{-i\left(\frac{t}{\hbar}\right)H} \tag{37.57}$$

where H is the Hamiltonian. The angular brackets in Eq. (37.52) denote an average over the canonical ensemble of the crystal.

The probability $P_{\downarrow}(\phi)$ that the ion of the experiments of Monroe et al. [33] was in the $\left|\downarrow\right\rangle_i$ state for a given value of ϕ is herein derived from the correlation function for the statistical average of large number of continuous Stern-Gerlach experiments (an ensemble) each detecting the spin state of a harmonic oscillating RF-trapped ion which is equivalent to that of the interaction of ultrasound with Mössbauer gamma rays. From Eq. (37.52), the correlation function $Q(t)$ of acoustically modulated gamma ray absorption by Mössbauer nuclei is

$$Q(t) = \left\langle \exp\left[-i\mathbf{k}\cdot\mathbf{u}(l;t)\right]\exp\left[i\mathbf{k}\cdot\mathbf{u}(l;0)\right]\right\rangle \tag{37.58}$$

In the present case, the position vector is given by Eq. (37.53) where $\mathbf{x}(l)$ is the position vector of the mean position of the trapped ion, and $\mathbf{u}(l)$ is its displacement from the mean position. In this case, $\mathbf{p}$ and $\mathbf{k}$ of Eq. (37.54) are the momentum and the wavenumber, respectively, of the ion corresponding to the spin flip, E of Eq. (37.55) is the energy of the harmonic oscillator, E_0 is the difference in energy between the $\left|\uparrow\right\rangle_i$ and $\left|\downarrow\right\rangle_i$ states, and $\mathbf{u}(l;t)$ of Eq. (37.57) is

$$\mathbf{u}(l;t) = e^{i\left(\frac{t}{\hbar}\right)E}\,\mathbf{u}(l;0)\,e^{-i\left(\frac{t}{\hbar}\right)E} \tag{37.59}$$

The matrix elements of Eq. (37.58) are calculated by using the theorem [39]

$$e^A e^B = e^{A+B}e^{\frac{1}{2}[A,B]} \qquad \text{if } \left[[A,B],A\right] = \left[[A,B],B\right] = 0 \tag{37.60}$$

For a harmonic oscillator, the commutator of $\mathbf{k}\cdot\mathbf{u}(l;t)$ and $\mathbf{k}\cdot\mathbf{u}(l;0)$ is a c number; thus,

$$Q(t) = \left\langle \exp\left[-i\mathbf{k}\ \mathbf{u}(l;t)\right]\exp\left[i\mathbf{k}\ \mathbf{u}(l;0)\right]\right\rangle$$
$$= \left\langle \exp\left[-i\mathbf{k}\ \left[\mathbf{u}(l;t)-\mathbf{u}(l;0)\right]\right]\right\rangle X \exp\left[\frac{1}{2}\left\langle\left[\mathbf{k}\ \mathbf{u}(l;t),\ \mathbf{k}\ \mathbf{u}(l;0)\right]\right\rangle\right] \quad (37.61)$$

Since the correlation function applies to an ensemble of harmonic oscillator states, the first thermodynamic average can be simplified as follows:

$$\left\langle \exp\left[-i\mathbf{k}\ \left[\mathbf{u}(l;t)-\mathbf{u}(l;0)\right]\right]\right\rangle = \exp\left[-\frac{1}{2}\left\langle\left\{\mathbf{k}\ \left[\mathbf{u}(l;t)-\mathbf{u}(l;0)\right]\right\}^2\right\rangle\right] \quad (37.62)$$

This theorem is known in lattice dynamics as Ott's theorem [40] or sometimes as Bloch's theorem [41]. Using the time independence of the harmonic potential, Eq. (37.62) is

$$\exp\left[-\frac{1}{2}\left\langle\left\{\mathbf{k}\ \left[\mathbf{u}(l;t)-\mathbf{u}(l;0)\right]\right\}^2\right\rangle\right] = \exp\left[-\frac{1}{2}\left\langle\left[\mathbf{k}\ \mathbf{u}(l;t)\right]^2\right\rangle + \frac{1}{2}\left\langle\left[\mathbf{k}\ \mathbf{u}(l;0)\right]^2\right\rangle\right] \quad (37.63)$$

$$= \exp-\left\langle\left[\mathbf{k}\ \mathbf{u}(l)\right]^2\right\rangle \quad (37.64)$$

Substitution of Eqs. (37.62-37.64) into Eq. (37.61) gives

$$Q(t) = \exp\left\langle-\left[\mathbf{k}\ \mathbf{u}(l;t)\right]^2\right\rangle X \exp\left[\frac{1}{2}\left\langle\left[\mathbf{k}\ \mathbf{u}(l;t),\ \mathbf{k}\ \mathbf{u}(l;0)\right]\right\rangle\right] \quad (37.65)$$

Expanding $\mathbf{u}_\alpha(l;t)$ in terms of the normal coordinates of the harmonic potential and the phonon operators of that harmonic potential gives

$$u_\alpha(l;t) = \left(\frac{\hbar}{2M_l}\right)^{\frac{1}{2}} \sum_s \frac{B_\alpha^{(s)}(l)}{(\omega_s)^{\frac{1}{2}}}\left(b_s e^{-i\omega_s t} + b_s^\dagger e^{i\omega_s t}\right) \quad (37.66)$$

where α labels the Cartesian components, M_l is the mass of the ion in the lth experiment, ω_s is the frequency of the sth normal mode, $B^{(s)}(l)$ is the associated unit eigenvector, and $b_s^\dagger$ and b_s are the phonon creation and destruction operators for the sth normal mode. By use of the coordinate expansion, the exponential of the correlation function appearing in Eq. (37.65) can be written as

$$e^{\langle \mathbf{k}\,\mathbf{u}(l;t)\mathbf{k}\,\mathbf{u}(l;0)\rangle} = e^{\sum_s -c_s^2\left(\frac{e^{i\omega_s t}}{(\gamma_s)^{\frac{1}{2}}} + (\gamma_s)^{\frac{1}{2}} e^{-i\omega_s t}\right)}$$
$$= \prod_s e^{-c_s^2\left(\frac{e^{i\omega_s t}}{(\gamma_s)^{\frac{1}{2}}} + (\gamma_s)^{\frac{1}{2}} e^{-i\omega_s t}\right)} \quad (37.67)$$
$$= \prod_s \left[J_0\left(2c_s^2\right) + \sum_{n=1}^{\infty} J_n\left(2c_s^2\right)\left(\frac{e^{i\omega_s t}}{(\gamma_s)^{\frac{1}{2}}} + (\gamma_s)^{\frac{1}{2}} e^{-i\omega_s t}\right)\right]$$

where the following substitutions were made:

$$\gamma_s = \frac{n_s + 1}{n_s} = e^{\frac{\hbar\omega_s}{kT}} \tag{37.68}$$

$$n_s = \frac{1}{e^{\frac{\hbar\omega_s}{kT}} - 1} \tag{37.69}$$

$$c_s^2 = \frac{\hbar}{2M_l} \frac{\left[k \; B^{(s)}(l)\right]^2}{\omega_s} \frac{e^{\frac{\hbar\omega_s}{2kT}}}{e^{\frac{\hbar\omega_s}{kT}} - 1} \tag{37.70}$$

and where the Bessel function relationship [42]

$$e^{\frac{1}{2}x\left(y+y^{-1}\right)} = \sum_{n=-\infty}^{\infty} J_n(x) y^n \tag{37.71}$$

was used. n_s is the mean number of phonons in the sth mode at temperature T. In the case of Monroe's experiments [33], the correlation function for the exchange of energy between a harmonic oscillator state and a spin state was independent of time--not a function of $e^{i\omega_s t}$ and $e^{-i\omega_s t}$. Thus, the time dependent factors are dropped in Eq. (37.67), and combining Eqs. (37.65-37.67) and Eq. (37.70) gives the correlation function as

$$Q\left(c_s^2\right) = \exp -\left[c_s^2\right] \prod_s J_0\left(2c_s^2\right) \tag{37.72}$$

For the experiment of Monroe et al. [33], the ion was laser-cooled so that the $\left|\downarrow\right\rangle_i \left|n_x = 0\right\rangle_e$ state was occupied about 95% of the time; thus, the partition function of Eq. (37.51) is equal to one. Eq. (37.70) is

$$c_s^2 = \frac{\hbar}{2M} \frac{\left[k \; B^{(s)}(l)\right]^2}{\omega_s} \tag{37.73}$$

The harmonic frequency was $\omega_s = \omega_x$ with $s = 1$ in Eq. (37.67) where the sum is over the ensemble of translational harmonic oscillator modes for a series of "Schrödinger cat" state experiments--each a specific Raman beam pulse sequence with measurement; therefore, the correlation function is

$$Q\left(c_s^2\right) = \exp -\left[c_s^2\right] J_0\left(2c_s^2\right) \tag{37.74}$$

Monroe et al. [33] measured the probability of spin state $\left|\downarrow\right\rangle_i$ as a function of the phase angle of the displacement lasers of steps 2 and 4. The probability $P_\downarrow(\phi)$ of detecting the $\left|\downarrow\right\rangle_i$ state as a function of phase angle, ϕ, can be derived from the correlation function, Eq. (37.74). The expansion of the Bessel function is

$$J_\nu(x) = \left(\frac{x}{2}\right)^\nu \sum_{m=0}^{\infty} \frac{\left(-\frac{x^2}{4}\right)^m}{\left[m!\Gamma(m+\nu+1)\right]}$$
$$J_0(x) = \sum_{m=0}^{\infty} \frac{\left(-\frac{x^2}{4}\right)^m}{\left[m!\Gamma(m+1)\right]} = \sum_{m=0}^{\infty} \frac{\left(-\frac{x^2}{4}\right)^m}{[m!m!]} \tag{37.75}$$

where $\Gamma(m+1) = m!$ was used. The probability distribution function of vibrational levels in a coherent state is Poissonian. The probability [43] of a spin flip with the emission of m phonons is

$$P_m = \frac{\langle n\rangle^m e^{-\langle n\rangle}}{m!} = \frac{\left(\alpha^2\right)^m e^{-\alpha^2}}{m!} = \frac{\alpha^{2m} e^{-\alpha^2}}{m!} \tag{37.76}$$

with mean number of vibrational quanta $\langle n\rangle = \alpha^2$ (Eq. (37.40)). The probability $P_\downarrow(\phi)$ can be derived by factoring Eq. (37.76) from the Bessel function of the correlation function (Eq. (37.74)) and its expansion which follows from Eq. (37.75).

$$J_0(x) = \sum_{m=0}^{\infty} \frac{\left(-\frac{x^2}{4}\right)^m}{[m!m!]};$$
$$J_0(\alpha x) = \sum_{m=0}^{\infty} \frac{\left(-\frac{(\alpha x)^2}{4}\right)^m}{m!m!} = \frac{1}{e^{-\alpha^2}} \sum_{m=0}^{\infty} \frac{\left(-\frac{x^2}{4}\right)^m}{m!} \frac{\alpha^{2m} e^{-\alpha^2}}{m!} \tag{37.77}$$

Combining Eq. (37.76) and Eq. (37.77) demonstrates that the probability $P_\downarrow(\phi)$ is proportional to

$$P_\downarrow(\alpha x) \quad \sum_{m=0}^{\infty} \frac{\left(-\frac{x^2}{4}\right)^m}{m!} \tag{37.78}$$

Let $x = y^2$, then the change of variable in Eq. (37.78) is

$$P_\downarrow(\alpha y) \quad \sum_{m=0}^{\infty} \frac{\left(-\frac{x}{4}\right)^m}{m!} = \sum_{m=0}^{\infty} \frac{\left(-\frac{x^2}{4}\right)^{m/2}}{m!} \tag{37.79}$$

Let $m' = m/2$, then the change of variable in Eq. (37.79) is

$$P_\downarrow(\alpha y) \quad \sum_{m=0}^{\infty} \frac{\left(-\frac{x^2}{4}\right)^{m/2}}{m!} \quad \sum_{m=0}^{\infty} \frac{\left(-\frac{x^2}{4}\right)^{m'}}{(2m')!} \tag{37.80}$$

The series expansion of $\cos(x)$ is

$$\cos(x) = \sum_{m=0}^{\infty} \frac{\left(-x^2\right)^m}{(2m)!} \tag{37.81}$$

Combining Eq. (37.74) and Eqs. (37.78-37.81) gives the probability $P_{\downarrow}(\phi)$ proportional to

$$P_{\downarrow}(\phi) \quad \cos\left(2\alpha\sqrt{c_s^2}\right) \tag{37.82}$$

where $y = \sqrt{x} = \sqrt{c_s^2}$. The quantization axis was at an angle of $\frac{\pi}{4}$ with respect to the x-axis. From Eqs. (37.40-37.42), Eq.(37.50), and Eq. (37.73),

$$c_s^2 = \alpha^2 \sin^2 \frac{\phi}{2} \tag{37.83}$$

Combining Eq. (37.82) and Eq. (37.83) gives the probability $P_{\downarrow}(\phi)$ proportional to

$$P_{\downarrow}(\phi) \quad \cos\left(2\alpha^2 \sin\frac{\phi}{2}\right) \tag{37.84}$$

Combining Eq. (37.74), Eq. (37.83), and Eq. (37.84) gives the probability $P_{\downarrow}(\phi)$ proportional to

$$P_{\downarrow}(\phi) \quad \exp\left[-\alpha^2 \sin^2\phi\right]\cos\left(2\alpha^2 \sin\frac{\phi}{2}\right) = \exp\left[-\alpha^2\left(\frac{1-\cos\phi}{2}\right)\right]\cos\left(2\alpha^2 \sin\frac{\phi}{2}\right) \tag{37.85}$$

The rotation of the magnetic moment with RF fields such that $\delta \neq 0$ with application of the displacement beams is equivalent to a phase shift of the correlation function given by Eq. (37.58)

$$Q(t) = \left\langle \exp i\delta \exp\left[-i\mathbf{k}\ \mathbf{u}(l;t)\right]\exp\left[i\mathbf{k}\ \mathbf{u}(l;0)\right]\right\rangle \tag{37.86}$$

Thus, Eq. (37.85) is phase shifted.

$$P_{\downarrow}(\phi,\delta) \quad \exp\left[-\alpha^2\left(\frac{1-\cos\phi}{2}\right)\right]\cos\left(\delta + 2\alpha^2 \sin\frac{\phi}{2}\right) \tag{37.87}$$

The probability of detecting either $|\downarrow\rangle_i$ or $|\uparrow\rangle_i$ is one. The initial state of the ion for each cycle is $|\downarrow\rangle_i$. Consider the $\frac{\pi}{2}$-pulses (steps 2 and 5). In the absence of interference between the oscillator states and the Stern-Gerlach transition with $\alpha \neq 0$, the probability of detecting $|\downarrow\rangle_i$ or $|\uparrow\rangle_i$ is the same--1/2. However, with interference, the spin flip to the higher energy state occurs, $|\downarrow\rangle_i \rightarrow |\uparrow\rangle_i$. The probability of detecting $|\downarrow\rangle_i$ with interference is given by 1/2 minus the probability function, Eq. (37.87), normalized to 1/2. The probability function for the detection of $|\downarrow\rangle_i$ with interference as a function of phase angle, ϕ, harmonic oscillator amplitude, α, and phase shift, δ, is

$$P_{\downarrow}(\phi,\delta) = \frac{1 - \exp\left[-\alpha^2\left(\frac{1-\cos\phi}{2}\right)\right]\cos\left(\delta + 2\alpha^2 \sin\frac{\phi}{2}\right)}{2} \tag{37.88}$$

The plot of the probability $P_{\downarrow}(\phi)$ of detecting the $|\downarrow\rangle_i$ state as a function of phase angle, ϕ, harmonic oscillator amplitude, α, and phase shift, δ, using the values of the curve fit parameters of Monroe et al. [33] are given in Figures 37.9 and 37.10. Monroe et al. report [33] on average the detection of one photon per measurement cycle when the ion is in the $|\downarrow\rangle_i$ state. The data represented an average of about 4000 measurements, or 1 second of integration.

Figure 37.9. The plot of the probability $P_{\downarrow}(\phi)$ (Eq. (37.88)) of detecting the $|\downarrow\rangle_i$ state as a function of phase angle, ϕ, for the harmonic oscillator amplitude, α, and phase shift, $\delta = 0$. Curves in (**A**) to (**D**) represent experiments with various values of τ (2, 3, 5, and 15 μs, respectively). The curves are fits of the measurements to the values of Monroe et al. [33] for the parameter α of α=0.84, 1.20, 1.92, and 2.97, respectively.

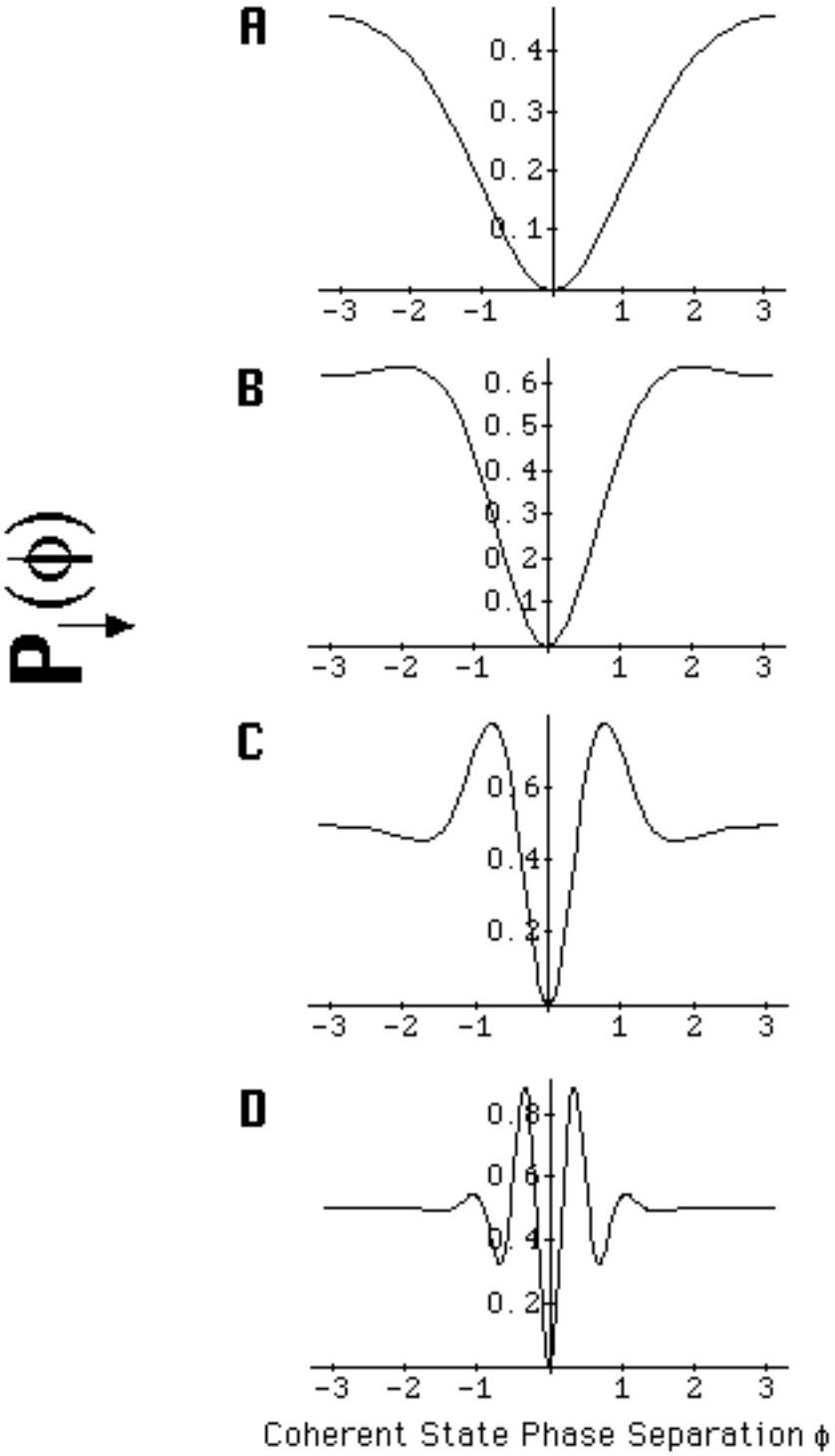

Figure 37.10. The plot of the probability $P_{\downarrow}(\phi)$ (Eq. (37.88)) of detecting the $|\downarrow\rangle_i$ state as a function of phase angle, ϕ, for the harmonic oscillator amplitude, $\alpha = 1.5$, and phase shift, δ. Curves in (**A**) to (**C**) are fits of the measurements to the values of Monroe et al. [33] for the parameter δ of $\delta = 1.03\pi$, 0.48π, and 0.06π, respectively.

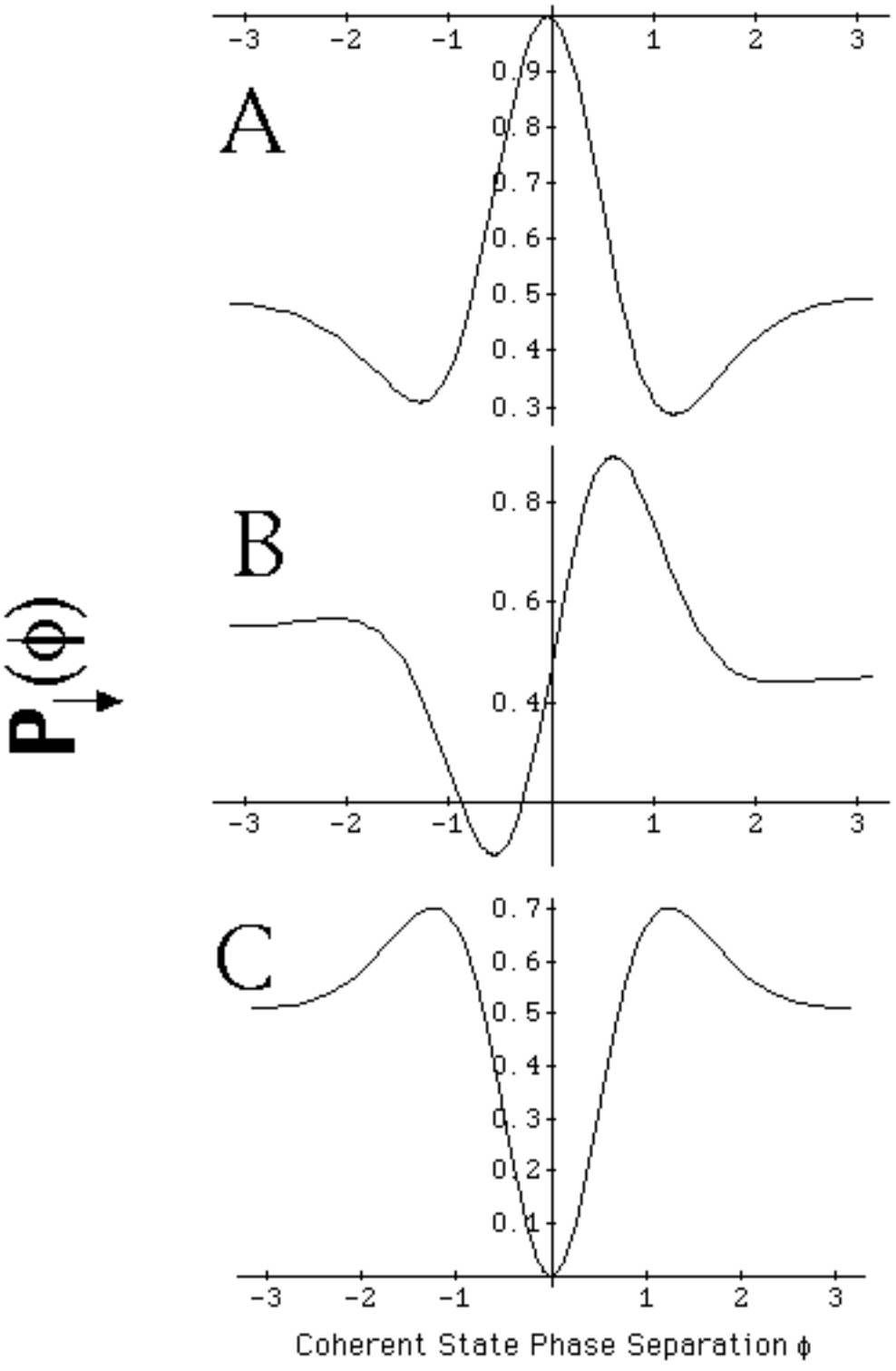

These results confirm that classical physics predicts the interference patterns observed by Monroe et al. [33] for a single $^{9}Be^{+}$ ion in a trap in a continuous Stern-Gerlach experiment without the requirement of Monroe [33] or Browne [32], "that an entire atom can simultaneously exist in two widely separated places".

SCHRÖDINGER FAT CATS-ANOTHER FLAWED INTERPRETATION

A recent report in The New York Times [44] entitled "Here, There and Everywhere: A Quantum State of Mind" states, "Physicists at Delft University of Technology have put a 5-micrometer-wide loop of superconducting wire into a "quantum superposition" of two contradictory possibilities: in one, the current flows clockwise; in the other, current flows counterclockwise." The article further states, "In the realm of atoms and smaller particles, objects exist not so much as objects as mists of possibilities being here there and everywhere at the same time-and then someone looks and the possibilities suddenly collapse into definite locations." The experiment was a simplified version of the concept of Schrödinger's cat. In 1935, Schrödinger [45] attempted to demonstrate the limitations of quantum mechanics using a thought experiment in which a cat is put in a quantum superposition of alive and dead states.

Instead of a cat, Friedman et al. [46] used a small square loop of superconducting wire linked to a SQUID (Superconducting Quantum Interference Device). A SQUID comprises a superconducting loop with a Josephson junction, a weak link that causes magnetic flux to be linked in integer units of the magnetic flux quantum. When the loop is placed in an external magnetic field, the loop spontaneously sets up an electrical current to cancel the field or generate an additional magnetic field, adjusting the magnetic field to a unit of the magnetic flux quantum, one of the allowed values. In the experiment of Friedman et al. [46], the loop was placed in a magnetic field equal to one half of the first allowed value, a magnetic flux quantum. Thus, the loop could set up either a current to raise the field strength to the first allowed value, or with equal probability, a current of equal magnitude flowing in the opposite direction to cancel out the external field. A pulse of microwaves was applied at the frequency to cause a transition of the magnetic moment of the current loop as an entirety. The absorption of microwaves caused the magnetic state of the SQUID to change and the current to reverse its direction.

Experimentally, a measurement always gave one of the two possible answers, clockwise or counterclockwise, never a zero cancellation. A difference in energy at which the flip transition occurred between the

two possibilities was detected by a group led by J. Lukens and J. Friedman at the State University of New York (SUNY) [46]. A simple explanation was that the microwaves simply flipped the current direction which had a energy bias in one direction versus the opposite based on the corresponding presence or absence of a magnetic flux quantum within the SQUID. Rather, they interpreted the results as experimental evidence that a SQUID can be put into a superposition of two magnetic flux states: one corresponding to a few microamperes of current flowing clockwise and the other corresponding to the same amount of current flowing anticlockwise. "Just as the cat is neither alive nor dead but a ghostly mix of the two possibilities, the current flows neither clockwise or counterclockwise, but is a mix of the two possibilities [44]." According to Friedman, "we can have two of these macroscopically well-defined states at the same time. Which is something of an affront to our classical intuitions about the world [44]."

Current running in both directions simultaneously is nonsensical. Current is a vector and must have only one direction. ***The energy difference observed by Friedman et al. can be explained CLASSICALLY.*** The experimental apparatus comprised a small SQUID coupled to a large current loop. A second SQUID magnetometer read the flux state of the first sample SQUID. The energy difference was not due to superposition of flux states. Rather, it was due to the nature of the electron which carries the superconducing current and links flux in units of the magnetic flux quantum. Consequently, the sample SQUID linked zero or one magnetic flux quantum. When excited by electromagnetic radiation of a resonant frequency, individual electrons undergo a spin-flip or Stern Gerlach transition corresponding to a reversal of the electron magnetic moment, angular moment, and current. The Stern Gerlach transition energies of electrons superimpose. ***The energy difference observed by Friedman et al. matches the energy corresponding to the flux linkage of the magnetic flux quantum by the ensemble of superconducting electrons in their entirety with a reversal of the corresponding macroscopic current.*** The linkage was caused by high power microwave excitation of a Stern Gerlach transition of the magnetically biased loop which caused a concomitant change in the flux state of the separately magnetically biased sample SQUID. In this case, the microwave frequency was kept constant, and the bias flux of the loop was scanned at a fixed magnetic bias of the sample SQUID until the resonance with the superposition of the Stern Gerlach transitions of the superconducting electrons in their entirety was achieved.

Superconducting Quantum Interference Device (SQUID)

The electron possesses an angular momentum of $\hbar$. As shown in the Electron g Factor Section, the electron angular momentum comprises kinetic and vector potential components. Angular momentum is conserved in the presence of an applied magnetic field when the electron links flux in units of the magnetic flux quantum, Φ_0.

$$\Phi_0 = \frac{h}{2e} \tag{37.89}$$

This occurs when the electron rotates by $\frac{\pi}{2}$ radians about an axis perpendicular to the axis parallel to the magnetic flux lines. This electron rotation corresponds to an $\frac{\hbar}{2}$ magnitude, 180° , rotation of the electron's angular momentum vector. In the case that the electrons carry current, this change in momentum of a given current carrying electron increases or decreases the current depending on the vector projection of the momentum change onto the direction of the current. Recently, it has been demonstrated that 50-nm-diameter rings of *InAs* on a *GaAs* surface have can host a single circulating electron in a pure quantum state, that is easily controlled by magnetic fields and voltages on nearby plates. The electrons were observed to link flux in the unit of the magnetic flux quantum with a gain in a unit of angular momentum in a specific direction with the linkage [47] as given in the Aharonov-Bohm Effect Section. Since the electron links flux in units of the magnetic flux quantum, the magnetic flux that links a superconducting loop with a weak link called a Josephson junction is the magnetic flux quantum. The factor of $2e$ in the denominator of the magnetic flux quantum (Eq. (37.89)) has been erroneously interpreted [48] as evidence that Cooper pairs are the superconducting current carriers which is central to the BCS theory of superconductors. However, single electrons, not electron pairs, are the carriers of the superconducting current.

The supercurrent and the linkage of flux is dissipationless; thus, the general form of the equation for the energy of a Josephson junction is harmonic function as given by Fowles [49]. Each electron links flux only in units of the magnetic flux quantum, Φ_0, given by Eq. (37.89). Thus, the natural frequency in terms of the applied flux, Φ, is the magnetic flux quantum, Φ_0.

The simplest SQUID (the radio frequency (r.f.) SQUID) is a superconducting loop of inductance L broken by a Josephson junction with capacitance C and critical current I_c. In equilibrium, a dissipationless supercurrent can flow around this loop, driven by the difference between the flux Φ that threads the loops and the external flux Φ_x applied to the loop. The dynamics of the SQUID can be

described in terms of the variable Φ and are analogous to those of a particle of "mass" C (and kinetic energy $\frac{1}{2}C\dot{\Phi}^2$) moving in a one-dimensional potential given by the sum of the magnetic energy of the loop and the Josephson coupling energy of the junction.

$$U = U_0\left[\frac{1}{2}\left(\frac{2\pi(\Phi-\Phi_x)}{\Phi_0}\right)^2 - \beta_L\cos\left(2\pi\frac{\Phi}{\Phi_0}\right)\right] \tag{37.90}$$

where

$$U_0 \equiv \frac{\Phi_0^2}{4\pi^2 L} \tag{37.91}$$

and

$$\beta_L \equiv \frac{2\pi L I_C}{\Phi_0} \tag{37.92}$$

For the parameters of the experiment, this is a double-well potential separated by a barrier with a height depending on I_c. When $\Phi_x = \frac{\Phi_0}{2}$ the potential is symmetric. Any change in Φ_x then tilts the potential. The flux state of the sample SQUID was zero or one fluxon. A static current flowed either clockwise or counterclockwise around the loop to cancel or augment Φ_x such that an allowed fluxon state was maintained.

Experimental Approach

The SUNY experiment was a macroscopic Stern-Gerlach experiment on a macroscopic current loop coupled to a small d.c. SQUID (sample SQUID). The SQUID and the current loop were independently biased with externally applied flux. The SQUID used in these experiments was made up of two $Nb/AlO_x/Nb$ tunnel junctions in parallel as shown in Figure 37.11. This essentially acted as a tunable junction in which I_c could be adjusted with a flux $\Phi_{xd.c.}$ applied to the small loop of the d.c. SQUID. Another flux Φ_x applied to the loop tuned the tilt ε of the potential wherein $\Phi_{xd.c.}$ tuned the barrier height ΔU_0 at $\varepsilon = 0$. The SQUID was biased such that it was in a zero or one fluxon state. A separate d.c. SQUID inductively coupled to the sample acted as a magnetometer, measuring the flux state of the sample SQUID: zero or one fluxon.

The sample SQUID used in the experiments was characterized by the following three energies: the charging energy

$$E_c \equiv \frac{e^2}{2C} = 9.0\ mK \tag{37.93}$$

the inductive energy

$$E_L \equiv \frac{\Phi_0^2}{2L} = 645\ K \tag{37.94}$$

and a tunable Josephson coupling energy

$$E_J \equiv \left(\frac{I_c \Phi_0}{2\pi}\right)\cos\left(\frac{\pi\Phi_{xd.c.}}{\Phi_0}\right) = 76\ K\cos\left(\frac{\pi\Phi_{xd.c.}}{\Phi_0}\right) \tag{37.95}$$

The plasma frequency ω_J associated with these parameters was, $1.5-1.8\ X\ 10^{11}\ rad\,s^{-1}(24-29\ GHz)$ depending on the value of $\Phi_{xd.c.}$. The fact that $E_c << E_L, E_J$ confirms that flux was the proper basis to describe the SQUID's dynamics.

The sample was encased in a PdAu shield that screened it from unwanted radiation. A coaxial cable entering the shield permitted the application of controlled external microwaves. The set-up was carefully filtered, and cooled to about 40 mK in a dilution refrigerator.

The flux Φ_x tilted the potential from being symmetric at $\Phi_x = \frac{\Phi_0}{2}$ according to Eq. (37.90). It was varied over the range $\frac{\Phi_0}{2} + 11.5\,m\Phi_0 < \Phi_0 < \frac{\Phi_0}{2} + 15.5\,m\Phi_0$. The barrier height ΔU_0 was varied over the range $8.559\,K \le \Delta U_0 \le 9.117\,K$. The SQUID was established in one state and excited with a pulse of high power 96.0 *GHz* (4.61 *K*) microwaves as Φ_x was scanned. The values of Φ_x at which photon absorption occurred with a change of flux state of the SQUID was recorded at a fixed barrier height ΔU_0. The experiment was repeated with ΔU_0 changed.

The system was initially prepared in a zero or one fluxon state with an energy barrier ΔU_0 and a tilt energy ε. Millisecond pulses of 96 GHz microwave radiation at a fixed power was then applied. When the energy difference between the initial and final states matched the resonance frequency as ε was varied for a given ΔU_0, the system had an appreciable probability of changing flux state which was detected by the magnetometer. The experiment was repeated for different values of ΔU_0.

Figure 37.11. The experimental setup.

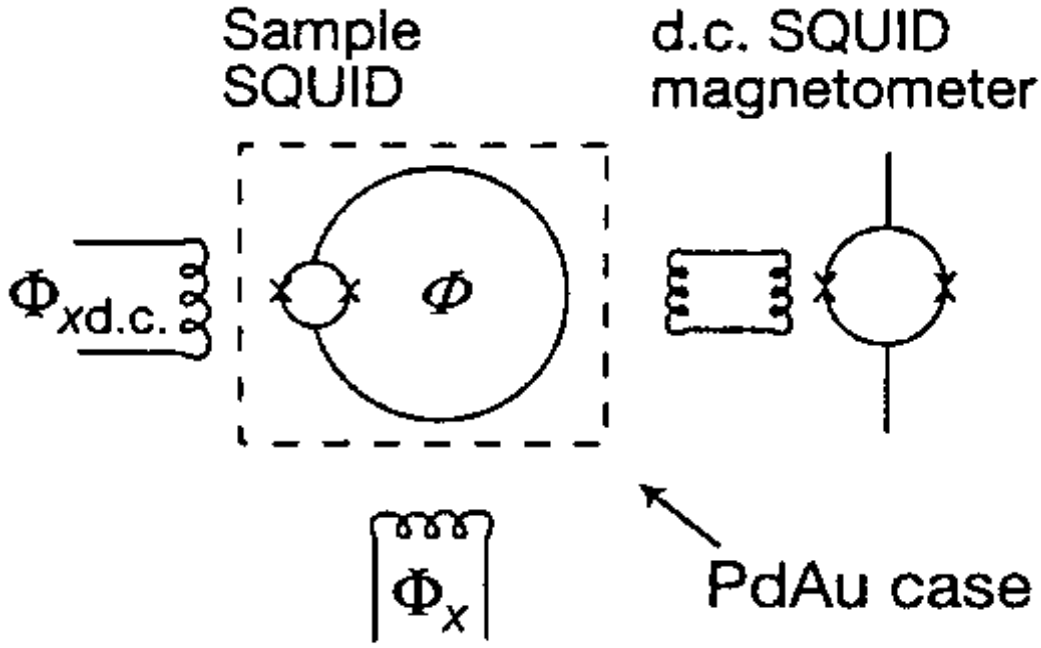

Data

The probability of the sample SQUID making a flux state transition when a millisecond pulse of 96.0 *GHz* (4.61 *K*) microwaves was applied was recorded as shown in Figure 37.12. For each ΔU_0, two peaks were observed as Φ_x was varied. As the energy barrier ΔU_0 was reduced, the observed peaks moved closer together and then separated without crossing. For $\Delta U_0 = 9.117\,K$ (thick solid curve), the right peak corresponds to level $|0\rangle$ which has a greater relative amplitude than the left peak which corresponds to level $|1\rangle$. When ΔU_0 was decreased to $8.956\,K$ (dotted curve), the peaks moved closer, and the asymmetry disappeared. As the barrier was decreased further ($8.797\,K$ is the dashed curve), the peaks moved apart again, and the asymmetry reappeared. But, in this case, the left larger peak corresponded to level $|0\rangle$. Thus, with a barrier change of about $2\,X\,0.14\,K$, the two levels passed through the point at which the levels were symmetrical according to Eq. (37.90) at about $\Delta U_0 = 8.956\,K$. and changed roles without actually intersecting. The insert shows the position of the peaks in the main figure (as well as other peaks) in the $\Delta U_0 - \Phi_x$ plane. Two examples of the convergence and divergence of the peaks in the $\Delta U_0 - \Phi_x$ plane at point where the levels were symmetrical according to Eq. (37.90) were observed. The dashed line in the insert represents the locus of points where the

calculated top of the energy barrier was 96 GHz above state $|i\rangle$. All of the data lies to the left of the dashed line and therefore, corresponds to levels that are below the top of the barrier according to Eq. (37.90).

Figure 37.12. The probability P_{switch} of making a flux state transition when a millisecond pulse of 96-GHz microwave radiation is applied. For clarity, each curve is shifted vertically by 0.3 relative to the pervious one. The insert shows the position of the observed peaks in the $\Delta U_0 - \Phi_x$ plane.

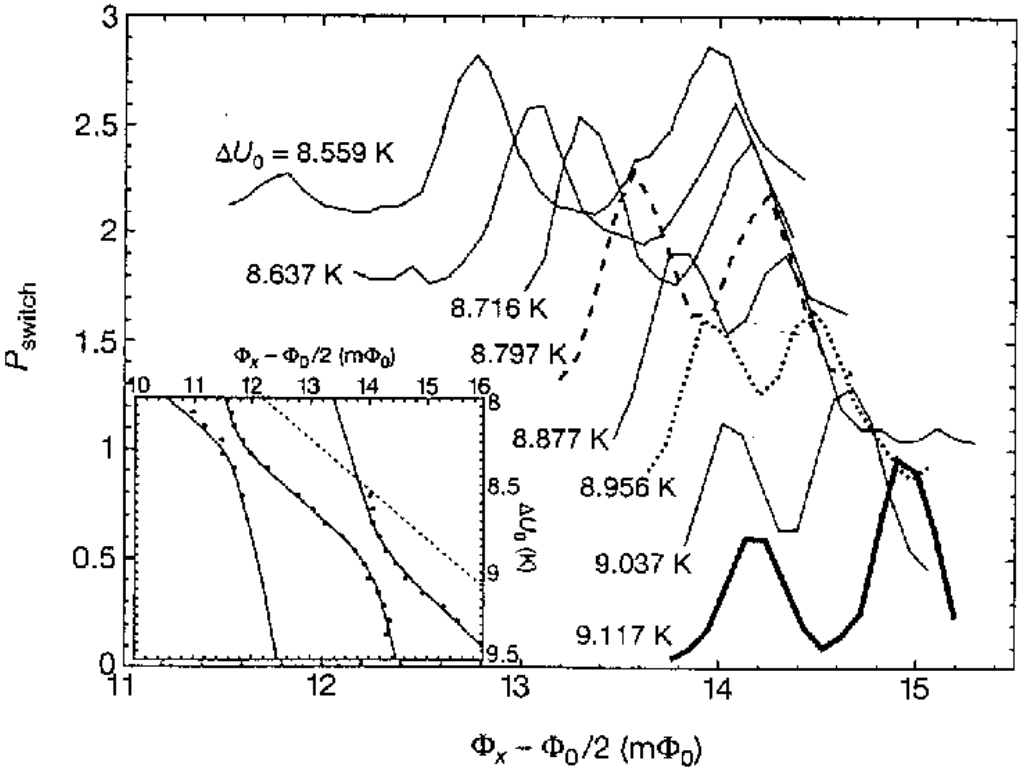

The inductance L and the impedance $Z \equiv \sqrt{L/C}$ of the loop, and the Josephson coupling parameter β_L of the sample SQUID were measured independently. The values were $L = 240 \pm 15\, pH$, $Z = 48.0 \pm 0.1\,\Omega$, and $\beta_L = 2.33 \pm 0.01$. The energy levels of the flux states $|0\rangle$ and $|1\rangle$ E_{level} as a function of ε relative to their mean energy $E_{mean}(\Delta U_0, \Phi_x)$ using the experimentally measured L, Z, and β_L are shown in Figure 37.13. At the middle at which point the levels were symmetrical according to Eq. (37.90), the two levels have a splitting of about $\Delta = 0.14\,K$ in energy and the upper level is about $\Delta = 0.14\,K$ below the top of the energy barrier as calculated from Eq. (37.90).

Figure 37.13. Energy of the measured peaks relative to the calculated

mean of the two levels as a function of ε .

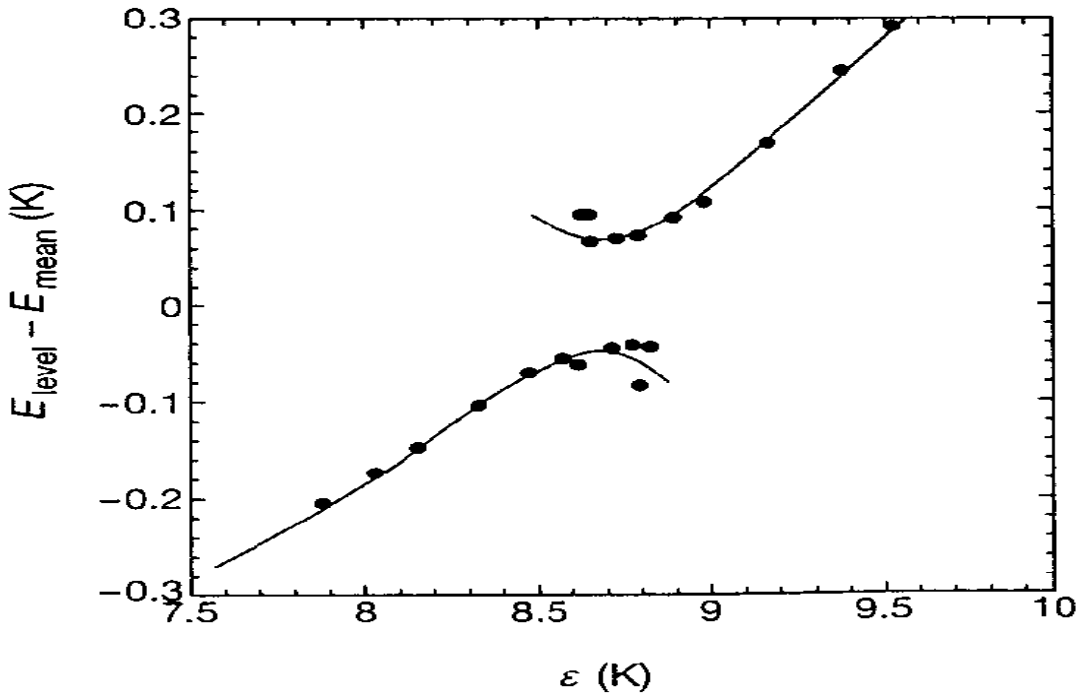

The quantum dynamics of the SQUID was determined by the flux through the loop, a collective phenomenon representing the superposition of about 10^{10} electrons acting in tandem. Since the experimental temperature was about 500 times smaller than the superconducting gap, almost all of the microscopic degrees of freedom were frozen out, and only the collective flux transition retained any dynamic relevance. The flux states $|0\rangle$ and $|1\rangle$ differed in flux by Φ_0 and differed in current by $2-3\,\mu A$.. Given the geometry of the SQUID this corresponded to a local magnetic moment of $10^{10}\ \mu_B$.

Quantum Interpretation

According to quantum theory, a superposition of fluxoid states $|0\rangle$ and $|1\rangle$ would manifest itself in an anticrossing defined as the lifting of the degeneracy of the energy levels of the two states at the point at which the states would be degenerate in the absence of coherence. Coherent tunneling lifts the degeneracy so that at the degeneracy point, the energy eigenstates are the symmetric and antisymmetric superposition of flux-basis states: $\frac{1}{\sqrt{2}}\left(|0\rangle + |1\rangle\right)$ and $\frac{1}{\sqrt{2}}\left(|0\rangle - |1\rangle\right)$. The energy difference ΔE between the two states is given approximately by

$$\Delta E = \sqrt{\varepsilon^2 + \Delta^2} \tag{37.96}$$

where Δ is known as the tunnel spitting. For a given ΔU_0, Eq. (37.90) predicts that two peaks would be observed as ε is varied by varying Φ_x. It further predicts that the peak separation should decrease and cross as the experiment is repeated for different values of ΔU_0. The lifting of degeneracy or splitting was anticipated to be observed as a decrease in peak separation and a reversal of the flux states in the $\Delta U_0 - \Phi_x$ plane without crossing. Friedman et al. sought to demonstrate the existence of such a splitting to support the notion of superposition of flux states corresponding to clockwise and counterclockwise currents simultaneously.

Classical Interpretation

Two sets of peaks are given by Eq. (37.90) which is derived from CLASSICAL PHYSICS. The nondegeneracy of the energy levels and the absence of crossing of the peaks was due to the linkage of flux by the electrons of the supercurrent.

As given in the Electron g Factor Section (Eq. (1.132), the angular momentum of the electron in the presence of an applied magnetic field is

$$\mathbf{L} = \mathbf{r} \times (m_e \mathbf{v} + e\mathbf{A}) \tag{37.97}$$

where $\mathbf{A}$ is the vector potential of the external field evaluated at the location of the electron. Conservation of angular momentum of the electron permits a discrete change of its "kinetic angular momentum" ($\mathbf{r} \times m\mathbf{v}$) by the field of $\frac{\hbar}{2}$, and concomitantly the "potential angular momentum" ($\mathbf{r} \times e\mathbf{A}$) must change by $-\frac{\hbar}{2}$. To conserve angular momentum in the presence of an applied magnetic field, the electron magnetic moment can be parallel or antiparallel to an applied field as observed with the Stern-Gerlach experiment, and the flip between orientations (a rotation of $\frac{\pi}{2}$) is accompanied by the "capture" of the magnetic flux quantum by the electron.

According to Eq. (1.136), the energy to flip the orientation of the orbitsphere due to its magnetic moment of a Bohr magneton, μ_B, is

$$\Delta E_{mag}^{spin} = 2\mu_B \mathbf{B} \tag{37.98}$$

where

$$\mu_B = \frac{e\hbar}{2m_e} \tag{37.99}$$

The energy change corresponding to the "capture" of the magnetic flux quantum is derived below. From Eq. (1.138), the energy stored in the magnetic field of the electron is

$$E_{mag} = \frac{\pi\mu_0 e^2\hbar^2}{(m_e)^2 r_n^3} \tag{37.100}$$

The orbitsphere is equivalent to a Josephson junction which can trap integer numbers of fluxons where the quantum of magnetic flux is $\Phi_0 = \frac{h}{2e}$. Thus, Eq. (1.148) gives

$$\Delta E_{mag}^{fluxon} = 2\frac{\alpha}{2\pi}\mu_B B \tag{37.101}$$

The principal energy of the transition of reorientation of the orbitsphere is given by Eq. (1.136). And, the total energy of the flip transition is the sum of Eq. (1.148), the energy of a fluxon treading the orbitsphere and Eq. (1.136), the energy of reorientation of the magnetic moment (Eqs. (1.149-1.151)).

$$\Delta E_{mag}^{spin} = 2\left(\mu_B \mathbf{B} + \frac{\alpha}{2\pi}\mu_B \mathbf{B}\right) \tag{37.102}$$

$$\Delta E_{mag}^{spin} = 2\left(1 + \frac{\alpha}{2\pi}\right)\mu_B \mathbf{B} \tag{37.103}$$

$$\Delta E_{mag}^{spin} = 2g\mu_B \mathbf{B} \tag{37.104}$$

The spin-flip transition can be considered as involving a magnetic moment of g times that of a Bohr magneton. The factor g is redesignated the fluxon g factor as opposed to the anomalous g factor and its value is 1.00116. The experimental value is 1.00116.

The energy difference Δ of the flux states $|0\rangle$ and $|1\rangle$ was not the tunnel spitting energy sought by Friedman et al. to support the notion of superposition of flux states corresponding to clockwise and counterclockwise currents simultaneously. The microwaves simply flipped the current direction which had a energy bias in one direction versus the opposite based on the corresponding presence or absence of a magnetic flux quantum within the SQUID. The energy difference was due to the linkage of flux by the current carrying superconducting electrons with a reversal of the current direction and a corresponding change in the flux state of the sample SQUID. The loop and SQUID transition resulted from a Stern Gerlach transition of a magnetic moment of 10^{10} μ_B that was equivalent to the superposition of 10^{10} electrons. The macroscopic spin-flip occurred by the absorption of high power microwave energy at the 96 GHz resonance frequency of the equivalent macroscopic magnetic moment. The energy of the 10^{10} electrons linking flux of $\frac{1}{2}\Phi_0$ is calculated from Eq. (37.101) by determining the magnetic flux due to 10^{10} electrons.

The magnetic moment of 10^{10} electrons μ is given by the number of electrons times a Bohr magneton μ_B of magnetic moment per electron.

$$\mu = \left(10^{10}\, electrons\right)\mu_B \tag{37.105}$$

The magnetic moment is equal to the current of the loop I times the area of the loop A.

$$\mu = \left(10^{10}\, electrons\right)\mu_B = IA \tag{37.106}$$

The magnetic flux B is given by one half the magnetic flux quantum Φ_0 divided by the area of the loop which is given by Eq. (37.106).

$$B = \frac{\frac{1}{2}\Phi_0}{A} = \frac{\frac{1}{2}\Phi_0}{\frac{\mu}{I}} = \frac{\frac{1}{2}\Phi_0}{\frac{\left(10^{10}\, electrons\right)\mu_B}{I}} \tag{37.107}$$

The energy of the 10^{10} electrons linking flux of $\frac{1}{2}\Phi_0$ by reversing the direction of supercurrent is calculated from Eq. (37.101) and Eq. (37.107) wherein the energy is one half that given by Eq. (37.101) because the flux state of the loop is initially biased at about the symmetrical point.

$$\begin{aligned}
\Delta E_{mag}^{fluxon} &= \left(10^{10}\, electrons\right)\frac{\alpha}{2\pi}\,\mu_B B \\
&= \left(10^{10}\, electrons\right)\frac{\alpha}{2\pi}\,\mu_B \frac{\frac{1}{2}\Phi_0}{\frac{\mu}{I}} \\
&= \left(10^{10}\, electrons\right)\frac{\alpha}{2\pi}\,\mu_B \frac{\frac{1}{2}\Phi_0}{\frac{\left(10^{10}\, electrons\right)\mu_B}{I}} \\
&= \frac{\alpha}{4\pi} I\Phi_0
\end{aligned} \tag{37.108}$$

The linkage of $\frac{1}{2}\Phi_0$ occurs when the electron rotates by $\frac{\pi}{2}$ radians about an axis perpendicular to the axis parallel to the magnetic flux lines. This electron rotation corresponds to an $\frac{\hbar}{2}$ magnitude, 180°, rotation of the electron's angular momentum vector. Since the electrons carry current, this reversal in momentum reverses the current according to the vector projection of the momentum change onto the direction of the current. Since the current reverses direction when a magnetic fluxon treads the loop of the SQUID, the current I is given by one half of the critical current I_c. The critical current I_c may be calculated from the Josephson coupling parameter β_L of the sample SQUID given by Eq. (37.92) using the independently measured value of $\beta_L = 2.33 \pm 0.01$ and the inductance

$L = 240 \pm 15\ pH$.

$$I_C \equiv \frac{\beta_L \Phi_0}{2\pi L} = \frac{(2.33)\Phi_0}{2\pi\left(240\ X\ 10^{-12}\ H\right)} = 3.2\ \mu A \qquad (37.109)$$

Substitution of one half I_c given by Eq. (37.109) into Eq. (37.108) gives the energy difference between the flux states.

$$\Delta E_{mag}^{fluxon} = \frac{1}{2}\left(\frac{\alpha}{2\pi}\right)\left(\frac{1}{2} I_c\right)\Phi_0 = \frac{1}{4}\left(\frac{\alpha}{2\pi}\right) I_c \Phi_0 = \frac{1}{4}\alpha \frac{I_c \Phi_0}{2\pi}$$

$$\Delta E_{mag}^{fluxon} = \frac{\alpha}{4\pi}\frac{\beta_L \Phi_0}{4\pi L}\Phi_0 = \frac{\alpha(2.33)\left(\Phi_0\right)^2}{(4\pi)^2\left(240\ X\ 10^{-12}\ H\right)} = 0.012\ meV = 0.139\ K \qquad (37.110)$$

Using Eqs. (37.90-37.92), the Josephson coupling energy of the junction U_J can be written in a form that is similar to that given by Eq. (37.110). From Eq. (37.90),

$$U_J = U_0 \beta_L \cos\left(2\pi \frac{\Phi}{\Phi_0}\right) \qquad (37.111)$$

Substitution of Eq. (37.91) for U_0 and Eq. (37.92) for β_L gives

$$U_J = U_0 \beta_L \cos\left(2\pi \frac{\Phi}{\Phi_0}\right) = \frac{\Phi_0^2}{4\pi^2 L}\beta_L \cos\left(2\pi \frac{\Phi}{\Phi_0}\right) = \frac{\Phi_0^2}{4\pi^2 L}\frac{2\pi L I_C}{\Phi_0}\cos\left(2\pi \frac{\Phi}{\Phi_0}\right) = \frac{I_C \Phi_0}{2\pi}\cos\left(2\pi \frac{\Phi}{\Phi_0}\right) \qquad (37.112)$$

The SQUID links flux in integer units of the magnetic flux quantum; thus, the Josephson coupling energy of the junction U_J is

$$U_J = \frac{I_C \Phi_0}{2\pi} \qquad (37.113)$$

The switch between Stern Gerlach states is predicted to be Lorentzian with a maximum transition intensity or probability at the energy level of 96 GHz difference between the states. The energy of the magnetic level $|0\rangle$ or $|1\rangle$ was tuned by the flux $\Phi_{xd.c.}$ which was tilted by flux Φ_x applied to the large current loop. In the case that the flux $\Phi_{xd.c.}$ corresponded to an energy level above the symmetrical case according to Eq. (37.90), the initial flux state $|0\rangle$ under went a transition to the state $|1\rangle$ at a higher flux Φ_x than in the case that $|1\rangle$ under went a transition to the state $|0\rangle$. In the case that the flux $\Phi_{xd.c.}$ corresponded to an energy level above the symmetrical case according to Eq. (37.90), the situation was reversed. The states were nondegenerate at the symmetrical point according to Eq. (37.90) because an energy bias existed based on the presence or absence of a magnetic flux quantum within the SQUID. Consequently, the energy difference of the peaks decreased to a minimum as the symmetrical point was approached, reversed assignments without crossing, and separated again. The data

demonstrate a difference in the energies of the flux states even at the point at which they were symmetrical according to Eq. (37.90). The difference was due to linking of flux by the superconducting electrons. The transition probability of state $|0\rangle$ to the state $|1\rangle$ occurred with slightly greater probability than the later since the potential energy of the state $|0\rangle$ was greater than the state $|1\rangle$. Thus, the intensity ratios of the peaks reversed also with the interchange of the assignments of the peaks as shown in Figure 37.12.

The energy of the 10^{10} electrons linking flux of $\frac{1}{2}\Phi_0$ is equivalent to the energy difference Δ of the flux states $|0\rangle$ and $|1\rangle$ of about $\Delta = 0.14\,K$ measured by Friedman et al as shown in Figure 37.13. The energy of the highest energy level is predicted to be about $\Delta = 0.14\,K$ below that given by Eq. (37.90) since the SQUID is biased by about $\frac{1}{2}\Phi_0$ with flux $\Phi_{xd.c.}$ which is perturbed by flux Φ_x. The measured value of about $\Delta = 0.14\,K$ is in good agreement with the predicted value.

The phenomenon observed by Friedman et al. [46] is similar to that of the Aharonov-Bohm Effect and the results of Monroe et al. [33] given in the Aharonov-Bohm Effect Section and the Schrödinger "Black" Cats Section, respectively. In the first case, the results of a damped harmonic oscillatory behavior of the ratio of the change in resistance and the resistance as a function of the flux applied to a current loop was erroneously interpreted as interference of electron wave-functions. The results were due to the linkage of flux by electrons in units of the magnetic flux quantum. In the latter case, the results were erroneously interpreted as demonstrating that an entire atom can simultaneously exist in two widely separated places and interfere with itself. The results were due to an interference between an oscillatory translational mode and a Stern Gerlach transition of the electron of a trapped charged ion. Similarly, the SUNY results confirm that classical physics predicts the splitting or difference in energy between flux states observed by Friedman et al. The behavior of a biased SQUID coupled to a biased macroscopic loop having the possibility of either clockwise or counterclockwise current that is interchanged by a Stern-Gerlach experiment is predicted quantitatively. The prediction is without the requirement of Friedman et al. [46] or Chang [44], that "Physicists have put a loop of superconducting wire into a "quantum superposition" of two contradictory possibilities: in one, the current flows clockwise; in the other, current flows counterclockwise".

PHYSICS IS NOT DIFFERENT ON THE ATOMIC SCALE

The central feature of Mills' theory is that all particles (atomic-size

particles and macroscopic particles) obey the same physical laws. Whereas Schrödinger postulated a boundary condition: $\Psi \rightarrow 0$ as $r \rightarrow \infty$, which leads to a purely mathematical model of the electron, the boundary condition in Mills' theory was derived from Maxwell's equations by Haus [50]:

> *For non-radiative states, the current-density function must not possess space-time Fourier components that are synchronous with waves traveling at the speed of light.*

Application of the latter boundary condition leads to an entirely different model of particles, atoms, molecules, and to a very different concept of the nature of the physical universe. ***The classical physical laws are unified and are shown to apply on all scales***.

The seemingly esoteric wave-particle duality of light and particles including the experimentally observed de Broglie relationship can be simply understood in terms of first principles. The independent variables of four dimensional space-time, the fundamental constants comprising the fine structure constant, α,

$$\alpha = \frac{1}{4\pi}\sqrt{\frac{\mu_o}{\varepsilon_o}}\frac{e^2}{\hbar} \tag{37.114}$$

the gravitational constant, G, the mass of the universe, and the spin of the electron neutrino determine the nature of the universe as shown in particular in the Gravity Section and the Unification of Spacetime, the Forces, Matter, and Energy Section. Photons and fundamental particles which arise from photons possess $\hbar$ of angular momentum and are two dimensional. As a consequence of this nature with first principle laws, absorption and emission of photons occurs in units or quanta of energy according to the Planck equation as described in particular in the One Electron Atom Section. Photons and electromagnetic fields arise from fundamental particles as given in the Photon Equation Section and superimpose due to the linearity of Maxwell's Equations and spacetime. Interference patterns, surface waves, diffraction, reflection, standing waves, and/or corpuscular behavior can be observed depending on the means of observation. These phenomena are explained according to first principles [51].

The wave-particle duality of the photon can be understood in terms of classical physics from the equation of the photon (Eq. (4.14)), a two dimensional orbitsphere, given in the Photon Equation Section. This function provides a photon angular momentum of $\hbar$, an energy given by the Planck relationship, a solution to the wave equation and Maxwell's Equations, a velocity of c, a zero rest mass, and linearly, circularly, or elliptically polarized light. Furthermore, photons superimpose in space and time to give a spherical wave described by the

Green Function, Eq. (4.22) which is consistent with the Airy pattern (Eq. (8.22)) in double slit diffraction experiments.

The wave-particle duality of the electron can be understood in terms of classical physics from the equation of the bound electron, a two dimensional orbitsphere, given in the One Electron Atom Section and from the equation of the free electron given in the Electron in Free Space Section. In both cases, the electron has an electric field equivalent to a point charge, e, has mass, m_e, the electron wavelength is given by the de Broglie relationship, the angular momentum of the electron is ($\hbar$, two possible orientations are possible in a magnetic field as observed in the Stern-Gerlach experiment, and the energy of the flip transition is proportional to the electron (fluxon) g factor (Eq. (1.151)). The ionized electron has its electron density in a plane (Eq. (3.7)), and the superposition of electrons provides a plane wave having the de Broglie wavelength which is consistent with the Davidson-Germer experiment given in the Electron Scattering by Helium Section. Furthermore, the correct prediction of the elastic scattering of electrons by helium atoms given in the Electron Scattering by Helium Section wherein the electron radius is a crucial parameter (Eq. (8.55)) and the excited state spectrum of hydrogen given in the Excited States of the One Electron atom (Quantization) Section (wherein ***the correspondence principle holds***) are direct verifications that the electron is an orbitsphere with the calculated radius.

Atoms are stable according to classical principles as shown in the Stability of Atoms and Hydrinos Section. The infinities of quantum electrodynamics are removed at once by having a finite electron radius as given in the One Electron Atom Section and the Electron in Free Space Section. In addition, the Lamb Shift is due to conservation of energy and linear momentum and arises from the radiation reaction force between the electron and the photon as given in the Resonant Line Shape and Lamb Shift Section. The negative result of the Michelson-Morley experiment rendered untenable the hypothesis of the ether by demonstrating that the ether had no measurable properties. And, the more recent related concepts of vacuum fluctuations, vacuum polarization, and virtual particles which are a source of infinities have no basis in physical reality; so, they are discarded.

References

1. Dyson, F., "Feynman's proof of Maxwell equations", Am. J. Phys., Vol. 58, (1990), pp. 209-211.
2. Horgan, J., "Quantum Philosophy", Scientific American, July, (1992), p. 96.
3. Beiser, A., Concepts of Modern Physics, Fourth Edition, McGraw-Hill, New

York, (1987),. pp. 44-86.
4. Beiser, A., Concepts of Modern Physics, Fourth Edition, McGraw-Hill, New York, (1987),. pp. 87-117.
5. S. Durr, T. Nonn, G. Rempe, Nature, September 3, (1998), Vol. 395, pp. 33-37.
6. Bohr, N. in *Albert Einstein: Philosopher-Scientist* (ed. Schilpp, P.A.)200-241 (Library of Living Philosophers, Evanston, 1949); reprinted in *Quantum Theory and Measurement* (eds. Wheeler, J. A. & Zurek, W. H.) 9-49 (Princeton University Press 1983).
7. Feynman, R., Leighton, R., & Sands, M. in *Feynman Lectures on Physics*, Vol. lll, Ch. l (Addison Wesley, Reading, 1965).
8. Weisskopf, V. F., Reviews of Modern Physics, Vol. 21, No. 2, (1949), pp. 305-315.
9. Dirac, P. A. M., From a Life of Physics, ed. A. Salam, et al., World Scientific, Singapore, (1989).
10. Milonni, P. W., The Quantum Vacuum, Academic Press, lnc., Boston, p. 90.
11. Dirac, P. A. M., Directions in Physics, ed. H. Hora and J. R. Shepanski, Wiley, New York, (1978), p. 36.
12. Horgan, J., "Quantum Philosophy", Scientific American, July, (1992), pp. 94-104.
13. Horgan, J., "Quantum Philosophy", Scientific American, July, (1992), p. 101.
14. Platt, D. E., Am. J. Phys., 60 (4), April, 1992, pp. 306-308.
15. Dehmelt, H. J., American Journal of Physics, Vol. 58, No. 1, January, (1990). pp. 17-27.
16. Einstein, A., Podolsky, B., Rosen, N., Phys. Rev., Vol. 47, (1935), p. 777.
17. Bell, J. S., Physics, Vol. 1, (1965), p. 195.
18. Bohm, D., Quantum Theory, Prentice-Hall, lnc., Englewood Cliffs, New Jersey, (1951), p. 614.
19. Aspect, A., Grangier, P., Gerard, R., Physical Review Letters, Vol. 47, No. 7, (1981), pp. 460-463.
20. Aspect, A., Grangier, P., Gerard, R., Physical Review Letters, Vol. 49, No. 2, (1982), pp. 91-94.
21. Aspect, A., Dalibard, J., , Gerard, R., Physical Review Letters, Vol. 49, No. 25, (1982), pp. 1804-1807.
22. Clauser, J., F., et al., Physical Review Letters, Vol. 23, No. 15, (1969), pp. 880-884.
23. Clauser, J., F., Horne, M., Physical Review D, Vol. 10, No. 2, (1974), pp. 526-535.
24. Horne, M., A., "Experimental Consequences of Local Hidden Variable Theories", thesis, Boston University, (1969).

25. Mermin, N. D., Physics Today, April , (1995), pp. 38-47.
26. Mermin, N. D., Physics Today, June, (1994), pp. 9-11.
27. Mermin, N. D., Physics Today, June, (1990), pp. 9-11.
28. Kong, J. A., Electromagnetic Wave Theory, Second Edition, John Wiley & Sons, Inc., New York,(1990).
29. Jackson, J. D., Classical Electrodynamics, Second Edition, John Wiley & Sons, New York, (1962), pp. 752-763.
30. Jackson, J. D., Classical Electrodynamics, Second Edition, John Wiley & Sons, New York, (1962), pp. 739-779.
31. Jackson, J. D., Classical Electrodynamics, Second Edition, John Wiley & Sons, New York, (1962), pp. 750-751.
32. M. W. Browne, "Physicist Put Atom in Two Places at Once", New York Times, Tuesday, May 28,1996, pp. B5-B6.
33. C. Monroe, D. M. Meekhof, B. E. King, D. J. Wineland, Science, Vol. 272, (1996), pp. 1131-1135.
34. G. Taubes, Science, Vol. 272, (1996), p. 1134.
35. S. R. Jefferts, C. Monroe, E. W. Bell, D. J. Wineland, Physical Review A, Vol. 51, No. 4, (1995), pp. 3112-3116.
36. C. Monroe, D. M. Meekhof, B. E. King, S. R. Jefferts, W. M. Itano, D. J. Wineland, Physical Review Letters, Vol. 75, No. 22, (1995), pp. 4011-4014.
37. C. P. Slichter, Principles of Magnetic Resonance, Harper & Row, New York, (1963), pp. 1-44.
38. A. A. Maradudin, Rev. Mod. Phys., Vol. 36, (1964), pp. 417-432.2.
39. A. Messiah, Quantum Mechanics, Vol. I, North-Holland Publishing Company, Amsterdam, (1961), p. 442.
40. H. Ott, Ann. Physik, Vol. 23, (1935), p. 169.
41. F. Bloch, Z. Physik, Vol. 74, (1932), p. 295.
42. G. N. Watson, Bessel Functions, Cambridge University Press, Cambridge, (1944), p. 14.
43. R. V. Hogg, E. A. Tanis, Probability and Statistical Inference, MacMillan Publishing Co., Inc., New York, (1977), pp. 78-82.
44. K. Chang, The New York Times, Tuesday, July 11, 2000, p. F3.
45. Schrödinger, E., "Die gegenwärtige situation in der quantenmechanik," Naturwissenschaften, Vol. 23, (1935), pp. 807-812, 823-828, 844-849.
46. J. R. Freedman, V. Patella, W. Hen, S. K. Tolpygo, J. E. Lukens, "Quantum superposition of distinct macroscopic states", Nature, Vol. 406, July, 6, (2000), pp. 43-45.
47. A. Lorke, R. J. Luyken, A. O. Govorov, J. P. Kotthaus, J. M. Garcia, and P. M. Petroff, Phys. Rev. Lett., Vol. 84, March 6, (2000), p. 2223.
48. Gough, C. E., Colclough, M. S., Forgan, E. M., Jordan, R. G., Keene, M., Muirhead, C. M., Rae, A. I. M., Thomas, N., Abell, J. S., Sutton, S., Nature, Vol. 326, (1987), P. 855.

49. Fowles, G. R., Analytical Mechanics, Third Edition, Holt, Rinehart, and Winston, New York, (1977), pp. 62-66.
50. Haus, H. A., "On the radiation from point charges", American Journal of Physics, 54, (1986), pp. 1126-1129.
51. James, M. B., Griffiths, D. J., Am. J. Phys., 60 (4), April, (1992), pp. 309-313.

THE HYDROGEN ATOM REVISITED

Randell L. Mills
BlackLight Power, Inc.
493 Old Trenton Road
Cranbury, NJ 08512

Abstract

Several myths about quantum mechanics exist due to a loss of awareness of its details since its inception in the beginning of the last century or based on recent experimental evidence. It is taught in textbooks that atomic hydrogen cannot go below the ground state. Atomic hydrogen having an experimental ground state of 13.6 eV can only exist in a vacuum or in isolation, and atomic hydrogen cannot go below this ground state in isolation. However, there is no known composition of matter containing hydrogen in the ground state of 13.6 eV. It is a myth that hydrogen has a theoretical ground state based on first principles. Historically there were many directions in which to proceed to solve a wave equation for hydrogen. The Schrödinger equation gives the observed spontaneously radiative states and the nonradiative energy level of atomic hydrogen. On this basis alone, it is justified despite its inconsistency with physical laws as well as with many experiments. A solution compatible with first principles and having first principles as the basis of quantization was never found. Scattering results required the solution to be interpreted as probability waves that give rise to the uncertainty principle which in turn forms the basis of the wave particle duality. The correspondence principal predicts that quantum predictions must approach classical predictions on a large scale. However, recent data has shown that the Heisenberg uncertainty principle as the basis of the wave particle duality and the correspondence principle taught in textbooks are experimentally incorrect.

Recently, a reconsideration of the postulates of quantum mechanics, has given rise to a closed form solution of a Schrödinger-like wave equation based on first principles [1]. Hydrogen at predicted lower energy levels has been identified in previous data. The transition of hydrogen to fractional quantum energy levels is reported by the assignment of soft X–ray emissions from the interstellar medium observed by Labov and Bowyer [2] and by the assignment of the source of 50 *eV* anomalous thermal broadening of the Balmer lines observed by Kuraica and Konjevic [3] during a glow discharge of hydrogen-argon mixtures which was not observed with neon-hydrogen mixtures or pure hydrogen irrespective of cathode material.

Certain inorganic ions predicted by Mills [1] serve as "transition catalysts" which resonantly accept energy from hydrogen atoms and release the energy to the surroundings. Argon ion is a catalyst that was present in the hydrogen glow discharge of Kuraica and Konjevic [3]. Lower-energy hydrogen atoms, hydrinos, can cause an autocatalytic acceleration of this "transition reaction" which is the mechanism corresponding to the interstellar lines.

The detection of the transition of atomic hydrogen from the traditional "ground" state ($n=1$) to the fractional quantum energy level $n=1/2$ below the traditional "ground" state—hydrinos— is further reported by the assignment of the anomalous 31 eV backward peak observed by Rudd, et al. [4] in the electron spectrum from collisions of 70 keV protons with hydrogen atoms. The transition occurs by a "resonant collision" mechanism predicted by Mills [1, 5]. Protons effect this transition of hydrogen by a resonant inelastic collision reaction. In this case, a backward 40.8 eV electron is produced which undergoes Franck-Hertz scattering [6] to give rise predominantly to a 30.6 eV backward peak, a 27.2 eV backward peak, and a 20.4 eV backward peak. Discontinuities in the back scattering spectrum at these energies were observed by Rudd, et al. [4] in the electron spectrum from collisions of 70 keV protons with hydrogen atoms. The maximum intensity of back scattering is predicted to be 165° falling to zero at 90° which is in agreement with the observed maximum at 160° which decreases with smaller angles to the absence of the backward scattering at 90°.

New evidence mandates that old theories be revised or abandoned. Recently line spectra of fractional quantum energy levels of atomic hydrogen have been measured by a 4 ° grazing incidence extreme ultraviolet spectrometer at INP Greifswald, Germany [7]. Intense EUV emission was observed by Mills et al. [7-12] at low temperatures (e.g. $<10^3\ K$) from atomic hydrogen and certain atomized pure elements or certain gaseous ions which ionize at integer multiples of the potential energy of atomic hydrogen. These atomized pure elements or gaseous ions comprise hydrogen catalysts to form lower energy hydrogen. New compositions of matter containing hydrogen at predicted lower energy levels have recently been observed in the laboratory, which energy levels are achieved using the novel catalysts. The Schrödinger wave equation solutions can not explain these results; thus, the theory must be modified.

Introduction

J. J. Balmer showed, in 1885, that the frequencies for some of the lines observed in the emission spectrum of atomic hydrogen could be expressed with a completely empirical relationship. This approach was later extended by J. R. Rydberg, who showed that all of the spectral lines of atomic hydrogen were given by the equation:

$$\bar{\nu} = R\left(\frac{1}{n_f^2} - \frac{1}{n_i^2}\right) \tag{38.1}$$

where $R = 109{,}677\ cm^{-1}$, $n_f = 1,2,3,...$, $n_i = 2,3,4,...$, and $n_i > n_f$. Niels Bohr, in 1913, developed a theory for atomic hydrogen based on an unprecedented postulate of stable circular orbits that do not radiate. Although no explanation was offered for the existence of stability for these orbits, the results gave energy levels in agreement with Rydberg's equation.

$$E_n = -\frac{e^2}{n^2 8\pi\varepsilon_o a_H} = -\frac{13.598\ eV}{n^2} \tag{38.2}$$

$$n = 1,2,3,... \tag{38.3}$$

where a_H is the Bohr radius for the hydrogen atom ($52.947\ pm$), e is the magnitude of the charge of the electron, and ε_o is the vacuum permittivity. Bohr's theory was a straightforward application of Newton's laws of motion and Coulomb's law of electric force - both pillars of classical physics and is in accord with the experimental observation that atoms are stable. However, it is not in accord with electromagnetic theory - another pillar of classical physics which predicts that accelerated charges radiate energy in the form of electromagnetic waves. An electron pursuing a curved path is accelerated and therefore should continuously lose energy, spiraling into the nucleus in a fraction of a second. The predictions of electromagnetic theory have always agreed with experiment, yet atoms do not collapse. To the early 20th century theoreticians, this contradiction could mean only one thing: The laws of physics that are valid in the macroworld do not hold true in the microworld of the atom. In 1923, de Broglie suggested that the motion of an electron has a wave aspect— $\lambda = \frac{h}{p}$. This concept seemed unlikely according to the familiar properties of electrons such as charge, mass and adherence to the laws of particle mechanics. But, the wave nature of the electron was confirmed by Davisson and Germer in 1927 by observing diffraction effects when electrons were reflected from metals. Schrödinger reasoned that if electrons have wave properties, there must be a wave equation that governs their motion. And in 1926, he proposed the

Schrödinger equation, $H\Psi = E\Psi$, where Ψ is the wave function, H is the wave operator, and E is the energy of the wave. This equation, and its associated postulates, is now the basis of ***quantum mechanics***, and it is the basis for the world view that the atomic realm including the electron and photon cannot be described in terms of "pure" wave and "pure" particle but in terms of a wave-particle duality. The wave-particle duality based on the fundamental principle that physics on an atomic scale is very different from physics on a macroscopic scale is central to present day atomic theory [1].

Development of Atomic Theory

Bohr Theory

In 1911, Rutherford proposed a planetary model for the atom where the electrons revolved about the nucleus (which contained the protons) in various orbits to explain the spectral lines of atomic hydrogen. There was, however, a fundamental conflict with this model and the prevailing classical physics. According to classical electromagnetic theory, an accelerated particle radiates energy (as electromagnetic waves). Thus, an electron in a Rutherford orbit, circulating at constant speed but with a continually changing direction of its velocity vector is being accelerated; thus, the electron should constantly lose energy by radiating and spiral into the nucleus.

An explanation was provided by Bohr in 1913, when he assumed that the energy levels were quantized and the electron was constrained to move in only one of a number of allowed states. Niels Bohr's theory for atomic hydrogen was based on an unprecedented postulate of stable circular orbits that do not radiate. Although no explanation was offered for the existence of stability for these orbits, the results gave energy levels in agreement with Rydberg's equation. Bohr's theory was a straightforward application of Newton's laws of motion and Coulomb's law of electric force. According to Bohr's model, the point particle electron was held to a circular orbit about the relatively massive point particle nucleus by the balance between the coulombic force of attraction between the proton and the electron and centrifugal force of the electron.

$$\frac{e^2}{4\pi\varepsilon_0 r^2} = \frac{m_e v^2}{r} \tag{38.4}$$

Bohr postulated the existence of stable orbits in defiance of classical physics (Maxwell's Equations), but he applied classical physics according to Eq. (38.4). Then Bohr realized that the energy formula Eqs. (38.2-38.3) was given by postulating nonradiative states with angular

momentum

$$L_z = m_e v r = n\hbar \qquad n = 1,2,3... \tag{38.5}$$

and by solving the energy equation classically. The Bohr radius is given by substituting the solution of Eq. (38.5) for v into Eq. (38.4).

$$r = \frac{4\pi\varepsilon_0\hbar^2 n^2}{m_e e^2} = n^2 a_0 \qquad n = 1,2,3... \tag{38.6}$$

The total energy is the sum of the potential energy and the kinetic energy. In the present case of an inverse squared central field, the total energy (which is the negative of the binding energy) is one half the potential energy [14]. The potential energy, $\phi(\mathbf{r})$, is given by Poisson's equation

$$\phi(\mathbf{r}) = -\int_{V'} \frac{\rho(\mathbf{r}')dv'}{4\pi\varepsilon_0|\mathbf{r}-\mathbf{r}'|} \tag{38.7}$$

For a point charge at a distance r from the nucleus the potential is

$$\phi(r) = -\frac{e^2}{4\pi\varepsilon_0 r} \tag{38.8}$$

Thus, the total energy is given by

$$E = -\frac{Z^2 e^2}{8\pi\varepsilon_o r} \tag{38.9}$$

where $Z = 1$. Substitution of Eq. (38.6) into Eq.(38.9) with the replacement of the electron mass by the reduced electron mass gives Eqs. (38.2-38.3).

Bohr's model was in agreement with the observed hydrogen spectrum, but it failed with the helium spectrum, and it could not account for chemical bonds in molecules. The prevailing wisdom was that the Bohr model failed because it was based on the application of Newtonian mechanics for discrete particles. And, its limited applicability was attributed to the unwarranted assumption that the energy levels are quantized.

Bohr's theory may also be analyzed according to the corresponding energy equation. Newton's differential equations of motion in the case of the central field such as a gravitational or electrostatic field are

$$m(\ddot{r} - r\dot{\theta}^2) = f(r) \tag{38.10}$$

$$m(2\dot{r}\dot{\theta} + r\ddot{\theta}) = 0 \tag{38.11}$$

where $\mathbf{f}(r)$ is the central force. The second or transverse equation, Eq. (38.11), gives the result that the angular momentum is constant.

$$r^2\dot{\theta} = \text{constant} = L/m \tag{38.12}$$

where $\mathbf{L}$ is the angular momentum. The central force equations can be transformed into an orbital equation by the substitution, $u = \frac{1}{r}$. The

differential equation of the orbit of a particle moving under a central force is

$$\frac{\delta^2 u}{\delta\theta^2} + u = \frac{-1}{\frac{mL^2u^2}{m^2}} f(u^{-1}) \tag{38.13}$$

Because the angular momentum is constant, motion in only one plane need be considered; thus, the orbital equation is given in polar coordinates. The solution of Eq. (38.13) for an inverse square force

$$f(r) = -\frac{k}{r^2} \tag{38.14}$$

is

$$r = r_0 \frac{1+e}{1+e\cos\theta} \tag{38.15}$$

$$e = A\frac{m\frac{L^2}{m^2}}{k} \tag{38.16}$$

$$r_0 = \frac{m\frac{L^2}{m^2}}{k(1+e)} \tag{38.17}$$

where e is the eccentricity and A is a constant. The equation of motion due to a central force can also be expressed in terms of the energies of the orbit. The square of the speed in polar coordinates is

$$v^2 = (\dot{r}^2 + r^2\dot{\theta}^2) \tag{38.18}$$

Since a central force is conservative, the total energy, E, is equal to the sum of the kinetic, T, and the potential, V, and is constant. The total energy is

$$\frac{1}{2}m(\dot{r}^2 + r^2\dot{\theta}^2) + V(r) = E = \text{ constant} \tag{38.19}$$

Substitution of the variable $u = \frac{1}{r}$ and Eq. (38.12) into Eq. (38.19) gives the orbital energy equation.

$$\frac{1}{2}m\frac{L^2}{m^2}[(\frac{\delta^2 u}{\delta\theta^2}) + u^2] + V(u^{-1}) = E \tag{38.20}$$

Because the potential energy function $V(r)$ for an inverse square force field is

$$V(r) = -\frac{k}{r} = -ku \tag{38.21}$$

the energy equation of the orbit, Eq. (38.20), is

$$\frac{1}{2}m\frac{L^2}{m^2}[(\frac{\delta^2 u}{\delta\theta^2}) + u^2] - ku = E \tag{38.22}$$

$$\left(\frac{\delta^2 u}{\delta\theta^2} + u^2\right) - \frac{2m}{L^2}[E + ku] = 0 \tag{38.23}$$

which has the solution

$$r = \frac{m\frac{L^2}{m^2}k^{-1}}{1+[1+2Em\frac{L^2}{m^2}k^{-2}]^{1/2}\ \cos\theta} \tag{38.24}$$

where the eccentricity, e, is

$$e = [1+2Em\frac{L^2}{m^2}k^{-2}]^{1/2} \tag{38.25}$$

Eq. (38.25) permits the classification of the orbits according to the total energy, E, as follows:

$E<0,$	$e<1$	ellipse
$E<0,$	$e=0$	circle (special case of ellipse)
$E=0,$	$e=1$	parabolic orbit
$E>0,$	$e>1$	hyperbolic orbit

(38.26)

Since $E=T+V$ and is constant, the closed orbits are those for which $T \lhd |V|$, and the open orbits are those for which $T \geq |V|$. It can be shown that the time average of the kinetic energy, $<T>$, for elliptic motion in an inverse square field is $1/2$ that of the time average of the potential energy, $<V>$. $<T>=1/2<V>$.

Bohr's solution is trivial in that he specified a circular bound orbit which determined that the eccentricity was zero, and he specified the angular momentum as a integer multiple of Planck's constant bar. Eq. (38.25) in CGS units becomes

$$E = -\frac{1}{2}\frac{me^4}{n^2\hbar^2} = -\frac{e^2}{2n^2a_0} \tag{38.27}$$

Schrödinger Theory of the Hydrogen Atom

In 1923, de Broglie suggested that the motion of an electron has a wave aspect— $\lambda = \frac{h}{p}$. This was confirmed by Davisson and Germer in 1927 by observing diffraction effects when electrons were reflected from metals. Schrödinger reasoned that if electrons have wave properties, there must be a wave equation that governs their motion. And, in 1926, he proposed the time independent Schrödinger equation

$$H\Psi = E\Psi \tag{38.28}$$

where Ψ is the wave function, H is the wave operator, and E is the energy of the wave. To give the sought three quantum numbers, the

Schrödinger equation solutions are three dimensional in space and four dimensional in spacetime

$$\left[\nabla^2 - \frac{1}{v^2}\frac{\delta^2}{\delta t^2}\right]\Psi(r,\theta,\phi,t) = 0 \tag{38.29}$$

where $\Psi(r,\theta,\phi,t)$ according to quantum theory is the probability density function of the electron as described below. When the time harmonic function is eliminated [15],

$$-\frac{\hbar^2}{2\mu}\left[\frac{1}{r^2}\frac{\delta}{\delta r}\left(r^2\frac{\delta\Psi}{\delta r}\right) + \frac{1}{r^2\sin\theta}\frac{\delta}{\delta\theta}\left(\sin\theta\frac{\delta\Psi}{\delta\theta}\right)_{r,\phi} + \frac{1}{r^2\sin^2\theta}\left(\frac{\delta^2\Psi}{\delta\phi^2}\right)_{r,\theta}\right] + V(r)\Psi(r,\theta,\phi) = E\Psi(r,\theta,\phi) \tag{38.30}$$

where the potential energy $V(r)$ in CGS units is

$$V(r) = -\frac{e^2}{r} \tag{38.31}$$

The Schrödinger equation (Eq. (38.30)) can be transformed into a sum comprising a part that depends only on the radius and a part that is a function of angle only obtained by separation of variables and linear superposition in spherical coordinates. The general form of the solutions for $\psi(r,\theta,\phi)$ are

$$\psi(r,\theta,\phi) = \sum_{l,m} R_{nlm}(r)Y_{lm}(\theta,\phi) \tag{38.32}$$

where l and m are separation constants. The azimuthal (theta) part of Eq. (38.30) is the generalized Legendre equation which is derived from the Laplace equation by Jackson (Eq. (3.9) of Jackson [16]). The solutions for the full angular part of Eq. (38.30), $Y_{lm}(\theta,\phi)$, are the spherical harmonics

$$Y_{lm}(\theta,\phi) = \sqrt{\frac{(2l+1)(l-m)!}{4\pi(l+m)!}}P_l^m(\cos\theta)e^{im\phi} \tag{38.33}$$

By substitution of the eigenvalues corresponding to the angular part [17], the Schrödinger equation becomes the radial equation, $R(r)$, given by

$$-\frac{\hbar^2}{2mr^2}\frac{d}{dr}\left(r^2\frac{dR}{dr}\right) + \left[\frac{\hbar^2 l(l+1)}{2mr^2} + V(r)\right]R(r) = ER(r) \tag{38.34}$$

The time independent Schrödinger equation is similar to Eq. (38.20) except that the solution is for the distribution of a spatial wavefunction in three dimensions rather than the dynamical motion of a point particle of mass m along a one dimensional trajectory. Electron motion is implicit in the Schrödinger equation. For wave propagation in three dimensions, the full time dependent Schrödinger equation is required; whereas, the classical case contains time derivatives. The kinetic energy of rotation is K_{rot} is given classically by

$$K_{rot} = \frac{1}{2} mr^2 \omega^2 \tag{38.35}$$

where m is the mass of the electron. In the time independent Schrödinger equation, the kinetic energy of rotation K_{rot} is given by

$$K_{rot} = \frac{\ell(\ell+1)\hbar^2}{2mr^2} \tag{38.36}$$

where

$$L = \sqrt{\ell(\ell+1)\hbar^2} \tag{38.37}$$

is the value of the electron angular momentum L for the state $Y_{lm}(\theta,\phi)$.

In the case of the ground state of hydrogen, the Schrödinger equation solution is trivial for an implicit circular bound orbit which determines that the eccentricity is zero, and with the specification that the electron angular momentum is Planck's constant bar. With $k = e^2$, Eq. (38.25) in CGS units becomes

$$E = -\frac{1}{2}\frac{me^4}{\hbar^2} = -\frac{e^2}{2a_0} \tag{38.38}$$

which corresponds to $n = 1$ in Eq. (38.27). Many problems in classical physics give three quantum numbers when three spatial dimensions are considered. In order to obtain three quantum numbers, the Schrödinger equation requires that the solution is for the distribution of a spatial wavefunction in three dimensions with implicit motion rather than a one dimensional trajectory of a point particle as shown below. However, this approach gives rise to predictions about the angular momentum and angular energy which are not consistent with experimental observations as well as a host of other problems which are summarized in the Discussion Section.

The radial equation may be written as

$$\frac{d}{dr}\left(r^2 \frac{dR}{dr}\right) + \frac{2mr^2}{\hbar^2}\left[E - V(r) - \frac{l(l+1)\hbar^2}{2mr^2}\right]R(r) = 0 \tag{38.39}$$

Let $U(r) = rR(r)$, then the radial equation reduces to

$$U'' + \frac{2m}{\hbar^2}\left[E - V(r) - \frac{l(l+1)\hbar^2}{2mr^2}\right]U = 0 \tag{38.40}$$

where

$$\psi = \frac{1}{r} U_{lm}(r) Y_{lm}(\theta,\phi) \tag{38.41}$$

Substitution of the potential energy given by Eq. (38.31) into Eq. (38.40) gives for sufficiently large r

$$U''_{\infty} - \left(\frac{\alpha}{2}\right)^2 U = 0 \tag{38.42}$$

provided we define

$$\left(\frac{\alpha}{2}\right)^2 = \frac{-2mE}{\hbar^2} \tag{38.43}$$

where α is the eigenvalue of the eigenfunction solution of the Schrödinger equation given *infra* having units of reciprocal length and E is the energy levels of the hydrogen atom. To arrive at the solution which represents the electron, a suitable boundary condition must be imposed. Schrödinger postulated a boundary condition: $\Psi \to 0$ as $r \to \infty$, which leads to a purely mathematical model of the electron. This equation is not based on first principles, has no validity as such, and should not be represented as so. The right hand side of Eq. (38.43) must be *postulated* in order that the Rydberg equation is obtained as shown below. The postulate is implicit since Eq. (38.43) arises from the Schrödinger which is postulated. It could be defined *arbitrarily*, but is justified because it gives the Rydberg formula. That Schrödinger guessed the accepted approach is not surprising since many approaches were contemplated at this time [18], and since none of these approaches were superior, Schrödinger's approach prevailed.

The solution of Eq. (38.42) that is consistent with the boundary condition is

$$U_\infty = c_1 e^{(\alpha/2)r} + c_2 e^{-(\alpha/2)r} \tag{38.44}$$

In the case that α is real, the energy of the particle is negative. In this case U_∞ will not have an integrable square if c_1 fails to vanish wherein the radial integral has the form

$$\int_0^\infty R^2 r^2 dr = \int U_\infty^2 dr \tag{38.45}$$

It is shown below that the solution of the Schrödinger corresponds to the case wherein c_1 fails to vanish. Thus, the solutions with sufficiently large r are infinite. The same problem arises in the case of a free electron that is ionized from hydrogen. If α is imaginary, which means that E is positive, Eq. (38.42) is the equation of a linear harmonic oscillator [19]. U_∞ shows sinusoidal behavior; thus, the wavefunction for the free electron can not be normalized and is infinite. In addition, the angular momentum of the free electron is infinite since it is given by $\ell(\ell+1)\hbar^2$ (Eq. (38.37)) where $\ell \to \infty$.

In order to solve the bound electron states, let

$$E = -W \tag{38.46}$$

so that W is positive. In Eq. (38.39), let $r = x/\alpha$ where α is given by Eq. (38.43).

$$x\frac{d^2R}{dx^2} + 2\frac{dR}{dx} + \left[\frac{2me^2}{\hbar^2\alpha} - \frac{x}{4} - \frac{l(l+1)}{x}\right]R = 0 \tag{38.47}$$

Eq. (38.47) is the differential equation for associated Laguerre functions

given in general form by

$$xy'' + 2y' + \left[n^* - \frac{k-1}{2} - \frac{x}{4} - \frac{k^2-1}{4x} \right] y = 0 \tag{38.48}$$

which has a solution possessing an integrable square of the form

$$y = e^{-x/2} x^{(k-1)/2} \frac{d^k}{dx^k} L_{n^*}(x) \tag{38.49}$$

provided that n^* and k are positive integers. However, n^* does not have to be an integer, it may be any *arbitrary* constant β. Then the corresponding solution is [20]

$$y = e^{-x/2} x^{(k-1)/2} \frac{d^k}{dx^k} L_{\beta}(x) \tag{38.50}$$

In the case that n^* is chosen to be an integer in order to obtain the Rydberg formula, $n^* - k \geq 0$ since otherwise $L^k_{n^*}(x)$ of Eq. (38.49) would vanish. By comparing Eq. (38.47) and Eq. (38.48),

$$\frac{k^2-1}{4} = \ell(\ell+1) \tag{38.51}$$

Thus,

$$k = 2\ell + 1 \tag{38.52}$$

and

$$n^* - \frac{k-1}{2} = n^* - \ell = \frac{me^2}{\hbar} \left(\frac{\alpha}{2} \right)^{-1} \tag{38.53}$$

Substitution of the value of α and solving for W gives

$$W = \frac{1}{2} \frac{me^4}{(n^* - \ell)^2 \hbar^2} \tag{38.54}$$

Because of the conditions on n^* and k, the quantity $n^* - \ell$ can not be zero. It is usually denoted by n and called the principal quantum number. The energy states of the hydrogen atom are

$$W_n = -E_n = \frac{1}{2} \frac{me^4}{n^2 \hbar^2} \tag{38.55}$$

and the corresponding eigenfunctions from Eq. (38.49) are

$$R_{n,\ell} = c_{n,\ell} e^{-x/2} x^{\ell} L^{2\ell+1}_{n+\ell}(x) \tag{38.56}$$

where the variable x is defined by

$$x = \alpha r = \frac{\sqrt{8mW}}{\hbar} r = \frac{2me^2}{n\hbar^2} r \tag{38.57}$$

In the Bohr theory of the hydrogen atom, the first orbital has a radius in CGS units given by

$$a_0 = \frac{\hbar^2}{me^2} = 0.53 \; X \; 10^{-8} \; cm \tag{38.58}$$

Thus, $\alpha = 2/na_0$ and

$$x = \frac{2}{n} \frac{r}{a_0} \tag{38.59}$$

The energy states of the hydrogen atom in CGS units in terms of the Bohr radius are given by Eq. (38.27). From Eq. (38.56), $R_{n,\ell}$ for the hydrogen atom ground state is

$$R_{1,0} = c_{1,0} e^{-r/a_0} L_1^1 = 2a_0^{-3/2} e^{-r/a_0} \tag{38.60}$$

For this state

$$Y_{00} = constant = (4\pi)^{-1/2} \tag{38.61}$$

when the function is normalized. Thus, the ground state function is

$$\psi_0 = (\pi a_0^3)^{-1/2} e^{-r/a_0} \tag{38.62}$$

Immediately further problems arise. Since ℓ must equal zero in the ground state, the predicted angular energy and angular momentum given by Eq. (38.36) and Eq. (38.37), respectively, are zero which are experimentally incorrect. In addition, different integer values of ℓ exist in the case of excited electron states. In these cases, the Schrödinger equation solutions, Eq. (38.36) and Eq. (38.37), predict that the excited state rotational energy levels are nondegenerate as a function of the ℓ quantum number even in the absence of an applied magnetic field. Consider the case of the excited state with $n = 2; \ell = 1$ compared to the experimentally degenerate state $n = 2; \ell = 0$. According to Eq. (38.37) the difference in angular energy of these two states is $3.4\ eV$ where the expectation radius, $4a_0$, is given by the squared integral of Eq. (38.70) over space. Thus, the predicted rotational energy in the absence of a magnetic field is over six orders of magnitude of the observed nondegenerate energy ($10^{-7} - 10^{-6}\ eV$) in the presence of a magnetic field.

Schrödinger realized that his equation was limited. It is not Lorentzian invariant; thus, it violates special relativity. It also does not comply with Maxwell's equations and other first principle laws. Schrödinger sought a resolution of the incompatibility with special relativity for the rest of his life. He was deeply troubled by the physical consequences of his equation and its solutions. His hope was that the resolution would make his equation fully compatible with classical physics and the quantization would arise from first principles.

Quantum mechanics failed to predict the results of the Stern-Gerlach experiment which indicated the need for an additional quantum number. Quantum electrodynamics was proposed by Dirac in 1926 to provide a generalization of quantum mechanics for high energies in conformity with the theory of special relativity and to provide a consistent treatment of the interaction of matter with radiation. From Weisskopf [21], "Dirac's quantum electrodynamics gave a more consistent derivation of the results of the correspondence principle, but it also brought about a number of new and serious difficulties." Quantum electrodynamics; 1.) does not explain nonradiation of bound electrons; 2.) contains an internal inconsistency with special relativity

regarding the classical electron radius - the electron mass corresponding to its electric energy is infinite; 3.) it admits solutions of negative rest mass and negative kinetic energy; 4.) the interaction of the electron with the predicted zero-point field fluctuations leads to infinite kinetic energy and infinite electron mass; 5.) Dirac used the unacceptable states of negative mass for the description of the vacuum; yet, infinities still arise.

A physical interpretation of Eq. (38.28) was sought. Schrödinger interpreted $e\Psi^*(x)\Psi(x)$ as the charge-density or the amount of charge between x and $x+dx$ (Ψ^* is the complex conjugate of Ψ). Presumably, then, he pictured the electron to be spread over large regions of space. Three years after Schrödinger's interpretation, Max Born, who was working with scattering theory, found that this interpretation led to logical difficulties, and he replaced the Schrödinger interpretation with the probability of finding the electron between r,θ,ϕ and $r+dr,\theta+d\theta,\phi+d\phi$ as

$$\int \Psi(r,\theta,\phi)\Psi^*(r,\theta,\phi)drd\theta d\phi \tag{38.63}$$

Born's interpretation is generally accepted. Nonetheless, interpretation of the wave function is a never-ending source of confusion and conflict. Many scientists have solved this problem by conveniently adopting the Schrödinger interpretation for some problems and the Born interpretation for others. This duality allows the electron to be everywhere at one time—yet have no volume. Alternatively, the electron can be viewed as a discrete particle that moves here and there (from $r=0$ to $r=\infty$), and $\Psi\Psi^*$ gives the time average of this motion.

Schrödinger was also troubled by the philosophical consequences of his theory since quantum mechanics leads to certain philosophical interpretations [22] which are not sensible. Some conjure up multitudes of universes including "mind" universes; others require belief in a logic that allows two contradictory statements to be true. The question addressed is whether the universe is determined or influenced by the possibility of our being conscious of it. The meaning of quantum mechanics is debated, but the Copenhagen interpretation is predominant. Its asserts that "what we observe is all we can know; any speculation about what a photon, an atom, or even a SQUID (Superconducting Quantum Interference Device) really is or what it is doing when we are not looking is just that speculation" [22]. As shown by Platt [23] in the case of the Stern-Gerlach experiment, "the postulate of quantum measurement [which] asserts that the process of measuring an observable forces the state vector of the system into an eigenvector of that observable, and the value measured will be the eigenvalue of that eigenvector". According to this interpretation every observable exists in

a state of superposition of possible states, and observation or the potential for knowledge causes the wavefunction corresponding to the possibilities to collapse into a definite.

According to the quantum mechanical view, a moving particle is regarded as a wave group. To regard a moving particle as a wave group implies that there are fundamental limits to the accuracy with which such "particle" properties as position and momentum can be measured. Quantum predicts that the particle may be located anywhere within its wave group with a probability $|\Psi|^2$. An isolated wave group is the result of superposing an infinite number of waves with different wavelengths. The narrower the wave group, the greater range of wavelengths involved. A narrow de Broglie wave group thus means a well-defined position (Δx smaller) but a poorly defined wavelength and a large uncertainty $\Delta \mathbf{p}$ in the momentum of the particle the group represents. A wide wave group means a more precise momentum but a less precise position. The infamous Heisenberg uncertainty principle is a formal statement of the standard deviations of properties implicit in the probability model of fundamental particles.

$$\Delta x \Delta \mathbf{p} \geq \frac{\hbar}{2} \tag{38.64}$$

According to the standard interpretation of quantum mechanics, the act of measuring the position or momentum of a quantum mechanical entity collapses the wave-particle duality because the principle forbids both quantities to be simultaneously known with precision.

The Wave-Particle Duality is Not Due to the Uncertainty Principle

Quantum entities can behave like particles or waves, depending on how they are observed. They can be diffracted and produce interference patterns (wave behavior) when they are allowed to take different paths from some source to a detector--in the usual example, electrons or photons go through two slits and form an interference pattern on the screen behind. On the other hand, with an appropriate detector put along one of the paths (at a slit, say), the quantum entities can be detected at a particular place and time, as if they are point-like particles. But any attempt to determine which path is taken by a quantum object destroys the interference pattern. Richard Feynman described this as the central mystery of quantum physics.

Bohr called this vague principle 'complementary', and explained it in terms of the uncertainty principle, put forward by Werner Heisenberg, his postdoc at the time. In an attempt to persuade Einstein that wave-particle duality is an essential part of quantum mechanics, Bohr constructed models of quantum measurements that showed the futility

of trying to determine which path was taken by a quantum object in an interference experiment. As soon as enough information is acquired for this determination, the quantum interferences must vanish, said Bohr, because any act of observing will impart uncontrollable momentum kicks to the quantum object. This is quantified by Heisenberg's uncertainty principle, which relates uncertainty in positional information to uncertainty in momentum--when the position of an entity is constrained, the momentum must be randomized to a certain degree.

More than 60 years after the famous debate between Niels Bohr and Albert Einstein on the nature of quantum reality, a question central to their debate --the nature of quantum interference--has resurfaced. The usual textbook explanation of wave-particle duality in terms of unavoidable 'measurement disturbances' is experimentally proven incorrect by an experiment reported in the September 3, 1998 issue of Nature [24] by Durr, Nonn, and Rempe. Durr, Nonn, and Rempe report on the interference fringes produced when a beam of cold atoms is diffracted by standing waves of light. Their interferometer displayed fringes of high contrast--but when they manipulated the electronic state within the atoms with a microwave field according to which path was taken, the fringes disappeared entirely. The interferometer produced a spatial distribution of electronic populations which were observed via fluorescence. The microwave field canceled the spatial distribution of electronic populations. The key to this new experiment was that although the interferences are destroyed, the initially imposed atomic momentum distribution left an envelope pattern (in which the fringes used to reside) at the detector. A careful analysis of the pattern demonstrated that it had not been measurably distorted by a momentum kick of the type invoked by Bohr, and therefore that any locally realistic momentum kicks imparted by the manipulation of the internal atomic state according to the particular path of the atom are too small to be responsible for destroying interference.

The Correspondence Principle Does Not Hold

Recent experimental results also dispel another doctrine of quantum mechanics [25, 26]. Bohr proposed a rule of thumb called the correspondence principle [27]. A form of the principle widely repeated in textbooks and lecture halls states that predictions of quantum mechanics and classical physics should match for the most energetic cases.

In the Nov. 22 Physical Review Letters [25], Bo Gao calculates possible energy states of any chilled, two-atom molecule, such as sodium, that's vibrating and rotating almost to the breaking point. He performs the calculations via quantum mechanical and so called

semiclassical methods and compares the results. Instead of the results agreeing better for increasingly energetic states. The opposite happens.

Classical Solution of the Schrödinger Equation

Mills has solved and published a solution of a Schrödinger type equation based on first principles [1]. The central feature of this theory is that all particles (atomic-size and macroscopic particles) obey the same physical laws. Whereas Schrödinger postulated a boundary condition: $\Psi \to 0$ as $r \to \infty$, the boundary condition in Mills' theory was derived from Maxwell's equations [28]:

> *For non-radiative states, the current-density function must not possess space-time Fourier components that are synchronous with waves traveling at the speed of light.*

Application of this boundary condition leads to a physical model of particles, atoms, molecules, and, in the final analysis, cosmology. The closed-form mathematical solutions contain fundamental constants only, and the calculated values for physical quantities agree with experimental observations. In addition, the theory predicts that Eq. (38.3), should be replaced by Eq. (38.65).

$$n = 1,2,3,..., \text{ and, } n = \frac{1}{2},\frac{1}{3},\frac{1}{4},... \tag{38.65}$$

Some revisions to standard quantum theory are implied. Quantum mechanics becomes a real physical description as opposed to a purely mathematical model where the old and the revised versions are interchangeable by a Fourier Transform operation [1].

The theories of Bohr, Schrödinger, and presently Mills all give the identical equation for the principal energy levels of the one electron atom.

$$E_{ele} = -\frac{Z^2 e^2}{8\pi\varepsilon_o n^2 a_H} = -\frac{Z^2}{n^2}\ X\ 2.1786\ X\ 10^{-18}\ J = -Z^2\ X\ \frac{13.598}{n^2}\ eV \tag{38.66}$$

The Mills theory solves the two dimensional wave equation for the charge density function of the electron. And, the Fourier transform of the charge density function is a solution of the three dimensional wave equation in frequency (k,ω) space. Whereas, the Schrödinger equation solutions are three dimensional in spacetime. The energy is given by

$$\int_{-\infty}^{\infty} \psi H \psi \, dv = E \int_{-\infty}^{\infty} \psi^2 dv; \tag{38.67}$$

$$\int_{-\infty}^{\infty} \psi^2 dv = 1 \tag{38.68}$$

Thus,

$$\int_{-\infty}^{\infty} \psi H \psi \, dv = E \tag{38.69}$$

In the case that the potential energy of the Hamiltonian, H, is a constant times the wavenumber, the Schrödinger equation is the well known Bessel equation. Then with one of the solutions for ψ, Eq. (38.69) is equivalent to an inverse Fourier transform. According to the duality and scale change properties of Fourier transforms, the energy equation of the present theory and that of quantum mechanics are identical, the energy of a radial Dirac delta function of radius equal to an integer multiple of the radius of the hydrogen atom (Eq. (38.66)). And, Bohr obtained the same energy formula by postulating nonradiative states with angular momentum

$$L_z = m\hbar \tag{38.70}$$

and solving the energy equation classically.

The mathematics for all three theories converge to Eq. (38.66). However, the physics is quite different. Only the Mills theory is derived from first principles and holds over a scale of spacetime of 45 orders of magnitude: it correctly predicts the nature of the universe from the scale of the quarks to that of the cosmos.

Mills revisions transform Schrödinger's and Heisenberg's quantum theory into what may be termed a ***classical quantum theory***. Physical descriptions flow readily from the theory. For example, in the old quantum theory the spin angular momentum of the electron is called the "intrinsic angular momentum". This term arises because it is difficult to provide a physical interpretation for the electron's spin angular momentum. Quantum Electrodynamics provides somewhat of a physical interpretation by proposing that the "vacuum" contains fluctuating electric and magnetic fields. In contrast, in Mills' theory, spin angular momentum results from the motion of negatively charged mass moving systematically, and the equation for angular momentum, $\mathbf{r} \times \mathbf{p}$, can be applied directly to the wave function (a current density function) that describes the electron. And, quantization is carried by the photon, rather than probability waves of the electron.

Fractional Quantum Energy Levels of Hydrogen

The nonradiative state of atomic hydrogen which is historically called the "ground state" forms the basis of the boundary condition of Mills theory [1] to solve the wave equation. Mills further predicts [1] that certain atoms or ions serve as catalysts to release energy from hydrogen to produce an increased binding energy hydrogen atom called a *hydrino atom* having a binding energy of

$$Binding\ Energy = \frac{13.6\ eV}{n^2} \tag{38.71}$$

where

$$n = \frac{1}{2}, \frac{1}{3}, \frac{1}{4}, ..., \frac{1}{p} \tag{38.72}$$

and p is an integer greater than 1, designated as $H\left(\frac{a_H}{p}\right)$ where a_H is the radius of the hydrogen atom. (Although it is purely mathematical, these stable energy levels are also given by both Bohr's and Schrödinger's theories by postulating integer values of the central charge. Justification may be based on notions such virtual particles which are acceptable in other applications of Schrödinger's equation.) Hydrinos are predicted to form by reacting an ordinary hydrogen atom with a catalyst having a net enthalpy of reaction of about

$$m\ \ 27.2\ eV \tag{38.73}$$

where m is an integer. This catalysis releases energy from the hydrogen atom with a commensurate decrease in size of the hydrogen atom, $r_n = na_H$. For example, the catalysis of $H(n=1)$ to $H(n=1/2)$ releases $40.8\ eV$, and the hydrogen radius decreases from a_H to $\frac{1}{2}a_H$.

It is taught in textbooks that atomic hydrogen cannot go below the ground state. Atomic hydrogen having an experimental ground state of 13.6 eV can only exist in a vacuum or in isolation, and atomic hydrogen cannot go below this ground state in isolation. However, there is no known composition of matter containing hydrogen in the ground state of 13.6 eV. Atomic hydrogen is radical and is very reactive. It may react to form a hydride ion or compositions of matter. It is a chemical intermediate which may be trapped as many chemical intermediates may be by methods such as isolation or cryogenically. A hydrino atom may be considered a chemical intermediate that may be trapped in vacuum or isolation. A hydrino atom may be very reactive to form a hydride ion or a novel composition of matter. Hydrogen at predicted lower energy levels, hydrino atoms, has been identified in the extreme ultraviolet emission spectrum from interstellar medium. In addition, new compositions of matter containing hydrogen at predicted lower energy levels have recently been observed in the laboratory, which energy levels are achieved using the novel catalysts.

The excited energy states of atomic hydrogen are also given by Eq. (38.71) except that

$$n = 1,2,3,... \tag{38.74}$$

The $n=1$ state is the "ground" state for "pure" photon transitions (the $n=1$ state can absorb a photon and go to an excited electronic state, but

it cannot release a photon and go to a lower-energy electronic state). However, an electron transition from the ground state to a lower-energy state is possible by a nonradiative energy transfer such as multipole coupling or a resonant collision mechanism. These lower-energy states have fractional quantum numbers, $n = \frac{1}{\text{integer}}$. Processes that occur without photons and that require collisions are common. For example, the exothermic chemical reaction of $H + H$ to form H_2 does not occur with the emission of a photon. Rather, the reaction requires a collision with a third body, M, to remove the bond energy- $H + H + M \rightarrow H_2 + M^*$ [29]. The third body distributes the energy from the exothermic reaction, and the end result is the H_2 molecule and an increase in the temperature of the system. Some commercial phosphors are based on nonradiative energy transfer involving multipole coupling [30]. For example, the strong absorption strength of Sb^{3+} ions along with the efficient nonradiative transfer of excitation from Sb^{3+} to Mn^{2+}, are responsible for the strong manganese luminescence from phosphors containing these ions. Similarly, the $n = 1$ state of hydrogen and the $n = \frac{1}{\text{integer}}$ states of hydrogen are nonradiative, but a transition between two nonradiative states is possible via a nonradiative energy transfer, say $n = 1$ to $n = 1/2$. In these cases, during the transition the electron couples to another electron transition, electron transfer reaction, or inelastic scattering reaction which can absorb the exact amount of energy that must be removed from the hydrogen atom. Thus, a catalyst provides a net positive enthalpy of reaction of $m\ 27.2\ eV$ (i.e. it absorbs $m\ 27.2\ eV$ where m is an integer). Certain atoms or ions serve as catalysts which resonantly accept energy from hydrogen atoms and release the energy to the surroundings to effect electronic transitions to fractional quantum energy levels.

Once formed hydrinos have a binding energy given by Eqs. (38.71-38.72); thus, they may serve as catalysts which provide a net enthalpy of reaction given by Eq. (38.73). Also, the simultaneous ionization of two hydrogen atoms may provide a net enthalpy given by Eq. (38.73). Since the surfaces of stars comprise significant amounts of atomic hydrogen, hydrinos may be formed as a source to interstellar space where further transitions may occur.

A number of experimental observations lead to the conclusion that atomic hydrogen can exist in fractional quantum states that are at lower energies than the traditional "ground" ($n = 1$) state. For example, the existence of fractional quantum states of hydrogen atoms explains the spectral observations of the extreme ultraviolet background emission

from interstellar space [2], which may characterize dark matter as demonstrated in Table 2. (In these cases, a hydrogen atom in a fractional quantum state, $H\left(n_i\right)$, collides, for example, with a $n=\frac{1}{2}$ hydrogen atom, $H\left(\frac{1}{2}\right)$, and the result is an even lower-energy hydrogen atom, $H\left(n_f\right)$, and $H\left(\frac{1}{2}\right)$ is ionized.

$$H\left(n_i\right)+H\left(\frac{1}{2}\right)\rightarrow H\left(n_f\right)+H^{+}+e^{-}+photon \qquad (38.75)$$

The energy released, as a photon, is the difference between the energies of the initial and final states given by Eqs. (38.71-38.72) minus the ionization energy of $H\left(\frac{1}{2}\right)$, $54.4\,eV$.) The catalysis of an energy state of hydrogen to a lower energy state wherein a different lower energy state atom of hydrogen serves as the catalyst is called disproportionation by Mills [1].

Identification of Lower-Energy Hydrogen by Soft X-rays from Dark Interstellar Medium

The first soft X-ray background was detected and reported [31] about 25 years ago. Quite naturally, it was assumed that these soft X-ray emissions were from ionized atoms within hot gases. In a more recent paper, a grazing incidence spectrometer was designed to measure and record the diffuse extreme ultraviolet background [2]. The instrument was carried aboard a sounding rocket and data were obtained between 80 $Å$ and 650 $Å$ (data points approximately every 1.5 $Å$). Here again, the data were interpreted as emissions from hot gases. However, the authors left the door open for some other interpretation with the following statement from their introduction:

> "It is now generally believed that this diffuse soft X-ray background is produced by a high-temperature component of the interstellar medium. However, evidence of the thermal nature of this emission is indirect in that it is based not on observations of line emission, but on indirect evidence that no plausible non-thermal mechanism has been suggested which does not conflict with some component of the observational evidence."

The authors also state that "if this interpretation is correct, gas at several temperatures is present." Specifically, emissions were attributed to gases in three ranges: $5.5 < \log T < 5.7$; $\log T = 6$; $6.6 < \log T < 6.8$.

The explanation proposed herein of the observed dark interstellar medium spectrum hinges on the possibility of energy states below the $n=1$ state, as given by Eqs. (38.71-38.72). Thus, lower-energy transitions of the type,

$$\Delta E = \left(\frac{1}{n_f^2} - \frac{1}{n_i^2}\right) X 13.6\ eV - 54.4\ eV \quad n = 1, \frac{1}{2}, \frac{1}{3}, \frac{1}{4}, \ldots, \quad \text{and } n_i > n_f \tag{38.76}$$

induced by a disproportionation reaction with $H\left(\frac{a_H}{2}\right)$ ought to occur. The wavelength is related to ΔE by

$$\lambda\ (in\ \text{Å}) = \frac{1.240\ X\ 10^4}{\Delta E(in\ eV)} \tag{38.77}$$

The energies and wavelengths of several of these proposed transitions are shown in Table 1. Note that the lower energy transitions are in the soft X-ray region.

Table 1. Energies (Eq. (38.76)) of several fractional-state transitions catalyzed by $H\left(\frac{a_H}{2}\right)$.

n_i	n_f	ΔE (eV)	λ (Å)
$\frac{1}{2}$	$\frac{1}{3}$	13.6	912
$\frac{1}{3}$	$\frac{1}{4}$	40.80	303.9
$\frac{1}{4}$	$\frac{1}{5}$	68.00	182.4
$\frac{1}{5}$	$\frac{1}{6}$	95.20	130.2
$\frac{1}{6}$	$\frac{1}{7}$	122.4	101.3
$\frac{1}{7}$	$\frac{1}{8}$	149.6	82.9

The Data And Its Interpretation

In their analysis of the data, Labov and Bowyer [2] established several tests to separate emission features from the background. There were seven features (peaks) that passed their criteria. The wavelengths and other aspects of these peaks are shown in Table 2. Peaks 2 and 5 were interpreted by Labov and Bowyer as instrumental second-order images of peaks 4 and 7, respectively. Peak 3, the strongest feature, is clearly a helium resonance line: $He(1s^1 2p^1 \rightarrow 1s^2)$. At issue here, is the interpretation of peaks 1, 4, 6, and 7. It is proposed that peaks 4, 6, and 7 arise from the $\frac{1}{3} \rightarrow \frac{1}{4}$, $\frac{1}{4} \rightarrow \frac{1}{5}$, and $\frac{1}{6} \rightarrow \frac{1}{7}$ hydrogen atoms transitions given by Eq. (38.76). It is also proposed that peak 1 arises from inelastic helium scattering of peak 4. That is, the $\frac{1}{3} \rightarrow \frac{1}{4}$ transition yields a 40.8 eV photon (303.9 $\AA$). When this photon strikes $He(1s^2)$, 21.2 eV is absorbed in the excitation to $He(1s^1 2p^1)$. This leaves a 19.6 eV photon (632.6 $\AA$), peak 1. For these four peaks, the agreement between the predicted values (Table 1) and the experimental values (Table 2) is remarkable.

Table 2. Emission features of the LaBov and Bowyer spectrum and their interpretation.

peak	λ (Å)	confidence limit (Å)	intensity photons $cm^{-2}\ s^{-1}\ sr^{-1}$	assignment (Labov & Bowyer)	assignment (Mills)	predicted λ (Eq. (76-77)) (Å)
1	633.0	-4.7 to +4.7	19,000	O^{4+}; Log T = 5.5	*He* scattering of 303.9 line (peak 4)	633.0
2	607.5	-4.9 to + 4.9	second order	second order of 302.5 line	second order of 303.9 line	607.8
3	584	-4.5 to +4.5	70,400	*He* resonance $(1s^1 2p^1 \rightarrow 1s^2)$	*He* resonance $(1s^1 2p^1 \rightarrow 1s^2)$	584
4	302.5	-6.0 to +5.9	2,080	He^+; $(2p^1$ to $1s^1)$	n = 1/3 to n = 1/4	303.9
5	200.6	-4.4 to + 5.3	second order	second order of 101.5 line	second order of 101.3 line	202.6
6	181.7	-4.6 to +5.1	1,030	Fe^{9+} and Fe^{10+}; Log T = 6	n = 1/4 to n = 1/5	182.3
7	101.5	-5.3 to + 4.2	790	Fe^{17+} and Fe^{18+}; Log T = 6.6-6.8	n = 1/6 to n = 1/7	101.3

One argument against this new interpretation of the data is that the transition $\frac{1}{5} \rightarrow \frac{1}{6}$ is missing—predicted at 130.2 $\AA$ by Eqs. (38.76-38.77). This missing peak cannot be explained into existence, but a reasonable rationale can be provided for why it might be missing from these data. The data obtained by Labov and Bowyer are outstanding when the region of the spectrum, the time allotted for data collection, and the logistics are considered. Nonetheless, it is clear that the signal-to-noise ratio is low and that considerable effort had to be expended to differentiate emission features from the background. This particular peak, $\frac{1}{5} \rightarrow \frac{1}{6}$, is likely to be only slightly stronger than the $\frac{1}{6} \rightarrow \frac{1}{7}$ peak (the intensities, Table 2, appear to decrease as n decreases), which has low intensity. Labov and Bowyer provided their data (wavelength, count, count error, background, and background error). The counts minus background values for the region of interest, $130.2 \pm 5\,\AA$, are shown in Table 3 (the confidence limits for the wavelength of about $\pm 5\,\AA$ are the single-side 1 confidence levels and include both the uncertainties in the fitting procedure and uncertainties in the wavelength calibration). Note that the largest peak (count – background) is at 129.64 $\AA$ and has a $counts - background = 8.72$. The $counts - background$ for the strongest signal of the other hydrino transitions are: $n = 1/3$ to $n = 1/4$, 20.05; $n = 1/4$ to $n = 1/5$, 11.36; $n = 1/6$ to $n = 1/7$, 10.40. Thus, there is fair agreement with the wavelength and the strength of the signal. This, of course, does not mean that there is a peak at 130.2 $\AA$. However, it is not unreasonable to conclude that a spectrum with a better signal-to-noise ratio might uncover the missing peak.

Table 3. Data (Labov & Bowyer) near the predicted $\frac{1}{5} \rightarrow \frac{1}{6}$ transition (130.2 *Å*).

l (Å)	counts	background	counts – background
125.82	26	21.58	4.42
127.10	22	21.32	0.68
128.37	18	19.50	–1.50
129.64	29	20.28	8.72
130.90	18	19.76	–1.76
132.15	20	19.50	0.50
133.41	19	19.50	–0.50
134.65	19	20.80	–1.80

Another, and more important, argument against this new interpretation is the fact that the proposed fractional-quantum-state hydrogen atoms have not been detected before. There are several explanations. Firstly, the transitions to these fractional states must be forbidden or must have very high activation energies—otherwise all hydrogen atoms would quickly go to these lower energy states (an estimated transition probability, based on the Labov and Bowyer data, is be between 10^{-15} and $10^{-17} s^{-1}$). In actuality, a catalyst is required in order to obtain emission. Secondly, the number of hydrogen *atoms* ($n=1$), the hydrogen-*atom* density, and the presence of an active catalyst under any conditions on Earth is exceeding low. The combination of extremely low population and extremely low transition probability makes the detection of these transitions especially difficult. Thirdly, this is a very troublesome region of the electromagnetic spectrum for detection because these wavelengths do not penetrate even millimeters of the atmosphere (i.e. this region is the vacuum ultraviolet which requires windowless spectroscopy at vacuum for detection). Lastly, no one

previously has been actively searching for these transitions. The Chandra X-ray Observatory is scheduled to perform similar experiments with detection at much better signal to noise than obtained by Labov and Bowyer.

Hydrogen Catalysts

The catalysis of hydrogen involves the nonradiative transfer of energy from atomic hydrogen to a catalyst which may then release the transferred energy by radiative and nonradiative mechanisms. As a consequence of the nonradiative energy transfer, the hydrogen atom becomes unstable and emits further energy until it achieves a lower-energy nonradiative state having a principal energy level given by Eqs. (38.71-38.72).

Potassium ions can provide a net enthalpy of a multiple of that of the potential energy of the hydrogen atom. The second ionization energy of potassium is $31.63\,eV$; and K^+ releases $4.34\,eV$ when it is reduced to K. The combination of reactions K^+ to K^{2+} and K^+ to K, then, has a net enthalpy of reaction of $27.28\,eV$, which is equivalent to $m = 1$ in Eq. (38.73).

$$27.28\,eV + K^+ + K^+ + H\left[\frac{a_H}{p}\right] \rightarrow K + K^{2+} + H\left[\frac{a_H}{(p+1)}\right] + [(p+1)^2 - p^2]\,X\,13.6\,eV \quad (38.78)$$

$$K + K^{2+} \rightarrow K^+ + K^+ + 27.28\,eV \quad (38.79)$$

The overall reaction is

$$H\left[\frac{a_H}{p}\right] \rightarrow H\left[\frac{a_H}{(p+1)}\right] + [(p+1)^2 - p^2]\,X\,13.6\,eV \quad (38.80)$$

Argon ion is a catalyst. The second ionization energy is $27.63\,eV$.

$$27.63\,eV + Ar^+ + H\left[\frac{a_H}{p}\right] \rightarrow Ar^{2+} + e^- + H\left[\frac{a_H}{(p+1)}\right] + [(p+1)^2 - p^2]X13.6\,eV \quad (38.81)$$

$$Ar^{2+} + e^- \rightarrow Ar^+ + 27.63\,eV \quad (38.82)$$

And, the overall reaction is

$$H\left[\frac{a_H}{p}\right] \rightarrow H\left[\frac{a_H}{(p+1)}\right] + [(p+1)^2 - p^2]X13.6\,eV \quad (38.83)$$

An argon ion and a proton can also provide a net enthalpy of a multiple of that of the potential energy of the hydrogen atom. The third ionization energy of argon is $40.74\,eV$, and H^+ releases $13.6\,eV$ when it is

reduced to H. The combination of reactions of Ar^{2+} to Ar^{3+} and H^+ to H, then, has a net enthalpy of reaction of $27.14\,eV$, which is equivalent to $m=1$ in Eq. (38.73).

$$27.14\,eV + Ar^{2+} + H^+ + H\left[\frac{a_H}{p}\right] \rightarrow H + Ar^{3+} + H\left[\frac{a_H}{(p+1)}\right] + [(p+1)^2 - p^2]X13.6\,eV \quad (38.84)$$

$$H + Ar^{3+} \rightarrow H^+ + Ar^{2+} + 27.14\,eV \quad (38.85)$$

And, the overall reaction is

$$H\left[\frac{a_H}{p}\right] \rightarrow H\left[\frac{a_H}{(p+1)}\right] + [(p+1)^2 - p^2]X13.6\,eV \quad (38.86)$$

Anomalous Thermal Broadening of the Atomic Hydrogen Emission Spectrum in a Gas Discharge Cell by the Presence of Argon

The observation by Kuraica and Konjevic [3] of hydrogen Balmer lines in argon-hydrogen, neon-hydrogen, and pure hydrogen mixtures revealed intense wing developments with argon present in the plasma of negative glow of a glow discharge irrespective of cathode material (carbon, copper, and silver). The authors offer a tentative explanation for hydrogen line shapes in the presence of argon which is based on a quasiresonace charge transfer between metastable argon ions and hydrogen molecules and the formation of a hydrogen molecular ion. According to the authors,

> "... it is essential that the H_2^+ or H_3^+ ion must gain energy in the electric field before dissociation. Otherwise, the large energy of excited hydrogen atoms (on the average 50 eV per atom) cannot be explained".

The source of $50\,eV$ anomalous thermal broadening of the Balmer lines observed by Kuraica and Konjevic [3] during a glow discharge of hydrogen-argon mixtures which was not observed with neon-hydrogen mixtures or pure hydrogen irrespective of cathode material is assigned to lower-energy hydrogen transitions. Transitions of hydrogen to lower-energy levels occurs in a hydrogen plasma discharge cell via a catalyst with a net enthalpy of about 27.2 electron volts including thermal broadening. The catalyst, Ar^+ ions (Eqs. (38.81-38.83)), or Ar^{2+} ions and protons (Eqs. (38.84-38.86)) are formed by the discharge which also produces reactant hydrogen atoms. The transitions to lower-energy levels catalyzed by argon ions result in the release of energy (Eqs. (38.81-38.86)). Hydrogen atoms in fractional quantum states can under go an autocatalytic reaction to further lower energy states. Line spectra in the extreme ultraviolet and soft x-ray regions corresponding to these

transitions have been observed by a 4 ° grazing incidence extreme ultraviolet spectrometer at INP, Greifswald, Germany [7]. The energy heats the plasma and causes thermal broadening of the hydrogen spectrum.

Backward Peak in the Electron Spectrum from Collisions of 70 keV Protons with Hydrogen Atoms

The energy removed by a scattering reaction is resonant with the hydrogen energy released to stimulate this transition. Consider the case wherein a proton undergoes a collision with an electron of a hydrogen atom to effect an electronic transition from $n=1$ to $n=1/2$. The initial and final electronic states are nonradiative; thus, the transition must occur without radiation. The end result is a lower-energy state for the hydrogen and backward scattered electron which is required to conserve energy, momentum, and satisfy the boundary condition for nonradiation. The energy of the hydrogen transition must be transferred to a backward free electron. The reaction for the $n=1$ to $n=1/2$ hydrogen transition effected by inelastic scattering of a 70 keV proton is

$$H^+(70\ keV)+H(n=1)+e^-(0\ eV)\rightarrow H^+(70\ keV)+H(n=1/2)+e^-(40.8\ eV) \quad (38.87)$$

The backward electron is Franck-Hertz [6] scattered by free hydrogen atoms. For hydrogen, the Franck-Hertz scattered peaks of hydrogen transitions, $n_i \rightarrow n_f$ is

$$E=\left(\frac{1}{n_f^2}-\frac{1}{n_i^2}\right)X13.6\ eV-10.2\ eV \quad (38.88)$$

(when this electron strikes $H(1s^1)$, $10.2\ eV$ is absorbed in the excitation to $H(2p^1)$). For the $n=1$ to $n=1/2$ hydrogen transition, a backward 40.8 eV electron is produced which undergoes Franck-Hertz scattering to give rise to a 30.6 eV backward peak. Franck-Hertz scattering of the 30.6 eV peak gives rise to a 20.4 eV backward peak. Or, the backward 40.8 eV electron ionizes a hydrogen atom to give rise to a 27.2 eV peak.

$$E=\left(\frac{1}{n_f^2}-\frac{1}{n_i^2}\right)X13.6\ eV-13.6\ eV \quad (38.89)$$

(when this electron strikes $H(1s^1)$, $13.6\ eV$ is absorbed in the ionization to $H^+ + e^-$). Other transitions will occur to a lesser extent. Discontinuities at the position of the major transitions of 40.8 eV, 30.6 eV, 27.2 eV, and 20.4 eV were observed by Rudd, et al. [4] in the electron spectrum from collisions of 70 keV protons with hydrogen atoms shown in Figure 1.

Figure 1. Spectrum of Rudd et al. [4] of electrons ejected at 160° from 70 keV proton impact on the target gas from the Slevin hydrogen atom source. Open circles, the RF excitation was on and the measured hydrogen dissociation fraction was 93%; solid circles, the RF excitation was off, making the target pure H_2.

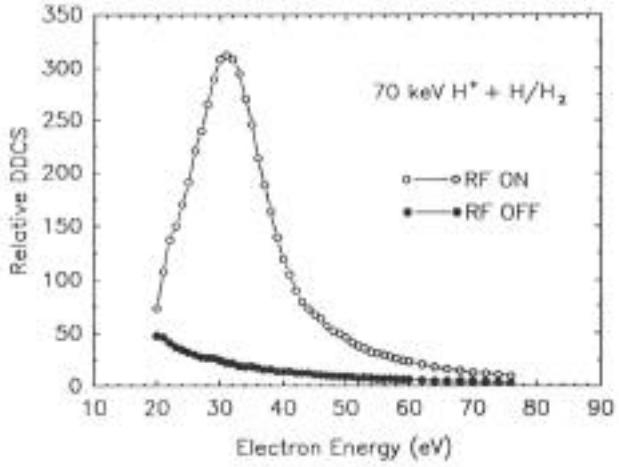

The angle of the maximum intensity of back scattering can be calculated via the boundary condition of nonradiation. The condition for radiation by a moving charge is derived from Maxwell's equations [28]. The condition for nonradiation of a moving charge-density function is that the spacetime Fourier transform of the current-density function must not possess waves synchronous with waves traveling at the speed of light, that is synchronous with $\frac{\omega_n}{c}$ or synchronous with $\frac{\omega_n}{c}\sqrt{\frac{\varepsilon}{\varepsilon_o}}$ where ε is the dielectric constant of the medium. The condition for nonradiation by a moving point charge is that its spacetime Fourier transform does not possess components that are synchronous with waves traveling at the speed of light, as shown by Haus [28]. The Haus derivation applies to a moving charge-density function as well because charge obeys superposition. The Haus derivation is summarized below.

The Fourier components of the current produced by the moving charge are derived. The electric field is found from the vector equation in Fourier space ($\mathbf{k}$, ω-space). The inverse Fourier transform is carried over the magnitude of $\mathbf{k}$. The resulting expression demonstrates that the radiation field is proportional to $\mathbf{J}\left(\frac{\omega}{c}\mathbf{n},\omega\right)$, where $\mathbf{J}(\mathbf{k},\omega)$ is the spacetime Fourier transform of the current perpendicular to $\mathbf{k}$ and

$\mathbf{n} \equiv \frac{\mathbf{k}}{|k|}$. Specifically,

$$\mathbf{E}(\mathbf{r},\omega)\frac{d\omega}{2\pi} = \frac{c}{2\pi}\int \rho(\omega,\Omega) d\omega d\Omega \sqrt{\frac{\mu_0}{\varepsilon_0}} \mathbf{n} \times \left(\mathbf{n} \times \mathbf{J}\left(\frac{\omega}{c}\mathbf{n},\omega\right) e^{i\left(\frac{\omega}{c}\mathbf{n}\cdot\mathbf{r}\right)}\right) \tag{38.90}$$

The field $\mathbf{E}(\mathbf{r},\omega)\frac{d\omega}{2\pi}$ is proportional to $\mathbf{J}\left(\frac{\omega}{c}\mathbf{n},\omega\right)$, namely, the Fourier component for which $\mathbf{k} = \frac{\omega}{c}$. Factors of ω that multiply the Fourier component of the current are due to the density of modes per unit volume and unit solid angle. An unaccelerated charge does not radiate in free space, not because it experiences no acceleration, but because it has no Fourier component $\mathbf{J}\left(\frac{\omega}{c}\mathbf{n},\omega\right)$.

Consider a 70 keV proton of position $\mathbf{r}_0(t)$. The charge density of the proton is described by

$$\rho(\mathbf{r},t) = e\delta(\mathbf{r} - \mathbf{r}_0(t)) \tag{38.91}$$

where $\delta(\mathbf{r} - \mathbf{r}_0(t))$ is the spatial unit impulse function. The current density is

$$\mathbf{J}(\mathbf{r},t) = e\dot{\mathbf{r}}_0(t)\delta(\mathbf{r} - \mathbf{r}_0(t)) \tag{38.92}$$

The spatial Fourier transform represents the current density as a superposition of spatial exponentials, $\exp -i\mathbf{k}\cdot\mathbf{r}$.

$$\begin{aligned}\mathbf{J}(\mathbf{k},t) &= \iiint d^3\mathbf{r} e\dot{\mathbf{r}}_0(t)\delta(\mathbf{r} - \mathbf{r}_0(t))\exp -i\mathbf{k}\cdot\mathbf{r} \\ &= e\dot{\mathbf{r}}_0(t)e^{-i\mathbf{k}\cdot\mathbf{r}_0}\end{aligned} \tag{38.93}$$

The full spacetime Fourier transform is

$$\begin{aligned}\mathbf{J}(\mathbf{k},\omega) &= \iiint dt e\mathbf{v}e^{-i\mathbf{k}\cdot\mathbf{v}t + i\omega t} \\ &= 2\pi e\mathbf{v}\delta(\omega - \mathbf{k}\cdot\mathbf{v})\end{aligned} \tag{38.94}$$

The only nonzero Fourier components are for

$$k_z = \frac{\omega}{v_z\cos\theta} > \frac{\omega}{c} \tag{38.95}$$

where θ is the angle between the wavenumber vector, $\mathbf{k}_z$, and the velocity vector, $\mathbf{v}_z$. Thus, no Fourier components that are synchronous with light velocity with the propagation constant $|\mathbf{k}_z| = \frac{\omega}{c}$ exist. Radiation due to charge motion does not occur when this boundary condition is met.

Consider the case wherein the proton undergoes a collision with the electron of a hydrogen atom to effect an electronic transition from $n = 1$ to $n = 1/2$. The initial and final electronic states are nonradiative; thus, the transition must occur without radiation. If the proton removes

the energy, then radiation will occur during the concomitant acceleration. With acceleration, the current density is

$$\mathbf{J}(\mathbf{r},t) = e\dot{\mathbf{r}}_0(t)\left(1-e^{-\alpha t}\right)\delta(\mathbf{r}-\mathbf{r}_0(t)) \tag{38.96}$$

where α is the transition decay constant. The spatial Fourier transform represents the current density as a superposition of spatial exponentials, $\exp -i\mathbf{k}\ \mathbf{r}$.

$$\begin{aligned}\mathbf{J}(\mathbf{k},t) &= \iiint d^3\mathbf{r}e\dot{\mathbf{r}}_0(t)\left(1-e^{-\alpha t}\right)\delta(\mathbf{r}-\mathbf{r}_0(t))\exp -i\mathbf{k}\ \mathbf{r} \\ &= e\dot{\mathbf{r}}_0(t)e^{-i\mathbf{k}\ \mathbf{r}_0}\left(1-e^{-\alpha t}\right)\end{aligned} \tag{38.97}$$

The full spacetime Fourier transform is

$$\begin{aligned}\mathbf{J}(\mathbf{k},\omega) &= \iiint dte\mathbf{v}e^{-i\mathbf{k}\ \mathbf{v}t+i\omega t-\alpha t} \\ &= \frac{2\pi e\mathbf{v}}{\alpha + i(\omega - \mathbf{k}\ \mathbf{v})}\end{aligned} \tag{38.98}$$

For Eq. (38.98), Fourier components that are synchronous with light velocity with the propagation constant $|\mathbf{k}_z| = \frac{\omega}{c}$ do exist.

However, nonradiation can be achieved during the transition by coupling between the proton and a free electron. During the transition from $n=1$ to $n=1/2$, a transfer of energy from a hydrogen atom causing a backward electron is required to satisfy the nonradiative boundary condition. In the limit, the current density function approaches that of a charge moving at constant velocity. This condition also applies to the backward electron. Thus, the condition for the final velocity of the backward electron is given by Eqs. (38.94) and (38.95). The boundary condition for the velocity of the proton, v_p, and the velocity of the backward electron, v_e, is

$$-v_e\cos\theta_e = v_p\cos\theta_p \tag{38.99}$$

where θ_e is the laboratory frame electron scattering angle and θ_p is the laboratory frame proton scattering angle. The velocity, v_e, of an electron as a function of the energy, E_e, is

$$v_e = \sqrt{\frac{2E_e}{m_e}} \tag{38.100}$$

where m_e is the mass of the electron. The velocity, v_p, of an electron as a function of the energy, E_p, is

$$v_p = \sqrt{\frac{2E_p}{m_p}} \tag{38.101}$$

where m_p is the mass of the proton. Substitution of Eqs. (38.100) and (38.101) into Eq. (38.99) gives

$$-\sqrt{\frac{2E_e}{m_e}}\cos\theta_e = \sqrt{\frac{2E_p}{m_p}}\cos\theta_p \qquad (38.102)$$

From the nonradiative boundary condition, the angle of the backward electron is

$$\theta = \cos^{-1}\left[-\sqrt{\frac{E_p m_e}{m_p E_e}}\cos\theta_p\right] \qquad (38.103)$$

In the case that the initial and final velocity vectors of the incident proton are equal, $E_{p_{initial}} = E_{p\,final} = 70\ keV$, and the initial and final energies of the electron are $E_{e_{initial}} = 0\ eV$ and $E_{e_{final}} = 40.8\ eV$, respectively, the maximum intensity of the peaks is predicted (Eq. (38.103)) to be 165°. This is in agreement with the observed maximum at about 160° [4]. For small proton scattering angles, Eq. (38.103) is also in agreement with the absence of the backward peaks at 90° [4]. The maximum intensity of the backward peaks from collisions of hydrogen atoms with 30 keV protons predicted from Eq. (38.103) is 130°. Thus, the intensity of the backward peaks at 160° with 30 keV protons is predicted to be less than that of 70 keV incident protons in agreement with Rudd [4].

Novel Energy States of Hydrogen Formed by a Catalytic Reaction

Typically the emission of extreme ultraviolet light from hydrogen gas is achieved via a discharge at high voltage, a high power inductively coupled plasma, or a plasma created and heated to extreme temperatures by RF coupling (e.g. $> 10^6\ K$) with confinement provided by a toroidal magnetic field. Intense EUV emission was observed by Mills et al. [7-12] at low temperatures (e.g. $< 10^3\ K$) from atomic hydrogen and certain atomized pure elements or certain gaseous ions which ionize at integer multiples of the potential energy of atomic hydrogen. The release of energy from hydrogen as evidenced by the EUV emission must result in a lower-energy state of hydrogen. The lower-energy hydrogen atom called a hydrino atom by Mills [1] would be expected to demonstrate novel chemistry. The formation of novel compounds based on hydrino atoms would be substantial evidence supporting catalysis of hydrogen as the mechanism of the observed EUV emission. A novel hydride ion called a hydrino hydride ion having extraordinary chemical properties given by Mills [1] is predicted to form by the reaction of an electron with a hydrino atom. Compounds containing hydrino hydride ions have been isolated as products of the reaction of atomic hydrogen with atoms and ions identified as catalysts in the Mills et al. EUV study [1, 7-12, 32-37]. The novel hydride compounds were identified analytically by techniques such as time of flight secondary ion mass

spectroscopy, X-ray photoelectron spectroscopy, and proton nuclear magnetic resonance spectroscopy. For example, the time of flight secondary ion mass spectroscopy showed a large hydride peak in the negative spectrum. The X-ray photoelectron spectrum showed large metal core level shifts due to binding with the hydride as well as novel hydride peaks. The proton nuclear magnetic resonance spectrum showed significantly upfield shifted peaks which corresponded to and identified novel hydride ions.

Discussion

The Schrödinger equation gives the observed spontaneously radiative energy levels and the nonradiative state of hydrogen. On this basis alone, it is justified despite its inconsistency with physicals laws and numerous experimental observations such as

• The appropriate eigenvalue must be postulated and the variables of the Laguerre differential equation must be defined as integers in order to obtain the Rydberg formula.

• The Schrödinger equation is not Lorentzian invariant.

• The Schrödinger equation violates first principles including special relativity and Maxwell's equations [1, 38].

• The Schrödinger equation gives no basis why excited states are radiative and the 13.6 eV state is stable [1]. Mathematics does not determine physics. It only models physics.

• The Schrödinger equation solutions, Eq. (38.36) and Eq. (38.37), predict that the ground state electron has zero angular energy and zero angular momentum, respectively.

• The Schrödinger equation solution, Eq. (38.36), predicts that the ionized electron may have infinite angular momentum.

• The Schrödinger equation solutions, Eq. (36) and Eq. (37), predict that the excited state rotational energy levels are nondegenerate as a function of the ℓ quantum number even in the absence of an applied magnetic field, and the predicted energy is over six orders of magnitude of the observed nondegenerate energy in the presence of a magnetic field. In the absence of a magnetic field, no preferred direction exists. In this case, the ℓ quantum number is a function of the orientation of the atom with respect to an arbitrary coordinate system.

Therefore, the nondegeneracy is nonsensical and violates conservation of angular momentum of the photon.

• The Schrödinger equation predicts that each of the functions that corresponds to a highly excited state electron is not integrable and can not be normalized; thus, each is infinite.

• The Schrödinger equation predicts that the ionized electron is sinusoidal over all space and can not be normalized; thus, it is infinite.

• The Heisenberg uncertainty principle arises as the standard deviation in the electron probability wave, but experimentally it is not the basis of wave particle duality.

• The correspondence principle does not hold experimentally.

• The Schrödinger equation does not predict the electron magnetic moment and misses the spin quantum number all together.

• The Schrödinger equation is not a wave equation since it gives the velocity squared proportional to the frequency.

• The Schrödinger equation is not consistent with conservation of energy in an inverse potential field wherein the binding energy is equal to the kinetic energy and the sum of the binding energy and the kinetic energy is equal to the potential energy [14].

• The Schrödinger equation permits the electron to exist in the nucleus which is a state that is physically nonsensical with infinite potential energy and infinite negative kinetic energy.

• The Schrödinger equation interpreted as a probability wave of a point particle can not explain neutral scattering of electrons from hydrogen [1].

• The Schrödinger equation interpreted as a probability wave of a point particle gives rise to infinite magnetic and electric energy in the corresponding fields of the electron.

• A modification of the Schrödinger equation was developed by Dirac to explain spin which relies on the unfounded notions of negative energy states of the vacuum, virtual particles, and gamma factors.

The success of quantum mechanics can be attributed to 1.) the lack of rigor and unlimited tolerance to ad hoc assumptions in violation of physical laws, 2.) fantastical experimentally immeasurable corrections such as virtual particles, vacuum polarizations, effective nuclear charge, shielding, ionic character, compactified dimensions, and renormalization, and 3.) curve fitting parameters that are justified solely on the basis that they force the theory to match the data. Quantum mechanics is now in a state of crisis with constantly modified versions of matter represented as undetectable minuscule vibrating strings that exist in many unobservable hyperdimensions, that can travel back and forth between undetectable interconnected parallel universes. And, recent data shows that the expansion of the universe is accelerating. This observation has shattered the long held unquestionable doctrine of the origin of the universe as a big bang [39]. It may be time to reconsider the roots of quantum theory, namely the theory of the hydrogen atom. Especially in light of the demonstration that the hydrogen atom can be solved in closed form from first principles, that new chemistry is predicted, and that the predictions have substantial experimental support. New evidence mandates that old theories be revised or abandoned. Recently line spectra of fractional quantum energy levels of atomic hydrogen have been measured by a 4 ° grazing incidence extreme ultraviolet spectrometer at INP, Greifswald, Germany [7]. The Schrödinger wave equation solutions can not explain the experimental results which confirm the existence of lower energy states of hydrogen; thus, the theory must be modified.

Billions of dollars have been spent to harness the energy of hydrogen through fusion using plasmas created and heated to extreme temperatures by RF coupling (e.g. $>10^6\ K$) with confinement provided by a toroidal magnetic field. Mills et al. [7-12] have demonstrated that energy may be released from hydrogen using a chemical catalyst at relatively low temperatures with an apparatus which is of trivial technological complexity compared to a tokomak. And, rather than producing radioactive waste, the reaction has the potential to produce compounds having extraordinary properties [32-37]. The implications are that a vast new energy source and a new field of hydrogen chemistry have been discovered.

References

1. R. Mills, The Grand Unified Theory of Classical Quantum Mechanics, January 1999 Edition, BlackLight Power, Inc., Cranbury, New Jersey, Distributed by Amazon.com.
2. Labov, S., Bowyer, S., "Spectral observations of the extreme ultraviolet background", The Astrophysical Journal, 371, (1991), pp. 810-819.

3. Kuraica, M., Konjevic, N., Physical Review A, Volume 46, No. 7, October (1992), pp. 4429-4432.
4. Rudd, M. E., Gealy, M. W., Kerby, G. W., Hsu, Ying-Yuan, Physical Review Letters, Vol. 68, No. 10, (1992), pp. 1504-1506.
5. R. Mills, W. Good, J. Phillips, A. Popov, Lower-Energy Hydrogen Methods and Structures, US Patent 6,024,935, issued February 15, 2000.
6. Beiser, A., Concepts of Modern Physics, Fourth Edition, McGraw-Hill Book Company, New York, (1978), pp. 312-354.
7. J. P. F. Conrads, R. Mills, "Observation of Extreme Ultraviolet Hydrogen and Hydrino Emission from Hydrogen-KI Plasmas Produced by a Hollow Cathode Discharge", in progress.
8. R. Mills, J. Dong, Y. Lu, "Observation of Extreme Ultraviolet Hydrogen Emission from Incandescently Heated Hydrogen Gas with Certain Catalysts", 1999 Pacific Conference on Chemistry and Spectroscopy and the 35th ACS Western Regional Meeting, Ontario Convention Center, California, (October 6-8, 1999).
9. R. Mills, J. Dong, Y. Lu, "Observation of Extreme Ultraviolet Hydrogen Emission from Incandescently Heated Hydrogen Gas with Certain Catalysts", Int. J. Hydrogen Energy, accepted.
10. J. P. F. Conrads, R. Mills, "Temporal Behavior of Light-Emission in the Visible Spectral Range from a Ti-K2CO3-H-Cell', in progress.
11. R. Mills, Y. Lu, and T. Onuma, "Formation of a Hydrogen Plasma from an Incandescently Heated Hydrogen-Potassium Gas Mixture and Plasma Decay Upon Removal of Heater Power", Int. J. Hydrogen Energy, submitted.
12. R. Mills, M. Nansteel, and Y. Lu, "Observation of Extreme Ultraviolet Hydrogen Emission from Incandescently Heated Hydrogen Gas with Strontium that Produced an Optically Measured Power Balance that was 4000 Times the Control", Int. J. Hydrogen Energy, submitted.
13. Beiser, A., Concepts of Modern Physics, Fourth Edition, McGraw-Hill, New York, (1987),. pp. 87-117.
14. Fowles, G. R., Analytical Mechanics, Third Edition, Holt, Rinehart, and Winston, New York, (1977), pp. 154-156.
15. McQuarrie, D. A., Quantum Chemistry, University Science Books, Mill Valley, CA, (1983), pp. 78-79.
16. Jackson, J. D., Classical Electrodynamics, Second Edition, John Wiley & Sons, New York, (1962), pp. 84-108.
17. McQuarrie, D. A., Quantum Chemistry, University Science Books, Mill Valley, CA, (1983), pp. 221-224.
18. W. Moore, Schrödinger life and thought, Cambridge University Press, (1989), p.198.
19. Fowles, G. R., Analytical Mechanics, Third Edition, Holt, Rinehart, and Winston, New York, (1977), pp. 57-60.

20. H. Margenau, G. M. Murphy, The Mathematics of Chemistry and Physics, D. Van Nostrand Company, Inc., New York, (1943), pp. 77-78.
21. Weisskopf, V. F., Reviews of Modern Physics, Vol. 21, No. 2, (1949), pp. 305-315.
22. Horgan, J., "Quantum Philosophy", Scientific American, July, (1992), pp. 94-104.
23. Platt, D. E., Am. J. Phys., 60 (4), April, 1992, pp. 306-308.
24. S. Durr, T. Nonn, G. Rempe, Nature, September 3, (1998), Vol. 395, pp. 33-37.
25. B. Gao, Phys. Rev. Lett., Vol. 83, No. 21, Nov. 22, (1999), pp. 4225-4228.
26. Science News, Vol. 156, November 27th 1999, p. 342, under "Physics rule of thumb gets thumbs down" 2nd & 3rd paragraphs.
27. Science News, 1/11/86, p. 26.
28. Haus, H. A., "On the radiation from point charges", American Journal of Physics, 54, (1986), pp. 1126-1129.
29. N. V. Sidgwick, The Chemical Elements and Their Compounds, Volume I, Oxford, Clarendon Press, (1950), p.17.
30. M. D. Lamb, Luminescence Spectroscopy, Academic Press, London, (1978), p. 68.
31. S. Bower, G. Field, and J. Mack, "Detection of an Anisotrophic Soft X-ray Background Flux," Nature, Vol. 217, (1968), p. 32.
32. R. Mills, B. Dhandapani, N. Greenig, J. He, "Synthesis and Characterization of Potassium Iodo Hydride", Int. J. of Hydrogen Energy, accepted.
33. R. Mills, "Novel Inorganic Hydride", Int. J. of Hydrogen Energy, Vol. 25, (2000), pp. 669-683.
34. R. Mills, "Novel Hydrogen Compounds from a Potassium Carbonate Electrolytic Cell", Fusion Technology, Vol. 37, No. 2, March, (2000), pp. 157-182.
35. R. Mills, J. He, and B. Dhandapani, "Novel Hydrogen Compounds", 1999 Pacific Conference on Chemistry and Spectroscopy and the 35th ACS Western Regional Meeting, Ontario Convention Center, California, (October 6-8, 1999).
36. R. Mills, B. Dhandapani, M. Nansteel, J. He, "Synthesis and Characterization of Novel Hydride Compounds", Int. J. of Hydrogen Energy, submitted.
37. R. Mills, "Highly Stable Novel Inorganic Hydrides", International Journal of Inorganic Materials, submitted.
38. C. A. Fuchs, A. Peres, "Quantum theory needs no 'interpretation'", Phys. Today, Vol. 53, March, (2000), No. 3, pp. 70-71.
39. N. A. Bahcall, J. P. Ostriker, S. Perlmutter, P. J. Steinhardt, Science, May 28, 1999, Vol. 284, pp. 1481-1488.

SECTION V

Prospect
Quarks to Cosmos to Consciousness

THE NATURE OF CONSCIOUSNESS

Consciousness arises from a "negative" entropy state of a being at the expense of its surroundings wherein the being increases the spontaneous decay rate of the surroundings. The relationship between the energy decay rate according to Maxwell's Equations, spacetime expansion due to energy decay with the rate given by General Relativity, entropy due to spacetime expansion, and the imaginary nature of coordinate time due to spacetime expansion permits the phenomenon of consciousness.

RELATIONSHIP OF SPACETIME AND THE ARROW OF TIME

The provision of the equivalence of inertial and gravitational mass by the Mills theory of fundamental particles wherein spacetime is Riemannian due to its relativistic correction with particle production permits the correct derivation of the General Theory. And, the former provision of the two-dimensional nature of matter permits the unification of atomic, subatomic, and cosmological gravitation. The unified theory of gravitation is derived by first establishing a metric.

A space in which the curvature tensor has the following form:

$$R_{\mu\nu,\alpha\beta} = K\ (g_{\nu\alpha}g_{\mu\beta} - g_{\mu\alpha}g_{\nu\beta}) \tag{39.1}$$

is called a space of constant curvature; it is a four-dimensional generalization of Friedmann-Lobachevsky space. The constant K is called the constant of curvature. *The curvature of spacetime results from a discontinuity of matter having curvature confined to two spatial dimensions. This is the property of all matter as an orbitsphere.* Consider an isolated orbitsphere and radial distances, r, from its center. *For r less than r_n there is no mass; thus, spacetime is flat or Euclidean.* The curvature tensor applies to all space of the inertial frame considered; thus, for r less than r_n, $K = 0$. At $r = r_n$ there exists a discontinuity of mass of the orbitsphere. This results in a discontinuity of the curvature tensor for radial distances greater than or equal to r_n. The discontinuity requires relativistic corrections to spacetime itself. It requires radial length contraction and time dilation that results in the curvature of spacetime. The gravitational radius of the orbitsphere and infinitesimal temporal displacement in spacetime which is curved by the presence of the orbitsphere are derived in the Gravity Section.

The Schwarzschild metric gives the relationship whereby matter causes relativistic corrections to spacetime that determines the curvature of spacetime and is the origin of gravity. The separation of proper time between two events x^μ and $x^\mu + dx^\mu$ given by Eq. (), the Schwarzschild metric [1-2], is

$$d\tau^2 = \left(1 - \frac{2Gm_0}{c^2 r}\right) dt^2 - \frac{1}{c^2}\left(1 - \frac{2Gm_0}{c^2 r}\right)^{-1} dr^2 + r^2 d\theta^2 + r^2 \sin^2\theta d\phi^2 \qquad (39.2)$$

Eq. (39.2) can be reduced to Newton's Theory of Gravitation for r_g, the gravitational radius of the particle, much less than r_α^*, the radius of the particle at production ($\frac{r_g}{r_\alpha^*} << 1$), where the radius of the particle is its Compton wavelength bar ($r_\alpha^* = \lambda\!\!\!^{-}_c$).

$$\mathbf{F} = \frac{Gm_1 m_2}{r^2} \qquad (39.3)$$

where G is the Newtonian gravitational constant. Eq. (39.2) relativistically corrects Newton's Gravitational Theory. In an analogous manner, Lorentz transformations correct Newton's Laws of Mechanics. Consider a general point in the xy plane having $dr = 0$; $d\theta = 0$; $\sin^2\theta = 1$. Substitution of these parameters into Eq. (39.2) gives

$$d\tau = dt\left(1 - \frac{2Gm_0}{c^2 r} - \frac{v^2}{c^2}\right)^{\frac{1}{2}} \qquad (39.4)$$

In the case of matter/energy conversion with $v^2 = c^2$, Eq. (39.4) becomes

$$\tau = ti\sqrt{\frac{2GM}{c^2 r}} = ti\sqrt{\frac{2GM}{c^2 r}} \qquad (39.5)$$

And, the particle energies are all equal to the particle production mass energy. The particle production energies given in the Gravity Section are the mass energy, the Planck energy, electric potential, magnetic energy, the gravitational potential energy, and the mass/spacetime metric energy.

$$m_o c^2 = \hbar\omega^* = V = E_{mag} = E_{grav} = E_{spacetime} \qquad (39.6)$$

$$m_0 c^2 = \hbar\omega^* = \frac{\hbar^2}{m_0 \lambda\!\!\!^{-2}_C} = \alpha^{-1}\frac{e^2}{4\pi\varepsilon_0 \lambda\!\!\!^{-}_C} = \alpha^{-1}\frac{\pi\mu_0 e^2\hbar^2}{\left(2\pi m_0\right)^2 \lambda\!\!\!^{-3}_C} = \alpha^{-1}\frac{\mu_0 e^2 c^2}{2h}\sqrt{\frac{Gm_0}{\lambda\!\!\!^{-}_C}}\sqrt{\frac{\hbar c}{G}} = \frac{\alpha h}{1\ \mathrm{sec}}\sqrt{\frac{\lambda\!\!\!^{-}_C c^2}{2Gm}} \qquad (39.7)$$

The equations which ***unify de Broglie's Equation, Planck's Equation, Maxwell's Equations, Newton's Equations, and Special and General Relativity define the mass of fundamental particles in terms of the spacetime metric***. Eqs. (39.6-39.7) gives the equivalence of particle production energies corresponding to mass, charge, current, and gravity according to the proportionality constants which are given in terms of a self consistent set of units. This equivalence is a consequence of equivalence of the gravitational mass and the inertial mass together with Special Relativity. According to Eqs. (39.6-39.7) matter, energy, and spacetime are conserved.

Period Equivalence

The Schwarzschild metric (Eq. (39.2)) with the equivalence of the particle production energies (Eqs. (39.6-39.7)) permit the equivalence of mass/energy ($E = mc^2$) and spacetime ($\frac{c^3}{4\pi G} = 3.22\ X\ 10^{34}\ \frac{kg}{\sec}$). Spacetime expands as mass is released as energy which provides the basis of the atomic, thermodynamic, and cosmological arrows of time. The proper time of the electron is given by Eq. (27.1), and the electron mass corresponding to this amount of time is given by Eq. (27.3). Thus, Q, the mass/energy to expansion/contraction quotient of spacetime is given by the ratio of Eq. (27.3) and Eq. (27.1) wherein Eq. (39.5) gives the General Relativistic factor which divides the electron mass and multiplies the electron proper time to give the corresponding spacetime expansion.

$$Q = \frac{\frac{m_e}{\sqrt{\frac{2GM}{c^2\lambda_c}}}}{\tau\sqrt{\frac{2GM}{c^2\lambda_c}}} = \frac{\left(\frac{h\alpha}{1\ \sec\ c^2}\right)^{\frac{1}{2}}\left(\frac{c\hbar}{2G}\right)^{\frac{1}{4}}}{2\pi\frac{\hbar}{m_e c^2}\frac{2Gm_e}{c^2\lambda_c}} = \frac{c^3}{4\pi G} = 3.22\ X\ 10^{34}\ \frac{kg}{\sec} \tag{39.8}$$

The universe undergoes time harmonic expansion and contraction corresponding to matter/energy conversion. The equation of the radius of the universe, R, which is derived in the Gravity Section is

$$R = \left(\frac{2Gm_U}{c^2} + \frac{\frac{cm_U}{c^3}}{\frac{c^3}{4\pi G}} - \frac{cm_U}{\frac{c^3}{4\pi G}}\right)\cos\left(\frac{2\pi t}{\frac{2\pi Gm_U}{c^3}\sec}\right)m \tag{39.9}$$

From Eq. (39.9), the period of the expansion/contraction cycle of the radius of the universe, T, is

$$T = \frac{2\pi Gm_U}{c^3}\ \sec \tag{39.10}$$

It was derived in the Unification of Spacetime, the Forces, Matter, and Energy Section that ***the periods of spacetime expansion/contraction and particle decay/production for the universe are equal***. It follows from the Poynting Power Theorem (Eq. (7.27)) with spherical radiation that the transition lifetimes are given by the ratio of energy and the power of the transition [3]. Magnetic energy is a Special Relativistic consequence of electric energy and kinetic energy. Thus, only transitions involving electric energy need be considered. The transition lifetime, τ, in the case of the electric multipole moment given by Jackson [4] as

$$Q_{lm} = \frac{3}{\ell + 3}e\left(r_n\right)^{\ell} \tag{39.11}$$

is [1]

$$\tau = \frac{energy}{power}$$

$$\tau = \frac{[\hbar\omega]}{\left[\frac{2\pi c}{[(2l+1)!!]^2}\left(\frac{l+1}{l}\right)k^{2l+1}|Q_{lm}+Q'_{lm}|^2\right]} = \frac{1}{2\pi}\left(\frac{h}{e^2}\right)\sqrt{\frac{\mu_0}{\varepsilon_0}}\frac{[(2l+1)!!]^2}{2\pi}\left(\frac{l}{l+1}\right)\left(\frac{l+3}{3}\right)^2\frac{1}{(kr_n)^{2l}\omega} \tag{39.12}$$

where in the exemplary case of an excited state of atomic hydrogen r_n is the radius of the electron orbitsphere which is na_0 (Eq. (27.17)). From Eq. (24.35), the transition lifetime is proportional to the ratio of η, the radiation resistance of free space.

$$\eta = \sqrt{\frac{\mu_0}{\varepsilon_0}} \tag{39.13}$$

and, the Quantum Hall resistance, $\frac{h}{e^2}$. The Quantum Hall resistance given in the Quantum Hall Effect Section was derived using the Poynting Power Theorem. Also, from Eq. (39.12), the transition lifetime is proportional to the fine structure constant, α,

$$\alpha = \frac{1}{4\pi}\sqrt{\frac{\mu_o}{\varepsilon_o}}\frac{e^2}{\hbar} \tag{39.14}$$

From Eq. (24.17) and Eq. (24.35), the lifetime an excited state of a hydrogen atom is inversely proportional to the frequency of the transition. This is also the case for the universe which is a 3-sphere universe. (More explicitly, the universe is a Riemannian three dimensional hyperspace plus time with a constant positive curvature). During an electromagnetic transition, the total energy of the system decays exponentially. Applying Eqs. (2.45) and (2.46) to the case of exponential decay,

$$h(t) = e^{-\frac{1}{T}t}u(t) \tag{39.15}$$

However, Eq. (39.5) determines that ***the coordinate time is imaginary*** because energy transitions are spacelike due to General Relativistic effects. For example, Eq. (27.2) gives the mass of the electron (a fundamental particle) in accordance with Eq. (39.5).

$$\frac{2\pi\lambda\!\!\!^{-}_C}{\sqrt{\frac{2Gm_e}{\lambda\!\!\!^{-}_C}}} = \frac{2\pi\lambda\!\!\!^{-}_C}{v_g} = i\alpha^{-1}\sec \tag{39.16}$$

where Newtonian gravitational velocity v_g is given by Eq. (23.35). Replacement of the coordinate time, t, of Eq. (39.15) by the spacelike

time, it, gives.

$$h(t) = e^{-i\frac{1}{T}t} = \cos\frac{2\pi}{T}t \tag{39.17}$$

where the period is T. The periods of spacetime expansion/contraction and particle decay/production for the universe are equal due to the Eq. (39.5) which determines the masses of fundamental particles, the equivalence of inertial and gravitational mass, the phase matching condition of mass to the speed of light and charge to the speed of light, and that the coordinate time is imaginary because energy transitions are spacelike due to General Relativistic effects. From Eq. (39.5)

$$\frac{\text{proper time}}{\text{coordinate time}} = \frac{\text{gravitational wave condition}}{\text{electromagnetic wave condition}} = \frac{\text{gravitational mass phase matching}}{\text{charge/inertial mass phase matching}}$$

$$\frac{\text{proper time}}{\text{coordinate time}} = i\frac{\sqrt{\frac{2Gm}{c^2\lambda\!\!\!^{-}_C}}}{\alpha} = i\frac{v_g}{\alpha c} \tag{39.18}$$

Eq. (24.24) gives the ratio of Eq. (39.18) in terms of the coordinate particle mass and the Grand Unification Mass/Energy.

$$\frac{\text{proper time}}{\text{coordinate time}} = \frac{m_0}{m_u} = \alpha^{-1}\frac{\mu_0 e^2 c}{2h}\frac{\sqrt{\frac{Gm_0}{\lambda\!\!\!^{-}_C}}}{c} = \alpha^{-1}\frac{\mu_0 e^2 c}{2h}\sqrt{\frac{Gm_0}{c^2\lambda\!\!\!^{-}_C}} = \alpha^{-1}\frac{\mu_0 e^2 c}{2h}\frac{v_G}{c} = \frac{v_G}{c} \tag{39.19}$$

As fundamental particles, atoms, molecules, and macroscopic configurations of fundamental particles, atoms, and molecules release energy, spacetime increases. The superposition of expanding spacetime arising at the atomic level over all scales of dimensions from the atomic to the cosmological gives rise to the observed expanding universe. The wavefront of energy and spacetime from matter to energy conversion travel at the speed of light. Consider Eq. (23.43). As given in the Gravity Section, at the present time in the cycle of the universe, the world line of the expanding spacetime and the released energy are approximately coincident. In terms of Eq. (23.38), the proper time and the coordinate time are approximately equal. The ratio of the gravitational radius, r_g given by Eq. (23.36), and the radius of the universe equal to one and the gravitational velocity given by Eq. (23.35) is the escape velocity. And, Q, (Eq. (23.140)) is equal to the matter to energy conversion rate of the time harmonic expansion/contraction cycle of the universe which permits light energy (photons) to propagate (escape the gravitational hole of the universe).

When the gravitational radius r_g is the radius of the universe, the proper time is equal to the coordinate time (Eq. (23.43)), and the gravitational velocity v_g of the universe is the escape velocity which is the speed of light.

Mass/energy must be conserved during the harmonic cycle of expansion and contraction. The gravitational potential energy E_{grav} of the universe is given by Eq. (24.43). In the case that the radius of the universe r is the gravitational radius r_G given by Eq. (23.22), the gravitational potential energy is equal to $m_U c^2$ which follows that given by Eq. (23.27). The gravitational velocity v_G is given by Eq. (23.33) wherein an electromagnetic wave of mass/energy equivalent to the mass of the universe travels in a circular orbit wherein the eccentricity is equal to zero (Eq. (26.20)), and the escape velocity from the universe can never be reached. The wavelength of the oscillation of the universe and the wavelength corresponding to the gravitational radius r_G must be equal. Electromagnetic energy and gravitational mass obey superposition, and both spacetime expansion/contraction and electromagnetic energy corresponding to particle decay/production travel at the speed of light and obey the wave relationship given by Eq. (20.4). The wavelength is given in terms of the radius by Eq. (2.2). Thus, ***the harmonic oscillation period***, T, is

$$T = \frac{2\pi r_G}{c} = \frac{2\pi G m_U}{c^3} = \frac{2\pi G\left(2\ X\ 10^{54}\ kg\right)}{c^3} = 3.10\ X\ 10^{19}\ \text{sec} = 9.83\ X\ 10^{11}\ \text{years} \tag{39.20}$$

where the mass of the universe, m_U.

The Arrow of Time and Entropy

The principle of entropy was invented to provide an explanation for the direction of time as it pertains to macroscopic processes. The present theory provides an explanation for the expanding universe which unifies the ***microscopic, thermodynamic, and cosmological arrows of time***.

Physical phenomena involve exchange of energy between matter and spacetime. Eq. (39.5) gives the relationship between ***the equivalence of mass/energy conversion and the contraction/expansion of spacetime***. This relationship provides the arrow of time. Thus, the creation of mass from energy causes an infinitesimal contraction or collapse of spacetime much like a dimple in

a plastic ball but in three dimensions plus time; whereas, the release of energy causes an expansion of spacetime. Time goes forward in the direction of lower energy states and greater entropy because these states correspond to an expansion of spacetime relative to the higher energy states of matter. Expanded space corresponds to a smaller cross section for reverse time as opposed to forward time. Thus, the arrow of time arising on the subatomic and atomic level gives rise to the Second Law of thermodynamics;

> *In an isolated system, spontaneous processes occur in the direction of increasing entropy.*

Stated mathematically:

> *The entropy change, dS, which is equal to the change in heat, dq, divided by the temperature, T, is greater than zero.*

$$dS = \frac{dq}{T} > 0 \tag{39.21}$$

The atomic arrow of time also applies to cosmology and provides for the expansion of spacetime on a cosmological scale. As fundamental particles, atoms, molecules, and macroscopic configurations of fundamental particles, atoms, and molecules release energy, spacetime increases. The superposition of expanding spacetime arising at the atomic level over all scales of dimensions from the atomic to the cosmological gives rise to the observed expanding universe which continues to increase in entropy.

The universe is a four dimensional hyperspace of constant positive curvature. The coordinates are spherical, and the space can be described as a series of spheres each of constant radius r whose centers coincide at the origin. The existence of the mass m_U causes the area of the spheres to be less than $4\pi r^2$ and causes the clock of each r-sphere to run so that it is no longer observed from other r-spheres to be at the same rate. Only in the case that the radius of the universe is equal to the gravitational radius, is the area given by $4\pi r^2$; otherwise, the area of the sphere corresponding to the radius of the universe is less than that given by $4\pi r^2$. The Schwarzschild metric given by Eq. (39.2) is the general form of the metric which allows for these effects. The proper area is given by solving Eq. (39.2) for the coordinate radius as a function of the proper radius followed by the substitution of the coordinate radius into the area equation, $4\pi r^2$. Eq. (39.5) determines that ***the coordinate time is imaginary*** because energy transitions are spacelike due to General Relativistic effects. This relation used in Eq. (39.17) and the linked relationship between the equivalence of mass/energy

conversion and the contraction/expansion of spacetime (Eq. (39.5)) have implications for the nature of consciousness.

CONSCIOUSNESS

A distinction exists between animate beings and inanimate objects. If the brain chemistry of conscious beings behaved as typical chemical reactions following an arrow of time according to typical enthalpy and concomitant entropy changes, then any information stored and processed by the brain would decrease over time, and consciousness would not be possible. The brain chemistry comprising ion channel conductance changes, ion flows, ion pump activity, metabolic reactions, etc., comprise an energy state in opposition to the thermodynamic arrow of time. Living beings produce negative entropy at the expense of their surroundings. Consciousness, the ability of a chemical reaction to be aware of itself arises from the relationship of energy changes to entropy. Eq. (39.6) also applies to the case of an excited state of matter. Thus, ultimately consciousness arises from the relationship between matter/energy conversion, spacetime expansion, and the arrow of time.

The time harmonic period of the universe for electromagnetic energy decay according to Maxwell's Equations and spacetime expansion and contraction according to General Relativity are equal (Eq. (39.20)). By Eq. (39.4), when the radius of the universe is the gravitational radius, r_g, (Eq. (23.147)) the coordinate time is equal to the proper time. Thereafter, a phase shift in the coordinate time relative to the proper time arises due to spacetime expansion effected by matter to energy conversion. The rates of spontaneous electromagnetic energy decay and spacetime expansion for the universe as a whole remain such that the harmonic rate equation is obeyed. However, animate matter can decrease its rate of decay at the expense of the surrounding matter. The unique feature of the phenomena of life and consciousness arises from a different coordinate time phase shift corresponding to matter/energy conversion to spacetime expansion of the life form with respect to that of the matter comprising the life form's environment due to an artificially increased energy state of the life form. Consider a being that simultaneously increases its energy state and state of order. The absorption of energy increases its mass. The corresponding excited energy state would decay according to Eq. (39.17) with concomitant spacetime expansion according to Eq. (39.8). Entropy would increase. However, living beings comprise chemical systems which increase the rate of decay of other parts of the universe to achieve a "charged" or high energy ordered state which deviates from the rate law given by Eq. (39.17). Whereas, the rate of the being's surroundings decays faster at the expense of the being such that their sum obeys the rate given by Eq.

(39.17). As a consequence of the time phase shift due to its "charged" energy state change, a living being follows a shifted thermodynamic arrow of time relative to that of the spontaneous reactions of their surroundings. ***The arrow of time for the beings is delayed with respect to that of the local universe. The phenomenon of consciousness is permitted from the time-phase difference.***

Information is a form of energy. The brain has the ability to process and assimilate energy permitted by its shifted thermodynamic arrow of time. The brain which comprises hundreds of billions of neurons is the center of consciousness. Neurons achieve an artificial high energy state in the form of ion gradients across their cell membranes. The fluctuations and patterns of discharge of the energy state is the mechanism of conscious experience. Unlike a conventional processor such as a Turing Machine, the brain constantly changes its state such that the output to a given input may not be identical. The brain is governed by the entropy principle of thermodynamics whereby the chemical system achieves a state representative of a predominant configuration, the most probable state in time. ***The brain must be active continuously as a predominant configuration. The predominant configuration is based on and represents the physical universe as described in the BlackLight Brainchild Section. This time dependent state based on the second law of thermodynamics and representative of the physical universe is the basis of consciousness.***

In addition to exploiting the second law of thermodynamics with the formation of a predominant configuration, the brain has evolved to exploit several fundamental signal processing principles to achieve consciousness. For example, the brain functions as an analog Fourier processor which represents and processes information as Fourier series in Fourier space. The brain exploits time directly and time indirectly via spatial segregation of information as a means to encode context. The brain associates information by exploiting the principle that cascaded stages such as association neurons give rise to delayed Gaussian filters. And, filtered signals may be associated based on the physics of energy exchange between two or more harmonic states. The workings of the brain and the underlining physics and signal processing theory are described for a digital processor or the brain in the BlackLight Brainchild Section. Given the evolutionary ascension of multicelluar organisms each producing a negative entropic states and having specialized cells with excitable membranes, the progress to consciousness and intelligence was inevitable.

Consciousness is shaped by and requires the environment with which the brain interacts. A conscious being is made of energy, quarks,

gluons, electrons, atoms, molecules, etc. that originate from and are part of the universe. For example, the elements of humans other than hydrogen originate in stars. Therefore, in broader terms, the physics of the universe dynamically gives rise to a conscious being, and it is implicit that the universe is aware of itself.

REASON AND INTELLIGENCE

The brain is capable of accepting input, and storing, retrieving, and processing data to form novel conceptual content. Reason and intelligence arise from the massive directional connectivity of the brain which functions as an analog Fourier processor. The neuronal response is a series of action potentials in time. The superposition of the neuronal responses of multiple neurons becomes a Fourier series, a superposition of trigonometric functions, in frequency space (k,ω −space) wherein information is digitized in amplitude, frequency, and phase. The Fourier series in k,ω −space is then modulated, sampled, associated, and ordered via the filtering properties of cascaded groups of association neurons with couplings governed by Poissonian probability. The processing of information depends on and dynamically alters (through feedback) the total state of stored information, the cascades of association neurons, and the hierarchical relationships of association neurons and stored information (memory). A strongly linked group of cascaded association neurons comprises an "association ensemble", and a strongly linked group of memory neurons comprises an "memory ensemble". Repetitive activation of a memory or association neuron increases its excitability. A configuration of couplings between "memory ensembles" and "association ensembles" increases the excitability of the configuration. Analogously to statistical thermodynamics, a predominant configuration arises from the ensemble level. Consider the brain globally. The firing history of each ensemble relates to a hierarchical relationship of coupled "memory and association ensembles" which gives rise to a precedence of higher order predominant configurations. Intelligence, the ability to associate information and create novel information, is a consequence. Learning arises by the feedback loop of sensory input to the coupled predominant configurations which increases the basis for intelligence. The basis of consciousness is the Predominant Configuration Layer given *infra*..

The features of the brain such as 1.) layer structure, 2.) components such as processor neurons, association neurons, memory neurons, and domains, 3.) systems such as association ensembles, and 4.) processes such as association and ordering of information may be simulated using systems and methods to produce alternative intelligence (AI). The systems and methods are given in Mills US Patent Application

[5]. The brain can be understood in customary terms with the following definitions applied to the Mills Patent Application *infra.*

"processor"	brain
"P element" (processor element)	processor neuron
"M element" (memory element)	memory neuron
"stage"	association neuron
"impulse response"	action potential
"register"	domain
exponential decay of input between "stages"	decay of neurotransmitter concentration at a synapse of association neurons

The switching time of the brain is limited by the physiology of neurons. The brain operates at 10's of hertz. The maximum amount of memory used by the brain at any instant based on the ability to recall a test list is about a megabyte. In contrast, microprocessors process signals at rates of 100's of megahertz with a comparatively unlimited memory capacity. The brain's wet chemistry which processes information can be simulated using solid state systems. The possibility of running a simulation of the brain's operations based on the same physical and signal processing principles holds great promise to reach advanced levels of abstraction, conceptualization, and understanding of the physical universe. The subsequent advancement of technology is anticipated.

BlackLight Brainchild

Abstract

The present invention provides a method and system for pattern recognition and processing. Information representative of physical characteristics or representations of physical characteristics is transformed into a Fourier series in Fourier space within an input

context of the physical characteristics that is encoded in time as delays corresponding to modulation of the Fourier series at corresponding frequencies. Associations are formed between Fourier series by filtering the Fourier series and by using a spectral similarity between the filtered Fourier series to determine the association based on Poissonian probability. The associated Fourier series are added to form strings of Fourier series. Each string is ordered by filtering it with multiple selected filters to form multiple time order formatted subset Fourier series, and by establishing the order through associations with one or more initially ordered strings to form an ordered string. Associations are formed between the ordered strings to form complex ordered strings that relate similar items of interest. The components of the invention are active based on probability using weighting factors based on activation rates.

610

A METHOD AND SYSTEM FOR PATTERN RECOGNITION AND PROCESSING

Cross Reference to Related Applications

This application claims the benefit of United States provisional application Serial No. 60/068,834, filed December 24, 1997.

Background Of the Invention

Attempts have been made to create pattern recognition systems using programming and hardware. The state of the art includes neural nets. Neural nets typically comprise three layers--an input layer, a hidden layer, and an output layer. The hidden layer comprises a series of nodes which serve to perform a weighted sum of the input to form the output. Output for a given input is compared to the desired output, and a back projection of the errors is carried out on the hidden layer by changing the weighting factors at each node, and the process is reiterated until a tolerable result is obtained. The strategy of neural nets is analogous to the sum of least squares algorithms. These algorithms are adaptive to provide reasonable output to variations in input, but they can not create totally unanticipated useful output or discover associations between multiple inputs and outputs. Their usefulness to create novel conceptual content is limited; thus, advances in pattern recognition systems using neural nets is limited.

SUMMARY OF THE INVENTION

The present invention is directed to a method and system for pattern recognition and processing involving processing information in Fourier space.

The system of the present invention includes an Input Layer for receiving data representative of physical characteristics or representations of physical characteristics capable of transforming the data into a Fourier series in Fourier space. The data is received within an input context representative of the physical characteristics that is encoded in time as delays corresponding to modulation of the Fourier series at corresponding frequencies. The system includes a memory that maintains a set of initial ordered Fourier series. The system also includes an Association Layer that receives a plurality of the Fourier series in Fourier space including at least one ordered Fourier series from the memory and forms a string comprising a sum of the Fourier series and stores the string in memory. The system also includes a String

Ordering Layer that receives the string from memory and orders the Fourier series contained in the string to form an ordered string and stores the ordered string in memory. The system also includes a Predominant Configuration Layer that receives multiple ordered strings from the memory, forms complex ordered strings comprising associations between the ordered strings, and stores the complex ordered strings to the memory. The components of the system are active based on probability using weighting factors based on activation rates.

One aspect of the present invention is directed to inputting information as data to the system within an input context and associating the data. This aspect of the invention includes encoding the data as parameters of at least two Fourier components in Fourier space, adding the Fourier components to form at least two Fourier series in Fourier space, the Fourier series representing the information, sampling at least one of the Fourier series in Fourier space with a filter to form a sampled Fourier series, and modulating the sampled Fourier series in Fourier space with the filter to form a modulated Fourier series. This aspect of the invention also includes determining a spectral similarity between the modulated Fourier series and another Fourier series, determining a probability expectation value based on the spectral similarity, and generating a probability operand having a value selected from a set of zero and one, based on the probability expectation value. These steps are repeated until the probability operand has a value of one. Once the probability operand has a value of one, the modulated Fourier series and the other Fourier series are added to form a string of Fourier series in Fourier space, and the string of Fourier series is stored in the memory.

Another aspect of the present invention is directed to ordering a string representing the information. This aspect of the invention utilizes a High Level Memory section of the memory that maintains an initial set of ordered Fourier series. This aspect of the invention includes obtaining a string from the memory and selecting at least two filters from a selected set of filters stored in the memory. This aspect also includes sampling the string with the filters such that each of the filters produce a sampled Fourier series. Each Fourier series comprises a subset of the string. This aspect also includes modulating each of the sampled Fourier series in Fourier space with the corresponding selected filter such that each of the filters produce an order formatted Fourier series. Furthermore, this aspect includes adding the order formatted Fourier series produced by each filter to form a summed Fourier series in Fourier space, obtaining an ordered Fourier series from the memory, determining a spectral similarity between the summed Fourier series and

the ordered Fourier series, determining a probability expectation value based on the spectral similarity, and generating a probability operand having a value selected from a set of zero and one, based on the probability expectation value. These steps are repeated until the probability operand has a value of one. Once the probability operand has a value of one, this aspect includes storing the summed Fourier series to an intermediate memory section. Thereafter, this aspect includes removing the selected filters from the selected set of filters to form an updated set of filters, removing the subsets from the string to obtain an updated string, and selecting an updated filter from the updated set of filters. This aspect further includes sampling the updated string with the updated filter to produce a sampled Fourier series comprising a subset of the string, modulating the sampled Fourier series in Fourier space with the corresponding selected updated filter to produce an updated order formatted Fourier series, recalling the summed Fourier series from the intermediate memory section, adding the updated order formatted Fourier series to the summed Fourier series to form an updated summed Fourier series in Fourier space, and obtaining an updated ordered Fourier series from the memory. This aspect further includes determining a spectral similarity between the updated summed Fourier series and the updated ordered Fourier series, determining a probability expectation value based on the spectral similarity, and generating a probability operand having a value selected from a set of zero and one, based on the probability expectation value. These steps are repeated until the probability operand has a value of one or all of the updated filters have been selected from the updated set of filters. If all of the updated filters have been selected before the probability operand has a value of one, then clearing the intermediate memory section and repeating the steps starting with selecting at least two filters from a selected set of filters. Once the probability operand has a value of one, the updated summed Fourier series is stored to the intermediate memory section and steps beginning with removing the selected filters from the selected set of filters to form an updated set of filters are repeated until one of the following set of conditions is satisfied: the updated set of filters is empty or the remaining subsets of the string is nil. If the remaining subsets of the string is nil, then the Fourier series in the intermediate memory section is stored in the High Level Memory section of the memory.

Another aspect of the present invention is directed to forming complex ordered strings by forming associations between a plurality of ordered strings. This aspect of the invention includes recording ordered strings to the High Level Memory section, forming associations of the ordered strings to form complex ordered strings, and recording the

complex ordered strings to the High Level Memory section. A further aspect of the invention is directed to forming a predominant configuration based on probability. This aspect of the invention includes generating an activation probability parameter, storing the activation probability parameter in the memory, generating an activation probability operand having a value selected from a set of zero and one, based on the activation probability parameter, activating any one or more components of the present invention such as matrices representing functions, data parameters, Fourier components, Fourier series, strings, ordered strings, components of the Input Layer, components of the Association Layer, components of the String Ordering Layer, and components of the Predominant Configuration Layer, the activation of each component being based on the corresponding activation probability parameter, and weighting each activation probability parameter based on an activation rate of each component.

DETAILED DESCRIPTION OF THE INVENTION

The present invention is directed to systems and methods for performing pattern recognition and association based upon receiving, storing, and processing information. The information is based upon physical characteristics or representations of physical characteristics and a relationship of the physical characteristics, hereinafter referred to as physical context, of an item of interest. The physical characteristics and physical context serve as a basis for stimulating a transducer. The transducer converts an input signal representative of the physical characteristics and the physical context into the information for processing. The information is data and an input context. The data is representative of the physical characteristics or the representations of physical characteristics and the input context corresponds to the physical context based upon the identity of a specific transducer and its particular transducer elements. The physical context maps on a one to one basis to the input context. The information defines a Fourier series in Fourier space that represents the item of interest. In other words, a Fourier series in Fourier space represents the information parameterized according to the data and the input context. In addition, the input context maps on a one to one basis to an Input Layer section of a memory. Thus, there is a one to one map of physical context to input context to Input Layer section of a memory. The representation of information as a Fourier series in Fourier space allows for the mapping.

As illustrated in Figure 1, at a high level, the system 10 includes several function specific layers. These include an Input Layer 12, an Association Layer 14, an String Ordering Layer 16 and a Predominant

Configuration Layer 18. The Input Layer 12 receives the data within the input context and transforms the data into the Fourier series in Fourier space representative of the information. The system 10 also includes a memory 20 for storing information. The Input Layer 12 also encodes the input context as delays in time corresponding to a modulation factor of the Fourier series at corresponding frequencies. The Association Layer 14 receives a plurality of Fourier series in Fourier space, including at least one ordered Fourier series from the memory 20, forms a string comprising a sum of the Fourier series and stores the string to the memory 20. The String Ordering Layer 16 receives the string from the memory 20, orders the Fourier series contained in the string to form an ordered string and stores the ordered string in the memory 20. The Predominant Configuration Layer 18 receives multiple ordered strings from the memory 20, forms associations between the ordered strings to form a complex ordered string, also referred to as a predominant configuration string, and stores the predominant configuration string to the memory 20. The memory 20 may be partitioned in several distinct sections for storing different types of information or distinctly classified types of information. Specifically, the memory may include a High Level Memory section, an intermediate level memory section, etc. as will be described in more detail below.

The following example illustrates how the present invention processes the physical characteristics of an item of interest, specifically a triangle. In flat geometry, the physical characteristics of a triangle are three connected lines at angles aggregating to 180°. The physical characteristics provide spatial variations of light scattering. In one embodiment, a light responsive transducer (not shown) of the system 10 transduces the light scattering into the data. An exemplary transducer is a charge coupled device ("CCD") array. One data element at a point in time may be a voltage of a particular CCD element of the CCD array. Each CCD element of the CCD array has a spatial identity. The physical context for the triangle is the relationship of the lines at the corresponding angles providing a spatial variation of light scattering. The input context is the identity of each CCD element that responds according to the physical context. For example, a CCD element (100,13) of a 512 by 512 CCD array will uniquely respond to light scattered by the lines and angular relations of the triangle relative to the other CCD elements of the CCD array. The response is stored in a specific memory register of an Input Layer section of the memory 20. The specific memory register is reflective of the input context. In the present invention, a Fourier series in Fourier space represents the information of the triangle parameterized according to the voltage and the CCD element identity.

Referring to FIGURE 2, in the first step, the Input Layer 12 receives the data from the transducer (not shown). A Fourier transform processor 22 encodes each data element as parameters of a Fourier component in Fourier space and stores the data parameter values to the Input Layer section 24 of the memory 20. Each Fourier component of the Fourier series may comprise a quantized amplitude, frequency, and phase angle. For example the Fourier series in Fourier space may be:

$$\sum_{m=1}^{M}\sum_{n=-\infty}^{\infty}\frac{4\pi}{1+\frac{k_z^2}{k_\rho^2}}a_{0_m}N_{m_{\rho_0}}N_{m_{z_0}}\sin\left(k_\rho-n\frac{2\pi}{\rho_{0_m}}\left(\frac{N_{m_{\rho 0}}\rho_{0_m}}{2}\right)\right)\sin\left(k_z-n\frac{2\pi}{z_{0_m}}\left(\frac{N_{m_{z_0}}z_{0_m}}{2}\right)\right)$$

having a quantized amplitude, frequency, and phase angle, wherein a_{0_m} is a constant, k_ρ and k_z are the frequency variables, n, m, and M are integers, and $N_{m_{\rho_0}}$, $N_{m_{z_0}}$, ρ_{0_m}, and z_{0_m} are the data parameters.

In a first embodiment, the data parameters $N_{m_{\rho_0}}$ and $N_{m_{z_0}}$ of the Fourier series component are proportional to the rate of change of the physical characteristic. Each of the data parameters ρ_{0_m} and z_{0_m} of each Fourier component is inversely proportional to the amplitude of the physical characteristic. In the triangle example, the amplitude of the voltage at a given CCD element relative to the neighboring CCD element defines the rate of change of the voltage which is converted into the data parameters $N_{m_{\rho_0}}$ and $N_{m_{z_0}}$. The inverse of the amplitude of the voltage of each CCD element is converted into the data parameters ρ_{0_m} and z_{0_m}. As illustrated in FIGURE 3 and described above, for each CCD element, the Fourier series, parameterized accordingly, are stored to a specific sub register 27 of a specific register 26 of the Input Layer section 24 of the memory 20. Since the structure of a Fourier series is known in the art, only the parameters need to be stored in a digital embodiment.

The number and types of transducers that may supply information to the system is only limited by available technology, hardware and economics, as is the number m of corresponding registers 26 for each transducer. Each register 26 may have any number d of subregisters 27, where the number d of subregisters of one register 26 is not necessarily the same as other registers 26. For example, "Level 1 " register "1 " may have thirty "Level 2 " subregisters 27 and "Level 1 " register "2 " may have one-hundred subregisters 27. Furthermore, each "Level 2 " register may have any number e of subregisters, where the number e of subregisters of one register 27 is not necessarily the same as other registers 27. For example, "Level 2 " register "1 " may have fifty "Level n" subregisters 29 and "Level 2 " register "2 " may have seventy "Level n" subregisters 29. Still further, each "Level n" register 29 may have any

number f of time buffer elements 31, where the number f of time buffer elements 31 is not necessarily the same as other time buffer elements 31.

In a second embodiment, each of the data parameters $N_{m_{\rho_0}}$ and $N_{m_{z_0}}$ of the Fourier series component is proportional to the amplitude of the physical characteristic. Each of the data parameters ρ_{0_m} and z_{0_m} of each Fourier component is inversely proportional to the rate of change of the physical characteristic. As in the first embodiment, for each CCD element, these parameters are stored in a specific sub register of the Input Layer section of the memory.

In a third embodiment, each of the data parameters $N_{m_{\rho_0}}$ and $N_{m_{z_0}}$ of the Fourier series component is proportional to the duration of the signal response of each transducer. Each of the data parameters ρ_{0_m} and z_{0_m} of each Fourier component is inversely proportional to the physical characteristic. As in the first embodiment, for each CCD element, these parameters are stored in a specific sub register of the Input Layer section of the memory.

As an alternative example, the Fourier series in Fourier space may be:

$$\sum_{m=1}^{M}\sum_{n=-\infty}^{\infty}\frac{4\pi}{1+\frac{k_z^2}{k_\rho^2}}\frac{4}{\rho_{0_m}z_{0_m}}a_{0_m}\sin\left(k_\rho-n\frac{2\pi}{\rho_{0_m}}\frac{N_{m_{\rho_0}}\rho_{0_m}}{2}\right)\sin\left(k_z-n\frac{2\pi}{z_{0_m}}\frac{N_{m_{z_0}}z_{0_m}}{2}\right)$$

having a quantized frequency, and phase angle, wherein a_{0_m} is a constant, k_ρ and k_z are the frequency variables, n, m, and M are integers, and $N_{m_{\rho_0}}$, $N_{m_{z_0}}$, ρ_{0_m}, and z_{0_m} are the data parameters. As described with respect to the previous example, for each CCD element, these parameters are stored in a specific sub register of the Input Layer section of the memory.

The physical context is conserved by mapping with a one to one basis between the physical context and the input context based on the identity of each transducer. The input context is conserved by mapping on a one to one basis to the Input Layer section 24 of memory 20. In an embodiment, the input context is encoded in time as a characteristic modulation frequency band in Fourier space of the Fourier series. The characteristic modulation frequency band in Fourier space represents the input context according to the identity of a specific transducer of the relationship of two transducer elements. The modulation within each frequency band may encode not only input context but context in a general sense. The general context may encode temporal order, cause and effect relationships, size order, intensity order, before-after order,

top-bottom order, left-right order, etc. all of which are relative to the transducer.

Still referring to FIGURE 3, the transducer has n levels of subcomponents. Each transducer is assigned a portion 26 of the Input Layer section 24 of the memory 20. The memory 20 is arranged in a hierarchical manner. Specifically, the memory is divided and assigned to correspond to a master time interval with $n+1$ sub time intervals. The hierarchy parallels the n levels of the transducer subcomponents. The n th level transducer sub component provides a data stream to the system 10. The data stream is recorded as a function of time in the $n+1$ sub time interval. The time intervals represent time delays which correspond to the characteristic modulation frequency band in Fourier space which in turn represents the input context according to the specific transducer or transducer subcomponent.

An exemplary complex transducer which may be represented by a data structure comprising a hierarchical set of time delay intervals is a CCD array of a video camera comprising a multitude of charge coupled devices (CCDs). Each CCD comprises a transducer element and is responsive to light intensity of a given wavelength band at a given spatial location in a grid. Another example of a transducer is an audio recorder comprising transducer elements each responsive to sound intensity of a given frequency band at a given spatial location or orientation. A signal within the band 300-400 MHz may encode and identify the signal as a video signal; whereas, a signal within the band 500-600 MHz may encode and identify the signal as an audio signal. Furthermore, a video signal within the band 315-325 MHz may encode and identify the signal as a video signal as a function of time of CCD element (100,13) of a 512 by 512 array of CCDs.

In one embodiment, the characteristic modulation having a frequency within the band in Fourier space is represented by $e^{-j2\pi ft_0}$. The modulation corresponds to the time delay $\delta(t-t_0)$ wherein f is the frequency variable, t is the time variable, and t_0 is the time delay. The characteristic modulation is encoded as a delay in time by storing the Fourier series in a specific portion of the Input Layer section of the memory wherein the specific portion has $n+1$ sub time intervals. Each sub time interval corresponds to a frequency band.

In an alternative embodiment, the characteristic modulation, having a frequency within the band is represented by $e^{-jk_\rho(\rho_{fb_m}+\rho_{t_m})}$. Thus, the Fourier series in Fourier space may be:

$$\sum_{m=1}^{M}\sum_{n=-\infty}^{\infty}\frac{4\pi}{1+\frac{k_z^2}{k_\rho^2}}a_{0_m}N_{m_{\rho_0}}N_{m_{z_0}}e^{-jk_\rho\left(\rho_{fb_m}+\rho_{t_m}\right)}\sin\left(k_\rho\frac{N_{m_{\rho 0}}\rho_{0_m}}{2}-n\frac{2\pi N_{m_{\rho 0}}}{2}\right)\sin\left(k_z\frac{N_{m_{z_0}}z_{0_m}}{2}-n\frac{2\pi N_{m_{z0}}}{2}\right)$$

wherein $\rho_{t_m}=v_{t_m}t_{t_m}$ is the modulation factor which corresponds to the physical time delay t_{t_m}, $\rho_{fb_m}=v_{fb_m}t_{fb_m}$ is the modulation factor which corresponds to the specific transducer time delay t_{fb_m}, v_{t_m} and v_{fb_m} are constants such as the signal propagation velocities, a_{0_m} is a constant, k_ρ and k_z are the frequency variables, n, m, and M are integers, and $N_{m_{\rho_0}}$, $N_{m_{z_0}}$, ρ_{0_m}, and z_{0_m} are data parameters. The data parameters are selected in the same manner as described above.

Transducer strings may be created by obtaining a Fourier series from at least two selected transducers and adding the Fourier series. Transducers that are active simultaneously may be selected. The transducer string may be stored in a distinct memory location of the memory. The characteristic modulation, having a frequency within the band in Fourier space can be represented by $e^{-j2\pi ft_0}$ which corresponds to the time delay $\delta\left(t-t_0\right)$ wherein f is the frequency variable, t is the time variable, and t_0 is the time delay.

Recalling any part of the transducer string from the distinct memory location may thereby cause additional Fourier series of the transducer string to be recalled. In other words the Fourier series are linked. Fourier series, in addition to those of transducer strings may be linked. In order to achieve linking of the Fourier series, the system generates a probability expectation value that recalling any part of one of the Fourier series from the memory causes at least another Fourier series to be recalled from the memory. The system stores the probability expectation value to memory. The system generates a probability operand having a value selected from a set of zero and one, based on the probability expectation value. The system recalls at least another Fourier series from the memory if the operand is one. The probability expectation value may increase with a rate of recalling any part of any of the Fourier series.

The system may be initialized by learning. The relationship between the data and the data parameters such as ρ_{0_m} and $N_{m_{\rho_0}}$ of each component of the Fourier series is learned by the system by applying standard physical signals. In the case of the triangle example, the standard physical signals are the scattered light from the physical characteristics of the triangle. The physical signals are applied to each transducer together with other information that is associated with the standard. A data base is established. This information that is associated

with the standard is recalled and comprises input into the Association Layer and the String Ordering Layer.

The data parameters and the input context are established and stored in the Input Layer section 24 of the memory 20.

Referring again to Figure 2, several parameterized Fourier components are input to the Association Layer to form associations of the Fourier series. The Fourier components may be stored in a Fourier component section 30 of a temporary memory section 28. The Fourier components are added to form multiple Fourier series which in turn may be stored in a Fourier series section 32 of the temporary memory section 28. At least one of the Fourier series stored in the Fourier series section 32 is input to a filter 34 wherein the filter 34 samples and modulates the Fourier series. The filtered Fourier series is input to a spectral similarity analyzer 36. The spectral similarity analyzer 36 determines the spectral similarity between the filtered Fourier series and another Fourier series stored in the Fourier series section 32 of the temporary memory section 28. A spectral similarity value is output from the spectral similarity analyzer 36 and input to a probability expectation analyzer 38. The probability expectation analyzer 38 determines a probability expectation value based on the spectral similarity value. The probability expectation value output from the probability expectation analyzer 38 is input to a probability operand generator 40. The probability operand generator 40 generates a probability operand value of one or zero based upon the probability expectation value. The probability operand value is output to a processor 42. If the probability operand value is zero, the processor 42 sends another Fourier series from the Fourier series section 32 of the temporary memory section 28 to the filter 34 and begins the process again. If the probability operand value is one, the filtered Fourier series and the other Fourier series are added to form a string and the string is stored in a string memory section 44.

The filter 34 can be a time delayed Gaussian filter in the time domain. The filter may be characterized in time by:

$$\frac{\alpha}{\sqrt{2\pi}} e^{-\frac{\left(t-\frac{\sqrt{N}}{\alpha}\right)^2}{\frac{2}{\alpha^2}}}$$

wherein $\frac{\sqrt{N}}{\alpha}$ is a delay parameter, α is a half-width parameter, and t is the time parameter. The Gaussian filter may comprise a plurality of cascaded stages each stage having a decaying exponential system function between stages. The filter, in frequency space, can be characterized by:

$$e^{-\frac{1}{2}\left(\frac{2\pi f}{\alpha}\right)^2} e^{-j\sqrt{N}\left(\frac{2\pi f}{\alpha}\right)}$$

wherein $\frac{\sqrt{N}}{\alpha}$ and α are a corresponding delay parameter and a half-width parameter in time, respectively, and f is the frequency parameter. The probability distribution may be Poissonian. Thus, the probability expectation value can be based upon Poissonian probability. The probability expectation value may be characterized by

$$\prod_s \left[p_{\uparrow_s} + \left(P - p_{\uparrow_s}\right) \exp\left[-\beta_s^{-2} \left(\frac{1 - \cos 2\phi_s}{2} \right) \right] \cos\left(\delta_s + 2\sin\phi_s\right) \right]$$

wherein P is the maximum probability of at least one other Fourier series being associated with a first Fourier series, $p_{\uparrow_s}$ is a probability of at least one other Fourier series being associated with a first Fourier series in the absence of coupling of the first Fourier series with the at least one other Fourier series, β_s^2 is a number that represents the amplitude of spectral similarity between at least two filtered or unfiltered Fourier series, ϕ_s represents the frequency difference angle between at least two filtered or unfiltered Fourier series, and δ_s, is a phase factor. β_s^2 may be characterized by

$$\beta_s^2 = (8\pi)^2 \frac{1}{\sqrt{2\pi}} \sqrt{\frac{\alpha_1^2 \alpha_s^2}{\alpha_1^2 + \alpha_s^2}}$$

$$\sum_{m_1=1}^{M_1} a_{0_{m_1}} N_{m_1} \sum_{m_s=1}^{M_s} a_{0_{m_s}} N_{m_s} \exp - \left\{ \frac{\alpha_1^2 \alpha_s^2}{\alpha_1^2 + \alpha_s^2} \left(\frac{\sqrt{N_1}}{\alpha_1} - \frac{\sqrt{N_s}}{\alpha_s} + \frac{N_{m_1}\rho_{0_{m_1}}}{2\nu_{m_1}} - \frac{N_{m_s}\rho_{0_{m_s}}}{2\nu_{m_s}} \right)^2 \right\}$$

$\frac{\sqrt{N_1}}{\alpha_1}$ and $\frac{\sqrt{N_s}}{\alpha_s}$ correspond to delay parameters of a first and s-th time delayed Gaussian filter, respectively, α_1 and α_s corresponding half-width parameters of a first and s-th time delayed Gaussian filter, respectively, M_1 and M_s are integers, $a_{0_{m_1}}$ and $a_{0_{m_s}}$ are constants, v_{m_1} and v_{m_s} are constants such as the signal propagation velocities, and N_{m_1}, N_{m_s}, $\rho_{0_{m_1}}$, and $\rho_{0_{m_s}}$ are data parameters. The data parameters are selected in the same manner as described above. ϕ_s may be characterized by

$$\phi_s = \frac{\pi \left(\frac{\sqrt{N_1}}{\alpha_1} - \frac{\sqrt{N_s}}{\alpha_s} + \sum_{m_1=1}^{M_1} \frac{N_{m_1}\rho_{0_{m_1}}}{2\nu_{m_1}} - \sum_{m_s=1}^{M_s} \frac{N_{m_s}\rho_{0_{m_s}}}{2\nu_{m_s}} \right)}{\frac{\sqrt{N_1}}{\alpha_1} + \sum_{m_1=1}^{M_1} \frac{N_{m_1}\rho_{0_{m_1}}}{2\nu_{m_1}}}$$

$\frac{\sqrt{N_1}}{\alpha_1}$ and $\frac{\sqrt{N_s}}{\alpha_s}$ correspond to delay parameters of a first and s-th time delayed Gaussian filter, respectively, α_1 and α_s corresponding half-width parameters of a first and s-th time delayed Gaussian filter, respectively, M_1 and M_s are integers, $a_{0_{m_1}}$ and $a_{0_{m_s}}$ are constants, v_{m_1} and v_{m_s} are constants such as the signal propagation velocities, and N_{m_1}, N_{m_s}, $\rho_{0_{m_1}}$, and $\rho_{0_{m_s}}$ are data parameters. The data parameters are selected in the same manner as described above.

An exemplary string with a characteristic modulation having a frequency within the band represented by $e^{-jk_\rho\left(\rho_{fb_m}+\rho_{t_m}\right)}$ is:

$$\sum_{s=1}^{S}\sum_{m=1}^{M_s}\sum_{n=-\infty}^{\infty}\frac{4\pi}{1+\frac{k_z^2}{k_\rho^2}}a_{0_{s,m}}N_{s,m_{\rho_0}}N_{s,m_{z_0}}e^{-jk_\rho\left(\rho_{fb_{s,m}}+\rho_{t_{s,m}}\right)}$$

$$\sin\left(k_\rho-n\frac{2\pi}{\rho_{0_{s,m}}}\left(\frac{N_{s,m_{\rho_0}}\rho_{0_{s,m}}}{2}\right)\right)\sin\left(k_z-n\frac{2\pi}{z_{0_{s,m}}}\left(\frac{N_{s,m_{z_0}}z_{0_{s,m}}}{2}\right)\right)$$

wherein $\rho_{t_{s,m}}=v_{t_{s,m}}t_{t_{s,m}}$ is the modulation factor which corresponds to the physical time delay $t_{t_{s,m}}$, $\rho_{fb_{s,m}}=v_{fb_{s,m}}t_{fb_{s,m}}$ is the modulation factor which corresponds to the specific transducer time delay $t_{fb_{s,m}}$, $v_{t_{s,m}}$ and $v_{fb_{s,m}}$ are constants such as the signal propagation velocities, $a_{0_{s,m}}$ is a constant, k_ρ and k_z are the frequency variables, n, m, s, M_s, and S are integers, and $N_{s,m_{\rho_0}}$, $N_{s,m_{z_0}}$, $\rho_{0_{s,m}}$, and $z_{0_{s,m}}$ are data parameters. The data parameters are selected in the same manner as described above.

An exemplary string with each Fourier series multiplied by the Fourier transform of the delayed Gaussian filter represented by $e^{-\frac{1}{2}\left(v_{s\rho 0}\frac{k_\rho}{\alpha_{s\rho 0}}\right)^2}e^{-j\frac{\sqrt{N_{s\rho 0}}}{\alpha_{s\rho 0}}\left(v_{s\rho 0}k_\rho\right)}e^{-\frac{1}{2}\left(v_{sz0}\frac{k_z}{\alpha_{sz0}}\right)^2}e^{-j\frac{\sqrt{N_{sz0}}}{\alpha_{sz0}}\left(v_{sz0}k_z\right)}$ that established the association to form the string is:

$$\sum_{s=1}^{S}\sum_{m=1}^{M_s}\sum_{n=-\infty}^{\infty}\frac{4\pi}{1+\frac{k_z^2}{k_\rho^2}}a_{0_{s,m}}N_{s,m_{\rho_0}}N_{s,m_{z_0}}e^{-\frac{1}{2}\left(v_{s\rho 0}\frac{k_\rho}{\alpha_{s\rho 0}}\right)^2}e^{-j\frac{\sqrt{N_{s\rho 0}}}{\alpha_{s\rho 0}}\left(v_{s\rho 0}k_\rho\right)}e^{-\frac{1}{2}\left(v_{sz0}\frac{k_z}{\alpha_{sz0}}\right)^2}e^{-j\frac{\sqrt{N_{sz0}}}{\alpha_{sz0}}\left(v_{sz0}k_z\right)}$$

$$e^{-jk_\rho\left(\rho_{fb_{s,m}}+\rho_{t_{s,m}}\right)}\sin\left(k_\rho-n\frac{2\pi}{\rho_{0_{s,m}}}\left(\frac{N_{s,m_{\rho_0}}\rho_{0_{s,m}}}{2}\right)\right)\sin\left(k_z-n\frac{2\pi}{v_{s,m}t_{0_{s,m}}}\left(\frac{N_{s,m_{z_0}}z_{0_{s,m}}}{2}\right)\right)$$

wherein $v_{s\rho 0}$ and v_{sz0} are constants such as the signal propagation velocities in the ρ and z directions, respectively, $\frac{\sqrt{N_{s\rho 0}}}{\alpha_{s\rho 0}}$ and $\frac{\sqrt{N_{sz0}}}{\alpha_{sz0}}$ are

delay parameters and α_{sp_0} and α_{sz_0} are half-width parameters of a corresponding Gaussian filter in the ρ and z directions, respectively, $\rho_{t_{s,m}} = v_{t_{s,m}} t_{s,m}$ is the modulation factor which corresponds to the physical time delay $t_{s,m}$, $\rho_{fb_{s,m}} = v_{fb_{s,m}} t_{fb_{s,m}}$ is the modulation factor which corresponds to the specific transducer time delay $t_{fb_{s,m}}$, $v_{t_{s,m}}$ and $v_{fb_{s,m}}$ are constants such as the signal propagation velocities, $a_{0_{s,m}}$ is a constant, k_ρ and k_z are the frequency variables, n, m, s, M_s, and S are integers, and $N_{s,m_{\rho_0}}$, $N_{s,m_{z_0}}$, $\rho_{0_{s,m}}$, and $z_{0_{s,m}}$ are data parameters. The data parameters are selected in the same manner as described above.

Therein, the Association Layer forms associations between Fourier series and sums the associated Fourier series to form a string. The string is then stored in the string memory section.

The next aspect of the present invention is the ordering of the strings stored in the string memory section 44. The ordering may be according to any one of the following: temporal order, cause and effect relationships, size order, intensity order, before-after order, top-bottom order, or left-right order. Referring to FIGURE 4, the method for ordering the strings stored in the string memory section 44 entails the following:

a.) obtaining a string from the string memory section 44 and storing the string to a temporary string memory section 46;

b.) selecting at least two filters 48, 50 from a selected set of filters 52;

c.) sampling the string with the filters 48, 50, each of the filters forming a sampled Fourier series, each Fourier series comprising a subset of the string;

d.) modulating each of the sampled Fourier series in Fourier space with the corresponding selected filter 48, 50, each forming an order formatted Fourier series;

e.) adding the order formatted Fourier series to form a summed Fourier series in Fourier space;

f.) obtaining an ordered Fourier series from the High Level Memory section 54;

g.) determining a spectral similarity with a spectral similarity analyzer 56 between the summed Fourier series and the ordered Fourier series;

h.) determining a probability expectation value, with a probability expectation value analyzer 58 based on the spectral similarity;

i.) generating a probability operand, with a probability operand generator 60 having a value selected from a set of zero and one, based on the probability expectation value;

j.) repeating steps b-i until the probability operand has a value of one as determined by the processor 42;

k.) storing the summed Fourier series to an intermediate memory section 62;

l.) removing the selected filters from the selected set of filters 52 to form an updated set of filters 52;

m.) removing the subsets from the string to obtain an updated string;

n.) selecting an updated filter 64 from the updated set of filters;

o.) sampling the updated string with the updated filter to form a sampled Fourier series comprising a subset of the string;

p.) modulating the sampled Fourier series in Fourier space with the corresponding selected updated filter to form an updated order formatted Fourier series;

q.) recalling the summed Fourier series from the intermediate memory section 62;

r.) adding the updated order formatted Fourier series to the summed Fourier series from the intermediate memory section to form an updated summed Fourier series in Fourier space;

s.) obtaining another ordered Fourier series from the High Level Memory section 54;

t.) determining a spectral similarity between the updated summed Fourier series and the another ordered Fourier series;

u.) determining a probability expectation value based on the spectral similarity;

v.) generating a probability operand having a value selected from a set of zero and one, based on the probability expectation value;

w.) repeating steps n-v until the probability operand has a value of one or all of the updated filters have been selected from the updated set of filters as determined by processor 42;

x.) if all of the updated filters have been selected before the probability operand has a value of one, then clearing the intermediate memory section and returning to step b;

y.) if the probability operand has a value of one, then clearing the intermediate memory section and storing the updated summed Fourier series to the intermediate memory section;

z.) repeating steps l-y until the one of the following set of conditions is satisfied: the updated set of filters is empty, or the remaining subsets of the string of step m.) is nil as determined by the processor 42;

aa.) storing the Fourier series of intermediate memory section to the High Level Memory section 54.

Each filter of the set of filters can be a time delayed Gaussian filter having a half-width parameter α which determines the amount of the string that is sampled. Each filter of the set of filters can be a time delayed Gaussian filter having a delay parameter $\frac{\sqrt{N}}{\alpha}$ which corresponds to a time point. Each Fourier series of the ordered string can be multiplied by the Fourier transform of the delayed Gaussian filter represented by $e^{-\frac{1}{2}\left(v_{s\rho 0}\frac{k_\rho}{\alpha_{s\rho 0}}\right)^2} e^{-j\frac{\sqrt{N_{s\rho 0}}}{\alpha_{s\rho 0}}\left(v_{s\rho 0}k_\rho\right)} e^{-\frac{1}{2}\left(v_{sz0}\frac{k_z}{\alpha_{sz0}}\right)^2} e^{-j\frac{\sqrt{N_{sz0}}}{\alpha_{sz0}}\left(v_{sz0}k_z\right)}$. The filter established the correct order. The ordered string can be represented by:

$$\sum_{s=1}^{S}\sum_{m=1}^{M_s}\sum_{n=-\infty}^{\infty}\frac{4\pi}{1+\frac{k_z^2}{k_\rho^2}}a_{0_{s,m}}N_{s,m_{\rho_0}}N_{s,m_{z_0}}e^{-\frac{1}{2}\left(v_{s\rho 0}\frac{k_\rho}{\alpha_{s\rho 0}}\right)^2}e^{-j\frac{\sqrt{N_{s\rho 0}}}{\alpha_{s\rho 0}}\left(v_{s\rho 0}k_\rho\right)}e^{-\frac{1}{2}\left(v_{sz0}\frac{k_z}{\alpha_{sz0}}\right)^2}e^{-j\frac{\sqrt{N_{sz0}}}{\alpha_{sz0}}\left(v_{sz0}k_z\right)}$$

$$e^{-jk_\rho\left(\rho_{fb_{s,m}}+\rho_{t_{s,m}}\right)}\operatorname{sinc}\left(k_\rho-n\frac{2\pi}{\rho_{0_{s,m}}}\frac{N_{s,m_{\rho 0}}\rho_{0_{s,m}}}{2}\right)\operatorname{sinc}\left(k_z-n\frac{2\pi}{v_{s,m}t_{0_{s,m}}}\frac{N_{s,m_{z_0}}z_{0_{s,m}}}{2}\right)$$

wherein $v_{s\rho 0}$ and v_{sz0} are constants such as the signal propagation velocities in the ρ and z directions, respectively, $\frac{\sqrt{N_{s\rho 0}}}{\alpha_{s\rho 0}}$ and $\frac{\sqrt{N_{sz0}}}{\alpha_{sz0}}$ are delay parameters and $\alpha_{s\rho 0}$ and α_{sz0} are half-width parameters of a corresponding Gaussian filter in the ρ and z directions, respectively, $\rho_{t_{s,m}}=v_{t_{s,m}}t_{s,m}$ is the modulation factor which corresponds to the physical time delay $t_{t_{s,m}}$, $\rho_{fb_{s,m}}=v_{fb_{s,m}}t_{fb_{s,m}}$ is the modulation factor which corresponds to the specific transducer time delay $t_{fb_{s,m}}$, $v_{t_{s,m}}$ and $v_{fb_{s,m}}$ are constants such as the signal propagation velocities, $a_{0_{s,m}}$ is a constant, k_ρ and k_z are the frequency variables, n, m, s, M_s, and S are integers, and $N_{s,m_{\rho_0}}$, $N_{s,m_{z_0}}$, $\rho_{0_{s,m}}$, and $z_{0_{s,m}}$ are data parameters. The data parameters are selected in the same manner as described above.

The probability expectation value may be based upon Poissonian probability. The probability expectation value is represented by

$$\prod_s\left[p_{\uparrow s}+\left(P-p_{\uparrow s}\right)\exp\left(-\beta_s^{-2}\left(\frac{1-\cos 2\phi_s}{2}\right)\right)\cos\left(\delta_s+2\sin\phi_s\right)\right]$$

wherein P is the maximum probability of at least one other Fourier series being associated with a first Fourier series, $p_{\uparrow s}$ is a probability of at least one other Fourier series being associated with a first Fourier series in the absence of coupling of the first Fourier series with the at least one other Fourier series, β_s^2 is a number that represents the amplitude of spectral similarity between at least two filtered or

unfiltered Fourier series, ϕ_s represents the frequency difference angle between at least two filtered or unfiltered Fourier series, and δ_s, is a phase factor. β_s^2 may be characterized by

$$\beta_s^2 = (8\pi)^2 \frac{1}{\sqrt{2\pi}} \sqrt{\frac{\alpha_1^2 \alpha_s^2}{\alpha_1^2 + \alpha_s^2}} \sum_{m_1=1}^{M_1} a_{0_{m_1}} N_{m_1} \sum_{m_s=1}^{M_s} a_{0_{m_s}} N_{m_s}$$

$$\exp - \left\{ \frac{\alpha_1^2 \alpha_s^2}{\alpha_1^2 + \alpha_s^2} \left(\frac{\sqrt{N_1}}{\alpha_1} - \frac{\sqrt{N_s}}{\alpha_s} + \left(\frac{N_{m_1} \rho_{0_{m_1}}}{2 v_{m_1}} + \frac{\rho_{fb_{m_1}}}{v_{fb_{m_1}}} + \frac{\rho_{t_{m_1}}}{v_{t_{m_1}}} \right) - \left(\frac{N_{m_s} \rho_{0_{m_s}}}{2 v_{m_s}} + \frac{\rho_{fb_{m_s}}}{v_{fb_{m_s}}} + \frac{\rho_{t_{m_s}}}{v_{t_{m_s}}} \right) \right)^2 \right\}$$

$$\frac{}{2}$$

wherein $\rho_{t_{m_1}} = v_{t_{m_1}} t_{t_{m_1}}$ and $\rho_{t_{m_s}} = v_{t_{m_s}} t_{t_{m_s}}$ are the modulation factors which corresponds to the physical time delays $t_{t_{m_1}}$ and $t_{t_{m_s}}$, respectively, $\rho_{fb_{m_1}} = v_{fb_{m_1}} t_{fb_{m_1}}$ and $\rho_{fb_{m_s}} = v_{fb_{m_s}} t_{fb_{m_s}}$ are the modulation factors which corresponds to the specific transducer time delay $t_{fb_{m_1}}$ and $t_{fb_{m_s}}$, respectively, $v_{t_{m_1}}$, $v_{t_{m_s}}$, $v_{fb_{m_1}}$, and $v_{fb_{m_s}}$ are constants such as the signal propagation velocities, $\frac{\sqrt{N_1}}{\alpha_1}$ and $\frac{\sqrt{N_s}}{\alpha_s}$ correspond to delay parameters of a first and s-th time delayed Gaussian filter, respectively, α_1 and α_s corresponding half-width parameters of a first and s-th time delayed Gaussian filter, respectively, M_1 and M_s are integers, $a_{0_{m_1}}$, $a_{0_{m_s}}$ are constants, v_{m_1} and v_{m_s} are constants such as the signal propagation velocities, and N_{m_1}, N_{m_s}, $\rho_{0_{m_1}}$, and $\rho_{0_{m_s}}$ are data parameters. The data parameters are selected in the same manner as described above. ϕ_s may be represented by

$$\phi_s = \frac{\pi \left(\frac{\sqrt{N_1}}{\alpha_1} - \frac{\sqrt{N_s}}{\alpha_s} + \sum_{m_1=1}^{M_1} \left(\frac{N_{m_1} \rho_{0_{m_1}}}{2 v_{m_1}} + \frac{\rho_{fb_{m_1}}}{v_{fb_{m_1}}} + \frac{\rho_{t_{m_1}}}{v_{t_{m_1}}} \right) - \sum_{m_s=1}^{M_s} \left(\frac{N_{m_s} \rho_{0_{m_s}}}{2 v_{m_s}} + \frac{\rho_{fb_{m_s}}}{v_{fb_{m_s}}} + \frac{\rho_{t_{m_s}}}{v_{t_{m_s}}} \right) \right)}{\frac{\sqrt{N_1}}{\alpha_1} + \sum_{m_1=1}^{M_1} \left(\frac{N_{m_1} \rho_{0_{m_1}}}{2 v_{m_1}} + \frac{\rho_{fb_{m_1}}}{v_{fb_{m_1}}} + \frac{\rho_{t_{m_1}}}{v_{t_{m_1}}} \right)}$$

wherein $\rho_{t_{m_1}} = v_{t_{m_1}} t_{t_{m_1}}$ and $\rho_{t_{m_s}} = v_{t_{m_s}} t_{t_{m_s}}$ are the modulation factors which corresponds to the physical time delays $t_{t_{m_1}}$ and $t_{t_{m_s}}$, respectively, $\rho_{fb_{m_1}} = v_{fb_{m_1}} t_{fb_{m_1}}$ and $\rho_{fb_{m_s}} = v_{fb_{m_s}} t_{fb_{m_s}}$ are the modulation factors which corresponds to the specific transducer time delay $t_{fb_{m_1}}$ and $t_{fb_{m_s}}$,

respectively, $v_{t_{m_1}}$, $v_{t_{m_s}}$, $v_{fb_{m_1}}$, and $v_{fb_{m_s}}$ are constants such as the signal propagation velocities, $\frac{\sqrt{N_1}}{\alpha_1}$ and $\frac{\sqrt{N_s}}{\alpha_s}$ correspond to delay parameters of a first and s-th time delayed Gaussian filter, respectively, α_1 and α_s corresponding half-width parameters of a first and s-th time delayed Gaussian filter, respectively, M_1, and M_s are integers, $a_{0_{m_1}}$ and $a_{0_{m_s}}$ are constants, v_{m_1} and v_{m_s} are constants such as the signal propagation velocities, and N_{m_1}, N_{m_s}, $\rho_{0_{m_1}}$, and $\rho_{0_{m_s}}$ are data parameters. The data parameters are selected in the same manner as described above.

The String Ordering Layer produces an ordered string of Fourier series, wherein the ordered string is stored in the High Level Memory section.

The next aspect of the present invention is the formation of a predominant configuration by forming complex ordered strings through the association of ordered strings. Referring to FIGURE 5, the method for forming the complex ordered strings from strings stored in the string memory section entails the following. The Predominant Configuration Layer 18 receives ordered strings from the High Level Memory section 54 and forms more complex ordered strings by forming associations between the ordered strings. The complex ordered strings are stored in the complex ordered string section 72 of the memory 20.

The Predominant Configuration Layer 18 also activates components within the Input Layer 12, the Association Layer 14, and the String Ordering Layer 16. The layers of the present invention may be treated and implemented as abstract data types in the art of computer science relating to object-oriented programming. The components of the layers therefore refer to all classes, instances, methods, attributes, behaviors, and messages of the layer abstractions as defined above. A class is the implementation of an abstract data type (ADT). It defines attributes and methods implementing the data structure and operations of the ADT, respectively. Instances of classes are called objects. Consequently, classes define properties and behavior of sets of objects. An object can be uniquely identified by its name and it defines a state which is represented by the values of its attributes at a particular time. The behavior of an object is defined by the set of methods which can be applied to it. A method is associated with a class. An object invokes a method as a reaction to receipt of a message.

Thus, the components of a layer comprise all entities in anyway related to or associated with the layer such as inputs, outputs, operands, matrices representing functions, systems, processes, methods, and probability parameters. In a digital embodiment, activation results in

the recall of the component from memory and may further result in processing steps such as matrix multiplication of matrices representing functions. Activation involves generating an activation probability parameter. The activation probability parameter is a parameter responsible for activating any component of the system and is dependent on a prior activation history of each component in the system.

The Predominant Configuration Layer 18 includes an activation probability parameter generator 66. The activation probability parameter generator 66 receives a listing of prior activation frequencies of all of the available components of the present invention such as matrices representing functions, data parameters, Fourier components, Fourier series, strings, ordered strings, components of the Input Layer, components of the Association Layer, components of the String Ordering Layer, and components of the Predominant Configuration Layer from an activation frequency memory section 68. The activation probability parameter generator 66 also receives a listing of all active components from the processor 42. Alternatively, the activation probability parameter generator 66 may receive a listing of all active components directly from the active components. The activation probability parameter is stored in memory 20. The activation probability parameter is input to an activation probability operand generator 70. The activation probability operand generator 70 generates a probability operand value of one or zero based upon the activation probability parameter. The probability operand value is output to the processor 42. Any one or more of the components are activated when the probability operand corresponding to each component has a value of one as determined by the processor 42. Thus, the activation of each component is based on the corresponding activation probability parameter. Each activation probability parameter is weighted based on the activation rate of the component. The activation process continues while the system is on. Thus, the activation process is akin to an operating system kernel in a forever loop.

Embodiments of the system for performing pattern recognition and processing may comprise a general purpose computer. Such a general purpose computer may have any number of basic configurations. For example, such a general purpose computer may comprise a central processing unit (CPU), one or more specialized processors, system memory, a mass storage device such as a magnetic disk, an optical disk, or other storage device, an input means such as a keyboard or mouse, a display device, and a printer or other output device. A system implementing the present invention can also comprise a special purpose computer or other hardware system and all should be included within its

scope.

Embodiments within the scope of the present invention also include computer program products comprising computer readable medium having embodied therein program code means. Such computer readable media can be any available media which can be accessed by a general purpose or special purpose computer. By way of example, and not limitation, such computer readable media can comprise RAM, ROM, EPROM, CD ROM, DVD or other optical disk storage, magnetic disk storage or other magnetic storage devices, or any other medium which can embody the desired program code means and which can be accessed by a general purpose or special purpose computer. Combinations of the above should also be included within the scope of computer readable media. Program code means comprises, for example, executable instructions and data which cause a general purpose computer or special purpose computer to perform a certain function of a group of functions.

The present invention may be embodied in other specific forms without departing from the spirit or essential attributes thereof and, accordingly, reference should be made to the appended claims, rather than to the foregoing specification, as indicating the scope of the invention.

Also, included as part of this application is a Support Appendix and associated sub-appendices. These include the following:

SUB-APPENDIX I is the derivation of the Input and the Band-Pass Filter of the Analog Fourier Processor according to the present invention;

SUB-APPENDIX II is the derivation of the Modulation and Sampling Gives the Input to the Association Mechanism and Basis of Reasoning according to the present invention;

SUB-APPENDIX III is the derivation of the Association Mechanism and Basis of Reasoning according to the present invention;

SUB-APPENDIX IV is the Ordering of Associations: Matrix Method according to the present invention;

SUB-APPENDIX V is the GENOMIC DNA SEQUENCING METHOD/MATRIX METHOD OF ANALYSIS according to the present invention;

SUB-APPENDIX VI is the derivation of the Input Context according to the present invention, and

SUB-APPENDIX VII is the derivation of the Comparison of Processing Activity to Statistical Thermodynamics/Predominant Configuration according to the present invention.

SUPPORT APPENDIX

The methods and systems of the present invention are herein defined as the "processor" which is capable of storing, retrieving, and

processing data to form novel conceptual content according to the present invention. The "processor" comprises systems and associated processes which serve specific functions which are collectively called "layers". The "layers" are organized so as to receive the appropriate inputs and produce the appropriate outputs according to the present invention. In a preferred embodiment, the memory layer is organized in a hierarchical manner according to the significance of the stored information. The significance may be measured by how frequently the information is recalled during processing, or it may be significant because it represents reference or standard information. The most significant information may be stored in a layer called "High Level Memory". Unlike a conventional processor such as a Turing Machine, the "processor" of the present invention may constantly change its state such that the output to a given input may not be identical. The "processor" may be governed by a principle similar to the entropy principle of thermodynamics whereby a chemical system achieves a state representative of a predominant configuration, most probable state in time. The "predominant configuration" of the present "processor" is the total systems of the "processor" and the total state of their components in time. The following invention of Pattern Recognition, Learning, and Processing Methods and Systems comprises analog or digital embodiments of:

1.) an Input Layer which receives data representative of physical characteristics or representations of physical characteristics of the environment and transforms it into a Fourier series in k,ω −space wherein input context is encoded in time as delays which corresponds to modulation of the Fourier series at corresponding frequencies. The derivation of the input comprising a Fourier series in k,ω −space is given in SUB-APPENDIX I--The Input and the Band-Pass Filter of the Analog Fourier Processor. The derivation of the encoding of input context in time as delays which corresponds to modulation of the Fourier series at corresponding frequencies is given in SUB-APPENDIX VI--Input Context. A flow diagram of an exemplary transducer data structure of a time delay interval subdivision hierarchy is shown in FIGURE 3. The corresponding derivations are also given in SUB-APPENDIX VI;

2.) an Association Filter Layer which receives multiple Fourier series from the Input layer, and High Level Memory, and forms a series (called a "string") of multiple Fourier series each representative of separate information by establishing "associations" between "string" member Fourier series. In k,ω −space, the Fourier series are sampled and modulated via time delayed Gaussian filters called "association filters" or "association ensembles" that provide input to form the "associations". The derivation of the time delayed Gaussian filters which provide

sampling and modulation (frequency shifting) of the Fourier series in k,ω −space is given in SUB-APPENDIX II--Modulation and Sampling Gives the Input to the Association Mechanism and Basis of Reasoning. The derivation of the "association" of Fourier series is given SUB-APPENDIX III--Association Mechanism and Basis of Reasoning;

3.) a "String" Ordering Layer which receives the "string" as input from the Association Filter Layer and orders the information represented by the "string" as a nested set of subsets of information with a Matrix Method of Analysis Algorithm via Poissonian probability based associations with input from High Level Memory. The methods of ordering the "string" comprising associated information are given SUB-APPENDIX IV--Ordering of Associations: Matrix Method, and

4.) an Output of the Ordered "String" to High Level Memory Layer with Formation of the "Predominant Configuration" which is analogous to statistical thermodynamics and arises spontaneously because the activation of any association filter, input to the Association Filter Layer to form a "string", and the input to the "String" Ordering Layer are based on their activation history whereby activation is effected by probability operators. The derivation of the predominant configuration structure is given in SUB-APPENDIX VII--Comparison of Processing Activity to Statistical Thermodynamics/Predominant Configuration.

A flow diagram of an exemplary hierarchical relationship between the characteristics and the processing and storage elements of the present "processor" is shown in FIGURE 18. FIGURE 19 is a flow diagram of an exemplary hierarchical relationship of the signals in Fourier space comprising "FCs", "SFCs", "groups of SFCs", and a "string" accordance with the present invention. An exemplary layer structure is shown in FIGURE 20. A flow diagram of an exemplary layer structure and exemplary signal format which demonstrates the relationships of the inputs and outputs of the processing layers is shown in FIGURE 21.

All layers comprise processor elements called "P elements" each with a system function response defined as the "impulse response" (Eqs. (39.22-39.24)) and an output (herein defined as the "P element response") shown in FIGURE 6 comprising a "pulse train of impulse responses"--an integer number of traveling dipole waveforms (each called an "impulse response"). The Fourier transform of this signal is the convolution of a sinc function with a periodic series of delta functions where the amplitude and the width of the sinc function is determined by the integer number of "impulse responses" of the signal. In a preferred embodiment, the amplitude of the "impulse response", the temporal and spatial spacing or repetition frequency of the "impulse responses", and the integer number of "impulse responses" of the "P element" signal is proportional to rate of voltage change called

"depolarization" of the "P element". This rate is determined by the amplitude and rate of change of the input. Thus, in the preferred embodiment, each "P element" is a linear differentiator--the output (pulse train of "impulse responses") is the sum (superposition) of the derivative of the inputs. Additionally in the embodiment, the "P element" has a threshold of "depolarization" to generate an output. In this case, the Fourier transform of "P element response" comprises a repeated series of a Fourier component herein defined as a "FC" with quantized frequency and phase angle. In another embodiment, the amplitude is also quantized. In $k,\omega-$space, the Fourier transform of the "impulse response" function filters the "FC" of a "P element" and is a band-pass when the spatial frequency of the "FC" is equal to the temporal frequency (i.e. the "FC" is band-passed when $k_\rho = k_z$).

An exemplary output signal of an analog "P element" to an input of the form given by Eq. (39.26) is given in time by Eq. (39.27) (the parameters ρ_0, z_0, and N may encode quantitative information such as intensity and rate of change of a physical parameter such as temperature) and in $k,\omega-$space by Eq. (39.32). The latter equation is that of a series of a Fourier component with information encoded in the parameters ρ_0 and N of the Fourier component. "P elements" are directionally massively interconnected in terms of the inputs and the outputs of the present invention which may superimpose. Multiple "P elements" input into any given "P element" which then outputs to multiple "P elements. The Fourier transform of the superposition of the output of multiple "P elements" is a repeating Fourier series--a repeating series of trigonometric functions comprising a series of Fourier components "FCs" herein referred to as a " SFCs". Exemplary representations are given by Eq. (39.33) and Eq. (39.33a). Thus, the present "processor" may function as an analog Fourier processor.

All layers also comprise memory elements called "M elements" that store an input such as a "P element response". The stored "P element response" may be recalled from the "M element". Each "M element" has a system function response defined as the "impulse response" (Eqs. (39.22-39.24)) and an output (herein defined as the "M element response") also shown in FIGURE 6 comprising a "pulse train of impulse responses"--an integer number of traveling dipole waveforms (each called an "impulse response"). In a preferred embodiment, the output, the "M element response", is the product of the "pulse train of impulse responses" and a time ramp. In this case, the Fourier transform of "M element response" comprises a repeated series of a Fourier component herein defined as a "FC" with quantized amplitude, frequency, and phase angle. An exemplary output signal of a group of analog "M elements" to

an input time ramp is given in k,ω −space by Eq. (39.33a) (the parameters ρ_{0_m}, z_{0_m}, $N_{m_{\rho_0}}$, and $N_{m_{z_0}}$ of the recalled function are typically the same as those stored). The "M elements" are directionally massively interconnected in terms of the inputs and the outputs of the present invention which may superimpose. Multiple "M elements" input into any given "M element" which then outputs to multiple "M elements". The collective of multiple "M elements" including their stored inputs is referred to as "memory" of the "processor". The collective storage of a signal such as a " SFCs" having an exemplary representation given by Eq. (39.33) to multiple "M elements" is called "store to memory". The collective activation of multiple "M elements" to provide a signal such as a " SFCs" having an exemplary representation given by Eq. (39.33a) is referred to as "recall from memory". An exemplary representation of information "recalled from memory" with input context encoded by specific modulation is given by Eq. (39.110).

The Association Layer and the "String" Ordering Layer comprise cascaded processor stages which are herein defined as "stages". The "stages" need not be identical. Let $h_i(t)$ be the impulse response of the i^{th} stage and assume that $h_i(t) \geq 0$, so that the step response of each stage (or indeed of any number of cascaded stages) is monotonic. Cascaded stages form filters. The Central Limit Theorem of probability theory states in effect that, under very general conditions, the cascade of a large number of linear-time-invariant (LTI) systems will tend to have a delayed Gaussian impulse response, almost independent of the characteristics of the systems cascaded. Sufficient conditions of the Central Limit Theorem are given by Eqs. (39.52-39.55) of SUB-APPENDIX II--Modulation and Sampling Gives the Input to the Association Mechanism and Basis of Reasoning. The collective of multiple cascaded "stages" comprises an "association ensemble" that receives input such as a " SFCs". Each "association ensemble" serves as a heterodyne having an exemplary representation given by Eq. (39.50) by modulating the Fourier series in k,ω −space. It further samples the Fourier series in k,ω −space. The modulation and sampling functions correspond to a delayed Gaussian filter in the time domain having an exemplary representation given by Eq. (39.51).

The "stages", "P elements", and "M elements" in one embodiment of the present "processor", are directionally massively interconnected in terms of the inputs and the outputs of the present invention which may superimpose. Multiple "stages", "P elements", and "M elements" input into any given "stage", "P element", or "M element" which then outputs to multiple "stages", "P elements", and "M elements".

The Input Layer comprises transducers that convert physical

signals from the environment into measurements called "data" which in an analog circuit embodiment, is processed into an analog time signal which corresponds to a Fourier series in k,ω −space. In a digital equivalent embodiment, the "data" is further transformed by a Fourier transform processor into a Fourier series in k,ω −space. According to the present invention information is encoded in a Fourier series in k,ω −space. Information is not limited to that corresponding to data, but is meant include all forms of information such as conceptual information, temporal order, cause and effect relationships, size order, intensity order, before-after order, top-bottom order, left-right order, and knowledge derived from study, experience, or instruction. Data which are transducer measurements is processed into a Fourier series in k,ω −space to form input to higher layers such as the Association Layer shown in FIGURE 21 whereby:

i.) "Data" such as the intensity and the rate of change of a physical signal such as the surface roughness, or the intensity of sound, light, or temperature recorded by a transducer is represented in terms of the frequency and amplitude parameters, ρ_{0_m} and $N_{m_{\rho_0}}$, of each component of the Fourier series (e.g. Eq. (39.33a)). Information is represented in terms of the parameters ρ_{0_m} and $N_{m_{\rho_0}}$ of each component of the Fourier series in the sense that if the transducer and Fourier processor were each a reciprocal device, then inputting the Fourier series into the output of the Fourier transform processor would yield the measured physical signals at the input of the transducers.

ii.) The input from the Input Layer to other layers can be an analog waveform in the analog case and a matrix in the digital case. Input context of a given transducer can be encoded in time as delays which correspond to modulation of the Fourier series in k,ω −space at corresponding frequencies whereby the data corresponding to each transducer maps to a distinct memory location called a "register" that encodes the input context by recording the data to corresponding specific time intervals of a time division structured memory.

iii.) Input context of a complex transducer system can be encoded in time by the mapping of data from the components of the transducer system to a memory structured according to a corresponding hierarchical set of time intervals representative of each transducer system with respect to different transducer systems, a transducer element's rank relationship relative to other transducer elements, and the response of a transducer element as a function of time. In terms of digital processing, the data from a transducer having n levels of subcomponents is assigned a master time interval with $n+1$ sub time intervals in a hierarchical manner wherein the data stream from the final

n th level transducer element is recorded as a function of time in the $n+1$ th time coded sub memory buffer. During processing the time intervals represent time delays which are transformed into modulation frequencies which encode input context. A flow diagram of an exemplary transducer data structure of a time delay interval subdivision hierarchy is shown in FIGURE 3. An exemplary complex transducer which may represented by a data structure comprising a hierarchical set of time delay intervals is a video camera which is comprised of a multitude of charge coupled devices (CCDs), transducer elements each responsive to light intensity of a given wavelength band at a given spatial location in a grid. Another example is an audio recorder comprising transducer elements each responsive to sound intensity of a given frequency band at a given spatial location or orientation. A signal within the band 300-400 MHz may encode and identify the signal as a video signal; whereas, a signal within the band 500-600 MHz may encode and identify the signal as an acoustic signal. Furthermore, a video signal within the band 315-325 MHz may encode and identify the signal as a video signal as a function of time of CCD element (100,13) of a 512 by 512 array of CCDs. An exemplary representation of a " SFCs" output of "P elements" or "M elements" with input context encoded by specific modulation is given by Eq. (39.110);

iv.) The relationship between the "data" and the parameters ρ_{0_m} and $N_{m_{\rho_0}}$ of each component of the Fourier series, may be learned by the "processor" by applying standard physical signals to each transducer together with other information that is "associated" with the standard. The information that is "associated" with the standard can be recalled and may comprise input to the Association Layer and the "String" Ordering Layer during processing according to the present invention.

The Association Filter Layer receives multiple Fourier series from the Input Layer, and High Level Memory, and forms a series (called a "string") of multiple Fourier series each representative of separate information by establishing associations between "string" member Fourier series. The "association" between one or more Fourier series that form the "string" occurs with Poissonian probability based on the spectral similarity of each association filtered Fourier series member with that of one or more others filtered by the same or different association filters as described further below.

The process of storing output from multiple transducers to memory further comprises creation of "transducer strings". In one embodiment of this case, associations occur at the transducer level, and "SFCs" are mapped to distinct "registers" from the corresponding distinct transducers responding simultaneously, for example. Consider a

"transducer string" made up of multiple "groups of SFCs" where each "SFCs" represents information of the transducer system with respect to different transducer systems, a transducer element's rank relationship relative to other transducer elements, and the response of a transducer element as a function of time. These aspects of each transducer are encoded via time delays corresponding to modulation in k,ω −space within a frequency band corresponding to each aspect of the transducer.

Two or more "transducer string" Fourier series such as two or more "SFCs" may become "linked" which is defined according to a corresponding linkage probability weighting parameter wherein activation of one "string" Fourier series may cause other "string" Fourier series to become active in according to the linkage probability weighting parameter. The probability that other "string" Fourier series are activated when any given "string" Fourier series is activated defines the "linkage". "Active" in this case of an analog embodiment is defined as providing an output signal; thus, "activate" is defined as causing an output signal. "Active" in a digital embodiment is defined as recalled from memory; thus, "activate" is defined according to causing a Fourier series to be recalled from memory.

In a general sense, the "string" in k,ω −space is analogous to a multidimensional Fourier series. The modulation within each frequency band may encode context in a general sense. In one embodiment, it encodes temporal order, cause and effect relationships, size order, intensity order, before-after order, top-bottom order, left-right order, etc. which is relative to the transducer. Further associations are established between "groups of SFCs" (i.e. a new "string" is created) by the Association Filter Layer.

The Association Filter Layer receives multiple Fourier series from the Input layer, and High Level Memory, and forms a series (called a "string") of multiple Fourier series each representative of separate information by establishing "associations" between "string" member Fourier series. FIGURE 19 is a flow diagram of an exemplary hierarchical relationship of the signals in Fourier space comprising "FCs", "SFCs", "groups of SFCs", and a "string" in accordance with the present invention. Each "FC" is "carried" (processed as a response to an input) by a "P element" or stored into and/or recalled from a "M element" as shown in FIGURE 18 which is a flow diagram of an exemplary hierarchical relationship between the characteristics and the processing and storage elements of the present "processor". Each Fourier series such as a "SFCs" representing information is filtered and delayed in the time domain (modulated and sampled in the frequency domain or k,ω −space) as it is recalled from memory and "carried" (processed as a response to the memory input) by a series of cascaded association "stages" called an

"association ensemble" or "association filter". Since the Fourier series is in k,ω −space, the modulation corresponds to a frequency shift. Each "association ensemble" is weakly linked with multiple other "association ensembles" at the level of the "stages". The "association ensembles" produce interference or "coupling" of the "SFCs" of one set of "stages" with that of another by producing frequency matched and phase locked Fourier series --sums of trigonometric waves that are frequency matched and periodically in phase--that give rise to "association" of the corresponding recalled or prior processed information.

"Coupling" gives rise to the formation of "associations" between one or more Fourier series that form the "string". "Coupling" refers to interference or energy exchange between "association ensembles" in an analog embodiment. In a digital embodiment, "coupling" refers to calculating an "association" probability parameter based on the spectral similarity of the each Fourier series such as a "SFCs" filtered by an "association filter" with that of one or more other Fourier series filtered by the same or different "association filters". The statistics may be Poissonian. "Association" refers to recording "coupled" Fourier series to memory based on the probability of the "coupling". In a digital embodiment, "association" refers to marking two or more Fourier series as associated based on a zero or one outcome of a probability operand applied to the "association" probability parameter and recording the "associated" Fourier series to memory. The "association" probability parameter based on Poissonian probability is derived from a correlation function in SUB-APPENDIX III--Association Mechanism and Basis of Reasoning. The "association" probability parameter has a "coupling cross section" amplitude and a "frequency difference angle" as parameters. The former is a weighting parameter of the spectral similarity of Fourier series which may become "associated". The "frequency difference angle" is the fractional difference in the frequencies of the Fourier series which may become "associated" expressed as an angle. The derivation of these parameters as well as the derivation of the "association" of Fourier series that "couple" with Poissonian probability is also found in SUB-APPENDIX III.

In a preferred embodiment, the "string" is formed by the Association Filter Layer with input context. In this case, "association" occurs whereby the "SFCs" or "groups of SFCs" such as those comprising "transducer strings" comprise a transducer specific frequency modulation factor. Exemplary representations of "string" outputs of "P elements" or "M elements" with input context encoded by specific modulation are given by Eq. (39.114) and Eq. (39.115). In this case, an exemplary representation of the "coupling cross section" amplitude and the "frequency difference angle" based on the spectral similarity of the

each "SFCs" filtered by an "association filter" with that of one or more other "SFCs" filtered by the same or different "association filters" is given by Eq. (39.111) and Eq. (39.112).

The "String" Ordering Layer receives the "string" as input from the Association Filter Layer and orders the information represented in the "string" via a method developed by Mills for sequencing DNA called the "Matrix Method" which is herein presented as a mechanism used by the "processor" to sequence information temporally, conceptually, or according to causality. First, the "string" (multiple Fourier series) is stored in memory. The "string" is recalled and processed by further sets of specific "association ensembles" that "couple" with other "higher level associations", information with conceptual significance established by a previous execution of the present procedure. In $k,\omega-$space, each specific "association ensemble" samples the "string", a Fourier series in $k,\omega-$space. It also serves as a heterodyne by modulating the Fourier series in $k,\omega-$space. The sampling in the frequency domain is dependent on the particular half-width parameter, α_s, of each specific "association ensemble". The collective sampling of the specific "association ensembles" provides a nested set of subsets of information where each subset maps to a specific time point corresponding to the specific delay, $\frac{\sqrt{N_s}}{\alpha_s}$, of the specific Gaussian filter of the "association ensemble" (Eqs. (39.50-39.51)). The nested set of subsets of information is ordered by the Matrix Method of Analysis Algorithm of Mills with Poissonian probability based associations with input from High Level Memory. Each "group of SFCs" of the input "string" has the corresponding time delay parameter, $\frac{\sqrt{N_s}}{\alpha_s}$, and the half-width parameter, α_s, of the Gaussian filter of the "association ensemble" (Eqs. (39.50-39.51)) that resulted in the "coupling" and "association" to form the "string". The process of ordering assigns a particular time delay, $\frac{\sqrt{N_{s'}}}{\alpha_{s'}}$, and half-width parameter, $\alpha_{s'}$, to each "group of SFCs" of the output "string". The half-width parameter, $\alpha_{s'}$ corresponds to each specific delayed Gaussian filter that samples the input "string" in the frequency domain to provide each "group of SFCs" of the output "ordered string". Each corresponding particular time delay, $\frac{\sqrt{N_{s'}}}{\alpha_{s'}}$, encodes and corresponds to the time domain order of each "group of SFCs" of the output "ordered string". An order processed "string" called a "P string" may comprise complex information having conceptual content.

The Output of the Ordered "String" to High Level Memory Layer with Formation of the Predominant Configuration receives ordered strings from the High Level Memory and forms more complex ordered strings as shown in FIGURE 20. This layer also activates components within other layers. The Output of the Ordered "String" to High Level Memory Layer with Formation of the Predominant Configuration is analogous to statistical thermodynamics and arises spontaneously because the activation of any "processor" component such as any "P element", "M element", "stage", "association ensemble", "SFCs", "string", "ordered string", "transducer string" having "linkages", Fourier series "linkage", input to the Association Filter Layer to form a "string", and the input to the "String" Ordering Layer are based on their past activation frequency whereby activation is effected by probability operators. In one embodiment, an activation probability parameter is generated and stored in memory for each "processor" component. A probability operand is generated having a value selected from a set of zero and one, based on the activation probability parameter. If the value is one, the component is activated. Thus, any "processor" component is randomly activated wherein the activation is based on the activation probability parameter. The activation probability parameter is weighted based on an activation rate. "Processor" components may become "linked" which is defined according to the corresponding probability weighting parameter wherein activation of one "processor" component may cause other "processor" components to become "active" according to the probability weighting parameter. The probability that other "processor" components are activated when any given "processor" component is activated defines the "linkage".

The processing of information depends on and dynamically alters (through feedback) the total state of stored information, the cascades of association "stages", and the hierarchical relationships of association "stages" and stored information (memory). "Memory linkages" occur whereby recalling any part of a string from a distinct memory location thereby causes additional Fourier series of the string to be recalled. "Linkages" between "stages" occur whereby activating any "stage" thereby causes additional "stages" to become "active". A strongly "linked group of cascaded association "stages" comprises an "association ensemble", and a strongly linked group of memory elements comprises a "memory ensemble". Repetitive activation of a "memory element" or association "stage" increases the probability of its future activation. A configuration of "couplings" between "memory ensembles" and "association ensembles" increases the probability of future activation of the configuration. Analogously to statistical thermodynamics, a predominant configuration arises from the ensemble level. Consider the

"processor" on a higher level. The activation history of each ensemble relates to a hierarchical relationship of coupled "memory and association ensembles" which gives rise to a precedence of higher order predominant configurations. Pattern recognition, learning, and the ability to associate information and create novel information is a consequence. Machine learning arises by the feedback loop of transducer input to the coupled predominant configurations which increases the basis for machine intelligence.

Pattern recognition and learning arise from the massive directional connectivity in terms of the output to input relationships of the "processor" which in one embodiment functions as an analog Fourier processor wherein a superposition of "P element responses" becomes a superposition of trigonometric functions in frequency space (k,ω −space). Information is digitized in amplitude, frequency, and phase in k,ω −space via the "P element response". It is then modulated, sampled, associated, and ordered via the properties of cascaded groups of association "stages" with "couplings" governed by Poissonian probability. For the "processor", since information is encoded in Fourier series in k,ω −space, specific time delays achieve the specific modulations equivalent to that of heterodynes of conventional signal processing circuits. In other words, a clock substitutes for a multitude of heterodyne circuits to encode input context wherein aspects of each transducer are encoded via time delays corresponding to modulation in k,ω −space within a frequency band corresponding to each aspect of the transducer. The modulation and sampling functions correspond to a delay and filter (delayed Gaussian filter) in the time domain analogous to the key components of amplitude modulation (AM) radio except that the Fourier series of the signal and its modulation occurs k,ω −space in the case of the present "processor" versus the time domain in the AM signal processing case. The filtering function occurs in the time domain in both cases. The unique processing features of the "processor" further permits ordering of information by a method developed by Mills for sequencing DNA called the "Matrix Method" which is herein presented as a mechanism used by the "processor" to sequence information temporally, conceptually, or according to causality. According to the Fourier theorem any waveform can be recreated by an infinite series of trigonometric functions, and any aspect of the universe can be represented by an infinite series of sine and cosine functions as processed by the "processor". For the "processor" of the present invention, the trigonometric function is the basis element of information. The quantity of information such as "inputs" that can be associated into ordered "strings" ("P strings") is essentially infinite based on it being encoded in Fourier series in k,ω −space. And, the number of

terms necessary to represent most objects is not overwhelming. In fact, even a potentially challenging object having sharp edges such as a square pulse poses no difficulty in that is fairly accurately represented by only seven terms of a Fourier series in the time domain comprising the prior art [6]. The same principle applies to information represented as a Fourier series in k,ω −space.

The following invention of Pattern Recognition, Learning, and Processing Methods and Systems comprises analog or digital embodiments. In one embodiment, analog circuit elements store, retrieve, and process input waveforms wherein the circuit elements have the system functions or impulse responses or comprise the operators and structures which transform input to output as described herein. In another embodiment, the mathematical functions corresponding to the waveforms of any stage of storage, retrieval, or processing are represented digitally, and the digital waveforms are digitally processed in a manner equivalent to the analog embodiment according to signal processing theory such as the Nyquist theorem. In a preferred embodiment, a digitally based "processor" comprises simulations methods and systems according to the analog systems and processes of the present invention. The Nyquist theorem states that all of the information in any waveform can be conserved and recovered by digital processing with frequency components equal to twice the maximum frequency of any waveform [7]. Thus, the analog and digital embodiments perform equivalently.

Exemplary Layer Structure and Exemplary Signal Format

FIGURE 20 shows an exemplary layer structure in accordance with the present invention. FIGURE 21 shows a flow diagram of an exemplary layer structure and exemplary signal format in accordance with the present invention. The present invention comprises an analog Fourier "processor" wherein the basis element of information in k,ω −*space* is the Fourier component. In a preferred embodiment, the analog systems and processes are implemented using the corresponding digital embodiments. The "processor" is applicable to standard computers comprising digital processors, and digital memory, storage, and retrieval systems where discrete values of the continuous functions evaluated at selected frequencies and/or at the Nyquist rate [7] form matrices upon which the operations of the exemplary signal format are performed in place of the continuous functions. Exemplary embodiments of the present invention according to the layer structure of FIGURE 20 and the exemplary layer structure and exemplary signal format of FIGURE 21 comprises:

Input Layer

The Input Layer receives data and transforms it into a Fourier series in k,ω −space wherein input context is encoded in time as delays which corresponds to modulation of the Fourier series at corresponding frequencies. Data is processed into a Fourier series in k,ω −space that represents information as given by Eq. (39.33) and Eq. (39.33a)

$$V_{\sum_m}\left(k_\rho,k_z\right)=\sum_{m=1}^{M}\sum_{n=-\infty}^{\infty}\frac{4\pi}{1+\frac{k_z^2}{k_\rho^2}}\frac{4}{\rho_{0_m}z_{0_m}}a_{0_m}\operatorname{sinc}\left(k_\rho-n\frac{2\pi}{\rho_{0_m}}\frac{N_{m_{\rho 0}}\rho_{0_m}}{2}\right)\operatorname{sinc}\left(k_z-n\frac{2\pi}{v_m t_{0_m}}\frac{N_{m_{z0}}z_{0_m}}{2}\right) \tag{39.33}$$

$$V_{\sum_m}\left(k_\rho,k_z\right)$$

$$=\sum_{m=1}^{M}\sum_{n=-\infty}^{\infty}\frac{4\pi}{1+\frac{k_z^2}{k_\rho^2}}\frac{4}{\rho_{0_m}z_{0_m}}a_{0_m}\frac{N_{m_{\rho 0}}\rho_{0_m}}{2}\frac{N_{m_{z0}}z_{0_m}}{2}\operatorname{sinc}\left(k_\rho-n\frac{2\pi}{\rho_{0_m}}\frac{N_{m_{\rho 0}}\rho_{0_m}}{2}\right)\operatorname{sinc}\left(k_z-n\frac{2\pi}{v_m t_{0_m}}\frac{N_{m_{z0}}z_{0_m}}{2}\right) \tag{39.33a}$$

$$=\sum_{m=1}^{M}\sum_{n=-\infty}^{\infty}\frac{4\pi}{1+\frac{k_z^2}{k_\rho^2}}a_{0_m}N_{m_{\rho 0}}N_{m_{z0}}\operatorname{sinc}\left(k_\rho-n\frac{2\pi}{\rho_{0_m}}\frac{N_{m_{\rho 0}}\rho_{0_m}}{2}\right)\operatorname{sinc}\left(k_z-n\frac{2\pi}{v_m t_{0_m}}\frac{N_{m_{z0}}z_{0_m}}{2}\right)$$

whereby i.) data such as intensity and rate of change recorded by a transducer is represented in terms of the parameters ρ_{0_m} and $N_{m_{\rho_0}}$ of each component of the Fourier series; ii.) input context is encoded in time by a hierarchical set of time delay intervals representative of each transducer system with respect to different transducer systems, a transducer element's rank relationship relative to other transducer elements, and the response of a transducer element as a function of time, and iii.) the input from the Input Layer to other layers shown in FIGURE 21 can be an analog waveform in the analog case and a matrix in the digital case wherein input context of a given transducer can be encoded in time as delays which correspond to modulation of the Fourier series in k,ω −space at corresponding frequencies as given by the terms $e^{-jk_\rho\left(\rho_{fb_{s,m}}+\rho_{t_{s,m}}\right)}$ of Eq. (39. 113)

$$V_{\sum_{s,m}}\left(k_\rho,k_z\right)=\sum_{s=1}^{S}\sum_{m=1}^{M_s}\sum_{n=-\infty}^{\infty}\frac{4\pi}{1+\frac{k_z^2}{k_\rho^2}}a_{0_{s,m}}N_{s,m_{\rho_0}}N_{s,m_{z_0}}e^{-jk_\rho\left(\rho_{\beta_{s,m}}+\rho_{t_{s,m}}\right)}$$

$$\sin\left(k_\rho-n\frac{2\pi}{\rho_{0_{s,m}}}\frac{N_{s,m_{\rho_0}}\rho_{0_{s,m}}}{2}\right)\sin\left(k_z-n\frac{2\pi}{v_{s,m}t_{0_{s,m}}}\frac{N_{s,m_{z_0}}z_{0_{s,m}}}{2}\right) \tag{39.113}$$

whereby the data corresponding to each transducer maps to a distinct memory location called a "register" that encodes the input context by recording the data to corresponding specific time intervals of a time division structured memory, and iv.) the relationship between the "data" and the parameters ρ_{0_m} and $N_{m_{\rho_0}}$ of each component of the Fourier series, may be learned by the "processor" by applying standard physical signals to each transducer together with other information that is associated with the standard. The information that is "associated" with the standard can be recalled and may comprise input into the Association Layer and the "String" Ordering Layer during processing according to the present invention. In terms of digital processing, the data from a transducer having n levels of subcomponents is assigned a master time interval with $n+1$ sub time intervals in a hierarchical manner wherein the data stream from the final n th level transducer element is recorded as a function of time in the $n+1$ th time coded memory buffer. During processing the time intervals represent time delays which are transformed into modulation frequencies which encode the input context. FIGURE 3 is a flow diagram of an exemplary transducer data structure of a time delay interval subdivision hierarchy wherein the data from a transducer having n levels of subcomponents numbering integer m per level is assigned a master time interval with $n+1$ sub time intervals in a hierarchical manner wherein the data stream from the final n th level transducer element is recorded as a function of time in the $n+1$ th time coded sub memory buffer in accordance with the present invention.

The process of storing output from multiple transducers to memory further comprises creation of "transducer strings". In one embodiment, associations occur at the transducer level, and "SFCs" are mapped to distinct "registers" from the corresponding distinct transducers responding simultaneously, for example. Consider a "transducer string" made up of multiple "groups of SFCs" where each "SFCs" represents information of the transducer system with respect to different transducer systems, a transducer element's rank relationship relative to other transducer elements, and the response of a transducer element as a function of time. These aspects of each transducer are encoded via delays corresponding to modulation in $k,\omega-$space (Eq.

(39.109)) within a frequency band corresponding to each aspect of the transducer.

$$x(t) = \int_{-\infty}^{\infty} X(f) e^{j 2\pi f t} df \qquad X(t) = \int_{-\infty}^{\infty} x(t) e^{-j 2\pi f t} dt$$

(39.109)

Delay	$\delta(t - t_0)$	$\Leftrightarrow$	$e^{-j 2\pi f t_0}$

Two or more "transducer string" Fourier series such as two or more "SFCs" may become "linked" which is defined according to a corresponding linkage probability weighting parameter wherein activation of one "string" Fourier series may cause other "string" Fourier series to become "active" according to the linkage probability weighting parameter. The probability that other "string" Fourier series are activated when any given "string" Fourier series is activated defines the "linkage".

The "string" in k,ω −space is analogous to a multidimensional Fourier series. The modulation within each frequency band may further encode context in a general sense. In one embodiment, it encodes temporal order, cause and effect relationships, size order, intensity order, before-after order, top-bottom order, left-right order, etc. which is relative to the transducer.

A "FC" of Eq. (39.32) is a series of a Fourier component. A distinct superposition or series of "FCs" is called a "SFCs" which further superimpose to form "groups of SFCs". The data is digitized according to the parameter N of Eqs. (39.33), (39.33a), and (39.87). Input to higher layers is in a Fourier series format in k,ω −space or data is processed with a FFT (Fast Fourier Transform) routine and stored in memory as a series of a Fourier component in k,ω −space with quantized amplitude, frequency, and phase angle (Eq. (39.33a)). Or, data is processed with a FFT (Fast Fourier Transform) routine and stored in memory as a series of a Fourier component in k,ω −space with quantized frequency, and phase angle of the form of Eq. (39.33). In this case, "groups of SFCs" representing information are recalled from memory with a time ramp multiplication of each "FC" of a "SFCs" to give the form of Eq. (39.33a). In the digital case, multiplication is performed via multiplication of corresponding matrices formed from the continuous functions by evaluating them at discrete frequency values. A summary of an exemplary method of inputting data follows:

a.) data is recorded by one or more transducers each having one

or more levels of component elements;

b.) the data recorded by each transducer is encoded as parameters such as ρ_{0_m} and $N_{m_{\rho_0}}$ of a Fourier series in Fourier space with input context representing the information based on the physical characteristics and the physical context;

c.) the data from a transducer having n levels of subcomponents is assigned a master time interval with $n+1$ sub time intervals in a hierarchical manner wherein the data stream from the final n th level transducer element is recorded as a function of time in the $n+1$ th time coded memory buffer;

d.) the time intervals represent time delays which are transformed into modulation frequencies which encode input context (e.g. the transducer element relationship of more than one transducer elements, its rank in the transducer hierarchy, and the time point of data recording);

e.) the representation of the data is given by Eq. (39.110)

$$V_{\sum_m}\left(k_\rho, k_z\right) = \sum_{m=1}^{M}\sum_{n=-\infty}^{\infty} \frac{4\pi}{1+\frac{k_z^2}{k_\rho^2}} a_{0_m} N_{m_{\rho 0}} N_{m_{z0}} e^{-jk_\rho\left(\rho_{fb_m}+\rho_{t_m}\right)} \sin\left(k_\rho \frac{N_{m_{\rho 0}}\rho_{0_m}}{2} - n\frac{2\pi N_{m_{\rho 0}}}{2}\right) \sin\left(k_z \frac{N_{m_{z0}} z_{0_m}}{2} - n\frac{2\pi N_{m_{z0}}}{2}\right) \quad (39.110)$$

f.) in the digital case, the function of Eq. (39.110) comprising a "SFCs" is evaluated at discrete frequencies at twice the rate of the highest discrete frequency ($\frac{N_m \rho_{0_m}}{2}$) to form a matrix for each "SFCs";

g.) "SFCs" are mapped to distinct "registers" from corresponding distinct transducers responding simultaneously to form "transducer strings" having a representation given by Eq. (39.113) wherein input context is encoded by the transducer modulation factor $e^{-jk_\rho\left(\rho_{fb_{s,m}}+\rho_{t_{s,m}}\right)}$;

h.) in the digital case comprising "memory linkages" of a "transducer string", recalling any part of a "transducer string" from a distinct memory location may thereby cause additional "linked" Fourier series of the "transducer string" to be recalled. In one embodiment, a linkage probability parameter is generated and stored

in memory for each "string" Fourier series such as a "SFCs". A probability operand is generated having a value selected from a set of zero and one, based on the linkage probability parameter. If the value is one, the corresponding Fourier series is recalled. Thus, when any part of a "transducer string" is recalled from memory, any other "string" Fourier series is randomly recalled wherein the recalling is based on the linkage probability parameter. The linkage probability parameter is weighted based on the linkage rate.

Association Filter Layer to Form a "String"

Each "SFCs" is filtered and delayed in the time domain (modulated and sampled in the frequency domain) as it is processed by a cascade of association filters (subprograms in the digital case) called an "association ensemble". Each "association ensemble" is weakly linked with multiple other such "association ensembles". These "association ensembles" produce interference or "coupling" of one "SFCs" with another by producing frequency matched and phase locked Fourier series --sums of trigonometric waves that are frequency matched and periodically in phase--that give rise to "association" of the recalled or prior processed information "carried" by the cascade. The Poissonian probability of such "association" (Eq. (39.106c)) is given by a correlation function given in the SUB-APPENDIX III--Association Mechanism and Basis of Reasoning wherein Eq. (39.87) and Eq. (39.89) are parameters.

$$P_A\left(\frac{\sqrt{N_1}}{\alpha_1},\frac{\sqrt{N_2}}{\alpha_2},...,\frac{\sqrt{N_s}}{\alpha_s},P,p_{\uparrow s},\delta_s\right) = \prod_s \left[p_{\uparrow s}+\left(P-p_{\uparrow s}\right)\exp\left[-\beta_s^{-2}\left(\frac{1-\cos 2\phi_s}{2}\right)\cos\left(\delta_s+2\sin\phi_s\right)\right]\right] \tag{39.106c}$$

$$\beta_s^2=(8\pi)^2\frac{1}{\sqrt{2\pi}}\sqrt{\frac{\alpha_1^2\alpha_s^2}{\alpha_1^2+\alpha_s^2}}$$

$$\sum_{m_1=1}^{M_1} a_{0_{m_1}} N_{m_1} \sum_{m_s=1}^{M_s} a_{0_{m_s}} N_{m_s} \exp\left\{-\left[\frac{\alpha_1^2\alpha_s^2}{\alpha_1^2+\alpha_s^2}\left(\frac{\sqrt{N_1}}{\alpha_1}-\frac{\sqrt{N_s}}{\alpha_s}+\frac{N_{m_1}\rho_{0_{m_1}}}{2\nu_{m_1}}-\frac{N_{m_s}\rho_{0_{m_s}}}{2\nu_{m_s}}\right)^2\right]\right\} \tag{39.87c}$$

$$\phi_s = \frac{\pi\left(\frac{\sqrt{N_1}}{\alpha_1} - \frac{\sqrt{N_s}}{\alpha_s} + \sum_{m_1=1}^{M_1} \frac{N_{m_1}\rho_{0_{m_1}}}{2\nu_{m_1}} - \sum_{m_s=1}^{M_s} \frac{N_{m_s}\rho_{0_{m_s}}}{2\nu_{m_s}}\right)}{\frac{\sqrt{N_1}}{\alpha_1} + \sum_{m_1=1}^{M_1} \frac{N_{m_1}\rho_{0_{m_1}}}{2\nu_{m_1}}} \tag{39.89}$$

The set of "associated" "groups of SFCs" is herein called a "string". The "string" comprises a Fourier series, a linear sum of "FCs". FIGURE 19 is a flow diagram of an exemplary hierarchical relationship of the signals in Fourier space comprising "FCs", "SFCs", "groups of SFCs", and a "string" in accordance with the present invention. Each "FC" is encoded by a "P element" or stored into and/or recalled from a "M element" as shown in FIGURE 18 which is a flow diagram of an exemplary hierarchical relationship between the characteristics and the processing and storage elements of the present "processor".

A summary of an exemplary method of establishing "associations" between "groups of SFCs" (i.e. a creating a "string") by "coupling" with Poissonian probability between "association ensembles" "carrying" the "groups of SFCs" comprising a transducer frequency band modulation factor according to Eq. (39.110) follows:

a.) n (n an integer) inputs each comprising a "SFCs", the function of Eq. (39.110) which in the digital case is evaluated at discrete frequencies at twice the rate of the highest discrete frequency ($\frac{N_m\rho_{0_m}}{2}$) to form a "SFCs" matrix, is recalled from memory;

b.) in the digital case, discrete values are determined at twice the rate of the highest discrete frequency ($\frac{N_m\rho_{0_m}}{2}$) of the Fourier series inputs of up to n different Fourier transforms of delayed Gaussian filters functions (39.50) to form up to n different association filter matrices;

c.) in the digital case, the discrete values of each of n (n an integer) inputs each comprising a "SFCs", the function of Eq. (39.110) which is evaluated at discrete frequencies to form a "SFCs" matrix, are multiplied on a matrix element by matrix element basis corresponding to the same frequency with one or more of the n different association filter matrices each comprising the Fourier transform of a delayed Gaussian filter (Eq. (39.50));

$$H_N(f) \approx e^{-\frac{1}{2}\left(\frac{2\pi f}{\alpha}\right)^2} e^{-j\sqrt{N}\left(\frac{2\pi f}{\alpha}\right)} \tag{39.50}$$

d.) the "coupling cross section" amplitude, β_s^2, and frequency difference angle, ϕ_s, of the harmonic "coupling", is calculated for two or more filtered inputs. In the case of input context, the amplitude, β_s^2, which follows from Eq. (39.87c) is given by Eq. (39.111b), and the frequency difference angle, ϕ_s, which follows from Eq. (39.89) is given by Eq. (39.112a);

$$\beta_s^2 = (8\pi)^2 \frac{1}{\sqrt{2\pi}} \sqrt{\frac{\alpha_1^2\alpha_s^2}{\alpha_1^2+\alpha_s^2}} \sum_{m_1=1}^{M_1} a_{0_{m_1}} N_{m_1} \sum_{m_s=1}^{M_s} a_{0_{m_s}} N_{m_s}$$

$$\exp\left\{-\frac{\frac{\alpha_1^2\alpha_s^2}{\alpha_1^2+\alpha_s^2}\left(\frac{\sqrt{N_1}}{\alpha_1}-\frac{\sqrt{N_s}}{\alpha_s}+\left(\frac{N_{m_1}\rho_{0_{m_1}}}{2\nu_{m_1}}+\frac{\rho_{fb_{m_1}}}{\nu_{fb_{m_1}}}+\frac{\rho_{t_{m_1}}}{\nu_{t_{m_1}}}\right)-\left(\frac{N_{m_s}\rho_{0_{m_s}}}{2\nu_{m_s}}+\frac{\rho_{fb_{m_s}}}{\nu_{fb_{m_s}}}+\frac{\rho_{t_{m_s}}}{\nu_{t_{m_s}}}\right)\right)^2}{2}\right\} \tag{39.111b}$$

$$\phi_s = \frac{\pi\left(\frac{\sqrt{N_1}}{\alpha_1}-\frac{\sqrt{N_s}}{\alpha_s}+\sum_{m_1=1}^{M_1}\left(\frac{N_{m_1}\rho_{0_{m_1}}}{2\nu_{m_1}}+\frac{\rho_{fb_{m_1}}}{\nu_{fb_{m_1}}}+\frac{\rho_{t_{m_1}}}{\nu_{t_{m_1}}}\right)-\sum_{m_s=1}^{M_s}\left(\frac{N_{m_s}\rho_{0_{m_s}}}{2\nu_{m_s}}+\frac{\rho_{fb_{m_s}}}{\nu_{fb_{m_s}}}+\frac{\rho_{t_{m_s}}}{\nu_{t_{m_s}}}\right)\right)}{\frac{\sqrt{N_1}}{\alpha_1}+\sum_{m_1=1}^{M_1}\left(\frac{N_{m_1}\rho_{0_{m_1}}}{2\nu_{m_1}}+\frac{\rho_{fb_{m_1}}}{\nu_{fb_{m_1}}}+\frac{\rho_{t_{m_1}}}{\nu_{t_{m_1}}}\right)} \tag{39.112a}$$

e.) the Poissonian probability of "association" is calculated (Eq. (39.106c)) with the "coupling cross section" amplitude, β_s^2, and frequency difference angle, ϕ_s, as parameters;

f.) a Poissonian probability operand with the expectation value given by the Poissonian probability of "association" (step e) is activated to return a value of zero or one;

g.) if the output of the Poissonian probability operand is one, then the two or more filtered inputs are marked as "associated" and this status is stored in memory;

h.) the process of forming "associations" (Steps a-g) are repeated

including processing the "SFCs" inputs and "associated" "SFCs" inputs with multiple "association ensembles" comprising Gaussian filters each of different delay, $\frac{\sqrt{N_s}}{\alpha_s}$, and half-width parameter, α_s to extend the number of associated "SFCs" to form a string;

i.) in one analog embodiment, the output $V_{\sum_m}$ in Fourier space is the "string" given by Eq. (39.113) comprising the superposition of S "groups of SFCs" wherein each "SFCs" corresponds to the response of M "M or P elements", with input context. In another embodiment, the output $V_{\sum_m}$ is the "string" of Eq. (39.114)

$$V_{\sum_{s,m}}\left(k_\rho,k_z\right)=\sum_{s=1}^{S}\sum_{m=1}^{M_s}\sum_{n=-\infty}^{\infty}\frac{4\pi}{1+\frac{k_z^2}{k_\rho^2}}a_{0_{s,m}}N_{s,m_{\rho_0}}N_{s,m_{z_0}}e^{-\frac{1}{2}\left(\frac{v_{s\rho 0}k_\rho}{\alpha_{s\rho 0}}\right)^2}e^{-j\frac{\sqrt{N_{s\rho 0}}}{\alpha_{s\rho 0}}\left(v_{s\rho 0}k_\rho\right)}e^{-\frac{1}{2}\left(\frac{v_{sz0}k_z}{\alpha_{sz0}}\right)^2}e^{-j\frac{\sqrt{N_{sz0}}}{\alpha_{sz0}}\left(v_{sz0}k_z\right)}$$

$$e^{-jk_\rho\left(\rho_{\beta s,m}+\rho_{ts,m}\right)}\sin c\left(k_\rho-n\frac{2\pi}{\rho_{0_{s,m}}}\right)\frac{N_{s,m_{\rho_0}}\rho_{0_{s,m}}}{2}\sin c\left(k_z-n\frac{2\pi}{v_{s,m}t_{0_{s,m}}}\right)\frac{N_{s,m_{z_0}}z_{0_{s,m}}}{2} \quad (39.114)$$

wherein each "SFCs" is multiplied by the Fourier transform of the delayed Gaussian filter (Eq. (39.50)) (i.e. the modulation factor $e^{-\frac{1}{2}\left(\frac{k_\rho}{\alpha_{s,m}}\right)^2}e^{-j\sqrt{N_{s,m}}\frac{k_\rho}{\alpha_{s,m}}}e^{-\frac{1}{2}\left(\frac{k_z}{\alpha_{s,m}}\right)^2}e^{-j\sqrt{N_{s,m}}\frac{k_z}{\alpha_{s,m}}}$) which gave rise to "coupling" and "association" to form the "string". In the digital case, the output $V_{\sum_m}$ in Fourier space is the "string" given by Eq. (39.113) comprising the superposition of S "groups of SFCs" wherein each "SFCs" corresponds to a matrix digitized according to Eq. (39.110), with input context. In another embodiment of the digital case, the output $V_{\sum_m}$ is the "string" of Eq. (39.114) wherein each "SFCs" corresponds to a matrix digitized according to Eq. (39.110) that is multiplied by a digitized matrix according to the Fourier transform of the delayed Gaussian filter (Eq. (39.50)) which gave rise to the "coupling" and "association" to form the "string".

"String" Ordering Layer

The "string" representing information is temporally or conceptually ordered via the Matrix Method of Analysis of Mills [8, 9]. Each "group of SFCs" of the input "string" has the corresponding time

delay parameter, $\frac{\sqrt{N_s}}{\alpha_s}$, and the half-width parameter, α_s, of the Gaussian filter of the "association ensemble" (Eq. (39.51)) that resulted in the "coupling" and "association" to form the "string".

$$h_N(t) \approx \frac{\alpha}{\sqrt{2\pi}} e^{-\frac{\left(t-\frac{\sqrt{N}}{\alpha}\right)^2}{\frac{2}{\alpha^2}}} \tag{39.51}$$

The "string" comprises a Fourier series, a linear sum of "FCs" each multiplied by its corresponding Gaussian filter modulation factor and modulation factor which encodes input context (Eq. (39.114)). Therefore, new series of "FCs", "SFCs" or "groups of SFCs", may be formed using additional "association filters" that sample the input "sting" in $k,\omega-space$. In a preferred embodiment, the string is sampled with specific "association ensembles" which provide a "nested set of subsets" of information comprised of a "SFCs" and "groups of SFCs" where each "subset" sampled from the input "string" maps to a specific time point corresponding to the specific delay, $\frac{\sqrt{N_s}}{\alpha_s}$, of the specific Gaussian filter of the "association ensemble" (Eqs. (39.50-39.51)). The process of ordering assigns a particular time delay, $\frac{\sqrt{N_{s'}}}{\alpha_{s'}}$, and half-width parameter, $\alpha_{s'}$, to each "subset" of the output "string" using the "nested set of subsets" as input to the Matrix Method which is herein presented as a mechanism used by the "processor" to sequence information temporally, conceptually, or according to causality.

Consider Eqs. (39.33) and (39.33a) which represent a "SFCs" in $k,\omega-space$ comprising a Fourier series. A "string" is a sum of Fourier series which follows from Eqs. (39.33) and (39.33a) and is given by Eqs. (39.107) and (39.108).

$$V_{\sum_{s,m}}\left(k_\rho,k_z\right) =$$

$$\sum_{s=1}^{S}\sum_{m=1}^{M_s}\sum_{n=-\infty}^{\infty}\frac{4\pi}{1+\frac{k_z^2}{k_\rho^2}}\frac{4}{\rho_{0_{s,m}}z_{0_{s,m}}}a_{0_{s,m}}\sin\left(k_\rho-n\frac{2\pi}{\rho_{0_{s,m}}}\frac{N_{s,m_{\rho 0}}\rho_{0_{s,m}}}{2}\right)\sin\left(k_z-n\frac{2\pi}{v_{s,m}t_{0_{s,m}}}\frac{N_{s,m_{z0}}z_{0_{s,m}}}{2}\right) \tag{39.107}$$

$$V_{\sum_{s,m}}\left(k_\rho,k_z\right)=\sum_{s=1}^{S}\sum_{m=1}^{M_s}\sum_{n=-\infty}^{\infty}\frac{4\pi}{1+\frac{k_z^2}{k_\rho^2}}\frac{4}{\rho_{0_{s,m}}z_{0_{s,m}}}a_{0_{s,m}}\frac{N_{s,m_{\rho_0}}\rho_{0_{s,m}}}{2}\frac{N_{s,m_{z_0}}z_{0_{s,m}}}{2}$$

$$\sin\left(k_\rho-n\frac{2\pi}{\rho_{0_{s,m}}}\frac{N_{s,m_{\rho_0}}\rho_{0_{s,m}}}{2}\right)\sin\left(k_z-n\frac{2\pi}{v_{s,m}t_{0_{s,m}}}\frac{N_{s,m_{z_0}}z_{0_{s,m}}}{2}\right)$$

$$=\sum_{s=1}^{S}\sum_{m=1}^{M_s}\sum_{n=-\infty}^{\infty}\frac{4\pi}{1+\frac{k_z^2}{k_\rho^2}}a_{0_{s,m}}N_{s,m_{\rho_0}}N_{s,m_{z_0}}\sin\left(k_\rho-n\frac{2\pi}{\rho_{0_{s,m}}}\frac{N_{s,m_{\rho_0}}\rho_{0_{s,m}}}{2}\right)\sin\left(k_z-n\frac{2\pi}{v_{s,m}t_{0_{s,m}}}\frac{N_{s,m_{z_0}}z_{0_{s,m}}}{2}\right)$$

(39.108)

The corresponding equations in the time domain are a sum of multiple finite series of traveling dipoles (each an "impulse response") wherein each dipole series is periodic in space and time. In frequency space, each time delayed Gaussian filter ("association ensemble" corresponding to a "SFCs") modulates and samples the Fourier series representing information. Thus, the time delayed Gaussian filter selects information from the "string" and provides input for the association mechanism as the "processor" implements the Matrix Method of Analysis to find the order of the associated pieces of information represented by each "SFCs" or "group of SFCs" of the "string".

Consider the time interval $t=t_i$ to $t=t_f$ of a "string" associated by "association ensembles" and recorded to memory. By processing the "string' with multiple "association ensembles" comprising Gaussian filters each of different delay, $\frac{\sqrt{N_s}}{\alpha_s}$, and half-width parameter, α_s, the "string" can be "broken" into "groups of SFCs" each having a center of mass at a time point corresponding to the delay $\frac{\sqrt{N_s}}{\alpha_s}$ and frequency composition corresponding to α_s which form a nested set of "sequential subsets" of "groups of SFCs" of the "string" in $k,\omega-$space which map to time points which are randomly positioned along the time interval from the $t=t_1$-side and the $t=t_2$-side as shown in FIGURES 8, 10, 12, and 14. This nested set of "sequential subsets" of random "groups of SFCs" mapping to random time points from the $t=t_i$-side and the $t=t_f$-side is analogous to the nested set of "sequential subsets" of random DNA fragments from the 5' end and the 3' end. The order in both cases can be solved by the Genomic DNA Sequencing Method/Matrix Method of Analysis of Mills [8, 9] described in SUB-APPENDIX V.

The output of an association filter is the convolution of the input "groups of SFCs" (each "SFCs" is given by Eqs. (39.33) and (39.33a)) of a

"string" (Eq. (39.108)) or the string itself with a delayed Gaussian. In terms of the matrix method of analysis (hereafter "MMA"), the filter parameter α of the time delayed Gaussian filter corresponds to the acquisition of the composition of a polynucleotide member of a nested set of subsets. The time delay (time domain) and modulation (frequency domain) parameter $\frac{\sqrt{N}}{\alpha}$ determines the center of mass of the output, and it corresponds to the terminal nucleotide data. By forming "associations" with input from "High Level Memory", the "processor" determines the relative position of the center of mass of each Fourier series such as a "group of SFCs" as either "before" or "after" the center of mass of the preceding and succeeding Fourier series "associated" with Fourier series input from "High Level Memory". The complete set of Fourier series "associated" with Fourier series input from "High Level Memory" covers all of the frequencies of the "string". By Parseval's theorem, by processing the entire interval in $k,\omega-$space, the information is entirely processed in the time domain. The order such as temporal order of the Fourier series representing information is determined using the MMA.

"Groups of SFCs" such as the "groups of SFCs" represented by Eq. (39.110) comprising a transducer frequency band modulation factor "carried" by "association ensembles" "couple" with Poissonian probability. "Associations" are established between "groups of SFCs" that result in the output of a second ordered "string" created from the input "string". In this case of input context, the "coupling cross section" amplitude, β_s^2, which follows from Eq. (39.87) is given by Eq. (39.111). And, the frequency difference angle, ϕ_s, of the "coupling" which follows from Eq. (39.89) is given by Eq. (39.112a).

Input to form "associations" is provided by changing the decay constant α and the number of "stages" in the cascade N, or by processing "a SFCs" of a "string" using an "association ensemble" with different parameters α and N over all "groups of SFCs" that make up the entire "string". Each "group of SFCs" is determined to be on the $t=t_i$-side or the $t=t_f$-side of the "axis" of the "string" corresponding to the 5'-side or 3'-side of the "axis" of a polynucleotide to be sequenced via the Matrix Method of Analysis. A feedback loop comprises sequentially switching to different "known", "set", or "hardwired" delayed Gaussian filters which corresponds to changing the decay constant, α_s, with a concomitant change in the half-width parameter, α_s, and the number of elements, N_s, with a concomitant change in the delay, $\frac{\sqrt{N_s}}{\alpha_s}$, where each

α_s and $\frac{\sqrt{N_s}}{\alpha_s}$ is "known" from past experiences and associations. The feedback loop whereby information from memory encoded in the "string" is filtered and delayed (modulated and sampled in frequency space) to provide "FCs", "SFCs" or "groups of SFCs" which are "associated" with input from "High Level Memory" provides the data acquisition and processing equivalent to the formation, acquisition, and analysis of the composition and terminal nucleotide data of a set of "sequential subsets" of the Matrix Method of Analysis. Changing the filters which process the "string" corresponds to changing the "guess" of the "known" nucleotides, $K_1K_2K_3K_4 \quad K_{n'}$, as well as the "unknown" nucleotides, $X_1, X_2, X_3, X_4 \quad$, of the Matrix Method of Analysis as applied to DNA sequencing. The order of the "groups of SFCs" of the "string" is established when "associations" with the "High Level Memory" are achieved for a given set of delayed Gaussian filters. Then each Fourier series of the ordered "string" is recorded to the "High Level Memory" wherein each Fourier series of the ordered "string" may be multiplied by the Fourier transform of the delayed Gaussian filter represented by $e^{-\frac{1}{2}\left(\frac{v_{s\rho 0}}{\alpha_{s\rho 0}}\frac{k_\rho}{}\right)^2} e^{-j\frac{\sqrt{N_{s\rho 0}}}{\alpha_{s\rho 0}}\left(v_{s\rho 0}k_\rho\right)} e^{-\frac{1}{2}\left(v_{sz0}\frac{k_z}{\alpha_{sz0}}\right)^2} e^{-j\frac{\sqrt{N_{sz0}}}{\alpha_{sz0}}\left(v_{sz0}k_z\right)}$ that established the correct order to form the ordered "string". The total output response $V_{\sum_m}$ in Fourier space comprising the superposition of S "groups of SFCs" wherein each "SFCs" corresponds to the response of M "M or P elements", with input context, is the "string" given by Eq. (39.113).

A summary of a method of ordering the nested set of subsets of Fourier series (e.g. each a "group of SFCs") follows:

a.) the "string" of the Association Filter Layer to Form a "String Section is recalled from memory;

b.) the recalled "string" is filtered and delayed (modulated and sampled in frequency space) to provide input to form "associations" with "High Level Memory" as given in the Association Filter Layer to Form a "String Section;

c.) a feedback loop is used to sequentially switch as described below to different "known", "standardized", "set", or "hardwired" delayed Gaussian filters which corresponds to changing the decay constant, α_s, with a concomitant change in the half-width parameter, α_s, and the number of elements, N_s, with a concomitant change in the

delay, $\frac{\sqrt{N_s}}{\alpha_s}$, where each α_s and $\frac{\sqrt{N_s}}{\alpha_s}$ is "known" or "standardized" from past "associations";

d.) "associations" are established between Fourier series by their "coupling" with Poissonian probability with Fourier series input from "High Level Memory" as given in the Association Filter Layer to Form a "String Section. The "associations" establish the relative position of the center of mass of each Fourier series such as a "group of SFCs" as either "before" or "after" the center of mass of the preceding and succeeding Fourier series "associated" with Fourier series input from "High Level Memory". The complete set of Fourier series "associated" with Fourier series input from "High Level Memory" covers all of the frequencies of the "string";

e.) "groups of SFCs" of a sequential "set of subsets" are sequentially mapped to a time line by being added to the "before" or "after" end of the emerging temporally, conceptually, or causally ordered "string" wherein assignment of each "group of SFCs" is consistent with the frequency compositional and center of mass data to arrive at the order of the entire "string";

f.) steps c)- e) are performed reiteratively until an order can be assigned without contradiction;

g.) the order of the associated "groups of SFCs" is established when "associations" with the "High Level Memory" are achieved for a given set of delayed Gaussian filters (i.e. the order is established when internal consistence is achieved with input from ordered "strings" of High Level Memory);

h.) the "groups of SFCs" of the " P string" of the form of Eqs. (39.113-39.115) that are parameterized according to their relative order are recorded to the "High Level Memory". For example, each Fourier series of the ordered string is recorded to the "High Level Memory" wherein each Fourier series of the ordered "string" is multiplied by the Fourier transform of the delayed Gaussian filter represented by $e^{-\frac{1}{2}\left(\frac{\nu_{sp0}}{\alpha_{sp0}}\frac{k_\rho}{}\right)^2} e^{-j\frac{\sqrt{N_{sp0}}}{\alpha_{sp0}}\left(\nu_{sp0}k_\rho\right)} e^{-\frac{1}{2}\left(\frac{\nu_{sz0}}{\alpha_{sz0}}\frac{k_z}{}\right)^2} e^{-j\frac{\sqrt{N_{sz0}}}{\alpha_{sz0}}\left(\nu_{sz0}k_z\right)}$ that established the correct order to form the ordered "string" represented by

$$V_{\sum_{s,m}}\left(k_\rho, k_z\right) = \sum_{s=1}^{S}\sum_{m=1}^{M_s}\sum_{n=-\infty}^{\infty} a_{0_{s,m}} N_{s,m_{\rho_0}} e^{-\frac{1}{2}\left(\frac{\nu_{s\rho 0}}{\alpha_{s\rho 0}}\frac{k_\rho}{}\right)^2} e^{-j\frac{\sqrt{N_{s\rho 0}}}{\alpha_{s\rho 0}}\left(\nu_{s\rho 0}k_\rho\right)} e^{-jk_\rho \rho_{fb_{s,m}}} \sin\left(k_\rho - n\frac{2\pi}{\rho_{0_{s,m}}}\right)\frac{N_{s,m_{\rho 0}}\rho_{0_{s,m}}}{2}$$

(39.115)

Output of the Ordered "String" to High Level Memory Layer with Formation of the Predominant Configuration

The activation of a "P element" increases its excitability or probability of future activation with input. Each "P element" has an activation memory with a finite half-life. Repetitive activation of a "P element" results in a longer half-life of the increased excitability; thus, the activation memory becomes long term. The same principle applies to cascade of association "stages" ("association ensembles") and M elements ("memory ensembles") and "configurations" of "couplings" of ensembles. For example, each "association ensemble" is comprised of "stages" in different states of "activity" where each state is equivalent to a microstate of statistical thermodynamics. A predominant configuration arises for any "association ensemble". Of the immense total number of microstates that can be assumed by an "association ensemble", an overwhelming proportion arises from one comparatively, small set of configurations centered on, and only minutely different from, the predominant configuration--with which they share an empirically identical set of macroscopic properties. On a higher level, a configuration of "couplings" between "association ensembles" increases the activation of the "stages" comprising the "association ensembles". Analogously to statistical thermodynamics, a predominant configuration arises from the "association ensemble" level. Consider the "processor" on a higher level. The activation history of each "association ensemble" relates to a hierarchical activation relationship of coupled "association ensembles" which gives rise to a precedence of higher order predominant configurations. The ability to associate information and create novel information, is a consequence. Machine learning arises by the feedback loop of transducer input to the coupled predominant configurations which increases the basis for creating information with novel conceptual content.

A summary of the method of Output of the Ordered "String" to High Level Memory Layer with Formation of the Predominant Configuration follows:

a.) the "groups of SFCs" of the " P string" of the form of Eqs. (39.113-39.115) that are parameterized according to their relative

order are recorded to the "High Level Memory";

b.) a counter corresponding to each "P string" and each "association ensemble" increases its stored count each time the "P string" or "association ensemble" is activated. In one embodiment, the count is also proportional to the length of time the "P string" or "association ensemble" is "active", and the count decays over time;

c.) the count is transformed into an expectation value and stored in a probability register which corresponds to each "string" and each "association ensemble";

d.) during the process of establishing "associations" a probability operand causes a given "P string" or "association ensemble" to become "active" with an expectation value according to the value stored in its corresponding probability register;

f.) on a lower level, the mechanism whereby past activation increases the probability of future activation applies to "P and M elements" as well;

e.) as more "P strings" are created, more "P elements", "M elements", and "stages" are activated, and more "association ensembles" are created and activated, the relationship of the probability of future activation based on past activation gives rise to a processing predominant configuration of the "processor" analogous to that of statistical thermodynamics.

SUB-APPENDIX I
The Input and the Band-Pass Filter of the Analog Fourier Processor

The "P element" "impulse response" is a traveling wave in one spatial dimension (ρ) plus time ($t = \frac{z}{v}$) where the wave function is a dipole traveling at a constant velocity v. The magnitude of the potential, V, in cylindrical spacetime coordinates at the point (ρ,z) due to an "impulse response" centered at the position (ρ_0, z_0) is

$$V = \frac{\left(2(z - z_0)^2 - (\rho - \rho_0)^2\right)}{[(\rho - \rho_0)^2 + (z - z_0)^2]^{5/2}} \tag{39.22}$$

$$V = \frac{\left(2z^2 - \rho^2\right)}{[\rho^2 + z^2]^{5/2}} \quad \delta(\rho - \rho_0, z - z_0) \tag{39.23}$$

where

$$z_0 = vt_0 \tag{39.24}$$

The potential is the convolution of the system function, $h(\rho,z)$, (the left-handed part of Eq. (39.23)) with the delta function (the right-hand part of Eq. (39.23)) at the position (ρ_0, z_0). A very important theorem of Fourier analysis states that the Fourier transform of a convolution is the product of the individual Fourier transforms, and the Fourier transform of a product is the convolution of the individual Fourier transforms [10]. The Fourier transform of the system function, $h(\rho,z)$, is given in Box 16.1 of the Superconductivity Section of Mills [11]. Also, see Mills [12].

An "impulse response" has the system function, $h(\rho,z)$, which has the Fourier transform, $H[k_\rho, k_z]$, which is shown in FIGURE 7.

$$H[k_\rho, k_z] = \frac{4\pi k_\rho^2}{k_z^2 + k_\rho^2} = \frac{4\pi}{1 + \frac{k_z^2}{k_\rho^2}} \tag{39.25}$$

The output of a "P element", V_{tr}, to an input of a pulse train of one or more "impulse responses" is another pulse train of "impulse responses". The spacetime "P element response", a pulse train function, is the convolution of the array pattern with the elemental pattern. The elemental pattern is the system function, $h(\rho,z)$,--the spacetime potential function of an "impulse response". And, the array pattern is a finite periodic array of delta functions each at the center position of an "impulse response".

$V_{tr}(\rho, z(t)) =$

$$\frac{\left(2z^2 - \rho^2\right)}{[\rho^2 + z^2]^{5/2}} \quad \sum_{n=1}^{\infty} a_n \delta(\rho - n\rho_0, z - nvt_0) X \left[U\left(\rho + \frac{N\rho_0}{2}, z + \frac{Nvt_0}{2}\right) - U\left(\rho - \frac{N\rho_0}{2}, z - \frac{Nvt_0}{2}\right) \right]$$

(39.26)

where a_n is a constant and $U\left(\rho+\frac{N\rho_0}{2},z+\frac{Nvt_0}{2}\right)$ is the unitary step function at $\rho=\frac{-N\rho_0}{2}$ *and* $z=\frac{-Nz_0}{2}=\frac{-Nvt_0}{2}$ and $U\left(\rho-\frac{N\rho_0}{2},z-\frac{Nvt_0}{2}\right)$ is the unitary step function at position $\rho=\frac{N\rho_0}{2}$ *and* $z=\frac{Nz_0}{2}=\frac{Nvt_0}{2}$. Multiple "P elements" input into any given "P element" which then outputs to multiple "P elements". And, the amplitude, frequency, and length of the "P element response" (pulse train) is proportional to the length and rate of voltage change--the amplitude and rate of change of the input. Thus, each "P element" is an linear differentiator--the output, V_{0ut}, is the sum (superposition) of the derivative of the inputs. An exemplary output signal of an analog "P element" to an input of the form given by Eq. (39.26) is

$$V_{Out}(\rho,z(t)) = \frac{\delta^2}{\delta\rho\delta z}\left[\frac{\left(2z^2-\rho^2\right)}{\left[\rho^2+z^2\right]^{5/2}}\sum_{n=1}^{\infty}a_n\delta\left(\rho-n\rho_0,z-nvt_0\right)\right] X\left[U\left(\rho+\frac{N\rho_0}{2},z+\frac{Nvt_0}{2}\right)-U\left(\rho-\frac{N\rho_0}{2},z-\frac{Nvt_0}{2}\right)\right] \quad (39.27)$$

The Fourier Transform of the periodic array of delta functions of Eq. (39.27) is also a periodic array of delta functions in $k,\omega-$space

$$\frac{1}{\rho_0 z_0}\sum_{n=-\infty}^{\infty}a_n\delta\left(k_\rho-n\frac{2\pi}{\rho_0},k_z-n\frac{2\pi}{vt_0}\right) \quad (39.28)$$

where $z_0=vt_0$. The Fourier Transform of the window function given by the difference of the unitary step functions of Eq. (39.27) is the product of two sinc functions in $k,\omega-$space

$$4\frac{\sin k_\rho\frac{N\rho_0}{2}}{k_\rho}\frac{\sin k_z\frac{Nz_0}{2}}{k_z} \quad (39.29)$$

By the Fourier Theorem, the Fourier Transform of Eq. (39.26) is the product of the Fourier Transform of the elemental function, system function given by Eq. (39.25), and the Fourier Transform of the array function given by Eq. (39.28) convolved with the Fourier transform of the window function given by Eq. (39.29).

$$\frac{4\pi}{1+\frac{k_z^2}{k_\rho^2}}\frac{1}{\rho_0 z_0}\sum_{n=-\infty}^{\infty}a_n\delta\left(k_\rho-n\frac{2\pi}{\rho_0},k_z-n\frac{2\pi}{vt_0}\right)\;4\frac{\sin k_\rho\frac{N\rho_0}{2}}{k_\rho}\frac{\sin k_z\frac{Nz_0}{2}}{k_z} \quad (39.30)$$

Each "P element" is an linear differentiator--the output is the sum (superposition) of the derivative of the inputs. The differentiation property of Fourier transforms [13] is

$$x(t) = \int_{-\infty}^{\infty} X(f) e^{j2\pi ft} df \qquad X(t) = \int_{-\infty}^{\infty} x(t) e^{-j2\pi ft} dt$$

(39.31)

$$\textit{Differentiation} \qquad \frac{dx(t)}{dt} \quad \Leftrightarrow \quad j2\pi f X(f)$$

From Eqs. (39.30) and (39.31), the Fourier transform of a "P element response", $V\left(k_\rho, k_z\right)$, called a "FC" is

$$V\left(k_\rho, k_z\right) = k_\rho k_z \frac{4\pi}{1+\frac{k_z^2}{k_\rho^2}} \frac{1}{\rho_0 z_0} \sum_{n=-\infty}^{\infty} a_n \delta\left(k_\rho - n\frac{2\pi}{\rho_0}, k_z - n\frac{2\pi}{vt_0}\right) 4\frac{\sin k_\rho \frac{N\rho_0}{2}}{k_\rho} \frac{\sin k_z \frac{Nz_0}{2}}{k_z}$$

$$= \frac{4\pi}{1+\frac{k_z^2}{k_\rho^2}} \frac{1}{\rho_0 z_0} \sum_{n=-\infty}^{\infty} a_n \delta\left(k_\rho - n\frac{2\pi}{\rho_0}, k_z - n\frac{2\pi}{vt_0}\right) 4\sin k_\rho \frac{N\rho_0}{2} \sin k_z \frac{Nz_0}{2} \qquad (39.32)$$

$$= \frac{4\pi}{1+\frac{k_z^2}{k_\rho^2}} \frac{4}{\rho_0 z_0} \sum_{n=-\infty}^{\infty} a_0 \sin\left(k_\rho - n\frac{2\pi}{\rho_0}\frac{N\rho_0}{2}\right) \sin\left(k_z - n\frac{2\pi}{vt_0}\frac{Nz_0}{2}\right)$$

Information "carried" by "P elements" may be represented by a Fourier series called a "SFCs" (series of Fourier components) comprising the superposition of the "P element responses" of multiple "P elements". Each "P element" contributes a Fourier component comprising an amplitude, a_{0_m}, at a specific frequency, $\frac{N_m\rho_{0_m}}{2}$, $\frac{N_m\rho_{0_m}}{2}$, which is repeated as a series with a specific phase, $\frac{nN_m}{2}$. A "SFCs" comprising the Fourier transform of the superposition of the "P element responses" of M "P elements", $V_{\sum_m}$, is represented by

$$V_{\sum_m}\left(k_\rho, k_z\right) = \sum_{m=1}^{M} \sum_{n=-\infty}^{\infty} \frac{4\pi}{1+\frac{k_z^2}{k_\rho^2}} \frac{4}{\rho_{0_m} z_{0_m}} a_{0_m} \sin\left(k_\rho - n\frac{2\pi}{\rho_{0_m}}\frac{N_{m_{\rho 0}}\rho_{0_m}}{2}\right) \sin\left(k_z - n\frac{2\pi}{vt_0}\frac{N_{m_{z0}} z_{0_m}}{2}\right)$$

(39.33)

Each "FC" of Eqs. (39.33) is a series of a Fourier component with quantized frequency and phase angle.

Consider the case that the amplitude of all "P element responses", are equal where each amplitude is represented by a_{0_m}. The "P element

response" function given by Eq. (39.33) corresponds to recording to memory ("writing"). Consider the case that memory elements are activated to read the stored information. In one embodiment, this "read" operation is effected by a voltage ramp that is linear with time. The Fourier transform of the response is given by the differentiation and duality properties of Fourier transforms [13]. The "read" total response $V_{\sum_m}$ in Fourier space comprising a "SFCs", the superposition of M "FCs" wherein each "FC" corresponds to the response of a "M or P element" is $V_{\sum_m}\left(k_\rho, k_z\right)$

$$= \sum_{m=1}^{M} \sum_{n=-\infty}^{\infty} \frac{4\pi}{1+\frac{k_z^2}{k_\rho^2}} \frac{4}{\rho_{0_m} z_{0_m}} a_{0_m} \frac{N_{m_{\rho 0}} \rho_{0_m}}{2} \frac{N_{m_{z0}} z_{0_m}}{2} \sin\left(k_\rho - n\frac{2\pi}{\rho_{0_m}}\frac{N_{m_{\rho 0}} \rho_{0_m}}{2}\right) \sin\left(k_z - n\frac{2\pi}{v_m t_{0_m}}\frac{N_{m_{z0}} z_{0_m}}{2}\right)$$

$$= \sum_{m=1}^{M} \sum_{n=-\infty}^{\infty} \frac{4\pi}{1+\frac{k_z^2}{k_\rho^2}} a_{0_m} N_{m_{\rho 0}} N_{m_{z0}} \sin\left(k_\rho - n\frac{2\pi}{\rho_{0_m}}\frac{N_{m_{\rho 0}} \rho_{0_m}}{2}\right) \sin\left(k_z - n\frac{2\pi}{v_m t_{0_m}}\frac{N_{m_{z0}} z_{0_m}}{2}\right) \tag{39.33a}$$

Each "FC" of Eqs. (39.33a) is a series of a Fourier component with quantized amplitude, frequency, and phase angle.

The relationship between $k,\omega-$space and real space is

$$\begin{aligned} k_\rho &= \frac{2\pi}{\lambda_\rho} = \frac{2\pi}{\rho} = \frac{2\pi}{n\rho_0} \\ k_z &= \frac{2\pi}{\lambda_z} = \frac{2\pi}{z} = \frac{2\pi}{nvt_0} \end{aligned} \tag{39.34}$$

In $k,\omega-$space, the Fourier transform of the "impulse response" function (the left-hand side of Eq. (39.33)) filters each "FC" of a "P element". In the special case that

$$k_\rho = k_z \tag{39.35}$$

the Fourier Transform of the system function (the left-hand side of Eq. (39.33)) is given by

$$H = 4\pi \tag{39.36}$$

Thus, the Fourier Transform of the system function band-passes the Fourier Transform of the time dependent "P element response" function when the spatial frequency of the "FC" is equal to the temporal frequency. In one embodiment, "FC" filtering may be provided by adjusting the "P element" response corresponding to k_ρ versus k_z such that the band-pass condition of Eq. (39.35) is not met. In an analog embodiment, the "FC" may be filtered by adjusting the "impulse response" frequency as a function of time and therefore space

corresponding to k_ρ since the "impulse response" is a traveling wave. In another analog embodiment, the "FC" may be filtered by adjusting the conduction velocity which alters the output corresponding to k_z.

When the band-pass condition is met (Eq. (39.35)), the Fourier transform of the superposition of a series of pulse trains of "impulse responses" of multiple "P elements" representing information is a series of trigonometric functions. Thus, in one embodiment of the present invention, the "processor" is an analog Fourier processor. According to the Fourier theorem any waveform can be recreated by an infinite series of trigonometric functions.

$$x(t) = a_0 + \sum_{n=1}^{\infty} a_n \cos\omega_n t + \sum_{n=1}^{\infty} b_n \sin\omega_n t \tag{39.37}$$

where a_0, a_n, and b_n are constants. And, any aspect of the universe can be represented by an infinite series of sine and cosine functions as processed by the "processor". For the present "processor", the trigonometric function is the basis element of information. And, the complexity or information content of any analog waveform or digital equivalent is reducible to the number of Fourier components required for its assimilation.

A unique feature of the present invention is that information is encoded in a Fourier series in k,ω −space versus a conventional Fourier series in time and space.

SUB-APPENDIX II
Modulation and Sampling Gives the Input to the Association Mechanism and Basis of Reasoning

Each "P element" connects to multiple other "P elements" which further connect to association "stages" that propagate the "P element responses" as input along these "stages" in a linear cascade. Consider an amplifier made up of cascaded stages. The stages need not be identical. Let $h_i(t)$ be the impulse response of the i^{th} stage and assume that $h_i(t) \geq 0$, so that the step response of each stage (or indeed of any number of cascaded stages) is monotonic. Assuming that both integrals exist, T_i, the normalized first moment of $h_i(t)$ is defined as

$$T_i = \frac{\int_{-\infty}^{\infty} t h_i(t) dt}{\int_{-\infty}^{\infty} h_i(t) dt} \tag{39.38}$$

which can be interpreted as the center of gravity of a mass distributed along the t-axis with density $h_i(t)$. If $h_i(t)$ is positive, it is analogous to a probability density function, and T_i corresponds to the statistical analog--the mean of $h_i(t)$. Thus, T_i is considered as the measure of the delay in the impulse or step response of the i^{th} stage. The delay resulting from a cascade of n stages is the sum of the delays of each stage [14]; that is if

$$h(t) = h_1(t) \quad h_2(t) \qquad h_n(t) \tag{39.39}$$

where is the convolution operator, then

$$T = T_1 + T_2 + \qquad T_n + \tag{39.40}$$

Similarly, assuming that both integrals exist, $\left(\frac{\Delta T_i}{2}\right)^2$, the normalized moment of inertia about a center of gravity of a mass distribution $h_i(t)$ is defined as

$$\begin{aligned} (\Delta T_i)^2 &= 4\left[\frac{\int_{-\infty}^{\infty} t^2 h_i(t) dt}{\int_{-\infty}^{\infty} h_i(t) dt} - T_i^2\right] \\ &= 4\frac{\int_{-\infty}^{\infty} (t - T_i)^2 h_i(t) dt}{\int_{-\infty}^{\infty} h_i(t) dt} \end{aligned} \tag{39.41}$$

If $h_i(t)$ is positive, it is analogous to a probability density function, and

$\left(\frac{\Delta T_i}{2}\right)^2$ can be interpreted as the statistical analog--the variance or dispersion of $h_i(t)$. ΔT_i is twice the radius of gyration of the mass distribution. Thus, ΔT_i is a measure of the duration of $h_i(t)$ or of the rise time of the step response of the i^{th} stage. The rise time resulting from a cascade of n stages is the sum of the rise times of each stage [15]; that is if $h(t)$ is given by Eq. (39.39), then

$$(\Delta T)^2 = (\Delta T_1)^2 + (\Delta T_2)^2 + \cdots + (\Delta T_n)^2 \tag{39.42}$$

Thus, in particular, for identical stages, the rise time is proportional to the square root of the number of stages. If $h_i(t)$ is not positive, rather than the definition of Eq. (39.41), the measure of duration is better defined as

$$\begin{aligned}(\Delta T)^2 &= 4\left[\frac{\int_{-\infty}^{\infty} t^2 h^2(t)\,dt}{\int_{-\infty}^{\infty} h^2(t)\,dt} - \left(\frac{\int_{-\infty}^{\infty} t h^2(t)\,dt}{\int_{-\infty}^{\infty} h^2(t)\,dt}\right)^2\right] \\ &= 4\frac{\int_{-\infty}^{\infty} (t - T_i)^2 h_i(t)\,dt}{\int_{-\infty}^{\infty} h_i(t)\,dt}\end{aligned} \tag{39.43}$$

In many ways ΔT of Eq. (39.43) is the most analytically satisfactory simple general measure of duration; for virtually any $h_i(t)$ for which the integrals exist, Eq. (39.43) will give a reasonable estimate of duration. Equivalently, possibly the best simple measure of bandwidth for real lowpass waveforms is

$$(\Delta W)^2 = 4\frac{\int_{-\infty}^{\infty} f^2 |H(f)|^2\,df}{\int_{-\infty}^{\infty} |H(f)|^2\,df} \tag{39.44}$$

From the definitions of ΔT and ΔW given by Eq. (39.43) and Eq. (39.44), respectively, it is possible to prove the following *Uncertainty Principle* [14]:

> For any real waveform for which ΔT and ΔW of Eq. (39.41) and Eq. (39.43) exist,
>
> $$\Delta T \Delta W \geq \frac{1}{\pi} \tag{39.45}$$

In other words, ΔT and ΔW cannot simultaneously be arbitrarily small: A

short duration implies a large bandwidth, and a small-bandwidth waveform must last for a long time.

Consider a cascade of association "stages". The Uncertainty Principle given by Eq. (39.45) applies to the "P element response" as it is transmitted from one "stage" to another in the cascade. In one embodiment, the "voltage" decays exponentially at the junction or linkage of any two "stages". The cascade forms a filter, and an ideal filter response is that which has the smallest duration-bandwidth product in the sense of Eqs. (39.43) and (39.44). Such a response is a Gaussian pulse which also has the same form in the time and space domain [14]. However, a Gaussian pulse cannot be the impulse response of any casual system, even with substantial delay. Consider, for example, an N-stage amplifier with the impulse response of each stage equal to

$$h(t) = \alpha\sqrt{N}e^{-\alpha\sqrt{N}t}u(t) \tag{39.46}$$

The frequency response of the cascade of N such stages is

$$H_N(f) = \left[H(f)\right]^N = \left(\frac{1}{1+\frac{j2\pi f}{\alpha\sqrt{N}}}\right)^N \tag{39.47}$$

The shape of $H_N(f)$ for large N can be determined by taking logarithms and using the power series expansion

$$\ln(1+x) = x - \frac{x^2}{2} + \frac{x^3}{3}... \tag{39.48}$$

The power series expansion of the $\ln H_N$ is

$$\begin{aligned} \ln H_N &= -N\left[\frac{j2\pi f}{\alpha\sqrt{N}} - \frac{1}{2}\left(\frac{j2\pi f}{\alpha\sqrt{N}}\right)^2 + \frac{1}{3}\left(\frac{j2\pi f}{\alpha\sqrt{N}}\right)^3 ...\right] \\ &\approx -j\frac{2\pi f}{\alpha}\sqrt{N} - \frac{1}{2}\left(\frac{2\pi f}{\alpha}\right)^2 \end{aligned} \tag{39.49}$$

where the remaining terms vanish as fast as $\frac{1}{\sqrt{N}}$ for large N. Thus, the frequency response tends to

$$H_N(f) \approx e^{-\frac{1}{2}\left(\frac{2\pi f}{\alpha}\right)^2} e^{-j\sqrt{N}\left(\frac{2\pi f}{\alpha}\right)} \tag{39.50}$$

for large N, and the impulse response of the cascade tends to

$$h_N(t) \approx \frac{\alpha}{\sqrt{2\pi}} e^{-\frac{\left(t-\frac{\sqrt{N}}{\alpha}\right)^2}{\frac{2}{\alpha^2}}} \tag{39.51}$$

that is, a Gaussian pulse delayed by $\frac{\sqrt{N}}{\alpha}$. This result is a very special

case of a remarkable theorem [15]--the Central Limit Theorem of probability theory--which states in effect that, under very general conditions, the cascade of a large number of linear-time-invariant (LTI) systems will tend to have a Gaussian impulse response, almost independent of the characteristics of the systems cascaded. Sufficient conditions of the Central Limit Theorem are that

1. The absolute third moments,

$$\int_{-\infty}^{\infty} |t|^3 h_i(t)dt \tag{39.52}$$

exist for all components of the systems and are uniformly bounded;

2. The durations, ΔT_i, of the component systems in the sense of Eq. (39.43) satisfy the relation

$$\lim_{N\to\infty} \frac{1}{N} \sum_{i=1}^{N} (\Delta T_i)^2 \neq 0 \tag{39.53}$$

For large N, the first condition allows the higher order terms in the expansion such as Eq. (39.49) to be ignored, and the second condition guarantees that no finite subset of the component systems will dominate the result because the remainder have relatively wide bandwidths. Given this theorem, it follows from Eqs. (39.38-39.45) [14] that the overall impulse response of N cascaded stages is approximately

$$h(t) \approx \frac{k}{\sqrt{2\pi}\Delta T} e^{\frac{(t-T)^2}{2(\Delta T)^2}} \tag{39.54}$$

where T and ΔT are given by Eq. (39.40) and Eq. (39.42), respectively, and

$$k = \prod_{i=1}^{N} \int_{-\infty}^{\infty} h_i(t)dt \tag{39.55}$$

Eq. (39.54) is a filter function. Consider Eq. (39.33) where the Fourier transform of the superposition of "P element responses" (the sum of multiple pulse trains of "impulse responses" representing information) is given by a series of trigonometric functions wherein the "processor" can be an analog Fourier processor. The input of information to the association mechanism arises as the Fourier series is modulated and sampled. Consider the output of a cascade of association "stages"--each with an "impulse response". The "stages" are cascaded as an N-stage amplifier with the transmission impulse response of each stage in one embodiment equal to that of a decaying exponential given by Eq. (39.46). The filtered signal is the sum of the convolution of the

response of each transmission stage of the cascade with each "P element response". Using the distributive, commutative, and associative laws of the convolution operation and using the Central Limit Theorem, the filtered signal is the convolution of the superposition of the "P element responses" over the cascade of "stages" also given by Eq. (39.27) with the Gaussian response given by Eq. (39.51). A very important theorem of Fourier analysis states that the Fourier transform of a convolution is the product of the individual Fourier transforms [10]. Thus, the output of a cascade of N stages each with a transmission decay constant α (corresponding to the transmission impulse response) is the product of Eq. (39.33) and Eq. (39.50). By changing the decay constant α and the number of "stages" N in the cascade, Fourier series representing information including that from memory can be filtered and delayed (modulated and sampled in frequency space) to provide input to form associations of the Association Filter Layer. For example, consider the result on exemplary filter functions and the corresponding Fourier transforms shown in FIGURES 8 to 15 as the decay constant α and the number of "stages" N of each corresponding cascade are altered. In frequency space, the time delayed Gaussian filter corresponds to modulation and sampling of the Fourier series representation of the memory output comprising the superposition of multiple "M element responses". Thus, the time delayed Gaussian filter selects memory output and provides input for the association mechanism and basis of reasoning.

In another embodiment, the time delayed Gaussian filter may be modulated in the time domain to effect a frequency shift in $k,\omega-$space. The shift follows from Eq. (39.109) and the duality property of Fourier transforms [13].

SUB-APPENDIX III
The Association Mechanism and Basis of Reasoning

"Coupling"

A cascade of association "stages" called an "association ensemble" is "activated" with input from "M elements", "P elements", or "stages" of a different "association ensemble". The "association ensemble" is "active" if it is "carrying" a Fourier series such as a "SFCs" wherein "active" in the digital case may refer to a recall of an "SFCs" from memory followed by steps a-i of the Association Filter Layer to Form a "String" Section. The "association ensemble" is "inactive" if it has no output and is not "carrying" a Fourier series such as a "SFCs" wherein "inactive" in the digital case may refer to no recall of an "SFCs" from memory.

In an analog embodiment, the "stages" of an "association ensemble" are intraconnected and interconnected. A first "active" cascade of association "stages" can interfere with and "couple" with a second set, third set, etc. The probability distribution function of "coupling" between a first "active" "association ensemble" and at least one other "active" "association ensemble" is Poissonian. Each "association ensemble" is comprised of a large number of cascaded association "stages" each weakly linked to one or more "stages" of the one or more different "association ensembles". (The "coupling" is analogous to interference between coherent or harmonic states.) The probability $P_{\uparrow}\left(\frac{\sqrt{N_1}}{\alpha_1},\frac{\sqrt{N_2}}{\alpha_2},...,\frac{\sqrt{N_s}}{\alpha_s}\right)$ that a first "active" cascade of association "stages" with modulation $e^{-j\sqrt{N_1}\left(\frac{2\pi f}{\alpha_1}\right)}$ given by Eq. (39.50) will interfere with and "couple" with s separate "active" cascades of association "stages" ("association ensembles") each with modulation $e^{-j\sqrt{N_s}\left(\frac{2\pi f}{\alpha_s}\right)}$ given by Eq. (39.50) can be derived from the correlation function (Eq. (39.78) for the statistical average of the large number of possible "couplings" between the individual weakly linked "stages".

The physical behavior of a large number of "active" cascaded association "stages" (an "association ensemble") each weakly linked to provide a Poissonian probability of "coupling" to one or more "stages" of one or more different "association ensembles" is equivalent to that of the interaction of ultrasound with Mössbauer gamma rays. Each "association ensemble" "carries" a Fourier series in k,ω −space such as a "M or P element response" which comprises a sum of harmonic functions. Thus, physically, the former case corresponds to interference

of a first Fourier series input filtered by an "association ensemble" with a second, third, or s th Fourier series input filtered by s th "association ensemble". The latter case corresponds to interference of an electronic transition and an oscillator transition. In both cases, a harmonic energized state interferes with another.

Consider the Lamb-Mössbauer formula for the absorption of a γ ray of energy E by a nucleus in a crystal given by Maradudin [16].

$$\sigma_a(E) = \frac{1}{4}\sigma_0\Gamma^2 \sum_{mn} e^{-\frac{\beta E_m}{Z}} X \frac{\langle m|e^{i\left(\frac{\mathbf{p}}{\hbar}\right)\cdot\mathbf{R}(l)}|n\rangle\langle n|e^{-i\left(\frac{\mathbf{p}}{\hbar}\right)\cdot\mathbf{R}(l)}|m\rangle}{\left(E_0 - E + E_n - E_m\right)^2 + \frac{1}{4}\Gamma^2} \tag{39.56}$$

In this equation, E_0 is the energy difference between the final and initial nuclear states of the absorbing nucleus, E_m and E_n are the energies of the eigenstates $|m\rangle$ and $|n\rangle$ of the crystal, respectively, Γ is the natural width of the excited state of the nucleus, $\mathbf{p}$ is the momentum of the γ ray, $\mathbf{R}(l)$ is the instantaneous position vector of the absorbing nucleus, Z is the crystal's partition function, $T = (k\beta)^{-1}$, and σ_0 is the resonance absorption cross section for the absorbing nucleus. By expressing the denominator of Eq. (39.56) as an integral, Eq. (39.56) is equivalent to

$$\sigma_a(E) = \frac{1}{2}\sigma_0\gamma \int_{-\infty}^{\infty} dt e^{i\omega t - \gamma|t|} X\left\langle \exp\left[-i\mathbf{k}\cdot\mathbf{u}(l;t)\right]\exp\left[i\mathbf{k}\cdot\mathbf{u}(l;0)\right]\right\rangle \tag{39.57}$$

wherein the position vector $\mathbf{R}(l)$ is

$$\mathbf{R}(l) = \mathbf{x}(l) + \mathbf{u}(l) \tag{39.58}$$

For, Eq. (39.58), $\mathbf{x}(l)$ is the position vector of the mean position of the absorbing nucleus, and $\mathbf{u}(l)$ is its displacement from the mean position. Eq. (39.57) follows from Eq. (39.56) with the following substitutions:

$$\left(\frac{1}{\hbar}\right)\mathbf{p} = \mathbf{k} \tag{39.59}$$

$$\hbar\omega = E - E_0 \tag{39.60}$$

$$\gamma = \frac{\Gamma}{2\hbar} \tag{39.61}$$

and $\mathbf{u}(l;t)$ denotes the Heisenberg operator,

$$\mathbf{u}(l;t) = e^{i\left(\frac{t}{\hbar}\right)H}\mathbf{u}(l;0)e^{-i\left(\frac{t}{\hbar}\right)H} \tag{39.62}$$

where H is the Hamiltonian. The angular brackets in Eq. (39.57) denote an average over the canonical ensemble of the crystal.

The correlation function for the statistical average of a large number of "active" cascaded association "stages" (an "association ensemble") each weakly coupled to one or more "stages" of one or more different "active" "association ensembles" is equivalent to that of the interaction of ultrasound with Mössbauer gamma rays. From Eq.

(39.57), the correlation function $Q(t)$ of acoustically modulated gamma ray absorption by Mössbauer nuclei is

$$Q(t) = \left\langle \exp\left[-i\mathbf{k}\ \mathbf{u}(l;t)\right] \exp\left[i\mathbf{k}\ \mathbf{u}(l;0)\right] \right\rangle \tag{39.63}$$

In the present case, $\mathbf{u}(l)$ corresponds to the delay of an "association ensemble" s comprising a time delayed Gaussian filter. In k,ω −space, the time delay corresponds to a modulation of the s th Fourier series (e.g. "P or M element response" given by Eq. (39.33)) that is "carried" by the "association ensemble" s). Since the Fourier series is a sum of trigonometric functions in k,ω −space, the modulation corresponds to a frequency shift of the Fourier series "carried" by the "association ensemble" s. $\mathbf{k}$ of Eq. (39.59) corresponds to the wavenumber of the frequency shifted s th Fourier series. $\frac{E - E_0}{\hbar}$ of Eq. (39.60) is the shifted frequency of a first Fourier series that is "carried" by a first "association ensemble".

In the case of acoustically modulated gamma ray absorption by Mössbauer nuclei, $\mathbf{u}(l;t)$ of Eq. (39.62) is

$$\mathbf{u}(l;t) = e^{i\left(\frac{E}{\hbar}\right)t}\,\mathbf{u}(l;0)\,e^{-i\left(\frac{E}{\hbar}\right)t} \tag{39.64}$$

The matrix elements of Eq. (39.63) are calculated by using the theorem [17]

$$e^A e^B = e^{A+B} e^{\frac{1}{2}[A,B]} \qquad \text{if } \left[[A,B],A\right] = \left[[A,B],B\right] = 0 \tag{39.65}$$

For a harmonic oscillator, the commutator of $\mathbf{k}\ \mathbf{u}(l;t)$ and $\mathbf{k}\ \mathbf{u}(l;0)$ is a c number; thus,

$$\begin{aligned} Q(t) &= \left\langle \exp\left[-i\mathbf{k}\ \mathbf{u}(l;t)\right] \exp\left[i\mathbf{k}\ \mathbf{u}(l;0)\right] \right\rangle \\ &= \left\langle \exp\left[-i\mathbf{k}\ \left[\mathbf{u}(l;t) - \mathbf{u}(l;0)\right]\right] \right\rangle X \exp\left[\frac{1}{2}\left\langle \left[\mathbf{k}\ \mathbf{u}(l;t),\ \mathbf{k}\ \mathbf{u}(l;0)\right] \right\rangle\right] \end{aligned} \tag{39.66}$$

Since the correlation function applies to an ensemble of harmonic oscillator states, the first thermodynamic average can be simplified as follows:

$$\left\langle \exp\left[-i\mathbf{k}\ \left[\mathbf{u}(l;t) - \mathbf{u}(l;0)\right]\right] \right\rangle = \exp\left[-\frac{1}{2}\left\langle \left\{\mathbf{k}\ \left[\mathbf{u}(l;t) - \mathbf{u}(l;0)\right]\right\}^2 \right\rangle\right] \tag{39.67}$$

This theorem is known in lattice dynamics as Ott's theorem [18] or sometimes as Bloch's theorem [19]. Using the time independence of the harmonic potential, Eq. (39.67) is

$$\exp\left[-\frac{1}{2}\left\langle \left\{\mathbf{k}\ \left[\mathbf{u}(l;t) - \mathbf{u}(l;0)\right]\right\}^2 \right\rangle\right] = \exp\left[-\frac{1}{2}\left\langle \left[\mathbf{k}\ \mathbf{u}(l;t)\right]^2 \right\rangle + \frac{1}{2}\left\langle \left[\mathbf{k}\ \mathbf{u}(l;0)\right]^2 \right\rangle\right] \tag{39.68}$$

$$= \exp\left[-\left\langle \left[\mathbf{k}\ \mathbf{u}(l)\right]^2 \right\rangle\right] \tag{39.69}$$

Substitution of Eqs. (39.67-39.69) into Eq. (39.66) gives

$$Q(t) = \exp\left\langle -\left[\mathbf{k}\ \mathbf{u}(l;t)\right]^2 \right\rangle X \exp\left[\frac{1}{2}\left\langle \left[\mathbf{k}\ \mathbf{u}(l;t),\ \mathbf{k}\ \mathbf{u}(l;0)\right]\right\rangle\right] \tag{39.70}$$

Expanding $\mathbf{u}_\alpha(l;t)$ in terms of the normal coordinates of the harmonic potential and the phonon operators of that harmonic potential gives

$$u_\alpha(l;t) = \left(\frac{\hbar}{2M_l}\right)^{\frac{1}{2}} \sum_s \frac{B_\alpha^{(s)}(l)}{(\omega_s)^{\frac{1}{2}}}\left(b_s e^{-i\omega_s t} + b_s^\dagger e^{i\omega_s t}\right) \tag{39.71}$$

where α labels the Cartesian components, M_l is the mass of the ion in the lth experiment, ω_s is the frequency of the sth normal mode, $B^{(s)}(l)$ is the associated unit eigenvector, and $b_s^\dagger$ and b_s are the phonon creation and destruction operators for the sth normal mode. By use of the coordinate expansion, the exponential of the correlation function appearing in Eq. (39.70) can be written as

$$\begin{aligned} e^{\langle \mathbf{k}\,\mathbf{u}(l;t)\mathbf{k}\,\mathbf{u}(l;0)\rangle} &= e^{\sum_s -c_s^2\left(\frac{e^{i\omega_s t}}{(\gamma_s)^{\frac{1}{2}}} + (\gamma_s)^{\frac{1}{2}} e^{-i\omega_s t}\right)} \\ &= \prod_s e^{-c_s^2\left(\frac{e^{i\omega_s t}}{(\gamma_s)^{\frac{1}{2}}} + (\gamma_s)^{\frac{1}{2}} e^{-i\omega_s t}\right)} \\ &= \prod_s \left[J_0\left(2c_s^2\right) + \sum_{n=1}^{\infty} J_n\left(2c_s^2\right)\left(\frac{e^{i\omega_s t}}{(\gamma_s)^{\frac{1}{2}}} + (\gamma_s)^{\frac{1}{2}} e^{-i\omega_s t}\right)^n\right] \end{aligned} \tag{39.72}$$

where the following substitutions were made:

$$\gamma_s = \frac{n_s + 1}{n_s} = e^{\frac{\hbar\omega_s}{kT}} \tag{39.73}$$

$$n_s = \frac{1}{e^{\frac{\hbar\omega_s}{kT}} - 1} \tag{39.74}$$

$$c_s^2 = \frac{\hbar}{2M_l}\frac{\left[k\ B^{(s)}(l)\right]^2}{\omega_s}\frac{e^{\frac{\hbar\omega_s}{2kT}}}{e^{\frac{\hbar\omega_s}{kT}} - 1} \tag{39.75}$$

and where the Bessel function relationship [20]

$$e^{\frac{1}{2}x\left(y+y^{-1}\right)} = \sum_{n=-\infty}^{\infty} J_n(x) y^n \tag{39.76}$$

was used. n_s is the mean number of phonons in the sth mode at temperature T.

In the case of "coupling" between a first "active" "association ensemble" and at least one other "active" "association ensemble", the correlation function is independent of time--not a function of $e^{i\omega_s t}$ and $e^{-i\omega_s t}$. Thus, the time dependent factors are dropped in Eq. (39.72), and combining Eqs. (39.70-39.72) and Eq. (39.75) gives the correlation

function as

$$Q\left(c_s^2\right) = \exp -c_s^2 \prod_s J_0\left(2c_s^2\right) \tag{39.77}$$

For the "coupling" of "active" "association ensembles", the partition function of Eq. (39.56) is equal to one. By the Central Limit Theorem, $s = 1$ in Eq. (39.72) corresponds to each cascade of association "stages" giving rise to a specific frequency shift. The correlation function for each "association ensemble" is

$$Q\left(c_s^2\right) = \exp -\left[c_s^2\right] J_0\left(2c_s^2\right) \tag{39.78}$$

The probability $P_{\uparrow}\left(\frac{\sqrt{N_1}}{\alpha_1}, \frac{\sqrt{N_2}}{\alpha_2}, ..., \frac{\sqrt{N_s}}{\alpha_s}\right)$ that a first "active" "association ensemble" will "couple" with s "active" "association ensembles" can be derived from the correlation function, Eq. (39.78). The expansion of the Bessel function is

$$\begin{aligned} J_\nu(x) &= \left(\frac{x}{2}\right)^\nu \sum_{m=0}^{\infty} \frac{\left(\frac{-x^2}{4}\right)^m}{\left[m!\Gamma(m+\nu+1)\right]} \\ J_0(x) &= \sum_{m=0}^{\infty} \frac{\left(\frac{-x^2}{4}\right)^m}{\left[m!\Gamma(m+1)\right]} = \sum_{m=0}^{\infty} \frac{\left(\frac{-x^2}{4}\right)^m}{[m!m!]} \end{aligned} \tag{39.79}$$

where $\Gamma(m+1) = m!$ was used. The probability distribution function of "coupling" between "association ensembles" (coherent states) is Poissonian. From SUB-APPENDIX II--Modulation and Sampling Gives the Input to the Association Mechanism and Basis of Reasoning, the output of a cascade of N "stages" with a transmission decay constant α is the product of Eq. (39.33) and Eq. (39.50). From Eqs. (39.40), (39.42), (39.46), (39.50), (39.51), and (39.54), the frequency shift of "association ensemble" one is $\frac{\sqrt{N_1}}{\alpha_1}$, and the frequency shift of "association ensemble" s is $\frac{\sqrt{N_s}}{\alpha_s}$ where the impulse response of each "stage" in both "association ensembles" is

$$h(t) = \alpha\sqrt{N} e^{-\alpha\sqrt{N}t} u(t) \tag{39.80}$$

"Coupling" of filtered Fourier series is based on their spectral similarity. In one embodiment, the "coupling cross section" amplitude, β_s^2, is given by the integral of the product of the spectrum of the first Fourier series sampled and modulated by the first "association ensemble" and the complex conjugate of the spectrum of the s th Fourier series sampled and modulated by the s th "association

ensemble". The spectrum of a Fourier series ("SFCs") sampled and modulated by an "association ensemble" is given by the product of Eq. (39.33) and Eq. (39.50). Thus, Eq. (39.75) is

$$\beta_s^2 = \int_0^\infty \int_0^\infty V_1\left(k_\rho, k_z(f)\right) V_s^*\left(k_\rho, k_z(f)\right) H_N(f)_1 H_N^*(f)_s \, df dk_\rho \tag{39.81}$$

$$\beta_s^2 = \int_0^\infty \int_0^\infty \left(\frac{4\pi}{1+\frac{k_z^2}{k_\rho^2}}\right)^2 e^{-\frac{1}{2}\left(\frac{2\pi f}{\alpha_1}\right)^2} e^{-j\sqrt{N_1}\left(\frac{2\pi f}{\alpha_1}\right)} e^{-\frac{1}{2}\left(\frac{2\pi f}{\alpha_s}\right)^2} e^{+j\sqrt{N_s}\left(\frac{2\pi f}{\alpha_s}\right)}$$

$$\sum_{m_1=1}^{M_1} \frac{4}{\rho_{0_{m_1}} z_{0_{m_1}}} a_{0_{m_1}} \sum_{n=-\infty}^{\infty} \sin\left(k_\rho - n\frac{2\pi}{\rho_{0_{m_1}}}\right)\frac{N_{m_1}\rho_{0_{m_1}}}{2} \sin\left(k_z - n\frac{2\pi}{v_{m_1} t_{0_{m_1}}}\right)\frac{N_{m_1} z_{0_{m_1}}}{2}$$

$$\sum_{m_s=1}^{M_s} \frac{4}{\rho_{0_{m_s}} z_{0_{m_s}}} a_{0_{m_s}} \sum_{n=-\infty}^{\infty} e^{-j\pi k_\rho} \sin\left(k_\rho - n\frac{2\pi}{\rho_{0_{m_s}}}\right)\frac{N_{m_s}\rho_{0_{m_s}}}{2} e^{-j\pi k_z} \sin\left(k_z - n\frac{2\pi}{v_{m_s} t_{0_{m_s}}}\right)\frac{N_{m_s} z_{0_{m_s}}}{2} df dk_\rho \tag{39.82}$$

Let $k_\rho = k_z$, then $\rho_0 = z_0 = vt_0$. Thus, Eq. (39.82) is

$$\beta_s^2 = \int_0^\infty (8\pi)^2 \sum_{m_1=1}^{M_1} \frac{4}{\rho_{0_{m_1}} z_{0_{m_1}}} a_{0_{m_1}} \sum_{n=-\infty}^{\infty} \sin\left(k_z - n\frac{2\pi}{v_{m_1} t_{0_{m_1}}}\right)\frac{N_{m_1} z_{0_{m_1}}}{2} e^{-\frac{1}{2}\left(\frac{2\pi f}{\alpha_1}\right)^2} e^{-j\sqrt{N_1}\left(\frac{2\pi f}{\alpha_1}\right)}$$

$$\sum_{m_s=1}^{M_s} \frac{4}{\rho_{0_{m_s}} z_{0_{m_s}}} a_{0_{m_s}} \sum_{n=-\infty}^{\infty} e^{-j\pi k_z} \sin\left(k_z - n\frac{2\pi}{v_{m_s} t_{0_{m_s}}}\right)\frac{N_{m_s} z_{0_{m_s}}}{2} e^{-\frac{1}{2}\left(\frac{2\pi f}{\alpha_s}\right)^2} e^{+j\sqrt{N_s}\left(\frac{2\pi f}{\alpha_s}\right)} df \tag{39.83}$$

Substitution of $k_z = \frac{2\pi f}{v}$ and $\sin\theta = e^{-j\theta}$ into Eq. (39.83) gives

$$\beta_s^2 = \int_0^\infty (8\pi)^2 \sum_{m_1=1}^{M_1} \frac{4}{\rho_{0_{m_1}} z_{0_{m_1}}} a_{0_{m_1}} \sum_{n=-\infty}^{\infty} e^{-j\left(\frac{2\pi f}{v_{m_1}} - n\frac{2\pi}{v_{m_1} t_{0_{m_1}}}\right)\frac{N_{m_1} z_{0_{m_1}}}{2}} e^{-\frac{1}{2}\left(\frac{2\pi f}{\alpha_1}\right)^2} e^{-j\sqrt{N_1}\left(\frac{2\pi f}{\alpha_1}\right)}$$

$$\sum_{m_s=1}^{M_s} \frac{4}{\rho_{0_{m_s}} z_{0_{m_s}}} a_{0_{m_s}} \sum_{n=-\infty}^{\infty} e^{+j\left(\frac{2\pi f}{v_{m_s}} - n\frac{2\pi}{v_{m_s} t_{0_{m_s}}}\right)\frac{N_{m_s} z_{0_{m_s}}}{2}} e^{-\frac{1}{2}\left(\frac{2\pi f}{\alpha_s}\right)^2} e^{+j\sqrt{N_s}\left(\frac{2\pi f}{\alpha_s}\right)} df \tag{39.84}$$

The integral of Eq. (39.84) is given by Hogg and Tanis [21]

$$\beta_s^2 = (8\pi)^2 \frac{1}{\sqrt{2\pi}} \sqrt{\frac{\alpha_1^2 \alpha_s^2}{\alpha_1^2 + \alpha_s^2}} \sum_{m_1=1}^{M_1} \frac{4}{\rho_{0_{m_1}} z_{0_{m_1}}} a_{0_{m_1}} \sum_{m_s=1}^{M_s} \frac{4}{\rho_{0_{m_s}} z_{0_{m_s}}} a_{0_{m_s}}$$

$$\sum_{n'=-\infty}^{\infty} \sum_{n=-\infty}^{\infty} \left| \cos 2\pi \left(\frac{nN_{m_1} z_{0_{m_1}}}{2v_{m_1} t_{0_{m_1}}} - \frac{n' N_{m_s} z_{0_{m_s}}}{2v_{m_s} t_{0_{m_s}}} \right) \right| \exp - \left\{ \frac{\frac{\alpha_1^2 \alpha_s^2}{\alpha_1^2 + \alpha_s^2} \left(\frac{\sqrt{N_1}}{\alpha_1} - \frac{\sqrt{N_s}}{\alpha_s} + \frac{N_{m_1} z_{0_{m_1}}}{2v_{m_1}} - \frac{N_{m_s} z_{0_{m_s}}}{2v_{m_s}} \right)^2}{2} \right\} \tag{39.85}$$

where $\sigma^2 = \frac{\alpha_1^2 \alpha_s^2}{\alpha_1^2 + \alpha_s^2}$ and $t = -j\left(\frac{\sqrt{N_1}}{\alpha_1} - \frac{\sqrt{N_s}}{\alpha_s} + \frac{N_{m_1} z_{0_{m_1}}}{2v_{m_1}} - \frac{N_{m_s} z_{0_{m_s}}}{2v_{m_s}} \right)$ in corresponding integrals. It was given previously (Eq. (39.83)) that $\rho_0 = z_0 = vt_0$; thus, Eq. (39.85) simplifies to

$$\beta_s^2 = (8\pi)^2 \frac{1}{\sqrt{2\pi}} \sqrt{\frac{\alpha_1^2 \alpha_s^2}{\alpha_1^2 + \alpha_s^2}} \sum_{m_1=1}^{M_1} \frac{4}{\rho_{0_{m_1}}^2} a_{0_{m_1}} \sum_{m_s=1}^{M_s} \frac{4}{\rho_{0_{m_s}}^2} a_{0_{m_s}}$$

$$\sum_{n'=-\infty}^{\infty} \sum_{n=-\infty}^{\infty} \left| \cos \pi \left(nN_{m_1} - n' N_{m_s} \right) \right| \exp - \left\{ \frac{\frac{\alpha_1^2 \alpha_s^2}{\alpha_1^2 + \alpha_s^2} \left(\frac{\sqrt{N_1}}{\alpha_1} - \frac{\sqrt{N_s}}{\alpha_s} + \frac{N_{m_1} t_{0_{m_1}}}{2} - \frac{N_{m_s} t_{0_{m_s}}}{2} \right)^2}{2} \right\} \tag{39.86}$$

where $\sigma^2 = \frac{\alpha_1^2 \alpha_s^2}{\alpha_1^2 + \alpha_s^2}$ and $t = -j\left(\frac{\sqrt{N_1}}{\alpha_1} - \frac{\sqrt{N_s}}{\alpha_s} + \frac{N_{m_1} t_{0_{m_1}}}{2} - \frac{N_{m_s} t_{0_{m_s}}}{2} \right)$ in corresponding integrals. Consider the case that the amplitude of all "P element responses" are equal, thus $a_{0_{m_1}} = a_{0_{m_s}}$ *for all* m_1 *and* m_s in Eq. (39.86). In the case that each "SFCs" is represented by Eq. (39.33a), Eq. (39.86) is

$$\beta_s^2 = (8\pi)^2 \frac{1}{\sqrt{2\pi}} \sqrt{\frac{\alpha_1^2 \alpha_s^2}{\alpha_1^2 + \alpha_s^2}} \sum_{m_1=1}^{M_1} a_{0_{m_1}} N_{m_1} \sum_{m_s=1}^{M_s} a_{0_{m_s}} N_{m_s}$$

$$\sum_{n'=-\infty}^{\infty} \sum_{n=-\infty}^{\infty} \left| \cos \pi \left(nN_{m_1} - n' N_{m_s} \right) \right| \exp - \left\{ \frac{\frac{\alpha_1^2 \alpha_s^2}{\alpha_1^2 + \alpha_s^2} \left(\frac{\sqrt{N_1}}{\alpha_1} - \frac{\sqrt{N_s}}{\alpha_s} + \frac{N_{m_1} t_{0_{m_1}}}{2} - \frac{N_{m_s} t_{0_{m_s}}}{2} \right)^2}{2} \right\} \tag{39.87a}$$

where $\sigma^2 = \frac{\alpha_1^2 \alpha_s^2}{\alpha_1^2 + \alpha_s^2}$ and $t = -j\left(\frac{\sqrt{N_1}}{\alpha_1} - \frac{\sqrt{N_s}}{\alpha_s} + \frac{N_{m_1} t_{0_{m_1}}}{2} - \frac{N_{m_s} t_{0_{m_s}}}{2}\right)$ in corresponding integrals.

In one embodiment, the present "processor" is an analog Fourier processor wherein the data is digitized according to the parameter N of Eqs. (39.33), (39.33a), and (39.87). Each "FC" of Eqs. (39.33) is a series of a Fourier component with quantized frequency and phase angle. Each "FC" of Eqs. (39.33a) is a series of a Fourier component with quantized amplitude, frequency, and phase angle. Each "SFCs" represented by Eq. (39.33) and Eq. (39.33a) is filtered and delayed in the time domain (modulated and sampled in the frequency domain) as it is recalled from memory and processed by an "association ensemble". "Association ensembles" produce interference or "coupling" of the "SFCs" of one set of "M or P elements" with that of another by producing frequency matched and phase locked Fourier series --sums of trigonometric waves that are frequency matched and periodically in phase--that give rise to "association" of the corresponding recalled or processed information. The Poissonian probability of such "coupling" (Eq. (39.106)) can be derived from the correlation function (Eq. (39.78) wherein Eq. (39.87) is a parameter. The magnitude of the "coupling cross section" of Eq. (39.87a) and Eq. (39.86) is independent of any phase matching condition because the phase angle is quantized. Thus, the argument of the cosine function of Eq. (39.87a) and Eq. (39.86) is zero or an integer multiple of π. Consequentially, in each case, the corresponding time convolution of Eq. (39.84) is a cyclic convolution, and the sum over n is eliminated. Whereas, the frequency matching condition provided by the frequency shifts of the cascades of association "stages" comprises the zero argument of the exponential function of Eq. (39.87a). Thus, the magnitude of the "coupling cross section" follows from Eq. (39.87a)

$$\beta_s^2 = (8\pi)^2 \frac{1}{\sqrt{2\pi}} \sqrt{\frac{\alpha_1^2 \alpha_s^2}{\alpha_1^2 + \alpha_s^2}}$$

$$\sum_{m_1=1}^{M_1} a_{0_{m_1}} N_{m_1} \sum_{m_s=1}^{M_s} a_{0_{m_s}} N_{m_s} \exp - \left\{ \frac{\frac{\alpha_1^2 \alpha_s^2}{\alpha_1^2 + \alpha_s^2} \left(\frac{\sqrt{N_1}}{\alpha_1} - \frac{\sqrt{N_s}}{\alpha_s} + \frac{N_{m_1} t_{0_{m_1}}}{2} - \frac{N_{m_s} t_{0_{m_s}}}{2} \right)^2}{2} \right\} \tag{39.87b}$$

In terms of the relationship $\rho_0 = z_0 = vt_0$, Eq. (39.87b) is

$$\beta_s^2 = (8\pi)^2 \frac{1}{\sqrt{2\pi}} \sqrt{\frac{\alpha_1^2 \alpha_s^2}{\alpha_1^2 + \alpha_s^2}}$$

$$\sum_{m_1=1}^{M_1} a_{0_{m_1}} N_{m_1} \sum_{m_s=1}^{M_s} a_{0_{m_s}} N_{m_s} \exp - \left\{ \frac{\frac{\alpha_1^2 \alpha_s^2}{\alpha_1^2 + \alpha_s^2} \left(\frac{\sqrt{N_1}}{\alpha_1} - \frac{\sqrt{N_s}}{\alpha_s} + \frac{N_{m_1} \rho_{0_{m_1}}}{2\nu_{m_1}} - \frac{N_{m_s} \rho_{0_{m_s}}}{2\nu_{m_s}} \right)^2}{2} \right\} \tag{39.87c}$$

"Coupling" between "active" "association ensembles" further depends on the frequency difference angle, ϕ_s, between the two or more Fourier series "carried" by the corresponding "association ensembles". In $k,\omega-space$, the information is represented as Fourier series which comprise sums of harmonic functions. Thus, the "coupling cross section" is a complex number with a projection in $k,\omega-space$ that is a function of the frequency shift $\frac{\sqrt{N_1}}{\alpha_1}$ of the first "association ensemble" and the frequency shift $\frac{\sqrt{N_s}}{\alpha_s}$ of the s th "association ensemble". The frequency shift of each "association ensemble" corresponds to the respective modulation function given by the Fourier transform of the delayed Gaussian filter (Eq. (39.50)). The resultant "coupling cross section", $\langle \beta_s^2(\phi_s) \rangle$, as a function of frequency difference angle, ϕ_s, is given by

$$\langle \beta_s^2(\phi_s) \rangle = \beta_s^2 e^{i2\phi_s} \tag{39.88}$$

where the frequency difference angle, ϕ_s, is

$$\phi_s = \frac{\pi \left(\frac{\sqrt{N_1}}{\alpha_1} - \frac{\sqrt{N_s}}{\alpha_s} + \sum_{m_1=1}^{M_1} \frac{N_{m_1} \rho_{0_{m_1}}}{2\nu_{m_1}} - \sum_{m_s=1}^{M_s} \frac{N_{m_s} \rho_{0_{m_s}}}{2\nu_{m_s}} \right)}{\frac{\sqrt{N_1}}{\alpha_1} + \sum_{m_1=1}^{M_1} \frac{N_{m_1} \rho_{0_{m_1}}}{2\nu_{m_1}}} \tag{39.89}$$

Thus, the "coupling cross section" given by Eq. (39.88) is a dimensionless complex number that comprises a "coupling cross section" amplitude, β_s^2, and frequency difference angle, ϕ_s, of the harmonic "coupling". In other embodiments of the present invention, further operations may be performed on $\langle \beta_s^2(\phi_s) \rangle$ such as phase shifting, normalizing to a given parameter, scaling, multiplication by a factor or parameter such as a gain factor, addition or subtraction of a given parameter or number such as an offset, etc. In a further embodiment,

$\left\langle \beta_s^2(\phi_s) \right\rangle$ may be represented by different equations than those such as Eq.(39.87c) and Eq. (39.81) that also represent the spectral similarity and difference of the frequencies of filtered or unfiltered Fourier series that may "couple".

In the case that $\rho_0 = z_0 = vt_0$, the frequency difference, ϕ_s, is

$$\phi_s = \frac{\pi\left(\frac{\sqrt{N_1}}{\alpha_1} - \frac{\sqrt{N_s}}{\alpha_s} + \sum_{m_1=1}^{M_1} \frac{N_{m_1} t_{0_{m_1}}}{2} - \sum_{m_s=1}^{M_s} \frac{N_{m_s} t_{0_{m_s}}}{2}\right)}{\frac{\sqrt{N_1}}{\alpha_1} + \sum_{m_1=1}^{M_1} \frac{N_{m_1} t_{0_{m_1}}}{2}} \tag{39.90}$$

The probability distribution of "coupling" between two "association ensembles" each "carrying" a Fourier series such as a "SFCs" is Poissonian with mean number of "stage" "couplings"

$$\langle n \rangle = \beta^2 \tag{39.91}$$

The probability [22] of "coupling" with a second "association ensemble" with m "couplings" between "stages" is

$$P_m = \frac{\langle n \rangle^m e^{-\langle n \rangle}}{m!} = \frac{\left(\beta^2\right)^m e^{-\beta^2}}{m!} = \frac{\beta^{2m} e^{-\beta^2}}{m!} \tag{39.93}$$

with mean number of "stage" "coupling" events $\langle n \rangle = \beta^2$. The probability $P_\uparrow\left(\frac{\sqrt{N_1}}{\alpha_1}, \frac{\sqrt{N_2}}{\alpha_2}, ..., \frac{\sqrt{N_s}}{\alpha_s}\right)$ can be derived by factoring Eq. (39.93) from the Bessel function of the correlation function (Eq. (39.78)) and its expansion which follows from Eq. (39.79).

$$\begin{aligned} J_0(x) &= \sum_{m=0}^{\infty} \frac{\left(\frac{-x^2}{4}\right)^m}{[m!m!]}; \\ J_0(\beta x) &= \sum_{m=0}^{\infty} \frac{\left(\frac{-(\beta x)^2}{4}\right)^m}{m!m!} = \frac{1}{e^{-\beta^2}} \sum_{m=0}^{\infty} \frac{\left(\frac{-x^2}{4}\right)^m}{m!} \frac{\beta^{2m} e^{-\beta^2}}{m!} \end{aligned} \tag{39.94}$$

Combining Eq. (39.93) and Eq. (39.94) demonstrates that the probability $P_\uparrow\left(\frac{\sqrt{N_1}}{\alpha_1}, \frac{\sqrt{N_s}}{\alpha_s}\right) = P_\uparrow(\beta x)$ is proportional to

$$P_\uparrow(\beta x) \quad \sum_{m=0}^{\infty} \frac{\left(\frac{-x^2}{4}\right)^m}{m!} \tag{39.95}$$

Let $x = y^2$, then the change of variable in Eq. (39.95) is

$$P_{\uparrow}(\beta y) \quad \sum_{m=0}^{\infty} \frac{\left(\frac{-x}{4}\right)^{m}}{m!} = \sum_{m=0}^{\infty} \frac{\left(\frac{-x^2}{4}\right)^{m/2}}{m!} \tag{39.96}$$

Let $m' = m/2$, then the change of variable in Eq. (39.96) is

$$P_{\uparrow}(\beta y) \quad \sum_{m=0}^{\infty} \frac{\left(\frac{-x^2}{4}\right)^{m/2}}{m!} \quad \sum_{m=0}^{\infty} \frac{\left(\frac{-x^2}{4}\right)^{m'}}{(2m')!} \tag{39.97}$$

The series expansion of $\cos(x)$ is

$$\cos(x) = \sum_{m=0}^{\infty} \frac{\left(-x^2\right)^{m}}{(2m)!} \tag{39.98}$$

Combining Eq. (39.78) and Eqs. (39.95-39.98) gives the probability $P_{\uparrow}\left(\frac{\sqrt{N_1}}{\alpha_1}, \frac{\sqrt{N_s}}{\alpha_s}\right)$ proportional to

$$P_{\uparrow}\left(\frac{\sqrt{N_1}}{\alpha_1}, \frac{\sqrt{N_s}}{\alpha_s}\right) \quad \cos\left(2\beta\sqrt{c_s^2}\right) \tag{39.99}$$

where $y = \sqrt{x} = \sqrt{c_s^2}$. From Eqs. (39.81-39.90),

$$c_s^2 = \beta^{-2}(\phi_s) = \beta_s^{-2}\sin^2\phi_s \tag{39.100}$$

Combining Eq. (39.99) and Eq. (39.100) gives the probability $P_{\uparrow}\left(\frac{\sqrt{N_1}}{\alpha_1}, \frac{\sqrt{N_s}}{\alpha_s}\right)$ proportional to

$$P_{\uparrow}\left(\frac{\sqrt{N_1}}{\alpha_1}, \frac{\sqrt{N_s}}{\alpha_s}\right) \quad \cos\left(2\sin\phi_s\right) \tag{39.101}$$

where ϕ_s is the frequency difference angle. Combining Eq. (39.78), Eq. (39.100), and Eq. (39.101) gives the probability $P_{\downarrow}(\phi)$ proportional to

$$P_{\uparrow}\left(\frac{\sqrt{N_1}}{\alpha_1}, \frac{\sqrt{N_s}}{\alpha_s}\right) \quad \exp\left[-\beta_s^{-2}\sin^2\phi_s\right]\cos\left(2\sin\phi_s\right) = \exp\left[-\beta_s^{-2}\left(\frac{1-\cos 2\phi_s}{2}\right)\right]\cos\left(2\sin\phi_s\right) \tag{39.102}$$

where ϕ_s is the frequency difference angle and β_s^2 is the "coupling cross section" amplitude.

According to the time delay property of Fourier transforms [13], a time delay, $\delta(t - t_0)$, during independent activation of a given "association ensemble" with recall from memory is equivalent to a phase shift of the correlation function given by Eq. (39.63)

$$Q(t) = \left\langle \exp i\delta \exp\left[-i\mathbf{k}\ \mathbf{u}(l;t)\right]\exp\left[i\mathbf{k}\ \mathbf{u}(l;0)\right]\right\rangle \tag{39.103}$$

Thus, Eq. (39.102) is phase shifted.

$$P_{\uparrow}\left(\frac{\sqrt{N_1}}{\alpha_1},\frac{\sqrt{N_s}}{\alpha_s},\delta_s\right) \quad \exp\left[-\beta_s^{-2}\left(\frac{1-\cos 2\phi_s}{2}\right)\right]\cos\left(\delta_s + 2\sin\phi_s\right) \qquad (39.104)$$

where ϕ_s is the frequency difference angle, β_s^2 is the "coupling cross section" amplitude, and δ_s is the phase shift.

In an analog embodiment, each of the *s* separate "association ensembles" that may "couple " with the first "active" "association ensemble" may be "inactive" before "coupling". The "coupling" causes the corresponding "association ensemble" to become "active". Eq. (39.104) represents the probability that a first "active" "association ensemble" will "couple" with *s* "active" "association ensembles" as a function of the frequency difference angle, ϕ_s, the "coupling cross section" amplitude, β_s^2, and the phase shift, δ_s. Eq. (39.104) also represents the probability that a first "active" "association ensemble" will "couple" with and "activate" *s* "inactive" "association ensembles" as a function of the frequency difference angle, ϕ_s, the "coupling cross section" amplitude, β_s^2, and the phase shift, δ_s. In the latter case, the Fourier series such as a "SFCs" "carried" by the "activated" *s* th "association ensemble" may be "linked" with the "association ensemble". The "linkage" is as described for "transducer strings" in SUB-APPENDIX VI--Input Context.

"Association"

Given that a first "association ensemble" is "active", the probability of the occurrence of either the "active" state or the "inactive" state of the *s* th "association ensemble" is one. In one embodiment, in the absence of interference (i.e. "coupling") between the "association ensembles", the probability of the occurrence of the "active" state of the *s* th "association ensemble" is the same as the probability of the occurrence of the "inactive" state--1/2. However, in the event that "coupling" between the first and *s* th "association ensemble" may occur, the *s* th "association ensemble" may be "activated". The probability of the occurrence of the "active" state of the *s* th "association ensemble" with the possibility of "coupling" with the first "active" "association ensemble" is 1/2 plus the probability function, Eq. (39.104), normalized to 1/2. Therefore, given that the first "active " "association ensemble" may "couple" with the *s* th "association ensemble", the probability function for the occurrence of the "active" state of the *s* th "association ensemble" is

$$P_A\left(\frac{\sqrt{N_1}}{\alpha_1},\frac{\sqrt{N_s}}{\alpha_s},\delta_s\right)=\frac{1+\exp\left[-\beta_s^{-2}\left(\frac{1-\cos 2\phi_s}{2}\right)\right]\cos\left(\delta_s+2\sin\phi_s\right)}{2} \quad (39.105)$$

where ϕ_s is the frequency difference angle, β_s^2 is the "coupling cross section" amplitude, and δ_s is the phase shift.

In an embodiment, the two Fourier series (e.g. each a "SFCs") are "associated" if they are "active" simultaneously. Thus, given that the first "active" "association ensemble" may "couple" with the s th "association ensemble", Eq. (39.105) is the probability function for the occurrence of the "association" of the Fourier series of the first "active" "association ensemble" with that which may be "carried" by the s th "association ensemble" as a function of the frequency difference angle, ϕ_s, the "coupling cross section" amplitude, β_s^2, and the phase shift, δ_s.

The probability of the occurrence of "association" between a first Fourier series and s other Fourier series $P_A\left(\frac{\sqrt{N_1}}{\alpha_1},\frac{\sqrt{N_2}}{\alpha_2},...,\frac{\sqrt{N_s}}{\alpha_s},\delta_s\right)$ wherein the first "active" "association ensemble" may "couple" with each of s "association ensembles" is the product of the probabilities

$$P_A\left(\frac{\sqrt{N_1}}{\alpha_1},\frac{\sqrt{N_2}}{\alpha_2},...,\frac{\sqrt{N_s}}{\alpha_s},\delta_s\right)=\prod_s\frac{1+\exp\left[-\beta_s^{-2}\left(\frac{1-\cos 2\phi_s}{2}\right)\right]\cos\left(\delta_s+2\sin\phi_s\right)}{2} \quad (39.106a)$$

wherein the first "association ensemble" provides modulation $e^{-j\sqrt{N_1}\left(\frac{2\pi f}{\alpha_1}\right)}$ given by Eq. (39.50), the s th "association ensembles" provides modulation $e^{-j\sqrt{N_s}\left(\frac{2\pi f}{\alpha_s}\right)}$ given by Eq. (39.50, ϕ_s is the frequency difference angle, β_s^2 is the "coupling cross section" amplitude, and δ_s is the phase shift. The plot of the probability $P_A\left(\frac{\sqrt{N_1}}{\alpha_1},\frac{\sqrt{N_2}}{\alpha_2},...,\frac{\sqrt{N_s}}{\alpha_s},\delta_s\right)$ of the occurrence of "association" of the first Fourier series with the s th Fourier series according to Eq. (39.106a) is given in FIGURES 16 A-C and FIGURES 17 A-D.

In another embodiment, in the absence of "coupling" between the "association ensembles", the probability of the occurrence of "association" is $p_\uparrow$. With the replacement of 1/2 of Eq.(39.106a) with $p_\uparrow$, the probability of the occurrence of "association" of the corresponding Fourier series based on a first "active" "association ensemble" "coupling" with s separate "association ensembles" is

$$P_A\left(\frac{\sqrt{N_1}}{\alpha_1},\frac{\sqrt{N_2}}{\alpha_2},...,\frac{\sqrt{N_s}}{\alpha_s},p_{\uparrow s},\delta_s\right)=\prod_s\left[p_{\uparrow s}+\left(1-p_{\uparrow s}\right)\exp\left[-\beta_s^{-2}\left(\frac{1-\cos 2\phi_s}{2}\right)\right]\cos\left(\delta_s+2\sin\phi_s\right)\right] \quad (39.106b)$$

where $p_{\uparrow s}$ is the probability of the occurrence of "association" in the absence of "coupling", ϕ_s is the frequency difference angle, β_s^2 is the "coupling cross section" amplitude, and δ_s is the phase shift.

Eq.(39.106b) gives one as the maximum probability of the occurrence of "association". In other embodiments, the probability maximum may be less than one. In this case, Eq. (39.106b) is

$$P_A\left(\frac{\sqrt{N_1}}{\alpha_1},\frac{\sqrt{N_2}}{\alpha_2},...,\frac{\sqrt{N_s}}{\alpha_s},P,p_{\uparrow s},\delta_s\right) \quad (39.106c)$$
$$=\prod_s\left[p_{\uparrow s}+\left(P-p_{\uparrow s}\right)\exp\left[-\beta_s^{-2}\left(\frac{1-\cos 2\phi_s}{2}\right)\right]\cos\left(\delta_s+2\sin\phi_s\right)\right]$$

where P is the maximum probability of the occurrence of "association". Eq. (39.105) and Eq. (39.106) represent the "association" probability parameter.

The probability of "association" of Fourier series was herein derived for Poissonian statistics using delayed Gaussian filters; however, the invention is not limited to Poissonian statistics and the use of Gaussian filters. In other embodiments, the "association" can be based on alternative statistics corresponding to their respective distributions. Examples are Gaussian or normal statistics, binomial statistics, Chi-square statistics, F statistics, and t statistics. Other statistical distributions are given in Hogg and Tanis [23] which are herein incorporated by reference. Furthermore, in other embodiments, the "association" can be base on alternative filters such as Butterworth, band pass, low pass, and high pass filters. Other filters are given in Siebert [24] which are herein incorporated by reference.

In an analog embodiment, "coupling" may potentiate the two or more Fourier series. For example, each signal in the time domain corresponding to the Fourier series $k,\omega-$space may repeat in time and therefore increase in duration. In an embodiment, potentiated Fourier series are recorded to memory as "associated" with a probability that depends of the potentiation. In an embodiment, the probability is given by Eq. (39.106c) wherein the potentiation is via "coupling".

Eq. (39.106c) also applies to the probability of "association" between a first "active" "association ensemble" and s "active" "association ensembles". In this case, an equivalent digital embodiment comprises the recall of Fourier series such as two or more "SFCs" from memory followed by steps a-i of the Association Filter Layer to Form a

"String" Section.

Eq. (39.106) gives the probability $P_A\left(\frac{\sqrt{N_1}}{\alpha_1},\frac{\sqrt{N_2}}{\alpha_2},...,\frac{\sqrt{N_s}}{\alpha_s},\delta_s\right)$ of the occurrence of "association" of the corresponding Fourier series based on a first "active" "association ensemble" with modulation $e^{-j\sqrt{N_1}\left(\frac{2\pi f}{\alpha_1}\right)}$ given by Eq. (39.50) "coupling" with s separate "association ensembles" each with modulation $e^{-j\sqrt{N_s}\left(\frac{2\pi f}{\alpha_s}\right)}$ given by Eq. (39.50) and independent phase shift, δ_s. The process of first establishing "associations" between different Fourier series representative of different pieces of information is the basis of producing information with novel conceptual content. The formation of "associations" is also the basis of reasoning. The generation of "associations" depends on the statistics of "coupling" of multiple "association ensembles" each comprised of cascaded association "stages". Then the "associated" information is ordered or further processed to provide general context such as cause and effect relationships by a mechanism involving the half-width parameters, α_s, the time delay parameters, $\frac{\sqrt{N_s}}{\alpha_s}$, and potentially the independent phase shifts, δ_s, of Eq. (39.106). The ordering of "associated" information is described in SUB-APPENDIX IV--Ordering of Associations: Matrix Method.

SUB-APPENDIX IV
Ordering of Associations: Matrix Method

The set of "associated" Fourier series such as at least two "groups of SFCs" and/or at least two "SFCs" is herein called a "string". The "string" is a superposition of Fourier series; thus, it comprises a Fourier series, a linear sum of "FCs". FIGURE 19 is a flow diagram of an exemplary hierarchical relationship of the signals in Fourier space comprising "FCs", "SFCs", "groups of SFCs", and a "string" in accordance with the present invention. Each "FC" is the output of a "P element" or is stored into and/or recalled from a "M element" as shown in FIGURE 18. The information of "string" may be ordered to provide cause and effect, chronology, and hierarchical relationships. The ordered "string" is retained in memory to provide successive associative reference or further ordering of information. The information of the "string" is ordered or sequenced temporally, conceptually, or according to causality via the Matrix Method of Analysis of Mills [8, 9].

Consider Eqs. (39.33) and (39.33a) where each represents a "SFCs" in $k,\omega-space$ comprising a Fourier series. A "string" is a sum of Fourier series which follows from Eqs. (39.33) and (39.33a) as follows:

$$V_{\sum_{s,m}}\left(k_\rho,k_z\right)=$$

$$\sum_{s=1}^{S}\sum_{m=1}^{M_s}\sum_{n=-\infty}^{\infty}\frac{4\pi}{1+\frac{k_z^2}{k_\rho^2}}\frac{4}{\rho_{0_{s,m}}z_{0_{s,m}}}a_{0_{s,m}}\sin\left(k_\rho-n\frac{2\pi}{\rho_{0_{s,m}}}\frac{N_{s,m_{\rho 0}}\rho_{0_{s,m}}}{2}\right)\sin\left(k_z-n\frac{2\pi}{v_{s,m}t_{0_{s,m}}}\frac{N_{s,m_{z0}}z_{0_{s,m}}}{2}\right) \tag{39.107}$$

$$V_{\sum_{s,m}}\left(k_\rho,k_z\right)=\sum_{s=1}^{S}\sum_{m=1}^{M_s}\sum_{n=-\infty}^{\infty}\frac{4\pi}{1+\frac{k_z^2}{k_\rho^2}}\frac{4}{\rho_{0_{s,m}}z_{0_{s,m}}}a_{0_{s,m}}\frac{N_{s,m_{\rho_0}}\rho_{0_{s,m}}}{2}\frac{N_{s,m_{z_0}}z_{0_{s,m}}}{2}$$

$$\sin\left(k_\rho-n\frac{2\pi}{\rho_{0_{s,m}}}\frac{N_{s,m_{\rho 0}}\rho_{0_{s,m}}}{2}\right)\sin\left(k_z-n\frac{2\pi}{v_{s,m}t_{0_{s,m}}}\frac{N_{s,m_{z0}}z_{0_{s,m}}}{2}\right)$$

$$=\sum_{s=1}^{S}\sum_{m=1}^{M_s}\sum_{n=-\infty}^{\infty}\frac{4\pi}{1+\frac{k_z^2}{k_\rho^2}}a_{0_{s,m}}N_{s,m_{\rho_0}}N_{s,m_{z_0}}\sin\left(k_\rho-n\frac{2\pi}{\rho_{0_{s,m}}}\frac{N_{s,m_{\rho_0}}\rho_{0_{s,m}}}{2}\right)\sin\left(k_z-n\frac{2\pi}{v_{s,m}t_{0_{s,m}}}\frac{N_{s,m_{z_0}}z_{0_{s,m}}}{2}\right) \tag{39.108}$$

The corresponding equations in the time domain are a sum of multiple finite series of traveling dipoles ("impulse responses") wherein each dipole series is periodic in space and time. In frequency space, each time delayed Gaussian filter ("association ensemble" corresponding to a

"SFCs") modulates and samples the Fourier series which encodes information. Thus, the time delayed Gaussian filter selects information from the "string" and provides input for the association mechanism as the "processor" implements the Matrix Method of Analysis to find the order of the associated pieces of information represented by each "SFCs" of the "string".

Consider the time interval $t=t_i$ to $t=t_f$ of a "string" associated by "association ensembles" and recorded to memory. By processing the "string' with multiple "association ensembles" comprising Gaussian filters each of different delay, $\frac{\sqrt{N_s}}{\alpha_s}$, and half-width parameter, α_s, the "string" can be "broken" into "groups of SFCs" each having a center of mass at a time point corresponding to the delay $\frac{\sqrt{N_s}}{\alpha_s}$ and frequency composition corresponding to α_s which form a nested set of "sequential subsets" of "groups of SFCs" of the "string" in $k,\omega-$space. The set members map to time points which are randomly positioned along the time interval from the $t=t_1$-side and the $t=t_2$-side as shown in FIGURES 8, 10, 12, and 14. This nested set of "sequential subsets" of random "groups of SFCs" mapping to random time points from the $t=t_i$-side and the $t=t_f$-side is analogous to the nested set of "sequential subsets" of random DNA fragments from the 5' end and the 3' end. The order in both cases can be solved by the Genomic DNA Sequencing Method/Matrix Method of Analysis of Mills [8, 9] described in SUB-APPENDIX V.

The output of an association filter is the convolution of the input "groups of SFCs" (each "SFCs" given by Eqs. (39.33) and (39.33a)) of a "string" (Eq. (39.108)) or the "string" itself with a delayed Gaussian. In terms of the matrix method of analysis (hereafter "MMA"), the filter parameter α of the time delayed Gaussian filter corresponds to the acquisition of the composition of a polynucleotide member of a nested set of subsets. The time delay (time domain) and modulation (frequency domain) parameter $\frac{\sqrt{N}}{\alpha}$ determines the center of mass of the output, and it corresponds to the terminal nucleotide data. By forming "associations" with input from "High Level Memory" as given in SUB-APPENDIX III--Association Mechanism and Basis of Reasoning, the "processor" determines the relative position of the center of mass of each Fourier series such as a "group of SFCs" as either "before" or "after" the center of mass of the preceding and succeeding Fourier series "associated" with Fourier series input from "High Level Memory". The

complete set of Fourier series "associated" with Fourier series input from "High Level Memory" covers all of the frequencies of the "string". By Parseval's theorem, by processing the entire interval in k,ω −space, the information is entirely processed in the time domain. The order such as temporal order of the Fourier series representing information is determined using the MMA.

Input to form associations is provided by changing the decay constant α and the number of "stages" in the cascade N, or by processing each "group of SFCs" of a "string" using an "association ensemble" with different parameters α and N over all "groups of SFCs" that make up the entire "string". Each "group of SFCs" is determined to be on the $t = t_i$-side or the $t = t_f$-side of the "axis" of the "string" corresponding to the 5'-side or 3'-side of the "axis" of a polynucleotide to be sequenced via the Matrix Method of Analysis. A feedback loop comprises sequentially switching to different "known", "set", or "hardwired" delayed Gaussian filters which corresponds to changing the decay constant, α_s, with a concomitant change in the half-width parameter, α_s, and the number of elements, N_s, with a concomitant change in the delay, $\frac{\sqrt{N_s}}{\alpha_s}$, where each α_s and $\frac{\sqrt{N_s}}{\alpha_s}$ is "known" from past experiences and associations. The feedback loop whereby information from memory encoded in the "string" is filtered and delayed (modulated and sampled in frequency space) to provide "FCs", "SFCs" or "groups of SFCs" which are associated with input from "High Level Memory" provides the data acquisition and processing equivalent to the formation, acquisition, and analysis of the composition and terminal nucleotide data of a set of "sequential subsets" of the Matrix Method of Analysis. Changing the filters which process the "string" corresponds to changing the "guess" of the "known" nucleotides, $K_1K_2K_3K_4 \quad K_{n'}$, as well as the "unknown" nucleotides, $X_1, X_2, X_3, X_4 \quad$, of the Matrix Method of Analysis as applied to DNA sequencing. The order of the "groups of SFCs" of the "string" is established when "associations" with the "High Level Memory" are achieved for a given set of delayed Gaussian filters (i.e. the order of Fourier series representing information is solved when internal consistence is achieved according to the MMA). Then each Fourier series of the ordered "string" is recorded to the "High Level Memory" wherein each Fourier series of the ordered "string" may be multiplied by the Fourier transform of the delayed Gaussian filter represented by $e^{-\frac{1}{2}\left(\nu_{sp0}\frac{k_p}{\alpha_{sp0}}\right)^2} e^{-j\frac{\sqrt{N_{sp0}}}{\alpha_{sp0}}\left(\nu_{sp0}k_p\right)} e^{-\frac{1}{2}\left(\nu_{sz0}\frac{k_z}{\alpha_{sz0}}\right)^2} e^{-j\frac{\sqrt{N_{sz0}}}{\alpha_{sz0}}\left(\nu_{sz0}k_z\right)}$ that established the correct order to form the ordered "string".

Also, multiple other cascades of association "stages" ("association ensembles") may act as delay-line memory actuators that produce a time delay, $\delta(t-t_0)$, during independent "activation" of a given "association ensemble" with recall from memory. In $k,\omega-$space, the time delay is equivalent to a modulation of the correlation function given by Eq. (39.63) corresponding to the independent phase shifts, δ_s, of the correlation function (Eq. (39.106)) of the separate "associated" "groups of SFCs". During "string" ordering by the Matrix Method of Analysis, the independent phase shifts, δ_s, may modify the order of the Fourier series of the "string" representing information. In addition, the independent phase shifts, δ_s, may initially modify the content of the "string" by altering the correlation function (Eq. (39.106)) to cause information to be "associated" which otherwise would not likely be or inhibit the "association" of information which otherwise would be. These mechanisms further provide for information with novel conceptual content.

SUB-APPENDIX V

GENOMIC DNA SEQUENCING METHOD/MATRIX METHOD OF ANALYSIS

Abstract

As an overview, the Mills method of sequencing DNA comprises the steps of:

a) preparing from segments of a DNA strand to be sequenced, families of polynucleotides, each family including all polynucleotides, complementary to at least a portion of the DNA segment and at least a portion of the 3' flanking DNA segment of the DNA strand to be sequenced, of the formula:

$$K_{n'} \quad K_4K_3K_2K_1X_1X_2X_3X_4 \quad X_n$$

ranging in length from K_1X_1 to $K_{n'} - X_n$ wherein $K_1K_2K_3K_4 \quad K_{n'}$ represents the nucleotides 5' to an internal reference point, the reference point defined as the dividing line between K_1 and X_1; wherein $X_1X_2X_3X_4 \quad X_n$ represents the nucleotides 3' to the internal reference point; wherein n and n' are integers and $n + n'$, the number of nucleotides in a polynucleotide, is less than or equal to the number of nucleotides in a polynucleotide of length within the analyzable limit of the method for determining base composition and identity of the 3' terminal nucleotide of a polynucleotide; and wherein each polynucleotide in the family conforms to the criterion that if the polynucleotide contains X_n it also contains $X_{n-1}, X_{n-2} \quad X_1$; and the criteria that if the polynucleotide contains K_n it also contains $K_{n'-1}, K_{n'-2} \quad K_1$;

b) determining the base composition (the number of A's, T's, C's, and G's) and the identity of the 3' terminal base of each polynucleotide of each family;

c) determining the base sequence of the longest polynucleotide in each family from the determined base composition and identity of the 3' terminal base of each polynucleotide in the family and derived change in base composition and terminal base between polynucleotides in each family; and

d) determining the base sequence of the entire DNA strand to be sequenced based upon the overlapping sequences of the longest polynucleotides in each family.

The base sequence of the longest polynucleotide of each family is determined by the Matrix Method of Analysis of the base composition of each polynucleotide in the family and the identity of the 3' terminal base of each polynucleotide.

The base sequence of the longest polynucleotide in each set is determined by:

a) setting up a matrix consisting of $\frac{1}{2}M + 1$ columns and $\frac{1}{2}M$ rows where M is the number of nucleotides in the longest polynucleotide of the set;

b) assigning the longest polynucleotide a coordinate position in the matrix of column 1, row 1;

c) assigning polynucleotides which are successively one nucleotide shorter on the 5' end to each column position and polynucleotides which are successively one nucleotide shorter on the 3' end to each row position;

d) determining all paths through the matrix from position 1,1 to position $\frac{1}{2}M + 1$, $\frac{1}{2}M$ which are consistent with the base composition and the 3' terminal base of the polynucleotide assigned to each position in the matrix and with the change in base composition and 3' terminal base between polynucleotides; and

e) from position $\frac{1}{2}M+1, \frac{1}{2}M$ determining the path back to position 1,1 which permits the assignment of specific bases at each step either the 5' or 3' end of a polynucleotide, consistent with the compositional and terminal base data, to arrive at the sequence of the longest polynucleotide wherein the $K_1K_2K_3K_4 \quad K_{n'}$ is guessed and steps d) and e) are performed reiteratively until a sequence can be assigned without contradiction.

Mills [8, 9] has developed a method of determining the nucleotide sequence of a DNA molecule of arbitrary length as a single procedure by sequencing portions of the molecule in a fashion such that the sequence of the 5' end of the succeeding contiguous portion is sequenced as the 3' end of its preceding portion is sequenced, for all portions, where the order of contiguous portions is determined by the sequence of the DNA molecule. Sequencing of the individual portions is accomplished by generating a family of polynucleotides under conditions which determine that the elements are partial copies of the portion and are of random nucleotide length on the 3' and 5' ends about a dinucleotide which is an internal reference point; determining the base composition and terminal base identity of each element of the family and solving for the sequence by a method of analysis wherein the base composition and terminal base data of each element is used to solve for a single base of the sequence by assigning the base to either the 5' or 3' end of the partial sequence about the internal reference point as the entire sequence of the portion is built up from a dinucleotide.

The molecules generated from the DNA to be sequenced comprise families of polynucleotides. Each family corresponds to a segment of the DNA to be sequenced and is made up of a longest polynucleotide (the length of which is selected to be within the analyzable limit of the procedure used to determine base composition and identity of the terminal base) and shorter polynucleotides which form a "sequential subset" of the longest polynucleotides. Grouped hierarchically from the longest to the shortest polynucleotide of the family is progressively one nucleotide shorter than the preceding polynucleotide and has the same sequence except that it lacks the one nucleotide. A further restraint on the elements of the family is that there is a specific dinucleotide of the sequence contained in each element. The molecules can be envisioned as being built around an "axis" which is at the mid position of the common dinucleotide. The "axis" constitutes an internal reference point. The polynucleotides vary around the "axis," each containing one less nucleotide on the 3' or 5' end than its longer predecessor in the group. All such molecules are included in the family, from the longest to the shortest, a dinucleotide.

The sequence of the DNA portion from which each family of polynucleotides has been made can be solved by determining the base

composition (the number of A's, T's, C's, and G's) and the identity of the 3' terminal base of each polynucleotide of the family. The composition and terminal nucleotide data of the elements of each family of polynucleotides are used to solve the sequence of the corresponding DNA portion template by a method of first generating all polynucleotides which can be obtained from a guessed solution of the sequence by successive removal of a 3' or 5' nucleotide consistent with the data of the change in composition between set elements and with the further constraint that a specific dinucleotide of the sequence must be present in all polynucleotides. The terminal nucleotide data is used to determine if a subset of the hypothetical family of polynucleotides exists such that the elements have a one to one correspondence with the data of terminal nucleotide as well as composition. If no such subset exists, the process is repeated for improved guesses until convergence to the correct solution for the sequence occurs.

A method which performs this analysis by testing for the validity of a guess for part of the sequence while solving for the remaining part using the composition and terminal base data independently to execute binary hypothesis testing decisions compatible with computer logic is the matrix method of analysis algorithm.

The matrix method of analysis is analogous to solving a system of n equations in n unknowns where the knowns are: 1) the structural properties of the polynucleotides, 2) the base composition and the identity of the terminal base, 3) the change in composition and change in terminal base between a polynucleotide and the next in the family. The method exploits the given information by implementing a reiterative procedure to find a path through a matrix of the possible polynucleotides having sequences consistent with the data. Final assignment of the sequence is made when the entire path finding procedure can be accomplished without contradictions between sequence assignment and actual data.

Strategy of the Sequencing Method

The strategy is to create a group of molecules which contain a reference point which is internal. Initially, location of the reference point is unknown, but it exists in all of the molecules. The molecules are a family of polynucleotides comprising complementary copies of a portion of the parent molecule from which they are generated and superimpose on the parent by alignment of this internal point of reference. The location of the point of reference or "axis," and the sequence of the parent molecule is solved for simultaneously by an algorithm called the matrix method of analysis.

The family of polynucleotides can be thought of as being all

molecules which result from the sequential loss of nucleotides from the 5' and 3' end of the longest polynucleotide of the group. An ordered pattern of terminal nucleotide change and nucleotide compositional change occurs between members of sequential subsets. This algorithm exploits the pattern of ordered systematic nucleotide compositional change and terminal nucleotide change that a designated longest polynucleotide with a given internal reference point and given nucleotide loss constraints can produce.

Criteria of Polynucleotides

The nucleotide sequence of a DNA strand can be solved by generating a family of polynucleotides overlapping portions of the DNA to be sequenced. Each family of polynucleotides forms a "sequential subset" of the longest polynucleotide of the group. The molecules are identical less one nucleotide from either the 5' or 3' end of a given molecule, and the former are defined as sequential subsets of the latter.

The molecules can be depicted as follows:

$$K_{n'} \ldots K_4 K_3 K_2 K_1 X_1 X_2 X_3 X_4 \ldots X_n$$

Where the series $K_1, K_2, K_3, K_4 \quad K_{n'}$ represent the nucleotides of the polynucleotide 5' to the internal reference point, or axis, and the series $X_1, X_2, X_3, X_4 \quad X_n$ represents the nucleotides of the polynucleotide on the 3' side of the axis. The 5' end with respect to the axis is designated as the "known" portion of the molecules (this does not necessarily imply that this sequence is initially known), and the 3' end of the polynucleotide is designated as the "unknown" portion . Thus, K_1, K_2, K_3, K_4 represent the "known" sequence and X_1, X_2, X_3, X_4 represent the "unknown" sequence. The distinction is that in the matrix, as described below K_1, K_2, K_3, K_4 appear as nucleotides, where as the X's represent variables. The nucleotides of the "known" portion can be known extrinsically or they can be guessed.

The polynucleotides are governed by the following constraints. No polynucleotide contains X_2 without containing X_1. In general terms, no polynucleotide contains X_n without containing $X_{n-1}, X_{n-2}, \quad X_1$. In addition, no polynucleotide contains K_2 without containing K_1. That is, polynucleotide contains an unknown with out containing all preceding unknowns and, every polynucleotide contains all succeeding knowns if it contains any given known. As a set, all the polynucleotides satisfy these criteria and vary randomly at the 3' and 5' ends.

The criteria can be represented symbolically as follows:

$X_n \rightarrow X_1$ (X_n implies X_1)

$K_n \rightarrow K_1$ ($K_{n'}$ implies K_1)

$K_{n'} - X_n$ (the polynucleotides are random at the 5' and 3'; ends; the knowns and unknowns are variables where K = Known, X = Unknown, $n' = 1 \text{ to } 4$ and $n = 1 \text{ to } 4$)

Principles of Matrix Method of Analysis

The matrix method of analysis entails setting up a rectangular matrix where the designated longest polynucleotide appears at position (1,1). The sequence of one half of this molecule is "known". The nucleotide sequence at the other one half of the molecule is designated "unknown" and is represented by variables. The term "known" does not necessarily imply that the nucleotide sequence of the parent molecule is known initially. The division between the "knowns" and "unknowns" is the internal reference point. The location of the internal reference point is not necessarily known initially and can be changed by changing the knowns so that this sequence superimposes a different region of the parent molecule. That is, when the sequence is solved, it will superimpose a region of the parent and the location of the internal reference point will be fixed. The location on the parent is at the line dividing the "knowns" and the "unknowns". If the 5' end of the sequence (and consequently the entire sequence) superimposes on a different region of the parent, the location of the internal reference point would be different. Thus, the location of the internal reference point relative to the parent molecule is determined by the "knowns".

An exemplary matrix is shown below for polynucleotides which conform to the criteria set forth. For a designated longest polynucleotide which contains a total of eight (8) nucleotides the matrix consists of 5 rows and 4 columns.

$$\begin{array}{cccccccc} K_4 & K_3 & K_2 & K_1 & X_1 & X_2 & X_3 & X_4 \end{array}$$

$$\begin{array}{cccc} K_4K_3K_2K_1X_1X_2X_3X_4 & K_4K_3K_2K_1X_1X_2X_3 & K_4K_3K_2K_1X_1X_2 & K_4K_3K_2K_1X_1 \\ K_3K_2K_1X_1X_2X_3X_4 & K_3K_2K_1X_1X_2X_3 & K_3K_2K_1X_1X_2 & K_3K_2K_1X_1 \\ K_2K_1X_1X_2X_3X_4 & K_2K_1X_1X_2X_3 & K_2K_1X_1X_2 & K_2K_1X_1 \\ K_1X_1X_2X_3X_4 & K_1X_1X_2X_3 & K_1X_1X_2 & K_1X_1 \\ X_1X_2X_3X_4 & X_1X_2X_3 & X_1X_2 & X_1 \end{array}$$

The matrix columns contain polynucleotides which have lost nucleotides at the 5' end; the rows are formed of polynucleotides which have lost nucleotides from the 3' end. Nucleotides are lost from the 5' end down any column and lost from the 3' end across any row. The matrix is constructed such that all the constraints governing the polynucleotides are satisfied, and all possible polynucleotides are recorded in the matrix according to the describe format.

The determination of the sequence of the polynucleotides proceeds as follows: starting at position (1,1) in the matrix, the base which has been lost is determined by the difference in base composition between the longest polynucleotide and the next longest of the set. The change is consistent with a move to position (1,2) and/or (2,1) of the matrix. The step is repeated for each polynucleotide of the family. These moves are down a column and/or across the row from left to right. Moves down a column or across a row from left to right are designated from/to moves. The result can be recorded, e.g. in a "lattice" which contains all coordinate positions arranged in levels such that each successive level from top to bottom corresponds to all possible from/to moves, and each successive level from bottom to top corresponds to all possible to/from moves. A to/from move is a movement up a column and/or across a row from right to left.

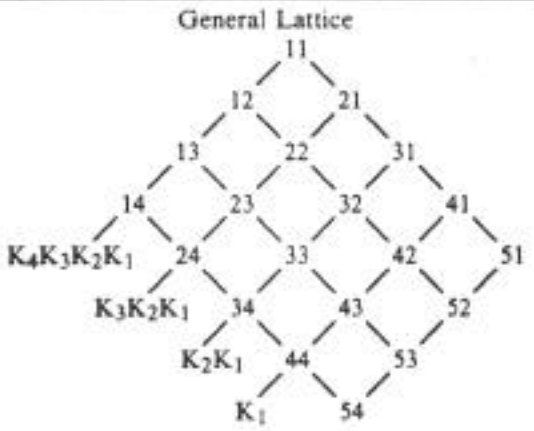

Polynucleotide	Lattice Coordinate position
$K_4K_3K_2K_1$	15
$K_3K_2K_1$	25
K_2K_1	35
K_1	45

For each step, the base which could have been lost from the 3' or 5' end is determined, and the appropriate move to a position in the matrix is made. This establishes the appropriate path in the matrix which can be designated by connecting the corresponding coordinates in the lattice. This procedure is repeated until all consistent from/to moves are recorded in the lattice. At least one path is formed from coordinate position (1,1) to a point of convergence, i. e., a coordinate position from which no further from/to moves can be made.

The next step is to determine which path is the correct path. This is accomplished by starting at a point of convergence and determining which to/from steps for all single or binary decisions are consistent with the terminal base data as moves are made back to position (1,1) from the point of convergence. Assignment of a base to the 3' or 5' end is made by a to/from move which does not contradict the change in base. For all to/from moves, if the path that is chosen from one coordinate to another corresponds to a move across a row from right to left, then the base is assigned to the 3' end which is consistent with the move. That is the base change determined from the data occurred from the 3' end. A contradiction arises if this assignment is inconsistent with terminal base data for the polynucleotide represented at the coordinate position or if the change in terminal base for this step is inconsistent with the data. For all to/from moves, if the path that is chosen from one coordinate to another corresponds to a move up a column then the base change for that step indicates which base to assign to the 5' end. A contradiction would arise if the next "known" up the column in the matrix is different

from that indicated by the base change.

The sequence is solved when at least one path is found from (1,1) to a point of convergence by from/to moves and to the (1,1) position from the point of convergence by to/from moves at each data step without contradictions. The matrix method of analysis yields a unique solution for a matrix of all possible polynucleotides of size $(\frac{1}{2}M+1, \frac{1}{2}M)$ that conform to the constraints for polynucleotides, for any set of data of $M-1$ polynucleotides that are successively one nucleotide less and are sequential subsets from $M-1$ nucleotides to a dinucleotide. (The longest polynucleotide is M nucleotides in length.)

The key to the matrix method of analyze is that there is convergence to at least one of the terminal possibilities (point in the matrix at which no further from/to moves can be made). It may converge to more than one (e.g., if the sequence contained only A, or T, or C, or G bases, then it would converge to all possible termini of the matrix that yields the solution of the sequence). Once any terminus is determined to be correct, it can serve as an initiation point, that is, a point, or coordinate position from which the initial to/from move is made. A terminus representing a single nucleotide or single variable in the matrix is correct if it is consistent with the data. The sequence can be deciphered by making decisions at branch points and by taking the return path that is determined to be correct by the data, i. e. the terminal base and the change in the terminal base at each step. If more than one path is correct, anyone of the correct paths will yield the sequence.

Examples of Solving Sequences by the Matrix Method of Analysis

To further illustrate the matrix method of determining sequence, examples of its application are given below. In each example a matrix for a polynucleotide family of eight nucleotides in length is shown. The lattice diagram shows all possible matrix from/to moves consistent with the change in composition data. The column labeled "path" represents the possible to/from moves in the matrix which are consistent with the terminal base data and the change in terminal base. The path which determines the solution to the sequence is read from bottom to top.

EXAMPLE 1

1 4 6 7 5 3 2
A T T C G C T A
$X_1X_2X_3X_4$

	1	2	3	4
1.	$ATTCX_1X_2X_3X_4$	$ATTCX_1X_2X_3$	$ATTCX_1X_2$	$ATTCX_1$
2.	$TTCX_1X_2X_3X_4$	$TTCX_1X_2X_3$	$TTCX_1X_2$	$TTCX_1$
3.	$TCX_1X_2X_3X_4$	$TCX_1X_2X_3$	TCX_1X_2	TCX_1
4.	$CX_1X_2X_3X_4$	$CX_1X_2X_3$	CX_1X_2	CX_1
5.	$X_1X_2X_3X_4$	$X_1X_2X_3$	X_1X_2	X_1

Lattice	Composition Data	Δ	Terminal Nucleotide	Path	Sequence
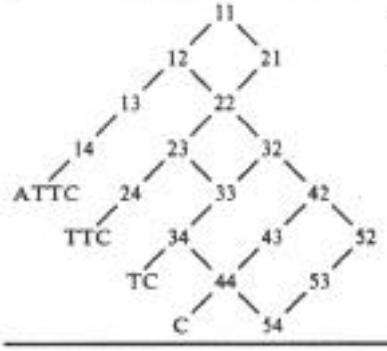	3T,2C,1G,2A		A	1,1	ATTCGCTA
	3T,2C,1G,1A	A	A	2,1	TTCGCTA
	3T,2C,1G	A	T	2,2	TTCGCT
	2T,2C,1G	T	C	2,3	TTCGC
	1T,2C,1G	T	C	3,3	TCGC
	1T,1C,1G	C	G	3,4	TCG
	1C,1G	T	G	4,4	CG
	1G	C	G	5,4	G

EXAMPLE 2

1 2 5 7 6 4 3
A G T C A T G
$X_1X_2X_3X_4$

	1	2	3	4
1.	$AGTCX_1X_2X_3X_4$	$AGTCX_1X_2X_3$	$AGTCX_1X_2$	$AGTCX_1$
2.	$GTCX_1X_2X_3X_4$	$GTCX_1X_2X_3$	$GTCX_1X_2$	$GTCX_1$
3.	$TCX_1X_2X_3X_4$	$TCX_1X_2X_3$	TCX_1X_2	TCX_1
4.	$CX_1X_2X_3X_4$	$CX_1X_2X_3$	CX_1X_2	CX_1
5.	$X_1X_2X_3X_4$	$X_1X_2X_3$	X_1X_2	X_1

Lattice	Composition Data	Δ	Terminal Nucleotide	Path	Sequence	
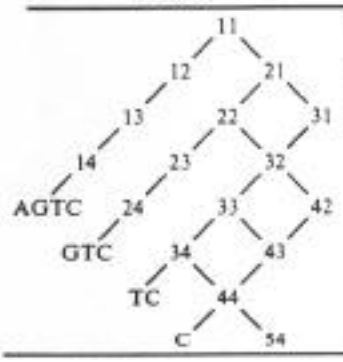	3T,2G,1C,2A		G	1,1 1,1	AGTCATTG	AGTCATTG
	3T,2G,1C,1A	A	G	2,1 2,1	GTCATTG	GTCATTG
	3T,1G,1C,1A	G	G	3,1 3,1	TCATTG	TCATTG
	3T,1C,1A	G	T	3,2 3,2	TCATT	TCATT
	2T,1C,1A	T	T	3,3 4,2	TCAT	CATT
	1T,1C,1A	T	T	4,3 4,3	CAT	CAT
	1C,1A	T	A	4,4 4,4	CA	CA
	1A	C	A	5,4 5,4	A	A

SUB-APPENDIX VI
Input Context

An Input Layer receives data and transforms it into a Fourier series in k,ω −space wherein input context is encoded in time as delays which corresponds to modulation of the Fourier series at corresponding frequencies. The Fourier series in Fourier space represents information parameterized according to the data and the input context. The information is the data and the input context. The information is based on physical characteristics or representations of physical characteristics and physical context. Data from transducers responding to an input signal representative of the physical characteristics and the physical context is used to parameterize the Fourier series in k,ω −space whereby

i.) "Data" such as intensity and rate of change recorded by a transducer is represented in terms of the parameters ρ_{0_m} and $N_{m_{\rho_0}}$ of each component of the Fourier series wherein the input context corresponds to the physical context based upon the identity of a specific transducer and its particular transducer elements. The physical context maps on a one to one basis to the input context. The processed signals from each transducer which can be input from the Input Layer to other layers such as the Association Layer and the "String" Ordering Layer, and the Predominant Configuration Layer comprises a Fourier series as given by Eq. (39.33) and Eq. (39.33a) wherein:

each of the factors $N_{m_{\rho_0}}$ and $N_{m_{z_0}}$ of the Fourier series component is proportional to the rate of change of the signal response of each transducer which is proportional to the rate of change of the physical signal such as the surface roughness, or the intensity of sound, light, or temperature; and

each of the factors ρ_{0_m} and z_{0_m} of each Fourier component is inversely proportional to the amplitude of the signal response of each transducer which is proportional to the physical signal such as the surface roughness, or the intensity of sound, light, or temperature; or

each of the factors $N_{m_{\rho_0}}$ and $N_{m_{z_0}}$ of the Fourier series component is proportional to the amplitude of the signal response of each transducer which is proportional to the physical signal such as the surface roughness, or the intensity of sound, light, or temperature; and

each of the factors ρ_{0_m} and z_{0_m} of each Fourier component is inversely proportional to the rate of change of the signal response of each transducer which is proportional to the rate of change of the physical signal such as the surface roughness, or the intensity of sound, light, or temperature; or

each of the factors $N_{m_{\rho_0}}$ and $N_{m_{z_0}}$ of the Fourier series component is proportional to the duration of the signal response of each transducer; and

each of the factors ρ_{0_m} and z_{0_m} of each Fourier component is inversely proportional to the amplitude of the signal response of each transducer which is proportional to the physical signal such as the surface roughness, or the intensity of sound, light, or temperature.

ii.) The input from the Input Layer to other layers shown in FIGURE 21 can be an analog waveform in the analog case and a matrix in the digital case. Input context of a given transducer can be encoded in time as delays which correspond to modulation of the Fourier series in k,ω −space at corresponding frequencies whereby the data corresponding to each transducer maps to a distinct memory location called a "register" that encodes the input context by recording the data to corresponding specific time intervals of a time division structured memory. The input context maps on a one to one basis to an Input Layer section of a memory. Thus, there is a one to one map of physical context to input context to Input Layer section of a memory. The representation of information as a Fourier series in Fourier space allows for the mapping.

iii.) Input context of a complex transducer system can be encoded in time by the mapping of data from the components of the transducer system to a memory structured according to a corresponding hierarchical set of time intervals representative of each transducer system with respect to different transducer systems, a transducer element's rank relationship relative to other transducer elements, and the response of a transducer element as a function of time. In terms of digital processing, the data from a transducer having n levels of subcomponents is assigned a master time interval with $n+1$ sub time intervals in a hierarchical manner wherein the data stream from the final n th level transducer element is recorded as a function of time in the $n+1$ th time coded memory buffer. During processing the time intervals represent time delays which are transformed into modulation frequencies which encode input context. FIGURE 3 is a flow diagram of an exemplary transducer data structure of a time delay interval subdivision hierarchy wherein the data from a transducer having n levels of subcomponents numbering integer m per level is assigned a master time interval with $n+1$ sub time intervals in a hierarchical manner wherein the data stream from the final n th level transducer element is recorded as a function of time in the $n+1$ th time coded sub memory buffer in accordance with the present invention.

The "processor" may be taught the relationship between the "data"

such as intensity and rate of change recorded by a transducer and the parameters such as ρ_{0_m} and $N_{m_{\rho_0}}$ of each component of the Fourier series by inputting standard physical signals to each transducer together with other information that is "associated" with the standards. A data base may be established. The information that is "associated" with the standard may be recalled and can comprise input into the Association Layer and the "String" Ordering Layer shown in FIGURE 20 and FIGURE 21 during "processing" according to the present invention.

The process of storing output from multiple transducers to memory further comprises creation of "transducer strings". In one embodiment, associations occur at the transducer level, and "SFCs" are mapped to distinct memory "registers" from the corresponding distinct transducers responding simultaneously, for example. In one embodiment, two or more Fourier series such as two or more "SFCs" of the "string" are "linked" whereby activation of any Fourier series such as a "SFCs" of the "string" may thereby activate other or all Fourier series of the "string" stored in the corresponding "registers". The activation may be based on probability. The activation probability may depend on the "strength of the linkage" which is defined in terms of a linkage probability parameter which increases with the linkage rate, the rate at which the activation of a Fourier series of a "string" thereby causes the activation of another Fourier series of the "string". Probability operators may activate other or all Fourier series of the "string" when any Fourier series of the "string" is "active" based on the linkage probability parameter.

In a digital embodiment comprising "memory linkages" of the "transducer string", recalling any part of a "transducer string" from a distinct memory location may thereby cause additional "linked" Fourier series of the "transducer string" to be recalled. In one embodiment, a linkage probability parameter is generated and stored in memory for each "string" Fourier series such as a "SFCs". A probability operand is generated having a value selected from a set of zero and one, based on the linkage probability parameter. If the value is one, the corresponding Fourier series is recalled. Thus, when any part of a "transducer string" is recalled from memory, any other "string" Fourier series is randomly recalled wherein the recalling is based on the linkage probability parameter. The linkage probability parameter is weighted based on the linkage rate.

$$x(t)=\int_{-\infty}^{\infty}X(f)e^{j2\pi ft}df \qquad X(t)=\int_{-\infty}^{\infty}x(t)e^{-j2\pi ft}dt$$

(39.109)

Delay $\delta(t-t_0) \quad \Leftrightarrow \quad e^{-j2\pi ft_0}$

Consider a "transducer string" made up of multiple "groups of SFCs" where each "SFCs" represents information of the transducer system with respect to different transducer systems, a transducer element's rank relationship relative to other transducer elements, and the response of a transducer element as a function of time, space, or space and time. (The latter case applies to a transducer which is responsive to changes in the intensity of a parameter over time and spatial position). These aspects of each transducer are encoded via delays corresponding to modulation in k,ω −space within a frequency band corresponding to each aspect of the transducer.

The "string" in k,ω −space is analogous to a multidimensional Fourier series. The modulation within each frequency band may further encode context in a general sense. In one embodiment, it encodes temporal order, cause and effect relationships, size order, intensity order, before-after order, top-bottom order, left-right order, etc. which is relative to the transducer.

Eq. (39.33a), the "read" total response $V_{\sum_m}$ in Fourier space comprising the superposition of M "FCs" wherein each "FC" corresponds to the response of a "M or P element" with input context encoded by the modulation factor $e^{-jk_\rho\left(\rho_{fb_{s,m}}+\rho_{t_{s,m}}\right)}$ becomes

$$V_{\sum_m}\left(k_\rho,k_z\right)=$$

$$\sum_{m=1}^{M}\sum_{n=-\infty}^{\infty}\frac{4\pi}{1+\frac{k_z^2}{k_\rho^2}}a_{0_m}N_{m_{\rho 0}}N_{m_{z0}}e^{-jk_\rho\left(\rho_{fb_m}+\rho_{t_m}\right)}\sin\left(k_\rho\frac{N_{m_{\rho 0}}\rho_{0_m}}{2}-n\frac{2\pi N_{m_{\rho 0}}}{2}\right)\sin\left(k_z\frac{N_{m_{z0}}z_{0_m}}{2}-n\frac{2\pi N_{m_{z0}}}{2}\right)$$

(39.110)

where $\rho_{t_m}=v_{t_m}t_{t_m}$ is the modulation factor which corresponds to the physical time delay t_{t_m} and $\rho_{fb_m}=v_{fb_m}t_{fb_m}$ is the modulation factor which corresponds to the specific transducer time delay t_{fb_m}. v_{t_m} and v_{fb_m} are constants such as the signal propagation velocities..

"Associations" are established between Fourier series such as "SFCs" and "groups of SFCs" (i.e. a "string" is created) by "coupling" with Poissonian probability between "association ensembles" "carrying" the

"SFCs" and "groups of SFCs". Input context is encoded by the transducer frequency band modulation factor $e^{-jk_\rho\left(\rho_{fb_{S,m}}+\rho_{t_{S,m}}\right)}$ according to Eq. (39.110). In this case, Eq. (39.87b) is

$$\beta_s^2=(8\pi)^2\frac{1}{\sqrt{2\pi}}\sqrt{\frac{\alpha_1^2\alpha_s^2}{\alpha_1^2+\alpha_s^2}}\sum_{m_1=1}^{M_1}a_{0_{m_1}}N_{m_1}\sum_{m_s=1}^{M_s}a_{0_{m_s}}N_{m_s}$$

$$\exp\left\{-\frac{\frac{\alpha_1^2\alpha_s^2}{\alpha_1^2+\alpha_s^2}\left(\frac{\sqrt{N_1}}{\alpha_1}-\frac{\sqrt{N_s}}{\alpha_s}+\left(\frac{N_{m_1}t_{0_{m_1}}}{2}+t_{fb_{m_1}}+t_{t_{m_1}}\right)-\left(\frac{N_{m_s}t_{0_{m_s}}}{2}+t_{fb_{m_s}}+t_{t_{m_s}}\right)\right)^2}{2}\right\} \tag{39.111a}$$

And, Eq. (39.87c) is

$$\beta_s^2=(8\pi)^2\frac{1}{\sqrt{2\pi}}\sqrt{\frac{\alpha_1^2\alpha_s^2}{\alpha_1^2+\alpha_s^2}}\sum_{m_1=1}^{M_1}a_{0_{m_1}}N_{m_1}\sum_{m_s=1}^{M_s}a_{0_{m_s}}N_{m_s}$$

$$\exp\left\{-\frac{\frac{\alpha_1^2\alpha_s^2}{\alpha_1^2+\alpha_s^2}\left(\frac{\sqrt{N_1}}{\alpha_1}-\frac{\sqrt{N_s}}{\alpha_s}+\left(\frac{N_{m_1}\rho_{0_{m_1}}}{2\nu_{m_1}}+\frac{\rho_{fb_{m_1}}}{\nu_{fb_{m_1}}}+\frac{\rho_{t_{m_1}}}{\nu_{t_{m_1}}}\right)-\left(\frac{N_{m_s}\rho_{0_{m_s}}}{2\nu_{m_s}}+\frac{\rho_{fb_{m_s}}}{\nu_{fb_{m_s}}}+\frac{\rho_{t_{m_s}}}{\nu_{t_{m_s}}}\right)\right)^2}{2}\right\} \tag{39.111b}$$

The corresponding frequency difference angle, ϕ_s, which follows from Eq. (39.89) is

$$\phi_s=\frac{\pi\left(\frac{\sqrt{N_1}}{\alpha_1}-\frac{\sqrt{N_s}}{\alpha_s}+\sum_{m_1=1}^{M_1}\left(\frac{N_{m_1}\rho_{0_{m_1}}}{2\nu_{m_1}}+\frac{\rho_{fb_{m_1}}}{\nu_{fb_{m_1}}}+\frac{\rho_{t_{m_1}}}{\nu_{t_{m_1}}}\right)-\sum_{m_s=1}^{M_s}\left(\frac{N_{m_s}\rho_{0_{m_s}}}{2\nu_{m_s}}+\frac{\rho_{fb_{m_s}}}{\nu_{fb_{m_s}}}+\frac{\rho_{t_{m_s}}}{\nu_{t_{m_s}}}\right)\right)}{\frac{\sqrt{N_1}}{\alpha_1}+\sum_{m_1=1}^{M_1}\left(\frac{N_{m_1}\rho_{0_{m_1}}}{2\nu_{m_1}}+\frac{\rho_{fb_{m_1}}}{\nu_{fb_{m_1}}}+\frac{\rho_{t_{m_1}}}{\nu_{t_{m_1}}}\right)} \tag{39.112a}$$

The corresponding frequency difference angle, ϕ_s, which follows from Eq. (39.90) is

$$\phi_s=\frac{\pi\left(\frac{\sqrt{N_1}}{\alpha_1}-\frac{\sqrt{N_s}}{\alpha_s}+\sum_{m_1=1}^{M_1}\left(\frac{N_{m_1}t_{0_{m_1}}}{2}+t_{fb_{m_1}}+t_{t_{m_1}}\right)-\sum_{m_s=1}^{M_s}\left(\frac{N_{m_s}t_{0_{m_s}}}{2}+t_{fb_{m_s}}+t_{t_{m_s}}\right)\right)}{\frac{\sqrt{N_1}}{\alpha_1}+\sum_{m_1=1}^{M_1}\left(\frac{N_{m_1}t_{0_{m_1}}}{2}+t_{fb_{m_1}}+t_{t_{m_1}}\right)} \tag{39.112b}$$

Eq. (39.108), the "read" total response $V_{\sum_m}$ in Fourier space comprising the superposition of S "SFCs" wherein each "SFCs" corresponds to the

response of M_s "M or P elements", with input context encoded by the modulation factor $e^{-jk_\rho\left(\rho_{fb_{s,m}}+\rho_{t_{s,m}}\right)}$, becomes the following "string".

$$V_{\sum_{s,m}}\left(k_\rho,k_z\right)=\sum_{s=1}^{S}\sum_{m=1}^{M_s}\sum_{n=-\infty}^{\infty}\frac{4\pi}{1+\frac{k_z^2}{k_\rho^2}}a_{0_{s,m}}N_{s,m_{\rho_0}}N_{s,m_{z_0}}e^{-jk_\rho\left(\rho_{fb_{s,m}}+\rho_{t_{s,m}}\right)}$$
$$\sin\left(k_\rho-n\frac{2\pi}{\rho_{0_{s,m}}}\right)\frac{N_{s,m_{\rho_0}}\rho_{0_{s,m}}}{2}\sin\left(k_z-n\frac{2\pi}{v_{s,m}t_{0_{s,m}}}\right)\frac{N_{s,m_{z_0}}z_{0_{s,m}}}{2} \quad (39.113)$$

where $\rho_{t_{s,m}}=v_{t_{s,m}}t_{t_{s,m}}$ is the modulation factor which corresponds to the physical time delay $t_{t_{s,m}}$ and $\rho_{fb_{s,m}}=v_{fb_{s,m}}t_{fb_{s,m}}$ is the modulation factor which corresponds to the specific transducer time delay $t_{fb_{s,m}}$. $v_{t_{s,m}}$ and $v_{fb_{s,m}}$ are constants such as the signal propagation velocities. In another embodiment, the output $V_{\sum_m}$ is the Gaussian sampled and modulated "string" of Eq. (39.113) wherein each "SFCs" is multiplied by the Fourier transform of the delayed Gaussian filter (Eq. (39.50)) (i.e. the modulation factor $e^{-\frac{1}{2}\left(v_{s\rho 0}\frac{k_\rho}{\alpha_{s\rho 0}}\right)^2}e^{-j\frac{\sqrt{N_{s\rho 0}}}{\alpha_{s\rho 0}}\left(v_{s\rho 0}k_\rho\right)}e^{-\frac{1}{2}\left(v_{sz0}\frac{k_z}{\alpha_{sz0}}\right)^2}e^{-j\frac{\sqrt{N_{sz0}}}{\alpha_{sz0}}\left(v_{sz0}k_z\right)}$) which gave rise to "coupling" and "association" to form the "string". $V_{\sum_m}$ is given by

$$V_{\sum_{s,m}}\left(k_\rho,k_z\right)=\sum_{s=1}^{S}\sum_{m=1}^{M_s}\sum_{n=-\infty}^{\infty}\frac{4\pi}{1+\frac{k_z^2}{k_\rho^2}}a_{0_{s,m}}N_{s,m_{\rho_0}}N_{s,m_{z_0}}e^{-\frac{1}{2}\left(v_{s\rho 0}\frac{k_\rho}{\alpha_{s\rho 0}}\right)^2}e^{-j\frac{\sqrt{N_{s\rho 0}}}{\alpha_{s\rho 0}}\left(v_{s\rho 0}k_\rho\right)}e^{-\frac{1}{2}\left(v_{sz0}\frac{k_z}{\alpha_{sz0}}\right)^2}e^{-j\frac{\sqrt{N_{sz0}}}{\alpha_{sz0}}\left(v_{sz0}k_z\right)}$$
$$e^{-jk_\rho\left(\rho_{fb_{s,m}}+\rho_{t_{s,m}}\right)}\sin\left(k_\rho-n\frac{2\pi}{\rho_{0_{s,m}}}\right)\frac{N_{s,m_{\rho_0}}\rho_{0_{s,m}}}{2}\sin\left(k_z-n\frac{2\pi}{v_{s,m}t_{0_{s,m}}}\right)\frac{N_{s,m_{z_0}}z_{0_{s,m}}}{2} \quad (39.114)$$

wherein input context is encoded by the modulation factor $e^{-jk_\rho\left(\rho_{fb_{s,m}}+\rho_{t_{s,m}}\right)}$. Eq. (39.114) is also an exemplary "string" with each Fourier series multiplied by the Fourier transform of the delayed Gaussian filter represented by $e^{-\frac{1}{2}\left(v_{s\rho 0}\frac{k_\rho}{\alpha_{s\rho 0}}\right)^2}e^{-j\frac{\sqrt{N_{s\rho 0}}}{\alpha_{s\rho 0}}\left(v_{s\rho 0}k_\rho\right)}e^{-\frac{1}{2}\left(v_{sz0}\frac{k_z}{\alpha_{sz0}}\right)^2}e^{-j\frac{\sqrt{N_{sz0}}}{\alpha_{sz0}}\left(v_{sz0}k_z\right)}$ that established the correct order to form the ordered "string" given in SUB-APPENDIX IV--Ordering of Associations: Matrix Method. The index over s is independent of m since each "FC" of a given "SFCs" is filtered by the same Gaussian filter. In embodiments, the index for the Gaussian filter is not independent of m. In one case, some "FCs" may be filtered by the same Gaussian filters; whereas, other "FCs" may be filtered by different Gaussian filters. In another case, each "FC" may be filtered by a different

Gaussian filter.

For the case where $v_{s,m}t_{0_{s,m}} = \rho_{0_{s,m}}$ and $k_\rho = k_z$., the "string" in Fourier space is one dimensional in terms of k_ρ and is given by

$$V_{\sum_{s,m}}\left(k_\rho, k_z\right) = \sum_{s=1}^{S}\sum_{m=1}^{M_s}\sum_{n=-\infty}^{\infty} a_{0_{s,m}} N_{s,m_{\rho_0}} e^{-\frac{1}{2}\left(v_{s\rho 0}\frac{k_\rho}{\alpha_{s\rho 0}}\right)^2} e^{-j\frac{\sqrt{N_{s\rho 0}}}{\alpha_{s\rho 0}}\left(v_{s\rho 0}k_\rho\right)} e^{-jk_\rho \rho_{p_{s,m}}} \operatorname{sinc}\left(k_\rho - n\frac{2\pi}{\rho_{0_{s,m}}}\frac{N_{s,m_{\rho 0}}\rho_{0_{s,m}}}{2}\right) \quad (39.115)$$

The "string" comprises a Fourier series, a linear sum of "FCs" each multiplied by its corresponding Gaussian filter modulation factor and modulation factor which encodes input context (Eqs. (39.114-39.115)). FIGURE 19 is a flow diagram of an exemplary hierarchical relationship of the signals in Fourier space comprising "FCs", "SFCs", "groups of SFCs", and a "string" in accordance with the present invention. Each "FC" is encoded by a "P element" or stored into and/or recalled from a "M element" as shown in FIGURE 18.

SUB-APPENDIX VII
Comparison of Processing Activity to Statistical Thermodynamics/Predominant Configuration

The quantity of information that can be "associated" into ordered "strings" called "P strings" is essentially infinite based on the input to the layers of the "processor" comprising Fourier series in k,ω −space. Consider Eq. (39.33a). In the case that the parameter $N_{s,m}$ spans 1 to 100, $\rho_{0_{s,m}}$ spans 1 to 1000, and there are 1000 modulation bands, the number of distinct inputs W is

$$W = 1000!1000!100! \tag{39.116}$$

Using Sterling's approximation

$$\ln N! = N \ln N - N \tag{39.117}$$

W is approximately

$$W = e^{12,360} \tag{39.118}$$

In essence an infinite amount of information can be represented as distinct Fourier series in k,ω −space according to this method of encoding it.

According to statistical thermodynamics [25], a macroscopic thermodynamic system is viewed as an assembly of myriad submicroscopic entities in ever changing quantum states. Consider the number of distinct ways each called a microstate that a set number quanta of energy can be distributed between a set number of energy levels. The total number of microstates W associated with any configuration involving N distinguishable units is

$$W = \frac{N!}{(\eta_a!)(\eta_b!)} \tag{39.119}$$

where η_a represents the number of units assigned the same number of energy quanta (and, hence, occupying the same quantum number), and η_b represents the number of units occupying some other quantum level. As the number of units increases, the total number of microstates skyrockets to unimaginable magnitudes. Thus, one can calculate that an assembly of 1000 localized harmonic oscillators sharing 1000 energy quanta possesses more than 10^{600} different microstates. This explosive expansion of the total number of microstates with increasing N is a direct consequence of the mathematics of permutations, from which arises also a second consequence of no less importance. Statistical analysis shows that the emergence of a *predominant configuration* is characteristic of any assembly with a large number (N) of units. Of the immense total number of microstates that can be assumed by a large assembly, an overwhelming proportion arises from one comparatively, small set of configurations centered on, and only minutely different

from, the predominant configuration--with which they share an empirically identical set of macroscopic properties.

Eq. (39.119) is equally valid for the number of distinct ways that a set of "active" states at any given time can be distributed over N "P elements" and "M elements" where η_a represents one set of indistinguishable "P elements", or "M elements", and η_b represents another set of indistinguishable "P elements", or "M elements". Eq. (39.119) is equally valid for the number of distinct ways that interference or "coupling" can occur between cascades of association "stages" at any given time distributed over N "links" where η_a represents one set of indistinguishable "links", and η_b represents another set of indistinguishable "links". Of the immense total number of microstates that can be assumed by a large assembly of "active" states distributed over a large set of "P or M elements" or by a large assembly of "couplings" distributed over many cascades of association "stages", an overwhelming proportion arises from one comparatively, small set of configurations centered on, and only minutely different from, the predominant configuration--with which they share an empirically identical set of macroscopic properties. Due to the large numbers of "P and M elements" and cascades of association "stages" involved in information processing, the present "processor's" performance is stable.

Consider the "processor" on a component level such as that of a "P element". In an embodiment, the activation of a "P element" increases its excitability or probability of future activation with input. Each "P element" has an "activation" memory with a finite half-life. Repetitive "activation" of a "P element" results in a longer half-life of the increased excitability; thus, the "activation" memory becomes long term. The same principle applies to ensembles of association "stages", "processor elements" ("P elements"), and "memory elements" ("M elements") and "configurations" of "couplings" of ensembles. Each ensemble is comprised of "stages", "P elements", or "M elements" in different states of "activity" where each state is equivalent to a microstate of statistical thermodynamics. A predominant configuration arises for any ensemble. Of the immense total number of microstates that can be assumed by an ensemble, an overwhelming proportion arises from one comparatively, small set of configurations centered on, and only minutely different from, the predominant configuration--with which they share an empirically identical set of macroscopic properties. On a higher level, a configuration of "couplings" between ensembles increases the activation of the "stages" "P elements", or "M elements" comprising the ensembles. Analogously to statistical thermodynamics, a predominant configuration arises from the ensemble level. Consider the "processor" on a higher

level. The activation history of each ensemble relates to a hierarchical activation relationship of "coupled" ensembles which gives rise to a precedence of higher order predominant configurations. The ability to associate information and create novel information, is a consequence. Machine learning arises by the feedback loop of transducer input to the coupled predominant configurations which increases the basis for creating information with novel conceptual content.

EXPERIMENTAL

The brain processes input data from each transducer such as an olfactory bulb as a Fourier series in k,ω −space. The Fourier series represents information with context. The context is encoded in time. The input is produced by its transducer and encoded to its transducer. The encoding occurs by each transducer having a characteristic modulation frequency band in k,ω −space. The input of each transducer maps to a distinct memory location called a "domain" such as a specific location in the olfactory lobe. The mapping encodes transducer context within the corresponding frequency band as a delay in time. The delay in time corresponds to the "domain". The process of storing "input" from multiple transducers to memory further comprises creation of "memory connections" called "transducer strings" in APPENDIX VI--Input Context.

Identifications of sensory "input" can be made by forming associations with memory. A cascade of association neurons ("stages") comprise an association assemble. As shown in APPENDIX II--Modulation and Sampling Gives the Input to the Association Mechanism and Basis of Reasoning, the cascade comprises a delayed Gaussian filter in the time domain. An important feature of the statistics of cascaded stages is that not all of the cascaded "stages" need to be active at any cycle to achieve essentially the same characteristic for large N as given by Eq. (39.50). The association neurons ("stages") of an association ensemble are weakly linked to the cascaded association neurons ("stages") of other association ensembles. Association ensembles carrying the corresponding Fourier series "couple" with Poissonian probability to form association of Fourier series. Each Fourier series has a specific transducer frequency band modulation factor. (See APPENDIX III--The Association Mechanism and Basis of Reasoning.) Each association ensemble modulates and samples the Fourier series in k,ω −space. In the time domain, each association ensemble, a delayed Gaussian filter, time delays and filters the sensory and memory time waveforms or functions. Each time domain function corresponding to an input "carried" by an "association ensemble" is a superposition of pairs of Gaussian pulses where each pair is active in a precise spatial and temporal sequence.

The phase of firing contains no information as given by Eq. (39.86) and Eq. (39.87a). Thus, a stimulus is predicted to evoke activity in dynamic (evolving) ensembles of transiently synchronized neurons. The active neurons composing these ensembles should change in a stimulus-specific manner and with a high degree of reliability on a cycle-by cycle basis during a stimulus response. Hence, information about a stimulus is contained not only in the neural assembly active at each oscillation cycle, but also in the precise temporal sequence in which these assemblies are updated during an a stimulus response. Neural coding with oscillations thus allows combinatorial representations in time as well as in space. This predicted stimulus response is consistent with the recent results of Wehr and Laurent [26] who measured the odour evoked response of the olfactory antennal lobe of the locust.

Wehr and Laurent report [26] in their Nature article entitled "Odour encoding by temporal sequences of firing in oscillating neural assemblies" that stimulus-evoked oscillatory synchronization of activity has been observed in many neural systems, including the cerebral cortex and the brain of insects. The possible functions of such rhythmic synchronization in neural coding, however, remain largely speculative. In the locust, odours evoke activity in dynamic (evolving) ensembles of transiently synchronized neurons. They report that the active neurons composing these ensembles change in a stimulus-specific manner and with a high degree of reliability on a cycle-by-cycle basis during an odour response. Hence, information about an odour is contained not only in the neural assembly active at each oscillation cycle, but also in the precise temporal sequence in which these assemblies are updated during an odour response. Neural coding with oscillations thus allows combinatorial representations in time as well as space.

Although stimulus-evoked oscillations of brain potentials caused by synchronized neural activity have been known for about 50 years, the roles, if any, they might play in information coding remain conjectural. Wehr and Laurent tested two functional hypotheses of temporal codes that use oscillations. The first proposes that oscillations, by virtue of their periodic nature, allow the phase of neural signals (that is, the timing of action potentials relative to a specific or common reference during each cycle) to be a coding parameter. Different and possibly coexisting stimuli could thus be represented by different neural assemblies, respectively defined by a common phase of activity. The hypothesis predicts that the neural assemblies activated by different stimuli should synchronize at different phases. The second hypothesis rather proposes that oscillations allow rank order (for example, cycles 1, 2, and 4 of the oscillation) of action potentials produced by participating neurons to be coding parameters. In this scheme, the

order of recruitment of neurons in an oscillating assembly should be stimulus-specific. To test these hypotheses, they used the olfactory antennal lobe of the locust, in which individual odours are represented combinatorially by oscillating and dynamic neural assemblies, each formed by about 10% of a total of about 800 projection neurons (PNs). They recorded simultaneously the responses of small ensembles of PNs--the analogues of the mitral-tufted cells of the vertebrate olfactory bulb--in vivo, to airborne odourants. Odours evoked reliable temporal response patterns in projection neurons, with tight oscillatory synchronization and neuron-specific modulation of period firing probability. The phase of firing contained no information (i.e. in no case did the phase of action potentials relative to the field potential or to action potentials of other participating neurons appear to vary with, and thus participate in encoding, the stimulus). Thus, the first hypothesis was inconsistent in the evidence, but the second hypothesis was. Stimulus identity is encoded in the temporal features of firing of groups of neurons. The results showed that odours can reliably evoke specific sequences of activity across neural assemblies. The fine temporal structure of PN responses to mixtures of odours were not simple or predictable combinations of their responses to the components presented separately. Each odour, however complex, apparently evoked activity in its own specific neuronal set and its own specific sequence of activity (coarse and fine levels of analysis). In reality, PN firing is probabilistic and average firing possibilities are not available to the animal on a single odour sampling. Information is, therefore, probably gathered from multiple neurons at once as well as over several oscillation cycles. Previous results indicate that odours are probably represented by about 100 neurons; only a subgroup of these are likely to be coactive during any given oscillation cycle.

In summary, Wehr and Laurent have shown that odours evoke activity in neural assemblies that are updated non-randomly at each cycle of an oscillatory response pattern. Information about the stimulus is found not in the phase of active neurons (which is statistically invariant when neurons synchronize to each other) but rather in their identity and in the temporal pattern in which they are recruited (this study [26]). The firing probability of individual neurons during one cycle of the response can be linked to that of other neurons during the same or other cycles, indicating deterministic and stimulus-specific sequential activation of groups of neurons. In principle, the timing of these odour-encoding sequences need not be precisely locked to the stimulus, although it is the feature which allowed their detection. Wehr and Laurent propose that oscillations are a means to encode stimuli in a temporal combinatorial fashion. In this hypothesis, stimuli are

represented both by spatial (instantaneous) ensembles, that is, the neurons activated together during any given cycle, and by temporal sequences, reflected in the responses of individual or groups of neurons over several cycles. Given the probabilistic nature of any neuron firing in any one cycle of the oscillatory response, the information provided by spatial ensembles alone is often ambiguous. Wehr and Laurent propose that the brain reduces the ambiguity by assigning "meaning" to the pattern in which these ensembles succeed each other. In particular, such a mechanism might aid reliable and rapid stimulus identification. In mammals, for example, each inspiration evokes 5-10 cycles of gamma frequency (30-60 Hz) oscillations in the olfactory bulb. In insects, behavioral studies indicate that odour identification is possible in a few hundred milliseconds, allowing in principle only 4-6 cycles of 20-30 Hz oscillations. Such a coding mechanism might also occur in any sensory system (cortical or not) expressing oscillatory synchronization, such as the visual and somatosensory cortices of mammals. Evidence from flies and from rat, cat, and primate neocortical neurons in vitro and in vivo is also consistent with the possibility that spike timing might play a role in information coding here, although previous studies did not consider spike timing within the context of oscillatory synchronization. Wehr and Laurent's study shows that oscillations can support combinatorial coding in time, and that information about a stimulus is contained in the precise temporal firing pattern of groups of neurons and is not dependent on phase.

References

1. Fock, V., The Theory of Space, Time, and Gravitation, The MacMillan Company, (1964).
2. Fang , L. Z., and Ruffini, R., Basic Concepts in Relativistic Astrophysics, World Scientific, (1983).
3. Jackson, J. D., Classical Electrodynamics, Second Edition, John Wiley & Sons, New York, (1962), pp. 758-763.
4. Jackson, J. D., Classical Electrodynamics, Second Edition, John Wiley & Sons, New York, (1962), pp. 758-763.
5. R. L. Mills, Provisional US Patent Application No. 60/068,834, "Pattern Recognition, Learning, and Processing Methods and Systems" filed December 24, 1997.
6. Siebert, W. McC., Circuits, Signals, and Systems, The MIT Press, Cambridge, Massachusetts, (1986), pp. 372-373.
7. Siebert, W. McC., Circuits, Signals, and Systems, The MIT Press, Cambridge, Massachusetts, (1986), pp. 435-439.
8. R. L. Mills, US Patent No. 5,064,754, "Genomic Sequencing Method", November 12, 1991.

9. R. L. Mills, US Patent No. 5,221,518, "DNA Sequencing Apparatus", June 22, 1993.
10. Reynolds, G. O., DeVelis, J. B., Parrent, G. B., Thompson, B. J., The New Physical Optics Notebook, SPIE Optical Engineering Press, (1990).
11. Mills, R., The Grand Unified Theory of Classical Quantum Mechanics, January 1999 Edition, Amazon.com.
12. Mills, R., Magnetic Susceptibility Imaging (MSI), U.S. Patent No. 5,073,858 (1991); Mills, R., Resonant Magnetic Susceptibility Imaging (ReMSI), Provisional US Patent Application No. 60/065,318, filed November 13, 1997.
13. Siebert, W. McC., Circuits, Signals, and Systems, The MIT Press, Cambridge, Massachusetts, (1986), p. 416.
14. Siebert, W. McC., Circuits, Signals, and Systems, The MIT Press, Cambridge, Massachusetts, (1986), pp. 491-497.
15. M. Fisz, Probability Theory and Mathematical Statistics, New York, New York, John Wiley, (1963). The version stated is a special case of Lyapunov's Theorem.
16. A. A. Maradudin, Rev. Mod. Phys., Vol. 36, (1964), pp. 417-432.2.
17. A. Messiah, Quantum Mechanics, Vol. I, North-Holland Publishing Company, Amsterdam, (1961), p. 442.
18. H. Ott, Ann. Physik, Vol. 23, (1935), p. 169.
19. F. Bloch, Z. Physik, Vol. 74, (1932), p. 295.
20. G. N. Watson, Bessel Functions, Cambridge University Press, Cambridge, (1944), p. 14.
21. R. V. Hogg, E. A. Tanis, Probability and Statistical Inference, MacMillan Publishing Co., Inc., New York, (1977), pp. 128-129.
22. R. V. Hogg, E. A. Tanis, Probability and Statistical Inference, MacMillan Publishing Co., Inc., New York, (1977), pp. 78-82.
23. R. V. Hogg, E. A. Tanis, Probability and Statistical Inference, MacMillan Publishing Co., Inc., New York, (1977).
24. Siebert, W. McC., Circuits, Signals, and Systems, The MIT Press, Cambridge, Massachusetts, (1986).
25. L. K. Nash, Chemthermo: A Statistical approach to Classical Chemical Thermodynamics, Addison-Wesley Publishing Company, Reading Massachusetts, (1976), pp. 1-44.
26. M. W. Wehr, G. Laurent, Nature, Vol. 384, No. 14, November, (1996), pp. 162-165.

708

FIGURE 1 is a high level block diagram illustrating an embodiment of the present "processor".

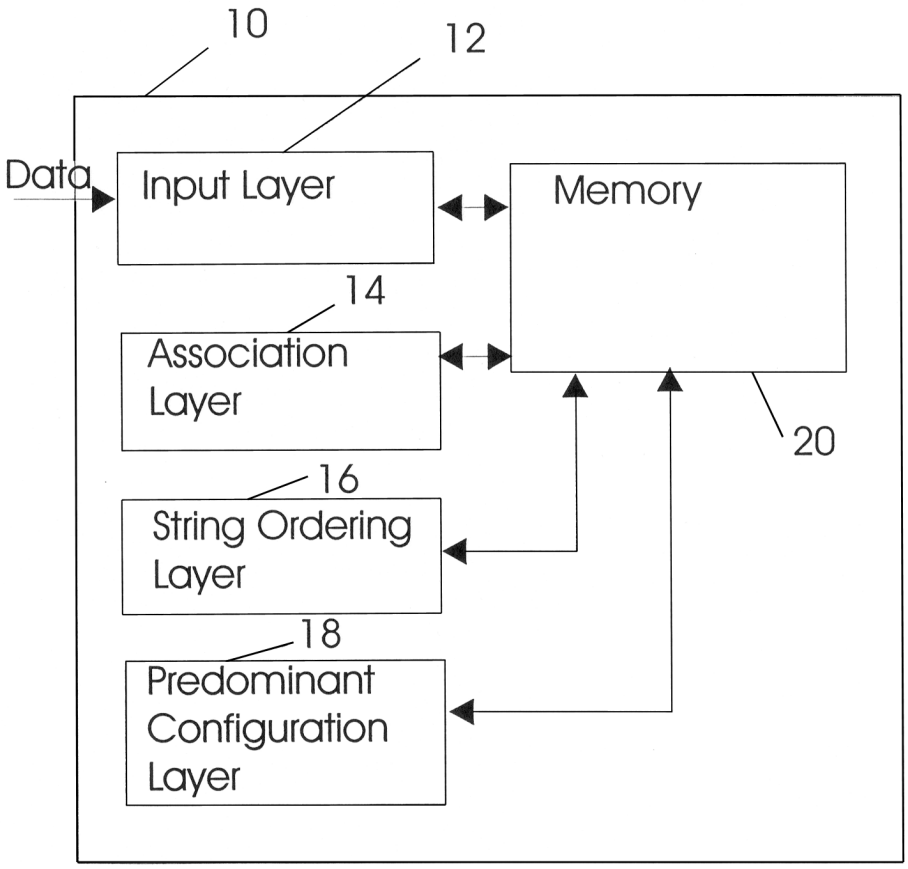

FIGURE 2 is a detailed block diagram illustrating an Input Layer, an Association Layer, and a memory layer of the embodiment of FIGURE 1.

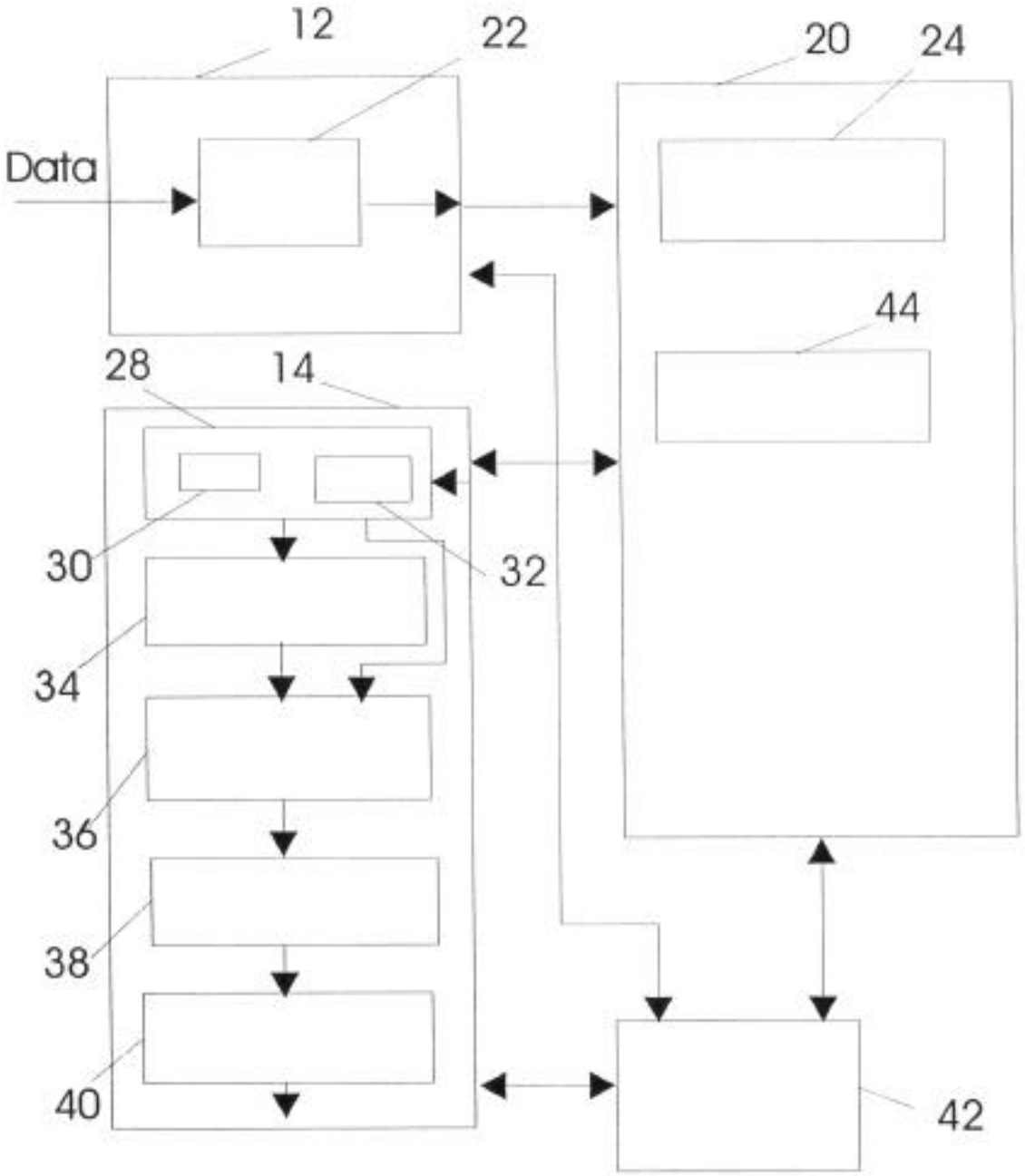

710

FIGURE 3 is a flow diagram of an exemplary transducer data structure of a time delay interval subdivision hierarchy wherein the data from a transducer having n levels of subcomponents numbering integer m per level is assigned a master time interval with $n+1$ sub time intervals in a hierarchical manner wherein the data stream from the final n th level transducer element is recorded as a function of time in the $n+1$ th time coded sub memory buffer.

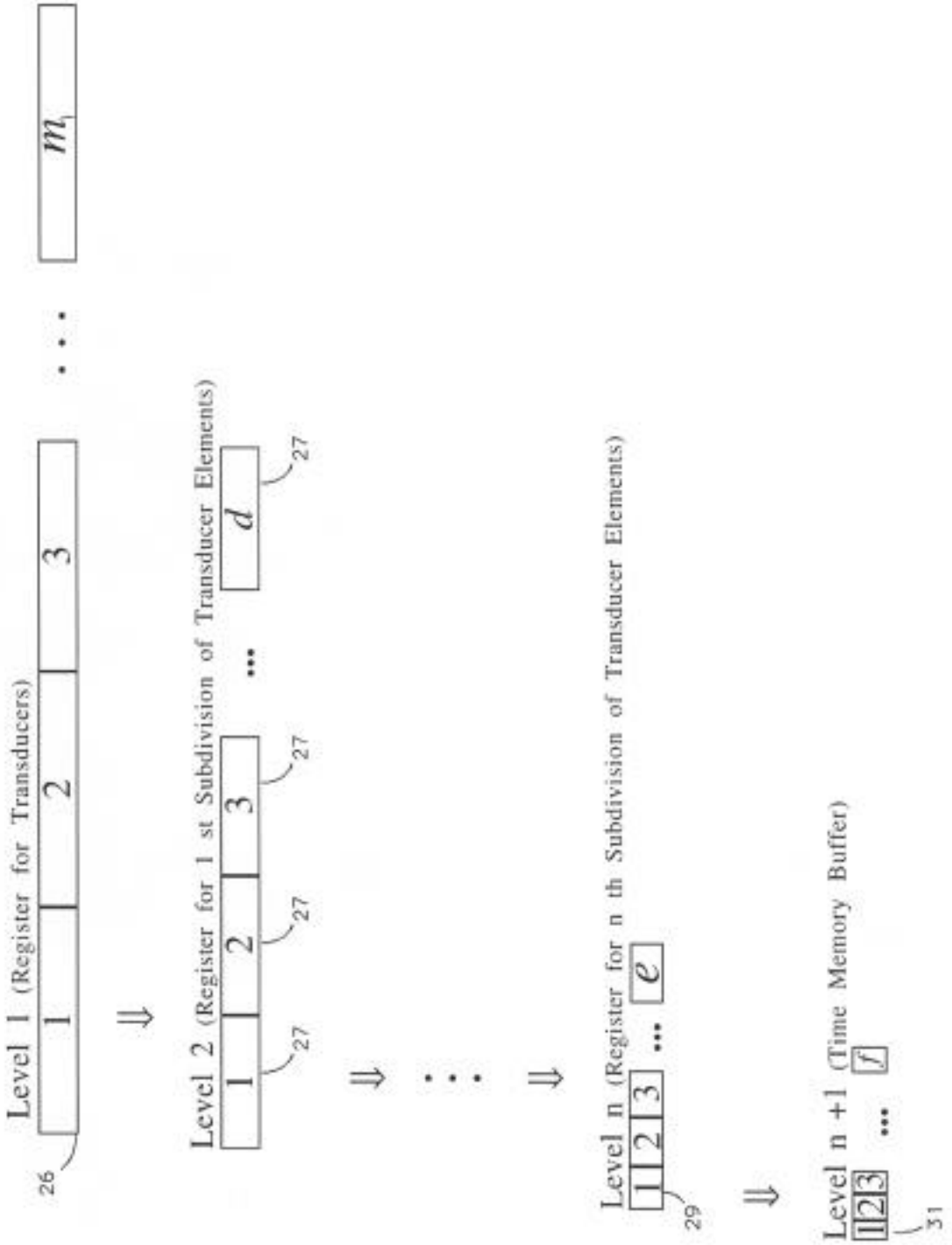

FIGURE 4 is a detailed block diagram illustrating an String Ordering Layer and the memory layer of the embodiment of FIGURE 1.

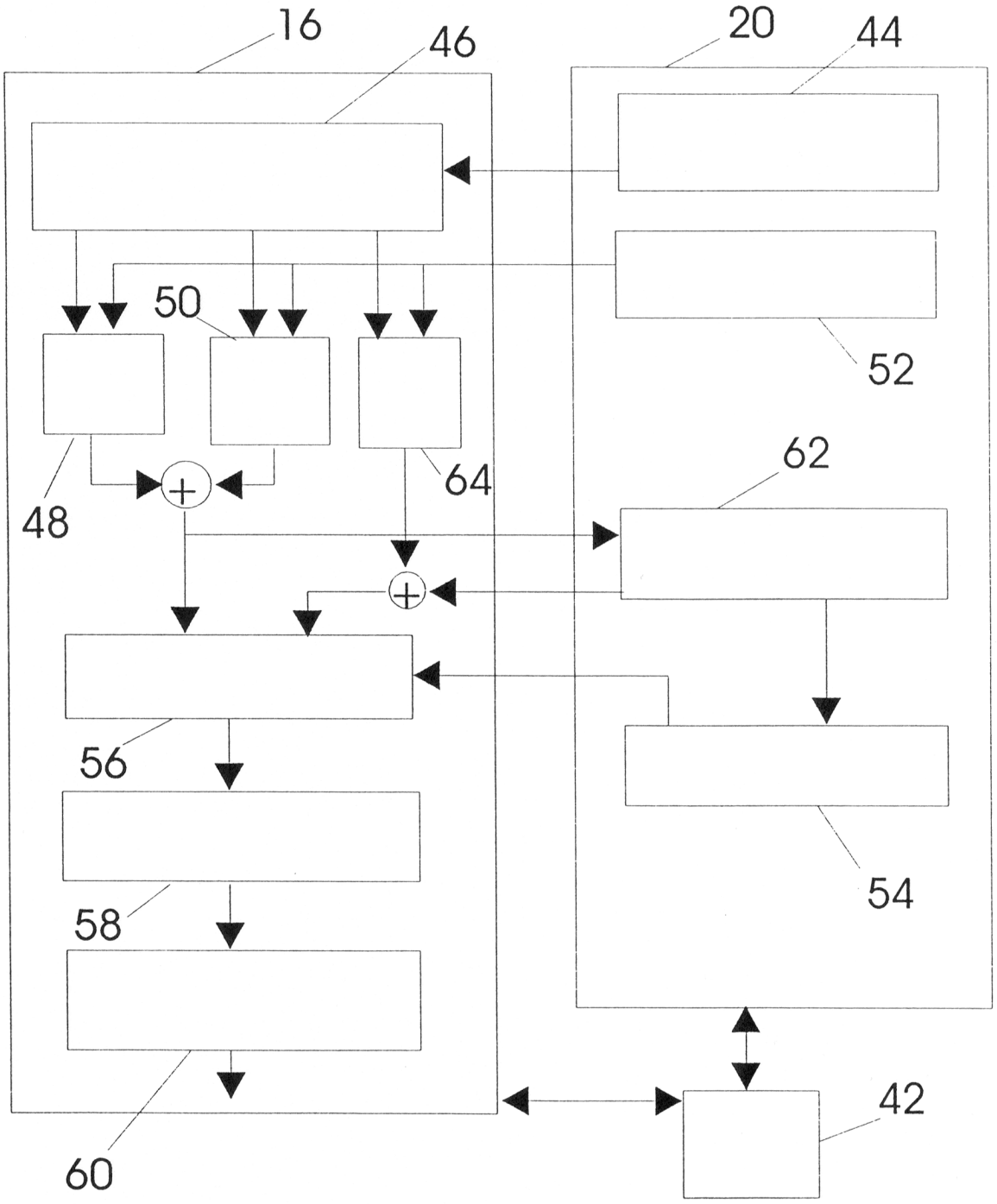

712

FIGURE 5 is a detailed block diagram illustrating a Predominant Configuration Layer and the memory of the embodiment of FIGURE 1 in relation to the Input Layer, the Association Layer, and the String Ordering Layer.

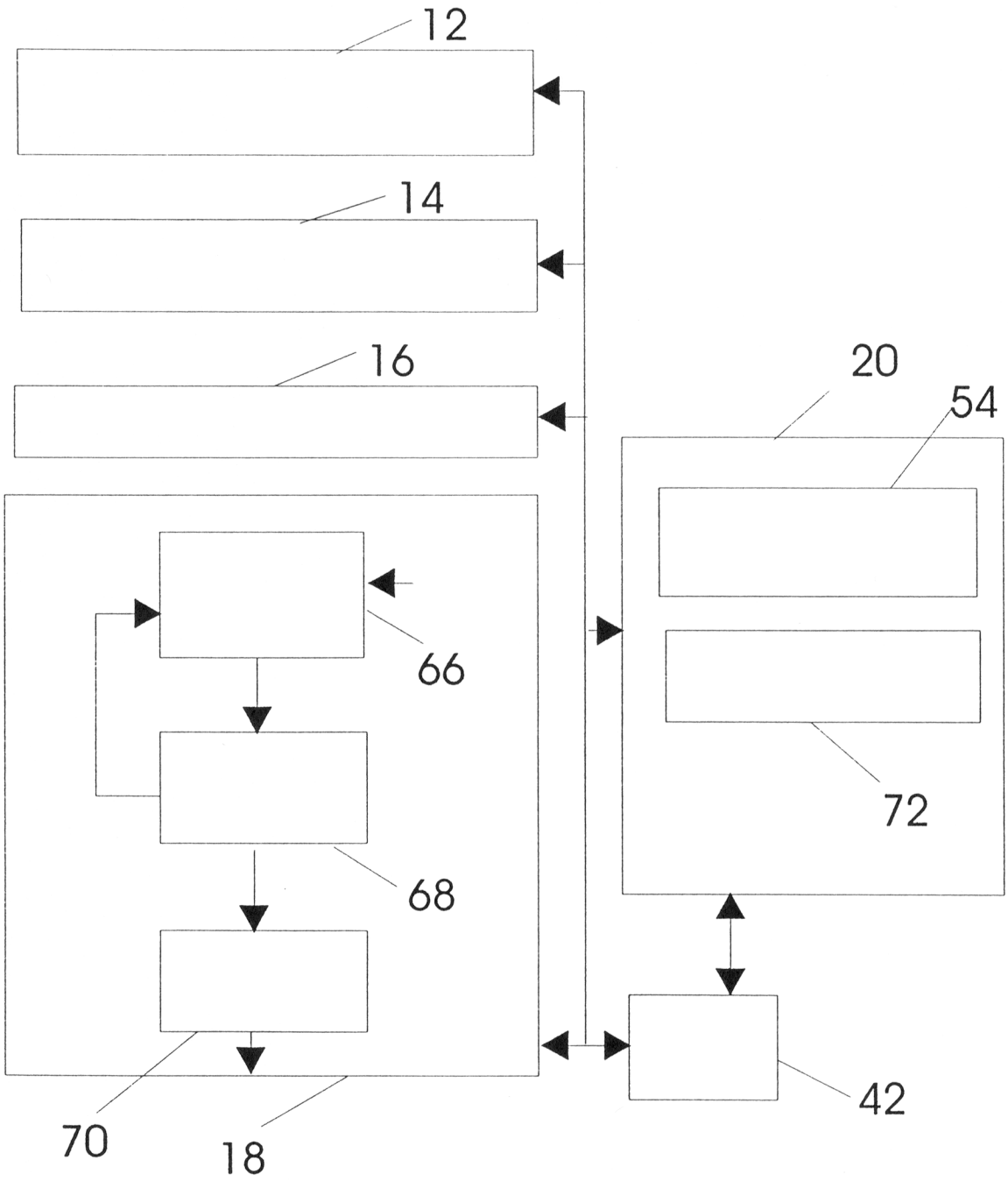

FIGURE 6 is a schematic drawing of the "P or M element response" comprised of a series of seven "impulse responses".

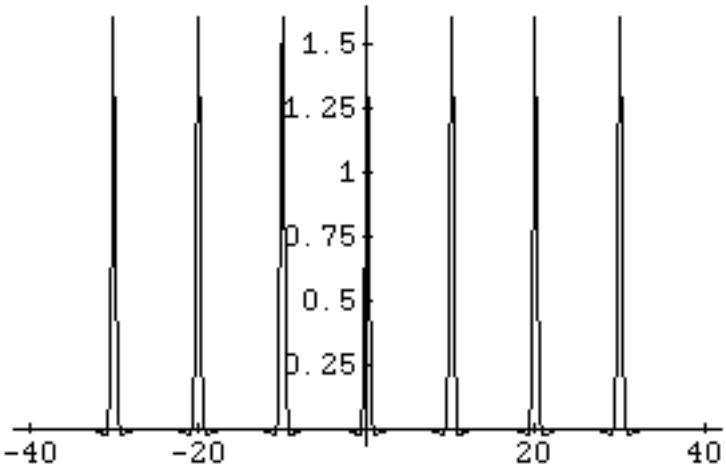

FIGURE 7 is a schematic drawing of the Fourier Transform $H[k_\rho, k_z]$ of the system function $h(\rho, z)$ corresponding to the "impulse response".

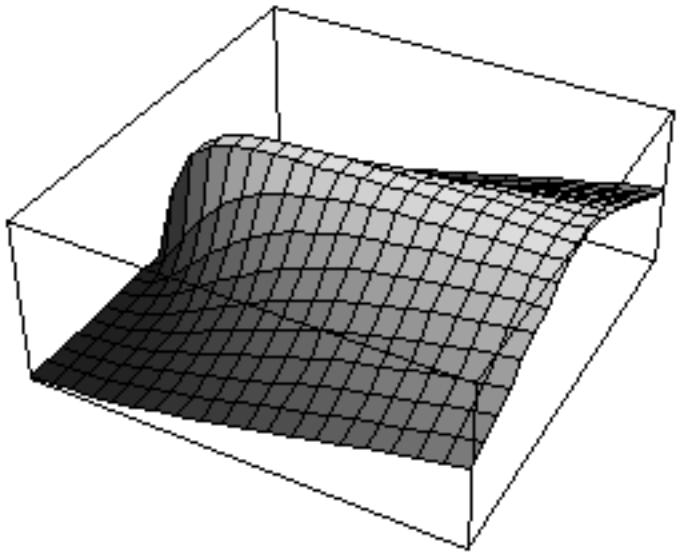

FIGURE 8 is a schematic of $h(t)$ given by Eq. (39.51) where $\alpha = 1$ and $N = 100$.

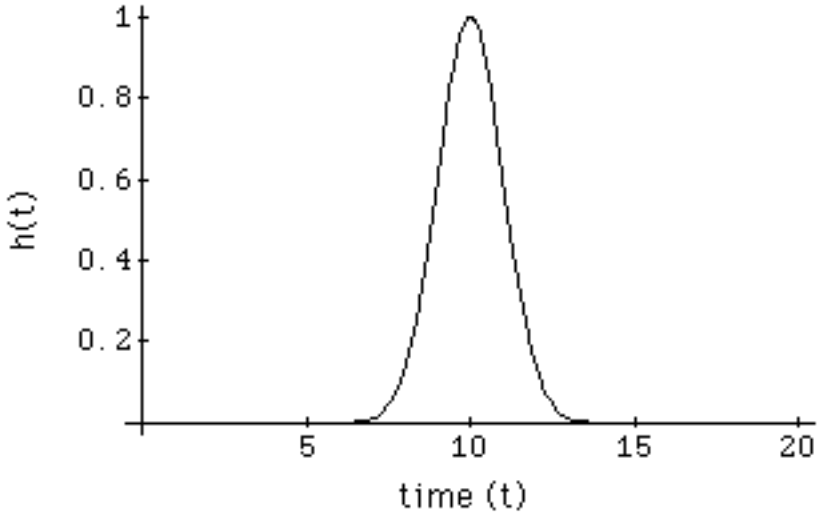

FIGURE 9 is a schematic of $H(f)$ given by Eq. (39.50) where $\alpha = 1$ and $N = 100$.

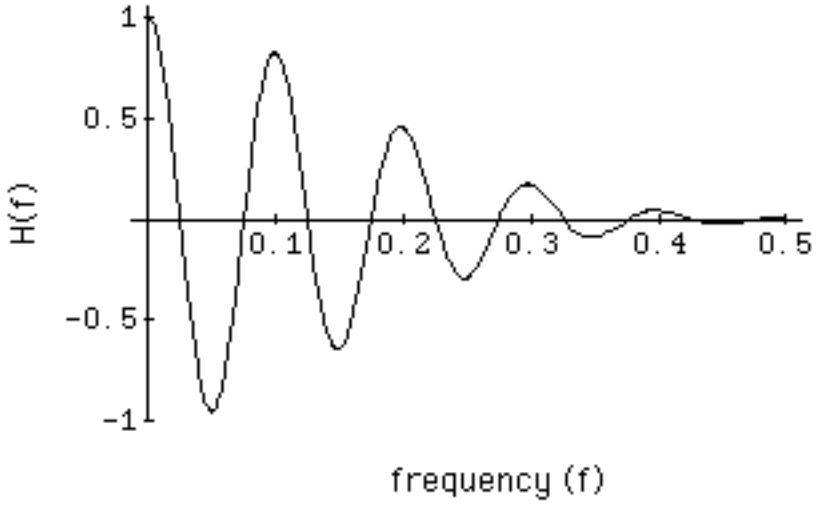

FIGURE 10 is a schematic of $h(t)$ given by Eq. (39.51) where $\alpha = 10$ and $N = 100$.

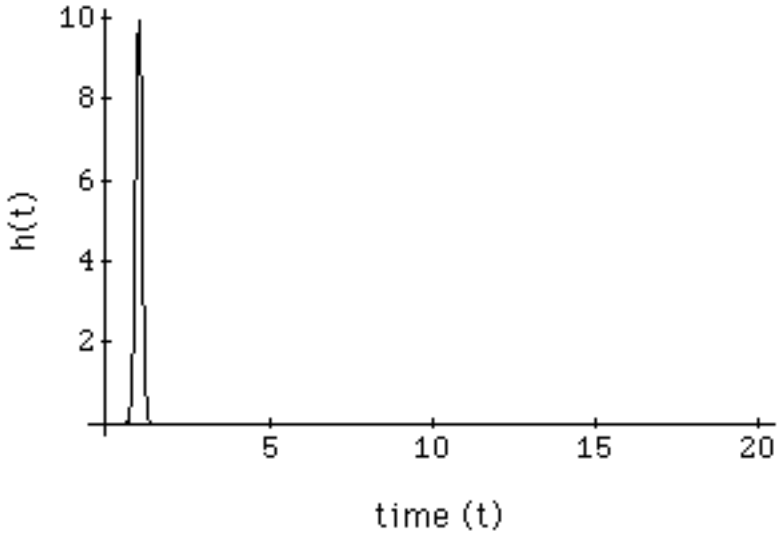

FIGURE 11 is a schematic of $H(f)$ given by Eq. (39.50) where $\alpha = 10$ and $N = 100$.

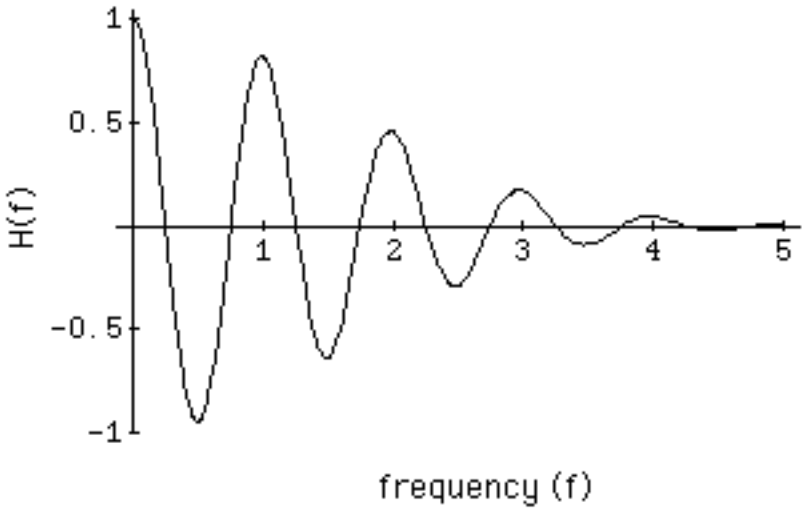

FIGURE 12 is a schematic of $h(t)$ given by Eq. (39.51) where $\alpha = 1$ and $N = 500$.

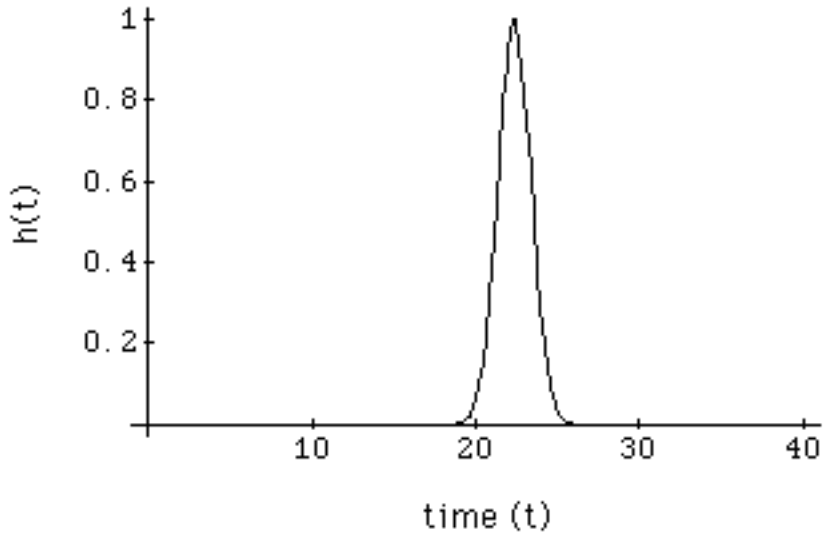

FIGURE 13 is a schematic of $H(f)$ given by Eq. (39.50) where $\alpha = 1$ and $N = 500$.

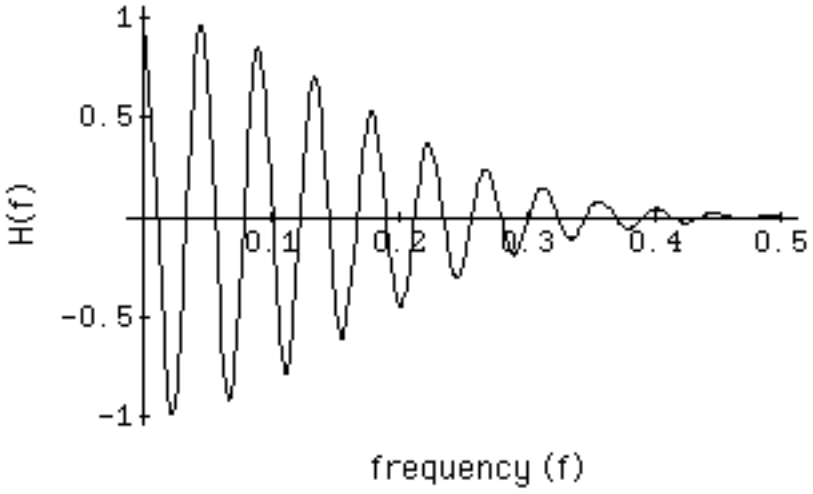

FIGURE 14 is a schematic of $h(t)$ given by Eq. (39.51) where $\alpha = 10$ and $N = 500$.

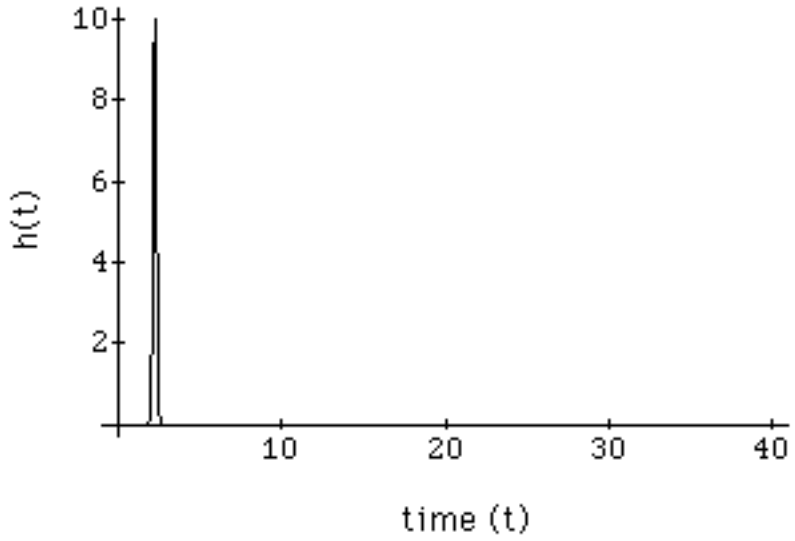

FIGURE 15 is a schematic of $H(f)$ given by Eq. (39.50) where $\alpha = 10$ and $N = 500$.

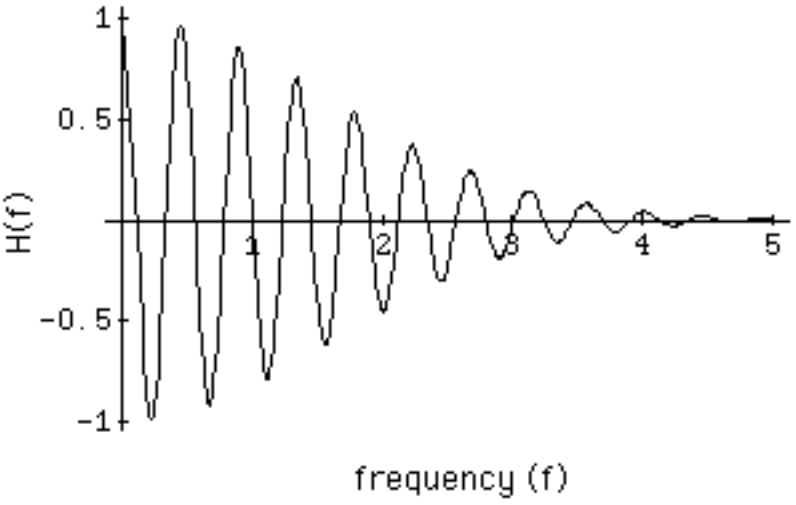

FIGURES 16A and 16B illustrate plots of the probability $P_A(\phi)$ (Eq. (39.106a)) of association of the corresponding Fourier series based on a first active association ensemble coupling with a second association ensemble as a function of frequency difference angle, ϕ_s, coupling cross section amplitude, β_s^2, and phase shift, $\delta_s = 0$ wherein the parameter β_s^2=0.01 and 0.25 respectively.

Fig. 16 **A**

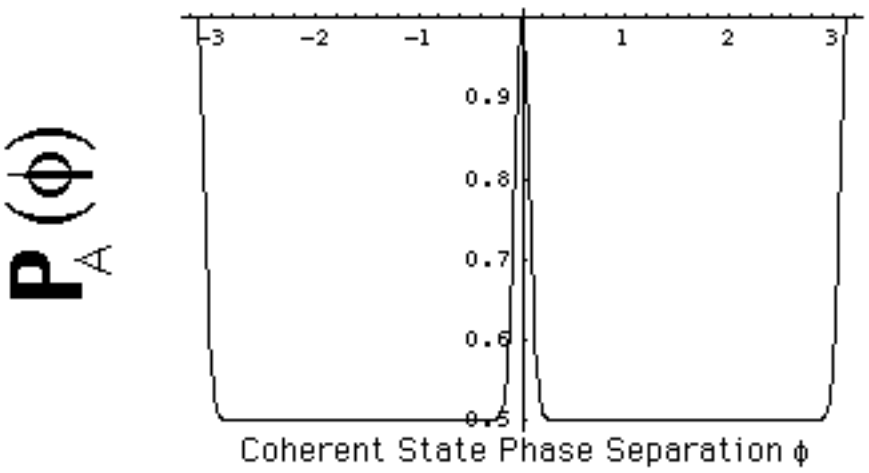

Fig. 16 **B**

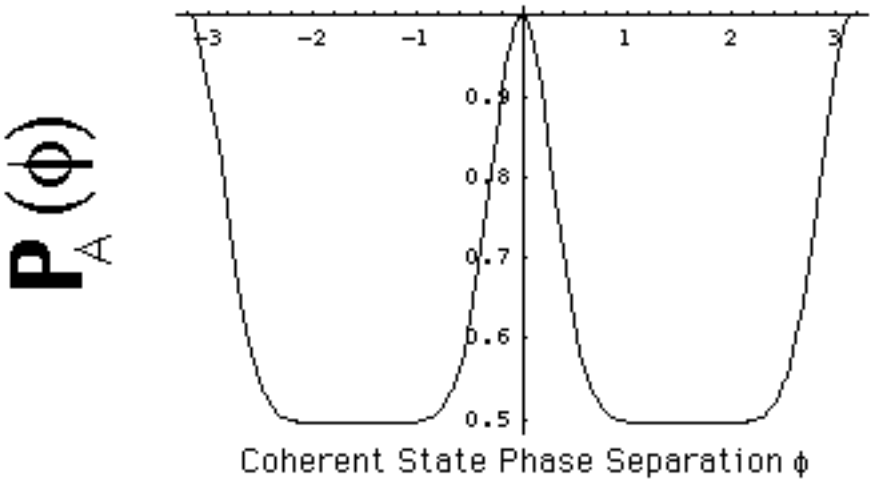

FIGURES 16C illustrates a plot of the probability $P_A(\phi)$ (Eq. (39.106a)) of association of the corresponding Fourier series based on a first active association ensemble coupling with a second association ensemble as a function of frequency difference angle, ϕ_s, coupling cross section amplitude, β_s^2, and phase shift, $\delta_s = 0$ wherein the parameter β_s^2=1.00.

Fig. 16 C

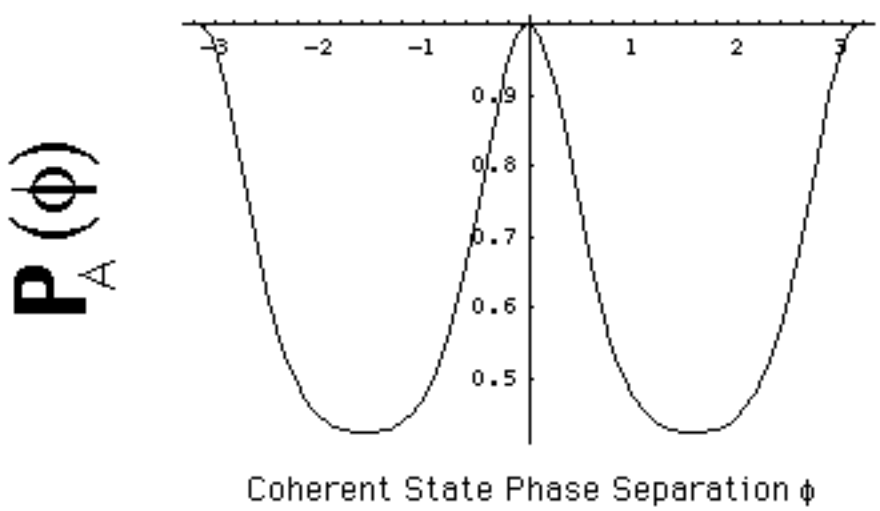

FIGURES 17A and 17B illustrate plots of the probability $P_A(\phi)$ (Eq. (39.106a)) of association of the corresponding Fourier series based on a first active association ensemble coupling with a second association ensemble as a function of frequency difference angle, ϕ_s, and phase shift, δ_s, for the coupling cross section amplitude, $\beta_s^2 = 0.25$, wherein the parameter $\delta_s = 0$ and 0.25π, respectively.

Fig. 17A

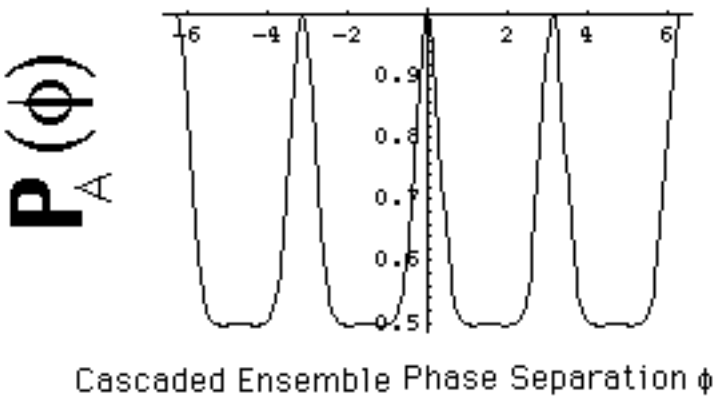

Fig. 17B

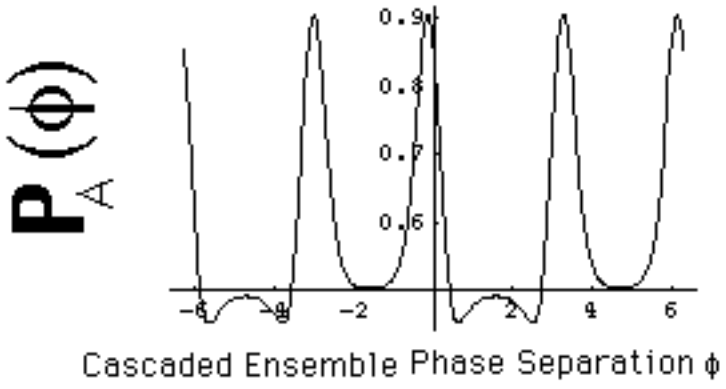

FIGURES 17C, and 17D illustrate plots of the probability $P_A(\phi)$ (Eq. (39.106a)) of association of the corresponding Fourier series based on a first active association ensemble coupling with a second association ensemble as a function of frequency difference angle, ϕ_s, and phase shift, δ_s, for the coupling cross section amplitude, $\beta_s^2 = 0.25$, wherein the parameter $\delta_s = 0.50\pi$, and π, respectively.

Fig. 17 **C**

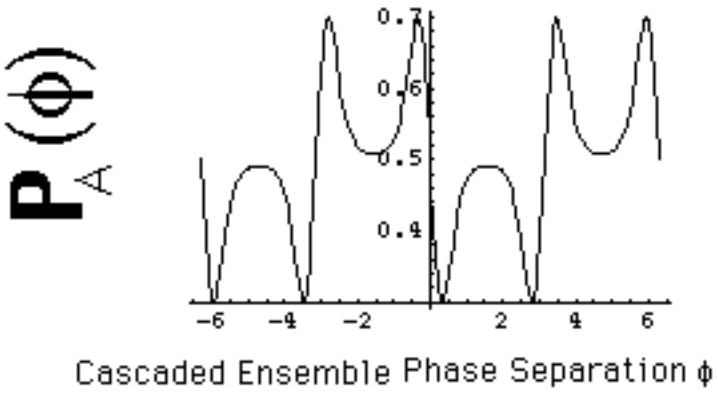

Fig. 17 **D**

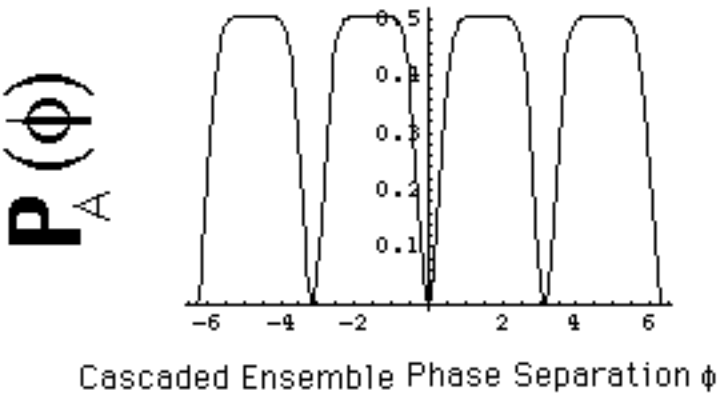

FIGURE 18 is a flow diagram of an exemplary hierarchical relationship between the characteristics and the processing and storage elements.

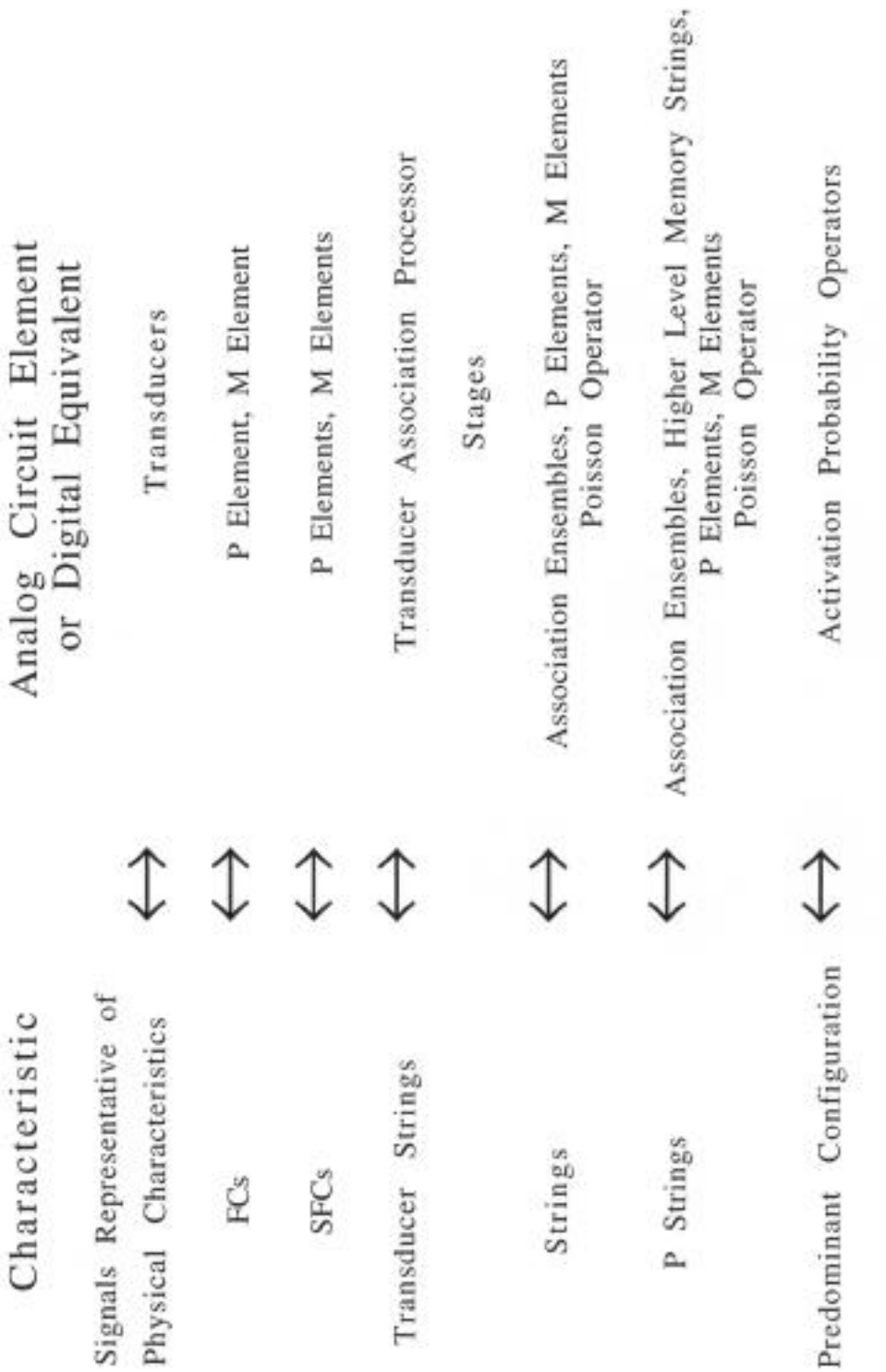

FIGURE 19 is a flow diagram of an exemplary hierarchical relationship of the signals in Fourier space comprising FCs, SFCs, groups of SFCs, and a string.

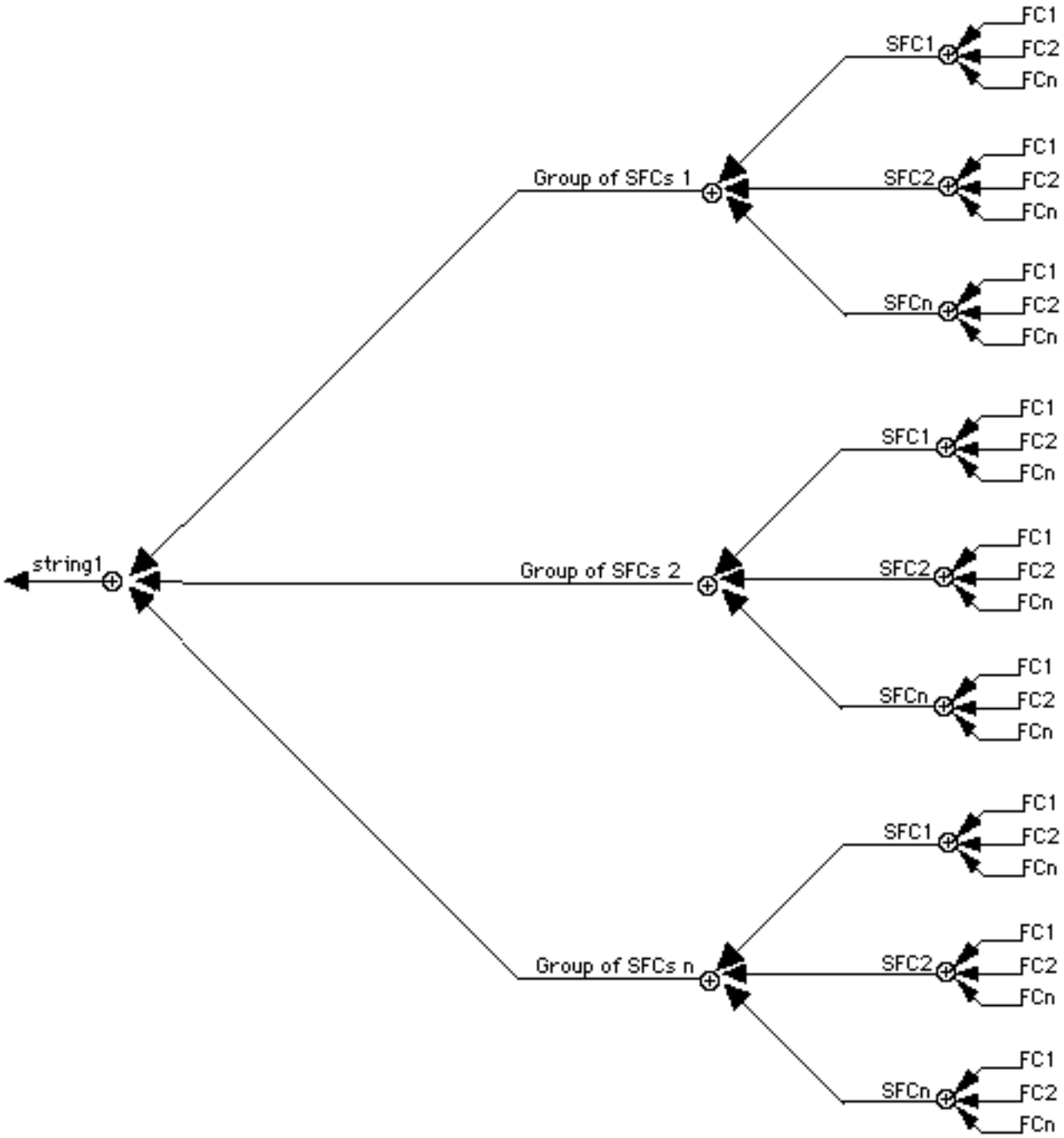

FIGURE 20 is an exemplary layer structure.

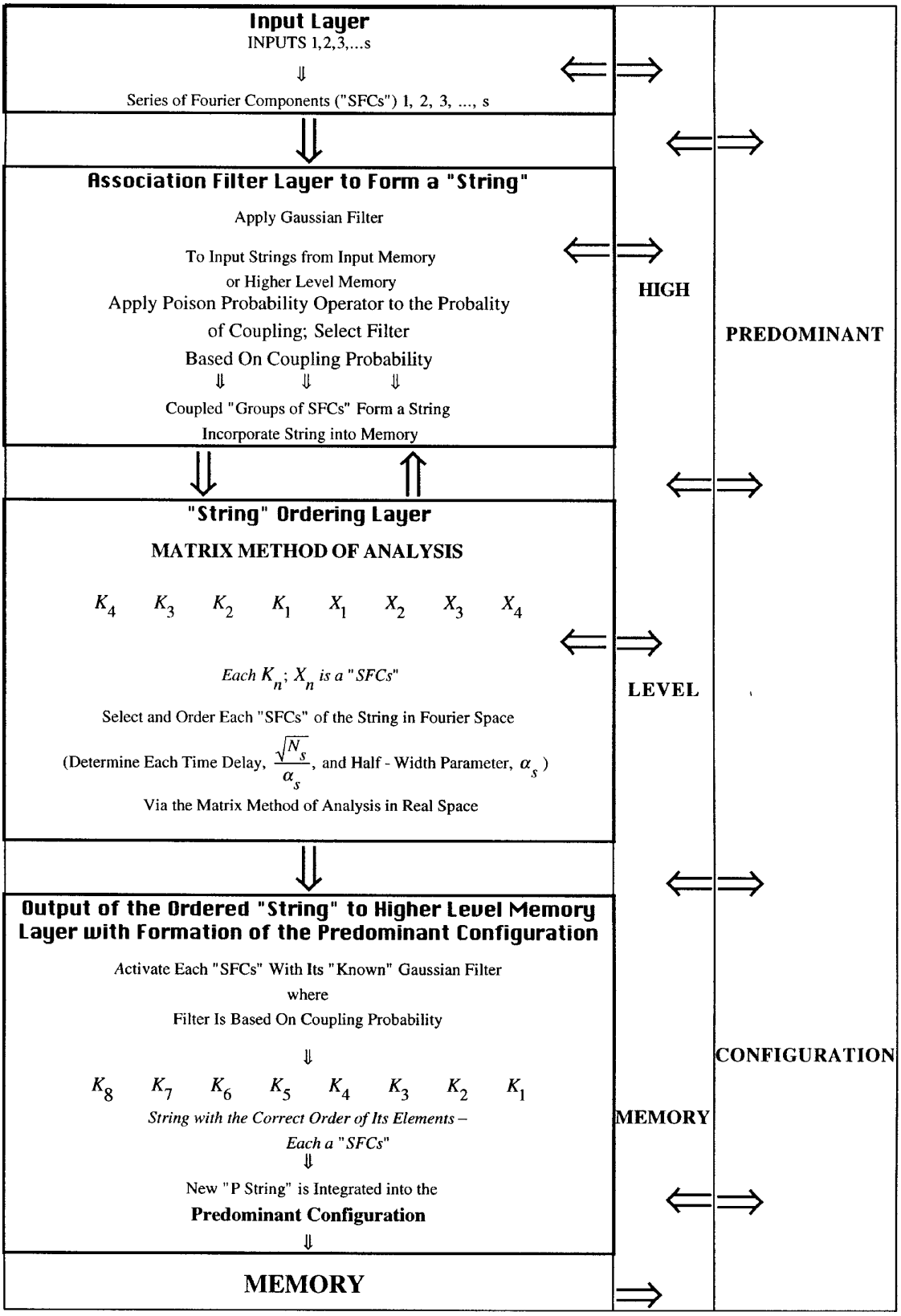

FIGURE 21 is a flow diagram of an exemplary layer structure and exemplary signal format.

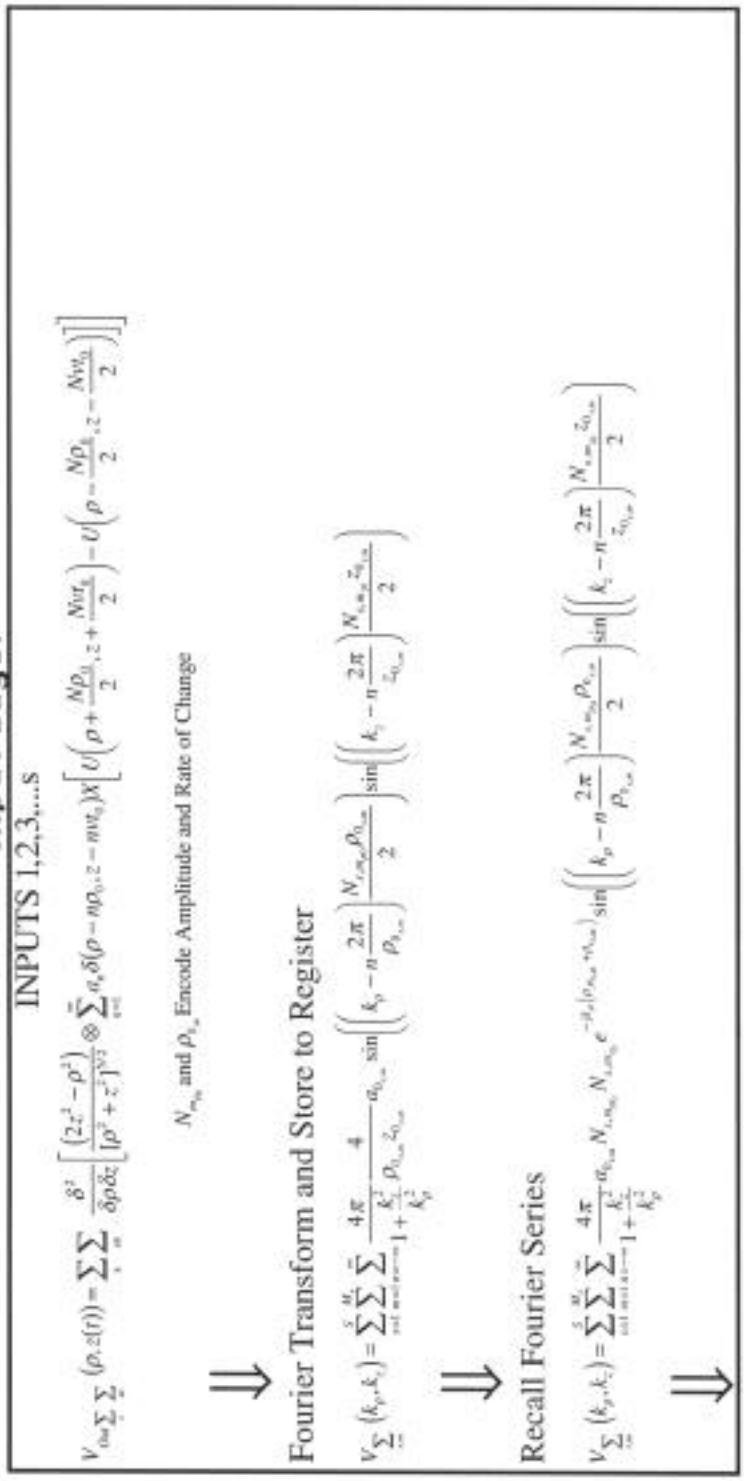

Fig. 21 Continued

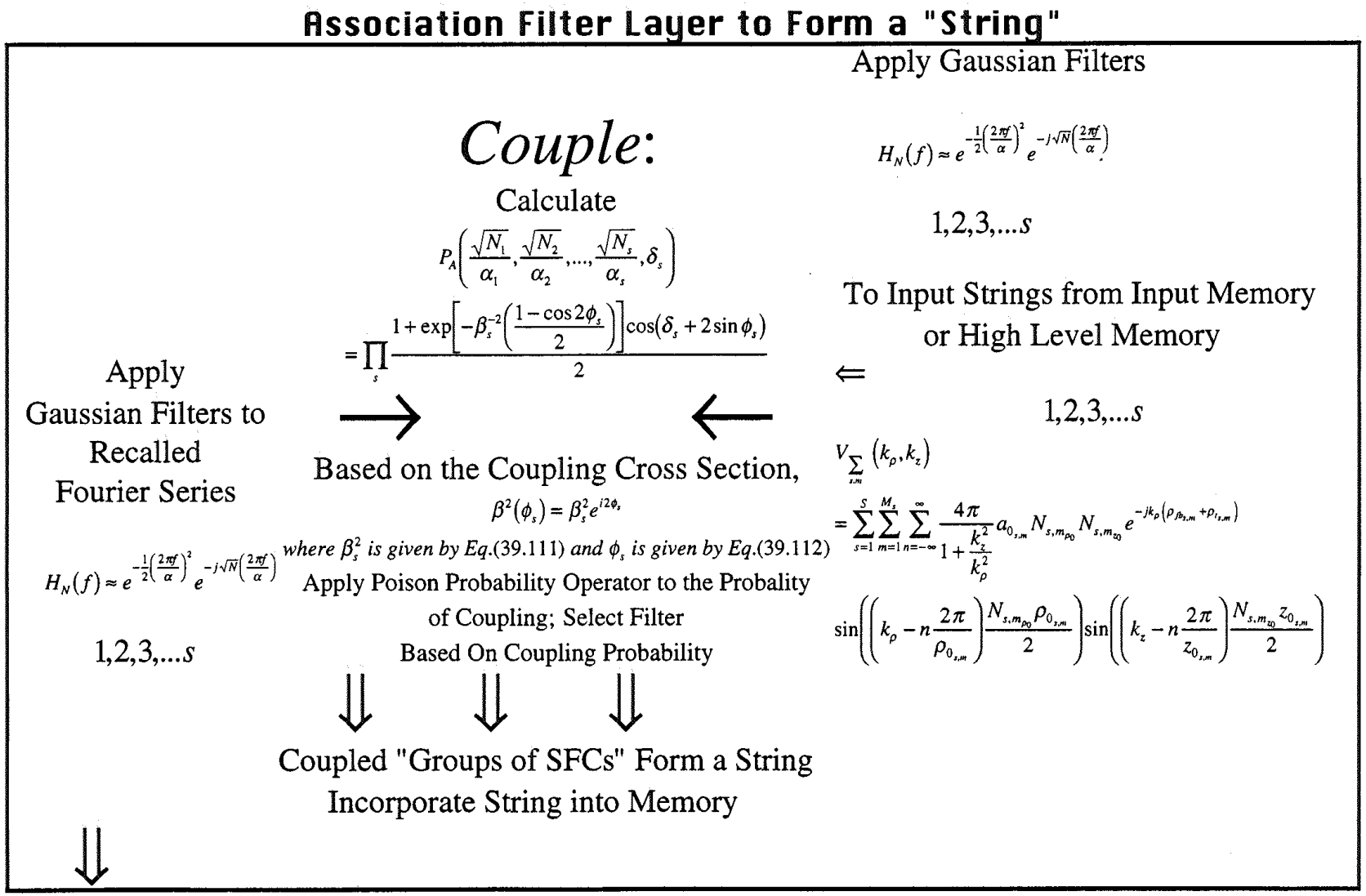

Fig. 21 Continued

"String" Ordering Layer

Recall String from Memory

$$V_{\sum_{s,m}}(k_\rho,k_z)=\sum_{s=1}^{S}\sum_{m=1}^{M_s}\sum_{n=-\infty}^{\infty}\frac{4\pi}{1+\frac{k_z^2}{k_\rho^2}}a_{0_{s,m}}N_{s,m_{\rho 0}}N_{s,m_{z0}}e^{-jk_\rho\left(\rho_{fb_{s,m}}+\rho_{1_{s,m}}\right)}$$

$$\sin\left(\left(k_\rho-n\frac{2\pi}{\rho_{0_{s,m}}}\right)\frac{N_{s,m_{\rho 0}}\rho_{0_{s,m}}}{2}\right)\sin\left(\left(k_z-n\frac{2\pi}{z_{0_{s,m}}}\right)\frac{N_{s,m_{z0}}z_{0_{s,m}}}{2}\right)$$

MATRIX METHOD OF ANALYSIS

$$K_4 \quad K_3 \quad K_2 \quad K_1 \quad X_1 \quad X_2 \quad X_3 \quad X_4$$

Each K_n; X_n is a "SFCs"

$$V_{\sum_{m}}(k_\rho,k_z)=\sum_{m=1}^{M}\sum_{n=-\infty}^{\infty}\frac{4\pi}{1+\frac{k_z^2}{k_\rho^2}}a_{0_m}N_{m_{\rho 0}}N_{m_{z0}}e^{-jk_\rho\left(\rho_{fb_m}+\rho_{1_m}\right)}\sin\left(k_\rho\frac{N_{m_{\rho 0}}\rho_{0_m}}{2}-n\frac{2\pi N_{m_{\rho 0}}}{2}\right)\sin\left(k_z\frac{N_{m_{z0}}z_{0_m}}{2}-n\frac{2\pi N_{m_{z0}}}{2}\right)$$

Select and Order Each "SFCs" of the String in Fourier Space

(Determine Each Time Delay, $\frac{\sqrt{N_s}}{\alpha_s}$, and Half-Width Parameter, α_s)

Via the Matrix Method of Analysis in Real Space

Fig. 21 Continued

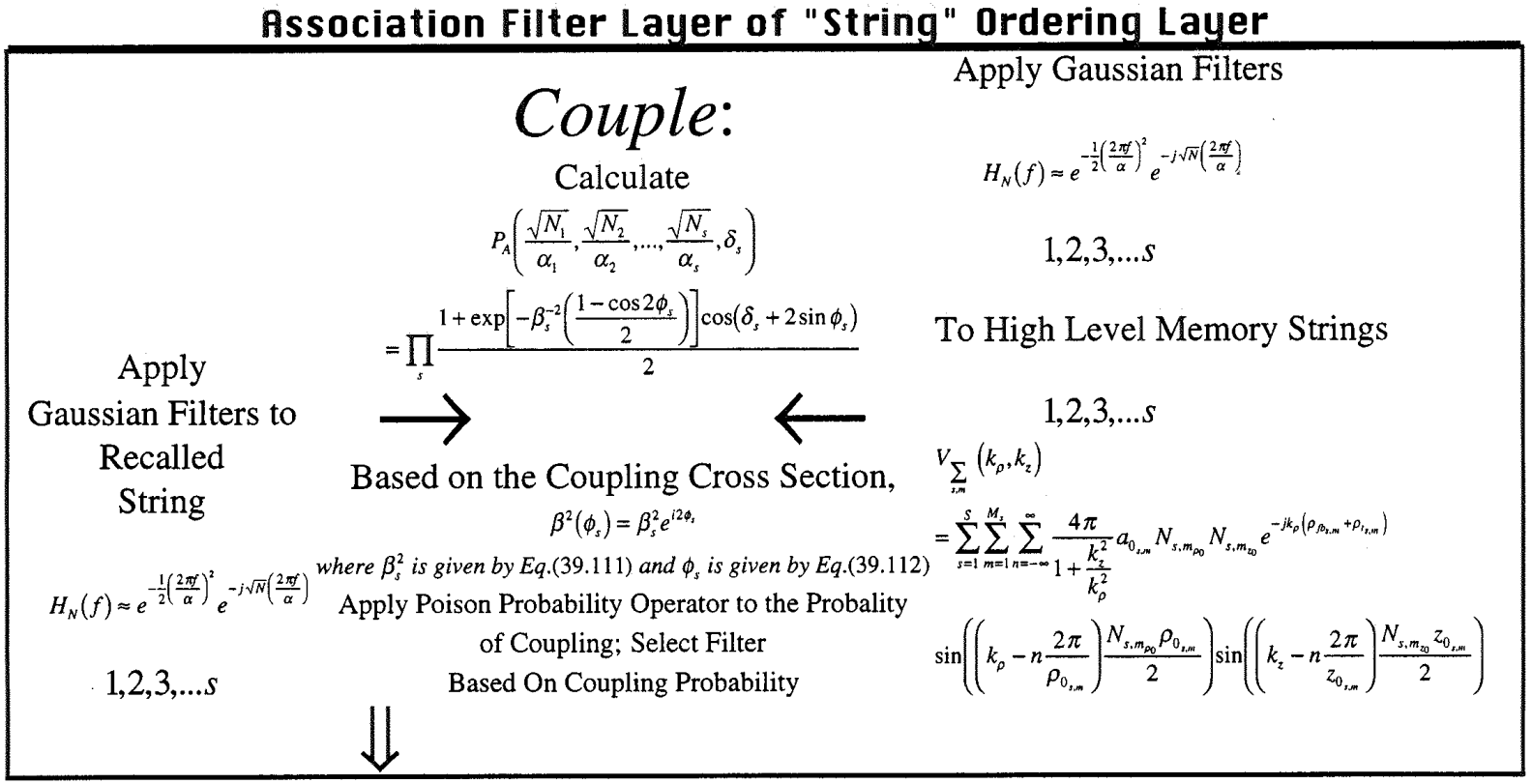

Fig. 21 Continued

Output of the Ordered "String" to Higher Level Memory Layer with Formation of the Predominant Configuration

Activate Each "SFCs" With Its "Known" Gaussian Filter

where

Filter Is Based On Coupling Probability

$$V_{\sum_{s,m}}\left(k_\rho,k_z\right)=\sum_{s=1}^{S}\sum_{m=1}^{M_s}\sum_{n=-\infty}^{\infty}\frac{4\pi}{1+\frac{k_z^2}{k_\rho^2}}a_{0_{s,m}}N_{s,m_{\rho 0}}N_{s,m_{z0}}e^{-\frac{1}{2}\left(v_{s\rho 0}\frac{k_\rho}{\alpha_{s\rho 0}}\right)^2}e^{-j\frac{\sqrt{N_{s\rho 0}}}{\alpha_{s\rho 0}}\left(v_{s\rho 0}k_\rho\right)}e^{-\frac{1}{2}\left(v_{sz0}\frac{k_z}{\alpha_{sz0}}\right)^2}e^{-j\frac{\sqrt{N_{sz0}}}{\alpha_{sz0}}\left(v_{sz0}k_z\right)}$$

$$e^{-jk_\rho\left(\rho_{fb_{s,m}}+\rho_{l_{s,m}}\right)}\sin\left(\left(k_\rho-n\frac{2\pi}{\rho_{0_{s,m}}}\right)\frac{N_{s,m_{\rho 0}}\rho_{0_{s,m}}}{2}\right)\sin\left(\left(k_z-n\frac{2\pi}{v_{s,m}t_{0_{s,m}}}\right)\frac{N_{s,m_{z0}}z_{0_{s,m}}}{2}\right)$$

⇓

K_8 K_7 K_6 K_5 K_4 K_3 K_2 K_1

String with the Correct Order of Its Elements– Each a "SFCs"

⇓

New "P String" is Integrated into the

Predominant Configuration

SECTION VI

Astrophysics

SPECTRAL DATA OF HYDRINOS FROM THE DARK INTERSTELLAR MEDIUM AND SPECTRAL DATA OF HYDRINOS, DIHYDRINOS, AND HYDRINO HYDRIDE IONS FROM THE SUN

Randell L. Mills

BlackLight Power, Inc.

493 Edinburg Road

Cranbury, NJ 08512

The detection of atomic hydrogen in fractional quantum energy levels below the traditional "ground" state—hydrinos—is reported by the assignment of soft x–ray emissions from the interstellar medium, the Sun, and stellar flares, and by assignment of certain lines obtained by the far-infrared absolute spectrometer (FIRAS) on the Cosmic Background Explorer. The detection of a new molecular species—the diatomic hydrino molecule—is reported by the assignment of certain infrared line emissions from the Sun. The detection of a new hydride species—hydrino hydride ion—is reported by the assignment of certain soft X-ray, ultraviolet (UV), and visible emissions from the Sun.

INTERSTELLAR MEDIUM

Hydrogen Transitions to Electronic Energy Levels Below the "Ground" State Corresponding to Fractional Quantum Numbers Match the Spectral Lines of the Extreme Ultraviolet Background of Interstellar Space.

Dark Matter

The Universe is predominantly comprised of hydrogen and a small amount of helium. These elements exist in interstellar regions of space, and they are expected to comprise the majority of interstellar matter. However, the observed constant angular velocity of many galaxies as the distance from the luminous galactic center increases can only be accounted for by the existence of nonluminous weakly interacting matter, dark matter. Dark matter exists at the cold fringes of galaxies and in cold interstellar space. It may account for the majority of the universal mass.

The identity of dark matter has been a cosmological mystery. Postulated assignments include τ neutrinos, but a detailed search for signature emissions has yielded nil [1]. It is anticipated that the emission spectrum of the extreme ultraviolet background of interstellar matter possesses the spectral signature of dark matter. In a recent paper, a grazing incidence spectrometer was designed to measure and record the diffuse extreme ultraviolet background [2]. The instrument was carried aboard a sounding rocket, and data were obtained between 80 *Å* and 650 *Å* (data points approximately every 1.5 *Å*). Several lines including an intense 635 *Å* emission associated with dark matter were observed [2].

> "Regardless of the origin, the 635 *Å* emission observed could be a major source of ionization. Reynolds (1983, 1984, 1985) has shown that diffuse Hα emission is ubiquitous throughout the Galaxy, and widespread sources of flux shortward of 912 *Å* are required. Pulsar dispersion measures (Reynolds 1989) indicate a high scale height for the associated ionized material. Since the path length for radiation shortward of 912 *Å* is low, this implies that the ionizing source must also have a large scale height and be widespread. Transient heating appears unlikely, and the steady state ionization rate is more than can be provided by cosmic rays, the soft X-ray background, B stars, or hot white dwarfs (Reynolds 1986; Brushweiler & Cheng 1988). Sciama (1990) and Salucci & Sciama (1990) have argued that a variety of observations can be explained by the presence of dark matter in the galaxy which decays with the emission of radiation below 912 *Å*.

The flux of 635 *Å* radiation required to produce hydrogen ionization is given by $F = \zeta_H / \sigma_\lambda = 4.3\ X\ 10^4 \zeta_{-13}\ photons\ cm^{-2} s^{-1}$, where ζ_{-13} is the ionizing rate in units of $10^{-13} s^{-1}$ per *H* atom. Reynolds (1986) estimates that in the immediate vicinity of the Sun, a steady state ionizing rate of ζ_{-13} between 0.4 and 3.0 is required. To produce this range of ionization, the 635 *Å* intensity we observe would have to be distributed over 7% - 54% of the sky."

Dark Matter Spectrum

In addition to the peak at 635 *Å*, the spectral data [2] show peaks at 85 *Å*, 101 *Å*, 117 *Å*, 130 *Å*, 140 *Å*, 163 *Å*, 182 *Å*, 200 *Å*, 234 *Å*, 261 *Å*, 303 *Å*, 460 *Å*, 584 *Å*, 608 *Å*, *and* 633 *Å*. The authors interpreted these data as soft X-ray emissions from ionized atoms within hot gases. However, the authors left the door open for some other interpretation with the following statement from their introduction:

> "It is now generally believed that this diffuse soft X-ray background is produced by a high-temperature component of the interstellar medium. However, evidence of the thermal nature of this emission is indirect in that it is based not on observations of line emission, but on indirect evidence that no plausible non-thermal mechanism has been suggested which does not conflict with some component of the observational evidence."

The authors also state that "if this interpretation is correct, gas at several temperatures is present." Specifically, emissions were attributed to gases in three ranges: $5.5 < \log T < 5.7$; $\log T = 6$; $6.6 < \log T < 6.8$.

Mills' Theory

Mills' theory provides an alternative explanation for the soft X-ray emissions of the dark interstellar medium observed by Labov and Bowyer [2] based on the predicted existence of fractional-quantum-energy-level hydrogen atoms, ***hydrinos***. J. J. Balmer showed in 1885 that the frequencies for some of the lines observed in the emission spectrum of atomic hydrogen could be expressed with a completely empirical relationship. This approach was later extended by J. R. Rydberg, who showed that all of the spectral lines of atomic hydrogen were given by the equation:

$$\bar{\nu} = R\left(\frac{1}{n_f^2} - \frac{1}{n_i^2}\right) \tag{40.1}$$

where $R = 109{,}677\ cm^{-1}$, $n_f = 1,2,3,...$, $n_i = 2,3,4,...$, *and* $n_i > n_f$. Niels Bohr, in 1913, developed a theory for atomic hydrogen that gave energy levels in agreement with Rydberg's equation. An identical equation, based on a totally different theory for the hydrogen atom, was developed by E. Schrödinger, and independently by W. Heisenberg, in 1926.

$$E_n = -\frac{e^2}{n^2 8\pi\varepsilon_o a_H} = \frac{13.598\ eV}{n^2} \tag{40.2a}$$

$$n = 1,2,3,... \tag{40.2b}$$

where a_H is the Bohr radius for the hydrogen atom ($52.947\ pm$), e is the magnitude of the charge of the electron, and ε_o is the vacuum permittivity. Mills' theory predicts that Eq. (40.2b), should be replaced by Eq. (40.2c).

$$n = 1,2,3,...,\ and,\ n = \frac{1}{2},\frac{1}{3},\frac{1}{4},... \tag{40.2c}$$

The $n = 1$ state is the "ground" state for "pure" photon transitions (the $n = 1$ state can absorb a photon and go to an excited electronic state, but it cannot release a photon and go to a lower-energy electronic state). However, an electron transition from the ground state to a lower-energy state is possible by a nonradiative energy transfer such as multipole coupling or a resonant collision mechanism. These lower-energy states have fractional quantum numbers, $n = \frac{1}{\text{integer}}$. Processes that occur without photons and that require collisions are common. For example, the exothermic chemical reaction of $H + H$ to form H_2 does not occur with the emission of a photon. Rather, the reaction requires a collision with a third body, M, to remove the bond energy- $H + H + M \rightarrow H_2 + M^*$. The third body distributes the energy from the exothermic reaction, and the end result is the H_2 molecule and an increase in the temperature of the system. Some commercial phosphors are based on nonradiative energy transfer involving multipole coupling. For example, the strong absorption strength of Sb^{3+} ions along with the efficient nonradiative transfer of excitation from Sb^{3+} to Mn^{2+}, are responsible for the strong manganese luminescence from phosphors containing these ions. Similarly, the $n = 1$ state of hydrogen and the $n = \frac{1}{\text{integer}}$ states of hydrogen are nonradiative, but a transition between two nonradiative states is possible via a nonradiative energy transfer, say $n = 1$ to $n = 1/2$. In these cases, during the transition the electron couples to another electron transition or electron transfer reaction which can

absorb the exact amount of energy that must be removed from the hydrogen atom, a resonant energy sink called an ***energy hole***. The reaction of hydrogen-type atoms to lower-energy states is referred to as a ***transition reaction***. Lower-energy hydrogen atoms, ***hydrinos***, can act as a source of energy holes that can cause a transition reaction with the absorption of an energy hole of $m\,X\,27.2\,eV$ (Eq.(5.5)). Thus, the transition cascade for the pth cycle of the hydrogen-type atom, $H\left[\frac{a_H}{p}\right]$, with the hydrogen-type atom, $H\left[\frac{a_H}{m'}\right]$, that is ionized as the source of energy holes to cause a the transition reaction is represented by

$$m\,X\,27.21\,eV + H\left[\frac{a_H}{m'}\right] + H\left[\frac{a_H}{p}\right] \rightarrow H^+ + e^- + H\left[\frac{a_H}{(p+m)}\right] + [(p+m)^2 - p^2 - (m'^2 - 2m)]X13.6\,eV \quad (40.3)$$

$$H^+ + e^- \rightarrow H\left[\frac{a_H}{1}\right] + 13.6\,eV \quad (40.4)$$

And, the overall reaction is

$$H\left[\frac{a_H}{m'}\right] + H\left[\frac{a_H}{p}\right] \rightarrow H\left[\frac{a_H}{1}\right] + H\left[\frac{a_H}{(p+m)}\right] + \left[2pm + m^2 - m'^2\right]X13.6\,eV + 13.6\,eV \quad (40.5)$$

Rather than undergoing internal conversion, the energy emitted by a hydrino which has nonradiatively transferred $m\,X\,27.2\,eV$ of energy to a second hydrino may be emitted as a spectral line since hydrinos may only accept energy by a nonradiative mechanism.

Line Assignments

In Table 1, the peaks recorded by Labov and Bowyer are assigned to the hydrogen electronic transitions to energy levels below the ground state corresponding to fractional quantum numbers that are induced by disproportionation reactions as described in the Disproportionation of Energy States Section (Eqs. (40.3-40.5)). Consider the case where $m' = 2$. A hydrogen atom in a fractional quantum state, $H(n_i)$, collides with a $n = \frac{1}{2}$ hydrogen atom, $H\left(\frac{1}{2}\right)$, and the result is an even lower-energy hydrogen atom, $H(n_f)$, and $H\left(\frac{1}{2}\right)$ is ionized.

$$H(n_i) + H\left(\frac{1}{2}\right) \rightarrow H(n_f) + H^+ + e^- + photon \quad (40.6)$$

The energy released, as a photon, is the difference between the energies of the initial and final states given by Eqs. (40.2a-40.2c) minus the ionization energy of $H\left(\frac{1}{2}\right)$, $54.4\ eV$. The agreement between the experimental data and the values predicted for the proposed transitions is remarkable. Furthermore, the $304\ Å$ ($40.8\ eV$) transition of hydrogen is scattered by interstellar neutral helium giving rise to a broad He I emission centered at $584\ Å$ ($21.21\ eV$) and a broad scattered hydrogen emission at about $634\ Å$ ($19.6\ eV$). When this photon strikes $He(1s^2)$, $21.2\ eV$ is absorbed in the excitation to $He(1s^1 2p^1)$. This leaves a $19.6\ eV$ photon ($632.6\ Å$). Similarly, the $114\ Å$ ($108.8\ eV$) transition of hydrogen is scattered by interstellar neutral helium giving rise to a broad He I emission centered at $584\ Å$ ($21.21\ eV$) and a broad scattered hydrogen emission at about $141\ Å$ ($87.6\ eV$). Also, the $182.3\ Å$ ($68\ eV$) transition of hydrogen is scattered by interstellar neutral helium giving rise to a broad He I emission centered at $584\ Å$ ($21.21\ eV$) and a broad scattered hydrogen emission at about $265\ Å$ ($46.8\ eV$). Conspicuously absent is the $256\ Å$ ($48.3\ eV$) line of He II which eliminates the assignment of the $303\ Å$ and the $234\ Å$ lines to the He II transitions.

As shown in Table 1, hydrogen transitions to electronic energy levels below the "ground" state corresponding to fractional quantum numbers predicted by Mills' theory match the spectral lines of the extreme ultraviolet background of interstellar space. And, hydrogen disproportionation reactions yield ionized hydrogen, energetic electrons, and hydrogen ionizing radiation. This assignment resolves the paradox of the identity of dark matter and accounts for many celestial observations such as: diffuse Hα emission is ubiquitous throughout the Galaxy, and widespread sources of flux shortward of $912\ Å$ are required [2].

Line Intensity

The intensity of the extreme ultraviolet emission, I, of disproportionation transitions of hydrinos can be calculated from the column density of hydrogen or hydrino atoms, $N(H)$, and the rate of the disproportionation reaction, $r_{m,m',p}$, given by Eq. (5.70) of the Interstellar Disproportionation Rate Section. Photons are emitted with equal probability in all directions; thus, Eq. (5.70) is multiplied by $\frac{1}{4\pi}$ to give

the rate constant in terms of the solid angle. The intensity is

$$I = \frac{1}{4\pi} A_{ul} N(H) = \frac{1}{\sqrt{2}} n_H \left(\frac{a_H}{p}\right)^2 \sqrt{\frac{3kT}{m_H}} N(H) \quad (40.7)$$

where A_{ul} is the Einstein A coefficient, and $N(H) = n_H \ell$ is the column density. The path length, ℓ, is calculated in steradians from its integral. In the case that $m = 1$, $m' = 2$, and $p = 3$ in Eqs. (5.50-5.52); $T = 50\ ^\circ K$, $g_{m,p} = 1$ (the result of Förster's theory for the efficiencies of dipole-dipole resonant energy transfers), and using $N(H) = 2\ X\ 10^{18}\ cm^{-2}$ as the column density of hydrino atoms, $H\left(\frac{a_H}{3}\right)$, which is estimated from typical values of the column density of H in diffuse hydrogen regions along the sight-line at b=48 deg and which corresponds to a density of lower-energy hydrogen atoms, $H\left(\frac{a_H}{3}\right)$, of $n_H = 4\ X\ 10^3\ atom / m^3$, the calculated intensity of the 304 $\AA$ line which is herein assigned as the $1/3 \rightarrow 1/4$ H transition is

$$I = 2000\ photons\ cm^{-2} s^{-1} sr^{-1} \quad (40.8)$$

The intensity reported by Labov and Bowyer for the 304 $\AA$ line is

$$I = 2080^{+740}_{-720}\ photons\ cm^{-2} s^{-1} sr^{-1} \quad (40.8a)$$

The experimental intensity is in agreement with the intensity calculated from Mills' theory.

Table 1. Observed emission data. (Raw extreme ultraviolet background spectral data taken from raw data and Figure 4 of Labov and Bowyer [2]).

Peak #	Observed Wavelength (Å)	Observed Energy (eV)	Peak Assignment	Predicted Energy[a] (eV)	Predicted Wavelength (Å)
1	84.8	146.2	1/7 → 1/8 H transtiton	149.6	82.9
2	101.5	122.2	1/6 → 1/7 H transition	122.4	101.3
3	116.8	106.2	1/2 → 1/4 H transition	108.8	114.0
4	129.6	95.6	1/5 → 1/6 H transition	95.2	130.2
5	139.6	88.8	He scattered peak #3	87.6	139.6
6	163.2	75.9	Second order of peak #1	74.8	163.2
7	181.7	68.3	1/4 → 1/5 H transition	68.0	182.3
8	200.6	61.8	Second order of peak #2	61.2	202.6
9*	233.8	53.0	1 → 1/3 H transition	54.4	227.9
10	261.2	47.5	He scattered peak #7	46.8	265.0
11	302.5	41.0	1/3 → 1/4 H transition	40.8	303.9
12	459.1	27.0	Second order of peak #9	27.2	455.8
13	584	21.2	He resonance scattered emission	21.2	584
14	607.5	20.4	Second order of peak #11	20.4	607.8
15	633.0	19.7	He scattered peak #11	19.6	633.0
16			1/2 → 1/3 H transition	13.6	912.3

For excited state hydrogen transitions, $n_i \rightarrow n_f \quad n = 1,2,3,...,$

$$E = \left(\frac{1}{n_f^2} - \frac{1}{n_i^2}\right) X 13.6\ eV$$

[a]For lower-energy transitions, $n = 1, \frac{1}{2}, \frac{1}{3}, \frac{1}{4}, ...,$ and $n_i > n_f$ induced by a disproportionation reaction with $H\left[\frac{a_H}{2}\right]$

$$E = \left(\frac{1}{n_f^2} - \frac{1}{n_i^2}\right) X 13.6\ eV - 54.4\ eV$$

[a]For helium inelastic scattered peaks of hydrogen transitions, $n_i \rightarrow n_f$

$$E = \left(\frac{1}{n_f^2} - \frac{1}{n_i^2}\right) X 13.6\ eV - 54.4\ eV - 21.21\ eV$$

* Bowyer and Labov used three monochrometers for maximal sensitivity in each energy range: 80-230Å, 230-430Å, and 430-650Å. The monochrometer change at 230Å resulted in the 6 Å discrepancy between the calculated and observed lines.

SOLAR DATA

Solar Neutrino Problem

Another two-decade-old cosmological mystery is the discrepancy between solar neutrino flux observed with the Homestake detector, 2.1 ± 0.03 *SNU*, and that predicted based on the Standard Solar Model, 7.9 ± 2.6 *SNU* [3-5]. According to the Standard Solar Model, the pp chain is the predominant energy source of main-sequence stars which commences with proton-proton fusion according to the following reaction [3];

$$^1H + {}^1H \rightarrow {}^2H + e^+ + \upsilon_e \tag{40.9}$$

And, according to this model, strong coupling exists between luminosity and neutrino flux because they are both based on nuclear reactions. A recent experiment with a radioactive solar surrogate at the Gallex solar neutrino detector in Italy supports the results that over the past several years the Gallex and Russia's SAGE , the other large gallium detector, see only about 60% of the solar neutrino signal predicted to within 1 to 2% by astrophysical models [6]. The paradox of the paucity of solar neutrinos to account for the solar energy output by the pp chain is resolved by assigning a major portion of the solar output to hydrogen transitions. Hydrogen transitions to electronic energy levels below the "ground" state corresponding to fractional quantum numbers can yield energies comparable to nuclear energies. For example, all transitions to the $n = \frac{1}{100}$ state of hydrogen taken together release 136 *keV*. Data strongly supporting this tenant is the observation by Labov and Bowyer of an intense 304 *Å* (40.8 *eV*) solar emission line corresponding to the transition given by Eqs. (5.44-5.46),

$$H\left(\frac{a_H}{3}\right) \xrightarrow{H\left(\frac{a_H}{2}\right)} H\left(\frac{a_H}{4}\right) \tag{40.10}$$

in the absence of the 256 *Å* (48.3 *eV*) line of He II which eliminates the assignment of the 304 *Å* line to the He II transition.

Temperature of the Solar Corona Problem

In addition to the questions of what powers the sun and why the solar neutrino flux is significantly deficient, there exists no satisfactory answer to two additional solar questions: The cause of sunspots and other solar activity and why the Sun emits X-rays is unknown [7]. In fact, a possible anticorrelation exists between the abundance of sunspots and the solar neutrino flux observed with the Homestake detector [8]. The cause of sunspots and other solar activity, and why the Sun emits X-rays can be explained by energy releasing transitions of hydrogen to

lower energy levels. The photosphere of the Sun is 6000 K; whereas, the temperature of the corona based on the assignment of the emitted X-rays to highly ionized heavy elements is in excess of 10^6 K. No satisfactory power transfer mechanism is known which explains the excessive temperature of the corona relative to that of the photosphere. The mechanism must explain the constant transfer over time of energy from the photosphere at 6000 K to the corona at 10^6 K which radiates energy into cold space. Further compounding the temperature mystery is the observation of a strong coronal hydrogen Lyman series, beginning with Lα at 1216 *Å* and ending at 912 *Å*, corresponding to unionized hydrogen atoms. The hydrogen lines would indicate that the corona is less than 10^4 K. The paradox is resolved by the existence of a power source associated with the corona. The energy which maintains the corona at a temperature in excess of 10^6 K is that released by disproportionation reactions of lower-energy hydrogen as given by Eqs. (40.3-40.5).

Disproportionation may be the predominant mechanism of hydrogen electronic transitions to lower energy levels of solar hydrogen and hydrinos. Hydrogen transitions to electronic energy levels below the "ground" state corresponding to fractional quantum numbers match lines of the solar emission spectrum in the extreme ultraviolet and X-ray regions. The solar lines that match the energy of disproportionation reactions of lower-energy hydrogen given by Eqs. (40.3-40.5) are given in Table 2. The energy of the emission line for the transition given by Eqs. (40.3-40.5) whereby $H\left(\frac{a_H}{m'}\right)$ is ionized as the source of the energy hole of $m\ X\ 27.2\ eV$ that causes a transition reaction is $\left[2pm+m^2-m'^2\right]X13.6\ eV+13.6\ eV$:

$$H\left(\frac{a_H}{m'}\right)+H\left(\frac{a_H}{p}\right)\rightarrow H\left(\frac{a_H}{1}\right)+H\left(\frac{a_H}{(p+m)}\right)+\left[2pm+m^2-m'^2\right]X13.6\ eV+13.6\ eV \tag{40.11}$$

For example, the line corresponding to the disproportionation reaction:

$$H\left(\frac{a_H}{2}\right)\xrightarrow{H\left(\frac{a_H}{2}\right)} H\left(\frac{a_H}{3}\right) \tag{40.12}$$

is 912 *Å*. Transitions of hydrogen to lower-energy states catalyzed by hydrogen gives rise to a broad band emission with an edge at 912 *Å* and a tail to shorter wavelengths as given in the Broadening of the Hydrogen 912 *Å* Line Problem Section. The coronal hydrogen Lyman series, beginning with Lα at 1217 *Å* and ending at 912 *Å*, corresponds to hydrogen scattering, and the helium series starting at 584 *Å* and ending on the

helium continuum at 504 $\AA$ corresponds to helium scattering of the EUV emitted from lower-energy hydrogen transitions as given in Table 2. This assignment resolves the mystery of the observation of a strong coronal hydrogen Lyman series, beginning with Lα at 1216 $\AA$ and ending at 912 $\AA$, corresponding to unionized hydrogen atoms. The hydrogen lines would indicate that the corona is less than 10^4 K; whereas, the actual temperature is in excess of 10^6 K. The excess intensity of these lines for the low number of scatters in the corona is due to the strong scattering at EUV wavelengths.

The energy released by the transition of the hydrino atom with the initial lower-energy state quantum number p and radius $\frac{a_H}{p}$ to the state with lower-energy state quantum number $(p+m)$ and radius $\frac{a_H}{(p+m)}$ catalyzed by a hydrino atom with the initial lower-energy state quantum number m', initial radius $\frac{a_H}{m'}$, and final radius a_H are given in Table 2.

The agreement between the calculated (nonrelativistic) and the experimental values is remarkable. Furthermore, many of the lines of Table 2 had no previous assignment, or the assignment was unsatisfactory. Some lines assigned in the literature may have been assigned incorrectly by trying to fit the spectrum to known lines. But, inconsistencies arise. For example, the intensity of the peak assigned to He II by Thomas [9] is extremely strong ($I = 62{,}200$). The laboratory He II transition intensities are: $I(303.780\ \AA) = 1000$; $I(303.786\ \AA) = 500$; $I(256\ \AA) = 300$. Therefore, the predicted peak intensity of the 256 $\AA$ (48.3 eV) line of He II is $I = 12{,}440$; whereas, the observed intensity is too weak ($I = 1580$) which eliminates the assignment of the 304 $\AA$ line to the He II transition. Several of the disproportionation lines are slightly broadened due to the collision and electron ejection mechanism (Eqs. (40.3-40.5)) and temperature broadening. The line intensities vary from strong to fairly weak, but in general the intensity of emission due to disproportionation is weakened due to energy transfer to the ionized electron versus photon emission (Eqs. (40.3-40.5)). The ejected electron energy is dissipated as synchrotron radiation. The line intensities are further weakened due to the high cross section for absorption and scattering at extreme UV wavelengths. In fact the disproportionation line intensities may be weaker than those of highly ionized heavy elements. Ionized heavy elements emit high in the corona at $2MK$ where the path length to space is much less than the path length for emission from disproportionation reaction regions such as at the solar surface. The

helium and hydrogen scattered peaks corresponding to disproportionation reactions are of different intensities depending on the concentration of unionized scatters in the region where the disproportionation emission occurs. The scattered line intensity is a function of temperature because that will determine the concentration of both unionized hydrino as well as unionized scattering atoms. Temporal variation in the disproportionation line intensities may reflect solar activity. For example, the coronal power is 0.01 % of the solar power in the case of a quite Sun and as high as 100 % of the solar power in the case of an active Sun [10]. Several lines which are assigned in Table 3 to transitions of lower-energy hydrogen in the Stellar Data Section greatly increase in intensity during a flare event which is evidence that lower-energy hydrogen transitions are the cause of solar flares.

Table 2. Observed line emission of the disproportionation reaction given by Eqs. (40.3-40.5). (Raw extreme ultraviolet solar spectral data taken from Figures 3a-k of [9], Figures 1a-d (observed lines from Table 1) of [11]; Figure 7.5 of [12], and Figure 4.10 of Phillips [13].)

Observed Line (Å)	[b]Predicted (Mills) (Å)	m, m' f	Assignment (Mills)	Ref	Assignment (Other)
1215.7	1215.67	d	$H(2p^1) \rightarrow H(1s^1) + 10.2\ eV$	12, 13	Collisional Excitation, Lα scattering
911.8	911.78	1, 1;1[c]	1 → 1/2 H transition	12, 13	$H^+ + e^- \rightarrow H + 13.6\ eV$ at $T > 20{,}000\ K$
		1, 2	1/2 → 1/3 H transition		
584.5	584.5	e	$He(1s^1 2p^1) \rightarrow He(1s^2) + 21.2\ eV$	12, 13	Collisional Excitation
373.7	373.73	2, 2	Inelastic Scattering (He) of 1 → 1/3 H transition	9	None
303.784	303.92	1, 2	1/3 → 1/4 transition	9	He II
280.2[a] 280.8[a]	280.54	2, 2	Inelastic Scattering (H) of 1 → 1/3 H transition	11	None

264.80	265.08	1, 2	Inelastic Scattering (He) of 1/4 → 1/5 H transition	11	Fe XIV
228[a]	227.95	2, 2	1 → 1/3 H transition	11	None
215.16	214.54	1, 2	Inelastic Scattering (H) of 1/4 → 1/5 H transition	11	S XII
182.16	182.36	1, 2	1/4 → 1/5 H transition	11	Fe XI
167.50	167.62	1, 2	Inelastic Scattering (He) of 1/5 → 1/6 H transition	11	Fe VIII
152.15	151.97	3, 3	1 → 1/4 H transition	11	Ni XII
145.9[a]	145.88	1, 2	Inelastic Scattering (H) of 1/5 → 1/6 H transition	11	None
141[a]	141.59	2, 2	Inelastic Scattering (He) of 1/2 → 1/4 H transition	11	None
129.87	130.26	1, 2	1/5 → 1/6 H transition	11	O VI
125.5[a]	125.76	2, 2	Inelastic Scattering (H) of 1/2 → 1/4 H transition	11	None
122.2[a]	122.56	1, 2	Inelastic Scattering (He) of 1/6 → 1/7 H transition	11	None
114[a]	113.97	2, 2	1/2 → 1/4 H transition	11	None
110.5[a]	110.52	1, 2	Inelastic Scattering (H) of 1/6 → 1/7 H transition	11	None
101.3[a]	101.31	1, 2	1/6 → 1/7 H transition	11	None
96.7[a]	96.59	1, 2	Inelastic Scattering (He) of 1/7 → 1/8 H transition	11	None
88.8	88.95	1, 2	Inelastic Scattering (H) of 1/7 → 1/8 H transition	11	None
87.0[a]	87.34	2, 2	Inelastic Scattering (He) of 1/3 → 1/5 H transition	11	None
82.9[a]	82.89	1, 2	1/7 → 1/8 H transition	11	None
81.1[a]	81.05	2, 2	Inelastic Scattering (H) of 1/3 → 1/5 H transition	11	None
79.58	79.70	1, 2	Inelastic Scattering (He) of 1/8 → 1/9 H transition	11	Fe XII

76.0[a]	75.98	2, 2	1/3 → 1/5 H transition	11	None
70.1[a]	70.14	1, 2	1/8 → 1/9 H transition	11	None
67.5[a]	67.84	1, 2	Inelastic Scattering (He) of 1/9 → 1/10 H transition	11	None
63.12	63.14	2, 2	Inelastic Scattering (He) of 1/4 → 1/6 H transition	11	Mg X
61.0[a]	60.78	1, 2	1/9 → 1/10 H transition	11	None
59.7[a]	59.79	2, 2	Inelastic Scattering (H) of 1/4 → 1/6 H transition	11	None

---

[a] Wavelength read from Figue 1 of [11]; wavelength not given in Table of [11];

[b] For lower-energy transitions, $n = 1, \frac{1}{2}, \frac{1}{3}, \frac{1}{4}, \ldots,$ and $n_i > n_f$ induced by a disproportionation reaction with $H\left[\frac{a_H}{2}\right]$, $E = \left(\frac{1}{n_f^2} - \frac{1}{n_i^2}\right) X 13.6\ eV - m'^2\, X 13.6\ eV$;

[b] For helium inelastic scattered peaks of hydrogen transitions, $n_i \rightarrow n_f$, $E = \left(\frac{1}{n_f^2} - \frac{1}{n_i^2}\right) X 13.6\ eV - m'^2\, X 13.6\ eV - 21.21\, eV$ (when this photon strikes $He(1s^2)$, $21.2\ eV$ is absorbed in the excitation to $He(1s^1 2p^1)$);

[b] For hydrogen inelastic scattered peaks of hydrogen transitions, $n_i \rightarrow n_f$, $E = \left(\frac{1}{n_f^2} - \frac{1}{n_i^2}\right) X 13.6\ eV - m'^2\, X 13.6\ eV - 10.2\ eV$ (when this photon strikes $H(1s^1)$, $10.2\ eV$ is absorbed in the excitation to $H(2p^1)$);

[c] $H[n=1] \rightarrow H\left[n = \frac{1}{2}\right] + h\nu\ (911.8\ \text{Å})$ (Eqs. 40.16-40.18);

[d] $H(2p^1) \rightarrow H(1s^1) + 10.2\ eV$ (excitation by emission of lower-energy hydrogen transitions);

[e] $He(1s^1 2p^1) \rightarrow He(1s^2) + 21.2\ eV$ (excitation by emission of lower-energy hydrogen transitions);

[f] Eqs. (40.3-40.5).

Disproportionation takes place at the surface and the corona of the Sun where the reactants, hydrogen and lower-energy hydrogen atoms, are present and where the gas is rarefied enough that the electron of the hydrino atom which provides the energy hole ionizes to vacuum versus to a plasma as in the case of the photosphere. With ionization to vacuum, the integral of Eq. (6.27) is one. The power, $P_{m,m',p}$,

from the disproportionation reaction of the transition of the hydrino atom with the initial lower-energy state quantum number p and radius $\frac{a_H}{p}$ to the state with lower-energy state quantum number $(p+m)$ and radius $\frac{a_H}{(p+m)}$ catalyzed by a hydrino atom with the initial lower-energy state quantum number m', initial radius $\frac{a_H}{m'}$, and final radius a_H is given in the Interstellar Disproportionation Rate Section.

$$P_{m,m',p} = \frac{N_H^2}{V} 4\pi\sqrt{2}\left(\frac{a_H}{p}\right)^2 \sqrt{\frac{3kT}{m_H}}\left[2pm + m^2 - m'^2 + 1\right] X 2.2\, X 10^{-18}\ W \quad (40.13)$$

where N_H is the total number of hydrogen or hydrino atoms, V is the volume, k is Boltzmann's constant, T is the absolute temperature, and m_H is the mass of the hydrogen or hydrino atom. The total number of hydrogen or hydrino atoms, N_H, is given by

$$N_H = \rho_H V \quad (40.14)$$

where ρ_H is the density of hydrogen or hydrino atoms. The volume V is

$$V = \frac{4}{3}\pi\left(R_C^3 - R_P^3\right) \quad (40.15)$$

where R_C is the radius of the corona and R_P is the radius of the photosphere. The density of hydrogen atoms at the surface of the photosphere is $10^{21}\ \frac{H\ atoms}{m^3}$. The density of hydrogen atoms in the corona varies as a function of height. It ranges from $10^{15}\ \frac{H\ atoms}{m^3}$ at the photosphere to vacuum at the edge of the corona which has a height of greater than $10^9\ m$. An estimate of the power of the Sun from disproportionation reactions is given by substitution of $\rho_H = 10^{15}\ \frac{H^*\ atoms}{m^3}$ (H^* refers to hydrino atoms), $R_C = 2\ X\ 10^9\ m$, $R_P = 1\ X\ 10^9\ m$, $T = 2\ X\ 10^6\ K$, $p = 2$, $m = 1$ and $m' = 2$ into Eqs. (40.22-40.24). The calculated maximum power of $4\ X\ 10^{26}\ W$ matches the observed maximum power output of $4\ X\ 10^{26}\ W$. Thus, a major part of the solar power can be attributed to disproportionation reactions using the same rate equation that predicts the observed line intensity (Eq. (40.8)) of the $40.8\ eV$ line of Labov and Bowyer [2] assigned to Eq. (40.10).

Broadening of the Hydrogen 911.8Å Line Problem

As shown in Figure 7.5 of [12], Figure 4.10 of Phillips [13], and Figure 9.5 of Stix [14] (See Figure 1), the extreme ultraviolet spectrum of the solar disk is a sharp line spectrum for hydrogen and helium except

for the continuum lines, the H I 911.8 $\AA$ line and the He I 504.3 $\AA$ line. In both cases, the continuum line has a sharp edge and a broad band on the shorter wavelength side only. Recombination at a continuum of very high electron energies is the mechanism proposed previously [15]. However, the broadening of the H I 911.8 $\AA$ line (911.8 $\AA$ *to* ≈ 600 $\AA$) is six times that predicted based on the thermal electron energy ($T = 6{,}000$ K in Eq. (40.25)) at the surface of the photosphere where the H I 911.8 $\AA$ continuum originates, and based on the relative width of the helium continuum lines, He I 504.3 $\AA$ (He I 504.3 $\AA$ *to* ≈ 530 $\AA$) and He II 227.9 $\AA$ (He II 227.9 $\AA$ *to* ≈ 225 $\AA$ [11]). The latter lines are proportionally much narrower; yet the corresponding temperatures of origin must be higher because the transitions are more energetic. Furthermore, the H 911.8 $\AA$ continuum line of the spectrum of a prominence is about one half the width of the same line of the quiet Sun spectrum as shown in Figure 1. Yet, the temperature rises to greater than 10,000 K in a prominence [16]. The proposed recombination continuum line also is inconsistent with the line shape shown in Figure 1. A plasma with a Maxwellian distribution would give a line of constant slope when plotted on a logarithmic scale; whereas, more than one slope is present in Figure 1. The problem of the anomalous spectral feature of the excessive broadening of the continuum line of hydrogen to higher energies can be resolved by assignment of the broadening mechanism to energetic disproportionation reactions involving hydrogen atoms as reactants.

The Sun itself is the source of lower-energy hydrogen for reactants for interstellar disproportionation reactions given by Eqs. (40.3-40.5). The source of energy holes in solar production are hydrogen and singly ionized helium, He^+. The ionization energy of hydrogen is 13.6 eV. Disproportionation can occur between three hydrogen atoms whereby two atoms provide an energy hole of 27.21 eV for the third hydrogen atom. Thus, the transition cascade for the pth cycle of the hydrogen-type atom, $H\left[\frac{a_H}{p}\right]$, with two hydrogen atoms, $H\left[\frac{a_H}{1}\right]$, as the source of energy holes that causes the transition reaction is represented by

$$27.21\ eV + 2H\left[\frac{a_H}{1}\right] + H\left[\frac{a_H}{p}\right] \rightarrow 2H^+ + 2e^- + H\left[\frac{a_H}{(p+1)}\right] + [(p+1)^2 - p^2]X13.6\ eV \quad (40.16)$$

$$2H^+ + 2e^- \rightarrow 2H\left[\frac{a_H}{1}\right] + 27.21\ eV \quad (40.17)$$

And, the overall reaction is

$$H\left[\frac{a_H}{p}\right] \rightarrow H\left[\frac{a_H}{(p+1)}\right] + [(p+1)^2 - p]X13.6\ eV \tag{40.18}$$

Helium II is one of the catalysts that can causes a transition reaction because the second ionization energy is $54.4\ eV$, $m = 2$ in Eq. (5.5). Thus, the transition cascade for the pth cycle is represented by

$$54.4\ eV + He^+ + H\left[\frac{a_H}{p}\right] \rightarrow He^{2+} + e^- + H\left[\frac{a_H}{(p+2)}\right] + [(p+2)^2 - p^2]X13.6\ eV \tag{40.19}$$

$$He^{2+} + e^- \rightarrow He^+ + 54.4\ eV \tag{40.20}$$

And, the overall reaction is

$$H\left[\frac{a_H}{p}\right] \rightarrow H\left[\frac{a_H}{(p+2)}\right] + [(p+2)^2 - p]X13.6\ eV \tag{40.21}$$

Also, Helium II is a catalyst that can cause a transition reaction with the absorption of an energy hole of $27.21\ eV$, $m = 1$ in Eq. (5.5). Thus, the transition cascade for the pth cycle is represented by

$$27.21\ eV + He^+ + H\left[\frac{a_H}{p}\right] \rightarrow He^{2+} + e^- + H\left[\frac{a_H}{(p+1)}\right] + [(p+1)^2 - p^2]X13.6\ eV - 27.21\ eV \tag{40.22}$$

$$He^{2+} + e^- \rightarrow He^+ + 54.4\ eV \tag{40.23}$$

And, the overall reaction is

$$H\left[\frac{a_H}{p}\right] \rightarrow H\left[\frac{a_H}{(p+1)}\right] + [(p+1)^2 - p]X13.6\ eV \tag{40.24}$$

In the case of the three body catalytic reaction given by Eqs. (40.16-40.18) with $p = 1$, the electronic transition of one of the hydrogen atoms from the "ground" state to the lower-energy state, $n = \frac{1}{2}$, is possible by a "resonant collision" mechanism wherein the emitted photon of $911.8\ Å$ is shifted to a continuum of shorter wavelengths between $911.8\ Å - 455.9\ Å$ via a mechanism analogous to that of a doubly excited state transition. In general, the reaction requires a collision with a body, M, to remove part of the transition energy-

$H + M \rightarrow H\left[n = \frac{1}{2}\right] + M^* + h\upsilon$. Consider the case that hydrogen atom one, $H(1)$, and two, $H(2)$, provide an energy hole of $27.21\,eV$ for hydrogen atom $H(3)$. $H(1)$ is ionized, serving as the body which removes energy in the resonant collision, and $H(2)$ remains in a continuum excited state. Then, $H(2)$ and $H(3)$ emit radiation simultaneously. Thus, the H I $911.8\,Å$ continuum line is broadened with a sharp edge at $911.8\,Å$ and a continuum tail of shorter wavelengths between $911.8\,Å - 455.9\,Å$. A second edge at $739\,Å$ would correspond to the superposition of the energy of the H I $911.8\,Å$ transition of $H(3)$ and the $3647\,Å$ Balmer continuum of $H(2)$. This second continuum edge at $739\,Å$ is observed as demonstrated in the quiet sun-center spectrum of Figure 1. The three-body-hydrogen catalytic reaction occurs on the surface of the photosphere where the temperature permits hydrogen atoms to form at sufficient concentrations for the occurrence of hydrogen-three-body collisions. This mechanism of broadening of the H I $911.8\,Å$ continuum line is not possible in the case that He^+ (Eqs. (40.19-40.21)) or (Eqs. (40.22-40.24)) is the source of the energy hole; thus, the corresponding helium continuum lines, He I $504.3\,Å$, and He II $227.9\,Å$, are not anomalous. The $911.8\,Å$ emission corresponding lower-energy hydrogen transition, $H[n = 1] \xrightarrow{He^+ \text{ or } He^{2+}} H\left[n = \frac{1}{2}\right] + h\nu\ (911.8\,Å)$, is sharp.

The disproportionation reactions of hydrogen wherein hydrogen atoms are the source of energy holes occur at the surface of the photosphere where the temperature is 6000 K. A major portion of the power of the Sun is due to solar emission in the region of the H I $911.8\,Å$ band [17] and longer wavelengths. The intensity of the H I $911.8\,Å$ band is weakened due to the high cross section for absorption and scattering at extreme UV wavelengths. In fact, the disproportionation line intensities may be weaker than those of highly ionized heavy elements. Ionized heavy elements emit high in the corona at $2MK$ where the path length to space is much less than the path length for emission from disproportionation reaction regions such as at the solar surface as shown in Figure 1.

The reaction product, lower-energy hydrogen, can be reionized as it is diffuses towards the center of the Sun which has a temperature of $15.8\,X\,10^6\,K$. Thus, lower-energy hydrogen provides a mechanism to transfer energy from the photosphere to the corona at a much higher temperature.

Figure 1a. (Top) Skylab extreme ultraviolet spectrum of the solar disk is a sharp line spectrum for hydrogen and helium except for the continuum lines, *He* I 504.3 *Å* and *H* I 911.8 *Å* line. The *H* I 911.8 *Å* line is excessively broad at short wavelengths. The hydrogen Lyman series, beginning with Lα at 1216 *Å* and ending at 912 *Å* is marked. The helium series starting at 584 *Å* and ending on the helium continuum at 504 *Å* is also marked. (Bottom) A similar spectrum, but observed in the corona above the solar limb. In this spectrum, the emission from chromospheric lines and continua is severely attenuated. The strongest lines in this spectrum are produced by high-temperature, multiply ionized ions such as the indicated doublets of Ne VIII, Mg X, or Si XII.

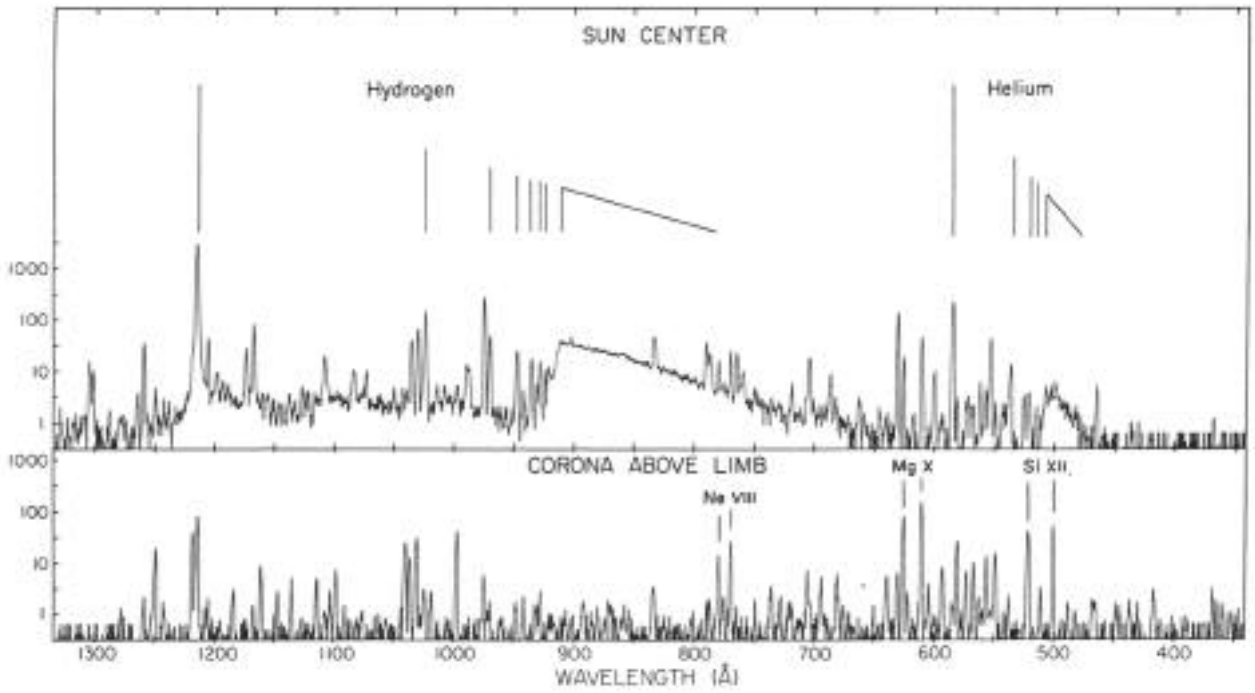

Figure 1b. (Top and Middle) Skylab (Harvard College Observatory spectrometer) extreme ultraviolet spectra of the solar disk and a prominence are each a sharp line spectrum for hydrogen and helium except for the continuum lines, *He* I 504.3 *Å* and *H* I 911.8 *Å* line. In the quiet Sun-center spectrum, the *H* I 911.8 *Å* line is excessively broad at short wavelengths. The hydrogen Lyman series, beginning with Lα at 1216 *Å* and ending at 912 *Å* is marked. The helium series starting at 584 *Å* and ending on the helium continuum at 504 *Å* is also marked. (Bottom) A similar spectrum, but observed in the corona above the solar limb. In this spectrum, the emission from chromospheric lines and continua is severely attenuated. The strongest lines in this spectrum are produced by high-temperature, multiply ionized ions such as the indicated doublets of Mg X, or Si XII.

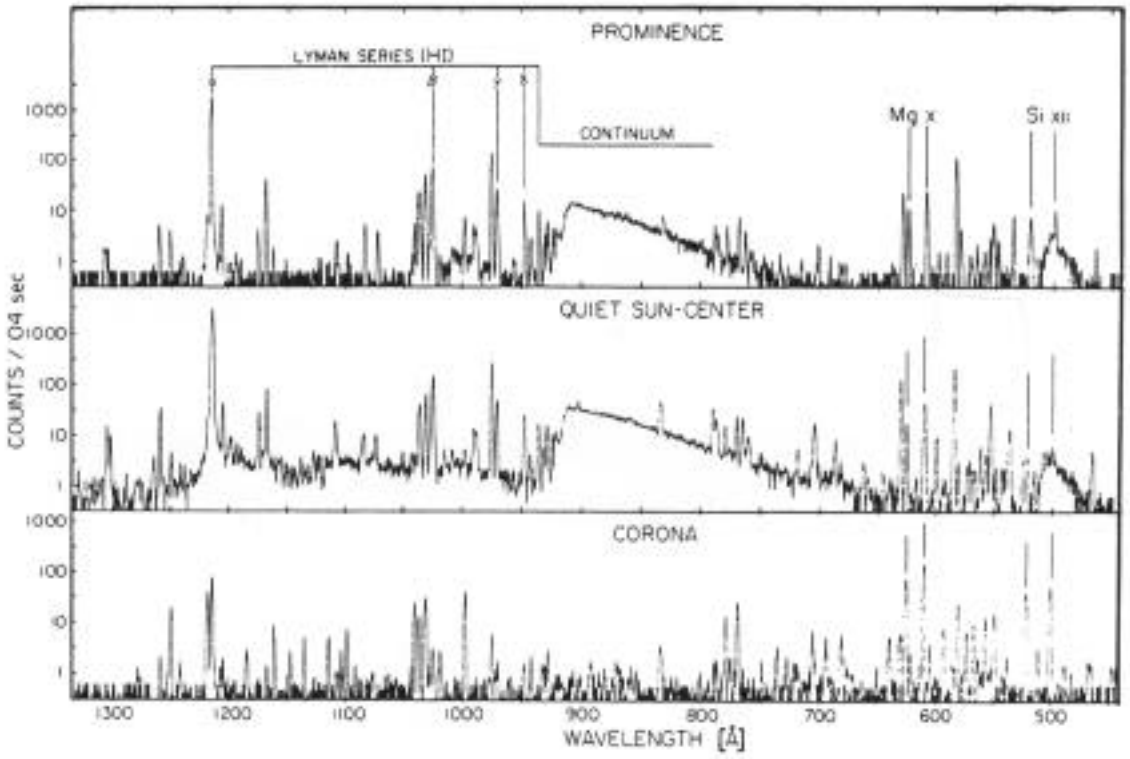

Temperature of the Transition from "Radiation Zone" to "Convection Zone" Problem

The reaction product, lower-energy hydrogen, can be reionized as it diffuses towards the center of the Sun. The abrupt change in the speed of sound and transition from "radiation zone" to "convection zone" at a radius of 0.7 the solar radius, $0.7R_S$, with a temperature of $2X10^6\ K$ matches the ionization temperature of lower-energy hydrogen. The central temperature of the Sun is $15.8X10^6\ K$. A stable "radiation zone" overlays the core where energy diffuses outward and stratification is governed by the opacity of matter to the passage of radiation. By $0.7R_S$, the temperature has dropped to about $2X10^6\ K$. The Sun becomes opaque to radiation for outward distances greater than $0.7R_S$, and the speed of sound abruptly changes at $0.7R_S$ [7]. This observation is consistent with the ionization of lower-energy hydrogen for radii shorter than $0.7R_S$ with a resulting strong increase in opacity. Previously, this observation was assigned to the onset of capture of electrons by highly ionized atoms. However, the Sun is composed of about 2% heavy elements for which various states of ionization are achieved essentially continuously for radii short of $0.7R_S$ to the surface. The average energy, $\bar{E}$, of an ideal gas atom given by Eq.(16.32) with three degrees of freedom is

$$\bar{E} = \frac{3}{2}kT \tag{40.25}$$

where k is Boltzmann's constant and T is the temperature. Substitution of $2X10^6\ K$ into Eq. (40.25) gives $260\ eV$ as the average kinetic energy of the atoms at the location of $0.7R_S$ which corresponds to the ionization temperature of lower-energy hydrogen of quantum number $n = \frac{1}{4}$ (Hydrinos tend to lower-energy states with time; therefore, the radius of this speed-of-sound-transition region decreases with time). The increase in opacity caused by the presence of unionized lower-energy hydrogen atoms initiates a "convection zone" reaching nearly to the surface wherein thermal convection is nearly adiabatic, until a rapid drop in density and temperature just beneath the visible surface produces a thin superadiabatic layer. The atmosphere and extended heliosphere above the surface are the sites of many amazing phenomenon including solar flares, the greatest explosions in the Solar System. Limb measurements of the transition-region ultraviolet lines point to the much of the emission coming from tiny (less than $100\ km$ across) structures not resolvable by any instrument so far used, and only a small part is due to the "true" transition region (the interface of the chromosphere and the corona). A sudden release of energy gives rise to exploding granules

[18]. These previously poorly understood phenomena are caused by disproportionation reactions which release a major portion of the Solar power. Disproportionation takes place at the surface and corona of the Sun where the gas is sufficiently rarefied such that the electron of the hydrino atom which provides the energy hole ionizes to vacuum versus to a plasma in the case of the photosphere. With ionization to vacuum, the integral of Eq. (6.27) is one corresponding to a high reaction rate.

Cool Carbon Monoxide Clouds Problem

Another spectroscopic mystery concerns an infrared absorption band of the chromosphere. According to Phillips [19]:

> "The most puzzling observations of the chromosphere have been made in the infrared, at a wavelength of 4.7 μm, where there are absorption bands (i.e. numerous spectral lines crowded together to form a continuous absorption feature) due to the molecule carbon monoxide. This appears to be present at altitudes well into the chromosphere, where the temperature has risen to 6000 K or more, yet the molecule can only exist at temperatures of about 4000 K-at higher temperatures it would break up into its constituent carbon and oxygen atoms. It seems that the chromosphere has pockets of much cooler gas. This has altered our perception of the chromosphere's nature..."

This problem can be resolved by assignment of the broad 4.7 μm feature to a temperature broadened rotational transition of a molecular ion of lower-energy hydrogen.

A hydrino atom can react with a proton to form a dihydrino molecular ion.

$$H\left(\frac{a_H}{p}\right) + H^+ \rightarrow H_2^*\left(2c' = \frac{2a_o}{p}\right)^+ \tag{40.26}$$

The energy released is the bond dissociation energy of the dihydrino molecular ion given by Eq. (12.90).

$$E_D = E\left(H\left(\frac{a_H}{p}\right)\right) - E_{T_{zeroorder}} - \frac{E_{vib}}{2} \tag{40.27}$$

where the total energy of the dihydrino molecular ion with zero order vibration, $E_{T_{zeroorder}}$, is given by Eqs. (12.76), (12.90), and (12.91). The binding energy of the hydrino atom is

$$E\left(H\left(\frac{a_H}{p}\right)\right) = p^2 13.6\ eV \tag{40.28}$$

From Eqs. (12.58) and (12.89), the vibrational energy, E_{vib}, without the

small correction do to the elongation of the molecular ion due to vibration is

$$E_{vib} = p^2 0.59\ eV \tag{40.29}$$

The effect of zero order vibration is a small contribution to the total energy, E_T, thus; the total energy of the hydrino molecular ion is approximately given by Eq. (12.76).

$$E_T = 13.6\ eV(-4p^2 \ln 3 + p^2 + 2p^2 \ln 3) \tag{40.30}$$

The energy, E, for the reaction (Eq. (40.26)) of the hydrino atom, $H\left(\frac{a_H}{p}\right)$, with a proton to form the hydrogen-type molecular ion, $H_2^*\left(2c' = \frac{2a_o}{p}\right)^+$, is approximately

$$E = E\left(H\left(\frac{a_H}{p}\right)\right) - E_T - \frac{E_{vib}}{2} \tag{40.31}$$

The rotational wavelength of the hydrogen-type molecular ion $H_2^*\left(2c' = \frac{2a_o}{p}\right)^+$ including vibration given by Eq. (14.33) is

$$\lambda = \frac{169}{p^2[J+1]}\ \mu m \tag{40.32}$$

where p is an integer. The wavelength calculated from Eq. (40.32) for the $J = 0$ to $J = 1$ transition of the hydrogen-type molecular ion $H_2^*\left(2c' = \frac{2a_o}{p}\right)^+$ for $p = 6$ is 4.7 μm. A broad 4.7 μm solar chromospheric absorption line is observed which was previously assigned to cool carbon monoxide clouds; however, the temperature of the chromosphere, $> 6000\ K$, is higher than that at which carbon monoxide completely decomposes into carbon and oxygen, $< 4000\ K$ [19]. The energy, E, for the reaction (Eq. (40.26)) of hydrino atom, $H\left(\frac{a_H}{6}\right)$, with a proton to form the hydrogen-type molecular ion $H_2^*\left(2c' = \frac{a_o}{3}\right)^+$ is equal to the bond dissociation energy, E_D given by Eqs (40.28-40.31). The calculated bond dissociation energy, E_D, of $H_2^*\left(2c' = \frac{a_o}{3}\right)^+$ is $E_D = 100\ eV$. The bond dissociation temperature of the hydrogen-type molecular ion $H_2^*\left(2c' = \frac{a_o}{3}\right)^+$ can be calculated from the relationship between the average kinetic energy, $\bar{E}$, of an ideal gas atom and the T. Substitution of $\bar{E} = 100\ eV$ into Eq. (40.25) gives $T = 7.7\ X\ 10^5\ K$ as the temperature

corresponding to the average kinetic energy of the atoms of the chromosphere which is equal to the bond dissociation energy of $H_2^*\left(2c'=\frac{a_o}{3}\right)^+$. The assignment of the 4.7 μm absorption line to the $J=0$ to $J=1$ transition rotational transition of $H_2^*\left(2c'=\frac{a_o}{3}\right)^+$ provides a resolution of the problem of cool carbon monoxide clouds.

Stellar Age Problem

Modeling how stars evolve leads to age estimates for some stars that are greater than the age of the universe [7]. Mills' theory predicts that presently, stars exist which are older than the elapsed time of the present expansion as stellar evolution occurred during the contraction phase. The maximum energy release of the universe given by Eq. (23.142) of the Gravity Section occurred at the beginning of the expansion phase. P_U, the maximum power radiated by the universe is

$$P_U = \frac{\frac{m_e c^2}{\sqrt{\frac{2GM}{c^2\lambda_c}}}}{\tau\sqrt{\frac{2GM}{c^2\lambda_c}}} = \frac{c^5}{4\pi G} = 2.89\ X\ 10^{51}\ W \qquad (40.33)$$

The observed power of the present universe from stellar mass to energy conversion calculated from the number of galaxies ($400\ billion$) times the number of stars per galaxy ($400\ billion$) times the average mass to energy conversion rate per star ($5\ billion\ kg\ c^2/\sec\ star$) is close to that given by Eq. (40.33). Thus, stars existed at the beginning of the present expansion.

Solar Rotation Problem

A further mystery concerns the rotation of the Sun [7]. First, the surface rotation decreases with increasing latitude, and rotation throughout the "convection zone" is unexpectedly similar to that at the surface. Second, the outer part of the "radiation zone" appears to rotate at a constant intermediate rate. Third, a significant amount of angular momentum loss was necessary for the Sun to form. Otherwise, the centrifugal force of gravity would have been too weak to collapse the gas cloud that contracted to form the Sun. Conservation of angular momentum would have caused the angular velocity of the gases to exceed the escape velocity. The outer layers of the Sun transferred most of the original angular momentum of the gas cloud to the solar wind. To conserve angular momentum, evolutionary models require that the core

must be spinning at a faster rate than the overlying layers. However, current helioseimology results indicate that the core may be the most slowly rotating part of the Sun. More angular momentum must have been lost from the core than from the outer layers which directly lose angular momentum to the solar wind. This solar rotation problem may be resolved by including the consequences of spacetime expansion affected by matter to energy conversion in the Sun (Eq. (23.140)) to the loss of angular momentum by the Sun. The expansion of spacetime is a mechanism to transfer angular momentum to the universe. For example, in the limit that a body is completely converted to energy, the body's total angular momentum is completely transferred to the universe. Fusion (mainly the pp chain (Eq. (40.9)) and disproportionation (Eqs. (40.3-40.5)) reactions are the sources of the Sun's output power. Both reactions convert matter into energy; thus, they cause spacetime to expand. The gravitational equation (Eq. (23.38)) with the equivalence of the particle production energies (Eqs. (23.48a-23.48b)) permit the equivalence of mass/energy ($E = mc^2$) and spacetime ($\frac{c^3}{4\pi G} = 3.22\ X\ 10^{34}\ \frac{kg}{\sec}$). Spacetime expands as mass is released as energy according to Eq. (23.140) which provides the basis of the atomic, thermodynamic, and cosmological arrows of time.

Solar energy is electromagnetic. The multipole fields of a radiating source can be used to calculate the energy and the angular momentum carried off by the radiation [20]. For harmonically varying fields, the time-averaged energy density is

$$u = \frac{1}{16\pi}\left(\mathbf{E}\cdot\mathbf{E}^* + \mathbf{B}\cdot\mathbf{B}^*\right) \tag{40.34}$$

The time-averaged angular-momentum density is

$$\mathbf{m} = \frac{1}{8\pi c}\,\mathrm{Re}\left[\mathbf{r}\times\left(\mathbf{E}\times\mathbf{B}^*\right)\right] \tag{40.35}$$

The ratio of the square of the angular momentum, M^2, to the square of the energy, U^2, for a pure (l,m) multipole follows from Eq. (2.25) and Eqs. (2.31-2.33)

$$\frac{M^2}{U^2} = \frac{m^2}{\omega^2} \tag{40.36}$$

The loss of the solar angular momentum can be calculated from the mass deficit over time with angular momentum transfer by photons propagating in the corresponding expanding spacetime. The relationship between proper time and coordinate time given by the Schwarzschild metric for the infinitesimal spatial temporal displacement [21], $d\tau^2$, is:

$$d\tau^2 = \left(1 - \frac{2Gm_0}{c^2 r}\right) dt^2 - \frac{1}{c^2}\left[\frac{dr^2}{1 - \frac{2Gm_0}{c^2 r}} + r^2 d\theta^2 + r^2 \sin^2\theta d\phi^2\right] \tag{40.37}$$

Consider a general point in the xy-plane having $dr = 0$; $d\theta = 0$; $\sin^2\theta = 1$. Substitution of these parameters into Eq. (40.37) gives

$$d\tau = dt\left(1 - \frac{2Gm_0}{c^2 r} - \frac{v^2}{c^2}\right)^{\frac{1}{2}} \tag{40.38}$$

with $v^2 = c^2$, Eq. (40.31) becomes

$$\tau = ti\sqrt{\frac{2GM}{c^2 r}} = ti\sqrt{\frac{2GM}{c^2 r}} \tag{40.39}$$

The unification of Maxwell's equations and general relativity give the following relationships which follow from Eq. (40.39)

$$\frac{\text{proper time}}{\text{coordinate time}} = \frac{\text{gravitational wave condition}}{\text{electromagnetic wave condition}} = \frac{\text{gravitational mass phase matching}}{\text{charge/inertial mass phase matching}}$$

$$\frac{\text{proper time}}{\text{coordinate time}} = i\frac{\sqrt{\frac{2Gm}{c^2 \lambda_C}}}{\alpha} = i\frac{v_g}{\alpha c} \tag{40.40}$$

Eq. (24.41) given in the Unification of Spacetime, the Forces, Matter, and Energy Section determines that the periods of spacetime expansion/contraction (General Relativity) and particle decay/production (Maxwell's Equations) for the universe are equal. The period, T, is

$$T = \frac{2\pi G m_U}{c^3} \text{ sec} \tag{40.41}$$

It is calculated in Gravity Section from the mass energy of the universe, $m_U c^2$, at the point where $v = c$ in Eq. (40.38) and the radius of the universe is equal to the gravitational radius (Eq. (23.147)).

$$r_g = \frac{2Gm}{c^2} \tag{40.42}$$

Thus, the proper time is equal to the coordinate time (Eq. (40.39). In the case of the Sun, $v << c$, and the radius of the Sun is much greater than its gravitational radius (Eq. (40.42)). In the case of Eq. (40.36), the relationship between the proper time corresponding to Maxwell's Equations and coordinate time corresponding to the solar mechanics effected by spacetime expansion is given by Eq. (40.38). The loss of the solar rotational kinetic energy can be calculated from the mass deficit over time with angular momentum transfer by photons propagating in

the corresponding expanding spacetime using the relationship between proper and coordinate time. The average rotation rate of the Sun is approximately 450 *nHz* [7]. The mass and the radius of the Sun are $1.99 \text{ X } 10^{30}$ *kg* and $6.96 \text{ X } 10^{8}$ *m*, respectively. The present angular momentum of the Sun can be estimated from the angular momentum of a sphere where the moment of inertia, I, is given by Fowles [22].

$$L = I\omega = \frac{2}{5} m R_S^2 \omega = \frac{2}{5}\left(2 \text{ X } 10^{30} \text{ kg}\right)\left(6.96 \text{ X } 10^{8} \text{ m}\right)^2 \left(2\pi \text{ X } 450 \text{ nHz}\right) = 1.1 \text{ X } 10^{42} \text{ Js} \tag{40.43}$$

where R_S is the solar radius. The rotational kinetic energy, K, of the Sun is

$$K = \frac{L^2}{2I} = I\omega = \frac{1}{5} m R_S^2 \omega^2 = \frac{1}{5}\left(2 \text{ X } 10^{30} \text{ kg}\right)\left(6.96 \text{ X } 10^{8} \text{ m}\right)^2 \left(2\pi \text{ X } 450 \text{ nHz}\right)^2 = 1.5 \text{ X } 10^{36} \text{ J} \tag{40.44}$$

The Sun comprises 99.85 % of the mass of the Solar System. Therefore, the angular momentum loss, ΔL, by the Solar System including the Sun is approximately equal to the angular momentum loss of the Sun. To conserve the angular momentum of the Solar System, the average angular frequency of the Sun was 52 times greater in the past [23, 24]. In this case, the initial rotational velocity of the Sun, v_i, was

$$v_i = R_S\omega = \left(6.96 \text{ X } 10^{8} \text{ m}\right)\left(52 \text{ X } 2\pi \text{ X } 450 \text{ nHz}\right) = 1.0 \text{ X } 10^{5} \frac{\text{m}}{\text{sec}} \tag{40.45}$$

Consider Eq. (40.36) which gives the ratio of the square of the angular momentum, M^2, to the square of the energy, U^2, for a pure (l,m) electromagnetic multipole. The relationship between the angular frequency change of the Sun, $\Delta\omega_{coordinate}$, corresponding to the loss of rotational energy to electromagnetic radiation and the angular frequency in Eq. (40.36), $\Delta\omega_{proper}$, corresponding to the electromagnetic radiation is

$$\frac{\Delta\omega_{coordinate}}{\Delta\omega_{proper}} = \left[\sqrt{1 - \frac{2Gm_S}{c^2 r}} - \sqrt{1 - \frac{2Gm_S}{c^2 r} - \frac{(\Delta v)^2}{c^2}}\right] \tag{40.46}$$

where Δv is the change in rotational velocity of the Sun. Eq. (40.36) is given in terms of the rotational energy by using Eq. (40.46).

$$\frac{M^2}{U^2} = \frac{1^2}{\omega^2} \tag{40.47}$$

$$\frac{I\Delta\omega_{coordinate}}{U_{coordinate}} = \frac{1}{\Delta\omega_{coordinate}}\left[\sqrt{1 - \frac{2Gm_S}{c^2 r}} - \sqrt{1 - \frac{2Gm_S}{c^2 r} - \frac{(\Delta v)^2}{c^2}}\right] \tag{40.48}$$

$$\Delta K = \frac{1}{2} I\left(\Delta\omega_{coordinate}\right)^2 = \frac{1}{2} U\left[\sqrt{1 - \frac{2Gm_S}{c^2 r}} - \sqrt{1 - \frac{2Gm_S}{c^2 r} - \frac{(\Delta v)^2}{c^2}}\right] \quad \frac{1}{4} U \frac{(\Delta v)^2}{c^2} \tag{40.49}$$

$$\Delta K \quad \frac{1}{4}\Delta m_S c^2 \frac{(\Delta v)^2}{c^2} \tag{40.50}$$

The velocity change over time, Δv, is essentially equal to the initial velocity given by Eq. (40.45). The power of the Sun is $4\ X\ 10^{26}\ W$, and the time span which the Sun has spent on the main sequence, converting hydrogen to helium is $4.6\ X\ 10^9$ *years* [24]. Thus, the energy released by the Sun over its life is $5.8\ X\ 10^{43}\ J$. In terms of the symmetry of energy emission, the Sun is a monopole; thus, $m = 1$ in Eq. (40.36). Substitution of the mass/energy deficit $5.8\ X\ 10^{43}\ J$ for $\Delta m_S c^2$ and the rotational velocity change $\Delta v = 1.0\ \mathrm{X}\ 10^5\ \frac{m}{\mathrm{sec}}$ gives the change in rotational energy of the Sun, ΔK, due to General Relativistic effects.

$$\Delta K \quad \frac{1}{4}\left(5.8\ X\ 10^{43}\ J\right)\left[\frac{1\ X\ 10^5\ m}{c}\right]^2 = 1.6\ X\ 10^{36}\ J \tag{40.51}$$

The lost rotational energy (angular momentum) due to matter to energy conversion with spacetime expansion is comparable with the present rotational energy (angular momentum) of the Sun.

The differential rates of matter to energy conversion predominantly by fusion within the core and by disproportionation reactions of lower-energy hydrogen in the outer layers of the Sun effect the relative rotation rates. The relative rotation rate for the core would be less than expected if the core was the predominant source of Solar power. Furthermore, the relative ratio of the radius of a reacting mass and its gravitational radius (Eqs. (40.42) and (40.49)) also effect the relative rotation rates. In the case that matter to energy conversion rates of the core ("radiation zone") and the "convection zone" are approximately equal, the transfer of angular momentum to the universe via general relativistic effects is greater for the core due to its significantly greater density. The core has the largest gravitational radius. General relativity provides a resolution to the problem of the loss of angular momentum of the core which is in agreement with the current Solar models and helioseismology data. The photon transfer of momentum to expanding spacetime mechanism provides a resolution to the solar rotation problem of the slowly rotating Solar core. The outer layers transfer momentum to the solar wind as a function of the latitude; thus, the equator rotates the fastest. A possible explanation of the absence of the change in the rotation with latitude of the core versus the outer layers is the general relativistic mechanism of angular momentum transfer. Due to the $\sin\theta$ dependence (Eqs. (40.37) and (40.49)), the transfer of angular momentum increases as a function of the distance from the rotation axis. In the case that the general relativistic angular momentum transfer is comparable to the angular momentum transfer to

the solar wind, the absence of a change in the rotation with latitude of the core would be predicted. This case agrees with the present observations.

STELLAR DATA

Further stellar evidence of disproportionation reactions is the emission of extreme ultraviolet radiation by young stars called A stars. They appear to have energetic, ultraviolet-emitting upper atmospheres, or coronas, even though astronomers believe such stars lack the ability to heat these regions [25].

Numerous late-type stars, particularly dM stars, are known to flare from time to time at visible and X-ray wavelengths. An extremely pronounced flare was observed by the Extreme Ultraviolet Explorer (EUVE) Deep Survey telescope on the star AU Microscopii at a count of 20 times greater than that at quiescence [26]. The flare consisted of a sharp peak in the level of the EUV emission that lasted for two hours followed by a decaying tail that lasted more than a day. The total energy of this event has been estimated to be $3X10^{27}\,J$, with an emission measure of $\approx 6X\,10^{53}\,cm^{-3}$ which indicates that large volumes of material are involved in the flaring process, with flare-loop lengths estimated to be the size of at least one solar radius. Emission lines in the extreme ultraviolet were observed for which there is no satisfactory assignment. These spectral lines match hydrogen transitions to electronic energy levels below the "ground" state corresponding to fractional quantum numbers as shown in Table 3. The lines assigned to lower-energy hydrogen transitions increased significantly in intensity during the flare event. The data is consistent with disproportionation reactions of lower-energy hydrogen as the mechanism of solar flare activity.

EQ Peg is a nearby visual binary system. Both components of the system are flare stars of spectral types dM4e and dM5e and visual magnitudes 10.38 and 12.4, respectively. The flare activity is very prominent, and the system exhibits frequent large flares in the U band. Extreme ultraviolet spectroscopic observations of the star EQ Pegasi were made with the Extreme Ultraviolet Explorer (EUVE) Deep Survey photometer [27]. Emission lines in the extreme ultraviolet were observed for which there is no satisfactory assignment. These spectral lines match hydrogen transitions to electronic energy levels below the "ground" state corresponding to fractional quantum numbers as shown in Table 4.

The energy released by the transition of the hydrino atom with the initial lower-energy state quantum number p and radius $\frac{a_H}{p}$ to the state

with lower-energy state quantum number $(p+m)$ and radius $\frac{a_H}{(p+m)}$ catalyzed by a hydrino atom with the initial lower-energy state quantum number m', initial radius $\frac{a_H}{m'}$, and final radius a_H are given in Tables 3 and 4.

The agreement between the calculated (nonrelativistic) and the experimental values is remarkable. Furthermore, many of the lines of Tables 3 and 4 had no previous assignment, or the assignment was unsatisfactory.

Table 3. Observed line emission of the disproportionation reaction given by Eqs. (40.3-40.5). (Raw extreme ultraviolet spectral data of stellar flare on AU Mic taken from Figure 1 of [26])

Observed Line (Å)	[a]Predicted (Mills) (Å)	m, m' [b]	Assignment (Mills)	Assignment (Other)
183	182.36	1, 2	1/4 → 1/5 H transition	None
168	167.62	1, 2	Inelastic Scattering (He) of 1/5 → 1/6 H transition	None
130	130.26	1, 2	1/5 → 1/6 H transition	None
126	125.76	2, 2	Inelastic Scattering (H) of 1/2 → 1/4 H transition	None
123	122.56	1, 2	Inelastic Scattering (He) of 1/6 → 1/7 H transition	None
114	113.97	2, 2	1/2 → 1/4 H transition	None
111	110.52	1, 2	Inelastic Scattering (H) of 1/6 → 1/7 H transition	None
101	101.31	1, 2	1/6 → 1/7 H transition	None
97	96.59	1, 2	Inelastic Scattering (He) of 1/7 → 1/8 H transition	None
90	88.95	1, 2	Inelastic Scattering (H) of 1/7 → 1/8 H transition	None
87	87.34	2, 2	Inelastic Scattering (He) of 1/3 → 1/5 H transition	None
83	82.89	1, 2	1/7 → 1/8 H transition	None
81	81.05	2, 2	Inelastic Scattering (H) of 1/3 → 1/5 H transition	None
79.5	79.70	1, 2	Inelastic Scattering (He) of 1/8 → 1/9 H transition	None
76	75.98	2, 2	1/3 → 1/5 H transition	None

[a] For lower-energy transitions, $n = 1, \frac{1}{2}, \frac{1}{3}, \frac{1}{4}, \ldots$, and $n_i > n_f$ induced by a disproportionation reaction with $H\left(\frac{a_H}{2}\right)$, $E = \left(\frac{1}{n_f^2} - \frac{1}{n_i^2}\right) X 13.6\ eV - 54.4\ eV$;

[a] For helium inelastic scattered peaks of hydrogen transitions, $n_i \rightarrow n_f$, $E = \left(\frac{1}{n_f^2} - \frac{1}{n_i^2}\right) X 13.6\ eV - 54.4\ eV - 21.21\ eV$ (when this photon strikes $He(1s^2)$, 21.2 eV is absorbed in the excitation to $He(1s^1 2p^1)$);

[a] For hydrogen Inelastic scattered peaks of hydrogen transitions, $n_i \rightarrow n_f$, $E = \left(\frac{1}{n_f^2} - \frac{1}{n_i^2}\right) X 13.6\ eV - 54.4\ eV - 10.2\ eV$ (when this photon strikes $H(1s^1)$, 10.2 eV is absorbed in the excitation to $H(2p^1)$);

[b] Eqs. (40.3-40.5).

Table 4. Observed line emission of the disproportionation reaction given by Eqs. (40.3-40.5) where $m = 1$ and $m' = 2$. (Raw extreme ultraviolet stellar spectral data of star EQ Pegasi taken from Figures 1-3 of [27])

Observed Line (Å)	[a]Predicted (Mills) (Å)	m, m' [b]	Assignment (Mills)	Assignment (Other)
304	303.93	1, 2	1/3 → 1/4 H transition	He II
265	265.08	1, 2	Inelastic Scattering (He) of 1/4 → 1/5 H transition	None
182	182.36	1, 2	1/4 → 1/5 H transition	None
130	130.26	1, 2	1/5 → 1/6 H transition	None
122.5	122.56	1,2	Inelastic Scattering (He) of 1/6 → 1/7 H transition	None
101.3	101.31	1, 2	1/6 → 1/7 H transition	None
89	88.95	1, 2	Inelastic Scattering (H) of 1/7 → 1/8 H transition	None
83	82.89	1, 2	1/7 → 1/8 H transition	None
81	81.05	2, 2	Inelastic Scattering (H) of 1/3 → 1/5 H transition	None

[a] For lower-energy transitions, $n = 1, \frac{1}{2}, \frac{1}{3}, \frac{1}{4}, \ldots$, and $n_i > n_f$ induced by a disproportionation reaction with $H\left(\frac{a_H}{2}\right)$, $E = \left(\frac{1}{n_f^2} - \frac{1}{n_i^2}\right) X 13.6\ eV - 54.4\ eV$;

[a] For helium inelastic scattered peaks of hydrogen transitions, $n_i \rightarrow n_f$, $E = \left(\frac{1}{n_f^2} - \frac{1}{n_i^2}\right) X 13.6\ eV - 54.4\ eV - 21.21 eV$ (when this photon strikes $He(1s^2)$, $21.2\ eV$ is absorbed in the excitation to $He(1s^1 2p^1)$);

[a] For hydrogen inelastic scattered peaks of hydrogen transitions, $n_i \rightarrow n_f$, $E = \left(\frac{1}{n_f^2} - \frac{1}{n_i^2}\right) X 13.6\ eV - 54.4\ eV - 10.2\ eV$ (when this photon strikes $H(1s^1)$, $10.2\ eV$ is absorbed in the excitation to $H(2p^1)$);

[b] Eqs. (40.3-40.5)

PLANETARY DATA

Planetary evidence of disproportionation reactions is the emission of energy by Jupiter and Uranus in excess of that absorbed from the Sun. Jupiter is gigantic ball of gaseous hydrogen. Saturn and Uranus are also largely comprised of hydrogen. H_3^+ is detected from all three planets by infrared emission spectroscopy [28]. Disproportionation reactions of hydrogen yield ionizing electrons, energy, and ionized hydrogen atoms. Ionizing electrons and protons can both react with molecular hydrogen to produce H_3^+. The reactions are as follows:

Lower-energy hydrogen atoms can act as a source of energy holes that can cause a transition reaction with the absorption of an energy hole of $m\,X\,27.2\,eV$ (Eq.(5.5)) with the release of significant energy. Thus, the transition cascade for the pth cycle of the hydrogen-type atom, $H\left(\frac{a_H}{p}\right)$, with the hydrogen-type atom, $H\left(\frac{a_H}{m'}\right)$, that is ionized as the source of energy holes that causes the transition reaction where the energetic ionized electron and proton lead to production of H_3^+ is represented by

$$m\,X\,27.21\,eV + H\left(\frac{a_H}{m'}\right) + H\left(\frac{a_H}{p}\right) \rightarrow H^+ + e^- + H\left(\frac{a_H}{(p+m)}\right) + [(p+m)^2 - p^2 - \left(m'^2 - 2m\right)]X13.6\,eV \quad (40.52)$$

$$1.86\,eV + H^+ + H_2 \rightarrow H_2^+ + H \quad (40.53)$$

$$15.46\,eV + e^- + H_2 \rightarrow H_2^+ + 2e^- \quad (40.54)$$

$$2H_2^+ + 2H_2 \rightarrow 2H_3^+ + 2H + 2(1.7\,eV) \quad (40.55)$$

And, the overall reaction is

$$4H_2 + H\left(\frac{a_H}{m'}\right) + H\left(\frac{a_H}{p}\right) \rightarrow 2H_3^+ + 2e^- + 3H\left(\frac{a_H}{1}\right) + H\left(\frac{a_H}{(p+m)}\right) + \left[2pm + m^2 - m'^2\right]X13.6\,eV - 13.92\,eV \quad (40.56)$$

An unsolved puzzle involves the energy source for the mid-latitude H_2 band emissions of Saturn. The Voyager 2 measurements show H_2 band emissions which must be electron excited. Yet insufficient energy is available from the solar flux alone, suggesting the existence of an additional source of energy [29]. Voyager 2 measurements show that the H_2 band intensity in the shadow of the rings is less than 15 percent of its value just north of the shadow. This fact, and the sharp edge of the ring shadow, are further evidence against excitation by precipitating magnetospheric particles. Also, high resolution measurements of Jupiter' northern

auroral ultraviolet emission show that the equatorial H_2 dayglow spectrum was 13% of the strength of the observed auroral emission, and secondary electron excitation is consistent with the observed Jovian northern FUV H_2 auroral emissions [30]. These observations indicate that disproportionation reactions of hydrogen comprise a planetary ionizing energy source.

Two unidentified lines in Jupiter's near-infrared K-band spectrum match the lowest energy vibrational transition of the dihydrino molecular ion $H_2^*\left[2c' = a_o\right]^+$ and this transition with the lowest energy rotational transition. Two occasions of exceptionally widespread but distinct emission activity have been observed in Jupiter's near-infrared K-band spectrum during September and November of 1988 as reported by Trafton and Watson [31]. Two distinct sets of emission features were involved on the two dates of observation. During these occasions, these normally absent emission features extended from the South polar limb to at least the equator, over a broad range of longitudes. Meanwhile, Jupiter's auroral H_2 and H_3^+ remained confined to their usual magnetic polar domains. The one emission feature at 2.22 μm matches the energy of the $n = 1$ to $n = 0$ vibrational transition of the dihydrino molecular ion, $H_2^*\left[2c' = a_o\right]^+$ given by Eq. (12.157). The other feature at 2.1055 μm matches the energy of the $n = 1$ to $n = 0$ vibrational transition of the dihydrino molecular ion, $H_2^*\left[2c' = a_o\right]^+$ given by Eq. (12.157) with the $J+1$ to J rotational transition given by Eq. (14.29). One potential source of these emissions is auroral excitation from precipitation of protons during Jovian magnetospheric storms. The reaction giving rise to the dihydrino molecular ion is

$$H\left[\frac{a_H}{2}\right] + H^+ \rightarrow H_2^*\left[2c' = a_o\right]^+ \tag{40.57}$$

The $n = 1$ to $n = 0$ vibrational transition of the corresponding dihydrino molecule $H_2^*\left[2c' = \frac{a_o}{\sqrt{2}}\right]$ is forbidden, but it may be seen with the presence of sufficient concentration. The Sun may be a source of the dihydrino molecular vibrational transition. The calculated energy is given by Eq. (12.172). This energy is very close to that of the coronal 'green' line at 530.3 nm which has a less than straightforward assignment [32]. And, many lines which correspond to dihydrino rotational transitions are observed in the infrared spectrum of the Sun as given in the Solar Infrared Data Section.

COSMIC BACKGROUND EXPLORER DATA

The spin/nuclear hyperfine structure transition energies of lower-

energy hydrogen match closely certain spectral lines obtained by COBE [33-35] for which no other satisfactory assignment exists. The far-infrared absolute spectrometer (FIRAS) on the Cosmic Background Explorer has carried out an all-sky survey in the far infrared region ($1 \; to \; 90 \; cm^{-1}$). Averaged over many positions in the Galaxy, spectral features are observed which correspond closely with the predicted hydrino hyperfine transition energies. The lines obtained by COBE that match the hyperfine structure transitions of lower-energy hydrogen as calculated in the Spin-Nuclear and Orbital-Nuclear Coupling of Hydrinos Section are given in Table 5. The energy, the wavelength, and the frequency corresponding to the spin-nuclear coupling energy of the hydrino atom with the lower energy state quantum numbers n and ℓ and with the radius $\frac{a_H}{n}$ are given in Table 5.

Table 5. The spin-nuclear coupling energy of the hydrino atom with the lower energy state quantum numbers n and ℓ and with the radius $\frac{a_H}{n}$.

n	ℓ	Energy[a] ($JX\,10^{23}$)	Lambda (cm)	Frequency (GHz)	Wave Number (cm^{-1})	Experimental Wave Number [33,34] (cm^{-1})
1	0	0.09592	20.71	1.447	0.04829	0.0485
2	0	1.918	1.0355	28.95	0.9657	0.965
2	1	5.051	0.3933	76.23	2.543	2.55
3	0	7.769	0.2557	117.2	3.911	3.90
4	0	19.95	0.09957	301.1	10.04	10.0
5	0	40.77	0.04873	615.2	20.52	20.5

[a]For the case that $\ell = 0$,

$$\Delta E_{total}^{\text{S/N O/N}} = n^2\, 2.878\ X\ 10^{-24}\ J - n^3\, 3.837\ X\ 10^{-24}\ J \tag{40.58}$$

[a]For the case that $\ell \neq 0$,

$$r_{1\pm} = \frac{a_H + \sqrt{a_H^2 \pm \frac{6\mu_o e\left(\sqrt{\ell(\ell+1)} + \sqrt{\frac{3}{4}}\right)\mu_P a_o}{\hbar}}}{2n} \tag{40.59}$$

$$\Delta E_{total}^{\text{S/N O/N}} = \frac{ne^2}{8\pi\varepsilon_o}\left(\frac{1}{r_{1-}} - \frac{1}{r_{1+}}\right)\left(\sqrt{\ell(\ell+1)} + \sqrt{\frac{3}{4}}\right)2\mu_P \frac{n^3\mu_0 e\hbar}{m_e a_H^3} \tag{40.60}$$

SOLAR INFRARED DATA

Diatomic Molecular Rotation of Hydrogen-Type Molecules

Two hydrogen atoms react to form a diatomic molecule, the hydrogen molecule.

$$2H\left[a_H\right] \rightarrow H_2\left[2c' = \sqrt{2}a_o\right] \tag{40.61}$$

where $2c'$ is the internuclear distance. Also, two hydrino atoms react to form a diatomic molecule, a dihydrino molecule.

$$2H\left[\frac{a_H}{n}\right] \rightarrow H_2^*\left[2c' = \frac{\sqrt{2}a_o}{n}\right] \tag{40.62}$$

where n is an integer. The rotational energy emitted by a hydrogen-type

molecule with the transition from the state with the rotational quantum number $J+1$ to one with the rotational quantum number J given by Eq. (14.29) is

$$\lambda = \frac{8.43\,X\,10^5}{n^2[J+1]}\ \text{Å} \tag{40.63}$$

where n is an integer which corresponds to, $\frac{1}{n}$, the fractional quantum number of the hydrogen-type molecule.

The rotational transition energies of lower-energy molecular hydrogen match closely certain spectral lines obtained by Livingston and Wallace [36] using the 1-m Fourier Transform Spectrometer at the McMath telescope on Kitt peak for which no other satisfactory assignment exists. Livingston and Wallace combined infrared solar spectra at different air masses to obtain a solar spectrum in the infrared from 1850 to 9000 cm^{-1} (1.1 to 5.4 μm) corrected for atmospheric absorption by a point-by point extrapolation to zero air mass. The spectra were obtained at disk center. The observed region was free of sunspots, and a 1-m out-of-focus image (~40 arc-sec diameter area) assured that any surface velocity and brightness structure was averaged over. The spectra band width was set at long wavelengths (~5.4 μm) by the response of the InSb detectors and at the short wavelength end (~1.1 μm) by a silicon filter. The infrared lines corrected for atmospheric absorption that match the rotational transitions of lower-energy molecular hydrogen are given in Table 6. Similar observations of spectral lines obtained by Brault et al. at Kitt Peak National Observatory [37], M. Migeotte made at Jungfraujoch International Scientific Station of Switzerland [38], and Cohen [39] recorded on Skylab with the NRL's Apollo Telescope also appear in Table 6. The frequency corresponding to the $J+1$ to J rotational transition of the dihydrino molecule (Eq. (40.63) where n is an integer which corresponds to $\frac{1}{n}$, the fractional quantum number of the hydrogen-type molecule) are given in Table 6. The assignment of additional lines to rotational transitions of lower-energy hydrogen molecules was limited by the range of the spectrum, the weakness of the spectrum in certain regions, and strong atmospheric components in some regions. The presence of all of the lines in order of energy over the region observed for $n \geq 5$ may be indicative of a greater population where states $n < 5$ are ionized at $0.7R_S$ as described in the Temperature of the Transition from "Radiation Zone" to "Convection Zone" Problem Section. Also, the intensity of these forbidden lines is indicative of a substantial abundance of dihydrino molecules in the Sun.

Table 6. The $J+1$ to J rotational energy of Solar dihydrino molecules.

Observed Line Wave Number (cm^{-1})	Predicted Mills (cm^{-1}) Eq. (40.63)	n Eq. (40. 62)	Assignment Mills Transition $J+1$ to J Eq. (40.63)	Ref.	Assignment (Other)
1898.2	1898.1	2	4 to 3	36	$CO,\ \Delta v = 1\ peak$
1897.9 1894.4	1898.1	2	4 to 3	37	None
1898.1	1898.1	2	4 to 3	38	Solar in origin CO
2846.8	2847.1	2	6 to 5	36	None
2847.7	2847.1	2	6 to 5	37	None
2847.1	2847.1	2	6 to 5	38	CH_4 (telluric)
3322	3321.6	2	7 to 6	36	None
3320.4 3322	3321.6	2	7 to 6	37	None
3321.6	3321.6	2	7 to 6	38	Solar in origin Not identified
4270.8	4270.7	2	9 to 8	36	$CO,\ \Delta v = 2\ peak$
4270.7	4270.7	2	9 to 8	37	None
4745.3	4745.2	2	10 to 9	37	None
1067.7	1067.7	3	1 to 0	38	O_3 (telluric)
2135.3	2135.3	3	2 to 1	36	$CO,\ \Delta v = 1\ peak$
2135.5	2135.3	3	2 to 1	37	None
2135.3	2135.3	3	2 to 1	38	CO (telluric)
3203.1	3203.0	3	3 to 2	37	None
3203.0	3203.0	3	3 to 2	38	Not identified
4270.8	4270.7	3	4 to 3	36	$CO,\ \Delta v = 2\ peak$
4270.7	4270.7	3	4 to 3	37	None

6406.18	6406.0	3	6 to 5	36	*Ni,* 6406.18
6406.2	6406.0	3	6 to 5	37	None
7473.7	7473.7	3	7 to 6	37	None
8540.9 8542.3	8541.4	3	8 to 7	37	None
1898.2	1898.1	4	1 to 0	36	*CO,* $\Delta v = 1$ *peak*
1897.8 1898.4	1898.1	4	1 to 0	37	None
5693.8	5694.2	4	3 to 2	36	None
5693.7 5694.4	5694.2	4	3 to 2	37	None
7592.2	7592.3	4	4 to 3	36	None
7592.6	7592.3	4	4 to 3	37	None
9490.5	9490.4	4	5 to 4	37	None
2967.12	2965.8	5	1 to 0	36	None
2965.7 2966	2965.8	5	1 to 0	37	None
2965.8	2965.8	5	1 to 0	38	H_2O, $2\nu_2$ (telluric)
5931.3	5931.5	5	2 to 1	36	None
5931.5	5931.5	5	2 to 1	37	None
8896.7	8897.3	5	3 to 2	36	None
8897.3	8897.3	5	3 to 2	37	None
4270.8	4270.7	6	1 to 0	36	*CO,* $\Delta v = 2$ *peak*
4270.7	4270.7	6	1 to 0	37	None
8540.9 8542.3	8541.4	6	2 to 1	37	None
5812.26 5814.2	5812.9	7	1 to 0	36	*Fe at* 5812.26 None
5812.7	5812.9	7	1 to 0	37	None

7592.2	7592.3	8	1 to 0	36	None
7592.6	7592.3	8	1 to 0	37	None
60,124	60,142	13	3 to 2	39	$Fe(II)$
69,783	69,750	14	3 to 2	39	None
53,362	53,381	15	2 to 1	39	Active region Unidentified
80,038	80,071	15	3 to 2	39	None
60,710	60,735	16	2 to 1	39	Active region Unidentified
68,582	68,564	17	2 to 1	39	$C(I)$
76,869	76,868	18	2 to 1	39	None

IDENTIFICATION OF HYDRINO HYDRIDE ENERGY LEVELS BY SOFT X-RAYS, ULTRAVIOLET (UV), AND VISIBLE EMISSIONS FROM THE SUN

Hydrino $H\left(\frac{a_H}{p}\right)$ reacts with an electron to form a corresponding ***hydrino hydride ion***, hereinafter designated as $H^-(n=1/p)$:

$$H\left(\frac{a_H}{p}\right)+e^- \rightarrow H^-(n=1/p) \tag{40.64}$$

The product is a hydride ion (H^-) having a binding energy given by the following formula (Eq. (7.58)) derived in the Hydrino Hydride Section

$$Binding\ Energy = \frac{\hbar^2\sqrt{s(s+1)}}{8\mu_e a_0^2\left[1+\frac{\sqrt{s(s+1)}}{p}\right]^2}-\frac{\pi\mu_0 e^2\hbar^2}{m_e^2 a_0^3}\left(1+\frac{2^2}{\left[1+\frac{\sqrt{s(s+1)}}{p}\right]^3}\right) \tag{40.65}$$

where p is an integer greater than one, $s=1/2$, π is pi, $\hbar$ is the Planck's constant bar, μ_o is the permeability of vacuum, m_e is the mass of the electron, μ_e is the reduced electron mass, a_o is the Bohr radius, and e is the elementary charge. Each hydride ion having fractional quantum energy level comprises two indistinguishable electrons bound to a proton where the radius of the two electrons of the hydrino hydride ion as a function of p (Eq. (7.57)) is

$$r_2 = r_1 = \frac{a_0}{p}\left(1+\sqrt{s(s+1)}\right);\ s=\frac{1}{2} \tag{40.66}$$

Solar Hydrino Hydride Lines

The Solar hydrino hydride emission lines were sought. For typical conditions in the photosphere Figure 2 [40] shows the continuous absorption coefficient $\kappa_C(\lambda)$ of the Sun. In the visible and infrared, the hydride ion H^- is the dominant absorber. Its free-free continuum starts at $\lambda = 1.645\ \mu m$, corresponding to the ionization energy of $0.745\ eV$ for H^- with strongly increasing absorption towards the far infrared.

Figure 2. Continuum absorption coefficient (per particle) in the solar atmosphere, at $\tau_{500} = 0.1$.

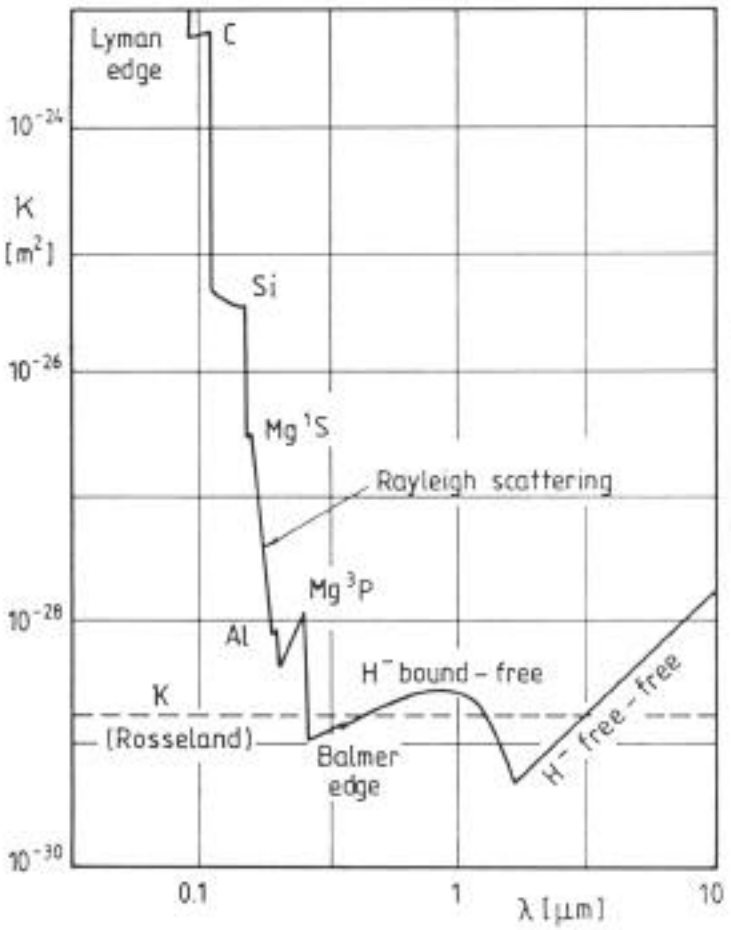

Hydrinos soft X-ray emissions from the dark interstellar medium observed by Labov and Bowyer [2] and the soft X-ray emissions of the

Sun [9,11-13] are given in the INTERSTELLAR MEDIUM Secton and the SOLAR DATA Section, respectively. In these cases, a hydrogen atom in a fractional quantum state, $H\left(n_i\right)$, collides, for example, with a $n=\frac{1}{2}$ hydrogen atom, $H\left(\frac{1}{2}\right)$, and the result is an even lower-energy hydrogen atom, $H\left(n_f\right)$, and $H\left(\frac{1}{2}\right)$ is ionized.

$$H\left(n_i\right)+H\left(\frac{1}{2}\right)\rightarrow H\left(n_f\right)+H^{+}+e^{-}+photon \tag{40.67}$$

The energy released, as a photon, is the difference between the energies of the initial and final states given by Eq. (40.2a) with Eq. (40.2c) minus the ionization energy of $H\left(\frac{1}{2}\right)$, $54.4\,eV$. For example, in Table 2, all of the transitions between different fractional quantum energy levels are present in order of energy from the $1\rightarrow 1/2$ H transition to the $1/9\rightarrow 1/10$ H transition. A solar hydrino atom $H\left(\frac{a_H}{p}\right)$ may react with free electrons in the Sun or ionize an atom of lower electron affinity to form the hydrino hydride $H^{-}\left(n=1/p\right)$ according to Eq. (40.64). The ionization energies of the hydrino hydride ion $H^{-}\left(n=1/p\right)$ as a function of p, where p, is an integer are shown in Table 7. These lines were sought in published solar spectra. Each predicted peak is a sharp emission peak in the case that the solar temperature is lower than the ionization energy of the hydrino hydride and a continuum absorption peak increasing to lower wavelengths of width corresponding to the local solar temperature in the case that the ionization energy is lower than the local solar temperature.

A. The Data and Hydrino Hydride Assignments

The calculated (Eq. (40.65) with Eq. (40.66)) and observed emission and continuum peaks at the ionization energy of the hydrino hydride ion $H^{-}\left(n=1/p\right)$ as a function of p, for $p=1$ to $p=10$ are given in Table 7.

Table 7. The calculated (Eq. (40.65) with Eq. (40.66)) and observed emission and continuum peaks at the ionization energy of the hydrino hydride ion $H^-(n=1/p)$ as a function of p, for $p=1$ to $p=10$. (Raw extreme ultraviolet (EUV) solar spectral data $(17-45\ nm)$ taken from Figures 3a-k of [9], Raw EUV solar spectral data $(20-170\ nm)$ taken from spectra of [41] and $(70-160\ nm)$ taken from spectra of [42]; Raw UV solar spectral data $(117.5-195\ nm)$ taken from spectra of [43]; Raw near UV/visible $(119.5-420.5\ nm)$ taken from spectra of [44]).

Hydride Ion	r_1 (a_o)[a]	Calculated Ionization Energy[b] (eV)	Calculated Wavelength (nm)	Experimental Wavelength (nm)	Ref.	Assignment (Other) & Comments
$H^-(n=1)$	1.866	0.754	1645	1645	45	$H^-(n=1)$
$H^-(n=1/2)$	0.9330	3.047	406.9	407	44	None Continuum Peak
$H^-(n=1/3)$	0.6220	6.610	187.57	187.58	43	Ratio of 1875.7 Å Peak to Fe II peak at 1876.838 Å increased by a factor of 25 in a Flare Versus the Quiet Sun
$H^-(n=1/4)$	0.4665	11.23	110.4	110.4	41; 42	None Continuum Peak 3 eV Width
$H^-(n=1/5)$	0.3732	16.70	74.23	74.23	41	None Continuum Peak 3 eV Width
$H^-(n=1/6)$	0.3110	22.81	54.36	54.36	41	None Continuum Peak 3 eV Width
$H^-(n=1/7)$	0.2666	29.34	42.26	42.26	9	Peak Indicated Unassignable
$H^-(n=1/8)$	0.2333	36.08	34.36	34.36	9	Peak Indicated Unassignable
$H^-(n=1/9)$	0.2073	42.83	28.95	28.92	9	Fe XIV Broad Peak
$H^-(n=1/10)$	0.1866	49.37	25.11	25.11	9	Fe XVI Sharp Peak on Top of Broad Peak

[a] Equation (40.66)
[b] Equation (40.65)

B. Discussion

As shown in Table 7 hydrino hydride ionization energies predicted by Mills' theory match the emission spectral lines of the Sun for high energies and match the continuum lines at lower energies. Two of the emission lines of Table 7 corresponding to $H^-(n=1/7)$ and $H^-(n=1/8)$ had no previous assignment. The continuum lines at 407 *nm*, 110.4 *nm*, 74.23 *eV*, and 54.36 *eV* corresponding to $H^-(n=1/2)$, $H^-(n=1/4)$, $H^-(n=1/5)$, $H^-(n=1/6)$, respectively, were previously unidentified. And, the width of the continuum lines corresponding to $H^-(n=1/4)$, $H^-(n=1/5)$, and $H^-(n=1/6)$ shown in Figure 3 and Figure 4 are each 3 *eV* wide indicating a very consistent local solar temperature of 23,000 °*K* [46]. The continuum line at 407 *nm* corresponding to $H^-(n=1/2)$ appears in Figure 5. The hydrino hydride continuum lines and the normal hydride continuum line shown in Figure 2 extends the series of Solar continuum lines from $H^-(n=1)$ to $H^-(n=1/6)$ with the exception of $H^-(n=1/3)$ for which no absolute intensity data is available. (Figure 5 covers the spectral range at the wavelength predicted for $H^-(n=1/3)$--187.58 *nm*, but the spectrometer was ground-based. Wavelengths short of 260 *nm* were essentially eliminated by nitrogen, oxygen and water vapor absorption.) The existence of the peaks at the predicted energies with the continuum features substantially identifies the 407 *nm*, 110.4 *nm*, 74.23 *eV*, and 54.36 *eV* peaks as hydrino hydride peaks. And, the 1875.8 *Å* peak can be substantially assigned to $H^-(n=1/3)$ by comparing the intensity of this peak during a flare versus the quiet Sun. Solar emission lines in the extreme ultraviolet were observed by the Extreme Ultraviolet Explorer (EUVE) Deep Survey telescope on the star AU Microscopii and the star EQ Pegasi for which there is no satisfactory assignment. These spectral lines match hydrino transitions as shown in Tables 3 and 4. The lines assigned to hydrino transitions increased significantly in intensity during the flare event. The data is consistent with disproportionation reactions of hydrinos as the mechanism of solar flare activity. Because flare activity is due to hydrino formation reactions and flares possess free electrons, hydrino hydride ions are predicted to form in abundance during a flare event. The 1875.8 *Å* peak at the ionization energy of the hydrino hydride ion $H^-(n=1/3)$ and the 1876.838 *Å* peak of Fe II from the quiet Sun spectrum and from a Solar flare spectrum recorded on Skylab with NRL's Apollo Telescope Mount Experiment are shown in Figures 6A and 6B, respectively. The ratio of the intensity above background of the $H^-(n=1/3)$ at 1875.8 *Å* relative to the Fe II peak at 1876.838 *Å* increases by a factor greater than 25 during a solar flare event. This is a "smoking

gun" of hydrino hydride formation. The agreement between the predicted and observed continuum series and increased intensity of the 1875.8 $\AA$ peak during a solar flare is remarkable.

Hydrino hydride compounds may be the source of the diffuse interstellar bands (DIBs) [47]. Compounds comprising hydrino hydride ion(s), hydrino atom(s), dihydrino molecular ion(s), and/or dihydrino molecule(s) as well as normal hydrogen atoms and molecules are given in the Additional Increased Binding Energy Hydrogen Compounds Section of Mills PCT Patent Appl. [48]. Many are predicted to have unique absorption features in the visible due energy shifts of elements other than hydrogen by lower-energy hydrogen. And, examples of the hydride $H^-(n=1/2)$ as a possible carrier of some DIBs due to its shifted free space continuum at 407 nm are the 4,430 DIB [49] and others in this wavelength region [47]. The source of the colors of Jupiter including the Red Spot is a mystery [50]. Hydrino Hydride compounds and the hydrino hydride ion $H^-(n=1/2)$ may be the carrier. A unique feature in the albedos of Jupiter is observed at the $H^-(n=1/2)$ bound-free continuum [51] wavelengths. And a broadband 410 nm filter generates the greatest contrast in global latitude-longitude maps [52] of Jupiter. Other emission features which can be assigned to hydrino hydride are observed in the spectra of Jupiter as well as the other hydrogen planets, Saturn and Neptune. For example, the 110 nm emission of $H^-(n=1/4)$ is seen in the case of Jupiter [53], Saturn [54], and Neptune [55].

Figure 3A. The continuum peaks at the ionization energy of the hydrino hydride ions $H^-(n=1/4)$, $H^-(n=1/5)$, and $H^-(n=1/6)$ from the Solar Extreme Ultraviolet Hichhiker (SEH) [41].

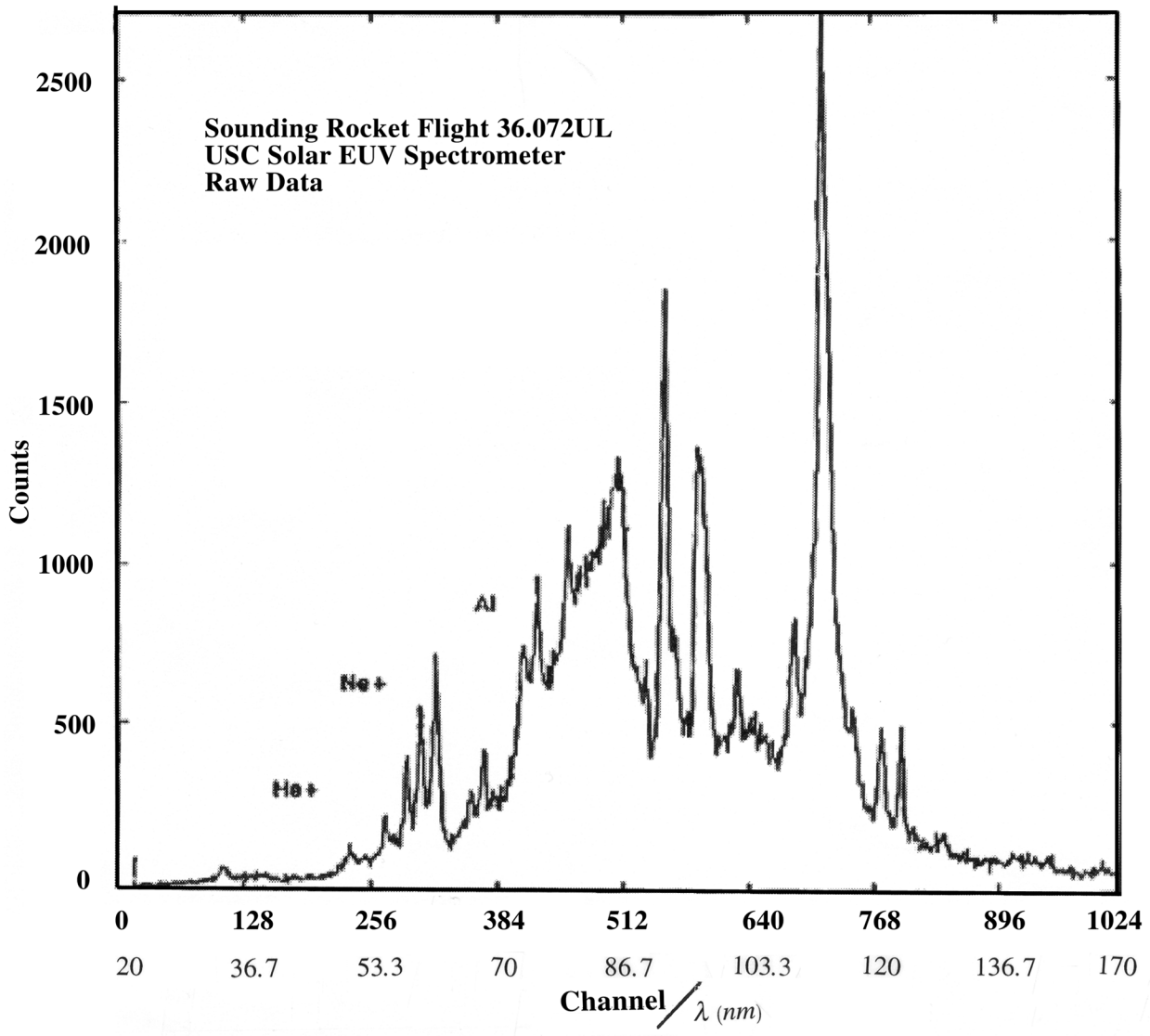

Figure 3B. The continuum peaks at the ionization energy of the hydrino hydride ions $H^-(n=1/4)$, $H^-(n=1/5)$, and $H^-(n=1/6)$ from the Solar Extreme Ultraviolet Hichhiker (SEH) [41].

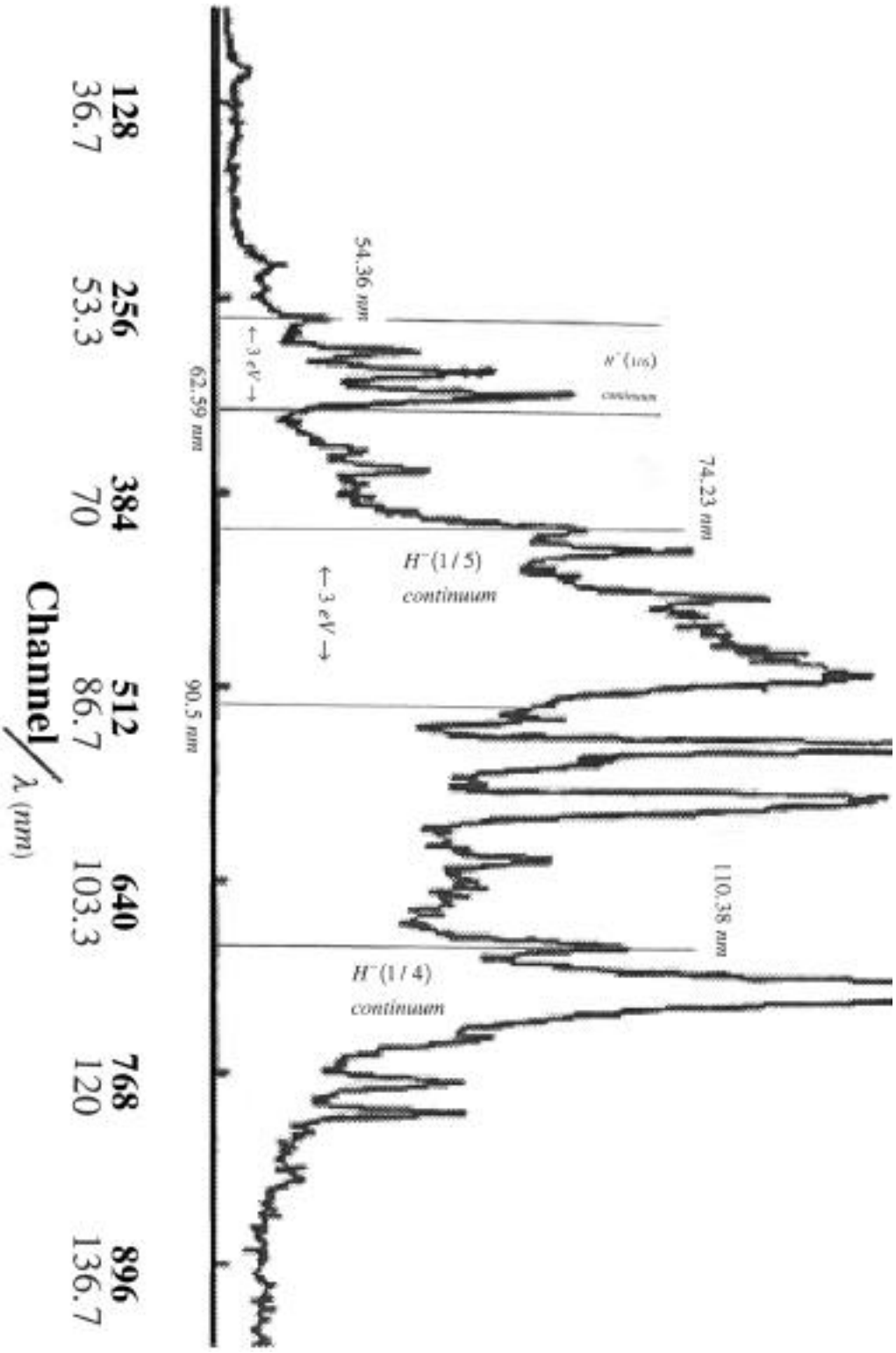

Figure 4. The continuum peaks at the ionization energy of the hydrino hydride ions $H^-(n=1/4)$ and $H^-(n=1/5)$ and from the SUMER EUV Spectrum: 25/30-Jan-1996 [42].

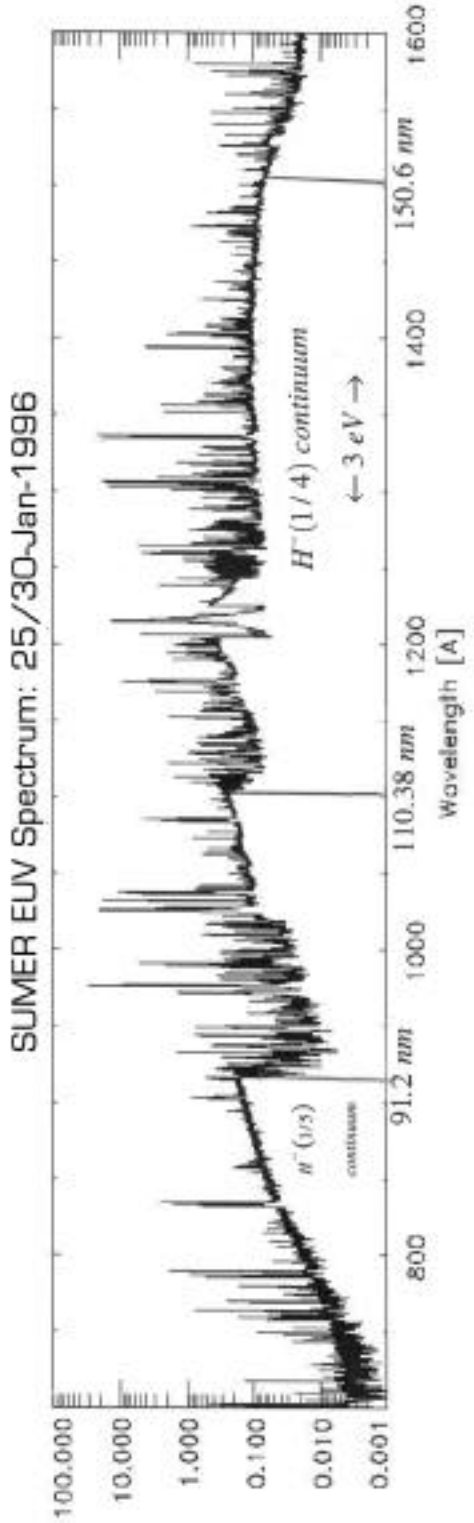

Figure 5. The continuum peak at the ionization energy of the hydrino hydride ion $H^-(n=1/2)$ from the ground-based UARS/SOLSTICE Irradiance 119.5 nm to 420.5 nm, 1 nm spectral resolution, UARS day 145 = 3 Feb 1992, UARS day 1250 = 12 Feb 1995 [44].

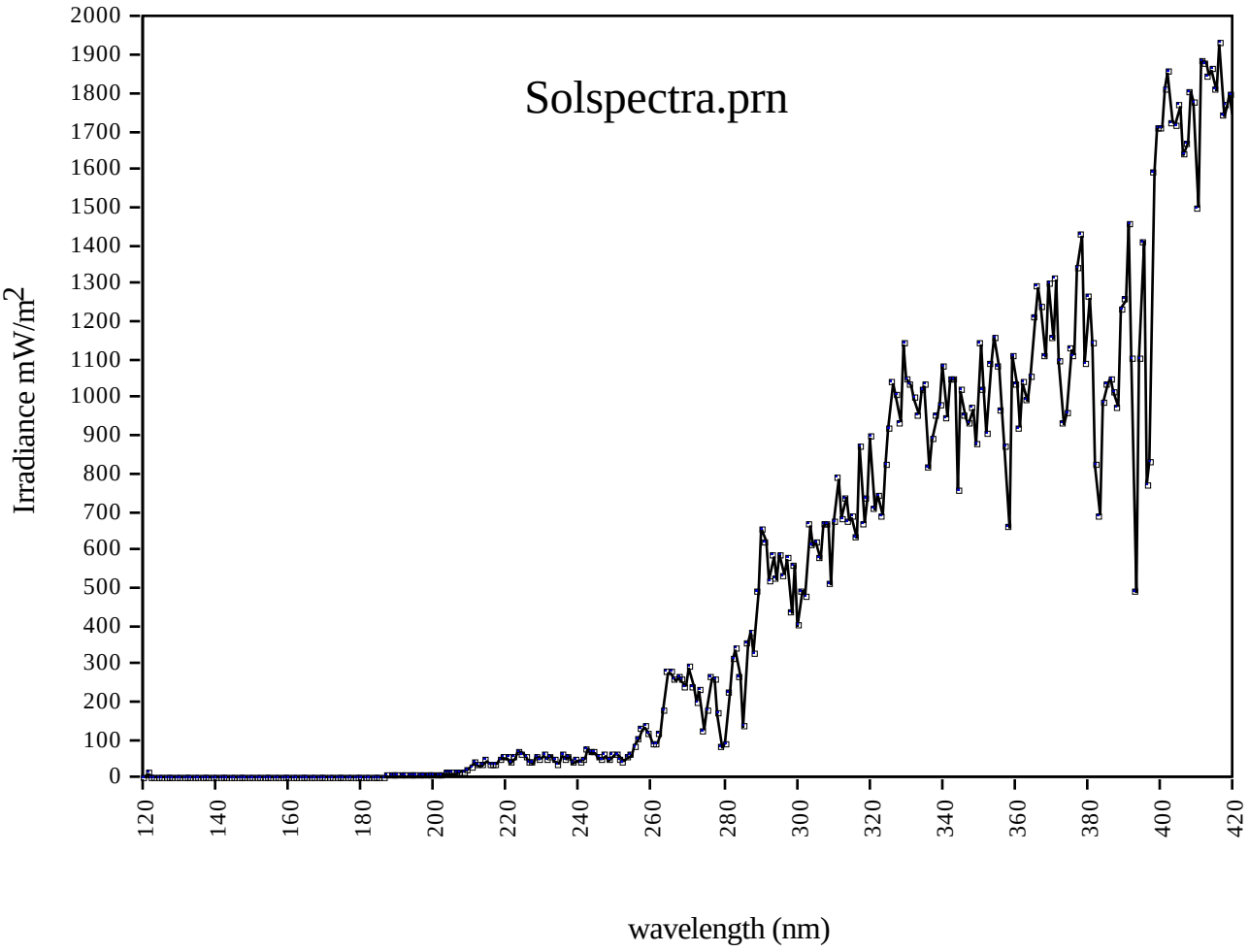

Figure 6A. The 1875.8 $\AA$ peak at the ionization energy of the hydrino hydride ion $H^-(n=1/3)$ and the 1876.838 $\AA$ peak of Fe II from the quiet Sun spectrum recorded on Skylab with NRL's Apollo Telescope Mount Experiment [43].

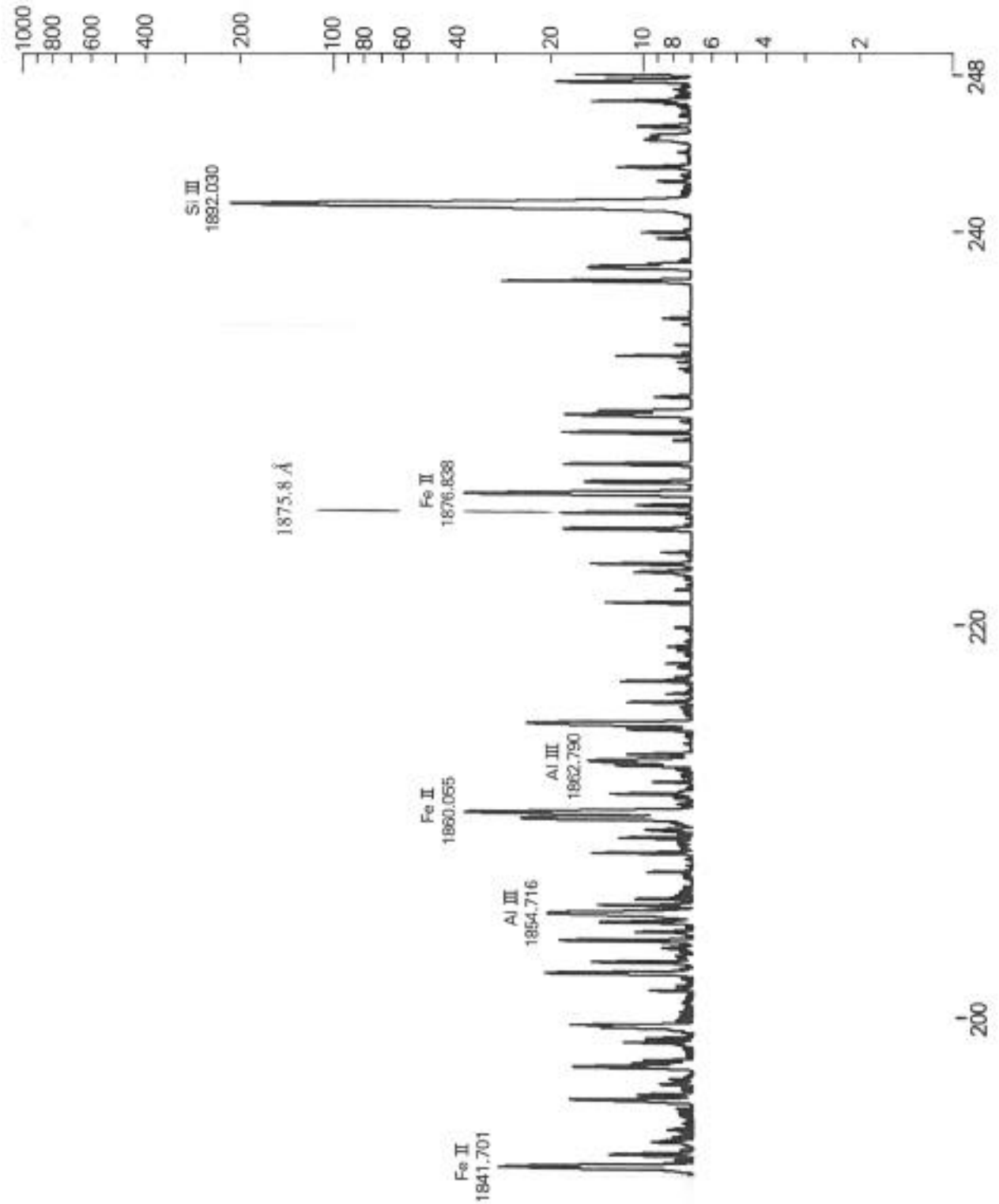

Figure 6B. The 1875.8 $\AA$ peak at the ionization energy of the hydrino hydride ion $H^-(n=1/3)$ and the 1876.838 $\AA$ peak of Fe II from a Solar flare spectrum recorded on Skylab with NRL's Apollo Telescope Mount Experiment [43].

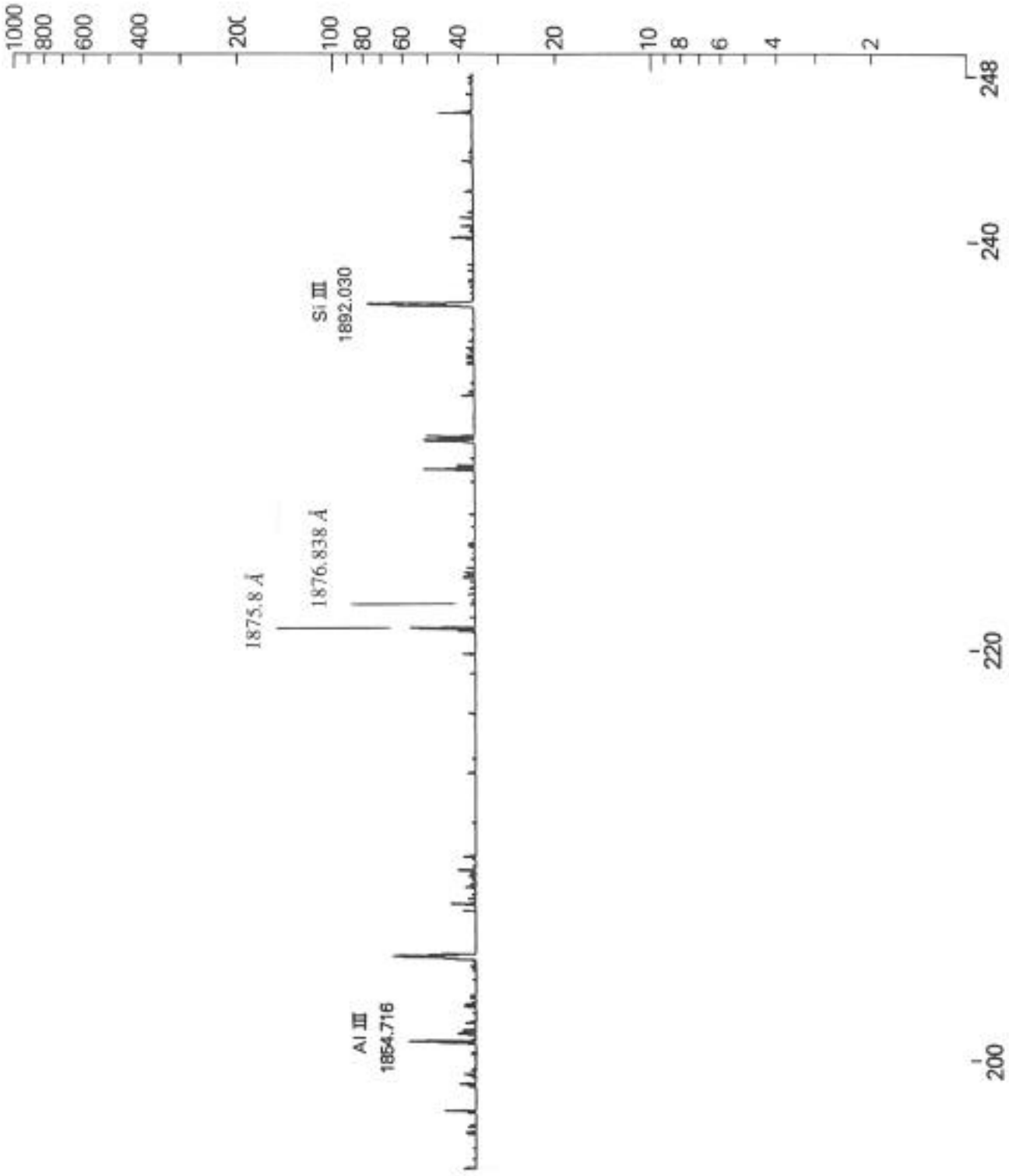

Acknowledgments

Special thanks to S. Labov and S. Bowyer for providing their raw digitized spectroscopic data and W. Good for bringing this paper to my attention and for identifying significant peaks in their raw data. Special thanks to J. Farrell for line assignments of solar data.

References

1. Davidsen, A., et al., "Test of the decaying dark matter hypothesis using the Hopkins ultraviolet telescope", Nature, 351, (1991), pp. 128-130.
2. Labov, S., Bowyer, S., "Spectral observations of the extreme ultraviolet background", The Astrophysical Journal, 371, (1991), pp. 810-819.
3. Bahcall, J., et al., "Solar neutrinos: a field in transition", Nature, 334, 11, (1988), pp. 487-493.
4. G., Taubes, Science, 256, (1992), pp. 1512-1513.
5. G., Taubes, Science, 256, (1992), pp. 731-733.
6. Schwarzschild, B., Physics Today, April, (1995), pp.19-21.
7. J., Harvey, Physics Today, October, (1995), pp. 32-38.
8. B., Schwarzschild, Physics Today, October, (1990), pp. 17-20.
9. Thomas, R. J., Neupert, W., M., Astrophysical Journal Supplement Series, Vol. 91, (1994), pp. 461-482.
10. Stix, M., The Sun, Springer-Verlag, Berlin, (1991), pp. 351-356.
11. Malinovsky, M., Heroux, L., Astrophysical Journal, Vol. 181, (1973), pp. 1009-1030.
12. Noyes, R., The Sun, Our Star, Harvard University Press, Cambridge, MA, (1982), p.172.
13. Phillips, J. H., Guide to the Sun, Cambridge University Press, Cambridge, Great Britain, (1992), pp. 118-119; 120-121; 144-145.
14. Stix, M., The Sun, Springer-Verlag, Berlin, (1991), p. 321.
15. Phillips, J. H., Guide to the Sun, Cambridge University Press, Cambridge, Great Britain, (1992), p. 119.
16. Phillips, J. H., Guide to the Sun, Cambridge University Press, Cambridge, Great Britain, (1992), p. 158.
17. Stix, M., The Sun, Springer-Verlag, Berlin, (1991), pp. 6-12; 347-350.
18. Phillips, J. H., Guide to the Sun, Cambridge University Press, Cambridge, Great Britain, (1992), pp. 107-130; 360.
19. Phillips, J. H., Guide to the Sun, Cambridge University Press, Cambridge, Great Britain, (1992), pp. 126-127; 360.
20. Jackson, J. D., Classical Electrodynamics, Second Edition, John Wiley & Sons, New York, (1962), pp. 739-752.
21. Fang , L. Z., and Ruffini, R., Basic Concepts in Relativistic Astrophysics, World Scientific, (1983).
22. Fowles, G. R., Analytical Mechanics, Third Edition, Holt, Rinehart, and Winston, New York, (1977), p196.

23. Lerner, E., The Big Bang Never Happened, Times Books, (1990), pp. 186-190.
24. Stix, M., The Sun, Springer-Verlag, Berlin, (1991), pp. 1-19.
25. R. Cowen, Science News, 141, (1992), pp. 344-346.
26. Bowyer, S., Science, Vol. 263, (1994), pp. 55-59.
27. Fossi, B. C. M., et al., Astrophysical Journal, 449, (1995), pp. 376-385.
28. J. Tennyson, Physics World, July, (1995), pp. 33-36.
29. Sandel, B. R., et al., Science, Vol. 215, January, (1982), pp. 548-553.
30. Trafton, L. M., Gerard, J. C., Munhoven, G., Waite, J. H., The Astrophysical Journal, Vol. 421, (1994) pp. 816-827.
31. Trafton, L. M., Watson, J. K. G., The Astrophysical Journal, 385, (1992), pp. 320-326.
32. Phillips, J. H., Guide to the Sun, Cambridge University Press, Cambridge, Great Britain, (1992), pp. 137-139.
33. W. T. Reach, et. al., The Astrophysical Journal, 451, (1995), pp. 188-199.
34. E. L. Wright, et. al., The Astrophysical Journal, 381, (1991), pp. 200-209.
35. J. C. Mather, et. al., The Astrophysical Journal, 420, (1994), pp. 439-444.
36. Livingston, W., Wallace, L., An Atlas of the Solar Spectrum in the Infrared from 1850 to 9000 cm^{-1} (1.1 to 5.4 μm) with Identifications of the Main Solar Features, published by the National Optical Astronomy Observatories, December 18, (1990).
37. L. Delbouille, G. Roland, J. Brault, L. Testerman, Photometric Atlas of the Solar Spectrum from 1,850 to 10,000 cm^{-1}, Kitt Peak National Observatory, Tucson, AZ.
38. M. Migeotte, L. Neven, J. Swensson, The Solar Spectrum from 2.8 to 23.7 Microns, Part II. Measurements and Identifications with W. S. Benedict, Comments on the Spectra of Telluric H_2O and CO_2 as Observed in the Solar Spectrum. 2.8-23.7 Microns, Institut D'Astrophysique De L'Universite' De Liege Observatoire Royal De Belgique, Technical Final Report-Phase A (Part II) Under Contract AF 61 (514)-432.
39. L. Cohen, An Atlas of Solar Spectra Between 1175 and 1950 Angstroms Recorded on Skylab with the NRL's Apollo Telescope Mount Experiment, Laboratory for Astronomy and Solar Physics, Goddard Space Flight Center, NASA Reference Publication 1069, March, (1981).
40. Stix, M., The Sun, Springer-Verlag, Berlin, (1991), p. 136.
41. Darrell Judge, University of Southern California Space Science Center, Solar Extreme Ultraviolet Hichhiker (SEH), http://sspp.gsfc.nasa.gov/seh.html.

42. hptt://umbra.nascom.nasa.gov, Solar Data Analysis Center (SDAC),SUMER EUV Spectrum: 25/30-Jan-1996, www.uio.no/~paalb/sumer_atlas.html.
43. Leonard Cohen, An Atlas of Spectra Between 1175 and 1950 Angstroms Recorded on Skylab with NRL's Apollo Telescope Mount Experiment, (NASA Ref. Pub. 1069) March 1981, NASA.
44. UARS/SOLSTICE Irradiance 119.5 nm to 420.5 nm, 1 nm spectral resolution, UARS day 145 = 3 Feb 1992, UARS day 1250 = 12 Feb 1995, hptt://umbra.nascom.nasa.gov, Solar Data Analysis Center (SDAC), ftp://umbra.nascom.nasa.gov/pub/uv_atlases/, solspectra.prn.
45. John A. Dean, Editor, Lange's Handbook of Chemistry, Thirteenth Edition, McGraw-Hill Book Company, New York, (1985), p. 3-10.
46. Stix, M., The Sun, Springer-Verlag, Berlin, (1991), p. 141.
47. P. Jenniskens, F. -X. Desert, Astron. Astrophys. Suppl. Ser., Vol. 106, (1994), pp. 39-78.
48. R. Mills, US Patent Application entitled, "Novel Hydride Compounds", PCT Patent Application, PCT US98/14029 filed on July 7, 1998.
49. C. Joblin, J. P. Maillard, L. d'Hendecourt, and A. Leger, Nature, 346, (1990), pp. 729-732.
50. R. Beebe, Jupiter The Giant Planet, Second Edition, Smithsonian Institute Press, Washington, (1997), pp. 64-65.
51. C. B. Pilcher, R. G. Prinn, T. B. McCord, Journal of the Atmospheric Sciences, Vol. 30, (1973), pp. 302-307.
52. A. A. Simon, R. F. Beebe, ICARUS, Vol. 121, (1996) pp. 319-330.
53. A. L. Broadfoot, et. al., Science, Vol. 204, June 1, (1979), pp. 979-982.
54. B. R. Sandel, et. al., Science, Vol. 215, January 29, (1982), pp. 548-553.
55. A. L. Broadfoot, et. al., Science, Vol. 246, December, (1989), pp. 1459-1466.